INSTRUMENTAL ANALYSIS (CHEM 311)



Deon Miles
Sewanee, the University of the South

LibreTexts™

Instrumental Analysis (CHEM 311)

This text is disseminated via the Open Education Resource (OER) LibreTexts Project (https://LibreTexts.org) and like the thousands of other texts available within this powerful platform, it is freely available for reading, printing, and "consuming."

The LibreTexts mission is to bring together students, faculty, and scholars in a collaborative effort to provide and accessible, and comprehensive platform that empowers our community to develop, curate, adapt, and adopt openly licensed resources and technologies; through these efforts we can reduce the financial burden born from traditional educational resource costs, ensuring education is more accessible for students and communities worldwide.

Most, but not all, pages in the library have licenses that may allow individuals to make changes, save, and print this book. Carefully consult the applicable license(s) before pursuing such effects. Instructors can adopt existing LibreTexts texts or Remix them to quickly build course-specific resources to meet the needs of their students. Unlike traditional textbooks, LibreTexts' web based origins allow powerful integration of advanced features and new technologies to support learning.



LibreTexts is the adaptable, user-friendly non-profit open education resource platform that educators trust for creating, customizing, and sharing accessible, interactive textbooks, adaptive homework, and ancillary materials. We collaborate with individuals and organizations to champion open education initiatives, support institutional publishing programs, drive curriculum development projects, and more.

The LibreTexts libraries are Powered by NICE CXone Expert and was supported by the Department of Education Open Textbook Pilot Project, the California Education Learning Lab, the UC Davis Office of the Provost, the UC Davis Library, the California State University Affordable Learning Solutions Program, and Merlot. This material is based upon work supported by the National Science Foundation under Grant No. 1246120, 1525057, and 1413739.

Any opinions, findings, and conclusions or recommendations expressed in this material are those of the author(s) and do not necessarily reflect the views of the National Science Foundation nor the US Department of Education.

Have questions or comments? For information about adoptions or adaptions contact info@LibreTexts.org or visit our main website at https://LibreTexts.org.

This text was compiled on 08/19/2025

TABLE OF CONTENTS

Licensing

1: Introduction to Analytical Chemistry

- 1.1: What is Analytical Chemistry
- 1.2: The Analytical Perspective
- 1.3: Common Analytical Problems
- 1.4: Types of Instrumental Methods
- 1.5: Problems
- 1.6: Additional Resources
- 1.7: Chapter Summary and Key Terms

2: Basic Tools of Analytical Chemistry

- 2.1: Measurements in Analytical Chemistry
- 2.2: Concentration
- 2.3: Stoichiometric Calculations
- 2.4: Basic Equipment
- 2.5: Preparing Solutions
- 2.6: Spreadsheets and Computational Software
- 2.7: The Laboratory Notebook
- 2.8: Problems
- 2.9: Additional Resources
- 2.10: Chapter Summary and Key Terms

3: The Vocabulary of Analytical Chemistry

- 3.1: Analysis, Determination, and Measurement
- 3.2: Techniques, Methods, Procedures, and Protocols
- 3.3: Classifying Analytical Techniques
- 3.4: Selecting an Analytical Method
- 3.5: Developing the Procedure
- 3.6: Protocols
- 3.7: The Importance of Analytical Methodology
- 3.8: Problems
- 3.9: Additional Resources
- 3.10: Chapter Summary and Key Terms

4: Evaluating Analytical Data

- 4.1: Characterizing Measurements and Results
- 4.2: Characterizing Experimental Errors
- 4.3: Propagation of Uncertainty
- 4.4: The Distribution of Measurements and Results
- 4.5: Statistical Analysis of Data
- 4.6: Statistical Methods for Normal Distributions
- 4.7: Detection Limits
- 4.8: Using Excel and R to Analyze Data
- 4.9: Problems
- 4.10: Additional Resources

- 4.11: Chapter Summary and Key Terms

5: Standardizing Analytical Methods

- 5.1: Analytical Signals
- 5.2: Calibrating the Signal
- 5.3: Determining the Sensitivity
- 5.4: Linear Regression and Calibration Curves
- 5.5: Compensating for the Reagent Blank
- 5.6: Using Excel and R for a Linear Regression
- 5.7: Problems
- 5.8: Additional Resources
- 5.9: Chapter Summary and Key Terms

6: Spectroscopic Methods

- 6.1: Overview of Spectroscopy
- 6.2: Spectrometer
  - 6.2.1: ATR-FTIR
- 6.3: Spectroscopy Based on Absorption
- 6.4: Lasers
  - 6.4.1: Gas Lasers
  - 6.4.2: Laser Theory
  - 6.4.3: Overview of Lasers
  - 6.4.4: Semiconductor and Solid-state lasers
  - 6.4.5: Semiconductors
- 6.5: UV/Vis and IR Spectroscopy
- 6.6: Signals and Noise
  - 6.6.1: The Signal-to-Noise Ratio
  - 6.6.2: Sources of Instrumental Noise
  - 6.6.3: Signal-to-Noise Enhancement
- 6.7: Emission Spectroscopy
- 6.8: Photoluminescent Spectroscopy
- 6.9: Analytical Chemiluminescence
  - 6.9.1: Introduction to Chemiluminescence
    - 6.9.1.1: Electronic transitions and luminescence
    - 6.9.1.2: Chemiluminescence Spectroscopy
  - 6.9.2: Instrumentation
    - 6.9.2.1: Detection of chemiluminescence
- 6.10: Detectors
  - 6.10.1: Detectors of Light
  - 6.10.2: Radiation Transducers
- 6.11: An Introduction to Infrared Spectrometry
  - 6.11.1: Theory of Infrared Absorption Spectrometry
  - 6.11.2: Infrared Sources and Transducers
  - 6.11.3: FTIR- Hardware
  - 6.11.4: Infrared Instruments
- 6.12: Applications of Infrared Spectrometry
  - 6.12.1: Mid-Infrared Absorption Spectometry
  - 6.12.2: Mid-Infrared Reflection Spectrometry

- 6.12.3: Near-Infrared and Far-Infrared Spectroscopy
- 6.13: Raman Spectroscopy
  - 6.13.1: Theory of Raman Spectroscopy
  - 6.13.2: Instrumentation
  - 6.13.3: Applications of Raman Spectroscopy
  - 6.13.4: Other Types of Raman Spectroscopy
- 6.14: Problems
- 6.15: Additional Resources
- 6.16: Chapter Summary and Key Terms

7: Nuclear Magnetic Resonance Spectroscopy

- 7.1: Theory of Nuclear Magnetic Resonance
- 7.2: Environmental Effects on NMR Spectra
  - 7.2.1: Spin-Spin Coupling
  - 7.2.2: The Basis for Differences in Chemical Shift
- 7.3: NMR Spectrometers
- 7.4: Applications of Proton NMR
- 7.5: Carbon-13 NMR
- 7.6: Two-Dimensional Fourier Transform NMR
- 7.7: Structure Determination - Nuclear Magnetic Resonance Spectroscopy
  - 7.7.1: Nuclear Magnetic Resonance Spectroscopy
  - 7.7.2: The Nature of NMR Absorptions
  - 7.7.3: The Chemical Shift
  - 7.7.4: Chemical Shifts in ^{1}H NMR Spectroscopy
  - 7.7.5: Integration of ^{1}H NMR Absorptions - Proton Counting
  - 7.7.6: Spin-Spin Splitting in ^{1}H NMR Spectra
  - 7.7.7: ^{1}H NMR Spectroscopy and Proton Equivalence
  - 7.7.8: More Complex Spin-Spin Splitting Patterns
  - 7.7.9: Uses of ^{1}H NMR Spectroscopy
  - 7.7.10: ^{13}C NMR Spectroscopy - Signal Averaging and FT-NMR
  - 7.7.11: Characteristics of ^{13}C NMR Spectroscopy
  - 7.7.12: DEPT ^{13}C NMR Spectroscopy
  - 7.7.13: Uses of ^{13}C NMR Spectroscopy
  - 7.7.S: Structure Determination - Nuclear Magnetic Resonance Spectroscopy (Summary)

8: Molecular Mass Spectrometry

- 8.1: General Features of Atomic Mass Spectrometry
- 8.2: Molecular Mass Spectra
- 8.3: How the Mass Spectrometer Works
- 8.4: Mass Spectrometers
- 8.5: Ion Sources
  - 8.5.1: Electrospray Ionization Mass Spectrometry
- 8.6: Mass Spectrometers
  - 8.6.1: Mass Analyzers (Mass Spectrometry)
- 8.7: Applications of Molecular Mass Spectrometry
  - 8.7.1: Interpreting a Mass Spectrum
  - 8.7.2: The Molecular Ion (M^{+}) Peak
  - 8.7.3: The M+1 Peak
  - 8.7.4: The Mass Spectra of Elements

- 8.7.5: Fragmentation Patterns in Mass Spectra
- 8.7.6: Mass Spectrometry - Fragmentation Patterns
- 8.7.7: Organic Compounds Containing Halogen Atoms

9: Atomic Spectroscopy

- 9.1: Introduction to Atomic Absorption Spectroscopy
- 9.2: Sample Atomization Techniques
- 9.3: Atomic Absorption Instrumentation
- 9.4: Interferences in Absorption Spectroscopy
- 9.5: Atomic Absorption Techniques
- 9.6: Atomic Absorption Spectroscopy
- 9.7: Atomic Emission Spectroscopy
  - 9.7.1: Emission Spectroscopy Based on Flame and Plasma Sources
  - 9.7.2: Atomic Emission Spectroscopy
  - 9.7.3: Inductively Coupled Plasma Mass Spectrometer

10: Chromatographic and Electrophoretic Methods

- 10.1: Introduction to Chromatographic Separations
  - 10.1.1: A General Description of Chromatography
  - 10.1.2: Migration Rates of Solutes
  - 10.1.3: Zone Broadening and Column Efficiency
  - 10.1.4: Chromatography
  - 10.1.5: Optimization and Column Performance
  - 10.1.6: Summary of Important Relationships for Chromatography
  - 10.1.7: Applications of Chromatography
- 10.2: Gas Chromatography
  - 10.2.1: Gas Chromatography
- 10.3: High-Performance Liquid Chromatography
  - 10.3.1: High Performance Liquid Chromatography
- 10.4: Other Forms of Chromatography
  - 10.4.1: Chromatographic Columns
- 10.5: Capillary Electrophoresis and Capillary Electrochromatography
  - 10.5.1: An Overview of Electrophoresis
  - 10.5.2: Capillary Electrophoresis
  - 10.5.3: Capillary Electrophoresis
    - 10.5.3.1: Ionic Mobility and Electrophoresis
  - 10.5.4: Applications of Capillary Electrophoresis
- 10.6: Problems
- 10.7: Additional Resources
- 10.8: Chapter Summary and Key Terms

11: Thermal Methods

- 11.1: Thermogravimetry
- 11.2: Differential Thermal Analysis and Differential Scanning Calorimetry

12: Equilibrium Chemistry

- 12.1: Reversible Reactions and Chemical Equilibria
- 12.2: Thermodynamics and Equilibrium Chemistry

- 12.3: Manipulating Equilibrium Constants
- 12.4: Equilibrium Constants for Chemical Reactions
- 12.5: Ladder Diagrams
- 12.6: Problems
- 12.7: Additional Resources
- 12.8: Chapter Summary and Key Terms

13: Electrochemical Methods

- 13.1: Overview of Electrochemistry
- 13.2: An Introduction to Electroanalytical Chemistry
  - 13.2.1: Electrochemical Cells
  - 13.2.2: Potentials in Electroanalytical Cells
  - 13.2.3: Electrode Potentials
  - 13.2.4: Calculation of Cell Potentials from Electrode Potentials
  - 13.2.5: Currents in Electrochemical Cells
  - 13.2.6: Types of Electroanalytical Methods
- 13.3: Potentiometry
  - 13.3.1: Standard Electrodes
  - 13.3.2: Standard Potentials
  - 13.3.3: Reference Electrodes
  - 13.3.4: Metallic Indicator Electrodes
  - 13.3.5: Membrane Ion-Selective Electrodes
  - 13.3.6: Molecular-Selective Electrode Systems
  - 13.3.7: Quantitative Potentiometry
- 13.4: Voltammetry
  - 13.4.1: Potential Excitation Signals and Currents in Voltammetry
  - 13.4.2: Voltammetric Instrumentation
  - 13.4.3: Linear Sweep Voltammetry
  - 13.4.4: Cyclic Voltammetry
  - 13.4.5: Polarography
  - 13.4.6: Stripping Methods
  - 13.4.7: Applications of Voltammetry
- 13.5: Problems
- 13.6: Additional Resources
- 13.7: Chapter Summary and Key Terms

14: Surface Characterization by Spectroscopy and Microscopy

- 14.1: Introduction to the Study of Surfaces
- 14.2: Scanning Electron Microscopy
  - 14.2.1: Scanning electron microscopy (SEM)
  - 14.2.2: Transmission Electron Microscopy
- 14.3: Scanning Probe Microscopes
  - 14.3.1: Scanning Tunneling Microscopy
  - 14.3.2: Scanning Tunneling Microscopy (STM)
  - 14.3.3: Atomic Force Microscopy
  - 14.3.4: Atomic Force Microscopy (AFM)
- 14.4: Spectroscopic Surface Methods
  - 14.4.1: X-ray Photoelectron Spectroscopy
  - 14.4.2: Auger Electron Spectroscopy

Index

Glossary

Detailed Licensing

Detailed Licensing

Licensing

*A detailed breakdown of this resource's licensing can be found in **Back Matter/Detailed Licensing**.*

CHAPTER OVERVIEW

1: INTRODUCTION TO ANALYTICAL CHEMISTRY

Chemistry is the study of matter, including its composition, its structure, its physical properties, and its reactivity. Although there are many ways to study chemistry, traditionally we divide it into five areas: organic chemistry, inorganic chemistry, biochemistry, physical chemistry, and analytical chemistry. This division is historical and, perhaps, arbitrary, as suggested by current interest in interdisciplinary areas, such as bioanalytical chemistry and organometallic chemistry. Nevertheless, these five areas remain the simplest division that spans the discipline of chemistry.

Each of these traditional areas of chemistry brings a unique perspective to how a chemist makes sense of the diverse array of elements, ions, and molecules (both small and large) that make up our physical environment. An undergraduate chemistry course, therefore, is much more than a collection of facts; it is, instead, the means by which we learn to see the chemical world from a different perspective. In keeping with this spirit, this chapter introduces you to the field of analytical chemistry and highlights the unique perspectives that analytical chemists bring to the study of chemistry.

1.1: What is Analytical Chemistry
1.2: The Analytical Perspective
1.3: Common Analytical Problems
1.4: Types of Instrumental Methods
1.5: Problems
1.6: Additional Resources
1.7: Chapter Summary and Key Terms

This page titled 1: Introduction to Analytical Chemistry is shared under a CC BY-NC-SA 4.0 license and was authored, remixed, and/or curated by David Harvey.

1.1: WHAT IS ANALYTICAL CHEMISTRY

"ANALYTICAL CHEMISTRY IS WHAT ANALYTICAL CHEMISTS DO."

This quote is attributed to C. N. Reilly (1925-1981) on receipt of the 1965 Fisher Award in Analytical Chemistry. Reilly, who was a professor of chemistry at the University of North Carolina at Chapel Hill, was one of the most influential analytical chemists of the last half of the twentieth century.

For another view of what constitutes analytical chemistry, see the article "Quo Vadis, Analytical Chemistry?", the full reference for which is Valcárcel, M. *Anal. Bioanal. Chem.* **2016**, *408*, 13-21.

Let's begin with a deceptively simple question: What is analytical chemistry? Like all areas of chemistry, analytical chemistry is so broad in scope and so much in flux that it is difficult to find a simple definition more revealing than that quoted above. In this chapter we will try to expand upon this simple definition by saying a little about what analytical chemistry is, as well as a little about what analytical chemistry is not.

Analytical chemistry often is described as the area of chemistry responsible for characterizing the composition of matter, both qualitatively (Is there lead in this paint chip?) and quantitatively (How much lead is in this paint chip?). As we shall see, this description is misleading.

Most chemists routinely make qualitative and quantitative measurements. For this reason, some scientists suggest that analytical chemistry is not a separate branch of chemistry, but simply the application of chemical knowledge [Ravey, M. *Spectroscopy*, **1990**, *5(7)*, 11]. In fact, you probably have performed many such quantitative and qualitative analyses in other chemistry courses.

> You might, for example, have determined the concentration of acetic acid in vinegar using an acid–base titration, or used a qualitative analysis scheme to identify which of several metal ions are in an aqueous sample.

Defining analytical chemistry as the application of chemical knowledge ignores the unique perspective that an analytical chemist bring to the study of chemistry. The craft of analytical chemistry is found not in performing a routine analysis on a routine sample—a task we appropriately call chemical analysis—but in improving established analytical methods, in extending these analytical methods to new types of samples, and in developing new analytical methods to measure chemical phenomena [de Haseth, J. *Spectroscopy*, **1990**, *5(7)*, 11].

Here is one example of the distinction between analytical chemistry and chemical analysis. A mining engineer evaluates an ore by comparing the cost of removing the ore from the earth with the value of its contents, which they estimate by analyzing a sample of the ore. The challenge of developing and validating a quantitative analytical method is the analytical chemist's responsibility; the routine, daily application of the analytical method is the job of the chemical analyst.

THE SEVEN STAGES OF AN ANALYTICAL METHOD

1. Conception of analytical method (birth).
2. Successful demonstration that the analytical method works.
3. Establishment of the analytical method's capabilities.
4. Widespread acceptance of the analytical method.
5. Continued development of the analytical method leads to significant improvements.
6. New cycle through steps 3–5.
7. Analytical method can no longer compete with newer analytical methods (death).

Steps 1–3 and 5 are the province of analytical chemistry; step 4 is the realm of chemical analysis.

The seven stages of an analytical method listed here are modified from Fassel, V. A. *Fresenius' Z. Anal. Chem.* **1986**, *324*, 511–518 and Hieftje, G. M. *J. Chem. Educ.* **2000**, *77*, 577–583.

Another difference between analytical chemistry and chemical analysis is that an analytical chemist works to improve and to extend established analytical methods. For example, several factors complicate the quantitative analysis of nickel in ores, including nickel's unequal distribution within the ore, the ore's complex matrix of silicates and oxides, and the presence of other metals that may interfere with the analysis. Figure 1.1.1 outlines one standard analytical method in use during the late nineteenth century [Fresenius. C. R. *A System of Instruction in Quantitative Chemical Analysis*; John Wiley and Sons: New York, 1881]. The need for many reactions, digestions, and filtrations makes this analytical method both time-consuming and difficult to perform accurately.

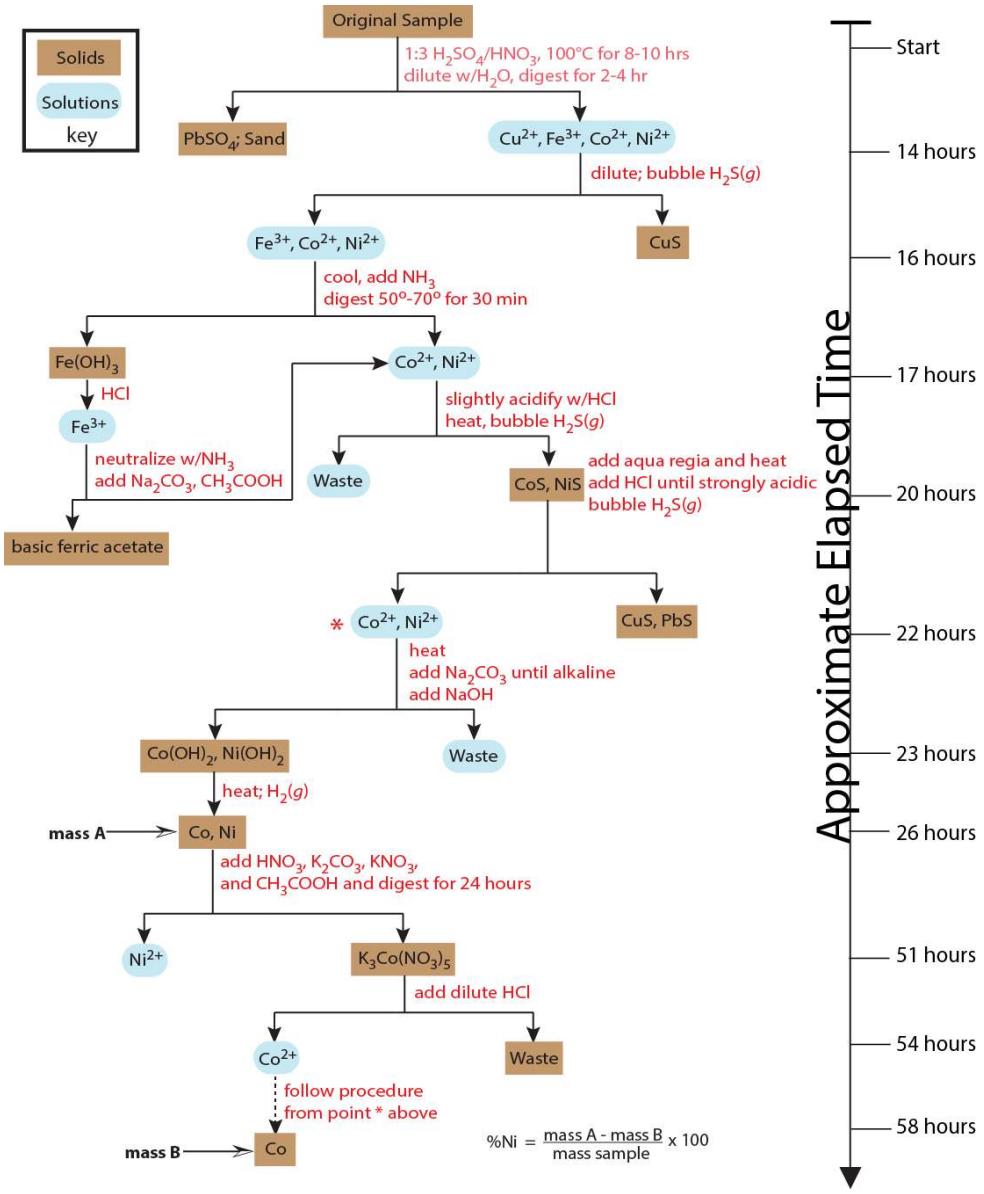


Figure 1.1.1 : Fresenius' analytical scheme for the gravimetric analysis of Ni in ores. After each step, the solid and the solution are separated by gravity filtration. Note that the mass of nickel is not determined directly. Instead, Co and Ni first are isolated and weighed together (**mass A**), and then Co is isolated and weighed separately (**mass B**). The timeline shows that it takes approximately 58 hours to analyze one sample. This scheme is an example of a gravimetric analysis, which is explored further in Chapter 8.

The discovery, in 1905, that dimethylglyoxime (dmg) selectively precipitates Ni^{2+} and Pd^{2+} led to an improved analytical method for the quantitative analysis of nickel [Kolthoff, I. M.; Sandell, E. B. *Textbook of Quantitative Inorganic Analysis*, 3rd Ed., The Macmillan Company: New York, 1952]. The resulting analysis, which is outlined in Figure 1.1.2 , requires fewer manipulations and less time. By the 1970s, flame atomic absorption spectrometry replaced gravimetry as the standard method for analyzing nickel in ores, resulting in an even more rapid analysis [Van Loon, J. C. *Analytical Atomic Absorption Spectroscopy*, Academic Press: New York, 1980]. Today, the standard analytical method utilizes an inductively coupled plasma optical emission spectrometer.

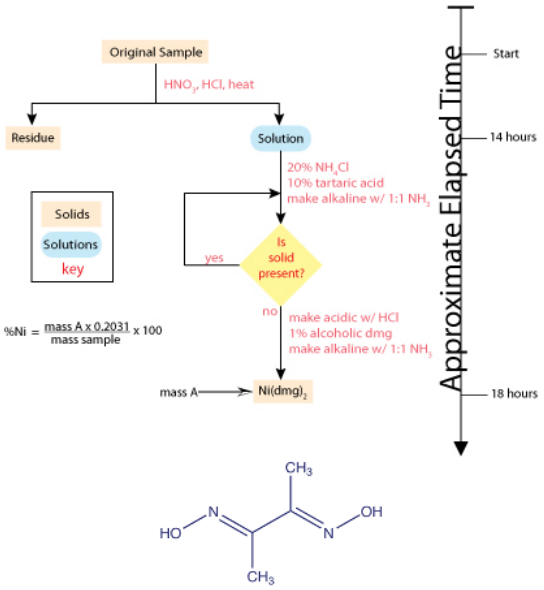


Figure 1.1.2 : Gravimetric analysis for Ni in ores by precipitating $Ni(dmg)_2$. The timeline shows that it takes approximately 18 hours to analyze a single sample, substantially less than 58 hours for the method in Figure 1.1.1 . The factor of 0.2301 in the equation for %Ni accounts for the difference in the formula weights of Ni and $Ni(dmg)_2$; see Chapter 8 for further details. The structure of dmg is shown below the method's flow chart.

Perhaps a more appropriate description of analytical chemistry is “the science of inventing and applying the concepts, principles, and...strategies for measuring the characteristics of chemical systems” [Murray, R. W. *Anal. Chem.* **1991**, *63*, 271A]. Analytical chemists often work at the extreme edges of analysis, extending and improving the ability of all chemists to make meaningful measurements on smaller samples, on more complex samples, on shorter time scales, and on species present at lower concentrations. Throughout its history, analytical chemistry has provided many of the tools and methods necessary for research in other traditional areas of chemistry, as well as fostering multidisciplinary research in, to name a few, medicinal chemistry, clinical chemistry, toxicology, forensic chemistry, materials science, geochemistry, and environmental chemistry.

> To an analytical chemist, the process of making a useful measurement is critical; if the measurement is not of central importance to the work, then it is not analytical chemistry.

You will come across numerous examples of analytical methods in this textbook, most of which are routine examples of chemical analysis. It is important to remember, however, that nonroutine problems prompted analytical chemists to develop these methods.

> An editorial in *Analytical Chemistry* entitled “Some Words about Categories of Manuscripts” highlights nicely what makes a research endeavor relevant to modern analytical chemistry. The full citation is Murray, R. W. *Anal. Chem.* **2008**, *80*, 4775; for a more recent editorial, see “The Scope of *Analytical Chemistry*” by Sweedler, J. V. et. al. *Anal. Chem.* **2015**, *87*, 6425.

This page titled 1.1: What is Analytical Chemistry is shared under a CC BY-NC-SA 4.0 license and was authored, remixed, and/or curated by David Harvey.

- **1.1: What is Analytical Chemistry** by David Harvey is licensed CC BY-NC-SA 4.0.

1.2: THE ANALYTICAL PERSPECTIVE

Having noted that each area of chemistry brings a unique perspective to the study of chemistry, let's ask a second deceptively simple question: What is the analytical perspective? Many analytical chemists describe this perspective as an analytical approach to solving problems.

> For different viewpoints on the analytical approach see (a) Beilby, A. L. *J. Chem. Educ.* **1970**, *47*, 237-238; (b) Lucchesi, C. A. *Am. Lab.* **1980**, October, 112-119; (c) Atkinson, G. F. *J. Chem. Educ.* **1982**, *59*, 201-202; (d) Pardue, H. L.; Woo, J. *J. Chem. Educ.* **1984**, *61*, 409-412; (e) Guarnieri, M. *J. Chem. Educ.* **1988**, *65*, 201-203, (f) Strobel, H. A. *Am. Lab.* **1990**, October, 17-24.

Although there likely are as many descriptions of the analytical approach as there are analytical chemists, it is convenient to define it as the five-step process shown in Figure 1.2.1 .

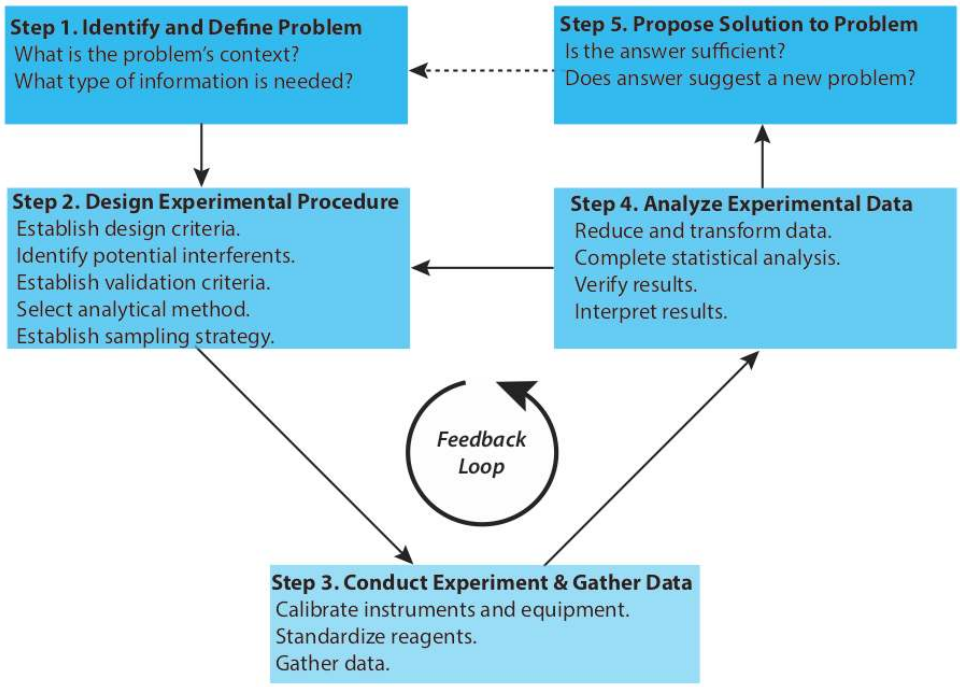


Figure 1.2.1 : Flow diagram showing one view of the analytical approach to solving problems (modified after Atkinson, G. F. *J. Chem. Educ.* **1982**, *59*, 201-202).

Three general features of this approach deserve our attention. First, in steps 1 and 5 analytical chemists have the opportunity to collaborate with individuals outside the realm of analytical chemistry. In fact, many problems on which analytical chemists work originate in other fields. Second, the heart of the analytical approach is a feedback loop (steps 2, 3, and 4) in which the result of one step requires that we reevaluate the other steps. Finally, the solution to one problem often suggests a new problem.

Analytical chemistry begins with a problem, examples of which include evaluating the amount of dust and soil ingested by children as an indicator of environmental exposure to particulate based pollutants, resolving contradictory evidence regarding the toxicity of perfluoro polymers during combustion, and developing rapid and sensitive detectors for chemical and biological weapons. At this point the analytical approach involves a collaboration between the analytical chemist and the individual or agency working on the problem. Together they determine what information is needed and clarify how the problem relates to broader research goals or policy issues, both essential to the design of an appropriate experimental procedure.

> These examples are taken from a series of articles, entitled the "Analytical Approach," which for many years was a regular feature of the journal *Analytical Chemistry*.

To design the experimental procedure the analytical chemist considers criteria, such as the required accuracy, precision, sensitivity, and detection limit, the urgency with which results are needed, the cost of a single analysis, the number of samples to analyze, and the amount of sample available for analysis. Finding an appropriate balance between these criteria frequently is complicated by their interdependence. For example, improving precision may require a larger amount of sample than is available. Consideration also is given to how to collect, store,

and prepare samples, and to whether chemical or physical interferences will affect the analysis. Finally a good experimental procedure may yield useless information if there is no method for validating the results.

The most visible part of the analytical approach occurs in the laboratory. As part of the validation process, appropriate chemical and physical standards are used to calibrate equipment and to standardize reagents.

The data collected during the experiment are then analyzed. Frequently the data first is reduced or transformed to a more readily analyzable form and then a statistical treatment of the data is used to evaluate accuracy and precision, and to validate the procedure. Results are compared to the original design criteria and the experimental design is reconsidered, additional trials are run, or a solution to the problem is proposed. When a solution is proposed, the results are subject to an external evaluation that may result in a new problem and the beginning of a new cycle.

> Chapter 3 introduces you to the language of analytical chemistry. You will find terms such accuracy, precision, and sensitivity defined there. Chapter 4 introduces the statistical analysis of data. Calibration and standardization methods, including a discussion of linear regression, are covered in Chapter 5. See Chapter 7 for a discussion of how to collect, store, and prepare samples for analysis. See Chapter 14 for a discussion about how to validate an analytical method.

As noted earlier some scientists question whether the analytical approach is unique to analytical chemistry. Here, again, it helps to distinguish between a chemical analysis and analytical chemistry. For an analytically-oriented scientist, such as a physical organic chemist or a public health officer, the primary emphasis is how the analysis supports larger research goals that involve fundamental studies of chemical or physical processes, or that improve access to medical care. The essence of analytical chemistry, however, is in developing new tools for solving problems, and in defining the type and quality of information available to other scientists.

? EXERCISE 1.2.1

As an exercise, let's adapt our model of the analytical approach to the development of a simple, inexpensive, portable device for completing bioassays in the field. Before continuing, locate and read the article

"Simple Telemedicine for Developing Regions: Camera Phones and Paper-Based Microfluidic Devices for Real-Time, Off-Site Diagnosis"

by Andres W. Martinez, Scott T. Phillips, Emanuel Carriho, Samuel W. Thomas III, Hayat Sindi, and George M. Whitesides. You will find it on pages 3699-3707 in Volume 80 of the journal *Analytical Chemistry*, which was published in 2008. As you read the article, pay particular attention to how it emulates the analytical approach and consider the following questions:

1. What is the analytical problem and why is it important?
2. What criteria did the authors consider in designing their experiments? What is the basic experimental procedure?
3. What interferences were considered and how did they overcome them? How did the authors calibrate the assay?
4. How did the authors validate their experimental method?
5. Is there evidence that steps 2, 3, and 4 in Figure 1.2.1 are repeated?
6. Was there a successful conclusion to the analytical problem?

Don't let the technical details in the paper overwhelm you; if you skim over these you will find the paper both well-written and accessible.

Answer

What is the analytical problem and why is it important?

A medical diagnoses often relies on the results of a clinical analysis. When you visit a doctor, they may draw a sample of your blood and send it to the lab for analysis. In some cases the result of the analysis is available in 10-15 minutes. What is possible in a developed country, such as the United States, may not be feasible in a country with less access to expensive lab equipment and with fewer trained personnel available to run the tests and to interpret the results. The problem addressed in this paper, therefore, is the development of a reliable device for rapidly performing a clinical assay under less than ideal circumstances.

What criteria did the authors consider in designing their experiments?

In considering a solution to this problem, the authors identify seven important criteria for the analytical method: (1) it must be inexpensive; (2) it must operate without the need for much electricity, so that it can be used in remote locations; (3) it must be adaptable to many types of assays; (4) its must not require a highly skilled technician; (5) it must be quantitative; (6) it must be accurate; and (7) it must produce results rapidly.

What is the basic experimental procedure?

The authors describe how they developed a paper-based microfluidic device that allows anyone to run an analysis simply by dipping the device into a sample (synthetic urine, in this case). The sample moves by capillary action into test zones containing reagents that react with specific species (glucose and protein, for this prototype device). The reagents react to produce a color whose intensity is proportional to the species' concentration. A digital photograph of the microfluidic device is taken using a cell phone camera and sent to an off-site physician who uses image editing software to analyze the photograph and to interpret the assay's result.

What interferences were considered and how did they overcome them?

In developing this analytical method the authors considered several chemical or physical interferences. One concern was the possibility of non-specific interactions between the paper and the glucose or protein, which might lead to non-uniform image in the test zones. A careful analysis of the distribution of glucose and protein in the test zones showed that this was not a problem. A second concern was the possibility that particulate materials in the sample might interfere with the analyses. Paper is a natural filter for particulate materials and the authors found that samples containing dust, sawdust, and pollen do not interfere with the analysis for glucose. Pollen, however, is an interferent for the protein analysis, presumably because it, too, contains protein.

How did the author's calibrate the assay?

To calibrate the device the authors analyzed a series of standard solutions that contained known concentrations of glucose and protein. Because an image's intensity depends upon the available light, a standard sample is run with the test samples, which allows a single calibration curve to be used for samples collected under different lighting conditions.

How did the author's validate their experimental method?

The test device contains two test zones for each analyte, which allows for duplicate analyses and provides one level of experimental validation. To further validate the device, the authors completed 12 analyses at each of three known concentrations of glucose and protein, obtaining acceptable accuracy and precision in all cases.

Is there any evidence of repeating steps 2, 3, and 4 in Figure 1.2.1?

Developing this analytical method required several cycles through steps 2, 3, and 4 of the analytical approach. Examples of this feedback loop include optimizing the shape of the test zones and evaluating the importance of sample size.

Was there a successful conclusion to the analytical problem?

Yes. The authors were successful in meeting their goals by developing and testing an inexpensive, portable, and easy-to-use device for running clinical samples in developing countries.

This exercise provides you with an opportunity to think about the analytical approach in the context of a real analytical problem. Practice exercises such as this provide you with a variety of challenges ranging from simple review problems to more open-ended exercises. You will find answers to practice exercises at the end of each chapter.

Use this link to access the article's abstract from the journal's web site. If your institution has an on-line subscription you also will be able to download a PDF version of the article.

This page titled 1.2: The Analytical Perspective is shared under a CC BY-NC-SA 4.0 license and was authored, remixed, and/or curated by David Harvey.

- **1.2: The Analytical Perspective** by David Harvey is licensed CC BY-NC-SA 4.0.

1.3: COMMON ANALYTICAL PROBLEMS

Many problems in analytical chemistry begin with the need to identify what is present in a sample. This is the scope of a ***qualitative analysis***, examples of which include identifying the products of a chemical reaction, screening an athlete's urine for a performance-enhancing drug, or determining the spatial distribution of Pb on the surface of an airborne particulate. An early challenge for analytical chemists was developing simple chemical tests to identify inorganic ions and organic functional groups. The classical laboratory courses in inorganic and organic qualitative analysis, still taught at some schools, are based on this work.

> See, for example, the following laboratory textbooks: (a) Sorum, C. H.; Lagowski, J. J. *Introduction to Semimicro Qualitative Analysis*, 5th Ed.; Prentice-Hall: Englewood, NJ, 1977; (b) Shriner, R. L.; Fuson, R. C.; Curtin, D. Y. *The Systematic Identification of Organic Compounds*, 5th Ed.; John Wiley and Sons: New York, 1964.

Modern methods for qualitative analysis rely on instrumental techniques, such as infrared (IR) spectroscopy, nuclear magnetic resonance (NMR) spectroscopy, and mass spectrometry (MS). Because these qualitative applications are covered adequately elsewhere in the undergraduate curriculum, typically in organic chemistry, they receive no further consideration in this text.

Perhaps the most common analytical problem is a ***quantitative analysis***, examples of which include the elemental analysis of a newly synthesized compound, measuring the concentration of glucose in blood, or determining the difference between the bulk and the surface concentrations of Cr in steel. Much of the analytical work in clinical, pharmaceutical, environmental, and industrial labs involves developing new quantitative methods to detect trace amounts of chemical species in complex samples. Most of the examples in this text are of quantitative analyses.

Another important area of analytical chemistry, which receives some attention in this text, are methods for characterizing physical and chemical properties. The determination of chemical structure, of equilibrium constants, of particle size, and of surface structure are examples of a ***characterization analysis***.

The purpose of a qualitative, a quantitative, or a characterization analysis is to solve a problem associated with a particular sample. The purpose of a ***fundamental analysis***, on the other hand, is to improve our understanding of the theory that supports an analytical method and to understand better an analytical method's limitations.

> A good resource for current examples of qualitative, quantitative, characterization, and fundamental analyses is *Analytical Chemistry's* annual review issue that highlights fundamental and applied research in analytical chemistry. Examples of review articles in the 2015 issue include "Analytical Chemistry in Archaeological Research," "Recent Developments in Paper-Based Microfluidic Devices," and "Vibrational Spectroscopy: Recent Developments to Revolutionize Forensic Science."

1.3: Common Analytical Problems is shared under a CC BY-NC-SA 4.0 license and was authored, remixed, and/or curated by LibreTexts.

- **1.3: Common Analytical Problems** is licensed CC BY-NC-SA 4.0.

1.4: Types of Instrumental Methods

It is useful to organize instrumental methods of analysis into several groups based on the chemical or physical properties that we use to generate a signal that we can measure and relate to the analyte of interest to us. One group of instrumental methods is based on the interaction of photons of electromagnetic radiation with matter, which we call collectively spectroscopy. We can divide spectroscopy into two broad classes of techniques. In one class of techniques there is a transfer of energy between the photon and the sample. Table 1.4.1 provides a list of several representative examples.

Table 1.4.1. Examples of Spectroscopic Instrumental Methods That Involve an Exchange of Energy Between a Photon and the Sample

type of energy transfer	region of electromagnetic spectrum	spectroscopic technique
absorption	γ-ray	Mossbauer spectroscopy
	X-ray	X-ray absorption spectroscopy
	UV/Vis	UV/Vis spectroscopy
	IR	infrared spectroscopy
	microwave	raman spectroscopy
	radio wave	electron spin resonance nuclear magnetic resonance
emission (thermal excitation)	UV/Vis	atomic emission spectroscopy
photoluminescence	X-ray	X-ray fluorescence
	UV/Vis	fluorescence spectroscopy phosphorescence spectroscopy atomic fluorescence spectroscopy
chemiluminescence	UV/Vis	chemiluminescence spectroscopy

In the second broad class of spectroscopic techniques, the electromagnetic radiation undergoes a change in amplitude, phase angle, polarization, or direction of propagation as a result of its refraction, reflection, scattering, diffraction, or dispersion by the sample. Several representative spectroscopic techniques are listed in Table 1.4.2.

Table 1.4.2. Examples of Other Spectroscopic Instrumental Methods

region of electromagnetic spectrum	type of interaction	spectroscopic technique
X-ray	diffraction	X-ray diffraction
UV/Vis	refraction	refractrometry
	scattering	nephelometry turbidimetry
	dispersion	optical rotary dispersion

A second group of instrumental methods is based on the measurement of current, charge, or potential at the surface of an electrode, sometimes while controlling one or both of the other two variables, and sometime while stirring the solution. Figure 1.4.1 provides a visual introduction to these methods.

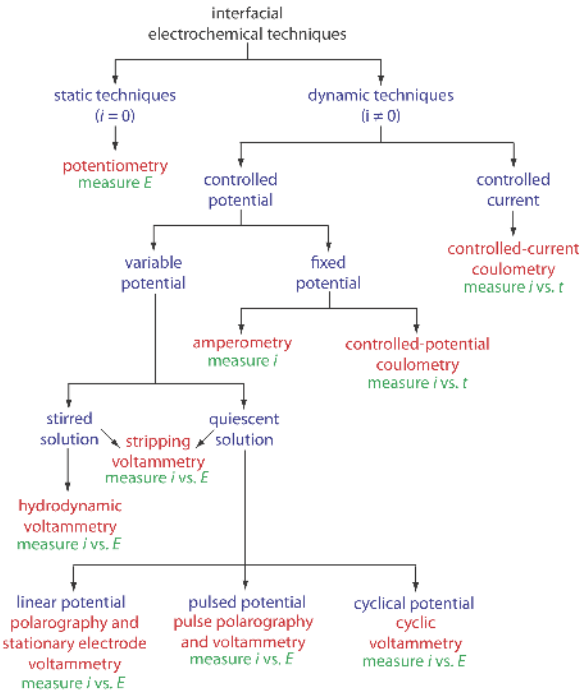


Figure 1.4.1 Family tree that highlights the similarities and differences between a number of interfacial electrochemical techniques. The specific instrumental methods are shown in red, the experimental conditions are shown in blue, and the analytical signals are shown in green.

Our third group of instrumental methods gathers together a variety of other measurements that can provide a useful analytical signal; these are summarized in Table 1.4.3.

Table 1.4.3. Additional Examples of Instrumental Methods of Analysis

type of measurement or phenomenon	instrumental method
piezoelectric effect	quartz crystal microbalance
mass-to-charge ratio	mass spectrometry
rate of chemical reaction or physical process	kinetic methods flow injection analysis neutron activation analysis isotope diution analysis
thermal energy	thermal gravimetry differential thermal analysis differential scanning calorimetry

Our last group of instrumental methods are used to separate mixtures based on either the equilibrium partitioning of species between two phases or the migration of species in response to an applied electrical field. These methods usally are paired with a suitable instrumental method from Table 1.4.1, Table 1.4.2, Table 1.4.3, or Figure 1.4.1 to provide a way to follow the separation.

Table 1.4.4. Examples of Instrumental Methods for Separating Mixtures.

basis of separation	instrumental method
equilibrium partitioning between two phases	gas chromatography liquid chromatography supercritical fluid chromatography
migration in response to applied electrical field	electrophoresis

This page titled 1.4: Types of Instrumental Methods is shared under a CC BY-NC-SA 4.0 license and was authored, remixed, and/or curated by David Harvey.

- **1.2: Types of Instrumental Methods** by David Harvey is licensed CC BY-NC-SA 4.0.

1.5: PROBLEMS

1. For each of the following problems indicate whether its solution requires a qualitative analysis, a quantitative analysis, a characterization analysis, and/or a fundamental analysis. More than one type of analysis may be appropriate for some problems.
   a. The residents in a neighborhood near a hazardous-waste disposal site are concerned that it is leaking contaminants into their groundwater.
   b. An art museum is concerned that a recently acquired oil painting is a forgery.
   c. Airport security needs a more reliable method for detecting the presence of explosive materials in luggage.
   d. The structure of a newly discovered virus needs to be determined.
   e. A new visual indicator is needed for an acid–base titration.
   f. A new law requires a method for evaluating whether automobiles are emitting too much carbon monoxide.
2. Read the article "When Machine Tastes Coffee: Instrumental Approach to Predict the Sensory Profile of Espresso Coffee," which discusses work completed at the Nestlé Research Center in Lausanne, Switzerland. You will find the article on pages 1574-1581 in Volume 80 of *Analytical Chemistry*, published in 2008. Prepare an essay that summarizes the nature of the problem and how it was solved. Do not worry about the nitty-gritty details of the mathematical model developed by the authors, which relies on a combination of an analysis of variance (ANOVA), a topic we will consider in Chapter 14, and a principle component regression (PCR), at topic that we will not consider in this text. Instead, focus on the results of the model by examining the visualizations in Figure 3 and Figure 4 of the paper. As a guide, refer to Figure 1.2.1 in this chapter for a model of the analytical approach to solving problems. Use this link to access the article's abstract from the journal's web site. If your institution has an on-line subscription you also will be able to download a PDF version of the article.

This page titled 1.5: Problems is shared under a CC BY-NC-SA 4.0 license and was authored, remixed, and/or curated by David Harvey.

- **1.4: Problems** by David Harvey is licensed CC BY-NC-SA 4.0.

1.6: ADDITIONAL RESOURCES

The role of analytical chemistry within the broader discipline of chemistry has been discussed by many prominent analytical chemists; several notable examples are listed here.

- Baiulescu, G. E.; Patroescu, C; Chalmers, R. A. *Education and Teaching in Analytical Chemistry*, Ellis Horwood: Chichester, 1982.
- de Haseth, J. "What is Analytical Chemistry?," *Spectroscopy* **1990**, *5*, 19–21.
- Heiftje, G. M. "The Two Sides of Analytical Chemistry," *Anal. Chem.* **1985**, *57*, 256A–267A.
- Heiftje, G. M. "But is it analytical chemistry?," *Am. Lab.* **1993**, October, 53–61.
- Kissinger, P. T. "Analytical Chemistry—What is It? Why Teach It?," *Trends Anal. Chem.* **1992**, *11*, 57–57.
- Laitinen, H. A.; Ewing, G. (eds.) *A History of Analytical Chemistry*, The Division of Analytical Chemistry of the American Chemical Society: Washington, D. C., 1972.
- Laitinen, H. A. "Analytical Chemistry in a Changing World," *Anal. Chem.* **1980**, *52*, 605A–609A.
- Laitinen, H. A. "History of Analytical Chemistry in the U. S. A.," *Talanta*, **1989**, *36*, 1–9.
- McLafferty, F. W. "Analytical Chemistry: Historic and Modern," *Acc. Chem. Res.* **1990**, *23*, 63–64.
- Mottola, H. A. "The Interdisciplinary and Multidisciplinary Nature of Contemporary Analytical Chemistry and its Core Components," *Anal. Chim. Acta* **1991**, *242*, 1–3.
- Noble, D. "From Wet Chemistry to Instrumental Analysis: A Perspective on Analytical Sciences," *Anal. Chem.* **1994**, *66*, 251A–263A.
- Tyson, J. *Analysis: What Analytical Chemists Do*, Royal Society of Chemistry: Cambridge, England 1988.

For additional discussion of clinical assays based on paper-based microfluidic devices, see the following papers.

- Ellerbee, A. K.; Phillips, S. T.; Siegel, A. C.; Mirica, K. A.; Martinez, A. W.; Striehl, P.; Jain, N.; Prentiss, M.; Whitesides, G. M. "Quantifying Colorimetric Assays in Paper-Based Microfluidic Devices by Measuring the Transmission of Light Through Paper," *Anal. Chem.* **2009**, *81*, 8447–8452.
- Martinez, A. W.; Phillips, S. T.; Whitesides, G. M. "Diagnostics for the Developing World: Microfluidic Paper-Based Analytical Devices," *Anal. Chem.* **2010**, *82*, 3–10.

This textbook provides one introduction to the discipline of analytical chemistry. There are other textbooks for introductory courses in analytical chemistry and you may find it useful to consult them when you encounter a difficult concept; often a fresh perspective will help crystallize your understanding. The textbooks listed here are excellent resources.

- Enke, C. *The Art and Science of Chemical Analysis*, Wiley: New York.
- Christian, G. D.; Dasgupta, P, K.; Schug; K. A. *Analytical Chemistry*, Wiley: New York.
- Harris, D. *Quantitative Chemical Analysis*, W. H. Freeman and Company: New York.
- Kellner, R.; Mermet, J.-M.; Otto, M.; Valcárcel, M.; Widmer, H. M. *Analytical Chemistry*, Wiley- VCH: Weinheim, Germany.
- Rubinson, J. F.; Rubinson, K. A. *Contemporary Chemical Analysis*, Prentice Hall: Upper Saddle River, NJ.
- Skoog, D. A.; West, D. M.; Holler, F. J. *Fundamentals of Analytical Chemistry*, Saunders: Philadelphia.

To explore the practice of modern analytical chemistry there is no better resource than the primary literature. The following journals publish broadly in the area of analytical chemistry.

- Analytical and Bioanalytical Chemistry
- Analytical Chemistry
- Analytical Chimica Acta
- Analyst
- Talanta

This page titled 1.6: Additional Resources is shared under a CC BY-NC-SA 4.0 license and was authored, remixed, and/or curated by David Harvey.

- **1.5: Additional Resources** by David Harvey is licensed CC BY-NC-SA 4.0.

1.7: CHAPTER SUMMARY AND KEY TERMS

CHAPTER SUMMARY

Analytical chemists work to improve the ability of chemists and other scientists to make meaningful measurements. The need to work with smaller samples, with more complex materials, with processes occurring on shorter time scales, and with species present at lower concentrations challenges analytical chemists to improve existing analytical methods and to develop new ones.

Typical problems on which analytical chemists work include qualitative analyses (What is present?), quantitative analyses (How much is present?), characterization analyses (What are the sample's chemical and physical properties?), and fundamental analyses (How does this method work and how can it be improved?).

KEY TERMS

- characterization analysis
- fundamental analysis
- qualitative analysis
- quantitative analysis

This page titled 1.7: Chapter Summary and Key Terms is shared under a CC BY-NC-SA 4.0 license and was authored, remixed, and/or curated by David Harvey.

- **1.6: Chapter Summary and Key Terms** by David Harvey is licensed CC BY-NC-SA 4.0.

CHAPTER OVERVIEW

2: BASIC TOOLS OF ANALYTICAL CHEMISTRY

In the chapters that follow we will explore many aspects of analytical chemistry. In the process we will consider important questions, such as “How do we extract useful results from experimental data?”, “How do we ensure our results are accurate?”, “How do we obtain a representative sample?”, and “How do we select an appropriate analytical technique?” Before we consider these and other questions, we first must review some basic tools of importance to analytical chemists.

2.1: Measurements in Analytical Chemistry
2.2: Concentration
2.3: Stoichiometric Calculations
2.4: Basic Equipment
2.5: Preparing Solutions
2.6: Spreadsheets and Computational Software
2.7: The Laboratory Notebook
2.8: Problems
2.9: Additional Resources
2.10: Chapter Summary and Key Terms

This page titled 2: Basic Tools of Analytical Chemistry is shared under a CC BY-NC-SA 4.0 license and was authored, remixed, and/or curated by David Harvey.

2.1: MEASUREMENTS IN ANALYTICAL CHEMISTRY

Analytical chemistry is a quantitative science. Whether determining the concentration of a species, evaluating an equilibrium constant, measuring a reaction rate, or drawing a correlation between a compound's structure and its reactivity, analytical chemists engage in "measuring important chemical things" [Murray, R. W. *Anal. Chem.* **2007**, *79*, 1765]. In this section we review briefly the basic units of measurement and the proper use of significant figures.

UNITS OF MEASUREMENT

A measurement usually consists of a unit and a number that expresses the quantity of that unit. We can express the same physical measurement with different units, which creates confusion if we are not careful to specify the unit. For example, the mass of a sample that weighs 1.5 g is equivalent to 0.0033 lb or to 0.053 oz. To ensure consistency, and to avoid problems, scientists use the common set of fundamental base units listed in Table 2.1.1 . These units are called SI units after the Système International d'Unités.

> It is important for scientists to agree upon a common set of units. In 1999, for example, NASA lost a Mars Orbiter spacecraft because one engineering team used English units in their calculations and another engineering team used metric units. As a result, the spacecraft came too close to the planet's surface, causing its propulsion system to overheat and fail.
>
> Some measurements, such as absorbance, do not have units. Because the meaning of a unitless number often is unclear, some authors include an artificial unit. It is not unusual to see the abbreviation AU—short for absorbance unit—following an absorbance value, which helps clarify that the measurement is an absorbance value.

Table 2.1.1 : Fundamental Base SI Units

Measurement	Unit	Symbol	Definition (1 unit is...)
mass	kilogram	kg	...the mass of the international prototype, a Pt-Ir object housed at the Bureau International de Poids and Measures at Sèvres, France. (Note: The mass of the international prototype changes at a rate of approximately 1 µg per year due to reversible surface contamination. The reference mass, therefore, is determined immediately after its cleaning using a specified procedure. Current plans call for retiring the international prototype and defining the kilogram in terms of Planck's constant; see this link for more details.)
distance	meter	m	...the distance light travels in $(299\ 792\ 458)^{-1}$ seconds.
temperature	kelvin	K	...equal to $(273.16)^{-1}$, where 273.16 K is the triple point of water (where its solid, liquid, and gaseous forms are in equilibrium. and where 0 is the lowest possible temperature).
time	second	s	...the time it takes for 9 192 631 770 periods of radiation corresponding to a specific transition of the ^{133}Cs atom.
current	ampere	A	...the current producing a force of 2×10^{-7} N/m between two straight parallel conductors of infinite length separated by one meter (in a vacuum).
amount of substance	mole	mol	...the amount of a substance containing as many particles as there are atoms in exactly 0.012 kilogram of ^{12}C.
light	candela	cd	...the luminous intensity of a source with a monochromatic frequency of 540×10^{12} hertz and a radiant power of $(683)^{-1}$ watts per steradian.

> There is some disagreement on the use of "amount of substance" to describe the measurement for which the mole is the base SI unit; see "What's in a Name? Amount of Substance, Chemical Amount, and Stoichiometric Amount," the full reference for which is Giunta, C. J. *J. Chem. Educ.* **2016**, *93*, 583–586.

We define other measurements using these fundamental SI units. For example, we measure the quantity of heat produced during a chemical reaction in joules, (J), where 1 J is equivalent to 1 m kg/s . Table 2.1.2 provides a list of some important derived SI units, as well as a few common non-SI units.

Table 2.1.2 : Derived SI Units and Non-SI Units of Importance to Analytical Chemistry

Measurement	Unit	Symbol	Equivalent SI Units
length	angstrom (non-SI)	Å	1 Å = 1 × 10^{-10} m
volume	liter (non-SI)	L	1 L = 10^{-3} m^3
force	newton (SI)	N	1 N = 1 m·kg/s^2
pressure	pascal (SI) atmosphere (non-SI)	Pa atm	1 Pa = 1 N/m^3 = 1 kg/(m·s^2) 1 atm = 101 325 Pa
energy, work, heat	joule (SI) calorie (non-SI) electron volt (non-SI)	J cal eV	1 J = 1 N·m = 1 m^2·kg/s^2 1 cal = 4.184 J 1 eV = 1.602 177 33 × 10^{-19} J
power	watt (SI)	W	1 W = 1 J/s = 1 m^2·kg/s^3
charge	coulomb (SI)	C	1 C = 1 A·s
potential	volt (SI)	V	1 V = 1 W/A = 1 m^2·kg/(s^3·A)
frequency	hertz (SI)	Hz	1 Hz = s^{-1}
temperature	Celcius (non-SI)	ºC	ºC = K – 273.15

Chemists frequently work with measurements that are very large or very small. A mole contains 602 213 670 000 000 000 000 000 particles and some analytical techniques can detect as little as 0.000 000 000 000 001 g of a compound. For simplicity, we express these measurements using scientific notation; thus, a mole contains 6.022 136 7 × 10^{23} particles, and the detected mass is 1 × 10^{-15} g. Sometimes we wish to express a measurement without the exponential term, replacing it with a prefix (Table 2.1.3). A mass of 1 × 10^{-15} g, for example, is the same as 1 fg, or femtogram.

> Writing a lengthy number with spaces instead of commas may strike you as unusual. For a number with more than four digits on either side of the decimal point, however, the recommendation from the International Union of Pure and Applied Chemistry is to use a thin space instead of a comma.

Table 2.1.3 : Common Prefixes for Exponential Notation

Prefix	Symbol	Factor	Prefix	Symbol	Factor	Prefix	Symbol	Factor
yotta	Y	10^{24}	kilo	k	10^{3}	micro	μ	10^{-6}
zetta	Z	10^{21}	hecto	h	10^{2}	nano	n	10^{-9}
eta	E	10^{18}	deka	da	10^{1}	pico	p	10^{-12}
peta	P	10^{15}	—	—	10^{0}	femto	f	10^{-15}
tera	T	10^{12}	deci	d	10^{-1}	atto	a	10^{-18}
giga	G	10^{9}	centi	c	10^{-2}	zepto	z	10^{-21}
mega	M	10^{6}	milli	m	10^{-3}	yocto	y	10^{-24}

UNCERTAINTY IN MEASUREMENTS

A measurement provides information about both its magnitude and its uncertainty. Consider, for example, the three photos in Figure 2.1.1 , taken at intervals of approximately 1 sec after placing a sample on the balance. Assuming the balance is properly calibrated, we are certain that the sample's mass is more than 0.5729 g and less than 0.5731 g. We are uncertain, however, about the sample's mass in the last decimal place since the final two decimal places fluctuate between 29, 30, and 31. The best we can do is to report the sample's mass as 0.5730 g ± 0.0001 g, indicating both its magnitude and its absolute uncertainty.



Figure 2.1.1 : When weighing a sample on a balance, the measurement fluctuates in the final decimal place. We record this sample's mass as 0.5730 g ± 0.0001 g.

SIGNIFICANT FIGURES

A measurement's significant figures convey information about a measurement's magnitude and uncertainty. The number of significant figures in a measurement is the number of digits known exactly plus one digit whose value is uncertain. The mass shown in Figure 2.1.1 , for example, has four significant figures, three which we know exactly and one, the last, which is uncertain.

Suppose we weigh a second sample, using the same balance, and obtain a mass of 0.0990 g. Does this measurement have 3, 4, or 5 significant figures? The zero in the last decimal place is the one uncertain digit and is significant. The other two zeros, however, simply indicates the decimal point's location. Writing the measurement in scientific notation, 9.90×10^{-2}, clarifies that there are three significant figures in 0.0990.

> In the measurement **0.0**99**0** g, the zero in **green** is a significant digit and the zeros in **red** are not significant digits.

EXAMPLE 2.1.1

How many significant figures are in each of the following measurements? Convert each measurement to its equivalent scientific notation or decimal form.

a. 0.0120 mol HCl
b. 605.3 mg $CaCO_3$
c. 1.043×10^{-4} mol Ag^+
d. 9.3×10^{4} mg NaOH

Solution

(a) Three significant figures; 1.20×10^{-2} mol HCl.

(b) Four significant figures; 6.053×10^{2} mg $CaCO_3$.

(c) Four significant figures; 0.000 104 3 mol Ag^+.

(d) Two significant figures; 93 000 mg NaOH.

There are two special cases when determining the number of significant figures in a measurement. For a measurement given as a logarithm, such as pH, the number of significant figures is equal to the number of digits to the right of the decimal point. Digits to the left of the decimal point are not significant figures since they indicate only the power of 10. A pH of 2.45, therefore, contains two significant figures.

> The log of 2.8×10^{2} is 2.45. The log of 2.8 is 0.45 and the log of 10^2 is 2. The 2 in 2.45, therefore, only indicates the power of 10 and is not a significant digit.

An exact number, such as a stoichiometric coefficient, has an infinite number of significant figures. A mole of $CaCl_2$, for example, contains exactly two moles of chloride ions and one mole of calcium ions. Another example of an exact number is the relationship between some units. There are, for example, exactly 1000 mL in 1 L. Both the 1 and the 1000 have an infinite number of significant figures.

Using the correct number of significant figures is important because it tells other scientists about the uncertainty of your measurements. Suppose you weigh a sample on a balance that measures mass to the nearest ±0.1 mg. Reporting the sample's mass as 1.762 g instead of 1.7623 g is incorrect because it does not convey properly the measurement's uncertainty. Reporting the sample's mass as 1.76231 g also is incorrect because it falsely suggests an uncertainty of ±0.01 mg.

SIGNIFICANT FIGURES IN CALCULATIONS

Significant figures are also important because they guide us when reporting the result of an analysis. When we calculate a result, the answer cannot be more certain than the least certain measurement in the analysis. Rounding an answer to the correct number of significant figures is important.

For addition and subtraction, we round the answer to the last decimal place in common for each measurement in the calculation. The exact sum of 135.621, 97.33, and 21.2163 is 254.1673. Since the last decimal place common to all three numbers is the hundredth's place

$$\begin{array}{r} 135.621 \\ 97.33 \\ 21.2163 \\ \hline 254.1673 \end{array}$$

we round the result to 254.17.

The last common decimal place shared by 135.621, 97.33, and 21.2163 is shown in **red**.

When working with scientific notation, first convert each measurement to a common exponent before determining the number of significant figures. For example, the sum of 6.17×10^7, 4.3×10^5, and 3.23×10^4 is 6.22×10^7.

$$\begin{array}{ll} 6.17 & \times 10^7 \\ 0.043 & \times 10^7 \\ \underline{0.00323 \times 10^7} & \\ 6.21623 \times 10^7 & \end{array}$$

The last common decimal place shared by 6.17×10^7, 4.3×10^5 and 3.23×10^4 is shown in **red**.

For multiplication and division, we round the answer to the same number of significant figures as the measurement with the fewest number of significant figures. For example, when we divide the product of 22.91 and 0.152 by 16.302, we report the answer as 0.214 (three significant figures) because 0.152 has the fewest number of significant figures.

$$\frac{22.91 \times 0.152}{16.302} = 0.2136 = 0.214$$

There is no need to convert measurements in scientific notation to a common exponent when multiplying or dividing.

It is important to recognize that the rules presented here for working with significant figures are generalizations. What actually is conserved is uncertainty, not the number of significant figures. For example, the following calculation

$$101/99 = 1.02$$

is correct even though it violates the general rules outlined earlier. Since the relative uncertainty in each measurement is approximately 1% (101 ± 1 and 99 ± 1), the relative uncertainty in the final answer also is approximately 1%. Reporting the answer as 1.0 (two significant figures), as required by the general rules, implies a relative uncertainty of 10%, which is too large. The correct answer, with three significant figures, yields the expected relative uncertainty. Chapter 4 presents a more thorough treatment of uncertainty and its importance in reporting the result of an analysis.

Finally, to avoid "round-off" errors, it is a good idea to retain at least one extra significant figure throughout any calculation. Better yet, invest in a good scientific calculator that allows you to perform lengthy calculations without the need to record intermediate values. When your calculation is complete, round the answer to the correct number of significant figures using the following simple rules.

1. Retain the least significant figure if it and the digits that follow are less than halfway to the next higher digit. For example, rounding 12.442 to the nearest tenth gives 12.4 since 0.442 is less than half way between 0.400 and 0.500.
2. Increase the least significant figure by 1 if it and the digits that follow are more than halfway to the next higher digit. For example, rounding 12.476 to the nearest tenth gives 12.5 since 0.476 is more than halfway between 0.400 and 0.500.
3. If the least significant figure and the digits that follow are exactly halfway to the next higher digit, then round the least significant figure to the nearest even number. For example, rounding 12.450 to the nearest tenth gives 12.4, while rounding 12.550 to the nearest tenth gives 12.6. Rounding in this manner ensures that we round up as often as we round down.

? EXERCISE 2.1.1

For a problem that involves both addition and/or subtraction, and multiplication and/or division, be sure to account for significant figures at each step of the calculation. With this in mind, report the result of this calculation to the correct number of significant figures.

$$\frac{0.250 \times (9.93 \times 10^{-3}) - 0.100 \times (1.927 \times 10^{-2})}{9.93 \times 10^{-3} + 1.927 \times 10^{-2}} =$$

Answer

The correct answer to this exercise is 1.9×10^{-2}. To see why this is correct, let's work through the problem in a series of steps. Here is the original problem

$$\frac{0.250 \times (9.93 \times 10^{-3}) - 0.100 \times (1.927 \times 10^{-2})}{9.93 \times 10^{-3} + 1.927 \times 10^{-2}} =$$

Following the correct order of operations we first complete the two multiplications in the numerator. In each case the answer has three significant figures, although we retain an extra digit, highlight in **red**, to avoid round-off errors.

$$\frac{2.482 \times 10^{-3} - 1.927 \times 10^{-3}}{9.93 \times 10^{-3} + 1.927 \times 10^{-2}} =$$

Completing the subtraction in the numerator leaves us with two significant figures since the last significant digit for each value is in the hundredths place.

$$\frac{0.555 \times 10^{-3}}{9.93 \times 10^{-3} + 1.927 \times 10^{-2}} =$$

The two values in the denominator have different exponents. Because we are adding together these values, we first rewrite them using a common exponent.

$$\frac{0.555 \times 10^{-3}}{0.993 \times 10^{-2} + 1.927 \times 10^{-2}} =$$

The sum in the denominator has four significant figures since each of the addends has three decimal places.

$$\frac{0.555 \times 10^{-3}}{2.920 \times 10^{-2}} =$$

Finally, we complete the division, which leaves us with a result having two significant figures.

$$\frac{0.555 \times 10^{-3}}{2.920 \times 10^{-2}} = 1.9 \times 10^{-2}$$

This page titled 2.1: Measurements in Analytical Chemistry is shared under a CC BY-NC-SA 4.0 license and was authored, remixed, and/or curated by David Harvey.

- **2.1: Measurements in Analytical Chemistry** by David Harvey is licensed CC BY-NC-SA 4.0.

2.2: CONCENTRATION

Concentration is a general measurement unit that reports the amount of solute present in a known amount of solution or solvent

$$\text{concentration} = \frac{\text{amount of solute}}{\text{amount of solution}} \tag{2.2.1}$$

Although we associate the terms "solute" and "solution" with liquid samples, we can extend their use to gas-phase and solid-phase samples as well. Table 2.2.1 lists the most common units of concentration.

Table 2.2.1 : Common Units for Reporting Concentration

Name	Units	Symbol
molarity	$\frac{\text{moles solute}}{\text{liters solution}}$	M
formality	$\frac{\text{moles solute}}{\text{liters solution}}$	F
normality	$\frac{\text{equivalents solute}}{\text{liters solution}}$	N
molality	$\frac{\text{moles solute}}{\text{kilograms solvent}}$	m
weight percent	$\frac{\text{grams solute}}{\text{100 grams solution}}$	% w/w
volume percent	$\frac{\text{mL solute}}{\text{100 mL solution}}$	% v/v
weight-to-volume percent	$\frac{\text{grams solute}}{\text{100 mL solution}}$	% w/v
parts per million	$\frac{\text{grams solute}}{10^6 \text{ grams solution}}$	ppm
parts per billion	$\frac{\text{grams solute}}{10^9 \text{ grams solution}}$	ppb

An alternative expression for weight percent is

$$\frac{\text{grams solute}}{\text{grams solution}} \times 100$$

You can use similar alternative expressions for volume percent and for weight-to-volume percent.

MOLARITY AND FORMALITY

Both molarity and formality express concentration as moles of solute per liter of solution; however, there is a subtle difference between them. ***Molarity*** is the concentration of a particular chemical species. ***Formality***, on the other hand, is a substance's total concentration without regard to its specific chemical form. There is no difference between a compound's molarity and formality if it dissolves without dissociating into ions. The formal concentration of a solution of glucose, for example, is the same as its molarity.

For a compound that ionizes in solution, such as $CaCl_2$, molarity and formality are different. When we dissolve 0.1 moles of $CaCl_2$ in 1 L of water, the solution contains 0.1 moles of Ca^{2+} and 0.2 moles of Cl^-. The molarity of $CaCl_2$, therefore, is zero since there is no undissociated $CaCl_2$ in solution; instead, the solution is 0.1 M in Ca^{2+} and 0.2 M in Cl^-. The formality of $CaCl_2$, however, is 0.1 F since it represents the total amount of $CaCl_2$ in solution. This more rigorous definition of molarity, for better or worse, largely is ignored in the current literature, as it is in this textbook. When we state that a solution is 0.1 M $CaCl_2$ we understand it to consist of Ca^{2+} and Cl^- ions. We will reserve the unit of formality to situations where it provides a clearer description of solution chemistry.

Molarity is used so frequently that we use a symbolic notation to simplify its expression in equations and in writing. Square brackets around a species indicate that we are referring to that species' molarity. Thus, $[Ca^{2+}]$ is read as "the molarity of calcium ions."

For a solute that dissolves without undergoing ionization, molarity and formality have the same value. A solution that is 0.0259 M in glucose, for example, is 0.0259 F in glucose as well.

NORMALITY

Normality is a concentration unit that no longer is in common use; however, because you may encounter normality in older handbooks of analytical methods, it is helpful to understand its meaning. ***Normality*** defines concentration in terms of an equivalent, which is the amount of one chemical species that reacts stoichiometrically with another chemical species. Note that this definition makes an equivalent, and thus

normality, a function of the chemical reaction in which the species participates. Although a solution of H_2SO_4 has a fixed molarity, its normality depends on how it reacts. You will find a more detailed treatment of normality in Appendix 1.

> One handbook that still uses normality is *Standard Methods for the Examination of Water and Wastewater*, a joint publication of the American Public Health Association, the American Water Works Association, and the Water Environment Federation. This handbook is one of the primary resources for the environmental analysis of water and wastewater.

MOLALITY

Molality is used in thermodynamic calculations where a temperature independent unit of concentration is needed. Molarity is based on the volume of solution that contains the solute. Since density is a temperature dependent property, a solution's volume, and thus its molar concentration, changes with temperature. By using the solvent's mass in place of the solution's volume, the resulting concentration becomes independent of temperature.

WEIGHT, VOLUME, AND WEIGHT-TO-VOLUME PERCENT

Weight percent (% w/w), ***volume percent*** (% v/v) and ***weight-to-volume percent*** (% w/v) express concentration as the units of solute present in 100 units of solution. A solution that is 1.5% w/v NH_4NO_3, for example, contains 1.5 gram of NH_4NO_3 in 100 mL of solution.

PARTS PER MILLION AND PARTS PER BILLION

Parts per million (ppm) and ***parts per billion*** (ppb) are ratios that give the grams of solute in, respectively, one million or one billion grams of sample. For example, a sample of steel that is 450 ppm in Mn contains 450 µg of Mn for every gram of steel. If we approximate the density of an aqueous solution as 1.00 g/mL, then we can express solution concentrations in ppm or ppb using the following relationships.

$$\text{ppm} = \frac{\mu\text{g}}{\text{g}} = \frac{\text{mg}}{\text{L}} = \frac{\mu\text{g}}{\text{mL}} \quad \text{ppb} = \frac{\text{ng}}{\text{g}} = \frac{\mu\text{g}}{\text{L}} = \frac{\text{ng}}{\text{mL}}$$

For gases a part per million usually is expressed as a volume ratio; for example, a helium concentration of 6.3 ppm means that one liter of air contains 6.3 µL of He.

> You should be careful when using parts per million and parts per billion to express the concentration of an aqueous solute. The difference between a solute's concentration in mg/L and ng/g, for example, is significant if the solution's density is not 1.00 g/mL. For this reason many organizations advise against using the abbreviation ppm and ppb (see section 7.10.3 at www.nist.gov). If in doubt, include the exact units, such as 0.53 µg Pb^{2+}/L for the concentration of lead in a sample of seawater.

CONVERTING BETWEEN CONCENTRATION UNITS

The most common ways to express concentration in analytical chemistry are molarity, weight percent, volume percent, weight-to-volume percent, parts per million and parts per billion. The general definition of concentration in Equation 2.2.1 makes it is easy to convert between concentration units.

✔ EXAMPLE 2.2.1

A concentrated solution of ammonia is 28.0% w/w NH_3 and has a density of 0.899 g/mL. What is the molar concentration of NH_3 in this solution?

Solution

$$\frac{28.0\text{ g NH}_3}{100\text{ g soln}} \times \frac{0.899\text{ g soln}}{\text{ml soln}} \times \frac{1\text{ mol NH}_3}{17.03\text{ g NH}_3} \times \frac{1000\text{mL}}{\text{L}} = 14.8\text{ M}$$

✔ EXAMPLE 2.2.2

The maximum permissible concentration of chloride ion in a municipal drinking water supply is 2.50×10^2 ppm Cl^-. When the supply of water exceeds this limit it often has a distinctive salty taste. What is the equivalent molar concentration of Cl^-?

Solution

$$\frac{2.50 \times 10^2\text{ mg Cl}^-}{\text{L}} \times \frac{1\text{ g}}{1000\text{ mg}} \times \frac{1\text{ mol Cl}^-}{35.453\text{ gCl}^-} = 7.05 \times 10^{-3}\text{ M}$$

EXERCISE 2.2.1

Which solution—0.50 M NaCl or 0.25 M $SrCl_2$—has the larger concentration when expressed in mg/mL?

Answer

The concentrations of the two solutions are

$$\frac{0.50 \text{ mol NaCl}}{\text{L}} \times \frac{58.44 \text{ g NaCl}}{\text{mol NaCl}} \times \frac{10^6 \ \mu\text{g}}{\text{g}} \times \frac{1\text{L}}{1000 \text{ mL}} = 2.9 \times 10^4 \ \mu\text{g/mL NaCl}$$

$$\frac{0.25 \text{ mol } SrCl_2}{\text{L}} \times \frac{158.5 \text{ g } SrCl_2}{\text{mol } SrCl_2} \times \frac{10^6 \ \mu\text{g}}{\text{g}} \times \frac{1\text{L}}{1000 \text{ mL}} = 4.0 \times 10^4 \ \mu\text{g/ml } SrCl_2$$

The solution of $SrCl_2$ has the larger concentration when it is expressed in µg/mL instead of in mol/L.

P-FUNCTIONS

Sometimes it is inconvenient to use the concentration units in Table 2.2.1 . For example, during a chemical reaction a species' concentration may change by many orders of magnitude. If we want to display the reaction's progress graphically we might wish to plot the reactant's concentration as a function of the volume of a reagent added to the reaction. Such is the case in Figure 2.2.1 for the titration of HCl with NaOH. The *y*-axis on the left-side of the figure displays the $[H^+]$ as a function of the volume of NaOH. The initial $[H^+]$ is 0.10 M and its concentration after adding 80 mL of NaOH is 4.3×10^{-13} M. We easily can follow the change in $[H^+]$ for the addition of the first 50 mL of NaOH; however, for the remaining volumes of NaOH the change in $[H^+]$ is too small to see.

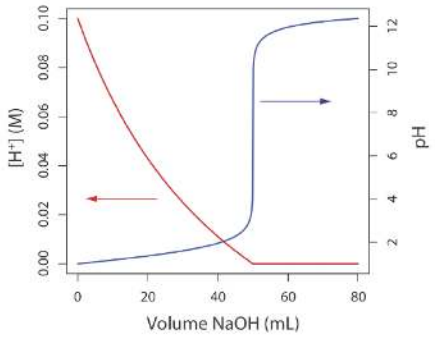


Figure 2.2.1 : Two curves showing the progress of a titration of 50.0 mL of 0.10 M HCl with 0.10 M NaOH. The $[H^+]$ is shown on the left *y*-axis and the pH on the right *y*-axis.

When working with concentrations that span many orders of magnitude, it often is more convenient to express concentration using a p-function. The p-function of *X* is written as p*X* and is defined as

$$\text{p}X = -\log(X)$$

The pH of a solution that is 0.10 M H^+ for example, is

$$\text{pH} = -\log[H^+] = -\log(0.10) = 1.00$$

and the pH of 4.3×10^{-13} M H^+ is

$$\text{pH} = -\log[H^+] = -\log(4.3 \times 10^{-13}) = 12.37$$

Figure 2.2.1 shows that plotting pH as a function of the volume of NaOH provides more useful information about how the concentration of H^+ changes during the titration.

A more appropriate equation for pH is $\text{pH} = -\log(a_{H^+})$ where a_{H^+} is the activity of the hydrogen ion. See Chapter 6.9 for more details. For now the approximate equation $\text{pH} = -\log[H^+]$ is sufficient.

EXAMPLE 2.2.3

What is pNa for a solution of 1.76×10^{-3} M Na_3PO_4?

Solution

Since each mole of Na_3PO_4 contains three moles of Na^+, the concentration of Na^+ is

$$[Na^+] = (1.76 \times 10^{-3}\ M) \times \frac{3\ mol\ Na^+}{mol\ Na_3PO_4} = 5.28 \times 10^{-3}\ M$$

and pNa is

$$pNa = -\log[Na^+] = -\log(5.28 \times 10^{-3}) = 2.277$$

Remember that a pNa of 2.777 has three, not four, significant figures; the 2 that appears in the one's place indicates the power of 10 when we write $[Na^+]$ as 0.528×10^{-2} M.

EXAMPLE 2.2.4

What is the $[H^+]$ in a solution that has a pH of 5.16?

Solution

The concentration of H^+ is

$$pH = -\log[H^+] = 5.16$$

$$\log[H^+] = -5.16$$

$$[H^+] = 10^{-5.16} = 6.9 \times 10^{-6}\ M$$

Recall that if $\log(X) = a$, then $X = 10^a$.

EXERCISE 2.2.2

What are the values for pNa and pSO_4 if we dissolve 1.5 g Na_2SO_4 in a total solution volume of 500.0 mL?

Answer

The concentrations of Na^+ and SO_4^{2-} are

$$\frac{1.5\ g\ Na_2SO_4}{0.500L} \times \frac{1\ mol\ Na_2SO_4}{142.0\ g\ Na_2SO_4} \times \frac{2\ mol\ Na^+}{mol\ molNa_2SO_4} = 4.23 \times 10^{-2}\ M\ Na^+$$

$$\frac{1.5\ g\ Na_2SO_4}{0.500L} \times \frac{1\ mol\ Na_2SO_4}{142.0\ g\ Na_2SO_4} \times \frac{1\ mol\ SO_4^{2-}}{mol\ molNa_2SO_4} = 2.11 \times 10^{-2}\ M\ SO_4^{2-}$$

The pNa and pSO_4 values are

$$pNa = -\log(4.23 \times 10^{-2}\ M\ Na^+) = 1.37$$

$$pSO_4 = -\log(2.11 \times 10^{-2}\ M\ SO_4^{2-}) = 1.68$$

This page titled 2.2: Concentration is shared under a CC BY-NC-SA 4.0 license and was authored, remixed, and/or curated by David Harvey.

- **2.2: Concentration** by David Harvey is licensed CC BY-NC-SA 4.0.

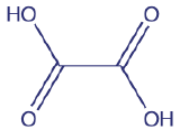
2.3: STOICHIOMETRIC CALCULATIONS

A balanced reaction, which defines the stoichiometric relationship between the moles of reactants and the moles of products, provides the basis for many analytical calculations. Consider, for example, an analysis for oxalic acid, $H_2C_2O_4$, in which Fe^{3+} oxidizes oxalic acid to CO_2

$$2Fe^{3+}(aq) + H_2C_2O_4(aq) + 2H_2O(l) \longrightarrow 2Fe^{2+}(aq) + 2CO_2(g) + 2H_3O^+(aq)$$

The balanced reaction shows us that one mole of oxalic acid reacts with two moles of Fe^{3+}. As shown in the following example, we can use this balanced reaction to determine the amount of $H_2C_2O_4$ in a sample of rhubarb if we know the moles of Fe^{3+} needed to react completely with oxalic acid.

In sufficient amounts, oxalic acid, the structure for which is shown below, is toxic. At lower physiological concentrations it leads to the formation of kidney stones. The leaves of the rhubarb plant contain relatively high concentrations of oxalic acid. The stalk, which many individuals enjoy eating, contains much smaller concentrations of oxalic acid.



In the examples that follow, note that we retain an extra significant figure throughout the calculation, rounding to the correct number of significant figures at the end. We will follow this convention in any calculation that involves more than one step. If we forget that we are retaining an extra significant figure, we might report the final answer with one too many significant figures. Here we mark the extra digit in **red** for emphasis. Be sure you pick a system for keeping track of significant figures.

EXAMPLE 2.3.1

The amount of oxalic acid in a sample of rhubarb was determined by reacting with Fe^{3+}. After extracting a 10.62 g of rhubarb with a solvent, oxidation of the oxalic acid required 36.44 mL of 0.0130 M Fe^{3+}. What is the weight percent of oxalic acid in the sample of rhubarb?

Solution

We begin by calculating the moles of Fe^{3+} used in the reaction

$$\frac{0.0130 \text{ mol } Fe^{3+}}{\text{L}} \times 0.03644 \text{ M} = 4.737 \times 10^{-4} \text{ mol } Fe^{3+}$$

The moles of oxalic acid reacting with the Fe^{3+}, therefore, is

$$4.737 \times 10^{-4} \text{ mol } Fe^{3+} \times \frac{1 \text{ mol } H_2C_2O_4}{2 \text{ mol } Fe^{3+}} = 2.368 \times 10^{-4} \text{ mol } H_2C_2O_4$$

Converting the moles of oxalic acid to grams of oxalic acid

$$2.368 \times 10^{-4} \text{ mol } H_2C_2O_4 \times \frac{90.03 \text{ g } H_2C_2O_4}{\text{mol } H_2C_2O_4} = 2.132 \times 10^{-2} \text{ g } H_2C_2O_4$$

and calculating the weight percent gives the concentration of oxalic acid in the sample of rhubarb as

$$\frac{2.132 \times 10^{-2} \text{ g } H_2C_2O_4}{10.62 \text{ g rhubarb}} \times 100 = 0.201\% \text{ w/w } H_2C_2O_4$$

EXERCISE 2.3.1

You can dissolve a precipitate of AgBr by reacting it with $Na_2S_2O_3$, as shown here.

$$AgBr(s) + 2Na_2S_2O_3(aq) \longrightarrow Ag(S_2O_3)_2^{3-}(aq) + Br^-(aq) + 4Na^+(aq)$$

How many mL of 0.0138 M $Na_2S_2O_3$ do you need to dissolve 0.250 g of AgBr?

Answer

First, we find the moles of AgBr

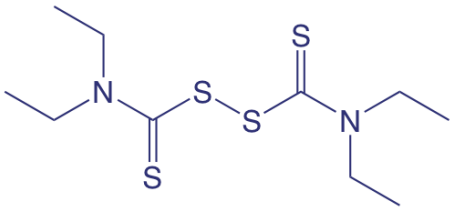
$$0.250 \text{ g AgBr} \times \frac{1 \text{ mol AgBr}}{187.8 \text{ g AgBr}} = 1.331 \times 10^{-3} \text{ mol AgBr}$$

and then the moles and volume of $Na_2S_2O_3$

$$1.331 \times 10^{-3} \text{ mol AgBr} \times \frac{2 \text{ mol } Na_2S_2O_3}{\text{mol AgBr}} = 2.662 \times 10^{-3} \text{ mol } Na_2S_2O_3$$

$$2.662 \times 10^{-3} \text{ mol } Na_2S_2O_3 \times \frac{1 \text{ L}}{0.0138 \text{ mol } Na_2S_2O_3} \times \frac{1000 \text{ mL}}{\text{L}} = 193 \text{ mL}$$

The analyte in Example 2.3.1 , oxalic acid, is in a chemically useful form because there is a reagent, Fe^{3+}, that reacts with it quantitatively. In many analytical methods, we first must convert the analyte into a more accessible form before we can complete the analysis. For example, one method for the quantitative analysis of disulfiram, $C_{10}H_{20}N_2S_4$—the active ingredient in the drug Antabuse, and whose structure is shown below—requires that we first convert the sulfur to SO_2 by combustion, and then oxidize the SO_2 to H_2SO_4 by bubbling it through a solution of H_2O_2. When the conversion is complete, the amount of H_2SO_4 is determined by titrating with NaOH.



To convert the moles of NaOH used in the titration to the moles of disulfiram in the sample, we need to know the stoichiometry of each reaction. Writing a balanced reaction for H_2SO_4 and NaOH is straightforward

$$H_2SO_4(aq) + 2NaOH(aq) \longrightarrow 2H_2O(l) + Na_2SO_4(aq)$$

but the balanced reactions for the oxidations of $C_{10}H_{20}N_2S_4$ to SO_2, and of SO_2 to H_2SO_4 are not as immediately obvious. Although we can balance these redox reactions, it is often easier to deduce the overall stoichiometry by using a little chemical logic.

EXAMPLE 2.3.2

An analysis for disulfiram, $C_{10}H_{20}N_2S_4$, in Antabuse is carried out by oxidizing the sulfur to H_2SO_4 and titrating the H_2SO_4 with NaOH. If a 0.4613-g sample of Antabuse requires 34.85 mL of 0.02500 M NaOH to titrate the H_2SO_4, what is the %w/w disulfiram in the sample?

Solution

Calculating the moles of H_2SO_4 is easy—first, we calculate the moles of NaOH used in the titration

$$(0.02500 \text{ M}) \times (0.03485 \text{ L}) = 8.7125 \times 10^{-4} \text{ mol NaOH}$$

and then we use the titration reaction's stoichiometry to calculate the corresponding moles of H_2SO_4.

$$8.7125 \times 10^{-4} \text{ mol NaOH} \times \frac{1 \text{ mol } H_2SO_4}{2 \text{ mol NaOH}} = 4.3562 \times 10^{-4} \text{ mol } H_2SO_4$$

Here is where we use a little chemical logic. Instead of balancing the reactions for the combustion of $C_{10}H_{20}N_2S_4$ to SO_2 and for the subsequent oxidation of SO_2 to H_2SO_4, we recognize that a conservation of mass requires that all the sulfur in $C_{10}H_{20}N_2S_4$ ends up in the H_2SO_4; thus

$$4.3562 \times 10^{-4} \text{ mol } H_2SO_4 \times \frac{1 \text{ mol S}}{\text{mol } H_2SO_4} \times \frac{1 \text{ mol } C_{10}H_{20}N_2S_4}{4 \text{ mol S}} = 1.0890 \times 10^{-4} \text{ mol } C_{10}H_{20}N_2S_4$$

$$1.0890 \times 10^{-4} \text{ mol } C_{10}H_{20}N_2S_4 \times \frac{296.54 \text{ g } C_{10}H_{20}N_2S_4}{\text{mol } C_{10}H_{20}N_2S_4} = 0.032293 \text{ g } C_{10}H_{20}N_2S_4$$

$$\frac{0.032293 \text{ g } C_{10}H_{20}N_2S_4}{0.4613 \text{ g sample}} \times 100 = 7.000\% \text{ w/w } C_{10}H_{20}N_2S_4$$

> A conservation of mass is the essence of stoichiometry!

This page titled 2.3: Stoichiometric Calculations is shared under a CC BY-NC-SA 4.0 license and was authored, remixed, and/or curated by David Harvey.

- **2.3: Stoichiometric Calculations** by David Harvey is licensed CC BY-NC-SA 4.0.

2.4: BASIC EQUIPMENT

The array of equipment available for making analytical measurements and working with analytical samples is impressive, ranging from the simple and inexpensive, to the complex and expensive. With three exceptions—the measurement of mass, the measurement of volume, and the drying of materials—we will postpone the discussion of equipment to later chapters where its application to specific analytical methods is relevant.

EQUIPMENT FOR MEASURING MASS

An object's mass is measured using a digital electronic analytical balance (Figure 2.4.1). An electromagnet levitates the sample pan above a permanent cylindrical magnet. When we place an object on the sample pan, it displaces the sample pan downward by a force equal to the product of the sample's mass and its acceleration due to gravity. The balance detects this downward movement and generates a counterbalancing force by increasing the current to the electromagnet. The current needed to return the balance to its original position is proportional to the object's mass. A typical electronic balance has a capacity of 100–200 g, and can measure mass to the nearest ±0.01 mg to ±1 mg.



Figure 2.4.1 : The photo shows a typical digital electronic balance capable of determining mass to the nearest ±0.1 mg. The sticker inside the balance's wind shield is its annual calibration certification. For a review of other types of electronic balances, see Schoonover, R. M. *Anal. Chem.* **1982**, *54*, 973A-980A.

Although we tend to use interchangeably, the terms "weight" and "mass," there is an important distinction between them. Mass is the absolute amount of matter in an object, measured in grams. Weight, *W*, is a measure of gravitational acceleration, *g*, acting on that mass, *m*:

$$W = m \times g$$

An object has a fixed mass but its weight depends upon the acceleration due to gravity, which varies subtly from location-to-location.

A balance measures an object's weight, not its mass. Because weight and mass are proportional to each other, we can calibrate a balance using a standard weight whose mass is traceable to the standard prototype for the kilogram. A properly calibrated balance gives an accurate value for an object's mass; see Appendix 9 for more details on calibrating a balance.

If the sample is not moisture sensitive, a clean and dry container is placed on the balance. The container's mass is called the ***tare*** and most balances allow you to set the container's tare to a mass of zero. The sample is transferred to the container, the new mass is measured and the sample's mass determined by subtracting the tare. A sample that absorbs moisture from the air is treated differently. The sample is placed in a covered weighing bottle and their combined mass is determined. A portion of the sample is removed and the weighing bottle and the remaining sample are reweighed. The difference between the two masses gives the sample's mass.

Several important precautions help to minimize errors when we determine an object's mass. To minimize the effect of vibrations, the balance is placed on a stable surface and in a level position. Because the sensitivity of an analytical balance is sufficient to measure the mass of a fingerprint, materials often are handled using tongs or laboratory tissues. Volatile liquid samples must be weighed in a covered container to avoid the loss of sample by evaporation. To minimize fluctuations in mass due to air currents, the balance pan often is housed within a wind shield, as seen in Figure 2.4.1 . A sample that is cooler or warmer than the surrounding air will create a convective air current that affects the measurement of its mass. For this reason, bring your samples to room temperature before determining their mass. Finally, samples dried in an oven are stored in a desiccator to prevent them from reabsorbing moisture from the atmosphere.

EQUIPMENT FOR MEASURING VOLUME

Analytical chemists use a variety of glassware to measure volume, including graduated cylinders, volumetric pipets, and volumetric flasks. The choice of what type of glassware to use depends on how accurately and how precisely we need to measure the volume and whether we are interested in containing or delivering the sample.

A ***graduated cylinder*** is the simplest device for delivering a known volume of a liquid reagent (Figure 2.4.2). The graduated scale allows you to deliver any volume up to the cylinder's maximum. Typical accuracy is ±1% of the maximum volume. A 100-mL graduated cylinder, for example, is accurate to ±1 mL.



Figure 2.4.2 : An example of a 250-mL graduated cylinder.

A ***volumetric pipet*** provides a more accurate method for delivering a known volume of solution. Several different styles of pipets are available, two of which are shown in Figure 2.4.3 . Transfer pipets provide the most accurate means for delivering a known volume of solution. A transfer pipet delivering less than 100 mL generally is accurate to the hundredth of a mL. Larger transfer pipets are accurate to a tenth of a mL. For example, the 10-mL transfer pipet in Figure 2.4.3 will deliver 10.00 mL with an accuracy of ±0.02 mL.

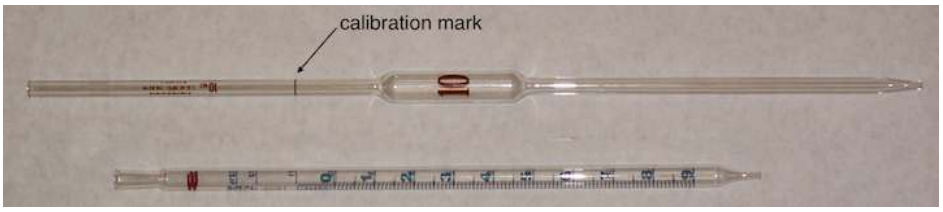


Figure 2.4.3 : Two examples of 10-mL volumetric pipets. The pipet on the top is a transfer pipet and the pipet on the bottom is a Mohr measuring pipet. The transfer pipet delivers a single volume of 10.00 mL when filled to its calibration mark. The Mohr pipet has a mark every 0.1 mL, allowing for the delivery of variable volumes. It also has additional graduations at 11 mL, 12 mL, and 12.5 mL.

> Scientists at the Brookhaven National Laboratory used a germanium nanowire to make a pipet that delivers a 35 zeptoliter (10^{-21} L) drop of a liquid gold-germanium alloy. You can read about this work in the April 21, 2007 issue of *Science News*.

To fill a transfer pipet, use a rubber suction bulb to pull the solution up past the calibration mark (*Never use your mouth to suck a solution into a pipet!*). After replacing the bulb with your finger, adjust the solution's level to the calibration mark and dry the outside of the pipet with a laboratory tissue. Allow the pipet's contents to drain into the receiving container with the pipet's tip touching the inner wall of the container. A small portion of the liquid remains in the pipet's tip and is not be blown out. With some measuring pipets any solution remaining in the tip must be blown out.

Delivering microliter volumes of liquids is not possible using transfer or measuring pipets. Digital micropipets (Figure 2.4.4), which come in a variety of volume ranges, provide for the routine measurement of microliter volumes.

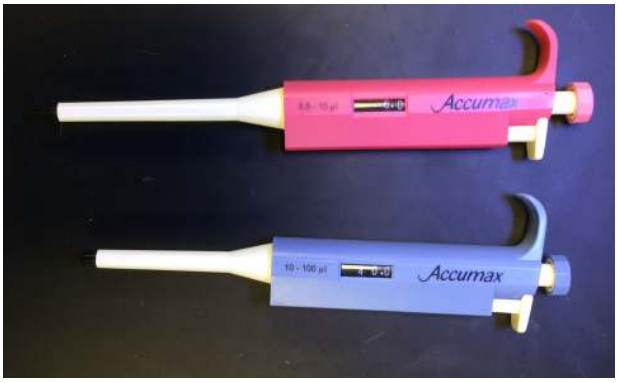


Figure 2.4.4 : A set of two digital micropipets. The pipet on the top delivers volumes between 0.5 mL and 10 µL and the pipet on the bottom delivers volumes between 10 mL and 100 µL.

Graduated cylinders and pipets deliver a known volume of solution. A ***volumetric flask***, on the other hand, contains a specific volume of solution (Figure 2.4.5). When filled to its calibration mark, a volumetric flask that contains less than 100 mL generally is accurate to the hundredth of a mL, whereas larger volumetric flasks are accurate to the tenth of a mL. For example, a 10-mL volumetric flask contains 10.00 mL ± 0.02 mL and a 250-mL volumetric flask contains 250.0 mL ± 0.12 mL.



Figure 2.4.5 : A collection of volumetric flasks with volumes of 10 mL, 50 mL, 100, mL, 250 mL, and 500 mL.

Because a volumetric flask contains a solution, it is used to prepare a solution with an accurately known concentration. Transfer the reagent to the volumetric flask and add enough solvent to bring the reagent into solution. Continue adding solvent in several portions, mixing thoroughly after each addition, and then adjust the volume to the flask's calibration mark using a dropper. Finally, complete the mixing process by inverting and shaking the flask at least 10 times.

If you look closely at a volumetric pipet or a volumetric flask you will see markings similar to those shown in Figure 2.4.6 . The text of the markings, which reads

$$10 \text{ mL T. D. at } 20\ ^{o}\text{C} \pm 0.02 \text{ mL}$$

indicates that the pipet is calibrated to deliver (T. D.) 10 mL of solution with an uncertainty of ±0.02 mL at a temperature of 20 ^{o}C. The temperature is important because glass expands and contracts with changes in temperatures; thus, the pipet's accuracy is less than ±0.02 mL at a higher or a lower temperature. For a more accurate result, you can calibrate your volumetric glassware at the temperature you are working by weighing the amount of water contained or delivered and calculating the volume using its temperature dependent density.



Figure 2.4.6 : Close-up of the 10-mL transfer pipet from Figure 2.4.3 .

> A volumetric flask has similar markings, but uses the abbreviation T. C. for "to contain" in place of T. D.

You should take three additional precautions when you work with pipets and volumetric flasks. First, the volume delivered by a pipet or contained by a volumetric flask assumes that the glassware is clean. Dirt and grease on the inner surface prevent liquids from draining evenly, leaving droplets of liquid on the container's walls. For a pipet this means the delivered volume is less than the calibrated volume, while drops of liquid above the calibration mark mean that a volumetric flask contains more than its calibrated volume. Commercially available cleaning solutions are available for cleaning pipets and volumetric flasks.

Second, when filling a pipet or volumetric flask the liquid's level must be set exactly at the calibration mark. The liquid's top surface is curved into a meniscus, the bottom of which should align with the glassware's calibration mark (Figure 2.4.7). When adjusting the meniscus, keep your eye in line with the calibration mark to avoid parallax errors. If your eye level is above the calibration mark you will overfill the pipet or the volumetric flask and you will underfill them if your eye level is below the calibration mark.



Figure 2.4.7 : Proper position of the solution's meniscus relative to the volumetric flask's calibration mark.

Finally, before using a pipet or volumetric flask rinse it with several small portions of the solution whose volume you are measuring. This ensures the removal of any residual liquid remaining in the pipet or volumetric flask.

EQUIPMENT FOR DRYING SAMPLES

Many materials need to be dried prior to their analysis to remove residual moisture. Depending on the material, heating to a temperature between 110 ^{o}C and 140 ^{o}C usually is sufficient. Other materials need much higher temperatures to initiate thermal decomposition.

Conventional drying ovens provide maximum temperatures of 160 ^{o}C to 325 ^{o}C, depending on the model. Some ovens include the ability to circulate heated air, which allows for a more efficient removal of moisture and shorter drying times. Other ovens provide a tight seal for the door, which allows the oven to be evacuated. In some situations a microwave oven can replace a conventional laboratory oven. Higher temperatures, up to as much as 1700 ^{o}C, require a muffle furnace (Figure 2.4.8).

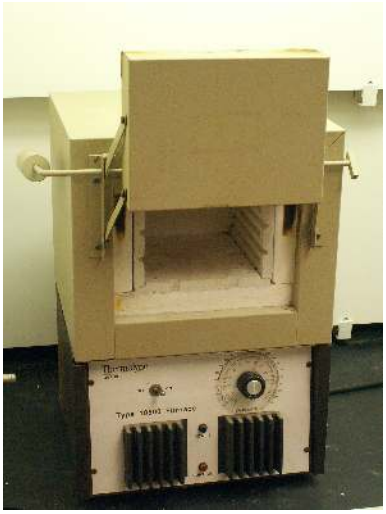


Figure 2.4.8 : Example of a muffle furnace.

After drying or decomposing a sample, it is cooled to room temperature in a desiccator to prevent the readsorption of moisture. A ***desiccator*** (Figure 2.4.9) is a closed container that isolates the sample from the atmosphere. A drying agent, called a ***desiccant***, is placed in the bottom of the container. Typical desiccants include calcium chloride and silica gel. A perforated plate sits above the desiccant, providing a shelf for storing samples. Some desiccators include a stopcock that allows them to be evacuated.



Figure 2.4.9 : Example of a desiccator. The solid in the bottom of the desiccator is the desiccant, which in this case is silica gel.

This page titled 2.4: Basic Equipment is shared under a CC BY-NC-SA 4.0 license and was authored, remixed, and/or curated by David Harvey.

- **2.4: Basic Equipment** by David Harvey is licensed CC BY-NC-SA 4.0.

2.5: PREPARING SOLUTIONS

Preparing a solution of known concentration is perhaps the most common activity in any analytical lab. The method for measuring out the solute and the solvent depend on the desired concentration and how exact the solution's concentration needs to be known. Pipets and volumetric flasks are used when we need to know a solution's exact concentration; graduated cylinders, beakers, and/or reagent bottles suffice when a concentrations need only be approximate. Two methods for preparing solutions are described in this section.

PREPARING STOCK SOLUTIONS

A ***stock solution*** is prepared by weighing out an appropriate portion of a pure solid or by measuring out an appropriate volume of a pure liquid, placing it in a suitable flask, and diluting to a known volume. Exactly how one measure's the reagent depends on the desired concentration unit. For example, to prepare a solution with a known molarity you weigh out an appropriate mass of the reagent, dissolve it in a portion of solvent, and bring it to the desired volume. To prepare a solution where the solute's concentration is a volume percent, you measure out an appropriate volume of solute and add sufficient solvent to obtain the desired total volume.

✔ EXAMPLE 2.5.1

Describe how to prepare the following three solutions: (a) 500 mL of approximately 0.20 M NaOH using solid NaOH; (b) 1 L of 150.0 ppm Cu^{2+} using Cu metal; and (c) 2 L of 4% v/v acetic acid using concentrated glacial acetic acid (99.8% w/w acetic acid).

Solution

(a) Because the desired concentration is known to two significant figures, we do not need to measure precisely the mass of NaOH or the volume of solution. The desired mass of NaOH is

$$\frac{0.20\text{ mol NaOH}}{\text{L}} \times \frac{40.0\text{ g NaOH}}{\text{mol NaOH}} \times 0.50\text{ L} = 4.0\text{ g NaOH}$$

To prepare the solution, place 4.0 grams of NaOH, weighed to the nearest tenth of a gram, in a bottle or beaker and add approximately 500 mL of water.

(b) Since the desired concentration of Cu^{2+} is given to four significant figures, we must measure precisely the mass of Cu metal and the final solution volume. The desired mass of Cu metal is

$$\frac{150.0\text{ mg Cu}}{\text{L}} \times 1.000\text{ M} \times \frac{1\text{ g}}{1000\text{ mg}} = 0.1500\text{ g Cu}$$

To prepare the solution, measure out exactly 0.1500 g of Cu into a small beaker and dissolve it using a small portion of concentrated HNO_3. To ensure a complete transfer of Cu^{2+} from the beaker to the volumetric flask—what we call a ***quantitative transfer***—rinse the beaker several times with small portions of water, adding each rinse to the volumetric flask. Finally, add additional water to the volumetric flask's calibration mark.

(c) The concentration of this solution is only approximate so it is not necessary to measure exactly the volumes, nor is it necessary to account for the fact that glacial acetic acid is slightly less than 100% w/w acetic acid (it is approximately 99.8% w/w). The necessary volume of glacial acetic acid is

$$\frac{4\text{ mL }CH_3COOH}{100\text{ mL}} \times 2000\text{ mL} = 80\text{ mL }CH_3COOH$$

To prepare the solution, use a graduated cylinder to transfer 80 mL of glacial acetic acid to a container that holds approximately 2 L and add sufficient water to bring the solution to the desired volume.

? EXERCISE 2.5.1

Provide instructions for preparing 500 mL of 0.1250 M $KBrO_3$.

Answer

Preparing 500 mL of 0.1250 M $KBrO_3$ requires

$$0.5000\text{ L} \times \frac{0.1250\text{ mol }KBrO_3}{\text{L}} \times \frac{167.00\text{ g }KBrO_3}{\text{mol }KBrO_3} = 10.44\text{ g }KBrO_3$$

Because the concentration has four significant figures, we must prepare the solution using volumetric glassware. Place a 10.44 g sample of $KBrO_3$ in a 500-mL volumetric flask and fill part way with water. Swirl to dissolve the $KBrO_3$ and then dilute with water

to the flask's calibration mark.

PREPARING SOLUTIONS BY DILUTION

Solutions are often prepared by diluting a more concentrated stock solution. A known volume of the stock solution is transferred to a new container and brought to a new volume. Since the total amount of solute is the same before and after dilution, we know that

$$C_o \times V_o = C_d \times V_d \tag{2.5.1}$$

where C_o is the stock solution's concentration, V_o is the volume of stock solution being diluted, C_d is the dilute solution's concentration, and V_d is the volume of the dilute solution. Again, the type of glassware used to measure V_o and V_d depends on how precisely we need to know the solution's concentration.

Note that Equation 2.5.1 applies only to those concentration units that are expressed in terms of the solution's volume, including molarity, formality, normality, volume percent, and weight-to-volume percent. It also applies to weight percent, parts per million, and parts per billion if the solution's density is 1.00 g/mL. We cannot use Equation 2.5.1 if we express concentration in terms of molality as this is based on the mass of solvent, not the volume of solution. See Rodríquez-López, M.; Carrasquillo, A. *J. Chem. Educ.* **2005**, *82*, 1327-1328 for further discussion.

EXAMPLE 2.5.2

A laboratory procedure calls for 250 mL of an approximately 0.10 M solution of NH_3. Describe how you would prepare this solution using a stock solution of concentrated NH_3 (14.8 M).

Solution

Substituting known values into Equation 2.5.1

$$14.8\ \text{M} \times V_o = 0.10\ \text{M} \times 250\ \text{mL}$$

and solving for V_o gives 1.7 mL. Since we are making a solution that is approximately 0.10 M NH_3, we can use a graduated cylinder to measure the 1.7 mL of concentrated NH_3, transfer the NH_3 to a beaker, and add sufficient water to give a total volume of approximately 250 mL.

Although usually we express molarity as mol/L, we can express the volumes in mL if we do so both for both V_o and V_d.

? EXERCISE 2.5.2

To prepare a standard solution of Zn^{2+} you dissolve a 1.004 g sample of Zn wire in a minimal amount of HCl and dilute to volume in a 500-mL volumetric flask. If you dilute 2.000 mL of this stock solution to 250.0 mL, what is the concentration of Zn^{2+}, in μg/mL, in your standard solution?

Answer

The first solution is a stock solution, which we then dilute to prepare the standard solution. The concentration of Zn^{2+} in the stock solution is

$$\frac{1.004\ \text{g Zn}^{2+}}{500.0\ \text{mL}} \times \frac{10^6\ \mu\text{g}}{\text{g}} = 2008\ \mu\text{g Zn}^{2+}/\text{mL}$$

To find the concentration of the standard solution we use Equation 2.5.1

$$\frac{2008\ \mu\text{g Zn}^{2+}}{\text{mL}} \times 2.000\ \text{mL} = C_d \times 250.0\ \text{mL}$$

where C_d is the standard solution's concentration. Solving gives a concentration of 16.06 μg Zn^{2+}/mL.

As shown in the following example, we can use Equation 2.5.1 to calculate a solution's original concentration using its known concentration after dilution.

EXAMPLE 2.5.3

A sample of an ore was analyzed for Cu^{2+} as follows. A 1.25 gram sample of the ore was dissolved in acid and diluted to volume in a 250-mL volumetric flask. A 20 mL portion of the resulting solution was transferred by pipet to a 50-mL volumetric flask and diluted to volume. An analysis of this solution gives the concentration of Cu^{2+} as 4.62 µg/mL. What is the weight percent of Cu in the original ore?

Solution

Substituting known values (with significant figures appropriate for pipets and volumetric flasks) into Equation 2.5.1

$$(C_{\text{Cu}})_o \times 20.00\ \text{mL} = 4.62\ \mu\text{g/mL Cu}^{2+} \times 50.00\ \text{mL}$$

and solving for $(C_{\text{Cu}})_o$ gives the original concentration as 11.55 µg/mL Cu^{2+}. To calculate the grams of Cu^{2+} we multiply this concentration by the total volume

$$\frac{11.55 \mu\text{g Cu}^{2+}}{\text{mL}} \times 250.0\ \text{mL} \times \frac{1\ \text{g}}{10^6\ \mu\text{g}} = 2.888 \times 10^{-3}\ \text{g Cu}^{2+}$$

The weight percent Cu is

$$\frac{2.888 \times 10^{-3}\ \text{g Cu}^{2+}}{1.25\ \text{g sample}} \times 100 = 0.231\%\ \text{w/w Cu}^{2+}$$

This page titled 2.5: Preparing Solutions is shared under a CC BY-NC-SA 4.0 license and was authored, remixed, and/or curated by David Harvey.

- **2.5: Preparing Solutions** by David Harvey is licensed CC BY-NC-SA 4.0.

2.6: SPREADSHEETS AND COMPUTATIONAL SOFTWARE

Analytical chemistry is a quantitative discipline. Whether you are completing a statistical analysis, trying to optimize experimental conditions, or exploring how a change in pH affects a compound's solubility, the ability to work with complex mathematical equations is essential. Spreadsheets, such as Microsoft Excel are an important tool for analyzing your data and for preparing graphs of your results. Scattered throughout this textbook you will find instructions for using spreadsheets.

> If you do not have access to Microsoft Excel or another commercial spreadsheet package, you might considering using Calc, a freely available open-source spreadsheet that is part of the OpenOffice.org software package at www.openoffice.org, or Google Sheets.

Although spreadsheets are useful, they are not always well suited for working with scientific data. If you plan to pursue a career in chemistry, you may wish to familiarize yourself with a more sophisticated computational software package, such as the freely available open-source program that goes by the name R, or commercial programs such as Mathematica or Matlab. You will find instructions for using R scattered throughout this textbook.

> You can download the current version of R from www.r-project.org. Click on the link for Download: CRAN and find a local mirror site. Click on the link for the mirror site and then use the link for Linux, MacOS X, or Windows under the heading "Download and Install R."

Despite the power of spreadsheets and computational programs, *don't forget that the most important software is behind your eyes and between your ears*. The ability to think intuitively about chemistry is a critically important skill. In many cases you will find that it is possible to determine if an analytical method is feasible or to approximate the optimum conditions for an analytical method without resorting to complex calculations. Why spend time developing a complex spreadsheet or writing software code when a "back-of-the-envelope" estimate will do the trick? Once you know the general solution to your problem, you can use a spreadsheet or a computational program to work out the specifics. Throughout this textbook we will introduce tools to help develop your ability to think intuitively.

> For an interesting take on the importance of intuitive thinking, see *Are You Smart Enough to Work at Google?* by William Poundstone (Little, Brown and Company, New York, 2012).

This page titled 2.6: Spreadsheets and Computational Software is shared under a CC BY-NC-SA 4.0 license and was authored, remixed, and/or curated by David Harvey.

- **2.6: Spreadsheets and Computational Software** by David Harvey is licensed CC BY-NC-SA 4.0.

2.7: THE LABORATORY NOTEBOOK

Finally, we can not end a chapter on the basic tools of analytical chemistry without mentioning the laboratory notebook. A laboratory notebook is your most important tool when working in the lab. If kept properly, you should be able to look back at your laboratory notebook several years from now and reconstruct the experiments on which you worked.

Your instructor will provide you with detailed instructions on how he or she wants you to maintain your notebook. Of course, you should expect to bring your notebook to the lab. Everything you do, measure, or observe while working in the lab should be recorded in your notebook as it takes place. Preparing data tables to organize your data will help ensure that you record the data you need, and that you can find the data when it is time to calculate and analyze your results. Writing a narrative to accompany your data will help you remember what you did, why you did it, and why you thought it was significant. Reserve space for your calculations, for analyzing your data, and for interpreting your results. Take your notebook with you when you do research in the library.

Maintaining a laboratory notebook may seem like a great deal of effort, but if you do it well you will have a permanent record of your work. Scientists working in academic, industrial and governmental research labs rely on their notebooks to provide a written record of their work. Questions about research carried out at some time in the past can be answered by finding the appropriate pages in the laboratory notebook. A laboratory notebook is also a legal document that helps establish patent rights and proof of discovery.

This page titled 2.7: The Laboratory Notebook is shared under a CC BY-NC-SA 4.0 license and was authored, remixed, and/or curated by David Harvey.

- **2.7: The Laboratory Notebook** by David Harvey is licensed CC BY-NC-SA 4.0.

2.8: PROBLEMS

1. Indicate how many significant figures are in each of the following numbers.

   a. 903

   b. 0.903

   c. 1.0903

   d. 0.0903

   e. 0.09030

   f. 9.03×10^2
2. Round each of the following to three significant figures.

   a. 0.89377

   b. 0.89328

   c. 0.89350

   d. 0.8997

   e. 0.08907
3. Round each to the stated number of significant figures.

   a. the atomic weight of carbon to 4 significant figures

   b. the atomic weight of oxygen to 3 significant figures

   c. Avogadro's number to 4 significant figures

   d. Faraday's constant to 3 significant figures
4. Report results for the following calculations to the correct number of significant figures.

   a. 4.591 + 0.2309 + 67.1 =

   b. 313 – 273.15 =

   c. 712×8.6 =

   d. 1.43/0.026 =

   e. $(8.314 \times 298)/96\,485$ =

   f. $\log(6.53 \times 10^{-5})$ =

   g. $10^{-7.14}$ =

   h. $(6.51 \times 10^{-5}) \times (8.14 \times 10^{-9})$
5. A 12.1374 g sample of an ore containing Ni and Co is carried through Fresenius' analytical scheme, as shown in Figure 1.1.1. At point A the combined mass of Ni and Co is 0.2306 g, while at point B the mass of Co is 0.0813 g. Report the weight percent Ni in the ore to the correct number of significant figures.

6. Figure 1.1.2 shows an analytical method for the analysis of Ni in ores based on the precipitation of Ni^{2+} using dimethylglyoxime. The formula for the precipitate is $Ni(C_4H_7N_2O_2)_2$. Calculate the precipitate's formula weight to the correct number of significant figures.
7. An analyst wishes to add 256 mg of Cl^- to a reaction mixture. How many mL of 0.217 M $BaCl_2$ is this?
8. The concentration of lead in an industrial waste stream is 0.28 ppm. What is its molar concentration?
9. Commercially available concentrated hydrochloric acid is 37.0% w/w HCl. Its density is 1.18 g/mL. Using this information calculate (a) the molarity of concentrated HCl, and (b) the mass and volume, in mL, of a solution that contains 0.315 moles of HCl.
10. The density of concentrated ammonia, which is 28.0% w/w NH_3, is 0.899 g/mL. What volume of this reagent should you dilute to 1.0×10^3 mL to make a solution that is 0.036 M in NH_3?
11. A 250.0 mL aqueous solution contains 45.1 µg of a pesticide. Express the pesticide's concentration in weight-to-volume percent, in parts per million, and in parts per billion.
12. A city's water supply is fluoridated by adding NaF. The desired concentration of F^- is 1.6 ppm. How many mg of NaF should you add per gallon of treated water if the water supply already is 0.2 ppm in F^-?
13. What is the pH of a solution for which the concentration of H^+ is 6.92×10^{-6} M ? What is the $[H^+]$ in a solution whose pH is 8.923?
14. When using a graduated cylinder, the absolute accuracy with which you can deliver a given volume is ±1% of the cylinder's maximum volume. What are the absolute and the relative uncertainties if you deliver 15 mL of a reagent using a 25 mL graduated cylinder? Repeat for a 50 mL graduated cylinder.
15. Calculate the molarity of a potassium dichromate solution prepared by placing 9.67 grams of $K_2Cr_2O_7$ in a 100-mL volumetric flask, dissolving, and diluting to the calibration mark.
16. For each of the following explain how you would prepare 1.0 L of a solution that is 0.10 M in K^+. Repeat for concentrations of 1.0×10^2 ppm K^+ and 1.0% w/v K^+.

    a. KCl

    b. K_2SO_4

    c. $K_3Fe(CN)_6$
17. A series of dilute NaCl solutions are prepared starting with an initial stock solution of 0.100 M NaCl. Solution A is prepared by pipeting 10 mL of the stock solution into a 250-mL volumetric flask and diluting to volume. Solution B is prepared by pipeting 25 mL of solution A into a 100-mL volumetric flask and diluting to volume. Solution C is prepared by pipeting 20 mL of solution B into a 500-mL volumetric flask and diluting to volume. What is the molar concentration of NaCl in solutions A, B and C?
18. Calculate the molar concentration of NaCl, to the correct number of significant figures, if 1.917 g of NaCl is placed in a beaker and dissolved in 50 mL of water measured with a graduated cylinder. If this solution is quantitatively transferred to a 250-mL volumetric flask and diluted to volume, what is its concentration to the correct number of significant figures?
19. What is the molar concentration of NO_3^- in a solution prepared by mixing 50.0 mL of 0.050 M KNO_3 with 40.0 mL of 0.075 M $NaNO_3$? What is pNO_3 for the mixture?
20. What is the molar concentration of Cl^- in a solution prepared by mixing 25.0 mL of 0.025 M NaCl with 35.0 mL of 0.050 M $BaCl_2$? What is pCl for the mixture?
21. To determine the concentration of ethanol in cognac a 5.00 mL sample of the cognac is diluted to 0.500 L. Analysis of the diluted cognac gives an ethanol concentration of 0.0844 M. What is the molar concentration of ethanol in the undiluted cognac?

This page titled 2.8: Problems is shared under a CC BY-NC-SA 4.0 license and was authored, remixed, and/or curated by David Harvey.

- **2.8: Problems** by David Harvey is licensed CC BY-NC-SA 4.0.

2.9: ADDITIONAL RESOURCES

The following two web sites contain useful information about the SI system of units.

- http://www.bipm.org/en/home/ – The home page for the Bureau International des Poids and Measures.
- http://physics.nist.gov/cuu/Units/index.html – The National Institute of Standards and Technology's introduction to SI units.

For a chemist's perspective on the SI units for mass and amount, consult the following papers.

- Davis, R. S. "What is a Kilogram in the Revised International System of Units (SI)?", *J. Chem. Educ.* **2015**, *92*, 1604–1609.
- Freeman, R. D. "SI for Chemists: Persistent Problems, Solid Solutions," *J. Chem. Educ.* **2003**, *80*, 16–20.
- Gorin, G. "Mole, Mole per Liter, and Molar: A Primer on SI and Related Units for Chemistry Students," *J. Chem. Educ.* **2003**, *80*, 103–104.

Discussions regarding possible changes in the SI base units are reviewed in these articles.

- Chao, L. S.; Schlamminger, S.; Newell, D. B.; Pratt, J. R.; Seifert, F.; Zhang, X.; Sineriz, M. L.; Haddad, D. "A LEGO Watt Balance: An Apparatus to Determine a Mass Based on the New SI," arXiv:1412.1699 [physics.ins-det].
- Fraundorf, P. "A Multiple of 12 for Avogadro," arXiv:1201.5537 [physics.gen-ph].
- Kemsley, J. "Rethinking the Mole and Kilogram," *C&E News*, August 25, 2014, p. 25.

The following are useful resources for maintaining a laboratory notebook and for preparing laboratory reports.

- Coghill, A. M.; Garson, L. M. (eds) *The ACS Style Guide: Effective Communication of Scientific Information*, 3rd Edition, American Chemical Society: Washington, D. C.; 2006.
- Kanare, H. M. *Writing the Laboratory Notebook*, American Chemical Society: Washington, D. C.; 1985.

The following texts provide instructions for using spreadsheets in analytical chemistry.

- de Levie, R. *How to Use Excel® in Analytical Chemistry and in General Scientific Data Analysis*, Cambridge University Press: Cambridge, UK, 2001.
- Diamond, D.; Hanratty, V. C. A., *Spreadsheet Applications in Chemistry*, Wiley-Interscience: New York, 1997.
- Feiser, H. *Concepts and Calculations in Analytical Chemistry: A Spreadsheet Approach*, CRC Press: Boca Raton, FL, 1992.

The following classic textbook emphasizes the application of intuitive thinking to the solving of problems.

- Harte, J. *Consider a Spherical Cow: A Course in Environmental Problem Solving*, University Science Books: Sausalito, CA, 1988.

This page titled 2.9: Additional Resources is shared under a CC BY-NC-SA 4.0 license and was authored, remixed, and/or curated by David Harvey.

- **2.9: Additional Resources** by David Harvey is licensed CC BY-NC-SA 4.0.

2.10: CHAPTER SUMMARY AND KEY TERMS

CHAPTER SUMMARY

There are a few basic numerical and experimental tools with which you must be familiar. Fundamental measurements in analytical chemistry, such as mass, use base SI units, such as the kilogram. Other units, such as energy, are defined in terms of these base units. When reporting a measurement, we must be careful to include only those digits that are significant, and to maintain the uncertainty implied by these significant figures when trans- forming measurements into results.

The relative amount of a constituent in a sample is expressed as a concentration. There are many ways to express concentration, the most common of which are molarity, weight percent, volume percent, weight-to-volume percent, parts per million and parts per billion. Concentrations also can be expressed using p-functions.

Stoichiometric relationships and calculations are important in many quantitative analyses. The stoichiometry between the reactants and the products of a chemical reaction are given by the coefficients of a balanced chemical reaction.

Balances, volumetric flasks, pipets, and ovens are standard pieces of equipment that you will use routinely in the analytical lab. You should be familiar with the proper way to use this equipment. You also should be familiar with how to prepare a stock solution of known concentration, and how to prepare a dilute solution from a stock solution.

KEY TERMS

analytical balance
concentration
desiccant
desiccator
dilution
formality
graduated cylinder
meniscus
molality
molarity
normality
parts per million
parts per billion
p-function
quantitative transfer
scientific notation
significant figures
SI units
stock solution
tare
volume percent
volumetric flask
volumetric pipet
weight percent
weight-to-volume percent

This page titled 2.10: Chapter Summary and Key Terms is shared under a CC BY-NC-SA 4.0 license and was authored, remixed, and/or curated by David Harvey.

- **2.10: Chapter Summary and Key Terms** by David Harvey is licensed CC BY-NC-SA 4.0.

CHAPTER OVERVIEW

3: THE VOCABULARY OF ANALYTICAL CHEMISTRY

If you browse through an issue of the journal *Analytical Chemistry*, you will discover that the authors and readers share a common vocabulary of analytical terms. You probably are familiar with some of these terms, such as accuracy and precision, but other terms, such as analyte and matrix, are perhaps less familiar to you. In order to participate in any community, one must first understand its vocabulary; the goal of this chapter, therefore, is to introduce some important analytical terms. Becoming comfortable with these terms will make the chapters that follow easier to read and to understand.

3.1: Analysis, Determination, and Measurement
3.2: Techniques, Methods, Procedures, and Protocols
3.3: Classifying Analytical Techniques
3.4: Selecting an Analytical Method
3.5: Developing the Procedure
3.6: Protocols
3.7: The Importance of Analytical Methodology
3.8: Problems
3.9: Additional Resources
3.10: Chapter Summary and Key Terms

This page titled 3: The Vocabulary of Analytical Chemistry is shared under a CC BY-NC-SA 4.0 license and was authored, remixed, and/or curated by David Harvey.

3.1: ANALYSIS, DETERMINATION, AND MEASUREMENT

The first important distinction we will make is among the terms analysis, determination, and measurement. An analysis provides chemical or physical information about a sample. The component in the sample of interest to us is called the ***analyte***, and the remainder of the sample is the matrix. In an analysis we determine the identity, the concentration, or the properties of an analyte. To make this determination we measure one or more of the analyte's chemical or physical properties.

An example will help clarify the difference between an ***analysis***, a ***determination*** and a ***measurement***. In 1974 the federal government enacted the Safe Drinking Water Act to ensure the safety of the nation's public drinking water supplies. To comply with this act, municipalities monitor their drinking water supply for potentially harmful substances, such as fecal coliform bacteria. Municipal water departments collect and analyze samples from their water supply. To determine the concentration of fecal coliform bacteria an analyst passes a portion of water through a membrane filter, places the filter in a dish that contains a nutrient broth, and incubates the sample for 22–24 hrs at 44.5 ºC ± 0.2 ºC. At the end of the incubation period the analyst counts the number of bacterial colonies in the dish and reports the result as the number of colonies per 100 mL (Figure 3.1.1). Thus, a municipal water department analyzes samples of water to determine the concentration of fecal coliform bacteria by measuring the number of bacterial colonies that form during a carefully defined incubation period

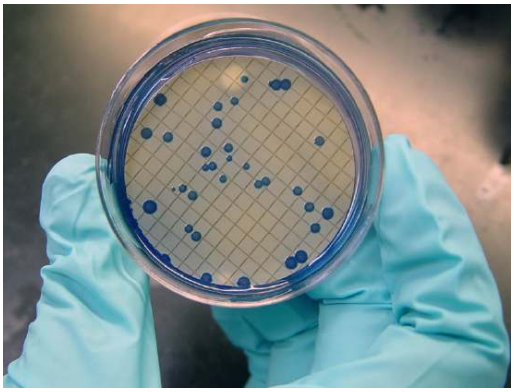


Figure 3.1.1 : Colonies of fecal coliform bacteria from a water supply. Source: Susan Boyer. Photo courtesy of ARS–USDA (www.ars.usda.gov).

A fecal coliform count provides a general measure of the presence of pathogenic organisms in a water supply. For drinking water, the current maximum contaminant level (MCL) for total coliforms, including fecal coliforms is less than 1 colony/100 mL. Municipal water departments must regularly test the water supply and must take action if more than 5% of the samples in any month test positive for coliform bacteria.

This page titled 3.1: Analysis, Determination, and Measurement is shared under a CC BY-NC-SA 4.0 license and was authored, remixed, and/or curated by David Harvey.

- **3.1: Analysis, Determination, and Measurement** by David Harvey is licensed CC BY-NC-SA 4.0.

3.2: TECHNIQUES, METHODS, PROCEDURES, AND PROTOCOLS

Suppose you are asked to develop an analytical method to determine the concentration of lead in drinking water. How would you approach this problem? To provide a structure for answering this question, it is helpful to consider four levels of analytical methodology: techniques, methods, procedures, and protocols [Taylor, J. K. *Anal. Chem.* **1983**, *55*, 600A–608A].

A ***technique*** is any chemical or physical principle that we can use to study an analyte. There are many techniques for that we can use to determine the concentration of lead in drinking water [Fitch, A.; Wang, Y.; Mellican, S.; Macha, S. *Anal. Chem.* **1996**, *68*, 727A–731A]. In graphite furnace atomic absorption spectroscopy (GFAAS), for example, we first convert aqueous lead ions into free atoms—a process we call atomization. We then measure the amount of light absorbed by the free atoms. Thus, GFAAS uses both a chemical principle (atomization) and a physical principle (absorption of light).

> See Chapter 10 for a discussion of graphite furnace atomic absorption spectroscopy.

A ***method*** is the application of a technique for a specific analyte in a specific matrix. As shown in Figure 3.2.1 , the GFAAS method for determining the concentration of lead in water is different from that for lead in soil or blood.

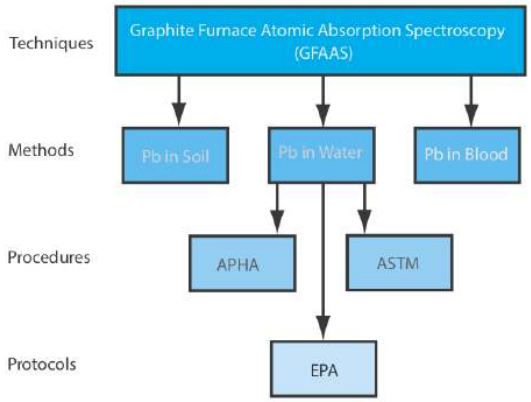


Figure 3.2.1 : Chart showing the hierarchical relationship between a technique, methods that use the technique, and procedures and protocols for a method. The abbreviations are APHA: American Public Health Association, ASTM: American Society for Testing Materials, EPA: Environmental Protection Agency.

A ***procedure*** is a set of written directions that tell us how to apply a method to a particular sample, including information on how to collect the sample, how to handle interferents, and how to validate results. A method may have several procedures as each analyst or agency adapts it to a specific need. As shown in Figure 3.2.1 , the American Public Health Agency and the American Society for Testing Materials publish separate procedures for determining the concentration of lead in water.

Finally, a ***protocol*** is a set of stringent guidelines that specify a procedure that an analyst must follow if an agency is to accept the results. Protocols are common when the result of an analysis supports or defines public policy. When determining the concentration of lead in water under the Safe Drinking Water Act, for example, the analyst must use a protocol specified by the Environmental Protection Agency.

There is an obvious order to these four levels of analytical methodology. Ideally, a protocol uses a previously validated procedure. Before developing and validating a procedure, a method of analysis must be selected. This requires, in turn, an initial screening of available techniques to determine those that have the potential for monitoring the analyte.

This page titled 3.2: Techniques, Methods, Procedures, and Protocols is shared under a CC BY-NC-SA 4.0 license and was authored, remixed, and/or curated by David Harvey.

- **3.2: Techniques, Methods, Procedures, and Protocols** by David Harvey is licensed CC BY-NC-SA 4.0.

3.3: CLASSIFYING ANALYTICAL TECHNIQUES

The analysis of a sample generates a chemical or physical signal that is proportional to the amount of analyte in the sample. This signal may be anything we can measure, such as volume or absorbance. It is convenient to divide analytical techniques into two general classes based on whether the signal is proportional to the mass or moles of analyte, or is proportional to the analyte's concentration

Consider the two graduated cylinders in Figure 3.3.1 , each of which contains a solution of 0.010 M $Cu(NO_3)_2$. Cylinder 1 contains 10 mL, or 1.0×10^{-4} moles of Cu^{2+}, and cylinder 2 contains 20 mL, or 2.0×10^{-4} moles of Cu^{2+}. If a technique responds to the absolute amount of analyte in the sample, then the signal due to the analyte S_A

$$S_A = k_A n_A \tag{3.3.1}$$

where n_A is the moles or grams of analyte in the sample, and k_A is a proportionality constant. Because cylinder 2 contains twice as many moles of Cu^{2+} as cylinder 1, analyzing the contents of cylinder 2 gives a signal twice as large as that for cylinder 1.



Figure 3.3.1 : Two graduated cylinders, each containing 0.10 M $Cu(NO_3)_2$. Although the cylinders contain the same concentration of Cu^{2+}, the cylinder on the left contains 1.0×10^{-4} mol Cu^{2+} and the cylinder on the right contains 2.0×10^{-4} mol Cu^{2+}.

A second class of analytical techniques are those that respond to the analyte's concentration, C_A

$$S_A = k_A C_A \tag{3.3.2}$$

Since the solutions in both cylinders have the same concentration of Cu^{2+}, their analysis yields identical signals.

A technique that responds to the absolute amount of analyte is a ***total analysis*** technique. Mass and volume are the most common signals for a total analysis technique, and the corresponding techniques are gravimetry (Chapter 8) and titrimetry (Chapter 9). With a few exceptions, the signal for a total analysis technique is the result of one or more chemical reactions, the stoichiometry of which determines the value of k_A in Equation 3.3.1 .

> Historically, most early analytical methods used a total analysis technique. For this reason, total analysis techniques are often called "classical" techniques.

Spectroscopy (Chapter 10) and electrochemistry (Chapter 11), in which an optical or an electrical signal is proportional to the relative amount of analyte in a sample, are examples of concentration techniques. The relationship between the signal and the analyte's concentration is a theoretical function that depends on experimental conditions and the instrumentation used to measure the signal. For this reason the value of k_A in Equation 3.3.2 is determined experimentally.

> Since most concentration techniques rely on measuring an optical or electrical signal, they also are known as "instrumental" techniques.

This page titled 3.3: Classifying Analytical Techniques is shared under a CC BY-NC-SA 4.0 license and was authored, remixed, and/or curated by David Harvey.

- **3.3: Classifying Analytical Techniques** by David Harvey is licensed CC BY-NC-SA 4.0.

3.4: SELECTING AN ANALYTICAL METHOD

A method is the application of a technique to a specific analyte in a specific matrix. We can develop an analytical method to determine the concentration of lead in drinking water using any of the techniques mentioned in the previous section. A gravimetric method, for example, might precipiate the lead as $PbSO_4$ or as $PbCrO_4$, and use the precipitate's mass as the analytical signal. Lead forms several soluble complexes, which we can use to design a complexation titrimetric method. As shown in Figure 3.2.1, we can use graphite furnace atomic absorption spectroscopy to determine the concentration of lead in drinking water. Finally, lead's multiple oxidation states (Pb^0, Pb^{2+}, Pb^{4+}) makes feasible a variety of electrochemical methods.

Ultimately, the requirements of the analysis determine the best method. In choosing among the available methods, we give consideration to some or all the following design criteria: accuracy, precision, sensitivity, selectivity, robustness, ruggedness, scale of operation, analysis time, availability of equipment, and cost.

ACCURACY

Accuracy is how closely the result of an experiment agrees with the "true" or expected result. We can express accuracy as an absolute error, e

$$e = \text{obtained result} - \text{expected result}$$

or as a percentage relative error, $\%e_r$

$$\%e_r = \frac{\text{obtained result} - \text{expected result}}{\text{expected result}} \times 100$$

A method's accuracy depends on many things, including the signal's source, the value of k_A in Equation 3.3.1 or Equation 3.3.2, and the ease of handling samples without loss or contamination. A total analysis technique, such as gravimetry and titrimetry, often produce more accurate results than does a concentration technique because we can measure mass and volume with high accuracy, and because the value of k_A is known exactly through stoichiometry.

> Because it is unlikely that we know the true result, we use an expected or accepted result to evaluate accuracy. For example, we might use a standard reference material, which has an accepted value, to establish an analytical method's accuracy. You will find a more detailed treatment of accuracy in Chapter 4, including a discussion of sources of errors.

PRECISION

When a sample is analyzed several times, the individual results vary from trial-to-trial. ***Precision*** is a measure of this variability. The closer the agreement between individual analyses, the more precise the results. For example, the results shown in the upper half of Figure 3.4.1 for the concentration of K^+ in a sample of serum are more precise than those in the lower half of Figure 3.4.1 . It is important to understand that precision does not imply accuracy. That the data in the upper half of Figure 3.4.1 are more precise does not mean that the first set of results is more accurate. In fact, neither set of results may be accurate.

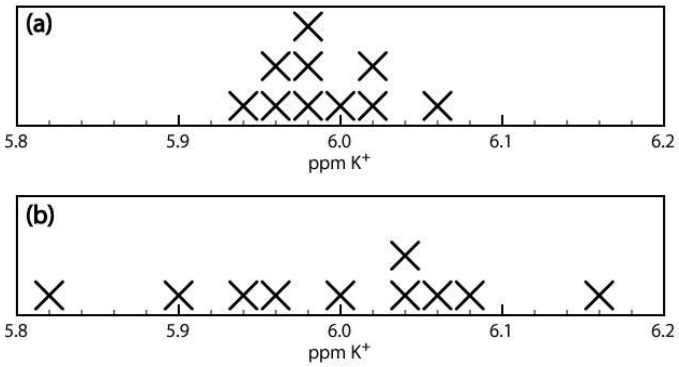


Figure 3.4.1 : Two determinations of the concentration of K^+ in serum, showing the effect of precision on the distribution of individual results. The data in (a) are less scattered and, therefore, more precise than the data in (b).

A method's precision depends on several factors, including the uncertainty in measuring the signal and the ease of handling samples reproducibly. In most cases we can measure the signal for a total analysis technique with a higher precision than is the case for a concentration method.

Confusing accuracy and precision is a common mistake. See Ryder, J.; Clark, A. *U. Chem. Ed.* **2002**, *6*, 1–3, and Tomlinson, J.; Dyson, P. J.; Garratt, J. *U. Chem. Ed.* **2001**, *5*, 16–23 for discussions of this and other common misconceptions about the meaning of error. You will find a more detailed treatment of precision in Chapter 4, including a discussion of sources of errors.

SENSITIVITY

The ability to demonstrate that two samples have different amounts of analyte is an essential part of many analyses. A method's ***sensitivity*** is a measure of its ability to establish that such a difference is significant. Sensitivity is often confused with a method's ***detection limit***, which is the smallest amount of analyte we can determine with confidence.

Confidence, as we will see in Chapter 4, is a statistical concept that builds on the idea of a population of results. For this reason, we will postpone our discussion of detection limits to Chapter 4. For now, the definition of a detection limit given here is sufficient.

Sensitivity is equivalent to the proportionality constant, k_A, in Equation 3.3.1 and Equation 3.3.2 [IUPAC Compendium of Chemical Terminology, Electronic version]. If ΔS_A is the smallest difference we can measure between two signals, then the smallest detectable difference in the absolute amount or the relative amount of analyte is

$$\Delta n_A = \frac{\Delta S_A}{k_A} \quad \text{or} \quad \Delta C_A = \frac{\Delta S_A}{k_A}$$

Suppose, for example, that our analytical signal is a measurement of mass using a balance whose smallest detectable increment is ±0.0001 g. If our method's sensitivity is 0.200, then our method can conceivably detect a difference in mass of as little as

$$\Delta n_A = \frac{\pm 0.0001 \text{ g}}{0.200} = \pm 0.0005 \text{ g}$$

For two methods with the same ΔS_A, the method with the greater sensitivity—that is, the method with the larger k_A—is better able to discriminate between smaller amounts of analyte.

SPECIFICITY AND SELECTIVITY

An analytical method is specific if its signal depends only on the analyte [Persson, B-A; Vessman, J. *Trends Anal. Chem.* **1998**, *17*, 117–119; Persson, B-A; Vessman, J. *Trends Anal. Chem.* **2001**, *20*, 526–532]. Although ***specificity*** is the ideal, few analytical methods are free from interferences. When an ***interferent*** contributes to the signal, we expand Equation 3.3.1 and Equation 3.3.2 to include its contribution to the sample's signal, S_{samp}

$$S_{samp} = S_A + S_I = k_A n_A + k_I n_I \tag{3.4.1}$$

$$S_{samp} = S_A + S_I = k_A C_A + k_I C_I \tag{3.4.2}$$

where S_I is the interferent's contribution to the signal, k_I is the interferent's sensitivity, and n_I and C_I are the moles (or grams) and the concentration of interferent in the sample, respectively.

Selectivity is a measure of a method's freedom from interferences [Valcárcel, M.; Gomez-Hens, A.; Rubio, S. *Trends Anal. Chem.* **2001**, *20*, 386–393]. A method's selectivity for an interferent relative to the analyte is defined by a ***selectivity coefficient***, $K_{A,I}$

$$K_{A,I} = \frac{k_I}{k_A} \tag{3.4.3}$$

which may be positive or negative depending on the signs of k_I and k_A. The selectivity coefficient is greater than +1 or less than –1 when the method is more selective for the interferent than for the analyte.

Although k_A and k_I usually are positive, they can be negative. For example, some analytical methods work by measuring the concentration of a species that remains after is reacts with the analyte. As the analyte's concentration increases, the concentration of the species that produces the signal decreases, and the signal becomes smaller. If the signal in the absence of analyte is assigned a value of zero, then the subsequent signals are negative.

Determining the selectivity coefficient's value is easy if we already know the values for k_A and k_I. As shown by Example 3.4.1 , we also can determine $K_{A,I}$ by measuring S_{samp} in the presence of and in the absence of the interferent.

✔ EXAMPLE 3.4.1

A method for the analysis of Ca^{2+} in water suffers from an interference in the presence of Zn^{2+}. When the concentration of Ca^{2+} is 100 times greater than that of Zn^{2+}, an analysis for Ca^{2+} has a relative error of +0.5%. What is the selectivity coefficient for this method?

Solution

Since only relative concentrations are reported, we can arbitrarily assign absolute concentrations. To make the calculations easy, we will let C_{Ca} = 100 (arbitrary units) and C_{Zn} = 1. A relative error of +0.5% means the signal in the presence of Zn^{2+} is 0.5% greater than the signal in the absence of Zn^{2+}. Again, we can assign values to make the calculation easier. If the signal for Cu^{2+} in the absence of Zn^{2+} is 100 (arbitrary units), then the signal in the presence of Zn^{2+} is 100.5.

The value of k_{Ca} is determined using Equation 3.3.2

$$k_{Ca} = \frac{S_{Ca}}{C_{Ca}} = \frac{100}{100} = 1$$

In the presence of Zn^{2+} the signal is given by Equation 3.4.2; thus

$$S_{samp} = 100.5 = k_{Ca}C_{Ca} + k_{Zn}C_{Zn} = (1 \times 100) + k_{Zn} \times 1$$

Solving for k_{Zn} gives its value as 0.5. The selectivity coefficient is

$$K_{Ca,Zn} = \frac{k_{Zn}}{k_{Ca}} = \frac{0.5}{1} = 0.5$$

If you are unsure why, in the above example, the signal in the presence of zinc is 100.5, note that the percentage relative error for this problem is given by

$$\frac{\text{obtained result} - 100}{100} \times 100 = +0.5\%$$

Solving gives an obtained result of 100.5.

? EXERCISE 3.4.1

Wang and colleagues describe a fluorescence method for the analysis of Ag^+ in water. When analyzing a solution that contains 1.0×10^{-9} M Ag^+ and 1.1×10^{-7} M Ni^{2+}, the fluorescence intensity (the signal) was +4.9% greater than that obtained for a sample of 1.0×10^{-9} M Ag^+. What is $K_{Ag,Ni}$ for this analytical method? The full citation for the data in this exercise is Wang, L.; Liang, A. N.; Chen, H.; Liu, Y.; Qian, B.; Fu, J. *Anal. Chim. Acta* **2008**, *616*, 170-176.

Answer

Because the signal for Ag^+ in the presence of Ni^{2+} is reported as a relative error, we will assign a value of 100 as the signal for 1×10^{-9} M Ag^+. With a relative error of +4.9%, the signal for the solution of 1×10^{-9} M Ag^+ and 1.1×10^{-7} M Ni^{2+} is 104.9. The sensitivity for Ag^+ is determined using the solution that does not contain Ni^{2+}; thus

$$k_{Ag} = \frac{S_{Ag}}{C_{Ag}} = \frac{100}{1 \times 10^{-9}\ \text{M}} = 1.0 \times 10^{11}\ \text{M}^{-1}$$

Substituting into Equation 3.4.2 values for k_{Ag}, S_{samp} , and the concentrations of Ag^+ and Ni^{2+}

$$104.9 = (1.0 \times 10^{11}\ \text{M}^{-1}) \times (1 \times 10^{-9}\ \text{M}) + k_{Ni} \times (1.1 \times 10^{-7}\ \text{M})$$

and solving gives k_{Ni} as 4.5×10^{7} M^{-1}. The selectivity coefficient is

$$K_{Ag,Ni} = \frac{k_{Ni}}{k_{Ag}} = \frac{4.5 \times 10^{7}\ \text{M}^{-1}}{1.0 \times 10^{11}\ \text{M}^{-1}} = 4.5 \times 10^{-4}$$

A selectivity coefficient provides us with a useful way to evaluate an interferent's potential effect on an analysis. Solving Equation 3.4.3 for k_I

$$k_I = K_{A,I} \times k_A \tag{3.4.4}$$

and substituting in Equation 3.4.1 and Equation 3.4.2, and simplifying gives

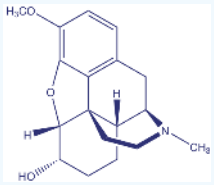
$$S_{samp} = k_A\{n_A + K_{A,I} \times n_I\} \tag{3.4.5}$$

$$S_{samp} = k_A\{C_A + K_{A,I} \times C_I\} \tag{3.4.6}$$

An interferent will not pose a problem as long as the term $K_{A,I} \times n_I$ in Equation 3.4.5 is significantly smaller than n_A, or if $K_{A,I} \times C_I$ in Equation 3.4.6 is significantly smaller than C_A.

EXAMPLE 3.4.2

Barnett and colleagues developed a method to determine the concentration of codeine (structure shown below) in poppy plants [Barnett, N. W.; Bowser, T. A.; Geraldi, R. D.; Smith, B. *Anal. Chim. Acta* **1996**, *318*, 309– 317]. As part of their study they evaluated the effect of several interferents. For example, the authors found that equimolar solutions of codeine and the interferent 6-methoxycodeine gave signals, respectively of 40 and 6 (arbitrary units).



(a) What is the selectivity coefficient for the interferent, 6-methoxycodeine, relative to that for the analyte, codeine.

(b) If we need to know the concentration of codeine with an accuracy of ±0.50%, what is the maximum relative concentration of 6-methoxy-codeine that we can tolerate?

Solution

(a) The signals due to the analyte, S_A, and the interferent, S_I, are

$$S_A = k_A C_A \qquad S_I = k_I C_I$$

Solving these equations for k_A and for k_I, and substituting into Equation 3.4.4 gives

$$K_{A,I} = \frac{S_I/C_I}{S_A/C_I}$$

Because the concentrations of analyte and interferent are equimolar ($C_A = C_I$), the selectivity coefficient is

$$K_{A,I} = \frac{S_I}{S_A} = \frac{6}{40} = 0.15$$

(b) To achieve an accuracy of better than ±0.50% the term $K_{A,I} \times C_I$ in Equation 3.4.6 must be less than 0.50% of C_A; thus

$$K_{A,I} \times C_I \leq 0.0050 \times C_A$$

Solving this inequality for the ratio C_I/C_A and substituting in the value for $K_{A,I}$ from part (a) gives

$$\frac{C_I}{C_A} \leq \frac{0.0050}{K_{A,I}} = \frac{0.0050}{0.15} = 0.033$$

Therefore, the concentration of 6-methoxycodeine must be less than 3.3% of codeine's concentration.

When a method's signal is the result of a chemical reaction—for example, when the signal is the mass of a precipitate—there is a good chance that the method is not very selective and that it is susceptible to an interference.

EXERCISE 3.4.2

Mercury (II) also is an interferent in the fluorescence method for Ag^+ developed by Wang and colleagues (see Practice Exercise 3.4.1). The selectivity coefficient, $K_{Ag,Hg}$ has a value of -1.0×10^{-3}.

(a) What is the significance of the selectivity coefficient's negative sign?

(b) Suppose you plan to use this method to analyze solutions with concentrations of Ag^+ no smaller than 1.0 nM. What is the maximum concentration of Hg^{2+} you can tolerate if your percentage relative errors must be less than ±1.0%?

Answer

(a) A negative value for $K_{Ag,Hg}$ means that the presence of Hg^{2+} decreases the signal from Ag^+.

(b) In this case we need to consider an error of –1%, since the effect of Hg^{2+} is to decrease the signal from Ag^{+}. To achieve this error, the term $K_{A,I} \times C_I$ in Equation 3.4.6 must be less than –1% of C_A; thus

$$K_{\text{Ag,Hg}} \times C_{\text{Hg}} = -0.01 \times C_{\text{Ag}}$$

Substituting in known values for $K_{\text{Ag,Hg}}$ and C_{Ag}, we find that the maximum concentration of Hg^{2+} is 1.0×10^{-8} M.

Problems with selectivity also are more likely when the analyte is present at a very low concentration [Rodgers, L. B. *J. Chem. Educ.* **1986**, *63*, 3–6].

Look back at Figure 1.1.1, which shows Fresenius' analytical method for the determination of nickel in ores. The reason there are so many steps in this procedure is that precipitation reactions generally are not very selective. The method in Figure 1.1.2 includes fewer steps because dimethylglyoxime is a more selective reagent. Even so, if an ore contains palladium, additional steps are needed to prevent the palladium from interfering.

ROBUSTNESS AND RUGGEDNESS

For a method to be useful it must provide reliable results. Unfortunately, methods are subject to a variety of chemical and physical interferences that contribute uncertainty to the analysis. If a method is relatively free from chemical interferences, we can use it to analyze an analyte in a wide variety of sample matrices. Such methods are considered ***robust***.

Random variations in experimental conditions introduces uncertainty. If a method's sensitivity, *k*, is too dependent on experimental conditions, such as temperature, acidity, or reaction time, then a slight change in any of these conditions may give a significantly different result. A ***rugged*** method is relatively insensitive to changes in experimental conditions.

SCALE OF OPERATION

Another way to narrow the choice of methods is to consider three potential limitations: the amount of sample available for the analysis, the expected concentration of analyte in the samples, and the minimum amount of analyte that will produce a measurable signal. Collectively, these limitations define the analytical method's scale of operations.

We can display the scale of operations visually (Figure 3.4.2) by plotting the sample's size on the *x*-axis and the analyte's concentration on the *y*-axis. For convenience, we divide samples into macro (>0.1 g), meso (10 mg–100 mg), micro (0.1 mg–10 mg), and ultramicro (<0.1 mg) sizes, and we divide analytes into major (>1% w/w), minor (0.01% w/w–1% w/w), trace (10^{-7}% w/w–0.01% w/w), and ultratrace (<10^{-7}% w/w) components. Together, the analyte's concentration and the sample's size provide a characteristic description for an analysis. For example, in a microtrace analysis the sample weighs between 0.1 mg and 10 mg and contains a concentration of analyte between 10^{-7}% w/w and 10^{-2}% w/w.

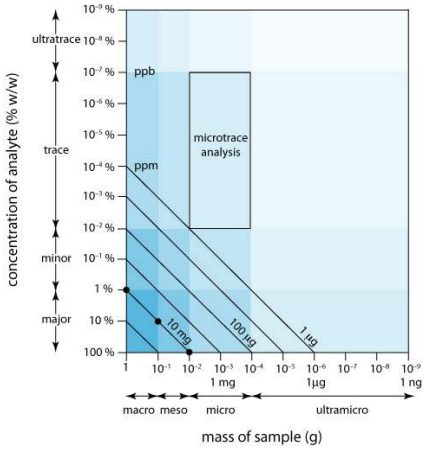


Figure 3.4.2 : Scale of operations for analytical methods. The shaded areas define different types of analyses. The boxed area, for example, represents a microtrace analysis. The diagonal lines show combinations of sample size and analyte concentration that contain the same mass of analyte. The three filled circles (•), for example, indicate analyses that use 10 mg of analyte. See Sandell, E. B.; Elving, P. J. in Kolthoff, I. M.; Elving, P. J., eds. *Treatise on Analytical Chem-istry*, Interscience: New York, Part I, Vol. 1, Chapter 1, pp. 3–6; (b) Potts, L. W. *Quantitative Analysis–Theory and Practice*, Harper and Row: New York, 1987, pp. 12 for more details.

The diagonal lines connecting the axes show combinations of sample size and analyte concentration that contain the same absolute mass of analyte. As shown in Figure 3.4.2 , for example, a 1-g sample that is 1% w/w analyte has the same amount of analyte (10 mg) as a 100-mg sample that is 10% w/w analyte, or a 10-mg sample that is 100% w/w analyte.

We can use Figure 3.4.2 to establish limits for analytical methods. If a method's minimum detectable signal is equivalent to 10 mg of analyte, then it is best suited to a major analyte in a macro or meso sample. Extending the method to an analyte with a concentration of 0.1% w/w requires a sample of 10 g, which rarely is practical due to the complications of carrying such a large amount of material through the analysis. On the other hand, a small sample that contains a trace amount of analyte places significant restrictions on an analysis. For example, a 1-mg sample that is 10^{-4}% w/w in analyte contains just 1 ng of analyte. If we isolate the analyte in 1 mL of solution, then we need an analytical method that reliably can detect it at a concentration of 1 ng/mL.

> It should not surprise you to learn that a total analysis technique typically requires a macro or a meso sample that contains a major analyte. A concentration technique is particularly useful for a minor, trace, or ultratrace analyte in a macro, meso, or micro sample.

EQUIPMENT, TIME, AND COST

Finally, we can compare analytical methods with respect to their equipment needs, the time needed to complete an analysis, and the cost per sample. Methods that rely on instrumentation are equipment-intensive and may require significant operator training. For example, the graphite furnace atomic absorption spectroscopic method for determining lead in water requires a significant capital investment in the instrument and an experienced operator to obtain reliable results. Other methods, such as titrimetry, require less expensive equipment and less training.

The time to complete an analysis for one sample often is fairly similar from method-to-method. This is somewhat misleading, however, because much of this time is spent preparing samples, preparing reagents, and gathering together equipment. Once the samples, reagents, and equipment are in place, the sampling rate may differ substantially. For example, it takes just a few minutes to analyze a single sample for lead using graphite furnace atomic absorption spectroscopy, but several hours to analyze the same sample using gravimetry. This is a significant factor in selecting a method for a laboratory that handles a high volume of samples.

The cost of an analysis depends on many factors, including the cost of equipment and reagents, the cost of hiring analysts, and the number of samples that can be processed per hour. In general, methods that rely on instruments cost more per sample then other methods.

MAKING THE FINAL CHOICE

Unfortunately, the design criteria discussed in this section are not mutually independent [Valcárcel, M.; Ríos, A. *Anal. Chem.* **1993**, *65*, 781A–787A]. Working with smaller samples or improving selectivity often comes at the expense of precision. Minimizing cost and analysis time may decrease accuracy. Selecting a method requires carefully balancing the various design criteria. Usually, the most important design criterion is accuracy, and the best method is the one that gives the most accurate result. When the need for a result is urgent, as is often the case in clinical labs, analysis time may become the critical factor.

In some cases it is the sample's properties that determine the best method. A sample with a complex matrix, for example, may require a method with excellent selectivity to avoid interferences. Samples in which the analyte is present at a trace or ultratrace concentration usually require a concentration method. If the quantity of sample is limited, then the method must not require a large amount of sample.

Determining the concentration of lead in drinking water requires a method that can detect lead at the parts per billion concentration level. Selectivity is important because other metal ions are present at significantly higher concentrations. A method that uses graphite furnace atomic absorption spectroscopy is a common choice for determining lead in drinking water because it meets these specifications. The same method is also useful for determining lead in blood where its ability to detect low concentrations of lead using a few microliters of sample is an important consideration.

This page titled 3.4: Selecting an Analytical Method is shared under a CC BY-NC-SA 4.0 license and was authored, remixed, and/or curated by David Harvey.

- **3.4: Selecting an Analytical Method** by David Harvey is licensed CC BY-NC-SA 4.0.

3.5: DEVELOPING THE PROCEDURE

After selecting a method, the next step is to develop a procedure that accomplish our goals for the analysis. In developing a procedure we give attention to compensating for interferences, to selecting and calibrating equipment, to acquiring a representative sample, and to validating the method.

COMPENSATING FOR INTERFERENCES

A method's accuracy depends on its selectivity for the analyte. Even the best method, however, may not be free from interferents that contribute to the measured signal. Potential interferents may be present in the sample itself or in the reagents used during the analysis.

When the sample is free of interferents, the total signal, S_{total}, is a sum of the signal due to the analyte, S_A, and the signal due to interferents in the reagents, S_{reag},

$$S_{total} = S_A + S_{reag} = k_A n_A + S_{reag} \tag{3.5.1}$$

$$S_{total} = S_A + S_{reag} = k_A C_A + S_{reag} \tag{3.5.2}$$

Without an independent determination of S_{reag} we cannot solve Equation 3.5.1 or 3.5.2 for the moles or concentration of analyte.

To determine the contribution of S_{reag} in Equations 3.5.1 and 3.5.2 we measure the signal for a ***method blank***, a solution that does not contain the sample. Consider, for example, a procedure in which we dissolve a 0.1-g sample in a portion of solvent, add several reagents, and dilute to 100 mL with additional solvent. To prepare the method blank we omit the sample and dilute the reagents to 100 mL using the solvent. Because the analyte is absent, S_{total} for the method blank is equal to S_{reag}. Knowing the value for S_{reag} makes it is easy to correct S_{total} for the reagent's contribution to the total signal; thus

$$(S_{total} - S_{reag}) = S_A = k_A n_A$$

$$(S_{total} - S_{reag}) = S_A = k_A C_A$$

By itself, a method blank cannot compensate for an interferent that is part of the sample's matrix. If we happen to know the interferent's identity and concentration, then we can be add it to the method blank; however, this is not a common circumstance and we must, instead, find a method for separating the analyte and interferent before continuing the analysis.

> A method blank also is known as a reagent blank. When the sample is a liquid, or is in solution, we use an equivalent volume of an inert solvent as a substitute for the sample.

CALIBRATION

A simple definition of a quantitative analytical method is that it is a mechanism for converting a measurement, the signal, into the amount of analyte in a sample. Assuming we can correct for interferents, a quantitative analysis is nothing more than solving Equation 3.3.1 or Equation 3.3.2 for n_A or for C_A.

To solve these equations we need the value of k_A. For a total analysis method usually we know the value of k_A because it is defined by the stoichiometry of the chemical reactions responsible for the signal. For a concentration method, however, the value of k_A usually is a complex function of experimental conditions. A ***calibration*** is the process of experimentally determining the value of k_A by measuring the signal for one or more standard samples, each of which contains a known concentration of analyte.

With a single standard we can calculate the value of k_A using Equation 3.3.1 or Equation 3.3.2. When using several standards with different concentrations of analyte, the result is best viewed visually by plotting S_A versus the concentration of analyte in the standards. Such a plot is known as a ***calibration curve***, an example of which is shown in Figure 3.5.1 .

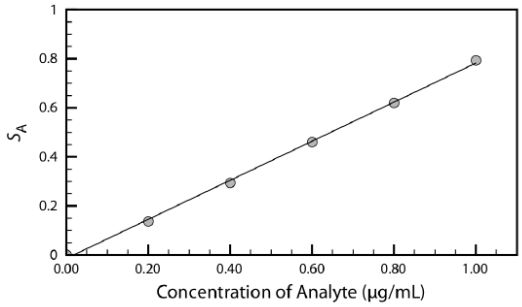


Figure 3.5.1 : Example of a calibration curve. The filled circles (•) are the results for five standard samples, each with a different concentration of analyte, and the line is the best fit to the data determined by a linear regression analysis. See Chapter 5 for a further discussion of calibration curves and an explanation of linear regression.

SAMPLING

Selecting an appropriate method and executing it properly helps us ensure that our analysis is accurate. If we analyze the wrong sample, however, then the accuracy of our work is of little consequence.

A proper sampling strategy ensures that our samples are representative of the material from which they are taken. Biased or nonrepresentative sampling, and contaminating samples during or after their collection are two examples of sampling errors that can lead to a significant error in accuracy. It is important to realize that sampling errors are independent of errors in the analytical method. As a result, we cannot correct a sampling error in the laboratory by, for example, evaluating a reagent blank.

> Chapter 7 provides a more detailed discussion of sampling, including strategies for obtaining representative samples.

VALIDATION

If we are to have confidence in our procedure we must demonstrate that it can provide acceptable results, a process we call ***validation***. Perhaps the most important part of validating a procedure is establishing that its precision and accuracy are appropriate for the problem we are trying to solve. We also ensure that the written procedure has sufficient detail so that different analysts or laboratories will obtain comparable results. Ideally, validation uses a standard sample whose composition closely matches the samples we will analyze. In the absence of appropriate standards, we can evaluate accuracy by comparing results to those obtained using a method of known accuracy.

> You will find more details about validating analytical methods in Chapter 14.

This page titled 3.5: Developing the Procedure is shared under a CC BY-NC-SA 4.0 license and was authored, remixed, and/or curated by David Harvey.

- **3.5: Developing the Procedure** by David Harvey is licensed CC BY-NC-SA 4.0.

3.6: PROTOCOLS

Earlier we defined a protocol as a set of stringent written guidelines that specify an exact procedure that we must follow if an agency is to accept the results of our analysis. In addition to the considerations that went into the procedure's design, a protocol also contains explicit instructions regarding internal and external quality assurance and quality control (***QA/QC***) procedures [Amore, F. *Anal. Chem.* **1979**, *51*, 1105A–1110A; Taylor, J. K. *Anal. Chem.* **1981**, *53*, 1588A–1593A]. The goal of internal QA/QC is to ensure that a laboratory's work is both accurate and precise. External QA/QC is a process in which an external agency certifies a laboratory.

As an example, let's outline a portion of the Environmental Protection Agency's protocol for determining trace metals in water by graphite furnace atomic absorption spectroscopy as part of its Contract Laboratory Program (CLP). The CLP protocol (see Figure 3.6.1) calls for an initial calibration using a method blank and three standards, one of which is at the detection limit. The resulting calibration curve is verified by analyzing initial calibration verification (ICV) and initial calibration blank (ICB) samples. The lab's result for the ICV sample must fall within ±10% of its expected concentration. If the result is outside this limit the analysis is stopped and the problem identified and corrected before continuing.

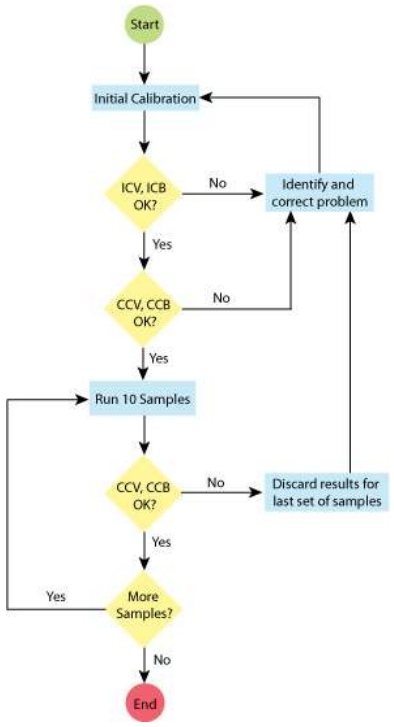


Figure 3.6.1 : Schematic diagram showing a portion of the EPA's protocol for determining trace metals in water using graphite furnace atomic absorption spectrometry. The abbreviations are ICV: initial calibration verification; ICB: initial calibration blank; CCV: continuing calibration verification; CCB: continuing calibration blank.

After a successful analysis of the ICV and ICB samples, the lab reverifies the calibration by analyzing a continuing calibration verification (CCV) sample and a continuing calibration blank (CCB). Results for the CCV also must be within ±10% of its expected concentration. Again, if the lab's result for the CCV is outside the established limits, the analysis is stopped, the problem identified and corrected, and the system recalibrated as described above. Additional CCV and the CCB samples are analyzed before the first sample and after the last sample, and between every set of ten samples. If the result for any CCV or CCB sample is unacceptable, the results for the last set of samples are discarded, the system is recalibrated, and the samples reanalyzed. By following this protocol, each result is bound by successful checks on the calibration. Although not shown in Figure 3.6.1 , the protocol also contains instructions for analyzing duplicate or split samples, and for using spike tests to verify accuracy.

This page titled 3.6: Protocols is shared under a CC BY-NC-SA 4.0 license and was authored, remixed, and/or curated by David Harvey.

- **3.6: Protocols** by David Harvey is licensed CC BY-NC-SA 4.0.

3.7: THE IMPORTANCE OF ANALYTICAL METHODOLOGY

The importance of the issues raised in this chapter is evident if we examine environmental monitoring programs. The purpose of a monitoring program is to determine the present status of an environmental system, and to assess long term trends in the system's health. These are broad and poorly defined goals. In many cases, an environmental monitoring program begins before the essential questions are known. This is not surprising since it is difficult to formulate questions in the absence of results. Without careful planning, however, a poor experimental design may result in data that has little value.

These concerns are illustrated by the Chesapeake Bay Monitoring Program. This research program, designed to study nutrients and toxic pollutants in the Chesapeake Bay, was initiated in 1984 as a cooperative venture between the federal government, the state governments of Maryland, Virginia, and Pennsylvania, and the District of Columbia. A 1989 review of the program highlights the problems common to many monitoring programs [D'Elia, C. F.; Sanders, J. G.; Capone, D. G. *Envrion. Sci. Technol.* **1989**, *23*, 768–774].

At the beginning of the Chesapeake Bay monitoring program, little attention was given to selecting analytical methods, in large part because the eventual use of the data was not yet specified. The analytical methods initially chosen were standard methods already approved by the Environmental Protection Agency (EPA). In many cases these methods were not useful because they were designed to detect pollutants at their legally mandated maximum allowed concentrations. In unpolluted waters, however, the concentrations of these contaminants often are well below the detection limit of the EPA methods. For example, the detection limit for the EPA approved standard method for phosphate was 7.5 ppb. Since the actual phosphate concentrations in Chesapeake Bay were below the EPA method's detection limit, it provided no useful information. On the other hand, the detection limit for a non-approved variant of the EPA method, a method routinely used by chemical oceanographers, was 0.06 ppb, a more realistic detection limit for their samples. In other cases, such as the elemental analysis for particulate forms of carbon, nitrogen and phosphorous, EPA approved procedures provided poorer reproducibility than nonapproved methods.

This page titled 3.7: The Importance of Analytical Methodology is shared under a CC BY-NC-SA 4.0 license and was authored, remixed, and/or curated by David Harvey.

- **3.7: The Importance of Analytical Methodology** by David Harvey is licensed CC BY-NC-SA 4.0.

3.8: PROBLEMS

1. When working with a solid sample, often it is necessary to bring the analyte into solution by digesting the sample with a suitable solvent. Any remaining solid impurities are removed by filtration before continuing with the analysis. In a typical total analysis method, the procedure might read

   "After digesting the sample in a beaker using approximately 25 mL of solvent, remove any solid impurities that remain by passing the solution the analyte through filter paper, collecting the filtrate in a clean Erlenmeyer flask. Rinse the beaker with several small portions of solvent, passing these rinsings through the filter paper and collecting them in the same Erlenmeyer flask. Finally, rinse the filter paper with several portions of solvent, collecting the rinsings in the same Erlenmeyer flask."

   For a typical concentration method, however, the procedure might state

   "After digesting the sample in a beaker using 25.00 mL of solvent, remove any solid impurities by filtering a portion of the solution containing the analyte. Collect and discard the first several mL of filtrate before collecting a sample of 5.00 mL for further analysis."

   Explain why these two procedures are different.
2. A certain concentration method works best when the analyte's concentration is approximately 10 ppb.

   (a) If the method requires a sample of 0.5 mL, about what mass of analyte is being measured?

   (b) If the analyte is present at 10% w/v, how would you prepare the sample for analysis?

   (c) Repeat for the case where the analyte is present at 10% w/w.

   (d) Based on your answers to parts (a)–(c), comment on the method's suitability for the determination of a major analyte.
3. An analyst needs to evaluate the potential effect of an interferent, *I*, on the quantitative analysis for an analyte, *A*. She begins by measuring the signal for a sample in which the interferent is absent and the analyte is present with a concentration of 15 ppm, obtaining an average signal of 23.3 (arbitrary units). When she analyzes a sample in which the analyte is absent and the interferent is present with a concentration of 25 ppm, she obtains an average signal of 13.7.

   (a) What is the sensitivity for the analyte?

   (b) What is the sensitivity for the interferent?

   (c) What is the value of the selectivity coefficient?

   (d) Is the method more selective for the analyte or the interferent?

   (e) What is the maximum concentration of interferent relative to that of the analyte if the error in the analysis is to be less than 1%?
4. A sample is analyzed to determine the concentration of an analyte. Under the conditions of the analysis the sensitivity is $17.2\ \text{ppm}^{-1}$. What is the analyte's concentration if S_{total} is 35.2 and S_{reag} is 0.6?
5. A method for the analysis of Ca^{2+} in water suffers from an interference in the presence of Zn^{2+}. When the concentration of Ca^{2+} is 50 times greater than that of Zn^{2+}, an analysis for Ca^{2+} gives a relative error of –2.0%. What is the value of the selectivity coefficient for this method?
6. The quantitative analysis for reduced glutathione in blood is complicated by many potential interferents. In one study, when analyzing a solution of 10.0 ppb glutathione and 1.5 ppb ascorbic acid, the signal was 5.43 times greater than that obtained for the analysis of 10.0 ppb glutathione [Jiménez-Prieto, R.; Velasco, A.; Silva, M; Pérez-Bendito, D. *Anal. Chem. Acta* **1992**, *269*, 273– 279]. What is the selectivity coefficient for this analysis? The same study found that analyzing a solution of 3.5×10^2 ppb methionine and 10.0 ppb glutathione gives a signal that is 0.906 times less than that obtained for the analysis of 10.0 ppb glutathione. What is the selectivity coefficient for this analysis? In what ways do these interferents behave differently?
7. Oungpipat and Alexander described a method for determining the concentration of glycolic acid (GA) in a variety of samples, including physiological fluids such as urine [Oungpipat, W.; Alexander, P. W. *Anal. Chim. Acta* **1994**, *295*, 36–46]. In the presence of only GA, the signal is

$$S_{samp,1} = k_{\text{GA}} C_{\text{GA}}$$

and in the presence of both glycolic acid and ascorbic acid (AA), the signal is

$$S_{samp,2} = k_{\text{GA}} C_{\text{GA}} + k_{\text{AA}} C_{\text{AA}}$$

When the concentration of glycolic acid is $1.0 \times 10^{-4}\ \text{M}$ and the concentration of ascorbic acid is $1.0 \times 10^{-5}\ \text{M}$, the ratio of their signals is

$$\frac{S_{samp,2}}{S_{samp,1}} = 1.44$$

(a) Using the ratio of the two signals, determine the value of the selectivity ratio $K_{\text{GA,AA}}$.

(b) Is the method more selective toward glycolic acid or ascorbic acid?

(c) If the concentration of ascorbic acid is $1.0 \times 10^{-5}\ \text{M}$, what is the smallest concentration of glycolic acid that can be determined such that the error introduced by failing to account for the signal from ascorbic acid is less than 1%?

8. Ibrahim and co-workers developed a new method for the quantitative analysis of hypoxanthine, a natural compound of some nucleic acids [Ibrahim, M. S.; Ahmad, M. E.; Temerk, Y. M.; Kaucke, A. M. *Anal. Chim. Acta* **1996**, *328*, 47–52]. As part of their study they evaluated the method's selectivity for hypoxanthine in the presence of several possible interferents, including ascorbic acid.

(a) When analyzing a solution of $1.12 \times 10^{-6}\ \text{M}$ hypoxanthine the authors obtained a signal of $7.45 \times 10^{-5}\ \text{amps}$. What is the sensitivity for hypoxanthine? You may assume the signal has been corrected for the method blank.

(b) When a solution containing $1.12 \times 10^{-6}\ \text{M}$ hypoxanthine and $6.5 \times 10^{-5}\ \text{M}$ ascorbic acid is analyzed a signal of $4.04 \times 10^{-5}\ \text{amps}$ is obtained. What is the selectivity coefficient for this method?

(c) Is the method more selective for hypoxanthine or for ascorbic acid?

(d) What is the largest concentration of ascorbic acid that may be present if a concentration of $1.12 \times 10^{-6}\ \text{M}$ hypoxanthine is to be determined within 1.0%?

9. Examine a procedure from *Standard Methods for the Analysis of Waters and Wastewaters* (or another manual of standard analytical methods) and identify the steps taken to compensate for interferences, to calibrate equipment and instruments, to standardize the method, and to acquire a representative sample.

This page titled 3.8: Problems is shared under a CC BY-NC-SA 4.0 license and was authored, remixed, and/or curated by David Harvey.

- **3.8: Problems** by David Harvey is licensed CC BY-NC-SA 4.0.

3.9: ADDITIONAL RESOURCES

The International Union of Pure and Applied Chemistry (IUPAC) maintains a web-based compendium of analytical terminology. You can find it at the following web site.

- old.iupac.org/publications/an...al_compendium/

The following papers provide alternative schemes for classifying analytical methods.

- Booksh, K. S.; Kowalski, B. R. "Theory of Analytical Chemistry," *Anal. Chem.* **1994**, *66*, 782A– 791A.
- Phillips, J. B. "Classification of Analytical Methods," *Anal. Chem.* **1981**, *53*, 1463A–1470A.
- Valcárcel, M.; Luque de Castro, M. D. "A Hierarchical Approach to Analytical Chemistry," *Trends Anal. Chem.* **1995**, *14*, 242–250.
- Valcárcel, M.; Simonet, B. M. "Types of Analytical Information and Their Mutual Relationships," *Trends Anal. Chem.* **1995**, *14*, 490–495.

Further details on criteria for evaluating analytical methods are found in the following series of papers.

- Wilson, A. L. "The Performance-Characteristics of Analytical Methods", Part I-*Talanta*, **1970**, *17*, 21–29; Part II-*Talanta*, **1970**, *17*, 31–44; Part III-*Talanta*, **1973**, *20*, 725–732; Part IV-*Talanta*, **1974**, *21*, 1109–1121.

For a point/counterpoint debate on the meaning of sensitivity consult the following two papers and two letters of response.

- Ekins, R.; Edwards, P. "On the Meaning of 'Sensitivity'," *Clin. Chem.* **1997**, *43*, 1824–1831.
- Ekins, R.; Edwards, P. "On the Meaning of 'Sensitivity:' A Rejoinder," *Clin. Chem.* **1998**, *44*, 1773–1776.
- Pardue, H. L. "The Inseparable Triangle: Analytical Sensitivity, Measurement Uncertainty, and Quantitative Resolution," *Clin. Chem.* **1997**, *43*, 1831–1837.
- Pardue, H. L. "Reply to 'On the Meaning of 'Sensitivity:' A Rejoinder'," *Clin. Chem.* **1998**, *44*, 1776–1778.

Several texts provide analytical procedures for specific analytes in well-defined matrices.

- Basset, J.; Denney, R. C.; Jeffery, G. H.; Mendham, J. *Vogel's Textbook of Quantitative Inorganic Analysis*, 4th Edition; Longman: London, 1981.
- Csuros, M. *Environmental Sampling and Analysis for Technicians*, Lewis: Boca Raton, 1994.
- Keith, L. H. (ed) *Compilation of EPA's Sampling and Analysis Methods*, Lewis: Boca Raton, 1996
- Rump, H. H.; Krist, H. *Laboratory Methods for the Examination of Water, Wastewater and Soil*, VCH Publishers: NY, 1988.
- *Standard Methods for the Analysis of Waters and Wastewaters*, 21st Edition, American Public Health Association: Washington, D. C.; 2005.

For a review of the importance of analytical methodology in today's regulatory environment, consult the following text.

- Miller, J. M.; Crowther, J. B. (eds) *Analytical Chemistry in a GMP Environment*, John Wiley & Sons: New York, 2000.

This page titled 3.9: Additional Resources is shared under a CC BY-NC-SA 4.0 license and was authored, remixed, and/or curated by David Harvey.

- **3.9: Additional Resources** by David Harvey is licensed CC BY-NC-SA 4.0.

3.10: CHAPTER SUMMARY AND KEY TERMS

CHAPTER SUMMARY

Every discipline has its own vocabulary and your success in studying ana- lytical chemistry will improve if you master this vocabulary. Be sure you understand the difference between an analyte and its matrix, between a technique and a method, between a procedure and a protocol, and between a total analysis technique and a concentration technique.

In selecting an analytical method we consider criteria such as accu- racy, precision, sensitivity, selectivity, robustness, ruggedness, the amount of available sample, the amount of analyte in the sample, time, cost, and the availability of equipment. These criteria are not mutually independent, and often it is necessary to find an acceptable balance between them.

In developing a procedure or protocol, we give consideration to compensating for interferences, calibrating the method, obtaining an appropriate sample, and validating the analysis. Poorly designed procedures and protocols produce results that are insufficient to meet the needs of the analysis.

KEY TERMS

accuracy	analysis	analyte
calibration	calibration curve	concentration technique
detection limit	determination	interferent
matrix	measurement	method
method blank	precision	procedure
protocol	QA/QC	robust
rugged	selectivity	selectivity coefficient
sensitivity	signal	specificity
technique	total analysis technique	validation

This page titled 3.10: Chapter Summary and Key Terms is shared under a CC BY-NC-SA 4.0 license and was authored, remixed, and/or curated by David Harvey.

- **3.10: Chapter Summary and Key Terms** by David Harvey is licensed CC BY-NC-SA 4.0.

CHAPTER OVERVIEW

4: EVALUATING ANALYTICAL DATA

When we use an analytical method we make three separate evaluations of experimental error. First, before we begin the analysis we evaluate potential sources of errors to ensure they will not adversely effect our results. Second, during the analysis we monitor our measurements to ensure that errors remain acceptable. Finally, at the end of the analysis we evaluate the quality of the measurements and results, and compare them to our original design criteria. This chapter provides an introduction to sources of error, to evaluating errors in analytical measurements, and to the statistical analysis of data.

4.1: Characterizing Measurements and Results
4.2: Characterizing Experimental Errors
4.3: Propagation of Uncertainty
4.4: The Distribution of Measurements and Results
4.5: Statistical Analysis of Data
4.6: Statistical Methods for Normal Distributions
4.7: Detection Limits
4.8: Using Excel and R to Analyze Data
4.9: Problems
4.10: Additional Resources
4.11: Chapter Summary and Key Terms

This page titled 4: Evaluating Analytical Data is shared under a CC BY-NC-SA 4.0 license and was authored, remixed, and/or curated by David Harvey.

4.1: CHARACTERIZING MEASUREMENTS AND RESULTS

Let's begin by choosing a simple quantitative problem that requires a single measurement: What is the mass of a penny? You probably recognize that our statement of the problem is too broad. For example, are we interested in the mass of a United States penny or of a Canadian penny, or is the difference relevant? Because a penny's composition and size may differ from country to country, let's narrow our problem to pennies from the United States.

There are other concerns we might consider. For example, the United States Mint produces pennies at two locations (Figure 4.1.1). Because it seems unlikely that a penny's mass depends on where it is minted, we will ignore this concern. Another concern is whether the mass of a newly minted penny is different from the mass of a circulating penny. Because the answer this time is not obvious, let's further narrow our question and ask "What is the mass of a circulating United States Penny?"



Figure 4.1.1 : An uncirculated 2005 Lincoln head penny. The "D" below the date indicates that this penny was produced at the United States Mint at Denver, Colorado. Pennies produced at the Philadelphia Mint do not have a letter below the date. Source: United States Mint image.

A good way to begin our analysis is to gather some preliminary data. Table 4.1.1 shows masses for seven pennies collected from my change jar. In examining this data we see that our question does not have a simple answer. That is, we can not use the mass of a single penny to draw a specific conclusion about the mass of any other penny (although we might reasonably conclude that all pennies weigh at least 3 g). We can, however, characterize this data by reporting the spread of the individual measurements around a central value.

Table 4.1.1 : Masses of Seven Circulating U. S. Pennies

Penny	Mass (g)
1	3.080
2	3.094
3	3.107
4	3.056
5	3.112
6	3.174
7	3.198

MEASURES OF CENTRAL TENDENCY

One way to characterize the data in Table 4.1.1 is to assume that the masses of individual pennies are scattered randomly around a central value that is the best estimate of a penny's expected, or "true" mass. There are two common ways to estimate central tendency: the mean and the median.

MEAN

The ***mean***, $\overline{X}$, is the numerical average for a data set. We calculate the mean by dividing the sum of the individual values by the size of the data set

$$\overline{X} = \frac{\sum_{i=1}^{n} X_i}{n}$$

where X_i is the ith measurement, and n is the size of the data set.

EXAMPLE 4.1.1

What is the mean for the data in Table 4.1.1 ?

Solution

To calculate the mean we add together the results for all measurements

$$3.080 + 3.094 + 3.107 + 3.056 + 3.112 + 3.174 + 3.198 = 21.821 \text{ g}$$

and divide by the number of measurements

$$\overline{X} = \frac{21.821 \text{ g}}{7} = 3.117 \text{ g}$$

The mean is the most common estimate of central tendency. It is not a robust estimate, however, because a single extreme value—one much larger or much smaller than the remainder of the data—influences strongly the mean's value [Rousseeuw, P. J. *J. Chemom.* **1991**, *5*, 1–20]. For example, if we accidently record the third penny's mass as 31.07 g instead of 3.107 g, the mean changes from 3.117 g to 7.112 g!

> An estimate for a statistical parameter is robust if its value is not affected too much by an unusually large or an unusually small measurement.

MEDIAN

The ***median***, $\widetilde{X}$, is the middle value when we order our data from the smallest to the largest value. When the data has an odd number of values, the median is the middle value. For an even number of values, the median is the average of the $n/2$ and the $(n/2) + 1$ values, where n is the size of the data set.

> When $n = 5$, the median is the third value in the ordered data set; for $n = 6$, the median is the average of the third and fourth members of the ordered data set.

EXAMPLE 4.1.2

What is the median for the data in Table 4.1.1 ?

Solution

To determine the median we order the measurements from the smallest to the largest value

$$3.056 \quad 3.080 \quad 3.094 \quad 3.107 \quad 3.112 \quad 3.174 \quad 3.198$$

Because there are seven measurements, the median is the fourth value in the ordered data; thus, the median is 3.107 g.

As shown by Example 4.1.1 and Example 4.1.2 , the mean and the median provide similar estimates of central tendency when all measurements are comparable in magnitude. The median, however, is a more robust estimate of central tendency because it is less sensitive to measurements with extreme values. For example, if we accidently record the third penny's mass as 31.07 g instead of 3.107 g, the median's value changes from 3.107 g to 3.112 g.

MEASURES OF SPREAD

If the mean or the median provides an estimate of a penny's expected mass, then the spread of individual measurements about the mean or median provides an estimate of the difference in mass among pennies or of the uncertainty in measuring mass with a balance. Although we often define the spread relative to a specific measure of central tendency, its magnitude is independent of the central value. Although shifting all measurements in the same direction by adding or subtracting a constant value changes the mean or median, it does not change the spread. There are three common measures of spread: the range, the standard deviation, and the variance.

> Problem 13 at the end of the chapter asks you to show that this is true.

RANGE

The ***range***, w, is the difference between a data set's largest and smallest values.

$$w = X_{\text{largest}} - X_{\text{smallest}}$$

The range provides information about the total variability in the data set, but does not provide information about the distribution of individual values. The range for the data in Table 4.1.1 is

$$w = 3.198 \text{ g} - 3.056 \text{ g} = 0.142 \text{ g}$$

STANDARD DEVIATION

The ***standard deviation***, s, describes the spread of individual values about their mean, and is given as

$$s = \sqrt{\frac{\sum_{i=1}^{n}(X_i - \overline{X})^2}{n-1}} \tag{4.1.1}$$

where X_i is one of the n individual values in the data set, and $\overline{X}$ is the data set's mean value. Frequently, we report the relative standard deviation, s_r, instead of the absolute standard deviation.

$$s_r = \frac{s}{\overline{X}}$$

The percent relative standard deviation, $\%s_r$, is $s_r \times 100$.

The relative standard deviation is important because it allows for a more meaningful comparison between data sets when the individual measurements differ significantly in magnitude. Consider again the data in Table 4.1.1 . If we multiply each value by 10, the absolute standard deviation will increase by 10 as well; the relative standard deviation, however, is the same.

EXAMPLE 4.1.3

Report the standard deviation, the relative standard deviation, and the percent relative standard deviation for the data in Table 4.1.1 ?

Solution

To calculate the standard deviation we first calculate the difference between each measurement and the data set's mean value (3.117), square the resulting differences, and add them together to find the numerator of Equation 4.1.1

$$\begin{aligned}(3.080 - 3.117)^2 &= (-0.037)^2 = 0.001369\\ (3.094 - 3.117)^2 &= (-0.023)^2 = 0.000529\\ (3.107 - 3.117)^2 &= (-0.010)^2 = 0.000100\\ (3.056 - 3.117)^2 &= (-0.061)^2 = 0.003721\\ (3.112 - 3.117)^2 &= (-0.005)^2 = 0.000025\\ (3.174 - 3.117)^2 &= (+0.057)^2 = 0.003249\\ (3.198 - 3.117)^2 &= (+0.081)^2 = \underline{0.006561}\\ &\qquad\qquad\qquad\qquad\quad 0.015554\end{aligned}$$

For obvious reasons, the numerator of Equation 4.1.1 is called a sum of squares. Next, we divide this sum of squares by $n - 1$, where n is the number of measurements, and take the square root.

$$s = \sqrt{\frac{0.015554}{7 - 1}} = 0.051 \text{ g}$$

Finally, the relative standard deviation and percent relative standard deviation are

$$s_r = \frac{0.051 \text{ g}}{3.117 \text{ g}} = 0.016$$

$$\%s_r = (0.016) \times 100 = 1.6\%$$

It is much easier to determine the standard deviation using a scientific calculator with built in statistical functions.

Many scientific calculators include two keys for calculating the standard deviation. One key calculates the standard deviation for a data set of n samples drawn from a larger collection of possible samples, which corresponds to Equation 4.1.1 . The other key calculates the standard deviation for all possible samples. The latter is known as the population's standard deviation, which we will cover later in this chapter. Your calculator's manual will help you determine the appropriate key for each.

VARIANCE

Another common measure of spread is the ***variance***, which is the square of the standard deviation. We usually report a data set's standard deviation, rather than its variance, because the mean value and the standard deviation share the same unit. As we will see shortly, the variance is a useful measure of spread because its values are additive.

EXAMPLE 4.1.4

What is the variance for the data in Table 4.1.1 ?

Solution

The variance is the square of the absolute standard deviation. Using the standard deviation from Example 4.1.3 gives the variance as

$$s^2 = (0.051)^2 = 0.0026$$

EXERCISE 4.1.1

The following data were collected as part of a quality control study for the analysis of sodium in serum; results are concentrations of Na^+ in mmol/L.

$$140 \quad 143 \quad 141 \quad 137 \quad 132 \quad 157 \quad 143 \quad 149 \quad 118 \quad 145$$

Report the mean, the median, the range, the standard deviation, and the variance for this data. This data is a portion of a larger data set from Andrew, D. F.; Herzberg, A. M. *Data: A Collection of Problems for the Student and Research Worker*, Springer-Verlag:New York, 1985, pp. 151–155.

Answer

Mean: To find the mean we add together the individual measurements and divide by the number of measurements. The sum of the 10 concentrations is 1405. Dividing the sum by 10, gives the mean as 140.5, or 1.40×10^2 mmol/L.

Median: To find the median we arrange the 10 measurements from the smallest concentration to the largest concentration; thus

$$118 \quad 132 \quad 137 \quad 140 \quad 141 \quad 143 \quad 143 \quad 145 \quad 149 \quad 157$$

The median for a data set with 10 members is the average of the fifth and sixth values; thus, the median is (141 + 143)/2, or 142 mmol/L.

Range: The range is the difference between the largest value and the smallest value; thus, the range is 157 – 118 = 39 mmol/L.

Standard Deviation: To calculate the standard deviation we first calculate the absolute difference between each measurement and the mean value (140.5), square the resulting differences, and add them together. The differences are

$$-0.5 \quad 2.5 \quad 0.5 \quad -3.5 \quad -8.5 \quad 16.5 \quad 2.5 \quad 8.5 \quad -22.5 \quad 4.5$$

and the squared differences are

$$0.25 \quad 6.25 \quad 0.25 \quad 12.25 \quad 72.25 \quad 272.25 \quad 6.25 \quad 72.25 \quad 506.25 \quad 20.25$$

The total sum of squares, which is the numerator of Equation 4.1.1, is 968.50. The standard deviation is

$$s = \sqrt{\frac{968.50}{10-1}} = 10.37 \approx 10.4$$

Variance: The variance is the square of the standard deviation, or 108.

This page titled 4.1: Characterizing Measurements and Results is shared under a CC BY-NC-SA 4.0 license and was authored, remixed, and/or curated by David Harvey.

- **4.1: Characterizing Measurements and Results** by David Harvey is licensed CC BY-NC-SA 4.0.

4.2: CHARACTERIZING EXPERIMENTAL ERRORS

Characterizing a penny's mass using the data in Table 4.1.1 suggests two questions. First, does our measure of central tendency agree with the penny's expected mass? Second, why is there so much variability in the individual results? The first of these questions addresses the accuracy of our measurements and the second addresses the precision of our measurements. In this section we consider the types of experimental errors that affect accuracy and precision.

ERRORS THAT AFFECT ACCURACY

Accuracy is how close a measure of central tendency is to its expected value, μ. We express accuracy either as an absolute error, e

$$e = \overline{X} - \mu \tag{4.2.1}$$

or as a percent relative error, $\%e$

$$\%e = \frac{\overline{X} - \mu}{\mu} \times 100 \tag{4.2.2}$$

Although Equation 4.2.1 and Equation 4.2.2 use the mean as the measure of central tendency, we also can use the median.

> The convention for representing a statistical parameter is to use a Roman letter for a value calculated from experimental data, and a Greek letter for its corresponding expected value. For example, the experimentally determined mean is $\overline{X}$ and its underlying expected value is μ. Likewise, the experimental standard deviation is s and the underlying expected value is σ.

We identify as determinate an error that affects the accuracy of an analysis. Each source of a ***determinate error*** has a specific magnitude and sign. Some sources of determinate error are positive and others are negative, and some are larger in magnitude and others are smaller in magnitude. The cumulative effect of these determinate errors is a net positive or negative error in accuracy.

> It is possible, although unlikely, that the positive and negative determinate errors will offset each other, producing a result with no net error in accuracy.

We assign determinate errors into four categories—sampling errors, method errors, measurement errors, and personal errors—each of which we consider in this section.

SAMPLING ERRORS

A determinate sampling error occurs when our sampling strategy does not provide a us with a representative sample. For example, if we monitor the environmental quality of a lake by sampling from a single site near a point source of pollution, such as an outlet for industrial effluent, then our results will be misleading. To determine the mass of a U. S. penny, our strategy for selecting pennies must ensure that we do not include pennies from other countries.

> An awareness of potential sampling errors especially is important when we work with heterogeneous materials. Strategies for obtaining representative samples are covered in Chapter 5.

METHOD ERRORS

In any analysis the relationship between the signal, S_{total}, and the absolute amount of analyte, n_A, or the analyte's concentration, C_A, is

$$S_{total} = k_A n_A + S_{mb} \tag{4.2.3}$$

$$S_{total} = k_A C_A + S_{mb} \tag{4.2.4}$$

where k_A is the method's sensitivity for the analyte and S_{mb} is the signal from the method blank. A ***method error*** exists when our value for k_A or for S_{mb} is in error. For example, a method in which S_{total} is the mass of a precipitate assumes that k is defined by a pure precipitate of known stoichiometry. If this assumption is not true, then the resulting determination of n_A or C_A is inaccurate. We can minimize a determinate error in k_A by calibrating the method. A method error due to an interferent in the reagents is minimized by using a proper method blank.

MEASUREMENT ERRORS

The manufacturers of analytical instruments and equipment, such as glassware and balances, usually provide a statement of the item's maximum ***measurement error***, or ***tolerance***. For example, a 10-mL volumetric pipet (Figure 4.2.1) has a tolerance of ±0.02 mL, which

means the pipet delivers an actual volume within the range 9.98–10.02 mL at a temperature of 20 °C. Although we express this tolerance as a range, the error is determinate; that is, the pipet's expected volume, μ, is a fixed value within this stated range.



Figure 4.2.1 : Close-up of a 10-mL volumetric pipet showing that it has a tolerance of ±0.02 mL at 20 °C.

Volumetric glassware is categorized into classes based on its relative accuracy. Class A glassware is manufactured to comply with tolerances specified by an agency, such as the National Institute of Standards and Technology or the American Society for Testing and Materials. The tolerance level for Class A glassware is small enough that normally we can use it without calibration. The tolerance levels for Class B glassware usually are twice that for Class A glassware. Other types of volumetric glassware, such as beakers and graduated cylinders, are not used to measure volume accurately. Table 4.2.1 provides a summary of typical measurement errors for Class A volumetric glassware. Tolerances for digital pipets and for balances are provided in Table 4.2.2 and Table 4.2.3 .

Table 4.2.1 : Measurement Errors for Type A Volumetric Glassware

Transfer Pipets		Volumetric Flasks		Burets	
Capacity (mL)	Tolerance (mL)	Capacity (mL)	Tolerance (mL)	Capacity (mL)	Tolerance (mL)
1	±0.006	5	±0.02	10	±0.02
2	±0.006	10	±0.02	25	±0.03
5	±0.01	25	±0.03	50	±0.05
10	±0.02	50	±0.05		
20	±0.03	100	±0.08		
25	±0.03	250	±0.12		
50	±0.05	500	±0.20		
100	±0.08	1000	±0.30		
		2000			

Table 4.2.2 : Measurement Errors for Digital Pipets

Pipet Range	Volume (mL or μL)	Percent Measurement Error
10–100 μL	10	±3.0%
	50	±1.0%
	100	±0.8%
100–1000 μL	100	±3.0%
	500	±1.0%
	1000	±0.6%
1–10 mL	1	±3.0%
	5	±0.8%
	10	±0.6%

The tolerance values for the volumetric glassware in Table 4.2.1 are from the ASTM E288, E542, and E694 standards. The measurement errors for the digital pipets in Table 4.2.2 are from www.eppendorf.com.

Table 4.2.3 : Measurement Errors for Selected Balances

Balance	Capacity (g)	Measurement Error
Precisa 160M	160	±1 mg
A & D ER 120M	120	±0.1 mg
Metler H54	160	±0.01 mg

We can minimize a determinate measurement error by calibrating our equipment. Balances are calibrated using a reference weight whose mass we can trace back to the SI standard kilogram. Volumetric glassware and digital pipets are calibrated by determining the mass of water delivered or contained and using the density of water to calculate the actual volume. It is never safe to assume that a calibration does not change during an analysis or over time. One study, for example, found that repeatedly exposing volumetric glassware to higher temperatures

during machine washing and oven drying, led to small, but significant changes in the glassware's calibration [Castanheira, I.; Batista, E.; Valente, A.; Dias, G.; Mora, M.; Pinto, L.; Costa, H. S. *Food Control* **2006**, *17*, 719–726]. Many instruments drift out of calibration over time and may require frequent recalibration during an analysis.

PERSONAL ERRORS

Finally, analytical work is always subject to ***personal error***, examples of which include the ability to see a change in the color of an indicator that signals the endpoint of a titration, biases, such as consistently overestimating or underestimating the value on an instrument's readout scale, failing to calibrate instrumentation, and misinterpreting procedural directions. You can minimize personal errors by taking proper care.

IDENTIFYING DETERMINATE ERRORS

Determinate errors often are difficult to detect. Without knowing the expected value for an analysis, the usual situation in any analysis that matters, we often have nothing to which we can compare our experimental result. Nevertheless, there are strategies we can use to detect determinate errors.

The magnitude of a constant ***determinate error*** is the same for all samples and is more significant when we analyze smaller samples. Analyzing samples of different sizes, therefore, allows us to detect a constant determinate error. For example, consider a quantitative analysis in which we separate the analyte from its matrix and determine its mass. Let's assume the sample is 50.0% w/w analyte. As we see in Table 4.2.4 , the expected amount of analyte in a 0.100 g sample is 0.050 g. If the analysis has a positive constant determinate error of 0.010 g, then analyzing the sample gives 0.060 g of analyte, or an apparent concentration of 60.0% w/w. As we increase the size of the sample the experimental results become closer to the expected result. An upward or downward trend in a graph of the analyte's experimental concentration versus the sample's mass (Figure 4.2.2) is evidence of a constant determinate error.

Table 4.2.4 : Effect of a Constant Determinate Error on the Analysis of a Sample That is 50.0% w/w Analyte

Mass of Sample (g)	Expected Mass of Analyte (g)	Constant Error (g)	Experimental Mass of Analyte (g)	Experimental Concentration of Analyte (% w/w)
0.100	0.050	0.010	0.060	60.0
0.200	0.100	0.010	0.110	55.0
0.400	0.200	0.010	0.210	52.5
0.800	0.400	0.010	0.410	51.2
1.600	0.800	0.010	0.810	50.6

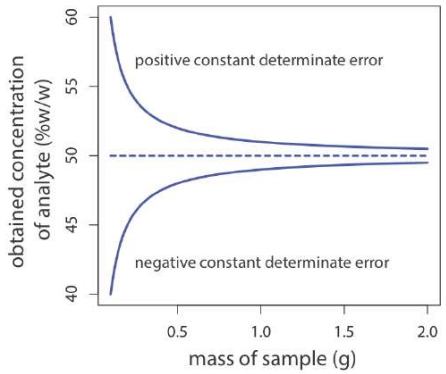


Figure 4.2.2 : Effect of a constant positive determinate error of +0.01 g and a constant negative determinate error of –0.01 g on the determination of an analyte in samples of varying size. The analyte's expected concentration of 50% w/w is shown by the dashed line.

A ***proportional determinate error***, in which the error's magnitude depends on the amount of sample, is more difficult to detect because the result of the analysis is independent of the amount of sample. Table 4.2.5 outlines an example that shows the effect of a positive proportional error of 1.0% on the analysis of a sample that is 50.0% w/w in analyte. Regardless of the sample's size, each analysis gives the same result of 50.5% w/w analyte.

Table 4.2.5 : Effect of a Proportional Determinate Error on the Analysis of a Sample That is 50.0% w/w Analyte

Mass of Sample (g)	Expected Mass of Analyte (g)	Proportional Error (%)	Experimental Mass of Analyte (g)	Experimental Concentration of Analyte (% w/w)
0.100	0.050	1.00	0.0505	50.5
0.200	0.100	1.00	0.101	50.5
0.400	0.200	1.00	0.202	50.5
0.800	0.400	1.00	0.404	50.5
1.600	0.800	1.00	0.808	50.5

One approach for detecting a proportional determinate error is to analyze a standard that contains a known amount of analyte in a matrix similar to our samples. Standards are available from a variety of sources, such as the National Institute of Standards and Technology (where they are called Standard Reference Materials) or the American Society for Testing and Materials. Table 4.2.6 , for example, lists certified values for several analytes in a standard sample of *Gingko biloba* leaves. Another approach is to compare our analysis to an analysis carried out using an independent analytical method that is known to give accurate results. If the two methods give significantly different results, then a determinate error is the likely cause.

Table 4.2.6 : Certified Concentrations for SRM 3246: *Gingko bilbo* (Leaves)

Class of Analyte	Analyte	Mass Fraction (mg/g or ng/g)
Flavonoids/Ginkgolide B (mass fraction in mg/g)	Qurecetin	2.69 ± 0.31
	Kaempferol	3.02 ± 0.41
	Isorhamnetin	$0.517 \pm 0.0.99$
	Total Aglycones	6.22 ± 0.77
Selected Terpenes (mass fraction in mg/g)	Ginkgolide A	0.57 ± 0.28
	Ginkgolide B	0.470 ± 0.090
	Ginkgolide C	0.59 ± 0.22
	Ginkgolide J	0.18 ± 0.10
	Bilobalide	1.52 ± 0.40
	Total Terpene Lactones	3.3 ± 1.1
Selected Toxic Elements (mass fraction in ng/g)	Cadmium	20.8 ± 1.0
	Lead	995 ± 30
	Mercury	23.08 ± 0.17

> The primary purpose of this Standard Reference Material is to validate analytical methods for determining flavonoids, terpene lactones, and toxic elements in *Ginkgo biloba* or other materials with a similar matrix. Values are from the official Certificate of Analysis available at www.nist.gov.

Constant and proportional determinate errors have distinctly different sources, which we can define in terms of the relationship between the signal and the moles or concentration of analyte (Equation 4.2.3 and Equation 4.2.4). An invalid method blank, S_{mb}, is a constant determinate error as it adds or subtracts the same value to the signal. A poorly calibrated method, which yields an invalid sensitivity for the analyte, k_A, results in a proportional determinate error.

ERRORS THAT AFFECT PRECISION

As we saw in Section 4.1, precision is a measure of the spread of individual measurements or results about a central value, which we express as a range, a standard deviation, or a variance. Here we draw a distinction between two types of precision: repeatability and reproducibility. ***Repeatability*** is the precision when a single analyst completes an analysis in a single session using the same solutions, equipment, and instrumentation. ***Reproducibility***, on the other hand, is the precision under any other set of conditions, including between analysts or between laboratory sessions for a single analyst. Since reproducibility includes additional sources of variability, the reproducibility of an analysis cannot be better than its repeatability.

> The ratio of the standard deviation associated with reproducibility to the standard deviation associated with repeatability is called the Horowitz ratio. For a wide variety of analytes in foods, for example, the median Horowtiz ratio is 2.0 with larger values for fatty acids and for trace elements; see Thompson, M.; Wood, R. "The 'Horowitz Ratio'–A Study of the Ratio Between Reproducibility and Repeatability in the Analysis of Foodstuffs," *Anal. Methods*, **2015**, *7*, 375–379.

Errors that affect precision are indeterminate and are characterized by random variations in their magnitude and their direction. Because they are random, positive and negative ***indeterminate errors*** tend to cancel, provided that we make a sufficient number of measurements. In such situations the mean and the median largely are unaffected by the precision of the analysis.

SOURCES OF INDETERMINATE ERROR

We can assign indeterminate errors to several sources, including collecting samples, manipulating samples during the analysis, and making measurements. When we collect a sample, for instance, only a small portion of the available material is taken, which increases the chance that small-scale inhomogeneities in the sample will affect repeatability. Individual pennies, for example, may show variations in mass from several sources, including the manufacturing process and the loss of small amounts of metal or the addition of dirt during circulation. These variations are sources of indeterminate sampling errors.

During an analysis there are many opportunities to introduce indeterminate method errors. If our method for determining the mass of a penny includes directions for cleaning them of dirt, then we must be careful to treat each penny in the same way. Cleaning some pennies more vigorously than others might introduce an indeterminate method error.

Finally, all measuring devices are subject to indeterminate measurement errors due to limitations in our ability to read its scale. For example, a buret with scale divisions every 0.1 mL has an inherent indeterminate error of ±0.01–0.03 mL when we estimate the volume to the hundredth of a milliliter (Figure 4.2.3).

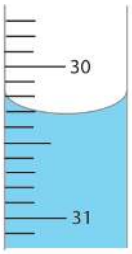


Figure 4.2.3 : Close-up of a buret showing the difficulty in estimating volume. With scale divisions every 0.1 mL it is difficult to read the actual volume to better than ±0.01–0.03 mL.

EVALUATING INDETERMINATE ERROR

Indeterminate errors associated with our analytical equipment or instrumentation generally are easy to estimate if we measure the standard deviation for several replicate measurements, or if we monitor the signal's fluctuations over time in the absence of analyte (Figure 4.2.4) and calculate the standard deviation. Other sources of indeterminate error, such as treating samples inconsistently, are more difficult to estimate.

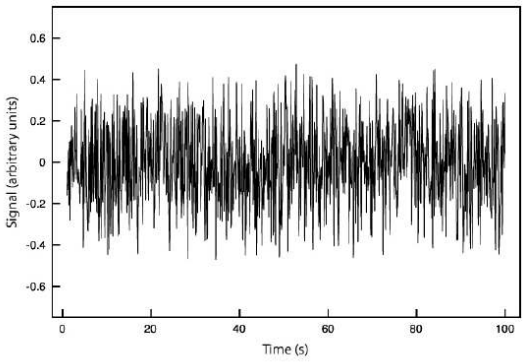


Figure 4.2.4 : Background noise in an instrument showing the random fluctuations in the signal.

To evaluate the effect of an indeterminate measurement error on our analysis of the mass of a circulating United States penny, we might make several determinations of the mass for a single penny (Table 4.2.7). The standard deviation for our original experiment (see Table 4.1.1) is 0.051 g, and it is 0.0024 g for the data in Table 4.2.7 . The significantly better precision when we determine the mass of a single penny suggests that the precision of our analysis is not limited by the balance. A more likely source of indeterminate error is a variability in the masses of individual pennies.

Table 4.2.7 : Replicate Determinations of the Mass of a Single Circulating U. S. Penny

Replicate	Mass (g)	Replicate	Mass (g)
1	3.025	6	3.023
2	3.024	7	3.022
3	3.028	8	3.021
4	3.027	9	3.026
5	3.028	10	3.024

In Section 4.5 we will discuss a statistical method—the *F*-test—that you can use to show that this difference is significant.

ERROR AND UNCERTAINTY

Analytical chemists make a distinction between error and uncertainty [Ellison, S.; Wegscheider, W.; Williams, A. *Anal. Chem.* **1997**, *69*, 607A–613A]. ***Error*** is the difference between a single measurement or result and its expected value. In other words, error is a measure of

bias. As discussed earlier, we divide errors into determinate and indeterminate sources. Although we can find and correct a source of determinate error, the indeterminate portion of the error remains.

Uncertainty expresses the range of possible values for a measurement or result. Note that this definition of uncertainty is not the same as our definition of precision. We calculate precision from our experimental data and use it to estimate the magnitude of indeterminate errors. Uncertainty accounts for all errors—both determinate and indeterminate—that reasonably might affect a measurement or a result. Although we always try to correct determinate errors before we begin an analysis, the correction itself is subject to uncertainty.

Here is an example to help illustrate the difference between precision and uncertainty. Suppose you purchase a 10-mL Class A pipet from a laboratory supply company and use it without any additional calibration. The pipet's tolerance of ±0.02 mL is its uncertainty because your best estimate of its expected volume is 10.00 mL ± 0.02 mL. This uncertainty primarily is determinate. If you use the pipet to dispense several replicate samples of a solution and determine the volume of each sample, the resulting standard deviation is the pipet's precision. Table 4.2.8 shows results for ten such trials, with a mean of 9.992 mL and a standard deviation of ±0.006 mL. This standard deviation is the precision with which we expect to deliver a solution using a Class A 10-mL pipet. In this case the pipet's published uncertainty of ±0.02 mL is worse than its experimentally determined precision of ±0.006 ml. Interestingly, the data in Table 4.2.8 allows us to calibrate this specific pipet's delivery volume as 9.992 mL. If we use this volume as a better estimate of the pipet's expected volume, then its uncertainty is ±0.006 mL. As expected, calibrating the pipet allows us to decrease its uncertainty [Kadis, R. *Talanta* **2004**, *64*, 167–173].

Table 4.2.8 : Experimental Results for Volume Dispensed by a 10–mL Class A Transfer Pipet

Replicate	Volume (ml)	Replicate	Volume (mL)
1	10.002	6	9.983
2	9.993	7	9.991
3	9.984	8	9.990
4	9.996	9	9.988
5	9.989	10	9.999

This page titled 4.2: Characterizing Experimental Errors is shared under a CC BY-NC-SA 4.0 license and was authored, remixed, and/or curated by David Harvey.

- **4.2: Characterizing Experimental Errors** by David Harvey is licensed CC BY-NC-SA 4.0.

4.3: PROPAGATION OF UNCERTAINTY

Suppose we dispense 20 mL of a reagent using the Class A 10-mL pipet whose calibration information is given in Table 4.2.8. If the volume and uncertainty for one use of the pipet is 9.992 ± 0.006 mL, what is the volume and uncertainty if we use the pipet twice?

As a first guess, we might simply add together the volume and the maximum uncertainty for each delivery; thus

$$(9.992\ \text{mL} + 9.992\ \text{mL}) \pm (0.006\ \text{mL} + 0.006\ \text{mL}) = 19.984 \pm 0.012\ \text{mL}$$

It is easy to appreciate that combining uncertainties in this way overestimates the total uncertainty. Adding the uncertainty for the first delivery to that of the second delivery assumes that with each use the indeterminate error is in the same direction and is as large as possible. At the other extreme, we might assume that the uncertainty for one delivery is positive and the other is negative. If we subtract the maximum uncertainties for each delivery,

$$(9.992\ \text{mL} + 9.992\ \text{mL}) \pm (0.006\ \text{mL} - 0.006\ \text{mL}) = 19.984 \pm 0.000\ \text{mL}$$

we clearly underestimate the total uncertainty.

So what is the total uncertainty? From the discussion above, we reasonably expect that the total uncertainty is greater than ±0.000 mL and that it is less than ±0.012 mL. To estimate the uncertainty we use a mathematical technique known as the propagation of uncertainty. Our treatment of the propagation of uncertainty is based on a few simple rules.

A FEW SYMBOLS

A ***propagation of uncertainty*** allows us to estimate the uncertainty in a result from the uncertainties in the measurements used to calculate that result. For the equations in this section we represent the result with the symbol *R*, and we represent the measurements with the symbols *A*, *B*, and *C*. The corresponding uncertainties are u_R, u_A, u_B, and u_C. We can define the uncertainties for *A*, *B*, and *C* using standard deviations, ranges, or tolerances (or any other measure of uncertainty), as long as we use the same form for all measurements.

> The requirement that we express each uncertainty in the same way is a critically important point. Suppose you have a range for one measurement, such as a pipet's tolerance, and standard deviations for the other measurements. All is not lost. There are ways to convert a range to an estimate of the standard deviation. See Appendix 2 for more details.

UNCERTAINTY WHEN ADDING OR SUBTRACTING

When we add or subtract measurements we propagate their absolute uncertainties. For example, if the result is given by the equation

$$R = A + B - C$$

the the absolute uncertainty in *R* is

$$u_R = \sqrt{u_A^2 + u_B^2 + u_C^2} \tag{4.3.1}$$

✔ EXAMPLE 4.3.1

If we dispense 20 mL using a 10-mL Class A pipet, what is the total volume dispensed and what is the uncertainty in this volume? First, complete the calculation using the manufacturer's tolerance of 10.00 mL±0.02 mL, and then using the calibration data from Table 4.2.8.

Solution

To calculate the total volume we add the volumes for each use of the pipet. When using the manufacturer's values, the total volume is

$$V = 10.00\ \text{mL} + 10.00\ \text{mL} = 20.00\ \text{mL}$$

and when using the calibration data, the total volume is

$$V = 9.992\ \text{mL} + 9.992\ \text{mL} = 19.984\ \text{mL}$$

Using the pipet's tolerance as an estimate of its uncertainty gives the uncertainty in the total volume as

$$u_R = \sqrt{(0.02)^2 + (0.02)^2} = 0.028\ \text{mL} = 0.028\ \text{mL}$$

and using the standard deviation for the data in Table 4.2.8 gives an uncertainty of

$$u_R = \sqrt{(0.006)^2 + (0.006)^2} = 0.0085\ \text{mL}$$

Rounding the volumes to four significant figures gives 20.00 mL ± 0.03 mL when we use the tolerance values, and 19.98 ± 0.01 mL when we use the calibration data.

UNCERTAINTY WHEN MULTIPLYING OR DIVIDING

When we multiple or divide measurements we propagate their relative uncertainties. For example, if the result is given by the equation

$$R = \frac{A \times B}{C}$$

then the relative uncertainty in R is

$$\frac{u_R}{R} = \sqrt{\left(\frac{u_A}{A}\right)^2 + \left(\frac{u_B}{B}\right)^2 + \left(\frac{u_C}{C}\right)^2} \tag{4.3.2}$$

EXAMPLE 4.3.2

The quantity of charge, Q, in coulombs that passes through an electrical circuit is

$$Q = i \times t$$

where i is the current in amperes and t is the time in seconds. When a current of 0.15 A ± 0.01 A passes through the circuit for 120 s ± 1 s, what is the total charge and its uncertainty?

Solution

The total charge is

$$Q = (0.15\ \text{A}) \times (120\ \text{s}) = 18\ \text{C}$$

Since charge is the product of current and time, the relative uncertainty in the charge is

$$\frac{u_R}{R} = \sqrt{\left(\frac{0.01}{0.15}\right)^2 + \left(\frac{1}{120}\right)^2} = 0.0672$$

and the charge's absolute uncertainty is

$$u_R = R \times 0.0672 = (18\ \text{C}) \times (0.0672) = 1.2\ \text{C}$$

Thus, we report the total charge as 18 C ± 1 C.

UNCERTAINTY FOR MIXED OPERATIONS

Many chemical calculations involve a combination of adding and subtracting, and of multiply and dividing. As shown in the following example, we can calculate the uncertainty by separately treating each operation using Equation 4.3.1 and Equation 4.3.2 as needed.

EXAMPLE 4.3.3

For a concentration technique, the relationship between the signal and the an analyte's concentration is

$$S_{total} = k_A C_A + S_{mb}$$

What is the analyte's concentration, C_A, and its uncertainty if S_{total} is 24.37 ± 0.02, S_{mb} is 0.96 ± 0.02, and k_A is $0.186 \pm 0.003\ \text{ppm}^{-1}$?

Solution

Rearranging the equation and solving for C_A

$$C_A = \frac{S_{total} - S_{mb}}{k_A} = \frac{24.37 - 0.96}{0.186\ \text{ppm}^{-1}} = \frac{23.41}{0.186\ \text{ppm}^{-1}} = 125.9\ \text{ppm}$$

gives the analyte's concentration as 126 ppm. To estimate the uncertainty in C_A, we first use Equation 4.3.1 to determine the uncertainty for the numerator.

$$u_R = \sqrt{(0.02)^2 + (0.02)^2} = 0.028$$

The numerator, therefore, is 23.41 ± 0.028. To complete the calculation we use Equation 4.3.2 to estimate the relative uncertainty in C_A.

$$\frac{u_R}{R} = \sqrt{\left(\frac{0.028}{23.41}\right)^2 + \left(\frac{0.003}{0.186}\right)^2} = 0.0162$$

The absolute uncertainty in the analyte's concentration is

$$u_R = (125.9 \text{ ppm}) \times (0.0162) = 2.0 \text{ ppm}$$

Thus, we report the analyte's concentration as 126 ppm ± 2 ppm.

EXERCISE 4.3.1

To prepare a standard solution of Cu^{2+} you obtain a piece of copper from a spool of wire. The spool's initial weight is 74.2991 g and its final weight is 73.3216 g. You place the sample of wire in a 500-mL volumetric flask, dissolve it in 10 mL of HNO_3, and dilute to volume. Next, you pipet a 1 mL portion to a 250-mL volumetric flask and dilute to volume. What is the final concentration of Cu^{2+} in mg/L, and its uncertainty? Assume that the uncertainty in the balance is ±0.1 mg and that you are using Class A glassware.

Answer

The first step is to determine the concentration of Cu^{2+} in the final solution. The mass of copper is

$$74.2991 \text{ g} - 73.3216 \text{ g} = 0.9775 \text{ g Cu}$$

The 10 mL of HNO_3 used to dissolve the copper does not factor into our calculation. The concentration of Cu^{2+} is

$$\frac{0.9775 \text{ g Cu}}{0.5000 \text{ L}} \times \frac{1.000 \text{ mL}}{250.0 \text{ mL}} \times \frac{1000 \text{ mg}}{\text{g}} = 7.820 \text{ mg Cu}^{2+}\text{/L}$$

Having found the concentration of Cu^{2+}, we continue with the propagation of uncertainty. The absolute uncertainty in the mass of Cu wire is

$$u_{\text{g Cu}} = \sqrt{(0.0001)^2 + (0.0001)^2} = 0.00014 \text{ g}$$

The relative uncertainty in the concentration of Cu^{2+} is

$$\frac{u_{\text{mg/L}}}{7.820 \text{ mg/L}} = \sqrt{\left(\frac{0.00014}{0.9775}\right)^2 + \left(\frac{0.20}{500.0}\right)^2 + \left(\frac{0.006}{1.000}\right)^2 + \left(\frac{0.12}{250.0}\right)^2} = 0.00603$$

Solving for $u_{\text{mg/L}}$ gives the uncertainty as 0.0472. The concentration and uncertainty for Cu^{2+} is 7.820 mg/L ± 0.047 mg/L.

UNCERTAINTY FOR OTHER MATHEMATICAL FUNCTIONS

Many other mathematical operations are common in analytical chemistry, including the use of powers, roots, and logarithms. Table 4.3.1 provides equations for propagating uncertainty for some of these function where *A* and *B* are independent measurements and where *k* is a constant whose value has no uncertainty.

Table 4.3.1 : Propagation of Uncertainty for Selected Mathematical Functions

Function	u_R	Function	u_R
$R = kA$	$u_R = ku_A$	$R = \ln(A)$	$u_R = \frac{u_A}{A}$
$R = A + B$	$u_R = \sqrt{u_A^2 + u_B^2}$	$R = \log(A)$	$u_R = 0.4343 \times \frac{u_A}{A}$
$R = A - B$	$u_R = \sqrt{u_A^2 + u_B^2}$	$R = e^A$	$\frac{u_R}{R} = u_A$
$R = A \times B$	$\frac{u_R}{R} = \sqrt{\left(\frac{u_A}{A}\right)^2 + \left(\frac{u_B}{B}\right)^2}$	$R = 10^A$	$\frac{u_R}{R} = 2.303 \times u_A$
$R = \frac{A}{B}$	$\frac{u_R}{R} = \sqrt{\left(\frac{u_A}{A}\right)^2 + \left(\frac{u_B}{B}\right)^2}$	$R = A^k$	$\frac{u_R}{R} = k \times \frac{u_A}{A}$

EXAMPLE 4.3.4

If the pH of a solution is 3.72 with an absolute uncertainty of ±0.03, what is the $[H^+]$ and its uncertainty?

Solution

The concentration of H^+ is

$$[H^+] = 10^{-\text{pH}} = 10^{-3.72} = 1.91 \times 10^{-4} \text{ M}$$

or 1.9×10^{-4} M to two significant figures. From Table 4.3.1 the relative uncertainty in $[H^+]$ is

$$\frac{u_R}{R} = 2.303 \times u_A = 2.303 \times 0.03 = 0.069$$

The uncertainty in the concentration, therefore, is

$$(1.91 \times 10^{-4}\ \text{M}) \times (0.069) = 1.3 \times 10^{-5}\ \text{M}$$

We report the $[H^+]$ as $1.9(\pm 0.1) \times 10^{-4}$ M, which is equivalent to $1.9 \times 10^{-4}\ \text{M} \pm 0.1 \times 10^{-4}\ \text{M}$.

EXERCISE 4.3.2

A solution of copper ions is blue because it absorbs yellow and orange light. Absorbance, *A*, is defined as

$$A = -\log T = -\log\left(\frac{P}{P_o}\right)$$

where, *T* is the transmittance, P_o is the power of radiation as emitted from the light source and *P* is its power after it passes through the solution. What is the absorbance if P_o is 3.80×10^2 and *P* is 1.50×10^2 ? If the uncertainty in measuring P_o and *P* is 15, what is the uncertainty in the absorbance?

Answer

The first step is to calculate the absorbance, which is

$$A = -\log T = -\log \frac{P}{P_o} = -\log \frac{1.50 \times 10^2}{3.80 \times 10^2} = 0.4037 \approx 0.404$$

Having found the absorbance, we continue with the propagation of uncertainty. First, we find the uncertainty for the ratio P/P_o, which is the transmittance, T.

$$\frac{u_T}{T} = \sqrt{\left(\frac{15}{3.80 \times 10^2}\right)^2 + \left(\frac{15}{1.50 \times 10^2}\right)^2} = 0.1075$$

Finally, from Table 4.3.1 the uncertainty in the absorbance is

$$u_A = 0.4343 \times \frac{u_T}{T} = (0.4343) \times (0.1075) = 4.669 \times 10^{-2}$$

The absorbance and uncertainty is 0.40 ± 0.05 absorbance units.

IS CALCULATING UNCERTAINTY ACTUALLY USEFUL?

Given the effort it takes to calculate uncertainty, it is worth asking whether such calculations are useful. The short answer is, yes. Let's consider three examples of how we can use a propagation of uncertainty to help guide the development of an analytical method.

One reason to complete a propagation of uncertainty is that we can compare our estimate of the uncertainty to that obtained experimentally. For example, to determine the mass of a penny we measure its mass twice—once to tare the balance at 0.000 g and once to measure the penny's mass. If the uncertainty in each measurement of mass is ±0.001 g, then we estimate the total uncertainty in the penny's mass as

$$u_R = \sqrt{(0.001)^2 + (0.001)^2} = 0.0014\ \text{g}$$

If we measure a single penny's mass several times and obtain a standard deviation of ±0.050 g, then we have evidence that the measurement process is out of control. Knowing this, we can identify and correct the problem.

We also can use a propagation of uncertainty to help us decide how to improve an analytical method's uncertainty. In Example 4.3.3 , for instance, we calculated an analyte's concentration as 126 ppm ± 2 ppm, which is a percent uncertainty of 1.6%. Suppose we want to decrease the percent uncertainty to no more than 0.8%. How might we accomplish this? Looking back at the calculation, we see that the concentration's relative uncertainty is determined by the relative uncertainty in the measured signal (corrected for the reagent blank)

$$\frac{0.028}{23.41} = 0.0012 \text{ or } 0.12\%$$

and the relative uncertainty in the method's sensitivity, k_A,

$$\frac{0.003 \text{ ppm}^{-1}}{0.186 \text{ ppm}^{-1}} = 0.016 \text{ or } 1.6\%$$

Of these two terms, the uncertainty in the method's sensitivity dominates the overall uncertainty. Improving the signal's uncertainty will not improve the overall uncertainty of the analysis. To achieve an overall uncertainty of 0.8% we must improve the uncertainty in k_A to ±0.0015 ppm^{-1}.

EXERCISE 4.3.3

Verify that an uncertainty of ±0.0015 ppm^{-1} for k_A is the correct result.

Answer

An uncertainty of 0.8% is a relative uncertainty in the concentration of 0.008; thus, letting u be the uncertainty in k_A

$$0.008 = \sqrt{\left(\frac{0.028}{23.41}\right)^2 + \left(\frac{u}{0.186}\right)^2}$$

Squaring both sides of the equation gives

$$6.4 \times 10^{-5} = \left(\frac{0.028}{23.41}\right)^2 + \left(\frac{u}{0.186}\right)^2$$

Solving for the uncertainty in k_A gives its value as 1.47×10^{-3} or ±0.0015 ppm^{-1}.

Finally, we can use a propagation of uncertainty to determine which of several procedures provides the smallest uncertainty. When we dilute a stock solution usually there are several combinations of volumetric glassware that will give the same final concentration. For instance, we can dilute a stock solution by a factor of 10 using a 10-mL pipet and a 100-mL volumetric flask, or using a 25-mL pipet and a 250-mL volumetric flask. We also can accomplish the same dilution in two steps using a 50-mL pipet and 100-mL volumetric flask for the first dilution, and a 10-mL pipet and a 50-mL volumetric flask for the second dilution. The overall uncertainty in the final concentration—and, therefore, the best option for the dilution—depends on the uncertainty of the volumetric pipets and volumetric flasks. As shown in the following example, we can use the tolerance values for volumetric glassware to determine the optimum dilution strategy [Lam, R. B.; Isenhour, T. L. *Anal. Chem.* **1980**, *52*, 1158–1161].

EXAMPLE 4.3.5 :

Which of the following methods for preparing a 0.0010 M solution from a 1.0 M stock solution provides the smallest overall uncertainty?

(a) A one-step dilution that uses a 1-mL pipet and a 1000-mL volumetric flask.

(b) A two-step dilution that uses a 20-mL pipet and a 1000-mL volumetric flask for the first dilution, and a 25-mL pipet and a 500-mL volumetric flask for the second dilution.

Solution

The dilution calculations for case (a) and case (b) are

$$\text{case (a)}: 1.0 \text{ M} \times \frac{1.000 \text{ mL}}{1000.0 \text{ mL}} = 0.0010 \text{ M}$$

$$\text{case (b)}: 1.0 \text{ M} \times \frac{20.00 \text{ mL}}{1000.0 \text{ mL}} \times \frac{25.00 \text{ mL}}{500.0 \text{mL}} = 0.0010 \text{ M}$$

Using tolerance values from Table 4.2.1, the relative uncertainty for case (a) is

$$u_R = \sqrt{\left(\frac{0.006}{1.000}\right)^2 + \left(\frac{0.3}{1000.0}\right)^2} = 0.006$$

and for case (b) the relative uncertainty is

$$u_R = \sqrt{\left(\frac{0.03}{20.00}\right)^2 + \left(\frac{0.3}{1000}\right)^2 + \left(\frac{0.03}{25.00}\right)^2 + \left(\frac{0.2}{500.0}\right)^2} = 0.002$$

> Since the relative uncertainty for case (b) is less than that for case (a), the two-step dilution provides the smallest overall uncertainty. Of course we must balance the smaller uncertainty for case (b) against the increased opportunity for introducing a determinate error when making two dilutions instead of just one dilution, as in case (a).

This page titled 4.3: Propagation of Uncertainty is shared under a CC BY-NC-SA 4.0 license and was authored, remixed, and/or curated by David Harvey.

- **4.3: Propagation of Uncertainty** by David Harvey is licensed CC BY-NC-SA 4.0.

4.4: THE DISTRIBUTION OF MEASUREMENTS AND RESULTS

Earlier we reported results for a determination of the mass of a circulating United States penny, obtaining a mean of 3.117 g and a standard deviation of 0.051 g. Table 4.4.1 shows results for a second, independent determination of a penny's mass, as well as the data from the first experiment. Although the means and standard deviations for the two experiments are similar, they are not identical. The difference between the two experiments raises some interesting questions. Are the results for one experiment better than the results for the other experiment? Do the two experiments provide equivalent estimates for the mean and the standard deviation? What is our best estimate of a penny's expected mass? To answer these questions we need to understand how we might predict the properties of all pennies using the results from an analysis of a small sample of pennies. We begin by making a distinction between populations and samples.

Table 4.4.1 : Results for Two Determinations of the Mass of a Circulating U. S. Penny

First Experiment		Second Experiment	
Penny	Mass (g)	Penny	Mass (g)
1	3.080	1	3.052
2	3.094	2	3.141
3	3.107	3	3.083
4	3.056	4	3.083
5	3.112	5	3.048
6	3.174		
7	3.198		
$\overline{X}$	3.117		3.081
s	0.051		0.037

POPULATIONS AND SAMPLES

A ***population*** is the set of all objects in the system we are investigating. For the data in Table 4.4.1 , the population is all United States pennies in circulation. This population is so large that we cannot analyze every member of the population. Instead, we select and analyze a limited subset, or ***sample*** of the population. The data in Table 4.4.1 , for example, shows the results for two such samples drawn from the larger population of all circulating United States pennies.

PROBABILITY DISTRIBUTIONS FOR POPULATIONS

Table 4.4.1 provides the means and the standard deviations for two samples of circulating United States pennies. What do these samples tell us about the population of pennies? What is the largest possible mass for a penny? What is the smallest possible mass? Are all masses equally probable, or are some masses more common?

To answer these questions we need to know how the masses of individual pennies are distributed about the population's average mass. We represent the distribution of a population by plotting the probability or frequency of obtaining a specific result as a function of the possible results. Such plots are called ***probability distributions***.

There are many possible probability distributions; in fact, the probability distribution can take any shape depending on the nature of the population. Fortunately many chemical systems display one of several common probability distributions. Two of these distributions, the binomial distribution and the normal distribution, are discussed in this section.

THE BINOMIAL DISTRIBUTION

The binomial distribution describes a population in which the result is the number of times a particular event occurs during a fixed number of trials. Mathematically, the binomial distribution is defined as

$$P(X,N) = \frac{N!}{X!(N-X)!} \times p^X \times (1-p)^{N-X}$$

where $P(X , N)$ is the probability that an event occurs X times during N trials, and p is the event's probability for a single trial. If you flip a coin five times, $P(2,5)$ is the probability the coin will turn up "heads" exactly twice.

> The term $N!$ reads as N-factorial and is the product $N \times (N-1) \times (N-2) \times \cdots \times 1$. For example, 4! is $4 \times 3 \times 2 \times 1 = 24$. Your calculator probably has a key for calculating factorials.

A binomial distribution has well-defined measures of central tendency and spread. The expected mean value is

$$\mu = Np$$

and the expected spread is given by the variance

$$\sigma^2 = Np(1-p)$$

or the standard deviation.

$$\sigma = \sqrt{Np(1-p)}$$

The binomial distribution describes a population whose members have only specific, discrete values. When you roll a die, for example, the possible values are 1, 2, 3, 4, 5, or 6. A roll of 3.45 is not possible. As shown in Worked Example 4.4.1 , one example of a chemical system that obeys the binomial distribution is the probability of finding a particular isotope in a molecule.

EXAMPLE 4.4.1

Carbon has two stable, non-radioactive isotopes, ^{12}C and ^{13}C, with relative isotopic abundances of, respectively, 98.89% and 1.11%.

(a) What are the mean and the standard deviation for the number of ^{13}C atoms in a molecule of cholesterol ($C_{27}H_{44}O$)?

(b) What is the probability that a molecule of cholesterol has no atoms of ^{13}C?

Solution

The probability of finding an atom of ^{13}C in a molecule of cholesterol follows a binomial distribution, where X is the number of ^{13}C atoms, N is the number of carbon atoms in a molecule of cholesterol, and p is the probability that an atom of carbon in ^{13}C.

For (a), the mean number of ^{13}C atoms in a molecule of cholesterol is

$$\mu = Np = 27 \times 0.0111 = 0.300$$

with a standard deviation of

$$\sigma = \sqrt{Np(1-p)} = \sqrt{27 \times 0.0111 \times (1 - 0.0111)} = 0.544$$

For (b), the probability of finding a molecule of cholesterol without an atom of ^{13}C is

$$P(0,27) = \frac{27!}{0!\,(27-0)!} \times (0.0111)^0 \times (1-0.0111)^{27-0} = 0.740$$

There is a 74.0% probability that a molecule of cholesterol will not have an atom of ^{13}C, a result consistent with the observation that the mean number of ^{13}C atoms per molecule of cholesterol, 0.300, is less than one.

A portion of the binomial distribution for atoms of ^{13}C in cholesterol is shown in Figure 4.4.1 . Note in particular that there is little probability of finding more than two atoms of ^{13}C in any molecule of cholesterol.

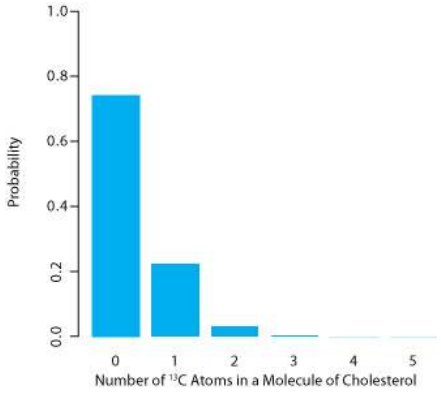


Figure 4.4.1 : Portion of the binomial distribution for the number of naturally occurring ^{13}C atoms in a molecule of cholesterol. Only 3.6% of cholesterol molecules contain more than one atom of ^{13}C, and only 0.33% contain more than two atoms of ^{13}C.

THE NORMAL DISTRIBUTION

A binomial distribution describes a population whose members have only certain discrete values. This is the case with the number of ^{13}C atoms in cholesterol. A molecule of cholesterol, for example, can have two ^{13}C atoms, but it can not have 2.5 atoms of ^{13}C. A population is continuous if its members may take on any value. The efficiency of extracting cholesterol from a sample, for example, can take on any value between 0% (no cholesterol is extracted) and 100% (all cholesterol is extracted).

The most common continuous distribution is the Gaussian, or ***normal distribution***, the equation for which is

$$f(X) = \frac{1}{\sqrt{2\pi\sigma^2}} e^{-\frac{(X-\mu)^2}{2\sigma^2}}$$

where μ is the expected mean for a population with n members

$$\mu = \frac{\sum_{i=1}^{n} X_i}{n}$$

and σ^2 is the population's variance.

$$\sigma^2 = \frac{\sum_{i=1}^{n} (X_i - \mu)^2}{n} \tag{4.4.1}$$

Examples of three normal distributions, each with an expected mean of 0 and with variances of 25, 100, or 400, respectively, are shown in Figure 4.4.2 . Two features of these normal distribution curves deserve attention. First, note that each normal distribution has a single maximum that corresponds to μ, and that the distribution is symmetrical about this value. Second, increasing the population's variance increases the distribution's spread and decreases its height; the area under the curve, however, is the same for all three distributions.

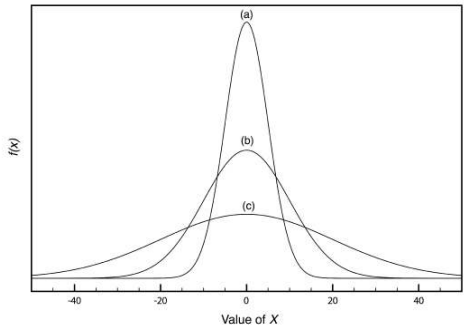


Figure 4.4.2 : Normal distribution curves for: (a) $\mu = 0$; $\sigma^2 = 25$ (b) $\mu = 0$; $\sigma^2 = 100$ (c) $\mu = 0$; $\sigma^2 = 400$.

The area under a normal distribution curve is an important and useful property as it is equal to the probability of finding a member of the population within a particular range of values. In Figure 4.4.2 , for example, 99.99% of the population shown in curve (a) have values of X between –20 and +20. For curve (c), 68.26% of the population's members have values of X between –20 and +20.

Because a normal distribution depends solely on μ and σ^2, the probability of finding a member of the population between any two limits is the same for all normally distributed populations. Figure 4.4.3 , for example, shows that 68.26% of the members of a normal distribution have a value within the range $\mu \pm 1\sigma$, and that 95.44% of population's members have values within the range $\mu \pm 2\sigma$. Only 0.27% members of a population have values that exceed the expected mean by more than $\pm 3\sigma$. Additional ranges and probabilities are gathered together in the probability table included in Appendix 3. As shown in Example 4.4.2 , if we know the mean and the standard deviation for a normally distributed population, then we can determine the percentage of the population between any defined limits.

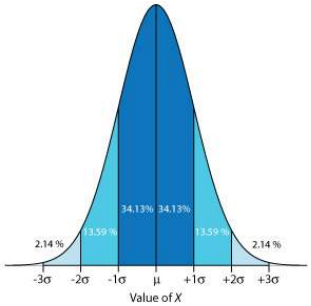


Figure 4.4.3 : Normal distribution curve showing the area under the curve for several different ranges of values of X.

EXAMPLE 4.4.2

The amount of aspirin in the analgesic tablets from a particular manufacturer is known to follow a normal distribution with $\mu = 250$ mg and $\sigma = 5$. In a random sample of tablets from the production line, what percentage are expected to contain between 243 and 262 mg of aspirin?

Solution

We do not determine directly the percentage of tablets between 243 mg and 262 mg of aspirin. Instead, we first find the percentage of tablets with less than 243 mg of aspirin and the percentage of tablets having more than 262 mg of aspirin. Subtracting these results from

100%, gives the percentage of tablets that contain between 243 mg and 262 mg of aspirin.

To find the percentage of tablets with less than 243 mg of aspirin or more than 262 mg of aspirin we calculate the deviation, *z*, of each limit from μ in terms of the population's standard deviation, σ

$$z = \frac{X - \mu}{\sigma}$$

where *X* is the limit in question. The deviation for the lower limit is

$$z_{lower} = \frac{243 - 250}{5} = -1.4$$

and the deviation for the upper limit is

$$z_{upper} = \frac{262 - 250}{5} = +2.4$$

Using the table in Appendix 3, we find that the percentage of tablets with less than 243 mg of aspirin is 8.08%, and that the percentage of tablets with more than 262 mg of aspirin is 0.82%. Therefore, the percentage of tablets containing between 243 and 262 mg of aspirin is

$$100.00\% - 8.08\% - 0.82\% = 91.10\%$$

Figure 4.4.4 shows the distribution of aspiring in the tablets, with the area in blue showing the percentage of tablets containing between 243 mg and 262 mg of aspirin.

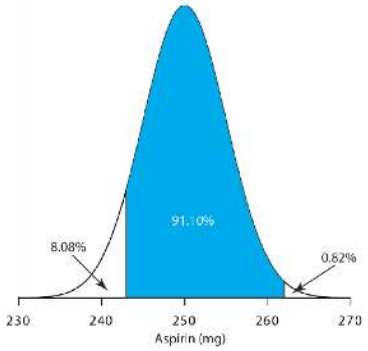


Figure 4.4.4 : Normal distribution for the population of aspirin tablets in Example 4.4.2 . The population's mean and standard deviation are 250 mg and 5 mg, respectively. The shaded area shows the percentage of tablets containing between 243 mg and 262 mg of aspirin.

? EXERCISE 4.4.1

What percentage of aspirin tablets will contain between 240 mg and 245 mg of aspirin if the population's mean is 250 mg and the population's standard deviation is 5 mg.

Answer

To find the percentage of tablets that contain less than 245 mg of aspirin we first calculate the deviation, *z*,

$$z = \frac{245 - 250}{5} = -1.00$$

and then look up the corresponding probability in Appendix 3, obtaining a value of 15.87%. To find the percentage of tablets that contain less than 240 mg of aspirin we find that

$$z = \frac{240 - 250}{5} = -2.00$$

which corresponds to 2.28%. The percentage of tablets containing between 240 and 245 mg of aspiring is 15.87% – 2.28% = 13.59%.

CONFIDENCE INTERVALS FOR POPULATIONS

If we select at random a single member from a population, what is its most likely value? This is an important question, and, in one form or another, it is at the heart of any analysis in which we wish to extrapolate from a sample to the sample's parent population. One of the most important features of a population's probability distribution is that it provides a way to answer this question.

Figure 4.4.3 shows that for a normal distribution, 68.26% of the population's members have values within the range $\mu \pm 1\sigma$. Stating this another way, there is a 68.26% probability that the result for a single sample drawn from a normally distributed population is in the interval $\mu \pm 1\sigma$. In general, if we select a single sample we expect its value, X_i is in the range

$$X_i = \mu \pm z\sigma \tag{4.4.2}$$

where the value of z is how confident we are in assigning this range. Values reported in this fashion are called ***confidence intervals***. Equation 4.4.2, for example, is the confidence interval for a single member of a population. Table 4.4.2 gives the confidence intervals for several values of z. For reasons discussed later in the chapter, a 95% confidence level is a common choice in analytical chemistry.

> When z = 1, we call this the 68.26% confidence interval.

Table 4.4.2 : Confidence Intervals for a Normal Distribution

z	Confidence Interval
0.50	38.30
1.00	68.26
1.50	86.64
1.96	95.00
2.00	95.44
2.50	98.76
3.00	99.73
3.50	99.95

✔ EXAMPLE 4.4.3

What is the 95% confidence interval for the amount of aspirin in a single analgesic tablet drawn from a population for which μ is 250 mg and for which σ is 5?

Solution

Using Table 4.4.2 , we find that z is 1.96 for a 95% confidence interval. Substituting this into Equation 4.4.2 gives the confidence interval for a single tablet as

$$X_i = \mu \pm 1.96\sigma = 250 \text{ mg} \pm (1.96 \times 5) = 250 \text{ mg} \pm 10\text{mg}$$

A confidence interval of 250 mg ± 10 mg means that 95% of the tablets in the population contain between 240 and 260 mg of aspirin.

Alternatively, we can rewrite Equation 4.4.2 so that it gives the confidence interval is for μ based on the population's standard deviation and the value of a single member drawn from the population.

$$\mu = X_i \pm z\sigma \tag{4.4.3}$$

✔ EXAMPLE 4.4.4

The population standard deviation for the amount of aspirin in a batch of analgesic tablets is known to be 7 mg of aspirin. If you randomly select and analyze a single tablet and find that it contains 245 mg of aspirin, what is the 95% confidence interval for the population's mean?

Solution

The 95% confidence interval for the population mean is given as

$$\mu = X_i \pm z\sigma = 245 \text{ mg} \pm (1.96 \times 7) \text{ mg} = 245 \text{ mg} \pm 14 \text{ mg}$$

Therefore, based on this one sample, we estimate that there is 95% probability that the population's mean, μ, lies within the range of 231 mg to 259 mg of aspirin.

Note the qualification that the prediction for μ is based on one sample; a different sample likely will give a different 95% confidence interval. Our result here, therefore, is an estimate for μ based on this one sample.

It is unusual to predict the population's expected mean from the analysis of a single sample; instead, we collect n samples drawn from a population of known σ, and report the mean, $\overline{X}$. The standard deviation of the mean, $\sigma_{\overline{X}}$, which also is known as the ***standard error of the mean***, is

$$\sigma_{\overline{X}} = \frac{\sigma}{\sqrt{n}}$$

The confidence interval for the population's mean, therefore, is

$$\mu = \overline{\overline{X}} \pm \frac{z\sigma}{\sqrt{n}}$$

EXAMPLE 4.4.5

What is the 95% confidence interval for the analgesic tablets in Example 4.4.4 , if an analysis of five tablets yields a mean of 245 mg of aspirin?

Solution

In this case the confidence interval is

$$\mu = 245 \text{ mg} \pm \frac{1.96 \times 7}{\sqrt{5}} \text{ mg} = 245 \text{ mg} \pm 6 \text{ mg}$$

We estimate a 95% probability that the population's mean is between 239 mg and 251 mg of aspirin. As expected, the confidence interval when using the mean of five samples is smaller than that for a single sample.

EXERCISE 4.4.2

An analysis of seven aspirin tablets from a population known to have a standard deviation of 5, gives the following results in mg aspirin per tablet:

$$246 \quad 249 \quad 255 \quad 251 \quad 251 \quad 247 \quad 250$$

What is the 95% confidence interval for the population's expected mean?

Answer

The mean is 249.9 mg aspirin/tablet for this sample of seven tablets. For a 95% confidence interval the value of z is 1.96, which makes the confidence interval

$$249.9 \pm \frac{1.96 \times 5}{\sqrt{7}} = 249.9 \pm 3.7 \approx 250 \text{ mg} \pm 4 \text{ mg}$$

PROBABILITY DISTRIBUTIONS FOR SAMPLES

In Examples 4.4.2 –4.4.5 we assumed that the amount of aspirin in analgesic tablets is normally distributed. Without analyzing every member of the population, how can we justify this assumption? In a situation where we cannot study the whole population, or when we cannot predict the mathematical form of a population's probability distribution, we must deduce the distribution from a limited sampling of its members.

SAMPLE DISTRIBUTIONS AND THE CENTRAL LIMIT THEOREM

Let's return to the problem of determining a penny's mass to explore further the relationship between a population's distribution and the distribution of a sample drawn from that population. The two sets of data in Table 4.4.1 are too small to provide a useful picture of a sample's distribution, so we will use the larger sample of 100 pennies shown in Table 4.4.3 . The mean and the standard deviation for this sample are 3.095 g and 0.0346 g, respectively.

Table 4.4.3 : Masses for a Sample of 100 Circulating U. S. Pennies

Penny	Weight (g)	Penny	Weight (g)	Penny	Weight (g)	Penny	Weight (g)
1	3.126	26	3.073	51	3.101	76	3.086
2	3.140	27	3.084	52	3.049	77	3.123
3	3.092	28	3.148	53	3.082	78	3.115
4	3.095	29	3.047	54	3.142	79	3.055
5	3.080	30	3.121	55	3.082	80	3.057
6	3.065	31	3.116	56	3.066	81	3.097
7	3.117	32	3.005	57	3.128	82	3.066
8	3.034	33	3.115	58	3.112	83	3.113
9	3.126	34	3.103	59	3.085	84	3.102
10	3.057	35	3.086	60	3.086	85	3.033
11	3.053	36	3.103	61	3.084	86	3.112
12	3.099	37	3.049	62	3.104	87	3.103
13	3.065	38	2.998	63	3.107	88	3.198
14	3.059	39	3.063	64	3.093	89	3.103
15	3.068	40	3.055	65	3.126	90	3.126
16	3.060	41	3.181	66	3.138	91	3.111
17	3.078	42	3.108	67	3.131	92	3.126
18	3.125	43	3.114	68	3.120	93	3.052
19	3.090	44	3.121	69	3.100	94	3.113
20	3.100	45	3.105	70	3.099	95	3.085
21	3.055	46	3.078	71	3.097	96	3.117
22	3.105	47	3.147	72	3.091	97	3.142
23	3.063	48	3.104	73	3.077	98	3.031
24	3.083	49	3.146	74	3.178	99	3.083
25	3.065	50	3.095	75	3.054	100	3.104

A ***histogram*** (Figure 4.4.5) is a useful way to examine the data in Table 4.4.3 . To create the histogram, we divide the sample into intervals, by mass, and determine the percentage of pennies within each interval (Table 4.4.4). Note that the sample's mean is the midpoint of the histogram.

Table 4.4.4 : Frequency Distribution for the Data in Table 4.4.3

Mass Interval	Frequency (as % of Sample)	Mass Interval	Frequency (as % of Sample)
2.991 – 3.009	2	3.105 – 3.123	19
3.010 – 3.028	0	3.124 – 3.142	12
3.029 – 3.047	4	3.143 – 3.161	3
3.048 – 3.066	19	3.162 – 3.180	1
3.067 – 3.085	14	3.181 – 3.199	2
3.086 – 3.104	24	3.200 – 3.218	0

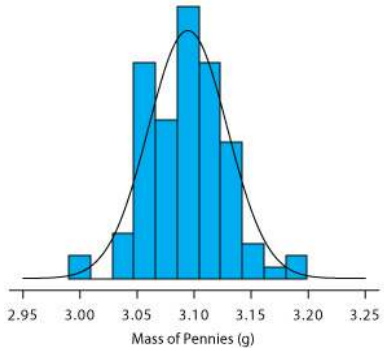


Figure 4.4.5 : The blue bars show a histogram for the data in Table 4.4.3 . The height of each bar corresponds to the percentage of pennies within one of the mass intervals in Table 4.4.4 . Superimposed on the histogram is a normal distribution curve based on the assumption that μ and σ^2 for the population are equivalent to $\overline{X}$ and σ^2 for the sample. The total area of the histogram's bars and the area under the normal distribution curve are equal.

Figure 4.4.5 also includes a normal distribution curve for the population of pennies, based on the assumption that the mean and the variance for the sample are appropriate estimates for the population's mean and variance. Although the histogram is not perfectly symmetric in shape, it provides a good approximation of the normal distribution curve, suggesting that the sample of 100 pennies is normally distributed. It is easy to imagine that the histogram will approximate more closely a normal distribution if we include additional pennies in our sample.

We will not offer a formal proof that the sample of pennies in Table 4.4.3 and the population of all circulating U. S. pennies are normally distributed; however, the evidence in Figure 4.4.5 strongly suggests this is true. Although we cannot claim that the results of all experiments are normally distributed, in most cases our data are normally distributed. According to the ***central limit theorem***, when a measurement is subject to a variety of indeterminate errors, the results for that measurement will approximate a normal distribution [Mark, H.; Workman, J. *Spectroscopy* **1988**, *3*, 44–48]. The central limit theorem holds true even if the individual sources of indeterminate error are not normally distributed. The chief limitation to the central limit theorem is that the sources of indeterminate error must be independent and of similar magnitude so that no one source of error dominates the final distribution.

An additional feature of the central limit theorem is that a distribution of means for samples drawn from a population with any distribution will approximate closely a normal distribution if the size of each sample is sufficiently large. For example, Figure 4.4.6 shows the distribution for two samples of 10 000 drawn from a uniform distribution in which every value between 0 and 1 occurs with an equal frequency. For samples of size n = 1, the resulting distribution closely approximates the population's uniform distribution. The distribution of the means for samples of size n = 10, however, closely approximates a normal distribution.

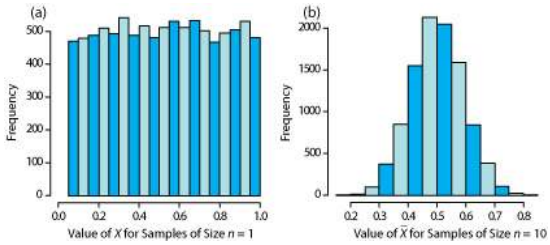


Figure 4.4.6 : Histograms for (a) 10 000 samples of size n = 1 drawn from a uniform distribution with a minimum value of 0 and a maximum value of 1, and (b) the means for 10000 samples of size n = 10 drawn from the same uniform distribution. For (a) the mean of the 10 000 samples is 0.5042, and for (b) the mean of the 10 000 samples is 0.5006. Note that for (a) the distribution closely approximates a uniform distribution in which every possible result is equally likely, and that for (b) the distribution closely approximates a normal distribution.

You might reasonably ask whether this aspect of the central limit theorem is important as it is unlikely that we will complete 10 000 analyses, each of which is the average of 10 individual trials. This is deceiving. When we acquire a sample of soil, for example, it consists of many individual particles each of which is an individual sample of the soil. Our analysis of this sample, therefore, gives the mean for this large number of individual soil particles. Because of this, the central limit theorem is relevant. For a discussion of circumstances where the central limit theorem may not apply, see "Do You Reckon It's Normally Distributed?", the full reference for which is Majewsky, M.; Wagner, M.; Farlin, J. *Sci. Total Environ.* **2016**, *548–549*, 408–409.

DEGREES OF FREEDOM

Did you notice the differences between the equation for the variance of a population and the variance of a sample? If not, here are the two equations:

$$\sigma^2 = \frac{\sum_{i=1}^{n}(X_i - \mu)^2}{n}$$

$$s^2 = \frac{\sum_{i=1}^{n}(X_i - \overline{X})^2}{n-1}$$

Both equations measure the variance around the mean, using μ for a population and $\overline{X}$ for a sample. Although the equations use different measures for the mean, the intention is the same for both the sample and the population. A more interesting difference is between the denominators of the two equations. When we calculate the population's variance we divide the numerator by the population's size, *n*; for the sample's variance, however, we divide by *n* – 1, where *n* is the sample's size. Why do we divide by *n* – 1 when we calculate the sample's variance?

A variance is the average squared deviation of individual results relative to the mean. When we calculate an average we divide the sum by the number of independent measurements, or ***degrees of freedom***, in the calculation. For the population's variance, the degrees of freedom is equal to the population's size, *n*. When we measure every member of a population we have complete information about the population.

When we calculate the sample's variance, however, we replace μ with $\overline{X}$, which we also calculate using the same data. If there are *n* members in the sample, we can deduce the value of the nth member from the remaining *n* – 1 members and the mean. For example, if \(*n* = 5\) and we know that the first four samples are 1, 2, 3 and 4, and that the mean is 3, then the fifth member of the sample must be

$$X_5 = (\overline{X} \times n) - X_1 - X_2 - X_3 - X_4 = (3 \times 5) - 1 - 2 - 3 - 4 = 5$$

Because we have just four independent measurements, we have lost one degree of freedom. Using *n* – 1 in place of *n* when we calculate the sample's variance ensures that s^2 is an unbiased estimator of σ^2.

> Here is another way to think about degrees of freedom. We analyze samples to make predictions about the underlying population. When our sample consists of *n* measurements we cannot make more than *n* independent predictions about the population. Each time we estimate a parameter, such as the population's mean, we lose a degree of freedom. If there are *n* degrees of freedom for calculating the sample's mean, then *n* – 1 degrees of freedom remain when we calculate the sample's variance.

CONFIDENCE INTERVALS FOR SAMPLES

Earlier we introduced the confidence interval as a way to report the most probable value for a population's mean, μ

$$\mu = \overline{X} \pm \frac{z\sigma}{\sqrt{n}} \tag{4.4.4}$$

where $\overline{X}$ is the mean for a sample of size *n*, and σ is the population's standard deviation. For most analyses we do not know the population's standard deviation. We can still calculate a confidence interval, however, if we make two modifications to Equation 4.4.4.

The first modification is straightforward—we replace the population's standard deviation, σ, with the sample's standard deviation, *s*. The second modification is not as obvious. The values of *z* in Table 4.4.2 are for a normal distribution, which is a function of $sigma^2$, not s^2. Although the sample's variance, s^2, is an unbiased estimate of the population's variance, σ^2, the value of s^2 will only rarely equal σ^2. To account for this uncertainty in estimating σ^2, we replace the variable *z* in Equation 4.4.4 with the variable *t*, where *t* is defined such that $t \geq z$ at all confidence levels.

$$\mu = \overline{X} \pm \frac{ts}{\sqrt{n}} \tag{4.4.5}$$

Values for *t* at the 95% confidence level are shown in Table 4.4.5 . Note that *t* becomes smaller as the number of degrees of freedom increases, and that it approaches *z* as *n* approaches infinity. The larger the sample, the more closely its confidence interval for a sample (Equation 4.4.5) approaches the confidence interval for the population (Equation 4.4.3). Appendix 4 provides additional values of *t* for other confidence levels.

Table 4.4.5 : Values of t for a 95% Confidence Interval

Degrees of Freedom	*t*	Degrees of Freedom	*t*	Degrees of Freedom	*t*	Degrees of Freedom	*t*
1	12.706	6	2.447	12	2.179	30	2.042
2	4.303	7	2.365	14	2.145	40	2.021
3	3.181	8	2.306	16	2.120	60	2.000
4	2.776	9	2.262	18	2.101	100	1.984
5	2.571	10	2.228	20	2.086	\(\infty	1.960

✔ EXAMPLE 4.4.6

What are the 95% confidence intervals for the two samples of pennies in Table 4.4.1 ?

Solution

The mean and the standard deviation for first experiment are, respectively, 3.117 g and 0.051 g. Because the sample consists of seven measurements, there are six degrees of freedom. The value of *t* from Table 4.4.5 , is 2.447. Substituting into Equation 4.4.5 gives

$$\mu = 3.117\ \text{g} \pm \frac{2.447 \times 0.051\ \text{g}}{\sqrt{7}} = 3.117\ \text{g} \pm 0.047\ \text{g}$$

For the second experiment the mean and the standard deviation are 3.081 g and 0.073 g, respectively, with four degrees of freedom. The 95% confidence interval is

$$\mu = 3.081\ \text{g} \pm \frac{2.776 \times 0.037\ \text{g}}{\sqrt{5}} = 3.081\ \text{g} \pm 0.046\ \text{g}$$

Based on the first experiment, the 95% confidence interval for the population's mean is 3.070–3.164 g. For the second experiment, the 95% confidence interval is 3.035–3.127 g. Although the two confidence intervals are not identical—remember, each confidence interval provides a different estimate for μ—the mean for each experiment is contained within the other experiment's confidence interval. There also is an appreciable overlap of the two confidence intervals. Both of these observations are consistent with samples drawn from the same population.

Note that our comparison of these two confidence intervals at this point is somewhat vague and unsatisfying. We will return to this point in the next section, when we consider a statistical approach to comparing the results of experiments.

? EXERCISE 4.4.3

What is the 95% confidence interval for the sample of 100 pennies in Table 4.4.3 ? The mean and the standard deviation for this sample are 3.095 g and 0.0346 g, respectively. Compare your result to the confidence intervals for the samples of pennies in Table 4.4.1 .

Answer

With 100 pennies, we have 99 degrees of freedom for the mean. Although Table 4.4.3 does not include a value for *t*(0.05, 99), we can approximate its value by using the values for *t*(0.05, 60) and *t*(0.05, 100) and by assuming a linear change in its value.

$$t(0.05, 99) = t(0.05, 60) - \frac{39}{40}\{t(0.05, 60) - t(0.05, 100\})$$

$$t(0.05, 99) = 2.000 - \frac{39}{40}\{2.000 - 1.984\} = 1.9844$$

The 95% confidence interval for the pennies is

$$3.095 \pm \frac{1.9844 \times 0.0346}{\sqrt{100}} = 3.095\ \text{g} \pm 0.007\ \text{g}$$

From Example 4.4.6 , the 95% confidence intervals for the two samples in Table 4.4.1 are 3.117 g ± 0.047 g and 3.081 g ± 0.046 g. As expected, the confidence interval for the sample of 100 pennies is much smaller than that for the two smaller samples of pennies. Note, as well, that the confidence interval for the larger sample fits within the confidence intervals for the two smaller samples.

A CAUTIONARY STATEMENT

There is a temptation when we analyze data simply to plug numbers into an equation, carry out the calculation, and report the result. This is never a good idea, and you should develop the habit of reviewing and evaluating your data. For example, if you analyze five samples and report an analyte's mean concentration as 0.67 ppm with a standard deviation of 0.64 ppm, then the 95% confidence interval is

$$\mu = 0.67\ \text{ppm} \pm \frac{2.776 \times 0.64\ \text{ppm}}{\sqrt{5}} = 0.67\ \text{ppm} \pm 0.79\ \text{ppm}$$

This confidence interval estimates that the analyte's true concentration is between –0.12 ppm and 1.46 ppm. Including a negative concentration within the confidence interval should lead you to reevaluate your data or your conclusions. A closer examination of your data may convince you that the standard deviation is larger than expected, making the confidence interval too broad, or you may conclude that the analyte's concentration is too small to report with confidence.

> We will return to the topic of detection limits near the end of this chapter.

Here is a second example of why you should closely examine your data: results obtained on samples drawn at random from a normally distributed population must be random. If the results for a sequence of samples show a regular pattern or trend, then the underlying population either is not normally distributed or there is a time-dependent determinate error. For example, if we randomly select 20 pennies and find that the mass of each penny is greater than that for the preceding penny, then we might suspect that our balance is drifting out of calibration.

This page titled 4.4: The Distribution of Measurements and Results is shared under a CC BY-NC-SA 4.0 license and was authored, remixed, and/or curated by David Harvey.

- **4.4: The Distribution of Measurements and Results** by David Harvey is licensed CC BY-NC-SA 4.0.

4.5: STATISTICAL ANALYSIS OF DATA

A confidence interval is a useful way to report the result of an analysis because it sets limits on the expected result. In the absence of determinate error, a confidence interval based on a sample's mean indicates the range of values in which we expect to find the population's mean. When we report a 95% confidence interval for the mass of a penny as 3.117 g ± 0.047 g, for example, we are stating that there is only a 5% probability that the penny's expected mass is less than 3.070 g or more than 3.164 g.

Because a confidence interval is a statement of probability, it allows us to consider comparative questions, such as these: "Are the results for a newly developed method to determine cholesterol in blood significantly different from those obtained using a standard method?" or "Is there a significant variation in the composition of rainwater collected at different sites downwind from a coal-burning utility plant?" In this section we introduce a general approach to the statistical analysis of data. Specific statistical tests are presented in Section 4.6.

> The reliability of significance testing recently has received much attention—see Nuzzo, R. "Scientific Method: Statistical Errors," *Nature*, **2014**, *506*, 150–152 for a general discussion of the issues—so it is appropriate to begin this section by noting the need to ensure that our data and our research question are compatible so that we do not read more into a statistical analysis than our data allows; see Leek, J. T.; Peng, R. D. "What is the Question? *Science*, **2015**, *347*, 1314-1315 for a use-ul discussion of six common research questions.
>
> In the context of analytical chemistry, significance testing often accompanies an exploratory data analysis (Is there a reason to suspect that there is a difference between these two analytical methods when applied to a common sample?) or an inferential data analysis (Is there a reason to suspect that there is a relationship between these two independent measurements?). A statistically significant result for these types of analytical research questions generally leads to the design of additional experiments better suited to making predictions or to explaining an underlying causal relationship. A significance test is the first step toward building a greater understanding of an analytical problem, not the final answer to that problem.

SIGNIFICANCE TESTING

Let's consider the following problem. To determine if a medication is effective in lowering blood glucose concentrations, we collect two sets of blood samples from a patient. We collect one set of samples immediately before we administer the medication, and collect the second set of samples several hours later. After analyzing the samples, we report their respective means and variances. How do we decide if the medication was successful in lowering the patient's concentration of blood glucose?

One way to answer this question is to construct a normal distribution curve for each sample, and to compare the two curves to each other. Three possible outcomes are shown in Figure 4.5.1 . In Figure 4.5.1 a, there is a complete separation of the two normal distribution curves, which suggests the two samples are significantly different from each other. In Figure 4.5.1 b, the normal distribution curves for the two samples almost completely overlap, which suggests that the difference between the samples is insignificant. Figure 4.5.1 c, however, presents us with a dilemma. Although the means for the two samples seem different, the overlap of their normal distribution curves suggests that a significant number of possible outcomes could belong to either distribution. In this case the best we can do is to make a statement about the probability that the samples are significantly different from each other.

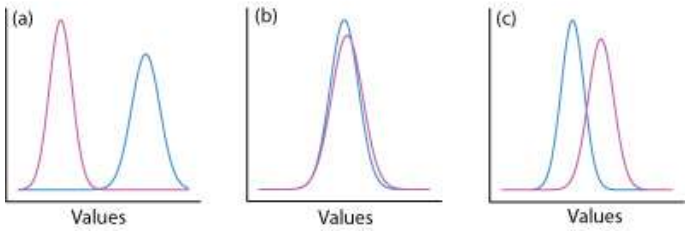


Figure 4.5.1 : Three examples of the possible relationships between the normal distribution curves for two samples. In (a) the curves do not overlap, which suggests that the samples are significantly different from each other. In (b) the two curves are almost identical, suggesting the samples are indistinguishable. The partial overlap of the curves in (c) means that the best we can do is evaluate the probability that there is a difference between the samples.

The process by which we determine the probability that there is a significant difference between two samples is called significance testing or hypothesis testing. Before we discuss specific examples we will first establish a general approach to conducting and interpreting a significance test.

CONSTRUCTING A SIGNIFICANCE TEST

The purpose of a ***significance test*** is to determine whether the difference between two or more results is sufficiently large that it cannot be explained by indeterminate errors. The first step in constructing a significance test is to state the problem as a yes or no question, such as "Is this medication effective at lowering a patient's blood glucose levels?" A null hypothesis and an alternative hypothesis define the two possible answers to our yes or no question. The ***null hypothesis***, H_0, is that indeterminate errors are sufficient to explain any differences between our results. The ***alternative hypothesis***, H_A, is that the differences in our results are too great to be explained by random error and that they must be determinate in nature. We test the null hypothesis, which we either retain or reject. If we reject the null hypothesis, then we must accept the alternative hypothesis and conclude that the difference is significant.

Failing to reject a null hypothesis is not the same as accepting it. We retain a null hypothesis because we have insufficient evidence to prove it incorrect. It is impossible to prove that a null hypothesis is true. This is an important point and one that is easy to forget. To appreciate this point let's return to our sample of 100 pennies in Table 4.4.3. After looking at the data we might propose the following null and alternative hypotheses.

H_0: The mass of a circulating U.S. penny is between 2.900 g and 3.200 g

H_A: The mass of a circulating U.S. penny may be less than 2.900 g or more than 3.200 g

To test the null hypothesis we find a penny and determine its mass. If the penny's mass is 2.512 g then we can reject the null hypothesis and accept the alternative hypothesis. Suppose that the penny's mass is 3.162 g. Although this result increases our confidence in the null hypothesis, it does not prove that the null hypothesis is correct because the next penny we sample might weigh less than 2.900 g or more than 3.200 g.

After we state the null and the alternative hypotheses, the second step is to choose a confidence level for the analysis. The confidence level defines the probability that we will reject the null hypothesis when it is, in fact, true. We can express this as our confidence that we are correct in rejecting the null hypothesis (e.g. 95%), or as the probability that we are incorrect in rejecting the null hypothesis. For the latter, the confidence level is given as α, where

$$\alpha = 1 - \frac{\text{confidence interval (\%)}}{100} \tag{4.5.1}$$

For a 95% confidence level, α is 0.05.

> In this textbook we use α to represent the probability that we incorrectly reject the null hypothesis. In other textbooks this probability is given as *p* (often read as "p- value"). Although the symbols differ, the meaning is the same.

The third step is to calculate an appropriate test statistic and to compare it to a critical value. The test statistic's critical value defines a breakpoint between values that lead us to reject or to retain the null hypothesis, which is the fourth, and final, step of a significance test. How we calculate the test statistic depends on what we are comparing, a topic we cover in Section 4.6. The last step is to either retain the null hypothesis, or to reject it and accept the alternative hypothesis.

> The four steps for a statistical analysis of data using a significance test:
>
> 1. Pose a question, and state the null hypothesis, H_0, and the alternative hypothesis, H_A.
> 2. Choose a confidence level for the statistical analysis.
> 3. Calculate an appropriate test statistic and compare it to a critical value.
> 4. Either retain the null hypothesis, or reject it and accept the alternative hypothesis.

ONE-TAILED AND TWO-TAILED SIGNIFICANCE TESTS

Suppose we want to evaluate the accuracy of a new analytical method. We might use the method to analyze a Standard Reference Material that contains a known concentration of analyte, μ. We analyze the standard several times, obtaining a mean value, $\overline{X}$, for the analyte's concentration. Our null hypothesis is that there is no difference between $\overline{X}$ and μ

$$H_0 \colon \overline{X} = \mu$$

If we conduct the significance test at $\alpha = 0.05$, then we retain the null hypothesis if a 95% confidence interval around $\overline{X}$ contains μ. If the alternative hypothesis is

$$H_A \colon \overline{X} \neq \mu$$

then we reject the null hypothesis and accept the alternative hypothesis if μ lies in the shaded areas at either end of the sample's probability distribution curve (Figure 4.5.2 a). Each of the shaded areas accounts for 2.5% of the area under the probability distribution curve, for a total

of 5%. This is a ***two-tailed significance test*** because we reject the null hypothesis for values of μ at either extreme of the sample's probability distribution curve.

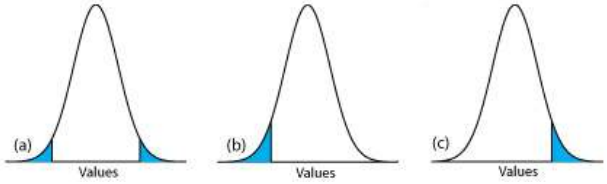


Figure 4.5.2 : Examples of (a) two-tailed, and (b, c) one-tailed, significance test of $\overline{X}$ and μ. The probability distribution curves, which are normal distributions, are based on the sample's mean and standard deviation. For α = 0.05, the blue areas account for 5% of the area under the curve. If the value of μ falls within the blue areas, then we reject the null hypothesis and accept the alternative hypothesis. We retain the null hypothesis if the value of μ falls within the unshaded area of the curve.

We also can write the alternative hypothesis in two additional ways

$$H_A: \overline{\overline{X}} > \mu$$

$$H_A: \overline{\overline{X}} < \mu$$

rejecting the null hypothesis if n falls within the shaded areas shown in Figure 4.5.2 b or Figure 4.5.2 c, respectively. In each case the shaded area represents 5% of the area under the probability distribution curve. These are examples of a ***one-tailed significance test***.

For a fixed confidence level, a two-tailed significance test is the more conservative test because rejecting the null hypothesis requires a larger difference between the parameters we are comparing. In most situations we have no particular reason to expect that one parameter must be larger (or must be smaller) than the other parameter. This is the case, for example, when we evaluate the accuracy of a new analytical method. A two-tailed significance test, therefore, usually is the appropriate choice.

We reserve a one-tailed significance test for a situation where we specifically are interested in whether one parameter is larger (or smaller) than the other parameter. For example, a one-tailed significance test is appropriate if we are evaluating a medication's ability to lower blood glucose levels. In this case we are interested only in whether the glucose levels after we administer the medication are less than the glucose levels before we initiated treatment. If a patient's blood glucose level is greater after we administer the medication, then we know the answer—the medication did not work—and do not need to conduct a statistical analysis.

ERROR IN SIGNIFICANCE TESTING

Because a significance test relies on probability, its interpretation is subject to error. In a significance test, a defines the probability of rejecting a null hypothesis that is true. When we conduct a significance test at $\alpha = 0.05$, there is a 5% probability that we will incorrectly reject the null hypothesis. This is known as a ***type 1 error***, and its risk is always equivalent to α. A type 1 error in a two-tailed or a one-tailed significance tests corresponds to the shaded areas under the probability distribution curves in Figure 4.5.2 .

A second type of error occurs when we retain a null hypothesis even though it is false. This is as a ***type 2 error***, and the probability of its occurrence is β. Unfortunately, in most cases we cannot calculate or estimate the value for β. The probability of a type 2 error, however, is inversely proportional to the probability of a type 1 error.

Minimizing a type 1 error by decreasing α increases the likelihood of a type 2 error. When we choose a value for α we must compromise between these two types of error. Most of the examples in this text use a 95% confidence level ($\alpha = 0.05$) because this usually is a reasonable compromise between type 1 and type 2 errors for analytical work. It is not unusual, however, to use a more stringent (e.g. $\alpha = 0.01$) or a more lenient (e.g. $\alpha = 0.10$) confidence level when the situation calls for it.

This page titled 4.5: Statistical Analysis of Data is shared under a CC BY-NC-SA 4.0 license and was authored, remixed, and/or curated by David Harvey.

- **4.5: Statistical Analysis of Data** by David Harvey is licensed CC BY-NC-SA 4.0.

4.6: STATISTICAL METHODS FOR NORMAL DISTRIBUTIONS

The most common distribution for our results is a normal distribution. Because the area between any two limits of a normal distribution curve is well defined, constructing and evaluating significance tests is straightforward.

COMPARING $\overline{X}$ TO μ

One way to validate a new analytical method is to analyze a sample that contains a known amount of analyte, μ. To judge the method's accuracy we analyze several portions of the sample, determine the average amount of analyte in the sample, $\overline{X}$, and use a significance test to compare $\overline{X}$ to μ. Our null hypothesis is that the difference between $\overline{X}$ and μ is explained by indeterminate errors that affect the determination of $\overline{X}$. The alternative hypothesis is that the difference between $\overline{X}$ and μ is too large to be explained by indeterminate error.

$$H_0: \overline{X} = \mu$$

$$H_A: \overline{X} \neq \mu$$

The test statistic is t_{exp}, which we substitute into the confidence interval for μ given by Equation 4.4.5

$$\mu = \overline{X} \pm \frac{t_{exp} s}{\sqrt{n}} \tag{4.6.1}$$

Rearranging this equation and solving for t_{exp}

$$t_{exp} = \frac{|\mu - \overline{X}|\sqrt{n}}{s} \tag{4.6.2}$$

gives the value for t_{exp} when μ is at either the right edge or the left edge of the sample's confidence interval (Figure 4.6.1 a)

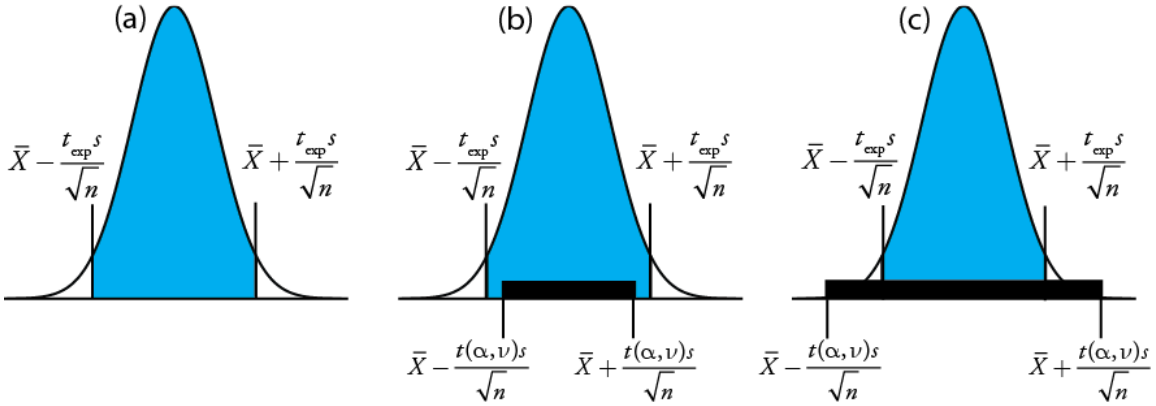


Figure 4.6.1 : Relationship between a confidence interval and the result of a significance test. (a) The shaded area under the normal distribution curve shows the sample's confidence interval for μ based on t_{exp}. The solid bars in (b) and (c) show the expected confidence intervals for μ explained by indeterminate error given the choice of α and the available degrees of freedom, ν. For (b) we reject the null hypothesis because portions of the sample's confidence interval fall outside the confidence interval explained by indeterminate error. In the case of (c) we retain the null hypothesis because the confidence interval explained by indeterminate error completely encompasses the sample's confidence interval.

To determine if we should retain or reject the null hypothesis, we compare the value of t_{exp} to a critical value, $t(\alpha,\nu)$, where α is the confidence level and ν is the degrees of freedom for the sample. The critical value $t(\alpha,\nu)$ defines the largest confidence interval explained by indeterminate error. If $t_{exp} > t(\alpha,\nu)$, then our sample's confidence interval is greater than that explained by indeterminate errors (Figure 4.6.1 b). In this case, we reject the null hypothesis and accept the alternative hypothesis. If $t_{exp} \leq t(\alpha,\nu)$, then our sample's confidence interval is smaller than that explained by indeterminate error, and we retain the null hypothesis (Figure 4.6.1 c). Example 4.6.1 provides a typical application of this significance test, which is known as a **t-test** of $\overline{X}$ to μ.

You will find values for $t(\alpha,\nu)$ in Appendix 4.

Another name for the *t*-test is Student's *t*-test. Student was the pen name for William Gossett (1876-1927) who developed the *t*-test while working as a statistician for the Guiness Brewery in Dublin, Ireland. He published under the name Student because the brewery did not want its competitors to know they were using statistics to help improve the quality of their products.

EXAMPLE 4.6.1

Before determining the amount of Na_2CO_3 in a sample, you decide to check your procedure by analyzing a standard sample that is 98.76% w/w Na_2CO_3. Five replicate determinations of the %w/w Na_2CO_3 in the standard gave the following results

$$98.71\% \quad 98.59\% \quad 98.62\% \quad 98.44\% \quad 98.58\%$$

Using $\alpha = 0.05$, is there any evidence that the analysis is giving inaccurate results?

Solution

The mean and standard deviation for the five trials are

$$\overline{X} = 98.59 \qquad s = 0.0973$$

Because there is no reason to believe that the results for the standard must be larger or smaller than μ, a two-tailed *t*-test is appropriate. The null hypothesis and alternative hypothesis are

$$H_0 \colon \overline{X} = \mu \qquad H_A \colon \overline{X} \neq \mu$$

The test statistic, t_{exp}, is

$$t_{exp} = \frac{|\mu - \overline{X}|\sqrt{n}}{s} = \frac{|98.76 - 98.59|\sqrt{5}}{0.0973} = 3.91$$

The critical value for *t*(0.05, 4) from Appendix 4 is 2.78. Since t_{exp} is greater than *t*(0.05, 4), we reject the null hypothesis and accept the alternative hypothesis. At the 95% confidence level the difference between $\overline{X}$ and μ is too large to be explained by indeterminate sources of error, which suggests there is a determinate source of error that affects the analysis.

There is another way to interpret the result of this *t*-test. Knowing that t_{exp} is 3.91 and that there are 4 degrees of freedom, we use Appendix 4 to estimate the α value corresponding to a *t*(α, 4) of 3.91. From Appendix 4, *t*(0.02, 4) is 3.75 and *t*(0.01, 4) is 4.60. Although we can reject the null hypothesis at the 98% confidence level, we cannot reject it at the 99% confidence level. For a discussion of the advantages of this approach, see J. A. C. Sterne and G. D. Smith "Sifting the evidence—what's wrong with significance tests?" *BMJ* **2001**, *322*, 226–231.

EXERCISE 4.6.1

To evaluate the accuracy of a new analytical method, an analyst determines the purity of a standard for which μ is 100.0%, obtaining the following results.

$$99.28\% \quad 103.93\% \quad 99.43\% \quad 99.84\% \quad 97.60\% \quad 96.70\% \quad 98.02\%$$

Is there any evidence at $\alpha = 0.05$ that there is a determinate error affecting the results?

Answer

The null hypothesis is $H_0 \colon \overline{X} = \mu$ and the alternative hypothesis is $H_A \colon \overline{X} \neq \mu$. The mean and the standard deviation for the data are 99.26% and 2.35%, respectively. The value for t_{exp} is

$$t_{exp} = \frac{|100.0 - 99.26|\sqrt{7}}{2.35} = 0.833$$

and the critical value for *t*(0.05, 6) is 2.477. Because t_{exp} is less than *t*(0.05, 6) we retain the null hypothesis and have no evidence for a significant difference between $\overline{X}$ and μ.

Earlier we made the point that we must exercise caution when we interpret the result of a statistical analysis. We will keep returning to this point because it is an important one. Having determined that a result is inaccurate, as we did in Example 4.6.1 , the next step is to identify and to correct the error. Before we expend time and money on this, however, we first should examine critically our data. For example, the smaller the value of *s*, the larger the value of t_{exp}. If the standard deviation for our analysis is unrealistically small, then the probability of a type 2 error increases. Including a few additional replicate analyses of the standard and reevaluating the *t*-test may strengthen our evidence for a determinate error, or it may show us that there is no evidence for a determinate error.

COMPARING s^2 TO σ^2

If we analyze regularly a particular sample, we may be able to establish an expected variance, σ^2, for the analysis. This often is the case, for example, in a clinical lab that analyze hundreds of blood samples each day. A few replicate analyses of a single sample gives a sample variance, s^2, whose value may or may not differ significantly from σ^2.

We can use an *F*-test to evaluate whether a difference between s^2 and σ^2 is significant. The null hypothesis is $H_0\text{: } s^2 = \sigma^2$ and the alternative hypothesis is $H_A\text{: } s^2 \neq \sigma^2$. The test statistic for evaluating the null hypothesis is F_{exp}, which is given as either

$$F_{exp} = \frac{s^2}{\sigma^2} \text{ if } s^2 > \sigma^2 \text{ or } F_{exp} = \frac{\sigma^2}{s^2} \text{ if } \sigma^2 > s^2 \tag{4.6.3}$$

depending on whether s^2 is larger or smaller than σ^2. This way of defining F_{exp} ensures that its value is always greater than or equal to one.

If the null hypothesis is true, then F_{exp} should equal one; however, because of indeterminate errors F_{exp} usually is greater than one. A critical value, $F(\alpha, \nu_{num}, \nu_{den})$, is the largest value of F_{exp} that we can attribute to indeterminate error given the specified significance level, α, and the degrees of freedom for the variance in the numerator, ν_{num}, and the variance in the denominator, ν_{den}. The degrees of freedom for s^2 is $n - 1$, where n is the number of replicates used to determine the sample's variance, and the degrees of freedom for σ^2 is defined as infinity, ∞. Critical values of *F* for $\alpha = 0.05$ are listed in Appendix 5 for both one-tailed and two-tailed *F*-tests.

EXAMPLE 4.6.2

A manufacturer's process for analyzing aspirin tablets has a known variance of 25. A sample of 10 aspirin tablets is selected and analyzed for the amount of aspirin, yielding the following results in mg aspirin/tablet.

254 249 252 252 249 249 250 247 251 252

Determine whether there is evidence of a significant difference between the sample's variance and the expected variance at $\alpha = 0.05$.

Solution

The variance for the sample of 10 tablets is 4.3. The null hypothesis and alternative hypotheses are

$$H_0\text{: } s^2 = \sigma^2 \qquad H_A\text{: } s^2 \neq \sigma^2$$

and the value for F_{exp} is

$$F_{exp} = \frac{\sigma^2}{s^2} = \frac{25}{4.3} = 5.8$$

The critical value for *F*(0.05, ∞, 9) from Appendix 5 is 3.333. Since F_{exp} is greater than *F*(0.05, ∞, 9), we reject the null hypothesis and accept the alternative hypothesis that there is a significant difference between the sample's variance and the expected variance. One explanation for the difference might be that the aspirin tablets were not selected randomly.

COMPARING VARIANCES FOR TWO SAMPLES

We can extend the *F*-test to compare the variances for two samples, *A* and *B*, by rewriting Equation 4.6.3 as

$$F_{exp} = \frac{s_A^2}{s_B^2}$$

defining *A* and *B* so that the value of *F*exp is greater than or equal to 1.

EXAMPLE 4.6.3

Table 4.4.1 shows results for two experiments to determine the mass of a circulating U.S. penny. Determine whether there is a difference in the variances of these analyses at $\alpha = 0.05$.

Solution

The standard deviations for the two experiments are 0.051 for the first experiment (*A*) and 0.037 for the second experiment (*B*). The null and alternative hypotheses are

$$H_0\text{: } s_A^2 = s_B^2 \qquad H_A\text{: } s_A^2 \neq s_B^2$$

and the value of F_{exp} is

$$F_{exp} = \frac{s_A^2}{s_B^2} = \frac{(0.051)^2}{(0.037)^2} = \frac{0.00260}{0.00137} = 1.90$$

From Appendix 5, the critical value for $F(0.05, 6, 4)$ is 9.197. Because $F_{exp} < F(0.05, 6, 4)$, we retain the null hypothesis. There is no evidence at $\alpha = 0.05$ to suggest that the difference in variances is significant.

EXERCISE 4.6.2

To compare two production lots of aspirin tablets, we collect an analyze samples from each, obtaining the following results (in mg aspirin/tablet).

$$\text{Lot 1: } 256 \quad 248 \quad 245 \quad 245 \quad 244 \quad 248 \quad 261$$

$$\text{Lot 2: } 241 \quad 258 \quad 241 \quad 244 \quad 256 \quad 254$$

Is there any evidence at $\alpha = 0.05$ that there is a significant difference in the variances for these two samples?

Answer

The standard deviations are 6.451 mg for Lot 1 and 7.849 mg for Lot 2. The null and alternative hypotheses are

$$H_0: s^2_{\text{Lot 1}} = s^2_{\text{Lot 2}} \qquad H_A: s^2_{\text{Lot 1}} \neq s^2_{\text{Lot 2}}$$

and the value of F_{exp} is

$$F_{exp} = \frac{(7.849)^2}{(6.451)^2} = 1.480$$

The critical value for $F(0.05, 5, 6)$ is 5.988. Because $F_{exp} < F(0.05, 5, 6)$, we retain the null hypothesis. There is no evidence at $\alpha = 0.05$ to suggest that the difference in the variances is significant.

COMPARING MEANS FOR TWO SAMPLES

Three factors influence the result of an analysis: the method, the sample, and the analyst. We can study the influence of these factors by conducting experiments in which we change one factor while holding constant the other factors. For example, to compare two analytical methods we can have the same analyst apply each method to the same sample and then examine the resulting means. In a similar fashion, we can design experiments to compare two analysts or to compare two samples.

It also is possible to design experiments in which we vary more than one of these factors. We will return to this point in Chapter 14.

Before we consider the significance tests for comparing the means of two samples, we need to make a distinction between ***unpaired data*** and ***paired data***. This is a critical distinction and learning to distinguish between these two types of data is important. Here are two simple examples that highlight the difference between unpaired data and paired data. In each example the goal is to compare two balances by weighing pennies.

- Example 1: We collect 10 pennies and weigh each penny on each balance. This is an example of paired data because we use the same 10 pennies to evaluate each balance.
- Example 2: We collect 10 pennies and divide them into two groups of five pennies each. We weigh the pennies in the first group on one balance and we weigh the second group of pennies on the other balance. Note that no penny is weighed on both balances. This is an example of unpaired data because we evaluate each balance using a different sample of pennies.

In both examples the samples of 10 pennies were drawn from the same population; the difference is how we sampled that population. We will learn why this distinction is important when we review the significance test for paired data; first, however, we present the significance test for unpaired data.

One simple test for determining whether data are paired or unpaired is to look at the size of each sample. If the samples are of different size, then the data must be unpaired. The converse is not true. If two samples are of equal size, they may be paired or unpaired.

UNPAIRED DATA

Consider two analyses, A and B with means of $\overline{X}_A$ and $\overline{X}_B$, and standard deviations of s_A and s_B. The confidence intervals for μ_A and for μ_B are

$$\mu_A = \overline{X}_A \pm \frac{t s_A}{\sqrt{n_A}} \tag{4.6.4}$$

$$\mu_B = \overline{X}_B \pm \frac{ts_B}{\sqrt{n_B}} \tag{4.6.5}$$

where n_A and n_B are the sample sizes for *A* and for *B*. Our null hypothesis, H_0: $\mu_A = \mu_B$, is that and any difference between μ_A and μ_B is the result of indeterminate errors that affect the analyses. The alternative hypothesis, H_A: $\mu_A \neq \mu_B$, is that the difference between $\mu_A$and μ_B is too large to be explained by indeterminate error.

To derive an equation for t_{exp}, we assume that μ_A equals μ_B, and combine Equation 4.6.4 and Equation 4.6.5

$$\overline{X}_A \pm \frac{t_{exp} s_A}{\sqrt{n_A}} = \overline{X}_B \pm \frac{t_{exp} s_B}{\sqrt{n_B}}$$

Solving for $|\overline{X}_A - \overline{X}_B|$ and using a propagation of uncertainty, gives

$$|\overline{X}_A - \overline{X}_B| = t_{exp} \times \sqrt{\frac{s_A^2}{n_A} + \frac{s_B^2}{n_B}} \tag{4.6.6}$$

Finally, we solve for t_{exp}

$$t_{exp} = \frac{|\overline{X}_A - \overline{X}_B|}{\sqrt{\frac{s_A^2}{n_A} + \frac{s_B^2}{n_B}}} \tag{4.6.7}$$

and compare it to a critical value, $t(\alpha, \nu)$, where α is the probability of a type 1 error, and ν is the degrees of freedom.

> Problem 9 asks you to use a propagation of uncertainty to show that Equation 4.6.6 is correct.

Thus far our development of this *t*-test is similar to that for comparing $\overline{X}$ to μ, and yet we do not have enough information to evaluate the *t*-test. Do you see the problem? With two independent sets of data it is unclear how many degrees of freedom we have.

Suppose that the variances s_A^2 and s_B^2 provide estimates of the same σ^2. In this case we can replace s_A^2 and s_B^2 with a pooled variance, s_{pool}^2, that is a better estimate for the variance. Thus, Equation 4.6.7 becomes

$$t_{exp} = \frac{|\overline{X}_A - \overline{X}_B|}{s_{pool} \times \sqrt{\frac{1}{n_A} + \frac{1}{n_B}}} = \frac{|\overline{X}_A - \overline{X}_B|}{s_{pool}} \times \sqrt{\frac{n_A n_B}{n_A + n_B}} \tag{4.6.8}$$

where s_{pool}, the pooled standard deviation, is

$$s_{pool} = \sqrt{\frac{(n_A - 1)s_A^2 + (n_B - 1)s_B^2}{n_A + n_B - 2}} \tag{4.6.9}$$

The denominator of Equation 4.6.9 shows us that the degrees of freedom for a pooled standard deviation is $n_A + n_B - 2$, which also is the degrees of freedom for the *t*-test. Note that we lose two degrees of freedom because the calculations for s_A^2 and s_B^2 require the prior calculation of $\overline{X}_A$ amd $\overline{X}_B$.

> So how do you determine if it is okay to pool the variances? Use an *F*-test.

If s_A^2 and s_B^2 are significantly different, then we calculate t_{exp} using Equation 4.6.7. In this case, we find the degrees of freedom using the following imposing equation.

$$\nu = \frac{\left(\frac{s_A^2}{n_A} + \frac{s_B^2}{n_B}\right)^2}{\frac{\left(\frac{s_A^2}{n_A}\right)^2}{n_A+1} + \frac{\left(\frac{s_B^2}{n_B}\right)^2}{n_B+1}} - 2 \tag{4.6.10}$$

Because the degrees of freedom must be an integer, we round to the nearest integer the value of ν obtained using Equation 4.6.10.

> Equation 4.6.10, which is from Miller, J.C.; Miller, J.N. *Statistics for Analytical Chemistry*, 2nd Ed., Ellis-Horward: Chichester, UK, 1988. In the 6th Edition, the authors note that several different equations have been suggested for the number of degrees of freedom for

t when s_A and s_B differ, reflecting the fact that the determination of degrees of freedom an approximation. An alternative equation—which is used by statistical software packages, such as R, Minitab, Excel—is

$$\nu = \frac{\left(\frac{s_A^2}{n_A} + \frac{s_B^2}{n_B}\right)^2}{\frac{\left(\frac{s_A^2}{n_A}\right)^2}{n_A - 1} + \frac{\left(\frac{s_B^2}{n_B}\right)^2}{n_B - 1}} = \frac{\left(\frac{s_A^2}{n_A} + \frac{s_B^2}{n_B}\right)^2}{\frac{s_A^4}{n_A^2(n_A - 1)} + \frac{s_B^4}{n_B^2(n_B - 1)}}$$

For typical problems in analytical chemistry, the calculated degrees of freedom is reasonably insensitive to the choice of equation.

Regardless of whether we calculate t_{exp} using Equation 4.6.7 or Equation 4.6.8, we reject the null hypothesis if t_{exp} is greater than $t(\alpha, \nu)$ and retain the null hypothesis if t_{exp} is less than or equal to $t(\alpha, \nu)$.

EXAMPLE 4.6.4

Table 4.4.1 provides results for two experiments to determine the mass of a circulating U.S. penny. Determine whether there is a difference in the means of these analyses at $\alpha = 0.05$.

Solution

First we use an *F*-test to determine whether we can pool the variances. We completed this analysis in Example 4.6.3 , finding no evidence of a significant difference, which means we can pool the standard deviations, obtaining

$$s_{pool} = \sqrt{\frac{(7-1)(0.051)^2 + (5-1)(0.037)^2}{7+5-2}} = 0.0459$$

with 10 degrees of freedom. To compare the means we use the following null hypothesis and alternative hypotheses

$$H_0: \mu_A = \mu_B \qquad H_A: \mu_A \neq \mu_B$$

Because we are using the pooled standard deviation, we calculate t_{exp} using Equation 4.6.8.

$$t_{exp} = \frac{|3.117 - 3.081|}{0.0459} \times \sqrt{\frac{7 \times 5}{7+5}} = 1.34$$

The critical value for *t*(0.05, 10), from Appendix 4, is 2.23. Because t_{exp} is less than *t*(0.05, 10) we retain the null hypothesis. For $\alpha = 0.05$ we do not have evidence that the two sets of pennies are significantly different.

EXAMPLE 4.6.5

One method for determining the %w/w Na_2CO_3 in soda ash is to use an acid–base titration. When two analysts analyze the same sample of soda ash they obtain the results shown here.

Analyst A:	86.82%	87.04%	86.93%	87.01%	86.20%	87.00%
Analyst B:	81.01%	86.15%	81.73%	83.19%	80.27%	83.93%

Determine whether the difference in the mean values is significant at $\alpha = 0.05$.

Solution

We begin by reporting the mean and standard deviation for each analyst.

$$\overline{X}_A = 86.83\% \qquad s_A = 0.32\%$$

$$\overline{X}_B = 82.71\% \qquad s_B = 2.16\%$$

To determine whether we can use a pooled standard deviation, we first complete an *F*-test using the following null and alternative hypotheses.

$$H_0: s_A^2 = s_B^2 \qquad H_A: s_A^2 \neq s_B^2$$

Calculating F_{exp}, we obtain a value of

$$F_{exp} = \frac{(2.16)^2}{(0.32)^2} = 45.6$$

Because F_{exp} is larger than the critical value of 7.15 for $F(0.05, 5, 5)$ from Appendix 5, we reject the null hypothesis and accept the alternative hypothesis that there is a significant difference between the variances; thus, we cannot calculate a pooled standard deviation.

To compare the means for the two analysts we use the following null and alternative hypotheses.

$$H_0: \overline{X}_A = \overline{X}_B \qquad H_A: \overline{X}_A \neq \overline{X}_B$$

Because we cannot pool the standard deviations, we calculate t_{exp} using Equation 4.6.7 instead of Equation 4.6.8

$$t_{exp} = \frac{|86.83 - 82.71|}{\sqrt{\frac{(0.32)^2}{6} + \frac{(2.16)^2}{6}}} = 4.62$$

and calculate the degrees of freedom using Equation 4.6.10.

$$\nu = \frac{\left(\frac{(0.32)^2}{6} + \frac{(2.16)^2}{6}\right)^2}{\frac{\left(\frac{(0.32)^2}{6}\right)^2}{6+1} + \frac{\left(\frac{(2.16)^2}{6}\right)^2}{6+1}} - 2 = 5.3 \approx 5$$

From Appendix 4, the critical value for $t(0.05, 5)$ is 2.57. Because t_{exp} is greater than $t(0.05, 5)$ we reject the null hypothesis and accept the alternative hypothesis that the means for the two analysts are significantly different at $\alpha = 0.05$.

? EXERCISE 4.6.3

To compare two production lots of aspirin tablets, you collect samples from each and analyze them, obtaining the following results (in mg aspirin/tablet).

Lot 1: 256 248 245 245 244 248 261

Lot 2: 241 258 241 244 256 254

Is there any evidence at $\alpha = 0.05$ that there is a significant difference in the variance between the results for these two samples? This is the same data from Exercise 4.6.2 .

Answer

To compare the means for the two lots, we use an unpaired t-test of the null hypothesis $H_0: \overline{X}_{\text{Lot 1}} = \overline{X}_{\text{Lot 2}}$ and the alternative hypothesis $H_A: \overline{X}_{\text{Lot 1}} \neq \overline{X}_{\text{Lot 2}}$. Because there is no evidence to suggest a difference in the variances (see Exercise 4.6.2) we pool the standard deviations, obtaining an s_{pool} of

$$s_{pool} = \sqrt{\frac{(7-1)(6.451)^2 + (6-1)(7.849)^2}{7+6-2}} = 7.121$$

The means for the two samples are 249.57 mg for Lot 1 and 249.00 mg for Lot 2. The value for t_{exp} is

$$t_{exp} = \frac{|249.57 - 249.00|}{7.121} \times \sqrt{\frac{7 \times 6}{7+6}} = 0.1439$$

The critical value for $t(0.05, 11)$ is 2.204. Because t_{exp} is less than $t(0.05, 11)$, we retain the null hypothesis and find no evidence at $\alpha = 0.05$ that there is a significant difference between the means for the two lots of aspirin tablets.

PAIRED DATA

Suppose we are evaluating a new method for monitoring blood glucose concentrations in patients. An important part of evaluating a new method is to compare it to an established method. What is the best way to gather data for this study? Because the variation in the blood glucose levels amongst patients is large we may be unable to detect a small, but significant difference between the methods if we use different patients to gather data for each method. Using paired data, in which the we analyze each patient's blood using both methods, prevents a large variance within a population from adversely affecting a t-test of means.

Typical blood glucose levels for most non-diabetic individuals ranges between 80–120 mg/dL (4.4–6.7 mM), rising to as high as 140 mg/dL (7.8 mM) shortly after eating. Higher levels are common for individuals who are pre-diabetic or diabetic.

When we use paired data we first calculate the difference, d_i, between the paired values for each sample. Using these difference values, we then calculate the average difference, $\bar{d}$, and the standard deviation of the differences, s_d. The null hypothesis, $H_0: d = 0$, is that there is no difference between the two samples, and the alternative hypothesis, $H_A: d \neq 0$, is that the difference between the two samples is significant.

The test statistic, t_{exp}, is derived from a confidence interval around $\bar{d}$

$$t_{exp} = \frac{|\bar{d}|\sqrt{n}}{s_d}$$

where n is the number of paired samples. As is true for other forms of the t-test, we compare t_{exp} to $t(\alpha, \nu)$, where the degrees of freedom, ν, is $n - 1$. If t_{exp} is greater than $t(\alpha, \nu)$, then we reject the null hypothesis and accept the alternative hypothesis. We retain the null hypothesis if t_{exp} is less than or equal to t(a, o). This is known as a ***paired t-test.***

EXAMPLE 4.6.6

Marecek et. al. developed a new electrochemical method for the rapid determination of the concentration of the antibiotic monensin in fermentation vats [Marecek, V.; Janchenova, H.; Brezina, M.; Betti, M. *Anal. Chim. Acta* **1991**, *244*, 15–19]. The standard method for the analysis is a test for microbiological activity, which is both difficult to complete and time-consuming. Samples were collected from the fermentation vats at various times during production and analyzed for the concentration of monensin using both methods. The results, in parts per thousand (ppt), are reported in the following table.

Sample	Microbiological	Electrochemical
1	129.5	132.3
2	89.6	91.0
3	76.6	73.6
4	52.2	58.2
5	110.8	104.2
6	50.4	49.9
7	72.4	82.1
8	141.4	154.1
9	75.0	73.4
10	34.1	38.1
11	60.3	60.1

Is there a significant difference between the methods at $\alpha = 0.05$?

Solution

Acquiring samples over an extended period of time introduces a substantial time-dependent change in the concentration of monensin. Because the variation in concentration between samples is so large, we use a paired t-test with the following null and alternative hypotheses.

$$H_0: \bar{d} = 0 \qquad H_A: \bar{d} \neq 0$$

Defining the difference between the methods as

$$d_i = (X_{\text{elect}})_i - (X_{\text{micro}})_i$$

we calculate the difference for each sample.

sample	1	2	3	4	5	6	7	8	9	10	11
d_i	2.8	1.4	–3.0	6.0	–6.6	–0.5	9.7	12.7	–1.6	4.0	–0.2

The mean and the standard deviation for the differences are, respectively, 2.25 ppt and 5.63 ppt. The value of t_{exp} is

$$t_{exp} = \frac{|2.25|\sqrt{11}}{5.63} = 1.33$$

which is smaller than the critical value of 2.23 for t(0.05, 10) from Appendix 4. We retain the null hypothesis and find no evidence for a significant difference in the methods at $\alpha = 0.05$.

EXERCISE 4.6.4

Suppose you are studying the distribution of zinc in a lake and want to know if there is a significant difference between the concentration of Zn^{2+} at the sediment-water interface and its concentration at the air-water interface. You collect samples from six locations—near the lake's center, near its drainage outlet, etc.—obtaining the results (in mg/L) shown in the table. Using this data, determine if there is a significant difference between the concentration of Zn^{2+} at the two interfaces at $\alpha = 0.05$. Complete this analysis treating the data as (a) unpaired and as (b) paired. Briefly comment on your results.

Location	Air-Water Interface	Sediment-Water Interface
1	0.430	0.415
2	0.266	0.238
3	0.457	0.390
4	0.531	0.410
5	0.707	0.605
6	0.716	0.609

Complete this analysis treating the data as (a) unpaired and as (b) paired. Briefly comment on your results.

Answer

Treating as Unpaired Data: The mean and the standard deviation for the concentration of Zn^{2+} at the air-water interface are 0.5178 mg/L and 0.1732 mg/L, respectively, and the values for the sediment-water interface are 0.4445 mg/L and 0.1418 mg/L, respectively. An *F*-test of the variances gives an F_{exp} of 1.493 and an $F(0.05, 5, 5)$ of 7.146. Because F_{exp} is smaller than $F(0.05, 5, 5)$, we have no evidence at $\alpha = 0.05$ to suggest that the difference in variances is significant. Pooling the standard deviations gives an s_{pool} of 0.1582 mg/L. An unpaired *t*-test gives t_{exp} as 0.8025. Because t_{exp} is smaller than $t(0.05, 11)$, which is 2.204, we have no evidence that there is a difference in the concentration of Zn^{2+} between the two interfaces.

Treating as Paired Data: To treat as paired data we need to calculate the difference, d_i, between the concentration of Zn^{2+} at the air-water interface and at the sediment-water interface for each location, where

$$d_i = \left([Zn^{2+}]_{\text{air-water}} \right)_i - \left([Zn^{2+}]_{\text{sed-water}} \right)_i$$

The mean difference is 0.07333 mg/L with a standard deviation of 0.0441 mg/L. The null hypothesis and the alternative hypothesis are

$$H_0 : \bar{d} = 0 \qquad H_A : \bar{d} \neq 0$$

and the value of t_{exp} is

$$t_{exp} = \frac{|0.07333|\sqrt{6}}{0.0441} = 4.073$$

Because t_{exp} is greater than $t(0.05, 5)$, which is 2.571, we reject the null hypothesis and accept the alternative hypothesis that there is a significant difference in the concentration of Zn^{2+} between the air-water interface and the sediment-water interface.

The difference in the concentration of Zn^{2+} between locations is much larger than the difference in the concentration of Zn^{2+} between the interfaces. Because out interest is in studying the difference between the interfaces, the larger standard deviation when treating the data as unpaired increases the probability of incorrectly retaining the null hypothesis, a type 2 error.

One important requirement for a paired *t*-test is that the determinate and the indeterminate errors that affect the analysis must be independent of the analyte's concentration. If this is not the case, then a sample with an unusually high concentration of analyte will have an unusually large d_i. Including this sample in the calculation of $\bar{d}$ and s_d gives a biased estimate for the expected mean and standard deviation. This rarely is a problem for samples that span a limited range of analyte concentrations, such as those in Example 4.6.6 or Exercise 4.6.4 . When paired data span a wide range of concentrations, however, the magnitude of the determinate and indeterminate sources of error may not be independent of the analyte's concentration; when true, a paired *t*-test may give misleading results because the paired data with the largest absolute determinate and indeterminate errors will dominate $\bar{d}$. In this situation a regression analysis, which is the subject of the next chapter, is more appropriate method for comparing the data.

OUTLIERS

Earlier in the chapter we examined several data sets consisting of the mass of a circulating United States penny. Table 4.6.1 provides one more data set. Do you notice anything unusual in this data? Of the 112 pennies included in Table 4.4.1 and Table 4.4.3, no penny weighed less than 3 g. In Table 4.6.1, however, the mass of one penny is less than 3 g. We might ask whether this penny's mass is so different from the other pennies that it is in error.

Table 4.6.1 : Mass (g) for Additional Sample of Circulating U. S. Pennies

3.067	2.514	3.094
3.049	3.048	3.109
3.039	3.079	3.102

A measurement that is not consistent with other measurements is called outlier. An ***outlier*** might exist for many reasons: the outlier might belong to a different population (Is this a Canadian penny?); the outlier might be a contaminated or otherwise altered sample (Is the penny damaged or unusually dirty?); or the outlier may result from an error in the analysis (Did we forget to tare the balance?). Regardless of its source, the presence of an outlier compromises any meaningful analysis of our data. There are many significance tests that we can use to identify a potential outlier, three of which we present here.

DIXON'S *Q*-TEST

One of the most common significance tests for identifying an outlier is ***Dixon's Q-test***. The null hypothesis is that there are no outliers, and the alternative hypothesis is that there is an outlier. The *Q*-test compares the gap between the suspected outlier and its nearest numerical neighbor to the range of the entire data set (Figure 4.6.2).

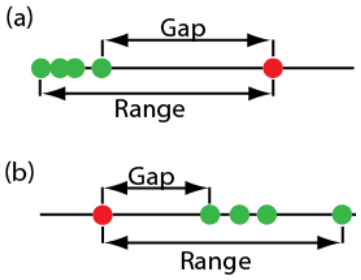


Figure 4.6.2 : Dotplots showing the distribution of two data sets containing a possible outlier. In (a) the possible outlier's value is larger than the remaining data, and in (b) the possible outlier's value is smaller than the remaining data.

The test statistic, Q_{exp}, is

$$Q_{\text{exp}} = \frac{\text{gap}}{\text{range}} = \frac{|\text{outlier's value} - \text{nearest value}|}{\text{largest value} - \text{smallest value}}$$

This equation is appropriate for evaluating a single outlier. Other forms of Dixon's *Q*-test allow its extension to detecting multiple outliers [Rorabacher, D. B. *Anal. Chem.* **1991**, *63*, 139–146].

The value of Q_{exp} is compared to a critical value, $Q(\alpha, n)$, where α is the probability that we will reject a valid data point (a type 1 error) and *n* is the total number of data points. To protect against rejecting a valid data point, usually we apply the more conservative two-tailed *Q*-test, even though the possible outlier is the smallest or the largest value in the data set. If Q_{exp} is greater than $Q(\alpha, n)$, then we reject the null hypothesis and may exclude the outlier. We retain the possible outlier when Q_{exp} is less than or equal to $Q(\alpha, n)$. Table 4.6.2 provides values for $Q(\alpha, n)$ for a data set that has 3–10 values. A more extensive table is in Appendix 6. Values for $Q(\alpha, n)$ assume an underlying normal distribution.

Table 4.6.2 : Dixon's Q-Test

n	*Q*(0.05, *n*)
3	0.970
4	0.829
5	0.710
6	0.625
7	0.568
8	0.526
9	0.493
10	0.466

GRUBB'S TEST

Although Dixon's *Q*-test is a common method for evaluating outliers, it is no longer favored by the International Standards Organization (ISO), which recommends the ***Grubb's test***. There are several versions of Grubb's test depending on the number of potential outliers. Here we will consider the case where there is a single suspected outlier.

> For details on this recommendation, see International Standards ISO Guide 5752-2 "Accuracy (trueness and precision) of measurement methods and results–Part 2: basic methods for the determination of repeatability and reproducibility of a standard measurement

method," 1994.

The test statistic for Grubb's test, G_{exp}, is the distance between the sample's mean, $\overline{X}$, and the potential outlier, X_{out}, in terms of the sample's standard deviation, s.

$$G_{exp} = \frac{|X_{out} - \overline{X}|}{s}$$

We compare the value of G_{exp} to a critical value $G(\alpha, n)$, where α is the probability that we will reject a valid data point and n is the number of data points in the sample. If G_{exp} is greater than $G(\alpha, n)$, then we may reject the data point as an outlier, otherwise we retain the data point as part of the sample. Table 4.6.3 provides values for $G(0.05, n)$ for a sample containing 3–10 values. A more extensive table is in Appendix 7. Values for $G(\alpha, n)$ assume an underlying normal distribution.

Table 4.6.3 : Grubb's Test

n	$G(0.05, n)$
3	1.115
4	1.481
5	1.715
6	1.887
7	2.020
8	2.126
9	2.215
10	2.290

CHAUVENET'S CRITERION

Our final method for identifying an outlier is ***Chauvenet's criterion***. Unlike Dixon's Q-Test and Grubb's test, you can apply this method to any distribution as long as you know how to calculate the probability for a particular outcome. Chauvenet's criterion states that we can reject a data point if the probability of obtaining the data point's value is less than $(2n)^{-1}$, where n is the size of the sample. For example, if n = 10, a result with a probability of less than $(2 \times 10)^{-1}$, or 0.05, is considered an outlier.

To calculate a potential outlier's probability we first calculate its standardized deviation, z

$$z = \frac{|X_{out} - \overline{X}|}{s}$$

where X_{out} is the potential outlier, $\overline{X}$ is the sample's mean and s is the sample's standard deviation. Note that this equation is identical to the equation for G_{exp} in the Grubb's test. For a normal distribution, we can find the probability of obtaining a value of z using the probability table in Appendix 3.

✔ EXAMPLE 4.6.7

Table 4.6.1 contains the masses for nine circulating United States pennies. One entry, 2.514 g, appears to be an outlier. Determine if this penny is an outlier using a Q-test, Grubb's test, and Chauvenet's criterion. For the Q-test and Grubb's test, let $\alpha = 0.05$.

Solution

For the Q-test the value for Qexp is

$$Q_{exp} = \frac{|2.514 - 3.039|}{3.109 - 2.514} = 0.882$$

From Table 4.6.2 , the critical value for $Q(0.05, 9)$ is 0.493. Because Q_{exp} is greater than $Q(0.05, 9)$, we can assume the penny with a mass of 2.514 g likely is an outlier.

For Grubb's test we first need the mean and the standard deviation, which are 3.011 g and 0.188 g, respectively. The value for G_{exp} is

$$G_{exp} = \frac{|2.514 - 3.011}{0.188} = 2.64$$

Using Table 4.6.3 , we find that the critical value for $G(0.05, 9)$ is 2.215. Because G_{exp} is greater than $G(0.05, 9)$, we can assume that the penny with a mass of 2.514 g likely is an outlier.

For Chauvenet's criterion, the critical probability is $(2 \times 9)^{-1}$, or 0.0556. The value of z is the same as G_{exp}, or 2.64. Using Appendix 3, the probability for z = 2.64 is 0.00415. Because the probability of obtaining a mass of 0.2514 g is less than the critical probability, we can assume the penny with a mass of 2.514 g likely is an outlier.

You should exercise caution when using a significance test for outliers because there is a chance you will reject a valid result. In addition, you should avoid rejecting an outlier if it leads to a precision that is much better than expected based on a propagation of uncertainty. Given these concerns it is not surprising that some statisticians caution against the removal of outliers [Deming, W. E. *Statistical Analysis of Data*; Wiley: New York, 1943 (republished by Dover: New York, 1961); p. 171].

> You also can adopt a more stringent requirement for rejecting data. When using the Grubb's test, for example, the ISO 5752 guidelines suggests retaining a value if the probability for rejecting it is greater than $\alpha = 0.05$, and flagging a value as a "straggler" if the probability for rejecting it is between $\alpha = 0.05$ and $\alpha = 0.01$. A "straggler" is retained unless there is compelling reason for its rejection. The guidelines recommend using $\alpha = 0.01$ as the minimum criterion for rejecting a possible outlier.

On the other hand, testing for outliers can provide useful information if we try to understand the source of the suspected outlier. For example, the outlier in Table 4.6.1 represents a significant change in the mass of a penny (an approximately 17% decrease in mass), which is the result of a change in the composition of the U.S. penny. In 1982 the composition of a U.S. penny changed from a brass alloy that was 95% w/w Cu and 5% w/w Zn (with a nominal mass of 3.1 g), to a pure zinc core covered with copper (with a nominal mass of 2.5 g) [Richardson, T. H. *J. Chem. Educ.* **1991**, *68*, 310–311]. The pennies in Table 4.6.1 , therefore, were drawn from different populations.

This page titled 4.6: Statistical Methods for Normal Distributions is shared under a CC BY-NC-SA 4.0 license and was authored, remixed, and/or curated by David Harvey.

- **4.6: Statistical Methods for Normal Distributions** by David Harvey is licensed CC BY-NC-SA 4.0.

4.7: DETECTION LIMITS

The International Union of Pure and Applied Chemistry (IUPAC) defines a method's detection limit as the smallest concentration or absolute amount of analyte that has a signal significantly larger than the signal from a suitable blank [IUPAC Compendium of Chemical Technology, Electronic Version]. Although our interest is in the amount of analyte, in this section we will define the detection limit in terms of the analyte's signal. Knowing the signal you can calculate the analyte's concentration, C_A, or the moles of analyte, n_A, using the equations

$$S_A = k_A C_A \text{ or } S_A = k_A n_A$$

where k is the method's sensitivity.

> See Chapter 3 for a review of these equations.

Let's translate the IUPAC definition of the detection limit into a mathematical form by letting S_{mb} represent the average signal for a method blank, and letting σ_{mb} represent the method blank's standard deviation. The null hypothesis is that the analyte is not present in the sample, and the alternative hypothesis is that the analyte is present in the sample. To detect the analyte, its signal must exceed S_{mb} by a suitable amount; thus,

$$(S_A)_{DL} = S_{mb} \pm z\sigma_{mb} \tag{4.7.1}$$

where $(S_A)_{DL}$ is the analyte's detection limit.

> If σ_{mb} is not known, we can replace it with s_{mb}; Equation 4.7.1 then becomes
>
> $$(S_A)_{DL} = S_{mb} \pm ts_{mb}$$
>
> You can make similar adjustments to other equations in this section. See, for example, Kirchner, C. J. "Estimation of Detection Limits for Environme tal Analytical Procedures," in Currie, L. A. (ed) *Detection in Analytical Chemistry: Importance, Theory, and Practice*; American Chemical Society: Washington, D. C., 1988.

The value we choose for z depends on our tolerance for reporting the analyte's concentration even if it is absent from the sample (a type 1 error). Typically, z is set to three, which, from Appendix 3, corresponds to a probability, α, of 0.00135. As shown in Figure 4.7.1 a, there is only a 0.135% probability of detecting the analyte in a sample that actually is analyte-free.

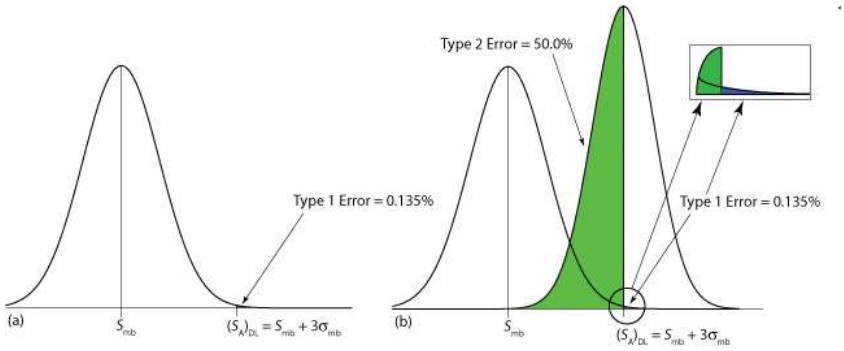


Figure 4.7.1 : Normal distribution curves showing the probability of type 1 and type 2 errors for the IUPAC detection limit. (a) The normal distribution curve for the method blank, with S_{mb} = 0 and σ_{mb} = 1. The minimum detectable signal for the analyte, $(S_A)_{DL}$, has a type 1 error of 0.135%. (b) The normal distribution curve for the analyte at its detection limit, $(S_A)_{DL}$= 3, is superimposed on the normal distribution curve for the method blank. The standard deviation for the analyte's signal, σ_A, is 0.8, The area in green represents the probability of a type 2 error, which is 50%. The inset shows, in blue, the probability of a type 1 error, which is 0.135%.

A detection limit also is subject to a type 2 error in which we fail to find evidence for the analyte even though it is present in the sample. Consider, for example, the situation shown in Figure 4.7.1 b where the signal for a sample that contains the analyte is exactly equal to $(S_A)_{DL}$. In this case the probability of a type 2 error is 50% because half of the sample's possible signals are below the detection limit. We correctly detect the analyte at the IUPAC detection limit only half the time. The IUPAC definition for the detection limit is the smallest signal for which we can say, at a significance level of α, that an analyte is present in the sample; however, failing to detect the analyte does not mean it is not present in the sample.

The detection limit often is represented, particularly when discussing public policy issues, as a distinct line that separates detectable concentrations of analytes from concentrations we cannot detect. This use of a detection limit is incorrect [Rogers, L. B. *J. Chem. Educ.*

1986, *63*, 3–6]. As suggested by Figure 4.7.1 , for an analyte whose concentration is near the detection limit there is a high probability that we will fail to detect the analyte.

An alternative expression for the detection limit, the ***limit of identification***, minimizes both type 1 and type 2 errors [Long, G. L.; Winefordner, J. D. *Anal. Chem.* **1983**, *55*, 712A–724A]. The analyte's signal at the limit of identification, $(S_A)_{\text{LOI}}$, includes an additional term, $z\sigma_A$, to account for the distribution of the analyte's signal.

$$(S_A)_{\text{LOI}} = (S_A)_{\text{DL}} + z\sigma_A = S_{mb} + z\sigma_{mb} + z\sigma_A$$

As shown in Figure 4.7.2 , the limit of identification provides an equal probability of a type 1 and a type 2 error at the detection limit. When the analyte's concentration is at its limit of identification, there is only a 0.135% probability that its signal is indistinguishable from that of the method blank.

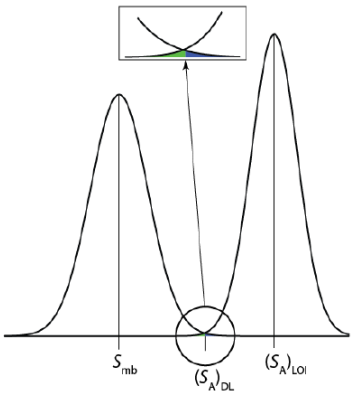


Figure 4.7.2 : Normal distribution curves for a method blank and for a sample at the limit of identification: $S_{mb} = 0$; $\sigma_{mb} = 1$; $\sigma_A = 0.8$; and $(S_A)_{\text{LOI}} = 0 + 3 \times 1 + 3 \times 0.8 = 5.4$. The inset shows that the probability of a type 1 error (0.135%) is the same as the probability of a type 2 error (0.135%).

The ability to detect the analyte with confidence is not the same as the ability to report with confidence its concentration, or to distinguish between its concentration in two samples. For this reason the American Chemical Society's Committee on Environmental Analytical Chemistry recommends the ***limit of quantitation***, $(S_A)_{\text{LOQ}}$ ["Guidelines for Data Acquisition and Data Quality Evaluation in Environmental Chemistry," *Anal. Chem.* **1980**, *52*, 2242–2249].

$$(S_A)_{\text{LOQ}} = S_{mb} + 10\sigma_{mb}$$

This page titled 4.7: Detection Limits is shared under a CC BY-NC-SA 4.0 license and was authored, remixed, and/or curated by David Harvey.

- **4.7: Detection Limits** by David Harvey is licensed CC BY-NC-SA 4.0.

4.8: USING EXCEL AND R TO ANALYZE DATA

Although the calculations in this chapter are relatively straightforward, it can be tedious to work problems using nothing more than a calculator. Both Excel and R include functions for many common statistical calculations. In addition, R provides useful functions for visualizing your data.

EXCEL

Excel has built-in functions that we can use to complete many of the statistical calculations covered in this chapter, including reporting descriptive statistics, such as means and variances, predicting the probability of obtaining a given outcome from a binomial distribution or a normal distribution, and carrying out significance tests. Table 4.8.1 provides the syntax for many of these functions; you can information on functions not included here by using Excel's Help menu.

Table 4.8.1 : Excel Functions for Statistics Calculations

Parameter	Excel Function
Descriptive Statistics	
mean	= average(data)
median	= median(data)
standard deviation for sample	= stdev.s(data)
standard deviation for populations	= stdev.p(data)
variance for sample	= var.s(data)
variance for population	= var.p(data)
maximum value	= max(data)
minimum value	= min(data)
Probability Distributions	
binomial distribution	= binom.dist(*X*, *N*, *p*, TRUE or FALSE)
normal distribution	= norm.dist(*x*, μ σ, TRUE or FALSE)
Significance Tests	
F-test	= f.test(data set 1, data set 2)
t-test	= t.test(data set 1, data set 2, tails = 1 or 2, type of *t*-test: 1 = paired; 2 = unpaired with equal variances; or 3 = unpaired with unequal variances)

DESCRIPTIVE STATISTICS

Let's use Excel to provide a statistical summary of the data in Table 4.1.1. Enter the data into a spreadsheet, as shown in Figure 4.8.1 . To calculate the sample's mean, for example, click on any empty cell, enter the formula

= **average**(b2:b8)

and press Return or Enter to replace the cell's content with Excel's calculation of the mean (3.117285714), which we round to 3.117. Excel does not have a function for the range, but we can use the functions that report the maximum value and the minimum value to calculate the range; thus

= **max**(b2:b8) – **min**(b2:b8)

returns 0.142 as an answer.

	A	B
1		mass (g)
2		3.080
3		3.094
4		3.107
5		3.056
6		3.112
7		3.174
8		3.198

Figure 4.8.1 : Portion of a spreadsheet containing data from Table 4.1.1.

PROBABILITY DISTRIBUTIONS

In Example 4.4.2 we showed that 91.10% of a manufacturer's analgesic tablets contained between 243 and 262 mg of aspirin. We arrived at this result by calculating the deviation, *z*, of each limit from the population's expected mean, μ, of 250 mg in terms of the population's

expected standard deviation, σ, of 5 mg. After we calculated values for z, we used the table in Appendix 3 to find the area under the normal distribution curve between these two limits.

We can complete this calculation in Excel using the **norm.dist** function As shown in Figure 4.8.2 , the function calculates the probability of obtaining a result less than x from a normal distribution with a mean of μ and a standard deviation of σ. To solve Example 4.4.2 using Excel enter the following formulas into separate cells

$$= \textbf{norm.dist}(243, 250, 5, \text{TRUE})$$

$$= \textbf{norm.dist}(262, 250, 5, \text{TRUE})$$

obtaining results of 0.080756659 and 0.991802464. Subtracting the smaller value from the larger value and adjusting to the correct number of significant figures gives the probability as 0.9910, or 99.10%.

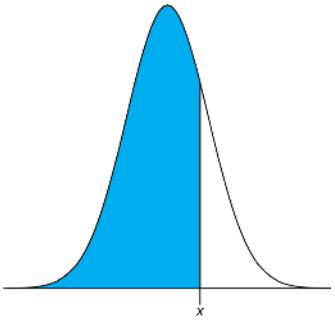


Figure 4.8.2 : Shown in blue is the area returned by the function norm.dist(x, μ σ, TRUE). The last parameter—TRUE—returns the cumulative distribution from $-\infty$ to x; entering FALSE gives the probability of obtaining a result greater than x. For our purposes, we want to use TRUE.

Excel also includes a function for working with binomial distributions. The function's syntax is

$$= \textbf{binom.dist}(X, N, p, \text{TRUE or FALSE})$$

where X is the number of times a particular outcome occurs in N trials, and p is the probability that X occurs in a single trial. Setting the function's last term to TRUE gives the total probability for any result up to X and setting it to FALSE gives the probability for X. Using Example 4.4.1 to test this function, we use the formula

$$= \textbf{binom.dist}(0, 27, 0.0111, \text{FALSE})$$

to find the probability of finding no atoms of ^{13}C atoms in a molecule of cholesterol, $C_{27}H_{44}O$, which returns a value of 0.740 after adjusting for significant figures. Using the formula

$$= \textbf{binom.dist}(2, 27, 0.0111, \text{TRUE})$$

we find that 99.7% of cholesterol molecules contain two or fewer atoms of ^{13}C.

SIGNIFICANCE TESTS

As shown in Table 4.8.1 , Excel includes functions for the following significance tests covered in this chapter:

- an *F*-test of variances
- an unpaired *t*-test of sample means assuming equal variances
- an unpaired *t*-test of sample means assuming unequal variances
- a paired *t*-test for of sample means

Let's use these functions to complete a *t*-test on the data in Table 4.4.1, which contains results for two experiments to determine the mass of a circulating U. S. penny. Enter the data from Table 4.4.1 into a spreadsheet as shown in Figure 4.8.3 .

	A	B	C
1		Set 1	Set 2
2		3.080	3.052
3		3.094	3.141
4		3.107	3.083
5		3.056	3.083
6		3.112	3.048
7		3.174	
8		3.198	

Figure 4.8.3 : Portion of a spreadsheet containing the data in Table 4.4.1.

Because the data in this case are unpaired, we will use Excel to complete an unpaired *t*-test. Before we can complete the *t*-test, we use an *F*-test to determine whether the variances for the two data sets are equal or unequal.

To complete the *F*-test, we click on any empty cell, enter the formula

= **f.test**(b2:b8, c2:c6)

and press Return or Enter, which replaces the cell's content with the value of α for which we can reject the null hypothesis of equal variances. In this case, Excel returns an α of 0.566 105 03; because this value is not less than 0.05, we retain the null hypothesis that the variances are equal. Excel's *F*-test is two-tailed; for a one-tailed *F*-test, we use the same function, but divide the result by two; thus

= **f.test**(b2:b8, c2:c6)/2

Having found no evidence to suggest unequal variances, we next complete an unpaired *t*-test assuming equal variances, entering into any empty cell the formula

= **t.test**(b2:b8, c2:c6, 2, 2)

where the first 2 indicates that this is a two-tailed *t*-test, and the second 2 indicates that this is an unpaired *t*-test with equal variances. Pressing Return or Enter replaces the cell's content with the value of α for which we can reject the null hypothesis of equal means. In this case, Excel returns an α of 0.211 627 646; because this value is not less than 0.05, we retain the null hypothesis that the means are equal.

> See Example 4.6.3 and Example 4.6.4 for our earlier solutions to this problem.

The other significance tests in Excel work in the same format. The following practice exercise provides you with an opportunity to test yourself.

? EXERCISE 4.8.1

Rework Example 4.6.5 and Example 4.6.6 using Excel.

Answer

You will find small differences between the values you obtain using Excel's built in functions and the worked solutions in the chapter. These differences arise because Excel does not round off the results of intermediate calculations.

R

R is a programming environment that provides powerful capabilities for analyzing data. There are many functions built into R's standard installation and additional packages of functions are available from the R web site (www.r-project.org). Commands in R are not available from pull down menus. Instead, you interact with R by typing in commands.

> You can download the current version of R from www.r-project.org. Click on the link for Download: CRAN and find a local mirror site. Click on the link for the mirror site and then use the link for Linux, MacOS X, or Windows under the heading "Download and Install R."

DESCRIPTIVE STATISTICS

Let's use R to provide a statistical summary of the data in Table 4.1.1. To do this we first need to create an object that contains the data, which we do by typing in the following command.

> penny1 = c(3.080, 3.094, 3.107, 3.056, 3.112, 3.174, 3.198)

> In R, the symbol '>' is a prompt, which indicates that the program is waiting for you to enter a command. When you press 'Return' or 'Enter,' R executes the command, displays the result (if there is a result to return), and returns the > prompt.

Table 4.8.2 lists some of the commands in R for calculating basic descriptive statistics. As is the case for Excel, R does not include stand alone commands for all descriptive statistics of interest to us, but we can calculate them using other commands. Using a command is easy—simply enter the appropriate code at the prompt; for example, to find the sample's variance we enter

> **var**(penny1)

[1] 0.002221918

Table 4.8.2 : R Functions for Descriptive Statistics

Parameter	Excel Function
mean	mean(object)
median	median(object)
standard deviation for sample	sd(object)
standard deviation for populations	sd(object) * ((length(object) – 1)/length(object))^0.5
variance for sample	var(object)
variance for population	var(object) * ((length(object) – 1)/length(object))
range	max(object) – min(object)

PROBABILITY DISTRIBUTIONS

In Example 4.4.2 we showed that 91.10% of a manufacturer's analgesic tablets contained between 243 and 262 mg of aspirin. We arrived at this result by calculating the deviation, *z*, of each limit from the population's expected mean, μ, of 250 mg in terms of the population's expected standard deviation, σ, of 5 mg. After we calculated values for *z*, we used the table in Appendix 3 to find the area under the normal distribution curve between these two limits.

We can complete this calculation in R using the function **pnorm**. The function's general format is

$$\textbf{pnorm}(x, \mu, \sigma)$$

where *x* is the limit of interest, μ is the distribution's expected mean, and σ is the distribution's expected standard deviation. The function returns the probability of obtaining a result of less than *x* (Figure 4.8.4).

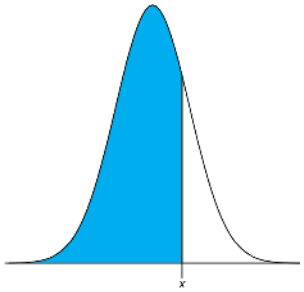


Figure 4.8.4 : Shown in blue is the area returned by the function **pnorm**(x, μ, σ).

Here is the output of an R session for solving Example 4.4.2.

> pnorm(243, 250, 5)

[1] 0.08075666

> pnorm(262, 250, 5)

[1] 0.9918025

Subtracting the smaller value from the larger value and adjusting to the correct number of significant figures gives the probability as 0.9910, or 99.10%.

R also includes functions for binomial distributions. To find the probability of obtaining a particular outcome, *X*, in *N* trials we use the **dbinom** function.

$$\textbf{dbinom}(X, N, p)$$

where *X* is the number of times a particular outcome occurs in *N* trials, and *p* is the probability that *X* occurs in a single trial. Using Example 4.4.1 to test this function, we find that the probability of finding no atoms of ^{13}C atoms in a molecule of cholesterol, $C_{27}H_{44}O$ is

> dbinom(0, 27, 0.0111)

[1] 0.7397997

0.740 after adjusting the significant figures. To find the probability of obtaining any outcome up to a maximum value of *X*, we use the **pbinom** function.

$$\textbf{pbinom}(X, N, p)$$

To find the percentage of cholesterol molecules that contain 0, 1, or 2 atoms of ^{13}C, we enter

> pbinom(2, 27, 0.0111)

[1] 0.9967226

and find that the answer is 99.7% of cholesterol molecules.

SIGNIFICANCE TESTS

R includes commands for the following significance tests covered in this chapter:

- *F*-test of variances
- unpaired *t*-test of sample means assuming equal variances
- unpaired *t*-test of sample means assuming unequal variances
- paired *t*-test for of sample means
- Dixon's *Q*-test for outliers
- Grubb's test for outliers

Let's use these functions to complete a *t*-test on the data in Table 4.4.1, which contains results for two experiments to determine the mass of a circulating U. S. penny. First, enter the data from Table 4.4.1 into two objects.

> penny1 = c(3.080, 3.094, 3.107, 3.056, 3.112, 3.174, 3.198)

> penny2 = c(3.052, 3.141, 3.083, 3.083, 3.048)

Because the data in this case are unpaired, we will use R to complete an unpaired *t*-test. Before we can complete a *t*-test we use an *F*-test to determine whether the variances for the two data sets are equal or unequal.

To complete a two-tailed *F*-test in R we use the command

var.test(*X*, *Y*)

where *X* and *Y* are the objects that contain the two data sets. Figure 4.8.5 shows the output from an R session to solve this problem.

```
> var.test(penny1, penny2)

        F test to compare two variances

data:  penny1 and penny2
F = 1.8726, num df = 6, denom df = 4, p-value = 0.5661
alternative hypothesis: true ratio of variances is not equal to 1
95 percent confidence interval:
 0.2036028 11.6609726
sample estimates:
ratio of variances
          1.872598
```

Figure 4.8.5 : Output of an R session for an *F*-test of variances. The *p*-value of 0.5661 is the probability of incorrectly rejecting the null hypothesis that the variances are equal (*note: R identifies* α *as a p-value*). The 95% confidence interval is the range of values for F_{exp} that are explained by random error. If this range includes the expected value for *F*, in this case 1.00, then there is insufficient evidence to reject the null hypothesis. Note that R does not adjust for significant figures.

Note that R does not provide the critical value for $F(0.05, 6, 4)$; instead it reports the 95% confidence interval for F_{exp}. Because this confidence interval of 0.204 to 11.661 includes the expected value for *F* of 1.00, we retain the null hypothesis and have no evidence for a difference between the variances. R also provides the probability of incorrectly rejecting the null hypothesis, which in this case is 0.5561.

For a one-tailed *F*-test the command is one of the following

var.test(*X*, *Y*, alternative = "greater")

var.test(*X*, *Y*, alternative = "less")

where "greater" is used when the alternative hypothesis is $s_X^2 > s_Y^2$, and "less" is used when the alternative hypothesis is $s_X^2 < s_Y^2$.

Having found no evidence suggesting unequal variances, we now complete an unpaired *t*-test assuming equal variances. The basic syntax for a two-tailed *t*-test is

t.test(*X*, *Y*, mu = 0, paired = FALSE, var.equal = FALSE)

where *X* and *Y* are the objects that contain the data sets. You can change the underlined terms to alter the nature of the *t*-test. Replacing "var.equal = FALSE" with "var.equal = TRUE" makes this a two-tailed *t*-test with equal variances, and replacing "paired = FALSE" with "paired = TRUE" makes this a paired *t*-test. The term "mu = 0" is the expected difference between the means, which for this problem is 0. You can, of course, change this to suit your needs. The underlined terms are default values; if you omit them, then R assumes you intend an unpaired two-tailed *t*-test of the null hypothesis that $X = Y$ with unequal variances. Figure 4.8.6 shows the output of an R session for this problem.

```
> t.test(penny1, penny2, var.equal=TRUE)
  Two Sample t-test
data:  penny1 and penny2
t = 1.3345, df = 10, p-value = 0.2116
alternative hypothesis: true difference in means is not equal to 0
95 percent confidence interval:
 -0.02403040  0.09580182
sample estimates:
mean of x mean of y
 3.117286  3.081400
```

Figure 4.8.6 : Output of an R session for an unpaired *t*-test with equal variances. The *p*-value of 0.2116 is the probability of incorrectly rejecting the null hypothesis that the means are equal (*note: R identifies α as a p-value*). The 95% confidence interval is the range of values for the difference between the means that is explained by random error. If this range includes the expected value for the difference, in this case zero, then there is insufficient evidence to reject the null hypothesis. Note that R does not adjust for significant figures.

We can interpret the results of this *t*-test in two ways. First, the *p*-value of 0.2116 means there is a 21.16% probability of incorrectly rejecting the null hypothesis. Second, the 95% confidence interval of –0.024 to 0.0958 for the difference between the sample means includes the expected value of zero. Both ways of looking at the results provide no evidence for rejecting the null hypothesis; thus, we retain the null hypothesis and find no evidence for a difference between the two samples.

The other significance tests in R work in the same format. The following practice exercise provides you with an opportunity to test yourself.

? EXERCISE 4.8.2

Rework Example 4.6.5 and Example 4.6.6 using R.

Answer

Shown here are copies of R sessions for each problem. You will find small differences between the values given here for t_{exp} and for F_{exp} and those values shown with the worked solutions in the chapter. These differences arise because R does not round off the results of intermediate calculations.

Example 4.6.5

```
> AnalystA = c(86.82, 87.04, 86.93, 87.01, 86.20, 87.00)
> AnalystB = c(81.01, 86.15, 81.73, 83.19, 80.27, 83.94)
> var.test(AnalystB, AnalystA)
F test to compare two variances
data: AnalystB and AnalystA
F = 45.6358, num df = 5, denom df = 5, p-value = 0.0007148
alternative hypothesis: true ratio of variances is not equal to 1
95 percent confidence interval:
6.385863 326.130970
sample estimates:
ratio of variances
45.63582
> t.test(AnalystA, AnalystB, var.equal=FALSE)
Welch Two Sample t-test
data: AnalystA and AnalystB
t = 4.6147, df = 5.219, p-value = 0.005177
alternative hypothesis: true difference in means is not equal to 0
95 percent confidence interval: 1.852919 6.383748
sample estimates: mean of x mean of y
86.83333 82.71500
```

Example 4.21

```
> micro = c(129.5, 89.6, 76.6, 52.2, 110.8, 50.4, 72.4, 141.4, 75.0, 34.1, 60.3)
> elect = c(132.3, 91.0, 73.6, 58.2, 104.2, 49.9, 82.1, 154.1, 73.4, 38.1, 60.1)
```

```
> t.test(micro,elect,paired=TRUE)
Paired t-test
data: micro and elect
t = -1.3225, df = 10, p-value = 0.2155
alternative hypothesis: true difference in means is not equal to 0
95 percent confidence interval:
-6.028684 1.537775
sample estimates:
mean of the differences
–2.245455
```

Unlike Excel, R also includes functions for evaluating outliers. These functions are not part of R's standard installation. To install them enter the following command within R (*note: you will need an internet connection to download the package of functions*).

> install.packages("outliers")

After you install the package, you must load the functions into R by using the following command (*note: you need to do this step each time you begin a new R session as the package does not automatically load when you start R*).

> library("outliers")

You need to install a package once, but you need to load the package each time you plan to use it. There are ways to configure R so that it automatically loads certain packages; see *An Introduction to R* for more information (click here to view a PDF version of this document).

Let's use this package to find the outlier in Table 4.6.1 using both Dixon's *Q*-test and Grubb's test. The commands for these tests are

dixon.test(*X*, type = 10, two.sided = TRUE)

grubbs.test(*X*, type = 10, two.sided = TRUE)

where *X* is the object that contains the data, "type = 10" specifies that we are looking for one outlier, and "two.sided = TRUE" indicates that we are using the more conservative two-tailed test. Both tests have other variants that allow for the testing of outliers on both ends of the data set ("type = 11") or for more than one outlier ("type = 20"), but we will not consider these here. Figure 4.8.7 shows the output of a session for this problem. For both tests the very small *p*-value indicates that we can treat as an outlier the penny with a mass of 2.514 g.

```
> penny3=c(3.067,3.049, 3.039, 2.514, 3.048, 3.079, 3.094, 3.109, 3.102)
> dixon.test(penny3, type=10, two.sided=TRUE)

  Dixon test for outliers

data:  penny3
Q = 0.8824, p-value < 2.2e-16
alternative hypothesis: lowest value 2.514 is an outlier

> grubbs.test(penny3, type=10, two.sided=TRUE)

  Grubbs test for one outlier

data:  penny3
G = 2.6430, U = 0.0177, p-value = 1.938e-06
alternative hypothesis: lowest value 2.514 is an outlier
```

Figure 4.8.7 : Output of an R session for Dixon's *Q*-test and Grubb's test for outliers. The *p*-values for both tests show that we can treat as an outlier the penny with a mass of 2.514 g.

VISUALIZING DATA

One of R's more useful features is the ability to visualize data. Visualizing data is important because it provides us with an intuitive feel for our data that can help us in applying and evaluating statistical tests. It is tempting to believe that a statistical analysis is foolproof, particularly if the probability for incorrectly rejecting the null hypothesis is small. Looking at a visual display of our data, however, can help us determine whether our data is normally distributed—a requirement for most of the significance tests in this chapter—and can help us identify potential outliers. There are many useful ways to look at data, four of which we consider here.

Visualizing data is important, a point we will return to in Chapter 5 when we consider the mathematical modeling of data.

To plot data in R, we will use the package “lattice,” which you will need to load using the following command.

> library(“lattice”)

To demonstrate the types of plots we can generate, we will use the object “penny,” which contains the masses of the 100 pennies in Table 4.4.3.

> You do not need to use the command install.package this time because lattice was automatically installed on your computer when you downloaded R.

Our first visualization is a histogram. To construct the histogram we use mass to divide the pennies into bins and plot the number of pennies or the percent of pennies in each bin on the *y*-axis as a function of mass on the *x*-axis. Figure 4.8.8 shows the result of entering the command

> **histogram**(penny, type = “percent”, xlab = “Mass (g)”, ylab = “Percent of Pennies”, main = “Histogram of Data in Table 4.4.3”)

A histogram allows us to visualize the data’s distribution. In this example the data appear to follow a normal distribution, although the largest bin does not include the mean of 3.095 g and the distribution is not perfectly symmetric. One limitation of a histogram is that its appearance depends on how we choose to bin the data. Increasing the number of bins and centering the bins around the data’s mean gives a histogram that more closely approximates a normal distribution (Figure 4.4.5).

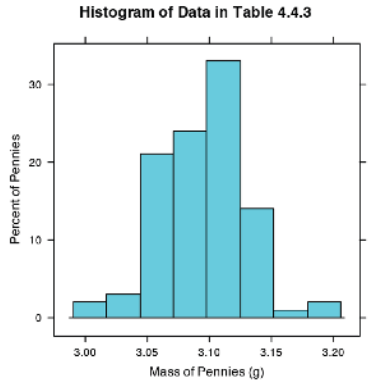


Figure 4.8.8 : Histogram of the data from Table 4.4.3.

An alternative to the histogram is a kernel density plot, which basically is a smoothed histogram. In this plot each value in the data set is replaced with a normal distribution curve whose width is a function of the data set’s standard deviation and size. The resulting curve is a summation of the individual distributions. Figure 4.8.9 shows the result of entering the command

> **densityplot**(penny, xlab = “Mass of Pennies (g)”, main = “Kernel Density Plot of Data in Table 4.4.3”)

The circles at the bottom of the plot show the mass of each penny in the data set. This display provides a more convincing picture that the data in Table 4.4.3 are normally distributed, although we see evidence of a small clustering of pennies with a mass of approximately 3.06 g.

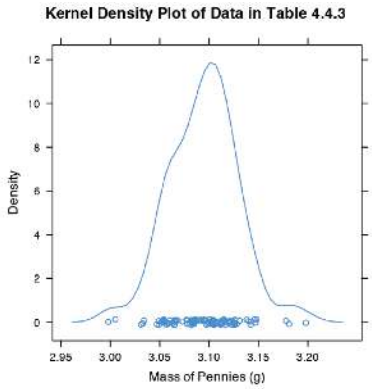


Figure 4.8.9 : Kernal plot of the data from Table 4.4.3.

We analyze samples to characterize the parent population. To reach a meaningful conclusion about a population, the samples must be representative of the population. One important requirement is that the samples are random. A dot chart provides a simple visual display that allows us to examine the data for non-random trends. Figure 4.8.10 shows the result of entering

> **dotchart**(penny, xlab = “Mass of Pennies (g)”, ylab = “Penny Number”, main = “Dotchart of Data in Table 4.4.3”)

In this plot the masses of the 100 pennies are arranged along the *y*-axis in the order in which they were sampled. If we see a pattern in the data along the *y*-axis, such as a trend toward smaller masses as we move from the first penny to the last penny, then we have clear evidence of non-random sampling. Because our data do not show a pattern, we have more confidence in the quality of our data.

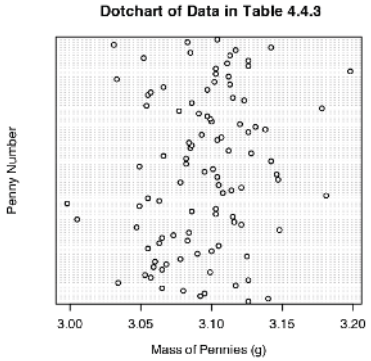


Figure 4.8.10 : Dot chart of the data from Table 4.4.3. Note that the dispersion of points along the *x*-axis is not uniform, with more points occurring near the center of the *x*-axis than at either end. This pattern is as expected for a normal distribution.

The last plot we will consider is a box plot, which is a useful way to identify potential outliers without making any assumptions about the data's distribution. A box plot contains four pieces of information about a data set: the median, the middle 50% of the data, the smallest value and the largest value within a set distance of the middle 50% of the data, and possible outliers. Figure 4.8.11 shows the result of entering

> **bwplot**(penny, xlab = "Mass of Pennies (g)", main = "Boxplot of Data in Table 4.4.3)"

The black dot (•) is the data set's median. The rectangular box shows the range of masses spanning the middle 50% of the pennies. This also is known as the interquartile range, or IQR. The dashed lines, which are called "whiskers," extend to the smallest value and the largest value that are within $\pm 1.5 \times \text{IQR}$ of the rectangular box. Potential outliers are shown as open circles (o). For normally distributed data the median is near the center of the box and the whiskers will be equidistant from the box. As is often the case in statistics, the converse is not true—finding that a boxplot is perfectly symmetric does not prove that the data are normally distributed.

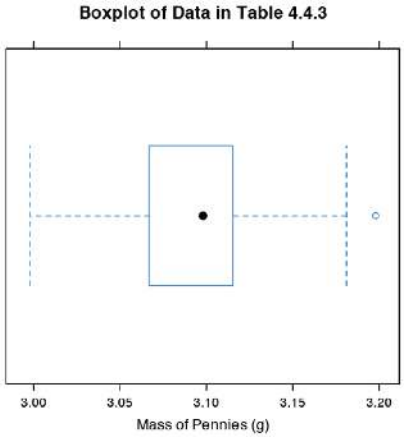


Figure 4.8.11 : Box plot of the data from Table 4.4.3.

To find the interquartile range you first find the median, which divides the data in half. The median of each half provides the limits for the box. The IQR is the median of the upper half of the data minus the median for the lower half of the data. For the data in Table 4.4.3 the median is 3.098. The median for the lower half of the data is 3.068 and the median for the upper half of the data is 3.115. The IQR is 3.115 – 3.068 = 0.047. You can use the command "summary(penny)" in R to obtain these values.

The lower "whisker" extend to the first data point with a mass larger than

$$3.068 - 1.5 \times \text{IQR} = 3.068 - 1.5 \times 0.047 = 2.9975$$

which for this data is 2.998 g. The upper "whisker" extends to the last data point with a mass smaller than

$$3.115 + 1.5 \times \text{IQR} = 3.115 + 1.5 \times 0.047 = 3.1855$$

which for this data is 3.181 g.

The box plot in Figure 4.8.11 is consistent with the histogram (Figure 4.8.8) and the kernel density plot (Figure 4.8.9). Together, the three plots provide evidence that the data in Table 4.4.3 are normally distributed. The potential outlier, whose mass of 3.198 g, is not sufficiently far away from the upper whisker to be of concern, particularly as the size of the data set (n = 100) is so large. A Grubb's test on the potential outlier does not provide evidence for treating it as an outlier.

? EXERCISE 4.8.3

Use R to create a data set consisting of 100 values from a uniform distribution by entering the command

> data = runif(100, min = 0, max = 100)

A uniform distribution is one in which every value between the minimum and the maximum is equally probable. Examine the data set by creating a histogram, a kernel density plot, a dot chart, and a box plot. Briefly comment on what the plots tell you about the your sample and its parent population.

Answer

Because we are selecting a random sample of 100 members from a uniform distribution, you will see subtle differences between your plots and the plots shown as part of this answer. Here is a record of my R session and the resulting plots.

> data = runif(100, min = 0, max = 0)

> data

[1] 18.928795 80.423589 39.399693 23.757624 30.088554

[6] 76.622174 36.487084 62.186771 81.115515 15.726404

[11] 85.765317 53.994179 7.919424 10.125832 93.153308

[16] 38.079322 70.268597 49.879331 73.115203 99.329723

[21] 48.203305 33.093579 73.410984 75.128703 98.682127

[26] 11.433861 53.337359 81.705906 95.444703 96.843476

[31] 68.251721 40.567993 32.761695 74.635385 70.914957

[36] 96.054750 28.448719 88.580214 95.059215 20.316015

[41] 9.828515 44.172774 99.648405 85.593858 82.745774

[46] 54.963426 65.563743 87.820985 17.791443 26.417481

[51] 72.832037 5.518637 58.231329 10.213343 40.581266

[56] 6.584000 81.261052 48.534478 51.830513 17.214508

[61] 31.232099 60.545307 19.197450 60.485374 50.414960

[66] 88.908862 68.939084 92.515781 72.414388 83.195206

[71] 74.783176 10.643619 41.775788 20.464247 14.547841

[76] 89.887518 56.217573 77.606742 26.956787 29.641171

[81] 97.624246 46.406271 15.906540 23.007485 17.715668

[86] 84.652814 29.379712 4.093279 46.213753 57.963604

[91] 91.160366 34.278918 88.352789 93.004412 31.055807

[96] 47.822329 24.052306 95.498610 21.089686 2.629948

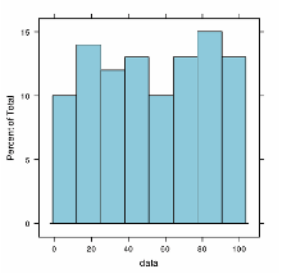
> histogram(data, type = "percent")

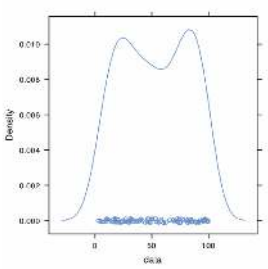
> densityplot(data)

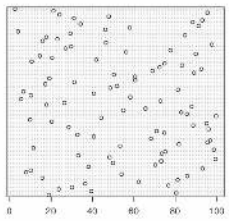
> dotchart(data)

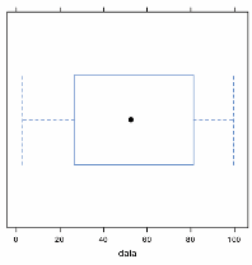
> bwplot(data)

The histogram (far left) divides the data into eight bins, each of which contains between 10 and 15 members. As we expect for a uniform distribution, the histogram's overall pattern suggests that each outcome is equally probable. In interpreting the kernel density plot (second from left), it is important to remember that it treats each data point as if it is from a normally distributed population (even though, in this case, the underlying population is uniform). Although the plot appears to suggest that there are two normally distributed populations, the individual results shown at the bottom of the plot provide further evidence for a uniform distribution. The dot chart (second from right) shows no trend along the y-axis, which indicates that the individual members of this sample were drawn at random from the population. The distribution along the x-axis also shows no pattern, as expected for a uniform distribution, Finally, the box plot (far right) shows no evidence of outliers.









This page titled 4.8: Using Excel and R to Analyze Data is shared under a CC BY-NC-SA 4.0 license and was authored, remixed, and/or curated by David Harvey.

- **4.8: Using Excel and R to Analyze Data** by David Harvey is licensed CC BY-NC-SA 4.0.

4.9: PROBLEMS

1. The following masses were recorded for 12 different U.S. quarters (all given in grams):

5.683	5.549	5.548	5.552
5.620	5.536	5.539	5.684
5.551	5.552	5.554	5.632

Report the mean, median, range, standard deviation and variance for this data.

2. A determination of acetaminophen in 10 separate tablets of Excedrin Extra Strength Pain Reliever gives the following results (in mg)

224.3	240.4	246.3	239.4	253.1
261.7	229.4	255.5	235.5	249.7

(a) Report the mean, median, range, standard deviation and variance for this data.

(b) Assuming that $\overline{X}$ and s^2 are good approximations for μ and for σ^2, and that the population is normally distributed, what percentage of tablets contain more than the standard amount of 250 mg acetaminophen per tablet?

The data in this problem are from Simonian, M. H.; Dinh, S.; Fray, L. A. *Spectroscopy* **1993**, *8(6)*, 37–47.

3. Salem and Galan developed a new method to determine the amount of morphine hydrochloride in tablets. An analysis of tablets with different nominal dosages gave the following results (in mg/tablet).

100-mg tablets	60-mg tablets	30-mg tablets	10-mg tablets
99.17	54.21	28.51	9.06
94.31	55.62	26.25	8.83
95.92	57.40	25.92	9.08
94.55	57.51	28.62	
93.83	52.59	24.93	

(a) For each dosage, calculate the mean and the standard deviation for the mg of morphine hydrochloride per tablet.

(b) For each dosage level, and assuming that $\overline{X}$ and s^2 are good approximations for μ and for σ^2, and that the population is normally distributed, what percentage of tablets contain more than the nominal amount of morphine hydro- chloride per tablet?

The data in this problem are from Salem, I. I.; Galan, A. C. Anal. Chim. Acta 1993, 283, 334–337.

4. Daskalakis and co-workers evaluated several procedures for digesting oyster and mussel tissue prior to analyzing them for silver. To evaluate the procedures they spiked samples with known amounts of silver and analyzed the samples to determine the amount of silver, reporting results as the percentage of added silver found in the analysis. A procedure was judged acceptable if its spike recoveries fell within the range 100±15%. The spike recoveries for one method are shown here.

105%	108%	92%	99%
101%	93%	93%	104%

Assuming a normal distribution for the spike recoveries, what is the probability that any single spike recovery is within the accepted range?

The data in this problem are from Daskalakis, K. D.; O'Connor, T. P.; Crecelius, E. A. *Environ. Sci. Technol.* **1997**, *31*, 2303– 2306. See Chapter 15 to learn more about using a spike recovery to evaluate an analytical method.

5. The formula weight (*FW*) of a gas can be determined using the following form of the ideal gas law

$$FW = \frac{g\mathrm{R}T}{PV}$$

where g is the mass in grams, R is the gas constant, T is the temperature in Kelvin, P is the pressure in atmospheres, and V is the volume in liters. In a typical analysis the following data are obtained (with estimated uncertainties in parentheses)

g = 0.118 g (± 0.002 g)

R = 0.082056 L atm mol^{-1} K^{-1} (± 0.000001 L atm mol^{-1} K^{-1})

T = 298.2 K (± 0.1 K)

P = 0.724 atm (± 0.005 atm)

V = 0.250 L (± 0.005 L)

(a) What is the compound's formula weight and its estimated uncertainty?

(b) To which variable(s) should you direct your attention if you wish to improve the uncertainty in the compound's molecular weight?

6. To prepare a standard solution of Mn^{2+}, a 0.250 g sample of Mn is dissolved in 10 mL of concentrated HNO_3 (measured with a graduated cylinder). The resulting solution is quantitatively transferred to a 100-mL volumetric flask and diluted to volume with distilled water. A 10-mL aliquot of the solution is pipeted into a 500-mL volumetric flask and diluted to volume.

(a) Express the concentration of Mn in mg/L, and estimate its uncertainty using a propagation of uncertainty.

(b) Can you improve the concentration's uncertainty by using a pipet to measure the HNO_3, instead of a graduated cylinder?

7. The mass of a hygroscopic compound is measured using the technique of weighing by difference. In this technique the compound is placed in a sealed container and weighed. A portion of the compound is removed and the container and the remaining material are reweighed. The difference between the two masses gives the sample's mass. A solution of a hygroscopic compound with a gram formula weight of 121.34 g/mol (±0.01 g/mol) is prepared in the following manner. A sample of the compound and its container has a mass of 23.5811 g. A portion of the compound is transferred to a 100-mL volumetric flask and diluted to volume. The mass of the compound and container after the transfer is 22.1559 g. Calculate the compound's molarity and estimate its uncertainty by a propagation of uncertainty.

8. Use a propagation of uncertainty to show that the standard error of the mean for n determinations is $\sigma/\sqrt{n}$.

9. Beginning with Equation 4.6.4 and Equation 4.6.5, use a propagation of uncertainty to derive Equation 4.6.6.

10. What is the smallest mass you can measure on an analytical balance that has a tolerance of ±0.1 mg, if the relative error must be less than 0.1%?

11. Which of the following is the best way to dispense 100.0 mL if we wish to minimize the uncertainty: (a) use a 50-mL pipet twice; (b) use a 25-mL pipet four times; or (c) use a 10-mL pipet ten times?

12. You can dilute a solution by a factor of 200 using readily available pipets (1-mL to 100-mL) and volumetric flasks (10-mL to 1000-mL) in either one step, two steps, or three steps. Limiting yourself to the glassware in Table 4.2.1, determine the proper combination of glassware to accomplish each dilution, and rank them in order of their most probable uncertainties.

13. Explain why changing all values in a data set by a constant amount will change $\overline{X}$ but has no effect on the standard deviation, s.

14. Obtain a sample of a metal, or other material, from your instructor and determine its density by one or both of the following methods:

Method A: Determine the sample's mass with a balance. Calculate the sample's volume using appropriate linear dimensions.

Method B: Determine the sample's mass with a balance. Calculate the sample's volume by measuring the amount of water it displaces by adding water to a graduated cylinder, reading the volume, adding the sample, and reading the new volume. The difference in volumes is equal to the sample's volume.

Determine the density at least five times.

(a) Report the mean, the standard deviation, and the 95% confidence interval for your results.

(b) Find the accepted value for the metal's density and determine the absolute and relative error for your determination of the metal's density.

(c) Use a propagation of uncertainty to determine the uncertainty for your method of analysis. Is the result of this calculation consistent with your experimental results? If not, suggest some possible reasons for this disagreement.

15. How many carbon atoms must a molecule have if the mean number of ^{13}C atoms per molecule is at least one? What percentage of such molecules will have no atoms of ^{13}C?

16. In Example 4.4.1 we determined the probability that a molecule of cholesterol, $C_{27}H_{44}O$, had no atoms of ^{13}C.

(a) Calculate the probability that a molecule of cholesterol, has 1 atom of ^{13}C.

(b) What is the probability that a molecule of cholesterol has two or more atoms of ^{13}C?

17. Berglund and Wichardt investigated the quantitative determination of Cr in high-alloy steels using a potentiometric titration of Cr(VI). Before the titration, samples of the steel were dissolved in acid and the chromium oxidized to Cr(VI) using peroxydisulfate. Shown here are the results (as %w/w Cr) for the analysis of a reference steel.

16.968	16.922	16.840	16.883
16.887	16.977	16.857	16.728

Calculate the mean, the standard deviation, and the 95% confidence interval about the mean. What does this confidence interval mean?

The data in this problem are from Berglund, B.; Wichardt, C. *Anal. Chim. Acta* **1990**, *236*, 399–410.

18. Ketkar and co-workers developed an analytical method to determine trace levels of atmospheric gases. An analysis of a sample that is 40.0 parts per thousand (ppt) 2-chloroethylsulfide gave the following results

43.3	34.8	31.9
37.8	34.4	31.9
42.1	33.6	35.3

(a) Determine whether there is a significant difference between the experimental mean and the expected value at $\alpha = 0.05$.

(b) As part of this study, a reagent blank was analyzed 12 times giving a mean of 0.16 ppt and a standard deviation of 1.20 ppt. What are the IUPAC detection limit, the limit of identification, and limit of quantitation for this method assuming $\alpha = 0.05$?

The data in this problem are from Ketkar, S. N.; Dulak, J. G.; Dheandhanou, S.; Fite, W. L. *Anal. Chim. Acta* **1991**, *245*, 267–270.

19. To test a spectrophotometer's accuracy a solution of 60.06 ppm $K_2Cr_2O_7$ in 5.0 mM H_2SO_4 is prepared and analyzed. This solution has an expected absorbance of 0.640 at 350.0 nm in a 1.0-cm cell when using 5.0 mM H_2SO_4 as a reagent blank. Several aliquots of the solution produce the following absorbance values.

0.639	0.638	0.640	0.639	0.640	0.639	0.638

Determine whether there is a significant difference between the experimental mean and the expected value at $\alpha = 0.01$.

20. Monna and co-workers used radioactive isotopes to date sediments from lakes and estuaries. To verify this method they analyzed a ^{208}Po standard known to have an activity of 77.5 decays/min, obtaining the following results.

77.09	75.37	72.42	76.84	77.84	76.69
78.03	74.96	77.54	76.09	81.12	75.75

Determine whether there is a significant difference between the mean and the expected value at $\alpha = 0.05$.

The data in this problem are from Monna, F.; Mathieu, D.; Marques, A. N.; Lancelot, J.; Bernat, M. *Anal. Chim. Acta* **1996**, *330*, 107–116.

21. A 2.6540-g sample of an iron ore, which is 53.51% w/w Fe, is dissolved in a small portion of concentrated HCl and diluted to volume in a 250-mL volumetric flask. A spectrophotometric determination of the concentration of Fe in this solution yields results of 5840, 5770, 5650, and 5660 ppm. Determine whether there is a significant difference between the experimental mean and the expected value at $\alpha = 0.05$.

22. Horvat and co-workers used atomic absorption spectroscopy to determine the concentration of Hg in coal fly ash. Of particular interest to the authors was developing an appropriate procedure for digesting samples and releasing the Hg for analysis. As part of their study they tested several reagents for digesting samples. Their results using HNO_3 and using a 1 + 3 mixture of HNO_3 and HCl are shown here. All concentrations are given as ppb Hg sample.

HNO_3:	161	165	160	167	166	
1 + 3 HNO_3 – HCl:	159	145	140	147	143	156

Determine whether there is a significant difference between these methods at $\alpha = 0.05$.

The data in this problem are from Horvat, M.; Lupsina, V.; Pihlar, B. *Anal. Chim. Acta* **1991**, *243*, 71–79.

23, Lord Rayleigh, John William Strutt (1842-1919), was one of the most well known scientists of the late nineteenth and early twentieth centuries, publishing over 440 papers and receiving the Nobel Prize in 1904 for the discovery of argon. An important turning point in Rayleigh's discovery of Ar was his experimental measurements of the density of N_2. Rayleigh approached this experiment in two ways: first by taking atmospheric air and removing O_2 and H_2; and second, by chemically producing N_2 by decomposing nitrogen containing compounds (NO, N_2O, and NH_4NO_3) and again removing O_2 and H_2. The following table shows his results for the density of N_2, as published in *Proc. Roy. Soc.* **1894**, *LV*, 340 (publication 210); all values are the grams of gas at an equivalent volume, pressure, and temperature.

atmospheric origin	chemical origin
2.31017	2.30143
2.30986	2.29890
2.31010	2.29816
2.31001	2.30182
2.31024	2.29869
2.31010	2.29940
2.31028	2.29849
	2.29889

Explain why this data led Rayleigh to look for and to discover Ar. You can read more about this discovery here: Larsen, R. D. *J. Chem. Educ.* **1990**, *67*, 925–928.

24. Gács and Ferraroli reported a method for monitoring the concentration of SO_2 in air. They compared their method to the standard method by analyzing urban air samples collected from a single location. Samples were collected by drawing air through a collection solution for 6 min. Shown here is a summary of their results with SO_2 concentrations reported in $\mu L/m^3$.

standard method	new method
21.62	21.54
22.20	20.51
24.27	22.31
23.54	21.30
24.25	24.62
23.09	25.72
21.02	21.54

Using an appropriate statistical test, determine whether there is any significant difference between the standard method and the new method at $\alpha = 0.05$.

The data in this problem are from Gács, I.; Ferraroli, R. *Anal. Chim. Acta* **1992**, *269*, 177–185.

25. One way to check the accuracy of a spectrophotometer is to measure absorbances for a series of standard dichromate solutions obtained from the National Institute of Standards and Technology. Absorbances are measured at 257 nm and compared to the accepted values. The results obtained when testing a newly purchased spectrophotometer are shown here. Determine if the tested spectrophotometer is accurate at $\alpha = 0.05$.

standard	measured absorbance	expected absorbance
1	0.2872	0.2871
2	0.5773	0.5760
3	0.8674	0.8677
4	1.1623	1.1608
5	1.4559	1.4565

26. Maskarinec and co-workers investigated the stability of volatile organics in environmental water samples. Of particular interest was establishing the proper conditions to maintain the sample's integrity between its collection and its analysis. Two preservatives were investigated—ascorbic acid and sodium bisulfate—and maximum holding times were determined for a number of volatile organics and water matrices. The following table shows results for the holding time (in days) of nine organic compounds in surface water.

compound	Ascorbic Acid	Sodium Bisulfate
methylene chloride	77	62
carbon disulfide	23	54
trichloroethane	52	51
benzene	62	42
1,1,2-trichlorethane	57	53
1,1,2,2-tetrachloroethane	33	85
tetrachloroethene	32	94
chlorbenzene	36	86

Determine whether there is a significant difference in the effectiveness of the two preservatives at $\alpha = 0.10$.

The data in this problem are from Maxkarinec, M. P.; Johnson, L. H.; Holladay, S. K.; Moody, R. L.; Bayne, C. K.; Jenkins, R. A. *Environ. Sci. Technol.* **1990**, *24*, 1665–1670.

27. Using X-ray diffraction, Karstang and Kvalhein reported a new method to determine the weight percent of kaolinite in complex clay minerals using X-ray diffraction. To test the method, nine samples containing known amounts of kaolinite were prepared and analyzed. The results (as % w/w kaolinite) are shown here.

actual	5.0	10.0	20.0	40.0	50.0	60.0	80.0	90.0	95.0
found	6.8	11.7	19.8	40.5	53.6	61.7	78.9	91.7	94.7

Evaluate the accuracy of the method at $\alpha = 0.05$.

The data in this problem are from Karstang, T. V.; Kvalhein, O. M. *Anal. Chem.* **1991**, *63*, 767–772.

28. Mizutani, Yabuki and Asai developed an electrochemical method for analyzing *l*-malate. As part of their study they analyzed a series of beverages using both their method and a standard spectrophotometric procedure based on a clinical kit purchased from Boerhinger Scientific. The following table summarizes their results. All values are in ppm.

Sample	Electrode	Spectrophotometric
Apple Juice 1	34.0	33.4
Apple Juice 2	22.6	28.4
Apple Juice 3	29.7	29.5
Apple Juice 4	24.9	24.8
Grape Juice 1	17.8	18.3
Grape Juice 2	14.8	15.4
Mixed Fruit Juice 1	8.6	8.5
Mixed Fruit Juice 2	31.4	31.9
White Wine 1	10.8	11.5
White Wine 2	17.3	17.6
White Wine 3	15.7	15.4
White Wine 4	18.4	18.3

The data in this problem are from Mizutani, F.; Yabuki, S.; Asai, M. *Anal. Chim. Acta* **1991**, *245*,145–150.

29. Alexiev and colleagues describe an improved photometric method for determining Fe^{3+} based on its ability to catalyze the oxidation of sulphanilic acid by KIO_4. As part of their study, the concentration of Fe^{3+} in human serum samples was determined by the improved method and the standard method. The results, with concentrations in $\mu\text{mol/L}$, are shown in the following table.

Sample	Improved Method	Standard Method
1	8.25	8.06
2	9.75	8.84
3	9.75	8.36
4	9.75	8.73
5	10.75	13.13
6	11.25	13.65
7	13.88	13.85
8	14.25	13.43

Determine whether there is a significant difference between the two methods at $\alpha = 0.05$.

The data in this problem are from Alexiev, A.; Rubino, S.; Deyanova, M.; Stoyanova, A.; Sicilia, D.; Perez Bendito, D. *Anal. Chim. Acta*, **1994**, *295*, 211–219.

30. Ten laboratories were asked to determine an analyte's concentration of in three standard test samples. Following are the results, in $\mu\text{g/ml}$.

Laboratory	Sample 1	Sample 2	Sample 3
1	22.6	13.6	16.0
2	23.0	14.2	15.9
3	21.5	13.9	16.9
4	21.9	13.9	16.9
5	21.3	13.5	16.7
6	22.1	13.5	17.4
7	23.1	13.5	17.5
8	21.7	13.5	16.8
9	22.2	12.9	17.2
10	21.7	13.8	16.7

Determine if there are any potential outliers in Sample 1, Sample 2 or Sample 3. Use all three methods—Dixon's *Q*-test, Grubb's test, and Chauvenet's criterion—and compare the results to each other. For Dixon's *Q*-test and for the Grubb's test, use a significance level of $\alpha = 0.05$.

The data in this problem are adapted from Steiner, E. H. "Planning and Analysis of Results of Collaborative Tests," in *Statistical Manual of the Association of Official Analytical Chemists*, Association of Official Analytical Chemists: Washington, D. C., 1975.

31.When copper metal and powdered sulfur are placed in a crucible and ignited, the product is a sulfide with an empirical formula of Cu_xS. The value of x is determined by weighing the Cu and the S before ignition and finding the mass of Cu_xS when the reaction is complete (any excess sulfur leaves as SO_2). The following table shows the Cu/S ratios from 62 such experiments (note that the values are organized from smallest-to-largest by rows).

1.764	1.838	1.865	1.866	1.872	1.877
1.890	1.891	1.891	1.897	1.899	1.900
1.906	1.908	1.910	1.911	1.916	1.919
1.920	1.922	1.927	1.931	1.935	1.936
1.936	1.937	1.939	1.939	1.940	1.941
1.941	1.942	1.943	1.948	1.953	1.955
1.957	1.957	1.957	1.959	1.962	1.963
1.963	1.963	1.966	1.968	1.969	1.973
1.975	1.976	1.977	1.981	1.981	1.988
1.993	1.993	1.995	1.995	1.995	2.017
2.029	2.042				

(a) Calculate the mean, the median, and the standard deviation for this data.

(b) Construct a histogram for this data. From a visual inspection of your histogram, do the data appear normally distributed?

(c) In a normally distributed population 68.26% of all members lie within the range $\mu \pm 1\sigma$. What percentage of the data lies within the range $\overline{X} \pm 1\sigma$? Does this support your answer to the previous question?

(d) Assuming that $\overline{X}$ and s^2 are good approximations for μ and for σ^2, what percentage of all experimentally determined Cu/S ratios should be greater than 2? How does this compare with the experimental data? Does this support your conclusion about whether the data is normally distributed?

(e) It has been reported that this method of preparing copper sulfide results in a non-stoichiometric compound with a Cu/S ratio of less than 2. Determine if the mean value for this data is significantly less than 2 at a significance level of $\alpha = 0.01$.

See Blanchnik, R.; Müller, A. "The Formation of Cu_2S From the Elements I. Copper Used in Form of Powders," *Thermochim. Acta*, **2000**, *361*, 31-52 for a discussion of some of the factors affecting the formation of non-stoichiometric copper sulfide. The data in this problem were collected by students at DePauw University.

32. Real-time quantitative PCR is an analytical method for determining trace amounts of DNA. During the analysis, each cycle doubles the amount of DNA. A probe species that fluoresces in the presence of DNA is added to the reaction mixture and the increase in fluorescence is monitored during the cycling. The cycle threshold, C_t, is the cycle when the fluorescence exceeds a threshold value. The data in the following table shows C_t values for three samples using real-time quantitative PCR. Each sample was analyzed 18 times.

Sample X		Sample Y		Sample Z	
24.24	25.14	24.41	28.06	22.97	23.43
23.97	24.57	27.21	27.77	22.93	23.66
24.44	24.49	27.02	28.74	22.95	28.79
24.79	24.68	26.81	28.35	23.12	23.77
23.92	24.45	26.64	28.80	23.59	23.98
24.53	24,48	27.63	27.99	23.37	23.56
24.95	24.30	28.42	28.21	24.17	22.80
24.76	24.60	25.16	28.00	23.48	23.29
25.18	24.57	28.53	28.21	23.80	23.86

Examine this data and write a brief report on your conclusions. Issues you may wish to address include the presence of outliers in the samples, a summary of the descriptive statistics for each sample, and any evidence for a difference between the samples.

The data in this problem is from Burns, M. J.; Nixon, G. J.; Foy, C. A.; Harris, N. *BMC Biotechnol.* **2005**, *5:31* (open access publication).

This page titled 4.9: Problems is shared under a CC BY-NC-SA 4.0 license and was authored, remixed, and/or curated by David Harvey.

- **4.9: Problems** by David Harvey is licensed CC BY-NC-SA 4.0.

4.10: ADDITIONAL RESOURCES

The following experiments provide useful introductions to the statistical analysis of data in the analytical chemistry laboratory.

- Bularzik, J. "The Penny Experiment Revisited: An Illustration of Significant Figures, Accuracy, Precision, and Data Analysis," *J. Chem. Educ.* **2007**, *84*, 1456–1458.
- Columbia, M. R. "The Statistics of Coffee: 1. Evaluation of Trace Metals for Establishing a Coffee's Country of Origin Based on a Means Comparison," *Chem. Educator* **2007**, *12*, 260–262.
- Cunningham, C. C.; Brown, G. R.; St Pierre, L. E. "Evaluation of Experimental Data," *J. Chem. Educ.* **1981**, *58*, 509–511.
- Edminston, P. L.; Williams, T. R. "An Analytical Laboratory Experiment in Error Analysis: Repeated Determination of Glucose Using Commercial Glucometers," *J. Chem. Educ.* **2000**, *77*, 377–379.
- Gordus, A. A. "Statistical Evaluation of Class Data for Two Buret Readings," *J. Chem. Educ.* **1987**, *64*, 376–377.
- Harvey, D. T. "Statistical Evaluation of Acid/Base Indicators," *J. Chem. Educ.* **1991**, *68*, 329–331.
- Hibbert, D. B. "Teaching modern data analysis with The Royal Austrian Chemical Institute's titration competition," *Aust. J. Ed. Chem.* **2006**, *66*, 5–11.
- Johll, M. E.; Poister, D.; Ferguson, J. "Statistical Comparison of Multiple Methods for the Determination of Dissolved Oxygen Levels in Natural Water," *Chem. Educator* **2002**, *7*, 146–148.
- Jordon, A. D. "Which Method is Most Precise; Which is Most Accurate?," *J. Chem. Educ.* **2007**, *84*, 1459–1460.
- Olsen, R. J. "Using Pooled Data and Data Visualization To Introduce Statistical Concepts in the General Chemistry Laboratory," *J. Chem. Educ.* **2008**, *85*, 544–545.
- O'Reilley, J. E. "The Length of a Pestle," *J. Chem. Educ.* **1986**, *63*, 894–896.
- Overway, K. "Population versus Sampling Statistics: A Spreadsheet Exercise," *J. Chem. Educ.* **2008** *85*, 749.
- Paselk, R. A. "An Experiment for Introducing Statistics to Students of Analytical and Clinical Chem- istry," *J. Chem. Educ.* **1985**, *62*, 536.
- Puignou, L.; Llauradó, M. "An Experimental Introduction to Interlaboratory Exercises in Analytical Chemistry," *J. Chem. Educ.* **2005**, *82*, 1079–1081.
- Quintar, S. E.; Santagata, J. P.; Villegas, O. I.; Cortinez, V. A. "Detection of Method Effects on Quality of Analytical Data," *J. Chem. Educ.* **2003**, *80*, 326–329.
- Richardson, T. H. "Reproducible Bad Data for Instruction in Statistical Methods," *J. Chem. Educ.* **1991**, *68*, 310–311.
- Salzsieder, J. C. "Statistical Analysis Experiment for Freshman Chemistry Lab," *J. Chem. Educ.* **1995**, *72*, 623.
- Samide, M. J. "Statistical Comparison of Data in the Analytical Laboratory," *J. Chem. Educ.* **2004**, *81*, 1641–1643.
- Sheeran, D. "Copper Content in Synthetic Copper Carbonate: A Statistical Comparison of Experimental and Expected Results," *J. Chem. Educ.* **1998**, *75*, 453–456.
- Spencer, R. D. "The Dependence of Strength in Plastics upon Polymer Chain Length and Chain Orientation," *J. Chem. Educ.* **1984**, *61*, 555–563.
- Stolzberg, R. J. "Do New Pennies Lose Their Shells? Hypothesis Testing in the Sophomore Analytical Chemistry Laboratory," *J. Chem. Educ.* **1998**, *75*, 1453–1455.
- Stone, C. A.; Mumaw, L. D. "Practical Experiments in Statistics," *J. Chem. Educ.* **1995**, *72*, 518– 524.
- Thomasson, K.; Lofthus-Merschman, S.; Humbert, M.; Kulevsky, N. "Applying Statistics in the Undergraduate Chemistry Laboratory: Experiments with Food Dyes," *J. Chem. Educ.* **1998**, *75*, 231–233.
- Vitha, M. F.; Carr, P. W. "A Laboratory Exercise in Statistical Analysis of Data," *J. Chem. Educ.* **1997**, *74*, 998–1000.

A more comprehensive discussion of the analysis of data, which includes all topics considered in this chapter as well as additional material, are found in many textbook on statistics or data analysis; several such texts are listed here.

- Anderson, R. L. *Practical Statistics for Analytical Chemists*, Van Nostrand Reinhold: New York; 1987.
- Graham, R. C. *Data Analysis for the Chemical Sciences*, VCH Publishers: New York; 1993.
- Mark, H.; Workman, J. *Statistics in Spectroscopy*, Academic Press: Boston; 1991.
- Mason, R. L.; Gunst, R. F.; Hess, J. L. *Statistical Design and Analysis of Experiments*; Wiley: New York, 1989.
- Massart, D. L.; Vandeginste, B. G. M.; Buydens, L. M. C.; De Jong, S.; Lewi, P. J.; Smeyers-Verbeke, J. *Handbook of Chemometrics and Qualimetrics*, Elsevier: Amsterdam, 1997.
- Miller, J. C.; Miller, J. N. *Statistics for Analytical Chemistry*, Ellis Horwood PTR Prentice-Hall: New York; 3rd Edition, 1993.
- *NIST/SEMATECH e-Handbook of Statistical Methods*, http://www.itl.nist.gov/div898/handbook/, 2006.
- Sharaf, M. H.; Illman, D. L.; Kowalski, B. R. *Chemometrics*, Wiley-Interscience: New York; 1986.

The importance of defining statistical terms is covered in the following papers.

- Analytical Methods Committee "Terminology—the key to understanding analytical science. Part 1: Accuracy, precision and uncertainty," AMC Technical Brief No. 13, Sept. 2003.

- Goedart, M. J.; Verdonk, A. H. “The Development of Statistical Concepts in a Design-Oriented Laboratory Course in Scientific Measuring,” *J. Chem. Educ.* **1991**, *68*, 1005–1009.
- Sánchez, J. M. “Teaching Basic Applied Statistics in University Chemistry Courses: Students’ Misconceptions,” *Chem. Educator* **2006**, *11*, 1–4.
- Thompson, M. “Towards a unified model of errors in analytical measurements,” *Analyst* **2000**, *125*, 2020–2025.
- Treptow, R. S. “Precision and Accuracy in Measurements,” *J. Chem. Educ.* **1998**, *75*, 992–995.

The detection of outliers, particularly when working with a small number of samples, is discussed in the following papers.

- Analytical Methods Committee “Robust Statistics—How Not To Reject Outliers Part 1. Basic Concepts,” *Analyst* **1989**, *114*, 1693–1697.
- Analytical Methods Committee “Robust Statistics—How Not to Reject Outliers Part 2. Inter-laboratory Trials,” *Analyst* **1989**, *114*, 1699–1702.
- Analytical Methods Committee “Rogues and Suspects: How to Tackle Outliers,” AMCTB 39, 2009.
- Analytical Methods Committee “Robust statistics: a method of coping with outliers,” AMCTB 6, 2001.
- Analytical Methods Committee “Using the Grubbs and Cochran tests to identify outliers,” *Anal. Meth- ods*, **2015**, *7*, 7948–7950.
- Efstathiou, C. “Stochastic Calculation of Critical Q-Test Values for the Detection of Outliers in Measurements,” *J. Chem. Educ.* **1992**, *69*, 773–736.
- Efstathiou, C. “Estimation of type 1 error probability from experimental Dixon’s Q parameter on testing for outliers within small data sets,” *Talanta* **2006**, *69*, 1068–1071.
- Kelly, P. C. “Outlier Detection in Collaborative Studies,” *Anal. Chem.* **1990**, *73*, 58–64.
- Mitschele, J. “Small Sample Statistics,” *J. Chem. Educ.* **1991**, *68*, 470–473.

The following papers provide additional information on error and uncertainty, including the propagation of uncertainty.

- Analytical Methods Committee “Optimizing your uncertainty—a case study,” AMCTB 32, 2008.
- Analytical Methods Committee “Dark Uncertainty,” AMCTB 53, 2012.
- Analytical Methods Committee “What causes most errors in chemical analysis?” AMCTB 56, 2013.
- Andraos, J. “On the Propagation of Statistical Errors for a Function of Several Variables,” *J. Chem. Educ*. **1996**, *73*, 150–154.
- Donato, H.; Metz, C. “A Direct Method for the Propagation of Error Using a Personal Computer Spreadsheet Program,” *J. Chem. Educ.* **1988**, *65*, 867–868.
- Gordon, R.; Pickering, M.; Bisson, D. “Uncertainty Analysis by the ‘Worst Case’ Method,” *J. Chem. Educ.* **1984**, *61*, 780–781.
- Guare, C. J. “Error, Precision and Uncertainty,” *J. Chem. Educ.* **1991**, *68*, 649–652.
- Guedens, W. J.; Yperman, J.; Mullens, J.; Van Poucke, L. C.; Pauwels, E. J. “Statistical Analysis of Errors: A Practical Approach for an Undergraduate Chemistry Lab Part 1. The Concept,” *J. Chem. Educ.* **1993**, *70*, 776–779
- Guedens, W. J.; Yperman, J.; Mullens, J.; Van Poucke, L. C.; Pauwels, E. J. “Statistical Analysis of Errors: A Practical Approach for an Undergraduate Chemistry Lab Part 2. Some Worked Examples,” *J. Chem. Educ.* **1993**, *70*, 838–841.
- Heydorn, K. “Detecting Errors in Micro and Trace Analysis by Using Statistics,” *Anal. Chim. Acta* **1993**, *283*, 494–499.
- Hund, E.; Massart, D. L.; Smeyers-Verbeke, J. “Operational definitions of uncertainty,” *Trends Anal. Chem.* **2001**, *20*, 394–406.
- Kragten, J. “Calculating Standard Deviations and Confidence Intervals with a Universally Applicable Spreadsheet Technique,” *Analyst* **1994**, *119*, 2161–2165.
- Taylor, B. N.; Kuyatt, C. E. “Guidelines for Evaluating and Expressing the Uncertainty of NIST Mea- surement Results,” NIST Technical Note 1297, 1994.
- Van Bramer, S. E. “A Brief Introduction to the Gaussian Distribution, Sample Statistics, and the Student’s t Statistic,” *J. Chem. Educ.* **2007**, *84*, 1231.
- Yates, P. C. “A Simple Method for Illustrating Uncertainty Analysis,” *J. Chem. Educ.* **2001**, *78*, 770–771.

Consult the following resources for a further discussion of detection limits.

- Boumans, P. W. J. M. “Detection Limits and Spectral Interferences in Atomic Emission Spectrometry,” *Anal. Chem.* **1984**, *66*, 459A–467A.
- Currie, L. A. “Limits for Qualitative Detection and Quantitative Determination: Application to Radiochemistry,” *Anal. Chem.* **1968**, *40*, 586–593.
- Currie, L. A. (ed.) *Detection in Analytical Chemistry: Importance, Theory and Practice*, American Chemical Society: Washington, D. C., 1988.
- Ferrus, R.; Egea, M. R. “Limit of discrimination, limit of detection and sensitivity in analytical systems,” *Anal. Chim. Acta* **1994**, *287*, 119–145.
- Fonollosa, J.; Vergara, A; Huerta, R.; Marco, S. “Estimation of the limit of detection using information theory measures,” *Anal. Chim. Acta* **2014**, *810*, 1–9.

- Glaser, J. A.; Foerst, D. L.; McKee, G. D.; Quave, S. A.; Budde, W. L. “Trace analyses for wastewaters,” *Environ. Sci. Technol.* **1981**, *15*, 1426–1435.
- Kimbrough, D. E.; Wakakuwa, J. “Quality Control Level: An Introduction to Detection Levels,” *Environ. Sci. Technol.* **1994**, *28*, 338–345.

The following articles provide thoughts on the limitations of statistical analysis based on significance testing.

- Analytical Methods Committee “Significance, importance, and power,” AMCTB 38, 2009.
- Analytical Methods Committee “An introduction to non-parametric statistics,” AMCTB 57, 2013.
- Berger, J. O.; Berry, D. A. “Statistical Analysis and the Illusion of Objectivity,” *Am. Sci.* **1988**, *76*, 159–165.
- Kryzwinski, M. “Importance of being uncertain,” *Nat. Methods* **2013**, *10*, 809–810.
- Kryzwinski, M. “Significance, P values, and t-tests,” *Nat. Methods* **2013**, *10*, 1041–1042.
- Kryzwinski, M. “Power and sample size,” *Nat. Methods* **2013**, *10*, 1139–1140.
- Leek, J. T.; Peng, R. D. “What is the question?,” *Science* **2015**, *347*, 1314–1315.

The following resources provide additional information on using Excel, including reports of errors in its handling of some statistical procedures.

- McCollough, B. D.; Wilson, B. “On the accuracy of statistical procedures in Microsoft Excel 2000 and Excel XP,” *Comput. Statist. Data Anal.* **2002**, *40*, 713–721.
- Morgon, S. L.; Deming, S. N. “Guide to Microsoft *Excel* for calculations, statistics, and plotting data,”
- (http://www.chem.sc.edu/faculty/morga...ide_Morgan.pdf).
- Kelling, K. B.; Pavur, R. J. “A Comparative Study of the Reliability of Nine Statistical Software Pack-ages,” *Comput. Statist. Data Anal.* **2007**, *51*, 3811–3831.

To learn more about using R, consult the following resources.

- Chambers, J. M. *Software for Data Analysis: Programming with R*, Springer: New York, 2008.
- Maindonald, J.; Braun, J. *Data Analysis and Graphics Using R*, Cambridge University Press: Cambridge, UK, 2003.
- Sarkar, D. *Lattice: Multivariate Data Visualization With R*, Springer: New York, 2008.

The following papers provide insight into visualizing data.

- Analytical Methods Committee “Representing data distributions with kernel density estimates,” AMC Technical Brief, March 2006.
- Frigge, M.; Hoaglin, D. C.; Iglewicz, B. “Some Implementations of the Boxplot,” *The American Statistician* **1989**, *43*, 50–54.

This page titled 4.10: Additional Resources is shared under a CC BY-NC-SA 4.0 license and was authored, remixed, and/or curated by David Harvey.

- **4.10: Additional Resources** by David Harvey is licensed CC BY-NC-SA 4.0.

4.11: CHAPTER SUMMARY AND KEY TERMS

SUMMARY

The data we collect are characterized by their central tendency (where the values cluster), and their spread (the variation of individual values around the central value). We report our data's central tendency by stating the mean or median, and our data's spread using the range, standard deviation or variance. Our collection of data is subject to errors, including determinate errors that affect the data's accuracy and indeterminate errors that affect its precision. A propagation of uncertainty allows us to estimate how these determinate and indeterminate errors affect our results.

When we analyze a sample several times the distribution of the results is described by a probability distribution, two examples of which are the binomial distribution and the normal distribution. Knowing the type of distribution allows us to determine the probability of obtaining a particular range of results. For a normal distribution we express this range as a confidence interval.

A statistical analysis allows us to determine whether our results are significantly different from known values, or from values obtained by other analysts, by other methods of analysis, or for other samples. We can use a *t*-test to compare mean values and an *F*-test to compare variances. To compare two sets of data you first must determine whether the data is paired or unpaired. For unpaired data you also must decide if you can pool the standard deviations. A decision about whether to retain an outlying value can be made using Dixon's *Q*-test, Grubb's test, or Chauvenet's criterion.

You should be sure to exercise caution if you decide to reject an outlier. Finally, the detection limit is a statistical statement about the smallest amount of analyte we can detect with confidence. A detection limit is not exact since its value depends on how willing we are to falsely report the analyte's presence or absence in a sample. When reporting a detection limit you should clearly indicate how you arrived at its value.

KEY TERMS

alternative hypothesis
bias
binomial distribution
box plot
central limit theorem
Chauvenet's criterion
confidence interval
constant determinate error
degrees of freedom
detection limit
determinate error
Dixon's *Q*-test
dot chart
error
F-test
Grubb's test
histogram
indeterminate error
kernel density plot
limit of identification
limit of quantitation
mean
median
measurement error
method error
normal distribution
null hypothesis
one-tailed significance test
outlier
paired data
paired t-test
personal error
population
probability distribution
propagation of uncertainty
proportional determinate error
range
repeatability
reproducibility
sample
sampling error
significance test
standard deviation
standard error of the mean
Standard Reference Material
tolerance
t-test
two-tailed significance test
type 1 error
type 2 error
uncertainty
unpaired data
variance

This page titled 4.11: Chapter Summary and Key Terms is shared under a CC BY-NC-SA 4.0 license and was authored, remixed, and/or curated by David Harvey.

- **4.11: Chapter Summary and Key Terms** by David Harvey is licensed CC BY-NC-SA 4.0.

CHAPTER OVERVIEW

5: STANDARDIZING ANALYTICAL METHODS

The American Chemical Society's Committee on Environmental Improvement defines standardization as the process of determining the relationship between the signal and the amount of analyte in a sample. In Chapter 3 we defined this relationship as

$$S_{total} = k_A n_A + S_{reag} \text{ or } S_{total} = k_A C_A + S_{reag}$$

where S_{total} is the signal, n_A is the moles of analyte, C_A is the analyte's concentration, k_A is the method's sensitivity for the analyte, and S_{reag} is the contribution to S_{total} from sources other than the sample. To standardize a method we must determine values for k_A and S_{reag}. Strategies for accomplishing this are the subject of this chapter.

5.1: Analytical Signals
5.2: Calibrating the Signal
5.3: Determining the Sensitivity
5.4: Linear Regression and Calibration Curves
5.5: Compensating for the Reagent Blank
5.6: Using Excel and R for a Linear Regression
5.7: Problems
5.8: Additional Resources
5.9: Chapter Summary and Key Terms

This page titled 5: Standardizing Analytical Methods is shared under a CC BY-NC-SA 4.0 license and was authored, remixed, and/or curated by David Harvey.

5.1: ANALYTICAL SIGNALS

To standardize an analytical method we use standards that contain known amounts of analyte. The accuracy of a standardization, therefore, depends on the quality of the reagents and the glassware we use to prepare these standards. For example, in an acid–base titration the stoichiometry of the acid–base reaction defines the relationship between the moles of analyte and the moles of titrant. In turn, the moles of titrant is the product of the titrant's concentration and the volume of titrant used to reach the equivalence point. The accuracy of a titrimetric analysis, therefore, is never better than the accuracy with which we know the titrant's concentration.

> See Chapter 9 for a thorough discussion of titrimetric methods of analysis.

PRIMARY AND SECONDARY STANDARDS

There are two categories of analytical standards: primary standards and secondary standards. A ***primary standard*** is a reagent that we can use to dispense an accurately known amount of analyte. For example, a 0.1250-g sample of $K_2Cr_2O_7$ contains 4.249×10^{-4} moles of $K_2Cr_2O_7$. If we place this sample in a 250-mL volumetric flask and dilute to volume, the concentration of $K_2Cr_2O_7$ in the resulting solution is 1.700×10^{-3} M . A primary standard must have a known stoichiometry, a known purity (or assay), and it must be stable during long-term storage. Because it is difficult to establishing accurately the degree of hydration, even after drying, a hydrated reagent usually is not a primary standard.

Reagents that do not meet these criteria are secondary standards. The concentration of a ***secondary standard*** is determined relative to a primary standard. Lists of acceptable primary standards are available (see, for instance, Smith, B. W.; Parsons, M. L. *J. Chem. Educ.* **1973**, *50*, 679–681; or Moody, J. R.; Green- burg, P. R.; Pratt, K. W.; Rains, T. C. *Anal. Chem.* **1988**, *60*, 1203A–1218A). Appendix 8 provides examples of some common primary standards.

> NaOH is one example of a secondary standard. Commercially available NaOH contains impurities of NaCl, Na_2CO_3, and Na_2SO_4, and readily absorbs H_2O from the atmosphere. To determine the concentration of NaOH in a solution, we titrate it against a primary standard weak acid, such as potassium hydrogen phthalate, $KHC_8H_4O_4$.

OTHER REAGENTS

Preparing a standard often requires additional reagents that are not primary standards or secondary standards, such as a suitable solvent or reagents needed to adjust the standard's matrix. These solvents and reagents are potential sources of additional analyte, which, if not accounted for, produce a determinate error in the standardization. If available, reagent grade chemicals that conform to standards set by the American Chemical Society are used [Committee on Analytical Reagents, *Reagent Chemicals*, 8th ed., American Chemical Society: Washington, D. C., 1993]. The label on the bottle of a reagent grade chemical (Figure 5.1.1) lists either the limits for specific impurities or provides an assay for the impurities. We can improve the quality of a reagent grade chemical by purifying it, or by conducting a more accurate assay. As discussed later in the chapter, we can correct for contributions to S_{total} from reagents used in an analysis by including an appropriate blank determination in the analytical procedure.



Figure 5.1.1 : Two examples of packaging labels for reagent grade chemicals. The label on the bottle on the right provides the manufacturer's assay for the reagent, NaBr. Note that potassium is flagged with an asterisk (*) because its assay exceeds the limit established by the American Chemical Society (ACS). The label for the bottle on the left does not provide an assay for impurities; however it indicates that the reagent meets ACS specifications by providing the maximum limits for impurities. An assay for the reagent, $NaHCO_3$, is provided.

PREPARING A STANDARD SOLUTION

It often is necessary to prepare a series of standards, each with a different concentration of analyte. We can prepare these standards in two ways. If the range of concentrations is limited to one or two orders of magnitude, then each solution is best prepared by transferring a known mass or volume of the pure standard to a volumetric flask and diluting to volume.

When working with a larger range of concentrations, particularly a range that extends over more than three orders of magnitude, standards are best prepared by a serial dilution from a single stock solution. In a ***serial dilution*** we prepare the most concentrated standard and then dilute a portion of that solution to prepare the next most concentrated standard. Next, we dilute a portion of the second standard to prepare a third standard, continuing this process until we have prepared all of our standards. Serial dilutions must be prepared with extra care because an error in preparing one standard is passed on to all succeeding standards.

This page titled 5.1: Analytical Signals is shared under a CC BY-NC-SA 4.0 license and was authored, remixed, and/or curated by David Harvey.

- **5.1: Analytical Signals** by David Harvey is licensed CC BY-NC-SA 4.0.

5.2: CALIBRATING THE SIGNAL

The accuracy with which we determine k_A and S_{reag} depends on how accurately we can measure the signal, S_{total}. We measure signals using equipment, such as glassware and balances, and instrumentation, such as spectrophotometers and pH meters. To minimize determinate errors that might affect the signal, we first calibrate our equipment and instrumentation by measuring S_{total} for a standard with a known response of S_{std}, adjusting S_{total} until

$$S_{total} = S_{std}$$

Here are two examples of how we calibrate signals; other examples are provided in later chapters that focus on specific analytical methods.

When the signal is a measurement of mass, we determine S_{total} using an analytical balance. To calibrate the balance's signal we use a reference weight that meets standards established by a governing agency, such as the National Institute for Standards and Technology or the American Society for Testing and Materials. An electronic balance often includes an internal calibration weight for routine calibrations, as well as programs for calibrating with external weights. In either case, the balance automatically adjusts S_{total} to match S_{std}.

> See Chapter 2.4 to review how an electronic balance works. Calibrating a balance is important, but it does not eliminate all sources of determinate error when measuring mass. See Appendix 9 for a discussion of correcting for the buoyancy of air.

We also must calibrate our instruments. For example, we can evaluate a spectrophotometer's accuracy by measuring the absorbance of a carefully prepared solution of 60.06 mg/L $K_2Cr_2O_7$ in 0.0050 M H_2SO_4, using 0.0050 M H_2SO_4 as a reagent blank [Ebel, S. *Fresenius J. Anal. Chem.* **1992**, *342*, 769]. An absorbance of 0.640 ± 0.010 absorbance units at a wavelength of 350.0 nm indicates that the spectrometer's signal is calibrated properly.

> Be sure to read and follow carefully the calibration instructions provided with any instrument you use.

This page titled 5.2: Calibrating the Signal is shared under a CC BY-NC-SA 4.0 license and was authored, remixed, and/or curated by David Harvey.

- **5.2: Calibrating the Signal** by David Harvey is licensed CC BY-NC-SA 4.0.

5.3: DETERMINING THE SENSITIVITY

To standardize an analytical method we also must determine the analyte's sensitivity, k_A, in Equation 5.3.1 or Equation 5.3.2 .

$$S_{total} = k_A n_A + S_{reag} \tag{5.3.1}$$

$$S_{total} = k_A C_A + S_{reag} \tag{5.3.2}$$

In principle, it is possible to derive the value of k_A for any analytical method if we understand fully all the chemical reactions and physical processes responsible for the signal. Unfortunately, such calculations are not feasible if we lack a sufficiently developed theoretical model of the physical processes or if the chemical reaction's evince non-ideal behavior. In such situations we must determine the value of k_A by analyzing one or more standard solutions, each of which contains a known amount of analyte. In this section we consider several approaches for determining the value of k_A. For simplicity we assume that S_{reag} is accounted for by a proper reagent blank, allowing us to replace S_{total} in Equation 5.3.1 and Equation 5.3.2 with the analyte's signal, S_A.

$$S_A = k_A n_A \tag{5.3.3}$$

$$S_A = k_A C_A \tag{5.3.4}$$

> Equation 5.3.3 and Equation 5.3.4 essentially are identical, differing only in whether we choose to express the amount of analyte in moles or as a concentration. For the remainder of this chapter we will limit our treatment to Equation 5.3.4. You can extend this treatment to Equation 5.3.3 by replacing C_A with n_A.

SINGLE-POINT VERSUS MULTIPLE-POINT STANDARDIZATIONS

The simplest way to determine the value of k_A in Equation 5.3.4 is to use a single-point standardization in which we measure the signal for a standard, S_{std}, that contains a known concentration of analyte, C_{std}. Substituting these values into Equation 5.3.4

$$k_A = \frac{S_{std}}{C_{std}} \tag{5.3.5}$$

gives us the value for k_A. Having determined k_A, we can calculate the concentration of analyte in a sample by measuring its signal, S_{samp}, and calculating C_A using Equation 5.3.6.

$$C_A = \frac{S_{samp}}{k_A} \tag{5.3.6}$$

A single-point standardization is the least desirable method for standardizing a method. There are two reasons for this. First, any error in our determination of k_A carries over into our calculation of C_A. Second, our experimental value for k_A is based on a single concentration of analyte. To extend this value of k_A to other concentrations of analyte requires that we assume a linear relationship between the signal and the analyte's concentration, an assumption that often is not true [Cardone, M. J.; Palmero, P. J.; Sybrandt, L. B. *Anal. Chem.* **1980**, *52*, 1187–1191]. Figure 5.3.1 shows how assuming a constant value of k_A leads to a determinate error in C_A if k_A becomes smaller at higher concentrations of analyte. Despite these limitations, single-point standardizations find routine use when the expected range for the analyte's concentrations is small. Under these conditions it often is safe to assume that k_A is constant (although you should verify this assumption experimentally). This is the case, for example, in clinical labs where many automated analyzers use only a single standard.

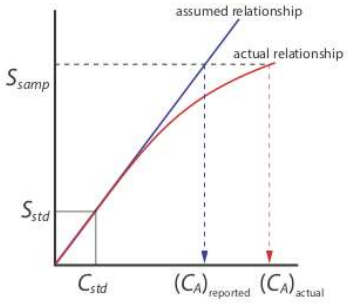


Figure 5.3.1 : Example showing how a single-point standardization leads to a determinate error in an analyte's reported concentration if we incorrectly assume that k_A is constant. The assumed relationship between S_{samp} and C_A is based on a single standard and is a straight-line; the actual relationship between S_{samp} and C_A becomes curved for larger concentrations of analyte.

The better way to standardize a method is to prepare a series of standards, each of which contains a different concentration of analyte. Standards are chosen such that they bracket the expected range for the analyte's concentration. A ***multiple-point standardization*** should

include at least three standards, although more are preferable. A plot of S_{std} versus C_{std} is called a ***calibration curve***. The exact standardization, or calibration relationship, is determined by an appropriate curve-fitting algorithm.

> Linear regression, which also is known as the method of least squares, is one such algorithm. Its use is covered in Section 5.4.

There are two advantages to a multiple-point standardization. First, although a determinate error in one standard introduces a determinate error, its effect is minimized by the remaining standards. Second, because we measure the signal for several concentrations of analyte, we no longer must assume k_A is independent of the analyte's concentration. Instead, we can construct a calibration curve similar to the "actual relationship" in Figure 5.3.1 .

EXTERNAL STANDARDS

The most common method of standardization uses one or more ***external standards***, each of which contains a known concentration of analyte. We call these standards "external" because they are prepared and analyzed separate from the samples.

> Appending the adjective "external" to the noun "standard" might strike you as odd at this point, as it seems reasonable to assume that standards and samples are analyzed separately. As we will soon learn, however, we can add standards to our samples and analyze both simultaneously.

SINGLE EXTERNAL STANDARD

With a single external standard we determine k_A using EEquation 5.3.5 and then calculate the concentration of analyte, C_A, using Equation 5.3.6.

EXAMPLE 5.3.1

A spectrophotometric method for the quantitative analysis of Pb^{2+} in blood yields an S_{std} of 0.474 for a single standard for which the concentration of lead is 1.75 ppb. What is the concentration of Pb^{2+} in a sample of blood for which S_{samp} is 0.361?

Solution

Equation 5.3.5 allows us to calculate the value of k_A using the data for the single external standard.

$$k_A = \frac{S_{std}}{C_{std}} = \frac{0.474}{1.75 \text{ ppb}} = 0.2709 \text{ ppb}^{-1}$$

Having determined the value of k_A, we calculate the concentration of Pb^{2+} in the sample of blood is calculated using Equation 5.3.6.

$$C_A = \frac{S_{samp}}{k_A} = \frac{0.361}{0.2709 \text{ ppb}^{-1}} = 1.33 \text{ ppb}$$

MULTIPLE EXTERNAL STANDARDS

Figure 5.3.2 shows a typical multiple-point external standardization. The volumetric flask on the left contains a reagent blank and the remaining volumetric flasks contain increasing concentrations of Cu^{2+}. Shown below the volumetric flasks is the resulting calibration curve. Because this is the most common method of standardization, the resulting relationship is called a ***normal calibration curve***.

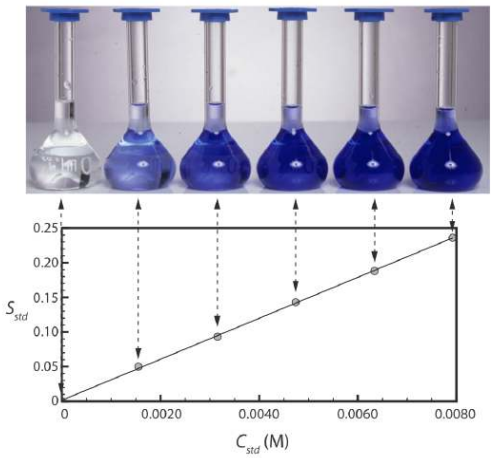


Figure 5.3.2 : The photo at the top of the figure shows a reagent blank (far left) and a set of five external standards for Cu^{2+} with concentrations that increase from left-to-right. Shown below the external standards is the resulting normal calibration curve. The absorbance of each standard, S_{std}, is shown by the filled circles.

When a calibration curve is a straight-line, as it is in Figure 5.3.2 , the slope of the line gives the value of k_A. This is the most desirable situation because the method's sensitivity remains constant throughout the analyte's concentration range. When the calibration curve is not a straight-line, the method's sensitivity is a function of the analyte's concentration. In Figure 5.3.1 , for example, the value of k_A is greatest when the analyte's concentration is small and it decreases continuously for higher concentrations of analyte. The value of k_A at any point along the calibration curve in Figure 5.3.1 is the slope at that point. In either case, a calibration curve allows to relate S_{samp} to the analyte's concentration.

EXAMPLE 5.3.2

A second spectrophotometric method for the quantitative analysis of Pb^{2+} in blood has a normal calibration curve for which

$$S_{std} = (0.296\ \text{ppb}^{-1} \times C_{std}) + 0.003$$

What is the concentration of Pb^{2+} in a sample of blood if S_{samp} is 0.397?

Solution

To determine the concentration of Pb^{2+} in the sample of blood, we replace S_{std} in the calibration equation with S_{samp} and solve for C_A.

$$C_A = \frac{S_{samp} - 0.003}{0.296\ \text{ppb}^{-1}} = \frac{0.397 - 0.003}{0.296\ \text{ppb}^{-1}} = 1.33\ \text{ppb}$$

It is worth noting that the calibration equation in this problem includes an extra term that does not appear in Equation 5.3.6. Ideally we expect our calibration curve to have a signal of zero when C_A is zero. This is the purpose of using a reagent blank to correct the measured signal. The extra term of +0.003 in our calibration equation results from the uncertainty in measuring the signal for the reagent blank and the standards.

EXERCISE 5.3.1

Figure 5.3.2 shows a normal calibration curve for the quantitative analysis of Cu^{2+}. The equation for the calibration curve is

$$S_{std} = 29.59\ \text{M}^{-1} \times C_{std} + 0.015$$

What is the concentration of Cu^{2+} in a sample whose absorbance, S_{samp}, is 0.114? Compare your answer to a one-point standardization where a standard of 3.16×10^{-3} M Cu^{2+} gives a signal of 0.0931.

Answer

Substituting the sample's absorbance into the calibration equation and solving for C_A give

$$S_{samp} = 0.114 = 29.59\ \text{M}^{-1} \times C_A + 0.015$$

$$C_A = 3.35 \times 10^{-3}\ \text{M}$$

For the one-point standardization, we first solve for k_A

$$k_A = \frac{S_{std}}{C_{std}} = \frac{0.0931}{3.16 \times 10^{-3}\ \text{M}} = 29.46\ \text{M}^{-1}$$

and then use this value of k_A to solve for C_A.

$$C_A = \frac{S_{samp}}{k_A} = \frac{0.114}{29.46\ \text{M}^{-1}} = 3.87 \times 10^{-3}\ \text{M}$$

When using multiple standards, the indeterminate errors that affect the signal for one standard are partially compensated for by the indeterminate errors that affect the other standards. The standard selected for the one-point standardization has a signal that is smaller than that predicted by the regression equation, which underestimates k_A and overestimates C_A.

An external standardization allows us to analyze a series of samples using a single calibration curve. This is an important advantage when we have many samples to analyze. Not surprisingly, many of the most common quantitative analytical methods use an external standardization.

There is a serious limitation, however, to an external standardization. When we determine the value of k_A using Equation 5.3.5, the analyte is present in the external standard's matrix, which usually is a much simpler matrix than that of our samples. When we use an external standardization we assume the matrix does not affect the value of k_A. If this is not true, then we introduce a proportional determinate error into our analysis. This is not the case in Figure 5.3.3 , for instance, where we show calibration curves for an analyte in the sample's matrix and in the standard's matrix. In this case, using the calibration curve for the external standards leads to a negative determinate error in analyte's reported concentration. If we expect that matrix effects are important, then we try to match the standard's matrix to that of the sample, a process known as ***matrix matching***. If we are unsure of the sample's matrix, then we must show that matrix effects are negligible or use an alternative method of standardization. Both approaches are discussed in the following section.

The matrix for the external standards in Figure 5.3.2 , for example, is dilute ammonia. Because the $Cu(NH_3)_4^{2+}$ complex absorbs more strongly than Cu^{2+}, adding ammonia increases the signal's magnitude. If we fail to add the same amount of ammonia to our samples, then we will introduce a proportional determinate error into our analysis.

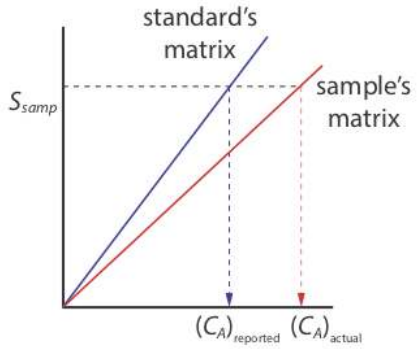


Figure 5.3.3 : Calibration curves for an analyte in the standard's matrix and in the sample's matrix. If the matrix affects the value of k_A, as is the case here, then we introduce a proportional determinate error into our analysis if we use a normal calibration curve.

STANDARD ADDITIONS

We can avoid the complication of matching the matrix of the standards to the matrix of the sample if we carry out the standardization in the sample. This is known as the ***method of standard additions***.

SINGLE STANDARD ADDITION

The simplest version of a standard addition is shown in Figure 5.3.4 . First we add a portion of the sample, V_o, to a volumetric flask, dilute it to volume, V_f, and measure its signal, S_{samp}. Next, we add a second identical portion of sample to an equivalent volumetric flask along with a spike, V_{std}, of an external standard whose concentration is C_{std}. After we dilute the spiked sample to the same final volume, we measure its signal, S_{spike}.

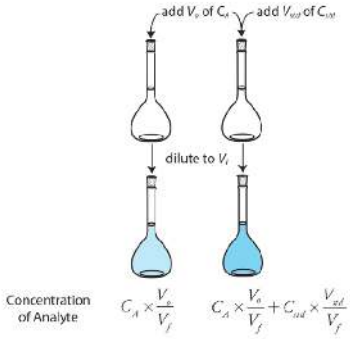


Figure 5.3.4 : Illustration showing the method of standard additions. The volumetric flask on the left contains a portion of the sample, V_o, and the volumetric flask on the right contains an identical portion of the sample and a spike, V_{std}, of a standard solution of the analyte. Both flasks are diluted to the same final volume, V_f. The concentration of analyte in each flask is shown at the bottom of the figure where C_A is the analyte's concentration in the original sample and C_{std} is the concentration of analyte in the external standard.

The following two equations relate S_{samp} and S_{spike} to the concentration of analyte, C_A, in the original sample.

$$S_{samp} = k_A C_A \frac{V_o}{V_f} \tag{5.3.7}$$

$$S_{spike} = k_A \left(C_A \frac{V_o}{V_f} + C_{std} \frac{V_{std}}{V_f} \right) \tag{5.3.8}$$

As long as V_{std} is small relative to V_o, the effect of the standard's matrix on the sample's matrix is insignificant. Under these conditions the value of k_A is the same in Equation 5.3.7 and Equation 5.3.8. Solving both equations for k_A and equating gives

$$\frac{S_{samp}}{C_A \frac{V_o}{V_f}} = \frac{S_{spike}}{C_A \frac{V_o}{V_f} + C_{std} \frac{V_{std}}{V_f}} \tag{5.3.9}$$

which we can solve for the concentration of analyte, C_A, in the original sample.

EXAMPLE 5.3.3

A third spectrophotometric method for the quantitative analysis of Pb^{2+} in blood yields an S_{samp} of 0.193 when a 1.00 mL sample of blood is diluted to 5.00 mL. A second 1.00 mL sample of blood is spiked with 1.00 mL of a 1560-ppb Pb^{2+} external standard and diluted to 5.00 mL, yielding an S_{spike} of 0.419. What is the concentration of Pb^{2+} in the original sample of blood?

Solution

We begin by making appropriate substitutions into Equation 5.3.9 and solving for C_A. Note that all volumes must be in the same units; thus, we first convert V_{std} from 1.00 mL to 1.00×10^{-3} mL.

$$\frac{0.193}{C_A \frac{1.00\text{ mL}}{5.00\text{ mL}}} = \frac{0.419}{C_A \frac{1.00\text{ mL}}{5.00\text{ mL}} + 1560\text{ ppb} \frac{1.00 \times 10^{-3}\text{ mL}}{5.00\text{ mL}}}$$

$$\frac{0.193}{0.200 C_A} = \frac{0.419}{0.200 C_A + 0.3120\text{ ppb}}$$

$$0.0386 C_A + 0.0602\text{ ppb} = 0.0838 C_A$$

$$0.0452 C_A = 0.0602\text{ ppb}$$

$$C_A = 1.33\text{ ppb}$$

The concentration of Pb^{2+} in the original sample of blood is 1.33 ppb.

It also is possible to add the standard addition directly to the sample, measuring the signal both before and after the spike (Figure 5.3.5). In this case the final volume after the standard addition is $V_o + V_{std}$ and Equation 5.3.7, Equation 5.3.8, and Equation 5.3.9 become

$$S_{samp} = k_A C_A$$

$$S_{spike} = k_A \left(C_A \frac{V_o}{V_o + V_{std}} + C_{std} \frac{V_{std}}{V_o + V_{std}} \right) \tag{5.3.10}$$

$$\frac{S_{samp}}{C_A} = \frac{S_{spike}}{C_A \frac{V_o}{V_o + V_{std}} + C_{std} \frac{V_{std}}{V_o + V_{std}}} \tag{5.3.11}$$

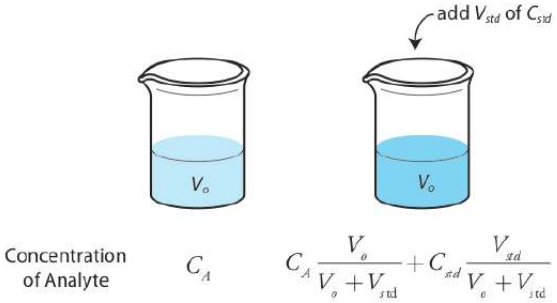


Figure 5.3.5 : Illustration showing an alternative form of the method of standard additions. In this case we add the spike of external standard directly to the sample without any further adjust in the volume.

EXAMPLE 5.3.4

A fourth spectrophotometric method for the quantitative analysis of Pb^{2+} in blood yields an S_{samp} of 0.712 for a 5.00 mL sample of blood. After spiking the blood sample with 5.00 mL of a 1560-ppb Pb^{2+} external standard, an S_{spike} of 1.546 is measured. What is the concentration of Pb^{2+} in the original sample of blood?

Solution

$$\frac{0.712}{C_A} = \frac{1.546}{C_A \frac{5.00\text{ mL}}{5.005\text{ mL}} + 1560\text{ ppb} \frac{5.00 \times 10^{-3}\text{ mL}}{5.005\text{ mL}}}$$

$$\frac{0.712}{C_A} = \frac{1.546}{0.9990 C_A + 1.558\text{ ppb}}$$

$$0.7113 C_A + 1.109\text{ ppb} = 1.546 C_A$$

$$C_A = 1.33\text{ ppb}$$

The concentration of Pb^{2+} in the original sample of blood is 1.33 ppb.

MULTIPLE STANDARD ADDITIONS

We can adapt a single-point standard addition into a multiple-point standard addition by preparing a series of samples that contain increasing amounts of the external standard. Figure 5.3.6 shows two ways to plot a standard addition calibration curve based on Equation 5.3.8. In Figure 5.3.6 a we plot S_{spike} against the volume of the spikes, V_{std}. If k_A is constant, then the calibration curve is a straight-line. It is easy to show that the *x*-intercept is equivalent to $-C_A V_o / C_{std}$.

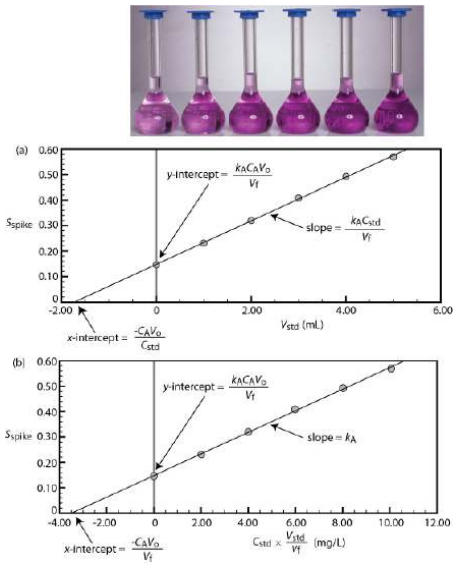


Figure 5.3.6 : Shown at the top of the figure is a set of six standard additions for the determination of Mn^{2+}. The flask on the left is a 25.00 mL sample diluted to 50.00 mL with water. The remaining flasks contain 25.00 mL of sample and, from left-to-right, 1.00, 2.00, 3.00, 4.00, and 5.00 mL spikes of an external standard that is 100.6 mg/L Mn^{2+}. Shown below are two ways to plot the standard additions calibration curve. The absorbance for each standard addition, S_{spike}, is shown by the filled circles.

EXAMPLE 5.3.5

Beginning with Equation 5.3.8 show that the equations in Figure 5.3.6 a for the slope, the *y*-intercept, and the *x*-intercept are correct.

Solution

We begin by rewriting Equation 5.3.8 as

$$S_{spike} = \frac{k_A C_A V_o}{V_f} + \frac{k_A C_{std}}{V_f} \times V_{std}$$

which is in the form of the equation for a straight-line

$$y = y\text{-intercept} + \text{slope} \times x\text{-intercept}$$

where *y* is S_{spike} and *x* is V_{std}. The slope of the line, therefore, is $k_A C_{std}/V_f$ and the *y*-intercept is $k_A C_A V_o/V_f$. The *x*-intercept is the value of *x* when *y* is zero, or

$$0 = \frac{k_A C_A V_o}{V_f} + \frac{k_A C_{std}}{V_f} \times x\text{-intercept}$$

$$x\text{-intercept} = -\frac{k_A C_A V_o / V_f}{K_A C_{std} / V_f} = -\frac{C_A V_o}{C_{std}}$$

EXERCISE 5.3.2

Beginning with Equation 5.3.8 show that the Equations in Figure 5.3.6 b for the slope, the *y*-intercept, and the *x*-intercept are correct.

Answer

We begin with Equation 5.3.8

$$S_{spike} = k_A \left(C_A \frac{V_o}{V_f} + C_{std} \frac{V_{std}}{V_f} \right)$$

rewriting it as

$$S_{spike} = \frac{k_A C_A V_o}{V_f} + k_A \left(C_{std} \frac{V_{std}}{V_f} \right)$$

which is in the form of the linear equation

$$y = y\text{-intercept} + \text{slope} \times x\text{-intercept}$$

where y is S_{spike} and x is $C_{std} \times V_{std}/V_f$. The slope of the line, therefore, is k_A, and the y-intercept is $k_A C_A V_o/V_f$. The x-intercept is the value of x when y is zero, or

$$x\text{-intercept} = -\frac{k_A C_A V_o/V_F}{k_A} = -\frac{C_A V_o}{V_f}$$

Because we know the volume of the original sample, V_o, and the concentration of the external standard, C_{std}, we can calculate the analyte's concentrations from the x-intercept of a multiple-point standard additions.

EXAMPLE 5.3.6

A fifth spectrophotometric method for the quantitative analysis of Pb^{2+} in blood uses a multiple-point standard addition based on Equation 5.3.8. The original blood sample has a volume of 1.00 mL and the standard used for spiking the sample has a concentration of 1560 ppb Pb^{2+}. All samples were diluted to 5.00 mL before measuring the signal. A calibration curve of S_{spike} versus V_{std} has the following equation

$$S_{spike} = 0.266 + 312\ \text{mL}^{-1} \times V_{std}$$

What is the concentration of Pb^{2+} in the original sample of blood?

Solution

To find the x-intercept we set S_{spike} equal to zero.

$$S_{spike} = 0.266 + 312\ \text{mL}^{-1} \times V_{std}$$

Solving for V_{std}, we obtain a value of -8.526×10^{-4} mL for the x-intercept. Substituting the x-intercept's value into the equation from Figure 5.3.6 a

$$-8.526 \times 10^{-4}\ \text{mL} = -\frac{C_A V_o}{C_{std}} = -\frac{C_A \times 1.00\ \text{mL}}{1560\ \text{ppb}}$$

and solving for C_A gives the concentration of Pb^{2+} in the blood sample as 1.33 ppb.

EXERCISE 5.3.3

Figure 5.3.6 shows a standard additions calibration curve for the quantitative analysis of Mn^{2+}. Each solution contains 25.00 mL of the original sample and either 0, 1.00, 2.00, 3.00, 4.00, or 5.00 mL of a 100.6 mg/L external standard of Mn^{2+}. All standard addition samples were diluted to 50.00 mL with water before reading the absorbance. The equation for the calibration curve in Figure 5.3.6 a is

$$S_{std} = 0.0854 \times V_{std} + 0.1478$$

What is the concentration of Mn^{2+} in this sample? Compare your answer to the data in Figure 5.3.6 b, for which the calibration curve is

$$S_{std} = 0.425 \times C_{std}(V_{std}/V_f) + 0.1478$$

Answer

Using the calibration equation from Figure 5.3.6 a, we find that the x-intercept is

$$x\text{-intercept} = -\frac{0.1478}{0.0854\ \text{mL}^{-1}} = -1.731\ \text{mL}$$

If we plug this result into the equation for the x-intercept and solve for C_A, we find that the concentration of Mn^{2+} is

$$C_A = -\frac{x\text{-intercept} \times C_{std}}{V_o} = -\frac{-1.731\ \text{mL} \times 100.6\ \text{mg/L}}{25.00\ \text{mL}} = 6.96\ \text{mg/L}$$

For Figure 5.3.6 b, the x-intercept is

$$x\text{-intercept} = -\frac{0.1478}{0.0425\ \text{mL/mg}} = -3.478\ \text{mg/mL}$$

and the concentration of Mn^{2+} is

$$C_A = -\frac{x\text{-intercept} \times V_f}{V_o} = -\frac{-3.478\ \text{mg/mL} \times 50.00\ \text{mL}}{25.00\ \text{mL}} = 6.96\ \text{mg/L}$$

Since we construct a standard additions calibration curve in the sample, we can not use the calibration equation for other samples. Each sample, therefore, requires its own standard additions calibration curve. This is a serious drawback if you have many samples. For example, suppose you need to analyze 10 samples using a five-point calibration curve. For a normal calibration curve you need to analyze only 15 solutions (five standards and ten samples). If you use the method of standard additions, however, you must analyze 50 solutions (each of the ten samples is analyzed five times, once before spiking and after each of four spikes).

USING A STANDARD ADDITION TO IDENTIFY MATRIX EFFECTS

We can use the method of standard additions to validate an external standardization when matrix matching is not feasible. First, we prepare a normal calibration curve of S_{std} versus C_{std} and determine the value of k_A from its slope. Next, we prepare a standard additions calibration curve using Equation 5.3.8, plotting the data as shown in Figure 5.3.6 b. The slope of this standard additions calibration curve provides an independent determination of k_A. If there is no significant difference between the two values of k_A, then we can ignore the difference between the sample's matrix and that of the external standards. When the values of k_A are significantly different, then using a normal calibration curve introduces a proportional determinate error.

INTERNAL STANDARDS

To use an external standardization or the method of standard additions, we must be able to treat identically all samples and standards. When this is not possible, the accuracy and precision of our standardization may suffer. For example, if our analyte is in a volatile solvent, then its concentration will increase if we lose solvent to evaporation. Suppose we have a sample and a standard with identical concentrations of analyte and identical signals. If both experience the same proportional loss of solvent, then their respective concentrations of analyte and signals remain identical. In effect, we can ignore evaporation if the samples and the standards experience an equivalent loss of solvent. If an identical standard and sample lose different amounts of solvent, however, then their respective concentrations and signals are no longer equal. In this case a simple external standardization or standard addition is not possible.

We can still complete a standardization if we reference the analyte's signal to a signal from another species that we add to all samples and standards. The species, which we call an ***internal standard***, must be different than the analyte.

Because the analyte and the internal standard receive the same treatment, the ratio of their signals is unaffected by any lack of reproducibility in the procedure. If a solution contains an analyte of concentration C_A and an internal standard of concentration C_{IS}, then the signals due to the analyte, S_A, and the internal standard, S_{IS}, are

$$S_A = k_A C_A$$

$$S_{IS} = k_{SI} C_{IS}$$

where k_A and k_{IS} are the sensitivities for the analyte and the internal standard, respectively. Taking the ratio of the two signals gives the fundamental equation for an internal standardization.

$$\frac{S_A}{S_{IS}} = \frac{k_A C_A}{k_{IS} C_{IS}} = K \times \frac{C_A}{C_{IS}} \tag{5.3.12}$$

Because K is a ratio of the analyte's sensitivity and the internal standard's sensitivity, it is not necessary to determine independently values for either k_A or k_{IS}.

SINGLE INTERNAL STANDARD

In a single-point internal standardization, we prepare a single standard that contains the analyte and the internal standard, and use it to determine the value of K in Equation 5.3.12.

$$K = \left(\frac{C_{IS}}{C_A}\right)_{std} \times \left(\frac{S_A}{S_{IS}}\right)_{std} \tag{5.3.13}$$

Having standardized the method, the analyte's concentration is given by

$$C_A = \frac{C_{IS}}{K} \times \left(\frac{S_A}{S_{IS}}\right)_{samp}$$

✔ EXAMPLE 5.3.7

A sixth spectrophotometric method for the quantitative analysis of Pb^{2+} in blood uses Cu^{2+} as an internal standard. A standard that is 1.75 ppb Pb^{2+} and 2.25 ppb Cu^{2+} yields a ratio of $(S_A/S_{IS})_{std}$ of 2.37. A sample of blood spiked with the same concentration of Cu^{2+}

gives a signal ratio, $(S_A/S_{IS})_{samp}$, of 1.80. What is the concentration of Pb^{2+} in the sample of blood?

Solution

Equation 5.3.13 allows us to calculate the value of K using the data for the standard

$$K = \left(\frac{C_{IS}}{C_A}\right)_{std} \times \left(\frac{S_A}{S_{IS}}\right)_{std} = \frac{2.25 \text{ ppb } Cu^{2+}}{1.75 \text{ ppb } Pb^{2+}} \times 2.37 = 3.05 \frac{\text{ppb } Cu^{2+}}{\text{ppb } Pb^{2+}}$$

The concentration of Pb^{2+}, therefore, is

$$C_A = \frac{C_{IS}}{K} \times \left(\frac{S_A}{S_{IS}}\right)_{samp} = \frac{2.25 \text{ ppb } Cu^{2+}}{3.05 \frac{\text{ppb } Cu^{2+}}{\text{ppb } Pb^{2+}}} \times 1.80 = 1.33 \text{ ppb } Pb^{2+}$$

MULTIPLE INTERNAL STANDARDS

A single-point internal standardization has the same limitations as a single-point normal calibration. To construct an internal standard calibration curve we prepare a series of standards, each of which contains the same concentration of internal standard and a different concentrations of analyte. Under these conditions a calibration curve of $(S_A/S_{IS})_{std}$ versus C_A is linear with a slope of K/C_{IS}.

> Although the usual practice is to prepare the standards so that each contains an identical amount of the internal standard, this is not a requirement.

EXAMPLE 5.3.8

A seventh spectrophotometric method for the quantitative analysis of Pb^{2+} in blood gives a linear internal standards calibration curve for which

$$\left(\frac{S_A}{S_{IS}}\right)_{std} = (2.11 \text{ ppb}^{-1} \times C_A) - 0.006$$

What is the ppb Pb^{2+} in a sample of blood if $(S_A/S_{IS})_{samp}$ is 2.80?

Solution

To determine the concentration of Pb^{2+} in the sample of blood we replace $(S_A/S_{IS})_{std}$ in the calibration equation with $(S_A/S_{IS})_{samp}$ and solve for C_A.

$$C_A = \frac{\left(\frac{S_A}{S_{IS}}\right)_{samp} + 0.006}{2.11 \text{ ppb}^{-1}} = \frac{2.80 + 0.006}{2.11 \text{ ppb}^{-1}} = 1.33 \text{ ppb } Pb^{2+}$$

The concentration of Pb^{2+} in the sample of blood is 1.33 ppb.

In some circumstances it is not possible to prepare the standards so that each contains the same concentration of internal standard. This is the case, for example, when we prepare samples by mass instead of volume. We can still prepare a calibration curve, however, by plotting $(S_A/S_{IS})_{std}$ versus C_A/C_{IS}, giving a linear calibration curve with a slope of K.

> You might wonder if it is possible to include an internal standard in the method of standard additions to correct for both matrix effects and uncontrolled variations between samples; well, the answer is yes as described in the paper "Standard Dilution Analysis," the full reference for which is Jones, W. B.; Donati, G. L.; Calloway, C. P.; Jones, B. T. *Anal. Chem.* **2015**, *87*, 2321-2327.

This page titled 5.3: Determining the Sensitivity is shared under a CC BY-NC-SA 4.0 license and was authored, remixed, and/or curated by David Harvey.

- **5.3: Determining the Sensitivity** by David Harvey is licensed CC BY-NC-SA 4.0.

5.4: LINEAR REGRESSION AND CALIBRATION CURVES

In a single-point external standardization we determine the value of k_A by measuring the signal for a single standard that contains a known concentration of analyte. Using this value of k_A and our sample's signal, we then calculate the concentration of analyte in our sample (see Example 5.3.1). With only a single determination of k_A, a quantitative analysis using a single-point external standardization is straightforward.

A multiple-point standardization presents a more difficult problem. Consider the data in Table 5.4.1 for a multiple-point external standardization. What is our best estimate of the relationship between S_{std} and C_{std}? It is tempting to treat this data as five separate single-point standardizations, determining k_A for each standard, and reporting the mean value for the five trials. Despite it simplicity, this is not an appropriate way to treat a multiple-point standardization.

Table 5.4.1 : Data for a Hypothetical Multiple-Point External Standardization

C_{std} (arbitrary units)	S_{std} (arbitrary units)	$k_A = S_{std}/C_{std}$
0.000	0.00	—
0.100	12.36	123.6
0.200	24.83	124.2
0.300	35.91	119.7
0.400	48.79	122.0
0.500	60.42	122.8
		mean k_A = 122.5

So why is it inappropriate to calculate an average value for k_A using the data in Table 5.4.1 ? In a single-point standardization we assume that the reagent blank (the first row in Table 5.4.1) corrects for all constant sources of determinate error. If this is not the case, then the value of k_A from a single-point standardization has a constant determinate error. Table 5.4.2 demonstrates how an uncorrected constant error affects our determination of k_A. The first three columns show the concentration of analyte in a set of standards, C_{std}, the signal without any source of constant error, S_{std}, and the actual value of k_A for five standards. As we expect, the value of k_A is the same for each standard. In the fourth column we add a constant determinate error of +0.50 to the signals, $(S_{std})_e$. The last column contains the corresponding apparent values of k_A. Note that we obtain a different value of k_A for each standard and that each apparent k_A is greater than the true value.

Table 5.4.2 : Effect of a Constant Determinate Error on the Value of k_A From a Single-Point Standardization

C_{std}	S_{std} (without constant error)	$k_A = S_{std}/C_{std}$ (actual)	$(S_{std})_e$ (with constant error)	$k_A = (S_{std})_e/C_{std}$ (apparent)
1.00	1.00	1.00	1.50	1.50
2.00	2.00	1.00	2.50	1.25
3.00	3.00	1.00	3.50	1.17
4.00	4.00	1.00	4.50	1.13
5.00	5.00	1.00	5.50	1.10
		mean k_A (true) = 1.00		mean k_A (apparent) = 1.23

How do we find the best estimate for the relationship between the signal and the concentration of analyte in a multiple-point standardization? Figure 5.4.1 shows the data in Table 5.4.1 plotted as a normal calibration curve. Although the data certainly appear to fall along a straight line, the actual calibration curve is not intuitively obvious. The process of determining the best equation for the calibration curve is called linear regression.

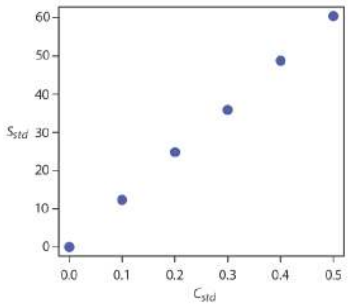


Figure 5.4.1 : Normal calibration curve data for the hypothetical multiple-point external standardization in Table 5.4.1 .

LINEAR REGRESSION OF STRAIGHT LINE CALIBRATION CURVES

When a calibration curve is a straight-line, we represent it using the following mathematical equation

$$y = \beta_0 + \beta_1 x \tag{5.4.1}$$

where y is the analyte's signal, S_{std}, and x is the analyte's concentration, C_{std}. The constants β_0 and β_1 are, respectively, the calibration curve's expected y-intercept and its expected slope. Because of uncertainty in our measurements, the best we can do is to estimate values for β_0 and β_1, which we represent as b_0 and b_1. The goal of a ***linear regression*** analysis is to determine the best estimates for b_0 and b_1. How we do this depends on the uncertainty in our measurements.

UNWEIGHTED LINEAR REGRESSION WITH ERRORS IN *Y*

The most common method for completing the linear regression for Equation 5.4.1 makes three assumptions:

1. that the difference between our experimental data and the calculated regression line is the result of indeterminate errors that affect y
2. that indeterminate errors that affect y are normally distributed
3. that the indeterminate errors in y are independent of the value of x

Because we assume that the indeterminate errors are the same for all standards, each standard contributes equally in our estimate of the slope and the y-intercept. For this reason the result is considered an ***unweighted linear regression***.

The second assumption generally is true because of the central limit theorem, which we considered in Chapter 4. The validity of the two remaining assumptions is less obvious and you should evaluate them before you accept the results of a linear regression. In particular the first assumption always is suspect because there certainly is some indeterminate error in the measurement of x. When we prepare a calibration curve, however, it is not unusual to find that the uncertainty in the signal, S_{std}, is significantly larger than the uncertainty in the analyte's concentration, C_{std}. In such circumstances the first assumption is usually reasonable.

HOW A LINEAR REGRESSION WORKS

To understand the logic of a linear regression consider the example shown in Figure 5.4.2 , which shows three data points and two possible straight-lines that might reasonably explain the data. How do we decide how well these straight-lines fit the data, and how do we determine the best straight-line?

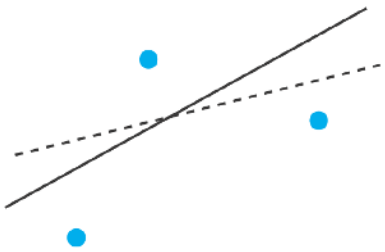


Figure 5.4.2 : Illustration showing three data points and two possible straight-lines that might explain the data. The goal of a linear regression is to find the mathematical model, in this case a straight-line, that best explains the data.

Let's focus on the solid line in Figure 5.4.2 . The equation for this line is

$$\hat{y} = b_0 + b_1 x \tag{5.4.2}$$

where b_0 and b_1 are estimates for the y-intercept and the slope, and $\hat{y}$ is the predicted value of y for any value of x. Because we assume that all uncertainty is the result of indeterminate errors in y, the difference between y and $\hat{y}$ for each value of x is the residual error, r, in our mathematical model.

$$r_i = (y_i - \hat{y}_i)$$

Figure 5.4.3 shows the residual errors for the three data points. The smaller the total residual error, R, which we define as

$$R = \sum_{i=1}^{n} (y_i - \hat{y}_i)^2 \tag{5.4.3}$$

the better the fit between the straight-line and the data. In a linear regression analysis, we seek values of b_0 and b_1 that give the smallest total residual error.

> The reason for squaring the individual residual errors is to prevent a positive residual error from canceling out a negative residual error. You have seen this before in the equations for the sample and population standard deviations. You also can see from this equation why

a linear regression is sometimes called the method of least squares.

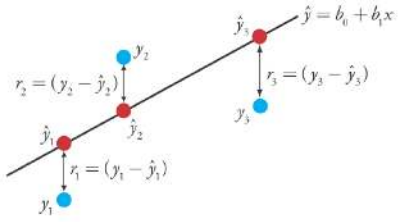


Figure 5.4.3 : Illustration showing the evaluation of a linear regression in which we assume that all uncertainty is the result of indeterminate errors in y. The points in blue, y , are the original data and the points in red, y_i , are the predicted values from the regression equation, $\hat{y} = b_0 + b_1 x$ .The smaller the total residual error (Equation 5.4.3), the better the fit of the straight-line to the data.

FINDING THE SLOPE AND Y-INTERCEPT

Although we will not formally develop the mathematical equations for a linear regression analysis, you can find the derivations in many standard statistical texts [See, for example, Draper, N. R.; Smith, H. Applied Regression Analysis, 3rd ed.; Wiley: New York, 1998]. The resulting equation for the slope, b_1, is

$$b_1 = \frac{n\sum_{i=1}^{n} x_i y_i - \sum_{i=1}^{n} x_i \sum_{i=1}^{n} y_i}{n\sum_{i=1}^{n} x_i^2 - \left(\sum_{i=1}^{n} x_i\right)^2} \tag{5.4.4}$$

and the equation for the y-intercept, b_0, is

$$b_0 = \frac{\sum_{i=1}^{n} y_i - b_1 \sum_{i=1}^{n} x_i}{n} \tag{5.4.5}$$

Although Equation 5.4.4 and Equation 5.4.5 appear formidable, it is necessary only to evaluate the following four summations

$$\sum_{i=1}^{n} x_i \quad \sum_{i=1}^{n} y_i \quad \sum_{i=1}^{n} x_i y_i \quad \sum_{i=1}^{n} x_i^2$$

Many calculators, spreadsheets, and other statistical software packages are capable of performing a linear regression analysis based on this model. To save time and to avoid tedious calculations, learn how to use one of these tools (and see Section 5.6 for details on completing a linear regression analysis using Excel and R.). For illustrative purposes the necessary calculations are shown in detail in the following example.

Equation 5.4.4 and Equation 5.4.5 are written in terms of the general variables x and y. As you work through this example, remember that x corresponds to C_{std}, and that y corresponds to S_{std}.

✔ EXAMPLE 5.4.1

Using the data from Table 5.4.1 , determine the relationship between S_{std} and C_{std} using an unweighted linear regression.

Solution

We begin by setting up a table to help us organize the calculation.

x_i	y_i	$x_i y_i$	x_i^2
0.000	0.00	0.000	0.000
0.100	12.36	1.236	0.010
0.200	24.83	4.966	0.040
0.300	35.91	10.773	0.090
0.400	48.79	19.516	0.160
0.500	60.42	30.210	0.250

Adding the values in each column gives

$$\sum_{i=1}^{n} x_i = 1.500 \quad \sum_{i=1}^{n} y_i = 182.31 \quad \sum_{i=1}^{n} x_i y_i = 66.701 \quad \sum_{i=1}^{n} x_i^2 = 0.550$$

Substituting these values into Equation 5.4.4 and Equation 5.4.5, we find that the slope and the *y*-intercept are

$$b_1 = \frac{(6 \times 66.701) - (1.500 \times 182.31)}{(6 \times 0.550) - (1.500)^2} = 120.706 \approx 120.71$$

$$b_0 = \frac{182.31 - (120.706 \times 1.500)}{6} = 0.209 \approx 0.21$$

The relationship between the signal and the analyte, therefore, is

$$S_{std} = 120.71 \times C_{std} + 0.21$$

For now we keep two decimal places to match the number of decimal places in the signal. The resulting calibration curve is shown in Figure 5.4.4 .

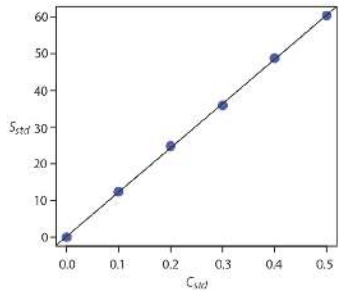


Figure 5.4.4 : Calibration curve for the data in Table 5.4.1 and Example 5.4.1 .

UNCERTAINTY IN THE REGRESSION ANALYSIS

As shown in Figure 5.4.4 , because indeterminate errors in the signal, the regression line may not pass through the exact center of each data point. The cumulative deviation of our data from the regression line—that is, the total residual error—is proportional to the uncertainty in the regression. We call this uncertainty the ***standard deviation about the regression***, s_r, which is equal to

$$s_r = \sqrt{\frac{\sum_{i=1}^{n} (y_i - \hat{y}_i)^2}{n-2}} \tag{5.4.6}$$

where y_i is the ith experimental value, and $\hat{y}_i$ is the corresponding value predicted by the regression line in Equation 5.4.2. Note that the denominator of Equation 5.4.6 indicates that our regression analysis has $n - 2$ degrees of freedom—we lose two degree of freedom because we use two parameters, the slope and the *y*-intercept, to calculate $\hat{y}_i$.

Did you notice the similarity between the standard deviation about the regression (Equation 5.4.6) and the standard deviation for a sample (Equation 4.1.1)?

A more useful representation of the uncertainty in our regression analysis is to consider the effect of indeterminate errors on the slope, b_1, and the *y*-intercept, b_0, which we express as standard deviations.

$$s_{b_1} = \sqrt{\frac{n s_r^2}{n\sum_{i=1}^{n} x_i^2 - \left(\sum_{i=1}^{n} x_i\right)^2}} = \sqrt{\frac{s_r^2}{\sum_{i=1}^{n} (x_i - \bar{x})^2}} \tag{5.4.7}$$

$$s_{b_0} = \sqrt{\frac{s_r^2 \sum_{i=1}^{n} x_i^2}{n\sum_{i=1}^{n} x_i^2 - \left(\sum_{i=1}^{n} x_i\right)^2}} = \sqrt{\frac{s_r^2 \sum_{i=1}^{n} x_i^2}{n\sum_{i=1}^{n} (x_i - \bar{x})^2}} \tag{5.4.8}$$

We use these standard deviations to establish confidence intervals for the expected slope, β_1, and the expected *y*-intercept, β_0

$$\beta_1 = b_1 \pm t s_{b_1} \tag{5.4.9}$$

$$\beta_0 = b_0 \pm t s_{b_0} \tag{5.4.10}$$

where we select *t* for a significance level of α and for $n - 2$ degrees of freedom. Note that Equation 5.4.9 and Equation 5.4.10 do not contain a factor of $(\sqrt{n})^{-1}$ because the confidence interval is based on a single regression line.

EXAMPLE 5.4.2

Calculate the 95% confidence intervals for the slope and *y*-intercept from Example 5.4.1 .

Solution

We begin by calculating the standard deviation about the regression. To do this we must calculate the predicted signals, $\hat{y}_i$, using the slope and *y*-intercept from Example 5.4.1 , and the squares of the residual error, $(y_i - \hat{y}_i)^2$. Using the last standard as an example, we find that the predicted signal is

$$\hat{y}_6 = b_0 + b_1 x_6 = 0.209 + (120.706 \times 0.500) = 60.562$$

and that the square of the residual error is

$$(y_i - \hat{y}_i)^2 = (60.42 - 60.562)^2 = 0.2016 \approx 0.202$$

The following table displays the results for all six solutions.

x_i	y_i	$\hat{y}_i$	$(y_i - \hat{y}_i)^2$
0.000	0.00	0.209	0.0437
0.100	12.36	12.280	0.0064
0.200	24.83	24.350	0.2304
0.300	35.91	36.421	0.2611
0.400	48.79	48.491	0.0894
0.500	60.42	60.562	0.0202

Adding together the data in the last column gives the numerator of Equation 5.4.6 as 0.6512; thus, the standard deviation about the regression is

$$s_r = \sqrt{\frac{0.6512}{6-2}} = 0.4035$$

Next we calculate the standard deviations for the slope and the *y*-intercept using Equation 5.4.7 and Equation 5.4.8. The values for the summation terms are from Example 5.4.1 .

$$s_{b_1} = \sqrt{\frac{6 \times (0.4035)^2}{(6 \times 0.550) - (1.500)^2}} = 0.965$$

$$s_{b_0} = \sqrt{\frac{(0.4035)^2 \times 0.550}{(6 \times 0.550) - (1.500)^2}} = 0.292$$

Finally, the 95% confidence intervals ($\alpha = 0.05$, 4 degrees of freedom) for the slope and *y*-intercept are

$$\beta_1 = b_1 \pm t s_{b_1} = 120.706 \pm (2.78 \times 0.965) = 120.7 \pm 2.7$$

$$\beta_0 = b_0 \pm t s_{b_0} = 0.209 \pm (2.78 \times 0.292) = 0.2 \pm 0.80$$

where *t*(0.05, 4) from Appendix 4 is 2.78. The standard deviation about the regression, s_r, suggests that the signal, S_{std}, is precise to one decimal place. For this reason we report the slope and the *y*-intercept to a single decimal place.

MINIMIZING UNCERTAINTY IN CALIBRATION MODEL

To minimize the uncertainty in a calibration curve's slope and *y*-intercept, we evenly space our standards over a wide range of analyte concentrations. A close examination of Equation 5.4.7 and Equation 5.4.8 help us appreciate why this is true. The denominators of both equations include the term $\sum_{i=1}^{n}(x_i - \overline{x}_i)^2$. The larger the value of this term—which we accomplish by increasing the range of *x* around its mean value—the smaller the standard deviations in the slope and the *y*-intercept. Furthermore, to minimize the uncertainty in the *y*-intercept, it helps to decrease the value of the term $\sum_{i=1}^{n} x_i$ in Equation 5.4.8, which we accomplish by including standards for lower concentrations of the analyte.

OBTAINING THE ANALYTE'S CONCENTRATION FROM A REGRESSION EQUATION

Once we have our regression equation, it is easy to determine the concentration of analyte in a sample. When we use a normal calibration curve, for example, we measure the signal for our sample, S_{samp}, and calculate the analyte's concentration, C_A, using the regression equation.

$$C_A = \frac{S_{samp} - b_0}{b_1} \tag{5.4.11}$$

What is less obvious is how to report a confidence interval for C_A that expresses the uncertainty in our analysis. To calculate a confidence interval we need to know the standard deviation in the analyte's concentration, s_{C_A}, which is given by the following equation

$$s_{C_A} = \frac{s_r}{b_1}\sqrt{\frac{1}{m} + \frac{1}{n} + \frac{\left(\overline{S}_{samp} - \overline{S}_{std}\right)^2}{(b_1)^2 \sum_{i=1}^{n}\left(C_{std_i} - \overline{C}_{std}\right)^2}} \tag{5.4.12}$$

where m is the number of replicate we use to establish the sample's average signal, S_{samp}, n is the number of calibration standards, S_{std} is the average signal for the calibration standards, and C_{std_1} and $\overline{C}_{std}$ are the individual and the mean concentrations for the calibration standards. Knowing the value of s_{C_A}, the confidence interval for the analyte's concentration is

$$\mu_{C_A} = C_A \pm t s_{C_A}$$

where μ_{C_A} is the expected value of C_A in the absence of determinate errors, and with the value of t is based on the desired level of confidence and $n - 2$ degrees of freedom.

Equation 5.4.12 is written in terms of a calibration experiment. A more general form of the equation, written in terms of x and y, is given here.

$$s_x = \frac{s_r}{b_1}\sqrt{\frac{1}{m} + \frac{1}{n} + \frac{\left(\overline{Y} - \overline{y}\right)^2}{(b_1)^2 \sum_{i=1}^{n}\left(x_i - \overline{x}\right)^2}}$$

A close examination of Equation 5.4.12 should convince you that the uncertainty in C_A is smallest when the sample's average signal, $\overline{S}_{samp}$, is equal to the average signal for the standards, $\overline{S}_{std}$. When practical, you should plan your calibration curve so that S_{samp} falls in the middle of the calibration curve. For more information about these regression equations see (a) Miller, J. N. *Analyst* **1991**, *116*, 3–14; (b) Sharaf, M. A.; Illman, D. L.; Kowalski, B. R. *Chemometrics*, Wiley-Interscience: New York, 1986, pp. 126-127; (c) Analytical Methods Committee "Uncertainties in concentrations estimated from calibration experiments," AMC Technical Brief, March 2006.

EXAMPLE 5.4.3

Three replicate analyses for a sample that contains an unknown concentration of analyte, yield values for S_{samp} of 29.32, 29.16 and 29.51 (arbitrary units). Using the results from Example 5.4.1 and Example 5.4.2 , determine the analyte's concentration, C_A, and its 95% confidence interval.

Solution

The average signal, $\overline{S}_{samp}$, is 29.33, which, using Equation 5.4.11 and the slope and the y-intercept from Example 5.4.1 , gives the analyte's concentration as

$$C_A = \frac{\overline{S}_{samp} - b_0}{b_1} = \frac{29.33 - 0.209}{120.706} = 0.241$$

To calculate the standard deviation for the analyte's concentration we must determine the values for $\overline{S}_{std}$ and for $\sum_{i=1}^{2}(C_{std_i} - \overline{C}_{std})^2$. The former is just the average signal for the calibration standards, which, using the data in Table 5.4.1 , is 30.385. Calculating $\sum_{i=1}^{2}(C_{std_i} - \overline{C}_{std})^2$ looks formidable, but we can simplify its calculation by recognizing that this sum-of-squares is the numerator in a standard deviation equation; thus,

$$\sum_{i=1}^{n}(C_{std_i} - \overline{C}_{std})^2 = (s_{C_{std}})^2 \times (n-1)$$

where $s_{C_{std}}$ is the standard deviation for the concentration of analyte in the calibration standards. Using the data in Table 5.4.1 we find that $s_{C_{std}}$ is 0.1871 and

$$\sum_{i=1}^{n}(C_{std_i} - \overline{C}_{std})^2 = (0.1872)^2 \times (6-1) = 0.175$$

Substituting known values into Equation 5.4.12 gives

$$s_{C_A} = \frac{0.4035}{120.706}\sqrt{\frac{1}{3} + \frac{1}{6} + \frac{(29.33 - 30.385)^2}{(120.706)^2 \times 0.175}} = 0.0024$$

Finally, the 95% confidence interval for 4 degrees of freedom is

$$\mu_{C_A} = C_A \pm t s_{C_A} = 0.241 \pm (2.78 \times 0.0024) = 0.241 \pm 0.007$$

Figure 5.4.5 shows the calibration curve with curves showing the 95% confidence interval for C_A.

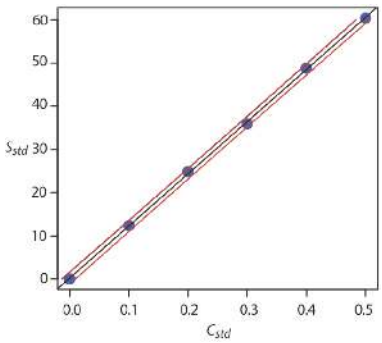


Figure 5.4.5 : Example of a normal calibration curve with a superimposed confidence interval for the analyte's concentration. The points in blue are the original data from Table 5.4.1 . The black line is the normal calibration curve as determined in Example 5.4.1 . The red lines show the 95% confidence interval for C_A assuming a single determination of S_{samp}.

In a standard addition we determine the analyte's concentration by extrapolating the calibration curve to the *x*-intercept. In this case the value of C_A is

$$C_A = x\text{-intercept} = \frac{-b_0}{b_1}$$

and the standard deviation in C_A is

$$s_{C_A} = \frac{s_r}{b_1}\sqrt{\frac{1}{n} + \frac{(\overline{S}_{std})^2}{(b_1)^2 \sum_{i=1}^{n}(C_{std_i} - \overline{C}_{std})^2}}$$

where n is the number of standard additions (including the sample with no added standard), and $\overline{S}_{std}$ is the average signal for the n standards. Because we determine the analyte's concentration by extrapolation, rather than by interpolation, s_{C_A} for the method of standard additions generally is larger than for a normal calibration curve.

? EXERCISE 5.4.1

Figure 5.4.2 shows a normal calibration curve for the quantitative analysis of Cu^{2+}. The data for the calibration curve are shown here.

$[Cu^{2+}]$ (M)	Absorbance
0	0
1.55×10^{-3}	0.050
3.16×10^{-3}	0.093
4.74×10^{-3}	0.143
6.34×10^{-3}	0.188
7.92×10^{-3}	0.236

Complete a linear regression analysis for this calibration data, reporting the calibration equation and the 95% confidence interval for the slope and the *y*-intercept. If three replicate samples give an S_{samp} of 0.114, what is the concentration of analyte in the sample and its 95% confidence interval?

Answer

We begin by setting up a table to help us organize the calculation

x_i	y_i	$x_i y_i$	x_i^2
0.000	0.000	0.000	0.000
1.55×10^{-3}	0.050	7.750×10^{-5}	2.403×10^{-6}
3.16×10^{-3}	0.093	2.939×10^{-4}	9.986×10^{-6}
4.74×10^{-3}	0.143	6.778×10^{-4}	2.247×10^{-5}
6.34×10^{-3}	0.188	1.192×10^{-3}	4.020×10^{-5}
7.92×10^{-3}	0.236	1.869×10^{-3}	6.273×10^{-5}

Adding the values in each column gives

$$\sum_{i=1}^{n} x_i = 2.371 \times 10^{-2} \quad \sum_{i=1}^{n} y_i = 0.710 \quad \sum_{i=1}^{n} x_i y_i = 4.110 \times 10^{-3} \quad \sum_{i=1}^{n} x_i^2 = 1.378 \times 10^{-4}$$

When we substitute these values into Equation 5.4.4 and Equation 5.4.5, we find that the slope and the *y*-intercept are

$$b_1 = \frac{6 \times (4.110 \times 10^{-3}) - (2.371 \times 10^{-2}) \times 0.710}{6 \times (1.378 \times 10^{-4}) - (2.371 \times 10^{-2})^2}) = 29.57$$

$$b_0 = \frac{0.710 - 29.57 \times (2.371 \times 10^{-2}}{6} = 0.0015$$

and that the regression equation is

$$S_{std} = 29.57 \times C_{std} + 0.0015$$

To calculate the 95% confidence intervals, we first need to determine the standard deviation about the regression. The following table helps us organize the calculation.

x_i	y_i	$\hat{y}_i$	$(y_i - \hat{y}_i)^2$
0.000	0.000	0.0015	2.250×10^{-6}
1.55×10^{-3}	0.050	0.0473	7.110×10^{-6}
3.16×10^{-3}	0.093	0.0949	3.768×10^{-6}
4.74×10^{-3}	0.143	0.1417	1.791×10^{-6}
6.34×10^{-3}	0.188	0.1890	9.483×10^{-6}
7.92×10^{-3}	0.236	0.2357	9.339×10^{-6}

Adding together the data in the last column gives the numerator of Equation 5.4.6 as 1.596×10^{-5}. The standard deviation about the regression, therefore, is

$$s_r = \sqrt{\frac{1.596 \times 10^{-5}}{6 - 2}} = 1.997 \times 10^{-3}$$

Next, we need to calculate the standard deviations for the slope and the *y*-intercept using Equation 5.4.7 and Equation 5.4.8.

$$s_{b_1} = \sqrt{\frac{6 \times (1.997 \times 10^{-3})^2}{6 \times (1.378 \times 10^{-4}) - (2.371 \times 10^{-2})^2}} = 0.3007$$

$$s_{b_0} = \sqrt{\frac{(1.997 \times 10^{-3})^2 \times (1.378 \times 10^{-4})}{6 \times (1.378 \times 10^{-4}) - (2.371 \times 10^{-2})^2}} = 1.441 \times 10^{-3}$$

and use them to calculate the 95% confidence intervals for the slope and the *y*-intercept

$$\beta_1 = b_1 \pm t s_{b_1} = 29.57 \pm (2.78 \times 0.3007) = 29.57\ \text{M}^{-1} \pm 0.84\ \text{M}^{-1}$$

$$\beta_0 = b_0 \pm t s_{b_0} = 0.0015 \pm (2.78 \times 1.441 \times 10^{-3}) = 0.0015 \pm 0.0040$$

With an average S_{samp} of 0.114, the concentration of analyte, C_A, is

$$C_A = \frac{S_{samp} - b_0}{b_1} = \frac{0.114 - 0.0015}{29.57\ \text{M}^{-1}} = 3.80 \times 10^{-3}\ \text{M}$$

The standard deviation in C_A is

$$s_{C_A} = \frac{1.997 \times 10^{-3}}{29.57}\sqrt{\frac{1}{3} + \frac{1}{6} + \frac{(0.114 - 0.1183)^2}{(29.57)^2 \times (4.408 \times 10^{-5})}} = 4.778 \times 10^{-5}$$

and the 95% confidence interval is

$$\mu = C_A \pm t s_{C_A} = 3.80 \times 10^{-3} \pm \{2.78 \times (4.778 \times 10^{-5})\}$$

$$\mu = 3.80 \times 10^{-3}\ \text{M} \pm 0.13 \times 10^{-3}\ \text{M}$$

EVALUATING A LINEAR REGRESSION MODEL

You should never accept the result of a linear regression analysis without evaluating the validity of the model. Perhaps the simplest way to evaluate a regression analysis is to examine the residual errors. As we saw earlier, the residual error for a single calibration standard, r_i, is

$$r_i = (y_i - \hat{y}_i)$$

If the regression model is valid, then the residual errors should be distributed randomly about an average residual error of zero, with no apparent trend toward either smaller or larger residual errors (Figure 5.4.6 a). Trends such as those in Figure 5.4.6 b and Figure 5.4.6 c provide evidence that at least one of the model's assumptions is incorrect. For example, a trend toward larger residual errors at higher concentrations, Figure 5.4.6 b, suggests that the indeterminate errors affecting the signal are not independent of the analyte's concentration. In Figure 5.4.6 c, the residual errors are not random, which suggests we cannot model the data using a straight-line relationship. Regression methods for the latter two cases are discussed in the following sections.

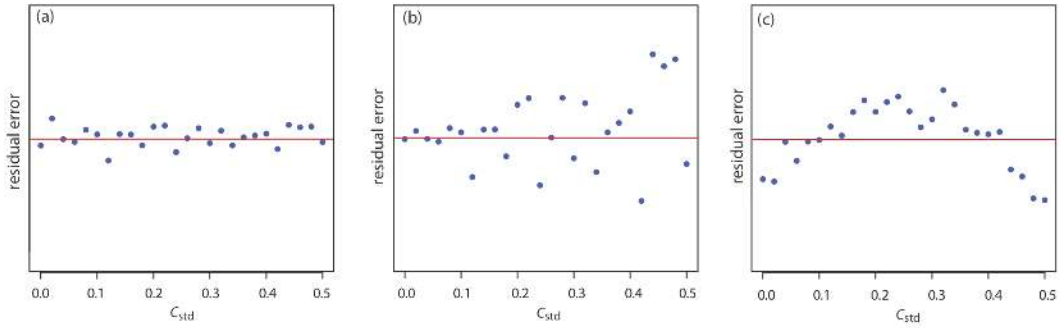


Figure 5.4.6 : Plots of the residual error in the signal, S_{std}, as a function of the concentration of analyte, C_{std}, for an unweighted straight-line regression model. The red line shows a residual error of zero. The distribution of the residual errors in (a) indicates that the unweighted linear regression model is appropriate. The increase in the residual errors in (b) for higher concentrations of analyte, suggests that a weighted straight-line regression is more appropriate. For (c), the curved pattern to the residuals suggests that a straight-line model is inappropriate; linear regression using a quadratic model might produce a better fit.

? EXERCISE 5.4.2

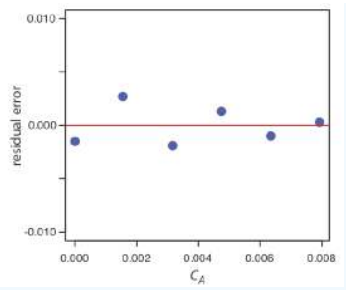
Using your results from Exercise 5.4.1 , construct a residual plot and explain its significance.

Answer

To create a residual plot, we need to calculate the residual error for each standard. The following table contains the relevant information.

x_i	y_i	$\hat{y}_i$	$y_i - \hat{y}_i$
0.000	0.000	0.0015	–0.0015
1.55×10^{-3}	0.050	0.0473	0.0027
3.16×10^{-3}	0.093	0.0949	–0.0019
4.74×10^{-3}	0.143	0.1417	0.0013
6.34×10^{-3}	0.188	0.1890	–0.0010
7.92×10^{-3}	0.236	0.2357	0.0003

The figure below shows a plot of the resulting residual errors. The residual errors appear random, although they do alternate in sign, and that do not show any significant dependence on the analyte's concentration. Taken together, these observations suggest that our regression model is appropriate.



WEIGHTED LINEAR REGRESSION WITH ERRORS IN *Y*

Our treatment of linear regression to this point assumes that indeterminate errors affecting *y* are independent of the value of *x*. If this assumption is false, as is the case for the data in Figure 5.4.6 b, then we must include the variance for each value of *y* into our determination of the *y*-intercept, b_0, and the slope, b_1; thus

$$b_0 = \frac{\sum_{i=1}^{n} w_i y_i - b_1 \sum_{i=1}^{n} w_i x_i}{n} \tag{5.4.13}$$

$$b_1 = \frac{n\sum_{i=1}^{n} w_i x_i y_i - \sum_{i=1}^{n} w_i x_i \sum_{i=1}^{n} w_i y_i}{n\sum_{i=1}^{n} w_i x_i^2 - \left(\sum_{i=1}^{n} w_i x_i\right)^2} \tag{5.4.14}$$

where w_i is a weighting factor that accounts for the variance in y_i

$$w_i = \frac{n(s_{y_i})^{-2}}{\sum_{i=1}^{n}(s_{y_i})^{-2}} \tag{5.4.15}$$

and s_{y_i} is the standard deviation for y_i. In a ***weighted linear regression***, each *xy*-pair's contribution to the regression line is inversely proportional to the precision of y_i; that is, the more precise the value of *y*, the greater its contribution to the regression.

EXAMPLE 5.4.4

Shown here are data for an external standardization in which *sstd* is the standard deviation for three replicate determination of the signal. This is the same data used in Example 5.4.1 with additional information about the standard deviations in the signal.

C_{std} (arbitrary units)	S_{std} (arbitrary units)	s_{std}
0.000	0.00	0.02
0.100	12.36	0.02
0.200	24.83	0.07
0.300	35.91	0.13
0.400	48.79	0.22
0.500	60.42	0.33

Determine the calibration curve's equation using a weighted linear regression. As you work through this example, remember that *x* corresponds to C_{std}, and that *y* corresponds to S_{std}.

Solution

We begin by setting up a table to aid in calculating the weighting factors.

C_{std} (arbitrary units)	S_{std} (arbitrary units)	s_{std}	$(s_{y_i})^{-2}$	w_i
0.000	0.00	0.02	2500.00	2.8339
0.100	12.36	0.02	250.00	2.8339
0.200	24.83	0.07	204.08	0.2313
0.300	35.91	0.13	59.17	0.0671
0.400	48.79	0.22	20.66	0.0234
0.500	60.42	0.33	9.18	0.0104

Adding together the values in the fourth column gives

$$\sum_{i=1}^{n}(s_{y_i})^{-2}$$

which we use to calculate the individual weights in the last column. As a check on your calculations, the sum of the individual weights must equal the number of calibration standards, *n*. The sum of the entries in the last column is 6.0000, so all is well. After we calculate the individual weights, we use a second table to aid in calculating the four summation terms in Equation 5.4.13 and Equation 5.4.14.

x_i	y_i	w_i	$w_i x_i$	$w_i y_i$	$w_i x_i^2$	$w_i x_i y_i$
0.000	0.00	2.8339	0.0000	0.0000	0.0000	0.0000
0.100	12.36	2.8339	0.2834	35.0270	0.0283	3.5027
0.200	24.83	0.2313	0.0463	5.7432	0.0093	1.1486
0.300	35.91	0.0671	0.0201	2.4096	0.0060	0.7229
0.400	48.79	0.0234	0.0094	1.1417	0.0037	0.4567
0.500	60.42	0.0104	0.0052	0.6284	0.0026	0.3142

Adding the values in the last four columns gives

$$\sum_{i=1}^{n} w_i x_i = 0.3644 \quad \sum_{i=1}^{n} w_i y_i = 44.9499 \quad \sum_{i=1}^{n} w_i x_i^2 = 0.0499 \quad \sum_{i=1}^{n} w_i x_i y_i = 6.1451$$

Substituting these values into the Equation 5.4.13 and Equation 5.4.14 gives the estimated slope and estimated *y*-intercept as

$$b_1 = \frac{(6 \times 6.1451) - (0.3644 \times 44.9499)}{(6 \times 0.0499) - (0.3644)^2} = 122.985$$

$$b_0 = \frac{44.9499 - (122.985 \times 0.3644)}{6} = 0.0224$$

The calibration equation is

$$S_{std} = 122.98 \times C_{std} + 0.2$$

Figure 5.4.7 shows the calibration curve for the weighted regression and the calibration curve for the unweighted regression in Example 5.4.1 . Although the two calibration curves are very similar, there are slight differences in the slope and in the *y*-intercept. Most notably, the *y*-intercept for the weighted linear regression is closer to the expected value of zero. Because the standard deviation for the signal, S_{std}, is smaller for smaller concentrations of analyte, C_{std}, a weighted linear regression gives more emphasis to these standards, allowing for a better estimate of the *y*-intercept.

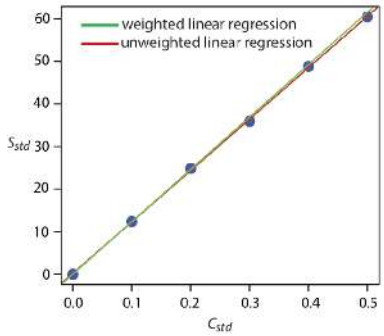


Figure 5.4.7 : A comparison of the unweighted and the weighted normal calibration curves. See Example 5.4.1 for details of the unweighted linear regression and Example 5.4.4 for details of the weighted linear regression.

Equations for calculating confidence intervals for the slope, the *y*-intercept, and the concentration of analyte when using a weighted linear regression are not as easy to define as for an unweighted linear regression [Bonate, P. J. *Anal. Chem.* **1993**, *65*, 1367–1372]. The confidence interval for the analyte's concentration, however, is at its optimum value when the analyte's signal is near the weighted centroid, y_c , of the calibration curve.

$$y_c = \frac{1}{n} \sum_{i=1}^{n} w_i x_i$$

WEIGHTED LINEAR REGRESSION WITH ERRORS IN BOTH *X* AND *Y*

If we remove our assumption that indeterminate errors affecting a calibration curve are present only in the signal (*y*), then we also must factor into the regression model the indeterminate errors that affect the analyte's concentration in the calibration standards (*x*). The solution for the resulting regression line is computationally more involved than that for either the unweighted or weighted regression lines. Although

we will not consider the details in this textbook, you should be aware that neglecting the presence of indeterminate errors in *x* can bias the results of a linear regression.

> See, for example, Analytical Methods Committee, "Fitting a linear functional relationship to data with error on both variable," AMC Technical Brief, March, 2002), as well as this chapter's Additional Resources.

CURVILINEAR AND MULTIVARIATE REGRESSION

A straight-line regression model, despite its apparent complexity, is the simplest functional relationship between two variables. What do we do if our calibration curve is curvilinear—that is, if it is a curved-line instead of a straight-line? One approach is to try transforming the data into a straight-line. Logarithms, exponentials, reciprocals, square roots, and trigonometric functions have been used in this way. A plot of log(*y*) versus *x* is a typical example. Such transformations are not without complications, of which the most obvious is that data with a uniform variance in *y* will not maintain that uniform variance after it is transformed.

> It is worth noting that the term "linear" does not mean a straight-line. A linear function may contain more than one additive term, but each such term has one and only one adjustable multiplicative parameter. The function
>
> $$y = ax + bx^2$$
>
> is an example of a linear function because the terms *x* and x^2 each include a single multiplicative parameter, *a* and *b*, respectively. The function
>
> $$y = x^b$$
>
> is nonlinear because *b* is not a multiplicative parameter; it is, instead, a power. This is why you can use linear regression to fit a polynomial equation to your data.
>
> Sometimes it is possible to transform a nonlinear function into a linear function. For example, taking the log of both sides of the nonlinear function above gives a linear function.
>
> $$\log(y) = b\log(x)$$

Another approach to developing a linear regression model is to fit a polynomial equation to the data, such as $y = a + bx + cx^2$. You can use linear regression to calculate the parameters *a*, *b*, and *c*, although the equations are different than those for the linear regression of a straight-line. If you cannot fit your data using a single polynomial equation, it may be possible to fit separate polynomial equations to short segments of the calibration curve. The result is a single continuous calibration curve known as a spline function.

> For details about curvilinear regression, see (a) Sharaf, M. A.; Illman, D. L.; Kowalski, B. R. *Chemometrics*, Wiley-Interscience: New York, 1986; (b) Deming, S. N.; Morgan, S. L. *Experimental Design: A Chemometric Approach*, Elsevier: Amsterdam, 1987.

The regression models in this chapter apply only to functions that contain a single independent variable, such as a signal that depends upon the analyte's concentration. In the presence of an interferent, however, the signal may depend on the concentrations of both the analyte and the interferent

$$S = k_A C_A + k_I CI + S_{reag}$$

where k_I is the interferent's sensitivity and C_I is the interferent's concentration. Multivariate calibration curves are prepared using standards that contain known amounts of both the analyte and the interferent, and modeled using multivariate regression.

> See Beebe, K. R.; Kowalski, B. R. *Anal. Chem.* **1987**, *59*, 1007A–1017A. for additional details, and check out this chapter's Additional Resources for more information about linear regression with errors in both variables, curvilinear regression, and multivariate regression.

This page titled 5.4: Linear Regression and Calibration Curves is shared under a CC BY-NC-SA 4.0 license and was authored, remixed, and/or curated by David Harvey.

- **5.4: Linear Regression and Calibration Curves** by David Harvey is licensed CC BY-NC-SA 4.0.

5.5: COMPENSATING FOR THE REAGENT BLANK

Thus far in our discussion of strategies for standardizing analytical methods, we have assumed that a suitable reagent blank is available to correct for signals arising from sources other than the analyte. We did not, however ask an important question: "What constitutes an appropriate reagent blank?" Surprisingly, the answer is not immediately obvious.

In one study, approximately 200 analytical chemists were asked to evaluate a data set consisting of a normal calibration curve, a separate analyte-free blank, and three samples with different sizes, but drawn from the same source [Cardone, M. J. *Anal. Chem.* **1986**, *58*, 433–438]. The first two columns in Table 5.5.1 shows a series of external standards and their corresponding signals. The normal calibration curve for the data is

$$S_{std} = 0.0750 \times W_{std} + 0.1250$$

where the *y*-intercept of 0.1250 is the calibration blank. A separate reagent blank gives the signal for an analyte-free sample.

Table 5.5.1 : Data Used to Study the Blank in an Analytical Method

W_{std}	S_{std}	Sample Number	W_{samp}	S_{samp}
1.6667	0.2500	1	62.4746	0.8000
5.0000	0.5000	2	82.7915	1.0000
8.3333	0.7500	3	103.1085	1.2000
11.6667	0.8413			
18.1600	1.4870		reagent blank	0.1000
19.9333	1.6200			
$S_{std} = 0.0750 \times W_{std} + 0.1250$				
W_{std}: weight of analyte used to prepare the external standard; diluted to a volume, V				
W_{samp}: weight of sample used to prepare sample as analyzed; diluted to a volume, V				

In working up this data, the analytical chemists used at least four different approaches to correct the signals: (a) ignoring both the calibration blank, *CB*, and the reagent blank, *RB*, which clearly is incorrect; (b) using the calibration blank only; (c) using the reagent blank only; and (d) using both the calibration blank and the reagent blank. The first four rows of Table 5.5.2 shows the equations for calculating the analyte's concentration using each approach, along with the reported concentrations for the analyte in each sample.

Table 5.5.2 : Equations and Resulting Concentrations of Analyte for Different Approaches to Correcting for the Blank

		Concentration of Analyte in...		
Approach for Correcting the Signal	Equation	Sample 1	Sample 2	Sample 3
ignore calibration and reagent blanks	$C_A = \frac{W_A}{W_{samp}} = \frac{S_{samp}}{k_A W_{samp}}$	0.1707	0.1610	0.1552
use calibration blank only	$C_A = \frac{W_A}{W_{samp}} = \frac{S_{samp} - CB}{k_A W_{samp}}$	0.1441	0.1409	0.1390
use reagent blank only	$C_A = \frac{W_A}{W_{samp}} = \frac{S_{samp} - RB}{k_A W_{samp}}$	0.1494	0.1449	0.1422
use both calibration and reagent blanks	$C_A = \frac{W_A}{W_{samp}} = \frac{S_{samp} - CB - RB}{k_A W_{samp}}$	0.1227	0.1248	0.1266
use total Youden blank	$C_A = \frac{W_A}{W_{samp}} = \frac{S_{samp} - TYB}{k_A W_{samp}}$	0.1313	0.1313	0.1313
$C_A =$ concentration of analyte; $W_A =$ weight of analyte; W_{samp} weight of sample; $k_A =$ slope of calibration curve (0.0750; slope of calibration equation); CB $=$ calibration blank (0.125; intercept of calibration equation); $RB =$ reagent blank (0.100); $TYB =$ total Youden blank (0.185; see text)				

That all four methods give a different result for the analyte's concentration underscores the importance of choosing a proper blank, but does not tell us which blank is correct. Because all four methods fail to predict the same concentration of analyte for each sample, none of these blank corrections properly accounts for an underlying constant source of determinate error.

To correct for a constant method error, a blank must account for signals from any reagents and solvents used in the analysis and any bias that results from interactions between the analyte and the sample's matrix. Both the calibration blank and the reagent blank compensate for signals from reagents and solvents. Any difference in their values is due to indeterminate errors in preparing and analyzing the standards.

> Because we are considering a matrix effect of sorts, you might think that the method of standard additions is one way to overcome this problem. Although the method of standard additions can compensate for proportional determinate errors, it cannot correct for a constant determinate error; see Ellison, S. L. R.; Thompson, M. T. "Standard additions: myth and reality," *Analyst*, **2008**, *133*, 992–997.

Unfortunately, neither a calibration blank nor a reagent blank can correct for a bias that results from an interaction between the analyte and the sample's matrix. To be effective, the blank must include both the sample's matrix and the analyte and, consequently, it must be determined using the sample itself. One approach is to measure the signal for samples of different size, and to determine the regression line for a plot of S_{samp} versus the amount of sample. The resulting *y*-intercept gives the signal in the absence of sample, and is known as the ***total Youden blank*** [Cardone, M. J. *Anal. Chem.* **1986**, *58*, 438–445]. This is the true blank correction. The regression line for the three samples in Table 5.5.1 is

$$S_{samp} = 0.009844 \times W_{samp} + 0.185$$

giving a true blank correction of 0.185. As shown in Table 5.5.2 , using this value to correct S_{samp} gives identical values for the concentration of analyte in all three samples.

The use of the total Youden blank is not common in analytical work, with most chemists relying on a calibration blank when using a calibration curve and a reagent blank when using a single-point standardization. As long we can ignore any constant bias due to interactions between the analyte and the sample's matrix, which is often the case, the accuracy of an analytical method will not suffer. It is a good idea, however, to check for constant sources of error before relying on either a calibration blank or a reagent blank.

This page titled 5.5: Compensating for the Reagent Blank is shared under a CC BY-NC-SA 4.0 license and was authored, remixed, and/or curated by David Harvey.

- **5.5: Compensating for the Reagent Blank** by David Harvey is licensed CC BY-NC-SA 4.0.

5.6: USING EXCEL AND R FOR A LINEAR REGRESSION

Although the calculations in this chapter are relatively straightforward—consisting, as they do, mostly of summations—it is tedious to work through problems using nothing more than a calculator. Both Excel and R include functions for completing a linear regression analysis and for visually evaluating the resulting model.

EXCEL

Let's use Excel to fit the following straight-line model to the data in Example 5.4.1.

$$y = \beta_0 + \beta_1 x$$

Enter the data into a spreadsheet, as shown in Figure 5.6.1 . Depending upon your needs, there are many ways that you can use Excel to complete a linear regression analysis. We will consider three approaches here.

	A	B
1	Cstd	Sstd
2	0.000	0.00
3	0.100	12.36
4	0.200	24.83
5	0.300	35.91
6	0.400	48.79
7	0.500	60.42

Figure 5.6.1 : Portion of a spreadsheet containing data from Example 5.4.1 (Cstd = C_{std}; Sstd = S_{std}).

USING EXCEL'S BUILT-IN FUNCTIONS

If all you need are values for the slope, β_1, and the *y*-intercept, β_0, you can use the following functions:

= intercept(*known_y's*, *known_x's*)

= slope(*known_y's*, *known_x's*)

where *known_y's* is the range of cells that contain the signals (*y*), and *known_x's* is the range of cells that contain the concentrations (*x*). For example, if you click on an empty cell and enter

= slope(B2:B7, A2:A7)

Excel returns exact calculation for the slope (120.705 714 3).

USING EXCEL'S DATA ANALYSIS TOOLS

To obtain the slope and the *y*-intercept, along with additional statistical details, you can use the data analysis tools in the Data Analysis ToolPak. The ToolPak is not a standard part of Excel's instillation. To see if you have access to the Analysis ToolPak on your computer, select **Tools** from the menu bar and look for the **Data Analysis...** option. If you do not see **Data Analysis...**, select **Add-ins...** from the **Tools** menu. Check the box for the **Analysis ToolPak** and click on **OK** to install them.

Select **Data Analysis...** from the **Tools** menu, which opens the *Data Analysis* window. Scroll through the window, select **Regression** from the available options, and press **OK**. Place the cursor in the box for *Input Y range* and then click and drag over cells B1:B7. Place the cursor in the box for *Input X range* and click and drag over cells A1:A7. Because cells A1 and B1 contain labels, check the box for *Labels*.

> Including labels is a good idea. Excel's summary output uses the *x*-axis label to identify the slope.

Select the radio button for *Output range* and click on any empty cell; this is where Excel will place the results. Clicking **OK** generates the information shown in Figure 5.6.2 .

SUMMARY OUTPUT

Regression Statistics	
Multiple R	0.99987244
R Square	0.9997449
Adjusted R Square	0.99968113
Standard Error	0.40329713
Observations	6

ANOVA

	df	SS	MS	F	Significance F
Regression	1	2549.727156	2549.72716	15676.296	2.4405E-08
Residual	4	0.650594286	0.16264857		
Total	5	2550.37775			

	Coefficients	Standard Error	t Stat	P-value	Lower 95%	Upper 95%	Lower 95.0%	Upper 95.0%
Intercept	0.20857143	0.29188503	0.71456706	0.51436267	-0.60183133	1.01897419	-0.60183133	1.01897419
Cstd	120.705714	0.964064525	125.205016	2.4405E-08	118.029042	123.382387	118.029042	123.382387

Figure 5.6.2 : Output from Excel's Regression command in the Analysis ToolPak. See the text for a discussion of how to interpret the information in these tables.

There are three parts to Excel's summary of a regression analysis. At the top of Figure 5.6.2 is a table of *Regression Statistics*. The *standard error* is the standard deviation about the regression, s_r. Also of interest is the value for *Multiple R*, which is the model's correlation coefficient, *r*, a term with which you may already be familiar. The correlation coefficient is a measure of the extent to which the regression model explains the variation in *y*. Values of *r* range from –1 to +1. The closer the correlation coefficient is to ±1, the better the model is at explaining the data. A correlation coefficient of 0 means there is no relationship between *x* and *y*. In developing the calculations for linear regression, we did not consider the correlation coefficient. There is a reason for this. For most straight-line calibration curves the correlation coefficient is very close to +1, typically 0.99 or better. There is a tendency, however, to put too much faith in the correlation coefficient's significance, and to assume that an *r* greater than 0.99 means the linear regression model is appropriate. Figure 5.6.3 provides a useful counterexample. Although the regression line has a correlation coefficient of 0.993, the data clearly is curvilinear. The take-home lesson here is simple: do not fall in love with the correlation coefficient!

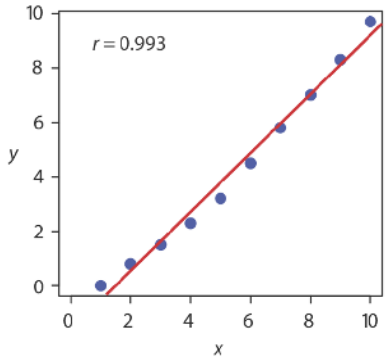


Figure 5.6.3 : Example of fitting a straight-line (in red) to curvilinear data (in blue).

The second table in Figure 5.6.2 is entitled *ANOVA*, which stands for analysis of variance. We will take a closer look at ANOVA in Chapter 14. For now, it is sufficient to understand that this part of Excel's summary provides information on whether the linear regression model explains a significant portion of the variation in the values of *y*. The value for *F* is the result of an *F*-test of the following null and alternative hypotheses.

H_0: the regression model does not explain the variation in *y*

H_A: the regression model does explain the variation in *y*

The value in the column for *Significance F* is the probability for retaining the null hypothesis. In this example, the probability is $2.5 \times 10^{-6}\%$, which is strong evidence for accepting the regression model. As is the case with the correlation coefficient, a small value for the probability is a likely outcome for any calibration curve, even when the model is inappropriate. The probability for retaining the null hypothesis for the data in Figure 5.6.3 , for example, is $9.0 \times 10^{-7}\%$.

> See Chapter 4.6 for a review of the *F*-test.

The third table in Figure 5.6.2 provides a summary of the model itself. The values for the model's coefficients—the slope, β_1, and the *y*-intercept, β_0—are identified as *intercept* and with your label for the *x*-axis data, which in this example is C_{std}. The standard deviations for the coefficients, s_{b_0} and s_{b_1}, are in the column labeled *Standard error*. The column *t Stat* and the column *P-value* are for the following *t*-tests.

$$\text{slope: } H_0\text{: } \beta_1 = 0 \quad H_A\text{: } \beta_1 \neq 0$$

y-intercept: $H_0: \beta_0 = 0 \quad H_A: \beta_0 \neq 0$

The results of these *t*-tests provide convincing evidence that the slope is not zero, but there is no evidence that the *y*-intercept differs significantly from zero. Also shown are the 95% confidence intervals for the slope and the *y*-intercept (*lower 95%* and *upper 95%*).

> See Chapter 4.6 for a review of the *t*-test.

PROGRAMMING THE FORMULAS YOURSELF

A third approach to completing a regression analysis is to program a spreadsheet using Excel's built-in formula for a summation

=sum(*first cell*:*last cell*)

and its ability to parse mathematical equations. The resulting spreadsheet is shown in Figure 5.6.4 .

	A	B	C	D	E	F
1	x	y	xy	x^2	n =	6
2	0.000	0.00	=A2*B2	=A2^2	slope =	=(F1*C8 - A8*B8)/(F1*D8-A8^2)
3	0.100	12.36	=A3*B3	=A3^2	y-int =	=(B8-F2*A8)/F1
4	0.200	24.83	=A4*B4	=A4^2		
5	0.300	35.91	=A5*B5	=A5^2		
6	0.400	48.79	=A6*B6	=A6^2		
7	0.500	60.42	=A7*B7	=A7^2		
8						
9	=sum(A2:A7)	=sum(B2:B7)	=sum(C2:C7)	=sum(D2:D7)	<--sums	

Figure 5.6.4 : Spreadsheet showing the formulas for calculating the slope and the *y*-intercept for the data in Example 5.4.1. The shaded cells contain formulas that you must enter. Enter the formulas in cells C3 to C7, and cells D3 to D7. Next, enter the formulas for cells A9 to D9. Finally, enter the formulas in cells F2 and F3. When you enter a formula, Excel replaces it with the resulting calculation. The values in these cells should agree with the results in Example 5.4.1. You can simplify the entering of formulas by copying and pasting. For example, enter the formula in cell C2. Select **Edit: Copy**, click and drag your cursor over cells C3 to C7, and select **Edit: Paste**. Excel automatically updates the cell referencing.

USING EXCEL TO VISUALIZE THE REGRESSION MODEL

You can use Excel to examine your data and the regression line. Begin by plotting the data. Organize your data in two columns, placing the *x* values in the left-most column. Click and drag over the data and select **Charts** from the ribbon. Select **Scatter**, choosing the option without lines that connect the points. To add a regression line to the chart, click on the chart's data and select **Chart: Add Trendline...** from the main men. Pick the straight-line model and click **OK** to add the line to your chart. By default, Excel displays the regression line from your first point to your last point. Figure 5.6.5 shows the result for the data in Figure 5.6.1 .

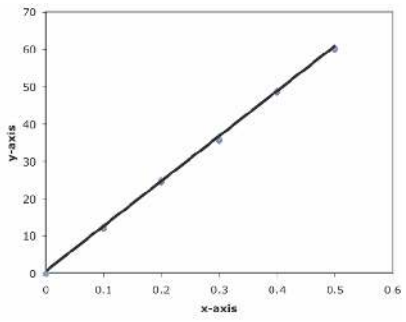


Figure 5.6.5 : Example of an Excel scatterplot showing the data and a regression line.

Excel also will create a plot of the regression model's residual errors. To create the plot, build the regression model using the Analysis ToolPak, as described earlier. Clicking on the option for *Residual plots* creates the plot shown in Figure 5.6.6 .

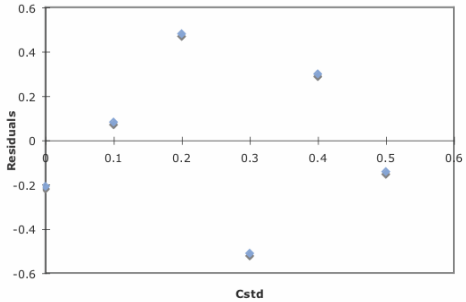


Figure 5.6.6 : Example of Excel's plot of a regression model's residual errors.

LIMITATIONS TO USING EXCEL FOR A REGRESSION ANALYSIS

Excel's biggest limitation for a regression analysis is that it does not provide a function to calculate the uncertainty when predicting values of x. In terms of this chapter, Excel can not calculate the uncertainty for the analyte's concentration, C_A, given the signal for a sample, S_{samp}. Another limitation is that Excel does not have a built-in function for a weighted linear regression. You can, however, program a spreadsheet to handle these calculations.

EXERCISE 5.6.1

Use Excel to complete the regression analysis in Exercise 5.4.1.

Answer

Begin by entering the data into an Excel spreadsheet, following the format shown in Figure 5.6.1 . Because Excel's Data Analysis tools provide most of the information we need, we will use it here. The resulting output, which is shown below, provides the slope and the y-intercept, along with their respective 95% confidence intervals.

SUMMARY OUTPUT

Regression Statistics	
Multiple R	0.99979366
R Square	0.99958737
Adjusted R Sq	0.99948421
Standard Erro	0.00199602
Observations	6

ANOVA

	df	*SS*	*MS*	*F*	*Significance F*
Regression	1	0.0386054	0.0386054	9689.9103	6.3858E-08
Residual	4	1.5936E-05	3.9841E-06		
Total	5	0.03862133			

	Coefficients	*Standard Error*	*t Stat*	*P-value*	*Lower 95%*	*Upper 95%*	*Lower 95.0%*	*Upper 95.0%*
Intercept	0.00139272	0.00144059	0.96677158	0.38840479	-0.00260699	0.00539242	-0.00260699	0.00539242
Cstd	29.5927329	0.30062507	98.437342	6.3858E-08	28.7580639	30.4274019	28.7580639	30.4274019

Excel does not provide a function for calculating the uncertainty in the analyte's concentration, C_A, given the signal for a sample, S_{samp}. You must complete these calculations by hand. With an S_{samp} of 0.114, we find that C_A is

$$C_A = \frac{S_{samp} - b_0}{b_1} = \frac{0.114 - 0.0014}{29.59\ \text{M}^{-1}} = 3.80 \times 10^{-3}\ \text{M}$$

The standard deviation in C_A is

$$s_{C_A} = \frac{1.996 \times 10^{-3}}{29.59} \sqrt{\frac{1}{3} + \frac{1}{6} + \frac{(0.114 - 0.1183)^2}{(29.59)^2 \times 4.408 \times 10^{-5})}} = 4.772 \times 10^{-5}$$

and the 95% confidence interval is

$$\mu = C_A \pm t s_{C_A} = 3.80 \times 10^{-3} \pm \{2.78 \times (4.772 \times 10^{-5})\}$$

$$\mu = 3.80 \times 10^{-3}\ \text{M} \pm 0.13 \times 10^{-3}\ \text{M}$$

R

Let's use R to fit the following straight-line model to the data in Example 5.4.1.

$$y = \beta_0 + \beta_1 x$$

ENTERING DATA AND CREATING THE REGRESSION MODEL

To begin, create objects that contain the concentration of the standards and their corresponding signals.

> conc = c(0, 0.1, 0.2, 0.3, 0.4, 0.5)

> signal = c(0, 12.36, 24.83, 35.91, 48.79, 60.42)

The command for a straight-line linear regression model is

$$\text{lm}(y \sim x)$$

where y and x are the objects the objects our data. To access the results of the regression analysis, we assign them to an object using the following command

> *model* = lm(signal ~ conc)

where *model* is the name we assign to the object.

> As you might guess, *lm* is short for linear model.
>
> You can choose any name for the object that contains the results of the regression analysis.

EVALUATING THE LINEAR REGRESSION MODEL

To evaluate the results of a linear regression we need to examine the data and the regression line, and to review a statistical summary of the model. To examine our data and the regression line, we use the **plot** command, which takes the following general form

plot(*x*, *y*, optional arguments to control style)

where *x* and *y* are the objects that contain our data, and the **abline** command

abline(*object*, optional arguments to control style)

where *object* is the object that contains the results of the linear regression. Entering the commands

> plot(conc, signal, pch = 19, col = “blue”, cex = 2)

> abline(model, col = “red”)

creates the plot shown in Figure 5.6.7 .

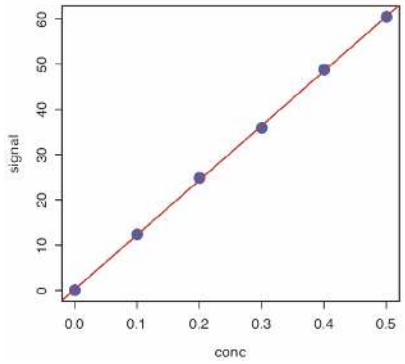


Figure 5.6.7 : Example of a regression plot in R showing the data (in blue) and the regression line (in red). You can customize your plot by adjusting the plot command’s optional arguments. For example, the argument *pch* controls the symbol used for plotting points, the argument *col* allows you to select a color for the points or the line, and the argument *cex* sets the size for the points. You can use the command *help(plot)* to learn more about the options for plotting data in R.

To review a statistical summary of the regression model, we use the **summary** command.

> summary(model)

The resulting output, shown in Figure 5.6.8 , contains three sections.

```
> model=lm(signal~conc)
> summary(model)

Call:
lm(formula = signal ~ conc)

Residuals:
     1          2         3         4         5         6
-0.20857  0.08086  0.48029 -0.51029  0.29914 -0.14143

Coefficients:
             Estimate   Std. Error   t value   Pr(>|t|)
(Intercept)  0.2086     0.2919       0.715     0.514
conc         120.7057   0.9641       125.205   2.44e-08 ***
---
Signif. codes:  0 ‘***’ 0.001 ‘**’ 0.01 ‘*’ 0.05 ‘.’ 0.1 ‘ ’ 1

Residual standard error: 0.4033 on 4 degrees of freedom
Multiple R-Squared: 0.9997,   Adjusted R-squared: 0.9997
F-statistic: 1.568e+04 on 1 and 4 DF,  p-value: 2.441e-08
```

Figure 5.6.8 : The summary of R’s regression analysis. See the text for a discussion of how to interpret the information in the output’s three sections.

The first section of R’s summary of the regression model lists the residual errors. To examine a plot of the residual errors, use the command

> plot(model, which = 1)

which produces the result shown in Figure 5.6.9 . Note that R plots the residuals against the predicted (fitted) values of *y* instead of against the known values of *x*. The choice of how to plot the residuals is not critical, as you can see by comparing Figure 5.6.9 to Figure 5.6.6 . The line in Figure 5.6.9 is a smoothed fit of the residuals.

The reason for including the argument *which = 1* is not immediately obvious. When you use R's *plot* command on an object created by the *lm* command, the default is to create four charts summarizing the model's suitability. The first of these charts is the residual plot; thus, *which = 1* limits the output to this plot.

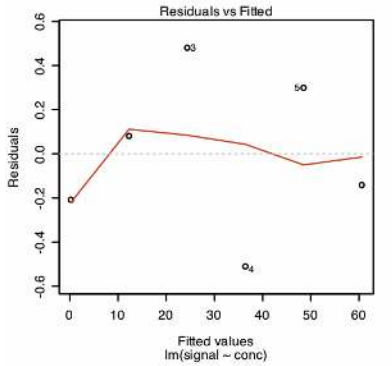


Figure 5.6.9 : Example showing R's plot of a regression model's residual error.

The second section of Figure 5.6.8 provides the model's coefficients—the slope, β_1, and the *y*-intercept, β_0—along with their respective standard deviations (*Std. Error*). The column *t value* and the column *Pr(>|t|)* are for the following *t*-tests.

$$\text{slope: } H_0\text{: } \beta_1 = 0 \quad H_A\text{: } \beta_1 \neq 0$$

$$y\text{-intercept: } H_0\text{: } \beta_0 = 0 \quad H_A\text{: } \beta_0 \neq 0$$

The results of these *t*-tests provide convincing evidence that the slope is not zero, but no evidence that the *y*-intercept differs significantly from zero.

The last section of the regression summary provides the standard deviation about the regression (*residual standard error*), the square of the correlation coefficient (*multiple R-squared*), and the result of an *F*-test on the model's ability to explain the variation in the *y* values. For a discussion of the correlation coefficient and the *F*-test of a regression model, as well as their limitations, refer to the section on using Excel's data analysis tools.

PREDICTING THE UNCERTAINTY IN C_A GIVEN S_{samp}

Unlike Excel, R includes a command for predicting the uncertainty in an analyte's concentration, C_A, given the signal for a sample, S_{samp}. This command is not part of R's standard installation. To use the command you need to install the "chemCal" package by entering the following command (*note: you will need an internet connection to download the package*).

> install.packages("chemCal")

After installing the package, you need to load the functions into R using the following command. (*note: you will need to do this step each time you begin a new R session as the package does not automatically load when you start R*).

> library("chemCal")

You need to install a package once, but you need to load the package each time you plan to use it. There are ways to configure R so that it automatically loads certain packages; see *An Introduction to R* for more information (click here to view a PDF version of this document).

The command for predicting the uncertainty in C_A is **inverse.predict**, which takes the following form for an unweighted linear regression

inverse.predict(*object*, *newdata*, alpha = *value*)

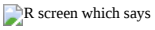
where *object* is the object that contains the regression model's results, *new-data* is an object that contains values for S_{samp}, and *value* is the numerical value for the significance level. Let's use this command to complete Example 5.4.3. First, we create an object that contains the values of S_{samp}

> sample = c(29.32, 29.16, 29.51)

and then we complete the computation using the following command

> inverse.predict(model, sample, alpha = 0.05)

producing the result shown in Figure 5.6.10 . The analyte's concentration, C_A, is given by the value *$Prediction*, and its standard deviation, s_{C_A}, is shown as *$`Standard Error`*. The value for *$Confidence* is the confidence interval, $\pm t s_{C_A}$, for the analyte's concentration, and *$`Confidence Limits`* provides the lower limit and upper limit for the confidence interval for C_A.



inverse.predict(model, sample, alpha=0.05); $Prediction; [1] 0.2412597; $`Standard Error`; [1] 0.002363588; $Confidence; [1] 0.006562373; $`Confidence Limits`; [1] 0.2346974 0.2478221." style="width: 328px; height: 243px;" width="328px" height="243px" src="/@api/deki/files/162725/Figure5.24.png">

Figure 5.6.10 : Output from R's command for predicting the analyte's concentration, C_A, from the sample's signal, S_{samp}.

USING R FOR A WEIGHTED LINEAR REGRESSION

R's command for an unweighted linear regression also allows for a weighted linear regression if we include an additional argument, *weights*, whose value is an object that contains the weights.

$$\text{lm}(y \sim x, \textit{weights} = \textit{object})$$

Let's use this command to complete Example 5.4.4. First, we need to create an object that contains the weights, which in R are the reciprocals of the standard deviations in y, $(s_{y_i})^{-2}$. Using the data from Example 5.4.4, we enter

> syi=c(0.02, 0.02, 0.07, 0.13, 0.22, 0.33)

> w=1/syi^2

to create the object that contains the weights. The commands

> modelw= lm(signal ~ conc, weights = w)

> summary(modelw)

generate the output shown in Figure 5.6.11 . Any difference between the results shown here and the results shown in Example 5.4.4 are the result of round-off errors in our earlier calculations.

> You may have noticed that this way of defining weights is different than that shown in Equation 5.4.15. In deriving equations for a weighted linear regression, you can choose to normalize the sum of the weights to equal the number of points, or you can choose not to —the algorithm in R does not normalize the weights.

```
> modelw=lm(signal~conc, weights = w)
> summary(modelw)

Call:
lm(formula = signal ~ conc, weights = w)

Residuals:
   1      2      3      4      5      6
-2.223  2.571  3.676 -7.129 -1.413 -2.864

Coefficients:
             Estimate   Std. Error  t value  Pr(>|t|)
(Intercept)  0.04446    0.08542     0.52     0.63
conc         122.64111  0.93590     131.04   2.03e-08 ***
---
Signif. codes:  0 '***' 0.001 '**' 0.01 '*' 0.05 '.' 0.1 ' ' 1

Residual standard error: 4.639 on 4 degrees of freedom
Multiple R-Squared: 0.9998,   Adjusted R-squared: 0.9997
F-statistic: 1.717e+04 on 1 and 4 DF,  p-value: 2.034e-08
```

Figure 5.6.11 : The summary of R's regression analysis for a weighted linear regression. The types of information shown here is identical to that for the unweighted linear regression in Figure 5.6.8 .

? EXERCISE 5.6.2

Use R to complete the regression analysis in Exercise 5.4.1.

Answer

The figure below shows the R session for this problem, including loading the *chemCal* package, creating objects to hold the values for C_{std}, S_{std}, and S_{samp}. Note that for S_{samp}, we do not have the actual values for the three replicate measurements. In place of the actual measurements, we just enter the average signal three times. This is okay because the calculation depends on the average signal and the number of replicates, and not on the individual measurements.

```
> library("chemCal")
> conc=c(0, 1.55e-3, 3.16e-3, 4.74e-3, 6.34e-3, 7.92e-3)
> signal=c(0, 0.050, 0.093, 0.143, 0.188, 0.236)
> model=lm(signal~conc)
> summary(model)

Call:
lm(formula = signal ~ conc)

Residuals:
      1           2           3           4           5           6
-0.0013927  0.0027385 -0.0019058  0.0013377 -0.0010106  0.0002328

Coefficients:
             Estimate   Std. Error   t value   Pr(>|t|)
(Intercept)  0.001393   0.001441     0.967     0.388
conc         29.592733  0.300625     98.437    6.39e-08 ***
---
Signif. codes:  0 '***' 0.001 '**' 0.01 '*' 0.05 '.' 0.1 ' ' 1

Residual standard error: 0.001996 on 4 degrees of freedom
Multiple R-Squared: 0.9996,   Adjusted R-squared: 0.9995
F-statistic:  9690 on 1 and 4 DF,  p-value: 6.386e-08

> samp=c(0.114, 0.114, 0.114)
> inverse.predict(model,samp,alpha=0.05)
$Prediction
[1] 0.003805234

$`Standard Error`
[1] 4.771723e-05

$Confidence
[1] 0.0001324843

$`Confidence Limits`
[1] 0.003672750 0.003937719
```

This page titled 5.6: Using Excel and R for a Linear Regression is shared under a CC BY-NC-SA 4.0 license and was authored, remixed, and/or curated by David Harvey.

- **5.6: Using Excel and R for a Linear Regression** by David Harvey is licensed CC BY-NC-SA 4.0.

5.7: PROBLEMS

1. Suppose you use a serial dilution to prepare 100 mL each of a series of standards with concentrations of 1.00×10^{-5}, 1.00×10^{-4}, 1.00×10^{-3}, and 1.00×10^{-2} M from a 0.100 M stock solution. Calculate the uncertainty for each solution using a propagation of uncertainty, and compare to the uncertainty if you prepare each solution as a single dilution of the stock solution. You will find tolerances for different types of volumetric glassware and digital pipets in Table 4.2.1 and Table 4.2.2. Assume that the uncertainty in the stock solution's molarity is ±0.0002.

2. Three replicate determinations of S_{total} for a standard solution that is 10.0 ppm in analyte give values of 0.163, 0.157, and 0.161 (arbitrary units). The signal for the reagent blank is 0.002. Calculate the concentration of analyte in a sample with a signal of 0.118.

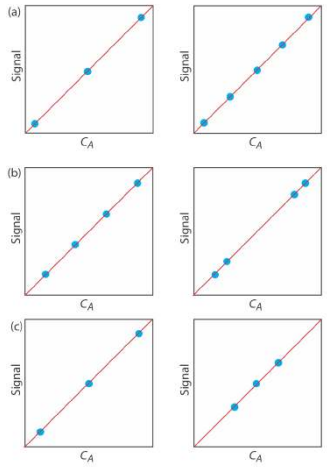
3. A 10.00-g sample that contains an analyte is transferred to a 250-mL volumetric flask and diluted to volume. When a 10.00 mL aliquot of the resulting solution is diluted to 25.00 mL it gives a signal of 0.235 (arbitrary units). A second 10.00-mL portion of the solution is spiked with 10.00 mL of a 1.00-ppm standard solution of the analyte and diluted to 25.00 mL. The signal for the spiked sample is 0.502. Calculate the weight percent of analyte in the original sample.

4. A 50.00 mL sample that contains an analyte gives a signal of 11.5 (arbitrary units). A second 50 mL aliquot of the sample, which is spiked with 1.00 mL of a 10.0-ppm standard solution of the analyte, gives a signal of 23.1. What is the analyte's concentration in the original sample?

5. A standard additions calibration curve based on Equation 5.3.10 places $S_{spike} \times (V_o + V_{std})$ on the *y*-axis and $C_{std} \times V_{std}$ on the *x*-axis. Derive equations for the slope and the *y*-intercept and explain how you can determine the amount of analyte in a sample from the calibration curve. In addition, clearly explain why you cannot plot S_{spike} on the *y*-axis and $C_{std} \times \{V_{std}/(V_o + V_{std})\}$ on the *x*-axis.

6. A standard sample contains 10.0 mg/L of analyte and 15.0 mg/L of internal standard. Analysis of the sample gives signals for the analyte and the internal standard of 0.155 and 0.233 (arbitrary units), respectively. Sufficient internal standard is added to a sample to make its concentration 15.0 mg/L. Analysis of the sample yields signals for the analyte and the internal standard of 0.274 and 0.198, respectively. Report the analyte's concentration in the sample.

7. For each of the pair of calibration curves shown ibelow, select the calibration curve that uses the more appropriate set of standards. Briefly explain the reasons for your selections. The scales for the *x*-axis and the *y*-axis are the same for each pair.



8. The following data are for a series of external standards of Cd^{2+} buffered to a pH of 4.6.

$[Cd^{2+}]$ (nM)	15.4	30.4	44.9	59.0	72.7	86.0
S_{spike} (nA)	4.8	11.4	18.2	26.6	32.3	37.7

(a) Use a linear regression analysis to determine the equation for the calibration curve and report confidence intervals for the slope and the *y*-intercept.

(b) Construct a plot of the residuals and comment on their significance.

At a pH of 3.7 the following data were recorded for the same set of external standards.

$[Cd^{2+}]$ (nM)	15.4	30.4	44.9	59.0	72.7	86.0
S_{spike} (nA)	15.0	42.7	58.5	77.0	101	118

(c) How much more or less sensitive is this method at the lower pH?

(d) A single sample is buffered to a pH of 3.7 and analyzed for cadmium, yielding a signal of 66.3 nA. Report the concentration of Cd^{2+} in the sample and its 95% confidence interval.

The data in this problem are from Wojciechowski, M.; Balcerzak, J. *Anal. Chim. Acta* **1991**, *249*, 433–445.

9. To determine the concentration of analyte in a sample, a standard addition is performed. A 5.00-mL portion of sample is analyzed and then successive 0.10-mL spikes of a 600.0 ppb standard of the analyte are added, analyzing after each spike. The following table shows the results of this analysis.

V_{spike} (mL)	0.00	0.10	0.20	0.30
S_{total} (arbitrary units)	15.0	42.7	58.5	77.0

Construct an appropriate standard additions calibration curve and use a linear regression analysis to determine the concentration of analyte in the original sample and its 95% confidence interval.

10. Troost and Olavsesn investigated the application of an internal standardization to the quantitative analysis of polynuclear aromatic hydrocarbons. The following results were obtained for the analysis of phenanthrene using isotopically labeled phenanthrene as an internal standard. Each solution was analyzed twice.

C_A/C_{IS}	0.50	1.25	2.00	3.00	4.00
S_A/S_{IS}	0.514	0.993	1.486	2.044	2.342
	0.522	1.024	1.471	2.080	2.550

(a) Determine the equation for the calibration curve using a linear regression, and report confidence intervals for the slope and the *y*-intercept. Average the replicate signals for each standard before you complete the linear regression analysis.

(b) Based on your results explain why the authors concluded that the internal standardization was inappropriate.

The data in this problem are from Troost, J. R.; Olavesen, E. Y. *Anal. Chem.* **1996**, *68*, 708–711.

11. In Chapter 4.6. we used a paired *t*-test to compare two analytical methods that were used to analyze independently a series of samples of variable composition. An alternative approach is to plot the results for one method versus the results for the other method. If the two methods yield identical results, then the plot should have an expected slope, β_1, of 1.00 and an expected *y*-intercept, β_0, of 0.0. We can use a *t*-test to compare the slope and the *y*-intercept from a linear regression to the expected values. The appropriate test statistic for the *y*-intercept is found by rearranging Equation 5.4.10.

$$t_{exp} = \frac{|\beta_0 - b_0|}{s_{b_0}} = \frac{|b_0|}{s_{b_0}}$$

Rearranging Equation 5.4.9 gives the test statistic for the slope.

$$t_{exp} = \frac{|\beta_1 - b_1}{s_{b_1}} = \frac{|b_1|}{s_{b_1}}$$

Reevaluate the data in Problem 25 from Chapter 4 using the same significance level as in the original problem.

> Although this is a common approach for comparing two analytical methods, it does violate one of the requirements for an unweighted linear regression—that indeterminate errors affect *y* only. Because indeterminate errors affect both analytical methods, the result of an unweighted linear regression is biased. More specifically, the regression underestimates the slope, b_1, and overestimates the *y*-intercept, b_0. We can minimize the effect of this bias by placing the more precise analytical method on the *x*-axis, by using more samples to increase the degrees of freedom, and by using samples that uniformly cover the range of concentrations.
>
> For more information, see Miller, J. C.; Miller, J. N. *Statistics for Analytical Chemistry*, 3rd ed. Ellis Horwood PTR Prentice-Hall: New York, 1993. Alternative approaches are found in Hartman, C.; Smeyers-Verbeke, J.; Penninckx, W.; Massart, D. L. *Anal. Chim. Acta* **1997**, *338*, 19–40, and Zwanziger, H. W.; Sârbu, C. *Anal. Chem.* **1998**, *70*, 1277–1280.

12. Consider the following three data sets, each of which gives values of *y* for the same values of *x*.

x	y_1	y_2	y_3
10.00	8.04	9.14	7.46
8.00	6.95	8.14	6.77
13.00	7.58	8.74	12.74
9.00	8.81	8.77	7.11
11.00	8.33	9.26	7.81
14.00	9.96	8.10	8.84
6.00	7.24	6.13	6.08
4.00	4.26	3.10	5.39
12.00	10.84	9.13	8.15
7.00	4.82	7.26	6.42
5.00	5.68	4.74	5.73

(a) An unweighted linear regression analysis for the three data sets gives nearly identical results. To three significant figures, each data set has a slope of 0.500 and a *y*-intercept of 3.00. The standard deviations in the slope and the *y*-intercept are 0.118 and 1.125 for each data set. All three standard deviations about the regression are 1.24. Based on these results for a linear regression analysis, comment on the similarity of the data sets.

(b) Complete a linear regression analysis for each data set and verify that the results from part (a) are correct. Construct a residual plot for each data set. Do these plots change your conclusion from part (a)? Explain.

(c) Plot each data set along with the regression line and comment on your results.

(d) Data set 3 appears to contain an outlier. Remove the apparent outlier and reanalyze the data using a linear regression. Comment on your result.

(e) Briefly comment on the importance of visually examining your data.

These three data sets are taken from Anscombe, F. J. “Graphs in Statistical Analysis,” *Amer. Statis.* **1973**, *27*, 17-21.

13. Fanke and co-workers evaluated a standard additions method for a voltammetric determination of Tl. A summary of their results is tabulated in the following table.

ppm Tl added	Instrument Response (μA)						
0.000	2.53	2.50	2.70	2.63	2.70	2.80	2.52
0.387	8.42	7.96	8.54	8.18	7.70	8.34	7.98
1.851	29.65	28.70	29.05	28.30	29.20	29.95	28.95
5.734	84.8	85.6	86.0	85.2	84.2	86.4	87.8

Use a weighted linear regression to determine the standardization relationship for this data.

The data in this problem are from Franke, J. P.; de Zeeuw, R. A.; Hakkert, R. *Anal. Chem.* **1978**, *50*, 1374–1380.

This page titled 5.7: Problems is shared under a CC BY-NC-SA 4.0 license and was authored, remixed, and/or curated by David Harvey.

- **5.7: Problems** by David Harvey is licensed CC BY-NC-SA 4.0.

5.8: ADDITIONAL RESOURCES

Although there are many experiments in the literature that incorporate external standards, the method of standard additions, or internal standards, the issue of choosing a method standardization is not the experiment's focus. One experiment designed to consider the issue of selecting a method of standardization is given here.

- Harvey, D. T. "External Standards or Standard Additions? Selecting and Validating a Method of Standardization," *J. Chem. Educ.* **2002**, *79*, 613–615.

In addition to the texts listed as suggested readings in Chapter 4, the following text provide additional details on linear regression.

- Draper, N. R.; Smith, H. *Applied Regression Analysis*, 2nd. ed.; Wiley: New York, 1981.

The following articles providing more details about linear regression.

- Analytical Methods Committee "Is my calibration linear?" AMC Technical Brief, December 2005.
- Analytical Methods Committee "Robust regression: an introduction, "AMCTB 50, 2012.
- Badertscher, M.; Pretsch, E. "Bad results from good data," *Trends Anal. Chem.* **2006**, *25*, 1131–1138.
- Boqué, R.; Rius, F. X.; Massart, D. L. "Straight Line Calibration: Something More Than Slopes, Intercepts, and Correlation Coefficients," *J. Chem. Educ.* **1993**, *70*, 230–232.
- Danzer, K.; Currie, L. A. "Guidelines for Calibration in Analytical Chemistry. Part 1. Fundamentals and Single Component Calibration," *Pure Appl. Chem.* **1998**, *70*, 993–1014.
- Henderson, G. "Lecture Graphic Aids for Least-Squares Analysis," *J. Chem. Educ.* **1988**, *65*, 1001–1003.
- Logan, S. R. "How to Determine the Best Straight Line," *J. Chem. Educ.* **1995**, *72*, 896–898.
- Mashkina, E.; Oldman, K. B. "Linear Regressions to Which the Standard Formulas do not Apply," *ChemTexts*, **2015**, *1*, 1–11.
- Miller, J. N. "Basic Statistical Methods for Analytical Chemistry. Part 2. Calibration and Regression Methods," *Analyst* **1991**, *116*, 3–14.
- Raposo, F. "Evaluation of analytical calibration based on least-squares linear regression for instrumental techniques: A tutorial review," *Trends Anal. Chem.* **2016**, *77*, 167–185.
- Renman, L., Jagner, D. "Asymmetric Distribution of Results in Calibration Curve and Standard Addition Evaluations," *Anal. Chim. Acta* **1997**, *357*, 157–166.
- Rodriguez, L. C.; Gamiz-Gracia; Almansa-Lopez, E. M.; Bosque-Sendra, J. M. "Calibration in chemical measurement processes. II. A methodological approach," *Trends Anal. Chem*. **2001**, *20*, 620–636.

Useful papers providing additional details on the method of standard additions are gathered here.

- Bader, M. "A Systematic Approach to Standard Addition Methods in Instrumental Analysis," *J. Chem. Educ.* **1980**, *57*, 703–706.
- Brown, R. J. C.; Roberts, M. R.; Milton, M. J. T. "Systematic error arising form 'Sequential' Standard Addition Calibrations. 2. Determination of Analyte Mass Fraction in Blank Solutions," *Anal. Chim. Acta* **2009**, *648*, 153–156.
- Brown, R. J. C.; Roberts, M. R.; Milton, M. J. T. "Systematic error arising form 'Sequential' Standard Addition Calibrations: Quantification and correction," *Anal. Chim. Acta* **2007**, *587*, 158–163.
- Bruce, G. R.; Gill, P. S. "Estimates of Precision in a Standard Additions Analysis," *J. Chem. Educ.* **1999**, *76*, 805–807.
- Kelly, W. R.; MacDonald, B. S.; Guthrie "Gravimetric Approach to the Standard Addition Method in Instrumental Analysis. 1." *Anal. Chem.* **2008**, *80*, 6154–6158.
- Meija, J.; Pagliano, E.; Mester, Z. "Coordinate Swapping in Standard Addition Graphs for Analytical Chemistry: A Simplified Path for Uncertainty Calculation in Linear and Nonlinear Plots," Anal. Chem. 2014, 86, 8563–8567.
- Nimura, Y.; Carr, M. R. "Reduction of the Relative Error in the Standard Additions Method," *Analyst* **1990**, *115*, 1589–1595.

Approaches that combine a standard addition with an internal standard are described in the following paper.

- Jones, W. B.; Donati, G. L.; Calloway, C. P.; Jones, B. T. "Standard Dilution Analysis," Anal. Chem. 2015, 87, 2321–2327.

The following papers discusses the importance of weighting experimental data when use linear regression.

- Analytical Methods Committee "Why are we weighting?" AMC Technical Brief, June 2007.
- Karolczak, M. "To Weight or Not to Weight? An Analyst's Dilemma," *Current Separations* **1995**, *13*, 98–104.

Algorithms for performing a linear regression with errors in both *X* and *Y* are discussed in the following papers. Also included here are papers that address the difficulty of using linear regression to compare two analytical methods.

- Irvin, J. A.; Quickenden, T. L. "Linear Least Squares Treatment When There are Errors in Both x and y," *J. Chem. Educ.* **1983**, *60*, 711–712.
- Kalantar, A. H. "Kerrich's Method for y = ax Data When Both y and x Are Uncertain," *J. Chem. Educ.* **1991**, *68*, 368–370.
- Macdonald, J. R.; Thompson, W. J. "Least-Squares Fitting When Both Variables Contain Errors: Pitfalls and Possibilities," *Am. J. Phys.* **1992**, *60*, 66–73.

- Martin, R. F. “General Deming Regression for Estimating Systematic Bias and Its Confidence Interval in Method-Comparison Studies,” *Clin. Chem.* **2000**, *46*, 100–104.
- Ogren, P. J.; Norton, J. R. “Applying a Simple Linear Least-Squares Algorithm to Data with Uncertain- ties in Both Variables,” *J. Chem. Educ.* **1992**, *69*, A130–A131.
- Ripley, B. D.; Thompson, M. “Regression Techniques for the Detection of Analytical Bias,” *Analyst* **1987**, *112*, 377–383.
- Tellinghuisen, J. “Least Squares in Calibration: Dealing with Uncertainty in *x*,” *Analyst*, **2010**, *135*, 1961–1969.

Outliers present a problem for a linear regression analysis. The following papers discuss the use of robust linear regression techniques.

- Glaister, P. “Robust Linear Regression Using Thiel’s Method,” *J. Chem. Educ.* **2005**, *82*, 1472–1473.
- Glasser, L. “Dealing with Outliers: Robust, Resistant Regression,” *J. Chem. Educ.* **2007**, *84*, 533–534.
- Ortiz, M. C.; Sarabia, L. A.; Herrero, A. “Robust regression techniques. A useful alternative for the detection of outlier data in chemical analysis,” *Talanta* **2006**, *70*, 499–512.

The following papers discusses some of the problems with using linear regression to analyze data that has been mathematically transformed into a linear form, as well as alternative methods of evaluating curvilinear data.

- Chong, D. P. “On the Use of Least Squares to Fit Data in Linear Form,” *J. Chem. Educ.* **1994**, *71*, 489–490.
- Hinshaw, J. V. “Nonlinear Calibration,” *LCGC* **2002**, *20*, 350–355.
- Lieb, S. G. “Simplex Method of Nonlinear Least-Squares - A Logical Complementary Method to Linear Least-Squares Analysis of Data,” *J. Chem. Educ.* **1997**, *74*, 1008–1011.
- Zielinski, T. J.; Allendoerfer, R. D. “Least Squares Fitting of Nonlinear Data in the Undergraduate Laboratory,” *J. Chem. Educ.* **1997**, *74*, 1001–1007.

More information on multivariate and multiple regression can be found in the following papers.

- Danzer, K.; Otto, M.; Currie, L. A. “Guidelines for Calibration in Analytical Chemistry. Part 2. Multispecies Calibration,” *Pure Appl. Chem.* **2004**, *76*, 1215–1225.
- Escandar, G. M.; Faber, N. M.; Goicoechea, H. C.; de la Pena, A. M.; Olivieri, A.; Poppi, R. J. “Second- and third-order multivariate calibration: data, algorithms and applications,” *Trends Anal. Chem.* **2007**, *26*, 752–765.
- Kowalski, B. R.; Seasholtz, M. B. “Recent Developments in Multivariate Calibration,” *J. Chemometrics* **1991**, *5*, 129–145.
- Lang, P. M.; Kalivas, J. H. “A Global Perspective on Multivariate Calibration Methods,” *J. Chemomet- rics* **1993**, *7*, 153–164.
- Madden, S. P.; Wilson, W.; Dong, A.; Geiger, L.; Mecklin, C. J. “Multiple Linear Regression Using a Graphing Calculator,” J. Chem. Educ. 2004, 81, 903–907.
- Olivieri, A. C.; Faber, N. M.; Ferré, J.; Boqué, R.; Kalivas, J. H.; Mark, H. “Uncertainty Estimation and Figures of Merit for Multivariate Calibration,” *Pure Appl. Chem.* **2006**, *78*, 633–661.

An additional discussion on method blanks, including the use of the total Youden blank, is found in the fol- lowing papers.

- Cardone, M. J. “Detection and Determination of Error in Analytical Methodology. Part II. Correc- tion for Corrigible Systematic Error in the Course of Real Sample Analysis,” *J. Assoc. Off. Anal. Chem.* **1983**, *66*, 1283–1294.
- Cardone, M. J. “Detection and Determination of Error in Analytical Methodology. Part IIB. Direct Calculational Technique for Making Corrigible Systematic Error Corrections,” *J. Assoc. Off. Anal. Chem.* **1985**, *68*, 199–202.
- Ferrus, R.; Torrades, F. “Bias-Free Adjustment of Analytical Methods to Laboratory Samples in Routine Analytical Procedures,” *Anal. Chem.* **1988**, *60*, 1281–1285.
- Vitha, M. F.; Carr, P. W.; Mabbott, G. A. “Appropriate Use of Blanks, Standards, and Controls in Chemical Measurements,” *J. Chem. Educ.* **2005**, *82*, 901–902.

There are a variety of computational packages for completing linear regression analyses. These papers provide details on there use in a variety of contexts.

- Espinosa-Mansilla, A.; de la Peña, A. M.; González-Gómez, D. “Using Univariate Linear Regression Calibration Software in the MATLAB Environment. Application to Chemistry Laboratory Practices,” *Chem. Educator* **2005**, *10*, 1–9.
- Harris, D. C. “Nonlinear Least-Squares Curve Fitting with Microsoft Excel Solver,” *J. Chem. Educ.* **1998**, *75*, 119–121.
- Kim, M. S.; Bukart, M.; Kim, M. H. “A Method Visual Interactive Regression,” *J. Chem. Educ.* **2006**, *83*, 1884.
- Machuca-Herrera, J. G. “Nonlinear Curve Fitting with Spreadsheets,” *J. Chem. Educ.* **1997**, *74*, 448–449.
- Smith, E. T.; Belogay, E. A.; Hõim “Linear Regression and Error Analysis for Calibration Curves and Standard Additions: An Excel Spreadsheet Exercise for Undergraduates,” Chem. Educator 2010, 15, 100–102.
- Smith, E. T.; Belogay, E. A.; Hõim “Using Multiple Linear Regression to Analyze Mixtures: An Excel Spreadsheet Exercise for Undergraduates,” *Chem. Educator* **2010**, *15*, 103–107.
- Young, S. H.; Wierzbicki, A. “Mathcad in the Chemistry Curriculum. Linear Least-Squares Regres- sion,” *J. Chem. Educ.* **2000**, *77*, 669.
- Young, S. H.; Wierzbicki, A. “Mathcad in the Chemistry Curriculum. Non-Linear Least-Squares Re- gression,” *J. Chem. Educ.* **2000**, *77*, 669.

This page titled 5.8: Additional Resources is shared under a CC BY-NC-SA 4.0 license and was authored, remixed, and/or curated by David Harvey.

- **5.8: Additional Resources** by David Harvey is licensed CC BY-NC-SA 4.0.

5.9: CHAPTER SUMMARY AND KEY TERMS

SUMMARY

In a quantitative analysis we measure a signal, S_{total}, and calculate the amount of analyte, n_A or C_A, using one of the following equations.

$$S_{total} = k_A n_A + S_{reag}$$

$$S_{total} = k_A C_A + S_{reag}$$

To obtain an accurate result we must eliminate determinate errors that affect the signal, S_{total}, the method's sensitivity, k_A, and the signal due to the reagents, S_{reag}.

To ensure that we accurately measure S_{total}, we calibrate our equipment and instruments. To calibrate a balance, for example, we use a standard weight of known mass. The manufacturer of an instrument usually suggests appropriate calibration standards and calibration methods.

To standardize an analytical method we determine its sensitivity. There are several standardization strategies available to us, including external standards, the method of standard addition, and internal standards. The most common strategy is a multiple-point external standardization and a normal calibration curve. We use the method of standard additions, in which we add known amounts of analyte to the sample, when the sample's matrix complicates the analysis. When it is difficult to reproducibly handle samples and standards, we may choose to add an internal standard.

Single-point standardizations are common, but are subject to greater uncertainty. Whenever possible, a multiple-point standardization is preferred, with results displayed as a calibration curve. A linear regression analysis provides an equation for the standardization.

A reagent blank corrects for any contribution to the signal from the reagents used in the analysis. The most common reagent blank is one in which an analyte-free sample is taken through the analysis. When a simple reagent blank does not compensate for all constant sources of determinate error, other types of blanks, such as the total Youden blank, are used.

KEY TERMS

calibration curve	external standard	internal standard
linear regression	matrix matching	method of standard additions
multiple-point standardization	normal calibration curve	primary standard
reagent grade	residual error	secondary standard
serial dilution	single-point standardization	standard deviation about the regression
total Youden blank	unweighted linear regression	weighted linear regression

This page titled 5.9: Chapter Summary and Key Terms is shared under a CC BY-NC-SA 4.0 license and was authored, remixed, and/or curated by David Harvey.

- **5.9: Chapter Summary and Key Terms** by David Harvey is licensed CC BY-NC-SA 4.0.

CHAPTER OVERVIEW

6: SPECTROSCOPIC METHODS

An early example of a colorimetric analysis is Nessler's method for ammonia, which was introduced in 1856. Nessler found that adding an alkaline solution of HgI_2 and KI to a dilute solution of ammonia produced a yellow-to-reddish brown colloid, in which the colloid's color depended on the concentration of ammonia. By visually comparing the color of a sample to the colors of a series of standards, Nessler was able to determine the concentration of ammonia. Colorimetry, in which a sample absorbs visible light, is one example of a spectroscopic method of analysis. At the end of the nineteenth century, spectroscopy was limited to the absorption, emission, and scattering of visible, ultraviolet, and infrared electromagnetic radiation. Since then, spectroscopy has expanded to include other forms of electromagnetic radiation—such as X-rays, microwaves, and radio waves—and other energetic particles—such as electrons and ions.

6.1: Overview of Spectroscopy
6.2: Spectrometer
6.2.1: ATR-FTIR
6.3: Spectroscopy Based on Absorption
6.4: Lasers
6.4.1: Gas Lasers
6.4.2: Laser Theory
6.4.3: Overview of Lasers
6.4.4: Semiconductor and Solid-state lasers
6.4.5: Semiconductors
6.5: UV/Vis and IR Spectroscopy
6.6: Signals and Noise
6.6.1: The Signal-to-Noise Ratio
6.6.2: Sources of Instrumental Noise
6.6.3: Signal-to-Noise Enhancement
6.7: Emission Spectroscopy
6.8: Photoluminescent Spectroscopy
6.9: Analytical Chemiluminescence
6.9.1: Introduction to Chemiluminescence
6.9.1.1: Electronic transitions and luminescence
6.9.1.2: Chemiluminescence Spectroscopy
6.9.2: Instrumentation
6.9.2.1: Detection of chemiluminescence
6.10: Detectors
6.10.1: Detectors of Light
6.10.2: Radiation Transducers
6.11: An Introduction to Infrared Spectrometry
6.11.1: Theory of Infrared Absorption Spectrometry
6.11.2: Infrared Sources and Transducers
6.11.3: FTIR- Hardware
6.11.4: Infrared Instruments
6.12: Applications of Infrared Spectrometry
6.12.1: Mid-Infrared Absorption Spectometry
6.12.2: Mid-Infrared Reflection Spectrometry
6.12.3: Near-Infrared and Far-Infrared Spectroscopy
6.13: Raman Spectroscopy

6.13.1: Theory of Raman Spectroscopy
6.13.2: Instrumentation
6.13.3: Applications of Raman Spectroscopy
6.13.4: Other Types of Raman Spectroscopy
6.14: Problems
6.15: Additional Resources
6.16: Chapter Summary and Key Terms

This page titled 6: Spectroscopic Methods is shared under a CC BY-NC-SA 4.0 license and was authored, remixed, and/or curated by David Harvey.

6.1: OVERVIEW OF SPECTROSCOPY

The focus of this chapter is on the interaction of ultraviolet, visible, and infrared radiation with matter. Because these techniques use optical materials to disperse and focus the radiation, they often are identified as optical spectroscopies. For convenience we will use the simpler term spectroscopy in place of optical ***spectroscopy***; however, you should understand we will consider only a limited piece of what is a much broader area of analytical techniques.

Despite the difference in instrumentation, all spectroscopic techniques share several common features. Before we consider individual examples in greater detail, let's take a moment to consider some of these similarities. As you work through the chapter, this overview will help you focus on the similarities between different spectroscopic methods of analysis. You will find it easier to understand a new analytical method when you can see its relationship to other similar methods.

WHAT IS ELECTROMAGNETIC RADIATION?

Electromagnetic radiation—light—is a form of energy whose behavior is described by the properties of both waves and particles. Some properties of electromagnetic radiation, such as its refraction when it passes from one medium to another (Figure 10.1.1), are explained best when we describe light as a wave. Other properties, such as absorption and emission, are better described by treating light as a particle. The exact nature of electromagnetic radiation remains unclear, as it has since the development of quantum mechanics in the first quarter of the 20th century [Home, D.; Gribbin, J. *New Scientist* 1991, 2 Nov. 30–33]. Nevertheless, this dual model of wave and particle behavior provide a useful description for electromagnetic radiation.



Figure 10.1.1 . The Golden Gate bridge as seen through rain drops. Refraction of light by the rain drops produces the distorted images. Source: Brocken Inaglory (commons. Wikipedia.org).

WAVE PROPERTIES OF ELECTROMAGNETIC RADIATION

Electromagnetic radiation consists of oscillating electric and magnetic fields that propagate through space along a linear path and with a constant velocity. In a vacuum, electromagnetic radiation travels at the speed of light, c, which is 2.99792×10^8 m/s. When electromagnetic radiation moves through a medium other than a vacuum, its velocity, v, is less than the speed of light in a vacuum. The difference between v and c is sufficiently small (<0.1%) that the speed of light to three significant figures, 3.00×10^8 m/s, is accurate enough for most purposes.

The oscillations in the electric field and the magnetic field are perpendicular to each other and to the direction of the wave's propagation. Figure 10.1.2 shows an example of plane-polarized electromagnetic radiation, which consists of a single oscillating electric field and a single oscillating magnetic field.

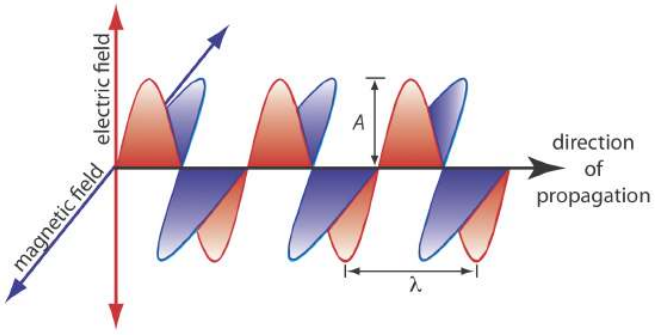


Figure 10.1.2 . Plane-polarized electromagnetic radiation showing the oscillating electric field in blue and the oscillating magnetic field in red. The radiation's amplitude, A, and its wavelength, λ, are shown. Normally, electromagnetic radiation is unpolarized, with oscillating electric and magnetic fields present in all possible planes perpendicular to the direction of propagation.

An electromagnetic wave is characterized by several fundamental properties, including its velocity, amplitude, frequency, phase angle, polarization, and direction of propagation [Ball, D. W. *Spectroscopy* **1994**, *9(5)*, 24–25]. For example, the amplitude of the oscillating

electric field at any point along the propagating wave is

$$A_t = A_e \sin(2\pi\nu t + \Phi)$$

where A_t is the magnitude of the electric field at time t, A_e is the electric field's maximum ***amplitude***, ν is the wave's ***frequency***—the number of oscillations in the electric field per unit time—and Φ is a ***phase angle*** that accounts for the fact that A_t need not have a value of zero at t = 0. The identical equation for the magnetic field is

$$A_t = A_m \sin(2\pi\nu t + \Phi)$$

where A_m is the magnetic field's maximum amplitude.

Other properties also are useful for characterizing the wave behavior of electromagnetic radiation. The ***wavelength***, λ, is defined as the distance between successive maxima (see Figure 10.1.2). For ultraviolet and visible electromagnetic radiation the wavelength usually is expressed in nanometers (1 nm = 10^{-9} m), and for infrared radiation it is expressed in microns (1 mm = 10^{-6} m). The relationship between wavelength and frequency is

$$\lambda = \frac{c}{\nu}$$

Another unit useful unit is the ***wavenumber***, $\bar{\nu}$, which is the reciprocal of wavelength

$$\bar{\nu} = \frac{1}{\lambda}$$

Wavenumbers frequently are used to characterize infrared radiation, with the units given in cm^{-1}.

When electromagnetic radiation moves between different media—for example, when it moves from air into water—its frequency, ν, remains constant. Because its velocity depends upon the medium in which it is traveling, the electromagnetic radiation's wavelength, λ, changes. If we replace the speed of light in a vacuum, c, with its speed in the medium, v, then the wavelength is

$$\lambda = \frac{v}{\nu}$$

This change in wavelength as light passes between two media explains the refraction of electromagnetic radiation shown in Figure 10.1.1 .

EXAMPLE 10.1.1

In 1817, Josef Fraunhofer studied the spectrum of solar radiation, observing a continuous spectrum with numerous dark lines. Fraunhofer labeled the most prominent of the dark lines with letters. In 1859, Gustav Kirchhoff showed that the D line in the sun's spectrum was due to the absorption of solar radiation by sodium atoms. The wavelength of the sodium D line is 589 nm. What are the frequency and the wavenumber for this line?

Solution

The frequency and wavenumber of the sodium D line are

$$\nu = \frac{c}{\lambda} = \frac{3.00 \times 10^8 \text{ m/s}}{589 \times 10^{-9} \text{ m}} = 5.09 \times 10^{14} \text{ s}^{-1}$$

$$\bar{\nu} = \frac{1}{\lambda} = \frac{1}{589 \times 10^{-9} \text{ m}} \times \frac{1 \text{ m}}{100 \text{ cm}} = 1.70 \times 10^4 \text{ cm}^{-1}$$

EXERCISE 10.1.1

Another historically important series of spectral lines is the Balmer series of emission lines from hydrogen. One of its lines has a wavelength of 656.3 nm. What are the frequency and the wavenumber for this line?

Answer

The frequency and wavenumber for the line are

$$\nu = \frac{c}{\lambda} = \frac{3.00 \times 10^8 \text{ m/s}}{656.3 \times 10^{-9} \text{ m}} = 4.57 \times 10^{14} \text{ s}^{-1}$$

$$\bar{\nu} = \frac{1}{\lambda} = \frac{1}{656.3 \times 10^{-9}\ \text{m}} \times \frac{1\ \text{m}}{100\ \text{cm}} = 1.524 \times 10^{4}\ \text{cm}^{-1}$$

PARTICLE PROPERTIES OF ELECTROMAGNETIC RADIATION

When matter absorbs electromagnetic radiation it undergoes a change in energy. The interaction between matter and electromagnetic radiation is easiest to understand if we assume that radiation consists of a beam of energetic particles called photons. When a ***photon*** is absorbed by a sample it is "destroyed" and its energy acquired by the sample [Ball, D. W. *Spectroscopy* **1994**, *9(6)* 20–21]. The energy of a photon, in joules, is related to its frequency, wavelength, and wavenumber by the following equalities

$$E = h\nu = \frac{hc}{\lambda} = hc\bar{\nu}$$

where *h* is Planck's constant, which has a value of 6.626×10^{-34} Js.

EXAMPLE 10.1.2

What is the energy of a photon from the sodium D line at 589 nm?

Solution

The photon's energy is

$$E = \frac{hc}{\lambda} = \frac{\left(6.626 \times 10^{-34}\ \text{Js}\right)\left(3.00 \times 10^{8}\ \text{m/s}\right)}{589 \times 10^{-7}\ \text{m}} = 3.37 \times 10^{-19}\ \text{J}$$

EXERCISE 10.1.2

What is the energy of a photon for the Balmer line at a wavelength of 656.3 nm?

Answer

The photon's energy is

$$E = \frac{hc}{\lambda} = \frac{\left(6.626 \times 10^{-34}\ \text{Js}\right)\left(3.00 \times 10^{8}\ \text{m/s}\right)}{656.3 \times 10^{-9}\ \text{m}} = 3.03 \times 10^{-19}\ \text{J}$$

THE ELECTROMAGNETIC SPECTRUM

The frequency and the wavelength of electromagnetic radiation vary over many orders of magnitude. For convenience, we divide electromagnetic radiation into different regions—the ***electromagnetic spectrum***—based on the type of atomic or molecular transitions that gives rise to the absorption or emission of photons (Figure 10.1.3). The boundaries between the regions of the electromagnetic spectrum are not rigid and overlap between spectral regions is possible.

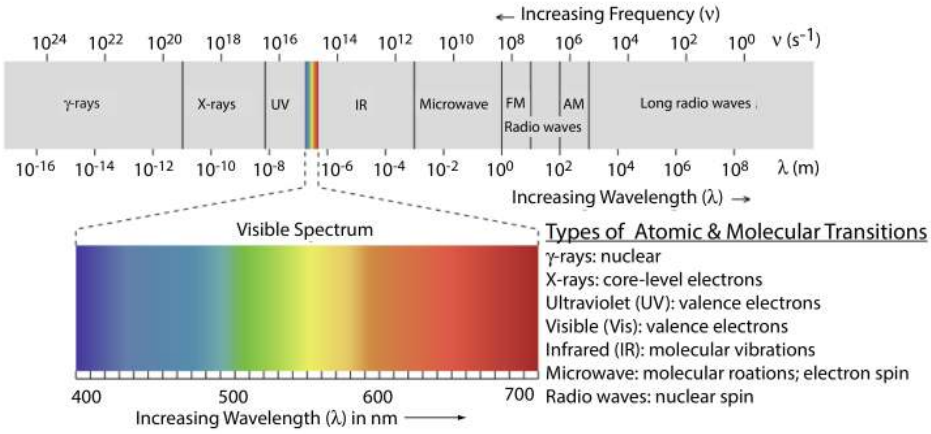


Figure 10.1.3 . The electromagnetic spectrum showing the boundaries between different regions and the type of atomic or molecular transitions responsible for the change in energy. The colored inset shows the visible spectrum. Source: modified from Zedh (www.commons.Wikipedia.org).

PHOTONS AS A SIGNAL SOURCE

In the previous section we defined several characteristic properties of electromagnetic radiation, including its energy, velocity, amplitude, frequency, phase angle, polarization, and direction of propagation. A spectroscopic measurement is possible only if the photon's interaction with the sample leads to a change in one or more of these characteristic properties.

We will divide spectroscopy into two broad classes of techniques. In one class of techniques there is a transfer of energy between the photon and the sample. Table 10.1.1 provides a list of several representative examples.

Table 10.1.1 . Examples of Spectroscopic Techniques That Involve an Exchange of Energy Between a Photon and the Sample

type of energy transfer	region of electromagnetic spectrum	spectroscopic technique
absorption	γ-ray	Mossbauer spectroscopy
	X-ray	X-ray absorption spectroscopy
	UV/Vis	*UV/Vis spectroscopy*
	IR	*infrared spectroscopy*
	microwave	raman spectroscopy
	radio wave	electron spin resonance nuclear magnetic resonance
emission (thermal excitation)	UV/Vis	*atomic emission spectroscopy*
photoluminescence	X-ray	X-ray fluorescence
	UV/Vis	*fluorescence spectroscopy* *phosphorescence spectroscopy* atomic fluorescence spectroscopy
chemiluminescence	UV/Vis	chemiluminescence spectroscopy
techniques discussed in this chapter are shown in *italics*		

In absorption spectroscopy a photon is absorbed by an atom or molecule, which undergoes a transition from a lower-energy state to a higher-energy, or excited state (Figure 10.1.4). The type of transition depends on the photon's energy. The electromagnetic spectrum in Figure 10.1.3 , for example, shows that absorbing a photon of visible light promotes one of the atom's or molecule's valence electrons to a higher-energy level. When an molecule absorbs infrared radiation, on the other hand, one of its chemical bonds experiences a change in vibrational energy.

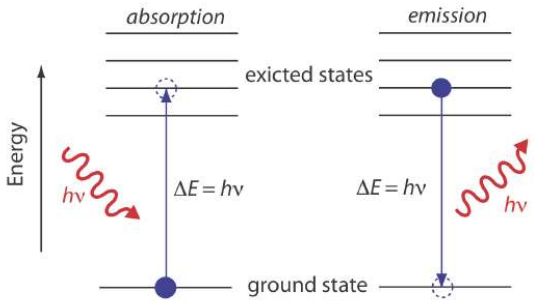


Figure 10.1.4 . A simplified energy diagram that shows the absorption and emission of a photon by an atom or a molecule. When a photon of energy $h\nu$ strikes the atom or molecule, absorption may occur if the difference in energy, ΔE, between the ground state and the excited state is equal to the photon's energy. An atom or molecule in an excited state may emit a photon and return to the ground state. The photon's energy, $h\nu$, equals the difference in energy, ΔE, between the two states.

When it absorbs electromagnetic radiation the number of photons passing through a sample decreases. The measurement of this decrease in photons, which we call ***absorbance***, is a useful analytical signal. Note that each energy level in Figure 10.1.4 has a well-defined value because each is quantized. Absorption occurs only when the photon's energy, $h\nu$, matches the difference in energy, ΔE, between two energy levels. A plot of absorbance as a function of the photon's energy is called an ***absorbance spectrum***. Figure 10.1.5 , for example, shows the absorbance spectrum of cranberry juice.

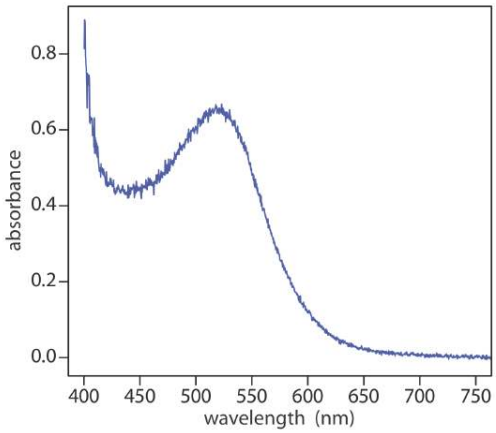


Figure 10.1.5 . Visible absorbance spectrum for cranberry juice. The anthocyanin dyes in cranberry juice absorb visible light with blue, green, and yellow wavelengths (see Figure 10.1.3). As a result, the juice appears red.

When an atom or molecule in an excited state returns to a lower energy state, the excess energy often is released as a photon, a process we call ***emission*** (Figure 10.1.4). There are several ways in which an atom or a molecule may end up in an excited state, including thermal energy, absorption of a photon, or as the result of a chemical reaction. Emission following the absorption of a photon is also called ***photoluminescence***, and that following a chemical reaction is called ***chemiluminescence***. A typical emission spectrum is shown in Figure 10.1.6 .

> Molecules also can release energy in the form of heat. We will return to this point later in the chapter.

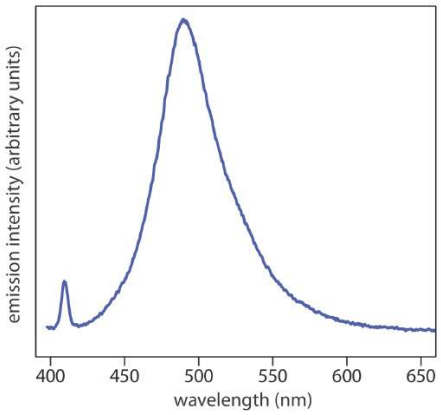


Figure 10.1.6 . Photoluminescence spectrum of the dye coumarin 343, which is incorporated in a reverse micelle suspended in cyclohexanol. The dye's absorbance spectrum (not shown) has a broad peak around 400 nm. The sharp peak at 409 nm is from the laser source used to excite coumarin 343. The broad band centered at approximately 500 nm is the dye's emission band. Because the dye absorbs blue light, a solution of coumarin 343 appears yellow in the absence of photoluminescence. Its photoluminescent emission is blue-green. Source: data from Bridget Gourley, Department of Chemistry & Biochemistry, DePauw University.

In the second broad class of spectroscopic techniques, the electromagnetic radiation undergoes a change in amplitude, phase angle, polarization, or direction of propagation as a result of its refraction, reflection, scattering, diffraction, or dispersion by the sample. Several representative spectroscopic techniques are listed in Table 10.1.2 .

Table 10.1.2 . Examples of Spectroscopic Techniques That Do Not Involve an Exchange of Energy Between a Photon and the Sample

region of electromagnetic spectrum	type of interaction	spectroscopic technique
X-ray	diffraction	X-ray diffraction
UV/Vis	refraction	refractrometry
	scattering	*nephelometry* *turbidimetry*
	dispersion	optical rotary dispersion
techniques discussed in this chapter are shown in *italics*		

BASIC COMPONENTS OF SPECTROSCOPIC INSTRUMENTS

The spectroscopic techniques in Table 10.1.1 and Table 10.1.2 use instruments that share several common basic components, including a source of energy, a means for isolating a narrow range of wavelengths, a detector for measuring the signal, and a signal processor that displays the signal in a form convenient for the analyst. In this section we introduce these basic components. Specific instrument designs are considered in later sections.

> You will find a more detailed treatment of these components in the additional resources for this chapter.

SOURCES OF ENERGY

All forms of spectroscopy require a source of energy. In absorption and scattering spectroscopy this energy is supplied by photons. Emission and photoluminescence spectroscopy use thermal, radiant (photon), or chemical energy to promote the analyte to a suitable excited state.

Sources of Electromagnetic Radiation. A source of electromagnetic radiation must provide an output that is both intense and stable. Sources of electromagnetic radiation are classified as either continuum or line sources. A ***continuum source*** emits radiation over a broad range of wavelengths, with a relatively smooth variation in intensity (Figure 10.1.7). A ***line source***, on the other hand, emits radiation at selected wavelengths (Figure 10.1.8). Table 10.1.3 provides a list of the most common sources of electromagnetic radiation.

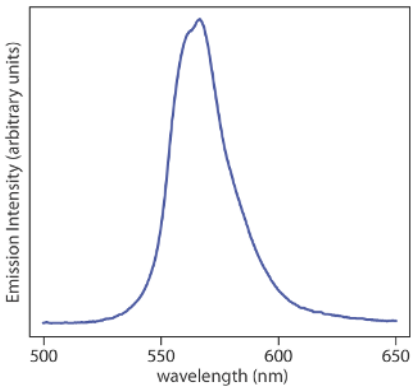


Figure 10.1.7 . Spectrum showing the emission from a green LED, which provides continuous emission over a wavelength range of approximately 530–640 nm.

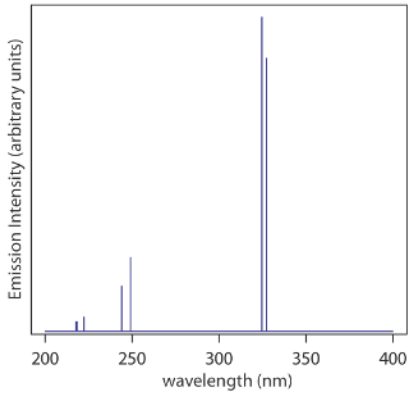


Figure 10.1.8 . Emission spectrum from a Cu hollow cathode lamp. This spectrum consists of seven distinct emission lines (the first two differ by only 0.4 nm and are not resolved at the scale shown in this spectrum). Each emission line has a width of approximately 0.01 nm at 1⁄2 of its maximum intensity.

Table 10.1.3 . Common Source of Electromagnetic Radiation

source	wavelength region	useful for...
H_2 and D_2 lamp	continuum source from 160–380 nm	molecular absorption
tungsten lamp	continuum source from 320–2400 nm	molecular absorption
Xe arc lamp	continuum source from 200–1000 nm	molecular fluorescence
nernst glower	continuum source from 0.4–20 μm	molecular absorption
globar	continuum source from 1–40 μm	molecular absorption
nichrome wire	continuum source from 0.75–20 μm	molecular absorption
hollow cathode lamp	line source in UV/Vis	atomic absorption
Hg vapor lamp	line source in UV/Vis	molecular fluorescence
laser	line source in UV/Vis/Ir	atomic and molecular absorption, fluorescence, and scattering

Sources of Thermal Radiation. The most common sources of thermal energy are flames and plasmas. A flame source uses a combustion of a fuel and an oxidant to achieve temperatures of 2000–3400 K. Plasmas, which are hot, ionized gases, provide temperatures of 6000–10000 K.

Chemical Sources of Energy. Exothermic reactions also may serve as a source of energy. In chemiluminescence the analyte is raised to a higher-energy state by means of a chemical reaction, emitting characteristic radiation when it returns to a lower-energy state. When the chemical reaction results from a biological or enzymatic reaction, the emission of radiation is called bioluminescence. Commercially available “light sticks” and the flash of light from a firefly are examples of chemiluminescence and bioluminescence.

WAVELENGTH SELECTION

In Nessler’s original colorimetric method for ammonia, which was described at the beginning of the chapter, the sample and several standard solutions of ammonia are placed in separate tall, flat-bottomed tubes. As shown in Figure 10.1.9 , after adding the reagents and allowing the color to develop, the analyst evaluates the color by passing ambient light through the bottom of the tubes and looking down through the solutions. By matching the sample’s color to that of a standard, the analyst is able to determine the concentration of ammonia in the sample.

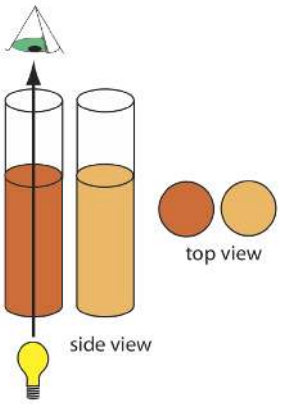


Figure 10.1.9 . Nessler’s original method for comparing the color of two solutions. Natural light passes upwards through the samples and standards and the analyst views the solutions by looking down toward the light source. The top view, shown on the right, is what the analyst sees. To determine the analyte’s concentration, the analyst exchanges standards until the two colors match.

In Figure 10.1.9 every wavelength of light from the source passes through the sample. This is not a problem if there is only one absorbing species in the sample. If the sample contains two components, then a quantitative analysis using Nessler’s original method is impossible unless the standards contains the second component at the same concentration it has in the sample.

To overcome this problem, we want to select a wavelength that only the analyte absorbs. Unfortunately, we can not isolate a single wavelength of radiation from a continuum source, although we can narrow the range of wavelengths that reach the sample. As seen in Figure 10.1.10 , a wavelength selector always passes a narrow band of radiation characterized by a ***nominal wavelength***, an ***effective bandwidth***, and a maximum throughput of radiation. The effective bandwidth is defined as the width of the radiation at half of its maximum throughput.

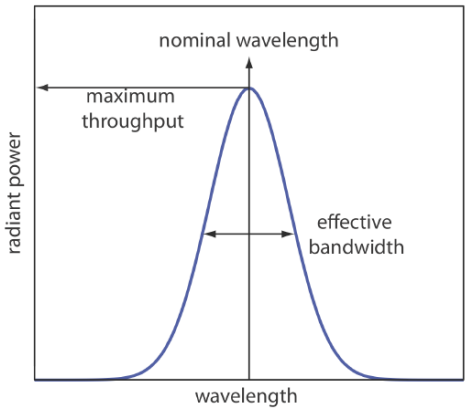


Figure 10.1.10 . Radiation exiting a wavelength selector showing the band's nominal wavelength and its effective bandwidth.

The ideal wavelength selector has a high throughput of radiation and a narrow effective bandwidth. A high throughput is desirable because the more photons that pass through the wavelength selector, the stronger the signal and the smaller the background noise. A narrow effective bandwidth provides a higher ***resolution***, with spectral features separated by more than twice the effective bandwidth being resolved. As shown in Figure 10.1.11 , these two features of a wavelength selector often are in opposition. A larger effective bandwidth favors a higher throughput of radiation, but provide less resolution. Decreasing the effective bandwidth improves resolution, but at the cost of a noisier signal [Jiang, S.; Parker, G. A. *Am. Lab.* **1981**, October, 38–43]. For a qualitative analysis, resolution usually is more important than noise and a smaller effective bandwidth is desirable; however, in a quantitative analysis less noise usually is desirable.

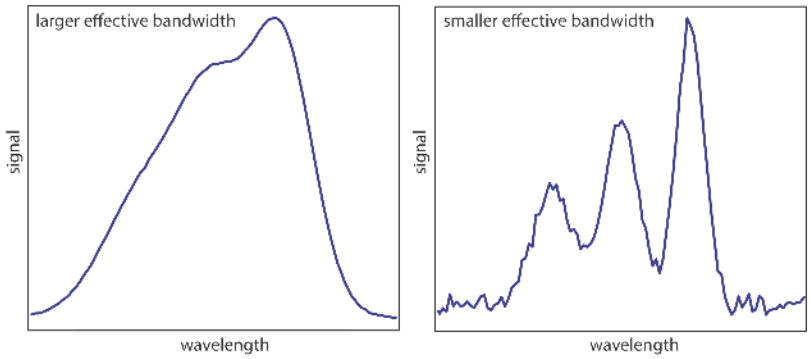


Figure 10.1.11 . Example showing the effect of the wavelength selector's effective bandwidth on resolution and noise. The spectrum with the smaller effective bandwidth (on the right) has a better resolution, allowing us to see the presence of three peaks, but at the expense of a noisier signal. The spectrum with the larger effective bandwidth (on the left) has less noise, but at the expense of less resolution between the three peaks.

Wavelength Selection Using Filters. The simplest method for isolating a narrow band of radiation is to use an absorption or interference ***filter***. Absorption filters work by selectively absorbing radiation from a narrow region of the electromagnetic spectrum. Interference filters use constructive and destructive interference to isolate a narrow range of wavelengths. A simple example of an absorption filter is a piece of colored glass. A purple filter, for example, removes the complementary color green from 500–560 nm.

Commercially available absorption filters provide effective bandwidths of 30–250 nm, although the throughput at the low end of this range often is only 10% of the source's emission intensity. Interference filters are more expensive than absorption filters, but have narrower effective bandwidths, typically 10–20 nm, with maximum throughputs of at least 40%.

Wavelength Selection Using Monochromators. A filter has one significant limitation—because a filter has a fixed nominal wavelength, if we need to make measurements at two different wavelengths, then we must use two different filters. A ***monochromator*** is an alternative method for selecting a narrow band of radiation that also allows us to continuously adjust the band's nominal wavelength.

The construction of a typical monochromator is shown in Figure 10.1.12 . Radiation from the source enters the monochromator through an entrance slit. The radiation is collected by a collimating mirror, which reflects a parallel beam of radiation to a diffraction grating. The diffraction grating is an optically reflecting surface with a large number of parallel grooves (see insert to Figure 10.1.12). The diffraction grating disperses the radiation and a second mirror focuses the radiation onto a planar surface that contains an exit slit. In some monochromators a prism is used in place of the diffraction grating.

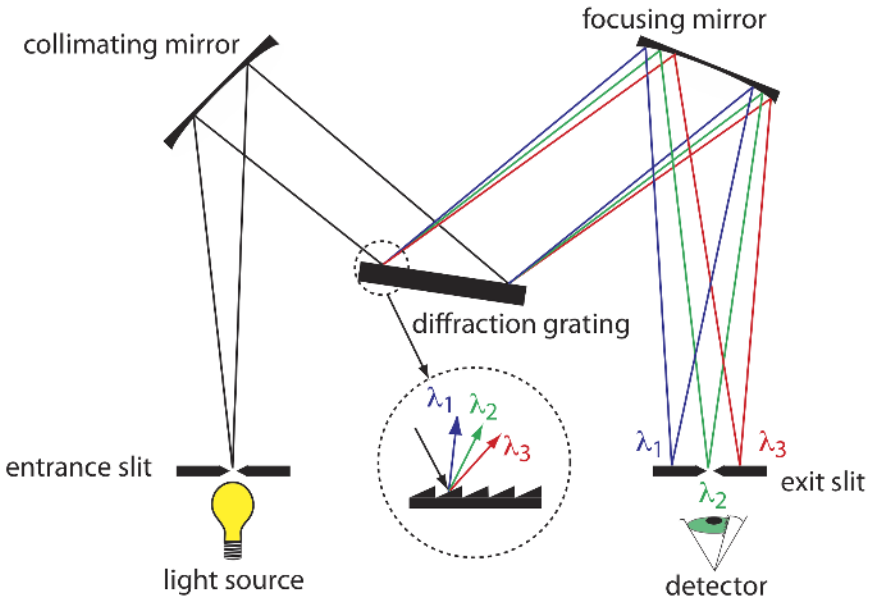


Figure 10.1.12 . Schematic diagram of a monochromator that uses a diffraction grating to disperse the radiation.

Radiation exits the monochromator and passes to the detector. As shown in Figure 10.1.12 , a monochromator converts a ***polychromatic*** source of radiation at the entrance slit to a ***monochromatic*** source of finite effective bandwidth at the exit slit. The choice of which wavelength exits the monochromator is determined by rotating the diffraction grating. A narrower exit slit provides a smaller effective bandwidth and better resolution than does a wider exit slit, but at the cost of a smaller throughput of radiation.

> Polychromatic means many colored. Polychromatic radiation contains many different wavelengths of light. Monochromatic means one color, or one wavelength. Although the light exiting a monochromator is not strictly of a single wavelength, its narrow effective bandwidth allows us to think of it as monochromatic.

Monochromators are classified as either fixed-wavelength or scanning. In a fixed-wavelength monochromator we manually select the wavelength by rotating the grating. Normally a fixed-wavelength monochromator is used for a quantitative analysis where measurements are made at one or two wavelengths. A scanning monochromator includes a drive mechanism that continuously rotates the grating, which allows successive wavelengths of light to exit from the monochromator. A scanning monochromator is used to acquire spectra, and, when operated in a fixed-wavelength mode, for a quantitative analysis.

Interferometers. An ***interferometer*** provides an alternative approach for wavelength selection. Instead of filtering or dispersing the electromagnetic radiation, an interferometer allows source radiation of all wavelengths to reach the detector simultaneously (Figure 10.1.13). Radiation from the source is focused on a beam splitter that reflects half of the radiation to a fixed mirror and transmits the other half to a moving mirror. The radiation recombines at the beam splitter, where constructive and destructive interference determines, for each wavelength, the intensity of light that reaches the detector. As the moving mirror changes position, the wavelength of light that experiences maximum constructive interference and maximum destructive interference also changes. The signal at the detector shows intensity as a function of the moving mirror's position, expressed in units of distance or time. The result is called an ***interferogram*** or a time domain spectrum. The time domain spectrum is converted mathematically, by a process called a Fourier transform, to a spectrum (a frequency domain spectrum) that shows intensity as a function of the radiation's energy.

> The mathematical details of the Fourier transform are beyond the level of this textbook. You can consult the chapter's additional resources for additional information.

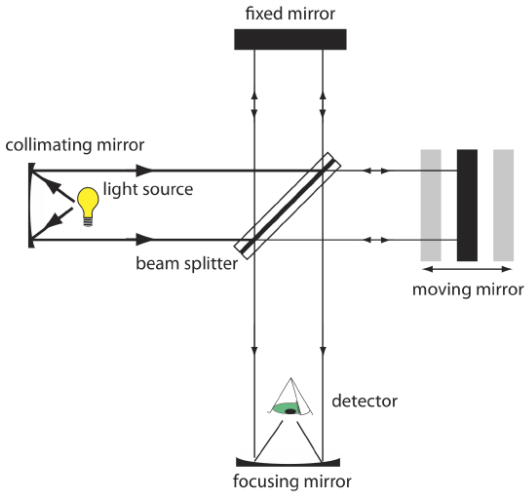


Figure 10.1.13 . Schematic diagram of an interferometers.

In comparison to a monochromator, an interferometer has two significant advantages. The first advantage, which is termed ***Jacquinot's advantage***, is the greater throughput of source radiation. Because an interferometer does not use slits and has fewer optical components from which radiation is scattered and lost, the throughput of radiation reaching the detector is $80-200\times$ greater than that for a monochromator. The result is less noise. The second advantage, which is called ***Fellgett's advantage***, is a savings in the time needed to obtain a spectrum. Because the detector monitors all frequencies simultaneously, a spectrum takes approximately one second to record, as compared to 10–15 minutes when using a scanning monochromator.

DETECTORS

In Nessler's original method for determining ammonia (Figure 10.1.9) the analyst's eye serves as the detector, matching the sample's color to that of a standard. The human eye, of course, has a poor range—it responds only to visible light—and it is not particularly sensitive or accurate. Modern detectors use a sensitive ***transducer*** to convert a signal consisting of photons into an easily measured electrical signal. Ideally the detector's signal, *S*, is a linear function of the electromagnetic radiation's power, *P*,

$$S = kP + D$$

where *k* is the detector's sensitivity, and *D* is the detector's ***dark current***, or the background current when we prevent the source's radiation from reaching the detector.

There are two broad classes of spectroscopic transducers: thermal transducers and photon transducers. Table 10.1.4 provides several representative examples of each class of transducers.

> Transducer is a general term that refers to any device that converts a chemical or a physical property into an easily measured electrical signal. The retina in your eye, for example, is a transducer that converts photons into an electrical nerve impulse; your eardrum is a transducer that converts sound waves into a different electrical nerve impulse.

Table 10.1.4 . Examples of Transducers for Spectroscopy

transducer	class	wavelength range	output signal
phototube	photon	200–1000 nm	current
photomultiplier	photon	110–1000 nm	current
Si photodiode	photon	250–1100 nm	current
photoconductor	photon	750–6000 nm	change in resistance
photovoltaic cell	photon	400–5000 nm	current or voltage
thermocouple	thermal	0.8–40 μm	voltage
thermistor	thermal	0.8–40 μm	change in resistance
pneumatic	thermal	0.8–1000 μm	membrane displacement
pyroelectric	thermal	0.3–1000 μm	current

Photon Transducers. Phototubes and photomultipliers use a photosensitive surface that absorbs radiation in the ultraviolet, visible, or near IR to produce an electrical current that is proportional to the number of photons reaching the transducer (Figure 10.1.14). Other photon detectors use a semiconductor as the photosensitive surface. When the semiconductor absorbs photons, valence electrons move to the semiconductor's conduction band, producing a measurable current. One advantage of the Si photodiode is that it is easy to miniaturize.

Groups of photodiodes are gathered together in a linear array that contains 64–4096 individual photodiodes. With a width of 25 μm per diode, a linear array of 2048 photodiodes requires only 51.2 mm of linear space. By placing a ***photodiode array*** along the monochromator's focal plane, it is possible to monitor simultaneously an entire range of wavelengths.

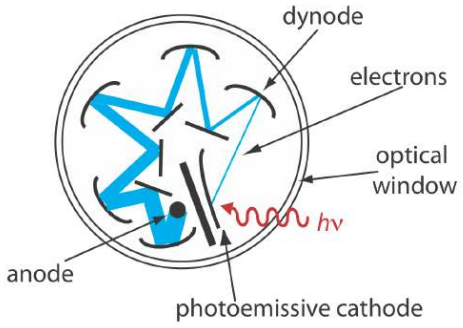


Figure 10.1.14 . Schematic of a photomultiplier. A photon strikes the photoemissive cathode producing electrons, which accelerate toward a positively charged dynode. Collision of these electrons with the dynode generates additional electrons, which accelerate toward the next dynode. A total of 10^6–10^7 electrons per photon eventually reach the anode, generating an electrical current.

Thermal Transducers. Infrared photons do not have enough energy to produce a measurable current with a photon transducer. A thermal transducer, therefore, is used for infrared spectroscopy. The absorption of infrared photons increases a thermal transducer's temperature, changing one or more of its characteristic properties. A pneumatic transducer, for example, is a small tube of xenon gas with an IR transparent window at one end and a flexible membrane at the other end. Photons enter the tube and are absorbed by a blackened surface, increasing the temperature of the gas. As the temperature inside the tube fluctuates, the gas expands and contracts and the flexible membrane moves in and out. Monitoring the membrane's displacement produces an electrical signal.

SIGNAL PROCESSORS

A transducer's electrical signal is sent to a ***signal processor*** where it is displayed in a form that is more convenient for the analyst. Examples of signal processors include analog or digital meters, recorders, and computers equipped with digital acquisition boards. A signal processor also is used to calibrate the detector's response, to amplify the transducer's signal, to remove noise by filtering, or to mathematically transform the signal.

> If the retina in your eye and the eardrum in your ear are transducers, then your brain is the signal processor.

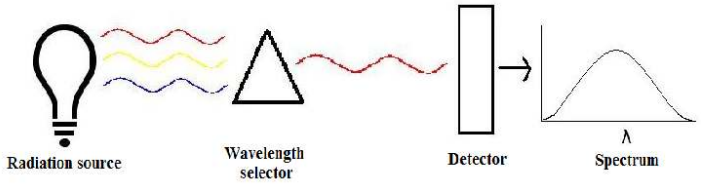
This page titled 6.1: Overview of Spectroscopy is shared under a CC BY-NC-SA 4.0 license and was authored, remixed, and/or curated by David Harvey.

- **10.1: Overview of Spectroscopy** by David Harvey is licensed CC BY-NC-SA 4.0.

6.2: Spectrometer

Strictly speaking, a spectrometer is any instrument used to view and analyze a range (or a *spectrum*) of a given characteristic for a substance (for example, a range of mass-to-charge values as in mass spectrometry), or a range of wavelengths as in absorption spectrometry like nuclear magnetic radiation spectroscopy or infrared spectroscopy). A spectro*photo*meter is a spectrometer that only measures the intensity of electromagnetic radiation (light) and is distinct from other spectrometers such as mass spectrometers.

A spectrometer is typically used to measure wavelengths of electromagnetic radiation (light) that has interacted with a sample. Incident light can be *reflected* off, *absorbed* by, or *transmitted* through a sample; the way the incident light changes during the interaction with the sample is characteristic of the sample. A spectrometer measures this change over a range of incident wavelengths (or at a specific wavelength).

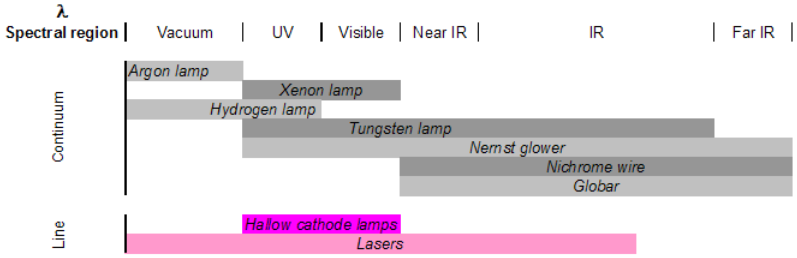


There are three main components in all spectrometers; these components can vary widely between instruments for specific applications and levels of resolution. Very generally, these components produce the electromagnetic radiation, somehow narrows the electromagnetic radiation to a specified range, and then detect the resulting electromagnetic radiation after is has interacted with the sample.

Sources of Radiation

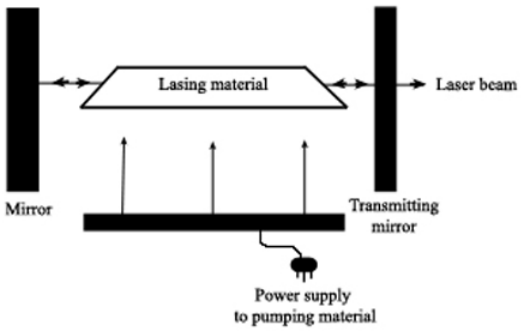
There are two classes of radiation sources used in spectrometry: continuum sources and line sources. The former are usually lamps or heated solid materials that emit a wide range of wavelengths that must be narrowed greatly using a wavelength selection element to isolate the wavelength of interest. The latter sources include lasers and specialized lamps, that are designed to emit discrete wavelengths specific to the lamp's material.

Electrode lamps are constructed of a sealed, gas-filled chamber that has one or more electrodes inside. Electrical current is passed through the electrode, which causes excitation of the gas. This excitation produces radiation at a wavelength or a range of wavelengths, specific to the gas. Examples include argon, xenon, hydrogen or deuterium, and tungsten lamps, which emit radiation in the following ranges.



There are also *non-electrode lamps* used as line sources that contain a gas and a piece of metal that will emit narrow radiation at the desired wavelength. Ionization of the gas occurs from radiation (usually in the radio or microwave frequencies). The metal atoms are then excited by a transfer of energy from the gas, thereby producing radiation at a very specific wavelength.

Laser (an acronym for *l*ight *a*mplification by *s*timulated *e*mission of *r*adiation) sources work by externally activating a lasing material so that photons of a specific energy are produced and aimed at the material. This triggers photon production within the material, with more and more photons being produced as they reflect inside the material. Because all the photons are of equal energy they are all in phase with each other so that energy (and wavelength) is isolated and enhanced. The photons are eventually focused into a narrow beam and then directed at the sample.



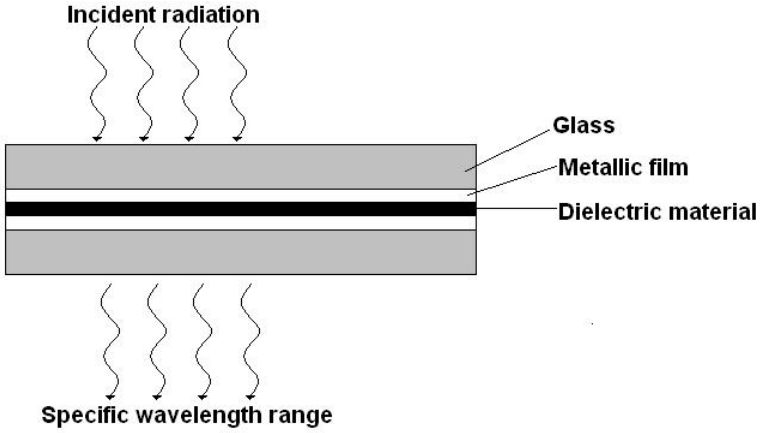
Wavelength Selection

There are three methods of narrowing the incident electromagnetic radiation down to the desired wavelength: dispersive or non-dispersive.

Non-dispersive Elements

Wavelength selection elements are non-dispersive materials that filter out the unwanted ranges of wavelengths from the incident light source, thereby allowing only a certain range of wavelengths to pass through. For example, UV filters (as used on cameras) work by absorbing the UV radiation (100-400nm) but allowing other wavelengths to be transmitted. This type of filter is not common in modern spectrometers now that there are more precise elements available for narrowing the radiation.

There are also interference filters that select wavelengths by causing interference effects between the incident and reflected radiation waves at each of the material boundaries in the filter. The filter has layers of a dielectric material, semitransparent metallic films, and glass; the incident light is partitioned according to the properties of each material as it passes through the layers (Ingle). If the light is of the proper wavelength when it encounters the second metallic film, then the reflected portion remains in phase with some of the incident light still entering that layer. This effectively isolates and enhances this particular wavelength while all others are removed via destructive interference.

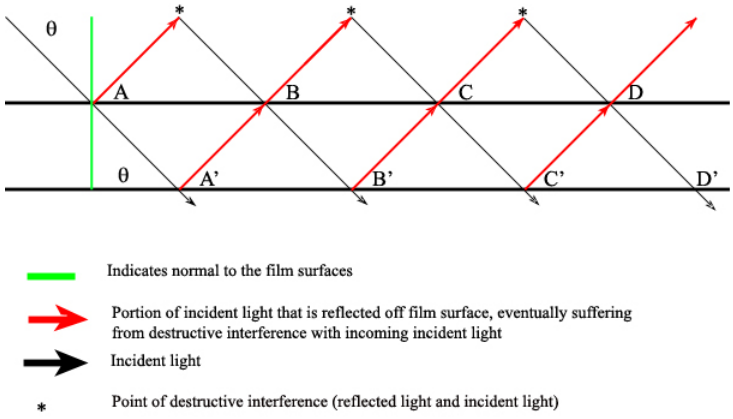


One filter can be adjusted to allow various wavelengths to pass through it by manually changing the angle of the incident radiation (θ) angle:

$$2d\sqrt{\epsilon^2-\sin^2} = m\lambda$$

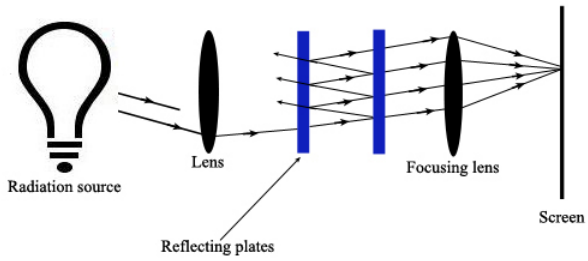
Where d is the thickness of the dialectic material (on the order of the wavelength of interest), ? is the refractive index of the material, m is the order of interference, and ? is the passable wavelength. This shows that for a given material (constant d, ϵ, and m) changing λ results in a different θ. Note that when the incident radiation is normal (perpendicular) to the filter surface, then the transmittable wavelength is independent of the radiation angle:

$$\theta = \frac{2d\lambda}{m}$$



Interferometers are also non-dispersive systems that use reflectors (usually mirrors) to direct the incident radiation along a specified path before being recombined and/or focused. Some systems also include a beam splitter that divides the incident beam and directs each portion along a different path before being recombined and directed to the detector. When the beams are recombined, only the radiation that is in phase when the beams recombine will be detected. All other radiation suffers destructive interference and is therefore removed from the spectrum. An interferogram is a photographic record produced by an interferometer.

A Fabry-Perot Interferometer allows the incident radiation to be reflected back and forth between a pair of reflective plates that are separated by an air gap (Ingle). Diffuse, multi-beam incident radiation passes through a lens and is directed to the plates. Some of the radiation reflects out of the plates back towards the incident source. The remaining radiation reflects back and forth between the plates and is eventually transmitted through the pair of plates towards a focusing lens. Here all constructively interfering radiation is focused onto a screen where it creates a dark or bright spot.



Constructive interference occurs when

$$2d\cos\theta' = m?$$

Where θ' equals the angle of refraction in the air gap. This air gap can be changed to isolate particular wavelengths.

The mathematics relationships of the Fabry-Perot Interferometer relates the difference in the optical path length, $\Delta(OPL)$, with the reflectance of the plate coatings:

$$\Delta(OPL) = 2d\lambda\cos\theta'$$

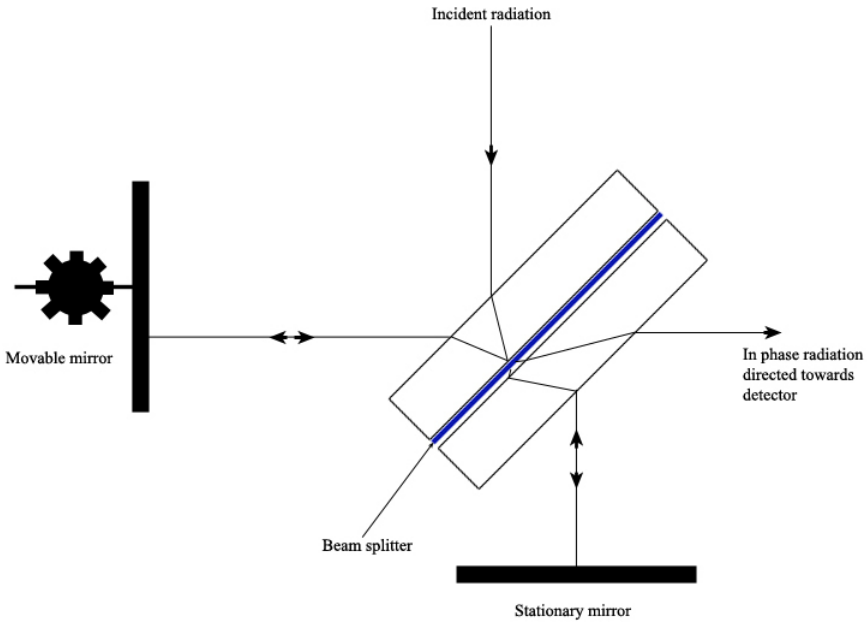
Phase difference = ? = 2? (2d? cos ?')/ ?

And ? ? 4?/(1- ?)^2

Where ? is the reflectance of the plate coating.

A Michelson Interferometer uses a beam splitter plate to divide the incident radiation into two beams of equal intensity. A pair of perpendicular mirrors then reflects the beams back to the splitter plate where they recombine and are directed towards the detector. One mirror is movable and the other is stationary. By moving one mirror, the path length of each beam is different, creating interference at the detector that can be measured as a function of the position of the movable mirror. At a certain distance from the splitter plate, the movable mirror causes constructive interference of the radiation at the detector such that a bright spot is detected.

By varying the distance from this location, the adjustable mirror causes the radiation to fluctuate sinusoidally between being “in phase” or “out of phase” at the detector (Ingle).

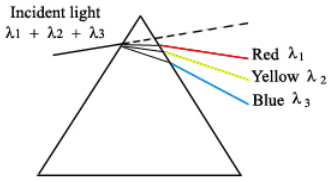


The sample material to be tested is placed in the path of one of the interferometer’s beams, which changes the path length difference between the two beams. It is the change in the interference pattern at the detector between the two beams that is measured.

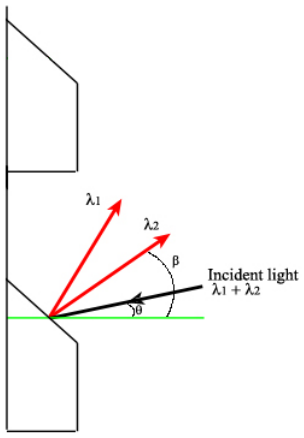
Other interferometers work in a similar manner, but change the angle of the mirrors rather than the position. These variations are found in the Sagnac Interferometer or the Mach-Zender Interferometer.

Dispersive Elements

These work by dispersing the incident radiation out spatially, creating a spectrum of wavelengths (Ingle). In a prism the diffuse radiation beam is separated because of the refractive index of the material. For example, when white light is shone onto a prism, a rainbow of colors is observed coming out the other side. This is a result of wavelength dependence on the refractive index of the prism material.



Gratings are also used to disperse incident light into component wavelengths. They work by reflecting the light off the angled grating surface, causing the wavelengths to be dispersed through constructive interference at wavelength-dependent diffraction angles (Ingle).



The condition for constructive interference (and therefore wavelength selection) on a grating surface is:

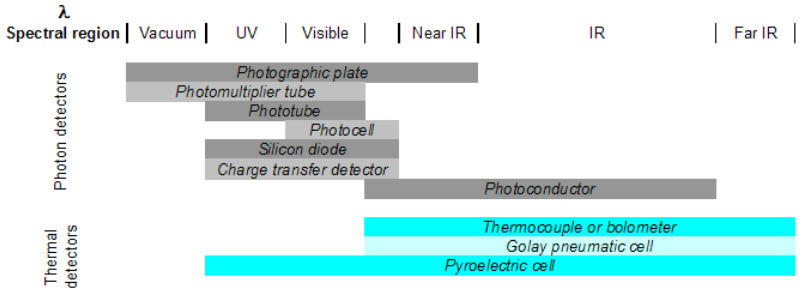
$$d(\sin\theta + \sin\theta) = m\theta$$

This relationship shows that the wavelength selection is not based on the grating material, but on the angle of incidence (θ). The angle θ can also be used to describe the angle between normal and $?_1$.

Detector

Detectors are transducers that transform the analog output of the spectrometer into an electrical signal that can be viewed and analyzed using a computer. There are two types: photon detectors and thermal detectors.

- **Photon detectors** work generally by either causing electrons to be emitted or development of current when photons strike the detector surface. Examples include *photovoltaic cells*, *phototubes*, and *charge-transfer transducers*. Photovoltaic cells generate electrical current on a semiconductor material when photons in the visible region are absorbed. Phototubes, however, emit electrons from a photon-sensitive material. Charge-transfer transducers (such as photodiodes) develop a charge from visible region photon-induced electron transfer reactions within a silicon material. In each case, it is the current, the number of electrons, or the charge that is actually detected (not the photons themselves) and is then related to the energy/quantity of photons that caused the change in the material.
- **Thermal detectors** detect a temperature change in a material due to photon absorption. *Thermocouples* work by measuring the difference in temperature between a pair of junctions (usually the reference against the sample) and are generally used for the infrared wavelengths. The temperature difference is related to a potential difference, which is the output signal. *Pyroelectric transducers* are used in infrared region and utilize a dielectric material that produces a current when its temperature is changed by radiation absorption.



References

1. Atkins, P and de Paula, J. Physical Chemistry for the Life Sciences. Oxford University Press. New York, 2006. Chapter 13.
2. Ingle, JD. Spectrochemical Analysis. Prentice Hall. London, 1988. Chapter 3.
3. Pavia, DL. Introduction to Spectroscopy , Third Edition. Thomas Learning, Inc. Singapore, 2001. Page 390.
4. Skoog, DA. Principles of Instrumental Analysis, Fifth Edition. Harcourt Brace. Philadelphia, 1998. Chapter 7.

6.2: Spectrometer is shared under a CC BY-NC-SA 4.0 license and was authored, remixed, and/or curated by Julie Bower.

- **Spectrometer** by Julie Bower is licensed CC BY-NC-SA 4.0.

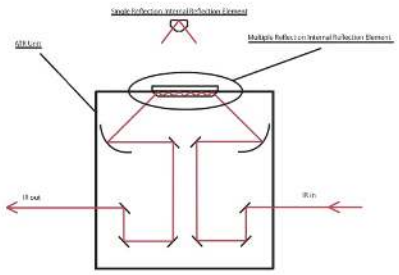
6.2.1: ATR-FTIR

This module will go over attenuated total reflectance Fourier transform infrared spectroscopy (ATR-FTIR). It will go over basic physics that describe and dictate the analytical technique. There will be a given example of how ATR-FTIR is used in biological studies. This example will be given in the format of real data and data analysis methods.

Introduction

ATR-FTIR is a tool that has been proven to be useful in various applications[1]. This technique is able to probe *in situ* single or multiple layers of adsorbed/deposited species at a solid/liquid interface[1,2]. It is for this reason that ATR-FTIR has been implemented in various different biological studies in order to probe chemical reactions/structure at the solid/liquid interface[2]. The reader should be aware that this module will not cover in depth about the physics that govern ATR-FTIR's ability to probe chemical species, but rather give the reader an introduction on the technique. This module will cover the basic experimental set-up that is currently being utilized in research, briefly go over essential equations that will help the reader better understand methods of experimentation, and finally provide an example of how ATR-FTIR can be utilized.

Experimental Setup



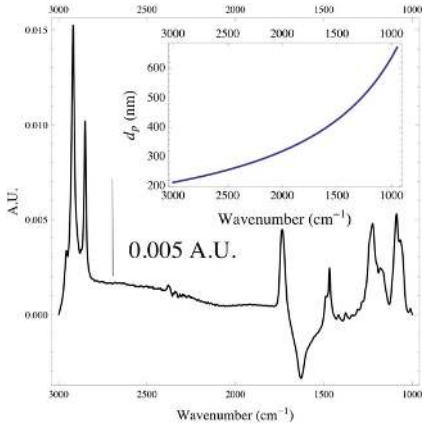
To the left is an image of what a typical ATR set-up includes. It shows the internal components found within a specific ATR setup which allows the infrared radiation to enter from the bottom of the ATR base and redirected by five different mirrors before the radiation enters then exits the internal reflection element (IRE) and continues towards the the detector. This setup allows for the infrared radiation to probe molecules at the interface of the IRE. The one shown above is an image of a multiple reflection internal reflection element. It is called a multiple reflection IRE because the radiation makes more than one reflection within the element prior to exiting towards the detector. There are advantages and disadvantages of using a multiple reflection element. One of the advantages is that the user is able to observe stronger absorbance by the sample due to the multiple points that the radiation is interacting, however the disadvantage of using a multiple reflection element is that the light absorbance is hard to quantify due to scattering that occurs with each reflection. One way for a user to overcome the disadvantage that multiple reflections brings is to use a single reflection IRE rather than a multiple reflection IRE.

ATR Basics

The infrared radiation that interacts with the adsorbed species is limited to a given depth, and is dependent on the wavelength and angle of the incoming radiation, refractive index of the IRE, and the refractive indices of the interacting layers at the IRE interface. This depth is known as the depth of penetration and the governing equation is shown below.

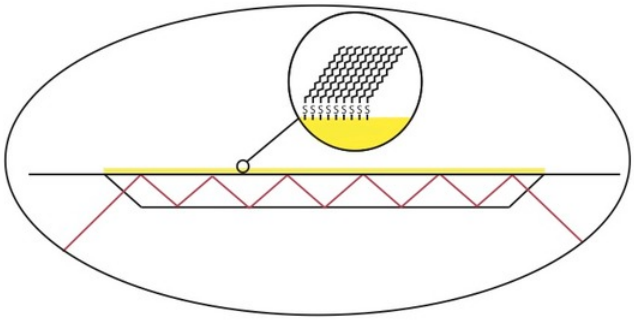
$$dp = \frac{\lambda}{2\pi\sqrt{n_1}}^{2} \sin[\theta]^2 - n_2^2 \tag{1}$$

It is good to keep in mind that the if working with systems that have more than one monolayer of adsorbed species that the depth of penetration is dependent on the wavelength of the incoming radiation. If this is the case the depth of penetration will be greater at higher wavelengths, and one will be probing deeper into the medium rather than at the interface of the IRE. Below is a spectrum of a monolayer of DPPC lipid vesicles adsorbed onto the surface of a ZnSe IRE. The inset plot shows the depth of penetration of the infrared radiation with respect to wavenumber.

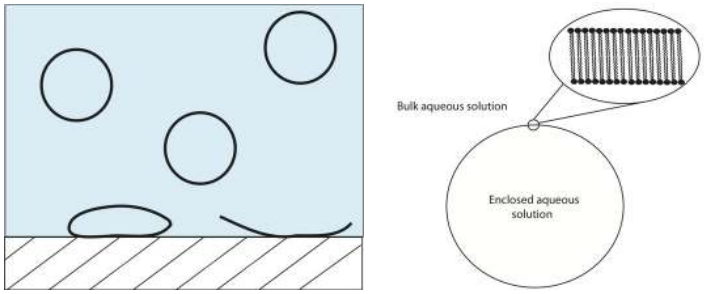


Vibrational Spectroscopy at the Solid/Liquid Interface

ATR-FTIR has been used to monitor and characterize organic thin film systems such as well formed self-assembled monolayers (SAM). This can be achieved forming a thin film of gold onto the IRE surface, exposing the gold surface to a thiol solution for a given amount of time. The figure below shows an example of an organic thin film formed on the surface of gold that was deposited on an IRE.

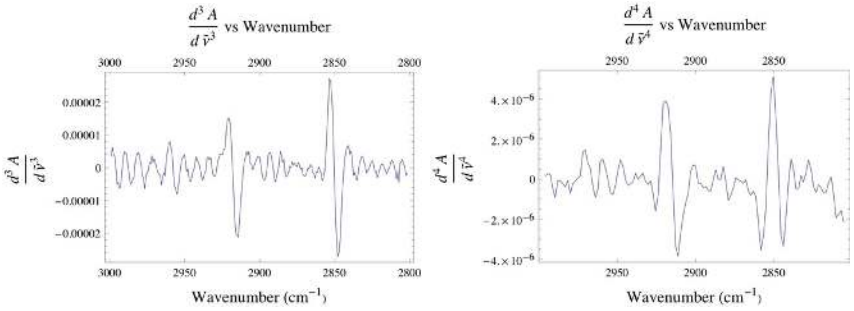


Lipid vesicles have received some attention over the years due to their ability to spontaneously form lipid aggregate spherical structures. These spherical structures have a wall made of lipids that separate the intracellular aqueous medium from the extracellular aqueous medium. They have been implemented in current forms of drug delivery systems, biological contrast agents, as well as serving as a model membrane. ATR-FTIR can be used to study these systems in a number of different ways. One such way to monitor the adsorption rate of these lipid vesicles from a bulk solution to a solid interface. Below is an example of one such experiment where 100 nm lipid vesicles were used to study the adsorption rate onto a ZnSe single reflection IRE.

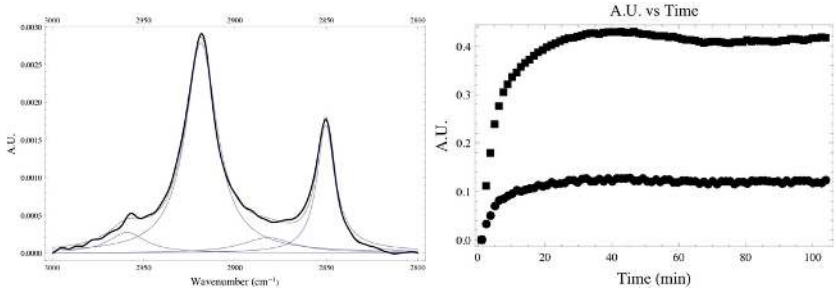


Below is the -C-H stretching region of DPPC found within the 2800 - 3000 cm^{-1}. The interval consists of the overlap of four different bands attributed to different -CH_2 and -CH_3 vibrational modes found within the acyl chain of DPPC. The bands found at 2850 and 2920 cm^{-1} are assigned to the -CH_2 symmetric and asymmetric vibrational modes, while the bands found at 2880 and 2960 cm^{-1} are assigned to the -CH_3 symmetric and asymmetric vibrational modes. Since the absorbance is proportional to the relative concentration of adsorbed lipid, it has been shown that if one monitors the absorbance under the -CH_2 bands one is able to attain precise adsorption rates of the lipid vesicles at the liquid/solid interface. Caution must be taken when finding the absorbance

of any absorption band, especially when dealing with overlapping absorption bands like the ones shown below. The proper way to analyze the data is to deconvolute the region of interest by identifying how many absorption bands are present by performing the proper 3rd and 4th derivative analysis on the spectrum, then fitting the data to the correct number of Gaussian/Lorentzian like bands.



Following the deconvolution and integration of the correct absorption bands one may create a time dependent absorbance plot similar to the one below. Where the top and bottom curve represent the time dependent absorbance of the asymmetric and symmetric -CH_2 bands.



References

1. What is the depth of penetration within water, if you are using a ZnSe internal reflection element, have an incident angle of 30º, and you are at 1000 cm^{-1}? (Hint: You will need the n_i for water and ZnSe.)

6.2.1: ATR-FTIR is shared under a CC BY-NC-SA 4.0 license and was authored, remixed, and/or curated by LibreTexts.

- **ATR-FTIR** is licensed CC BY-NC-SA 4.0.

6.3: SPECTROSCOPY BASED ON ABSORPTION

In absorption spectroscopy a beam of electromagnetic radiation passes through a sample. Much of the radiation passes through the sample without a loss in intensity. At selected wavelengths, however, the radiation's intensity is attenuated. This process of attenuation is called absorption.

ABSORPTION SPECTRA

There are two general requirements for an analyte's absorption of electromagnetic radiation. First, there must be a mechanism by which the radiation's electric field or magnetic field interacts with the analyte. For ultraviolet and visible radiation, absorption of a photon changes the energy of the analyte's valence electrons. A bond's vibrational energy is altered by the absorption of infrared radiation.

> Figure 10.1.3 provides a list of the types of atomic and molecular transitions associated with different types of electromagnetic radiation.

The second requirement is that the photon's energy, $h\nu$, must exactly equal the difference in energy, ΔE, between two of the analyte's quantized energy states. Figure 10.1.4 shows a simplified view of a photon's absorption, which is useful because it emphasizes that the photon's energy must match the difference in energy between a lower-energy state and a higher-energy state. What is missing, however, is information about what types of energy states are involved, which transitions between energy states are likely to occur, and the appearance of the resulting spectrum.

We can use the energy level diagram in Figure 10.2.1 to explain an absorbance spectrum. The lines labeled E_0 and E_1 represent the analyte's ground (lowest) electronic state and its first electronic excited state. Superimposed on each electronic energy level is a series of lines representing vibrational energy levels.

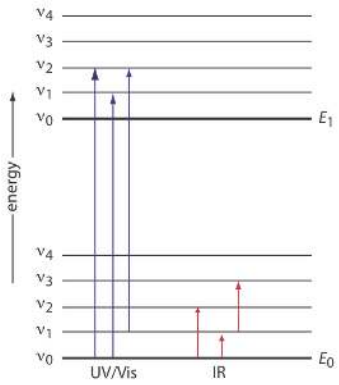


Figure 10.2.1 . Diagram showing two electronic energy levels (E_0 and E_1), each with five vibrational energy levels ν_{0-4}. Absorption of ultraviolet and visible radiation (shown by the blue arrows) leads to a change in the analyte's electronic energy levels and, possibly, a change in vibrational energy as well. A change in vibrational energy without a change in electronic energy levels occurs with the absorption of infrared radiation (shown by the red arrows).

INFRARED SPECTRA FOR MOLECULES AND POLYATOMIC IONS

The energy of infrared radiation produces a change in a molecule's or a polyatomic ion's vibrational energy, but is not sufficient to effect a change in its electronic energy. As shown in Figure 10.2.1 , vibrational energy levels are quantized; that is, a molecule or polyatomic ion has only certain, discrete vibrational energies. The energy for an allowed vibrational mode, E_ν, is

$$E_\nu = \nu + \frac{1}{2} h\nu_0$$

where ν is the vibrational quantum number, which has values of 0, 1, 2, ..., and ν_0 is the bond's fundamental vibrational frequency. The value of ν_0, which is determined by the bond's strength and by the mass at each end of the bond, is a characteristic property of a bond. For example, a carbon-carbon single bond (C–C) absorbs infrared radiation at a lower energy than a carbon-carbon double bond (C=C) because a single bond is weaker than a double bond.

At room temperature most molecules are in their ground vibrational state ($\nu = 0$) . A transition from the ground vibrational state to the first vibrational excited state ($\nu = 1$) requires absorption of a photon with an energy of $h\nu_0$. Transitions in which $\Delta\nu = \pm 1$ give rise to the fundamental absorption lines. Weaker absorption lines, called overtones, result from transitions in which $\Delta\nu$ is ±2 or ±3. The number of possible normal vibrational modes for a linear molecule is $3N - 5$, and for a non-linear molecule is $3N - 6$, where N is the number of atoms in the molecule. Not surprisingly, infrared spectra often show a considerable number of absorption bands. Even a relatively simple

molecule, such as ethanol (C_2H_6O), for example, has $3 \times 9 - 6$, or 21 possible normal modes of vibration, although not all of these vibrational modes give rise to an absorption. The IR spectrum for ethanol is shown in Figure 10.2.2 .

> Why does a non-linear molecule have $3N - 6$ vibrational modes? Consider a molecule of methane, CH_4. Each of methane's five atoms can move in one of three directions (x, y, and z) for a total of $5 \times 3 = 15$ different ways in which the molecule's atoms can move. A molecule can move in three ways: it can move from one place to another, which we call translational motion; it can rotate around an axis, which we call rotational motion; and its bonds can stretch and bend, which we call vibrational motion. Because the entire molecule can move in the x, y, and z directions, three of methane's 15 different motions are translational. In addition, the molecule can rotate about its x, y, and z axes, accounting for three additional forms of motion. This leaves 15 – 3 – 3 = 9 vibrational modes. A linear molecule, such as CO_2, has $3N - 5$ vibrational modes because it can rotate around only two axes.

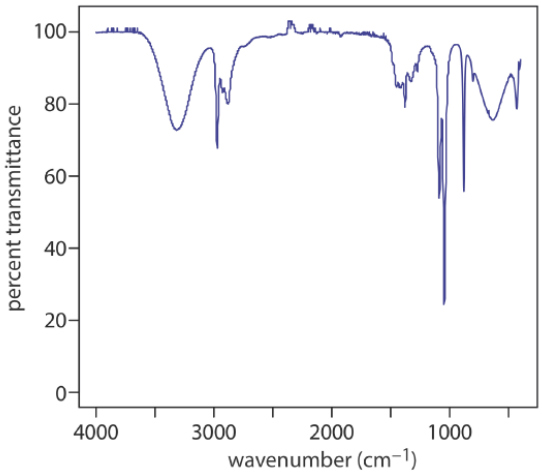


Figure 10.2.2 . Infrared spectrum of ethanol.

UV/VIS SPECTRA FOR MOLECULES AND IONS

The valence electrons in organic molecules and polyatomic ions, such as CO_3^{2-}, occupy quantized sigma bonding (σ), pi bonding (π), and non-bonding (n) molecular orbitals (MOs). Unoccupied sigma antibonding (σ^*) and pi antibonding (π^*) molecular orbitals are slightly higher in energy. Because the difference in energy between the highest-energy occupied MOs and the lowest-energy unoccupied MOs corresponds to ultraviolet and visible radiation, absorption of a photon is possible.

Four types of transitions between quantized energy levels account for most molecular UV/Vis spectra. Table 10.2.1 lists the approximate wavelength ranges for these transitions, as well as a partial list of bonds, functional groups, or molecules responsible for these transitions. Of these transitions, the most important are $n \rightarrow \pi^*$ and $\pi \rightarrow \pi^*$ because they involve important functional groups that are characteristic of many analytes and because the wavelengths are easily accessible. The bonds and functional groups that give rise to the absorption of ultraviolet and visible radiation are called ***chromophores***.

Table 10.2.1 . Electronic Transitions Involving n, σ, and π Molecular Orbitals

transition	wavelength range	examples
$\sigma \rightarrow \sigma^*$	<200 nm	C—C, C—H
$n \rightarrow \sigma^*$	160–260 nm	H_2O, CH_3OH, CH_3Cl
$\pi \rightarrow \pi^*$	200–500 nm	C=C, C=O, C=N, C≡C
$n \rightarrow \pi^*$	250–600 nm	C=O, C=N, N=N, N=O

Many transition metal ions, such as Cu^{2+} and Co^{2+}, form colorful solutions because the metal ion absorbs visible light. The transitions that give rise to this absorption are valence electrons in the metal ion's d-orbitals. For a free metal ion, the five d-orbitals are of equal energy. In the presence of a complexing ligand or solvent molecule, however, the d-orbitals split into two or more groups that differ in energy. For example, in an octahedral complex of $Cu(H_2O)_6^{2+}$ the six water molecules perturb the d-orbitals into the two groups shown in Figure 10.2.3 . The resulting $d \rightarrow d$ transitions for transition metal ions are relatively weak.

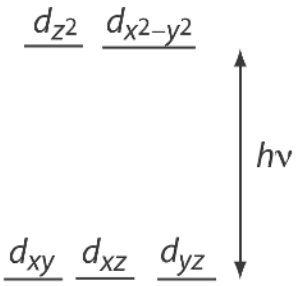


Figure 10.2.3 . Splitting of the *d*-orbitals in an octahedral field.

A more important source of UV/Vis absorption for inorganic metal–ligand complexes is charge transfer, in which absorption of a photon produces an excited state in which there is transfer of an electron from the metal, *M*, to the ligand, *L*.

$$M - L + h\nu \rightarrow \left(M^{+} - L^{-}\right)^{*}$$

Charge-transfer absorption is important because it produces very large absorbances. One important example of a charge-transfer complex is that of *o*-phenanthroline with Fe^{2+}, the UV/Vis spectrum for which is shown in Figure 10.2.4 . Charge-transfer absorption in which an electron moves from the ligand to the metal also is possible.

Why is a larger absorbance desirable? An analytical method is more sensitive if a smaller concentration of analyte gives a larger signal.

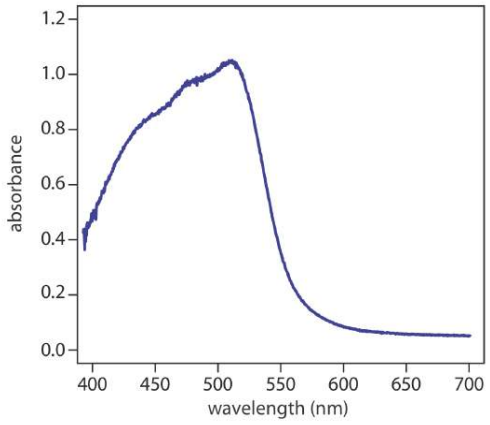


Figure 10.2.4 . UV/Vis spectrum for the metal–ligand complex $\mathrm{Fe(phen)}_3^{2+}$, where phen is the ligand *o*-phenanthroline.

Comparing the IR spectrum in Figure 10.2.2 to the UV/Vis spectrum in Figure 10.2.4 shows us that UV/Vis absorption bands are often significantly broader than those for IR absorption. We can use Figure 10.2.1 to explain why this is true. When a species absorbs UV/Vis radiation, the transition between electronic energy levels may also include a transition between vibrational energy levels. The result is a number of closely spaced absorption bands that merge together to form a single broad absorption band.

UV/VIS SPECTRA FOR ATOMS

The energy of ultraviolet and visible electromagnetic radiation is sufficient to cause a change in an atom's valence electron configuration. Sodium, for example, has a single valence electron in its 3*s* atomic orbital. As shown in Figure 10.2.5 , unoccupied, higher energy atomic orbitals also exist.

The valence shell energy level diagram in Figure 10.2.5 might strike you as odd because it shows that the 3*p* orbitals are split into two groups of slightly different energy. The reasons for this splitting are unimportant in the context of our treatment of atomic absorption. For further information about the reasons for this splitting, consult the chapter's additional resources.

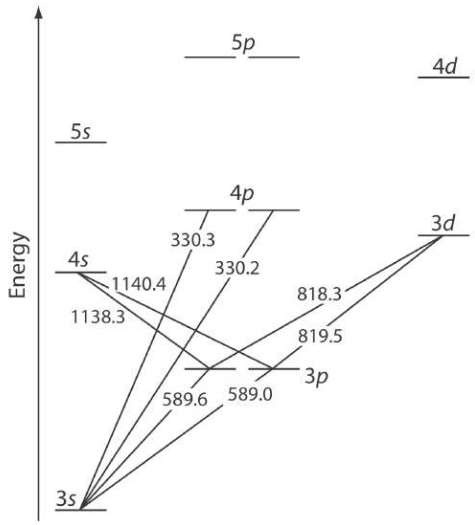


Figure 10.2.5 . Valence shell energy level diagram for sodium. The wavelengths (in wavenumbers) corresponding to several transitions are shown.

Absorption of a photon is accompanied by the excitation of an electron from a lower-energy atomic orbital to an atomic orbital of higher energy. Not all possible transitions between atomic orbitals are allowed. For sodium the only allowed transitions are those in which there is a change of ±1 in the orbital quantum number (l); thus transitions from $s \rightarrow p$ orbitals are allowed, but transitions from $s \rightarrow s$ and from $s \rightarrow d$ orbitals are forbidden.

The atomic absorption spectrum for Na is shown in Figure 10.2.6 , and is typical of that found for most atoms. The most obvious feature of this spectrum is that it consists of a small number of discrete absorption lines that correspond to transitions between the ground state (the 3*s* atomic orbital) and the 3*p* and the 4*p* atomic orbitals. Absorption from excited states, such as the $3p \rightarrow 4s$ and the $3p \rightarrow 3d$ transitions included in Figure 10.2.5 , are too weak to detect. Because an excited state's lifetime is short—an excited state atom typically returns to a lower energy state in 10^{-7} to 10^{-8} seconds—an atom in the exited state is likely to return to the ground state before it has an opportunity to absorb a photon.

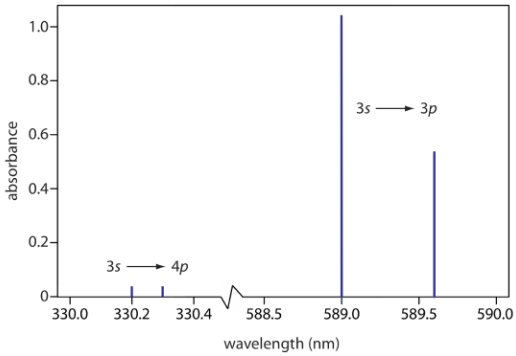


Figure 10.2.6 . Atomic absorption spectrum for sodium. Note that the scale on the *x*-axis includes a break.

Another feature of the atomic absorption spectrum in Figure 10.2.6 is the narrow width of the absorption lines, which is a consequence of the fixed difference in energy between the ground state and the excited state, and the lack of vibrational and rotational energy levels. Natural line widths for atomic absorption, which are governed by the uncertainty principle, are approximately 10^{-5} nm. Other contributions to broadening increase this line width to approximately 10^{-3} nm.

TRANSMITTANCE AND ABSORBANCE

As light passes through a sample, its power decreases as some of it is absorbed. This attenuation of radiation is described quantitatively by two separate, but related terms: transmittance and absorbance. As shown in Figure 10.2.7 a, transmittance is the ratio of the source radiation's power as it exits the sample, P_T, to that incident on the sample, P_0.

$$T = \frac{P_T}{P_0} \tag{6.3.1}$$

Multiplying the transmittance by 100 gives the percent transmittance, %*T*, which varies between 100% (no absorption) and 0% (complete absorption). All methods of detecting photons—including the human eye and modern photoelectric transducers—measure the transmittance of electromagnetic radiation.

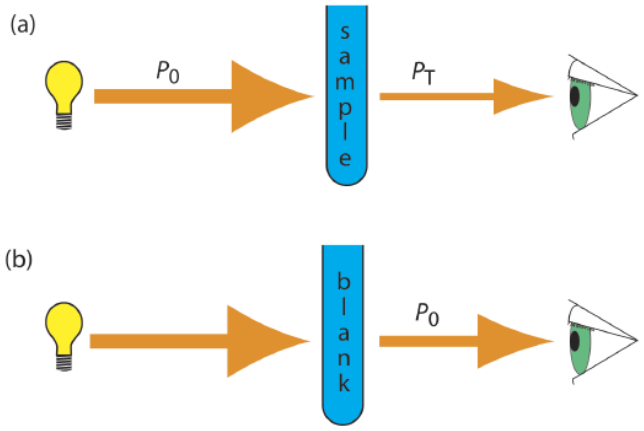


Figure 10.2.7 . (a) Schematic diagram showing the attenuation of radiation passing through a sample; P_0 is the source's radiant power and P_T is the radiant power transmitted by the sample. (b) Schematic diagram showing how we redefine P_0 as the radiant power transmitted by the blank. Redefining P_0 in this way corrects the transmittance in (a) for the loss of radiation due to scattering, reflection, absorption by the sample's container, and absorption by the sample's matrix.

Equation 6.3.1 does not distinguish between different mechanisms that prevent a photon emitted by the source from reaching the detector. In addition to absorption by the analyte, several additional phenomena contribute to the attenuation of radiation, including reflection and absorption by the sample's container, absorption by other components in the sample's matrix, and the scattering of radiation. To compensate for this loss of the radiation's power, we use a method blank. As shown in Figure 10.2.7 b, we redefine P_0 as the power exiting the method blank.

An alternative method for expressing the attenuation of electromagnetic radiation is absorbance, A, which we define as

$$A = -\log T = -\log \frac{P_T}{P_0} \tag{6.3.2}$$

Absorbance is the more common unit for expressing the attenuation of radiation because it is a linear function of the analyte's concentration.

> We will show that this is true in the next section when we introduce Beer's law.

EXAMPLE 10.2.1

A sample has a percent transmittance of 50%. What is its absorbance?

Solution

A percent transmittance of 50.0% is the same as a transmittance of 0.500. Substituting into Equation 6.3.2 gives

$$A = -\log T = -\log(0.500) = 0.301$$

EXERCISE 10.2.1

What is the %T for a sample if its absorbance is 1.27?

Answer

To find the transmittance, T, we begin by noting that

$$A = 1.27 = -\log T$$

Solving for T

$$-1.27 = \log T$$
$$10^{-1.27} = T$$

gives a transmittance of 0.054, or a %T of 5.4%.

Equation 6.3.1 has an important consequence for atomic absorption. As we learned from Figure 10.2.6 , atomic absorption lines are very narrow. Even with a high quality monochromator, the effective bandwidth for a continuum source is $100 - 1000\times$ greater than the width of

an atomic absorption line. As a result, little radiation from a continuum source is absorbed when it passes through a sample of atoms; because $P_0 \approx P_T$ the measured absorbance effectively is zero. For this reason, atomic absorption requires that we use a line source instead of a continuum source.

ABSORBANCE AND CONCENTRATION: BEER'S LAW

When monochromatic electromagnetic radiation passes through an infinitesimally thin layer of sample of thickness *dx*, it experiences a decrease in its power of *dP* (Figure 10.2.8).

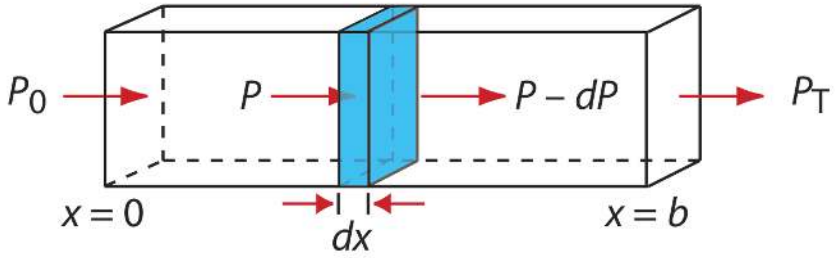


Figure 10.2.8 . Factors used to derive the Beer's law.

This fractional decrease in power is proportional to the sample's thickness and to the analyte's concentration, *C*; thus

$$-\frac{dP}{P} = \alpha C dx \tag{6.3.3}$$

where *P* is the power incident on the thin layer of sample and α is a proportionality constant. Integrating the left side of Equation 6.3.3 over the sample's full thickness

$$-\int_{P=P_0}^{P=P_t} \frac{dP}{P} = \alpha C \int_{x=0}^{x=b} dx$$

$$\ln \frac{P_0}{P_T} = \alpha b C$$

converting from ln to log, and substituting into Equation 6.3.2, gives

$$A = abC \tag{6.3.4}$$

where *a* is the analyte's ***absorptivity*** with units of cm^{-1} $conc^{-1}$. If we express the concentration using molarity, then we replace *a* with the ***molar absorptivity***, ε, which has units of cm^{-1} M^{-1}.

$$A = \varepsilon bC \tag{6.3.5}$$

The absorptivity and the molar absorptivity are proportional to the probability that the analyte absorbs a photon of a given energy. As a result, values for both *a* and ε depend on the wavelength of the absorbed photon.

EXAMPLE 10.2.2

A 5.00×10^{-4} M solution of analyte is placed in a sample cell that has a pathlength of 1.00 cm. At a wavelength of 490 nm, the solution's absorbance is 0.338. What is the analyte's molar absorptivity at this wavelength?

Solution

Solving Equation 6.3.5 for ϵ and making appropriate substitutions gives

$$\varepsilon = \frac{A}{bC} = \frac{0.338}{(1.00\text{ cm})\left(5.00 \times 10^{-4}\text{ M}\right)} = 676\text{ cm}^{-1}\text{ M}^{-1}$$

EXERCISE 10.2.2

A solution of the analyte from Example 10.2.2 has an absorbance of 0.228 in a 1.00-cm sample cell. What is the analyte's concentration?

Answer

Making appropriate substitutions into Beer's law

$$A = 0.228 = \varepsilon bC = \left(676\ \text{M}^{-1}\ \text{cm}^{-1}\right)(1\ \text{cm})C$$

and solving for C gives a concentration of 3.37×10^{-4} M.

Equation 6.3.4 and Equation 6.3.5, which establish the linear relationship between absorbance and concentration, are known as Beer's law. Calibration curves based on Beer's law are common in quantitative analyses.

As is often the case, the formulation of a law is more complicated than its name suggests. This is the case, for example, with Beer's law, which also is known as the Beer-Lambert law or the Beer-Lambert-Bouguer law. Pierre Bouguer, in 1729, and Johann Lambert, in 1760, noted that the transmittance of light decreases exponentially with an increase in the sample's thickness.

$$T \propto e^{-b}$$

Later, in 1852, August Beer noted that the transmittance of light decreases exponentially as the concentration of the absorbing species increases.

$$T \propto e^{-C}$$

Together, and when written in terms of absorbance instead of transmittance, these two relationships make up what we know as Beer's law.

BEER'S LAW AND MULTICOMPONENT SAMPLES

We can extend Beer's law to a sample that contains several absorbing components. If there are no interactions between the components, then the individual absorbances, A_i, are additive. For a two-component mixture of analyte's X and Y, the total absorbance, A_{tot}, is

$$A_{tot} = A_X + A_Y = \varepsilon_X bC_X + \varepsilon_Y bC_Y$$

Generalizing, the absorbance for a mixture of n components, A_{mix}, is

$$A_{mix} = \sum_{i=1}^{n} A_i = \sum_{i=1}^{n} \varepsilon_i bC_i \tag{6.3.6}$$

LIMITATIONS TO BEER'S LAW

Beer's law suggests that a plot of absorbance vs. concentration—we will call this a Beer's law plot—is a straight line with a y-intercept of zero and a slope of ab or εb. In some cases a Beer's law plot deviates from this ideal behavior (see Figure 10.2.9), and such deviations from linearity are divided into three categories: fundamental, chemical, and instrumental.

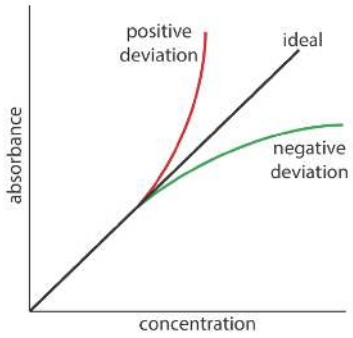


Figure 10.2.9 . Plots of absorbance vs. concentration showing positive and negative deviations from the ideal Beer's law relationship, which is a straight line.

FUNDAMENTAL LIMITATIONS TO BEER'S LAW

Beer's law is a limiting law that is valid only for low concentrations of analyte. There are two contributions to this fundamental limitation to Beer's law. At higher concentrations the individual particles of analyte no longer are independent of each other. The resulting interaction between particles of analyte may change the analyte's absorptivity. A second contribution is that an analyte's absorptivity depends on the solution's refractive index. Because a solution's refractive index varies with the analyte's concentration, values of a and ε may change. For sufficiently low concentrations of analyte, the refractive index essentially is constant and a Beer's law plot is linear.

CHEMICAL LIMITATIONS TO BEER'S LAW

A chemical deviation from Beer's law may occur if the analyte is involved in an equilibrium reaction. Consider, for example, the weak acid, HA. To construct a Beer's law plot we prepare a series of standard solutions—each of which contains a known total concentration of HA—and then measure each solution's absorbance at the same wavelength. Because HA is a weak acid, it is in equilibrium with its conjugate weak base, A^-.

> In the equations that follow, the conjugate weak base A^- is written as A as it is easy to mistake the symbol for anionic charge as a minus sign.

$$HA(aq) + H_2O(l) \rightleftharpoons H_3O^+(aq) + A^-(aq)$$

If both HA and A^- absorb at the selected wavelength, then Beer's law is

$$A = \varepsilon_{HA} b C_{HA} + \varepsilon_A b C_A \tag{6.3.7}$$

Because the weak acid's total concentration, C_{total}, is

$$C_{total} = C_{HA} + C_A$$

we can write the concentrations of HA and A^- as

$$C_{HA} = \alpha_{HA} C_{total} \tag{6.3.8}$$

$$C_A = (1 - \alpha_{HA}) C_{total} \tag{6.3.9}$$

where α_{HA} is the fraction of weak acid present as HA. Substituting Equation 6.3.8 and Equation 6.3.9 into Equation 6.3.7 and rearranging, gives

$$A = \left(\varepsilon_{HA}\alpha_{HA} + \varepsilon_A - \varepsilon_A\alpha_A\right) b C_{total} \tag{6.3.10}$$

To obtain a linear Beer's law plot, we must satisfy one of two conditions. If ε_{HA} and ε_A have the same value at the selected wavelength, then Equation 6.3.10 simplifies to

$$A = \varepsilon_A b C_{total} = \varepsilon_{HA} b C_{total}$$

Alternatively, if α_{HA} has the same value for all standard solutions, then each term within the parentheses of Equation 6.3.10 is constant—which we replace with *k*—and a linear calibration curve is obtained at any wavelength.

$$A = k b C_{total}$$

Because HA is a weak acid, the value of α_{HA} varies with pH. To hold α_{HA} constant we buffer each standard solution to the same pH. Depending on the relative values of α_{HA} and α_A, the calibration curve has a positive or a negative deviation from Beer's law if we do not buffer the standards to the same pH.

INSTRUMENTAL LIMITATIONS TO BEER'S LAW

There are two principal instrumental limitations to Beer's law. The first limitation is that Beer's law assumes that radiation reaching the sample is of a single wavelength—that is, it assumes a purely monochromatic source of radiation. As shown in Figure 10.1.10, even the best wavelength selector passes radiation with a small, but finite effective bandwidth. Polychromatic radiation always gives a negative deviation from Beer's law, but the effect is smaller if the value of ε essentially is constant over the wavelength range passed by the wavelength selector. For this reason, as shown in Figure 10.2.10 , it is better to make absorbance measurements at the top of a broad absorption peak. In addition, the deviation from Beer's law is less serious if the source's effective bandwidth is less than one-tenth of the absorbing species' natural bandwidth [(a) Strong, F. C., III *Anal. Chem.* **1984**, *56*, 16A–34A; Gilbert, D. D. *J. Chem. Educ.* **1991**, *68*, A278–A281]. When measurements must be made on a slope, linearity is improved by using a narrower effective bandwidth.

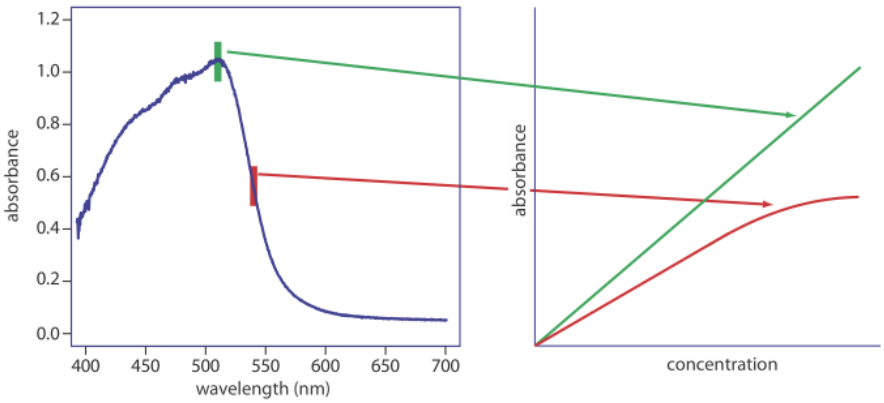


Figure 10.2.10 . Effect of wavelength selection on the linearity of a Beer's law plot. Another reason for measuring absorbance at the top of an absorbance peak is that it provides for a more sensitive analysis. Note that the green Beer's law plot has a steeper slope—and, therefore, a greater sensitivity—than the red Beer's law plot. A Beer's law plot, of course, is equivalent to a calibration curve.

Stray radiation is the second contribution to instrumental deviations from Beer's law. Stray radiation arises from imperfections in the wavelength selector that allow light to enter the instrument and to reach the detector without passing through the sample. Stray radiation adds an additional contribution, P_{stray}, to the radiant power that reaches the detector; thus

$$A = -\log \frac{P_{\text{T}} + P_{\text{stray}}}{P_0 + P_{\text{stray}}}$$

For a small concentration of analyte, P_{stray} is significantly smaller than P_0 and P_{T}, and the absorbance is unaffected by the stray radiation. For higher concentrations of analyte, less light passes through the sample and P_{T} and P_{stray} become similar in magnitude. This results is an absorbance that is smaller than expected, and a negative deviation from Beer's law.

This page titled 6.3: Spectroscopy Based on Absorption is shared under a CC BY-NC-SA 4.0 license and was authored, remixed, and/or curated by David Harvey.

- **10.2: Spectroscopy Based on Absorption** by David Harvey is licensed CC BY-NC-SA 4.0.

SECTION OVERVIEW

6.4: Lasers

LASER is an acronym for Light Amplification by Stimulated Emission of Radiation. Laser is a type of light source which has the unique characteristics of directionality, brightness, and monochromaticity. The goal of this module is to explain how a laser operates (stimulated or spontaneous emission), describe important components, and give some examples of types of lasers and their applications.

6.4.1: Gas Lasers

6.4.2: Laser Theory

6.4.3: Overview of Lasers

6.4.4: Semiconductor and Solid-state lasers

6.4.5: Semiconductors

6.4: Lasers is shared under a CC BY-NC-SA 4.0 license and was authored, remixed, and/or curated by LibreTexts.

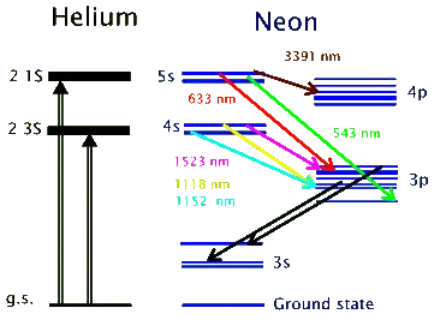
6.4.1: Gas Lasers

In these lasers the lasing medium is made-up of one or a mixture of gases or vapors. Gas lasers can be classified in terms of the type of transitions that lead to their operation: atomic or molecular. The most common of all gas lasers is the helium-neon (He-Ne) laser. The presence of two atomic species (helium and neon) in this gas laser might suggest that the medium is made of molecules, but these two species of atoms do not form a stable molecule. In fact, all inert atoms like helium, argon, krypton, etc. (those in the last column of the Periodic Table) hold tightly to their own electron clouds and seldom form a molecule or react with other atoms (hence the name: inert). In the He-Ne laser the transition that produces the output light is an atomic transition. Gas lasers that employ molecular gas or vapor for their lasing medium use molecular transitions for their lasing operation. Molecular transitions tend to be more complex than atomic ones. As a consequence the laser light produced by molecular lasers tends to have a wider and more varied collection of properties. Examples of some common molecular gas lasers are carbon monoxide (CO), carbon dioxide (CO2), excimer, and nitrogen (N2) lasers.

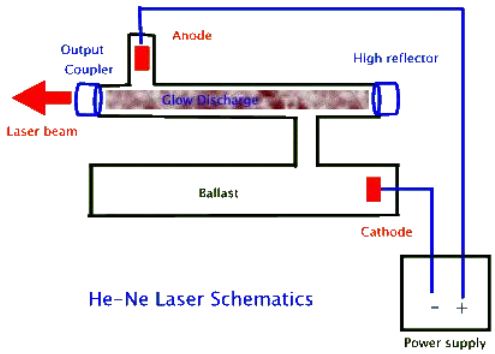
Helium Neon (He-Ne) Lasers

The He-Ne laser was the first continuous wave (cw) laser invented. A few months after Maiman announced his invention of the pulsed ruby laser, Ali Javan and his associates W. R. Bennet and D. R. Herriott announced their creation of a cw He-Ne laser. This gas laser is a four-level laser that use helium atoms to excite neon atoms. It is the atomic transitions in the neon that produces the laser light. The most commonly used neon transition in these lasers produces red light at 632.8 nm. But these lasers can also produce green and yellow light in the visible as well as UV and IR (Javan's first He-Ne operated in the IR at 1152.3 nm). By using highly reflective mirrors designed for one of these many possible lasing transitions, a given He-Ne's output is made to operate at a single wavelength.

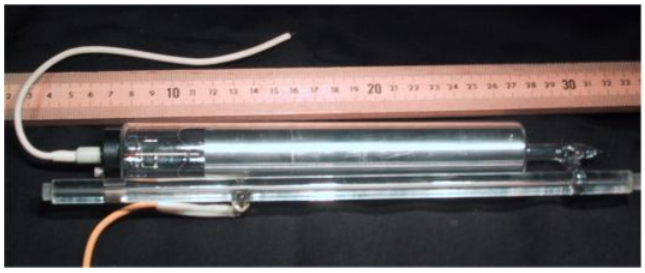
He-Ne lasers typically produce a few to tens of mW (milli-Watt, or 10^{-3} W) of power. They are not sources of high power laser light. Probably one of the most important features of these lasers is that they are highly stable, both in terms of their wavelength (mode stability) and intensity of their output light (low jitter in power level). For these reasons, He-Ne lasers are often used to stabilize other lasers. They are also used in applications, such as holography, where mode stability is important. Until the mid 1990's, He-Ne lasers were the dominant type of lasers produced for low power applications - from range finding to scanning to optical transmission, to laser pointers, etc. Recently, however, other types of lasers, most notably the semiconductor lasers, seem to have won the competition because of reduced costs.



The above energy level diagram shows the two excited states of helium atom, the 2 3S and 2 1S, that get populated as a result of the electromagnetic pumping in the discharge. Both of these states are metastable and do not allow de-excitations via radiative transitions. Instead, the helium atoms give off their energy to neon atoms through collisional excitation. In this way the 4s and 5s levels in neon get populated. These are the two upper lasing levels, each for a separate set of lasing transitions. Radiative decay from the 5s to the 4s levels are forbidden. So, the 4p and 3p levels serve as the lower lasing levels and rapidly decay into the metastable 3s level. In this way population inversion is easily achieved in the He-Ne. The 632.8 nm laser transition, for example, involves the 5s and 3p levels, as shown above.



In most He-Ne lasers the gas, a mixture of 5 parts helium to 1 part neon, is contained in a sealed glass tube with a narrow (2 to 3 mm diameter) bore that is connected to a larger size tube called a ballast, as shown above. Typically the laser's optical cavity mirrors, the high reflector and the output coupler, form the two sealing caps for the narrow bore tube. High voltage electrodes create a narrow electric discharge along the length of this tube, which then leads to the narrow beam of laser light. The function of the ballast is to maintain the desired gas mixture. Since some of the atoms may get imbedded in the glass and/or the electrodes as they accelerate within the discharge, in the absence of a ballast the tube would not last very long. To further prolong tube lifetime some of these lasers also use "getters", often metals such as titanium, that absorb impurities in the gas.



Above photograph shows a commercial He-Ne tube. The thicker cylinder closest to the meter-stick (shown for scale) is the ballast. The thinner tube houses the resonant cavity where the lasing occurs. Notice the two mirrors that seal the two ends of the bore. For mode stability reasons, these mirrors are concave; they serve as the output coupler and the high reflector.

A typical commercially available He-Ne produces about a few mW of 632.8 nm light with a beam width of a few millimeters at an overall efficiency of near 0.1%. This means that for every 1 Watt of input power from the power supply, 1 mW of laser light is produced. Still, because of their long operating lifetime of 20,000 hours or more and their relatively low manufacturing cost, He-Ne lasers are among the most popular gas lasers.

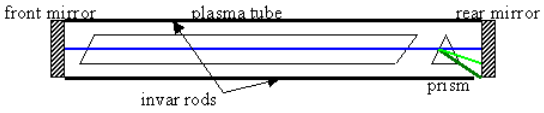
Argon-ion Lasers

Another commonly used gas laser is the argon-ion laser. In these lasers, as in the He-Ne the lasing transition type is atomic. But instead of a neutral atom, here the lasing is the result of the de-excitations of the ion. It takes more energy to ionize an atom than to excite it. By the same token, more energy can be obtained from the de-excitation of the ion. So, doubly (Ar++) and singly ionized (Ar+) argon atoms can radiate shorter wavelength light than could the neutral argon atom, Ar. Because of this, argon-ion lasers can produce uv light with a wavelength as short as 334 nm. In addition, these lasers can produce much more power than He-Ne lasers. Argon-ion lasers typically range in output power from one to as much as 20 W. At the higher power levels their output is multi-mode, i.e. contains several distinct wavelengths. Some of these wavelengths are:

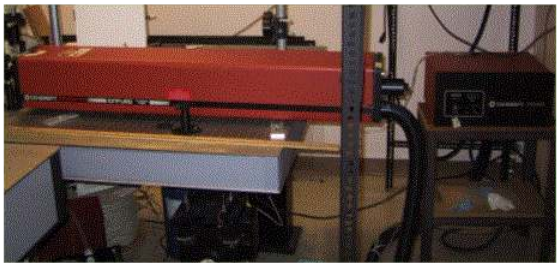
- 334 nm, UV
- 351 nm, UV
- 364 nm, UV
- 458 nm, violet
- 477 nm , violet
- 488 nm, (strong) blue
- 497 nm, blue-green
- 514 nm, (strongest) green

Because of these two reasons, high power and multicolor output, argon-ion is one of the most commonly used lasers in laser light shows, as well as in a variety of applications.

The make-up of a typical argon-ion laser is very similar to a He-Ne's, but with a few slight differences. First, these lasers are much larger in size. A typical Ar++ laser tube is about one meter long, as compared to just 20 cm for that of a He-Ne. Second, the optical cavity of these lasers is built external to the tube. This is partly because of the high power operation of the laser and partly because such external arrangement allows for the use of optional wavelength selection optics within the optical cavity. A prism or a diffraction grating located just before the high reflecting mirror selects only one of the lasing transitions for amplification within the cavity; other wavelengths are deflected out of the resonant cavity. In this way these ion lasers can operate in a so called single mode.



With this arrangement the two mirrors holders on opposite sides of the laser tube are typically attached together with an invar rod for thermal stabilization (Invar is a steel alloy that contains nickel). Its most valued property is that it expands and contracts very little when its temperature changes. As a result, when the laser's temperature changes as it heats up due to the large electric current within the electromagnetic pump discharge, the optical path length, and therefore the modal character of the laser output, remains relatively unchanged. Finally, because of their high power argon-ion lasers require active cooling. This is most commonly accomplished by circulating water, either directly from tap or from commercially produced chillers, in closed coils that surround the plasma (a gas of charged ions) tube and parts of the electric power supply. Some of the lower powered argon-ion lasers are just air cooled using a fan, which makes them less cumbersome to use.



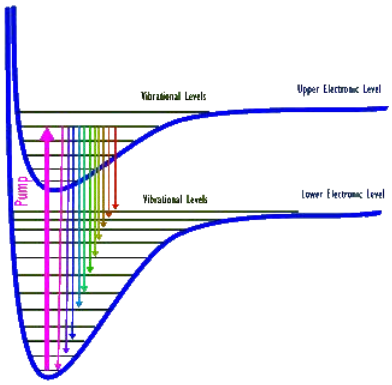


The above two photographs show a 5 W argon-ion laser. Notice the one-meter long laser tube, the large ballast, and the umbilical cord that connects to the laser power supply. This cord contains not only the power line that supplies the laser with the electric power to generate the plasma, but also the water lines that circulate water to cool the laser.

Another type of ion laser, the krypton laser, operates very much the same as the argon-ion laser. To take advantage of all the colors available in both argon and krypton lasers, manufacturers make argon-krypton ion lasers by using a suitable mixture of these two gases. The mixed gas lasers are very useful for entertainment applications because, in addition to many colors, they can also produce a "white" beam. (Why is the word "white" in quotations?)

Carbon-dioxide (CO_2) and Carbon-monoxide (CO) Lasers

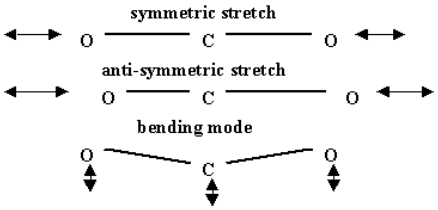
In both of these lasers the gaseous medium is made-up of molecules, which in addition to electronic energy levels of atoms also have both molecular vibrational and rotational energy levels. The vibrational energy levels are similar to finer spaced ladder rungs that span two rungs of the electronic energy levels. The rotational levels are still more finely spaced rungs that span the vibrational rungs! In these gas lasers the lasing transitions occur among the vibrational levels, typically belonging to different electronic levels.



Above diagram shows two electronic and several of their associated vibrational levels for a hypothetical molecule. (Electronic levels are shown as "bent rungs" because in the molecule atoms can change their separation distance and therefore their electronic energy. Also, note that rotational levels are not shown.) A thick arrow depicts a pump that excites the molecule from its lowest vibrational level belonging to the lower electronic level to the 5th highest vibrational level of the next upper electronic level. The excited molecule can then de-excite out of this upper level into many possible vibrational levels. Each one of these de-excitations produces a photon whose energy, and therefore its wavelength, corresponds to that specific de-excitation. As a result, when a collection of these molecules are all excited by this pump they generate a number (eleven, in this drawing) of different wavelength photons.

Specifically, CO_2 lasers can generate an output wavelength from about 9 micro-meters (mm, or microns) to about 11 microns (1 micron is one millionth of a meter, or 1000 nm.) These outputs generally contain many closely spaced wavelengths, if the laser is used for high power output. But for more wavelength specific applications the optical cavity of the laser is designed to amplify just one or a few of the vibrational radiative decay lines. The wavelength range for the CO laser is lower, from about 5 to 6 mm. Another feature of these gas lasers that make them one of the most versatile of all gas lasers is that they can be made to operate over a large range of power outputs, either in a pulsed or cw mode. The CO_2 laser, in particular, ranges in cw power from few Watts to kWs, making these lasers ideal for many industrial applications including welding and drilling.

Molecular vibrations for CO_2, a linear molecule, are shown in the figure below. Other combinations of these are possible but these three are fundamental. There are different varieties of CO_2 lasers that flow fresh gases through the resonant cavity area in order both to remove heat and to provide lots of gas to achieve high laser powers. For these lasers in the cw mode powers can reach as high as 100 kW. These intense laser beams are essentially tremendous invisible "heat" beams that can cut through thick pieces of metal and are used extensively in industrial applications.



We mention two interesting tidbits about these lasers. First, since glass in not very transparent to IR light, the mirrors are actually made of special crystalline materials that are transparent to the IR. Second, recall that IR light is invisible to our eyes and so special precautions are needed to protect people working around these lasers. It turns out that although these lasers can easily cut through metal, they cannot pass through a thin sheet of clear plexiglass, and so often these systems are housed in a plexiglass shell to block any stray reflected IR light.

Other types of gas lasers include the nitrogen laser (N2), excimers, copper-vapor, gold-vapor, and chemical lasers. Of these the excimer lasers and the chemical lasers are the most different from the ones we have already discussed above.

Excimer Lasers

Similar to CO_2, CO, and N_2 lasers, these gas lasers also use molecular transitions for their lasing operation. What makes them especially different is that the molecular gas used for these lasers has no ground state! Typically these molecules include an atom belonging to the inert gas family (argon, xenon, krypton) and one from the halide group (chlorine, fluorine, and bromine). The inert

gas atoms (also known as the rare gases) do not want to interact with any other atoms. On the other hand, the halide gases are highly reactive. Still, they cannot bond with the inert gases to form a molecule. But when sufficient energy is provided to these atoms they bind together in a short-lived excited state that soon (few nanoseconds) decays back into the original two separate atoms (i.e. the molecule dissociates). Because of this rapid molecular dissociation, these lasers obtain population inversion just by excitation alone! In fact, the word excimer is short for "excited dimer," although most excimer lasers do not use two identical atoms as a strict dimer would.

The excimer molecules are created from a mixture of inert gases along with one of the halides. Typically a few percent of Ar, Kr and Xe are mixed with a few percent of a halide to form excimer molecules: ArF, KrF , and XeF. The other 90% of the gas mix consists of other inert gases such as He and Ne which act simply as a buffer and do not take part in the reaction. A large electric pulse is often used for the excitation and formation of the excimer molecule. The rapid decay of the short-lived molecule then leads to a very short laser pulse lasting 10 - 100 ns (10-8 - 10-7 s). So, another unusual feature of the excimers is that they do not require an optical amplifier. They are very efficiently formed in the reaction with an efficiency of around 30% so that the gain is extremely high. A high reflector and a glass (really quartz - why?) window is sufficient for laser light production. This means that only about 4% of the light is reflected back into the cavity at the front window, but the gain is so high that only a single pass through the cavity is needed to produce lots of uv light. Typically about 1 Joule of energy is in a 10 ns pulse, so that the pulse power is 1J/10ns = 100 MW. If this power were steadily produced it would be equivalent to powers generated by large power plants. However, only about 1 - 100 pulses are produced per second, so that the average power produced is about 1 - 100 W.

Because of the highly reactive nature of the halide gas used in these lasers, excimers are not very easy to operate. The halides tend to be very corrosive and therefore add a great deal to the operational cost (as well as the danger!) of these lasers. But still these lasers are very much in use because their output wavelength is in the UV, from 350 nm down to as low as 193 nm; all with a good deal of power.

Chemical Lasers

In these lasers the energy of excitation comes from a chemical reaction that takes place in the medium itself. In this sense, then, chemical lasers are self-pumped. Even more interesting is the operation of one of the most common of these lasers, the hydrogen-fluoride laser that operates in the IR at 4.6 microns. The added intrigue is due to the chain reaction that takes place to excite the laser molecule, HF. A mixture of hydrogen (molecular) gas, H_2, and fluorine gas, F_2, is subjected to an electric discharge to start the chain reaction, which results in the production of a hydrogen-fluoride molecule in an excited vibrational level (excited state is denoted by a starred superscript: HF^*) and the dissociative production of H or F for the next reaction:

$$\mathrm{F} + \mathrm{H}_2 \rightarrow \mathrm{HF}^{\cdot} + \mathrm{H}$$

$$\mathrm{F}_2 + \mathrm{H} \rightarrow \mathrm{HF}^{\cdot} + \mathrm{F}$$

$$\mathrm{F} + \mathrm{H}_2 \rightarrow \mathrm{HF}^{\cdot} + \mathrm{H}$$

$$\mathrm{F}_2 + \mathrm{H} \rightarrow \mathrm{HF}^{\cdot} + \mathrm{F}$$

etc.

So, the medium in these lasers is used up as a fuel to generate their laser light. Therefore, practical limitations aside, the power of these lasers depends on the amount of the chemical (gas volume) that is used in the laser. Because of their conceivably limitless power output, these lasers have been studied mostly for their military applications. The most famous of these is the US Army's Mid-Infrared Advanced Chemical Laser, MIRACL, located at White Sands Missile Range, New Mexico. This is a formidable chemical laser that has been developed as part of the Department of Defense's efforts for its Strategic Defense Initiative (SDI).

MIRACL is the US's most powerful laser. It operates in a band from 3.6 to 4.2 microns producing megawatts of CW output for as long as 70 seconds. For its fuel it burns ethylene, C_2H_4, with nitrogen trifluoride, NF3. The resulting free fluorine atoms combine with deuterium gas that is injected to this burning fuel to form deuterium fluoride molecules (DF), which ultimately provide the laser light. In this laser the beam within the optical cavity is about 21 cm high and 3 cm wide, resulting in a 14 cm2 output beam. For testing purposes this laser is used with an aiming and focusing telescope system called the SEALITE Beam Director (SLBD) which was first developed by the Navy. The moving part of SLBD that is capable of fast rotations and high accelerations weighs about 18,000 pounds. Its telescope can focus the beam to any target that is located within a range of a minimum of 400 meters up to infinity.

Contributors

- Jay Newman and Seyffie Maleki (Union College)

6.4.1: Gas Lasers is shared under a CC BY-NC-SA 4.0 license and was authored, remixed, and/or curated by LibreTexts.

- **Gas Lasers** is licensed CC BY-NC-SA 4.0.

6.4.2: Laser Theory

Energy State Populations

For reasons that we cannot explain, it appears that all things in nature prefer to go to the lowest energy state available to them. This seems to be how nature behaves. Apples fall all the way to the ground, once they are let go by the tree branches they grew on. Of course unless they fall into a hole, in which case they go even lower than the ground level - to the bottom of the hole. To raise the energy of the fallen apple someone, or something, has to intervene. A child must pick it up off the ground, for example. Otherwise, the apple will remain at its lowest point. Similarly, atoms tend to prefer to always stay in their ground state, unless some intervening force causes them to reach an excited state. In the language used in the study of lasers, any process that feeds energy into a collection of atoms or molecules and causes them to vacate their ground state is referred to as an energy pump, or simply as a pump.

In most lamps electricity is used, by one mechanism or other, to pump atoms out of their ground-state into some excited state. We have already seen that incandescent bulbs produce light from Radiative transitions after excitation via collisions of the electrons in an electric current with the filament atoms. As we've also seen, other light sources, like the fluorescent lamps or neon tubes, use gas or vapor for their medium of excitation instead of a solid filament. In most lamps, the pumping mechanism is electricity. This is also the case for most lasers, but in some lasers optical pumping is the mechanism that is used to cause excitation. In optical pumping a light source generates photons with enough energy that they are able to get absorbed by the atoms in the lasing medium and cause them to go into an excited state.

Evidently, all excitations occur "instantaneously", but de-excitations can lag by a measurable time interval that depends on the properties of the excited state. That is to say, an atom in an excited state does not instantaneously de-excite. The time that it spends, on average, in that excited level is called the lifetime of that state. Lifetimes can vary in duration depending on the atom and on the energy level. Excited state lifetimes are typically a few nanoseconds (10-9 s, or a billionth of a second), but they could be as short as a picosecond (10-12 s, or a thousand times shorter still) or as long as a few milliseconds (10-3 s). The ground state, of course, has an infinitely long lifetime since an atom in its ground state can no longer decrease its energy. So, the most stable of states is the ground state. Long-lived states are referred to as meta-stable states.

In the case of Radiative emission, atoms happen to take two very distinctly different approaches: spontaneous emission, or stimulated emission. Spontaneous emission refers to the case when the excited atom de-excites, rather randomly whenever it "feels like it", and emits a photon. This photon has an energy equal to the difference between the two energy levels of the transition, but its direction of travel and its other properties, such as polarization are random. Stimulated emission was first theorized by Albert Einstein in 1917. For stimulated emission to occur a second, non-participating yet stimulating, photon must be present. The energy of this second photon must exactly match the allowed energy of the transition. Then the emitted photon will not only have the same energy as the stimulating one, but it will also travel in the same direction, and will be essentially identical to it.

So, independent of what type of medium is used in a laser, in the absence of a pump the atoms or molecules are almost all in their ground state. Let us imagine that we could count the number of atoms in our laser medium that are in each energy state and denote the ones which are in their ground state by Ngs , those in the first excite state by N1, those in the second excited state by N2 , and so on. Then in the absence of a pump we are mostly certain that N1= N2 = ... = 0, and Ngs = total number of all the atoms in the medium. Once the pump is turned on it will deplete the number of atoms that were originally in the ground state and increases the number of atoms in the excited states that it is pumping to. Because excited atoms de-excite quickly and return to their ground states by spontaneous emission, in almost all lasers even when the pump is feeding energy into the medium the number of atoms in their ground state remains many times more than atoms in any other energy state. That is to say, almost always we could safely state that:

$$N_{\text{ground state}} \text{ much bigger than } N_{\text{any other state}} .$$

To make a laser we need to not only excite the atoms in the laser medium, but somehow encourage them to undergo a decay through stimulated emission. In stimulated emission a passer-by photon which has an energy exactly equal to the transition energy stimulates the atom to emit a photon, identical to the passer-by photon, instantly. The problem with this is that the same passer-by photon could instead get absorbed by a de-excited atom. So, aside from pumping the atoms to excited states, we need to use clever procedures to insure that there are more excited atoms that could use the passer-by photon for stimulated emission than there are de-excited atoms which could absorb it; i.e. we need to generate a population inversion. Although Einstein predicted stimulation

emission in 1917, it was not found experimentally for over 10 years and took over another 30 years just to predict the possibility of a laser. This is basically because it was not considered possible to produce a population inversion because of the above inequality.

Lasing in Two-Level Systems

For the sake of our studies, let's first consider a laser medium whose atoms have only two energy states: a ground state and one excited state. In such an idealized atom the only possible transitions are excitation from the ground state to the excited state, and de-excitation from the excited state back into ground state. Could such an atom be used to make a laser?

There are several important conditions that our laser must satisfy. First of all, the light that it produces must be coherent. That is to say, it must emit photons that are in-phase with one another. Secondly, it should emit monochromaticlight, i.e. photons of the same frequency (or wavelength).Thirdly, it would be desirable if our laser's output were collimated, producing a sharply defined "pencil-like" beam of light (this is not crucial, but clearly a desirable condition). Lastly, it would also be desirable for our laser to be efficient, i.e. the higher the ratio of output energy - to - input energy, the better.

Let us begin by examining the requirements for our first condition for lasing, coherence. This condition is satisfied only when the lasing transition occurs through stimulated emission. As we have already seen, stimulated emission produces identical photons that are of equal energy and phase and travel in the same direction. But for stimulated emission to take place a "passer-by" photon whose energy is just equal to the de-excitation energy must approach the excited atom before it de-excites via spontaneous emission. Typically, a photon emitted by the spontaneous emission serves as the seed to trigger a collection of stimulated emissions. Still, if the lifetime of the excited state is too short, then there will not be enough excited atoms around to undergo stimulated emission. So, the first criteria that we need to satisfy is that the upper lasing state must have a relatively long lifetime, otherwise known as a meta-stablestate, with typical lifetimes in the milliseconds range. In addition to the requirement of a long lifetime, we need to ensure that the likelihood of absorption of the "passer-by" photons is minimized. This likelihood is directly related to the ratio of the atoms in their ground state versus those in the excited state. The smaller this ratio, the more likely that the "passer-by" photon will cause a stimulated emission rather than get absorbed. So, to satisfy this requirement, we need to produce a population inversion: create more atoms in the excited state than those in the ground state.

Achieving population inversion in a two-level atom is not very practical. Such a task would require a very strong pumping transition that would send any decaying atom back into its excited state. This would be similar to reversing the flow of water in a water fall. It can be done, but is very energy costly and inefficient. In a sense, the pumping transition would have to work against the lasing transition.

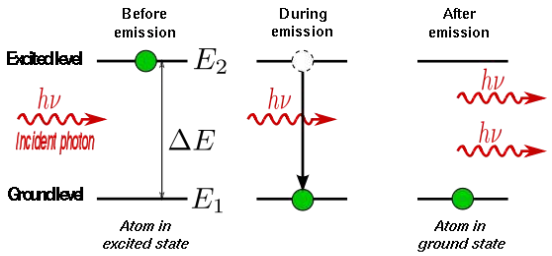
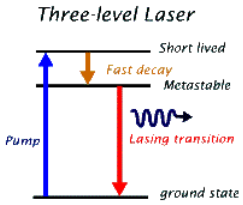


Figure 1: Stimulated emission in a two-level transition. (CC BY-SA 4.0; V1adis1av)

It is clear, from the above diagram, that in the two-level atom the pump is, in a way, the laser itself! Such a two-level laser would work only in jolts. That is to say, once the population inversion is achieved the laser would lase. But immediately it would end up with more atoms in the lower level. Such two-level lasers involve a more complicated process. We will see, in later material, examples of these in the context of excimer lasers, which are pulsed lasers. For a continuous laser action we need to consider other possibilities, such as a three-level atom.

Lasing in Three-Level Systems

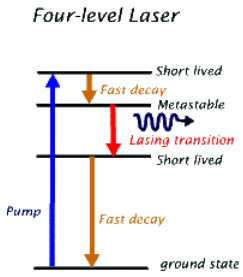
In fact, the first laser that was demonstrated to operate was a three-level laser, Maiman's ruby laser.



In the above diagram of a three level laser the pump causes an excitation from the ground state to the second excited state. This state is a rather short-lived state, so that the atom quickly decays into the first excited level. [Decays back to the ground state also occur, but these atoms can be pumped back to the second excited state again.] The first excited state is a long-lived (i.e. metastable) state which allows the atom to "wait" for the "passer-by" photon while building up a large population of atoms in this state. The lasing transition, in this laser, is due to the decay of the atom from this first excited metastable state to the ground state. If the number of atoms in the ground state exceeds the number of atoms that are pumped into the excited state, then there is a high likelihood that the "lasing photon" will be absorbed and we will not get sustained laser light. The fact that the lower lasing transition is the ground state makes it rather difficult to achieve efficient population inversion. In a ruby laser this task is accomplished by providing the ruby crystal with a very strong pulsating light source, called a flash lamp. The flash lamp produces a very strong pulse of light that is designed to excite the atoms from their ground state into any short-lived upper level.t In this way the ground state is depopulated and population inversion is achieved until a pulse of laser light is emitted. In the ruby laser the flash lamp light lasts for about 1/1000 of a second (1 ms) and can be repeated about every second. The duration of the laser pulse is shorter than this, typically 0.1 ms. In some pulsed lasers the pulse duration can be tailored using special methods to be much shorter than this, down to about 10 fs (where 1 fs = 10-15 s or one thousandth of a millionth of a millionth of a second). So, the output of a three-level laser is not continuous, but consists of pulses of laser light.

Lasing in Four-Level Systems

To achieve a continuous beam of laser light a four-level laser is required.



Here, the lower laser level is not the ground state. As a result, even a pump that may not be very efficient could produce population inversion, so long as the upper level of the laser transition is longer lived than the lower level. Of course, all attempts are made to design a pump that maximizes the number of excited atoms. A typical four-level laser is the helium-neon (He-Ne) gas laser. In these lasers electric pumping excites helium atoms to an excited state whose energy is roughly the same as the upper short-lived state in the neon atom. The sole purpose of the helium atoms is to exchange energy with neon atoms via collisional excitation. As it turns out, this is a very efficient way of getting neon atoms to lase.

Laser components

All lasers have three primary components:

- Medium
- Pump
- Resonant Cavity

The laser medium can be gaseous, liquid, or a solid. These could include atoms, molecules, or collections of atoms that would be involved in a laser transition. Typically, a laser is distinguished by its medium, even though two lasers using different media may have more in common than two which have similar media.

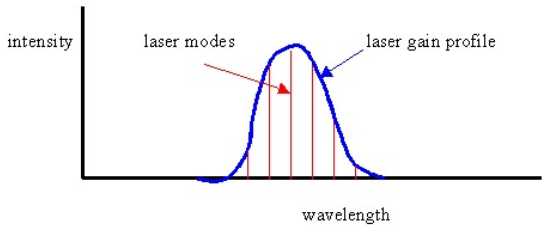
There are three different laser pumps: electromagnetic, optical, and chemical. Most lasers are pumped electro-magnetically, meaning via collisions with either electrons or ions. Dye lasers and many solid state lasers are pumped optically; however, solid state lasers are typically pumped with a broad band (range of wavelengths) flash-lamp type light source, or with a narrow band semiconductor laser. Chemically pumped lasers, using chemical reactions as an energy source, are not very efficient. So far, these lasers have been made to work not so much for their usefulness as for their curious operation.

Up to now in our discussion of laser theory we have not really seen how the beam is generated. We know that photons emitted by stimulated emission travel coherently in the same direction, but what is it that defines the beam direction and what allows the intensity of the laser light to get large? The answer to these two questions is coupled together in the resonant cavity. Laser resonant cavities usually have two flat or concave mirrors, one on either end, that reflect lasing photons back and forth so that stimulated emission continues to build up more and more laser light. The "back" mirror is made as close to 100% reflective as possible, while the "front" mirror typically is made only 95 - 99% reflective so that the rest of the light is transmitted by this mirror and leaks out to make up the actual laser beam outside the laser device.

The resonant cavity thus accounts for the directionality of the beam since only those photons that bounce back and forth between the mirrors lead to amplification of the stimulated emission. Once the beam escapes through the front mirror it continues as a well-directed laser beam. However, as the beam exits the laser it undergoes diffraction and does have some degree of spreading. Typically this beam divergence is as small as 0.05o but even this small amount will be apparent if the beam travels long distances.

Even more, the resonant cavity also accounts for the amplification of the light since the path through the laser medium is elongated by repeated passes back and forth. Typically this amplification grows exponentially, similar to the way compound interest works in a bank. The more money in your bank account, with compound interest, the faster you earn more interest dollars. Similarly, the more photons there are to produce stimulated emission, the larger the rate at which new coherent photons are produced. The term used for laser light is gain, or the number of additional photons produced per unit path length.

The last question to address in this section is: why is the resonant cavity called by that name? What does resonance have to do with having mirrors on either end of a region containing the laser medium? Recall that when we discussed resonance on a string, we spoke about the wave traveling one way along the string (say to the right) interfering with the wave reflected at the end traveling back to the left. At a resonant frequency, there are points at which the two waves exactly add or cancel all the time, leading to a standing wave. At other frequencies the waves will randomly add or cancel and the wave will not have a large amplitude. The case of a light wave traveling back and forth in the resonant cavity is exactly analogous in that only at certain resonant frequencies will the light wave be amplified. The required condition is easy to see. The mirror separation distance, L, must be equal to a multiple of half a wavelength of light, just as we saw in the case of a string. In symbols, we have that L = nl/2, where l is the wavelength of the light and n is some integer. In the case of light, because of the small wavelength n is a very large number, implying that there are a huge number of resonant frequencies. On the other hand, only those resonant frequencies that are amplified by the laser medium will have large amplitudes and so usually there are only a few so-called laser modes or laser resonant frequencies present in the light from a laser, as shown in the figure.



Questions on Laser Components

- What are the three primary components of a laser?
- What different types of laser medium are used?
- What is a pump? Describe the different types of pumps.
- What is a resonant cavity?
- Describe how the resonant cavity produces a collimated laser beam.
- What is the beam divergence of a laser caused by? What is a typical value for it?
- What does the term gain mean? Is it related to pain?
- Describe why a typical laser has only a few modes, while the resonant cavity produces a huge number of them.

Contributors

- Jay Newman and Seyffie Maleki (Union College)

6.4.2: Laser Theory is shared under a CC BY-NC-SA 4.0 license and was authored, remixed, and/or curated by LibreTexts.

- **Laser Theory** is licensed CC BY-NC-SA 4.0.

6.4.3: Overview of Lasers

LASER is an acronym for Light Amplification by Stimulated Emission of Radiation. Laser is a type of light source which has the unique characteristics of directionality, brightness, and monochromaticity. The goal of this module is to explain how a laser operates (stimulated or spontaneous emission), describe important components, and give some examples of types of lasers and their applications.

Introduction

The word LASER is an acronym for Light Amplification by Stimulated Emission of Radiation. In 1916, Albert Einstein discovered the physical principle responsible for this amplification, and the foundation principle is called stimulated emission. It was widely accepted at that time that laser would represent a big leap in science and technology, even before Theodore H. Maiman built the first one in 1960. The 1951 Nobel Prize in physics was shared by Charles H. Townes, Nokolay Basov, and Aleksandr Prokhorov, in citation, “For Fundamental work in the field of quantum electronics, which has led to the construction of oscillator and amplifiers based on the maser-laser principle”.

The early lasers developed in the 1950s by Charles H. Townes and Arthur Shawlow were gas and solid-state lasers for use in spectroscopy. The principles of lasers were adapted from masers. MASER is an acronym that stands for Microwave Amplification by Stimulated Emission of Radiation. It uses the idea of stimulated emission and population inversion to produce a coherent amplified radiation of light in the microwave region. Stimulated emission is when an electron in an excited state falls back to ground state after absorbing energy from an incident photon. Amplified radiation or light is produced with the same direction and energy as the incident light. Population inversion is when you have a greater population of electrons in the excited state than in ground state. Population inversion is achieved through various pumping mechanisms. The laser uses these same ideas except that the electromagnetic wave created is in the visible light region. When emission begins the light oscillates within the resonant cavity and gains magnitude. Once enough light has been acquired, the laser beam is produced. This allows lasers to be used as a powerful light source. Three unique characteristics of a laser are its properties of monochromaticity, directionality, and brightness.

The monochromaticity of lasers is due to the fact that lasers are highly selective in the wavelength of light produced, which in itself is due to the resonant frequency inside the active material. Resonant frequency means that the light is oscillating in a single mode creating a monochromatic beam of light. The property of directionality depends on the angle of which the light propagates out of the source. Since lasers have large spatial and temporal coherence directionality is maximized. Temporal coherence is when there are small fluctuations in the phase. Spatial coherence has small changes in the amplitude of the emitted light. Like monochromaticity, directionality is dependent on the resonant cavity of the active material. The property of brightness is a result of the directionality and the coherence of the light. Due to these properties, lasers today are used in simple laser pointers, cutting devices, the development of military technologies, spectroscopy, and medical treatments. Their direct application to spectroscopy has allowed scientists to measure lifetimes of excited state molecules, structural analysis, probing far regions of the atmosphere, photochemistry and their use as ionization sources.

History

One of the most important characteristics of light is that it has wave-like properties and that it is an electromagnetic wave. Experiments on the blackbody radiation demonstrated a comprehensive idea of emission and absorption of electromagnetic waves. In 1900, Max Plank developed the theory that electromagnetic waves can only exist in distinct quantities of energy, which are directly proportional to a given frequency (ν). In 1905, Albert Einstein proposed the dual nature of light, having both wave-like and particle-like properties. He used the photoelectric effect to show that light acts as a particle, with energy inversely proportional to the wavelength of light. This is important, because the number of particles is directly related to how intense a light beam will be. In 1915, Einstein introduced the idea of stimulated emission- a key concept to lasers.

In 1957, Townes and Shawlow proposed the concept of lasers in the infrared and optical region by adapting the concept of masers to produce monochromatic and coherent radiation. In 1953, Townes was the first to build a maser with an ammonia gas source. Masers use stimulated emission to generate microwaves. Townes and other scientists wanted to develop the optical maser to generate light. Optical masers would soon adopt the name LASER: Light Amplification by Stimulated Emission of Radiation. An optical maser would need more energy than what can be provided by microwave frequencies and a resonant cavity of the order of 1μm or less. Townes and Shawlow proposed the use of a Fabry-Pérot interferometer equipped with parallel mirrors, where Interference of radiation which is traveling back and forth between parallel mirrors in the cavity allowed for selection of certain wavelengths. Townes built an optical maser with potassium gas. That failed because the mirrors degraded over time. In 1957,

Gordon Gould improved upon Townes' and Shawlow's laser concept. It was Gould who renamed the optical maser to laser. In April 1959, Gould filed a patent for the laser and later in March 1960, Townes and Shawlow had also made a request for a patent. Since Gould's notebook was officially dated the idea was his first, but he did not receive the patent until 1977.

Components

A laser consists of three main components: a lasing medium, a resonant or optical cavity, and an output coupler. The lasing medium consists of a group of atoms, molecules , or ions in solid, liquid or gaseous form, which acts as an amplifier for light waves. For amplification, the medium has to achieve population inversion, which means in a state in which the number of atoms in the upper energy level is greater than the number of atoms in the lower energy level. The output coupler serves as energy source which provides for obtaining such a state of population inversion between a pair of energy levels of the atomic system. When the active medium is placed inside an optical resonator, the system acts as an oscillator.

Figure 1. Diagram of a typical laser, showing the three major parts.

Lasing Medium

The lasing medium is the component used to achieve lasing, such as chromium in the aluminum oxide crystal-found in a ruby laser. Helium and neon gas are two materials most commonly used in gas lasers. These are only a few examples of lasing mediums or materials that have been used in the past and present states of the laser. For further information about different types of lasing mediums please refer to the section where *Types of Lasers* is discussed.

Optical Cavity and Output Coupler

Rays of light moving along an optical path tend to diverge over time, because the energy of radiation has very high frequency. Therefore an optical cavity is needed to refocus the light. **Figure 1**, represents the basics of an optical cavity where the light inside moves back and forth between two mirrors. These redirect and focus the light each time it hits the surface of the mirrors. There are two types of cavities: stable cavities and unstable cavities. A stable cavity is when the ray of light does not diverge far from the optical axis. An unstable cavity is when the ray of light bounces off and away from a mirrors surface. The importance of the cavities is that it allows for the laser to have properties of directionality, monochromaticity and brightness.

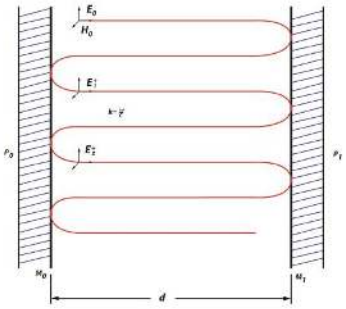


Figure 2. an optical cavity where the light inside moves back and forth between two mirrors

Light oscillating between the first mirror (M_o) and the second mirror (M_1) separated by distance, d, will have a round-trip phase shift (RTPS) of $2\theta=2kd=q2\pi-\phi$. In **Figure 1**, a round-trip can be described as the beam traveling from M_o to M_1back to M_o. Resonance occurs in the cavity because the light propagating between the two mirrors is uniform. The ABCD law describes that an optical cavity has a field distribution, because it reproduces itself as it is making these round-trips between the two parallel mirrors. The ABCD law was first applied to a Gaussian beam with a beam parameter, q, which is described as

$$q_2 = \frac{(Aq_1 + B)}{(Cq_1 + D)}$$

This law states that the beam, which is oscillating through an optical system, will experience some changing as it moves in the cavity. Fields that are created in an optical cavity have analogous shape and phase as they make each trip back and forth. However, the one thing that changes is the size of the field because the electromagnetic wave is unrestricted, unlike a wave in a short-circuited coaxial cable used to build a resonator or a microwave cavity mode. Since there is a field distribution of $E_o$at the surface of M_o, it can be said that there is a field distribution at the surface of M_1. Since there will be a change in size of the field this means that the electromagnetic wave will have change in amplitude by $\rho_0*\rho_1$ and a phase factor of $e^{-}jk2d$, creating additional fields.

This is an example of a phasorial addition of all fields between M_o and $M_{1,}$ creating a total field E_T (**Figure 2**). Phasorial addition is described by RTPS, where each additional E_n will have a delay of angle ϕ which is related to kd.

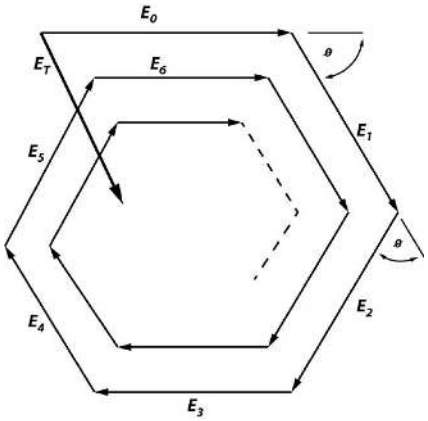


Figure 3. Totle field E_T

E_T will always be greater than $E_o$only if ρ_0 and $\rho_1$are not greater than 1 and ϕ=0. In this case, when ϕ=0 resonance is enhanced because all factors such as E_T travelling between M_o and M_1, the intensity of the electromagnetic waves, number of photons traveling between $M_o$and $M_{1,}$ and the amount of energy that is stored are maximized. The resonant wavelength can also be determined by using the relationship between RTPS, and because

$$k = \frac{\omega n}{c} = \frac{2\pi}{\lambda}$$

Using $2\theta = 2kd = q2\pi$

$$\frac{2\pi 2d}{\lambda} = q2\pi$$

$$d = \frac{q\lambda}{2}$$

Where the wavelength of interest is given by $\lambda = \lambda_0/n$, where n is the index of refraction and λ_0 is the free-space wavelength .

Since we are dealing with light as a wave, the light in the resonant cavity can be described in terms of frequency, ν. Where

$$k2d = \omega\frac{2nd}{c} = 2\pi\nu\frac{2nd}{c} = q(2\pi)$$

$$\nu = q\frac{c}{2nd}$$

A Fabry-Pérot interferometer is a prime example of an optical cavity used in a laser. The Fabry-Pérot is equipped with two parallel mirrors, one that is completely reflective and the other that is partially reflective. As light is accumulating in the cavity after taking several round trips between the two mirrors, some light is transmitted through the partially reflective mirror and a laser beam is produced. The beam can be in pulsed mode or continuous-wave (CW) mode. To increase the performance of the resonant cavity, the length of the cavity (d) must be considered as a way to avoid a decrease in the laser beam intensity due to any diffraction losses. The size of the aperture of the cavity is also important because it determines the strength or the intensity of the laser beam. In fact, determining the best length of a resonant cavity will enhance the coupling conditions of the output coupler by producing a frequency that is stable, which ultimately generates a laser beam that is coherent and has high power.

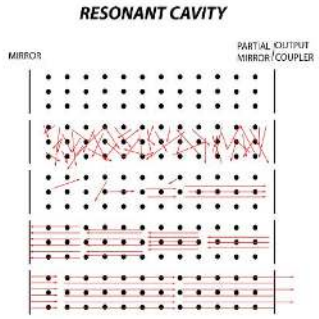


Figure 4. The first stage shows that all molecules present are in the ground state since there is no excitation energy present in the cavity. In the second stage, molecules become excited causing spontaneous emission of photons. In the third stage, photons collide with excited molecules causing an amplification of the light. This results in stimulated emission where the photon that is released has the same energy and direction of the photon that created it. Last is the fourth stage, where stimulated emission causes amplification of the light, and those photons that are traveling parallel to the cavities axis will hit one of the parallel mirrors and will be reflected back along the same axis. As the light is building up from the back and forth movement from one mirror to another, some of the light will pass through the partial mirror or the output coupler as a beam of rays. The remaining light in the cavity will continue producing more photons as long as there is a population inversion.

There are essentially six stages in the lasing process. First is the ground state where there is no excitation of the lasing medium. Second is pumping, which is applied to the medium where spontaneous emission occurs. Then the third stage is when emitted photons collide with an excited molecule where stimulated emission occurs. In the fourth stage the photons are produced in multiples, however those moving parallel in the cavity will hit a mirror and then hit the second mirror. During the fifth stage this process continues until there is an accumulation of light that is coherent and of a specific frequency. Finally, the sixth stage is when the light or laser beam exits the partially reflective mirror which is also known as the output coupler. An output coupler is the last important component of a laser because it must be efficient to produce an output of light with maximum intensity. If the output coupler is too transparent than there is much more loss of electromagnetic waves and this will decrease lasing significantly because population inversion will no longer be maintained. If the output coupler or partially reflective mirror is too reflective, then all the accumulated light that is built up in the resonant cavity will be trapped in the cavity. The beam will not pass through the output coupler, producing little to no light making the laser ineffective.

Emission

Lasers create a high energy beam of light by stimulated emission or spontaneous emission. Within in a molecule there are discrete energy levels. A simple molecular description has a low energy ground state (E_1) and a high energy excited state (E_2). When an electromagnetic wave, referred to as the incident light, irradiates a molecule there are two processes that can occur: absorption and stimulated emission.

Absorption occurs when the energy of the incident light matches the energy difference between the ground and excited state, causing the population in the ground state to be promoted to the excited state. The rate of absorption is given by the equation:

$$\frac{dN_1}{dt} = -W_{12}N_1$$

Where N_1 is the population in E_1, and W_{12} is the probability of this transition. The probability of the transition can also be related to the photon flux (intensity of incident light):

$$W_{12} = \sigma_{12}F$$

Where F is the photon flux and σ_{12} is the cross section of the transition with units of area. When absorption occurs photons are removed from the incident light and the intensity of the light is decreased.

Stimulated emission is the reverse of absorption. Stimulated emission has two main requirements: there must be population in the excited state and the energy of the incident light must match the difference between the excited and ground state. When these two requirements are met, population from the excited state will move to the ground energy level. During this process a photon is emitted with the same energy and direction as the incident light. Unlike absorption, stimulated emission adds to the intensity of the incident light. The rate for stimulated emission is similar to the rate of absorption, except that it uses the population of the higher energy level:

$$W_{21} = \sigma_{21}F$$

Like absorption the probability of the transition is related to the photon flux of the incident light through the equation:

$$\frac{dN_2}{dt} = -W_{21}N_2$$

When absorption and stimulated emission occur simultaneously in a system the photon flux of the incident light can increase or decrease. The change in the photon flux is a combination of the rate equations for absorption and stimulated emission. This is given by the equation:

$$dF = \sigma F(N_2 - N_1)d\tau$$

Spontaneous emission has the same characteristics as stimulated emission except that no incident light is required to cause the transition from the excited to ground state. Population in the excited state is unstable and will decay to the ground state through several processes. Most decays involve non-radiative vibrational relaxation, but some molecules will decay while emitting a photon matching the energy of the energy difference between the two states. The rate of spontaneous emission is given by:

$$\frac{dN_2}{dt} = -AN_2$$

Where A is the spontaneous emission probability which depends on the transition involved. The coefficient A is an Einstein coefficient obtained from the spontaneous emission lifetime. Since spontaneous emission is not competing with absorption, the photon flux is based solely on the rate of spontaneous emission.

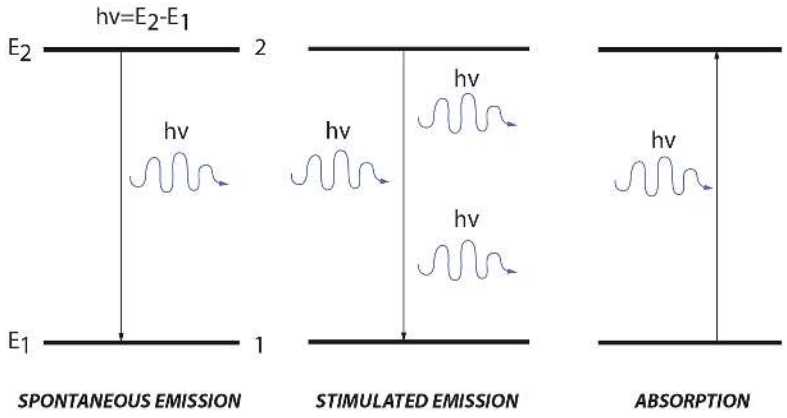


Figure 5. Diagram of spontaneous emission, stimulated emission and absorption in a two energy level system

The population ratio of a molecule or atom is found using the Boltzmann distribution and the energy of the ground state (E_1) and the excited state (E_2):

$$\frac{N_2}{N_1} = e^{\frac{-(E_2 - E_1)}{kT}}$$

Under normal conditions, the majority, if not all, of the population is in the lower energy level (E_1). This is because the energy of the excited is greater than the ground state. Normal thermal energy available (kT) is not enough to overcome the difference, and the ratio of population favors the ground state. For example, if the difference in energy between two states absorbes light at 500nm, the ratio of N_1 to N_2 is 5.1×10^{41}:1. The photon flux of the incident light is directly proportional to the difference in populations. Since the ground state has more populations, the photon flux decreases: there is more absorption occurring than stimulated emission. In order to increase the photon flux there must be more population in the excited state than in the ground state, generally known as a population inversion.

In a two level energy system it is impossible to create the population inversion needed for a laser. Instead three or four level energy systems are generally used (**Figure 5**).

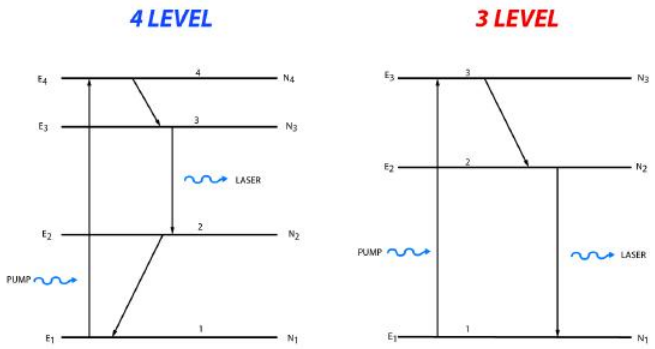


Figure 6. Three and four level energy system

Three level processes involve pumping of population from the lowest energy level to the highest, third energy state. The population can then decay down to the second energy level or back down to the first energy level. The population that makes it to the second energy level is available for stimulated emission. Light matching the energy difference between the second and first energy level will cause a stimulated emission. Four level systems follow roughly the same process except that population is moved from the lowest state to the highest fourth level. Then it decays to the third level and lasing happens when the incident light matches the energy between the third and second level. After lasing there is decay to the first level.

Pumping Process

Pumping is the movement of population from the ground state to a higher excited state. The general rate at which this is done is given by:

$$(\frac{dN_g}{dt})_p = W_p N_g$$

Where N_g is the population in the ground level and W_p is the pump rate. Pumping can be done optically, electronically, chemically (see chemical laser), using gases at high flow rates, and nuclear fission. Only optical and electrical pumping will be discussed in detail.

Optical Pumping

Optical pumping uses light to create the necessary population inversion for a laser. Usually high pressure xenon or krypton lamps are used to excite solid or liquid laser systems. The active material in the laser absorbs the light from the pump lamp, promoting the population from the ground state to the higher energy state. The material used in the laser can be continuously exposed to the pumping light which creates a continuous wave laser (CW). A pulsed laser can be created by using flashes of pumping light.

In optical pumping there are three types of efficiency: transfer, lamp radiative, and pump quantum efficiency. Transfer efficiency is the ratio of the energy created by the lamp and the power of the light emitted by the laser. The lamp radiative efficiency is the measure of how much electrical power is converted into light in the optical lamp. Pump quantum efficiency accounts for the ratio of population that decays to the correct energy level and population that decays either back to the ground state or another incorrect energy level. For example, the overall pumping rate of the first ruby laser was around 1.1%.

The average pump rate for optical pumping depends on the total efficiency of the pump (η_p), volume of the laser material (V), ground state population (N_g), power input (P), and frequency of the lasing transition (ν_0):

$$\langle W_p \rangle = \eta_p (P/(V N_g \hbar \nu_0))$$

Electrical Pumping

Electrical pumping is a much more complicated process than optical pumping. Usually used for gas and semiconducting lasers, electrical pumping uses electrical current to excite and promote the ground state population. In a simple gas laser that contains only

one species (A), current passes through the gas medium and creates electrons that collide with the gas molecules to produce excited state molecules (A^*):

$$A + e \longrightarrow A^* + e$$

During electron impact either an ion or an excited state can be created. The ability to make the excited state depends mostly on the material used in the laser and not the electrical pumping source making it difficult to describe the efficiency of the pumping. Total efficiencies have been calculated and tabulated for most active materials used in electrical pumping. Where eficiencies range from a < 0.1% N_2 gas laser to 70% for some CO_2 gas lasers.

Like the pumping rate of optical pumps, the rate of electrical pumping is found using the overall efficiency of the pump, power applied, and population of the ground state. However instead of using the frequency of the ground to upper state transition, electrical pumping uses the energy of the upper state ($\hbar\omega_p$) and the volume of the electron discharge (V):

$$\langle W_p \rangle = \eta_p (P/(V N_g \hbar \omega_p))$$

Pulsed operation

Q-Switching

The technique of Q switching allows the generation of laser pulses of short duration from a few nanoseconds to a few tens of nanoseconds and high peak power from a few megawatts to a few tens of megawatts.

Suggest we put a shutter into the laser cavity. If the shutter is closed, laser action cannot occur and the population inversion can be very high. If the shutter is opened suddenly, the stored energy will be released in a short and intense light pulse. This technique is known as Q-switching. Q here denotes the ratio of the energy stored to the energy dissipated in the cavity. This technique is used in many types of solid-stat lasers and CO_2 lasers to get a high-power pulsed output.

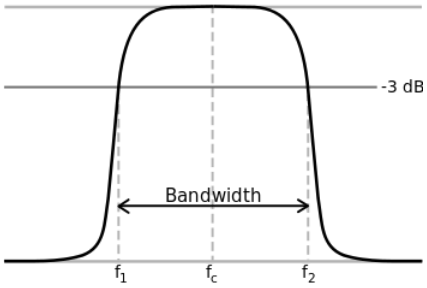


Figure 7. The bandwidth, Δf , or f1 to f2, of a damped oscillator is shown on a graph of energy versus frequency. The Q factor of the damped oscillator, or filter, is $f_c/\Delta f$. The higher the Q, the narrower and 'sharper' the peak is.

To produce high inversion required for Q-switching, four requirements must be satisfied.

1. The lifetime of the upper level must be longer than cavity buildup time.
2. The pumping flux duration must be longer than the cavity build up time.
3. The initial cavity losses must be high enough during the pumping duration to prevent oscillation occurring.
4. The cavity losses must be reduced instantaneously.

Mode-Locking

The technique of mode locking allows the generation of laser pulses of ultrashort duration from less than a picosecond to femtoseconds and very high peak, a few gigawatts.

Mode-locking is achieved by inducing the different longitudinal modes of a laser to a locked mode. When combining the electromagnetic waves modes with different frequencies and random phases, they produce a random and average output. When the modes are added in phase, they combine to produce a total amplitude and intensity output with a repeated pulse.

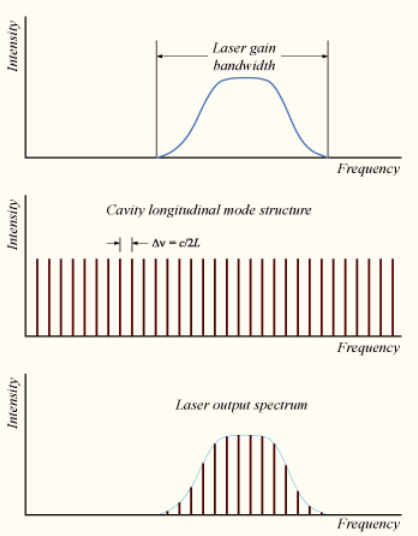


FIgure 8:Laser mode structure

Types of Lasers

There are many different types of lasers with a wide range applications, and below is a brief description of some of the main types.

Solid State Lasers

A solid-state laser is one that uses a solid active medium generally in a rod shape. Inside the active material is a dopant that acts as the light emitting source. Optical pumping is used to create population inversion of the active material. Solid-state lasers generally use stimulated emission as the mechanism for creating the high energy beam.

Ruby Laser

The ruby laser was the first operating laser and was built in 1960. It has a three-level (**Figure 6**) energy system that uses aluminum oxide with some of the aluminum atom replaced with chromium as its active material. The chromium in the aluminum oxide crystal is the active part of the laser. Electrons in the ground state of chromium absorb the incident light and become promoted to higher energy states. The short lived excited state relaxes down to a metastable state with a longer lifetime. Laser emission happens when there is relaxation from the metastable state back to the ground state.

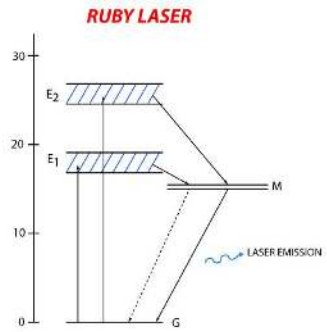


Figure 9. Schematic of Ruby laser

A xenon flash lamp emitting light at wavelengths of 6600Å and 4000Å (matching the energy needed to excite the chromium atoms). In order to create resonance of the incident light in the active material silver platting was put at both ends of the ruby rod. One end was completely covered while the other end was partially covered so lasing light could exit the system.

Nd: YAG Laser

Nd: YAG laser are the most popular type of solid state laser. The laser medium is a crystal of $Y_3Al_5O_{12}$ which are commonly called YAG, an acronym for yttrium aluminum garnet. A simplified energy-level scheme for Nd:YAG is shown in Fig. 9. The λ=1.06 μm laser transition is the strongest of the $4F_{3/2} \rightarrow 4I_{11/2}$ transitions.

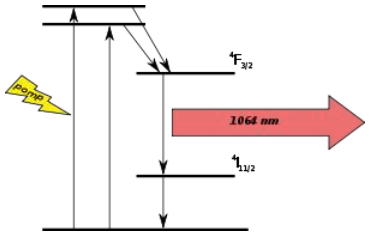


Figure 10. Simplified energy level diagram of the$^4F_{3/2}$---$4I_{11/2}$ laser transition in Nd:YAG showing the four- level nature of the system

The major application of the Nd laser is in various form of material processing: drilling, spot welding, and laser marking. Because they can be focused to a very small spot, the laser are also used in resistor trimming and in circuit mask , memory repair and also in cutting out specialized circuits. Medical applications include many types of surgeries. Many medical applications take advantage of low-loss optical fiber delivery systems that can be inserted into the body to wherever is needed. Nd lasers are also used in military applications such as range finding and target designation. High power pilsed versions are also used for X-ray spectral regions. In addition, Nd lasers are used in scientific lab as good sources for pumping dye laser and other types of lasers.

Semiconductor Laser

The semiconductor laser is another type of solid state laser that uses a semiconducting material like germanium or silicon. When the temperature of the semiconducting material is increased, electrons move from the valence band to the conducting band creating holes in the valence band (**Figure 7**). In between the conducting band and valence band is a region where there are no energy levels, called the band gap. Applying a voltage to the semiconductor causes electrons to move to the conduction band creating a population inversion. Irradiating a semiconductor with incident light matching the energy of the forbidden area causes a large transition from the conduction band to the valence band, increasing and amplifying the incident light.

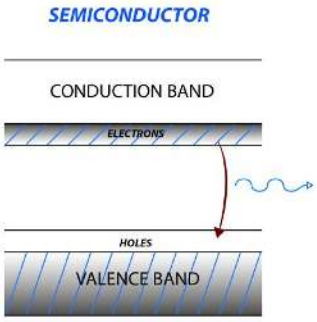


Figure 11. Schematic of semicondecor laser

Gas Lasers

A gas laser contains active material composed of a mixture of gases with similar energy states inside a small gas chamber. Electrical pumping is used to create the population inversion where one gas is excited through collisions with electrons and in turn excites the other gas through collisions.

Helium-Neon Laser

The helium-neon laser was the first gas laser. It consists of a long narrow tube that contains He and Ne gas. Mirrors are placed at both ends of the gas tube to form the resonant cavity with one of the mirrors partially reflecting the incident light. Stimulated emission of the gas mixture is carried out by first exciting the He gas to a higher energy state through electron collision with electrons from the electronic pumping source (electrical pumping). Then the excited He atoms collide with the Ne atoms transferring their energy and exciting them to a higher energy level. The Ne atoms in the higher energy level will then relax to a lower metastable energy state. Lasing occurs when there is relaxation from the metastable state to a lower energy state causing spontaneous emission. The Ne gas then returns to the ground state when it collides with the outer walls of the gas tube (**Figure 8**).

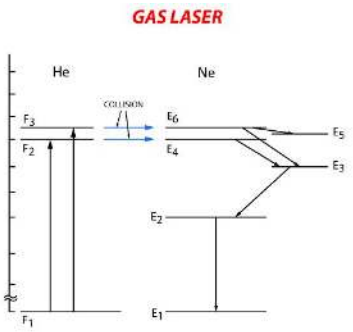


Figure 12. Schematic of gas laser

Carbon Dioxide Laser

The carbon dioxide laser is a gas laser that uses the energy difference between rotational-vibrational energy levels. Within the vibrational levels of CO_2 there are rotational sub-energy levels. A mixture of N_2 and CO_2 gas are placed inside a chamber. The N_2 atoms are excited through an electrical pumping mechanism. The excited atoms then collide with the CO_2 atoms transfer energy. This transfer of energy causes the CO_2 to go into a higher vibrational level. The excited CO_2 molecules then go through spontaneous emission when they are relaxed to lower rotational-vibrational levels increasing the signal of the incident light (**Figure 9**). Carbon dioxide lasers are extremely efficient, around 70%, and powerful compared to other gas lasers making them useful for welding and cutting.

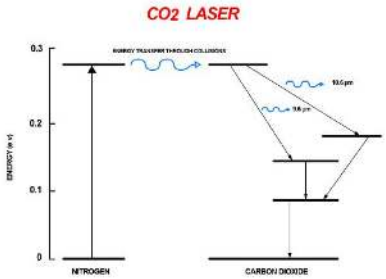


Figure 13. Schematic of carbondioxide laser

Liquid Lasers

Liquid lasers consist of a liquid active material usually composed of an organic dye compound. The most common type of liquid laser uses rhodamine 6G (**Figure 10**) dye mixed with alcohol and is excited by different types of lasers, such as an argon-ion laser or a nitrogen laser. Organic dyes are large compounds that have absorption bands in the UV or visible region with a strong intense fluorescence spectrum. The free π electrons of the dye are excited using an optical pumping source and the transition from the S_1 to the S_0 state creates the lasing light (see Jablonski diagrams). Liquids are generally used because they can easily be tuned to emit a certain wavelength by changing the resonant frequency within the cavity. Wavelengths from the visible to the infrared can be covered. There are many benefits of liquid lasers, some include that they can be cooled in a relative amount of time, they cannot be damaged unlike a solid-laser, and their production is cost-effective. The efficiency of liquid lasers is low because the lifetime of the excited state is relatively short; there are many non-radiative decay processes, and the material degrades over time. Liquid lasers tend to be used only as a pulse laser when tunability is required. Liquid lasers can be used for high-resolution spectroscopy since they are easily tuned over a wide range of wavelengths. They can also be used because they have concentrations which are manageable when dissolved in solids or other liquids.

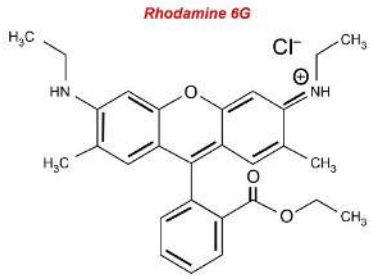


Figure 14. Rhodamine 6G molecule

Chemical Lasers

Chemical lasers are different from other lasers because the population inversion is the direct product of a chemical reaction when energy is released as a result of an exothermic reaction. Usually reactions involve gases where the energy created is used to make vibrationally excited molecules. Light used for lasing is then created from vibrational-rotational relaxation like in the CO_2 gas laser. An example of a chemical laser is the HF gas laser. Inside the gas chamber fluorine and hydrogen react to form an excited HF molecule:

$F + H_2 \rightarrow HF + H$

The excess energy from the reaction allows HF to stay in its excited state. As it relaxes, light is emitted through spontaneous emission. Deuterium can also be used in place of hydrogen. Deterium fluoride is useds for applications that require high-power. For example, MIRACL was built for military research and was known to produce 2.2 megawatts of power. The uniqueness of a chemical laser is that the power required for lasing is produced in the reaction itself.

Laser Applications

The applications of lasers are numerous and cover scientific and technological fields. In general, these applications are a direct consequence of the special characteristics of lasers. Below are a few examples of the laser applications, for a complete list please go to en.Wikipedia.org/wiki/List_of...ons_for_lasers

Lidar

Lidar is short for light detection and ranging which is an optical remote sensing technology can be used for monitoring the environment. A typical lidar system involves a transmitter of laser radiation and a receiver for the detection and analysis of backscattered light. A beam expander is usually used at transmitter to reduce divergence of the laser beam before it propagates into the atmosphere. The receiver includes a wavelength filter, a photo detector, and computers and electronics for data acquisition and analysis.

Lidar system dates back to the 1930, because of the laser, it has become one of the primary tools in atmospheric and environmental research. Other than that, Lidar has been put into various uses. In agriculture, lidar can be used to create topographic map to help farmer to decide appropriate amount of fertilizing to achieve a better crop yield. In Archaeology, lidar can be used to create a geographic information system to help archaeologists to find sites. In transportation, lidar has been used in autonomous cruise control system to prevent road accident and policemen are also using lidar speed gun to enforce the speed limit regulation.

Laser in Material Processing

The beam of a laser is usually a few millimeters in diagram. For most material processing applications, lenses are used to increase the intensity of the beam. The beam from a laser is either plane or spherical. After passing through a lens, the beam should get focused to a point. But in actual practice, diffraction effects have to be taken into consideration, the incoming will focus into a region of radius. If λ is the wavelength of the laser light, a is the radius of the beam, and f is the focal length of the lens, then the radius of the region is

$$b = \frac{\lambda f}{a}$$

If P represents the power of the laser beam, the intensity I, obtained at the focused region would be given by,

$$I = \frac{P}{\pi b^2} = \frac{Pa^2}{\pi\pi\lambda^2 f^2}$$

The high-power (P>100w) laser are widely used in material processing such as welding, drilling, cutting, surface treatment, and alloying. The main advantage of the laser beam can be summarized as follow: (1) The heating produced by the laser is less than that in conventional process. Material distortion is considerably reduced. (2) Possibility of working in inaccessible region. Any region which can be seen can be processed by a laser. (3) The process can be better controlled and easily automatized. However, against all these advantages, the disadvantages are: (1) high cost of the laser system. (2) Reliability and reproducibility problems of the laser system. (3) Safety problems.

Laser in Medicine

In field of medicine, the major use of lasers is for surgery such as laser eye surgery commonly known as LASIK. Besides that, there are also a few diagnosetic applications such as clinical use of flow microfluormeters, Doppler velocimetry to measure the blood velocity, laser fluorescence bronchoscope to detect tumors in their early phase.

For surgery, the laser beams are used instead of a conventional scalpel. The infrared beam from the CO^2 laser is strongly absorbed by water molecules in the tissue. It produces a rapid evaporation of these molecules, consequently cutting the tissue. The main advantage of laser beam surgery can be summarized as follows: (1) High precision. The incision can be made with a high precision particularly when the beam is directed by means of a microscope. (2) Possibility of operating in inaccessible region. Laser surgery can be operated in any region of the body which can be observed by means of an optical system. (4) Limited damage to blood vessel and adjacent tissue. However, the disadvantages are: (1) considerable cost. (2) Smaller velocity of the laser scalpel. (3) Reliability and safety problems associated with the laser procedure.

References

1. Arias, P., Jaeckey, J., Redondo, J., & Ringwald, A. (2010). Optimizing light-shining-through-a-wall experiments for axion and other weakly interacting slim particle searches. *The American Physical Society*, *82*(11), DOI: 10.1103/PhysRevD.82.11501
2. Bertolotti, M. (1999). *The History of the Laser.* Philadelphia, PA: Institute of Physics Publishing.
3. Ferrai, G., et al. (2010). Coherent Addition of Laser Beams in Resonant Passive Optical Cavities. *OpticsInfoBase*, *35(18)*, DOI: 10.1364/OL.35.003105
4. Hecht, J. (1992). *Laser pioneers*. San Diego, CA: Academic Press Limited.
5. Horn, D. T. (1988). *Laser experimenter's handbook*. Blue Ridge Summit, PA: Tab Books Inc.
6. Kenichi, I. (1988). *Fundamentals of Laser Optics.* Yokohama, Japan: Plenum Press.
7. Khanin, Y. (1995). *Principles of Laser Dynamics.* (P. Press, Ed.) New York, NY: Elsevier.
8. Verdeyen, J. (1989). *Laser Electronics.* Englewood Cliffs, NJ: Prentice-Hall, Inc.
9. Milonni,P.,Eberly, J., (2010) *Laser Physics*.Hoboken NJ:John Wiley&Sons, Inc.
10. Silfvast,W.,(1996) *Laser Fundamentals*. New York,NY: the Press Syndicate of the university of Cambridge.
11. Thyagarajan, K. (1981) *Lasers: Theory and Application.* New York, NY: Plenum Press.
12. Hooker,S., Webb,C., (2010) Laser Physics. Oxford, NY:Oxford University Press.
13. Svelto, O. (1982). *Principles of Lasers.* (2nd, Ed.) New York, NY: Plenum Press.
14. Coherent, I. (Ed.). (1980). *Lasers Operation, Equipment, Application and Design.* Palo Alto, CA: McGraw-Hill.

Outside Links

- http://en.Wikipedia.org/wiki/Laser
- en.Wikipedia.org/wiki/List_of_laser_types
- en.Wikipedia.org/wiki/Q_factor
- en.Wikipedia.org/wiki/Mode-locking

Problems

1. Determine the free-space wavelength (λ_0) in Å, and frequency of the resonant cavity for a beam parameter q_1 that is 632,110 and q_2 that is 632,111 in a helium-neon gas laser at 1 atm. The index of refraction n is 1.00, the length of the resonant cavity is 20 cm and the wavelength region of interest is 6328Å.
2. What wavelength of light will be released by the spontaneous emission of Ne gas, where the the energy difference between the excited and ground state is 9.9 x 10^{-19} J.
3. What is the population ratio of the above question at 300K.

Answers

1. For q_1 $\lambda_0 = 6328.0125 \angstrom$Å, q_2 $\lambda_0 = 6328.0025 \angstrom$Å, and v=474 THz for both q values
2. 200 nm
3. N_2/N_1=1.9 x 10^{-105}

Contributors and Attributions

- Greg Allen (UCD), Arpana Vaniya (UCD), Zheng Zhang (UC Davis)

6.4.3: Overview of Lasers is shared under a CC BY-NC-SA 4.0 license and was authored, remixed, and/or curated by LibreTexts.

- **Overview of Lasers** is licensed CC BY-NC-SA 4.0.

6.4.4: Semiconductor and Solid-state lasers

In both solid-state and semiconductor lasers the lasing medium is a solid. Aside from this similarity, however, these two laser types are very different from each other. In the case of the solid-state lasers the lasing species is typically an impurity that resides in a solid host, a crystal of some sort. The crystal modifies some of the quantized energy levels of the impurity, but still the lasing is almost atomic - similar to gas lasers. The physics of the quantization, in the case of semiconductor lasers, is very different. In addition, solid-state lasers are always optically pumped, whereas semiconductor lasers are excited by the passage of electric current through them.

We have already seen how atomic energy levels become modified when two or more atoms bind to form a molecule. The energy quantization picture becomes more complex when atoms bind together to form a solid. Below, we will first examine energy quantization in solids before we begin a more detailed examination of solid-state and semiconductor lasers.

Crystals and Energy Bands

You may recall from high school chemistry that a model that is very successful in explaining the electronic composition of stable atomic species is called the shell model. In this model, very similar to the planetary model, the atom is thought to be made of shells of different types. Each shell-type can accommodate a certain number of electrons. For example, an "s-shell" can be occupied by no more than two electrons, whereas p-shells can have up to six electrons in them, etc. To "make stable atoms" we start by filling electrons in these shells starting in "level" 1, then level-2, etc., following the specified hierarchy: 1s; 2s, 2p; 3s, 3p; 4s, 3d, 4p; 5s, 4d, 5p; etc. (Remember that the chemistry of materials is due to electromagnetic interactions alone, so for this we only need to concern ourselves with electrons.) We start with the innermost shell, an s-shell. Our first atom-type has one electron in its s-shell; that's of course the hydrogen atom, H. The next atom has two electrons in its s-shell; that's He. The third atom on our list (see the Periodic Table) has three electrons, two in its 1 s-shell and then one in its 2 s-shell; and so on. According to this model, which incidentally is very well supported by the more rigorous and fundamental laws of Quantum Mechanics, atoms prefer to fill their outer most shell. Inert gases, for example, all (except for He) have a completely filled outer p-shell. Those atoms that manage this are energetically very stable. Those that don't would then prefer to interact with another atom of the correct type to allow an exchange of electrons so that they come closer to fulfilling this desire for closed shells in order to reduce their overall energy. A bond between two types of atoms by this give-and-take is strongest when both atoms get the most fulfillment - both end up with closed shells.

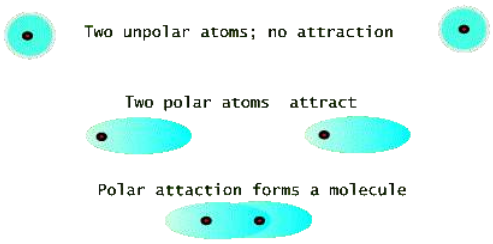
A good example of this is the case of table-salt: NaCl. Sodium atoms, Na, are hydrogenic (hydrogen-like); i.e. they have one electron in their outermost shell, which is an s-shell just outside an inert gas shell. So, to emulate the rare gases, all they need to do is to get rid of this electron. They cannot do this on their own (why?), but they can bind with an atom that wants an additional electron to complete its outer most shell. This happens to be true for the chlorine atom that has 5 electrons in its outermost shell, a p-shell. By sharing this electron with chlorine, the sodium atom still remains neutral, but now it, as well as the Cl, both end up with "filled" outer shells. In more ways than one, this is a happy marriage. Of course, in a grain of salt there are many Na and Cl atoms. (One grain of salt has roughly about 1 mg of mass. One proton is about 10-27 kg. How many atoms are then in one grain?) These atoms arrange themselves in a very organized pattern, called a crystal. These are rows and columns of atoms, as in a three-dimensional array, with interchanging Na and Cl species. In a salt crystal, a Na atom shares its electron with several Cl atoms, and yet because of the geometry of the crystal each Cl atom ends up with a net total of one extra and each Na atom with only one fewer electron (how?).

The electric attraction of the electrons to the atom's positively charged nucleus is the primary force that holds the atom together as a whole. So, in our shell model of the atom we must also account for the difference in attraction of electrons in different shells as well as the repulsion among the electrons themselves. Electrons in outer shells are further away from the nucleus, so their force of attraction is weaker than the inner shell electrons. In this respect, those electrons that belong to the unfilled outermost shell are the most loosely bound electrons in the atom. These electrons are the ones that are mostly responsible for the atom's interaction with another atom, so they are given a special name: the valence electrons.

How is the shell model related to our picture of atomic energy levels? It is primarily the valence electrons that connect these two pictures. Each atom species has its own unique energy levels, but its shell structure is not unique. When it is in its ground state, then its shells are filled according to the shell model's recipe, mentioned above. But once the atom is excited, then its electron configuration will change. The first excited state, for example, could require the valence electron to jump into the next higher shell.

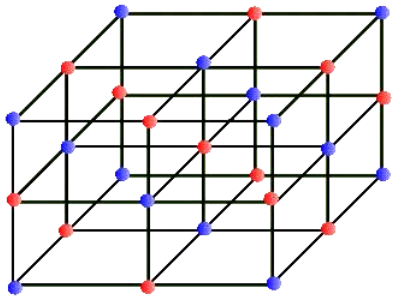
Further excitation of the atom could lead to even more drastic changes in its shell structure. But each of the excited energy levels corresponds to a different occupation of the accessible shells by the atom's electrons.

If atoms were made of (stationary) electrostatic charges, then most atomic species would have no reason to get together to make molecules or solids. But fortunately for us, this is not the case. Two neutral atoms can attract each other simply by changing their charge distribution so that they each become polar, i.e. the electron cloud of charges shifts over so that its center is not at the positive nucleus (see the figure below). In this sense even atoms of the same species find it energetically favorable to form a molecule. Because of this two totally neutral atoms of nitrogen prefer to form an N2 molecule even in the gas form. See the model drawing, below, which shows three time frames. The top frame shows two atoms with spherically symmetric charge distributions. These atoms do not initially interact with each other. But a momentary polarization of one atom can cause the other atom to polarize as well. This is the picture in the middle frame. The bottom frame the shows that two polarized atoms attract and form a molecule in which the electronic clouds of the two atoms overlaps.



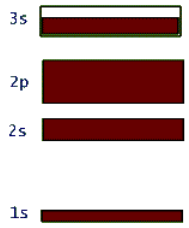
When we cool a gas, the ease with which it makes a liquid has a great deal to do with how easily the atoms in the gas form a molecule. Things get even more interesting when the liquid is further cooled to make a solid. The form, i.e. atomic structure, in the solid has not only to do with the atoms wanting to share electrons, but also with a totally different aspect of energy for a large collection of atoms. This relates to the probability of arrangements, or the so called entropy. What concerns us here is that for some species of atoms the lowest possible energy is reached when the atoms arrange themselves is a very regular and repeatable array of positions, called a crystal.

In every-day terminology the word "crystal" usually refers to a glassy and transparent object. But in our sense of the "regular network" a crystal may be totally opaque. In fact, most metals are crystalline in structure and are not at all transparent (at least in the visible range). Why should atoms form a regular array and make up a crystal? Why shouldn't they just clump together? In most substances atoms clump randomly, forming a solid. But in some special situations atoms crystallize to make very regular network structures. These networks can have different geometrical regularities. For example, in some crystals, the network structure is a simple cube that repeats in all directions. One atom sits at each corner of the cube, making up a simple cubic crystal. In a variation of this, in addition to the simple cubic structure each face of the cube has an atom at its center; this is called a face centered cubic crystal, etc. The salt crystal of NaCl has the simple cubic structure in which Cl and Na atoms occupy alternate corners of the cube, shown below:



This network structure in the crystal is called a lattice. The atoms in the lattice are not motionless. They jiggle and oscillate, but on average remain at a fixed site. The higher the temperature of the solid, the more vigorous is the jiggling oscillation of the lattice atoms. In the case of metals, which are electric conductors, the electron clouds of the lattice atoms overlap allowing the valence electrons to jump from lattice site to site when an electric potential (or voltage) is applied to the metal. So conductors allow these electrons to move freely - they are called "free electrons" - and make up an electric current, or flow of electric charge. Insulators, on the other hand, do not share their electrons and they are not free to migrate around. These materials, such as glass, wood, rubber,

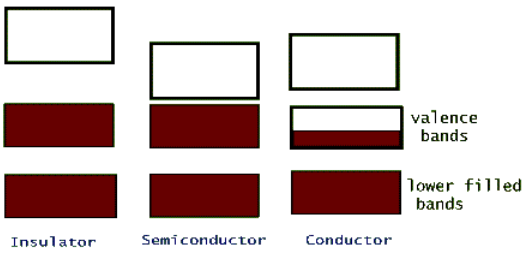
most plastic, and pure water, do not support electric currents under normal circumstances. What happens to the quantized energy levels of an atom when it is influenced by the presence of all the other lattice atoms in the crystal? It turns out that the idea of quantized energy levels still remains valid, but in a totally different picture. Instead of each atom having its own set of energy levels the solid as a whole can be described by a set of so called energy bands. In this picture the bands represent the quantized energy of the whole crystal. This is represented by the number of the energy bands, their energy widths, the gap between the bands, and whether the band is full, partially full, or empty. So, in a way these bands in the crystal play a similar role to the shells in the case of individual atoms. Just as in the atomic shell model we "fill" energy bands in a solid with electrons. Depending on the atomic species that make up the crystal, these bands get filled or not. For example, in the case of the sodium atom that we examined above, the corresponding energy band picture for its solid form is shown below:



Again it should be stressed that this band picture is really a combination of the energy-level-diagram and the occupancy picture of the shell model. So, here the large gap between the 1s and 2s bands represents the relatively large amount of energy that is necessary to promote an electron in a single atom of sodium from the 1s to the 2s shell. Also the filled 1s, 2s, and 2p bands indicate Na's shell structure. At the same time, the unfilled 3s band shows that these valence electrons in solid sodium can continuously change their energy within this band. This is totally due to the huge number of atoms in the solid structure and was not allowed in the quantized single atom.

Insulators, Semiconductors, and Conductors

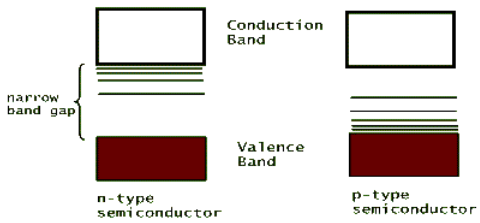
The electric conductivity of different materials is a consequence of their individual band structure. Metals, such as sodium, copper, aluminum, etc. have a crystalline band structure in which the upper most energy band, the valence band, is partially filled (or better yet, partially empty!). Electrons in this band can gain energy from an applied external electric potential, such as a battery, without the restriction of quantization. Insulators, on the other hand, have full valence bands, so for an electron to be promoted to its next higher available energy it has to leave this band and jump into the upper empty band. This is possible, but it takes a huge electric potential to make it happen (that's why lightning can pass through walls and kill people, but typical wiring is safe with just a thin plastic insulation over it). Semiconductors are intermediate between insulators and conductors. Their band structure is the same as an insulators' but the separating gap between their valance band and the next empty band, the conduction band, is very narrow.



Because of this narrow so called band gap, semiconductors can use the thermal energy of their lattice (collisions between the valence electrons and the oscillating lattice atoms) to promote a few of their valence electrons to the conduction band. In this way these material can conduct electricity, but because of the limited number of electrons that get promoted, they are not very good conductors. Examples of crystalline materials with narrow band gaps are silicon (Si) and germanium (Ge). In both of these materials the outermost shell is a partially filled p-shell with only two (out of a maximum of 6) electrons in it. In these crystals the two valence p-shell electrons are shared by the other neighboring atoms in the lattice.

To make a better conductor out of these semiconductors, atom impurities are introduced in the crystal formation through a process called doping. If one of the silicon atoms in the lattice is replaced by an arsenic (As) atom, which has three p-shell valence electrons, then the extra electron becomes loosely attached to its mother atom. This loose electron can take part in the electric

conduction and therefore increases the conductivity of the crystal. Strangely enough, a similar process can occur if one of the silicon atoms is replaced by a gallium (Ga) atom, which has only one p-shell valence electron. In this case, the Ga impurity strongly attracts one of the p-shell electrons from one of its Si neighbors. This leads to the production of a so called "electron hole". The resulting electron vacancy (hole) can travel in the crystal just as an electron would - but in the opposite direction - and results in an increased conductivity. Doped Si crystals with extra electrons, negative carriers, are referred to as n-type; those with holes are called p-type. These impurities modify the crystals' energy band structure by introducing atomic-type energy levels between the valance and conduction bands of the crystal and thus further reduce the band gap. This is shown below:



Semiconductor Devices

Diodes are the most basic of semiconductor devices. They are simply one-way conductors. By suitably doping a Si crystal, its conductivity can be altered to make it behave as a conductor in one direction and an insulator in the other direction! This is commonly done in a p-n junction. When the crystal is being formed it is first introduced to a donor-type impurity (say As for an Si crystal). As the crystal grows the concentration of the donar impurity is reduced and replaced with a growing concentration of an acceptor impurity (say Ga for an Si crystal). So, the resulting crystal begins at one end as an n-type and eventually becomes a p-type at the other end. The n-type portion has a large concentration of electrons and the p-type end a large concentration of holes. This variation causes this device to act as an effective insulator for the flow of electricity in it from the n to the p-side, but a very good conductor in the opposite direction. So, unlike a regular conductor that allows internal flow of electricity in both directions, this device acts like a unidirectional valve. An electronic component that allows electricity to flow in one way (the forward bias), but not the opposite way (reverse bias) is called a diode.

Transistors are the most common of semiconductor devices. They are controllable switches made from either p-n-p or n-p-n arrays of doped silicon. Today's technology can put millions of transistors together into single integrated modules, or chips, to make a large variety of different types of devices such as computer memory chips or microprocessors.

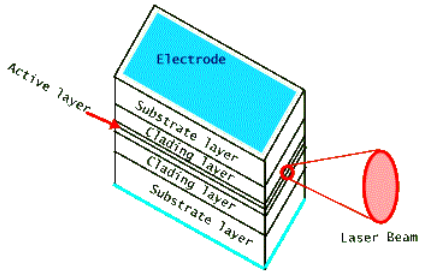
Another semiconductor device is the familiar solar cell. This is also a p-n junction with variations in the hole and electron concentrations along the crystal. When light strikes this device it excites bound electrons from the valence band into the conduction band. This creates not only a mobile electron, but a hole in the valence band. Both the electron and the oppositely traveling hole produce electric current. So, when light strikes this device it behaves as a source of electricity, just like a battery. In the case of a battery chemical energy is used to produce free electrons and thereby the electric current. In solar cells photon energy is converted into the production of electron-hole pairs and the resulting electric current in the junction.

Light Emitting Diodes (LEDs) behave just the opposite of solar cells. In these devices, also having a p-n junction, the combination of hole-electron pairs, created by an applied source of electricity, give off light. So, light is produced when a free electron fills a hole, i.e. a vacancy, in the crystal that is created by the presence of a p-type impurity. The light generated by LEDs is very broad-band and not of a single wavelength. It is also generated in all directions, so these devices do not make laser light. But they are useful light sources in that they are very compact and consume little electric power. To make them more efficient and reduce absorption of the generated light by the crystal's lattice, typically the junction is made near the surface. These light sources were first made in the early 1960's. Their creation soon lead to the discovery of semiconductor lasers.

Semiconductor Lasers

Also known as diode-lasers, these are by far the most inexpensive and commonly used lasers in the world. The first diode-laser was invented in 1962 at the General Electric Research and Development Center, in Niskayuna, New York - just a few miles from the Union College campus. But it was not until the early 1980's, with the development of innovative semiconductor chip manufacturing techniques, that their mass production reached the consumer market. Similar to their LED cousins, these semiconductor devices generate light from the energy extracted when electron-hole pairs recombine. Also, as in the case of LEDs, the electron-hole pairs in the semiconductor lasers are produced by the flow of electric current in the junction - this is called the

injection current. The primary difference between these lasers and photodiodes is that at high injection currents the electron-hole pair densities increase to produce population inversion, which leads to lasing. These lasers, in fact, behave very much like LEDs until the critical injection current, called the threshold current, is reached.



A typical semiconductor laser, shown above, is about a few hundred microns in dimension, much smaller than a grain of table salt. (Recall that a human hair is about 100 microns thick.) It produces light from an active area which is still smaller, a few tenths of one micron, perpendicular to the flow of electric current. Therefore (recall that diffraction from a very small exit aperture leads to a large angular spread of the beam) its laser light is very divergent and requires the use of a lens to collimate it. Most commonly used diode lasers are made of several different layers of compound semiconductors, often GaAlAs. Both the doping and thickness designs of these layers are used to control the confinement of laser light in the active lasing region. For some applications reflective coatings are deposited on the front and back facets to increase the efficiency of the optical amplification by acting as mirrors. But in most cases simple cleaving of the output facets leads to sufficient light amplification for lasing action. One of the drawbacks of the diode laser's small size is that it has a short coherence length. This limits its use in applications that require large coherence lengths, such as interferometry and holography. But the portability of its size makes it far more useful in many other applications. Below are two photographs of typical diode laser modules, shown in comparison with a typical writing pen or with a quarter. Notice that the laser's packaging "can" has a glass window to protect the fragile diode laser housed inside it. This package also includes a diagnostic photodiode detector that measures the output laser light leaking from the back facet of the laser chip.

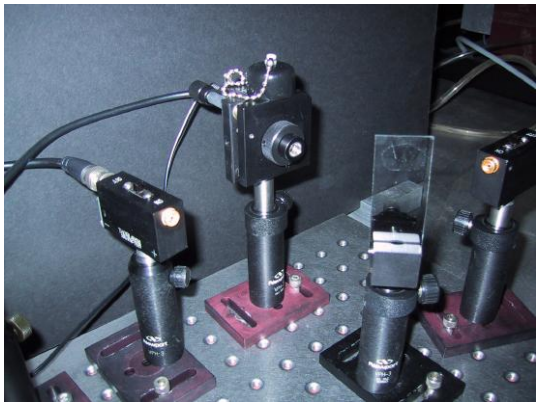




Diode lasers operate in several modes. Their wavelength depends primarily on the size of the band gap of the semiconductor. But the design of the semiconductor layers, as well as active feedback into the laser can generate band-widths of a few hundred kHz. Since changing the temperature of the diode expands or contracts the crystal and in this way changes the dimensions of the laser's

optical cavity, the laser's wavelength can be changed either by adjusting the injection current or by directly changing diode's temperature with another device. Wavelength tunability of a typical diode laser is about a few nm over a temperature range of about 10 oC. (This is very small compared to tunable dye lasers, for example.) Room temperature diode lasers have been manufactured with wavelength outputs from a few microns in the IR all the way to the green in the visible. Researchers are currently producing blue diode lasers, but these are not yet mass produced.

These lasers have a very high efficiency and are manufactured to produce laser light from a few mW to several tenths of a Watt. They can be made to operate in cw as well as in a pulsed mode. Because of their compact size an array of these can be manufactured on single chips, called laser diode arrays, that can generate output powers in the Watt range. But the single property that makes these lasers extremely useful is that their output light can be modulated at very fast rates. Because of this, and the very narrow band-width light that they can produce, diode lasers have overtaken all other lasers used in the communication industry.

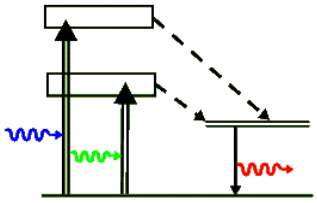


Measurement of the speed of light using a GHz pulsed diode laser (center) with its beam split by the glass slide to either directly enter the fast photodiode detector on the right or to travel several meters distance before being steered to enter the second photodiode detector on the left. By measuring the total path traveled and the time between the arrival of the two pulses, the speed of light can be measured on a table top to better than 1% accuracy.

Solid-state Lasers

The first laser ever made, the ruby laser, was a solid-state laser. In this laser the lasing is a result of atomic transitions of an impurity atom in a crystalline host. Even though the atomic levels of the lasing species are often modified because of the host crystal, the lasing process is atomic and very different from that in semiconductor lasers. All solid-state lasers are pumped optically. So, in these lasers the host must be transparent to the pumping radiation. (Why?) Also, the host must be a good heat conductor in order for it to effectively dissipate waste energy that is not used for lasing. Below we will review two of the most commonly used solid-state lasers: the ruby and YAG lasers.

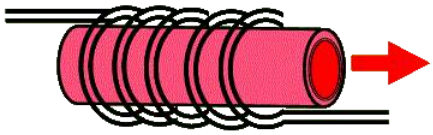
Ruby is an aluminum oxide (Al_2O_3) crystal, called sapphire, with a small amount of chromium oxide (Cr_2O_3) added to it. Sapphire is colorless and transparent, but the chromium doped crystal is pinkish-red in color because it strongly absorbs both in the green and in the blue. When this crystal is excited through the absorption of blue and/or green light it soon causes excitation of a meta-stable energy state of the chromium ion (Cr^{3+}). After a typical lifetime of a few milliseconds this state de-excites to the ground state with the emission of a 694.3 nm photon, which is visibly red in color. So, the primary role of the aluminum oxide crystal, aside from hosting the chromium ion, is to absorb the pump energy and to excite the ion through collisions.



The above simplified energy-level diagram shows the two optically pumped broad levels that quickly decay into the upper metastable lasing levels via non-radiative transitions (shown with dashed arrows). The energy of these non-radiative transitions is lost to the crystal as heat. Finally, the chromium ion de-excites back to its ground state by emitting the laser's 694.3 nm photon.

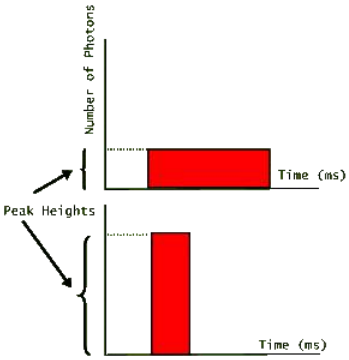
Note that Ruby is a 3-level laser and as such it requires a good deal of pump energy to achieve a population inversion. It can not produce a cw beam but produces a series of bright laser pulses.

To achieve population inversion, a strong pulse of broadband light is used to excite most chromium ions to their excited state. This is typically accomplished with the use of a helical flashlamp that surrounds a cylindrical ruby crystal. The two ends of this cylinder are coated (using evaporation techniques) to reflect the red 694.3 nm light. Because the wavelength output of the ruby laser is narrow-band and the pulse of light can be strong, this laser is one of the most preferred for holography. The following diagram shows a ruby rod surrounded with a helical flashtube. The cylindrical ends are coated for reflectivity in the red to form the optical cavity of the laser.



Typical ruby rods range in length from about 10 cm to 1/4 m and in diameter from a few to about 25 mm. The standard ruby lasers produce a few ms long duration pulses that range in energy from 10 to 100 J. But because ruby rods degrade quickly from excessive heating, these lasers are often operated at rather slow repetition rates (rep-rate) of few pulses per second (few Hz).

Applications that require large numbers of photons in a short period of time, benefit from laser pulses that are short in duration, but have a high peak. The following graph shows two pulses of light that carry equal number of photons (equal areas under their graphs), but have very different peak heights.



The one that has the higher peak, then has the shortest duration. (Note that for simplicity these pulses are depicted as rectangular in shape suggesting that lasing turns on and off at precise instants. In reality, however, laser pulses look more like hills; gradually increasing, reaching a peak, and then gradually decreasing before fully turning off.) Since the energy of each photon is fixed depending on the value of its wavelength (or its frequency), then both of these pulses carry the same amount of energy. For example, if we are told that the above pulses each have N photons emitted by a ruby laser, then we could easily calculate the pulse energies:

$$\text{pulse energy} = (\text{number of photons in the pulse}) \times (\text{energy of a single photon})$$

i.e. pulse energy = N x (hn) = N x (hc / l) = N x { (6.63 x 10-34) (3.00 x 108) / (694.3 x 10-9) }

$$= N \times (2.87 \times 10^{-19}) Joules.$$

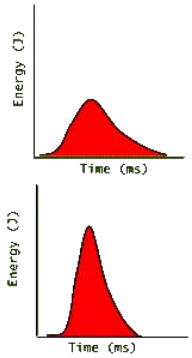
Alternatively, if we were told that each of the above ruby laser pulses is a 10 J pulse, then we could easily calculate the number of photons in each pulse:

number of photons = N = (pulse energy) / (energy of a single photon)

or,

$$N = \frac{10}{2.87 \times 10^{-19}} = 3.5 \times 10^{19}$$

Devices that measure laser light energies do not count the number of photons. Instead, they measure the energy that the photons produce in the device. (For example, photodiodes, which work like solar cells, absorb the photon energy and create electron-hole pairs, which produce a voltage across the p-n junction. This voltage is proportional to the absorbed energy and is displayed by the device indicating the pulse energy.) The following graphs are more realistic depictions of pulse energy measurements:



Here again we see two graphs of roughly equal areas and therefore equal pulse energies. The top pulse creates "less energy for a longer time" while the lower one creates "more energy for a shorter time". Since power is defined as:

power = (energy) / (time) (with units of 1 Watt = 1 Joule / 1 second)

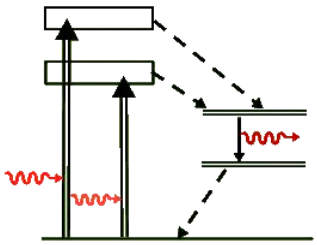
Then the pulse shown on the lower graph has much more power than the top one. (Why?) This is called the pulse power, or the peak power. For comparison with a cw laser it is convenient to average the energy of the pulse over not just its duration, but also over the time that the laser is on but there is not light emitted from it. To do this, all we need do is divide the total pulse energy by the time interval from when a pulse begins until the time that the next pulse begins; i.e. the "pulse-to-pulse time":

average power = (pulse energy) / (pulse-to-pulse time)

In pulsed lasers there are several ways to achieve a large peak power. One of these is called Q-switching, which refers to an increase in the efficiency of the optical cavity. The Q of an amplifier is just a measure of its efficiency. An amplifier that uses little energy for its amplification is said to have a large-Q. In pulsed lasers a method of increasing efficiency is to simply increase peak power. This can happen when instead of producing a long pulse one makes the laser produce a shorter pulse with a larger peak energy. One method for doing this is, instead of causing stimulated emission, to let the medium buildup more and more of a population inversion in its metastable state. This can be done rather easily by "blocking" one of the optical cavity's reflective mirrors for long enough that the maximum number of the atoms are in the upper laser level. Then to cause all of the atoms in the upper lasing level to undergo stimulated emission "all at once" a very quick "unblocking" of the reflective mirror results in many atoms to undergo stimulated emission simultaneously; therefore the resulting laser pulse has a high peak power. In this way Q-switched lasers can produce very high peak powers, in the hundreds of megawatts!

YAG Lasers

Yttrium-Aluminum-Garnet ($Y_3Al_5O_{12}$), YAG, is a clear and transparent crystal that is most commonly used as the host crystal for neodymium impurity atoms in Nd:YAG lasers. Even though the lasing transition occurs in the Neodymium (Nd) ions, these lasers are often called YAG lasers. Typically 1 - 2% of the Y is replaced by Nd in these lasers. Similar to the ruby laser, here again the crystal not only hosts the atom, but also its broad absorption bands (in the presence of the Nd-impurity) effectively absorb optical radiation - mostly around 700 nm and 800 nm. This energy is then transferred to the impurity ions through non-radiative processes.



Similar to the level diagram for the ruby laser, the above diagram is a simplified representation of the transitions for the neodymium ion, Nd+++, that take place in the YAG laser. Again, the dashed arrows indicate non-radiative transitions, where the energy lost in them is transferred as heat to the crystal. But unlike the ruby laser, the Nd:YAG is a four-level laser and has much more efficient lasing transitions than the ruby laser. Because of this efficiency in population inversion it can be pumped to produce a wide variety of laser output energies and can be operated in the cw as well as pulsed modes. The lasing photon has a wavelength of 1064 nm, well in the IR range.

Another host used for Nd is plain glass, but its optical and thermal properties are not as desirable as YAG's. The trade off is that growing large YAG crystals is not easy. A typical YAG rod, which is drilled out of a crystal block, is smaller than 1 cm in diameter and from a few to 10 cm in length. Still, these lasers can produce high output powers by using several rods in tandem. Pulsed YAG lasers can produce high peak powers by Q-switching and/or by using several rods as amplifiers. When used as amplifiers, the rods are not coated for reflectivity to produce optical amplification in the rod. Instead, the output of the first rod (the oscillator) is used as a Q-switch to generate stimulated emission in the next rod (the amplifier), and so on.

In the cw mode YAG lasers are pumped either by an arc lamp or a semiconductor laser. Pumping with a diode laser is more efficient because the diode's wavelength can be chosen to closely match the absorption of the YAG. Flashlamps are often used for pulsed operation of these lasers. In this mode Q-switching the laser can produce ns pulses with relatively high peak powers. But, to reach very high powers, like that generated by the NOVA laser, many rod amplifications are necessary.

YAG lasers are extremely versatile. They are used in applications from welding and drilling to range finding. Because their output wavelength is not visible, YAG lasers are used in many applications that require secrecy; from military to security applications. It is now possible to convert IR radiation into the visible range using so called non-linear crystals (also known as second-harmonic-generators). When high density photons impinge on such a crystal, the non-linear properties of its index of refraction causes the crystal to absorb two long wavelength photons and generate, in their place, one photon with twice their energy and therefore half their wavelength. Using these crystals, the YAG laser wavelength can be shortened to 532 nm (1064 nm/2), which is seen by the eye as green light. Today's green-colored laser pointers are diode-pumped YAG lasers with doubling crystals.

Although we can change the wavelength of the YAG laser from IR to green (and even further into UV, via another second harmonic generation), this is not a continuous tuning. Other interesting solid-state lasers, called vibronic lasers, use effective bands as their lower lasing level. In this way these lasers can produce a tunable output; i.e. one with a continually changeable wavelength. The most commonly used laser of this type is the Ti:sapphire laser, which is an aluminum oxide crystal, the same as ruby's host, but doped with titanium instead of chromium atoms.

Questions on Semiconductor & Solid-state lasers

1. What does the shell-model of the atom describe?
2. How is the shell-model related to the energy-level model of the atom?
3. What is the valence electron in an atom?
4. How can two neutral atoms form a bound molecule? Give an example of this.
5. Describe what a crystal is.
6. What are energy bands? How are they similar to and different from the energy levels/shell model?
7. What is the valence band in a crystal?
8. What are the differences in the energy band configurations between conductors, insulators, and semiconductors?
9. What is a p-n junction? What is a transistor?
10. What kind of transition leads to the production of light in a semiconductor p-n junction?
11. Describe what a semiconductor laser is and how it operates.
12. Give a few examples of the uses and advantages of semiconductor lasers.
13. What are some of the output wavelengths and powers of semiconductor lasers?
14. In what ways are the transitions in solid-state lasers different from atomic ones?
15. What is ruby? What is its color and what species of atom is involved in lasing in a ruby laser?
16. How are ruby lasers made to laser, i.e. please explain their pump, medium, and laser cavity?
17. What is the color of ruby laser light? Is its output cw or pulsed? Why?
18. What is Q-switching and what is its function?
19. What are ruby lasers used for?
20. What are the required properties of the host crystal in solid-state lasers?
21. What is a YAG laser? What is the host and what is its lasing species in the YAG?

22. What is the typical output wavelength of a YAG laser?
23. What are some of the advantages of YAG lasers? Some of its applications?
24. What is a Ti:sapphire laser? How is it different from a ruby laser in make-up and in operation?

Contributors

- Jay Newman and Seyffie Maleki (Union College)

6.4.4: Semiconductor and Solid-state lasers is shared under a CC BY-NC-SA 4.0 license and was authored, remixed, and/or curated by LibreTexts.

- **Semiconductor and Solid-state lasers** is licensed CC BY-NC-SA 4.0.

6.4.5: Semiconductors

A semiconductor is a material whose resistivity to the movement of charge falls somewhere between that of a conductor, through which we can move a charge easily, and an insulator, which resists the movement of charge. Some semiconductors are elemental, such as silicon and germanium (both of which we examine more closely in this section) and some are multielemental, such as silicon carbide.

Properties of Silicon and Germanium Semiconductors

A conductor, such as aluminum or copper, has a resistivity on the order of $10^{-8} - 10^{-6}\ \Omega \cdot m$, which means that its resistance to the movement of electrons is sufficiently small that it carries a current without much effort. An insulator, such as the mineral quartz, SiO_2, has a resistivity on the order of $10^{15} - 10^{19}\ \Omega \cdot m$. Silicon, on the other hand, has a resistivity of approximately $640\ \Omega \cdot m$ and germainum has a resistivity of about $0.46\ \Omega \cdot m$.

> **Note**
>
> The inverse of resistivity is conductivity.

Silicon and germanium are in the same group as carbon. If we use a simplified view of atoms, we can treat silicon and germanium as having four valence electrons and an effective nuclear charge, Z_{eff}, of

$$\begin{aligned}(Z_{eff})_{\text{Si}} &= Z - \text{ number of core electrons}\\ &= 14 - 10\\ &= +4\\ (Z_{eff})_{\text{Ge}} &= Z - \text{ number of core electrons}\\ &= 32 - 28\\ &= +4\end{aligned}$$

We can increase the conductivity of silicon and germanium by adding to them—this is called doping—a small amount of an impurity. Adding a small amount of In or Ga, which have three valence electrons instead of four valence electrons, leaves a small number of vacancies, or holes, in which an electron is missing. Adding a small amount of As or Sb, which have five valence electrons instead of four valence electrons, leaves a small number of extra electrons. Figure 6.4.5.1shows all three possibilities.

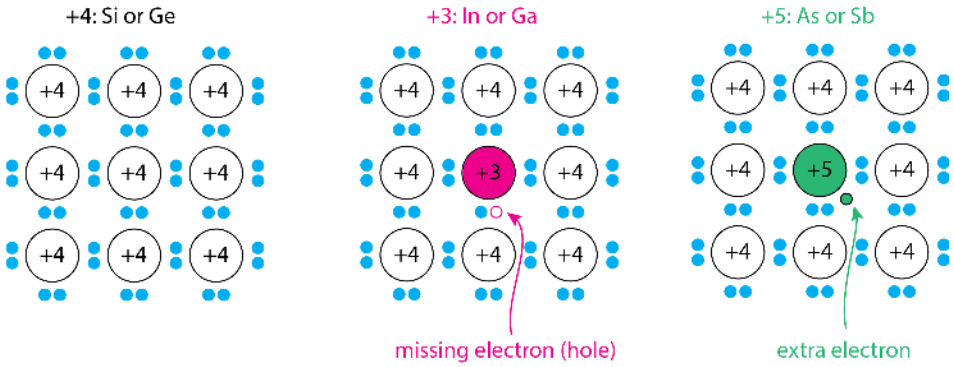


Figure 6.4.5.1. Illustration showing a two-dimensional cross-section through (left) a single crystal of silicon or germanium; (middle) a single crystal of silicon or germanium doped with indium or gallium; and (right) a single crystal of silicon or germanium doped with arsenic or antimony. Doping with indium or gallium leaves a hole where an electron is missing, and doping with arsenic or antimony leaves an extra electron. Patterned after figures in Diefenderfer, A. J. **Principles of Electronic Instrumentation**, W. B. Saunders (1972).

If we apply a potential across the semiconductor doped with As or Sb, the extra electron moves toward the positive pole, creating a small current, and leaving behind a vacancy, or hole. If we apply a potential across the semiconductor doped with In or Ga, electrons enter the semiconductor from the negative pole, occupying the vacancies, or holes, and creating a small current. In both cases, electrons move toward the positive pole and holes move toward the negative pole. We call an As or Sb doped semiconductor

an *n*-type semiconductor because the primary carrier of charge is an electron; we call an In or Ga doped semiconductor an *p*-type semiconductor because the primary carrier of charge is the hole.

Semiconductor Diodes

A diode is an electrical device that is more conductive in one direction than in the opposite direction. A diode takes advantage of the properties of the junction between a *p*-type and an *n*-type semiconductor.

Properties of *pn* Junctions

Let's use Figure 6.4.5.2to make sense of how a semiconductor diode works. The figure is divided into two parts: the left side of the figure, parts (a), (b), and (c), show the behavior of the semiconductor diode when a foward bias is applied, and the right side of the figure, parts (d), (e), and (f), show its behavior when a reverse bias is applied. For both, the semiconductor diode consists of a junction between a *n*-type semiconductor, which has an excess of electrons and carries a negative charge, and a *p*-type semiconductor, which has an excess of holes and, thus, a positive charge; this is shown in (a) and (d). How the semiconductor is manufactured is not of important to us.

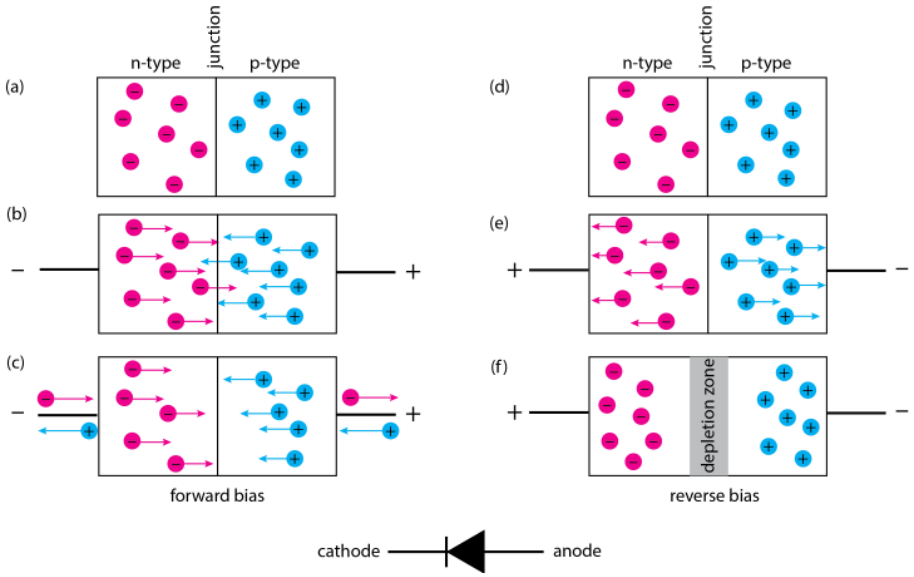


Figure 6.4.5.2. The behavior of a semiconductor diode under forward bias and reverse bias, and symbol for a semiconductor diode. See the text for additional details.

To effect a forward bias, we apply a positive potential to the *p*-type region and apply a negative potential to the *n*-type region. As we see in (b), the holes in the *p*-region move toward the junction and the electrons in the *n*-region move toward the junction as well. When holes and electrons meet they combine and are eliminated, which is why we see fewer holes and electrons in (c). Additional electrons flow into the *n*-region and electrons are pulled away from the *p*-region, as seen in (c), resulting in a current. To effect a reverse bias, we switch the applied potentials so that the *p*-region has the negative potential and the *n*-region has the positive potential. The result, as seen in (e) is a brief current as the holes and electrons move away from each other. leaving behind, in (f), a depletion zone that has essentially no electrons or holes.

Current-Voltage Curves for Semiconductor Diodes

Figure 6.4.5.3 shows a plot of current as a function of voltage for a semiconductor diode. In forward bias mode the current increases exponentially with an increase in applied voltage, but remains at essentially zero when operated under a reverse bias. The use of a sufficiently large negative potential, however, does result in an sudden and dramatic increase in current; the potential at which this happens is called the breakdown voltage.

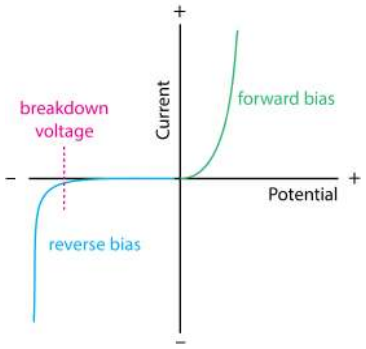


Figure 6.4.5.3. Current-voltage curve for a semiconductor diode under forward bias and under reverse bias.

This page titled 6.4.5: Semiconductors is shared under a CC BY-NC-SA 4.0 license and was authored, remixed, and/or curated by David Harvey.

- **2.4: Semiconductors** by David Harvey is licensed CC BY-NC-SA 4.0.

6.5: UV/VIS AND IR SPECTROSCOPY

In Figure 10.1.9 we examined Nessler's original method for matching the color of a sample to the color of a standard. Matching colors is a labor intensive process for the analyst and, not surprisingly, spectroscopic methods of analysis were slow to find favor. The 1930s and 1940s saw the introduction of photoelectric transducers for ultraviolet and visible radiation, and thermocouples for infrared radiation. As a result, modern instrumentation for absorption spectroscopy routinely became available in the 1940s—further progress has been rapid ever since.

INSTRUMENTATION

Frequently an analyst must select from among several instruments of different design, the one instrument best suited for a particular analysis. In this section we examine several different instruments for molecular absorption spectroscopy, with an emphasis on their advantages and limitations. Methods of sample introduction also are covered in this section.

INSTRUMENT DESIGNS FOR MOLECULAR UV/VIS ABSORPTION

Filter Photometer. The simplest instrument for molecular UV/Vis absorption is a ***filter photometer*** (Figure 10.3.1), which uses an absorption or interference filter to isolate a band of radiation. The filter is placed between the source and the sample to prevent the sample from decomposing when exposed to higher energy radiation. A filter photometer has a single optical path between the source and detector, and is called a ***single-beam*** instrument. The instrument is calibrated to 0% T while using a shutter to block the source radiation from the detector. After opening the shutter, the instrument is calibrated to 100% T using an appropriate blank. The blank is then replaced with the sample and its transmittance measured. Because the source's incident power and the sensitivity of the detector vary with wavelength, the photometer is recalibrated whenever the filter is changed. Photometers have the advantage of being relatively inexpensive, rugged, and easy to maintain. Another advantage of a photometer is its portability, making it easy to take into the field. Disadvantages of a photometer include the inability to record an absorption spectrum and the source's relatively large effective bandwidth, which limits the calibration curve's linearity.

> The percent transmittance varies between 0% and 100%. As we learned from Figure 10.2.7, we use a blank to determine P_0, which corresponds to 100%T. Even in the absence of light the detector records a signal. Closing the shutter allows us to assign 0%T to this signal. Together, setting 0% T and 100%T calibrates the instrument. The amount of light that passes through a sample produces a signal that is greater than or equal to 0%T and smaller than or equal to 100%T.

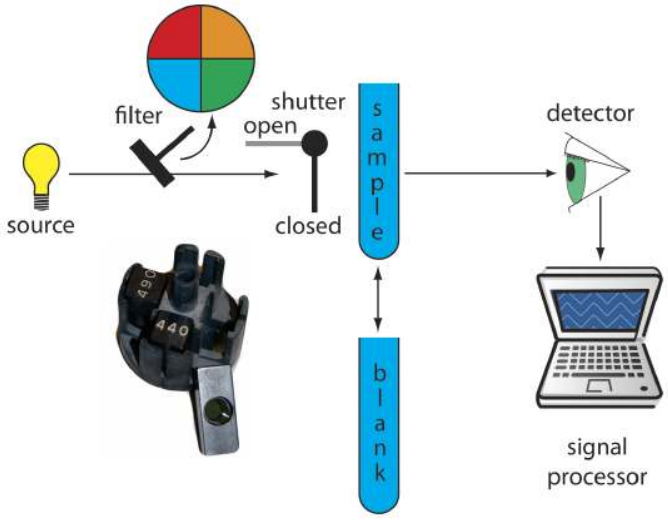


Figure 10.3.1 . Schematic diagram of a filter photometer. The analyst either inserts a removable filter or the filters are placed in a carousel, an example of which is shown in the photographic inset. The analyst selects a filter by rotating it into place.

Single-Beam Spectrophotometer. An instrument that uses a monochromator for wavelength selection is called a ***spectrophotometer***. The simplest spectrophotometer is a single-beam instrument equipped with a fixed-wavelength monochromator (Figure 10.3.2). Single-beam spectrophotometers are calibrated and used in the same manner as a photometer. One example of a single-beam spectrophotometer is Thermo Scientific's Spectronic 20D+, which is shown in the photographic insert to Figure 10.3.2 . The Spectronic 20D+ has a wavelength range of 340–625 nm (950 nm when using a red-sensitive detector), and a fixed effective bandwidth of 20 nm. Battery-operated, hand-held single-beam spectrophotometers are available, which are easy to transport into the field. Other single-beam spectrophotometers also are

available with effective bandwidths of 2–8 nm. Fixed wavelength single-beam spectrophotometers are not practical for recording spectra because manually adjusting the wavelength and recalibrating the spectrophotometer is awkward and time-consuming. The accuracy of a single-beam spectrophotometer is limited by the stability of its source and detector over time.

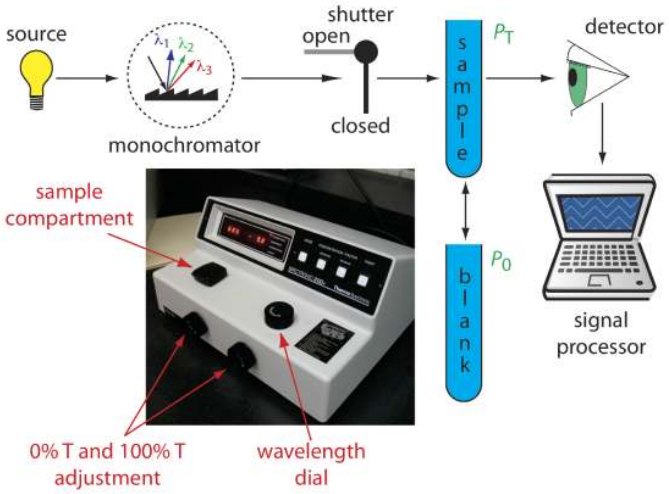


Figure 10.3.2 . Schematic diagram of a fixed-wavelength, single-beam spectrophotometer. The photographic inset shows a typical instrument. The shutter remains closed until the sample or blank is placed in the sample compartment. The analyst manually selects the wavelength by adjusting the wavelength dial. Inset photo modified from: Adi (www.commons.Wikipedia.org).

Double-Beam Spectrophotometer. The limitations of a fixed-wavelength, single-beam spectrophotometer is minimized by using a ***double-beam*** spectrophotometer (Figure 10.3.3). A chopper controls the radiation's path, alternating it between the sample, the blank, and a shutter. The signal processor uses the chopper's speed of rotation to resolve the signal that reaches the detector into the transmission of the blank, P_0, and the sample, P_T. By including an opaque surface as a shutter, it also is possible to continuously adjust 0%T. The effective bandwidth of a double-beam spectrophotometer is controlled by adjusting the monochromator's entrance and exit slits. Effective bandwidths of 0.2–3.0 nm are common. A scanning monochromator allows for the automated recording of spectra. Double-beam instruments are more versatile than single-beam instruments, being useful for both quantitative and qualitative analyses, but also are more expensive and not particularly portable.

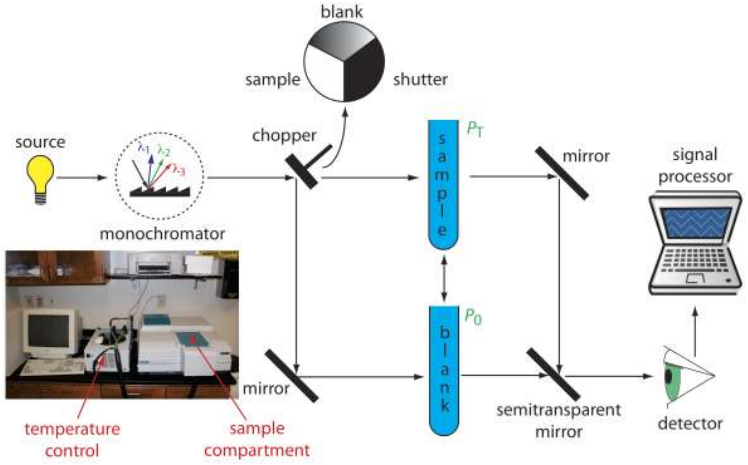


Figure 10.3.3 . Schematic diagram of a scanning, double-beam spectrophotometer. A chopper directs the source's radiation, using a transparent window to pass radiation to the sample and a mirror to reflect radiation to the blank. The chopper's opaque surface serves as a shutter, which allows for a constant adjustment of the spectrophotometer's 0%T. The photographic insert shows a typical instrument. The module in the middle of the photo is a temperature control unit that makes it possible to heat or cool the sample to a constant temperature.

Diode Array Spectrometer. An instrument with a single detector can monitor only one wavelength at a time. If we replace a single photomultiplier with an array of photodiodes, we can use the resulting detector to record a full spectrum in as little as 0.1 s. In a diode array spectrometer the source radiation passes through the sample and is dispersed by a grating (Figure 10.3.4). The photodiode array detector is situated at the grating's focal plane, with each diode recording the radiant power over a narrow range of wavelengths. Because we replace a full monochromator with just a grating, a diode array spectrometer is small and compact.

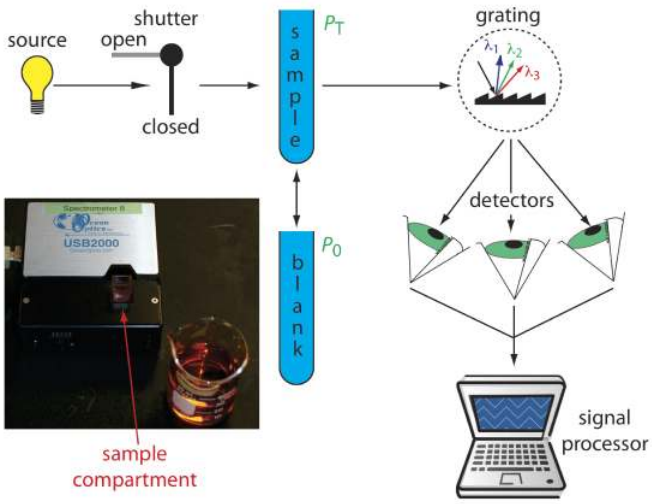


Figure 10.3.4 . Schematic diagram of a diode array spectrophotometer. The photographic insert shows a typical instrument. Note that the 50-mL beaker provides a sense of scale. Because the spectrometer is small and compact, it is easy to transport into the field.

One advantage of a diode array spectrometer is the speed of data acquisition, which allows us to collect multiple spectra for a single sample. Individual spectra are added and averaged to obtain the final spectrum. This ***signal averaging*** improves a spectrum's signal-to-noise ratio. If we add together n spectra, the sum of the signal at any point, x, increases as nS_x, where S_x is the signal. The noise at any point, N_x, is a random event, which increases as $\sqrt{n}N_x$ when we add together n spectra. The ***signal-to-noise ratio*** after n scans, $(S/N)_n$ is

$$\left(\frac{S}{N}\right)_n = \frac{nS_x}{\sqrt{n}N_x} = \sqrt{n}\frac{S_x}{N_x}$$

where S_x/N_x is the signal-to-noise ratio for a single scan. The impact of signal averaging is shown in Figure 10.3.5 . The first spectrum shows the signal after one scan, which consists of a single, noisy peak. Signal averaging using 4 scans and 16 scans decreases the noise and improves the signal-to-noise ratio. One disadvantage of a photodiode array is that the effective bandwidth per diode is roughly an order of magnitude larger than that for a high quality monochromator.

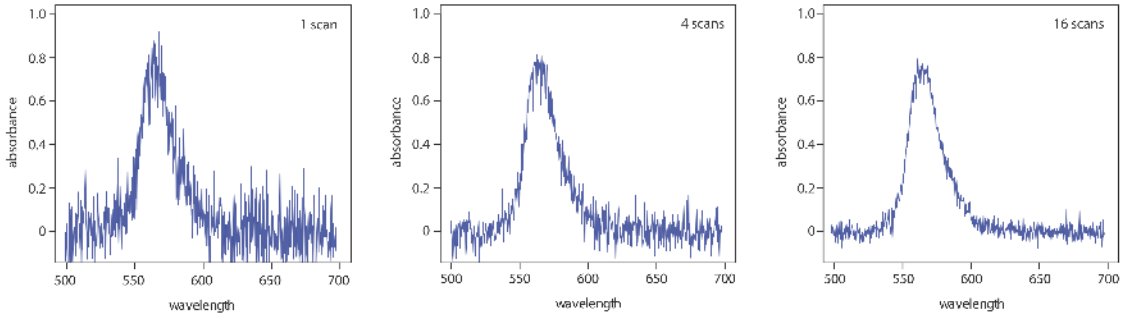


Figure 10.3.5 . Effect of signal averaging on a spectrum's signal-to-noise ratio. From top to bottom: spectrum for a single scan; average spectrum after four scans; and average spectrum after adding 16 scans.

For more details on signals and noise, see Introduction to Signals and Noise by Steven Petrovic, an on-line resource that is part of the Analytical Sciences Digital Library.

Sample Cells. The sample compartment provides a light-tight environment that limits stray radiation. Samples normally are in a liquid or solution state, and are placed in cells constructed with UV/Vis transparent materials, such as quartz, glass, and plastic (Figure 10.3.6). A quartz or fused-silica cell is required when working at a wavelength <300 nm where other materials show a significant absorption. The most common pathlength is 1 cm (10 mm), although cells with shorter (as little as 0.1 cm) and longer pathlengths (up to 10 cm) are available. Longer pathlength cells are useful when analyzing a very dilute solution or for gas samples. The highest quality cells allow the radiation to strike a flat surface at a 90° angle, minimizing the loss of radiation to reflection. A test tube often is used as a sample cell with simple, single-beam instruments, although differences in the cell's pathlength and optical properties add an additional source of error to the analysis.

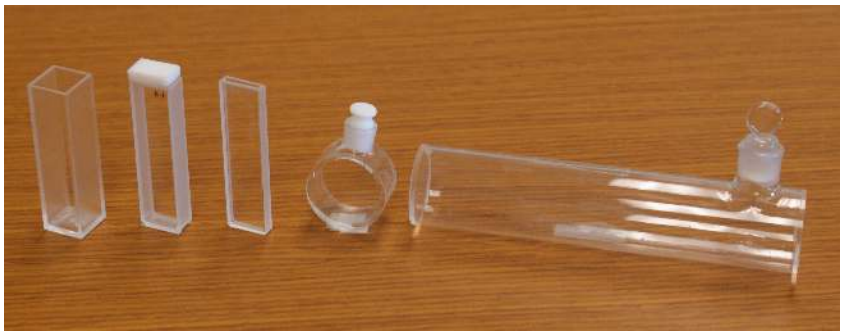


Figure 10.3.6 . Examples of sample cells for UV/Vis spectroscopy. From left to right (with path lengths in parentheses): rectangular plastic cuvette (10.0 mm), rectangular quartz cuvette (5.000 mm), rectangular quartz cuvette (1.000 mm), cylindrical quartz cuvette (10.00 mm), cylindrical glass cuvette with quartz windows (100.0 mm). Cells often are available as a matched pair, which is important when using a double-beam instrument.

If we need to monitor an analyte's concentration over time, it may not be possible to remove samples for analysis. This often is the case, for example, when monitoring an industrial production line or waste line, when monitoring a patient's blood, or when monitoring an environmental system, such as stream. With a ***fiber-optic probe*** we can analyze samples *in situ*. An example of a remote sensing fiber-optic probe is shown in Figure 10.3.7 . The probe consists of two bundles of fiber-optic cable. One bundle transmits radiation from the source to the probe's tip, which is designed to allow the sample to flow through the sample cell. Radiation from the source passes through the solution and is reflected back by a mirror. The second bundle of fiber-optic cable transmits the nonabsorbed radiation to the wavelength selector. Another design replaces the flow cell shown in Figure 10.3.7 with a membrane that contains a reagent that reacts with the analyte. When the analyte diffuses into the membrane it reacts with the reagent, producing a product that absorbs UV or visible radiation. The nonabsorbed radiation from the source is reflected or scattered back to the detector. Fiber optic probes that show chemical selectivity are called optrodes [(a) Seitz, W. R. *Anal. Chem.* **1984**, *56*, 16A–34A; (b) Angel, S. M. *Spectroscopy* **1987**, *2(2)*, 38–48].

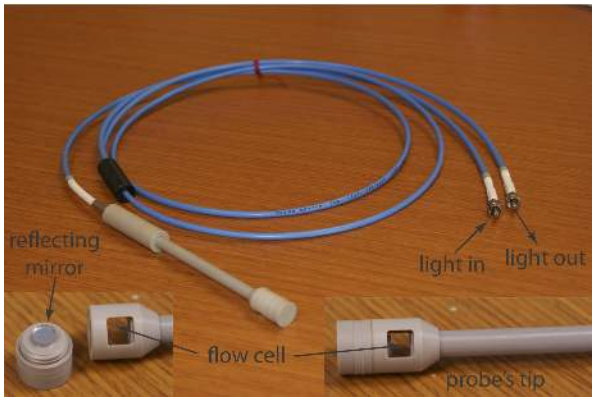


Figure 10.3.7 . Example of a fiber-optic probe. The inset photographs at the bottom of the figure provide close-up views of the probe's flow cell and the reflecting mirror.

INSTRUMENT DESIGNS FOR INFRARED ADSORPTION

Filter Photometer. The simplest instrument for IR absorption spectroscopy is a filter photometer similar to that shown in Figure 10.3.1 for UV/Vis absorption. These instruments have the advantage of portability and typically are used as dedicated analyzers for gases such as HCN and CO.

Double-beam spectrophotometer. Infrared instruments using a monochromator for wavelength selection use double-beam optics similar to that shown in Figure 10.3.3 . Double-beam optics are preferred over single-beam optics because the sources and detectors for infrared radiation are less stable than those for UV/Vis radiation. In addition, it is easier to correct for the absorption of infrared radiation by atmospheric CO_2 and H_2O vapor when using double-beam optics. Resolutions of 1–3 cm^{-1} are typical for most instruments.

Fourier transform spectrometer. In a Fourier transform infrared spectrometer, or FT–IR, the monochromator is replaced with an interferometer (Figure 10.1.13). Because an FT-IR includes only a single optical path, it is necessary to collect a separate spectrum to compensate for the absorbance of atmospheric CO_2 and H_2O vapor. This is done by collecting a background spectrum without the sample and storing the result in the instrument's computer memory. The background spectrum is removed from the sample's spectrum by taking the ratio the two signals. In comparison to other instrument designs, an FT–IR provides for rapid data acquisition, which allows for an enhancement in signal-to-noise ratio through signal-averaging.

Sample Cells. Infrared spectroscopy routinely is used to analyze gas, liquid, and solid samples. Sample cells are made from materials, such as NaCl and KBr, that are transparent to infrared radiation. Gases are analyzed using a cell with a pathlength of approximately 10 cm. Longer pathlengths are obtained by using mirrors to pass the beam of radiation through the sample several times.

A liquid sample may be analyzed using a variety of different sample cells (Figure 10.3.8). For non-volatile liquids a suitable sample is prepared by placing a drop of the liquid between two NaCl plates, forming a thin film that typically is less than 0.01 mm thick. Volatile liquids are placed in a sealed cell to prevent their evaporation.

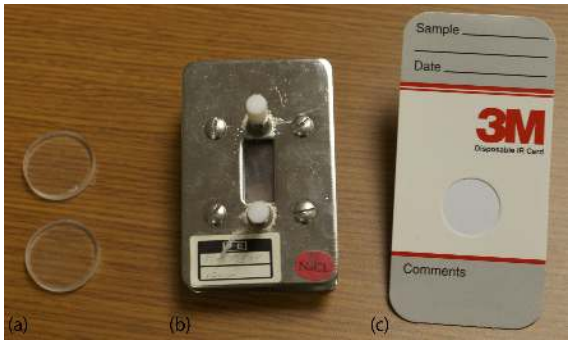


Figure 10.3.8 . Three examples of IR sample cells: (a) NaCl salts plates; (b) fixed pathlength (0.5 mm) sample cell with NaCl windows; (c) disposable card with a polyethylene window that is IR transparent with the exception of strong absorption bands at 2918 cm^{-1} and 2849 cm^{-1}.

The analysis of solution samples is limited by the solvent's IR absorbing properties, with CCl_4, CS_2, and $CHCl_3$ being the most common solvents. Solutions are placed in cells that contain two NaCl windows separated by a Teflon spacer. By changing the Teflon spacer, pathlengths from 0.015–1.0 mm are obtained.

Transparent solid samples are analyzed by placing them directly in the IR beam. Most solid samples, however, are opaque, and are first dispersed in a more transparent medium before recording the IR spectrum. If a suitable solvent is available, then the solid is analyzed by preparing a solution and analyzing as described above. When a suitable solvent is not available, solid samples are analyzed by preparing a mull of the finely powdered sample with a suitable oil. Alternatively, the powdered sample is mixed with KBr and pressed into an optically transparent pellet.

The analysis of an aqueous sample is complicated by the solubility of the NaCl cell window in water. One approach to obtaining an infrared spectrum of an aqueous solution is to use ***attenuated total reflectance*** instead of transmission. Figure 10.3.9 shows a diagram of a typical attenuated total reflectance (ATR) FT–IR instrument. The ATR cell consists of a high refractive index material, such as ZnSe or diamond, sandwiched between a low refractive index substrate and a lower refractive index sample. Radiation from the source enters the ATR crystal where it undergoes a series of internal reflections before exiting the crystal. During each reflection the radiation penetrates into the sample to a depth of a few microns, which results in a selective attenuation of the radiation at those wavelengths where the sample absorbs. ATR spectra are similar, but not identical, to those obtained by measuring the transmission of radiation.

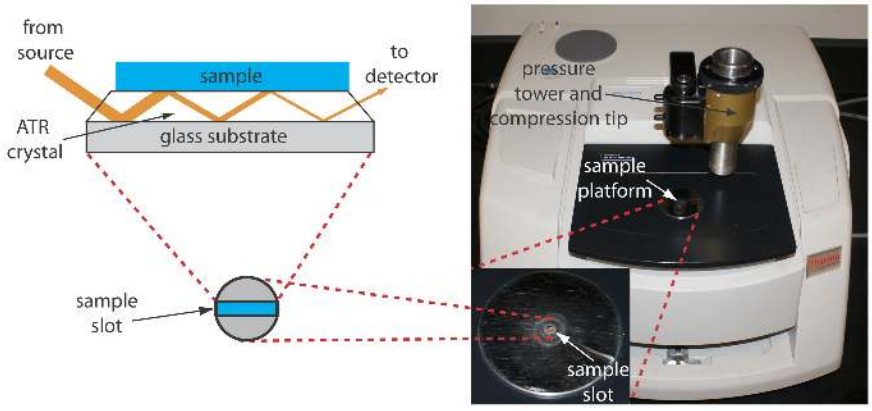


Figure 10.3.9 . FT-IR spectrometer equipped with a diamond ATR sample cell. The inserts show a close-up photo of the sample platform, a sketch of the ATR's sample slot, and a schematic showing how the source's radiation interacts with the sample. The pressure tower is used to ensure proper contact of a solid sample with the ATR crystal.

Solid samples also can be analyzed using an ATR sample cell. After placing the solid in the sample slot, a compression tip ensures that it is in contact with the ATR crystal. Examples of solids analyzed by ATR include polymers, fibers, fabrics, powders, and biological tissue samples. Another reflectance method is diffuse reflectance, in which radiation is reflected from a rough surface, such as a powder. Powdered samples are mixed with a non-absorbing material, such as powdered KBr, and the reflected light is collected and analyzed. As

with ATR, the resulting spectrum is similar to that obtained by conventional transmission methods. Further details about these, and other methods for preparing solids for infrared analysis can be found in this chapter's additional resources.

QUANTITATIVE APPLICATIONS

The determination of an analyte's concentration based on its absorption of ultraviolet or visible radiation is one of the most frequently encountered quantitative analytical methods. One reason for its popularity is that many organic and inorganic compounds have strong absorption bands in the UV/Vis region of the electromagnetic spectrum. In addition, if an analyte does not absorb UV/Vis radiation—or if its absorbance is too weak—we often can react it with another species that is strongly absorbing. For example, a dilute solution of Fe^{2+} does not absorb visible light. Reacting Fe^{2+} with *o*-phenanthroline, however, forms an orange–red complex of $Fe(phen)_3^{2+}$ that has a strong, broad absorbance band near 500 nm. An additional advantage to UV/Vis absorption is that in most cases it is relatively easy to adjust experimental and instrumental conditions so that Beer's law is obeyed.

A quantitative analysis based on the absorption of infrared radiation, although important, is encountered less frequently than with UV/Vis absorption. One reason is the greater tendency for instrumental deviations from Beer's law when using infrared radiation. Because an infrared absorption band is relatively narrow, any deviation due to the lack of monochromatic radiation is more pronounced. In addition, infrared sources are less intense than UV/Vis sources, which makes stray radiation more of a problem. Differences between the pathlengths for samples and for standards when using thin liquid films or KBr pellets are a problem, although an internal standard can correct for any difference in pathlength. Finally, establishing a 100%T ($A = 0$) baseline often is difficult because the optical properties of NaCl sample cells may change significantly with wavelength due to contamination and degradation. We can minimize this problem by measuring absorbance relative to a baseline established for the absorption band. Figure 10.3.10 shows how this is accomplished.

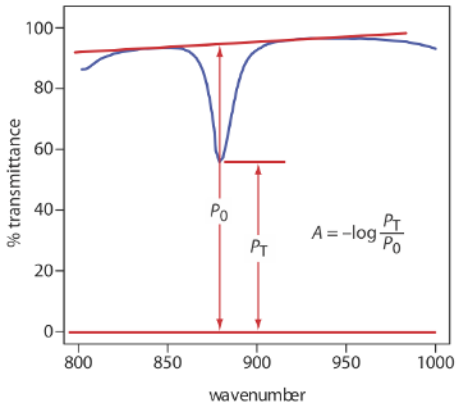


Figure 10.3.10 . Method for determining absorbance from an IR spectrum.

> Another approach is to use a cell with a fixed pathlength, such as that shown in Figure 10.3.8 b.

ENVIRONMENTAL APPLICATIONS

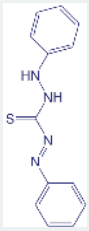
The analysis of waters and wastewaters often relies on the absorption of ultraviolet and visible radiation. Many of these methods are outlined in Table 10.3.1 . Several of these methods are described here in more detail.

Table 10.3.1 . Examples of Molecular UV/Vis Analysis of Waters and Wastewaters

analyte	method	λ (nm)
	trace metals	
aluminum	react with Eriochrome cyanide R dye at pH 6; forms red to pink complex	535
arsenic	reduce to AsH_3 using Zn and react with silver diethyldithiocarbamate; forms red complex	535
cadmium	extract into $CHCl_3$ containing dithizone from a sample made basic with NaOH; forms pink to red complex	518
chromium	oxidize to Cr(VI) and react with diphenylcarbazide; forms 540 red-violet product	540
copper	react with neocuprine in neutral to slightly acid solution and extract into $CHCl_3/CH_3OH$; forms yellow complex	457
iron	reduce to Fe^{2+} and react with *o*-phenanthroline; forms orange-red complex	510
lead	extract into $CHCl_3$ containing dithizone from sample made basic with NH_3/ NH_4^+ buffer; forms cherry red complex	510
manganese	oxidize to MnO_4^- with persulfate; forms purple solution	525
mercury	extract into $CHCl_3$ containing dithizone from acidic sample; forms orange complex	492
zinc	react with zincon at pH 9; forms blue complex	620
	inorganic nonmetals	
ammonia	reaction with hypochlorite and phenol using a manganous 630 salt catalyst; forms blue indophenol as product	630
cyanide	react with chloroamine-T to form CNCl and then with a pyridine-barbituric acid; forms a red-blue dye	578
fluoride	react with red Zr-SPADNS lake; formation of ZrF_6^{2-} decreases color of the red lake	570
chlorine (residual)	react with leuco crystal violet; forms blue product	592
nitrate	react with Cd to form NO_2^- and then react with sulfanilamide and *N*-(1-napthyl)-ethylenediamine; forms red azo 543 dye	543
phosphate	react with ammonium molybdate and then reduce with $SnCl_2$; forms molybdenum blue	690
	organics	
phenol	react with 4-aminoantipyrine and $K_3Fe(CN)_6$; forms yellow antipyrine dye	460
anionic surfactants	react with cationic methylene blue dye and extract into $CHCl_3$; forms blue ion pair	652

Although the quantitative analysis of metals in waters and wastewaters is accomplished primarily by atomic absorption or atomic emission spectroscopy, many metals also can be analyzed following the formation of a colored metal–ligand complex. One advantage to these spectroscopic methods is that they easily are adapted to the analysis of samples in the field using a filter photometer. One ligand used for the analysis of several metals is diphenylthiocarbazone, also known as dithizone. Dithizone is not soluble in water, but when a solution of dithizone in $CHCl_3$ is shaken with an aqueous solution that contains an appropriate metal ion, a colored metal–dithizonate complex forms that is soluble in $CHCl_3$. The selectivity of dithizone is controlled by adjusting the sample's pH. For example, Cd^{2+} is extracted from solutions made strongly basic with NaOH, Pb^{2+} from solutions made basic with an NH_3/ NH_4^+ buffer, and Hg^{2+} from solutions that are slightly acidic.

The structure of dithizone is shown below. See Chapter 7 for a discussion of extracting metal ions using dithizone.

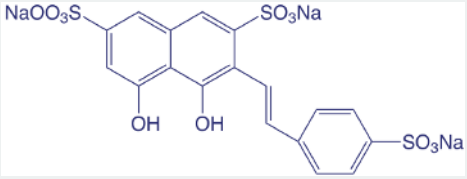


When chlorine is added to water the portion available for disinfection is called the chlorine residual. There are two forms of chlorine residual. The free chlorine residual includes Cl_2, HOCl, and OCl^-. The combined chlorine residual, which forms from the reaction of NH_3 with HOCl, consists of monochloramine, NH_2Cl, dichloramine, $NHCl_2$, and trichloramine, NCl_3. Because the free chlorine residual is more efficient as a disinfectant, there is an interest in methods that can distinguish between the total chlorine residual's different forms. One such method is the leuco crystal violet method. The free residual chlorine is determined by adding leuco crystal violet to the sample, which instantaneously oxidizes to give a blue-colored compound that is monitored at 592 nm. Completing the analysis in less than five minutes prevents a possible interference from the combined chlorine residual. The total chlorine residual (free + combined) is determined by reacting a separate sample with iodide, which reacts with both chlorine residuals to form HOI. When the reaction is complete, leuco crystal violet is added and oxidized by HOI, giving the same blue-colored product. The combined chlorine residual is determined by difference.

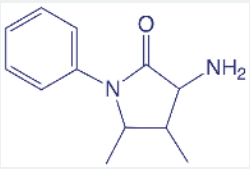
In Chapter 9 we explored how the total chlorine residual can be determined by a redox titration; see Representative Method 9.4.1 for further details. The method described here allows us to divide the total chlorine residual into its component parts.

The concentration of fluoride in drinking water is determined indirectly by its ability to form a complex with zirconium. In the presence of the dye SPADNS, a solution of zirconium forms a red colored compound, called a lake, that absorbs at 570 nm. When fluoride is added, the formation of the stable ZrF_6^{2-} complex causes a portion of the lake to dissociate, decreasing the absorbance. A plot of absorbance versus the concentration of fluoride, therefore, has a negative slope.

SPADNS, the structure of which is shown below, is an abbreviation for the sodium salt of 2-(4-sulfophenylazo)-1,8-dihydroxy-3,6-napthalenedisulfonic acid, which is a mouthful to say.



Spectroscopic methods also are used to determine organic constituents in water. For example, the combined concentrations of phenol and ortho- and meta-substituted phenols are determined by using steam distillation to separate the phenols from nonvolatile impurities. The distillate reacts with 4-aminoantipyrine at pH 7.9 ± 0.1 in the presence of $K_3Fe(CN)_6$ to a yellow colored antipyrine dye. After extracting the dye into $CHCl_3$, its absorbance is monitored at 460 nm. A calibration curve is prepared using only the unsubstituted phenol, C_6H_5OH. Because the molar absorptivity of substituted phenols generally are less than that for phenol, the reported concentration represents the minimum concentration of phenolic compounds.



4-aminoantipyrene

Molecular absorption also is used for the analysis of environmentally significant airborne pollutants. In many cases the analysis is carried out by collecting the sample in water, converting the analyte to an aqueous form that can be analyzed by methods such as those described in Table 10.3.1 . For example, the concentration of NO_2 is determined by oxidizing NO_2 to NO_3^-. The concentration of NO_3^- is then determined by first reducing it to NO_2^- with Cd, and then reacting NO_2^- with sulfanilamide and *N*-(1-naphthyl)-ethylenediamine to form a red azo dye. Another important application is the analysis for SO_2, which is determined by collecting the sample in an aqueous solution of $HgCl_4^{2-}$ where it reacts to form $Hg(SO_3)_2^{2-}$. Addition of *p*-rosaniline and formaldehyde produces a purple complex that is monitored at 569 nm. Infrared absorption is useful for the analysis of organic vapors, including HCN, SO_2, nitrobenzene, methyl mercaptan, and vinyl chloride. Frequently, these analyses are accomplished using portable, dedicated infrared photometers.

CLINICAL APPLICATIONS

The analysis of clinical samples often is complicated by the complexity of the sample's matrix, which may contribute a significant background absorption at the desired wavelength. The determination of serum barbiturates provides one example of how this problem is overcome. The barbiturates are first extracted from a sample of serum with $CHCl_3$ and then extracted from the $CHCl_3$ into 0.45 M NaOH (pH ≈ 13). The absorbance of the aqueous extract is measured at 260 nm, and includes contributions from the barbiturates as well as other components extracted from the serum sample. The pH of the sample is then lowered to approximately 10 by adding NH_4Cl and the absorbance remeasured. Because the barbiturates do not absorb at this pH, we can use the absorbance at pH 10, $A_{\text{pH 10}}$, to correct the absorbance at pH 13, $A_{\text{pH 13}}$

$$A_{\text{barb}} = A_{\text{pH 13}} - \frac{V_{\text{samp}} + V_{\text{NH}_4\text{Cl}}}{V_{\text{samp}}} \times A_{\text{pH 10}}$$

where A_{barb} is the absorbance due to the serum barbiturates and V_{samp} and $V_{\text{NH}_4\text{Cl}}$ are the volumes of sample and NH_4Cl, respectively. Table 10.3.2 provides a summary of several other methods for analyzing clinical samples.

Table 10.3.2 . Examples of the Molecular UV/Vis Analysis of Clinical Samples

analyte	method	λ (nm)
total serum protein	react with NaOH and Cu^{2+}; forms blue-violet complex	540
serum cholesterol	react with Fe^{3+} in presence of isopropanol, acetic acid, and H_2SO_4; forms blue-violet complex	540
uric acid	react with phosphotungstic acid; forms tungsten blue	710
serum barbituates	extract into $CHCl_3$ to isolate from interferents and then extract into 0.45 M NaOH	260
glucose	react with *o*-toludine at 100ºC; forms blue-green complex	630
protein-bound iodine	decompose protein to release iodide, which catalyzes redox reaction between Ce^{3+} and As^{3+}; forms yellow colored Ce^{4+}	420

INDUSTRIAL APPLICATIONS

UV/Vis molecular absorption is used for the analysis of a diverse array of industrial samples including pharmaceuticals, food, paint, glass, and metals. In many cases the methods are similar to those described in Table 10.3.1 and in Table 10.3.2 . For example, the amount of iron in food is determined by bringing the iron into solution and analyzing using the *o*-phenanthroline method listed in Table 10.3.1 .

Many pharmaceutical compounds contain chromophores that make them suitable for analysis by UV/Vis absorption. Products analyzed in this fashion include antibiotics, hormones, vitamins, and analgesics. One example of the use of UV absorption is in determining the purity of aspirin tablets, for which the active ingredient is acetylsalicylic acid. Salicylic acid, which is produced by the hydrolysis of acetylsalicylic acid, is an undesirable impurity in aspirin tablets, and should not be present at more than 0.01% w/w. Samples are screened for unacceptable levels of salicylic acid by monitoring the absorbance at a wavelength of 312 nm. Acetylsalicylic acid absorbs at 280 nm, but absorbs poorly at 312 nm. Conditions for preparing the sample are chosen such that an absorbance of greater than 0.02 signifies an unacceptable level of salicylic acid.

FORENSIC APPLICATIONS

UV/Vis molecular absorption routinely is used for the analysis of narcotics and for drug testing. One interesting forensic application is the determination of blood alcohol using the Breathalyzer test. In this test a 52.5-mL breath sample is bubbled through an acidified solution of $K_2Cr_2O_7$, which oxidizes ethanol to acetic acid. The concentration of ethanol in the breath sample is determined by a decrease in the absorbance at 440 nm where the dichromate ion absorbs. A blood alcohol content of 0.10%, which is above the legal limit, corresponds to 0.025 mg of ethanol in the breath sample.

DEVELOPING A QUANTITATIVE METHOD FOR A SINGLE COMPONENT

To develop a quantitative analytical method, the conditions under which Beer's law is obeyed must be established. First, the most appropriate wavelength for the analysis is determined from an absorption spectrum. In most cases the best wavelength corresponds to an absorption maximum because it provides greater sensitivity and is less susceptible to instrumental limitations. Second, if the instrument has adjustable slits, then an appropriate slit width is chosen. The absorption spectrum also aids in selecting a slit width by choosing a width that is narrow enough to avoid instrumental limita- tions to Beer's law, but wide enough to increase the throughput of source radiation. Finally, a calibration curve is constructed to determine the range of concentrations for which Beer's law is valid. Additional considerations that are important in any quantitative method are the effect of potential interferents and establishing an appropriate blank.

REPRESENTATIVE METHOD 10.3.1: DETERMINATION OF IRON IN WATER AND WASTEWATER

The best way to appreciate the theoretical and the practical details discussed in this section is to carefully examine a typical analytical method. Although each method is unique, the following description of the determination of iron in water and waste- water provides an instructive example of a typical procedure. The description here is based on Method 3500-Fe B as published in *Standard Methods for the Examination of Water and Wastewater*, 20th Ed., American Public Health Association: Washington, D. C., 1998.

Description of Method

Iron in the +2 oxidation state reacts with *o*-phenanthroline to form the orange-red $\mathrm{Fe(phen)_3^{2+}}$ complex. The intensity of the complex's color is independent of the solution's acidity between a pH of 3 and 9. Because the complex forms more rapidly at lower pH levels, the reaction usually is carried out within a pH range of 3.0–3.5. Any iron present in the +3 oxidation state is reduced with hydroxylamine before adding *o*-phenanthroline. The most important interferents are strong oxidizing agents, polyphosphates, and metal ions such as Cu^{2+}, Zn^{2+}, Ni^{2+}, and Cd^{2+}. An interference from oxidizing agents is minimized by adding an excess of hydroxylamine, and an interference from polyphosphate is minimized by boiling the sample in the presence of acid. The absorbance of samples and standards are measured at a wavelength of 510 nm using a 1-cm cell (longer pathlength cells also may be used). Beer's law is obeyed for concentrations of within the range of 0.2–4.0 mg Fe/L.

Procedure

For a sample that contains less than 2 mg Fe/L, directly transfer a 50-mL portion to a 125-mL Erlenmeyer flask. Samples that contain more than 2 mg Fe/L are diluted before acquiring the 50-mL portion. Add 2 mL of concentrated HCl and 1 mL of hydroxylamine to the sample. Bring the solution to a boil and continue boiling until the solution's volume is reduced to between 15 and 20 mL. After cooling to room temperature, transfer the solution to a 50-mL volumetric flask, add 10 mL of an ammonium acetate buffer, 2 mL of a 1000 ppm solution of

o-phenanthroline, and dilute to volume. Allow 10–15 minutes for color development before measuring the absorbance, using distilled water to set 100% T. Calibration standards, including a blank, are prepared by the same procedure using a stock solution that contains a known concentration of Fe^{2+}.

Questions

1. Explain why strong oxidizing agents are interferents and why an excess of hydroxylamine prevents the interference.

A strong oxidizing agent will oxidize some Fe^{2+} to Fe^{3+}. Because $Fe(phen)_3^{3+}$ does not absorb as strongly as $Fe(phen)_3^{2+}$, the absorbance is smaller than expected, which produces a negative determinate error. The excess hydroxylamine reacts with the oxidizing agents, removing them from the solution.

2. The color of the complex is stable between pH levels of 3 and 9. What are some possible complications at more acidic or at more basic pH's?

Because *o*-phenanthroline is a weak base, its conditional formation constant for $Fe(phen)_3^{2+}$ becomes smaller at more acidic pH levels, where *o*-phenanthroline is present in its protonated form. The result is a decrease in absorbance and a less sensitive analytical method. When the pH is greater than 9, competition between OH^- and *o*-phenanthroline for Fe^{2+} also decreases the absorbance. In addition, if the pH is sufficiently basic there is a risk that the iron will precipitate as $Fe(OH)_2$.

3. Cadmium is an interferent because it forms a precipitate with *o*-phenanthroline. What effect does the formation of precipitate have on the determination of iron?

Because *o*-phenanthroline is present in large excess (2000 µg of *o*-phenanthroline for 100 µg of $Fe2^+$), it is not likely that the interference is due to an insufficient amount of *o*-phenanthroline being available to react with the Fe^{2+}. The presence of a precipitate in the sample cell results in the scattering of radiation, which causes an apparent increase in absorbance. Because the measured absorbance increases, the reported concentration is too high. Although scattering is a problem here, it can serve as the basis of a useful analytical method. See Chapter 10.8 for further details.

4. Even high quality ammonium acetate contains a significant amount of iron. Why is this source of iron not a problem?

Because all samples and standards are prepared using the same volume of ammonium acetate buffer, the contribution of this source of iron is accounted for by the calibration curve's reagent blank.

QUANTITATIVE ANALYSIS FOR A SINGLE SAMPLE

To determine the concentration of an analyte we measure its absorbance and apply Beer's law using any of the standardization methods described in Chapter 5. The most common methods are a normal calibration curve using external standards and the method of standard additions. A single point standardization also is possible, although we must first verify that Beer's law holds for the concentration of analyte in the samples and the standard.

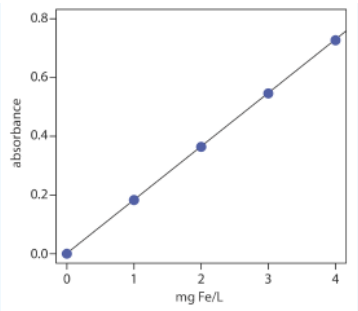
✔ EXAMPLE 10.3.1

The determination of iron in an industrial waste stream is carried out by the *o*-phenanthroline described in Representative Method 10.3.1. Using the data in the following table, determine the mg Fe/L in the waste stream.

mg Fe/L	absorbance
0.00	0.000
1.00	0.183
2.00	0.364
3.00	0.546
4.00	0.727
sample	0.269

Solution

Linear regression of absorbance versus the concentration of Fe in the standards gives the calibration curve and calibration equation shown here



$$A = 0.0006 + \left(0.1817\ \text{mg}^{-1}\text{L}\right) \times (\text{mgFe/L})$$

Substituting the sample's absorbance into the calibration equation gives the concentration of Fe in the waste stream as 1.48 mg Fe/L

? EXERCISE 10.3.1

The concentration of Cu^{2+} in a sample is determined by reacting it with the ligand cuprizone and measuring its absorbance at 606 nm in a 1.00-cm cell. When a 5.00-mL sample is treated with cuprizone and diluted to 10.00 mL, the resulting solution has an absorbance of 0.118. A second 5.00-mL sample is mixed with 1.00 mL of a 20.00 mg/L standard of Cu^{2+}, treated with cuprizone and diluted to 10.00 mL, giving an absorbance of 0.162. Report the mg Cu^{2+}/L in the sample.

Answer

For this standard addition we write equations that relate absorbance to the concentration of Cu^{2+} in the sample before the standard addition

$$0.118 = \varepsilon b \left[C_{\text{Cu}} \times \frac{5.00\ \text{mL}}{10.00\ \text{mL}} \right]$$

and after the standard addition

$$0.162 = \varepsilon b \left(C_{\text{Cu}} \times \frac{5.00\ \text{mL}}{10.00\ \text{mL}} + \frac{20.00\ \text{mg Cu}}{\text{L}} \times \frac{1.00\ \text{mL}}{10.00\ \text{mL}} \right)$$

in each case accounting for the dilution of the original sample and for the standard. The value of εb is the same in both equation. Solving each equation for εb and equating

$$\frac{0.162}{C_{\text{Cu}} \times \frac{5.00\ \text{mL}}{10.00\ \text{mL}} + \frac{20.00\ \text{mg Cu}}{\text{L}} \times \frac{1.00\ \text{mL}}{10.00\ \text{mL}}} = \frac{0.118}{C_{\text{Cu}} \times \frac{5.00\ \text{mL}}{10.00\ \text{mL}}}$$

leaves us with an equation in which C_{Cu} is the only variable. Solving for C_{Cu} gives its value as

$$\frac{0.162}{0.500 \times C_{\text{Cu}} + 2.00\ \text{mg Cu/L}} = \frac{0.118}{0.500 \times C_{\text{Cu}}}$$

$$0.0810 \times C_{\text{Cu}} = 0.0590 \times C_{\text{Ca}} + 0.236\ \text{mg Cu/L}$$

$$0.0220 \times C_{\text{Cu}} = 0.236\ \text{mg Cu/L}$$

$$C_{\text{Cu}} = 10.7\ \text{mg Cu/L}$$

QUANTITATIVE ANALYSIS OF MIXTURES

Suppose we need to determine the concentration of two analytes, *X* and *Y*, in a sample. If each analyte has a wavelength where the other analyte does not absorb, then we can proceed using the approach in Example 10.3.5 . Unfortunately, UV/Vis absorption bands are so broad that frequently it is not possible to find suitable wavelengths. Because Beer's law is additive the mixture's absorbance, A_{mix}, is

$$(A_{mix})_{\lambda_1} = (\varepsilon_x)_{\lambda_1} bC_X + (\varepsilon_Y)_{\lambda_1} bC_Y \tag{6.5.1}$$

where λ_1 is the wavelength at which we measure the absorbance. Because Equation 6.5.1 includes terms for the concentration of both *X* and *Y*, the absorbance at one wavelength does not provide enough information to determine either C_X or C_Y. If we measure the absorbance at a second wavelength

$$(A_{mix})_{\lambda_2} = (\varepsilon_x)_{\lambda_2} bC_X + (\varepsilon_Y)_{\lambda_2} bC_Y \tag{6.5.2}$$

then we can determine C_X and C_Y by solving simultaneously Equation 6.5.1 and Equation 6.5.2. Of course, we also must determine the value for ε_X and ε_Y at each wavelength. For a mixture of *n* components, we must measure the absorbance at *n* different wavelengths.

EXAMPLE 10.3.2

The concentrations of Fe^{3+} and Cu^{2+} in a mixture are determined following their reaction with hexacyanoruthenate (II), $Ru(CN)_6^{4-}$, which forms a purple-blue complex with Fe^{3+} (λ_{max} = 550 nm) and a pale-green complex with Cu^{2+} (λ_{max} = 396 nm) [DiTusa, M. R.; Schlit, A. A. *J. Chem. Educ.* **1985**, *62*, 541–542]. The molar absorptivities (M^{-1} cm^{-1}) for the metal complexes at the two wavelengths are summarized in the following table.

analyte	ε_{550}	ε_{396}
Fe^{3+}	9970	84
Cu^{2+}	34	856

When a sample that contains Fe^{3+} and Cu^{2+} is analyzed in a cell with a pathlength of 1.00 cm, the absorbance at 550 nm is 0.183 and the absorbance at 396 nm is 0.109. What are the molar concentrations of Fe^{3+} and Cu^{2+} in the sample?

Solution

Substituting known values into Equation 6.5.1 and Equation 6.5.2 gives

$$\begin{aligned} A_{550} &= 0.183 = 9970C_{Fe} + 34C_{Cu} \\ A_{396} &= 0.109 = 84C_{Fe} + 856C_{Cu} \end{aligned}$$

To determine C_{Fe} and C_{Cu} we solve the first equation for C_{Cu}

$$C_{Cu} = \frac{0.183 - 9970C_{Fe}}{34}$$

and substitute the result into the second equation.

$$\begin{aligned} 0.109 &= 84C_{Fe} + 856 \times \frac{0.183 - 9970C_{Fe}}{34} \\ &= 4.607 - \left(2.51 \times 10^5\right) C_{Fe} \end{aligned}$$

Solving for C_{Fe} gives the concentration of Fe^{3+} as 1.8×10^{-5} M. Substituting this concentration back into the equation for the mixture's absorbance at 396 nm gives the concentration of Cu^{2+} as 1.3×10^{-4} M.

Another approach to solving Example 10.3.2 is to multiply the first equation by 856/34 giving

$$4.607 = 251009C_{Fe} + 856C_{Cu}$$

Subtracting the second equation from this equation

$$\begin{aligned} 4.607 &= 251009C_{Fe} + 856C_{Cu} \\ -0.109 &= 84C_{Fe} + 856C_{Cu} \end{aligned}$$

gives

$$4.498 = 250925C_{Fe}$$

and we find that C_{Fe} is 1.8×10^{-5}. Having determined C_{Fe} we can substitute back into one of the other equations to solve for C_{Cu}, which is 1.3×10^{-5}.

EXERCISE 10.3.2

The absorbance spectra for Cr^{3+} and Co^{2+} overlap significantly. To determine the concentration of these analytes in a mixture, its absorbance is measured at 400 nm and at 505 nm, yielding values of 0.336 and 0.187, respectively. The individual molar absorptivities (M^{-1} cm^{-1}) for $Cr3^+$ are 15.2 at 400 nm and 0.533 at 505 nm; the values for Co^{2+} are 5.60 at 400 nm and 5.07 at 505 nm.

Answer

Substituting into Equation 6.5.1 and Equation 6.5.2 gives

$$A_{400} = 0.336 = 15.2C_{Cr} + 5.60C_{Co}$$

$$A_{400} = 0187 = 0.533C_{Cr} + 5.07C_{Co}$$

To determine C_{Cr} and C_{Co} we solve the first equation for C_{Co}

$$C_{Co} = \frac{0.336 - 15.2C_{Co}}{5.60}$$

and substitute the result into the second equation.

$$0.187 = 0.533C_{Cr} + 5.07 \times \frac{0.336 - 15.2C_{Co}}{5.60}$$

$$0.187 = 0.3042 - 13.23C_{Cr}$$

Solving for C_{Cr} gives the concentration of Cr^{3+} as 8.86×10^{-3} M. Substituting this concentration back into the equation for the mixture's absorbance at 400 nm gives the concentration of Co^{2+} as 3.60×10^{-2} M.

To obtain results with good accuracy and precision the two wavelengths should be selected so that $\varepsilon_X > \varepsilon_Y$ at one wavelength and $\varepsilon_X < \varepsilon_Y$ at the other wavelength. It is easy to appreciate why this is true. Because the absorbance at each wavelength is dominated by one analyte, any uncertainty in the concentration of the other analyte has less of an impact. Figure 10.3.11 shows that the choice of wavelengths for Practice Exercise 10.3.2 are reasonable. When the choice of wavelengths is not obvious, one method for locating the optimum wavelengths is to plot $\varepsilon_X/\varepsilon_y$ as function of wavelength, and determine the wavelengths where $\varepsilon_X/\varepsilon_y$ reaches maximum and minimum values [Mehra, M. C.; Rioux, J. *J. Chem. Educ.* **1982**, *59*, 688–689].

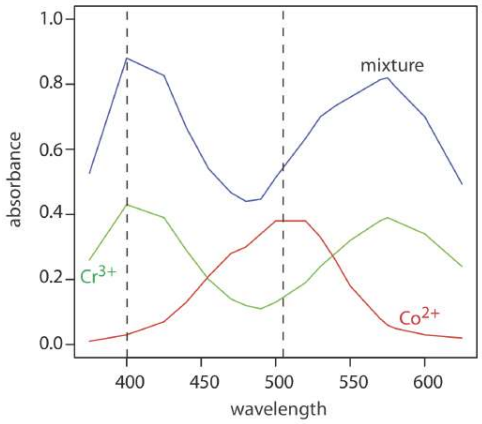


Figure 10.3.11 . Visible absorption spectra for 0.0250 M Cr^{3+}, 0.0750 M Co^{2+}, and for a mixture of Cr^{3+} and Co^{2+}. The two wavelengths used to analyze the mixture of Cr^{3+} and Co^{2+} are shown by the dashed lines. The data for the two standards are from Brewer, S. *Solving Problems in Analytical Chemistry*, John Wiley & Sons: New York, 1980.

When the analyte's spectra overlap severely, such that $\varepsilon_X \approx \varepsilon_Y$ at all wavelengths, other computational methods may provide better accuracy and precision. In a multiwavelength linear regression analysis, for example, a mixture's absorbance is compared to that for a set of standard solutions at several wavelengths [Blanco, M.; Iturriaga, H.; Maspoch, S.; Tarin, P. *J. Chem. Educ.* **1989**, *66*, 178–180]. If A_{SX} and A_{SY} are the absorbance values for standard solutions of components *X* and *Y* at any wavelength, then

$$A_{SX} = \varepsilon_X b C_{SX} \tag{6.5.3}$$

$$A_{SY} = \varepsilon_Y b C_{SY} \tag{6.5.4}$$

where C_{SX} and C_{SY} are the known concentrations of *X* and *Y* in the standard solutions. Solving Equation 6.5.3 and Equation 6.5.4 for ε_X and for ε_Y, substituting into Equation 6.5.1, and rearranging, gives

$$\frac{A_{mix}}{A_{SX}} = \frac{C_X}{C_{SX}} + \frac{C_Y}{C_{SY}} \times \frac{A_{SY}}{A_{SX}}$$

To determine C_X and C_Y the mixture's absorbance and the absorbances of the standard solutions are measured at several wavelengths. Graphing A_{mix}/A_{SX} versus A_{SY}/A_{SX} gives a straight line with a slope of C_Y/C_{SY} and a *y*-intercept of C_X/C_{SX}. This approach is particularly helpful when it is not possible to find wavelengths where $\varepsilon_X > \varepsilon_Y$ and $\varepsilon_X < \varepsilon_Y$.

The approach outlined here for a multiwavelength linear regression uses a single standard solution for each analyte. A more rigorous approach uses multiple standards for each analyte. The math behind the analysis of such data—which we call a multiple linear regression—is beyond the level of this text. For more details about multiple linear regression see Brereton, R. G. *Chemometrics: Data Analysis for the Laboratory and Chemical Plant*, Wiley: Chichester, England, 2003.

EXAMPLE 10.3.3

Figure $PageIndex{10.11}$ shows visible absorbance spectra for a standard solution of 0.0250 M Cr^{3+}, a standard solution of 0.0750 M Co^{2+}, and a mixture that contains unknown concentrations of each ion. The data for these spectra are shown here.

λ (nm)	A_{Cr}	A_{Cu}	A_{mix}	λ (nm)	A_{Cr}	A_{Cu}	A_{mix}
375	0.26	0.01	0.53	520	0.19	0.38	0.63
400	0.43	0.03	0.88	530	0.24	0.33	0.70
425	0.39	0.07	0.83	540	0.28	0.26	0.73
440	0.29	0.13	0.67	550	0.32	0.18	0.76
455	0.20	0.21	0.54	570	0.38	0.08	0.81
470	0.14	0.28	0.47	575	0.39	0.06	0.82
480	0.12	0.30	0.44	580	0.38	0.05	0.79
490	0.11	0.34	0.45	600	0.34	0.03	0.70
500	0.13	0.38	0.51	625	0.24	0.02	0.49

Use a multiwavelength regression analysis to determine the composition of the unknown.

Solution

First we need to calculate values for A_{mix}/A_{SX} and for A_{SY}/A_{SX}. Let's define X as Co^{2+} and Y as Cr^{3+}. For example, at a wavelength of 375 nm A_{mix}/A_{SX} is 0.53/0.01, or 53 and A_{SY}/A_{SX} is 0.26/0.01, or 26. Completing the calculation for all wavelengths and graphing A_{mix}/A_{SX} versus A_{SY}/A_{SX} gives the calibration curve shown in Figure 10.3.12 . Fitting a straight-line to the data gives a regression model of

$$\frac{A_{\text{mix}}}{A_{SX}} = 0.636 + 2.01 \times \frac{A_{SY}}{A_{SX}}$$

Using the *y*-intercept, the concentration of Co^{2+} is

$$\frac{C_X}{C_{SX}} = \frac{[\text{Co}^{2+}]}{0.0750\text{M}} = 0.636$$

or $[Co^{2+}]$ = 0.048 M; using the slope the concentration of Cr^{3+} is

$$\frac{C_Y}{C_{SY}} = \frac{[\text{Cr}^{3+}]}{0.0250\text{M}} = 2.01$$

or $[Cr^{3+}]$ = 0.050 M.

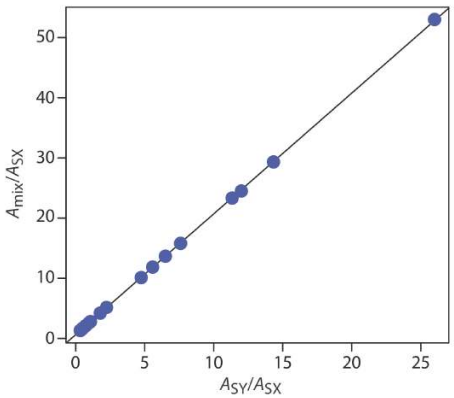


Figure 10.3.12 . Multiwavelength linear regression analysis for the data in Example 10.3.3 .

EXERCISE 10.3.3

A mixture of MnO_4^- and $Cr_2O_7^{2-}$, and standards of 0.10 mM $KMnO_4$ and of 0.10 mM $K_2Cr_2O_7$ give the results shown in the following table. Determine the composition of the mixture. The data for this problem is from Blanco, M. C.; Iturriaga, H.; Maspoch, S.; Tarin, P. *J. Chem. Educ.* **1989**, *66*, 178–180.

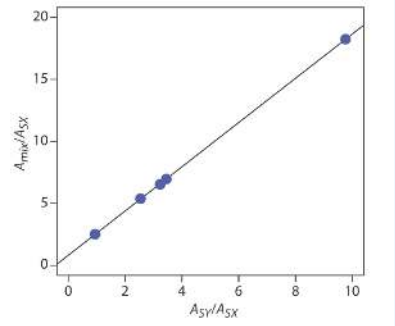
λ (nm)	A_{Mn}	A_{Cr}	A_{mix}
266	0.042	0.410	0.766
288	0.082	0.283	0.571
320	0.168	0.158	0.422
350	0.125	0.318	0.672
360	0.036	0.181	0.366

Answer

Letting *X* represent MnO_4^- and letting *Y* represent $Cr_2O_7^{2-}$, we plot the equation

$$\frac{A_{mix}}{A_{SX}} = \frac{C_X}{C_{SX}} + \frac{C_Y}{C_{SY}} \times \frac{A_{SY}}{A_{SX}}$$

placing A_{mix}/A_{SX} on the *y*-axis and A_{SY}/A_{SX} on the *x*-axis. For example, at a wavelength of 266 nm the value A_{mix}/A_{SX} of is 0.766/0.042, or 18.2, and the value of A_{SY}/A_{SX} is 0.410/0.042, or 9.76. Completing the calculations for all wavelengths and plotting the data gives the result shown here



Fitting a straight-line to the data gives a regression model of

$$\frac{A_{\text{mix}}}{A_{\text{SX}}} = 0.8147 + 1.7839 \times \frac{A_{SY}}{A_{SX}}$$

Using the *y*-intercept, the concentration of MnO_4^- is

$$\frac{C_X}{C_{SX}} = 0.8147 = \frac{[MnO_4^-]}{1.0 \times 10^{-4}\ \text{M}\ MnO_4^-}$$

or 8.15×10^{-5} M MnO_4^-, and using the slope, the concentration of $Cr_2O_7^{2-}$ is

$$\frac{C_Y}{C_{SY}} = 1.7839 = \frac{[Cr_2O_7^{2-}]}{1.00 \times 10^{-4}\ \text{M}\ Cr_2O_7^{2-}}$$

or 1.78×10^{-4} M $Cr_2O_7^{2-}$.

QUALITATIVE APPLICATIONS

As discussed in Chapter 10.2, ultraviolet, visible, and infrared absorption bands result from the absorption of electromagnetic radiation by specific valence electrons or bonds. The energy at which the absorption occurs, and the intensity of that absorption, is determined by the chemical environment of the absorbing moiety. For example, benzene has several ultraviolet absorption bands due to $\pi \rightarrow \pi^*$ transitions. The position and intensity of two of these bands, 203.5 nm (ε = 7400 M^{-1} cm^{-1}) and 254 nm (ε = 204 M^{-1} cm^{-1}), are sensitive to substitution. For benzoic acid, in which a carboxylic acid group replaces one of the aromatic hydrogens, the two bands shift to 230 nm (ε = 11600 M^{-1} cm^{-1}) and 273 nm (ε = 970 M^{-1} cm^{-1}). A variety of rules have been developed to aid in correlating UV/Vis absorption bands to chemical structure. Similar correlations are available for infrared absorption bands. For example a carbonyl's C=O stretch is sensitive to adjacent functional groups, appearing at 1650 cm^{-1} for acids, 1700 cm^{-1} for ketones, and 1800 cm^{-1} for acid chlorides. The interpretation of UV/ Vis and IR spectra receives adequate coverage elsewhere in the chemistry curriculum, notably in organic chemistry, and is not considered further in this text.

With the availability of computerized data acquisition and storage it is possible to build digital libraries of standard reference spectra. The identity of an a unknown compound often can be determined by comparing its spectrum against a library of reference spectra, a process known as ***spectral searching***. Comparisons are made using an algorithm that calculates the cumulative difference between the sample's spectrum and a reference spectrum. For example, one simple algorithm uses the following equation

$$D = \sum_{i=1}^{n} |(A_{sample})_i - (A_{reference})_i|$$

where D is the cumulative difference, A_{sample} is the sample's absorbance at wavelength or wavenumber i, $A_{reference}$ is the absorbance of the reference compound at the same wavelength or wavenumber, and n is the number of digitized points in the spectra. The cumulative difference is calculated for each reference spectrum. The reference compound with the smallest value of D is the closest match to the unknown compound. The accuracy of spectral searching is limited by the number and type of compounds included in the library, and by the effect of the sample's matrix on the spectrum.

Another advantage of computerized data acquisition is the ability to subtract one spectrum from another. When coupled with spectral searching it is possible to determine the identity of several components in a sample without the need of a prior separation step by repeatedly searching and sub- tracting reference spectra. An example is shown in Figure 10.3.13 in which the composition of a two-component mixture is determined by successive searching and subtraction. Figure 10.3.13 a shows the spectrum of the mixture. A search of the spectral library selects cocaine•HCl (Figure 10.3.13 b) as a likely component of the mixture. Subtracting the reference spectrum for cocaine•HCl from the mixture's spectrum leaves a result (Figure 10.3.13 c) that closely matches mannitol's reference spectrum (Figure 10.3.13 d). Subtracting the reference spectrum for mannitol leaves a small residual signal (Figure 10.3.13 e).

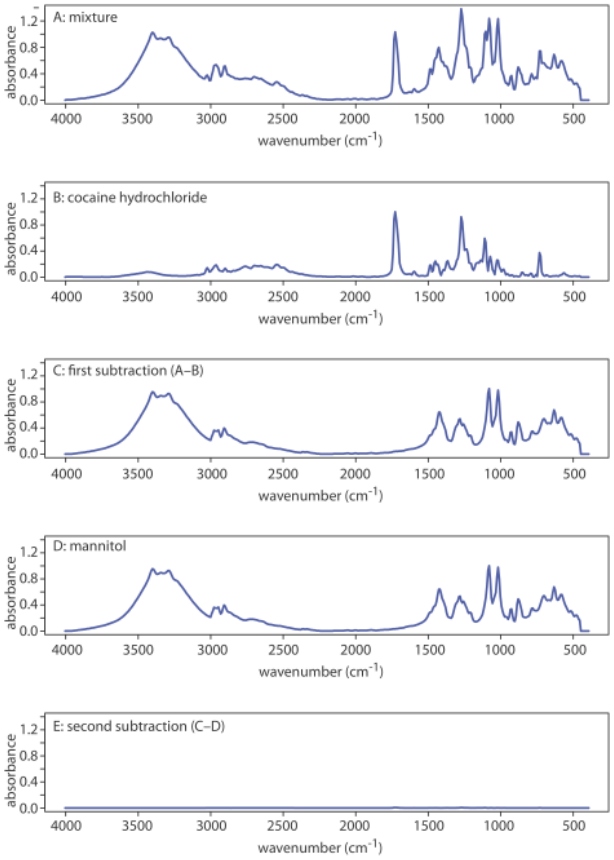


Figure 10.3.13 . Identifying the components of a mixture by spectral searching and subtracting. (a) IR spectrum of the mixture; (b) Reference IR spectrum of cocaine•HCl; (c) Result of subtracting the spectrum of cocaine•HCl from the mixture's spectrum; (d) Reference IR spectrum of mannitol; and (e) The residual spectrum after removing mannitol's contribution to the mixture's spectrum. IR spectra traditionally are displayed using percent transmittance, %T, along the *y*-axis (for example, see Figure 10.2.2). Because absorbance—not percent transmittance—is a linear function of concentration, spectral searching and spectral subtraction, is easier to do when displaying absorbance on the *y*-axis.

CHARACTERIZATION APPLICATIONS

Molecular absorption, particularly in the UV/Vis range, has been used for a variety of different characterization studies, including determining the stoichiometry of metal–ligand complexes and determining equilibrium constants. Both of these examples are examined in

this section.

STOICHIOMETRY OF A METAL-LIGAND COMPLEX

We can determine the stoichiometry of the metal–ligand complexation reaction

$$\mathrm{M} + y\mathrm{L} \rightleftharpoons \mathrm{ML}_y$$

using one of three methods: the method of continuous variations, the mole-ratio method, and the slope-ratio method. Of these approaches, the ***method of continuous variations***, also called Job's method, is the most popular. In this method a series of solutions is prepared such that the total moles of metal and of ligand, n_{total}, in each solution is the same. If $(n_{\mathrm{M}})_i$ and $(n_{\mathrm{L}})_i$ are, respectively, the moles of metal and ligand in solution i, then

$$n_{\text{total}} = (n_{\mathrm{M}})_i + (n_{\mathrm{L}})_i$$

The relative amount of ligand and metal in each solution is expressed as the mole fraction of ligand, $(X_{\mathrm{L}})i$, and the mole fraction of metal, $(X_{\mathrm{M}})_i$,

$$(X_{\mathrm{L}})_i = \frac{(n_{\mathrm{L}})_i}{n_{\text{total}}}$$

$$(X_M)_i = 1 - \frac{(n_{\mathrm{L}})_i}{n_{\text{total}}} = \frac{(n_{\mathrm{M}})_i}{n_{\text{total}}}$$

The concentration of the metal–ligand complex in any solution is determined by the limiting reagent, with the greatest concentration occurring when the metal and the ligand are mixed stoichiometrically. If we monitor the complexation reaction at a wavelength where only the metal–ligand complex absorbs, a graph of absorbance versus the mole fraction of ligand has two linear branches—one when the ligand is the limiting reagent and a second when the metal is the limiting reagent. The intersection of the two branches represents a stoichiometric mixing of the metal and the ligand. We use the mole fraction of ligand at the intersection to determine the value of y for the metal–ligand complex ML_y.

$$y = \frac{n_{\mathrm{L}}}{n_{\mathrm{M}}} = \frac{X_{\mathrm{L}}}{X_{\mathrm{M}}} = \frac{X_{\mathrm{L}}}{1 - X_{\mathrm{L}}}$$

> You also can plot the data as absorbance versus the mole fraction of metal. In this case, y is equal to $(1 - X_{\mathrm{M}})/X_{\mathrm{M}}$.

EXAMPLE 10.3.4

To determine the formula for the complex between Fe^{2+} and *o*-phenanthroline, a series of solutions is prepared in which the total concentration of metal and ligand is held constant at 3.15×10^{-4} M. The absorbance of each solution is measured at a wavelength of 510 nm. Using the following data, determine the formula for the complex.

X_{L}	absorbance	X_{L}	absorbance
0.000	0.000	0.600	0.693
0.100	0.116	0.700	0.809
0.200	0.231	0.800	0.693
0.300	0.347	0.900	0.347
0.400	0.462	1.000	0.000
0.500	0.578		

Solution

A plot of absorbance versus the mole fraction of ligand is shown in Figure 10.3.14 . To find the maximum absorbance, we extrapolate the two linear portions of the plot. The two lines intersect at a mole fraction of ligand of 0.75. Solving for y gives

$$y = \frac{X_L}{1 - X_L} = \frac{0.75}{1 - 0.75} = 3$$

The formula for the metal–ligand complex is $\mathrm{Fe(phen)}_3^{2+}$.

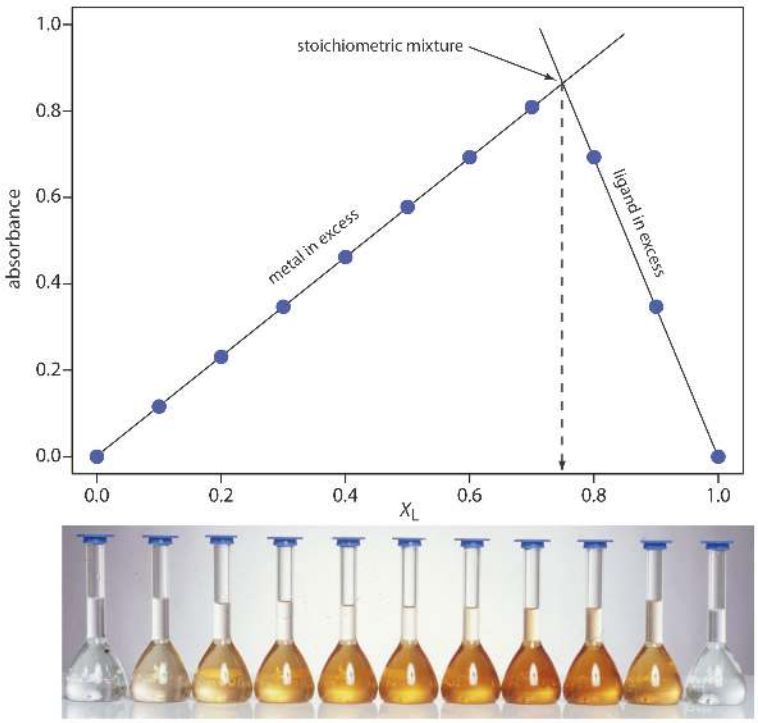


Figure 10.3.14 . Continuous variations plot for Example 10.3.4 . The photo shows the solutions used to gather the data. Each solution is displayed directly below its coresponding point on the continuous variations plot. To prepare these solutions I first prepared a solution of 3.15×10^{-4} M Fe^{2+} and a solution of 3.15×10^{-4} M *o*-phenanthroline. Because the two stock solutions have the same concentration, diluting a portion of one solution with the other solution gives a mixture in which the combined concentration of *o*-phenanthroline and Fe^{2+} is 3.15×10^{-4} M. Because each solution has the same volume, each solution also contains the same total moles of metal and ligand.

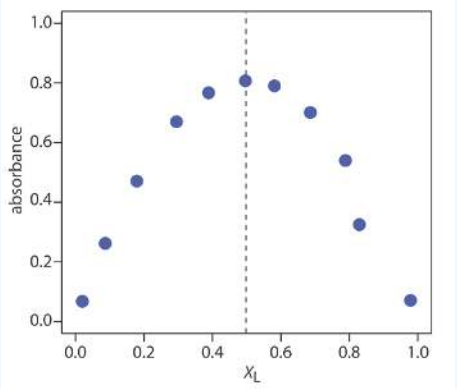
? EXERCISE 10.3.4

Use the continuous variations data in the following table to determine the formula for the complex between Fe^{2+} and SCN^{-}. The data for this problem is adapted from Meloun, M.; Havel, J.; Högfeldt, E. *Computation of Solution Equilibria*, Ellis Horwood: Chichester, England, 1988, p. 236.

X_L	absorbance	X_L	absorbance	X_L	absorbance	X_L	absorbance
0.0200	0.068	0.2951	0.670	0.5811	0.790	0.8923	0.324
0.0870	0.262	0.3887	0.767	0.6860	0.701	0.9787	0.071
0.1792	0.471	0.4964	0.807	0.7885	0.540		

Answer

The figure below shows a continuous variations plot for the data in this exercise. Although the individual data points show substantial curvature—enough curvature that there is little point in trying to draw linear branches for excess metal and excess ligand —the maximum absorbance clearly occurs at $X_L \approx 0.5$. The complex's stoichiometry, therefore, is $Fe(SCN)^{2+}$.



Several precautions are necessary when using the method of continuous variations. First, the metal and the ligand must form only one metal–ligand complex. To determine if this condition is true, plots of absorbance versus X_L are constructed at several different wavelengths and for several different values of n_{total}. If the maximum absorbance does not occur at the same value of X_L for each set of conditions, then more than one metal–ligand complex is present. A second precaution is that the metal–ligand complex's absorbance must obey Beer's law. Third, if the metal–ligand complex's formation constant is relatively small, a plot of absorbance versus X_L may show significant curvature. In this case it often is difficult to determine the stoichiometry by extrapolation. Finally, because the stability of a metal–ligand complex may be influenced by solution conditions, it is necessary to control carefully the composition of the solutions. When the ligand is a weak base, for example, each solutions must be buffered to the same pH.

In the ***mole-ratio method*** the moles of one reactant, usually the metal, is held constant, while the moles of the other reactant is varied. The absorbance is monitored at a wavelength where the metal–ligand complex absorbs. A plot of absorbance as a function of the ligand-to-metal mole ratio, n_L/n_M, has two linear branches that intersect at a mole–ratio corresponding to the complex's formula. Figure 10.3.15 a shows a mole-ratio plot for the formation of a 1:1 complex in which the absorbance is monitored at a wavelength where only the complex absorbs. Figure 10.3.15 b shows a mole-ratio plot for a 1:2 complex in which all three species—the metal, the ligand, and the complex—absorb at the selected wavelength. Unlike the method of continuous variations, the mole-ratio method can be used for complexation reactions that occur in a stepwise fashion if there is a difference in the molar absorptivities of the metal–ligand complexes, and if the formation constants are sufficiently different. A typical mole-ratio plot for the step-wise formation of ML and ML_2 is shown in Figure 10.3.15 c.

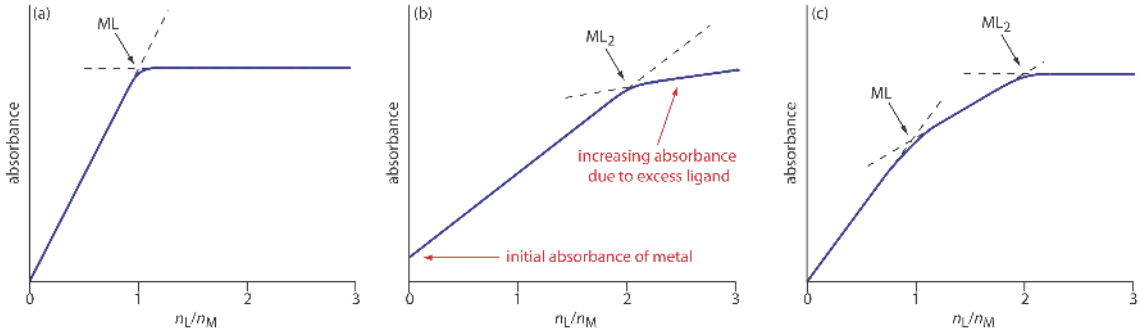


Figure 10.3.15 . Mole-ratio plots for: (a) a 1:1 metal–ligand complex in which only the complex absorbs; (b) a 1:2 metal–ligand complex in which the metal, the ligand, and the complex absorb; and (c) the stepwise formation of a 1:1 and a 1:2 metal–ligand complex.

For both the method of continuous variations and the mole-ratio method, we determine the complex's stoichiometry by extrapolating absorbance data from conditions in which there is a linear relationship between absorbance and the relative amounts of metal and ligand. If a metal–ligand complex is very weak, a plot of absorbance versus X_L or n_L/n_M becomes so curved that it is impossible to determine the stoichiometry by extrapolation. In this case the slope-ratio is used.

In the ***slope-ratio method*** two sets of solutions are prepared. The first set of solutions contains a constant amount of metal and a variable amount of ligand, chosen such that the total concentration of metal, C_M, is much larger than the total concentration of ligand, C_L. Under these conditions we may assume that essentially all the ligand reacts to form the metal–ligand complex. The concentration of the complex, which has the general form M_xL_y, is

$$[M_xL_y] = \frac{C_L}{y}$$

If we monitor the absorbance at a wavelength where only M_xL_y absorbs, then

$$A = \varepsilon b [M_xL_y] = \frac{\varepsilon b C_L}{y}$$

and a plot of absorbance versus C_L is linear with a slope, s_L, of

$$s_L = \frac{\varepsilon b}{y}$$

A second set of solutions is prepared with a fixed concentration of ligand that is much greater than a variable concentration of metal; thus

$$[M_xL_y] = \frac{C_M}{x}$$

$$A = \varepsilon b [M_xL_y] = \frac{\varepsilon b C_M}{x}$$

$$s_M = \frac{\varepsilon b}{x}$$

A ratio of the slopes provides the relative values of *x* and *y*.

$$\frac{s_{\mathrm{M}}}{s_{\mathrm{L}}} = \frac{\varepsilon b/x}{\varepsilon b/y} = \frac{y}{x}$$

An important assumption in the slope-ratio method is that the complexation reaction continues to completion in the presence of a sufficiently large excess of metal or ligand. The slope-ratio method also is limited to systems in which only a single complex forms and for which Beer's law is obeyed.

DETERMINATION OF EQUILIBRIUM CONSTANTS

Another important application of molecular absorption spectroscopy is the determination of equilibrium constants. Let's consider, as a simple example, an acid–base reaction of the general form

$$\mathrm{HIn}(aq) + \mathrm{H_2O}(l) \rightleftharpoons \mathrm{H_3O^+}(aq) + \mathrm{In^-}(aq)$$

where HIn and In^- are the conjugate weak acid and weak base forms of an acid–base indicator. The equilibrium constant for this reaction is

$$K_{\mathrm{a}} = \frac{\left[\mathrm{H_3O^+}\right]\left[\mathrm{A^-}\right]}{[\mathrm{HA}]}$$

To determine the equilibrium constant's value, we prepare a solution in which the reaction is in a state of equilibrium and determine the equilibrium concentration for H_3O^+, HIn, and In^-. The concentration of H_3O^+ is easy to determine by measuring the solution's pH. To determine the concentration of HIn and In^- we can measure the solution's absorbance.

If both HIn and In^- absorb at the selected wavelength, then, from Beer's law, we know that

$$A = \varepsilon_{\mathrm{Hln}} b[\mathrm{HIn}] + \varepsilon_{\mathrm{ln}} b[\mathrm{In^-}] \tag{6.5.5}$$

where $\varepsilon_{\mathrm{HIn}}$ and $\varepsilon_{\mathrm{In}}$ are the molar absorptivities for HIn and In^-. The indicator's total concentration, *C*, is given by a mass balance equation

$$C = [\mathrm{HIn}] + [\mathrm{In^-}] \tag{6.5.6}$$

Solving Equation 6.5.6 for [HIn] and substituting into Equation 6.5.5 gives

$$A = \varepsilon_{\mathrm{Hln}} b\left(C - \left[\mathrm{In^-}\right]\right) + \varepsilon_{\mathrm{ln}} b\left[\mathrm{In^-}\right]$$

which we simplify to

$$A = \varepsilon_{\mathrm{Hln}} bC - \varepsilon_{\mathrm{Hln}} b\left[\mathrm{In^-}\right] + \varepsilon_{\mathrm{ln}} b\left[\mathrm{In^-}\right]$$

$$A = A_{\mathrm{HIn}} + b\left[\mathrm{In^-}\right]\left(\varepsilon_{\mathrm{ln}} - \varepsilon_{\mathrm{HIn}}\right) \tag{6.5.7}$$

where A_{HIn}, which is equal to $\varepsilon_{\mathrm{HIn}} bC$, is the absorbance when the pH is acidic enough that essentially all the indicator is present as HIn. Solving Equation 6.5.7 for the concentration of In^- gives

$$\left[\mathrm{In^-}\right] = \frac{A - A_{\mathrm{Hln}}}{b\left(\varepsilon_{\mathrm{ln}} - \varepsilon_{\mathrm{HIn}}\right)} \tag{6.5.8}$$

Proceeding in the same fashion, we derive a similar equation for the concentration of HIn

$$[\mathrm{HIn}] = \frac{A_{\mathrm{In}} - A}{b\left(\varepsilon_{\mathrm{ln}} - \varepsilon_{\mathrm{Hln}}\right)} \tag{6.5.9}$$

where A_{In}, which is equal to $\varepsilon_{\mathrm{In}} bC$, is the absorbance when the pH is basic enough that only In^- contributes to the absorbance. Substituting Equation 6.5.8 and Equation 6.5.9 into the equilibrium constant expression for HIn gives

$$K_a = \frac{[\mathrm{H_3O^+}][\mathrm{In^-}]}{[\mathrm{HIn}]} = [\mathrm{H_3O^+}] \times \frac{A - A_{\mathrm{HIn}}}{A_{\mathrm{In}} - A} \tag{6.5.10}$$

We can use Equation 6.5.10 to determine K_{a} in one of two ways. The simplest approach is to prepare three solutions, each of which contains the same amount, *C*, of indicator. The pH of one solution is made sufficiently acidic such that [HIn] >> [In^-]. The absorbance of this solution gives A_{HIn}. The value of A_{In} is determined by adjusting the pH of the second solution such that [In^-] >> [HIn]. Finally, the pH of the third solution is adjusted to an intermediate value, and the pH and absorbance, *A*, recorded. The value of K_{a} is calculated using Equation 6.5.10.

✔ EXAMPLE 10.3.5

The acidity constant for an acid–base indicator is determined by preparing three solutions, each of which has a total concentration of indicator equal to 5.00×10^{-5} M. The first solution is made strongly acidic with HCl and has an absorbance of 0.250. The second solution is made strongly basic and has an absorbance of 1.40. The pH of the third solution is 2.91 and has an absorbance of 0.662. What is the value of K_a for the indicator?

Solution

The value of K_a is determined by making appropriate substitutions into 10.20 where $[H_3O^+]$ is 1.23×10^{-3}; thus

$$K_a = \left(1.23 \times 10^{-3}\right) \times \frac{0.662 - 0.250}{1.40 - 0.662} = 6.87 \times 10^{-4}$$

EXERCISE 10.3.5

To determine the K_a of a merocyanine dye, the absorbance of a solution of 3.5×10^{-4} M dye was measured at a pH of 2.00, a pH of 6.00, and a pH of 12.00, yielding absorbances of 0.000, 0.225, and 0.680, respectively. What is the value of K_a for this dye? The data for this problem is adapted from Lu, H.; Rutan, S. C. *Anal. Chem.*, **1996**, *68*, 1381–1386.

Answer

The value of K_a is

$$K_a = \left(1.00 \times 10^{-6}\right) \times \frac{0.225 - 0.000}{0.680 - 0.225} = 4.95 \times 10^{-7}$$

A second approach for determining K_a is to prepare a series of solutions, each of which contains the same amount of indicator. Two solutions are used to determine values for A_{HIn} and A_{In}. Taking the log of both sides of Equation 6.5.10 and rearranging leave us with the following equation.

$$\log \frac{A - A_{HIn}}{A_{In^-} - A} = \text{pH} - \text{p}K_a \tag{6.5.11}$$

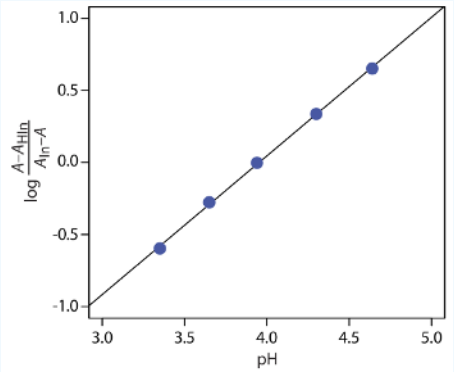
A plot of $\log[(A - A_{HIn})/(A_{In} - A)]$ versus pH is a straight-line with a slope of +1 and a *y*-intercept of $-\text{p}K_a$.

EXERCISE 10.3.6

To determine the K_a for the indicator bromothymol blue, the absorbance of each a series of solutions that contain the same concentration of bromothymol blue is measured at pH levels of 3.35, 3.65, 3.94, 4.30, and 4.64, yielding absorbance values of 0.170, 0.287, 0.411, 0.562, and 0.670, respectively. Acidifying the first solution to a pH of 2 changes its absorbance to 0.006, and adjusting the pH of the last solution to 12 changes its absorbance to 0.818. What is the value of K_a for bromothymol blue? The data for this problem is from Patterson, G. S. *J. Chem. Educ.*, **1999**, *76*, 395–398.

Answer

To determine K_a we use Equation 6.5.11, plotting $\log[(A - A_{HIn})/(A_{In} - A)]$ versus pH, as shown below.



Fitting a straight-line to the data gives a regression model of

$$\log \frac{A - A_{HIn}}{A_{In} - A} = -3.80 + 0.962\text{pH}$$

The *y*-intercept is $-\text{p}K_a$; thus, the $\text{p}K_a$ is 3.80 and the K_a is 1.58×10^{-4}.

In developing these approaches for determining K_a we considered a relatively simple system in which the absorbance of HIn and In^- are easy to measure and for which it is easy to determine the concentration of H_3O^+. In addition to acid–base reactions, we can adapt these approaches to any reaction of the general form

$$X(aq) + Y(aq) \rightleftharpoons Z(aq)$$

including metal–ligand complexation reactions and redox reactions, provided we can determine spectrophotometrically the concentration of the product, *Z*, and one of the reactants, either *X* or *Y*, and that we can determine the concentration of the other reactant by some other method. With appropriate modifications, a more complicated system in which we cannot determine the concentration of one or more of the reactants or products also is possible [Ramette, R. W. *Chemical Equilibrium and Analysis*, Addison-Wesley: Reading, MA, 1981, Chapter 13].

EVALUATION OF UV/VIS AND IR SPECTROSCOPY

SCALE OF OPERATIONS

Molecular UV/Vis absorption routinely is used for the analysis of trace analytes in macro and meso samples. Major and minor analytes are determined by diluting the sample before analysis, and concentrating a sample may allow for the analysis of ultratrace analytes. The scale of operations for infrared absorption is generally poorer than that for UV/Vis absorption.

ACCURACY

Under normal conditions a relative error of 1–5% is easy to obtained with UV/Vis absorption. Accuracy usually is limited by the quality of the blank. Examples of the type of problems that are encountered include the pres- ence of particulates in the sample that scatter radiation, and the presence of interferents that react with analytical reagents. In the latter case the interferent may react to form an absorbing species, which leads to a positive determinate error. Interferents also may prevent the analyte from reacting, which leads to a negative determinate error. With care, it is possible to improve the accuracy of an analysis by as much as an order of magnitude.

PRECISION

In absorption spectroscopy, precision is limited by indeterminate errors—primarily instrumental noise—which are introduced when we measure absorbance. Precision generally is worse for low absorbances where $P_0 \approx P_T$, and for high absorbances where P_T approaches 0. We might expect, therefore, that precision will vary with transmittance.

We can derive an expression between precision and transmittance by applying the propagation of uncertainty as described in Chapter 4. To do so we rewrite Beer's law as

$$C = -\frac{1}{\varepsilon b}\log T \tag{6.5.12}$$

Table 4.3.1 in Chapter 4 helps us complete the propagation of uncertainty for Equation 6.5.12; thus, the absolute uncertainty in the concentration, s_C, is

$$s_c = -\frac{0.4343}{\varepsilon b} \times \frac{s_T}{T} \tag{6.5.13}$$

where s_T is the absolute uncertainty in the transmittance. Dividing Equation 6.5.13 by Equation 6.5.12 gives the relative uncertainty in concentration, s_C/C, as

$$\frac{s_c}{C} = \frac{0.4343 s_T}{T \log T}$$

If we know the transmittance's absolute uncertainty, then we can determine the relative uncertainty in concentration for any measured transmittance.

Determining the relative uncertainty in concentration is complicated because s_T is a function of the transmittance. As shown in Table 10.3.3 , three categories of indeterminate instrumental error are observed [Rothman, L. D.; Crouch, S. R.; Ingle, J. D. Jr. *Anal. Chem.* **1975**, *47*, 1226–1233]. A constant s_T is observed for the uncertainty associated with reading $\%T$ on a meter's analog or digital scale. Typical values are ±0.2–0.3% (a k_1 of ±0.002–0.003) for an analog scale and ±0.001% a (k_1 of ±0.00001) for a digital scale.

Table 10.3.3 . Effect of Indeterminate Errors on Relative Uncertainty in Concentration

category	sources of indeterminate error	relative uncertainty in concentration
$s_T = k_1$	%T readout resolution noise in thermal detectors	$\frac{s_C}{C} = \frac{0.4343 k_1}{T \log T}$
$s_T = k_2 \sqrt{T^2 + T}$	noise in photon detectors	$\frac{s_C}{C} = \frac{0.4343 k_2}{\log T} \sqrt{1 + \frac{1}{T}}$
$s_T = k_3 T$	positioning of sample cell fluctuations in source intensity	$\frac{s_C}{C} = \frac{0.4343 k_3}{\log T}$

A constant s_T also is observed for the thermal transducers used in infrared spectrophotometers. The effect of a constant s_T on the relative uncertainty in concentration is shown by curve A in Figure 10.3.16 . Note that the relative uncertainty is very large for both high absorbances and low absorbances, reaching a minimum when the absorbance is 0.4343. This source of indeterminate error is important for infrared spectrophotometers and for inexpensive UV/Vis spectrophotometers. To obtain a relative uncertainty in concentration of ±1–2%, the absorbance is kept within the range 0.1–1.

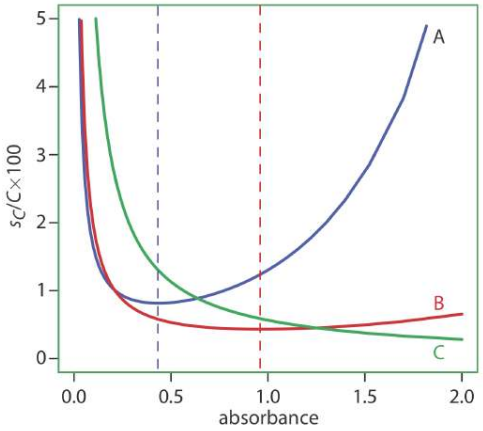


Figure 10.3.16 . Percent relative uncertainty in concentration as a function of absorbance for the categories of indeterminate errors in Table 6.5.10.3. A: k_1 = ±0.0030; B: k_2 = ±0.0030; and C: k_3= ±0.0130. The dashed lines correspond to the minimum uncertainty for curve A (absorbance of 0.4343) and for curve B (absorbance of 0.963).

Values of s_T are a complex function of transmittance when indeterminate errors are dominated by the noise associated with photon detectors. Curve B in Figure 10.3.16 shows that the relative uncertainty in concentration is very large for low absorbances, but is smaller at higher absorbances. Although the relative uncertainty reaches a minimum when the absorbance is 0.963, there is little change in the relative uncertainty for absorbances between 0.5 and 2. This source of indeterminate error generally limits the precision of high quality UV/Vis spectrophotometers for mid-to-high absorbances.

Finally, the value of s_T is directly proportional to transmittance for indeterminate errors that result from fluctuations in the source's intensity and from uncertainty in positioning the sample within the spectrometer. The latter is particularly important because the optical properties of a sample cell are not uniform. As a result, repositioning the sample cell may lead to a change in the intensity of transmitted radiation. As shown by curve C in Figure 10.3.16 , the effect is important only at low absorbances. This source of indeterminate errors usually is the limiting factor for high quality UV/Vis spectrophotometers when the absorbance is relatively small.

When the relative uncertainty in concentration is limited by the %T readout resolution, it is possible to improve the precision of the analysis by redefining 100% T and 0% T. Normally 100% T is established using a blank and 0% T is established while preventing the source's radiation from reaching the detector. If the absorbance is too high, precision is improved by resetting 100% T using a standard solution of analyte whose concentration is less than that of the sample (Figure 10.3.17 a). For a sample whose absorbance is too low, precision is improved by redefining 0% T using a standard solution of the analyte whose concentration is greater than that of the analyte (Figure 10.3.17 b). In this case a calibration curve is required because a linear relationship between absorbance and concentration no longer exists. Precision is further increased by combining these two methods (Figure 10.3.17 c). Again, a calibration curve is necessary since the relation- ship between absorbance and concentration is no longer linear.

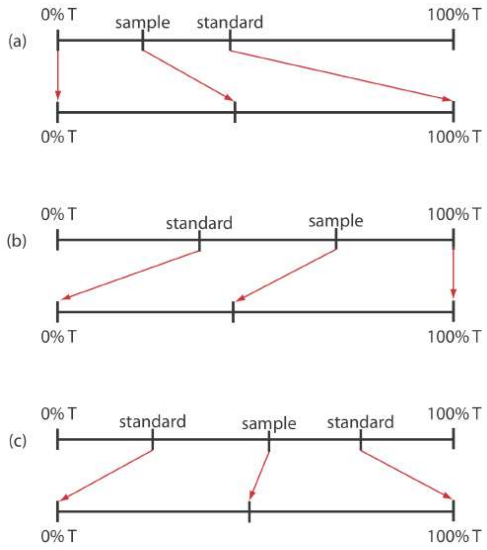


Figure 10.3.17 . Methods for improving the precision of absorption methods: (a) high-absorbance method; (b) low-absorbance method; (c) maximum precision method.

SENSITIVITY

The sensitivity of a molecular absorption method, which is the slope of a Beer's law calibration curve, is the product of the analyte's absorptivity and the pathlength of the sample cell (εb). You can improve a method's sensitivity by selecting a wavelength where absorbance is at a maximum or by increasing pathlength.

> See Figure 10.2.10 for an example of how the choice of wavelength affects a calibration curve's sensitivity.

SELECTIVITY

Selectivity rarely is a problem in molecular absorption spectrophotometry. In many cases it is possible to find a wavelength where only the analyte absorbs. When two or more species do contribute to the measured absorbance, a multicomponent analysis is still possible, as shown in Example 10.3.2 and Example 10.3.3 .

TIME, COST, AND EQUIPMENT

The analysis of a sample by molecular absorption spectroscopy is relatively rapid, although additional time is required if we need to convert a nonabsorbing analyte into an absorbing form. The cost of UV/Vis instrumentation ranges from several hundred dollars for a simple filter photometer, to more than $50,000 for a computer-controlled, high-resolution double-beam instrument equipped with variable slit widths, and operating over an extended range of wavelengths. Fourier transform infrared spectrometers can be obtained for as little as $15,000–$20,000, although more expensive models are available.

This page titled 6.5: UV/Vis and IR Spectroscopy is shared under a CC BY-NC-SA 4.0 license and was authored, remixed, and/or curated by David Harvey.

- **10.3: UV/Vis and IR Spectroscopy** by David Harvey is licensed CC BY-NC-SA 4.0.

SECTION OVERVIEW

6.6: Signals and Noise

When we try to calibrate an analytical method or to optimize an analytical system, our ability to do so successfully is limited by the uncertainty, or noise, in our measurements and by background signals that interfere with our ability to measure the signal of interest to us. In this chapter we will consider how we characterize noise, example of sources of noise, and ways to clean up our data by decreasing the contribution of noise to our measurements and by correcting for the presence of background signals.

6.6.1: The Signal-to-Noise Ratio

6.6.2: Sources of Instrumental Noise

6.6.3: Signal-to-Noise Enhancement

This page titled 6.6: Signals and Noise is shared under a CC BY-NC-SA 4.0 license and was authored, remixed, and/or curated by David Harvey.

6.6.1: The Signal-to-Noise Ratio

When we make a measurement it is the sum of two parts, a determinate, or fixed contribution that arises from the analyte and an indeterminate, or random, contribution that arises from uncertainty in the measurement process. We call the first of these the signal and we call the latter the noise. There are two broad categories of noise: that associated with obtaining samples and that associated with making measurements. Our interest here is in the latter.

What is Noise?

Noise is a random event characterized by a mean and standard deviation. There are many types of noise, but we will limit ourselves for now to noise that is stationary, in that its mean and its standard deviation are independent of time, and that is heteroscedastic, in that its mean and its variance (and its standard deviation) are independent of the signal's magnitude. Figure $6.6.1.1a$ shows an example of a noisy signal that meets these criteria. The *x*-axis here is shown as time—perhaps a chromatogram—but other units, such as wavelength (spectroscopy) or potential (electrochemistry), are possible. Figure $6.6.1.1b$ shows the underlying noise and Figure $6.6.1.1c$ shows the underlying signal. Note that the noise in Figure $6.6.1.1b$ appears consistent in its central tendency (mean) and its spread (variance) along the *x*-axis and is independent of the signal's strength.

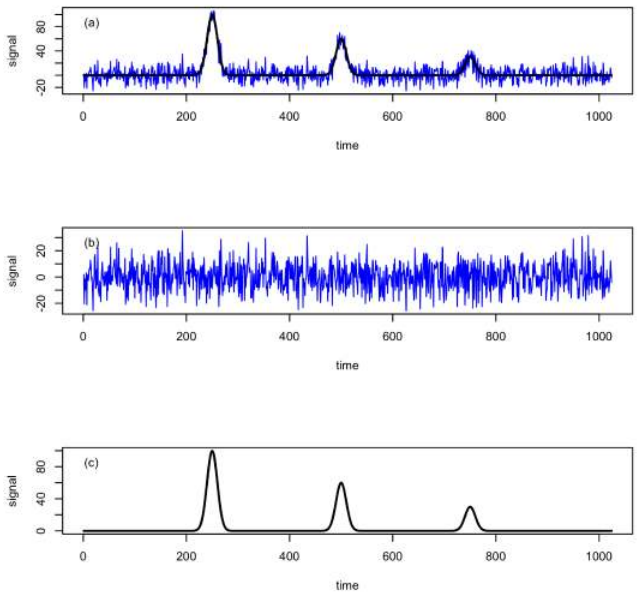


Figure 6.6.1.1: Plots showing (a) the signal and the noise in blue with the signal superimposed as a smooth line; (b) the noise only; and (c) the signal only. The signal consists of three peaks at times of 250, 500, and 750, and with maximum values of 100, 60, and 30, respectively. The noise is drawn at random from a normal distribution with a mean of 0 and a standard deviation of 10.

How Do We Characterize the Signal and the Noise?

Although we characterize noise by its mean and its standard deviation, the most important benchmark is the signal-to-noise ratio, S/N, which we define as

$$S/N = \frac{S_{\text{analyte}}}{s_{\text{noise}}}$$

where S_{analyte} is the signal's value at particular location on the *x*-axis and s_{noise} is the standard deviation of the noise using a signal-free portion of the data. As general rules-of-thumb, we can measure the signal with some confidence when $S/N \geq 3$ and we can detect the signal with some confidence when $3 \geq S/N \geq 2$. For the data in Figure $6.6.1.1$, and using the information in the figure caption, the signal-to-noise ratios are, from left-to-right, 10, 6, and 3.

Note

To measure the signal with confidence implies we can use the signal's value in a calculation, such as constructing a calibration curve. To detect the signal with confidence means we are certain that a signal is present (and that an analyte responsible for the signal is present) even if we cannot measure the signal with sufficient confidence to allow for a meaningful calculation.

This page titled 6.6.1: The Signal-to-Noise Ratio is shared under a CC BY-NC-SA 4.0 license and was authored, remixed, and/or curated by David Harvey.

- **5.1: The Signal-to-Noise Ratio** by David Harvey is licensed CC BY-NC-SA 4.0.

6.6.2: Sources of Instrumental Noise

When we make an analytical measurement, we are interested in both the accuracy and the precision of our results. Noise, as we learned in the previous section, is a random fluctuation in the signal that limits our ability to detect the presence of the underlying signal. There are a variety of ways in which noise can enter into our measurements. Some of these sources of noise are related to the process of collecting and processing samples for analysis; these sources of noise, which we might collectively call chemical sources of noise, are important and receive consideration in those sections of this textbook that consider the application of analytical methods. In this chapter, we will limit ourselves to considering sources of noise that arise from the instruments we use to make measurements. We call these sources of instrumental noise.

Thermal Noise

Even when an external voltage is not applied to an electrical circuit, a small current is present due to the random motion of electrons that arises from the temperature of the surroundings; we can this thermal (or, sometimes, Johnson) noise. The magnitude of this noise in any electrical element increases with temperature, of course, but it also is affected by its resistance, and by how quickly it responds to a change in the signal. Mathematically, we express this as the root-mean-square voltage, ν_{rms}, which is given as

$$\nu_{\text{rms}} = \sqrt{4kTR\Delta f} \tag{6.6.2.1}$$

where k is Boltzmann's constant, T is the temperature in Kelvin, R is the resistance in ohms, and Δf is the bandwidth. The latter term is a measure of how quickly the electrical element responds to a change in its input by changing its output from 10% to 90% of its final value, which is called the rise time, t_r, where

$$\Delta f = \frac{1}{3t_r}$$

For example, if a change in the input increases the output by 1, then the rise time is how long it takes the output to increase from 0.1 to 0.9.

A close look at Equation 6.6.2.1 shows that we can reduce thermal noise by decreasing the temperature, by decreasing the resistance of the electrical circuit, and by decreasing the bandwidth; the latter, of course, comes at the cost of an increase in the response time, which means the instrument responds more slowly to a change in the signal. Of these, it is often easiest to reduce the temperature by cooling, for example, the instrument's detector.

Shot Noise

As its name implies, shot noise is a discrete event that happens in response to an event, such as the movement of an electron through the space between two surfaces of opposite charge. These events are random and quantized, and generate random furcations in the current that have a root-mean-square value, i_{rms}, which is given by

$$i_{\text{rms}} = \sqrt{2Ie\Delta f} \tag{6.6.2.2}$$

where I is the average current, e is the charge on the electron in Coulombs, and Δf is the bandwidth. Of these terms, the only one under our control is the bandwidth; again, decreasing the bandwidth comes at the cost of an instrument that responds more slowly to a change in the signal.

Flicker Noise

Unlike thermal noise or shot noise, flicker noise is related to the frequency of the signal being measured, f, instead of the signal's bandwidth. The sources of flicker noise are not well understood, but it is known that it is inversely proportional to the signal's frequency; thus, flicker noise is sometimes called $1/f$ noise. Because of the inverse relationship, flicker noise is more important at low frequencies, where it appears as a long-term drift in the signal. It is less important at higher frequencies where thermal noise and shot noise are more important.

Environmental Noise

Our instruments normally do not operate in an environment free from external signals, each of which has a frequency that can be picked up by the instrument. Television signals, cell-phone signals, radio signals, power lines are obvious examples of high-to-

moderate frequencies that can serve as noise. Less obvious are lower frequency sources of noise, such as the change in temperature during the day or through the year.

This page titled 6.6.2: Sources of Instrumental Noise is shared under a CC BY-NC-SA 4.0 license and was authored, remixed, and/or curated by David Harvey.

- **5.2: Sources of Instrumental Noise** by David Harvey is licensed CC BY-NC-SA 4.0.

6.6.3: Signal-to-Noise Enhancement

There are two broad approaches we can use to improve the signal-to-noise ratio: hardware and software. Hardware approaches are built into the instrument and include decisions on how the instrument is set-up for making measurements (for example, the choice of a scan rate or a slit width), and how the signal is processed by the instrument (for example, using electronic filters). A few approaches are briefly considered here; others are included with the discussion of individual instruments. Software solutions are computational approaches in which we manipulate the data either while we are collecting it or after data acquisition is complete.

Hardware Solutions

One way to reduce noise is to focus on the circuitry, or hardware, used to measure the signal.

Shielding

One way to reduce environmental noise is to prevent it from entering into the instrument's electronic circuitry. One approach is to use a Faraday cage in which the instrument sits within a room or space covered with a conductive material. Electromagnetic radiation from the environment is absorbed by the conductive material and then shunted away to the ground. Rather than encasing the entire instrument in a Faraday cage, particularly sensitive portions of the circuitry can be shielded.

Differential Amplifier

A difference amplifier (see Chapter 3) is an electrical circuit used to determine the difference between two input voltages or currents and to return that difference as a larger voltage or current. As the magnitude of the noise in the two input signals is generally similar in value—that is, it is in phase—while the signal of interest is not, much of the noise's contribution to the signal is subtracted out.

Filtering

When the frequency of the noise is quite different from the frequency of the signal, a simple electrical circuit can be used to remove the high frequency noise and pass the low frequency signal; this is called a low-pass filter. See Chapter 2 for details on low-pass filters.

Modulation

When the signal of interest has a low frequency, the effect of flicker noise becomes significant because a technique that removes low frequency noise will remove the signal as well. Modulation is a process of increasing the frequency of the signal. When complete, a high-pass filter is used to remove the noise. Reversing the modulation returns the original signal, but with much of the noise removed.

Software Solutions

In this section we will consider three common computational tools for improving the signal-to-noise ratio: signal averaging, digital smoothing, and Fourier filtering.

Signal Averaging

The most important difference between the signal and the noise is that a signal is determinate (fixed in value) and the noise is indeterminate (random in value). If we measure a pure signal several times, we expect its value to be the same each time; thus, if we add together *n* scans, we expect that the net signal, S_n, is defined as

$$S_n = nS$$

where S is the signal for a single scan. Because noise is random, its value varies from one run to the next, sometimes with a value that is larger and sometimes with a value that is smaller, and sometimes with a value that is positive and sometimes with a value that is negative. On average, the standard deviation of the noise increases as we make more scans, but it does so at a slower rate than for the signal

$$s_n = \sqrt{n}s$$

where s is the standard deviation for a single scan and s_n is the standard deviation after *n* scans. Combining these two equations, shows us that the signal-to-noise ratio, S/N, after *n* scans increases as

$$(S/N)_n = \frac{S_n}{s_n} = \frac{nS}{\sqrt{n}s} = \sqrt{n}(S/N)_{n=1}$$

where $(S/N)_{n=1}$ is the signal-to-noise ratio for the initial scan. Thus, when $n = 4$ the signal-to-noise ratio improves by a factor of 2, and when $n = 16$ the signal-to-noise ratio increases by a factor of 4. Figure $6.6.3.1$ shows the improvement in the signal-to-noise ratio for 1, 2, 4, and 8 scans.

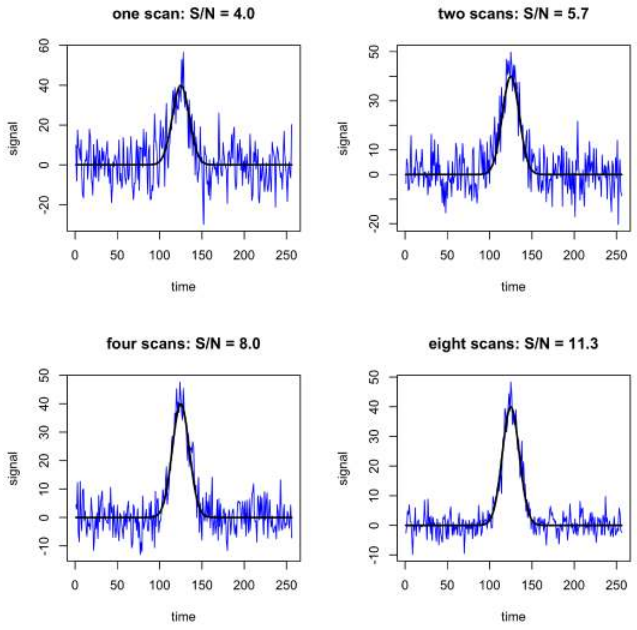


Figure 6.6.3.1: Improvement in the signal-to-noise ratio through signal averaging using 1, 2, 4, and 8 scans. Each plot shows the noisy signal in blue with the pure signal superimposed in black. The total signal is divided by the number of scans so that each *y*-axis has the same scale.

Signal averaging works well when the time it takes to collect a single scan is short and when the analyte's signal is stable with respect to time both because the sample is stable and the instrument is stable; when this is not the case, then we risk a time-dependent change in S_{analyte} and/or s_{noise} Because the equation for $(S/N)_n$ is proportional to the $\sqrt{n}$, the relative improvement in the signal-to-noise ratio decreases as n increases; for example, 16 scans gives a $4\times$ improvement in the signal-to-noise ratio, but it takes an additional 48 scans (for a total of 64 scans) to achieve a $8\times$ improvement in the signal-to-noise ratio.

Digital Smoothing Filters

One characteristic of noise is that its magnitude fluctuates rapidly in contrast to the underlying signal. We see this, for example, in Figure $6.6.3.1$ where the underlying signal either remains constant or steadily increases or decreases while the noise fluctuates chaotically. Digital smoothing filters take advantage of this by using a mathematical function to average the data for a small range of consecutive data points, replacing the range's middle value with the average signal over that range.

Moving Average Filters

For a moving average filter, also called a boxcar filter, we replace each point by the average signal for that point and an equal number of points on either side; thus, a moving average filter has a width, w, of 3, 5, 7, ... points. For example, suppose the first five points in a sequence are

0.80	0.30	0.80	0.20	1.00

then a three-point moving average $(w = 3)$ returns values of

NA	0.63	0.43	0.67	NA

where, for example, 0.63 is the average of 0.80, 0.30, and 0.80. Note that we lose $(w-1)/2 = (3-1)/2 = 1$ points at each end of the data set because we do not have a sufficient number of data points to complete a calculation for the first and the last point.

Figure 6.6.3.2shows the improvement in the S/N ratio when using moving average filters with widths of 5, 9, and 13.

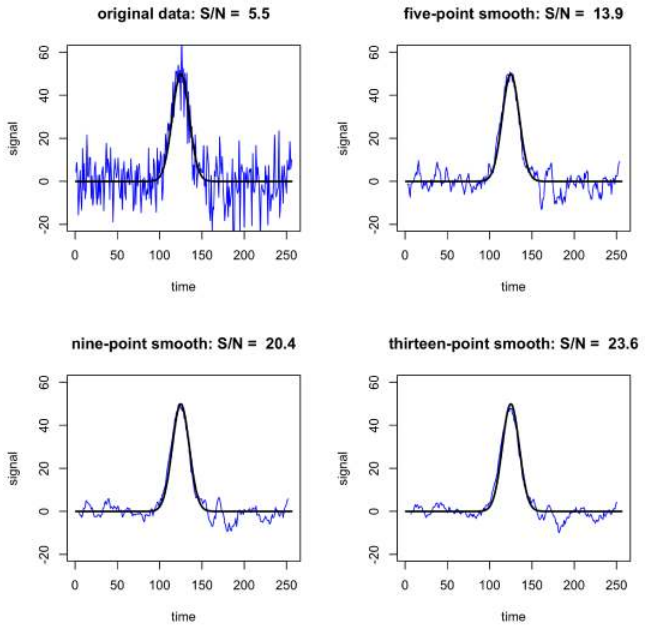


Figure 6.6.3.2: Improvement in the signal-to-noise ratio using moving average filters with ranges of 5, 9, and 13 on the original data shown in the upper left quadrant. Each plot shows the noisy signal in blue with the pure signal superimposed in black.

One limitation to a moving average filter is that it distorts the original data by removing points from both ends, although this is not a serious concern if the points in question are just noise. Of greater concern is the distortion in a signal's height if we use a range that is too wide; for example, Figure 6.6.3.3 shows how a 23-point moving average filter (shown in blue) applied to the noisy signal in the upper left quadrant of Figure 6.6.3.2 reduces the height of the original signal (shown in black). Because the filter's width—shown by the red bar—is similar to the peak's width, as the filter passes through the peak it systematically reduces the signal by averaging together values that are mostly smaller than the maximum signal.

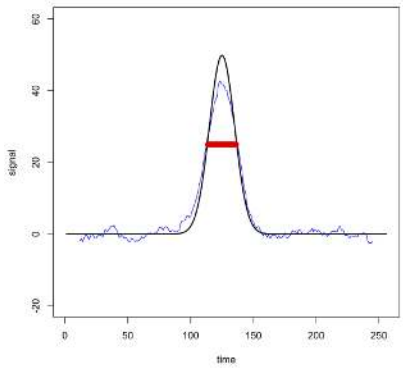


Figure 6.6.3.3: Example that shows how a moving average filter can distort the signal when applied to the noisy signal in the upper left quadrant of Figure 6.6.3.2. The original pure signal is shown in black and the signal after applying a 23-point moving average filter is shown in blue. The width of the moving average filter is shown by the red bar.

Savitzky-Golay Filters

A moving average filter weights all points equally; that is, points near the edges of the filter contribute to the average as a level equal to points near the filter's center. A Savitzky-Golay filter uses a polynomial model that weights each point differently, placing more weight on points near the center of the filter and less weight on points at the edge of the filter. Specific values depend on the size of the window and the polynomial model; for example, a five-point filter using a second-order polynomial has weights of

$$-3/35 \qquad 12/35 \qquad 17/35 \qquad 12/35 \qquad -3/35$$

For example, suppose the first five points in a sequence are

0.80	0.30	0.80	0.20	1.00

then this Savitzky-Golay filter returns values of

NA	NA	0.41	NA	NA

where, for example, the value for the middle point is

$$0.80 \times \frac{-3}{35} + 0.30 \times \frac{12}{35} + 0.80 \times \frac{17}{35} + 0.20 \times \frac{12}{35} + 1.00 \times \frac{-3}{35} = 0.406 \approx 0.41$$

Note that we lose $(w-1)/2 = (5-1)/2 = 2$ points at each end of the data set, where w is the filter's range, because we do not have a sufficient number of data points to complete the calculations. For other Savitzky-Golay smoothing filters, see Savitzky, A.; Golay, M. J. E. *Anal Chem*, **1964**, *36*, 1627-1639. Figure 6.6.3.4 shows the improvement in the S/N ratio when using Savitzky-Golay filters using a second-order polynomial with 5, 9, and 13 points.

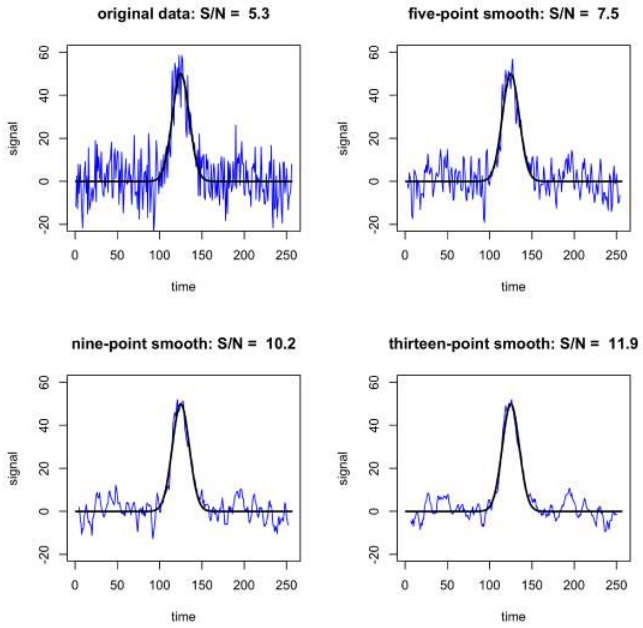


Figure 6.6.3.4: Improvement in the signal-to-noise ratio using Savitzky-Golay filters of ranges of 5, 9, and 13 on the original data shown in the upper left quadrant. Each plot shows the noisy signal in blue with the pure signal superimposed in black.

Because a Savitzky-Golay filter weights points differently than does a moving average smoothing filter, a Savitzky-Golay filter introduces less distortion to the signal, as we see in the following figure.

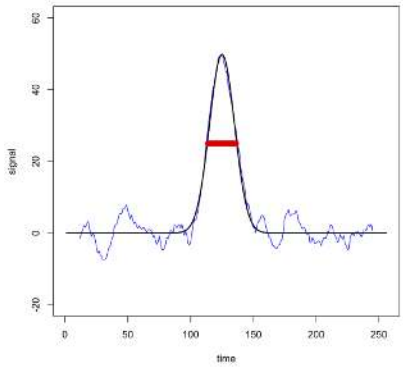


Figure 6.6.3.5: A Savitzky-Golay filter is less aggressive than a moving average filter. Applying a 23-point Savitzky-Golay filter to the noisy signal in the upper left quadrant of Figure 6.6.3.4 results in little distortion of the signal. Contrast this with Figure 6.6.3.3 where a 23-point moving average filter results in substantial distortion of the signal. The original pure signal is shown in black and the signal after applying a 23-point Savitzky-Golay filter is shown in blue. The width of the Savitzky-Golay filter is shown by the red bar.

Fourier Filtering

This approach to improving the signal-to-noise ratio takes advantage of a mathematical technique called a Fourier transform (FT). The basis of a Fourier transform is that we can express a signal in two separate domains. In the first domain the signal is characterized by one or more peaks, each defined by its position, its width, and its area; this is called the frequency domain. In the second domain, which is called the time domain, the signal consists of a set of oscillations, each defined by its frequency, its amplitude, and its decay rate. The Fourier transform—and the inverse Fourier transform—allow us to move between these two domains.

Note

The mathematical details behind the Fourier transform are beyond the level of this textbook; for a more in-depth treatment, consult this series of articles from the *Journal of Chemical Education*:

- Glasser, L. "Fourier Transforms for Chemists: Part I. Introduction to the Fourier Transform," *J. Chem. Educ.* **1987**, *64*, A228–A233.
- Glasser, L. "Fourier Transforms for Chemists: Part II. Fourier Transforms in Chemistry and Spectroscopy," *J. Chem. Educ.* **1987**, *64*, A260–A266.
- Glasser, L. "Fourier Transforms for Chemists: Part III. Fourier Transforms in Data Treatment," *J. Chem. Educ.* **1987**, *64*, A306–A313.

Figure 6.6.3.6*a* shows a single peak in the frequency domain and Figure 6.6.3.6*b* shows its equivalent time domain signal. There are correlations between the two domains:

- the further a peak in the frequency domain is from the origin, the greater it corresponding oscillation frequency in the time domain
- the broader a peak's width in the frequency domain, the faster its decay rate in the time domain
- the greater the area under a peak in the frequency domain, the higher its initial intensity in the time domain

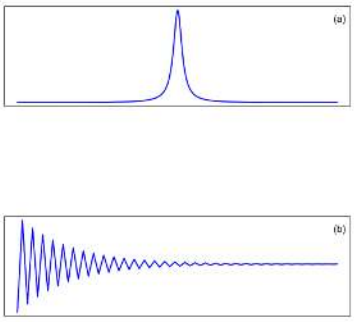


Figure 6.6.3.6: The plot in (a) shows a frequency domain consisting of a single peak defined by its position along the *x*-axis, its width, and its area. The plot in (b) shows the corresponding time domain that consists of a single oscillating signal defined by its oscillation frequency, its initial intensity, and its decay rate.

We can use a Fourier transform to improve the signal-to-noise ratio because the signal is a single broad peak and the noise appears as a multitude of very narrow peaks. As noted above, a broad peak in the frequency domain has a fast decaying signal in the time domain, which means that while the beginning of the time domain signal includes contributions from the signal and the noise, the latter part of the time domain signal includes contributions from noise only. The figure below shows how we can take advantage of this to reduce the noise and improve the signal-to-noise ratio for the noisy signal in Figure 6.6.3.7*a*, which has 256 points along the *x*-axis and has a signal-to-noise ratio of 5.1. First, we use the Fourier transform to convert its original domain into the new domain, the first 128 points of which are shown in Figure 6.6.3.7*b* (note: the first half of the data contains the same information as the second half of the data, so we only need to look at the first half of the data). The points at the beginning are dominated by the signal, which is why there is a systematic decrease in the intensity of the oscillations; the remaining points are dominated by noise, which is why the variation in intensity is random. To filter out the noise we retain the first 24 points as they are and set the intensities of the remaining points to zero (the choice of how many points to retain may require some adjustment). As shown in Figure 6.6.3.7*c*, we repeat this for the remaining 128 points, retaining the last 24 points as they are. Finally, we use an inverse Fourier transform to return to our original domain, with the result in Figure 6.6.3.7*d*, with the signal-to-noise ratio improving from 5. 1 for the original noisy signal to 11.2 for the filtered signal.

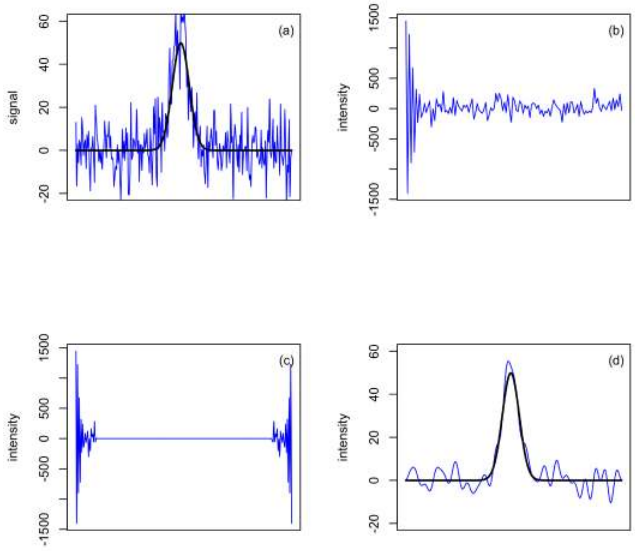


Figure 6.6.3.7: Example of removing noise using a Fourier filter. The original noisy signal with $S/N = 5.1$ is shown in (a) and is similar to the noisy signal in Figure 6.6.3.2*a* and Figure 6.6.3.4*a*. The first half of the Fourier transformed data is shown in (b). The Fourier transformed data is shown in (c) after zeroing out all but the first and the last 24 points. Returning to the original domain gives the final filtered signal with $S/N = 11.1$.

This page titled 6.6.3: Signal-to-Noise Enhancement is shared under a CC BY-NC-SA 4.0 license and was authored, remixed, and/or curated by David Harvey.

- **5.3: Signal-to-Noise Enhancement** by David Harvey is licensed CC BY-NC-SA 4.0.

6.7: EMISSION SPECTROSCOPY

An analyte in an excited state possesses an energy, E_2, that is greater than its energy when it is in a lower energy state, E_1. When the analyte returns to its lower energy state—a process we call relaxation—the excess energy, ΔE

$$\Delta E = E_2 - E_1$$

is released. Figure 10.1.4 shows a simplified picture of this process.

The amount of time an analyte, *A*, spends in its excited state—what we call the excited state's ***lifetime***—is short, typically 10^{-5}–10^{-9} s for an electronic excited state and 10–15 s for a vibrational excited state. Relaxation of the analyte's excited state, *A**, occurs through several mechanisms, including collisions with other species in the sample, photochemical reactions, and the emission of photons. In the first process, which we call vibrational relaxation or nonradiative relaxation, the excess energy is released as heat.

$$A^* \longrightarrow A + \text{ heat}$$

Relaxation by a photochemical reaction may involve simple decomposition

$$A^* \longrightarrow X + Y$$

or a reaction between *A** and another species

$$A^* + Z \longrightarrow X + Y$$

In both cases the excess energy is used up in the chemical reaction or released as heat.

In the third mechanism, the excess energy is released as a photon of electromagnetic radiation.

$$A^* \longrightarrow A + h\nu$$

The release of a photon following thermal excitation is called emission and that following the absorption of a photon is called photoluminescence. In chemiluminescence and bioluminescence, excitation results from a chemical or a biochemical reaction, respectively. Spectroscopic methods based on photoluminescence are the subject of the next section and atomic emission is covered in Chapter 10.7.

This page titled 6.7: Emission Spectroscopy is shared under a CC BY-NC-SA 4.0 license and was authored, remixed, and/or curated by David Harvey.

- **10.5: Emission Spectroscopy** by David Harvey is licensed CC BY-NC-SA 4.0.

6.8: PHOTOLUMINESCENT SPECTROSCOPY

Photoluminescence is divided into two categories: fluorescence and phosphorescence. A pair of electrons that occupy the same electronic ground state have opposite spins and are in a singlet spin state (Figure 10.6.1 a).

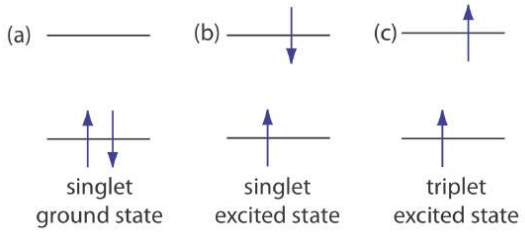


Figure 10.6.1 . Electron configurations for (a) a singlet ground state; (b) a singlet excited state; and (c) a triplet excited state.

When an analyte absorbs an ultraviolet or a visible photon, one of its valence electrons moves from the ground state to an excited state with a conservation of the electron's spin (Figure 10.6.1 b). Emission of a photon from a ***singlet excited state*** to the singlet ground state—or between any two energy levels with the same spin—is called ***fluorescence***. The probability of fluorescence is very high and the average lifetime of an electron in the excited state is only 10^{-5}–10^{-8} s. Fluorescence, therefore, rapidly decays once the source of excitation is removed.

In some cases an electron in a singlet excited state is transformed to a ***triplet excited state*** (Figure 10.6.1 c) in which its spin no is longer paired with the ground state. Emission between a triplet excited state and a singlet ground state—or between any two energy levels that differ in their respective spin states–is called ***phosphorescence***. Because the average lifetime for phosphorescence ranges from 10^{-4}–10^{4} s, phosphorescence may continue for some time after we remove the excitation source.

The use of molecular fluorescence for qualitative analysis and for semi-quantitative analysis dates to the early to mid 1800s, with more accurate quantitative methods appearing in the 1920s. Instrumentation for fluorescence spectroscopy using a filter or a monochromator for wavelength selection appeared in, respectively, the 1930s and 1950s. Although the discovery of phosphorescence preceded that of fluorescence by almost 200 years, qualitative and quantitative applications of molecular phosphorescence did not receive much attention until after the development of fluorescence instrumentation.

> As you might expect, the persistence of long-lived phosphorescence made it more noticeable.

FLUORESCENCE AND PHOSPHORESCENCE SPECTRA

To appreciate the origin of fluorescence and phosphorescence we must consider what happens to a molecule following the absorption of a photon. Let's assume the molecule initially occupies the lowest vibrational energy level of its electronic ground state, which is the singlet state labeled S_0 in Figure 10.6.2 . Absorption of a photon excites the molecule to one of several vibrational energy levels in the first excited electronic state, S_1, or the second electronic excited state, S_2, both of which are singlet states. Relaxation to the ground state occurs by a number of mechanisms, some of which result in the emission of a photon and others that occur without the emission of a photon. These relaxation mechanisms are shown in Figure 10.6.2 . The most likely relaxation pathway from any excited state is the one with the shortest lifetime.

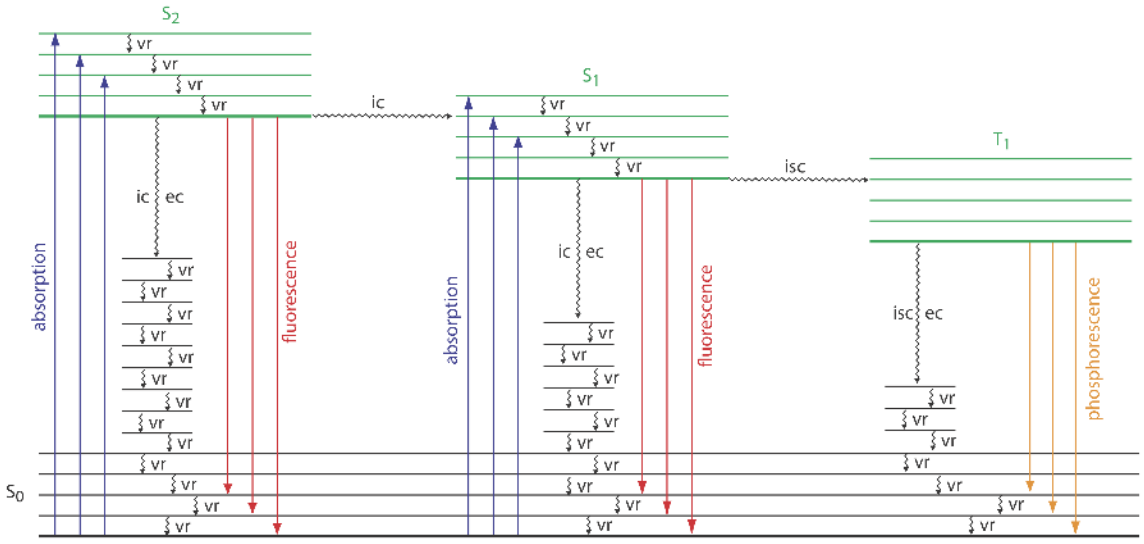


Figure 10.6.2 . Energy level diagram for a molecule that shows pathways for the deactivation of an excited state: ***vr*** is vibrational relaxation; ***ic*** is internal conversion; ***ec*** is external conversion; and ***isc*** is an intersystem crossing. The lowest vibrational energy for each electronic state is indicated by the thicker line. The electronic ground state is shown in black and the three electronic excited states are shown in green. The absorption, fluorescence, and phosphorescence of photons also are shown.

RADIATIONLESS DEACTIVATION

When a molecule relaxes without emitting a photon we call the process ***radiationless deactivation***. One example of radiationless deactivation is ***vibrational relaxation***, in which a molecule in an excited vibrational energy level loses energy by moving to a lower vibrational energy level in the same electronic state. Vibrational relaxation is very rapid, with an average lifetime of $<10^{-12}$ s. Because vibrational relaxation is so efficient, a molecule in one of its excited state's higher vibrational energy levels quickly returns to the excited state's lowest vibrational energy level.

Another form of radiationless deactivation is an ***internal conversion*** in which a molecule in the ground vibrational level of an excited state passes directly into a higher vibrational energy level of a lower energy electronic state of the same spin state. By a combination of internal conversions and vibrational relaxations, a molecule in an excited electronic state may return to the ground electronic state without emitting a photon. A related form of radiationless deactivation is an ***external conversion*** in which excess energy is transferred to the solvent or to another component of the sample's matrix.

> Let's use Figure 10.6.2 to illustrate how a molecule can relax back to its ground state without emitting a photon. Suppose our molecule is in the highest vibrational energy level of the second electronic excited state. After a series of vibrational relaxations brings the molecule to the lowest vibrational energy level of S_2, it undergoes an internal conversion into a higher vibrational energy level of the first excited electronic state. Vibrational relaxations bring the molecule to the lowest vibrational energy level of S_1. Following an internal conversion into a higher vibrational energy level of the ground state, the molecule continues to undergo vibrational relaxation until it reaches the lowest vibrational energy level of S_0.

A final form of radiationless deactivation is an ***intersystem crossing*** in which a molecule in the ground vibrational energy level of an excited electronic state passes into one of the higher vibrational energy levels of a lower energy electronic state with a different spin state. For example, an intersystem crossing is shown in Figure 10.6.2 between the singlet excited state S_1 and the triplet excited state T_1.

RELAXATION BY FLUORESCENCE

Fluorescence occurs when a molecule in an excited state's lowest vibrational energy level returns to a lower energy electronic state by emitting a photon. Because molecules return to their ground state by the fastest mechanism, fluorescence is observed only if it is a more efficient means of relaxation than a combination of internal conversions and vibrational relaxations.

A quantitative expression of fluorescence efficiency is the fluorescent ***quantum yield***, Φ_f, which is the fraction of excited state molecules that return to the ground state by fluorescence. The fluorescent quantum yields range from 1 when every molecule in an excited state undergoes fluorescence, to 0 when fluorescence does not occur.

The intensity of fluorescence, I_f, is proportional to the amount of radiation absorbed by the sample, $P_0 - P_T$, and the fluorescent quantum yield

$$I_f = k\Phi_f (P_0 - P_T) \tag{6.8.1}$$

where k is a constant that accounts for the efficiency of collecting and detecting the fluorescent emission. From Beer's law we know that

$$\frac{P_T}{P_0} = 10^{-\varepsilon bC} \tag{6.8.2}$$

where C is the concentration of the fluorescing species. Solving Equation 6.8.2 for P_T and substituting into Equation 6.8.1 gives, after simplifying

$$I_f = k\Phi_f P_0 \left(1 - 10^{-\varepsilon bC}\right) \tag{6.8.3}$$

When $\varepsilon bC < 0.01$, which often is the case when the analyte's concentration is small, Equation 6.8.3 simplifies to

$$I_f = 2.303k\Phi_f \varepsilon bCP_0 = k'P_0 \tag{6.8.4}$$

where k' is a collection of constants. The intensity of fluorescence, therefore, increases with an increase in the quantum efficiency, the source's incident power, and the molar absorptivity and the concentration of the fluorescing species.

Fluorescence generally is observed when the molecule's lowest energy absorption is a $\pi \rightarrow \pi^*$ transition, although some $n \rightarrow \pi^*$ transitions show weak fluorescence. Many unsubstituted, nonheterocyclic aromatic compounds have a favorable fluorescence quantum yield, although substitutions on the aromatic ring can effect Φ_f significantly. For example, the presence of an electron-withdrawing group, such as –NO_2, decreases Φ_f, while adding an electron-donating group, such as –OH, increases Φ_f. Fluorrescence also increases for aromatic ring systems and for aromatic molecules with rigid planar structures. Figure 10.6.3 shows the fluorescence of quinine under a UV lamp.



Figure 10.6.3 . Tonic water, which contains quinine, is fluorescent when placed under a UV lamp. Source: Splarka (commons.Wikipedia.org).

A molecule's fluorescent quantum yield also is influenced by external variables, such as temperature and solvent. Increasing the temperature generally decreases Φ_f because more frequent collisions between the molecule and the solvent increases external conversion. A decrease in the solvent's viscosity decreases Φ_f for similar reasons. For an analyte with acidic or basic functional groups, a change in pH may change the analyte's structure and its fluorescent properties.

As shown in Figure 10.6.2 , fluorescence may return the molecule to any of several vibrational energy levels in the ground electronic state. Fluorescence, therefore, occurs over a range of wavelengths. Because the change in energy for fluorescent emission generally is less than that for absorption, a molecule's fluorescence spectrum is shifted to higher wavelengths than its absorption spectrum.

RELAXATION BY PHOSPHORESCENCE

A molecule in a triplet electronic excited state's lowest vibrational energy level normally relaxes to the ground state by an intersystem crossing to a singlet state or by an external conversion. Phosphorescence occurs when the molecule relaxes by emitting a photon. As shown in Figure 10.6.2 , phosphorescence occurs over a range of wavelengths, all of which are at lower energies than the molecule's absorption band. The intensity of phosphorescence, I_p, is given by an equation similar to Equation 6.8.4 for fluorescence

$$I_P = 2.303k\Phi_P \varepsilon bCP_0 \tag{6.8.5}$$

$$= k'P_0 \tag{6.8.6}$$

where Φ_p is the ***phosphorescent quantum yield***.

Phosphorescence is most favorable for molecules with $n \rightarrow \pi^*$ transitions, which have a higher probability for an intersystem crossing than $\pi \rightarrow \pi^*$ transitions. For example, phosphorescence is observed with aromatic molecules that contain carbonyl groups or heteroatoms. Aromatic compounds that contain halide atoms also have a higher efficiency for phosphorescence. In general, an increase in phosphorescence corresponds to a decrease in fluorescence.

Because the average lifetime for phosphorescence can be quite long, ranging from 10^{-4}–10^{4} s, the phosphorescent quantum yield usually is quite small. An improvement in Φ_p is realized by decreasing the efficiency of external conversion. This is accomplished in several ways, including lowering the temperature, using a more viscous solvent, depositing the sample on a solid substrate, or trapping the molecule in solution. Figure 10.6.4 shows an example of phosphorescence.

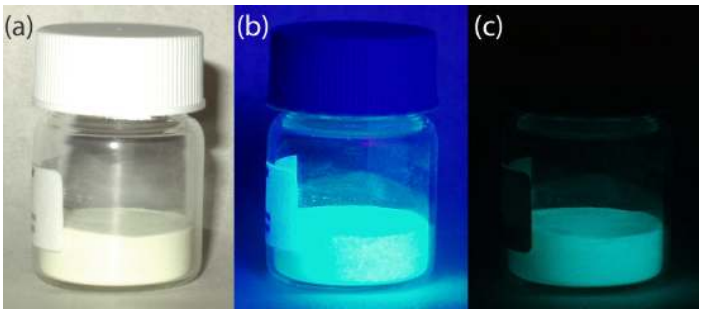


Figure 10.6.4 . An europium doped strontium silicate-aluminum oxide powder under (a) natural light, (b) a long-wave UV lamp, and (c) in total darkness. The photo taken in total darkness shows the phosphorescent emission. Source: modified from Splarka (commons.Wikipedia.org).

EXCITATION VERSUS EMISSION SPECTRA

Photoluminescence spectra are recorded by measuring the intensity of emitted radiation as a function of either the excitation wavelength or the emission wavelength. An ***excitation spectrum*** is obtained by monitoring emission at a fixed wavelength while varying the excitation wavelength. When corrected for variations in the source's intensity and the detector's response, a sample's excitation spectrum is nearly identical to its absorbance spectrum. The excitation spectrum provides a convenient means for selecting the best excitation wavelength for a quantitative or qualitative analysis.

In an ***emission spectrum*** a fixed wavelength is used to excite the sample and the intensity of emitted radiation is monitored as function of wavelength. Although a molecule has a single excitation spectrum, it has two emission spectra, one for fluorescence and one for phosphorescence. Figure 10.6.5 shows the UV absorption spectrum and the UV fluorescence emission spectrum for quinine.

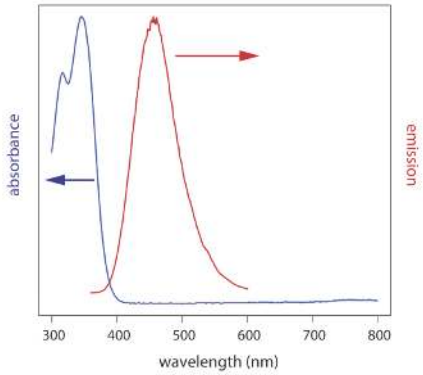


Figure 10.6.5 . Absorbance spectrum and fluorescence emission spectrum for quinine in 0.05 M H_2SO_4. The emission spectrum uses an excitation wavelength of 350 nm with a bandwidth of 20 nm. Both spectra are normalized so that the maximum absorbance is 1.00 and the maximum emission is 1.00. The actual maximum absorbance is 0.444 and the actual maximum emission is 126747. Source: data from Daniel Scott, Department of Chemistry & Biochemistry, DePauw University.

INSTRUMENTATION

The basic instrumentation for monitoring fluorescence and phosphorescence—a source of radiation, a means of selecting a narrow band of radiation, and a detector—are the same as those for absorption spectroscopy. The unique demands of fluorescence and phosphorescence, however, require some modifications to the instrument designs seen earlier in Figure 10.3.1 (filter photometer), Figure 10.3.2 (single-beam spectrophotometer), Figure 10.3.3 (double-beam spectrophotometer), and Figure 10.3.4 (diode array spectrometer). The most important difference is that the detector cannot be placed directly across from the source. Figure 10.6.6 shows why this is the case. If we place the detector along the source's axis it receives both the transmitted source radiation, P_T, and the fluorescent, I_f, or phosphorescent, I_p, radiation. Instead, we rotate the director and place it at 90º to the source.

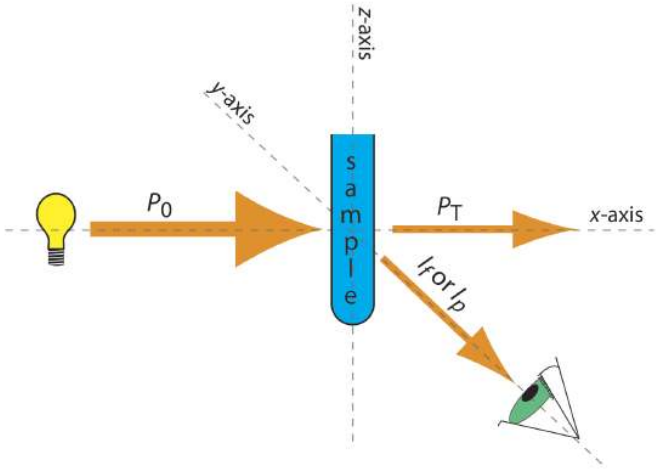


Figure 10.6.6 . Schematic diagram showing the orientation of the source and the detector when measuring fluorescence and phosphorescence. Contrast this to Figure 10.2.7, which shows the orientation for absorption spectroscopy.

INSTRUMENTS FOR MEASURING FLUORESCENCE

Figure 10.6.7 shows the basic design of an instrument for measuring fluorescence, which includes two wavelength selectors, one for selecting the source's excitation wavelength and one for selecting the analyte's emission wavelength. In a ***fluorimeter*** the excitation and emission wavelengths are selected using absorption or interference filters. The excitation source for a fluorimeter usually is a low-pressure Hg vapor lamp that provides intense emission lines distributed throughout the ultraviolet and visible region. When a monochromator is used to select the excitation and the emission wavelengths, the instrument is called a ***spectrofluorometer***. With a monochromator the excitation source usually is a high-pressure Xe arc lamp, which has a continuous emission spectrum. Either instrumental design is appropriate for quantitative work, although only a spectrofluorometer can record an excitation or emission spectrum.

> A Hg vapor lamp has emission lines at 254, 312, 365, 405, 436, 546, 577, 691, and 773 nm.

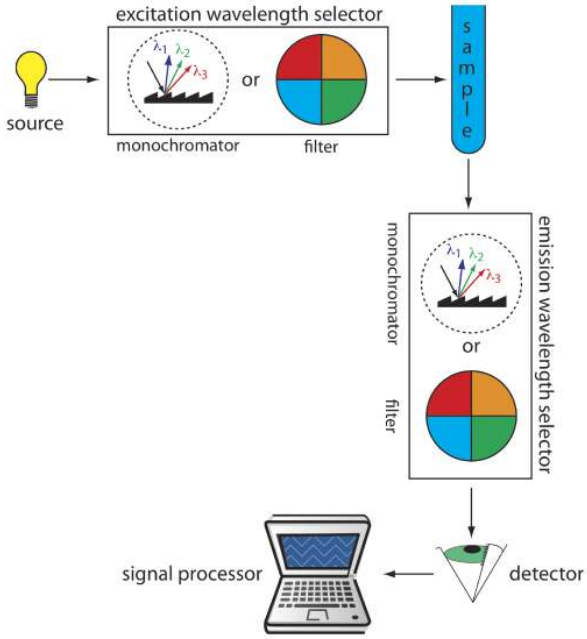


Figure 10.6.7 . Schematic diagram for measuring fluorescence showing the placement of the wavelength selectors for excitation and emission. When a filter is used the instrument is called a fluorimeter and when a monochromator is used the instrument is called a spectrofluorimeter.

The sample cells for molecular fluorescence are similar to those for molecular absorption (see Figure 10.3.6). Remote sensing using a fiber optic probe (see Figure 10.3.7) is possible using with either a fluorimeter or spectrofluorometer. An analyte that is fluorescent is monitored directly. For an analyte that is not fluorescent, a suitable fluorescent probe molecule is incorporated into the tip of the fiber optic probe. The analyte's reaction with the probe molecule leads to an increase or decrease in fluorescence.

INSTRUMENTS FOR MEASURING PHOSPHORESCENCE

An instrument for molecular phosphorescence must discriminate between phosphorescence and fluorescence. Because the lifetime for fluorescence is shorter than that for phosphorescence, discrimination is achieved by incorporating a delay between exciting the sample and measuring the phosphorescent emission. Figure 10.6.8 shows how two out-of-phase choppers allow us to block fluorescent emission from reaching the detector when the sample is being excited and to prevent the source radiation from causing fluorescence when we are measuring the phosphorescent emission.

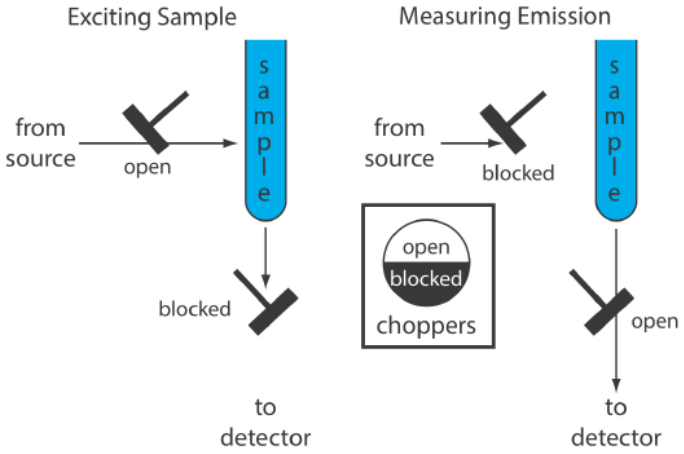


Figure 10.6.8 . Schematic diagram showing how choppers are used to prevent fluorescent emission from interfering with the measurement of phosphorescent emission.

Because phosphorescence is such a slow process, we must prevent the excited state from relaxing by external conversion. One way this is accomplished is by dissolving the sample in a suitable organic solvent, usually a mixture of ethanol, isopentane, and diethylether. The resulting solution is frozen at liquid-N_2 temperatures to form an optically clear solid. The solid matrix minimizes external conversion due to collisions between the analyte and the solvent. External conversion also is minimized by immobilizing the sample on a solid substrate, making possible room temperature measurements. One approach is to place a drop of a solution that contains the analyte on a small disc of filter paper. After drying the sample under a heat lamp, the sample is placed in the spectrofluorometer for analysis. Other solid substrates include silica gel, alumina, sodium acetate, and sucrose. This approach is particularly useful for the analysis of thin layer chromatography plates.

QUANTITATIVE APPLICATIONS

Molecular fluorescence and, to a lesser extent, phosphorescence are used for the direct or indirect quantitative analysis of analytes in a variety of matrices. A direct quantitative analysis is possible when the analyte's fluorescent or phosphorescent quantum yield is favorable. If the analyte is not fluorescent or phosphorescent, or if the quantum yield is unfavorable, then an indirect analysis may be feasible. One approach is to react the analyte with a reagent to form a product that is fluorescent or phosphorescent. Another approach is to measure a decrease in fluorescence or phosphores- cence when the analyte is added to a solution that contains a fluorescent or phosphorescent probe molecule. A decrease in emission is observed when the reaction between the analyte and the probe molecule enhances radiationless deactivation or results in a nonemitting product. The application of fluorescence and phosphorescence to inorganic and organic analytes are considered in this section.

INORGANIC ANALYTES

Except for a few metal ions, most notably UO_2^+, most inorganic ions are not sufficiently fluorescent for a direct analysis. Many metal ions are determined indirectly by reacting with an organic ligand to form a fluorescent or, less commonly, a phosphorescent metal–ligand complex. One example is the reaction of Al^{3+} with the sodium salt of 2, 4, 3′-trihydroxyazobenzene-5′-sulfonic acid—also known as alizarin garnet R—which forms a fluorescent metal–ligand complex (Figure 10.6.9). The analysis is carried out using an excitation wavelength of 470 nm, with fluorescence monitored at 500 nm. Table 10.6.1 provides additional examples of chelating reagents that form fluorescent metal–ligand complexes with metal ions. A few inorganic nonmetals are determined by their ability to decrease, or quench, the fluorescence of another species. One example is the analysis for F^- based on its ability to quench the fluorescence of the Al^{3+}–alizarin garnet R complex.

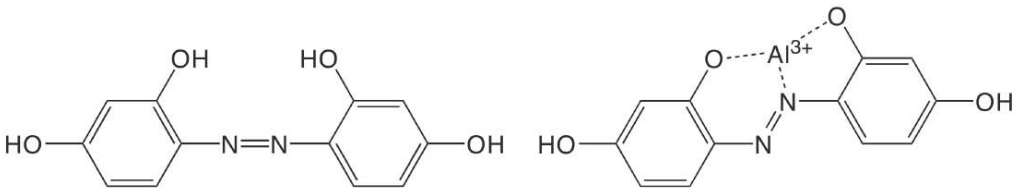


Figure 10.6.9 . Structure of alizarin garnet R and its metal–ligand complex with Al^{3+}.

Table 10.6.1 . Chelating Agents for the Fluorescent Analysis of Metal Ions

chelating agent	metal ions
8-hydroxyquinoline	Al^{3+}, Be^{2+}, Zn^{2+}, Li^{+}, Mg^{2+} (and others)
flavonal	Zr^{2+}, Sn^{4+}
benzoin	$B_4O_6^{2-}$, Zn^{2+}
$2',3',4',5,7-$ pentahydroxylflavone	Be^{2+}
2-(*o*-hydroxyphenyl) benzoxazole	Cd^{2+}

ORGANIC ANALYTES

As noted earlier, organic compounds that contain aromatic rings generally are fluorescent and aromatic heterocycles often are phosphorescent. Table 10.6.2 provides examples of several important biochemical, pharmaceutical, and environmental compounds that are analyzed quantitatively by fluorimetry or phosphorimetry. If an organic analyte is not naturally fluorescent or phosphorescent, it may be possible to incorporate it into a chemical reaction that produces a fluorescent or phosphorescent product. For example, the enzyme creatine phosphokinase is determined by using it to catalyze the formation of creatine from phosphocreatine. Reacting the creatine with ninhydrin produces a fluorescent product of unknown structure.

Table 10.6.2 . Examples of Naturally Photoluminescent Organic Analytes

class	compounds (F = fluorescence, P = phosphorescence)
aromatic amino acids	phenylalanine (F) tyrosine (F) tryptophan (F, P)
vitamins	vitamin A (F) vitamin B2 (F) vitamin B6 (F) vitamin B12 (F) vitamin E (F) folic acid (F)
catecholamines	dopamine (F) norepinephrine (F)
pharmaceuticals and drugs	quinine (F) salicylic acid (F, P) morphine (F) barbiturates (F) LSD (F) codeine (P) caffeine (P) sulfanilamide (P)
environmental pollutants	pyrene (F) benzo[a]pyrene (F) organothiophosphorous pesticides (F) carbamate insecticides (F) DDT (P)

STANDARDIZING THE METHOD

From Equation 6.8.4 and Equation 6.8.6 we know that the intensity of fluorescence or phosphorescence is a linear function of the analyte's concentration provided that the sample's absorbance of source radiation ($A = \varepsilon bC$) is less than approximately 0.01. Calibration curves often are linear over four to six orders of magnitude for fluorescence and over two to four orders of magnitude for phosphorescence. For higher concentrations of analyte the calibration curve becomes nonlinear because the assumptions that led to Equation 6.8.4 and Equation 6.8.6 no longer apply. Nonlinearity may be observed for smaller concentrations of analyte fluorescent or phosphorescent contaminants are present. As discussed earlier, quantum efficiency is sensitive to temperature and sample matrix, both of which must be con- trolled when using external standards. In addition, emission intensity depends on the molar absorptivity of the photoluminescent species, which is sensitive to the sample matrix.

REPRESENTATIVE METHOD 10.6.1: DETERMINATION OF QUININE IN URINE

The best way to appreciate the theoretical and the practical details discussed in this section is to carefully examine a typical analytical method. Although each method is unique, the following description of the determination of quinine in urine provides an instructive example of a typical procedure. The description here is based on Mule, S. J.; Hushin, P. L. *Anal. Chem.* **1971**, *43*, 708–711, and O'Reilly, J. E.; *J. Chem. Educ.* **1975**, *52*, 610–612. Figure 10.6.3 shows the fluorescence of the quinine in tonic water.

Description of the Method

Quinine is an alkaloid used to treat malaria. It is a strongly fluorescent compound in dilute solutions of H_2SO_4 ($\Phi_f = 0.55$). Quinine's excitation spectrum has absorption bands at 250 nm and 350 nm and its emission spectrum has a single emission band at 450 nm. Quinine is excreted rapidly from the body in urine and is determined by measuring its fluorescence following its extraction from the urine sample.

Procedure

Transfer a 2.00-mL sample of urine to a 15-mL test tube and use 3.7 M NaOH to adjust its pH to between 9 and 10. Add 4 mL of a 3:1 (v/v) mixture of chloroform and isopropanol and shake the contents of the test tube for one minute. Allow the organic and the aqueous (urine) layers to separate and transfer the organic phase to a clean test tube. Add 2.00 mL of 0.05 M H_2SO_4 to the organic phase and shake the contents for one minute. Allow the organic and the aqueous layers to separate and transfer the aqueous phase to the sample cell. Measure the fluorescent emission at 450 nm using an excitation wavelength of 350 nm. Determine the concentration of quinine in the urine sample using a set of external standards in 0.05 M H_2SO_4, prepared from a 100.0 ppm solution of quinine in 0.05 M H_2SO_4. Use distilled water as a blank.

Questions

1. Chloride ion quenches the intensity of quinine's fluorescent emission. For example, in the presence of 100 ppm NaCl (61 ppm Cl^-) quinine's emission intensity is only 83% of its emission intensity in the absence of chloride. The presence of 1000 ppm NaCl (610 ppm Cl^-) further reduces quinine's fluorescent emission to less than 30% of its emission intensity in the absence of chloride. The concentration of chloride in urine typically ranges from 4600–6700 ppm Cl^-. Explain how this procedure prevents an interference from chloride.

The procedure uses two extractions. In the first of these extractions, quinine is separated from urine by extracting it into a mixture of chloroform and isopropanol, leaving the chloride ion behind in the original sample.

2. Samples of urine may contain small amounts of other fluorescent compounds, which will interfere with the analysis if they are carried through the two extractions. Explain how you can modify the procedure to take this into account?

One approach is to prepare a blank that uses a sample of urine known to be free of quinine. Subtracting the blank's fluorescent signal from the measured fluorescence from urine samples corrects for the interfering compounds.

The fluorescent emission for quinine at 450 nm can be induced using an excitation frequency of either 250 nm or 350 nm. The fluorescent quantum efficiency is the same for either excitation wavelength. Quinine's absorption spectrum shows that ε_{250} is greater than ε_{350}. Given that quinine has a stronger absorbance at 250 nm, explain why its fluorescent emission intensity is greater when using 350 nm as the excitation wavelength.

From Equation 6.8.4 we know that I_f is a function of the following terms: k, Φ_f, P_0, ε, b, and C. We know that Φ_f, b, and C are the same for both excitation wavelengths and that ε is larger for a wavelength of 250 nm; we can, therefore, ignore these terms. The greater emission intensity when using an excitation wavelength of 350 nm must be due to a larger value for P_0 or k . In fact, P_0 at 350 nm for a high-pressure Xe arc lamp is about 170% of that at 250 nm. In addition, the sensitivity of a typical photomultiplier detector (which contributes to the value of k) at 350 nm is about 140% of that at 250 nm.

EXAMPLE 10.6.1

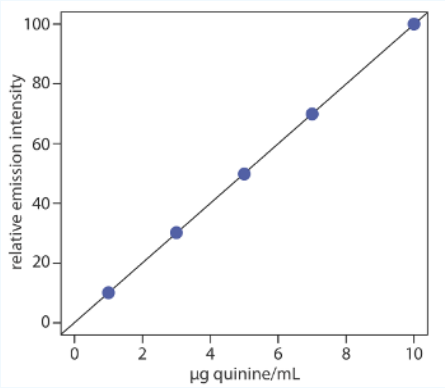
To evaluate the method described in Representative Method 10.6.1, a series of external standard are prepared and analyzed, providing the results shown in the following table. All fluorescent intensities are corrected using a blank prepared from a quinine-free sample of urine. The fluorescent intensities are normalized by setting I_f for the highest concentration standard to 100.

[quinine] (μg/mL)	I_f
1.00	10.11
3.00	30.20
5.00	49.84
7.00	69.89
10.00	100.0

After ingesting 10.0 mg of quinine, a volunteer provides a urine sample 24-h later. Analysis of the urine sample gives a relative emission intensity of 28.16. Report the concentration of quinine in the sample in mg/L and the percent recovery for the ingested quinine.

Solution

Linear regression of the relative emission intensity versus the concentration of quinine in the standards gives the calibration curve shown below and the following calibration equation.



$$I_f = 0.122 + 9.978 \times \frac{\text{g quinine}}{\text{mL}}$$

Substituting the sample's relative emission intensity into the calibration equation gives the concentration of quinine as 2.81 µg/mL. Because the volume of urine taken, 2.00 mL, is the same as the volume of 0.05 M H_2SO_4 used to extract the quinine, the concentration of quinine in the urine also is 2.81 µg/mL. The recovery of the ingested quinine is

$$\frac{\frac{2.81\,\mu\text{g quinine}}{\text{mL urine}} \times 2.00\text{ mL urine} \times \frac{1\text{mg}}{1000\,\mu\text{g}}}{10.0\text{ mg quinine ingested}} \times 100 = 0.0562\%$$

It can take 10–11 days for the body to completely excrete quinine so it is not surprising that such a small amount of quinine is recovered from this sample of urine.

EVALUATION OF PHOTOLUMINESCENCE SPECTROSCOPY

SCALE OF OPERATION

Photoluminescence spectroscopy is used for the routine analysis of trace and ultratrace analytes in macro and meso samples. Detection limits for fluorescence spectroscopy are influenced by the analyte's quantum yield. For an analyte with $\Phi_f > 0.5$, a picomolar detection limit is possible when using a high quality spectrofluorometer. For example, the detection limit for quinine sulfate, for which Φ is 0.55, generally is between 1 part per billion and 1 part per trillion. Detection limits for phosphorescence are somewhat higher, with typical values in the nanomolar range for low-temperature phosphorimetry and in the micromolar range for room-temperature phosphorimetry using a solid substrate.

ACCURACY

The accuracy of a fluorescence method generally is between 1–5% when spectral and chemical interferences are insignificant. Accuracy is limited by the same types of problems that affect other optical spectroscopic methods. In addition, accuracy is affected by interferences that affect the fluorescent quantum yield. The accuracy of phosphorescence is somewhat greater than that for fluorescence.

PRECISION

The relative standard deviation for fluorescence usually is between 0.5–2% when the analyte's concentration is well above its detection limit. Precision usually is limited by the stability of the excitation source. The precision for phosphorescence often is limited by reproducibility in preparing samples for analysis, with relative standard deviations of 5–10% being common.

SENSITIVITY

From Equation 6.8.4 and Equation 6.8.6 we know that the sensitivity of a fluorescent or a phosphorescent method is affected by a number of parameters. We already have considered the importance of quantum yield and the effect of temperature and solution composition on Φ_f and Φ_p. Besides quantum yield, sensitivity is improved by using an excitation source that has a greater emission intensity, P_0, at the desired wavelength, and by selecting an excitation wavelength for which the analyte has a greater molar absorptivity, ε. Another approach for improving sensitivity is to increase the volume from which emission is monitored. Figure 10.6.10 shows how rotating a monochromator's slits from their usual vertical orientation to a horizontal orientation increases the sampling volume. The result can in- crease the emission from the sample by $5 - 30\times$.

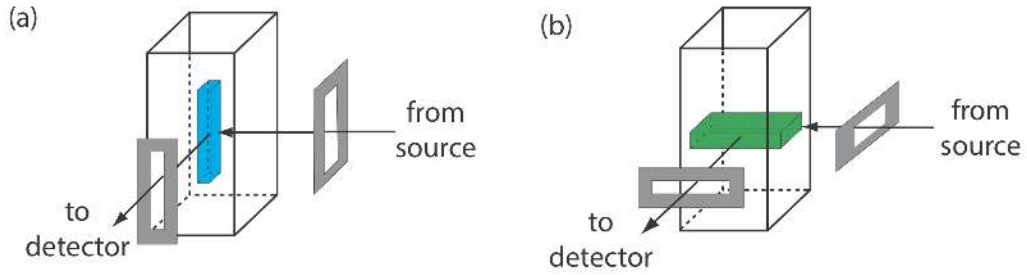


Figure 10.6.10 . Use of slit orientation to change the volume from which fluorescence is measured: (a) vertical slit orientation; (b) horizontal slit orientation. Suppose the slit's dimensions are 0.1 mm × 3 mm. In (a) the dimensions of the sampling volume are 0.1 mm × 0.1 mm × 3 mm, or 0.03 mm^3. For (b) the dimensions of the sampling volume are 0.1 mm × 3 mm × 3 mm, or 0.9 mm^3, a 30-fold increase in the sampling volume.

SELECTIVITY

The selectivity of fluorescence and phosphorescence is superior to that of absorption spectrophotometry for two reasons: first, not every compound that absorbs radiation is fluorescent or phosphorescent; and, second, selectivity between an analyte and an interferent is possible if there is a difference in either their excitation or their emission spectra. The total emission intensity is a linear sum of that from each fluorescent or phosphorescent species. The analysis of a sample that contains *n* analytes, therefore, is accomplished by measuring the total emission intensity at *n* wavelengths.

TIME, COST, AND EQUIPMENT

As with other optical spectroscopic methods, fluorescent and phosphorescent methods provide a rapid means for analyzing samples and are capable of automation. Fluorimeters are relatively inexpensive, ranging from several hundred to several thousand dollars, and often are satisfactory for quantitative work. Spectrofluorometers are more expensive, with models often exceeding $50,000.

This page titled 6.8: Photoluminescent Spectroscopy is shared under a CC BY-NC-SA 4.0 license and was authored, remixed, and/or curated by David Harvey.

- **10.6: Photoluminescent Spectroscopy** by David Harvey is licensed CC BY-NC-SA 4.0.

6.9: Analytical Chemiluminescence

The aim of the book is to give a comprehensive account of the chemiluminescence subject suitable for students, research workers, professional analytical chemists and life scientists. The chemistry of each reagent that has been used in chemiluminescence is explained and the techniques for increasing the magnitude of the emitted signal are discussed. Further sections describe the different instrumental methods that have been used and examine the sort of work that has been carried out with them. The final sections discuss the applications of chemiluminescence in some of the major areas of analytical chemistry.

This content originates from an Analytical Chemiluminescence Wikibook and is licensed via a Creative Commons Attribution-ShareAlike License.

SECTION OVERVIEW

6.9.1: Introduction to Chemiluminescence

6.9.1.1: Electronic transitions and luminescence

6.9.1.2: Chemiluminescence Spectroscopy

6.9.1: Introduction to Chemiluminescence is shared under a CC BY-SA 4.0 license and was authored, remixed, and/or curated by LibreTexts.

6.9.1.1: Electronic transitions and luminescence

Luminescence is the emission of light due to transitions of electrons from molecular orbitals of higher energy to those of lower energy, usually the ground state or the lowest unoccupied molecular orbitals. Such transitions are referred to as relaxations. Figure A1.1 shows four electronic energy levels (S_0,S_1, S_2 and T_1) and the possible transitions between them. S_0 represents the ground state, while S_1, S_2 and T_1 represent higher-energy excited states;S_0, S_1 and S_2 are singlet states in which all the electrons form pairs of opposed spins whereas T_1 is a triplet excited state, in which not all electrons are paired off in this way.

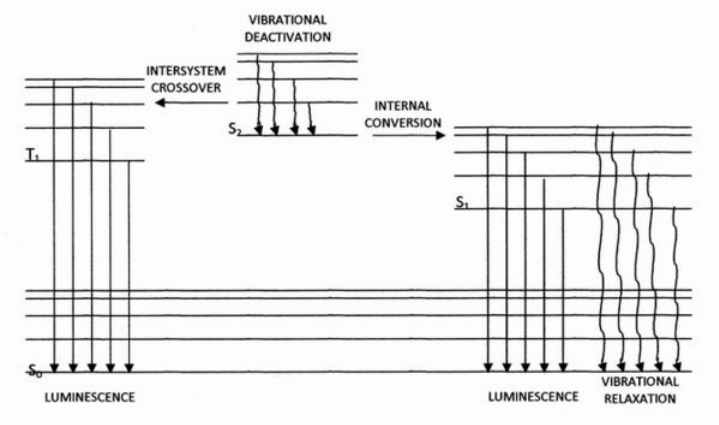


Figure A1.1 – Jablonski diagram showing four electronic energy levels S_0, S_1, S_2 and T_1, with their vibrational fine structure and the transitions between them that affect luminescence.

Each energy level is subdivided into a number of vibrational states, each characterised by an amount of vibrational energy that accompanies the potential energy of the electrons occupying the orbitals. Luminescence is classified according to the excited state that gives rise to it and to the source of the energy that caused the excited state to be populated with electrons. The promotion of electrons to an excited state is called excitation. In many cases, this is brought about by absorption of visible or ultraviolet radiation. In such a case, if the luminescence arises because electrons are relaxing from a singlet excited state to a singlet ground state, then it is called **fluorescence**, and generally occurs within 10^{-11} to 10^{-5} s. The transition is very fast because it involves no reversal of electron spin. If, however, it arises due to relaxation from a triplet excited state, then the luminescence is called **phosphorescence**, which generally occurs within 10^{-4} to 100 s. If the excitation is the result of energy released in a chemical reaction, the luminescence is called **chemiluminescence**. A subset of chemiluminescence occurring in the biosphere as a result of biological processes is called **bioluminescence**. **Electrochemiluminescence** is another distinct subset of chemiluminescence phenomena, made up of those reactions in which the excited species is produced at an electrode during electrolysis.

Before luminescence occurs, there is a non-radiative loss of energy (due to collisions between molecules) as the excited state relaxes to a lower vibrational state while remaining at the same electronic energy level. This type of transition is called **vibrational deactivation**. It has to occur even more rapidly than fluorescence and typically occurs within 10^{-12} s of excitation. Therefore the luminescence involves the emission of photons of lower energy (higher wavelength) than would otherwise be the case. Another possible transition is **internal conversion**, in which an electron transfers from a lower vibrational state of a higher electronic energy level to a higher vibrational state of a lower electronic energy level, without any significant gain or loss of energy; such a transition, $S_2 \rightarrow S_1$, is shown schematically in Figure 1.1. In **intersystem crossing**, internal conversion would involve also reversal of the spin of the electron as in a transition from a singlet to a triplet state; the transition $S_2 \rightarrow T_1$ in Figure 1.1 is of this type. Such transitions can give rise to phosphorescence. Finally, luminescence is not inevitable. The intensity of the emission compared with the number of molecules in the excited state is called the **quantum yield**(Φ_F). This can be calculated for fluorescent emission by dividing the number of emitted photons by the number of absorbed photons. Φ_F in a chemiluminescence phenomenon should be the same as in the fluorescence phenomenon involving the same excited state, but, because chemiluminescence does not depend on the absorption of photons, it can be calculated in the same way only by performing a separate fluorescence experiment. The intensity of chemiluminescence emission is more meaningfully compared with the number of reactant molecules; this measure is called the **chemiluminescence quantum yield** (Φ_{CL}). It is related to Φ_F by the equation:

$$\Phi_{CL} = \Phi_C \Phi_E \Phi_F$$

where Φ_C is the proportion of reactant molecules converted into product and Φ_E is the proportion of product molecules formed in the excited state. Φ_{CL} has values from 0 to 1 and reaches 0.88 for firefly luciferin *in vitro*[1].

Because Φ_{CL} depends on Φ_F it would be reasonable to suppose that chemiluminescence is affected by substitution in product molecules in the same way as is fluorescence. In that case, Φ_{CL}would be increased by electron donors and decreased by electron acceptors. There would also be an increase in Φ_{CL} (and a bathochromic shift in emission wavelength) due to conjugated systems and in rigidly planar molecules having facilitated π-bond delocalisation. Such generalisations must be used with great care, for the only product species to which they can apply are the molecules that are actually emitting; it is by no means obvious what these are in any particular case.

This content originates from an Analytical Chemiluminescence Wikibook and is licensed via a Creative Commons Attribution-ShareAlike License.

6.9.1.1: Electronic transitions and luminescence is shared under a CC BY-SA 4.0 license and was authored, remixed, and/or curated by LibreTexts.

- **1.1: Electronic transitions and luminescence** is licensed CC BY-SA 4.0.

6.9.1.2: Chemiluminescence Spectroscopy

The wavelengths of chemiluminescence emission that are analytically useful depend on the characteristics of the detector. Visible emission (though it is seldom visible to the naked eye) has a wavelength range of about 400-750 nm, corresponding to enthalpy changes of exothermic reactions of between 180 and 300 kJ mol^{-1}, provided that there is a pathway to an excited state that relaxes with the loss of a photon (see Figure 1.1). Emission intensity is proportional to the concentration of the emitting species, which is either an intermediate or a product in an electronically excited state. This concentration depends on the rate of the reaction producing it. Analytical detection of chemiluminescence usually involves no wavelength selection, i.e., it is emission photometry rather than emission spectrophotometry. Selectivity is achieved by on-line treatments rather than by processing of the signal, which has little fine-structure[1].

Because of this, the importance of chemiluminescence spectroscopy lies more in elucidating the mechanisms of chemiluminescence reactions rather than in analytical applications. In particular, spectroscopic investigations have been found useful for the identification of the emitter species in particular chemiluminescence reactions. Thus, experimental evidence has shown that manganese(II) ion is a common emitter in chemiluminescence arising due to the reduction either of permanganate or of other higher oxidation states of manganese[2]. Using a variety of reductants, chemiluminescence spectra, corrected for wavelength-related differences in detector sensitivity, showed maximum emission at 689 nm (in hexametaphosphate) and 734 nm, (in phosphate/orthophosphoric acid) which corresponds to the emission maxima of manganese(II) phosphorescence, and is clearly distinguishable from the intense emission at 634 nm and 703 nm from singlet oxygen, which had been earlier proposed as the emitter. Diagnosis of the emitter usually cannot be based on spectroscopic evidence alone, but must make use of chemical evidence also. Identifying the emitting species in luminol chemiluminescence in aqueous solutions is an example of such an investigation. The product of the oxidation of luminol is 3-aminophthalate. The maximum emission wavelength in these conditions is 424 nm, which corresponds to the maximum wavelength of fluorescence emission from the 3-aminophthalate dianion and this species was originally accepted as the emitter. However, chemical evidence suggests that emission is from the monoanion, which has a fluorescence maximum of 451 nm. Closer examination of the chemiluminescence reaction[3] suggests that the emitter is one particular conformer of the 3-aminophthalate monoanion that has a maximum emission wavelength resembling that of the dianion.

This content originates from an Analytical Chemiluminescence Wikibook and is licensed via a Creative Commons Attribution-ShareAlike License.

6.9.1.2: Chemiluminescence Spectroscopy is shared under a CC BY-SA 4.0 license and was authored, remixed, and/or curated by LibreTexts.

- **1.2: Chemiluminescence Spectroscopy** is licensed CC BY-SA 4.0.

SECTION OVERVIEW

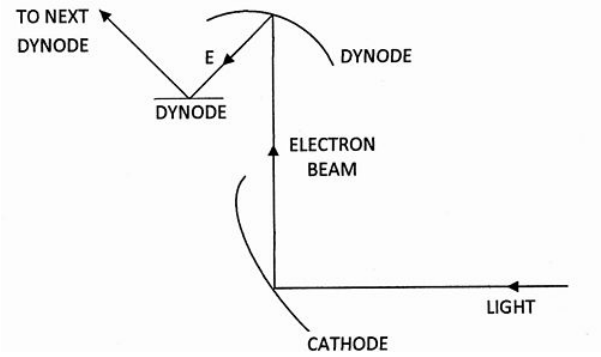
6.9.2: Instrumentation

6.9.2.1: Detection of chemiluminescence

6.9.2: Instrumentation is shared under a CC BY-SA 4.0 license and was authored, remixed, and/or curated by LibreTexts.

6.9.2.1: Detection of chemiluminescence

The detector of choice for chemiluminescence is the photomultiplier tube, a development of the vacuum phototube that permits considerable amplification of the signal. Figure D1.1 shows how the photomultiplier works. The surface of the cathode supports a photoemissive layer that ejects electrons in direct proportion to the intensity of the incident light; several electrons are emitted for each photon and are attracted towards a positively-charged dynode. When the electron beam meets the dynode several electrons (E in figure D1.1) are ejected for each incident electron and these are attracted to a second dynode at a higher positive potential. This process is repeated along a series of dynodes, the intensity of the electron beam increasing continually until when it reaches the anode (at the greatest positive potential) there are over a million electrons for each photon incident at the cathode. The resulting current can be amplified electronically. In the absence of light, the photomultiplier generates a dark current, chiefly due to thermal emission. Thermal dark currents can be eliminated by cooling to −30°C.



Principle of the photomultiplier (see text).

Diodes are also used for chemiluminescence detection[1], especially in low-cost applications. Photographic detection was also used in very early work[2].

6.9.2.1: Detection of chemiluminescence is shared under a CC BY-SA 4.0 license and was authored, remixed, and/or curated by LibreTexts.

- **4.1: Detection of chemiluminescence** is licensed CC BY-SA 4.0.

6.10: Detectors

Spectroscopy is the study of how light interacts with matter, and a necessity for these studies is the ability to detect light. To do this, spectroscopists use a wide variety of detectors, which are devices that convert incident photons into a measurable signal. Presented here is a discussion of the fundamental concepts that define a detector, and an examination of several detectors commonly used in spectroscopy.

Introduction

All spectroscopic measurements are made through the use of a detector, which converts photons into a measurable signal. A ubiquitous example of a photon detector is the human eye, which can detect visible light with wavelengths in the range of ~390-700 nanometers. Some of the earliest non-biological photon detectors were photographic plates, in which absorbed photons cause chemical reactions that manifest as color changes in the film. A vast majority of modern detectors act as photon transducers, which transform electromagnetic radiation into electrical signals which can be amplified and processed for final interpretation. The manner by which photons are converted to electrical signals varies widely, but detectors can be divided into two broad categories: those that function via the photoelectric effect, and those that are based on the solid-state properties of semiconductors.

The photoelectric effect is a physical phenomenon through which absorbed photons can eject electrons from the surface of a conductor, provided the photons have energies greater than the work function of the material. The kinetic energy of the ejected electron, termed a photoelectron, is given by

$$KE_{electron} = h\nu - \phi \tag{6.10.1}$$

in which h is Planck's constant, ν is the frequency of the incident photons, and ϕ is the work function. Many detectors exploit this effect, as the ejected photoelectrons can be collected at an anode and measured as a current.

Semiconductor-based detectors rely on a similar effect, though instead of ejecting photoelectrons from the surface of a conductor, absorbed photons excite electrons from the valence band of a semiconductor into the conduction band. This excitation results in an electon-hole pair, which allows current to flow through the semiconductor; this current can be quantified and interpreted with an appropriate circuit.

Fundamental Characteristics of Detectors

All detectors can be evaluated in terms of their various fundamental characteristics, including spectral response, linearity, quantum efficiency, dynamic range, response time, and susceptibility to noise. Certain types of detectors are better suited to particular applications based on how well they perform in these areas.

Spectral Response and Linearity

The ideal detector would be able to convert incident photons of any energy into an electrical signal, and would have a perfectly linear response, such that the magnitude of the current produced is directly proportional to the number of photons striking the detector. The spectral response of a real detector is limited to a fairly small region of the electromagnetic spectrum, and the response can deviate significantly from linearity, as shown in **Figure 1**. The spectral response of a detector largely determines its usefulness for various applications; silicon photodiodes are used in the UV and visible regions but are not sensitive beyond 1100 nm, while germanium photodiodes are insensitive to UV light, but can detect longer wavelengths up to 1800 nm.

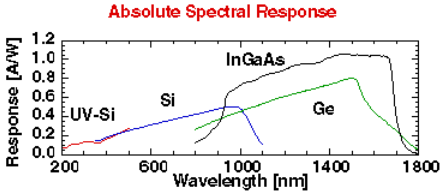


Figure 1: Response curves for several semiconductor photodiodes. The response, given in amps per watt of incident radiation, is not only limited by the semiconductor material, but varies with photon energy as well. Image from NIST.

Quantum Efficiency

Quantum efficiency is a measure of how well a detector can convert photons into an electrical signal. It is often reported as the ratio, η, of the number of electrons generated by the detector divided by the number of incident photons, but can also be reported as

the percent of incident photons that will be translated into a measurable signal; the latter definition takes into account the effects of noise and other signal losses within the system, and represents a more accurate measure of the efficiency of a detector. An ideal detector would have a quantum efficiency of 100%, and there exist several types of real detectors that approach this limit, with the ability to detect the absorption of single photons.

Dynamic Range

The dynamic range of a detector is a measure of its ability to generate a reliable signal relative to the intensity of incident radiation. A detector with a very high dynamic range will be able to measure both extremely weak and extremely strong photon sources, but this is often connected to a decrease in overall sensitivity. As the range of measurable intensities increases, the ratio of a signal to the maximum possible signal becomes smaller, which leads to a smaller change in signal for the same incident intensity, and thus a lower sensitivity. Conversely, extremely sensitive detectors tend to have relatively small dynamic ranges; the photomultiplier tube, which is capable of detecting single photons, can be easily damaged or destroyed when exposed to even moderate levels of incident radiation.

Response Time

The generation of an electrical signal from an incident photon occurs on a very fast, but measurable timescale, which varies by detector type. The response time is the amount of time necessary before a detector is able to generate another signal; the faster the response time, the more quickly variations in incident radiation can be resolved. An ideal detector would have zero response time, though this is an impossibility in real detectors. Some detectors, such as photodiode arrays, which use multiple detector elements arranged to gather spatial information, can have response times on the order of milliseconds, whereas conventional photocathode detectors have response times on the order of nanoseconds. Specialized detectors, such a streak cameras, can have temporal resolutions as low as 0.5 picoseconds, allowing for the study of extremely short-lived events.

Noise

All detectors generate small signals that do not correspond to absorption of a photon, and these signals are collectively termed noise. Noise does not contain any useful information, and therefore it is important to minimize signals due to noise relative to the overall signal; the higher the signal-to-noise ratio, the more sensitive the detector. There are many forms of noise, including shot noise, dark current noise, thermal noise, generation-recombination noise, and read-out noise, all of which arise from different factors. Various detectors are more or less susceptible to certain types of noise, and both experimental conditions and detector design can be modified to reduce noise to a minimum.

Shot Noise

Shot noise is a direct consequense of the discrete nature of photons, and how a detector generates a discrete number of photoelectrons through its interaction with photons. In any counting experiment of N trials, the standard deviation associated with the measurement is $\sqrt{N}$. In photon detectors, the signal is directly proportional to the number of incident photons, and the associated uncertainty in this measurement arises from the statistical probability of whether or not a photoelectron will be emitted when a photon is absorbed. This uncertainty gives rise to random fluctuations in the signal, and manifests as noise. Therefore, when N photons are incident on a detector, the signal-to-noise ratio is:

$$\frac{signal}{noise} = \frac{N}{\sqrt{N}} \times \frac{\sqrt{N}}{\sqrt{N}} = \frac{N\sqrt{N}}{N} = \sqrt{N} \tag{6.10.2}$$

In detectors with quantum efficiencies less than unity, the shot noise is slightly greater than this value, but in most experiments the number of incident photons is very large, and thus the signal-to-noise ratio is also large, making the shot noise imperceptibly small when compared to the overall signal. Shot noise is present in all measurements, due to the quantum nature of light, and is not dependent on temperature or the energy of the photon absorbed. Shot noise only becomes a significant contributor to overall noise when the number of incident photons is extremely small, such as in single-photon-counting experiments, and when other forms of noise are almost entirely eliminated.

Thermal Noise

Thermal noise, also known as Johnson-Nyquist noise, is intrinsic to all conductive materials, regardless of relative conductivity or applied voltage. The band structure of conductors allows for the free motion of charge carriers; the random motions of the charge carriers produce small current fluctuations in the system, which appear as a Gaussian distribution on top of the overall signal. As

the speed with which these charge carriers move is proportional to temperature of the system, thermal noise can be significantly reduced by lowering the temperature of the detector.

Dark Current Noise

Dark current noise is the current generated by photon detectors in the complete absence of photons. This type of noise is also thermally generated, but instead of current fluctuations due to the random motion of charge carriers, dark current noise is created by thermionic emission of electrons from photocathodes, or thermal generation of electron-hole pairs within a semiconductor. In the case of photocathodes, thermionic electrons are indistinguishable from photoelectrons, and are measured as an additional current on top of the photon-induced current. In the case of semiconductors, the generation of electron-hole pairs changes the conductivity of the semiconductor, and more current can flow through the circuit; when the pairs recombine, the conductivity drops to its initial value. This manifests as a fluctuation of the measured current above and below the real signal. In both cases, the event that generate the noise are discrete, such that dark current noise has the same properties as shot noise; unlike shot noise, however, dark currents are thermally generated, and can be significantly reduced by cooling the system.

Generation-Recombination Noise

Another form of noise affecting only semiconductor-based detectors is generation-recombination noise. Generation-recombination noise arises from the fact that when photons excite photoelectrons in a semiconductor, the number of electron-hole pairs generated fluctuates due to the statistical probability of the excitation occuring. The relative number of electron-hole pairs changes the conductivity of the semiconductor, which gives rise to current fluctuations similar to those created by dark current, with characteristics of shot noise. However, generation-recombination noise is not thermally generated, and cannot be reduced by cooling the system.

Read-Out Noise

Read-out noise is only a factor in detectors that integrate signals, such as charge coupled devices (CCDs) and complementary metal-oxide-semiconductor (CMOS) sensors. These detectors collect and store charge over an extended period of time, and when the charge collection is complete, the accumulated charge is "read off" the collection grid, a process which involves moving packets of charge between multiple electrodes for measurement, or converting charge signals into voltages using operational amplifiers. Each movement or conversion of a packet is subject to the gain or loss of a small number of electrons, and the changes in the number of electrons in each packet give rise to the read-out noise. Read-out noise is not dependent on temperature, but increases with the number of packet movements or conversions, as well as the speed with which the packets are moved and read.

Types of Detectors

The number of types of detectors and their variants employed in spectroscopy is exceedingly large, with new detectors constantly being developed for better performance characteristics and use in novel sensing applications. As can be seen in **Figure 2**, different types of detectors are sensitive to different regions of the electromagnetic spectrum, and the region of interest may dictate which detector type is utilized. Here, a selection of some of the more common detectors are discussed in more detail, including the design, function, and performance of each.

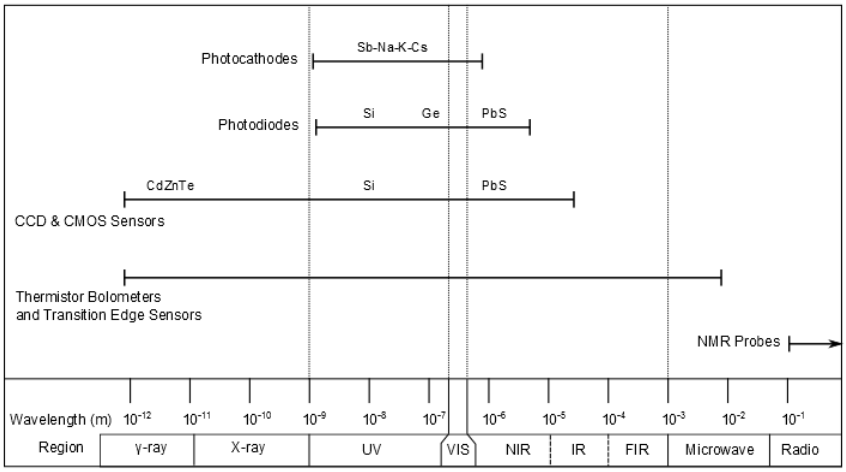


Figure 2: Representative detector sensitivity by photon energy. Note that while the detectors are sensitive to the regions shown, they may not be equally sensitive across the entire range.

Scintillators

While not technically photon detectors by themselves, scintillators are an integral component in many types of detectors, especially of high-energy photons, and it is instructive to understand what they are and how they work before discussing their use in conjunction with other technologies. A scintillator is a material that absorbs a photon of a given energy, and then undergoes fluorescence, re-emitting a photon of a lower energy. In this way, scintillators can be used to absorb photons that fall outside the normal energy range of a detector, and re-emit photons of wavelengths that can be detected.

Many scintillators used in photon detectors employ crystalline inorganic compounds, each of which have characteristic sensitivities, emission wavelengths, and relaxations times. For example, the most commonly used scintillator material is NaI(Tl), crystalline sodium iodide doped with thallium. This compound has a peak fluorescence of 415 nm, a relaxation time of 250 nanoseconds, and emits 38 photons per keV gamma ray absorbed. A newer alternative is $LaBr_3$(Ce), lanthanum bromide doped with cerium, which has nearly double the efficiency of NaI(Tl), and a relaxation time of only 16 nanoseconds. However, $LaBr_3$(Ce) is much more expensive, and is extremely hygroscopic, requiring special handling to protect the scintillator from moisture.

Photocathodes and Photomultiplier Tubes

Photocathodes

Photocathodes are among the simplest photon detectors, relying on only the photoelectric effect to generate a signal. A photon strikes and is absorbed by the photocathode, ejecting a photoelectron in the process. This photoelectron is accelerated through an electric field and is collected at an anode, where it is read as a current. In actual construction, the photocathode is a low work function metal, which is held at a positive potential relative to the collection anode. This assembly is usually housed in a vacuum tube, to limit the interference of air and water vapor and to increase the mean free path of the electrons, thus increasing the quantum efficiency of the detector.

Photocathodes are generally sensitive to radiation from ~180-900 nm, though certain materials are capable of detecting near IR light up to 1600 nm. The most common materials used as photocathodes for broadband spectrometers are multi-alkali alloys of antimony, such as Sb-Na-K-Cs, which is sensitive to photons of energies ranging from vacuum UV to near IR. In addition to their fairly broad spectral response, photocathodes also exhibit very large dynamic ranges, and have a nearly linear response across the entire range. Furthermore, photocathodes have response times on the order of 1-2 nanoseconds, and are only subject to small amounts of shot noise and thermal noise. However, noise from dark current can become a problem for particularly low work function photocathodes, as thermionic emission of electrons can generate current in the absence of photons. Additionally, their overall sensitivity is quite limited, as there is no internal signal gain in the detector. An external amplifier can be used to increase the magnitude of the signal, but this does not improve the signal-to-noise ratio, and generates a certain amount of noise itself.

Photomultiplier Tubes

Photomultiplier tubes (PMTs) are the direct successors to photocathodes, and function in exactly the same way with one key difference: instead of accelerating photoelectrons directly to the anode, a PMT amplifies the number of photoelectrons through the use of a dynode chain. A dynode, usually made from BeO or MgO, is held at a positive potential, such that when it is struck by a single energetic electron, the dynode will emit several electrons. The next dynode in the chain is held at a slightly lower potential, such that an electric field accelerates electrons liberated from the first dynode towards the second, where the electrons again liberate additional electrons. The process continues in a cascading fashion until the final anode is reached; if 6-8 dynodes are chained together, then a single photoelectron incident on the first can generate 10^6-10^8 electrons at the anode.

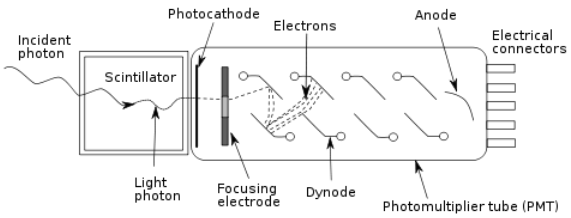


Figure 3: A schematic of a photomultiplier tube. In this case, a scintillator is used to convert incident radiation into photons of the appropriate wavelentgh for the greatest sensitivity of the photomultiplier.

This method of amplification overcomes a number of problems inherent in conventional photocathodes. The primary advantage of a PMT is the dramatically increased sensitivity due to the internal signal gain; modern PMTs are capable of reliably detecting

single photons. Additionally, through the use of the high-voltage dynode chain, the signal is amplified but thermal noise is not, as thermal noise is independent of applied voltage. In this sense, the thermal noise is diminished to essentially nothing, and the signal becomes shot noise dominated, allowing the detector to reach theoretical limits of sensitivity, with a quantum efficiency of 100%, provided that the dark current is minimized by lowering the temperature of the system.

PMTs respond best when used to detect radiation in the UV and visible regions, but they are used as detectors in a wide variety of instruments, from gamma and X-ray spectrometers to near IR spectrometers. This is possible through the use of a variety of scintillators, discussed above, placed between the incoming photons and the photocathode. Scintillators are capable of converting higher energy photons into visible photons, which can be efficiently amplified by the PMT. With a modest decrease in response time and a slight increase in noise, the addition of a scintillator allows for the superior sensitivity and signal of a PMT in spectral regions where they would otherwise be insensitive.

Photodiodes and Photodiode Arrays

Photodiodes and Arrays

Photodiodes exemplify the simplest of the solid-state detectors, and are built upon semiconductor p-n junctions. An individual p-n junction is constructed from the union of a positively-doped material with a negatively-doped material, and contact between the two surfaces results in the local motion of major charge carriers. Electrons near the junction drift towards the p-type material, and holes drift towards the n-type material, resulting in a depletion zone that has an intrinsic electric field, which creates a potential barrier across the junction.

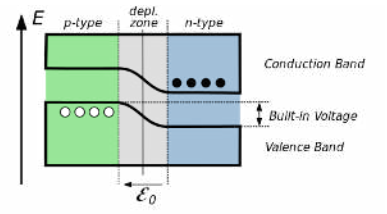


Figure 4: An unbiased p-n junction.

This junction is known as a diode, and will allow current to flow through it in only one direction. When the diode is subjected to an external potential, called a bias, the energies of the p- and n-type materials are shifted relative to each other, changing the magnitude of the potential barrier. When a positive voltage is applied to the p-type side and a negative voltage to the n-type side, the holes in the p-type and the electrons in the n-type sides are forced into the depletion zone. This is known as a forward bias, and when it is large enough, the depletion zone and its potential barrier will disappear and the diode will allow current to flow through it. However, if the potentials are reversed, into what is called a reverse bias, the electrons in the n-type side and the holes in the p-type side are pulled away from each other, widening the depletion zone, and increasing the potential barrier across the junction, preventing current from flowing through the diode.

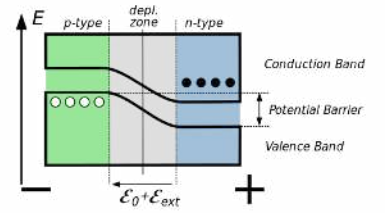


Figure 5: A reverse-biased p-n junction.

In photodiode detectors, the diode is held under reverse bias, which maintains a fairly large electric field throughout the depletion zone that will sweep free electrons towards the anode and free holes towards the cathode. When a diode is illuminated with electromagnetic radiation with energy sufficient to excite an electron from the valence band to the conduction band of the semiconductor, electron-hole pairs are generated. As these electron-hole pairs are separated and accelerated in opposite directions by the electric field, a photocurrent is produced, by which the incident radiation can be quantified.

The spectral response of a photodiode can be tuned to different regions by carefully selecting the materials used to make the p-n junction. For example, silicon-based photodiodes are sensitive to radiation between 190-1100 nm, making them useful for UV, visible, and limited near-IR spectroscopies, while lead sulfide photodiodes are sensitive in the range of ~1000-3500 nm, enabling detection in both near-IR and short-wave-IR. Additionally, solid-state photodiodes provide a very nearly linear response throughout

a large dynamic range. These properties, coupled with the fact that photodiodes do not require high-voltage power supplies and are physically small, relatively inexpensive to manufacture, and much more robust than photocathodes makes them an excellent choice for use in many spectroscopic instruments.

One additional advantage that stems from the small size of photodiodes is the ability to arrange multiple detectors into an array, known as a photodiode array (PDA). These arrays can take any shape and contain any number of detector elements, but are often arranged in a linear fashion, enabling the detection and encoding of spatial data as well as the energy and intensity of the incident light. As these arrays can be read out in parallel, a PDA has the same response time as an individual detector, allowing for the collection of much more data with the same response time.

However, there are certain aspects of photodiode detectors, such as overall sensitivity, response time, and noise levels, that prevent them from being completely superior to photocathode technologies. Conventionally operated photodiodes, even with quantum efficiencies around 80%, do not have any internal gain, and thus cannot compete with photomultiplier tubes in terms of the ability to detect very small numbers of photons. Furthermore, photodiodes generally have slower response times than similar photocathode detectors, on the order of microseconds, as there is a small but significant time-lag for the electron-hole pairs to be swept from the depletion zone to the electrical contacts. Finally, while shot, thermal, and dark current noise is present in all detectors, photodiodes are also subject to generation-recombination noise, though most photodiodes are limited by thermal noise and dark current noise. Many photodiode detectors must be cooled to reduce overall noise to acceptable levels.

Avalanche Photodiodes

One improvement can be made to photodiode detectors to bring their overall sensitivity into the same range as conventional photomultiplier tubes. When a diode held in reverse bias is subjected to a critical overpotential, the diode will break down and allow current to flow across it; this critical voltage is referred to as the breakdown voltage. In the absence of current, a photodiode can be held at a potential well above the breakdown voltage (known as being operated in Geiger mode), such that as soon as a photon is absorbed and an electron-hole pair generated, the diode will undergo breakdown and allow current to flow in the reverse direction. In order to achieve the sensitivity of a PMT, there must be significant internal signal gain, and this is realized through what is called an avalanche breakdown. The electron and hole generated by the absorption of a photon are accelerated very rapidly towards the cathode and anode by the very high potential difference across the photodiode. The electron and hole can gain enough kinetic energy that they are capable of causing impact ionizations within the semiconductor, generating additional electron-hole pairs. As each new pair is generated, they too are accelerated towards the electrodes, and cause additional ionizations; this chain reaction results in an avalanche of electrons moving towards the cathode and holes moving towards the anode, such that when they arrive, a very intense current pulse is measured. In this way, single photon absorptions can be detected in much the same way that they can with PMTs, but with a much lower overall voltage requirement. Where avalanche photodiodes still cannot compete with conventional PMTs is in response time; as the avalanche breakdown in a photodiode is a self-sustaining event, it must be stopped, or quenched, by lowering the potential across the junction to well below the breakdown voltage, and then raised back up before another absorption can be detected. This effectively means that while time resolution for single-photon events can be very good, on the order of 0.6 nanoseconds, it can take 10s of nanoseconds to reset the detector to a useable state, compared to the 1-2 nanosecond response times of PMTs.

CCDs and CMOS Sensors

CCD and CMOS sensors fall into the category of focal plane array (FPA) sensors, in which multiple light sensing elements are arranged, usually into a grid, in order to gather spatial information in addition to spectral information. These sensors differ from photodiode arrays in their architecture; PDAs are comprised of multiple discrete sensors, connected through external circuitry, whereas CCD and CMOS sensors are monolithic arrays, fabricated on a single semiconductor wafer, much in the same way that modern microprocessors are produced. Additionally, CCD and CMOS sensors are integrative sensors, collecting light for an extended period of time, called an exposure, before processing the light into a signal. CCDs differ from CMOS sensors in how charge is transferred and converted into a signal, with each form offering several advantages and disadvantages.

Charge Coupled Devices (CCDs)

Charge coupled devices are two-dimensional arrays of metal-oxide-semiconductor structures. On a substrate of p-type silicon (or another semiconductor for more specialized applications), a thin layer of silicon dioxide is deposited to act as an insulating barrier. A grid of discrete metal contacts, or gates, is then deposited on the oxide layer, completing the basic structure, known as a pixel. Modern sensors can have as few as 4096 pixels for very small sensors, to as many as 10^9 pixels for very large sensors.

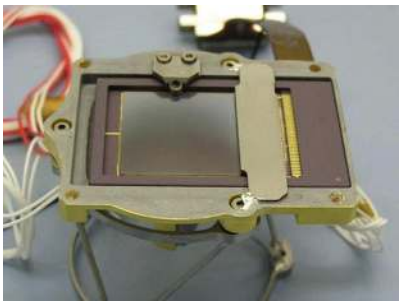


Figure 6: The CheMin CCD detector on the Curiosity Rover, sensitive to X-rays, which is integral to the X-ray diffraction and X-ray fluorescence spectroscopy used to determine the composition of Martian soil samples. The sensor is the size of a postage stamp. Image from NASA/Ames/JPL-Caltech.

When the metal gates are held at a positive voltage relative to the p-type silicon, the positively charged holes in the silicon are pushed away from the gates, creating a depletion zone that acts as a potential well for any free electrons in the substrate. Each metal-oxide-semiconductor structure thus acts as a capacitor, in which charge, in the form of electrons, can be trapped and stored. Upon exposure to a light source, incident photons are absorbed by the p-type silicon substrate, generating electron-hole pairs. The electrons are drawn into the potential wells nearest to where they were generated, and are collected there in packets until the sensor is read out. This process, as illustrated in **Figure 7**, is accomplished by sequentially changing the potential of the metal gates along rows, moving the charge packets from gate to gate until they reach the edge of the array. Once at the edge, each individual column is quickly shifted down to the corner of the array, packet by packet, into an external circuit that measures the amount of charge contained in each packet. As the packets are localized to a specific point on the detector array, a two-dimensional image can be reconstructed from the signal, pixel by pixel; this technology forms the basis for many high-end camera sensors, including the sensors in the Hubble Space Telescope.

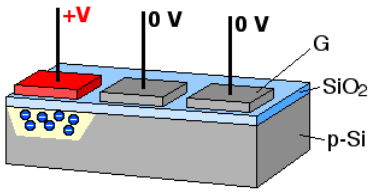


Figure 7:An animation showing the charge-transfer process along a row of detector elements in a charge coupled device. Animation by Michael Schmid.

One of the main benefits of a CCD detector is its adaptability to a variety of different tasks. The semiconductor substrate can be changed to access alternate regions of the electromagnetic spectrum; silicon is prominent for use in the soft X-ray to near-IR region, while cadmium zinc telluride is a common material for higher energy X-rays and gamma rays, and lead sulfide is used in the lower energy IR region. Furthermore, a scintillator can be placed in front of a CCD, allowing for detection in virtually any region of the spectrum. CCDs also exhibit extremely linear spectral responses, and have very large dynamic ranges. There is however a limit to how much light a CCD can integrate, as the metal-oxide-semiconductor capacitors have upper limits to how much charge they can store. Surpassing this limit causes charge to spill over into neighboring pixels, which causes unwanted blooming around the brightest spots in images. Additionally, CCDs suffer from fairly long response times, as the charge packets under each individual gate must be moved off the grid and converted from a charge to a voltage, an operation performed by an external output amplifier. Another inherent drawback to CCDs is the read-out noise associated with moving the charge packets off the grid and processing them through an amplifier into a usable signal.

Complementary Metal-Oxide-Semiconductor (CMOS) Sensors

Complementary metal-oxide-semiconductor sensors represent a newer approach to focal plane array detectors, incorporating technology that was not fully realized when the first CCDs were developed. A detailed analysis of the architecture and circuitry of modern CMOS sensors is beyond the scope of this discussion, but the fundamental difference between CMOS sensors and CCDs can be understood through two key changes: in a CMOS sensor, the packets of charge are not moved before they are measured, and signal amplification does not occur in an external circuit. Light is collected in the same manner in both CCDs and CMOS sensors, but instead of moving these packets to an external amplifier as a CCD does, each pixel in a CMOS sensor has its own built-in operational amplifier, which provides a significant amount of signal gain on-chip as it converts the charge of a packet to a voltage. The fact that each pixel has an associated voltage allows for an alternative method of read-out that is much faster and introduces far

less noise; in a process known as signal multiplexing, a common bus is sequentially connected to each pixel in a column, and the voltage is recorded. The bus is then shifted to the next column, and the process is repeated until all columns have been read. After measurement, a reset transistor built into each pixel drains the accumulated charge, and the sensor is ready to integrate another signal.

In addition to lower response times and less intrinsic noise as compared to CCDs, CMOS sensors are also much less expensive to produce, as they can be manufactured in current microprocessor fabrication facilities without any retooling. However, CMOS sensors have several disavantages; the addition of the operational amplifier and other electrical components necessary for operation blocks some of the active space on the chip, reducing the photosensitive area of each pixel. Furthermore, current manufacturing facilities are designed for microprocessors, which are by definition very small, and this places a limit on the maximum size of a CMOS sensor. In applications that call for small sensors, such as consumer-sized digital cameras, virtually all devices rely on CMOS sensors, but when larger format sensors are required, most devices utilize CCDs, which can be very large -- the primary sensor in the James Webb Space Telescope is a CCD that measures one meter across.

Other Detectors

Discussed here are several examples of photon detectors that operate in very different ways from those covered above, and are adapted for specific applications.

NMR Probes

All previously mentioned detectors require some form of electronic transition to occur in a substance; however, a great deal of spectroscopy occurs at energies far below those required for electronic excitations. One example of this is nuclear magnetic resonance spectroscopy, which measures how magnetic moments are shifted by applied electromagnetic radiation. This radiation often has frequencies on the order of several hundred megahertz, corresponding to wavelengths between 0.3 and 3 meters. None of the previously mentioned detectors are sensitive in this region, and a completely different form of detection is required. NMR probes are extremely simple in their construction: they are made from a coiled non-magnetic conductor, which acts as an antenna. An oscillating electromagnetic wave, such as a radio wave, exerts a Lorentz force on electrons within a conductor, and induces an oscillating electric current. When this process is reversed, and an electric current is applied through the coil, the probe will generate an electromagnetic wave, which can interact with a sample. In most modern NMR spectrometers, this current takes the form of a pulse, which serves to shift the bulk magnetization of a sample. When the bulk magnetization lies in the xy plane, it begins to precess about the z-axis, perpendicular to the coil. Ignoring any T_2^* relaxations, this precession gives rise to an oscillating magnetic field, which in turn induces an electromotive force (EMF) in the coil via the Lorentz force, manifesting as an oscillating current. This current can be directly measured, allowing for the quantization of a wide range of low-energy radiation. Operation of a probe as both a radiation source and a detector is know as quadrature detection.

The response time of the NMR coil is on the order of several hundred microseconds. This is due to the fact that the coil is a transciever; it both applies the pulse and then detects the signal. Converting from transducer to reciever takes time, as the coil will oscillate after the pulse. This is known as ringdown, and its duration is based on the amount of power sent through the coil on the pulse. If the NMR signal is detected before ringdown stops, then the resulting Fourier Transform of the spectrum will be significantly broadend by the oscillitory motion of the NMR coil. To circumvent these issues, an echo is often used. Additionanlly, the coil may be cooled to reduce thermal noise.

Thermistor Bolometers and Transition Edge Sensors

In addition to detecting photons through excitation of electrons or the induction of a current in a coil, there are several types of detector that function by measuring changes in temperature. One class of these detectors are thermistor bolometers, which exploit the fact that the resistance of a semiconductor is temperature dependent. The absorption of a photon of almost any energy will cause the temperature of the absorbing material to rise, although only slightly. However, certain semiconductors have very large changes in resistance for correspondingly small changes in temperature, allowing for the detection and quantization of small numbers of absorbed photons, in some cases as few as 10-100. In addition to being reasonably sensitive across an extroardinarily broad spectral range, thermistor bolometers are relatively inexpensive, as they are essentially made from a resistor and an ohmmeter. The primary difficulties with thermistor bolometers are response time, which requires the detector to reach thermal equilibrium after absorbing a photon, and thermal noise, which can dominate the signal at conventional temperatures. In order to get a reliable signal from a thermistor bolometer, the sensor must be kept very cold, and the temperature must be controlled with extreme precision.

An interesting subset of thermistor bolometers are transition edge sensors, or superconducting bolometers, which can reach single-photon sensitivity by taking advantage of a physical phenomenon intrinsic to superconductors. Superconducting materials are characterized by a critical temperature, below which their resistance drops to zero very suddenly. The theory behind a transition edge sensor is to measure the resistance across a superconductor held exactly at the lower edge of its critical temperature; before absorption, there is no resistance, but when even a single photon is absorbed, the temperature is raised far enough to exceed the critical temperature, and the resistance reappears and rises sharply. Transition edge sensors are some of the most sensitive detectors in existence (i.e. quantum efficiencies at or very near to 100%, with the ability to count the number of photons absorbed, even simultaneously), but the relative expense of the superconducting materials, combined with the fact that most need to be maintained at temperatures below 10 K limits their use to a small number of specialized applications.

Streak Cameras

Streak cameras are detectors designed for one purpose, and one purpose only: speed. Streak cameras allow for the observation of some of the fastest and shortest-lived processes known, with temporal resolutions down to 0.1 picoseconds. Streak cameras make this possible through the conversion of a time-resolved signal into space-resolved data. A stream of photons is absorbed by a conventional photocathode, ejecting photoelectrons into a cathode ray tube, where they are accelerated towards a CCD detector by an electric field. During this acceleration, however, the electrons pass through an electric field perpendicular to the direction they are moving. A set of plates on either side of the cathode ray tube are held at a potential that causes the electrons in the tube to deflect sideways. By applying a time-varying potential difference across the plates, the electrons experience a time-dependent deflection, causing them to form a streak moving from one side of the CCD to the other. In this way, the time at which a photon was absorbed, and a photoelectron emitted, is directly related to the lateral position of the signal on the CCD detector. As the potential difference between the plates can be varied extremely quickly, and CCD detectors can be made relatively large, astonishing time resolution is possible. It has been demonstrated that streak cameras can directly observe and track a laser pulse propagating through air.

References

1. Barbarino, G.; Asmundis, R.; De Rosa, G.; Fiorillo, G.; Gallo, V.; Russo, S. A new high-gain vacuum photomultiplier based upon the amplification of a Geiger-mode p-n junction. *Nucl. Instrum. Meth. A.* **2008**, *594*, 326–331. DOI: 10.1016/j.nima.2008.06.026.
2. Eisaman, M. D.; Fan, J.; Migdall, A.; Polyakov, S. V. Single-photon sources and detectors. *Rev. Sci. Instrum.* **2011**, *82*, 071101. DOI: 10.1063/1.3610677.
3. Grossman, W. E. L. A comparison of optical detectors for the visible and ultraviolet. *J. Chem. Ed.* **1989**, *66*, 697-700.
4. Hungerford, G.; Birch, D. J. S. Single-photon timing detectors for fluorescence lifetime spectroscopy. *Meas. Sci. Technol.* **1996**, *7*, 121-135. DOI: 10.1088/0957-0233/7/2/002.
5. Irwin, K. D.; Hilton, G. C. Transition edge sensors. *Top. Appl. Phys.* **2005,** *99*, 63-149.
6. Jach, T.; Ullom, J. N.; Elam, W. T. The microcalorimeter X-ray detector: A true paradigm shift in X-ray spectroscopy. *Eur. Phys. J. Spec. Top.* **2009**, *169*, 237-242. DOI: 10.1140/epjst/e2009-00998-3.
7. Renker, D.; Lorenz, E. Advances in solid state photon detectors. *J. Instrum.* **2009**, *4*, P04004. DOI: 10.1088/1748-0221/4/04/P04004.
8. Rogalski, A. Progress in focal plane array technologies. *Prog. Quant. Electron.* **2012**, *36*, 342-473. DOI: 10.1016/j.pquantelec.2012.07.001.
9. Townsend, P. D. Photocathodes—past performance and future potential. *Contemp. Phys*. **2003**, *44*, 17-34. DOI: 10.1080/00107510302717.

Problems

1. What physical phenomenon is the basis for photocathode detectors, and how is this different from solid-state semiconductor detectors?
2. How does dynamic range differ from the range of spectral response?
3. Of the types of noise discussed, which can be lessened by lowering the temperature of the detector, and why?
4. What is one advantage and one disadvantage of a CCD over a CMOS sensor?
5. What allows a streak camera to attain such mind-boggling temporal resolution?

Answers

1. The photoelectric effect, or the ejection of an electron from the surface of a conductor upon absorption of a photon, is the basis for photocathode detectors. Solid-state semiconductor detectors are based on the generation of electron-hole within a solid semiconductor; the excited electrons are not ejected from the material.
2. A spectral response range is the variety of photon energies (varying wavelength, constant photon flux) to which the detector is sensitive, whereas a dynamic range is the variety of photon intensities (varying photon flux, constant wavelength) for which the detector can generate a reliable signal.
3. Thermal noise and dark current noise are temperature-dependent, and can be reduced by cooling the detector. For each type of noise, the speed of random charge migration or generation of thermionic electrons or electron-hole pairs is possible due to the distribution of thermal energy in the detector; if the thermal energy is lessened, both the speed of charge carriers and the statistical probability of an electronic excitation are reduced, lowering the overall thermal noise.
4. One advantage of a CCD over a CMOS sensor is the ability to create very large pixel arrays, capable of extremely high resolutions. One disadvantage is that CCD detectors are invariably more expensive than comparable CMOS sensors.
5. The conversion of time-domain data into spatial data allows for the relative expansion of the dataset onto a larger frame of reference. For example, if an electron beam is swept across a 1,000 pixel CCD in one nanosecond, then the time difference between individual pixels corresponds to one picosecond.

Contributors and Attributions

- Josh Greenfield, UC Davis

6.10: Detectors is shared under a CC BY-NC-SA 4.0 license and was authored, remixed, and/or curated by LibreTexts.

- **Detectors** is licensed CC BY-NC-SA 4.0.

6.10.1: Detectors of Light

The human eye is a low resolution detector of white visible light. Most well-resolved light detectors are essentially photon transducers, or instruments that detect electromagnetic radiation, and convert it into an electrical signal which can be amplified and transformed into an interpretable spectrum. An array of detectors exist, covering the various regions of the electromagnetic (EM) spectrum, but this module only discusses photon detectors for ultraviolet, visible, and near infrared radiation.

Introduction

Light has a dual nature, exhibiting both wave and particle like behavior. Here, light will be treated quantum mechanically, and represented as a particle phenomenon where it exists in packets of energy called photons. A photon has a discrete energy of

$$E = hc/\lambda$$

where h is Planck's constant (= 6.626 x 10^{-34} J s), c is the speed of light (= 2.998 x 10^{8} m s^{-1}), and λ is the wavelength of the EM wave. Photoelectric detectors are the main detectors used in the visible and ultraviolet regions of the EM spectrum. Phototubes and photodiodes make up one main class of photodetector types, and they are based on the photoelectric effect, which states that an electron will be liberated from a metal surface if the energy of the photon striking the surface is greater than the the work function of the surface. A liberated electron's maximum kinetic energy is given by

$$KE_{electron} = hv - \phi$$

where v is the frequency of the EM wave, and ϕ is the work function of the metal surface. The lower the work function is, the easier it is to eject an electron. Therefore, materials with low work functions are employed in photodetectors.

Another principle photodetector type is semiconductor based. When the energy of a photon is greater than that of the bandgap energy of a semiconductor material, then the photon energy is sufficient to break a bond and lift an electron into the conduction band. This creates an electron-hole pair that will allow current to flow (see Figure 2, middle), and detection occurs by measuring the current intensity.

Parameters that Characterize Good Detectors

Spectral Bandwidth

Spectral bandwidth refers to the wavelength range over which photons can be detected. Before light reaches the detector, it passes through a monochromator. It may be helpful here to briefly review the details of spectrophotometry. When a monochromator is set to a particular wavelength, light will come out at the exit slit with a Gaussian profile. **Figure 1** shows a distribution of the light intensities that reach the sample, and on the figure λ^* is the set wavelength. The spectral bandwidth is defined as the width of the band of light at the full width at half maximum (FWHM).

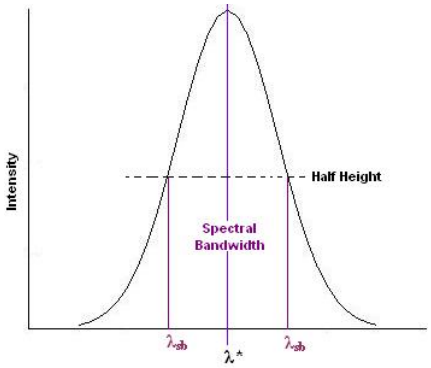


Figure 1. The distribution of light intensities that reach the sample. Spectral bandwidth at the FWHM is shown in purple.

The spectral bandwidth of a spectrophotometer is related to the physical slit-width of the monochromator, and thus, to the instruments resolution capabilities. By optimizing the spectral bandwidth, one can optimize the resolution. Resolution here refers to how well the spectrophotometer can separate light into distinct wavelength regions that vary from one another.

Quantum Efficiency

The quantum efficiency, η, for a photodiode is generally a function of wavelength, and is defined as

η = Number of photoelectrons liberated/Number of incident photons

The value of η for a detector is determined by the conduction and light absorption properties of the material is made of. The solid state properties will be discussed. Good photodetectors are those that have large values for η. If η is low, it means that the incident photons are not being absorbed. Due to the non-directional nature of photoexcitation, an excited electron can move in any possible direction, and will not necessarily move towards the material that can liberate electrons if provided with enough energy. Instead, a significant number of excited electrons will lose their energy through premature scattering. Therefore, the quantum efficiency is limited by the non-directional nature of the excitation light.

Spectral Response

The wavelength of incident light affects the amount of current generated by the photodiode. For example, silicon photodiodes see a response from the UV/Visible regions, and even into the near infrared. Spectral response can be characterized by the short-circuit photocurrent generated by the photodiode divided by the energy, or power, of the incident light. The value obtained is called the radiometric sensitivity, and is mathematically given by

$$S_R = I_{SC} / \phi$$

where S_R is the radiometric sensitivity in Amps/Watts, I_{SC} is the short-circuit photocurrent in Amps, and ϕ is the radiant flux in Watts.

Noise and Signal-to-Noise Ratios

A good detector detector exhibits high signal to noise ratios. The various types of noise present in photodetectors are discussed below.

Photon Shot Noise

Since current is carried by discrete charges, namely electrons, the current flowing through electrical conductors will undergo random fluctuations, and give rise to a type of background called shot noise. This is especially predominant in semiconductor diodes that rely on p-n junctions. Shot noise is given by

$$\langle I^2_{noise} \rangle = 2q^2 \phi \eta \, df$$

where q is the charge of an electron. From the formula, shot noise is proportional to the square root of the signal.

Dark Current Noise

So far, light energy has been introduced as a way to liberate electrons from a metal. Electrons can also be liberated by thermal energy, and since all molecules have a blackbody curve, they possess thermal energy even at room temperature. If that energy happens to be enough to excite electrons within the molecule into excited states, they may fluoresce if they are not non-radiatively deactivated as they relax back down to the ground state. This will lead to a background noise present in the absence of an excitation light source. Dark current noise can be greatly reduced by decreasing the temperature to help eliminate as much thermal motion as possible.

Read-Out Noise

Read-out noise is caused by the electronics in the CCD (charge-coupled device) output transistor and in the external circuitry. The CCD electronics do not measure the amount of charge in each packet of electrons perfectly. A small, but measurable amount of noise is added during the measurement process. This noise is termed read-out noise, and is expressed in units of electrons. Typically, the read-out noise for a CCD is around two to three electrons.

Thermal Noise

In a conductor, charge is completely free to move. Again, everything has a blackbody curve, and thus possess thermal energy at room temperature, and below. Thermal noise, also known as Johnson-Nyquist noise, is caused by the thermal (random) movement of the charge carriers inside the conductor. This electrical noise is inherent, and is present in all conductors (i.e. totally independent of the resistance). The formula for noise power is given by

$$P = k_B T b$$

where P is the total noise power, k is the Boltzmann constant (= 1.38065×10^{-23} J/K), T is the temperature, and b is the bandwidth.

General Recombination Noise

General recombination noise arrises from fluctuations in the number of conduction band electron holes and valence band holes available to conduct flow of electric charge. The photocurrent passing through the conductor material will have pulses that fluctuate randomly to cause general recombination noise.

Response Time

Response time essentially refers to time resolution, and refers to the minimum time interval over which changes in photon rates are detectable. Three main factors controlling the response time of a photodetector include the amount of time photocarriers spend in the depletion region, the diffusion time of photocarriers outside the depletion region, and the RC time constant of the circuit. The time spent in the depletion region depends on the carrier drift velocity, v_d, and the width of the depletion layer, w, and is given by

$$t_d = w/v_d$$

There is a trade-off between quantum efficiency and response time.

Linearity

It is desirable for the response to be linearly proportional to the incident photons. In a detector with linear response, the sensitivity remains constant at all sample concentrations. Examples of linear detectors are the photomultiplier tube and the CCD.

Dynamic Range

Dynamic range refers to the maximum variation in signal over which the detector output can represent photons without loss of signal. It is optimal to maximize the ratio of the largest measurable value to the smallest value.

Solid-State Properties

Semiconductors play an important role in detecting light. **Figure 2** shows band diagrams of an insulator, semiconductor, and a conducting metal. The valence states and conduction states can be seen as ground and excited states of an atom. In order for charge to flow, there must be available states in the conduction band. Since the band gap is very large for the insulator, no charge will flow because there is not enough energy. The states overlap in the conductor, so charge flows very easily. However, in the semiconductor, which is more like an insulator, the band gap is relatively small. Therefore, electrons can be elevated into the conduction band much more easily than in the case of the insulator. This will leave holes in the valence band, which are effectively positive charge. When these holes are present in the material, charge can flow, and a current can be detected.

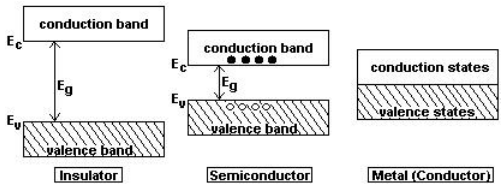


Figure 2. The band diagrams of an insulator, semiconductor, and conductor. The black circles represent electrons and the empty circles represent positively charged holes.

Photon Detectors

Vacuum Phototubes

The vacuum phototube is a very basic photon-detecting deviece that consists of two metal electrodes with a high voltage in between them, and it operates based on the photoelectric effect. Briefly, incident photons strike a photocatchode, and generate electrons that are attracted to an anode. Although phototubes do not have the dynodes, as shown in **Figure 3**, the operating principles are essentially the same, aside from the amplification factor.

Photomultiplier Tubes

Photomultiplier tubes (PMT's) utilize the photoelectric effect and the secondary emission of electrons to provide high current gains upon initial detection of a photon. Briefly, incident photons are directed towards a photocathode made up of a low work-function metal or semiconductor material. If the photon energy is greater than the work function of the cathode material, an electron has a high probability of being liberated from the material's surface. Once the electron is ejected from the cathode, it is accelerated by an applied electric field towards a series of dynodes, or electrodes. The dynodes are coated with a material that is likely to generate secondary emission of electrons and they are connected in series between resistors, causing a negative bias to form along the

dynodes. The number of electrons quickly multiply through secondary emission, and this leads to an electrical current, which can be further amplified using an operational amplifier.

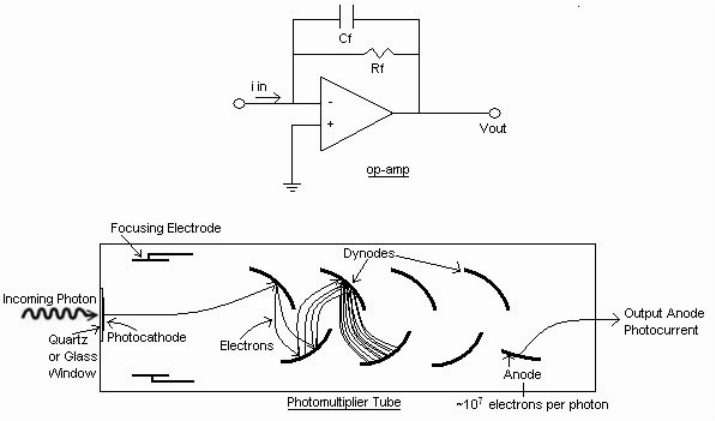


Figure 3. Operational Amplifier (top); Photomultiplier Tube (bottom)

The PMT is extremely sensitive, and thus useful when a very low flux of photons is being measured. Even single photons yield measurable pulses with relatively high quantum efficiency. A disadvantage to this is that exposure to even low levels of light can destroy an operating PMT.

Photodiodes

Photodiodes involve a p-n junction, which consists of two semiconductor materials that are oppositely doped. P-type refers to a positively doped semiconductor, while n-type refers to a negatively doped material. When the oppositely doped regions are place next to each other to create the junction, holes near the junction will tend to move across to the N-type space, while electrons in the N-type space will move towards the p-type space to occupy some of the holes. Thus, charge flow in a diode not connected to a battery will quickly come to a stop because the potential barrier builds up due to the charges that already migrated to opposite regions. No current will flow without placing a bias on the system. Now if a potential is placed across the material, then you will either have forward or reverse bias. If the positive side of the battery is connected to the p-type and the negative end to the n-type, then the electric field from the external potential difference can easily overcome the small internal field in the depletion zone that was caused by the initial drifting of charges. An applied field then attracts electrons to flow from the n to the p-type space and more holes from the p to the n-type space. This forward biased situation is a working diode. A second situation can arrise if the batter were to be switched so that the positive end was connected to the n-type rather than the p-type. Here, an external field will push electrons back into the n-type space while more holes move to the p-type space. This results in not net current flow, unless the reverse bias becomes so large that avalanche break down occurs to give current flow in the opposite direction. Depending on the wavelengths of interest, different semiconductor materials are used in constructing photodiodes. To observe photocurrent, the light energy provided must be sufficient to excite electrons across a material's bandgap. Silicon and Germanium are two materials that are used often, and they cover wavelength ranges of 190-1100nm and 400-1700nm respectively. Silicon is use most commonly because it has a greater bandgap, and therefore produces less dark current noise.

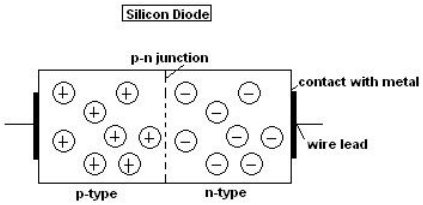


Figure 4. A Silicon Diode

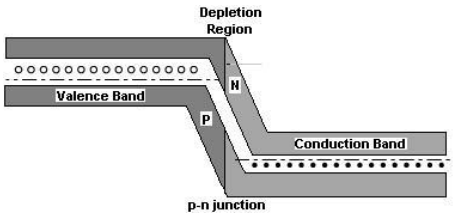


Figure 5. P-N Energy bands. In the reverse bias case, electrons would not move to the p-type space because it would have to go to a higher energy level, an extremely unfavorable move.

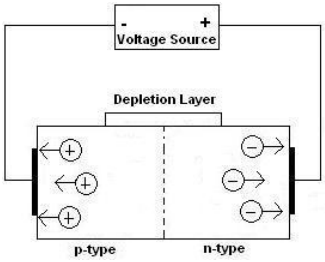


Figure 6. Reverse bias case with formation of depletion layer.

Charge-coupled Device (CCD)

A CCD essentially operates in the same manner as a silicon photodiode, except that an array of potential wells with n number of rows and columns are involved. When photons hit the surface in a CCD, they are converted into an electric charge pattern. **Figure 7** gives an illustration of the CCD cross section. Three electrodes are involved, two of which assist only with transferring charge. When a positive voltage is applied to the third electrode, the negatively charged electrons are attracted by the positively charged potential towards the electrode. Positively charged "holes" as seen in **Figure 2** of the solid state properties section are repelled from the negatively charged area, thus creating a potential well where electrons are stored. The potential wells are grouped in a fixed pixel array, and so each pixel represents a set of charge that will come out together to be converted into a voltage. The pixels, or potential wells, are shown in **Figure 8**. As an increasing number of photons hit the CCD, the potential well surrounding the electrode attracts more electrons, up until the point where the well is completely saturated (filled) with charge. The charge pattern is slowly moved towards the output by changing the potentials of the wells. The coupled charge patterns are read out, set by set, or column by column, until the last column is read. The resolution of a CCD depends on the pixel width as well as the pixel separation, which is defined as the distance from the center of one well to the the center of an adjacent well.

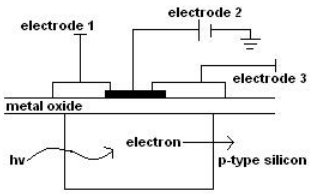


Figure 7. Cross section of a charge-coupled device.

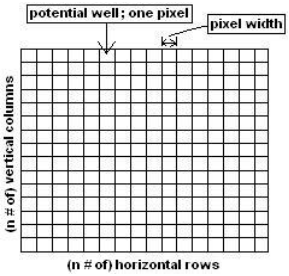


Figure 8. An array of potential wells in a CCD consisting of n number rows and columns.

References

1. R. George, Detection of Light From the Ultraviolet to the Submillimeter, 2nd Edition (2003)
2. D. Skoog, F. Holler, S. Crouch, Principles of Instrumental Analysis (2007)

Outside Links

1. http://hyperphysics.phy-astr.gsu.edu...c/photdet.html
2. en.Wikipedia.org/wiki/Photodiode
3. en.Wikipedia.org/wiki/Photomultiplier
4. en.Wikipedia.org/wiki/Charge-coupled_device
5. en.Wikipedia.org/wiki/Pn_junction

Problems

1. How would you construct a diode? Is a potential needed to make charge flow? What direction does the potential need to be for current to flow?

   A semiconductor material such as silicon must be doped with a material of one charge less and one charge more to create p and n type materials. When placed adjacent to each other, they form a p-n junction, which when connected to a battery with the positive side connected to the p-type material, will give forward bias.
2. Why can't a conductor be used in constructing a diode?

   Conductors reflect better than they absorb.
3. Define dark current, and how you would reduce it.

   Dark current arises from the fact that everything has thermal energy, and this thermal energy is sometimes enough to promote electrons to higher energy states from which they must return to the ground state. If they do so by way of a radiative process like fluorescence, then a background noise signal will be detected. This can be reduced quite a bit by cooling the detector.
4. What are some disadvantages of the vacuum phototube and the photomultiplier tube?

   Both devices are sensitive to low intensities, and have a fast response. However, they both cause a lot of light damage to the sample. Another disadvantage is that the semiconductor material only conducts under certain conditions. In the case of reverse-bias set up, no current will flow.
5. How is quantum efficiency related to spectral response?

   The quantum efficiency is the number of liberated electrons compared to the number of incident photons, while the spectral response is the ratio of the generated current to the incident power.

Contributors and Attributions

- Jennifer Lien

6.10.1: Detectors of Light is shared under a CC BY-NC-SA 4.0 license and was authored, remixed, and/or curated by LibreTexts.

- **Detectors of Light** is licensed CC BY-NC-SA 4.0.

6.10.2: Radiation Transducers

Introduction

In Nessler's original method for determining ammonia (see Section 7.4) the analyst's eye serves as the detector, matching the sample's color to that of a standard. The human eye, of course, has a poor range—it responds only to visible light—and it is not particularly sensitive or accurate. Modern detectors use a sensitive transducer to convert a signal consisting of photons into an easily measured electrical signal. Ideally the detector's signal, S, is a linear function of the electromagnetic radiation's power, P,

$$S = kP + D \tag{6.10.2.1}$$

where k is the detector's sensitivity, and D is the detector's dark current, or the background current when we prevent the source's radiation from reaching the detector. There are two broad classes of spectroscopic transducers: photon transducers and thermal transducers, although we will subdivide the photon transducers given their rich variety. Table 6.10.2.1 provides several representative examples of each class of transducers.

> Transducer is a general term that refers to any device that converts a chemical or a physical property into an easily measured electrical signal. The retina in your eye, for example, is a transducer that converts photons into an electrical nerve impulse; your eardrum is a transducer that converts sound waves into a different electrical nerve impulse.

Table 6.10.2.1. Examples of Transducers for Spectroscopy

transducer	class	wavelength range	output signal
photovoltaic cell	photon	350–750 nm	current
phototube	photon	200–1000 nm	current
photomultiplier	photon	110–1000 nm	current
Si photodiode	photon	250–1100 nm	current
photoconductor	photon	750–6000 nm	change in resistance
photovoltaic cell	photon	400–5000 nm	current or voltage
thermocouple	thermal	0.8–40 μm	voltage
thermistor	thermal	0.8–40 μm	change in resistance
pneumatic	thermal	0.8–1000 μm	membrane displacement
pyroelectric	thermal	0.3–1000 μm	current

Photon Transducers

A photon transducer takes a photon and converts it into an electrical signal, such as a current, a change in resistance, or a voltage. Many such detectors use a semiconductor as the photosensitive surface. When the semiconductor absorbs photons, valence electrons move to the semiconductor's conduction band, producing a measurable current.

Photovoltaic Cells

A photovoltaic cell (Figure 6.10.2.1) consists of a thin film of a semiconducting material, such as selenium sandwiched between two electrodes: a base electrode of iron or copper and a thin semi-transparent layer of silver or gold that serves as the collector electrode. When a photon of visible light falls on the photovoltaic cell it generates an electron and a hole with a positive charge within the semiconductor. Movement of the electrons from the collector electrode to the base electrode generates a current that is proportional to the power of the incoming radiation and that serves as the signal.

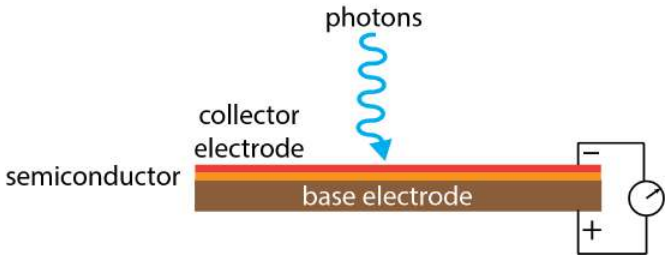


Figure 6.10.2.1: Schematic diagram of a photovoltaic cell that consists of a semiconducting thin film of selenium placed between two electrodes. When a photon strikes the semiconductor, it generates an electron and a hole that carries a positive charge. The movement of the electron from the collector electrode to the base electrode generates a measureable current.

Phototubes and Photomultipliers

Phototubes and photomultipliers use a photosensitive surface that absorbs radiation in the ultraviolet, visible, or near IR to produce an electrical current that is proportional to the number of photons that reach the transducer (see Figure 6.10.2.2). The current results from applying a negative potential to the photoemissive surface and a positive potential to a wire that serves as the anode. In a photomultiplier tube, a series of positively charged dynodes serves to amplify the current, producing 10^6–10^7 electrons per photon.

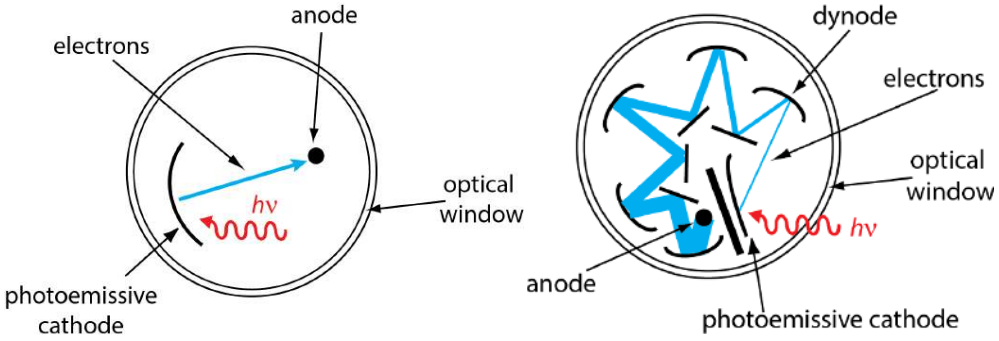


Figure 6.10.2.2.Schematic of a phototube (left) and a photomultiplier tube (right). In both, a photon strikes the photoemissive cathode producing electrons. In the phototube, the electrons that are drawn toward a positively charged anode, generating a current. In the photomultiplier tube, the electrons accelerate toward a positively charged dynode. Collision of these electrons with the dynode generates additional electrons, which accelerate toward the next dynode. A total of 10^6–10^7 electrons per photon eventually reach the anode, generating an electrical current.

Silicon Photodiodes

Applying a reverse biased voltage to the *pn* junction of a silicon semiconductor creates a depletion zone in which conductance is close to zero (see Chapter 2 for an earlier discussion of semiconductors). When a photon of light of sufficient energy impinges on the depletion zone, an electron-hole pair is formed. Movement of the electron through the *n*–region and of the hole through the *p*–region generates a current that is proportional to the number of photons reaching the detector. A silicon photodiode has a wide spectral range from approximately 190 nm to 1100 nm, which makes it versatile; however, a photodiode is less sensitive than a photomultiplier.

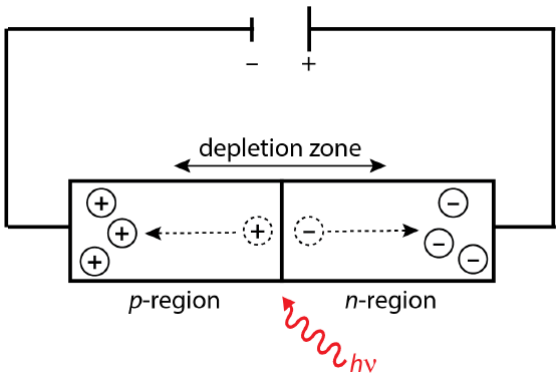


Figure 6.10.2.3: Illustration of silicon photodiode. See the text for a description of how the deterctor works.

Multichannel Photon Transducers

The photon transducers discussed above detect light at a single wavelength passed by the monochromator to the detector. If we wish to record a complete spectrum then we must continually adjust the monochromator either manually or by using a servo motor. In a multichannel instrument we create a one-dimensional or two-dimensional array of detectors that allow us to monitor simultaneously radiation spanning a broad range of wavelengths.

Photodiode Arrays

An individual silicon photodiode is quite small, typically with a width of approximately 0.025 mm. As a result, a linear (one-dimensional) array that consists of 1024 individual photodiodes has a width of just 25.6 mm. Figure 6.10.2.4 for example, shows the UV detector from an HPLC. Light from the deuterium lamp passes through a flow cell, is dispersed by a diffraction grating, and then focused onto a linear array of photodiodes. The close-up on the right shows the active protion of the photodiode array covered by an optical window. The active width of this photodiode array is approximately 6 mm and includes more than 200 individual photodiodes, sufficient to provide 1 nm resolution from 180 nm to 400 nm.

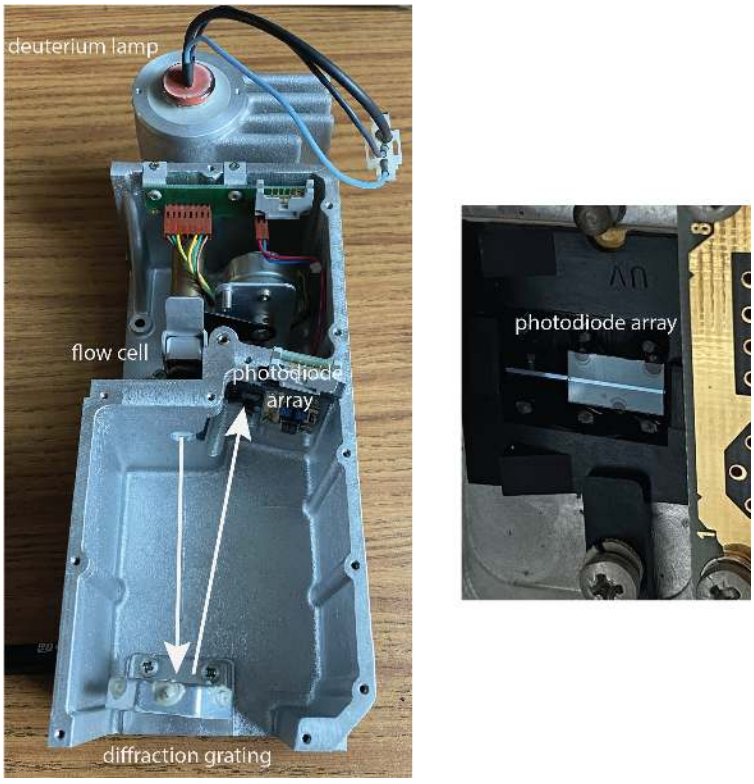


Figure 6.10.2.4: The photo on the left shows the UV detector from an HPLC and the photo on the right shows a close-up view of the its linear photodiode array deterctor. The bright line, from reflected light, is the photodiode array. The active portion of this detector is covered by an optically transparent window.

Charge-Transfer Devices

One way to increase the sensitivity of a detector is to collect and store charges before counting them. This is the approach taken with two types of charge-transfer devices: charged-coupled detectors and charge-injection detectors. Individual detectors, or pixels, consist of a layer of silicon dioxide coated on top of semiconductor. When a photon impinges on the detector it creates an electron-hole pair. An electrode on top of the silicon dioxide layer collects and stores either the negatively charged electrons or the positively charged holes. After a sufficient time, during which 10,000-100,000 charges are collected, the total accumulated charge is measured. Because individual pixels are small, typically 10 μm, they can be arranged in either a linear, one-dimensional array or a two-dimensional array. A charge-transfer device with 1024 x 1024 pixels will be approximately 10 mm x 10 mm in size.

Note

There are two important charge-transfer devices used as detectors: a charge-coupled device (CCD), which is discussed below, and a charge-injection device (CID), which is discussed in Chapter 10. Both types of devices use a two-dimensional arrays of individual detectors that store charge. The two devices differ primarily in how the accumulated charges are read.

Figure 6.10.2.5 shows a cross-section of a single detector (pixel) in a charge-coupled device (CCD) where individual pixels are arranged in a two-dimensional array. Electron-hole pairs are created in a layer of *p*-doped silicon. The holes migrate to the *n*-doped silicon layer and the electrons are drawn to the area below a positively charged electrode. When it is time to record the accumulated charges, the charge is read in the upper-right corner of the array with charges in the same row measured by shifting them from left-to-right. When the first row is read, the charges in the remaining rows are shifted up and recorded. In a charge-injection device, the roles of the electrons and holes are reversed and the accumulated positive charged are recorded.

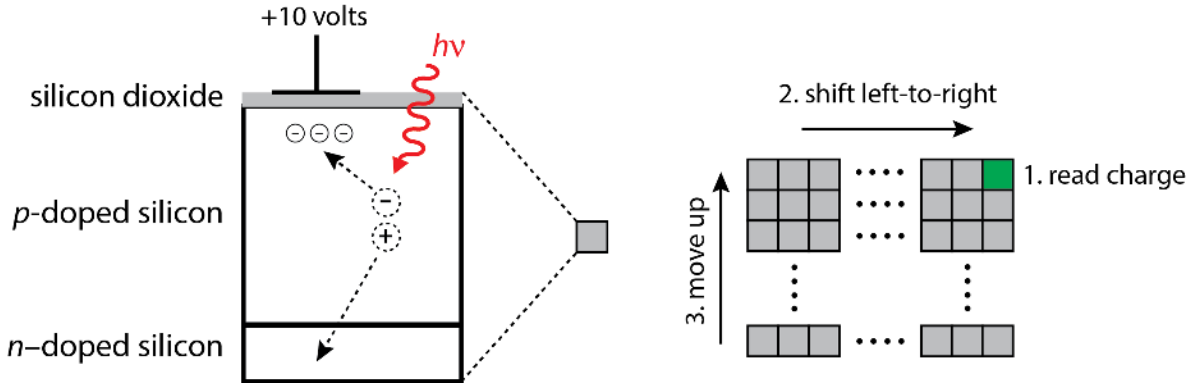


Figure 6.10.2.5: Schematic diagram of a charge-coupled device (CCD). The figure on the left shows a single detector, or pixel. When a photon impinges on the detector it generates an electron-hole pair in the *p*-doped layer. The electrons migrate and accumulate beneath a positively charged electrode. Individual pixels are arranged in an array, as shown on the right. This array may be a single row (a linear, or one-dimensional array) or in a series of rows. The charge in each pixels is recorded by shifting the pixels from left-to-right and by moving rows of pixels up.

Figure 6.10.2.6 shows an example of spectrophotometer equipped with a linear CCD detector that includes 2048 individual elements with a wavelength range from 200 nm to 1100 nm. The spectrometer is housed in a compact space of 90 mm x 60 mm



Figure 6.10.2.6: Example of a spectrophotometer equipped with a linear CCD detector.

Thermal Transducers

Infrared photons do not have enough energy to produce a measurable current with a photon transducer. A thermal transducer, therefore, is used for infrared spectroscopy. The absorption of infrared photons increases a thermal transducer's temperature,

changing one or more of its characteristic properties. A pneumatic transducer, for example, is a small tube of xenon gas with an IR transparent window at one end and a flexible membrane at the other end. Photons enter the tube and are absorbed by a blackened surface, increasing the temperature of the gas. As the temperature inside the tube fluctuates, the gas expands and contracts and the flexible membrane moves in and out. Monitoring the membrane's displacement produces an electrical signal.

This page titled 6.10.2: Radiation Transducers is shared under a CC BY-NC-SA 4.0 license and was authored, remixed, and/or curated by David Harvey.

- **7.5: Radiation Transducers** by David Harvey is licensed CC BY-NC-SA 4.0.

SECTION OVERVIEW

6.11: An Introduction to Infrared Spectrometry

6.11.1: Theory of Infrared Absorption Spectrometry

6.11.2: Infrared Sources and Transducers

6.11.3: FTIR- Hardware

6.11.4: Infrared Instruments

This page titled 6.11: An Introduction to Infrared Spectrometry is shared under a CC BY-NC-SA 4.0 license and was authored, remixed, and/or curated by David Harvey.

6.11.1: Theory of Infrared Absorption Spectrometry

Understanding the IR Spectrum

Figure 6.11.1.1 shows the infrared spectrum for ethanol. Unlike a UV/Vis absorbance spectrum, the *y*-axis is displayed as percent transmittance (%T) instead of absorbance, reflecting the fact that IR is used more for qualitative purposes than for quantitative purposes, where Beer's law, which is a linear function of concentration ($A = \epsilon bC$) makes absorbance the more useful measurement. The *x*-axis for an IR spectrum usually is given in wavenumbers, $\bar{\nu} = \lambda^{-1}$, with units of cm^{-1}. The peaks in an IR spectrum are inverted relative to absorbance spectrum; that is, they descend from a baseline of 100%T instead of rising from a baseline of zero absorbance.

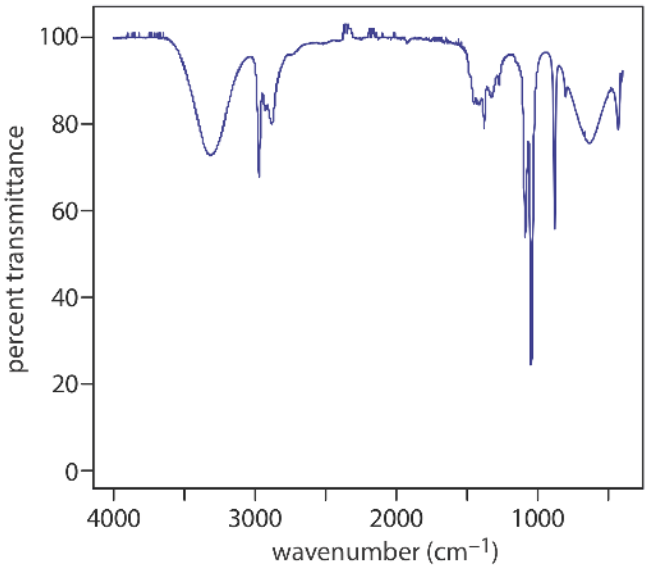


Figure 6.11.1.1: Infrared (IR) spectrum for ethanol.

Dipole Changes

The energy of a photon of infrared radiation (see Figure 6.11.1.2) is not sufficient to affect a change in the electronic energy levels of electrons, as in the UV/Vis atomic or molecular absorption or emission spectroscopies covered in Chapters 9, 10, and 12–15. Instead, infrared radiation is confined to changes in the vibrational energy states of molecules and molecular ions. To absorb an IR photon, the absorbing species must experience a change in its dipole moment, which allows the oscillation in the photon's electrical field to interact with an oscillation in charge within the absorbing species. If the two oscillations have the same frequency, then absorption is possible.

Note

Each vibrational energy state in Figure 6.11.1.2 also has a set of rotational energy states, which means that the peak for a particular change in vibrational energy levels may consist of a series of closely spaced lines, one for each of several changes in rotational energy. Because rotation is difficult for analytes that in liquid or solid forms, we usually see just a single, broad absorption line; for this reason, we will consider only vibrational transitions in this chapter.

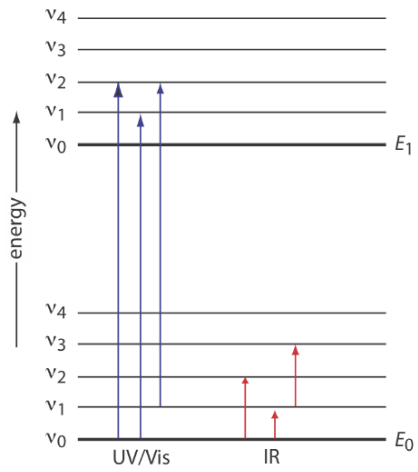


Figure 6.11.1.2: Diagram showing two electronic energy levels, E_0 and E_1, each with five vibrational energy levels, $\nu_0 - \nu_1$. Absorption of ultraviolet and visible radiation (shown by the blue arrows) leads to a change in the analyte's electronic energy levels and, possibly, a change in vibrational energy as well. A change in vibrational energy without a change in electronic energy levels occurs with the absorption of infrared radiation (shown by the red arrows).

Types of Molecular Vibrations

Although we tend to think of the atoms in a molecule as being rigidly fixed in space relative to each other, the individual atoms are in a constant state of motion: bond lengths increase and decrease by stretching and compressing, and bond angles change as the result of the bending of the bonds relative to each other. Figure 6.11.1.3 shows two different types of stretching (symmetric and asymmetric) and four different types of bending (in-plane rocking, in-plane scissoring, out-of-plane wagging, and out-of-plane twisting).

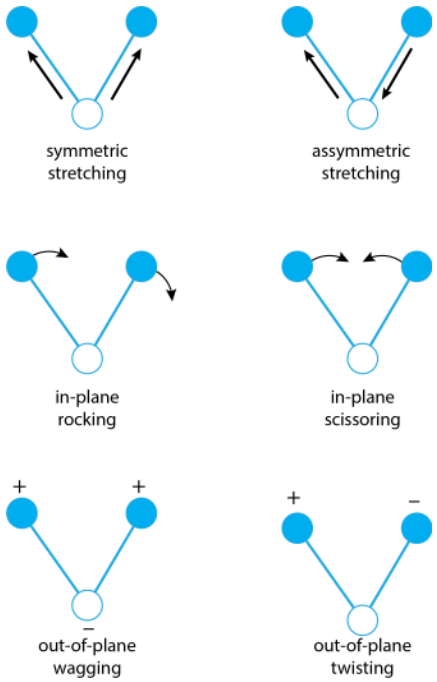


Figure 6.11.1.3: The six types of stretching and bending motions. For out-of-plane wagging and out-of-plane twisting, the plus sign $(+)$ indicates that the atom is moving toward the viewer and the minus sign $(-)$ indicate that the atom is moving away from the viewer.

Even a simple molecule can have many vibrational modes that give rise to a peak in the IR spectrum, as is the case for ethanol (Figure 6.11.1.1). The number of possible normal vibrational modes for a linear molecule is $3N - 5$, where N is the number of atoms, and $3N - 6$ for a non-linear molecule. Ethanol, for example, has $3 \times 9 - 6 = 21$ possible vibrational modes. As we will

see later in this section, some of these modes may not lead to a change in dipole moment, decreasing the number of peaks in the IR spectrum.

> **Note**
>
> Why does a non-linear molecule have $3N-6$ vibrational modes? Consider a molecule of methane, CH_4. Each of methane's five atoms can move in one of three directions (*x*, *y*, and *z*) for a total of $3\times5=15$ different ways in which the molecule's atoms can move. A molecule can move in three ways: it can move from one place to another, which we call translational motion; it can rotate around an axis, which we call rotational motion; and its bonds can stretch and bend, which we call vibrational motion. Because the entire molecule can move in the *x*, *y*, and *z* directions, three of methane's 15 different ways of moving are translational. In addition, the molecule can rotate about its *x*, *y*, and *z* axes, accounting for three additional forms of motion. This leaves $15-3-3=9$ vibrational modes. A linear molecule, such as CO_2, has $3N-5$ vibrational modes because it can rotate around only two axes.

Mechanical Model of Stretching in a Diatomic Molecule

The simplest model system for the the stretching and compressing of a bond is a weight with a mass, *m*, attached to an ideal spring that hangs from the ceiling as shown in Figure $6.11.1.4a$ If we pull on the mass and then release it, we initiate a simple oscillating harmonic motion that we can model using Hooke's law. If we displace the weight by a distance, *y*, then the force, *F*, that acts on the weight is

$$F=-ky \tag{6.11.1.1}$$

where k is the spring's force constant—a measure of the spring's springiness. The negative sign in Equation 6.11.1.1 indicates that this is the force needed to restore the spring to its original position; that is, the force is in the direction opposite to our action of pulling down on the weight.

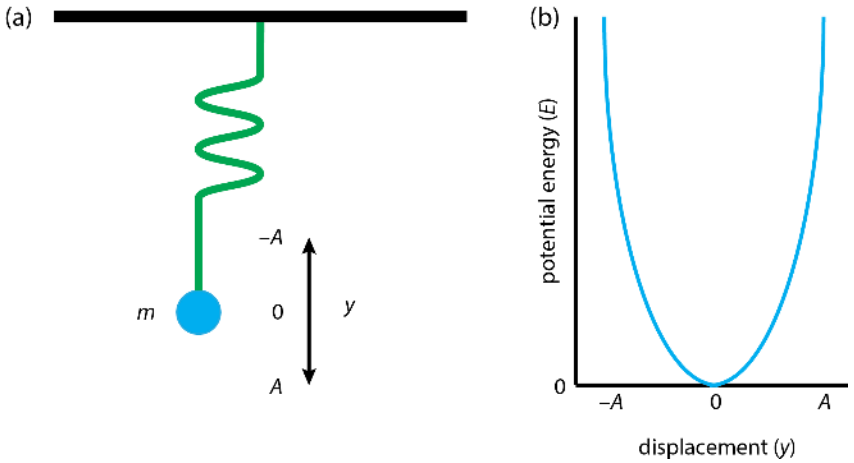


Figure 6.11.1.4: The model for a simple harmonic oscillator is shown in (a) and its potential energy as a function of displacement is shown in (b).

Potential Energy of a Harmonic Oscillator

Let's take the potential energy, *E*, of the spring and weight as 0 when they are at rest (*y* = 0). If we pull down on the weight by a distance of dy, then the change in the system's potential energy, dE, must increase by the product of force and distance

$$dE=-F\times dy=-ky\times dy \tag{6.11.1.2}$$

Integrating Equation 6.11.1.2 from $E=0$ to $E=E$ and from $y=0$ to $y=y$

$$\int_0^E dE=-k\int_0^y ydy \tag{6.11.1.3}$$

gives the energy as

$$E=\frac{1}{2}ky^2 \tag{6.11.1.4}$$

Figure 6.11.1.4*b* shows the resulting potential energy curve, for which the maximum potential energy is $\frac{1}{2}kA^2$ when the weight is at its maximum displacement. Note that the potential energy curve is a parabola.

Vibrational Frequency

The simple harmonic oscillator described above and shown in Figure 6.11.1.4 vibrates with a frequency, ν_0, given by the equation

$$\nu_0 = \frac{1}{2\pi}\sqrt{\frac{k}{m}} \tag{6.11.1.5}$$

where k is the spring's force constant and m is the weight's mass. We can extend this to a spring that connects two weights to each other by substituting for the mass, m, the system's reduced mass, μ

$$\mu = \frac{m_1 \times m_2}{m_1 + m_2} \tag{6.11.1.6}$$

where m_1 and m_2 are the masses of the two weights. Substituting Equation 6.11.1.6 into Equation 6.11.1.5 gives

$$\nu_0 = \frac{1}{2\pi}\sqrt{\frac{k}{\mu}} = \frac{1}{2\pi}\sqrt{\frac{k(m_1+m_2)}{m_1 \times m_2}} \tag{6.11.1.7}$$

If we make the assumption that Equation 6.11.1.7 applies to simple diatomic molecules, then we can estimate the bond's force constant, k, by measuring its vibrational frequency.

Quantum Treatment of Vibrations

Equations 6.11.1.4 and 6.11.1.7 are based on a classical mechanics treatment of the simple harmonic oscillator in which any displacement, and, thus, any energy is possible. Molecular vibrations, however, are quantized; thus

$$E = \left(v + \frac{1}{2}\right) \times h \times \frac{1}{2\pi}\sqrt{\frac{k}{\mu}} = \left(v + \frac{1}{2}\right) h\nu_0 \tag{6.11.1.8}$$

where v is the vibrational quantum number, which has allowed values of $0, 1, 2, \ldots$. The difference in energy, ΔE, between any two consecutive vibrational energy levels is $h\nu_0$. As allowed transitions in quantum mechanics are limited to $\Delta\nu = \pm 1$ and as the difference in energy is limited to $\Delta E = h\nu_0$, any particular mode of vibration should give rise to a single peak.

Anharmonic Behavior

The ideal behavior described in the last section, in which each vibrational motion that produces a change in dipole moment results in a single peak, does not hold due to a variety of reasons, including the coulombic interactions between the atoms as they move toward and away from each other. One result of these non-ideal behaviors is that the value ΔE does not remain constant for all values of the vibrational quantum number v. For larger values of v, the value of ΔE becomes smaller and transitions where $\Delta v = \pm 2$ or $\Delta v = \pm 3$ become possible giving rise to what are called overtone lines at frequencies that are $2\times$ or $3\times$ that for ν_0.

Why Do We See More or Fewer Vibrational Peaks Than Expected?

Figure 6.11.1.5 shows the IR spectrum for carbon dioxide, CO_2, which consists of three clusters of peaks located at approximately 670 cm^{-1}, 2350 cm^{-1}, and 3700 cm^{-1}. As carbon dioxide is a linear molecule that consists of two carbon-oxygen double bonds (O=C=O), it has $3 \times 3 - 5 = 9 - 5 = 4$ vibrational modes. So why do we see just three clusters of peaks?

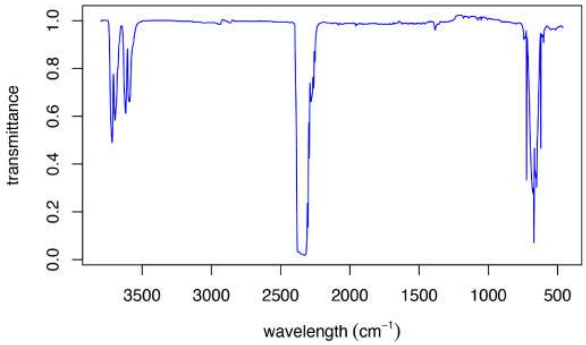


Figure 6.11.1.5: IR spectrum for CO_2. The raw data is from NIST.

One of the requirements for the absorption of infrared radiation, is that the vibrational motion must result in a change in dipole moment. Figure 6.11.1.6 shows the four vibrational modes for CO_2. Of these four vibrational modes, the symmetric stretch does not result in a change in dipole moment. Although this appears to explain why we see just three clusters of peaks, a close examination of the two bending motions in Figure 6.11.1.6 should convince you that they are identical and, therefore, will appear as a single peak.

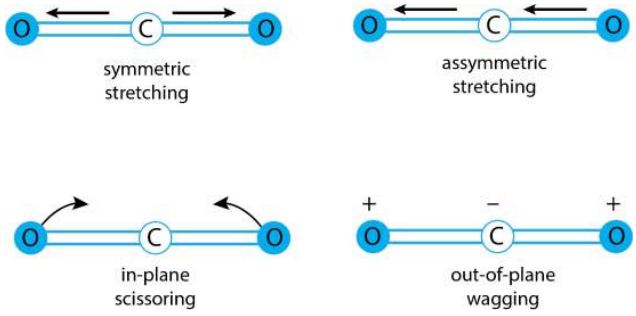


Figure 6.11.1.6: The four vibrational modes for CO_2. The symmetric stretch is not IR active as it does not involve a change in the molecules dipole moment. The asymmetric stretch occurs at 2349 cm^{-1}. The two bending motions are identical (or degenerate to each other) and appear at 667 cm^{-1}.

So what is the source of the cluster of peaks around 3700 cm^{-1}? Sometimes the absorption of a single photon excites two or more vibrational modes. In this case, the wavenumber for this absorption band is equivalent to the sum of the wavenumbers for the asymmetric stretch and the two degenerate bending modes (2349 + 667 = 3016 cm^{-1}, and 2349 + 667 + 667 = 3683 cm^{-1}). These are called combination bands.

Another source of additional peaks are overtone bands in which $\Delta v = \pm 2$ or $\Delta v = \pm 3$. Figure 6.11.1.7 shows the IR spectrum for carbonyl sulfide, OCS, which is analagous to CO_2 in which one of the oxygens is replaced with sulfur. The peak at 520 cm^{-1} is for its two degenerate bending motions and is labeled ν_2. The asymmetric stretch at 2062 cm^{-1} (ν_3) and the symmetric stretch at 859 cm^{-1} (ν_1) are the other two fundamental absorption bands. The remaining peaks are overtones, such as the peak labeled $2\nu_2$ at 1040 cm^{-1}, or combination bands, such as the peak labeled $\nu_3 + \nu_1$ at 2921 cm^{-1}. Many of the peaks appear as two peaks; this is the result of changes in rotational energy as well.

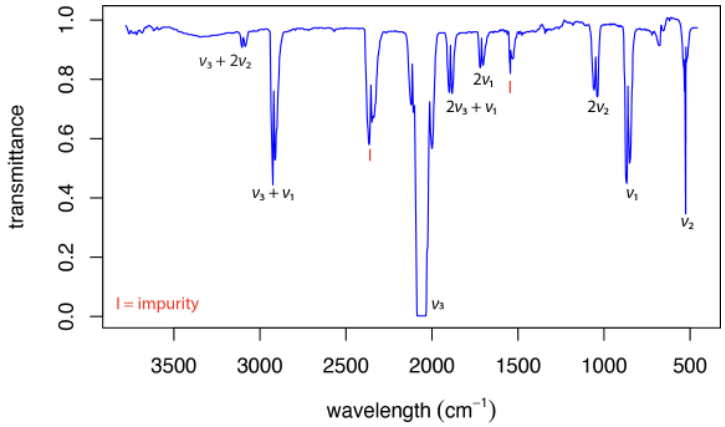


Figure 6.11.1.7: IR spectrum for OCS. The raw data is form NIST. The peak labeled as I (in red) is an impurity.

This page titled 6.11.1: Theory of Infrared Absorption Spectrometry is shared under a CC BY-NC-SA 4.0 license and was authored, remixed, and/or curated by David Harvey.

- **16.1: Theory of Infrared Absorption Spectrometry** by David Harvey is licensed CC BY-NC-SA 4.0.

6.11.2: Infrared Sources and Transducers

Instrumentation for IR spectroscopy requires a source of infrared radiation and a transducer for detecting the radiation after it passes through the sample.

Infrared Sources

Most IR sources consist of a solid material that emits radiation when heated by passing a current through the device. The intensity of emitted light typically is greatest at 5900–5000 cm^{-1} and then decreases steadily to 500 cm^{-1}. Common examples of IR sources include the Nernst glower (a ceramic rod heated to 1200–2200 K), a globar (a silicon carbide rod heated to 1300–1500 K), an incandescent wire (a nichrome wire heated to approximately 1100 K).

Infrared Transducers

Because IR radiation has a much lower energy than visible and ultraviolet light, the types of detectors used in UV/Vis spectroscopy are not suitable for recording IR spectra. Most IR detectors measure heat either directly or by a temperature-dependent change in one of its properties.

When two different metals, M_1 and M_2, are connected to each other in a closed loop, forming two M_1–M_2 junctions, a potential difference exists between the two junctions. The magnitude of this difference in potential depends on the difference in the temperatures of the two junctions. If the temperature of one junction is held constant or, if the source radiation is chopped—see Chapter 9.2 for a discussion of chopping—then the change in temperature of the other junction can be measured. The active junction is usually coated with a dark material to enhance the absorbance of thermal energy, and is small in size. A high-quality thermocouple is sensitive temperature differences as small as 10^{-6} K.

A bolometer is fashioned from materials for which the resistance is temperature dependent. As is true for a thermocouple, the active part of the detector is coated with a dark material and kept small in size.

Triglycerine sulfate, $(NH_2CH_2COOH)_3 \cdot H_2SO_4$, TGS, is a crystalline pyroelectric material. It usually is partially deuterated (DTGS) and, perhaps, doped with *L*-alanine (DLaTGS). The pyroelectric material is placed between two electrodes, one of which is optically transparent to infrared radiation. The absorption of infrared radiation results in a change in temperature and a resulting change in the detector's capacitance and, therefore, the current that flows.

This page titled 6.11.2: Infrared Sources and Transducers is shared under a CC BY-NC-SA 4.0 license and was authored, remixed, and/or curated by David Harvey.

- **16.2: Infrared Sources and Transducers** by David Harvey is licensed CC BY-NC-SA 4.0.

6.11.3: FTIR- Hardware

Below you will discover a detailed review of the physical components of a Fourier Transform Infrared (FTIR) Spectrometer. This module focuses on the physical equipments/components which make up the instrument, and not the mathematical aspects of analyzing the resulting data. For the mathematical treatment of FTIR data please see FTIR: Computational.

Introduction

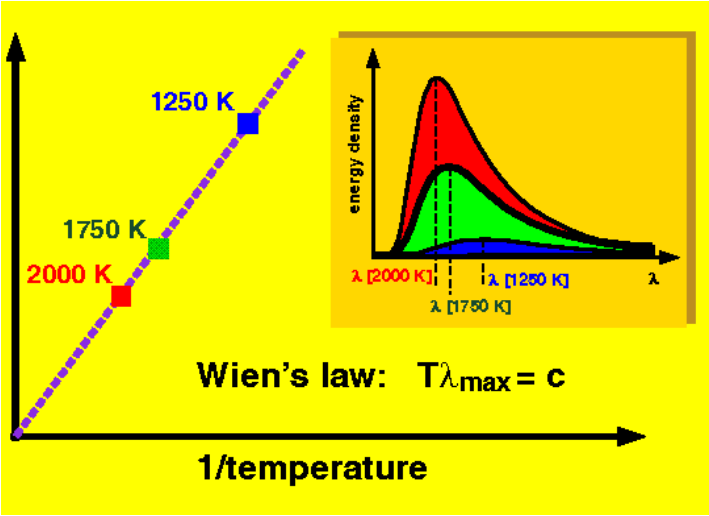
The history of the FTIR is a twisted and somewhat confusing tale, involving the development of technology, math, and materials. The beginnings of the first commercial FTIR spectrometer have been attributed to the work of M.J. Block and his research team in the small company 'Digilab'. Block's personal memoirs of the experience are both interesting and entertaining, involving highly classified information, money laundering, and fraud charges (follow the link if you wish to discover for yourself s-a-s.org/epstein/block/index.htm). Otherwise let it be enough to say that once the FTIR spectrometer was developed, its impact on the scientific community was paramount. Suddenly it was possible to acquire extremely accurate data in a much shorter amount of time than with traditional IR, as well as allowing for the analysis of exceedingly dilute samples. The device itself is surprisingly simple, with only one moving part. It’s no surprise that the instrument has been growing in popularity ever since its introduction, finding applications in chemistry, biology, materials science, process engineering, pharmaceutical science, and many other professions. FTIR instruments are relatively inexpensive, sturdy, stable, flexible, and fast. Through the years, this instrument have steadily evolved and new applications is continually being developed. Expanded computer power, the trend towards miniaturization, and more sophisticated imaging have all inspired some important new innovations.

FTIR measurements are conducted in the time domain. This is accomplished by directing the radiation from a broadband IR source to a beam splitter, which divides the light into two optical paths. Mirrors in the paths reflect the light back to the beam splitter, where the two beams recombine, and this modulated beam passes through the sample and hits the detector. In a typical interferometer, one mirror remains fixed, and the other retreats from the beam splitter at a constant speed. As the mirror moves, the beams go in and out of phase with each other, which generates a repeating interference pattern—a plot of intensity versus optical path difference—called an interferogram. The interferogram can be converted into the frequency domain via a Fourier transform, which yields the familiar single beam spectrum. The resolution of this spectrum is determined by the distance that the moving mirror traveled. Analyses generally fall into three categories, which are determined by the wavelengths of the radiation. Midrange IR covers the wavenumbers 1400 nm–3000 nm, where strong absorptions from fundamental molecular vibrations are measured. Near-IR (NIR) ranges from 700 nm–1400 nm. Far IR ranges from 3000 nm–1 mm.

Sources of Infrared Radiation

1. Theory

Infrared radiation is a relatively low energy light. All physical objects give of infrared radiation, the wavelength of which is dependent upon the temperature of the object. This phenomenon is known as black body radiation. The ideal IR source would emit radiation across the entire IR spectrum. As this is very difficult, a good compromise is a source which emits continuous mid-infrared radiation. Thankfully this can be achieved by most high temperature black bodies. Black body radiation was studied in depth by Max Planck, and it is through his equations that that the spectral energy density at a given wave number from a blackbody source of a given temperature can be calculated. Not to mention he was the discoverer of the properties of energy quanta. For this Max Planck received the 1918 Nobel Prize in Physics in recognition of the services he rendered to the advancement of Science. Now take a moment to examine the plot of energy density vs. max wave length below.



At first glance it would seem that the source temperature should be as high as possible to maximize the results—this is rarely the case. For example consider a typical incandescent light bulb. The tungsten filament glows at a temperature of 3000k, which would emit massive amounts of IR. The bulb portion of a light bulb is responsible for their lack of use as an IR source. The Bulb is made of glass which seals the tungsten filament in a vacuum. The vacuum is necessary to keep the tungsten from oxidizing at such high temperature, but the glass serves as an IR absorber, blocking its path to the sample. Any source we choose must be in direct contact with the atmosphere, because of this there are drastic limits on the temperature that we may operate an IR source.

There are several other limiting facts that require consideration when choosing an IR source. The material should be thermodynamically stable; otherwise it would quickly break down and need replacing. This would obviously be an expensive and undesired approach. There is also the possibility that the source may produce an excess of IR radiation. This would saturate the detector and possibly over load the analog-to-digital converter.

2. Silicon Carbide Rod (Globar)

The most ubiquitous IR source used in FTIR is a resistively heated silicon carbide rod (see image below). This device is commonly and somewhat simply referred to as a Globar.



An electric current is passed through the bar which become very hot, prducing large amounts of IR raidiation.

A Globar can reach temperatures of 1300K, and in the past required water cooling to keep from damaging the electrical components. Advances in ceramic metal alloys have lead to the production of Globars that no longer require water cooling. However these newer Globars are typically not operated at as high a temperature as 1300K.

3. Nichrome and Kanthanl wire Coils

Nichrome and Kanthanl wire coils where also once popular IR sources. They too did not require water cooling, ran at lower temperatures than a Globar, and possessed lower emissivity.

4. Nerst Glowers

Nernst Glowers are an IR source that is capable of hotter temperatures than a Globar. Nernst Glowers are fabricated from a mixture of refractory oxides. Despite being capable of higher temperature than a globar, the Nernst Glower is not capable of producing IR radiation above 2000 cm-1. As long as the frequency of IR needing to be examined is below 2000 cm-1 The Nernst Glower is an exceptional IR source, but if the entire mid IR range is necessary then using a Nernst Glower would result in low signal to noise ratios.

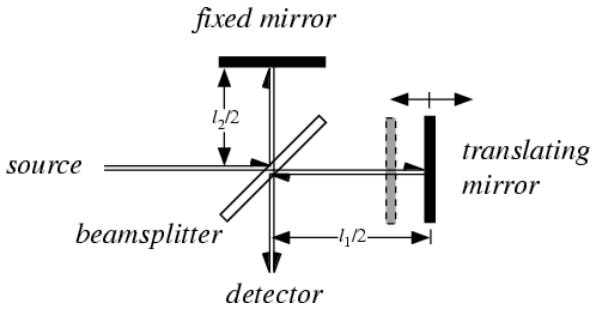
5. CarbonArcs (an unsuitable IR source)

It should be noted that the carbon IR sources used in many spectrometers today, similar to the Globar discussed above are different then the carbon arcs that you may be familiar with. A carbon arc occurs when an electrical discharge occurs between to carbon electrodes. These sparks are incredibly bright reaching temperature as hot at 6000 K. IR sources capitalizing on the large IR output of these arcs have ultimately shown to possess more draw backs than advantages. Because the carbon electrodes are consumed in the arcing process it would be necessary to continuously feed new rod forward to maintain the arc. The rods would also require an inert atmosphere to avoid combustion of the carbon. These limiting features and add complication of carbon archs makes them unfit as IR sources.

Michaleson Interferometer

History

The creation of today's FTIR would not have been possible had it not been for the existence of the Michelson interferometer. This essential piece of optical equipment was invented by Albert Abraham Michelson. He received the Nobel Prize in 1907 for his accurate measurements of the wavelengths of light. His Nobel winning experiments were made possible by his invention of the interferometer. Albert Michelson was in fact the first member of the United States of America to receive the Nobel Prize, solidifying the U.S as a world leader in science. Michelson did not invent the interferometer to perform infrared spectroscopy; in fact his experiments had nothing to do with any kind of spectroscopy. Michelson's goal was to discover evidence for luminiferous aether, the material once believed to permeate the universe allowing for the propagation of light waves. Of course it is now known that no such aether exists and that light is capable of propagating in vacuum. For more information on the extraordinary achievement of Michelson and his invention of the interferometer go to http://en.Wikipedia.org/wiki/Michels...ley_experiment.

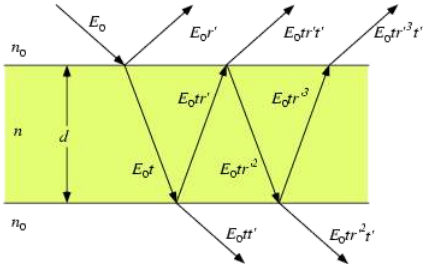


Above is a digram of the basic concepts and components of a Michelson Interferometer.

Each portion of the aboved digram will be discussed in turn and with further detail.

1. Beam Splitter

The beam splitter is made of a special material that transmits half of the radiation striking it and reflects the other half. Radiation from the source strikes the beam splitter and separates into two beams. One beam is transmitted through the beam splitter to the fixed mirror and the second is reflected off the beam splitter to the moving mirror. The fixed and moving mirrors reflect the radiation back to the beamsplitter. Again, half of this reflected radiation is transmitted and half is reflected at the beam splitter, resulting in one beam passing to the detector and the second back to the source.

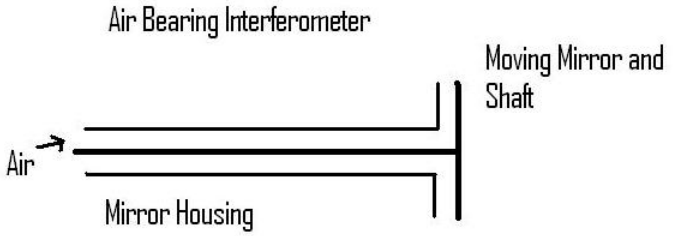


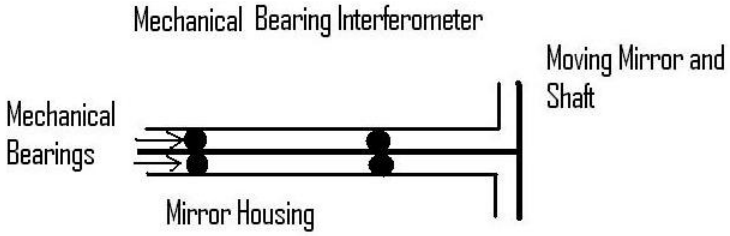
2. Stationary Mirror

The stationary mirror in an FTIR interferometer is nothing more than a flat highly reflective surface.

3. Moving Mirror

The beauty of the FTIR spectrometers design lies in its simplicity. There is present only one moving part in an FTIR spectrometer, its oscillating mirror. Air bearings are used in FTIR spectrometers because of the higher speed that the oscillating mirror is required to move at. The air bearings eliminate friction that would inevitable cause the moving parts of the mirror to break down, as is the case for the mechanical bearings. The air bearing has nearly replaced the mechanical bearing in all modern FTIR spectrometers. The older mechanical bearings required expensive ruby ball bearings, as they were the only material strong enough to endure the high physical demands of oscillating once every millisecond.





Detectors

Infrared detectors are classified into two categories; thermal, and quantum models. A thermal detector uses the energy of the infrared beam as heat, while the quantum mechanical detector uses the IR beam as light and provides for a more sensitive detector.

Thermo Detecto

A thermal detector operates by detecting the changes in temperature of an absorbing material. Their output may be in the form of an electromotive force (thermocouples), a change in resistance of a conductor (bolometer) or semiconductor (thermistor bolometer), or the movement of a diaphragm caused by the expansion of a gas (pneumatic detector). There exist major limitations to these forms of IR detectors. Their response time is much slower (several milliseconds) than the vibrational frequency of the oscillating mirror in FTIR. The mirror is moving with a frequency of approximately 1.25 kHz, there for the response time for an IR detector employed in FTIR must have a response time of less than 1ms. A response time of less than one millisecond is obtainable with cryogenically cooled thermo detectors. These detectors are commonly too expensive to be desired over other forms of detectors.

Pyroelectric Bolometer

There is one kind of thermo detector that is both inexpensive and possesses a response time fast enough to be appropriate, as well as the additional benefit of operating at room temperature. This detector is the Pyroelectric bolometer detector. These detectors incorporate as their heat sensing element ferroelectric materials that exhibit a large spontaneous electrical polarization at temperatures below their curie point. If the temperature of the ferroelectric material is changed the degree of polarization also changes causing an electric current. Pyroelectric bolometer is based on a Pyroelectric crystal (usually LiTaO3 or PZT) covered by absorbing layer (silver or silver blackened with carbon)

Quantum Well Detector

Because of their higher sensitivity, and faster response times, quantum well detectors are much more ubiquitous to FTIR. The detection mechanism of Quantum Well Infrared Photodetector (QWIP) involves photoexcitation of electrons between ground and first excited states of single or a multiquantum well structure. The parameters are designed so that these photo excited carriers can escape from the well and be collected as photocurrent. These quantum wells can be realized by placing thin layers of two different high bandgap semiconductor materials alternately where the bandgap discontinuity creates potential wells associated with conduction bands and valence bands. When IR photons strick these materials they induce a current that is then transformed into a digital signal via a analog digital converter.

These detector work more effectively (increased sensitivity) when at lower temperature. This is in part due to the higher degree of instrumental noise associated with a higher thermal back ground. Today there are available a wide range of these photo detecting diodes that do not require cooling. The finer details of the detector are numerous and dependent on the parameters of the equipment, there for beyond the scope of this module.

References

1. Berthomieu, C, & Hienerwadel, R. (2009). Fourier transform infrared (FTIR) spectroscopy. Photosynthesis research, 101(2-3), 157-170.
2. James P. Smith and Vicki Hinson-Smith. Product Review: The Endearing FTIR Spectrophotometer, *Analytical Chemistry* 2003 75 (1), 37 A-39 A

Problems

Theoretical Promblems

1. Why is it necesary for there to be a moving mirror in an interferometer?
2. What Other Sources of IR radiation can you imagen might work for FTIR? Explain you reasoning.
3. Explain the Purpose of the refrence laser in FTIR. Why use a lazer instead of any other form of light?
4. What region of the IR spectrum would light with a wavelength of: a) 900nm b) 1500nm c) 3000nm.

Calculations

1. Determine the wavenumber for the wavelengths given in problem 4. of the theoretical questions
2. Calculate the photon energy of laser light with a wavelength of 632.9nm, why might this be the chosen wavelenth for an FTIR refrence lazer?

6.11.3: FTIR- Hardware is shared under a CC BY-NC-SA 4.0 license and was authored, remixed, and/or curated by Jeffrey Rossini.

- **FTIR: Hardware** by Jeffrey Rossini is licensed CC BY-NC-SA 4.0.

6.11.4: Infrared Instruments

Instrumentation for infrared spectroscopy use one of three common optical benches: non-dispersive instruments, dispersive instruments, and Fourier transform instruments. As we have already examined non-dispersive and dispersive instruments in Chapter 13, and because they are no longer as common as they once were, we give them only a brief consideration here. Fourier transform instruments, which dominate the current marketplace, receive a more detailed treatment.

Non-Dispersive Instruments

The simplest instrument for IR absorption spectroscopy is a filter photometer similar to that shown earlier in Figure 13.4.1 for UV/Vis absorption. These instruments have the advantage of portability, which makes the useful in the field, and typically are used as dedicated analyzers for gases such as HCN and CO.

Dispersive Instruments

Infrared instruments using a monochromator for wavelength selection use double-beam optics similar to that shown earlier in Figure 13.4.3. Double-beam optics are preferred over single-beam optics because the sources and detectors for infrared radiation are less stable than those for UV/Vis radiation. In addition, it is easier to correct for the absorption of infrared radiation by atmospheric CO_2 and H_2O vapor when using double-beam optics. Resolutions of 1–3 cm^{-1} are typical for most instruments.

Fourier Transform Instruments

We covered the basic concepts of the Fourier transform in Chapter 7, which you may wish to review. In this section we take a more detailed look at the application of Fourier transforms to infrared instrumentation.

Components of a FT-IR

In a Fourier transform infrared spectrometer, or FT–IR, the monochromator is replaced with an interferometer (Figure 6.11.4.1). There are four key components that make up the interfometer: the drive mechanism that moves the moving mirror, the beam splitter, the light source, and the detector.

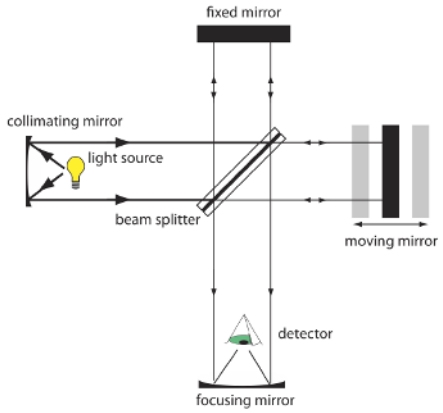


Figure 6.11.4.1: Schematic diagram of an interferometer. This is the same figure as Figure 7.7.1. The sample is positioned between the beam splitter and the detector.

Drive Mechanism

As we learned in Chapter 7, the Fourier transform encodes information about the wavelength or frequency of source radiation absorbed by the sample by observing how the signal reaching the detector varies with time. As the moving mirror is displaced in space, some frequencies of light experience complete constructive interference, some frequencies of light experience complete destructive interference, and other frequencies fall somewhere in between giving rise to a time domain spectrum. As the signal is monitored as function of time and the moving mirror is traversing a variable distance, the drive mechanism must allow for a precise and accurate relationship between the two. The mechanism of the moving mirror must be capable of moving the mirror through a distance of up to 20 cm at a scan rate as fast as 10 cm/s; it must also accomplish this while maintaining the mirror's orientation relative to the axis of its movement. To maintain accuracy, a HeNe laser, which emits visible light with a wavelength of 632.8 nm, is aligned with the light source so that they follow the same optical path.

Beam Splitter

The beam splitter is designed to reflect 50% of the source radiation to the fixed mirror and to pass the remaining 50% of the source radiation to the moving mirror. The materials used to construct the beam splitter depends on the range of wavelengths being used. The most common range of wavelengths, which is called mid-IR, runs from approximately 670 cm^{-1} to 4000 cm^{-1}. Instruments for mid-IR use a beam splitter that consists of silicon or germanium coated onto a substrate of KBr or NaCl.

Sources and Transducers

The most common sources for FT-IR are those discussed in the previous section, such as a Nernst glower. The most common transducer for FT-IR is pyroelectric triglycine sulfate.

This page titled 6.11.4: Infrared Instruments is shared under a CC BY-NC-SA 4.0 license and was authored, remixed, and/or curated by David Harvey.

- **16.3: Infrared Instruments** by David Harvey is licensed CC BY-NC-SA 4.0.

SECTION OVERVIEW

6.12: Applications of Infrared Spectrometry

Infrared spectroscopy finds wide use for both qualitative and quantitative analysis. Our organization of IR applications follows that traditionally used by others by dividing the broad range of infrared radiation into three distinct units: the near-IR (4000 cm^{-1} to 14,000 cm^{-1}, or 2,500 nm to 700 nm), the mid-IR (670 cm^{-1} to 4000 cm^{-1}, or 15 µm to 2.5 µm), and the far-IR (670 cm^{-1} to 10 cm^{-1}, or 1000 µm to 15 µm). Note that the near in near-IR means that it is nearest to the visible range of light. Of these, the most important in terms of the breadth of applications is the mid-IR.

6.12.1: Mid-Infrared Absorption Spectometry

6.12.2: Mid-Infrared Reflection Spectrometry

6.12.3: Near-Infrared and Far-Infrared Spectroscopy

This page titled 6.12: Applications of Infrared Spectrometry is shared under a CC BY-NC-SA 4.0 license and was authored, remixed, and/or curated by David Harvey.

6.12.1: Mid-Infrared Absorption Spectometry

Mid-infrared spectrometry is used for the routine qualitative analysis and, to a lesser extent, the quantitative analysis of organic molecules. In this section we consider absorption spectrometry in which we measure the absorbance of IR light as it passes through a gas, solution, liquid, or solid sample. In Section 17.2 we consider reflectance spectrometry in which we measure the absorbance of IR light as it reflects off the surface of a solid sample or a thin film of a liquid sample.

Sample Handling

Infrared spectroscopy is routinely used to analyze gas, liquid, and solid samples. We know from Beer's law, $A = \epsilon b C$, that absorbance is a linear function of the analyte's concentration, C, and the distance, b, the light travels through the sample. The challenge with obtaining an IR spectrum, is rarely the analyte's concentration or path length; instead it is finding materials and solvents that are transparent to IR radiation. The optical windows in IR cells are made from materials, such as NaCl and KBr, that are transparent to infrared radiation.

Gas Phase Samples

The cell for analyzing a sample in the gas phase generally is a 5–10 cm glass cylinder fitted with optically transparent windows. For an analyte with a particularly small concentration, the sample cell is designed with reflective surfaces that allow the infrared radiation to make several passes through the cell before it exits the sample cell, increasing the pathlength and, therefore, the absorbance.

Solution Solutions

The analysis of a sample in solution is limited by the solvent's IR absorbing properties, with carbon tetrachloride, CCl_4, carbon disulfide, CS_2, and chloroform, $CHCl_3$, being common solvents. A typical solution cell is shown in Figure 6.12.1.1. It is fashioned with two NaCl windows separated by a spacer. By changing the spacer, pathlengths from 0.015–1.0 mm are obtained. The sample is introduced into the cell using a syringe and the sample inlet port.

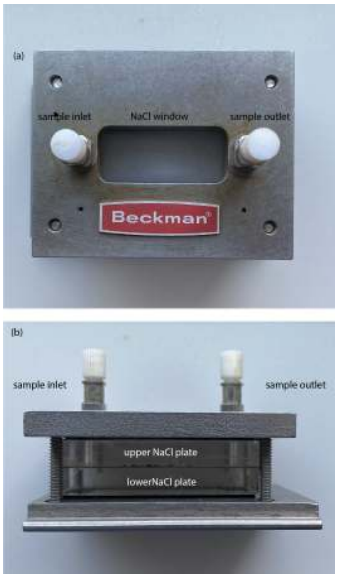


Figure 6.12.1.1: IR cell for analytes that are in solution. (a) View from above showing the sample inlet, the sample outlet, and the NaCl window. (b) View from the side showing the two NaCl plates.

Liquid Phase Samples

A sample that is a volatile liquid may be analyzed using the solution cell in Figure 6.12.1.1. For a non-volatile liquid sample, however, a suitable sample for qualitative work can be prepared by placing a drop of the liquid between the two NaCl plates shown in Figure 6.12.1.2*a*, forming a thin film that typically is less than 0.01 mm thick. An alternative approach is to place a drop of the sample on a disposable card equipped with a polyethylene "window" that IR transparent with the exception of strong absorption bands at 2918 cm^{-1} and 2849 cm^{-1} (Figure 6.12.1.2*b*).



Figure 6.12.1.2: Two examples of IR sample cells for liquid samples: (a) NaCl salts plates; (b) disposable card with a polyethylene window that is IR transparent with the exception of strong absorption bands at 2918 cm^{-1} and 2849 cm^{-1}.

Solid Phase Samples

Transparent solid samples are analyzed by placing them directly in the IR beam. Most solid samples, however, are opaque, and are first dispersed in a more transparent medium before recording the IR spectrum. If a suitable solvent is available, then the solid is analyzed by preparing a solution and analyzing as described above. When a suitable solvent is not available, solid samples are analyzed by preparing a mull of the finely powdered sample with a suitable oil and then smearing it on a NaCl salt plate or a disposable IR card (Figure 6.12.1.2). Alternatively, the powdered sample is mixed with KBr and pressed, under high pressure, into a thin, optically transparent pellet, as shown in Figure 6.12.1.3

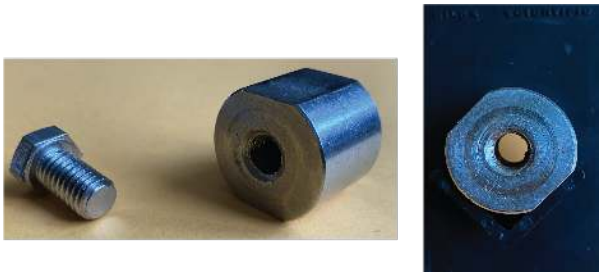


Figure 6.12.1.3: KBr press for preparing a solid sample for an IR analysis. The photo on the left shows the press. A threaded bolt is screwed into the back of the press (hidden from view). A portion of the sample, mixed with KBr, is added to the press and the second threaded bolt is screwed into the press. The two bolts are tightened by turning against each other, forming an optically transparent pellet, as shown by the photo on the right that looks through the pellet. With the threaded bolts removed, the press sits in a holder and placed in the spectrometer's optical path.

Qualitative Analysis

The most important application of mid-infrared spectroscopy is in the qualitative identification of organic molecules. Figure 6.12.1.4 shows mid-IR solution spectra for four simple alcohols: methanol, CH_3OH, ethanol, CH_3CH_2OH, propanol, $CH_3CH_2CH_2OH$, and isopropanol, $(CH_3)_2CHOH$. Clearly there are similarities and differences in these four spectra: similarities that might lead us to expect that each molecule contains the same functional groups and differences that appear as features unique to a particular molecule. The similarities in these four spectra appear at the higher wavenumber end of the *x*-axis scale; we call the peaks we find there group frequencies. The differences in these four spectra occur below approximately 1500 cm^{-1} in what we call the fingerprint region.

Note

The fingerprint region is defined here as beginning at 1500 cm^{-1}, extending to the lowest wavenumber shown on the *x*-axis. If you do some searching on the fingerprint region you will see that there is no broad agreement on where it begins. In my searching, I found sources that place the beginning of the fingerprint region as 1500 cm^{-1}, 1450 cm^{-1}, 1300 cm^{-1}, 1200 cm^{-1}, and 1000 cm^{-1}.

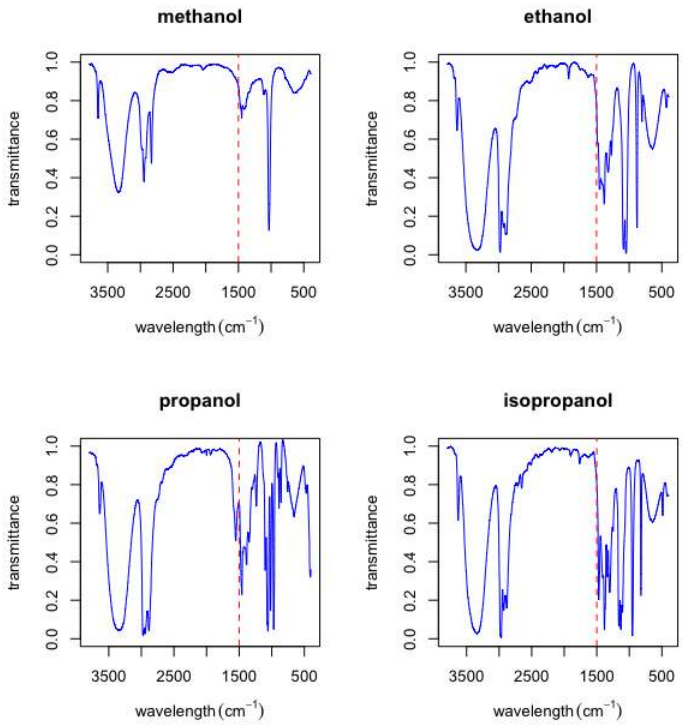


Figure 6.12.1.4: IR spectra for four simple alcohols: methanol, CH_3OH, ethanol, CH_3CH_2OH, propanol, $CH_3CH_2CH_2OH$, and iso-propanol, $(CH_3)_2CHOH$. Samples were prepared using carbon tetrachloride as a solvent. The vertical dashed red line at 1500 cm^{-1} marks the beginning of the fingerprint region. The original data for these spectra are from NIST.

Group Frequencies

All four of the spectra in Figure 6.12.1.4 share a small intensity, sharp peak at approximately 3650 cm^{-1}, a strong intensity, broad peak at approximately 3350 cm^{-1}, and two medium intensity, sharp peaks at 2950 cm^{-1} and 3850 cm^{-1}. By comparing spectra for these and other compounds, we know that the presence of a broad peak between approximately 3200 cm^{-1} and 3600 cm^{-1} is good evidence that the compound contains a hydrogen-bonded –OH functional group. The sharp peak at approximately 3650 cm^{-1} also is evidence of an –OH functional group, but one that is not hydrogen-bonded. The two sharp peaks at 2950 cm^{-1} and 3850 cm^{-1} are consistent with C–H bonds. All four of these peaks are for stretching vibrations. Tables of group frequencies are routinely available.

The "Fingerprint" Region

Figure 6.12.1.5 shows a close-up of the fingerprint region for the alcohol samples in Figure 6.12.1.4 Of particular interest with this set of samples is the increasing complexity of the spectra as we move from the simplest of these alcohols (methanol), to the most complex of these alcohols (propanol and isopropanol). Also of interest is that each spectrum is unique in a way that allows us to confirm a sample by matching it against a library of recorded spectra. There are a number of accessible collections of spectra that are available for this purpose. One such collection of spectra is the NIST Webbook—NIST is the National Institute of Standards and Technology—which is the source of the data used to display the spectra included in this section's figures and which includes spectra for over 16,000 compounds.

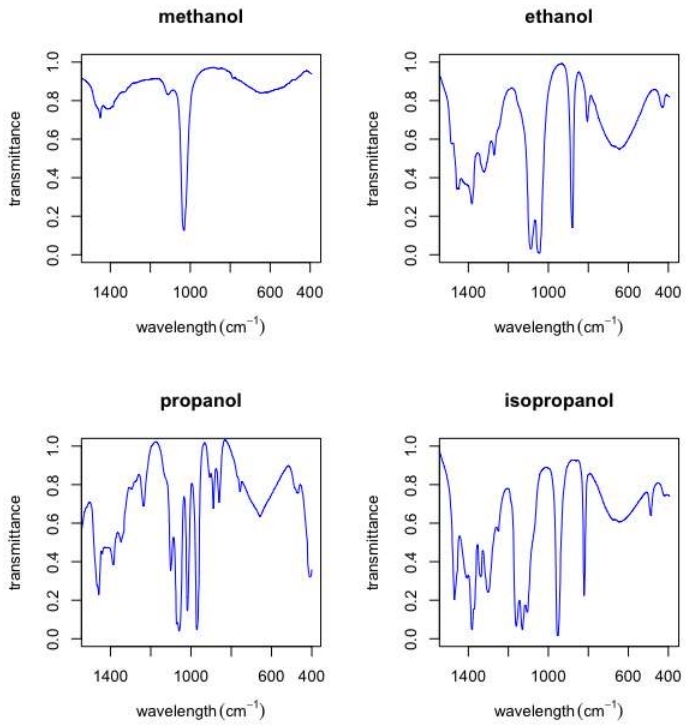


Figure 6.12.1.5: IR spectra in the fingerprint region for four simple alcohols: methanol, CH_3OH, ethanol, CH_3CH_2OH, propanol, $CH_3CH_2CH_2OH$, and iso-propanol, $(CH_3)_2CHOH$. Samples were prepared using carbon tetrachloride as a solvent. The original data for these spectra are from NIST.

Computer Search Systems

With the availability of computerized data acquisition and storage it is possible to build digital libraries of standard reference spectra. The identity of an a unknown compound often can be determined by comparing its spectrum against a library of reference spectra, a process known as spectral searching. Comparisons are made using an algorithm that calculates the cumulative difference between the sample's spectrum and a reference spectrum. For example, one simple algorithm uses the following equation

$$D = \sum_{i=1}^{n} |(A_{sample})_i - (A_{reference})_i| \tag{6.12.1.1}$$

where D is the cumulative difference, A_{sample} is the sample's absorbance at wavelength or wavenumber i, $A_{reference}$ is the absorbance of the reference compound at the same wavelength or wavenumber, and n is the number of digitized points in the spectra. Note that the spectra are defined here by absobrance instead of transmittance as absorbance is directly proportional to concentration. The cumulative absolute difference is calculated for each reference spectrum. The reference compound with the smallest value of D is the closest match to the unknown compound. The accuracy of spectral searching is limited by the number and type of compounds included in the library, and by the effect of the sample's matrix on the spectrum.

Another advantage of computerized data acquisition is the ability to subtract one spectrum from another. When coupled with spectral searching it is possible to determine the identity of several components in a sample without the need of a prior separation step by repeatedly searching and subtracting reference spectra. An example is shown in Figure 6.12.1.6 in which the composition of a two-component mixture is determined by successive searching and subtraction. Figure 6.12.1.6*a* shows the spectrum of the mixture. A search of the spectral library selects cocaine•HCl (Figure 6.12.1.6*b*) as a likely component of the mixture. Subtracting the reference spectrum for cocaine•HCl from the mixture's spectrum leaves a result (Figure 6.12.1.6*c*) that closely matches mannitol's reference spectrum (Figure 6.12.1.6*d*). Subtracting the reference spectrum for mannitol leaves a small residual signal (Figure 6.12.1.6*e*).

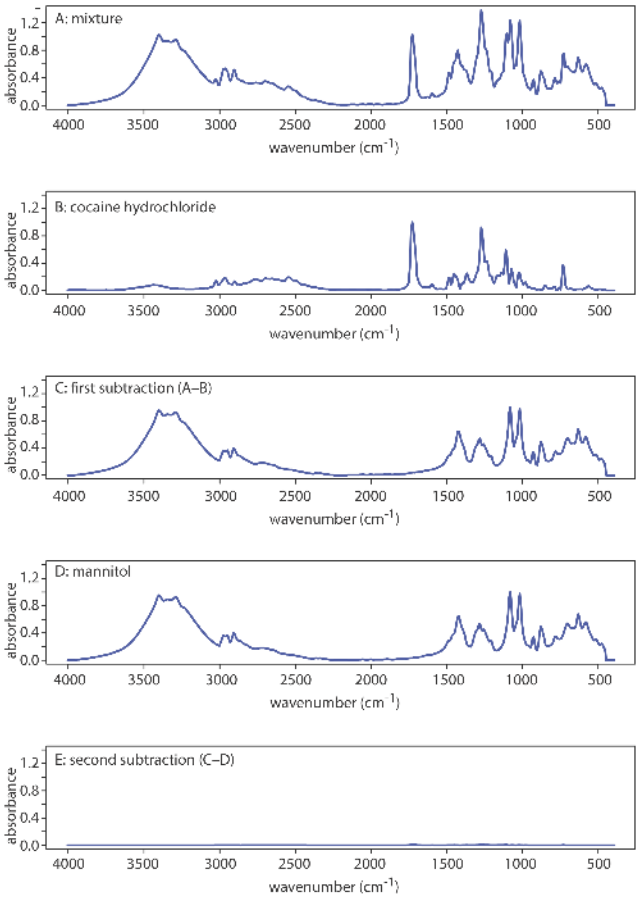


Figure 6.12.1.6: Identifying the components of a mixture by spectral searching and subtracting. (a) IR spectrum of the mixture; (b) Reference IR spectrum of cocaine•HCl; (c) Result of subtracting the spectrum of cocaine•HCl from the mixture's spectrum; (d) Reference IR spectrum of mannitol; and (e) The residual spectrum after removing mannitol's contribution to the mixture's spectrum. IR spectra traditionally are displayed using percent transmittance, %T, along the *y*-axis. Because absorbance—not percent transmittance—is a linear function of concentration, spectral searching and spectral subtraction, is easier to do when displaying absorbance on the *y*-axis.

Quantitative Applications

A quantitative analysis based on the absorption of infrared radiation, although important, is encountered less frequently than with UV/Vis absorption, primarily due to the three issues raised here.

Deviations from Beer's Law

One challenge for quantitative IR is the greater tendency for instrumental deviations from Beer's law when using infrared radiation. Because an infrared absorption band is relatively narrow, any deviation due to the lack of monochromatic radiation is more pronounced. In addition, infrared sources are less intense than UV/Vis sources, which makes stray radiation more of a problem. Differences between the path lengths for samples and for standards when using thin liquid films or KBr pellets are a problem, although an internal standard can correct for any difference in pathlength; alternatively, we can use the cell shown in Figure 6.12.1.1to maintain a constant path length.

Background Correction

The water and carbon dioxide in air have strong absorbances in the mid-IR. A double-beam dispersive instrument corrects for the contributions of CO_2 and H_2O vapor because they are present in both pathways through the instrument. An FT-IR, however, includes only a single optical path, so it is necessary to collect a separate spectrum to compensate for the absorbance of atmospheric CO_2 and H_2O vapor. This is done by collecting a background spectrum without the sample and storing the result in the instrument's computer memory. The background spectrum is removed from the sample's spectrum by taking the ratio the two signals. Another approach is to flush the sample compartment with nitrogren.

Measuring Absorbance

Another challenge for quantitative IR is that establishing a 100% T ($A = 0$) baseline often is difficult because the optical properties of NaCl sample cells may change significantly with wavelength due to contamination and degradation. We can minimize this problem by measuring absorbance relative to a baseline established for the absorption band. Figure 6.12.1.7 shows how this is accomplished.

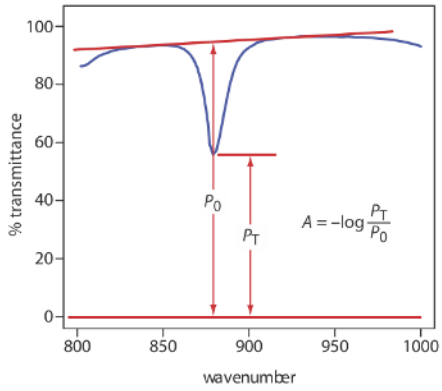


Figure 6.12.1.7: Method for determining absorbance from an IR spectrum.

Typical Applications

A recent review paper [Fahelelbom, K. M.; Saleh, A.; Al-Tabakha, M. A.; Ashames, A. A. *Rev. Anal. Chem.* **2022**, *41*, 21–33] summarizes the rich literature in quantitative mid-infrared spectrometry. Among the areas covered are the analysis of pharmaceuticals, including antibiotics, antihypertensives, antivirals, and counterfeit drugs. Mid-infrared spectrometry also finds use for the analysis of environmentally significant gases, such as methane, CH_4, hydrogen chloride, HCl, sulfur dioxide, SO_2, and nitric oxide, NO.

This page titled 6.12.1: Mid-Infrared Absorption Spectometry is shared under a CC BY-NC-SA 4.0 license and was authored, remixed, and/or curated by David Harvey.

- **17.1: Mid-Infrared Absorption Spectometry** by David Harvey is licensed CC BY-NC-SA 4.0.

6.12.2: Mid-Infrared Reflection Spectrometry

The first section of this chapter considered mid-IR absorption spectrometry in which we measure the amount of light that is transmitted by the sample, which we can convert, if we wish, into absorbance values. In the process, we examined both transmittance (Figure 7.1.4 and Figure 7.1.5) and absorbance (Figure 7.1.6) spectra. In this section, we consider experiments in which we measure the reflection of infrared radiation by a sample.

Types of Reflections

There are two broad classes of reflection: internal and external. As shown in Figure 6.12.2.1, internal reflection occurs when light encounters an interface between two media—here identified as the sample and the support—that have different refractive indicies, *n*. When the refractive index of the support is greater than the refractive index of the sample, then some of the light reflects off the interface. Attenuated total reflectance spectrometry is one example of an instrumental method that relies on internal reflection.

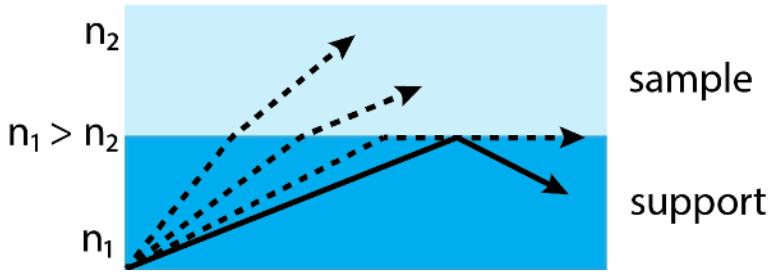


Figure 6.12.2.1: Internal reflection occurs at the interface between a support that has a greater refractive index than an overlying sample. For small angles of incidence (dashed lines), the light experiences refraction and crosses the interface. For a sufficiently large angle of incidence, the light experiences total reflection, as shown by the solid line.

External reflectance occurs when light reflects off of the sample's surface. As shown in Figure 6.12.2.2, the way in which light reflects depends on the nature of the sample's surface. In specular reflectance, the angle of reflection is the same at all locations because the sample's surface is smooth; in diffuse reflectance, the angle of reflection varies between locations due to the roughness of the sample's surface. Diffuse reflectance spectrometry is one example of an instrumental method that relies on external reflection.

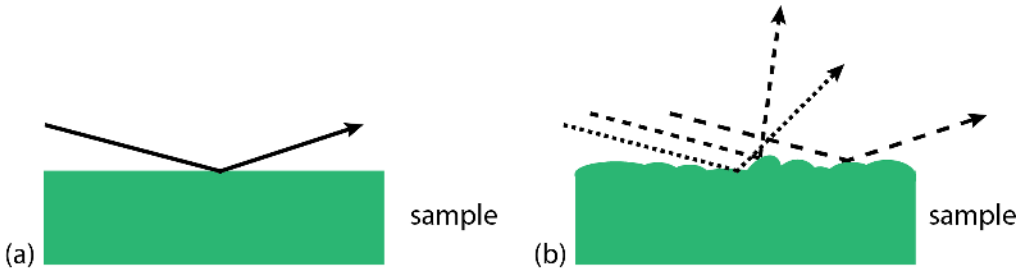


Figure 6.12.2.2: (a) Specular reflectance at a smooth surface and (b) diffuse reflectance from a rough surface.

Attenuated Total Reflectance Spectrometry

The analysis of an aqueous sample is complicated by the solubility of the NaCl cell window in water. One approach to obtaining an infrared spectrum of an aqueous solution is to use attenuated total reflectance instead of transmission. Figure 6.12.2.3 shows a diagram of a typical attenuated total reflectance (ATR) FT–IR instrument. The ATR cell consists of a high refractive index material, such as ZnSe or diamond, sandwiched between a low refractive index substrate and a lower refractive index sample. Radiation from the source enters the ATR crystal where it undergoes a series of internal reflections before exiting the crystal. During each reflection the radiation penetrates a short distance into the sample. This depth of penetration, d_p, depends on the wavelength of the light, λ, the refractive index of the ATR crystal, n_1, the refractive index of the sample, n_2, and the angle of the incident radiation, θ.

$$d_p = \frac{\lambda}{2\pi\sqrt{n_1^2 \sin^2\theta - n_2^2}} \qquad (6.12.2.1)$$

For example, when using ZnSe as the ATR crystal ($n_1 = 2.4$) and an angle of incidence of 45°, light of 1000 cm^{-1} penetrates to a depth of 2.0 μm in a sample with a refractive index similar to that for KBr ($n_2 = 1.5$).

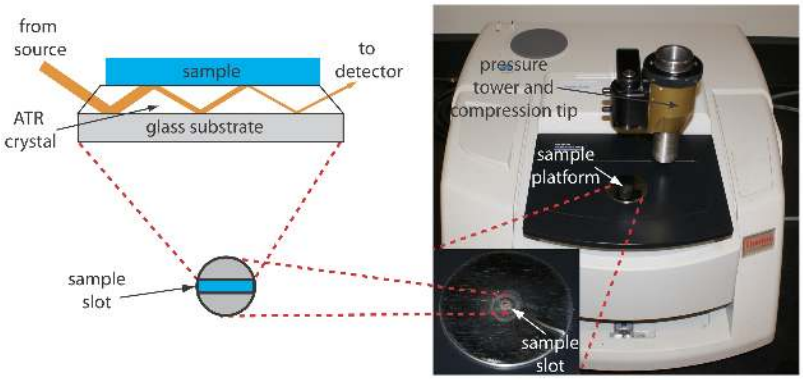


Figure 6.12.2.3. FT-IR spectrometer equipped with a diamond ATR sample cell. The inserts show a close-up photo of the sample platform, a sketch of the ATR's sample slot, and a schematic showing how the source's radiation interacts with the sample. The pressure tower is used to ensure proper contact of a solid sample with the ATR crystal.

Solid samples also can be analyzed using an ATR sample cell. After placing the solid in the sample slot, a compression tip ensures that it is in contact with the ATR crystal. Examples of solids analyzed by ATR include polymers, fibers, fabrics, powders, and biological tissue samples. ATR spectra are similar, but not identical, to those obtained by measuring transmission. An important contribution to this is the wavelength-dependent depth of penetration of the infrared radiation where a decrease in wavenumber (longer wavelength) results in a greater depth of penetration, which changes the intensity and width of absorption bands.

Diffuse Reflectance Spectrometry

Another reflectance method is diffuse reflectance, in which radiation is reflected from a rough surface, such as a powder. Powdered samples are mixed with a non-absorbing material, such as powdered KBr, and the reflected light is collected and analyzed. As with ATR, the resulting spectrum is similar to that obtained by conventional transmission methods. Figure 6.12.2.4 shows the IR spectrum for urea obtained using transmission and diffuse reflectance (both collected using an FT-IR). Both spectra show similar features between 1000 cm^{-1} and 2000 cm^{-1}, although there are differences in relative peak heights and background absorption.

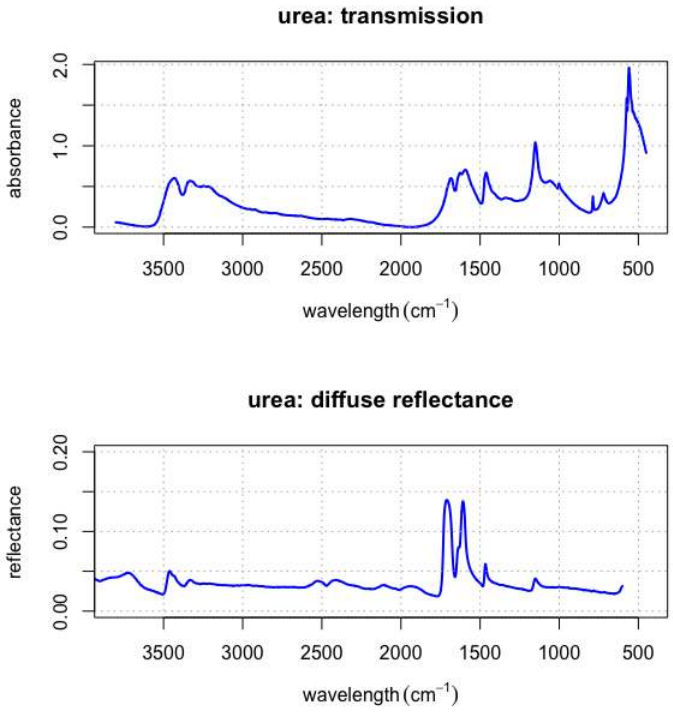


Figure 6.12.2.4: Diffuse reflection spectra for urea recorded using a FT-IR operating in transmission sample cell (top) or using a diffuse reflectance sample cell (bottom). The *y*-axis for the transmission spectrum is –log(T), where *T* is the transmittance, and the *y*-axis for the diffuse reflectance spectrum is –log(*R*), where *R* is the reflectance.

This page titled 6.12.2: Mid-Infrared Reflection Spectrometry is shared under a CC BY-NC-SA 4.0 license and was authored, remixed, and/or curated by David Harvey.

- **17.2: Mid-Infrared Reflection Spectrometry** by David Harvey is licensed CC BY-NC-SA 4.0.

6.12.3: Near-Infrared and Far-Infrared Spectroscopy

At the beginning of this chapter we divided infrared radiation into three areas: the near-IR, the mid-IR, and the far-IR. The mid-IR, which runs from 4000 cm^{-1} to 670 cm^{-1} (2.5 μm to 15 μm) is the most analytical useful region and was the subject of the previous two sections. Here we briefly turn our attention to applications using the near-IR and the far-IR.

Near-Infrared (NIR) Spectroscopy

The near-IR extends from approximately 13,000 cm^{-1} (a wavelength of 770 nm or 0.77 μm, the upper wavelength limit of visible light) to 4000 cm^{-1} (a wavelength of 2,500 nm or 2.5 μm). Earlier we noted that absorption bands in the region that extends from 1500 cm^{-1} to 4000 cm^{-1} are called group frequencies. The absorption bands in the near-infrared often are overtones and combination bands of these group frequencies. Of particular importance are functional groups that include hydrogen: OH, CH, and NH are examples. Absorption bands generally are less intense and less broad. Compared to mid-IR, the NIR is more useful for a quantitative analysis of aqueous samples because the OH absorption bands are much weaker. The instrumentation for NIR spectroscopy, both in transmission mode and in reflectance mode, is similar to that for UV/visible spectrometers and for mid-IR spectrometry.

Far-Infrared (FIR) Spectroscopy

The far-IR extends from approximately 670 cm^{-1} (a wavelength of 15 μm) to 10 cm^{-1} (a wavelength of 1000 μm or 1 mm). FIR spectroscopy finds applications in the analysis of materials that include metals, including metal oxides, metal sulfides, and metal-ligand complexes. FIR spectroscopy has also been applied to the analysis of polyamides, peptides, and proteins. Because the FIR merges into the microwave region, it also finds use in the analysis of the rotational energies of gases.

This page titled 6.12.3: Near-Infrared and Far-Infrared Spectroscopy is shared under a CC BY-NC-SA 4.0 license and was authored, remixed, and/or curated by David Harvey.

- **17.3: Near-Infrared and Far-Infrared Spectroscopy** by David Harvey is licensed CC BY-NC-SA 4.0.

SECTION OVERVIEW

6.13: Raman Spectroscopy

6.13.1: Theory of Raman Spectroscopy

6.13.2: Instrumentation

6.13.3: Applications of Raman Spectroscopy

6.13.4: Other Types of Raman Spectroscopy

This page titled 6.13: Raman Spectroscopy is shared under a CC BY-NC-SA 4.0 license and was authored, remixed, and/or curated by David Harvey.

6.13.1: Theory of Raman Spectroscopy

The blue color of the sky during the day and the red color of the sun at sunset are the result of the scattering of light by small particles of dust, by molecules of water vapor, and by other gases in the atmosphere. The efficiency of a photon's scattering depends on its wavelength. We see the sky as blue during the day because violet and blue light scatter to a greater extent than other, longer wavelengths of light. For the same reason, the sun appears red at sunset because red light scatters less efficiently and is more likely to pass through the atmosphere than other wavelengths of light. If we send a focused, monochromatic beam of radiation with a wavelength of λ through a medium of particles—whether solid particulates or individual molecules—that have dimensions $< 1.5\lambda$, then the radiation scatters in all directions. For example, infrared light in the near-IR with a wavelength of 700 nm will scatter from any particle whose longest dimension is less than 1,300 nm. Even in an otherwise transparent sample, scattering from molecules occurs.

Raman Spectra

There are two general classes of scattering: elastic scattering and inelastic scattering. In elastic scattering, a photon is first absorbed by a particle and then emitted without a change in its energy ($\Delta E = 0$); this is called Rayleigh scattering. With inelastic scattering, a photon is first absorbed by a particle and then emitted with a change in its energy ($\Delta E \neq 0$); this is called Raman scattering. A plot that shows the intensity of scattered radiation as a function of the scattered photon's energy, expressed as a change in the wavenumber, $\Delta\bar{\nu}$, is called a Raman spectrum and values of $\Delta\bar{\nu}$ are called Raman shifts.

Figure 6.13.1.1 shows a portion of the Raman spectrum for carbon tetrachloride and illustrates several important features. First, Rayleigh scattering produces an intense peak at $\Delta\bar{\nu} = 0$. Although the peak is intense, it carries no useful information as the absolute energy is just that for the source. Second, Raman scattering has two components—Stokes lines and the anti-Stokes lines—that have identical absolute shifts relative to the line for Rayleigh scattering, but that have different signs. The Stokes lines have positive values for $\Delta\bar{\nu}$ and the anti-Stokes lines have negative values for $\Delta\bar{\nu}$. Third, each of the Stokes lines is more intense than the corresponding anti-Stokes line. Fourth, because we measure the shift in a peak's wavenumber relative to the source radiation, the spectrum is independent of the source radiation.

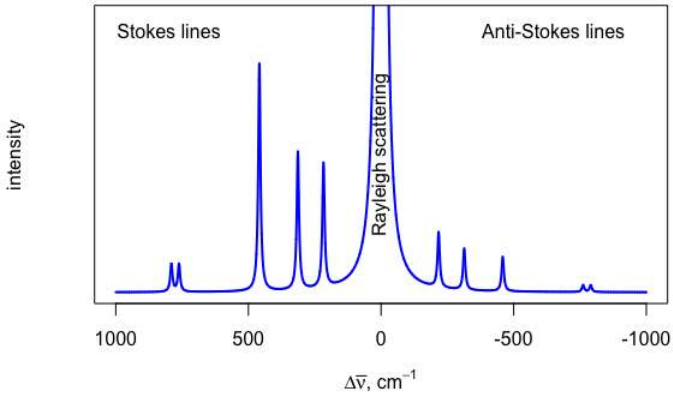


Figure 6.13.1.1: The Raman spectrum for carbon tetrachloride, CCl_4, showing the intense peak for Rayleigh scattering at $\Delta\bar{\nu} = 0$ and five lines each for Stokes and anti-Stokes scattering with $\Delta\bar{\nu} = \pm 217.0\ \text{cm}^{-1}$, $\Delta\bar{\nu} = \pm 313.5\ \text{cm}^{-1}$, $\Delta\bar{\nu} = \pm 458.7\ \text{cm}^{-1}$, $\Delta\bar{\nu} = \pm 761.7\ \text{cm}^{-1}$, and $\Delta\bar{\nu} = \pm 790.4\ \text{cm}^{-1}$. The values for these lines are from NIST; the spectrum itself is simulated.

Note

The energy—and, thus, the wavenumber—of a photon that experiences Stokes scattering is less than the energy—and, thus, the wavenumber—of the source radiation, which begs the question of why a Stokes shift is reported as a positive value instead of a negative value. Although you will find most Raman spectra with positive values for the Stokes shift, you also will find examples where Stokes shifts are reported with negative values. Because the Stokes lines are more intense than the anti-Stokes lines, and, therefore, more useful, and because their respective shifts result from the same changes in vibrational energy states

that we find in IR spectroscopy, it is convenient to report the Stokes lines as positive values so that we can align a species's Raman and IR spectra. See the next two sections for additional details.

Mechanism of Raman and Rayleigh Scattering

In Chapter 6 we examined the mechanism by which absorption and emission occur. In subsequent chapters we explored atomic absorption and atomic emission spectrometry, ultraviolet and visible molecular absorption spectrometry, molecular luminescence spectrometry, and infrared molecular absorption spectrometry. In each case we began by considering an energy level diagram that explains the origin of absorption and emission. Figure 6.13.1.2 provides an energy diagram that we can use to explain the origin of the lines that make up a Raman spectrum, such as the spectrum for carbon tetrachloride in Figure 6.13.1.1.

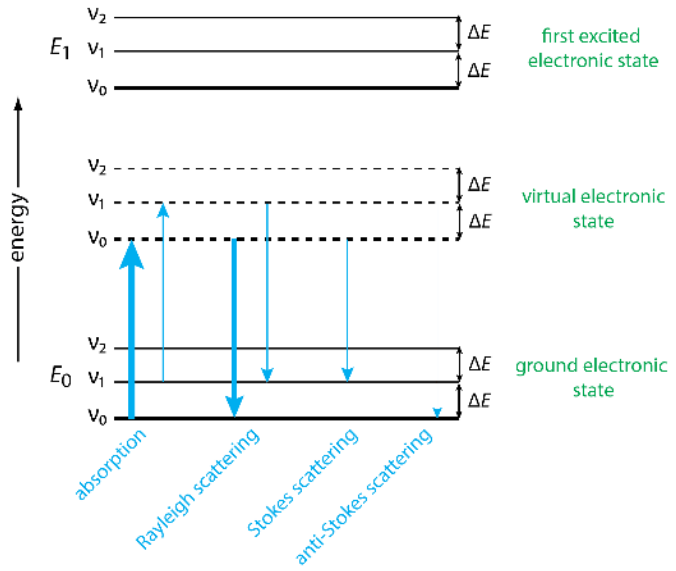


Figure 6.13.1.2: Energy level diagram that shows the origin of Rayleigh, Stokes, and anti-Stokes scattering. The thickness of the individual arrows provides a sense of the relative number of photons absorbed or emitted—the thicker the arrow, the greater the number of photons—although the individual thicknesses are not to scale.

The first thing to note about the energy level diagram in Figure 6.13.1.2 is that, in addition to showing the ground electronic state and the first excited electronic state—each with three vibrational energy levels—it also shows a virtual electronic state, something we did not encounter with other methods (see, for example, the energy diagram for UV and IR molecular absorption spectrometry in Figure 6.4.2). The ground and the first excited electronic states are quantized, which means that absorption cannot happen if the source's energy does not match exactly the change in energy between the two electronic states. The energy of an emitted photon also is fixed by the difference in the energy of the two electronic states. A virtual electronic state, however, is not quantized and is determined by the energy of the source radiation. The source of radiation, therefore, does not need to match a particular change in energy.

Absorption of a photon of source radiation moves the analyte from the ground electronic state to a virtual electronic state without a change in vibrational energy state, as seen by the two arrows at the far left of the diagram. Because the ground vibrational energy state, ν_0, is more populated than the vibrational energy state, ν_1, more of the analyte ends up in a virtual electronic state's lowest vibrational energy than in a higher vibrational energy state, which is shown here by the relative thickness of the two arrows.

Once in a virtual electronic state, the analyte can return to the ground excited state in one of three ways. It can do so without a change in the vibrational energy level. In this case, the energy of absorption and the energy of emission are the same and $\Delta E = 0$ and $\Delta \bar{\nu} = 0$. This is Rayleigh scattering and, as suggested by the combined thickness of the two arrows in Figure 6.13.1.2, it is the most important mechanism of relaxation.

When relaxation includes a change in the vibrational energy level, the result is an absolute change in energy equivalent to the difference in energy, ΔE, between adjacent vibrational energy levels. For Stokes scattering, relaxation is to a higher vibrational energy level, such as $\nu_0 \rightarrow \nu_1$ and, for anti-Stokes scattering, relaxation to a lower vibrational energy level, such as $\nu_1 \rightarrow \nu_0$. As suggested by the thickness of the lines for Stokes and anti-Stokes scattering in Figure 6.13.1.2, the Stokes lines are more intense than the anti-Stokes lines because they begin in a more heavily populated excited state.

Relationship Between IR and Raman Spectra

One important feature of Figure 6.13.1.2 is that the transition that gives rise to a particular Stokes line or anti-Stokes line is the same transition that will give rise to a corresponding IR band. If the selection rules for these transitions are the same for a particular species, then we expect that its IR spectrum and its Raman spectrum will have peaks at the same (or similar) values of $\bar{\nu}$ and $\Delta\bar{\nu}$ for its fundamental vibrations; however, as we see in Table 6.13.1.1 for carbon tetrachloride, CCl_4, there are five fundamental vibrations in its Raman spectrum, but just three in its IR spectrum.

Table 6.13.1.1: Fundamental Vibrational Energies for CCl_4 (values from NIST).

Infrared ($\bar{\nu}$, cm^{-1})	Raman ($\Delta\bar{\nu}$, cm^{-1})
—	217.0 (*l*)
309.9 (*l*) weak	313.5 (*l*)
—	458.7 (*l*)
768 (*g*); very strong	761.7 (*l*)
789 (*g*); very strong	790.4 (*l*)

The designations (*g*) and (*l*) indicate the sample's phase where (*g*) is gas phase and (*l*) is liquid phase. The designations of weak and very strong for the IR peaks indicates the relative extent of absorption: very strong means a relatively small %T (and a strong absorbance) and weak means a relatively large %T (and a weak absorbance). See Figure 6.13.1.1 for the relative amount of scattering in the Raman spectrum for CCl_4.

In Chapter 16 we learned that in IR spectroscopy a compound's fundamental vibrational energy is active—that is, we see a peak in its IR spectrum—only if the corresponding stretch or bend results in a change in the compound's dipole moment. For Raman spectroscopy, a compound's fundamental vibrational energy is active only if the corresponding stretch or bend results in a change in the polarizability of its electrons. Polarizability essentially is a measure of how easy it is to distort a compound's electron cloud by applying an external electric field, such as when a photon from the source is absorbed; in general, polarizability increases when a stretching or bending motion increases the compound's volume as the electrons are then spread over a greater amount of space.

Figure 6.13.1.3 shows the four stretching and bending modes for CCl_4. The stretching motion in (a), in which all four C–Cl bond lengths increase and decrease together, means the molecule's volume increases and decreases; thus, this vibrational mode is Raman active. The symmetry of the stretching motion, however, means there is no change in the molecule's dipole moment and the vibrational mode is IR inactive. The asymmetric stretch in (b), on the other hand, is both IR and Raman active. The bending motion in (c) results in the molecule becoming more or less compact in size, and is Raman active; the symmetry of the scissoring motions, however, means that the vibrational mode is IR inactive. The bending motions in (d) are both IR and Raman active.

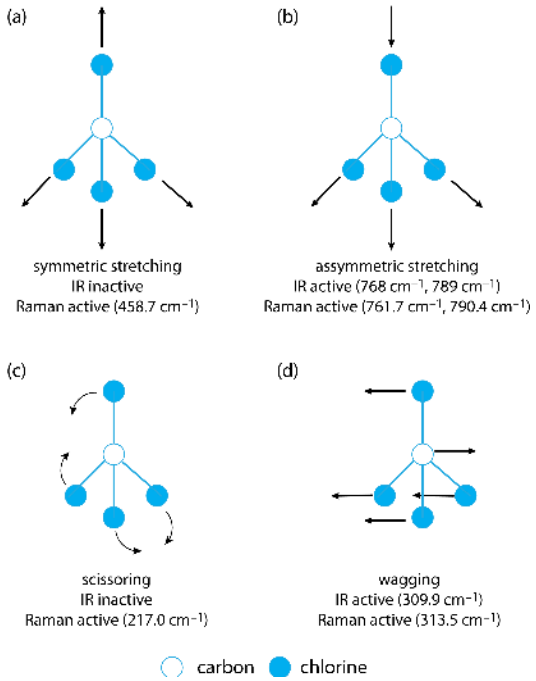


Figure 6.13.1.3. The four fundamental types of vibrational motions for CCl_4. The molecule has a tetrahedral shape. The black arrows show the direction of movement of the individual atoms. A molecule of CCl_4 has $3 \times 5 - 6 = 15 - 6 = 9$ vibrational modes. The bending motion in (d) and the stretching motion in (b) are triply degenerate, the bending motion in (c) is doubly degenerate, and the stretching motion in (a) is singly degenerate; this accounts for the nine possible vibrational modes. The asymmetric stretching motion in (b) gives rise to a split peak for reasons we will not consider here.

In general, symmetric stretching and bending modes result in relatively strong Raman scattering peaks, but no absorption in the IR, while symmetric stretching and bending modes result in both IR and Raman peaks. As a result, IR and Raman are complementary techniques.

Raman Depolarization Ratios

If the source of electromagnetic radiation is plane-polarized, then it is possible to collect a Raman spectrum using light scattered in a plane that is parallel to the source and, separately, in a plane that is perpendicular to the source. The ratio of a line's intensity of scattering in the perpendicular spectrum, $I_{\perp}$, to the intensity of scattering in the parallel spectrum, $I_{||}$, is called the depolarization ratio, p.

$$p = \frac{I_{\perp}}{I_{||}} \tag{6.13.1.1}$$

A Raman line that originates from a vibrational mode that does not change the molecules shape will result in a depolarization ratio close to zero and an absence of the line in the perpendicular spectrum. Figure 6.13.1.4shows the Raman spectrum when collecting data parallel (top) and perpendicular (bottom) to the light source. The absence of the peak at 458.7 cm^{-1} in the perpendicular spectrum confirms that this is the symmetric stretch illustrated in Figure 6.13.1.3a

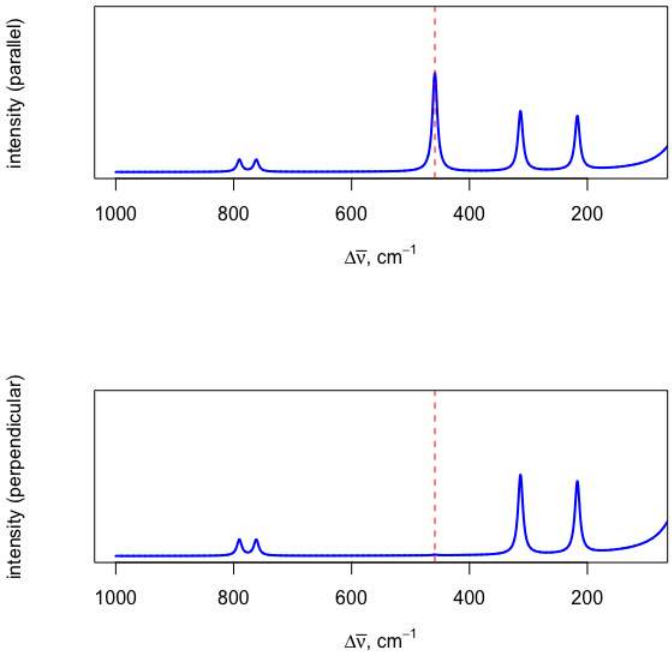


Figure 6.13.1.4: Raman spectrum for CCl_4 measured (top) parallel to the plane-polarized light source and (bottom) perpendicular to the plane-polarized source. The dashed red line shows the position of the symmetric stretch at 458.7 cm^{-1}; the absence of this peak in the perpendicular spectrum—the depolarization ratio, p is 0.005—confirms that this is the symmetric stretch. The remaining peaks have depolarization ratios of 0.75. The slope of increasing intensity below 200 cm^{-1} is from the Rayleigh scattering peak. The values for these lines are from NIST; the spectrum itself is simulated.

This page titled 6.13.1: Theory of Raman Spectroscopy is shared under a CC BY-NC-SA 4.0 license and was authored, remixed, and/or curated by David Harvey.

- **18.1: Theory of Raman Spectroscopy** by David Harvey is licensed CC BY-NC-SA 4.0.

6.13.2: Instrumentation

The basic instrumentation for Raman spectroscopy is similar to that for other spectroscopic techniques: a source or radiation, an optical bench for bringing the source to the sample, and a suitable detector.

Sources

One of the notable features of the Raman spectrum for CCl_4 (see Figure 18.1.1) is the low intensity of the Stokes lines and the anti-Stokes lines relative to the line for Rayleigh scattering. The low intensity of these lines requires that we use a high intensity source so that there are a sufficient number of scattered photons to collect. For this reason, a laser is the most common source for Raman spectroscopy, providing a high intensity, monochromatic source. Table $6.13.2.1$summarizes some of the more common lasers.

Table 6.13.2.1. Examples of Laser Sources for Raman Spectroscopy

type of laser	wavelengths (nm)
Ar ion	488.0 or 514.5
Kr ion	530.9 or 647.1
He/Ne	632.8
Near Infrared (NIR) Diode Laser	785 or 830
Nd/YAG	532 or 1064

The intensity of Raman scattering is proportional to $\frac{1}{\lambda^4}$, where λ is the wavelength of the source radiation; thus, the smaller the wavelength, the more intense the intensity of scattered light. For example, the intensity of scattering using an Ar ion laser at 488.0 nm is almost $23\times$ greater than the intensity of scattering using a Nd/YAG laser at 1064 nm

$$\frac{(1/480)^4}{(1/1064)^4} = 22.6$$

The increased scattering when using a smaller wavelength laser comes at a cost, however, of an interference from fluorescence from species that are promoted into excited electronic states by the source. The NIR diode laser and Nd/YAG laser, when operated at 1064 cm^{-1}, discriminate against fluorescence and are useful, therefore, for samples where fluorescence is a problem.

Samples

Raman spectroscopy has several advantages over infrared spectroscopy. Because water does not exhibit much Raman scattering it is possible to analyze aqueous samples; this is a serious limitation for IR spectroscopy where water absorbs strongly. The ability to focus a laser onto a small area makes it possible to analyze very small samples. A liquid sample, for example, can be held in the tip of a 1-mm inner diameter capillary tube, such as that used for measuring melting points. Solid samples and gaseous samples can be sampled using the same types of cells used in IR and FT-IR (see Chapter 17). Fiber optic probes make it possible to collect samples remotely. Figure $6.13.2.1$ shows the basic set-up. A small bundle of fibers (shown in blue) brings light from the source to the sample where a second bundle of fibers (shown in green) brings the scattered light to the slit that passes light onto the detector.

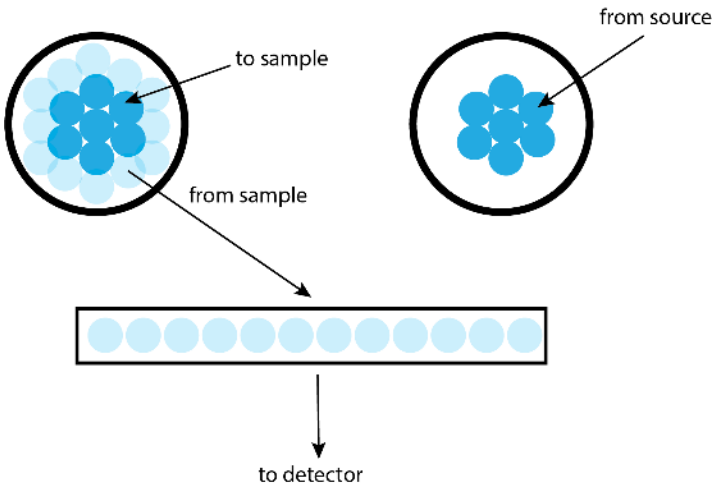


Figure 6.13.2.1: Illustration of a fiber optic probe for Raman spectroscopy. The darker blue circles are cross-sections of individual fibers that bring light from the source to the sample, and the lighter blue circles are cross-sections of individual fibers that collect scattered light from the sample and bring it to the detector. The circular arrangement of the collection fibers are gathered into a linear array and focused onto the entrance slit of the instrument's detector.

Optical Bench

Raman spectrometers use optical benches similar to those for UV/Vis or IR spectroscopy, which were covered in Chapter 7. Dispersive instruments place the laser source and the detector at 90° to each other so that any unscattered high intensity emission from the laser source is not collected by the detector. A filter is used to remove the Rayleigh scattering. To record a spectrum one either uses a scanning monochromator or a multichannel detector. Fourier transform instruments are similar to those used in FT-IR and include a filter to isolate the Stokes lines.

This page titled 6.13.2: Instrumentation is shared under a CC BY-NC-SA 4.0 license and was authored, remixed, and/or curated by David Harvey.

- **18.2: Instrumentation** by David Harvey is licensed CC BY-NC-SA 4.0.

6.13.3: Applications of Raman Spectroscopy

Raman spectroscopy is useful for both qualitative and quantitative analyses, examples of which are provided in this section.

Qualitative Applications

There are numerous databases that provide reference spectra for inorganic compounds, for minerals, for synthetic organic pigments, for natural and synthetic inorganic and organic pigments, and for carbohydrates. Such data bases are often searchable by not only name and formula, but by the prominent Raman scattering lines. Examples of spectra are included here using data from the databases linked to above.

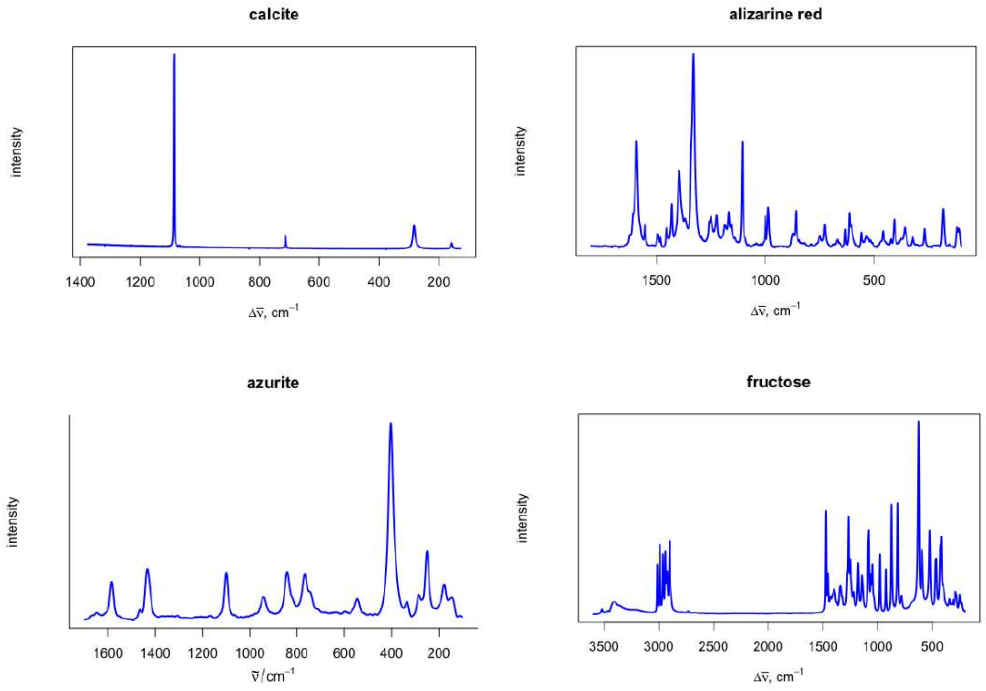


Figure 6.13.3.1: Examples of Raman spectra for the mineral calcite ($CaCO_3$), the organic pigment alizarine red ($C_{14}H_7NaO_7S$), the inorganic pigment azurite ($Cu_3(CO_3)_2(OH)_2$), and the carbohydrate fructose ($C_6H_{12}O_6$). The data for these spectra were obtained from the databases linked to at the beginning of this section.

Quantitative Applications

The intensity of Raman scattering, $I(\nu)_R$, is directly proportional to the intensity of the source radiation, I_l, and the concentration of the scattering species, C. The direct proportionality between $I(\nu)_R$ and I_l is important given that each photon experiencing Raman scattering requires approximately 10^8 excitation photons. Using a laser as a source of radiation and increasing its power leads to an improvement in sensitivity. The direct proportionality between $I(\nu)_R$ and the concentration of the scattering species means that a calibration curve of band intensity (or band area) is a linear function of concentration, allowing for a quantitative analysis.

This page titled 6.13.3: Applications of Raman Spectroscopy is shared under a CC BY-NC-SA 4.0 license and was authored, remixed, and/or curated by David Harvey.

- **18.3: Applications of Raman Spectroscopy** by David Harvey is licensed CC BY-NC-SA 4.0.

6.13.4: Other Types of Raman Spectroscopy

Traditional Raman spectroscopy has several limitations, perhaps the most important of which is that the probability of Raman scattering is much less than that for Rayleigh scattering, which leads to low sensitivity with detection limits often as large as 0.1 M. Here we briefly describe two forms of Raman spectroscopy that allow for significant improvements in detection limits.

Resonance Raman Spectroscopy (RRS)

If the wavelength of the source is similar to the wavelength needed to move the species from its ground electronic state to its first electronic excited state (not the virtual excited state shown in Figure 18.1.2), then the lines associated with the symmetric fundamental vibrations increase in intensity by a factor of 10^2 to 10^6. The improvement in sensitivity results in a substantial reduction in detection limits as low as 10^{-8} M. The use of a tunable laser makes it possible to adjust the wavelength of light emitted by the source to maximize the intensity of scattering.

Surface-Enhanced Raman Spectroscopy (SERS)

For reasons that are poorly understood, the intensity of Raman scattering lines is enhanced when the scattering species is absorbed to the surface of colloidal particles of metals such as Ag, Au, or Cu, or to the surface of etched metals. The phenomenon is not limited to just a few lines—as is the case for RRS—and results in a 10^3 to 10^6) improvement in the intensity of scattering. If a tunable laser is used for the source, allowing for both RRS and SERS, detection limits of 10^{-9} M to 10^{-12} M are possible.

This page titled 6.13.4: Other Types of Raman Spectroscopy is shared under a CC BY-NC-SA 4.0 license and was authored, remixed, and/or curated by David Harvey.

- **18.4: Other Types of Raman Spectroscopy** by David Harvey is licensed CC BY-NC-SA 4.0.

6.14: PROBLEMS

1. Provide the missing information in the following table.

wavelength (m)	frequency (s^{-1})	wavenumber (cm^{-1})	energy (J)
4.50×10^{-9}			
	1.33×10^{15}		
		3215	
			7.20×10^{-19}

2. Provide the missing information in the following table.

[analyte] (M)	absorbance	$\%T$	molar absorptivity (M^{-1} cm^{-1})	pathlength (cm)
1.40×10^{-4}			1120	1.00
	0.563		750	1.00
2.56×10^{-4}	0.225		456540	
1.55×10^{-3}	0.167		1550	5.00
		33.3		1.00
4.35×10^{-3}		21.2		
1.20×10^{-4}		81.3		10.00

3. A solution's transmittance is 35.0%. What is the transmittance if you dilute 25.0 mL of the solution to 50.0 mL?

4. A solution's transmittance is 85.0% when measured in a cell with a pathlength of 1.00 cm. What is the %T if you increase the pathlength to 10.00 cm?

5. The accuracy of a spectrophotometer is evaluated by preparing a solution of 60.06 ppm $K_2Cr_2O_7$ in 0.0050 M H_2SO_4, and measuring its absorbance at a wavelength of 350 nm in a cell with a pathlength of 1.00 cm. The expected absorbance is 0.640. What is the expected molar absorptivity of $K_2Cr_2O_7$ at this wavelength?

6. A chemical deviation to Beer's law may occur if the concentration of an absorbing species is affected by the position of an equilibrium reaction. Consider a weak acid, HA, for which K_a is 2×10^{-5}. Construct Beer's law calibration curves of absorbance versus the total concentration of weak acid (C_{total} = [HA] + [A^-]), using values for C_{total} of 1.0×10^{-5}, 3.0×10^{-5}, 5.0×10^{-5}, 7.0×10^{-5}, 9.0×10^{-5}, 11×10^{-5}, and 13×10^{-5} M for the following sets of conditions and comment on your results:

(a) $\varepsilon_{HA} = \varepsilon_{A^-} = 2000$ M^{-1} cm^{-1}; unbuffered solution.

(b) $\varepsilon_{HA} = 2000$ M^{-1} cm^{-1}; $\varepsilon_{A^-} = 500$ M^{-1} cm^{-1}; unbuffered solution.

(c) $\epsilon_{HA} = 2000$ M^{-1} cm^{-1}; $\epsilon_{A^-} = 500$ M^{-1} cm^{-1}; solution buffered to a pH of 4.5.

Assume a constant pathlength of 1.00 cm for all samples.

7. One instrumental limitation to Beer's law is the effect of polychromatic radiation. Consider a line source that emits radiation at two wavelengths, λ' and λ''. When treated separately, the absorbances at these wavelengths, A' and A'', are

$$A' = -\log \frac{P'_T}{P'_0} = \varepsilon' bC \qquad A'' = -\log \frac{P''_T}{P''_0} = \varepsilon'' bC$$

If both wavelengths are measured simultaneously the absorbance is

$$A = -\log \frac{\left(P'_T + P''_T\right)}{\left(P'_0 + P''_0\right)}$$

(a) Show that if the molar absorptivities at λ' and λ'' are the same ($\varepsilon' = \varepsilon'' = \varepsilon$), then the absorbance is equivalent to

$$A = \varepsilon bC$$

(b) Construct Beer's law calibration curves over the concentration range of zero to 1×10^{-4} M using $\varepsilon' = 1000$ M^{-1} cm^{-1} and $\varepsilon'' = 1000$ M^{-1} cm^{-1}, and $\varepsilon' = 1000$ M^{-1} cm^{-1} and $\varepsilon'' = 100$ M^{-1} cm^{-1}. Assume a value of 1.00 cm for the pathlength and that $P'_0 = P''_0 = 1$. Explain the difference between the two curves.

8. A second instrumental limitation to Beer's law is stray radiation. The following data were obtained using a cell with a pathlength of 1.00 cm when stray light is insignificant (P_{stray} = 0).

[analyte] (mM)	absorbance
0.00	0.00
2.00	0.40
4.00	0.80
6.00	1.20
8.00	1.60
10.00	3.00

Calculate the absorbance of each solution when P_{stray} is 5% of P_0, and plot Beer's law calibration curves for both sets of data. Explain any differences between the two curves. (*Hint*: Assume P_0 is 100).

9. In the process of performing a spectrophotometric determination of iron, an analyst prepares a calibration curve using a single-beam spectrophotometer similar to that shown in Figure 10.3.2. After preparing the calibration curve, the analyst drops and breaks the cuvette. The analyst acquires a new cuvette, measures the absorbance of the sample, and determines the %w/w Fe in the sample. Does the change in cuvette lead to a determinate error in the analysis? Explain.

10. The spectrophotometric methods for determining Mn in steel and for determining glucose use a chemical reaction to produce a colored spe- cies whose absorbance we can monitor. In the analysis of Mn in steel, colorless Mn^{2+} is oxidized to give the purple MnO_4^- ion. To analyze for glucose, which is also colorless, we react it with a yellow colored solution of the $Fe(CN)_6^{3-}$, forming the colorless $Fe(CN)_6^{4-}$ ion. The directions for the analysis of Mn do not specify precise reaction conditions, and samples and standards are treated separately. The conditions for the analysis of glucose, however, require that the samples and standards are treated simultaneously at exactly the same temperature and for exactly the same length of time. Explain why these two experimental procedures are so different.

11. One method for the analysis of Fe^{3+}, which is used with a variety of sample matrices, is to form the highly colored Fe^{3+}–thioglycolic acid complex. The complex absorbs strongly at 535 nm. Standardizing the method is accomplished using external standards. A 10.00-ppm Fe^{3+} working standard is prepared by transferring a 10-mL aliquot of a 100.0 ppm stock solution of Fe^{3+} to a 100-mL volumetric flask and diluting to volume. Calibration standards of 1.00, 2.00, 3.00, 4.00, and 5.00 ppm are prepared by transferring appropriate amounts of the 10.0 ppm working solution into separate 50-mL volumetric flasks, each of which contains 5 mL of thioglycolic acid, 2 mL of 20% w/v ammonium citrate, and 5 mL of 0.22 M NH_3. After diluting to volume and mixing, the absorbances of the external standards are measured against an appropriate blank. Samples are prepared for analysis by taking a portion known to contain approximately 0.1 g of Fe^{3+}, dissolving it in a minimum amount of HNO_3, and diluting to volume in a 1-L volumetric flask. A 1.00-mL aliquot of this solution is transferred to a 50-mL volumetric flask, along with 5 mL of thioglycolic acid, 2 mL of 20% w/v ammonium citrate, and 5 mL of 0.22 M NH_3 and diluted to volume. The absorbance of this solution is used to determine the concentration of $Fe3^+$ in the sample.

(a) What is an appropriate blank for this procedure?

(b) Ammonium citrate is added to prevent the precipitation of Al^{3+}. What is the effect on the reported concentration of iron in the sample if there is a trace impurity of Fe^{3+} in the ammonium citrate?

(c) Why does the procedure specify that the sample contain approximately 0.1 g of Fe^{3+}?

(d) Unbeknownst to the analyst, the 100-mL volumetric flask used to prepare the 10.00 ppm working standard of Fe^{3+} has a volume that is significantly smaller than 100.0 mL. What effect will this have on the reported concentration of iron in the sample?

12. A spectrophotometric method for the analysis of iron has a linear calibration curve for standards of 0.00, 5.00, 10.00, 15.00, and 20.00 mg Fe/L. An iron ore sample that is 40–60% w/w is analyzed by this method. An approximately 0.5-g sample is taken, dissolved in a minimum of concentrated HCl, and diluted to 1 L in a volumetric flask using distilled water. A 5.00 mL aliquot is removed with a pipet. To what volume—10, 25, 50, 100, 250, 500, or 1000 mL—should it be diluted to minimize the uncertainty in the analysis? Explain.

13. Lozano-Calero and colleagues developed a method for the quantitative analysis of phosphorous in cola beverages based on the formation of the blue-colored phosphomolybdate complex, $(NH_4)_3[PO_4(MoO_3)_{12}]$ [Lozano-Calero, D.; Martín-Palomeque, P.; Madueño-Loriguillo, S. *J. Chem. Educ.* **1996**, *73*, 1173–1174]. The complex is formed by adding $(NH_4)_6Mo_7O_{24}$ to the sample in the presence of a reducing agent, such as ascorbic acid. The concentration of the complex is determined spectrophotometrically at a wavelength of 830 nm, using an external standards calibration curve.

In a typical analysis, a set of standard solutions that contain known amounts of phosphorous is prepared by placing appropriate volumes of a 4.00 ppm solution of P_2O_5 in a 5-mL volumetric flask, adding 2 mL of an ascorbic acid reducing solution, and diluting to volume with distilled water. Cola beverages are prepared for analysis by pouring a sample into a beaker and allowing it to stand for 24 h to expel the dissolved CO_2. A 2.50-mL sample of the degassed sample is transferred to a 50-mL volumetric flask and diluted to volume. A 250-µL aliquot of the diluted sample is then transferred to a 5-mL volumetric flask, treated with 2 mL of the ascorbic acid reducing solution, and diluted to volume with distilled water.

(a) The authors note that this method can be applied only to noncol- ored cola beverages. Explain why this is true.

(b) How might you modify this method so that you can apply it to any cola beverage?

(c) Why is it necessary to remove the dissolved gases?

(d) Suggest an appropriate blank for this method?

(e) The author's report a calibration curve of

$$A = -0.02 + \left(0.72\ \text{ppm}^{-1}\right) \times C_{\text{P}_2\text{O}_5}$$

A sample of Crystal Pepsi, analyzed as described above, yields an absorbance of 0.565. What is the concentration of phosphorous, reported as ppm P, in the original sample of Crystal Pepsi?

> Crystal Pepsi was a colorless, caffeine-free soda produced by PepsiCo. It was available in the United States from 1992 to 1993.

14. EDTA forms colored complexes with a variety of metal ions that may serve as the basis for a quantitative spectrophotometric method of analysis. The molar absorptivities of the EDTA complexes of Cu^{2+}, Co^{2+}, and Ni^{2+} at three wavelengths are summarized in the following table (all values of ε are in M^{-1} cm^{-1}).

metal ion	$\varepsilon_{462.9}$	$\varepsilon_{732.0}$	$\varepsilon_{378.7}$
Co^{2+}	15.8	2.11	3.11
Cu^{2+}	2.32	95.2	7.73
Ni^{2+}	1.79	3.03	13.5

Using this information determine the following, assuming a pathlength, *b*, of 1.00 cm for all measurements:

(a) The concentration of Cu^{2+} in a solution that has an absorbance of 0.338 at a wavelength of 732.0 nm.

(b) The concentrations of Cu^{2+} and Co^{2+} in a solution that has an absorbance of 0.453 at a wavelength of 732.0 nm and 0.107 at a wavelength of 462.9 nm.

(c) The concentrations of Cu^{2+}, Co^{2+}, and Ni^{2+} in a sample that has an absorbance of 0.423 at a wavelength of 732.0 nm, 0.184 at a wavelength of 462.9 nm, and 0.291 at a wavelength of 378.7 nm.

15. The concentration of phenol in a water sample is determined by using steam distillation to separate the phenol from non-volatile impurities, followed by reacting the phenol in the distillate with 4-aminoantipyrine and $K_3Fe(CN)_6$ at pH 7.9 to form a colored antipyrine dye. A phenol standard with a concentration of 4.00 ppm has an absorbance of 0.424 at a wavelength of 460 nm using a 1.00 cm cell. A water sample is steam distilled and a 50.00-mL aliquot of the distillate is placed in a 100-mL volumetric flask and diluted to volume with distilled water. The absorbance of this solution is 0.394. What is the concentration of phenol (in parts per million) in the water sample?

16. Saito describes a quantitative spectrophotometric procedure for iron based on a solid-phase extraction using bathophenanthroline in a poly(vinyl chloride) membrane [Saito, T. *Anal. Chim. Acta* **1992**, *268*, 351–355]. In the absence of Fe^{2+} the membrane is colorless, but when immersed in a solution of Fe^{2+} and I^-, the membrane develops a red color as a result of the formation of an Fe^{2+}–bathophenanthroline complex. A calibration curve determined using a set of external standards with known concentrations of Fe^{2+} gave a standardization relationship of

$$A = \left(8.60 \times 10^3\ \text{M}^{-1}\right) \times \left[\text{Fe}^{2+}\right]$$

What is the concentration of iron, in mg Fe/L, for a sample with an absorbance of 0.100?

17. In the DPD colorimetric method for the free chlorine residual, which is reported as mg Cl_2/L, the oxidizing power of free chlorine converts the colorless amine N,N-diethyl-*p*-phenylenediamine to a colored dye that absorbs strongly over the wavelength range of 440–580 nm. Analysis of a set of calibration standards gave the following results.

mg Cl_2/L	absorbance
0.00	0.000
0.50	0.270
1.00	0.543
1.50	0.813
2.00	1.084

A sample from a public water supply is analyzed to determine the free chlorine residual, giving an absorbance of 0.113. What is the free chlorine residual for the sample in mg Cl_2/L?

18. Lin and Brown described a quantitative method for methanol based on its effect on the visible spectrum of methylene blue [Lin, J.; Brown, C. W. *Spectroscopy* **1995**, *10(5)*, 48–51]. In the absence of methanol, methylene blue has two prominent absorption bands at 610 nm and 663 nm, which correspond to the monomer and the dimer, respectively. In the presence of methanol, the intensity of the dimer's absorption band decreases, while that for the monomer increases. For concentrations of methanol between 0 and 30% v/v, the ratio of the

two absorbance, A_{663}/A_{610}, is a linear function of the amount of methanol. Use the following standardization data to determine the %v/v methanol in a sample if A_{610} is 0.75 and A_{663} is 1.07.

%v/v methanol	A_{663}/A_{610}	%v/v methanol	A_{663}/A_{610}
0.0	1.21	20.0	1.62
5.0	1.29	25.0	1.74
10.0	1.42	30.0	1.84
15.0	1.52		

19. The concentration of the barbiturate barbital in a blood sample is determined by extracting 3.00 mL of blood with 15 mL of $CHCl_3$. The chloroform, which now contains the barbital, is extracted with 10.0 mL of 0.45 M NaOH (pH ≈ 13). A 3.00-mL sample of the aqueous extract is placed in a 1.00-cm cell and an absorbance of 0.115 is measured. The pH of the sample in the absorption cell is then adjusted to approximately 10 by adding 0.50 mL of 16% w/v NH_4Cl, giving an absorbance of 0.023. When 3.00 mL of a standard barbital solution with a concentration of 3 mg/100 mL is taken through the same procedure, the absorbance at pH 13 is 0.295 and the absorbance at a pH of 10 is 0.002. Report the mg barbital/100 mL in the sample.

20. Jones and Thatcher developed a spectrophotometric method for analyzing analgesic tablets that contain aspirin, phenacetin, and caffeine [Jones, M.; Thatcher, R. L. *Anal. Chem.* **1951**, *23*, 957–960]. The sample is dissolved in $CHCl_3$ and extracted with an aqueous solution of $NaHCO_3$ to remove the aspirin. After the extraction is complete, the chloroform is transferred to a 250-mL volumetric flask and diluted to volume with $CHCl_3$. A 2.00-mL portion of this solution is then diluted to volume in a 200-mL volumetric flask with $CHCl_3$. The absorbance of the final solution is measured at wavelengths of 250 nm and 275 nm, at which the absorptivities, in $ppm^{-1}\ cm^{-1}$, for caffeine and phenacetin are

analyte	ε_{250}	ε_{275}
caffeine	0.0131	0.0485
phenacetin	0.0702	0.0159

Aspirin is determined by neutralizing the $NaHCO_3$ in the aqueous solution and extracting the aspirin into $CHCl_3$. The combined extracts are diluted to 500 mL in a volumetric flask. A 20.00-mL portion of the solution is placed in a 100-mL volumetric flask and diluted to volume with $CHCl_3$. The absorbance of this solution is measured at 277 nm, where the absorptivity of aspirin is 0.00682 $ppm^{-1}\ cm^{-1}$. An analgesic tablet treated by this procedure is found to have absorbances of 0.466 at 250 nm, 0.164 at 275 nm, and 0.600 at 277 nm when using a cell with a 1.00 cm pathlength. Report the milligrams of aspirin, caffeine, and phenacetin in the analgesic tablet.

21. The concentration of SO_2 in a sample of air is determined by the *p*-rosaniline method. The SO_2 is collected in a 10.00-mL solution of $HgCl_4^{2-}$, where it reacts to form $Hg(SO_3)_2$, by pulling air through the solution for 75 min at a rate of 1.6 L/min. After adding *p*-rosaniline and formaldehyde, the colored solution is diluted to 25 mL in a volumetric flask. The absorbance is measured at 569 nm in a 1-cm cell, yielding a value of 0.485. A standard sample is prepared by substituting a 1.00-mL sample of a standard solution that contains the equivalent of 15.00 ppm SO_2 for the air sample. The absorbance of the standard is found to be 0.181. Report the concentration of SO_2 in the air in mg SO_2/L. The density of air is 1.18 g/liter.

22. Seaholtz and colleagues described a method for the quantitative analysis of CO in automobile exhaust based on the measurement of infrared radiation at 2170 cm^{-1} [Seaholtz, M. B.; Pence, L. E.; Moe, O. A. Jr. *J. Chem. Educ.* **1988**, *65*, 820–823]. A calibration curve is prepared by filling a 10-cm IR gas cell with a known pressure of CO and measuring the absorbance using an FT-IR, giving a calibration equation of

$$A = -1.1 \times 10^{-4} + \left(9.9 \times 10^{-4}\right) \times P_{CO}$$

Samples are prepared by using a vacuum manifold to fill the gas cell. After measuring the total pressure, the absorbance at 2170 cm^{-1} is measured. Results are reported as %CO (P_{CO}/P_{total}). The analysis of five exhaust samples from a 1973 coupe gives the following results.

P_{total} (torr)	absorbance
595	0.1146
354	0.0642
332	0.0591
233	0.0412
143	0.0254

Determine the %CO for each sample, and report the mean and the 95% confidence interval.

23. Figure 10.3.8 shows an example of a disposable IR sample card made using a thin sheet of polyethylene. To prepare an analyte for analysis, it is dissolved in a suitable solvent and a portion of the sample placed on the IR card. After the solvent evaporates, leaving the analyte behind as a thin film, the sample's IR spectrum is obtained. Because the thickness of the polyethylene film is not uniform, the

primary application of IR cards is for a qualitative analysis. Zhao and Malinowski reported how an internal standardization with KSCN can be used for a quantitative IR analysis of polystyrene [Zhao, Z.; Malinowski, E. R. *Spectroscopy* **1996**, *11(7)*, 44–49]. Polystyrene is monitored at 1494 cm^{-1} and KSCN at 2064 cm^{-1}. Standard solutions are prepared by placing weighed portions of polystyrene in a 10-mL volumetric flask and diluting to volume with a solution of 10 g/L KSCN in methyl isobutyl ketone. A typical set of results is shown here.

g polystyrene	0.1609	0.3290	0.4842	0.6402	0.8006
A_{1494}	0.0452	0.1138	0.1820	0.3275	0.3195
A_{2064}	0.1948	0.2274	0.2525	0.3580	0.2703

When a 0.8006-g sample of a poly(styrene/maleic anhydride) copolymer is analyzed, the following results are obtained.

replicate	A_{1494}	A_{2064}
1	0.2729	0.3582
2	0.2074	0.2820
3	0.2785	0.3642

What is the %w/w polystyrene in the copolymer? Given that the reported %w/w polystyrene is 67%, is there any evidence for a determinate error at $\alpha = 0.05$?

24. The following table lists molar absorptivities for the Arsenazo complexes of copper and barium [Grossman, O.; Turanov, A. N. *Anal. Chim. Acta* **1992**, *257*, 195–202]. Suggest appropriate wavelengths for analyzing mixtures of copper and barium using their Arsenzao complexes.

wavelength (nm)	ε_{Cu} (M^{-1} cm^{-1})	ε_{Ba} (M^{-1} cm^{-1})
595	11900	7100
600	15500	7200
607	18300	7400
611	19300	6900
614	19300	7000
620	17800	7100
626	16300	8400
635	10900	9900
641	7500	10500
645	5300	10000
650	3500	8600
655	2200	6600
658	1900	6500
665	1500	3900
670	1500	2800
680	1800	1500

25. Blanco and colleagues report several applications of multiwavelength linear regression analysis for the simultaneous determination of two-component mixtures [Blanco, M.; Iturriaga, H.; Maspoch, S.; Tarin, P. *J. Chem. Educ.* **1989**, *66*, 178–180]. For each of the following, determine the molar concentration of each analyte in the mixture.

(a) Titanium and vanadium are determined by forming complexes with H_2O_2. Results for a mixture of Ti(IV) and V(V) and for stan-dards of 63.1 ppm Ti(IV) and 96.4 ppm V(V) are listed in the following table.

wavelength (nm)	$A_{Ti(V)\ Std}$	$A_{V(V)\ Std}$	A_{mix}
390	0.895	0.326	0.651
430	0.884	0.497	0.743
450	0.694	0.528	0.665
470	0.481	0.512	0.547
510	0.173	0.374	0.314

(b) Copper and zinc are determined by forming colored complexes with 2-pyridyl-azo-resorcinol (PAR). The absorbances for PAR, a mixture of Cu^{2+} and Zn^{2+}, and standards of 1.00 ppm Cu^{2+} and 1.00 ppm Zn^{2+} are listed in the following table. Note that you must correct the absorbances for the each metal for the contribution from PAR.

wavelength (nm)	A_{PAR}	$A_{Cu\ Std}$	$A_{Zn\ Std}$	A_{mix}
480	0.211	0.698	0.971	0.656
496	0.137	0.732	1.018	0.668
510	0.100	0.732	0.891	0.627
526	0.072	0.602	0.672	0.498
540	0.056	0.387	0.306	0.290

26. The stoichiometry of a metal–ligand complex, ML_n, is determined by the method of continuous variations. A series of solutions is prepared in which the combined concentrations of M and L are held constant at 5.15×10^{-4} M. The absorbances of these solutions are measured at a wavelength where only the metal–ligand complex absorbs. Using the following data, determine the formula of the metal–ligand complex.

mole fraction of M	mole fraction of L	absorbance
1.0	0.0	0.001
0.9	0.1	0.126
0.8	0.2	0.260
0.7	0.3	0.389
0.6	0.4	0.515
0.5	0.5	0.642
0.4	0.6	0.775
0.3	0.7	0.771
0.2	0.8	0.513
0.1	0.9	0.253
0.0	1.0	0.000

27. The stoichiometry of a metal–ligand complex, ML_n, is determined by the mole-ratio method. A series of solutions are prepared in which the metal's concentration is held constant at 3.65×10^{-4} M and the ligand's concentration is varied from 1×10^{-4} M to 1×10^{-3} M. Using the following data, determine the stoichiometry of the metal-ligand complex.

[ligand] (M)	absorbance	[ligand] (M)	absorbance
1.0×10^{-4}	0.122	6.0×10^{-4}	0.752
2.0×10^{-4}	0.251	7.0×10^{-4}	0.873
3.0×10^{-4}	0.376	8.0×10^{-4}	0.937
4.0×10^{-4}	0.496	9.0×10^{-4}	0.962
5.0×10^{-4}	0.625	1.0×10^{-3}	1.002

28. The stoichiometry of a metal–ligand complex, ML_n, is determined by the slope-ratio method. Two sets of solutions are prepared. For the first set of solutions the metal's concentration is held constant at 0.010 M and the ligand's concentration is varied. The following data are obtained at a wavelength where only the metal–ligand complex absorbs.

[ligand] (M)	absorbance
1.0×10^{-5}	0.012
2.0×10^{-5}	0.029
3.0×10^{-5}	0.042
4.0×10^{-5}	0.055
5.0×10^{-5}	0.069

For the second set of solutions the concentration of the ligand is held constant at 0.010 M, and the concentration of the metal is varied, yielding the following absorbances.

[metal] (M)	absorbance
1.0×10^{-5}	0.040
2.0×10^{-5}	0.085
3.0×10^{-5}	0.125
4.0×10^{-5}	0.162
5.0×10^{-5}	0.206

Using this data, determine the stoichiometry of the metal-ligand complex.

29. Kawakami and Igarashi developed a spectrophotometric method for nitrite based on its reaction with 5, 10, 15, 20-tetrakis(4-aminophenyl) porphrine (TAPP). As part of their study they investigated the stoichiometry of the reaction between TAPP and NO_2^-. The

following data are derived from a figure in their paper [Kawakami, T.; Igarashi, S. *Anal. Chim. Acta* **1996**, *333*, 175–180].

[TAPP] (M)	$[NO_2^-]$ (M)	absorbance
8.0×10^{-7}	0	0.227
8.0×10^{-7}	4.0×10^{-8}	0.223
8.0×10^{-7}	8.0×10^{-8}	0.211
8.0×10^{-7}	1.6×10^{-7}	0.191
8.0×10^{-7}	3.2×10^{-7}	0.152
8.0×10^{-7}	4.8×10^{-7}	0.127
8.0×10^{-7}	6.4×10^{-7}	0.107
8.0×10^{-7}	8.0×10^{-7}	0.092
8.0×10^{-7}	1.6×10^{-6}	0.058
8.0×10^{-7}	2.4×10^{-6}	0.045
8.0×10^{-7}	3.2×10^{-6}	0.037
8.0×10^{-7}	4.0×10^{-6}	0.034

What is the stoichiometry of the reaction?

30. The equilibrium constant for an acid–base indicator is determined by preparing three solutions, each of which has a total indicator concentration of 1.35×10^{-5} M. The pH of the first solution is adjusted until it is acidic enough to ensure that only the acid form of the indicator is present, yielding an absorbance of 0.673. The absorbance of the second solution, whose pH is adjusted to give only the base form of the indicator, is 0.118. The pH of the third solution is adjusted to 4.17 and has an absorbance of 0.439. What is the acidity constant for the acid–base indicator?

31. The acidity constant for an organic weak acid is determined by measuring its absorbance as a function of pH while maintaining a constant total concentration of the acid. Using the data in the following table, determine the acidity constant for the organic weak acid.

pH	absorbance	pH	absorbance
1.53	0.010	4.88	0.193
2.20	0.010	5.09	0.227
3.66	0.035	5.69	0.288
4.11	0.072	7.20	0.317
4.35	0.103	7.78	0.317
4.75	0.169		

32. Suppose you need to prepare a set of calibration standards for the spectrophotometric analysis of an analyte that has a molar absorptivity of 1138 M^{-1} cm^{-1} at a wavelength of 625 nm. To maintain an acceptable precision for the analysis, the %T for the standards should be between 15% and 85%.

(a) What is the concentration for the most concentrated and for the least concentrated standard you should prepare, assuming a 1.00-cm sample cell.

(b) Explain how you will analyze samples with concentrations that are 10 μM, 0.1 mM, and 1.0 mM in the analyte.

33. When using a spectrophotometer whose precision is limited by the uncertainty of reading %T, the analysis of highly absorbing solutions can lead to an unacceptable level of indeterminate errors. Consider the analysis of a sample for which the molar absorptivity is 1.0×10^4 M^{-1} cm^{-1} and for which the pathlength is 1.00 cm.

(a) What is the relative uncertainty in concentration for an analyte whose concentration is 2.0×10^{-4} M if s_T is ±0.002?

(b) What is the relative uncertainty in the concentration if the spectrophotometer is calibrated using a blank that consists of a 1.0×10^{-4} M solution of the analyte?

34. Hobbins reported the following calibration data for the flame atomic absorption analysis for phosphorous [Hobbins, W. B. “Direct Determination of Phosphorous in Aqueous Matricies by Atomic Absorption,” Varian Instruments at Work, Number AA-19, February 1982].

mg P/L	absorbance
2130	0.048
4260	0.110
6400	0.173
8530	0.230

To determine the purity of a sample of Na_2HPO_4, a 2.469-g sample is dissolved and diluted to volume in a 100-mL volumetric flask. Analysis of the resulting solution gives an absorbance of 0.135. What is the purity of the Na_2HPO_4?

35. Bonert and Pohl reported results for the atomic absorption analysis of several metals in the caustic suspensions produced during the manufacture of soda by the ammonia-soda process [Bonert, K.; Pohl, B. "The Determination of Cd, Cr, Cu, Ni, and Pb in Concentrated $CaCl_2$/NaCl solutions by AAS," AA Instruments at Work (Varian) Number 98, November, 1990].

(a) The concentration of Cu is determined by acidifying a 200.0-mL sample of the caustic solution with 20 mL of concentrated HNO_3, adding 1 mL of 27% w/v H_2O_2, and boiling for 30 min. The resulting solution is diluted to 500 mL in a volumetric flask, filtered, and analyzed by flame atomic absorption using matrix matched standards. The results for a typical analysis are shown in the following table.

solution	mg Cu/L	absorbance
blank	0.000	0.007
standard 1	0.200	0.014
standard 2	0.500	0.036
standard 3	1.000	0.072
standard 4	2.000	0.146
sample		0.027

Determine the concentration of Cu in the caustic suspension.

(b) The determination of Cr is accomplished by acidifying a 200.0-mL sample of the caustic solution with 20 mL of concentrated HNO_3, adding 0.2 g of Na_2SO_3 and boiling for 30 min. The Cr is isolated from the sample by adding 20 mL of NH_3, producing a precipitate that includes the chromium as well as other oxides. The precipitate is isolated by filtration, washed, and transferred to a beaker. After acidifying with 10 mL of HNO_3, the solution is evaporated to dryness. The residue is redissolved in a combination of HNO_3 and HCl and evaporated to dryness. Finally, the residue is dissolved in 5 mL of HCl, filtered, diluted to volume in a 50-mL volumetric flask, and analyzed by atomic absorption using the method of standard additions. The atomic absorption results are summarized in the following table.

sample	mg Cr_{added}/L	absorbance
blank		0.001
sample		0.045
standard addition 1	0.200	0.083
standard addition 2	0.500	0.118
standard addition 3	1.000	0.192

Report the concentration of Cr in the caustic suspension.

36. Quigley and Vernon report results for the determination of trace metals in seawater using a graphite furnace atomic absorption spectrophotometer and the method of standard additions [Quigley, M. N.; Vernon, F. *J. Chem. Educ.* **1996**, *73*, 671–673]. The trace metals are first separated from their complex, high-salt matrix by coprecipitating with Fe^{3+}. In a typical analysis a 5.00-mL portion of 2000 ppm Fe^{3+} is added to 1.00 L of seawater. The pH is adjusted to 9 using NH_4OH, and the precipitate of $Fe(OH)_3$ allowed to stand overnight. After isolating and rinsing the precipitate, the $Fe(OH)_3$ and coprecipitated metals are dissolved in 2 mL of concentrated HNO_3 and diluted to volume in a 50-mL volumetric flask. To analyze for Mn^{2+}, a 1.00-mL sample of this solution is diluted to 100 mL in a volumetric flask. The following samples are injected into the graphite furnace and analyzed.

sample	absorbance
2.5-µL sample + 2.5 µL of 0 ppb Mn^{2+}	0.223
2.5-µL sample + 2.5 µL of 2.5 ppb Mn^{2+}	0.294
2.5-µL sample + 2.5 µL of 5.0 ppb Mn^{2+}	0.361

Report the ppb Mn^{2+} in the sample of seawater.

37. The concentration of Na in plant materials are determined by flame atomic emission. The material to be analyzed is prepared by grinding, homogenizing, and drying at 103ºC. A sample of approximately 4 g is transferred to a quartz crucible and heated on a hot plate to char the organic material. The sample is heated in a muffle furnace at 550ºC for several hours. After cooling to room temperature the residue is dissolved by adding 2 mL of 1:1 HNO_3 and evaporated to dryness. The residue is redissolved in 10 mL of 1:9 HNO_3, filtered and diluted to 50 mL in a volumetric flask. The following data are obtained during a typical analysis for the concentration of Na in a 4.0264-g sample of oat bran.

sample	mg Na/L	emission (arbitrary units)
blank	0.00	0.0
standard 1	2.00	90.3
standard 2	4.00	181
standard 3	6.00	272
standard 4	8.00	363
standard 5	10.00	448
sample		238

Report the concentration of μg Na/g sample.

38. Yan and colleagues developed a method for the analysis of iron based its formation of a fluorescent metal–ligand complex with the ligand 5-(4-methylphenylazo)-8-aminoquinoline [Yan, G.; Shi, G.; Liu, Y. *Anal. Chim. Acta* **1992**, *264*, 121–124]. In the presence of the surfactant cetyltrimethyl ammonium bromide the analysis is carried out using an excitation wavelength of 316 nm with emission monitored at 528 nm. Standardization with external standards gives the following calibration curve.

$$I_f = -0.03 + \left(1.594\ \text{mg}^{-1}\ \text{L}\right) \times \frac{\text{mg Fe}^{3+}}{\text{L}}$$

A 0.5113-g sample of dry dog food is ashed to remove organic materials, and the residue dissolved in a small amount of HCl and diluted to volume in a 50-mL volumetric flask. Analysis of the resulting solution gives a fluorescent emission intensity of 5.72. Determine the mg Fe/L in the sample of dog food.

39. A solution of 5.00×10^{-5} M 1,3-dihydroxynaphthelene in 2 M NaOH has a fluorescence intensity of 4.85 at a wavelength of 459 nm. What is the concentration of 1,3-dihydroxynaphthelene in a solution that has a fluorescence intensity of 3.74 under identical conditions?

40. The following data is recorded for the phosphorescent intensity of several standard solutions of benzo[a]pyrene.

[benzo[a]pyrene] (M)	emission intensity
0	0.00
1.00×10^{-5}	0.98
3.00×10^{-5}	3.22
6.00×10^{-5}	6.25
1.00×10^{-4}	10.21

What is the concentration of benzo[a]pyrene in a sample that yields a phosphorescent emission intensity of 4.97?

41. The concentration of acetylsalicylic acid, $C_9H_8O_4$, in aspirin tablets is determined by hydrolyzing it to the salicylate ion, $C_7H_5O_2^-$, and determining its concentration spectrofluorometrically. A stock standard solution is prepared by weighing 0.0774 g of salicylic acid, $C_7H_6O_2$, into a 1-L volumetric flask and diluting to volume. A set of calibration standards is prepared by pipeting 0, 2.00, 4.00, 6.00, 8.00, and 10.00 mL of the stock solution into separate 100-mL volumetric flasks that contain 2.00 mL of 4 M NaOH and diluting to volume. Fluorescence is measured at an emission wavelength of 400 nm using an excitation wavelength of 310 nm with results shown in the following table.

mL of stock solution	emission intensity
0.00	0.00
2.00	3.02
4.00	5.98
6.00	9.18
8.00	12.13
10.00	14.96

Several aspirin tablets are ground to a fine powder in a mortar and pestle. A 0.1013-g portion of the powder is placed in a 1-L volumetric flask and diluted to volume with distilled water. A portion of this solution is filtered to remove insoluble binders and a 10.00-mL aliquot transferred to a 100-mL volumetric flask that contains 2.00 mL of 4 M NaOH. After diluting to volume the fluorescence of the resulting solution is 8.69. What is the %w/w acetylsalicylic acid in the aspirin tablets?

42. Selenium (IV) in natural waters is determined by complexing with ammonium pyrrolidine dithiocarbamate and extracting into $CHCl_3$. This step serves to concentrate the Se(IV) and to separate it from Se(VI). The Se(IV) is then extracted back into an aqueous matrix using HNO_3. After complexing with 2,3-diaminonaphthalene, the complex is extracted into cyclohexane. Fluorescence is measured at 520 nm following its excitation at 380 nm. Calibration is achieved by adding known amounts of Se(IV) to the water sample before beginning the analysis. Given the following results what is the concentration of Se(IV) in the sample.

[Se(IV)] added (nM)	emission intensity
0.00	323
2.00	597
4.00	862
6.00	1123

43. Fibrinogen is a protein that is produced by the liver and found in human plasma. Its concentration in plasma is clinically important. Many of the analytical methods used to determine the concentration of fibrinogen in plasma are based on light scattering following its precipitation. For example, da Silva and colleagues describe a method in which fibrino- gen precipitates in the presence of ammonium sulfate in a guanidine hydrochloride buffer [da Silva, M. P.; Fernandez-Romero, J. M.; Luque de Castro, M. D. *Anal. Chim. Acta* **1996**, *327*, 101–106]. Light scattering is measured nephelometrically at a wavelength of 340 nm. Analysis of a set of external calibration standards gives the following calibration equation

$$I_s = -4.66 + 9907.63C$$

where I_s is the intensity of scattered light and C is the concentration of fibrinogen in g/L. A 9.00-mL sample of plasma is collected from a patient and mixed with 1.00 mL of an anticoagulating agent. A 1.00-mL aliquot of this solution is diluted to 250 mL in a volumetric flask and is found to have a scattering intensity of 44.70. What is the concentration of fibrinogen, in gram per liter, in the plasma sample?

This page titled 6.14: Problems is shared under a CC BY-NC-SA 4.0 license and was authored, remixed, and/or curated by David Harvey.

- **10.9: Problems** by David Harvey is licensed CC BY-NC-SA 4.0.

6.15: ADDITIONAL RESOURCES

The following set of experiments introduce students to the applications of spectroscopy. Experiments are grouped into five categories: UV/Vis spectroscopy, IR spectroscopy, atomic absorption and atomic emission, fluorescence and phosphorescence, and signal averaging.

UV/Vis Spectroscopy

- Abney, J. R.; Scalettar, B. A. "Saving Your Students' Skin. Undergraduate Experiments That Probe UV Protection by Sunscreens and Sunglasses," *J. Chem. Educ.* **1998**, *75*, 757–760.
- Ainscough, E. W.; Brodie, A. M. "The Determination of Vanillin in Vanilla Extract," *J. Chem. Educ.* **1990**, *67*, 1070–1071.
- Allen, H. C.; Brauers, T.; Finlayson-Pitts, B. J. "Illustrating Deviations in the Beer-Lambert Law in an Instrumental Analysis Laboratory: Measuring Atmospheric Pollutants by Differential Optical Absorption Spectrometry," *J. Chem. Educ.* **1997**, *74*, 1459–1462.
- Blanco, M.; Iturriaga, H.; Maspoch, S.; Tarîn, P. "A Simple Method for Spectrophotometric Determination of Two-Components with Overlapped Spectra," *J. Chem. Educ.* **1989**, *66*, 178–180.
- Bonicamp, J. M.; Martin, K. L.; McBride, G. R.; Clark, R. W. "Beer's Law is Not a Straight Line: Amplification of Errors by Transformation," *Chem. Educator* **1999**, *4*, 81–88.
- Bruneau, E.; Lavabre, D.; Levy, G.; Micheau, J. C. "Quantitative Analysis of Continuous-Variation Plots with a Comparison of Several Methods," *J. Chem. Educ.* **1992**, *69*, 833–837.
- Cappas, C.; Hoffman, N.; Jones, J.; Young, S. "Determination of Concentrations of Species Whose Absorption Bands Overlap Extensively," *J. Chem. Educ.* **1991**, *68*, 300–303.
- Crisp, P. T.; Eckert, J. M.; Gibson, N. A. "The Determination of Anionic Surfactants in Natural and Waste Waters," *J. Chem. Educ.* **1983**, *60*, 236–238.
- Dilbeck, C. W.; Ganske, J. A. "Detection of NOx in Automobile Exhaust: An Applied Experiment in Atmospheric/Environmental Chemistry for the General Chemistry Laboratory," *Chem. Educator* **2008**, *13*, 1–5.
- Domínguez, A., Fernández, A.; González, N.; Iglesias, E.; Montenegro, L. "Determination of Critical Micelle Concentration of Some Surfactants by Three Techniques," *J. Chem. Educ.* **1997**, *74*, 1227– 1231.
- Gilbert, D. D. "Determining Optimum Spectral Bandwidth," *J. Chem. Educ.* **1991**, *68*, A278– A281.
- Han, J.; Story, T.; Han, G. "A Spectrophotometric Method for Quantitative Determination of Bromine Using Tris(2-carboxyethyl)phophine," *J. Chem. Educ.* **1999**, *76*, 976–977.
- Higginbotham, C.; Pike, C. F.; Rice, J, K. "Spectroscopy in Sol-Gel Matricies," *J. Chem. Educ.* **1998**, *75*, 461–464.
- Hill, Z. D.; MacCarthy, P. "Novel Approach to Job's Method," *J. Chem. Educ.* **1986**, *63*, 162–167.
- Ibañez, G. A.; Olivieri, A. C.; Escandar, G. M. "Determination of Equilibrium Constants of Metal Complexes from Spectrophotometric Measurements," *J. Chem. Educ.* **1999**, *76*, 1277–1281.
- Long, J. R.; Drago, R. S. "The Rigorous Evaluation of Spectrophotometric Data to Obtain an Equilibrium Constant," *J. Chem. Educ.* **1982**, *59*, 1037–1039.
- Lozano-Calero; D.; Martin-Palomeque, P. "Determination of Phosphorous in Cola Drinks," *J. Chem. Educ.* **1996**, *73*, 1173–1174.
- Maloney, K. M.; Quiazon, E. M.; Indralingam, R. "Measurement of Iron in Egg Yolk: An Instrumental Analysis Measurement Using Biochemical Principles," *J. Chem. Educ.* **2008**, *85*, 399–400.
- Mascotti, D. P.; Waner, M. J. "Complementary Spectroscopic Assays for Investigation Protein-Ligand Binding Activity: A Project for the Advanced Chemistry Laboratory," *J. Chem. Educ.* **2010**, *87*, 735– 738.
- McClain, R. L. "Construction of a Photometer as an Instructional Tool for Electronics and Instrumentation," *J. Chem. Educ.* **2014**, *91*, 747–750.
- McDevitt, V. L.; Rodriquez, A.; Williams, K. R. "Analysis of Soft Drinks: UV Spectrophotometry, Liquid Chromatography, and Capillary Electrophoresis," *J. Chem. Educ.* **1998**, *75*, 625–629.
- Mehra, M. C.; Rioux, J. "An Analytical Chemistry Experiment in Simultaneous Spectrophotometric Determination of Fe(III) and Cu(II) with Hexacyanoruthenate(II) Reagent," *J. Chem. Educ.* **1982**, *59*, 688–689.
- Mitchell-Koch, J. T.; Reid, K. R.; Meyerhoff, M. E. "Salicylate Detection by Complexation with Iron(III) and Optical Absorbance Spectroscopy," *J. Chem. Educ.* **2008**, *85*, 1658–1659.
- Msimanga, H. Z.; Wiese, J. "Determination of Acetaminophen in Analgesics by the Standard Addition Method: A Quantitative Analytical Chemistry Laboratory," *Chem. Educator* **2005**, *10*, 1–7.
- Örstan, A.; Wojcik, J. F. "Spectroscopic Determination of Protein-Ligand Binding Constants," *J. Chem. Educ.* **1987**, *64*, 814–816.
- Pandey, S.; Powell, J. R.; McHale, M. E. R.; Acree Jr., W. E. "Quantitative Determination of Cr(III) and Co(II) Using a Spectroscopic H-Point Standard Addition," *J. Chem. Educ.* **1997**, *74*, 848–850.
- Parody-Morreale, A.; Cámara-Artigas, A.; Sánchez-Ruiz, J. M. "Spectrophotometric Determination of the Binding Constants of Succinate and Chloride to Glutamic Oxalacetic Transaminase," *J. Chem. Educ.* **1990**, *67*, 988–990.
- Ravelo-Perez, L. M.; Hernández-Borges, J.; Rodríguez-Delgado, M. A.; Borges-Miquel, T. "Spectrophotometric Analysis of Lycopene in Tomatoes and Watermelons: A Practical Class," *Chem. Educator* **2008**, *13*, 1–3.

- Russell, D. D.; Potts, J.; Russell, R. M.; Olson, C.; Schimpf, M. "Spectroscopic and Potentiometric Investigation of a Diprotic Acid: An Experimental Approach to Understanding Alpha Functions," *Chem. Educator* **1999**, *4*, 68–72.
- Smith, E. T.; Matachek, J. R. "A Colorful Investigation of a Diprotic Acid: A General Chemistry Laboratory Exercise," *Chem. Educator* **2002**, *7*, 359–363
- Tello-Solis, S. R. "Thermal Unfolding of Lysozyme Studied by UV Difference Spectroscopy," *Chem. Educator* **2008**, *13*, 16–18.
- Tucker, S.; Robinson, R.; Keane, C.; Boff, M.; Zenko, M.; Batish, S.; Street, Jr., K. W. "Colorimetric Determination of pH," *J. Chem. Educ.* **1989**, *66*, 769–771.
- Vitt, J. E. "Troubleshooting 101: An Instrumental Analysis Experiment," *J. Chem. Educ.* **2008**, *85*, 1660–1662.
- Williams, K. R.; Cole, S. R.; Boyette, S. E.; Schulman, S. G. "The Use of Dristan Nasal Spray as the Unknown for Simultaneous Spectrophotometric Analysis of a Mixture," *J. Chem. Educ.* **1990**, *67*, 535.
- Walmsley, F. "Aggregation in Dyes: A Spectrophotometric Study," *J. Chem. Educ.* **1992**, *69*, 583. Wells, T. A. "Construction of a Simple Myoglobin-Based Optical Biosensor," *Chem. Educator* **2007**, *12*, 1–3.
  Yarnelle, M. K.; West, K. J. "Modification of an Ultraviolet Spectrophotometric Determination of the Active Ingredients in APC Tablets," *J. Chem. Educ.* **1989**, *66*, 601–602.

IR Spectroscopy

- Dragon, S.; Fitch, A. "Infrared Spectroscopy Determination of Lead Binding to Ethylenediaminetetraacetic Acid," *J. Chem. Educ.* **1998**, *75*, 1018–1021.
- Frohlich, H. "Using Infrared Spectroscopy Measurements to Study Intermolecular Hydrogen Bonding," *J. Chem. Educ.* **1993**, *70*, A3–A6.
- Garizi, N.; Macias, A.; Furch, T.; Fan, R.; Wagenknecht, P.; Singmaster, K. A. "Cigarette Smoke Analysis Using an Inexpensive Gas-Phase IR Cell," *J. Chem. Educ.* **2001**, *78*, 1665–1666.
- Indralingam, R.; Nepomuceno, A. I. "The Use of Disposable IR Cards for Quantitative Analysis Using an Internal Standard," *J. Chem. Educ.* **2001**, *78*, 958–960.
- Mathias, L. J.; Hankins, M. G.; Bertolucci, C. M.; Grubb, T. L.; Muthiah, J. "Quantitative Analysis by FTIR: Thin Films of Copolymers of Ethylene and Vinyl Acetate," *J. Chem. Educ.* **1992**, *69*, A217– A219.
- Schuttlefield, J. D.; Grassian, V. H. "ATR-FTIR Spectroscopy in the Undergraduate Chemistry Laboratory. Part I: Fundamentals and Examples," *J. Chem. Educ.* **2008**, *85*, 279–281.
- Schuttlefield, J. D.; Larsen, S. C.; Grassian, V. H. "ATR-FTIR Spectroscopy in the Undergraduate Chemistry Laboratory. Part II: A Physical Chemistry Laboratory Experiment on Surface Adsorption," *J. Chem. Educ.* **2008**, *85*, 282–284.
- Seasholtz, M. B.; Pence, L. E.; Moe Jr., O. A. "Determination of Carbon Monoxide in Automobile Exhaust by FTIR Spectroscopy," *J. Chem. Educ.* **1988**, *65*, 820–823.

Atomic Absorption and Atomic Emission Spectroscopy

- Amarasiriwardena, D. "Teaching analytical atomic spectroscopy advances in an environmental chemistry class using a project-based laboratory approach: investigation of lead and arsenic distributions in a lead arsenate contaminated apple orchard," *Anal. Bioanal. Chem.* **2007**, *388*, 307–314.
- Bazzi, A.; Bazzi, J.; Deng, Y.' Ayyash, M. "Flame Atomic Absorption Spectroscopic Determination of Iron in Breakfast Cereals: A Validated Experiment for the Analytical Chemistry Laboratory," *Chem. Educator* **2014**, *19*, 283–286.
- Buffen, B. P. "Removal of Heavy Metals from Water: An Environmentally Significant Atomic Absorption Spectrometry Experiment," *J. Chem. Educ.* **1999**, *76*, 1678–1679.
- Dockery, C. R.; Blew, M. J.; Goode, S. R. "Visualizing the Solute Vaporization Interference in Flame Atomic Absorption Spectroscopy," *J. Chem. Educ.* **2008**, *85*, 854–858.
- Donas, M. K.; Whissel, G.; Dumas, A.; Golden, K. "Analyzing Lead Content in Ancient Bronze Coins by Flame Atomic Absorption Spectroscopy," *J. Chem. Educ.* **2009**, *86*, 343–346.
- Finch, L. E.; Hillyer, M. M.; Leopold, M. C. "Quantitative Analysis of Heavy Metals in Children's Toys and Jewelry: A Multi-Instrument, Multitechnique Exercise in Analytical Chemistry and Public Health," *J. Chem. Educ.* **2015**, *92*, 849–854.
- Garrison, N.; Cunningham, M.; Varys, D.; Schauer, D. J. "Discovering New Biosorbents with Atomic Absorption Spectroscopy: An Undergraduate Laboratory Experiment," *J. Chem. Educ.* **2014**, *91*, 583–585.
- Gilles de Pelichy, L. D.; Adams, C.; Smith, E. T. "Analysis of the Essential Nutrient Strontium in Marine Aquariums by Atomic Absorption Spectroscopy," *J. Chem. Educ.* **1997**, *74*, 1192–1194.
- Hoskins, L. C.; Reichardt, P. B.; Stolzberg, R. J. "Determination of the Extraction Constant for Zinc Pyrrolidinecarbodithioate," *J. Chem. Educ.* **1981**, *58*, 580–581.
- Kooser, A. S.; Jenkins, J. L.; Welch, L. E. "Inductively Coupled Plasma-Atomic Emission Spectroscopy: Two Laboratory Activities for the Undergraduate Instrumental Analysis Course," *J. Chem. Educ.* **2003**, *80*, 86–88.

- Kostecka, K. S. “Atomic Absorption Spectroscopy of Calcium in Foodstuffs in Non-Science-Major Courses,” *J. Chem. Educ.* **2000**, *77*, 1321–1323.
- Kristian, K. E.; Friedbauer, S.; Kabashi, D.; Ferencz, K. M.; Barajas, J. C.; O’Brien, K. “A Simplified Digestion Protocol for the Analysis of Hg in Fish by Cold Vapor Atomic Absorption Spectroscopy,” *J. Chem. Educ.* **2015**, *92*, 698–702.
- Lehman, T. A.; Everett, W. W. “Solubility of Lead Sulfate in Water and in Sodium Sulfate Solutions,” *J. Chem. Educ.* **1982**, *59*, 797.
- Markow, P. G. “Determining the Lead Content of Paint Chips,” *J. Chem. Educ.* **1996**, *73*, 178–179.
- Masina, M. R.; Nkosi, P. A.; Rasmussen, P. W.; Shelembe, J. S.; Tyobeka, T. E. “Determination of Metal Ions in Pineapple Juice and Effluent of a Fruit Canning Industry,” *J. Chem. Educ.* **1989**, *66*, 342–343.
- Quigley, M. N. “Determination of Calcium in Analgesic Tablets using Atomic Absorption Spectrophotometry,” *J. Chem. Educ.* **1994**, *71*, 800.
- Quigley, M. N.; Vernon, F. “Determination of Trace Metal Ion Concentrations in Seawater,” *J. Chem. Educ.* **1996**, *73*, 671–675.
- Quigley, M. N.; Vernon, F. “A Matrix Modification Experiment for Use in Electrothermal Atomic Absorption Spectrophotometry,” *J. Chem. Educ.* **1996**, *73*, 980–981.
- Palkendo, J. A.; Kovach, J.; Betts, T. A. “Determination of Wear Metals in Used Motor Oil by Flame Atomic Absorption Spectroscopy,” *J. Chem. Educ.* **2014**, *91*, 579–582.
- Rheingold, A. L.; Hues, S.; Cohen, M. N. “Strontium and Zinc Content in Bones as an Indication of Diet,” *J. Chem. Educ.* **1983**, *60*, 233–234.
- Rocha, F. R. P.; Nóbrega, J. A. “Effects of Solution Physical Properties on Copper and Chromium Signals in Flame Atomic Absorption Spectrometry,” *J. Chem. Educ.* **1996**, *73*, 982–984.

Fluorescence and Phosphorescence Spectroscopy

- Bigger, S. W.; Bigger, A. S.; Ghiggino, K. P. “*FluSpec*: A Simulated Experiment in Fluorescence Spectroscopy,” *J. Chem. Educ.* **2014**, *91*, 1081–1083.
- Buccigross, J. M.; Bedell, C. M.; Suding-Moster, H. L. “Fluorescent Measurement of TNS Binding to Calmodulin,” *J. Chem. Educ.* **1996**, *73*, 275–278.
- Henderleiter, J. A.; Hyslopo, R. M. “The Analysis of Riboflavin in Urine by Fluorescence,” *J. Chem. Educ.* **1996**, *73*, 563–564.
- Koenig, M. H.; Yi, E. P.; Sandridge, M. J.; Mathew, A. S.; Demas, J. N. “Open-Box Approach to Measuring Fluorescence Quenching Using an iPad Screen and Digital SLR Camera,” *J. Chem. Educ.* **2015**, *92*, 310–316.
- Lagoria, M. G.; Román, E. S. “How Does Light Scattering Affect Luminescence? Fluorescence Spectra and Quantum Yields in the Solid Form,” *J. Chem. Educ.* **2002**, *79*, 1362–1367.
- Richardson, D. P.; Chang, R. “Lecture Demonstrations of Fluorescence and Phosphorescence,” *Chem. Educator* **2007**, *12*, 272–274.
- Seixas de Melo, J. S.; Cabral, C.; Burrows, H. D. “Photochemistry and Photophysics in the Laboratory. Showing the Role of Radiationless and Radiative Decay of Excited States,” *Chem. Educator* **2007**, *12*, 1–6.
- Sheffield, M. C.; Nahir, T. M. “Analysis of Selenium in Brazil Nuts by Microwave Digestion and Fluorescence Detection,” *J. Chem. Educ.* **2002**, *79*, 1345–1347.

Signal Averaging

- Blitz, J. P.; Klarup, D. G. “Signal-to-Noise Ratio, Signal Processing, and Spectral Information in the Instrumental Analysis Laboratory,” *J. Chem. Educ.* **2002**, *79*, 1358–1360.
- Stolzberg, R. J. “Introduction to Signals and Noise in an Instrumental Method Course,” *J. Chem. Educ.* **1983**, *60*, 171–172.
- Tardy, D. C. “Signal Averaging. A Signal-to-Noise Enhancement Experiment for the Advanced Chemistry Laboratory,” *J. Chem. Educ.* **1986**, *63*, 648–650.

The following sources provide additional information on spectroscopy in the following areas: general spectroscopy, Beer’s law, instrumentation, Fourier transforms, IR spectroscopy, atomic asorption and emission, luminescence, and applications.

General Spectroscopy

- Ball, D. W. “Units! Units! Units!” *Spectroscopy* **1995**, *10(8)*, 44–47.
- *A History of Analytical Chemistry, Laitinen, H. A.; Ewing, G. W, Eds. The Division of Analytical Chemistry of the American Chemical Society: Washington, D. C., 1977, p103–243.*
- Ingle, J. D.; Crouch, S. R. *Spectrochemical Analysis*, Prentice Hall, Englewood Cliffs, N. J.; 1988.
- Macomber, R. S. “A Unifying Approach to Absorption Spectroscopy at the Undergraduate Level,” *J. Chem. Educ.* **1997**, *74*, 65–67.
- Orchin, M.; Jaffe, H. H. *Symmetry, Orbitals and Spectra*, Wiley-Interscience: New York, 1971.
- Thomas, N. C. “The Early History of Spectroscopy,” *J. Chem. Educ.* **1991**, *68*, 631–633.

Beer’s Law

- Lykos, P. “The Beer-Lambert Law Revisited: A Development without Calculus,” *J. Chem. Educ.* **1992**, *69*, 730–732.

- Ricci, R. W.; Ditzler, M. A.; Nestor, L. P. "Discovering the Beer-Lambert Law," *J. Chem. Educ.* **1994**, *71*, 983–985.

Instrumentation

• Altermose, I. R. "Evolution of Instrumentation for UV-Visible Spectrophotometry: Part I," *J. Chem. Educ.* **1986**, *63*, A216–A223.

- Altermose, I. R. "Evolution of Instrumentation for UV-Visible Spectrophotometry: Part II," *J. Chem. Educ.* **1986**, *63*, A262–A266.
- Grossman, W. E. L. "The Optical Characteristics and Production of Diffraction Gratings," *J. Chem. Educ.* **1993**, *70*, 741–748.
- Jones, D. G. "Photodiode Array Detectors in UV-Vis Spectroscopy: Part I," *Anal. Chem.* **1985**, *57*,1057A–1073A.
- Jones, D. G. "Photodiode Array Detectors in UV-Vis Spectroscopy: Part II," *Anal. Chem.* **1985**, 11, 1207A–1214A.
- Palmer, C. "Diffraction Gratings," *Spectroscopy*, **1995**, *10(2)*, 14–15.

Fourier Transforms

- Bracewell, R. N. "The Fourier Transform," *Sci. American* **1989**, *260(6)*, 85–95.
- Glasser, L. "Fourier Transforms for Chemists: Part I. Introduction to the Fourier Transform," *J. Chem. Educ.* **1987**, *64*, A228–A233.
- Glasser, L. "Fourier Transforms for Chemists: Part II. Fourier Transforms in Chemistry and Spectroscopy," *J. Chem. Educ.* **1987**, *64*, A260–A266.
- Glasser, L. "Fourier Transforms for Chemists: Part III. Fourier Transforms in Data Treatment," *J. Chem. Educ.* **1987**, *64*, A306–A313.
- Graff, D. K. "Fourier and Hadamard: Transforms in Spectroscopy," *J. Chem. Educ.* **1995**, *72*, 304–309.
- Griffiths, P. R. *Chemical Fourier Transform Spectroscopy*, Wiley-Interscience: New York, 1975.
- *Transform Techniques in Chemistry, Griffiths, P. R. Ed., Plenum Press: New York, 1978.*
- Perkins, W. E. "Fourier Transform Infrared Spectroscopy: Part I. Instrumentation," *J. Chem. Educ.* **1986**, *63*, A5–A10.
- Perkins, W. E. "Fourier Transform Infrared Spectroscopy: Part II. Advantages of FT-IR," *J. Chem. Educ.* **1987**, *64*, A269–A271.
- Perkins, W. E. "Fourier Transform Infrared Spectroscopy: Part III. Applications," *J. Chem. Educ.* **1987**, *64*, A296–A305.
- Strong III, F. C. "How the Fourier Transform Infrared Spectrophotometer Works," *J. Chem. Educ.* **1979**, *56*, 681–684.

IR Spectroscopy.

- *Optical Spectroscopy: Sampling Techniques Manual, Harrick Scientific Corporation: Ossining, N. Y., 1987.*
- Leyden, D. E.; Shreedhara Murthy, R. S. "Surface-Selective Sampling Techniques in Fourier Transform Infrared Spectroscopy," *Spectroscopy* **1987**, *2(2)*, 28–36.
- Porro, T. J.; Pattacini, S. C. "Sample Handling for Mid-Infrared Spectroscopy, Part I: Solid and Liquid Sampling," *Spectroscopy* **1993**, *8(7)*, 40–47.
- Porro, T. J.; Pattacini, S. C. "Sample Handling for Mid-Infrared Spectroscopy, Part II: Specialized Techniques," *Spectroscopy* **1993**, *8(8)*, 39–44.

Atomic Absorption and Emission

- Blades, M. W.; Weir, D. G. "Fundamental Studies of the Inductively Coupled Plasma," *Spectroscopy* **1994**, *9*, 14–21.
- Greenfield, S. "Invention of the Annular Inductively Coupled Plasma as a Spectroscopic Source," *J. Chem. Educ.* **2000**, *77*, 584–591.
- Hieftje, G. M. "Atomic Absorption Spectrometry - Has it Gone or Where is it Going?" *J. Anal. At. Spectrom.* **1989**, *4*, 117–122.
- Jarrell, R. F. "A Brief History of Atomic Emission Spectrochemical Analysis, 1666–1950," *J. Chem. Educ.* **2000**, *77*, 573–576
- Koirtyohann, S. R. "A History of Atomic Absorption Spectrometry From an Academic Perspective,"*Anal. Chem.* **1991**, *63*, 1024A–1031A.
- L'Vov, B. V. "Graphite Furnace Atomic Absorption Spectrometry," *Anal. Chem.* **1991**, *63*, 924A–931A.
- Slavin, W. "A Comparison of Atomic Spectroscopic Analytical Techniques," *Spectroscopy*, **1991**, *6*, 16–21.
- Van Loon, J. C. *Analytical Atomic Absorption Spectroscopy*, Academic Press: New York, 1980.
- Walsh, A. "The Development of Atomic Absorption Methods of Elemental Analysis 1952–1962," *Anal. Chem.* **1991**, *63*, 933A–941A.
- Welz, B. *Atomic Absorption Spectroscopy*, VCH: Deerfield Beach, FL, 1985.

Luminescence Spectroscopy

- Guilbault, G. G. *Practical Fluorescence*, Decker: New York, 1990.
- Schenk, G. "Historical Overview of Fluorescence Analysis to 1980," *Spectroscopy* **1997**, *12*, 47–56.
- Vo-Dinh, T. *Room-Temperature Phosphorimetry for Chemical Analysis*, Wiley-Interscience: New York, 1984.
- Winefordner, J. D.; Schulman, S. G.; O'Haver, T. C. *Luminescence Spectroscopy in Analytical Chemistry*, Wiley-Interscience: New York, 1969.

Applications

- *Trace Analysis and Spectroscopic Methods for Molecules, Christian, G. D.; Callis, J. B. Eds., Wiley-Interscience: New York, 1986.*
- Vandecasteele, C.; Block, C. B. *Modern Methods for Trace Element Determination*, Wiley: Chichester, England, 1994.
- Skoog, D. A.; Holler, F. J.; Nieman, T. A. *Principles of Instrumental Analysis*, Saunders: Philadelphia, 1998.

- Van Loon, J. C. *Selected Methods of Trace Metal Analysis: Biological and Environmental Samples*, Wiley- Interscience: New York, 1985.

Gathered here are resources and experiments for analyzing multicomponent samples using mathematical techniques not covered in this textbook.

- Aberasturi, F.; Jimenez, A. I.; Jimenez, F.; Arias, J. J. "UV-Visible First-Derivative Spectrophotometry Applied to an Analysis of a Vitamin Mixture," *J. Chem. Educ.* **2001**, *78*, 793–795.
- Afkhami, A.; Abbasi-Tarighat, M.; Bahram, M.; Abdollahi, H. "A new strategy for solving matrix effect in multivariate calibration standard addition data using combination of H-point curve isolation and H-point standard addition methods," *Anal. Chim. Acta* **2008**, *613*, 144–151.
- Brown, C. W.; Obremski, R. J. "Multicomponent Quantitative Analysis," *Appl. Spectrosc. Rev.* **1984**, *20*, 373–418.
- Charles, M. J.; Martin, N. W.; Msimanga, H. Z. "Simultaneous Determination of Aspirin, Salicylamide, and Caffeine in Pain Relievers by Target Factor Analysis," *J. Chem. Educ.* **1997**, *74*, 1114–1117.
- Dado, G.; Rosenthal, J. "Simultaneous Determination of Cobalt, Copper, and Nickel by Multivariate Linear Regression," *J. Chem. Educ.* **1990**, *67*, 797–800.
- DiTusa, M. R.; Schilt, A. A. "Selection of Wavelengths for Optimum Precision in Simultaneous Spectrophotometric Determinations," *J. Chem. Educ.* **1985**, *62*, 541–542.
- Gómez, D. G.; de la Peña, A. M.; Mansilla, A. E.; Olivieri, A. C. "Spectrophotometric Analysis of Mixtures by Classical Least-Squares Calibration: An Advanced Experiment Introducing MATLAB," *Chem. Educator* **2003**, *8*, 187–191.
- Harvey, D. T.; Bowman, A. "Factor Analysis of Multicomponent Samples," *J. Chem. Educ.* **1990**, *67*, 470–472.
- Lucio-Gutierrez, J. R.; Salazar-Cavazos, M. L.; de Torres, N. W. "Chemometrics in the Teaching Lab. Quantification of a Ternary Mixture of Common Pharmaceuticals by First- and Second-Derivative IR Spectroscopy," *Chem. Educator* **2004**, *9*, 234–238.
- Padney, S.; McHale, M. E. R.; Coym, K. S.; Acree Jr., W. E. "Bilinear Regression Analysis as a Means to Reduce Matrix Effects in Simultaneous Spectrophotometric Determination of Cr(III) and Co(II)," *J. Chem. Educ.* **1998**, *75*, 878–880.
- Raymond, M.; Jochum, C.; Kowalski, B. R. "Optimal Multicomponent Analysis Using the Generalized Standard Addition Method," *J. Chem. Educ.* **1983**, *60*, 1072–1073.
- Ribone, M. E.; Pagani, A. P.; Olivieri, A. C.; Goicoechea, H. C. "Determination of the Active Principle in a Spectrophotometry and Principal Component Regression Analysis," *J. Chem. Educ.* **2000**, *77*, 1330–1333.
- Rojas, F. S.; Ojeda, C. B. "Recent developments in derivative ultraviolet/visible absorption spectrophotometry: 2004–2008," *Anal. Chim. Acta* **2009**, *635*, 22–44.

This page titled 6.15: Additional Resources is shared under a CC BY-NC-SA 4.0 license and was authored, remixed, and/or curated by David Harvey.

- **10.10: Additional Resources** by David Harvey is licensed CC BY-NC-SA 4.0.

6.16: CHAPTER SUMMARY AND KEY TERMS

CHAPTER SUMMARY

The spectrophotometric methods of analysis covered in this chapter include those based on the absorption, emission, or scattering of electromagnetic radiation. When a molecule absorbs UV/Vis radiation it undergoes a change in its valence shell electron configuration. A change in vibrational energy results from the absorption of IR radiation. Experimentally we measure the fraction of radiation transmitted, *T*, by the sample. Instrumentation for measuring absorption requires a source of electromagnetic radiation, a means for selecting a wavelength, and a detector for measuring transmittance. Beer's law relates absorbance to both transmittance and to the concentration of the absorbing species ($A = -\log T = \varepsilon bC$).

In atomic absorption we measure the absorption of radiation by gas phase atoms. Samples are atomized using thermal energy from either a flame or a graphite furnace. Because the width of an atom's absorption band is so narrow, the continuum sources common for molecular absorption are not used. Instead, a hollow cathode lamp provides the necessary line source of radiation. Atomic absorption suffers from a number of spectral and chemical interferences. The absorption or scattering of radiation from the sample's matrix are important spectral interferences that are minimized by background correction. Chemical interferences include the formation of nonvolatile forms of the analyte and ionization of the analyte. The former interference is minimized by using a releasing agent or a protecting agent, and an ionization suppressor helps minimize the latter interference.

When a molecule absorbs radiation it moves from a lower energy state to a higher energy state. In returning to the lower energy state the molecule may emit radiation. This process is called photoluminescence. One form of photoluminescence is fluorescence in which the analyte emits a photon without undergoing a change in its spin state. In phosphorescence, emission occurs with a change in the analyte's spin state. For low concentrations of analyte, both fluorescent and phosphorescent emission intensities are a linear function of the analyte's concentration. Thermally excited atoms also emit radiation, forming the basis for atomic emission spectroscopy. Thermal excitation is achieved using either a flame or a plasma.

Spectroscopic measurements also include the scattering of light by a particulate form of the analyte. In turbidimetry, the decrease in the radiation's transmission through the sample is measured and related to the ana- lyte's concentration through an equation similar to Beer's law. In nephelometry we measure the intensity of scattered radiation, which varies linearly with the analyte's concentration.

KEY TERMS

absorbance
amplitude
background correction
chromophore
double-beam
electromagnetic spectrum
excitation spectrum
fiber-optic probe
fluorescence
frequency
interferometer
ionization suppressor
line source
mole-ratio method
nephelometry
phosphorescence
photoluminescence
polychromatic
relaxation
self-absorption
signal-to-noise ratio
slope-ratio method
spectrophotometer
transducer
turbidimetry
wavenumber
absorbance spectrum
attenuated total reflectance
Beer's law
continuum source
effective bandwidth
emission
external conversion
filter
fluorescent quantum yield
graphite furnace
internal conversion
Jacquinot's advantage
method of continuous variations
monochromatic
nominal wavelength
phosphorescent quantum yield
photon
protecting agent
releasing agent
signal averaging
single-beam
spectral searching
spectroscopy
transmittance
vibrational relaxation
absorptivity
atomization
chemiluminescence
dark current
electromagnetic radiation
emission spectrum
Fellgett's advantage
filter photometer
fluorimeter
interferogram
intersystem crossing
lifetime
molar absorptivity
monochromator
phase angle
photodiode array
plasma
radiationless deactivation
resolution
signal processor
singlet excited state
spectrofluorometer
stray radiation
triplet excited state
wavelength

This page titled 6.16: Chapter Summary and Key Terms is shared under a CC BY-NC-SA 4.0 license and was authored, remixed, and/or curated by David Harvey.

- **10.11: Chapter Summary and Key Terms** by David Harvey is licensed CC BY-NC-SA 4.0.

CHAPTER OVERVIEW

7: Nuclear Magnetic Resonance Spectroscopy

7.1: Theory of Nuclear Magnetic Resonance
7.2: Environmental Effects on NMR Spectra
7.2.1: Spin-Spin Coupling
7.2.2: The Basis for Differences in Chemical Shift
7.3: NMR Spectrometers
7.4: Applications of Proton NMR
7.5: Carbon-13 NMR
7.6: Two-Dimensional Fourier Transform NMR
7.7: Structure Determination - Nuclear Magnetic Resonance Spectroscopy
7.7.1: Nuclear Magnetic Resonance Spectroscopy
7.7.2: The Nature of NMR Absorptions
7.7.3: The Chemical Shift
7.7.4: Chemical Shifts in ^{1}H NMR Spectroscopy
7.7.5: Integration of ^{1}H NMR Absorptions - Proton Counting
7.7.6: Spin-Spin Splitting in ^{1}H NMR Spectra
7.7.7: ^{1}H NMR Spectroscopy and Proton Equivalence
7.7.8: More Complex Spin-Spin Splitting Patterns
7.7.9: Uses of ^{1}H NMR Spectroscopy
7.7.10: ^{13}C NMR Spectroscopy - Signal Averaging and FT-NMR
7.7.11: Characteristics of ^{13}C NMR Spectroscopy
7.7.12: DEPT ^{13}C NMR Spectroscopy
7.7.13: Uses of ^{13}C NMR Spectroscopy
7.7.S: Structure Determination - Nuclear Magnetic Resonance Spectroscopy (Summary)

This page titled 7: Nuclear Magnetic Resonance Spectroscopy is shared under a CC BY-NC-SA 4.0 license and was authored, remixed, and/or curated by David Harvey.

7.1: Theory of Nuclear Magnetic Resonance

As is the case with other forms of optical spectroscopy, the signal in nuclear magnetic resonance (NMR) spectroscopy arises from a difference in the energy levels occupied by the nuclei in the analyte. In this section we develop a general theory of nuclear magnetic resonance spectroscopy that draws on quantum mechanics and on classical mechanics to explain these energy levels.

Quantum Mechanical Description of NMR

The quantum mechanical description of an electron is given by four quantum numbers: the principal quantum number, n, the angular momentum quantum number, l, the magnetic quantum number, m_l, and the spin quantum number, m_s. The first three of these quantum numbers tell us something about where the electron is relative to the nucleus and something about the electron's energy. The last of these four quantum numbers, the spin quantum number, tells us something about the ability of an electron to interact with an applied magnetic field. An electron has possible spins of +1/2 or of –1/2, which we often refer to as spin up, using an upwards arrow, ↑, to represent it, or as spin down, using a downwards arrow, ↓, to represent it.

A nucleus, like an electron, carries a charge and has a spin quantum number. The overall spin, I, of a nucleus is a function of the number of protons and neutrons that make up the nucleus. Here are three simple rules for nuclear spin states:

- If the number of neutrons and the number of protons are both even numbers, then the nucleus does not have a spin; thus, ^{12}C, with six protons and six neutrons, has no overall spin and $I = 0$.
- If the number of neutrons plus the number of protons is an odd number, then the nucleus has a half-integer spin, such as 1/2 or 3/2; thus, ^{13}C, with six protons and seven neutrons, has an overall spin of $I = 1/2$; this also is true for ^{1}H.
- If the number of neutrons and the number of protons are both odd numbers, then the nucleus has an integer spin, such as 1 or 2; thus, ^{2}H, with one proton and one neutron, has an overall spin of $I = 1$.

Note

Predicting that ^{13}C has a spin of $I = 1/2$, but that ^{127}I has a spin of $I = 3/2$ and that ^{17}O has a spin of $I = 5/2$ is not trivial. A periodic table that provides spin states for elements is available here.

The total number of spin states—that is, the total number of possible orientations of the spin—is equal to $(2 \times I) + 1$. To be NMR active, a nucleus must have at least two spin states so that a change in spin states, and, therefore, a change in energy, is possible; thus, ^{12}C, for which there are $(2 \times 0) + 1 = 1$ spin states, is NMR inactive, but ^{13}C, for which there are $(2 \times 1/2) + 1 = 2$ spin states with values of $m = +1/2$ and of $m = -1/2$, is NMR active, as is ^{2}H for which there are $(2 \times 1) + 1 = 3$ spin states with values of $m = +1/2$, $m = 0$, and $m = -1/2$. As our interest in this chapter is in the NMR spectra for ^{1}H and for ^{13}C, we will limit ourselves to considering $I = 1/2$ and spin states of $m = +1/2$ and of $m = -1/2$.

Energy Levels in an Applied Magnetic Field

Suppose we have a large population of ^{1}H atoms. In the absence of an applied magnetic field the atoms are divided equally between their possible spin states: 50% of the atoms have a spin of +1/2 and 50% of the atoms have a spin of –1/2. Both spin states have the same energy, as is the case on the left side of Figure 7.1.1, and neither absorption nor emission occurs.

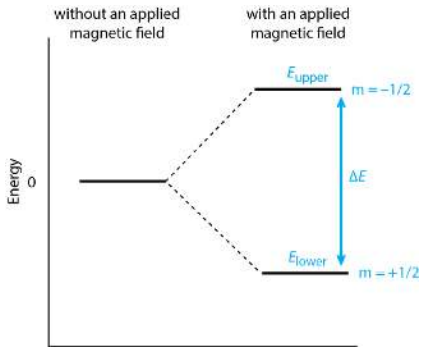


Figure 7.1.1. Energy level diagram for a proton, ^{1}H, in the absence (left) and in the presence (right) of an applied magnetic field.

In the presence of an applied magnetic field, as on the right side of Figure 7.1.1, the nuclei are either aligned with the magnetic field with spins of $m = +1/2$, or aligned against the magnetic field with spins of $m = -1/2$. The energies in these two spin

states, E_{lower} and E_{upper}, are given by the equations

$$E_{\text{lower}} = -\frac{\gamma h}{4\pi} B_0 \tag{7.1.1}$$

$$E_{\text{upper}} = +\frac{\gamma h}{4\pi} B_0 \tag{7.1.2}$$

where γ is the magnetogyric ratio for the nucleus, h is Planck's constant, and B_0 is the strength of the applied magnetic field. The difference in energy, ΔE, between the two states is

$$\Delta E = E_{\text{upper}} - E_{\text{lower}} = +\frac{\gamma h}{4\pi} B_0 - \left(-\frac{\gamma h}{4\pi} B_0\right) = \frac{\gamma h}{2\pi} B_0 \tag{7.1.3}$$

Substituting Equation 7.1.3 into the more familiar equation $\Delta E = h\nu$ gives the frequency, ν, of electromagnetic radiation needed to effect a change in spin state as

$$\nu = \frac{\gamma B_0}{2\pi} \tag{7.1.4}$$

This is called the Larmor frequency for the nucleus. For example, if the magnet has a field strength of 11.74 Tesla, then the frequency needed to effect a change in spin state for ^{1}H, for which γ is 2.68×10^8 rad $\text{T}^{-1}\text{s}^{-1}$, is

$$\nu = \frac{(2.68 \times 10^8 \text{rad T}^{-1}\text{s}^{-1})(11.74 \text{ T})}{2\pi} = 5.01 \times 10^8 \text{ s}^{-1}$$

or 500 MHz, which is in the radio frequency (RF) range of the electromagnetic spectrum. This is the Larmor frequency for ^{1}H.

Population of Spin States

The relative population of the upper spin state, N_{upper}, and of the lower spin state, N_{lower}, is given by the Boltzmann equation

$$\frac{N_{\text{upper}}}{N_{\text{lower}}} = e^{-\Delta E/kT} \tag{7.1.5}$$

where k is Boltzmann's constant (1.38066×10^{-23} J/K) and T is the temperature in Kelvin. Substituting in Equation 7.1.3 for ΔE gives this ratio as

$$\frac{N_{\text{upper}}}{N_{\text{lower}}} = e^{-\gamma h B_0/2\pi kT} \tag{7.1.6}$$

IF we place a population of ^{1}H atoms in a magnetic field with a strength of 11.74 Tesla, the ratio $\frac{N_{\text{upper}}}{N_{\text{lower}}}$ at 298 K is

$$\frac{N_{\text{upper}}}{N_{\text{lower}}} = e^{-\frac{(2.68\times10^8 \text{ rad s}^{-1})(6.626\times10^{-34} \text{ Js})(11.74 \text{ T})}{(2\pi)(1.38\times10^{-23} \text{ JK}^{-1})(298 \text{ K})}} = 0.99992$$

If this ratio is 1:1, then the probability of absorption and emission are equal and there is no net signal. In this case, the difference in the populations is on the order of 8 per 100,000, or 80 per 1,000,000, or 80 ppm. The small difference in the two populations means that NMR is less sensitive than many other spectroscopic methods.

Classical Description of NMR

To understand the classical description of an NMR experiment we draw upon Figure 7.1.2. For simplicity, let's assume that in the population of nuclei available to us, there is an excess of just one nucleus with a spin state of +1/2. In Figure 7.1.2*a*, we see that the spin of this nucleus is not perfectly aligned with the applied magnetic field, B_0, which is aligned with the *z*-axis; instead the nucleus precesses around the *z*-axis at an angle of theta, Θ. As a result, the net magnetic moment along the *z*-axis, μ_z, is less than the magnetic moment, μ, of the nucleus. The precession occurs with an angular velocity, ω_0, of γB_0.

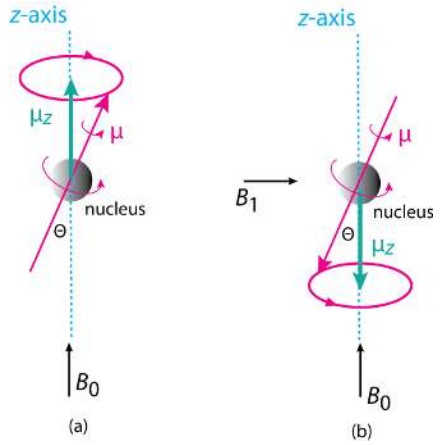


Figure 7.1.2. Illustration that shows in (a) the magnetic moment, μ, of a nucleus whose spin is aligned with the applied magnetic field, B_0. Application of the magnetic field, B_1 flips the spin of the nucleus, as shown in (b).

If we apply a source of radio frequency (RF) electromagnetic radiation along the *x*-axis such that its magnetic field component, B_1, is perpendicular to B_0, then it will generate its own angular velocity in the *xy*-plane. When the angular velocity of the precessing nucleus matches the angular velocity of B_1, absorption takes place and the spin flips, as seen in Figure 7.1.2*b*.

Relaxation

When the magnetic field B_1 is removed, the nucleus returns to its original state, as seen in Figure 7.1.2*a*, a process called relaxation. In the absence of relaxation, the system is saturated with equal populations of the two spin states and absorption approaches zero. This process of relaxation has two separate mechanisms: spin-lattice relaxation and spin-spin relaxation.

In spin-lattice relaxation the nucleus in its higher energy spin state, Figure 7.1.2*b*, returns to its lower energy state spin state, Figure 7.1.2*a*, by transferring energy to other species present in the sample (the lattice in spin-lattice). Spin-lattice relaxation is characterized by first-order exponential decay with a characteristic relaxation time of T_1 that is a measure of the average time the nucleus remains in its higher energy spin state. Smaller values for T_1 result in more efficient relaxation.

If two nuclei of the same type, but in different spin states, are in close proximity to each other, they can trades places in which the nucleus in the higher energy spin state gives up its energy to the nucleus in the lower energy spin state. The result is a decrease in the average life-time of an excited state. This is called spin-spin relaxation and it is characterized by a relaxation time of T_2.

Continuous Wave NMR vs. Fourier Transform NMR

In Chapter 16 we learned that we can record an infrared spectrum by using a scanning monochromator to pass, sequentially, different wavelengths of IR radiation through a sample, obtaining a spectrum of absorbance as a function of wavelength. We also learned that we can obtain the same spectrum by passing all wavelengths of IR radiation through the sample at the same time using an interferometer, and then use a Fourier transform to convert the resulting interferogram into a spectrum of absorbance as a function of wavelength. Here we consider their equivalents for NMR spectroscopy.

Continuous Wave NMR

If we scan B_1 while holding B_0 constant—or scan B_0 while holding B_1 constant—then we can identify the Larmor frequencies where a particular nucleus absorbs. The result is an NMR spectrum that shows the intensity of absorption as a function of the frequency at which that absorption takes place. Because we record the spectrum by scanning through a continuum of frequencies, the method is known as continuous wave NMR. Figure 7.1.2 provides a useful visualization for this experiment.

Fourier Transform NMR

In Fourier transform NMR, the magnetic field B_1 is applied as a brief pulse of radio frequency (RF) electromagnetic radiation centered at a frequency appropriate for the nucleus of interest and for the strength of the primary magnetic field, B_0. The pulse typically is 1-10 μs in length and applied in the *xy*-plane. From the Heisenberg uncertainty principle, a short pulse of Δt results in a broad range of frequencies as $\Delta f = 1/\Delta t$; this ensures that the pulse spans a sufficient range of frequencies such that the nucleus of interest to us will absorb energy and enter into an excited state.

Before we apply the pulse, the population of nuclei are aligned parallel to the applied magnetic field, B_0, some with a spin of +1/2 and others with a spin of –1/2. As we learned above, there is a slight excess of nuclei with spins of +1/2, which we can represent as a single vector that shows their combined magnetic moments along the *z*-axis, μ_z, as shown in Figure 7.1.3*a*. When we apply a pulse of RF electromagnetic radiation with a magnetic field strength of B_1, the spin states of the nuclei tip away from the *z*-axis by an angle that depends on the nucleus's magnetogyric ratio, γ, the value of B_1, and the length of the pulse. If, for example, a pulse of 5 μs tips the the magnetic vector by 45° (Figure 7.1.3*b*), then a pulse of 10 μs will tip the magnetic vector by 90° degrees (Figure 7.1.3*c*), so that it now lies completely within the *xy*-plane.

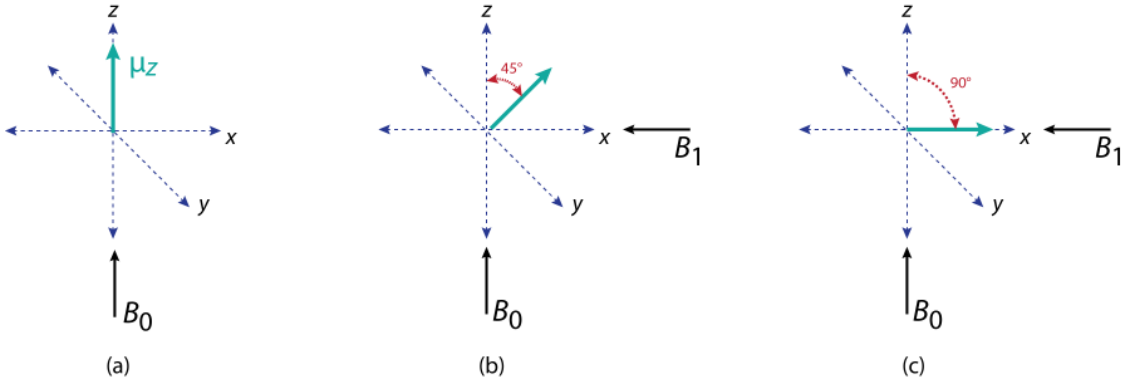


Figure 7.1.3. Illustration that shows (a) the net magnetic moment on the *z*-axis for a population of nuclei in an applied magnetic field with a field strength of B_0. Application of a pulsed RF field, B_1, tips the magnetic moment (b) away from the *z*-axis. The longer the pulse of RF, the greater the angle of tipping, as shown in (c).

At the end of the pulse, the nuclei begin to relax back to their original state. Figure 7.1.4 shows that this relaxation occurs both in the *xy*-plane (spin-spin relaxation) and along the *z*-axis (spin-lattice relaxation). If we were to trace the path of the magnetic vector with time, we would see that it follows a spiral-like motion as its contribution in the *xy*-plane decreases and its contribution along the *z*-axis increases. We measure this signal—called the free induction decay, or FID—during this period of relaxation.

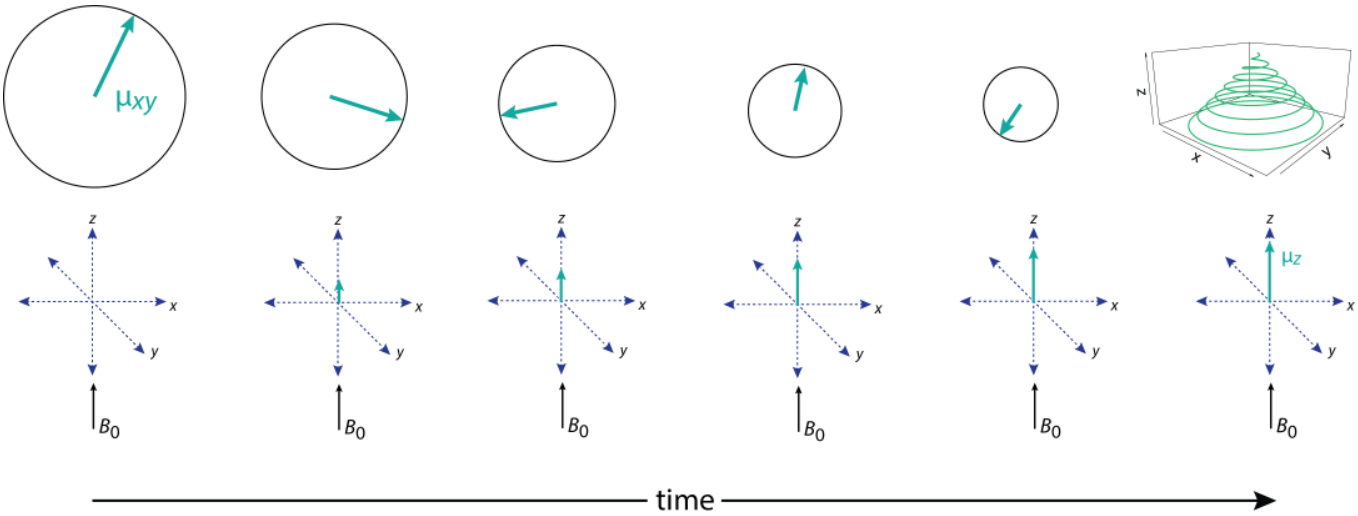


Figure 7.1.4. Illustration showing the process of relaxation during an NMR experiment. The bottom row shows the net magnetic moment aligned with the *z*-axis, μ_z, as a function of time. The top row shows the net magnetic moment in the *xy*-plane with the figure on the top right showing the overall change in the net magnetic moment in three dimensions.

The FID for a system that consists of only one type of nucleus is the simple exponentially damped oscillating signal in Figure 7.1.5*a*. The Fourier transform of this simple FID gives the spectrum in Figure 7.1.5*b* that has a single peak. A sample with a more than one type of nucleus yields a more complex FID pattern, such as that in Figure 7.1.5*c*, and a more complex spectrum, such as the two peaks in Figure 7.1.5*d*. Note that, as we learned in an earlier treatment of the Fourier transform in Chapter 7, a broader peak in the frequency domain results in a faster decay in the time domain.

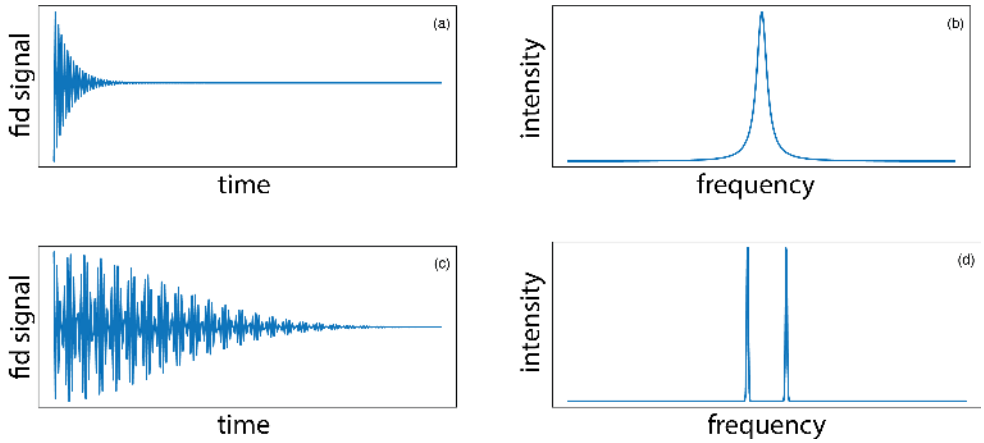


Figure 7.1.5. Panels (a) and (b) show the FID signal for a sample that yields single peak and the result of taking the FT of the FID. Panels (c) and (d) show the FID signal for a sample that consists of two peaks and the result of taking the FT of the FID.

Figure 7.1.6 shows a typical pulse sequence highlighting the total cycle time and its component parts: the pulse width, the acquisition time during which the FID is recorded, and a recycle delay before applying the next pulse and beginning the next cycle.

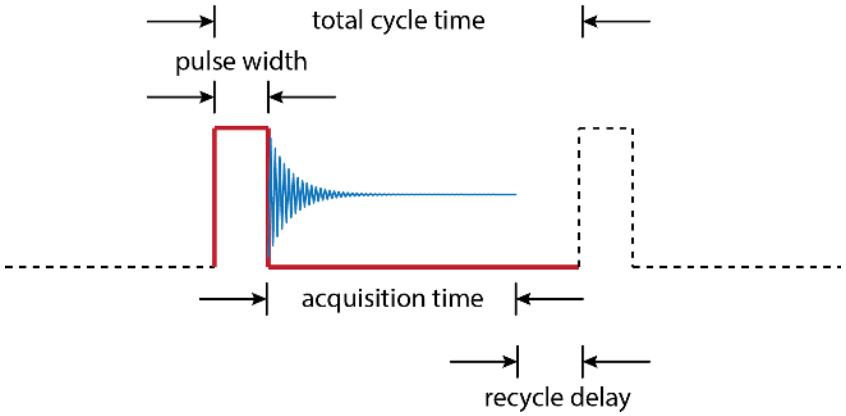


Figure 7.1.1: Example of a pulse sequence.

This page titled 7.1: Theory of Nuclear Magnetic Resonance is shared under a CC BY-NC-SA 4.0 license and was authored, remixed, and/or curated by David Harvey.

- **19.1: Theory of Nuclear Magnetic Resonance** by David Harvey is licensed CC BY-NC-SA 4.0.

7.2: Environmental Effects on NMR Spectra

In the previous section we showed that there is a relationship between the Larmor frequency for a nucleus, ν, its magnetogyric ratio, γ, and the primary applied magnetic field strength, B_0

$$\nu = \frac{\gamma B_0}{2\pi} \tag{7.2.1}$$

and we used this equation to show that the Larmor frequency for the ^{1}H nucleus in a magnetic field of $B_0 = 11.74$ T is 500 MHz. If this is the only thing that determines the frequency where absorption takes place, then all compounds that contain hydrogens will yield a ^{1}H NMR spectrum with a single peak at the same frequency. If all spectra are identical, then NMR provides little in the way of useful information. The NMR spectrum for propane (CH_3–CH_2—CH_3) in Figure 7.2.1 shows two clusters of peaks that give us confidence in the utility of NMR. In this case, it seems likely that the cluster of peaks between 250 Hz and 300 Hz, which have a greater total intensity, are for the six hydrogens in the two methyl groups (–CH_3) and that the cluster of peaks around 400 Hz are due to the methylene group (–CH_2–). In this section we will consider why the location of a nucleus within a molecule—what we call its environment—might affect the frequency at which it absorbs and why a particular absorption line might appear as a cluster of individual peaks instead of as a single peak.

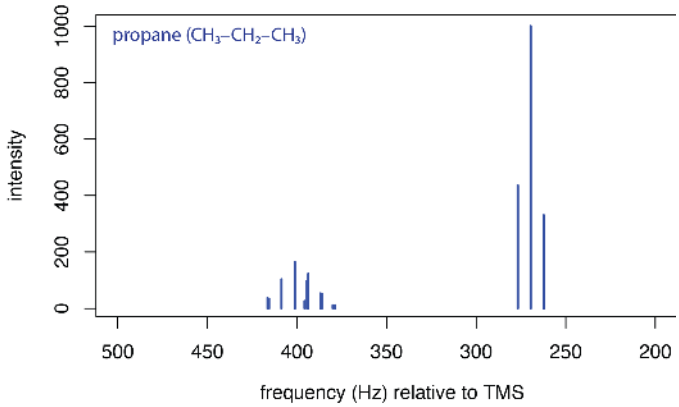


Figure 7.2.1: ^{1}H NMR spectrum for propane. The original data used to construct this spectrum is here and was obtained on a 300 MHz instrument.

The NMR Spectrum's Scale

Before we consider how a nucleus's environment affects the frequencies at which it absorbs, let's take a moment to become familiar with the scale used to plot a NMR spectrum. The label on the *x*-axis of the NMR spectrum for propane in Figure 7.2.1 raises several questions that we will answer here.

Why is the Scale Relative?

From Equation 7.2.1 we see that the frequency at which a nucleus absorbs is a function of the magnet's field strength, B_0. This means the frequency of a peak in an NMR spectrum depends on the value of B_0. One complication is that instruments with identical nominal values for B_0 likely will have slightly different actual values, which leads to small variations in the frequency at which a particular hydrogen absorbs on different instruments. We can overcome this problem by referencing a hydrogen's measured frequency to a reference compound that is set to a frequency of 0. The difference between the two frequencies should be the same on different instruments. For example, the most intense peak in the NMR spectrum for propane, Figure 7.2.1, has a frequency of 269.57 Hz when measured on an NMR with a nominal field strength of 300 MHz, which means that its frequency is 269.57 Hz greater than the reference, which is identified as TMS.

What is TMS?

The reference compound is tetramethylsilane, TMS, which has the chemical formula of $(CH_3)_4Si$ in which four methyl groups are in a tetrahedral arrangement about the central silicon. TMS has the advantage of having all of its hydrogens in the same environment, which yields a single peak. Its hydrogen atoms also absorbs at a low frequency that is well removed from the frequency at which most other hydrogen atoms absorb, which makes it easy to identify its peak in the NMR spectrum.

How Can We Create a Universal Scale?

An additional complication with the spectrum in Figure 7.2.1 is that the frequency at which a particular hydrogen absorbs is different when using a 60 MHz NMR than it is when using a 300 MHz NMR, a consequence of Equation 7.2.1. To create a single scale that is independent of B_0 we divide the peak's frequency, relative to TMS, by B_0, expressing both in Hz, and then report the result on a part-per-million scale by multiplying by 10^6. For example, the most intense peak in the NMR spectrum for propane, Figure 7.2.1, has a frequency of 269.57 Hz; the NMR on which the spectrum was recorded had a field strength of 300 MHz. On a parts-per-million scale, which we identify as delta, δ, the peak appears at

$$\delta = \frac{269.57 \text{ Hz}}{300 \times 10^6 \text{ Hz}} \times 10^6 = 0.899 \text{ ppm}$$

If we record the spectrum of propane on a 60 MHz instrument, then we expect that this peak to appear at 0.899 ppm, or a frequency of

$$\nu = \frac{0.899 \text{ ppm} \times (60 \times 10^6 \text{ Hz})}{10^6} = 53.9 \text{ Hz}$$

relative to TMS.

Most hydrogens have values of δ between 1 and 13. Figure 7.2.2 shows the ^{1}H NMR for propane using a ppm scale. The right side of the ppm scale is described as being upfield, with absorption occurring at a lower frequency, and with a smaller difference in energy, ΔE, between the ground state and the excited state. The left side of the ppm scale is described as being downfield, with absorption occurring at a higher frequency, and with a greater difference in energy, ΔE, between the ground state and the excited state.

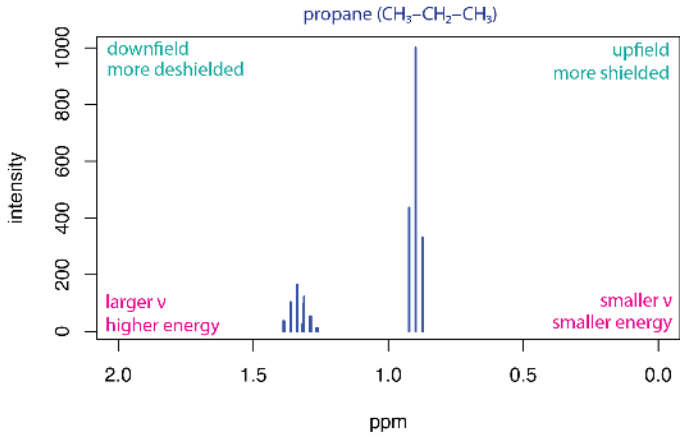


Figure 7.2.2: ^{1}H NMR spectrum for propane expressed in ppm. The original data used to construct this spectrum is here and was obtained on a 300 MHz instrument. The peak for TMS is not shown.

Types of Environmental Effects

The NMR spectrum for propane in Figure 7.2.2 shows two important features: the peaks for the two types of hydrogen in propane are shifted downfield relative to the reference and the methylene hydrogens are shifted further downfield than the methyl hydrogens. Both groups appear as clusters of peaks instead of as single peaks. In this section we consider the source of these two phenomena.

Chemical Shifts

In the presence of a magnetic field, the electrons in a molecule circulate, generating a secondary magnetic field, B_e, that usually, but not always, opposes the primary applied magnetic field, B_{appl}. The result is that the nucleus is partially shielded by the electrons such that the field it experiences, B_0, usually is smaller than the applied field and

$$B_0 = B_{\text{appl}} - B_e \tag{7.2.2}$$

The greater the shielding, the smaller the value of B_0 and the further to the right the peak appears in the NMR spectrum. For example, in the NMR spectrum for propane in Figure 7.2.2 the cluster of peaks for the –CH_3 hydrogens centered at 0.899 ppm shows greater shielding than the cluster of peaks for the –CH_2– hydogens that is centered at 1.337 ppm.

Chemical shifts are useful for determining structural information for molecules. A few examples are listed in the following table and more extensive tables here. Note that the range of chemical shifts for the methyl and the methylene groups encompass the values for propane in Figure 7.2.2.

Table 7.2.1. ^{1}H Shifts in ppm

type of hydrogen	example	range of chemical shifts (ppm)
primary alkyl	$R-CH_3$	0.7 – 1.3
secondary alkyl	$R-CH_2-R$	1.2 – 1.6
tertiary alkyl	R_3CH	1.4 – 1.8
methyl ketone	$R-C(=O)-CH_3$	2.0 – 2.4
aromatic methyl	$C_6H_5-CH_3$	2.4 – 2.7
alkynyl	$R-C\equiv C-H$	2.5 – 3.0
alkyl halide (X = F, Cl, Br, I)	R_2X-CH	2.5 – 4.0
alcohol	R_3-C-OH	2.5 – 5.0
vinylic	$R_2-C=C(-R)-H$	4.5 – 6.5
aryl	C_6H_5-H	6.5 – 8.0
aldehyde	$R-C(=O)-H$	9.7 – 10.0
carboxylic acid	$R-C(=O)-OH$	11.0 – 12.0

Spin-Spin Coupling

Chemical shifts are the result of shielding from the magnetic field associated with a molecule's circulating electrons. The splitting of a peak into a multiplet of peaks is the result of the shielding of one nucleus by the nuclei on adjacent atoms, and is called spin-spin coupling. Consider the NMR for propane in Figure 7.2.2, which consists of two clusters of peaks. The six hydrogens in the two methyl groups are sufficiently close to the two hydrogens in the methylene group that the spins of the methylene hydrogens can affect the frequency at which the methyl hydrogens absorb. Figure 7.2.3a shows how this works. Each of the two methylene hydrogens has a spin and those spins can both be aligned with the magnetic field, B_0, both be aligned against B_0, or two configurations in which one is aligned with B_0 and one is aligned against B_0, as seen by the arrows. When the two spins are aligned with B_0, the frequency at which the methyl hydrogens absorb is shifted downfield, and when the two spins are aligned against B_0, the frequency at which the methyl hydrogens absorb is shifted upfield; in the remaining two cases, there is no change in the ferquency at with the methyl hydrogens absorb. The result, as seen in Figure 7.2.3a is a triplet of peaks in a 1:2:1 intensity ratio.

The analysis for the effect of the six methyl hydrogens on the two methylene hydrogens is a bit more complex, but works in the same way. Figure 7.2.3b, for example, shows that there are 15 ways to arrange the spins of the six methyl hydrogens such that two are spin down and four are spin up. Figure 7.2.3c show the resulting NMR spectrum, which is a set of seven peaks in a 1:6:15:20:15:6:1 intensity ratio.

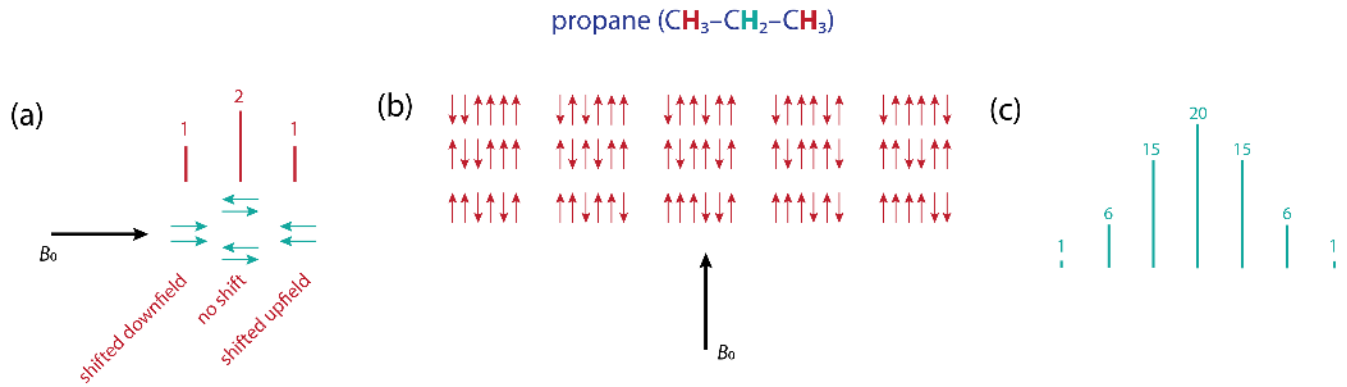


Figure 7.2.3. Illustration that shows the origin of spin-spin splitting: (a) The methyl hydrogens in propone split into three peaks by the spins of the two hydrogens on the adjacent methylene carbon; (b) The 15 different ways in which the six methyl hydrogens in propane have two nuclei that are spin down and four that are spin up; (c) The methylene hydrogens in propane are split into seven peaks by the six methyl hydrogens.

Figure 7.2.4 provides the splitting pattern observed for nuclei with $I = +1/2$, such as ^{1}H. The pattern is defined by the coefficients of a binomial distribution—asking how many different ways you can get *X* outcomes in *Y* attempts is at the heart of a binomial distribution—this is easy to represent using Pascal's triangle—which shows us that for six equivalent nuclei we expect to find seven peaks with relative peak areas (or other measure of the signal) of 1:6:15:20:15:6:1. Note that the first and the last entry in any row is 1 and that all other entries in a row, as illustrated for the third entry in the seventh row, are the sum of the two entries in the row immediately above. The pattern also is know as the $N+1$ rule as the N equivalent hydrogens will split the peak for an adjacent hydrogen into $N+1$ peaks.

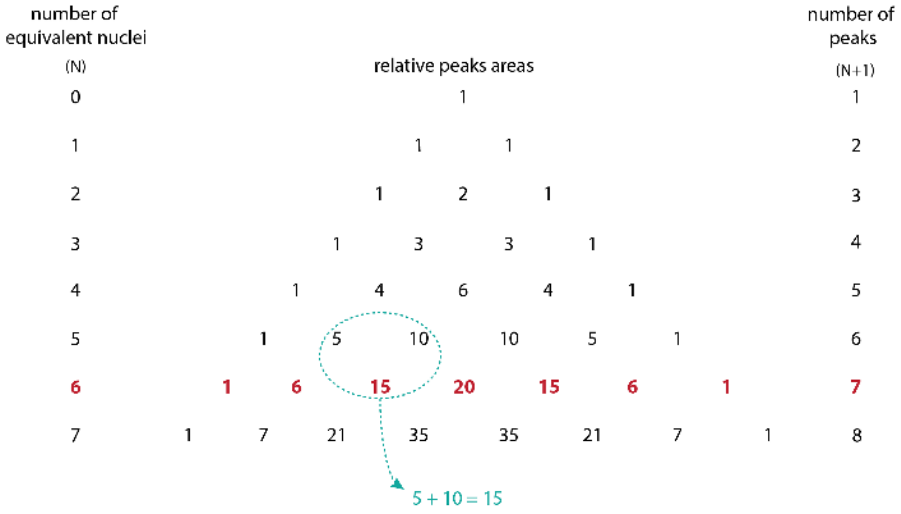


Figure 7.2.4. Pascal's triangle defines the splitting patterns in ^{1}H NMR. The annotation shows how the values in any row of Pascal's triangle give are derived from the previous row.

Figure 7.2.5 compares the experimental NMR for propane with its simulatd spectrum based on spin-spin splitting and the 2:6 ratio of methylene hydrogens relative to methyl hydrogens. The overall agreement between the two spectra is pretty good. The splitting of the individual peaks is designated by the coupling constant, *J*, which is shown in Figure 7.2.5 for both the experimental and the calculated spectra. Note that the coupling constant is the same whether we are considering the effect of the methyl hydrogens on the methylene hydrogens, or the effect of the methylene hydrogens on the methyl hydrogens. Values of the coupling constant become smaller the greater the distance between the nuclei.

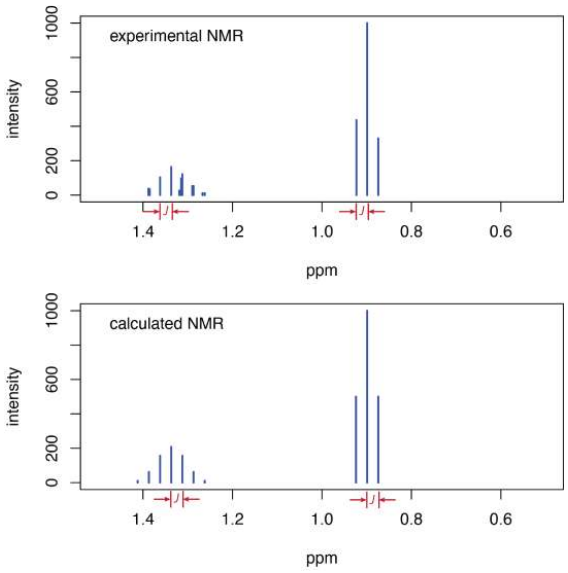


Figure 7.2.5: Experimental and calculated ^{1}H NMR spectra for propane. The original data used to construct this spectrum is here and was obtained on a 300 MHz instrument. The peak for TMS is not shown.

The treatment of spin-spin coupling above works well if the difference in the chemical shifts for the two nuclei is significantly greater than the magnitude of their coupling constant. When this is not true, the splitting patterns can become much more complex and often are difficult to interpret. There are a variety of to simplify spectra, one of which, decoupling, is outlined in Figure 7.2.6. The original spectrum (top) shows two doublets, suggesting that we have two individual nuclei that are coupled to each other. If we irradiate the nucleus on the right at its frequency, we can saturate its ground and excited states such that it ceases to absorb. As a result, the nucleus on the left no longer shows evidence of spin-spin coupling to the nucleus on the right (middle) and appears as a singlet. When we turn off the decoupler (bottom) the spin-spin coupling between the two nuclei returns more quickly than relaxation returns the signal for the nucleus on the right.

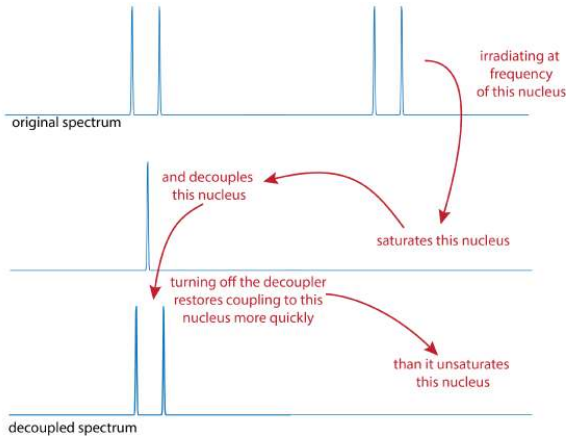


Figure 7.2.6. Illustration showing the effect of decoupling on an NMR spectrum. See the text for additional details.

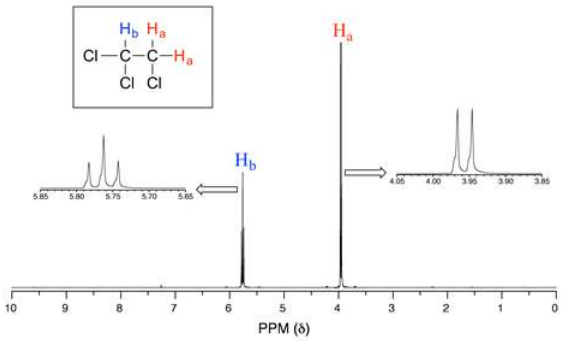
This page titled 7.2: Environmental Effects on NMR Spectra is shared under a CC BY-NC-SA 4.0 license and was authored, remixed, and/or curated by David Harvey.

- **19.2: Environmental Effects on NMR Spectra** by David Harvey is licensed CC BY-NC-SA 4.0.

7.2.1: Spin-Spin Coupling

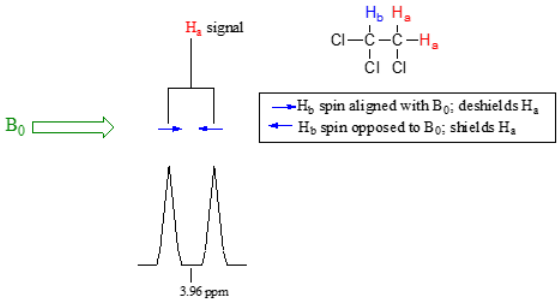
The ^1H-NMR spectra that we have seen so far (of methyl acetate and 1,4-dimethylbenzene) are somewhat unusual in the sense that in both of these molecules, each set of protons generates a single NMR signal. In fact, the ^1H-NMR spectra of most organic molecules contain proton signals that are 'split' into two or more sub-peaks. Rather than being a complication, however, this splitting behavior is actually very useful because it provides us with more information about our sample molecule.

Consider the spectrum for 1,1,2-trichloroethane. In this and in many spectra to follow, we show enlargements of individual signals so that the signal splitting patterns are recognizable.

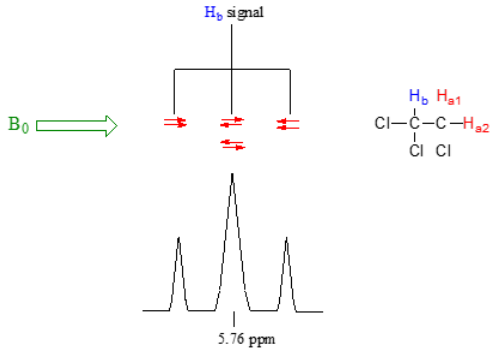


The signal at 3.96 ppm, corresponding to the two H_a protons, is split into two subpeaks of equal height (and area) – this is referred to as a doublet. The H_b signal at 5.76 ppm, on the other hand, is split into three sub-peaks, with the middle peak higher than the two outside peaks - if we were to integrate each subpeak, we would see that the area under the middle peak is twice that of each of the outside peaks. This is called a triplet.

The source of signal splitting is a phenomenon called spin-spin coupling, a term that describes the magnetic interactions between neighboring, non-equivalent NMR-active nuclei. (The terms 'splitting' and 'coupling' are often used interchangeably when discussing NMR.) In our 1,1,2 trichloromethane example, the H_a and H_b protons are spin-coupled to each other. Here's how it works, looking first at the H_a signal: in addition to being shielded by nearby valence electrons, each of the H_a protons is also influenced by the small magnetic field generated by H_b next door (remember, each spinning proton is like a tiny magnet). The magnetic moment of H_b will be aligned with B_0 in slightly more than half of the molecules in the sample, while in the remaining molecules it will be opposed to B_0. The Beff 'felt' by H_a is a slightly weaker if H_b is aligned against B_0, or slightly stronger if H_b is aligned with B_0. In other words, in half of the molecules H_a is shielded by H_b (thus the NMR signal is shifted slightly upfield) and in the other half H_a is deshielded by H_b (and the NMR signal shifted slightly downfield). What would otherwise be a single H_a peak has been split into two sub-peaks (a doublet), one upfield and one downfield of the original signal. These ideas an be illustrated by a splitting diagram, as shown below.

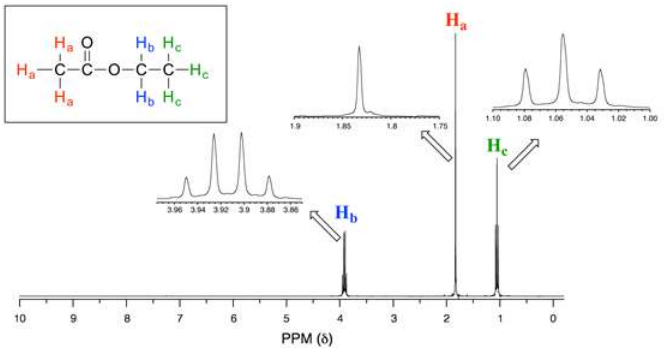


Now, let's think about the H_b signal. The magnetic environment experienced by H_b is influenced by the fields of both neighboring H_a protons, which we will call H_a1 and H_a2. There are four possibilities here, each of which is equally probable. First, the magnetic fields of both H_a1 and H_a2 could be aligned with B_0, which would deshield H_b, shifting its NMR signal slightly downfield. Second, both the H_a1 and H_a2 magnetic fields could be aligned opposed to B_0, which would shield H_b, shifting its resonance signal slightly upfield. Third and fourth, H_a1 could be with B_0 and H_a2 opposed, or H_a1 opposed to B_0 and H_a2 with B_0. In each of the last two cases, the shielding effect of one H_a proton would cancel the deshielding effect of the other, and the chemical shift of H_b would be unchanged.



So in the end, the signal for H_b is a triplet, with the middle peak twice as large as the two outer peaks because there are two ways that H_a1 and H_a2 can cancel each other out.

Consider the spectrum for ethyl acetate:



We see an unsplit 'singlet' peak at 1.83 ppm that corresponds to the acetyl (H_a) protons – this is similar to the signal for the acetate protons in methyl acetate that we considered earlier. This signal is unsplit because there are no adjacent protons on the molecule. The signal at 1.06 ppm for the H_c protons is split into a triplet by the two H_b protons next door. The explanation here is the same as the explanation for the triplet peak we saw previously for 1,1,2-trichloroethane.

The Hb protons give rise to a quartet signal at 3.92 ppm – notice that the two middle peaks are taller then the two outside peaks. This splitting pattern results from the spin-coupling effect of the three adjacent Hc protons, and can be explained by an analysis similar to that which we used to explain the doublet and triplet patterns.

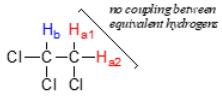
? Exercise 5.6.1

a. Explain, using a splitting diagram, the possible combinations of nuclear spin states for the H_c protons in ethyl acetate, and why the H_b signal is split into a quartet.
b. The integration ratio of the two 'sub-peaks' in a doublet is 1:1, and in triplets it is 1:2:1. What is the integration ratio of the H_b quartet in ethyl acetate? (Hint – use the illustration that you drew in part a to answer this question.)

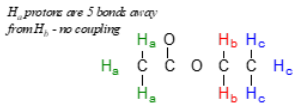
By now, you probably have recognized the pattern which is usually referred to as the n + 1 rule: if a set of protons has n neighboring, non-equivalent protons, it will be split into n + 1 subpeaks. Thus the two H_b protons in ethyl acetate split the H_c signal into a triplet, and the three H_c protons split the H_b signal into a quartet. H_a, with zero neighboring protons, is a singlet. This is very useful information if we are trying to determine the structure of an unknown molecule: if we see a triplet signal, we know that the corresponding proton or set of protons has two `neighbors`. When we begin to determine structures of unknown compounds using ^1H-NMR spectral data, it will become more apparent how this kind of information can be used.

Four important points need to be emphasized at this point.

First, signal splitting only occurs between non-equivalent protons – in other words, H_a1 in 1,1,2-trichloroethane is not split by H_a2, and vice-versa.



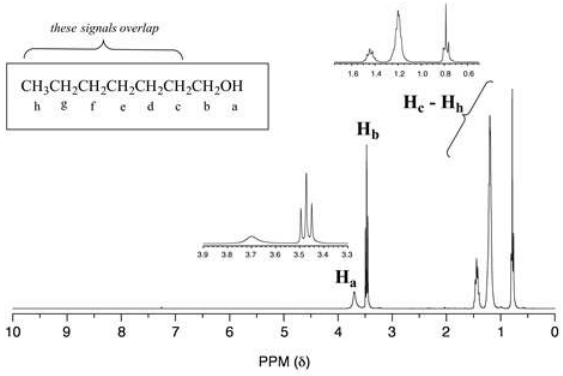
Second, splitting occurs primarily between protons that are separated by three or fewer bonds. This is why the H_a protons in ethyl acetate form a singlet– the nearest proton neighbors are five bonds away, too far for coupling to occur.



With more sensitive instruments we will sometimes see 4-bond and even 5-bond splitting, but in our treatment of NMR, for the sake of simplicity we will always assume that only three-bond splitting is seen.

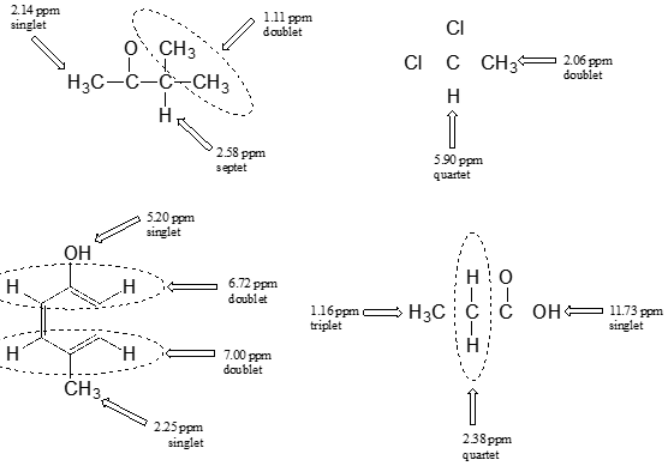
Third, protons that are bonded to oxygen or nitrogen generally do not split - and are not split by - adjacent protons. OH and NH protons are acidic enough to rapidly exchange between different molecules, so the neighboring protons never actually 'feels' their influence.

The spectrum of 1-heptanol has a characteristically broad alcohol proton signal at 3.7 ppm (labeled Ha below).



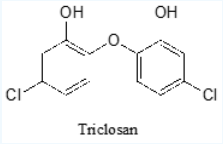
Notice in this spectrum that H_b is a triplet, coupled to the two H_c protons but not coupled to H_a. The signals corresponding to H_c through Hh are complex due to overlapping - when this happens (as it often does!), detailed analysis becomes more challenging.

Below are a few more examples of chemical shift and splitting pattern information for some relatively simple organic molecules.



Exercise 5.6.2

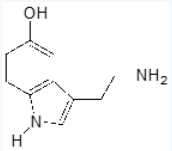
How many proton signals would you expect to see in the ^1H-NMR spectrum of triclosan (a common antimicrobial agent in soap)? For each of the proton signals, predict the splitting pattern, assuming that you can see only 3-bond splitting.



Triclosan

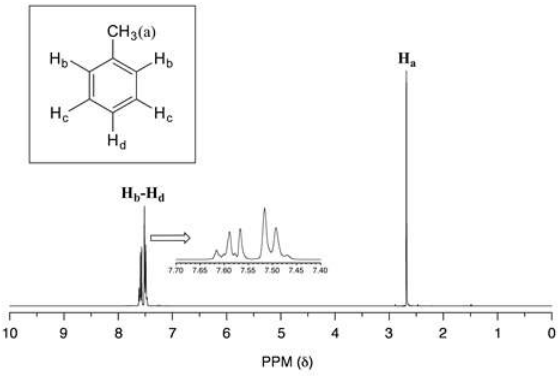
? Exercise 5.6.3

How many proton signals would you expect to see in the ^1H-NMR spectrum of the neurotransmitter serotonin? For each of the proton signals, predict the splitting pattern, again assuming only 3-bond splitting.



serotonin

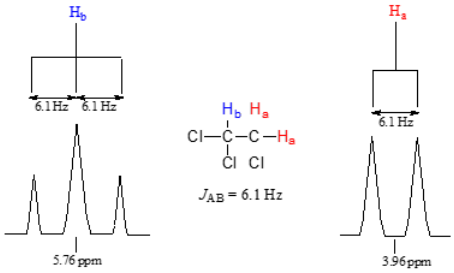
In an ideal world, all NMR spectra would be as easy to interpret as those we have seen so far: every peak would be separated from the others, the peak integration would be obvious, and the multiplicity (singlet, doublet, etc.) would be easy to recognize. The real world, unfortunately, is not always so pretty: peaks with similar chemical shifts overlap, making interpretation much more difficult. We have already seen this is the spectrum of 1-heptanol above. In the spectrum of methylbenzene, we would expect the signal for H_a to be a singlet, H_b to be a doublet, and H_c and H_d to be triplets. Looking at relative integration values for the four peaks, we would expect to see a 3:2:2:1 ratio.



In practice, however, the three aromatic proton sets H_b, H_c and H_d have very similar chemical shifts so their signals overlap substantially, and we cannot recognize doublet or triplet splitting patterns. In this case, we would refer to the aromatic part of the spectrum as a multiplet. We can report the integration ratio of the H_a peak compared to the combined aromatic peaks as 3 to 5, or the equivalent 1 to 1.67.

The magnitude of spin-spin coupling can be expressed using the coupling constant, abbreviated with the capital letter J. The coupling constant is simply the difference, expressed in Hz, between two adjacent sub-peaks in a split signal, and is a measure of the extent to which one nucleus 'feels' the magnetic dipole of its neighbor.

For our doublet in the 1,1,2-trichloroethane spectrum, for example, the two subpeaks are separated by 6.1 Hz, and thus we write $^3J_{a-b} = 6.1Hz$.

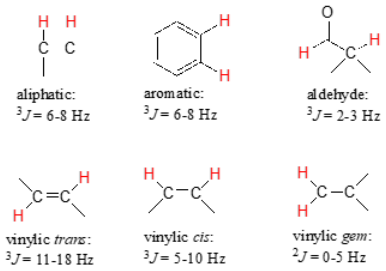


The superscript '3' tells us that this is a three-bond coupling interaction, and the 'a-b' subscript tells us that we are talking about coupling between H_a and H_b. Unlike the chemical shift value, the coupling constant, expressed in Hz, is the same regardless of the applied field strength of the NMR magnet. The strength of the magnetic moment of a neighboring proton, which is the source of the spin-spin coupling phenomenon, does not depend on the applied field strength. For this reason, coupling constants are normally given in Hz, not ppm.

When we look closely at the triplet signal in 1,1,2-trichloroethane, we see that the coupling constant - the 'gap' between subpeaks - is 6.1 Hz, the same as for the doublet. The coupling constant ${}^3J_{a-b}$ quantifies the magnetic interaction between the Ha and Hb hydrogen sets, and this interaction is of the same magnitude in either direction. In other words, spin-spin coupling is reciprocal: H_a influences H_b to the same extent that H_b influences H_a.

Coupling constants between proton sets on neighboring sp^3-hybridized carbons is typically in the region of 6-8 Hz. Coupling constants for neighboring vinylic protons can range from 0 Hz (no coupling at all) to 18 Hz, depending on the bonding arrangement.

Typical proton-proton coupling constants



For vinylic protons in a trans configuration, we see coupling constants in the range of ${}^3J = 11 - 18Hz$, while cis protons couple in the ${}^3J = 5 - 10Hz$ range. The 2-bond coupling between protons on the same alkene carbon (referred to as geminal protons) is very fine, generally 5 Hz or lower.

Fine coupling (2-3 Hz) is often seen between an aldehyde proton and a three-bond neighbor.

? Exercise 5.6.4

Give the expected splitting patterns and approximate coupling constants for the labeled protons in the compound below.

Presenting NMR data in table format

Information from NMR can be recorded conveniently in a condensed form without having to reproduce the actual spectrum. For example, the information from the ${}^1H$-NMR specta of ethyl acetate and methylbenzene (see earlier figures) can be presented in tabular format, listing the chemical shift, the peak splitting pattern, and the relative area under peaks (usually, the smallest peak is set to 1). Coupling constant information is not shown in the example tables below.

Table 5.6.1 : ${}^1H$-NMR spectrum of ethyl acetate

ppm	splitting	integration
3.92	q	1

ppm	splitting	integration
1.83	s	1.5
1.06	t	1.5

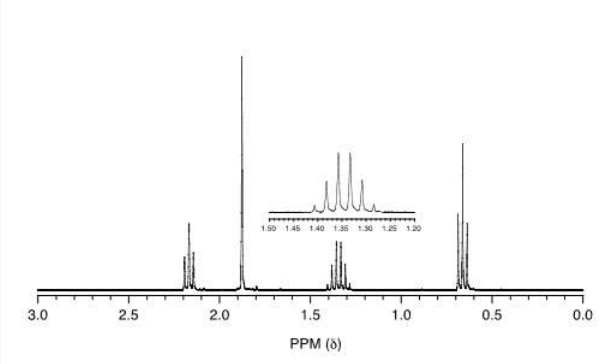
Table 5.6.2 : ^1H-NMR spectrum of methylbenzene.

ppm	splitting	integration
7.45 - 7.63	m	1.67
2.64	s	1

(abbreviations: s = singlet, d = doublet, t = triplet, q = quartet, m = multiplet)

Exercise 5.6.5

Match the ^1H-NMR spectrum below to its corresponding compound, and assign all of the signals.



a) cyclopentanone b) 3-pentanone c) butaldehyde

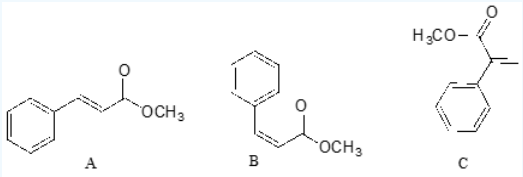
d) 2-pentanone e) 4-heptanone f) 1-butene

Exercise 5.6.6

a. Which of the compounds in the previous exercise is expected to have an ^1H-NMR spectrum consisting of two triplets and a sextet?
b. Which would have a spectrum consisting of two triplets?
c. Which would have a spectrum that includes a signal above 8 ppm?

Exercise 5.6.7

Explain how you could distinguish among the ^1H-NMR spectra of the three isomers below.



Video tutorials: proton NMR spectroscopy

Video of an actual NMR experiment

This page titled 7.2.1: Spin-Spin Coupling is shared under a CC BY-NC-SA 4.0 license and was authored, remixed, and/or curated by Tim Soderberg via source content that was edited to the style and standards of the LibreTexts platform.

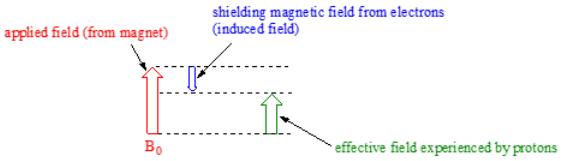
- **5.6: Spin-Spin Coupling** by Tim Soderberg is licensed CC BY-NC-SA 4.0. Original source: https://digitalcommons.morris.umn.edu/chem_facpubs/1/.

7.2.2: The Basis for Differences in Chemical Shift

Diamagnetic shielding and deshielding

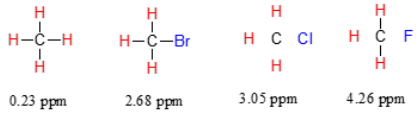
We come now to the question of why nonequivalent protons have different resonance frequencies and thus different chemical shifts. The chemical shift of a given proton is determined primarily by interactions with the nearby electrons. The most important thing to understand is that when electrons are subjected to an external magnetic field, they form their own small induced magnetic fields in opposition to the external field.

Consider the methane molecule (CH_4) in which the four equivalent protons have a chemical shift of 0.23 ppm (this is a value we can look up in any chemistry reference source). The valence electrons around the methyl carbon, when subjected to B0, generate their own very small induced magnetic field that opposes B_0. This induced field, to a small but significant degree, shields the nearby protons from experiencing the full force of B_0, an effect known as local diamagnetic shielding. In other words, the methane protons do not quite experience the full force of B_0 - what they experience is called B_{eff}, or the effective field, which is slightly weaker than B_0 due to the influence of the nearby electrons.



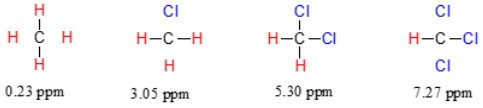
Because B_{eff} is slightly weaker than B0, the resonance frequency (and thus the chemical shift) of the methane proton is slightly lower than what it would be if it did not have electrons nearby and was feeling the full force of B_0. (You should note that the figure above is not to scale: the applied field is generated by a superconducting magnet and is extremely strong, while the opposing induced field from the electrons is comparatively very small.)

Now consider methyl fluoride, CH3F, in which the protons have a chemical shift of 4.26 ppm, significantly higher than that of methane. This is caused by something called the deshielding effect. Recall that fluorine is very electronegative: it pulls electrons towards itself, effectively decreasing the electron density around each of the protons. For the protons, being in a lower electron density environment means less diamagnetic shielding, which in turn means a greater overall exposure to B_0, a stronger B_{eff}, and a higher resonance frequency. Put another way, the fluorine, by pulling electron density away from the protons, is deshielding them, leaving them more exposed to B_0. As the electronegativity of the substituent increases, so does the extent of deshielding, and so does the chemical shift. This is evident when we look at the chemical shifts of methane and three halomethane compounds (remember that electronegativity increases as we move up a column in the periodic table, so flourine is the most electronegative and bromine the least).

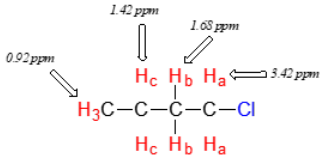


To a large extent, then, we can predict trends in chemical shift by considering how much deshielding is taking place near a proton.

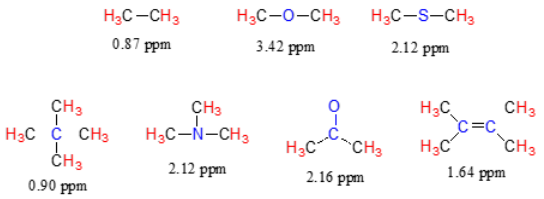
The chemical shift of trichloromethane (common name chloroform) is, as expected, higher than that of dichloromethane, which is in turn higher than that of chloromethane.



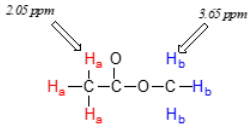
The deshielding effect of an electronegative substituent diminishes sharply with increasing distance:



The presence of an electronegative oxygen, nitrogen, sulfur, or sp^2-hybridized carbon also tends to shift the NMR signals of nearby protons slightly downfield:

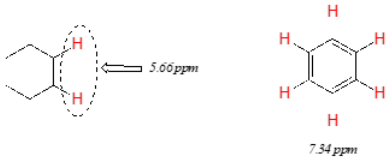


Now we can finally assign the two peaks in the the ^1H-NMR spectrum of methyl acetate. We can predict that the methyl ester protons (H_b), which are deshielded by the adjacent oxygen atom, will have a higher chemical shift than the acetate protons (H_a), which are deshielded to a lesser extent by the carbonyl group. Therefore, the signal at 3.7 must correspond to H_b, and the signal at 2.0 to H_a.



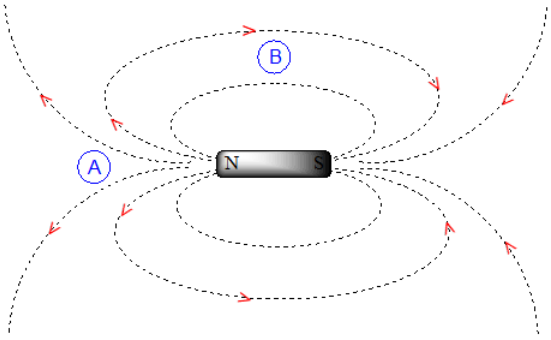
Diamagnetic anisotropy

Vinylic protons (those directly bonded to an alkene carbon) and aromatic protons resonate much further downfield than can be accounted for simply by the deshielding effect of nearby electronegative atoms. Note the chemical shifts of the vinylic and aromatic protons in cyclohexene and benzene:



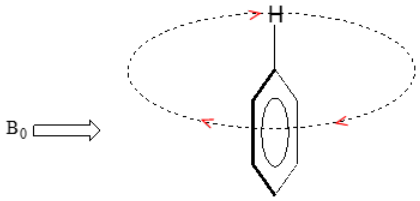
We'll consider the aromatic proton first. Recall that in benzene and many other aromatic structures, a sextet of p electrons is delocalized around the ring. When the molecule is exposed to B_0, these p electrons begin to circulate in a ring current, generating their own induced magnetic field that opposes B_0. In this case, however, the induced field of the p electrons does not shield the aromatic protons from B_0 as you might expect– rather, it causes the protons to experience a stronger magnetic field in the direction of B_0 – in other words, it adds to B_0 rather than subtracting from it.

To understand how this happens, we need to understand the concept of diamagnetic anisotropy (anisotropy means `non-uniformity`). So far, we have been picturing magnetic fields as being oriented in a uniform direction. This is only true over a small area. If we step back and take a wider view, however, we see that the lines of force in a magnetic field are actually anisotropic. They start in the 'north' direction, then loop around like a snake biting its own tail.



If we are at point A in the figure above, we feel a magnetic field pointing in a northerly direction. If we are at point B, however, we feel a field pointing to the south.

In the induced field generated by the aromatic ring current, the aromatic protons are at the equivalent of 'point B' – this means that the induced current in this region of space is oriented in the same direction as B_0, so it adds to B_0 rather than subtracting from it.



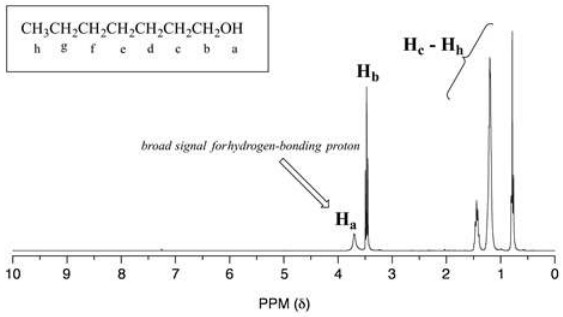
end result is that aromatic protons, due to the anisotropy of the induced field generated by the pi ring current, appear to be highly deshielded. Their chemical shift is far downfield, in the 6.5-8 ppm region.

Diamagnetic anisotropy is also responsible for the downfield chemical shifts of vinylic protons (4.5-6.5 ppm) and aldehyde protons (9-10 ppm). These groups are not aromatic and thus do not generate ring currents does benzene, but the p electrons circulate in such a way as to generate a magnetic field that adds to B_0 in the regions of space occupied by the protons. Carboxylic acid protons are very far downfield (10-12 ppm) due to the combined influence of the electronegative oxygen atom and the nearby pi bond.

Hydrogen bonded protons

Protons that are directly bonded to oxygen or nitrogen have chemical shifts that can vary widely depending on solvent and concentration. These protons can participate to varying degrees in hydrogen bonding interactions, and the degree hydrogen bonding greatly influences the electron density around the proton - and thus the chemical shift. Signals for hydrogen bonding protons also tend to be broader than those of hydrogens bonded to carbon, a phenomenon that is also due to hydrogen bonding.

Alcohol protons, for example, will usually show broad signals anywhere between 1-5 ppm. The signal for H_a in the spectrum of 1-heptanol is a typical example of a broadened NMR signal for an alcohol proton.



The table below provides a summary of approximate chemical shift ranges for protons in different bonding arrangements. A more detailed table can be found in the appendix.

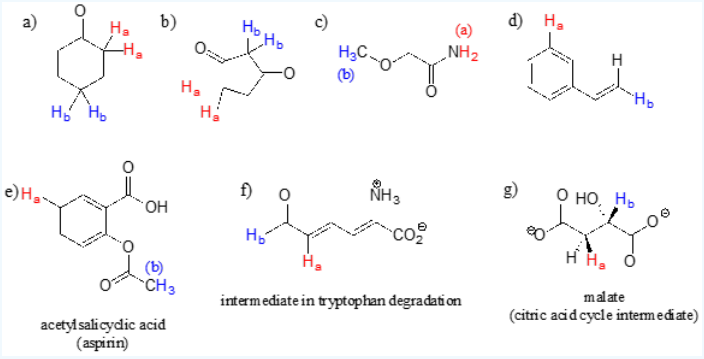
Table 5.5.1 : Typical chemical shift ranges in ^1H-NMR.

Type of proton	Chemical shift range (ppm)
bonded to sp^3 carbon	0.5 - 4
bonded to N (amine)	1 - 3
bonded to O (alcohol)	1 - 5
alkene/ vinylic	3.5 - 6.5
terminal alkyne	2 - 3
bonded to N (amide)	5 - 9

Type of proton	Chemical shift range (ppm)
aromatic	6 - 9
aldehyde	9.5 - 10
carboxylic acid	10 - 13

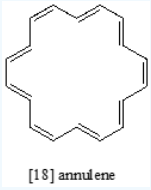
Exercise 5.5.1

For each pair of protons colored red (H_a) and blue (H_b) in the structures below, state which is expected to have the higher chemical shift in ^1H-NMR. For some of these it will be helpful to consult Table 2 at the back of the book.



Exercise 5.5.2

The ^1H-NMR spectrum of the aromatic compound [18] annulene has two peaks, at 8.9 ppm and -1.8 ppm (a negative chemical shift, upfield of TMS!) with an integration ratio of 2:1. Explain the unusual chemical shift of the latter peak.



This page titled 7.2.2: The Basis for Differences in Chemical Shift is shared under a CC BY-NC-SA 4.0 license and was authored, remixed, and/or curated by Tim Soderberg via source content that was edited to the style and standards of the LibreTexts platform.

- **5.5: The Basis for Differences in Chemical Shift** by Tim Soderberg is licensed CC BY-NC-SA 4.0. Original source: https://digitalcommons.morris.umn.edu/chem_facpubs/1/.

7.3: NMR Spectrometers

Earlier in this chapter, we noted that there are two basic experimental designs for recording a NMR spectrum. One is a continuous-wave instrument in which the range of frequencies over which the nucleus of interest absorb is scanned linearly, exciting the different nuclei sequentially. Most instruments, however, use pulses of RF radiation to excite all nuclei at the same time and then use a Fourier transform to recover the signals from the individual nuclei. Our attention in this chapter is limited to instruments for FT-NMR.

Components of Fourier Transform Spectrometers

Figure 7.3.1 includes a photograph of 400 MHz NMR and a cut-away illustration of the instrument; together, these show the key components of a FT-NMR: a magnet that provides the applied magnetic field, B_0, a nucleus-dependent probe that provides the radio-frequency signal that yields the magnetic field, B_1, and a way to insert the sample into the instrument. The NMR in the photograph also is equipped with a sample changer that allows the user to load 30 or more samples that are analyzed sequentially.

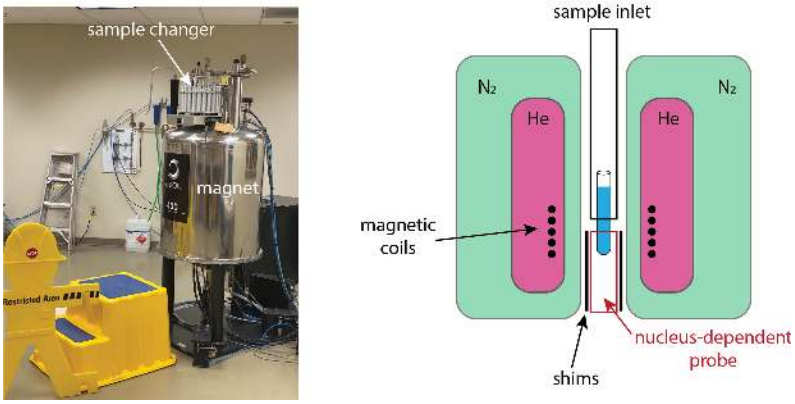


Figure 7.3.1. Photograph of a 400 MHz NMR and an illustration of the magnet's housing and the location of the sample.

Magnets

The NMR in Figure 7.3.1 is described as having a frequency, ν, of 400 MHz. The relationship between frequency and the magnet's field strength, B_0, is given by the equation

$$\nu = \frac{\gamma B_0}{2\pi} \tag{7.3.1}$$

where γ is the magnetogyric ratio for the nucleus. A NMR's frequency is defined in terms of a nucleus of ^{1}H; thus, a 400 MHz NMR has a magnet with a field strength of

$$B_0 = \frac{(2\pi) \times \nu}{\gamma} = \frac{(2\pi) \times (400 \times 10^6 \text{ s}^{-1})}{2.68 \times 10^8 \text{ rad T}^{-1} \text{ s}^{-1}} = 9.4 \text{ T}$$

Early instruments used a permanent magnet and were limited to field strengths of 0.7, 1.4, and 2.1 T, or 30, 60, and 90 MHz. As higher frequencies provide for greater sensitivity and resolution, modern instruments use a tightly wrapped coil of wire—typically a niobium/tin alloy or a niobium/titanium wire—that becomes superconducting when cooled to the temperature of liquid He (4.2 K). The result is a magnetic field strength of as much as 21 T or 900 MHz for ^{1}H NMR. The magnetic coil is held within a reservoir of liquid He, which, itself, is held within a reservoir of liquid N_2.

To be useful, the magnetic field must remain stable—that is, it must not drift—and it must be homogeneous throughout the sample. These are accomplished by using a reference to lock the magnetic field in place and by shimming.

Locking the Magnetic Field

Samples for NMR are prepared using a solvent in which the protons are replaced with deuterium. For example, instead of using chloroform, $CHCl_3$, as a solvent, we use deuterated chloroform, $CDCl_3$, where D is equivalent to ^{2}H. This has the benefit of providing a solvent that will not contribute to the signals in the NMR spectrum. It also has the benefit that ^{2}H has a spin of $I = 1$,

and a corresponding Larmor frequency. By monitoring the frequency at which ^{2}H absorbs, the instrument can use a feed-back loop to maintain its value by adjusting the magnet's field strength.

Shimming

A magnetic field that is not homogeneous is like a table with four legs, one of which is just a bit shorter than the others. To balance the table, we place a small wedge, or shim, under the shorter leg. When a magnetic field is not homogeneous, small, localized adjustments are made to the magnetic field using a set of shimming coils arranged around the sample. Shimming can be accomplished by the operator by monitoring the quality of the signal for a particular nucleus, however, most instruments use an algorithm that allows the instrument to shim itself.

The Sample Inlet and the Sample Probe

The center of the instrument, which runs from the sample input at the top to the sample probe at the bottom, is open to the laboratory environment and is at room temperature. The sample is placed in a cylindrical tube (Figure 7.3.2*a*), that is made from thin-walled borosilicate glass and is 180 mm long and 5 mm in diameter. The tube is then inserted into a teflon sleeve—called a spinner—as shown in Figure 7.3.2*b*, which is designed to both situate the sample at the proper depth within the sample probe, and to spin the sample about its long axis. This spinning is used to ensure that the sample averages out any inhomogeneities in the magnetic field not resovled by shimming.

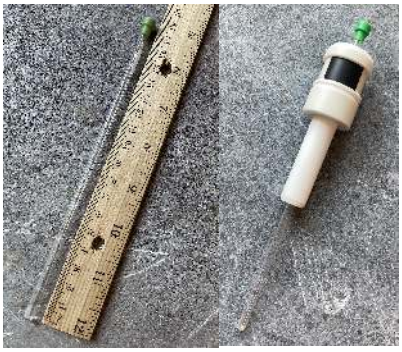


Figure 7.3.2. Photographs showing an NMR sample tube (left) and the spinner assembly (right).

The sample probe contains the coils needed to excite the sample and to detect the NMR signal as the excited states undergo relaxation. Figure 7.3.3 shows two configurations for this; in both configurations, the same coil is used for both excitation and detection. In the design on the left, which uses a permanent magnet, the applied magnetic field, B_0, is oriented horizontally across the sample's diameter and the radio frequency electromagnetic radiation and its field, B_1 is oriented vertically using a spiral coil. In the design on the right, which is used with a superconducting magnet, the applied magnetic field, B_0, is oriented vertically and the pulse of radio frequency electromagnetic radiation and its field, B_1, is oriented horizontally using a saddle coil.

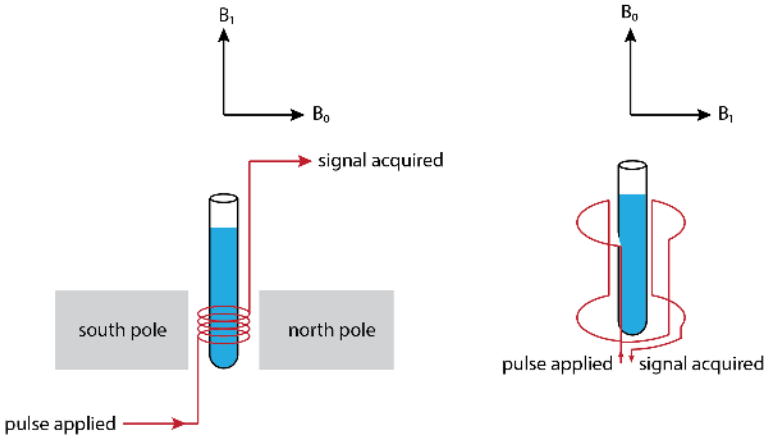


Figure 7.3.3. Two configurations for applying the magnetic fields B_0 and B_1. The configuration on the left is used with a permanent, such as a continuous wave instrument or a benchtop FT-NMR. The configuration on the right is used with a superconducting magnet, such as the instrument in Figure 7.3.1.

Data Processing

In Chapter 19.1 we used the following figure to describe a pulse NMR experiment. Following a pulse that is applied for 1–10 μs, the free-induction decay, FID, is recorded for a period of time that may range from as little as 0.1 seconds to as long as 10 seconds, depending on the nucleus being probed.

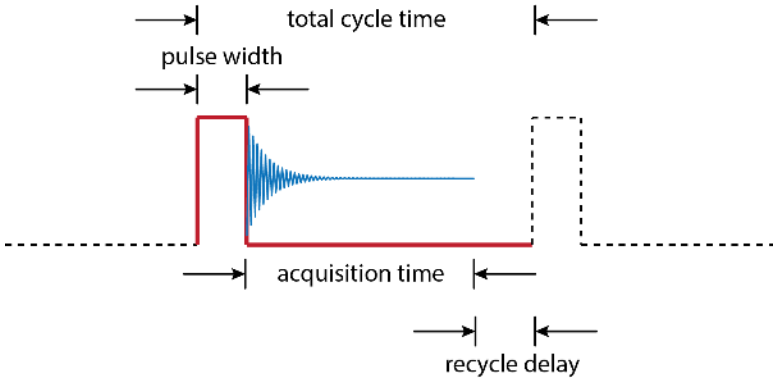


Figure 7.3.4. An example of a pulse sequence for FT-NMR. See the text for a description of the terms shown here.

The FID is an analog signal in the form of a voltage, typically in the μV range. This analog signal must be converted into a digital signal for data processing, which is called an analog-to-digital conversion, ADC. Two important considerations are needed here: how to ensure that the signal—more specifically, the location of the peaks in the NMR spectrum—is not distorted, and how to accomplish the ADC when the frequencies are on the order of hundreds of MHz.

Analog-to-Digital Conversion

An analog-to-digital converter maps the signal onto a limited number of possible values—expressed in binary notation—and are characterized by the number of available bits. A 2-bit ADC convertor, for example, is limited to $2^2 = 4$ possible binary values of 00, 01, 10, and 11 that correspond to the decimal numbers 1, 2, 3, and 4. Having only four possible values, of course, would distort the FID pattern in Figure 7.3.4 from a smoothly varying oscillating signal into a series of steps. Using an ADC convertor with 16 bits allows for 65,536 unique digital values, a significant improvement. Another form of distortion occurs if we do not sample the FID with sufficient frequency. Consider, for example, the simple sine wave in Figure 7.3.5*a* that is shown as a solid line. If we sample this signal only five times over a period of less than four complete cycles, as shown by the five equally-spaced dots in Figure 7.3.5*a*, then the apparent signal is that shown by the dadshed line.

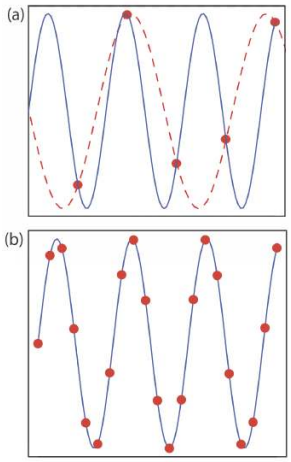


Figure 7.3.5: Effect of sampling frequency when monitoring a periodic signal. Individual samples are shown by the red dots (•). In (a) the sampling frequency is approximately 1.5 samples per period. The dashed red line shows the apparent signal based on five samples and the solid blue line shows the true signal. In (b) a sampling frequency of six samples per period accurately reproduces the true signal.

According to the Nyquist theorem, to determine accurately the frequency of a periodic signal, we must sample the signal at least twice during each cycle or period. Given a sampling rate of Δ, the following equation

$$\Delta = \frac{1}{2\nu_{\max}} \tag{7.3.2}$$

defines the highest frequency, $\nu_{\max}$, that we can monitor accurately. A sampling rate of six samples per period is more than sufficient to reproduce the real signal in Figure 7.3.5.

A peak with a frequency that is greater than $\nu_{\max}$ is not absent from the spectrum; instead, it simply appears at a different location. For example, suppose we can monitor accurately any frequency within the window shown in Figure 7.3.6 and that we only measure frequencies within this window. A peak with a frequency that is greater than what we can measure accurately by $\Delta\nu$ appears at an apparent frequency that is $\Delta\nu$ greater than the frequency window's lower limit. This is called folding.

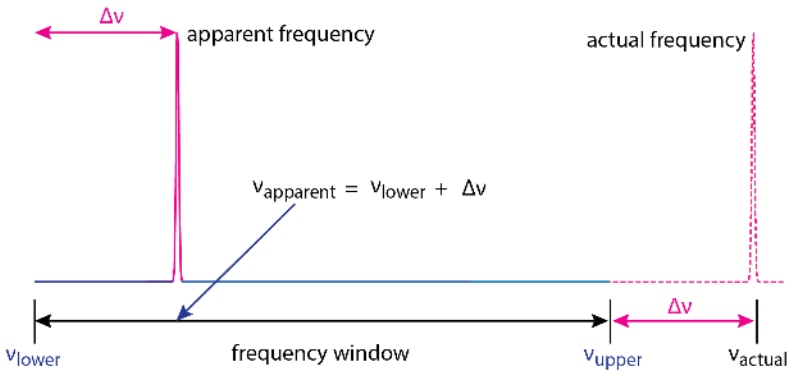


Figure 7.3.6. Illustration showing the origin of folding in which a peak in the NMR spectrum appears at a value of δ that is different from its actual value.

Managing MHz Signals

The instrument in Figure 7.3.1 is a 400 MHz NMR. This is a range of frequencies that is too large for an analog-to-digital convertor to handle with accuracy. The frequency window of interest to us, however, is typically 10 ppm for ^{1}H NMR (see Chapter 19.2 to review the NMR scale). For a 400 MHz NMR this corresponds to just 4000 Hz, with the useful range running from 400.000 MHz to 400.004 MHz. Subtracting the instrument's frequency of 400 MHz from the signal's frequency limits the latter to the range of 0–4000 Hz, a range that is easy for an ADC to handle.

Signal Integrators

Integrating to determine the area under the peaks provides a way to gain some quantitative information about the sample. Figure 7.3.7 shows the integration of the NMR of propane first seen in Chapter 19.2. Integration of the peak for the two methyl groups gives a result of 1766 and integration of the peak for the methylene group gives a result of 710. The ratio of the two is

$$\frac{1766}{710} = 2.5$$

which is somewhat smaller than the expected 3:1 ratio.

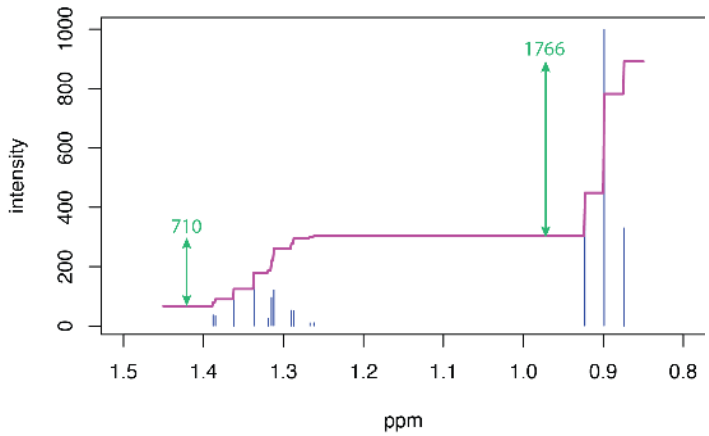


Figure 7.3.1. Illustration of integration. The original data used to construct this spectrum is here and was obtained on a 300 MHz instrument.

https://chem.libretexts.org/@go/page/526811

This page titled 7.3: NMR Spectrometers is shared under a CC BY-NC-SA 4.0 license and was authored, remixed, and/or curated by David Harvey.

- **19.3: NMR Spectrometers** by David Harvey is licensed CC BY-NC-SA 4.0.

7.4: Applications of Proton NMR

Proton (^{1}H) NMR finds use for both qualitative analyses and quantitative analyses; in this section we briefly consider each of these areas.

Identification of Compounds

Proton NMR is an essential tool for the qualitative analysis of organic, inorganic, and biochemical compounds. Figure 7.4.1 provides a simple example that shows the relationship between structure and a ^{1}H NMR's peaks. The spectra in this figure are for a set of four simple organic molecules, each of which has a chain of three carbons and an oxygen: 1-propanol, $CH_3CH_2CH_2OH$, 2-propanol, $CH_3CH(OH)CH_3$, propanal, CH_3CH_2CHO, and propanoic acid, CH_3CH_2COOH. The first two of these molecules are alcohols, the third is an aldehyde, and the last is an acid. The main spectrum runs from 0–14 ppm, with insets showing the spectra over a narrower range of 0–5 ppm.

Each of these molecules has a terminal $–CH_3$ group that is the most upfield peak in its spectrum, appearing between 0.94 – 1.20 ppm. Each of these molecules has a hydrogen that either is bonded to an oxygen or a hydrogen bonded to the same carbon as the oxygen. The hydrogens in the –OH groups of the two alcohols have similar shifts of 2.16 ppm and 2.26 ppm, but the aldehyde hydrogen in the –CHO group and the acid hydrogen in –COOH are shifted further downfield appearing at 9.793 ppm and 11.73 ppm, respectively. The hydrogens in the two $–CH_2–$ groups of 1-propanol have very different shifts, with the one adjacent to the –OH group appearing more downfield at 3.582 ppm than the one next to the $–CH_3$ group at 1.57 ppm. Not surprisingly, the –CH– hydrogen in 2-proponal, which is adjacent to the –OH group appears at 4.008 ppm.

Comparisons such of this make it possible to build tables of chemical shifts—see Table 19.2.1 in Chapter 19.2 for an example—that can help in determining the identify of the molecule giving rise to a particular NMR spectrum. As this receives extensive coverage in other courses, particularly courses in organic chemistry, we will not provide a more extensive coverage here.

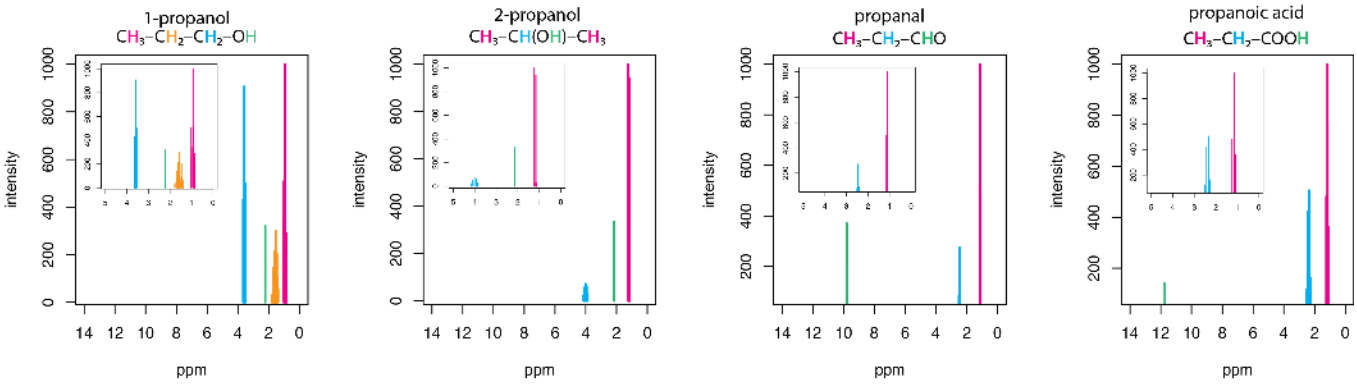


Figure 7.4.1. ^{1}H NMR spectra for 1-propanol, 2-propanol, propanal, and propanoic acid. The full spectrum are shown using the scale at the bottom of each figure. The insets show close-ups of the NMR spectra from 0 – 5 ppm. The original data used to construct these spectra are found here. The spectrum for propanal was recorded on a 300 MHz instrument; the other three spectra were recorded on a 90 MHz instrument.

Quantitative Analysis

A quantitative analysis requires a method of standardization, which for NMR usually makes use of an internal standard. A good internal standard should have high purity and should have a relatively simple NMR spectrum with peaks that do not overlap with the analyte or other species present in the sample. If we are interested in only the relative concentrations of the analyte and the internal standard, then we can use the following formula

$$\frac{M_a}{M_{is}} = \frac{I_a}{I_{is}} \times \frac{N_{is}}{N_a} \tag{7.4.1}$$

where M is the molar concentration of the analyte or internal standard, I is the intensity of the NMR peak for the analyte or internal standard, and N is the number of nuclei giving rise to the NMR peak for the analyte and the internal standard. Even if we don't know the exact concentration of the internal standard, if we know that its concentration is the same in all samples, then we can determine the relative concentration of analyte in a collection of samples.

If we are interested in determining the absolute concentration of analyte in a sample, then we must know the absolute concentration of the internal standared; when true, then Equation 7.4.1 becomes

$$M_a = \frac{I_a}{I_{is}} \times \frac{N_{is}}{N_a} \times M_{is} \tag{7.4.2}$$

Determining the purity of an analyte, P_a, in a sample, we can use the equation

$$P_a = \frac{I_a}{I_{is}} \times \frac{N_{is}}{N_a} \times \frac{M_a}{M_{is}} \times \frac{W_{is}}{W_a} \times P_{is} \tag{7.4.3}$$

where W is the weight of the internal standard or the sample that contains our analyte.

This page titled 7.4: Applications of Proton NMR is shared under a CC BY-NC-SA 4.0 license and was authored, remixed, and/or curated by David Harvey.

- **19.4: Applications of Proton NMR** by David Harvey is licensed CC BY-NC-SA 4.0.

7.5: Carbon-13 NMR

The relatively slow development of instrumentation for ^{13}C NMR spectra is the result of its limited sensitivity compared to ^{1}H NMR. This difference in sensitivity is due to two key differences between the nuclei ^{1}H and ^{13}C: their relative abundances and their relative magnetogyric ratios. While ^{1}H comprises 99% of all hydrogen, ^{13}C accounts for just 1% of all carbon. The strength of an NMR signal also depends on the difference in energy, ΔE, between the ground state and the excited state, which is a function of the magnetogyric ratio, γ

$$\Delta E = h\nu = \frac{\gamma B_0}{2\pi} \tag{7.5.1}$$

The greater the difference in energy, the greater the difference in the population between the ground and the excited states, and the greater the signal. The magnetogyric ratio, γ, for ^{1}H is $4\times$ greater than that for ^{13}C. As a result of these two factors, ^{1}H NMR is approximately $6400\times$ more senstitive than ^{13}C. The development of magnets with higher field strengths and the capabilities of signal averaging (see Chapter 5 on signals and noise) when using Fourier transforms to gather and analyze data, make ^{13}C feasible.

Figure 7.5.1 shows ^{13}C NMR spectrum for three related molecules: *p*-nitrophenol, *o*-nitrophenol, and *m*-nitrophenol. There are three things to make note of from this figure. First, each spectrum consists of a set of peaks, each of which is a singlet, suggesting that no spin-spin coupling is taking place. Second, the number of peaks in each spectrum is the same as the number of unique types of carbon—four unique carbons for *p*-nitrophenol and six each for *m*-nitrophenol and *o*-nitrophenol—which suggests that chemical shifts in ^{13}C provide useful information about the environment of the carbon atoms and, therefore, the molecule's structure. And, third, unlike ^{1}H, there is no relationship between the intensity of a ^{13}C peak and the number of carbon atoms. This is particularly evident when comparing the intensity of the peaks for the carbon bonded to the $–NO_2$ group and the carbon bonded to the –OH group, which are significantly less intense than the peaks for other carbons. We will consider each of these observations in the remainder of this section.

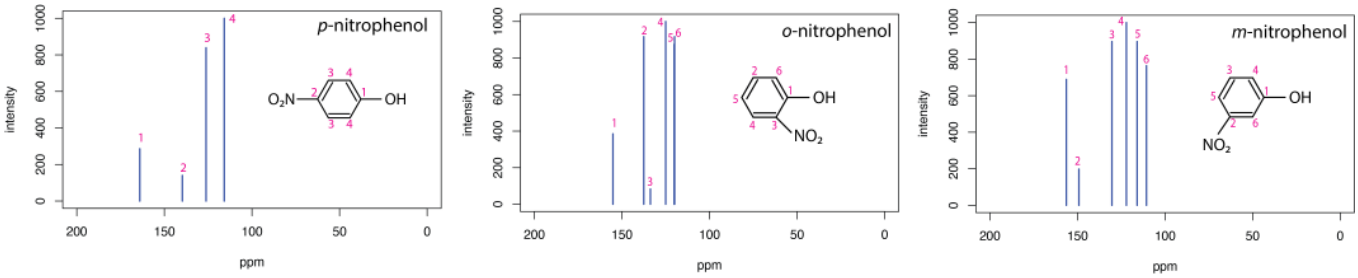


Figure 7.5.1. ^{13}C NMR spectra for three nitrophenols. The original data used to construct these spectra are found here. The spectra were recorded on a 15 MHz instrument (with respect to ^{13}C, or 60 MHz with respect to ^{1}H).

Proton Decoupling

In ^{13}C NMR there is no coupling between adjacent carbon atoms because it is unlikely that both are ^{13}C, the only isotope of carbon that is NMR active (the odds that two adjacent carbons are both ^{13}C is 0.01×0.01, or 0.0001 or 0.010%). Coupling does take place between ^{13}C and ^{1}H when the hydrogen atoms are attached to the carbon atom. Such coupling follows the same N+1 rule as in ^{1}H NMR; thus, a quartenary carbon (R_4C) appears as a singlet, a methine carbon (R_3CH) appears as a doublet, a methylene carbon (R_2CH_2) appears as a triplet, and a methyl carbon (RCH_3) appears as a quartet. Even with the extensive range of ppm values over which ^{13}C peaks appear—chemical shifts for ^{13}C spectra run from 250 – 0 ppm instead of 14 – 0 ppm for ^{1}H spectra—a compound with many different types of carbon atoms, each with 1 – 3 hydrogen atoms results in a complex spectrum. For this reason, ^{13}C NMR spectra are acquired in a way that prevents coupling between ^{13}C and ^{1}H. This is called proton decoupling.

The most common method of proton decoupling is to use a second RF generator to irradiate the sample with a broad-band of RF signals that spans the range of frequencies for the protons. As described earlier in Section 19.3, the effect is to saturate the proton's ground and excited states, which prevents the protons from absorbing energy and from coupling with each other and with the carbons atoms. The ^{13}C spectra in Figure 7.5.1 are examples of decoupled spectra.

Qualitative Applications of ^{13}C NMR

Just as with ^{1}H NMR spectra, tables of chemical shifts for ^{13}C peaks aids in determining a molecules structure. Table 7.5.1 provides ranges of chemical shifts for different types of carbon atom. A set of tables is available here.

Table 7.5.1. ^{13}C Shifts in ppm

type of carbon atom	example	range of chemical shifts (ppm)
primary alkyl	$R-CH_3$	10 – 30
secondary alkyl	$R-CH_2-R$	15 – 55
tertiary alkyl	R_3CH	20 – 60
quaternary alkyl	R_4C	30 – 40
alkynl	$R-C\equiv C-H$	65 – 90
alkenyl	$R-C=C-H$	100 – 150
aromatic	C_6H_6	110 – 170
ester	$R-C(=O)-O-R$	165 – 175
amide	$R-C(=O)-N-R_2$	165 – 175
carboxylic acid	$R-C(=O)-OH$	175 – 185
aldehyde	$R-C(=O)-H$	190 – 220
ketone	$R-C(=O)-R$	205 – 220
attached to iodine	$C-I$	0 – 40
attached to bromine	$C-Br$	25 – 65
attached to chlorine	$C-Cl$	35 – 80
attached to oxygen	$C-O$	40 – 80
attached to nitrogen	$C-N$	40 – 60

Nuclear Overhauser Enhancement

The most intense peak in the ^{13}C NMR spectrum for *m*-nitrophenol (see Figure 7.5.1 above) is the carbon in the benzene ring labeled as position 4, with an intensity of 1000 (the intensity scale is normalized here to a maximum value of 1000, but for this section, let's take it as an absolute value). Because the spectrum was acquired with proton decoupling turned on, the peak for this carbon appears as a singlet. If we turn proton decoupling off, then we expect the peak to appear as a doublet as this carbon has one hydrogen attached to it. We might reasonably expect to find that each peak has an intensity of 500, giving a total intensity of 1000. The actual intensities of the peaks for this carbon, however, are smaller than expected. Put another way, when we turn proton decoupling on, the intensity of a ^{13}C line increases more than expected and the more hydrogens, the greater the effect. This is called nuclear overhauser enhancement (NOE).

NOE is the result of the relative populations of the ground and excited states. The technical details are more than we will consider here, but the extent of the total enhancement of the peak intensities is proportional to the ratio of the magnetogyric ratios of the irradiated nucleus (^1H) and the observed nucleus (^{13}C), which for a ^1H decoupled ^{13}C NMR results in a total enhancement of the intensity of approximately 200%. As magnetogyric ratios can be negative, as is the case for ^{15}N, a decoupled spectrum can result in less intense peaks. One important consequence of NOE, is that integrated peak areas are not proportional to the number of identical carbon atoms, which is a loss of information.

Note

Although our focus in this chapter is on ^1H and ^{13}C NMR, other nuclei, such as ^{31}P, ^{19}F, and ^{15}N are useful for the study of chemically and biochemically important molecules.

This page titled 7.5: Carbon-13 NMR is shared under a CC BY-NC-SA 4.0 license and was authored, remixed, and/or curated by David Harvey.

- **19.5: Carbon-13 NMR** by David Harvey is licensed CC BY-NC-SA 4.0.

7.6: Two-Dimensional Fourier Transform NMR

The ^{1}H and ^{13}C spectra up to this point are shown in one dimension (1D), which is the frequency absorbed by the analyte's nuclei expressed in ppm. These spectra were acquired by applying a brief RF pulse to the sample, recording the resulting FID, and then using a Fourier transform to obtain the NMR spectrum. In addition to 1D experiments, there are a host of 2D experiments in which we apply a sequence of two or more pulses, recording the resulting FID after applying the last pulse. In this section we will consider one example of a 2D NMR experiment in some detail: ^{1}H – ^{1}H correlation spectroscopy, or ^{1}H – ^{1}H COSY.

Figure 7.6.1 shows the basic experimental details for the COSY experiment. The pulse train is shown in (a) and consists of a first pulse that is followed by a delay time, t_1, in which the nuclear spins are allowed to precess and relax. This is followed by the application of a second pulse and the measurement of the resulting FID during the acquisition period, t_2, that consists of n_{t_2} individual data points. The COSY experiment consists of a sequence of n_{t_1} individual pulse trains, each with a different t_1. The result (b) is a matrix with n_{t_1} rows and n_{t_2} columns. To process the data, each row in this matrix is Fourier transformed, the resulting $n_{t_1} \times n_{t_2}$ matrix is transposed to a $n_{t_2} \times n_{t_1}$ matrix and then Fourier transformed again to give (c) a $n_{t_2} \times n_{t_2}$ matrix that shows the intensity of the signal for all possible combinations of applied frequencies.

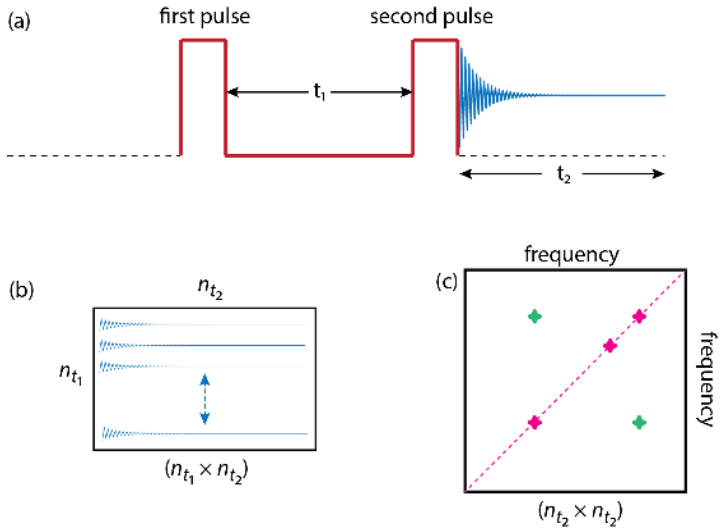


Figure 7.6.1. Details of a COSY experiment: (a) the pulse sequence; (b) the data matrix; and (c) the COSY spectrum. See the text for additional details.

Figure 7.6.2 shows the ^{1}H – ^{1}H COSY spectrum for ethyl acetate. Instead of just annotating the two axes with numerical values of the frequencies, they are displayed by superimposing the 1D ^{1}H NMR spectrum for ethyl acetate in ppm. The points that fall on the diagonal line are just the three frequencies where ethyl acetate has ^{1}H peaks. Of more interest are the points that fall on either side of the diagonal line—these are called cross peaks—as these show pairs of hydrogens that are coupled (or correlated) to each other. The cross peaks in the COSY spectrum are symmetrical about the diagonal line and show the correlation between the hydrogens on the methyl carbon and and the methylene carbon that are adjacent to each other (the ethyl part of ethyl acetate). The remaining methyl group is not coupled to the other hydrogen's in the ethyl acetate, so there is no cross peak at the intersection of $\delta = 2.038$ ppm and $\delta = 1.260$ ppm. The information about coupling from cross peaks assists in interpreting complex ^{1}H NMR spectra.

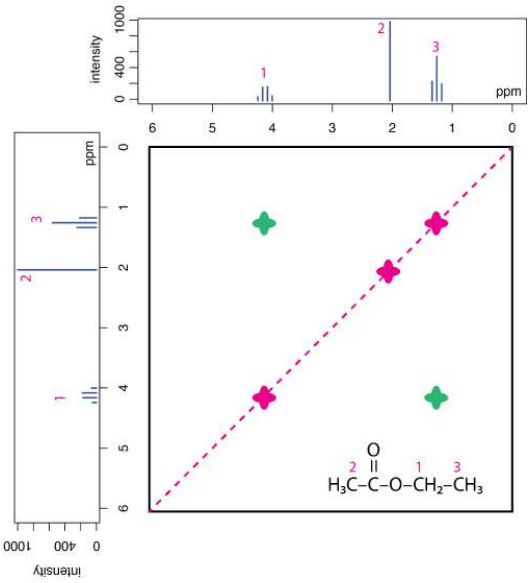


Figure 7.6.2. The COSY spectrum for ethyl acetate. The original data used to create the two ^{1}H NMR spectra is available here and was obtained using a 300 MHz NMR. The COSY spectrum is simulated.

COSY is one example of a homonuclear 2D NMR experiment because it examines coupling between identical nuclei, such as ^{1}H in Figure 7.6.2. There are many other 2D NMR experiments, each of which uses a sequence of pulses—some that use two pulses, as in COSY, and others that use three or more pulses—and a data analysis algorithm. Table 7.6.1 provides details on some of these methods.

Table 7.6.1. Selected examples of 2D NMR experiments.

method	information obtained from cross peaks
correlation spectroscopy (COSY)	coupling between two protons (^{1}H – ^{1}H) that are within three chemical bonds of each other
total correlation spectroscopy (TOCSY)	coupling between all protons (^{1}H) in the molecule
heteronuclear correlation spectroscopy (HETCOR)	coupling between a proton (^{1}H) and another nucleus, such as carbon (^{1}H – ^{13}C) or nitrogen (^{1}H – ^{15}N)
nuclear overhauser and exchange spectroscopy (NOESY)	coupling between two protons (^{1}H – ^{1}H) that are within approximately 5 Å of each other
heteronuclear single quantum correlation (HSQC)	coupling between a proton (^{1}H) and another nucleus, such as carbon (^{1}H – ^{13}C) or nitrogen (^{1}H – ^{15}N)
heteronuclear multiple bond coherence spectroscopy (HMBC)	coupling between a proton and a carbon (^{1}H – ^{13}C) that are two or three bonds apart
incredible natural abundance double-quantum transfer (INADEQUATE)	coupling between adjacent carbon atoms (^{13}C – ^{13}C)
double quantum filtered correlation spectroscopy (DQF–COSY)	suppresses signals from water

This page titled 7.6: Two-Dimensional Fourier Transform NMR is shared under a CC BY-NC-SA 4.0 license and was authored, remixed, and/or curated by David Harvey.

- **19.6: Two-Dimensional Fourier Transform NMR** by David Harvey is licensed CC BY-NC-SA 4.0.

SECTION OVERVIEW

7.7: STRUCTURE DETERMINATION - NUCLEAR MAGNETIC RESONANCE SPECTROSCOPY

LEARNING OBJECTIVES

- fulfillall of the detailed objectives listed under each individual section.
- solve road-map problems which may require the interpretation of ^{1}H NMR spectra in addition to other spectral data.
- define, and use in context, the key terms introduced.

In Chapter 12, you learned how an organic chemist could use two spectroscopic techniques, mass spectroscopy and infrared spectroscopy, to assist in determining the structure of an unknown compound. This chapter introduces a third technique, nuclear magnetic resonance (NMR). The two most common forms of NMR spectroscopy, ^{1}H NMR and ^{13}C NMR, will be discussed, the former in much more detail than the latter. Nuclear magnetic resonance spectroscopy is a very powerful tool, particularly when used in combination with other spectroscopic techniques.

7.7.1: NUCLEAR MAGNETIC RESONANCE SPECTROSCOPY

7.7.2: THE NATURE OF NMR ABSORPTIONS

7.7.3: THE CHEMICAL SHIFT

7.7.4: CHEMICAL SHIFTS IN ^{1}H NMR SPECTROSCOPY

7.7.5: INTEGRATION OF ^{1}H NMR ABSORPTIONS - PROTON COUNTING

7.7.6: SPIN-SPIN SPLITTING IN ^{1}H NMR SPECTRA

7.7.7: ^{1}H NMR SPECTROSCOPY AND PROTON EQUIVALENCE

7.7.8: MORE COMPLEX SPIN-SPIN SPLITTING PATTERNS

7.7.9: USES OF ^{1}H NMR SPECTROSCOPY

7.7.10: ^{13}C NMR SPECTROSCOPY - SIGNAL AVERAGING AND FT-NMR

7.7.11: CHARACTERISTICS OF ^{13}C NMR SPECTROSCOPY

7.7.12: DEPT ^{13}C NMR SPECTROSCOPY

7.7.13: USES OF ^{13}C NMR SPECTROSCOPY

7.7.S: STRUCTURE DETERMINATION - NUCLEAR MAGNETIC RESONANCE SPECTROSCOPY (SUMMARY)

This page titled 7.7: Structure Determination - Nuclear Magnetic Resonance Spectroscopy is shared under a CC BY-SA 4.0 license and was authored, remixed, and/or curated by Steven Farmer & Dietmar Kennepohl.

7.7.1: NUCLEAR MAGNETIC RESONANCE SPECTROSCOPY

OBJECTIVES

After completing this section, you should be able to

1. discuss the principles of NMR spectroscopy.
2. identify the two magnetic nuclei that are most important to an organic chemist.

KEY TERMS

Make certain that you can define, and use in context, the key term below.

- resonance

STUDY NOTES

Notice that the word “resonance” has a different meaning when we are discussing nuclear magnetic resonance spectroscopy than it does when discussing molecular structures.

INTRODUCTION

Some types of atomic nuclei act as though they spin on their axis similar to the Earth. Since they are positively charged they generate an electromagnetic field just as the Earth does. So, in effect, they will act as tiny bar magnetics. Not all nuclei act this way, but fortunately both ^{1}H and ^{13}C do have nuclear spins and will respond to this technique.



NMR Spectrometer

In the absence of an external magnetic field the direction of the spin of the nuclei will be randomly oriented (see figure below left). However, when a sample of these nuclei is place in an external magnetic field, the nuclear spins will adopt specific orientations much as a compass needle responses to the Earth’s magnetic field and aligns with it. Two possible orientations are possible, with the external field (*i.e.* parallel to and in the same direction as the external field) or against the field (*i.e.* antiparallel to the external field) - see Figure 7.7.1.1 .

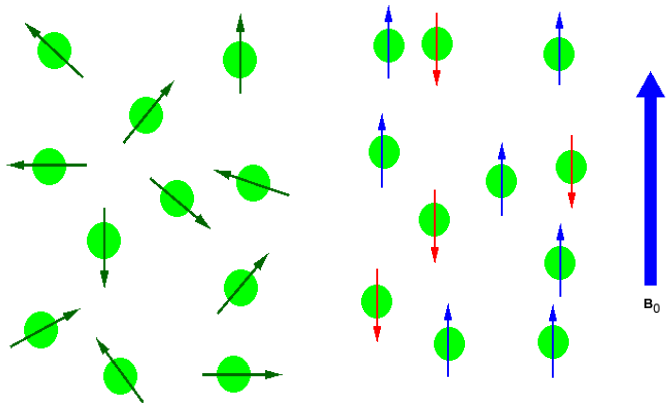
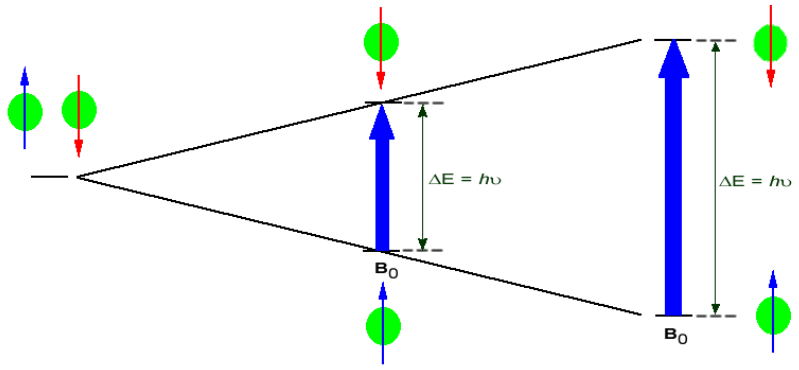


Figure 7.7.1.1: (Left) Random nuclear spin without an external magnetic field. (Right) Ordered nuclear spin in an external magnetic field

If the ordered nuclei are now subjected to EM radiation of the proper frequency the nuclei aligned with the field will absorb energy and "spin-flip" to align themselves against the field, a higher energy state. When this spin-flip occurs the nuclei are said to be in "resonance" with the field, hence the name for the technique, **N**uclear **M**agentic **R**esonance or NMR.

The amount of energy, and hence the exact frequency of EM radiation required for resonance to occur is dependent on both the strength of the magnetic field applied and the type of the nuclei being studied. As the strength of the magnetic field increases the energy difference between the two spin states increases and a higher frequency (more energy) EM radiation needs to be applied to achieve a spin-flip (see image below).



Superconducting magnets can be used to produce very strong magnetic field, on the order of 21 tesla (T). Lower field strengths can also be used, in the range of 4 - 7 T. At these levels the energy required to bring the nuclei into resonance is in the MHz range and corresponds to radio wavelength energies, *i.e.* at a field strength of 4.7 T 200 MHz bring ^{1}H nuclei into resonance and 50 MHz bring ^{13}C into resonance. This is considerably less energy then is required for IR spectroscopy, ~10^{-4} kJ/mol versus ~5 - ~50 kJ/mol.

^{1}H and ^{13}C are not unique in their ability to undergo NMR. All nuclei with an odd number of protons (^{1}H, ^{2}H, ^{14}N, ^{19}F, ^{31}P ...) or nuclei with an odd number of neutrons (*i.e.* ^{13}C) show the magnetic properties required for NMR. Only nuclei with even number of both protons and neutrons (^{12}C and ^{16}O) do not have the required magnetic properties.

? EXERCISE 7.7.1.1

If in a field strength of 4.7 T, H^1 requires 200 MHz of energy to maintain resonance. If atom X requires 150 MHz, calculate the amount of energy required to spin flip atom X's nucleus. Is this amount greater than the energy required for hydrogen?

Answer

$E = h\upsilon$

$E = (6.62 \times 10^{-34})(150\ \text{MHz})$

$E = 9.93 \times 10^{-26}$ J

The energy is equal to 9.93x10^{-26} J. This value is smaller than the energy required for hydrogen (1.324×10^{-25} J).

EXERCISE 7.7.1.1

Calculate the energy required to spin flip at 400 MHz. Does changing the frequency to 500 MHz decrease or increase the energy required? What about 300 MHz.

Answer

$E = h\upsilon$

$E = (6.62 \times 10^{-34})(400\ \text{MHz})$

$E = 2.648 \times 10^{-25}\ \text{J}$

The energy would increase if the frequency would increase to 500 MHz, and decrease if the frequency would decrease to 300 MHz.

This page titled 7.7.1: Nuclear Magnetic Resonance Spectroscopy is shared under a CC BY-SA 4.0 license and was authored, remixed, and/or curated by Steven Farmer, Richard Spinney, Dietmar Kennepohl, & Dietmar Kennepohl.

- **13.0: Nuclear Magnetic Resonance Spectroscopy** by Dietmar Kennepohl, Richard Spinney, Steven Farmer is licensed CC BY-SA 4.0.

7.7.2: THE NATURE OF NMR ABSORPTIONS

OBJECTIVES

After completing this section, you should be able to

1. explain, in general terms, the origin of shielding effects in NMR spectroscopy.
2. explain the number of peaks occurring in the ^{1}H or ^{13}C NMR spectrum of a simple compound, such as methyl acetate.
3. describe, and sketch a diagram of, a simple NMR spectrometer.
4. explain the difference in time scales of NMR and infrared spectroscopy.
5. predict the number of peaks expected in the ^{1}H or ^{13}C NMR spectrum of a given compound.

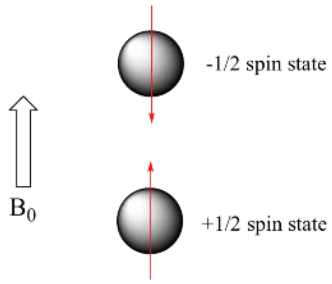
STUDY NOTES

Before you go on, make sure that you understand that each signal in the ^{1}H NMR spectrum shown for methyl acetate is due to a different proton environment. The three protons on the same methyl group are equivalent and appear in the spectrum as one signal. However, the two methyl groups are in two different environments (one is more deshielded) and so we see two signals in the whole spectrum (aside from the TMS reference peak).

Methyl acetate has a very simple ^{1}H NMR spectrum, because there is no proton-proton coupling, and therefore no splitting of the signals. In later sections, we discuss splitting patterns in ^{1}H NMR spectra and how they help a chemist determine the structure of organic compounds.

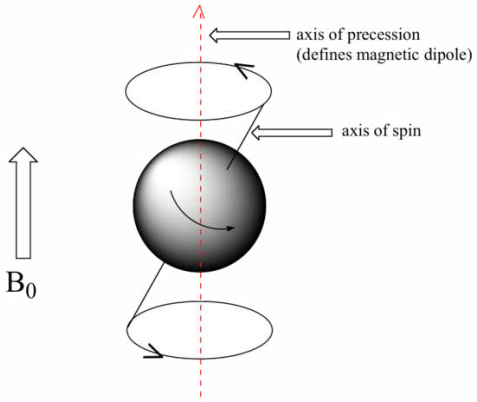
NUCLEAR PRECESSION, SPIN STATES, AND THE RESONANCE CONDITION

When a sample of an organic compound is sitting in a flask on a laboratory benchtop, the magnetic moments of its hydrogen atoms are randomly oriented. When the same sample is placed within the field of a very strong magnet in an NMR instrument (this field is referred to by NMR spectroscopists as the **applied field**, abbreviated $\mathbf{B_0}$) each hydrogen will assume one of two possible **spin states**. In what is referred to as the +½ spin state, the hydrogen's magnetic moment is aligned *with* the direction of B_0, while in the -½ spin state it is aligned *opposed to* the direction of B_0.



Because the +½ spin state is slightly lower in energy, in a large population of organic molecules slightly more than half of the hydrogen atoms will occupy this state, while slightly less than half will occupy the –½ state. *The difference in energy between the two spin states increases with increasing strength of B_0.*This last statement is in italics because it is one of the key ideas in NMR spectroscopy, as we shall soon see.

At this point, we need to look a little more closely at how a proton spins in an applied magnetic field. You may recall playing with spinning tops as a child. When a top slows down a little and the spin axis is no longer completely vertical, it begins to exhibit **precessional motion**, as the spin axis rotates slowly around the vertical. In the same way, hydrogen atoms spinning in an applied magnetic field also exhibit precessional motion about a vertical axis. It is this axis (which is either parallel or antiparallel to B_0) that defines the proton's magnetic moment. In the figure below, the proton is in the +1/2 spin state.

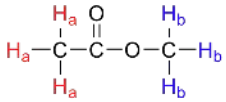


The **frequency of precession** (also called the **Larmour frequency,** abbreviated ω_L) is simply the number of times per second that the proton precesses in a complete circle. A proton`s precessional frequency increases with the strength of B_0.

If a proton that is precessing in an applied magnetic field is exposed to electromagnetic radiation of a frequency ν that matches its precessional frequency ω_L, we have a condition called **resonance**. *In the resonance condition, a proton in the lower-energy +½ spin state (aligned with B_0) will transition (flip) to the higher energy –½ spin state (opposed to B_0). In doing so, it will absorb radiation at this resonance frequency* $\nu = \omega_L$. This frequency, as you might have already guessed, corresponds to the energy difference between the proton's two spin states. With the strong magnetic fields generated by the superconducting magnets used in modern NMR instruments, the resonance frequency for protons falls within the radio-wave range, anywhere from 100 MHz to 800 MHz depending on the strength of the magnet.

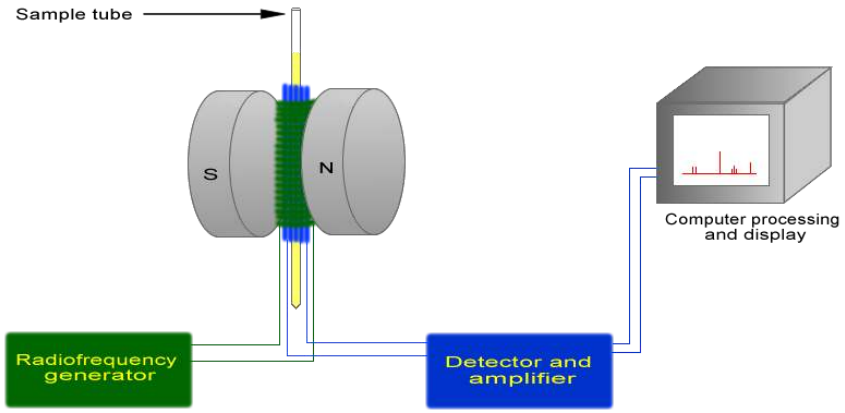
THE BASICS OF AN NMR EXPERIMENT

So far, you may have the impression that all ^1H nuclei in a molecule would absorb the same frequency. However, this would be of little use to organic chemists if that were the case. It turns out that not all ^1H nuclei absorb the same frequency and this is the same for all other NMR active nuclei. It turns out that chemically nonequivalent protons (or other nuclei) have different resonance frequencies in the same applied magnetic field. Nonequivalent protons are in different chemical environments. This allows NMR spectroscopy to provide us with useful information about the structure of an organic molecule. A full explanation of how a modern NMR instrument functions is beyond the scope of this text, but here is what happens. First, a sample compound (we'll use methyl acetate) is placed inside a very strong applied magnetic field (B_0). There are two types of protons in methyl acetate. H_a are bonded to a C that is then bonded to a carbonyl, whereas H_b are bonded to a carbon that is then bonded to an oxygen atom. This difference in bonding leads to different types of environments for H_a and H_b. All the H_a protons are the same since they all have the same type of bonding and will be in the same chemical environment and the same is true for H_b.



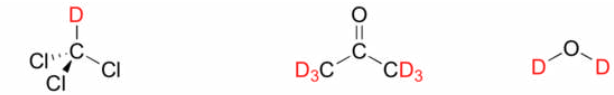
methyl acetate

The basic arrangement of an NMR spectrometer is displayed below. A sample (in a small glass tube, where the methyl acetate is in solution) is placed between the poles of a strong magnet. A radio frequency generator pulses the sample and excites the nuclei causing a spin-flip. The spin flip is detected by the detector and the signal sent to a computer where it is processed.



In the magnet, all of the protons begin to precess: the H_a protons at precessional frequency ω_a, the H_b protons at ω_b. At first, the magnetic moments of (slightly more than) half of the protons are aligned with B_0, and half (slightly less than half) are aligned against B_0. Then, the sample is hit with electromagnetic radiation in the radio frequency range. The two specific frequencies which match ω_a and ω_b (i.e. the resonance frequencies) cause those H_a and H_b protons which are aligned *with* B_0 to 'flip' so that they are now aligned *against* B_0. In doing so, the protons absorb radiation at the two resonance frequencies. The NMR instrument records which frequencies were absorbed, as well as the intensity of each absorbance.

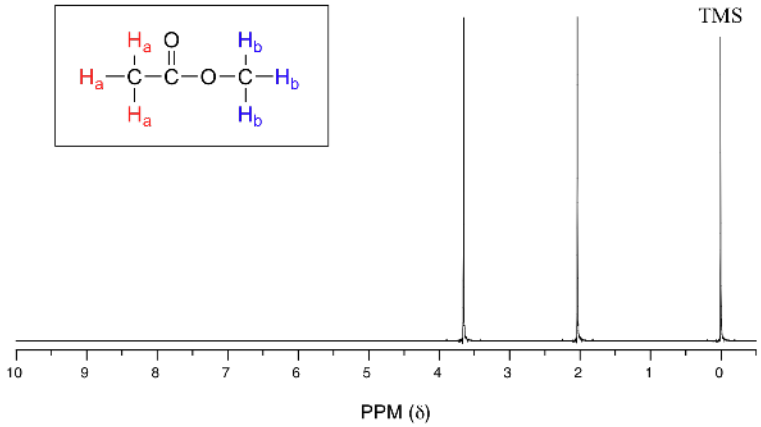
In most cases, a sample being analyzed by NMR is in solution. If we used a common laboratory solvent (diethyl ether, acetone, dichloromethane, ethanol, water, etc.) to dissolve our NMR sample, however, we run into a problem – there many more solvent protons in solution than there are sample protons, therefore the signals from the sample protons will be overwhelmed. To get around this problem, we use special NMR solvents in which all protons have been replaced by deuterium. Recall that deuterium is NMR-active, but its resonance frequency is very different from that of protons, and thus it is `invisible` in ^{1}H-NMR. Some common NMR solvents are shown below. There are multiple deuterated solvents since molecules have different solubilities, so one molecule may dissolve in deuterated chloroform while others may not.



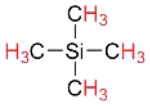
deuterated chloroform ($CDCl_3$) | d_6-acetone | D_2O

THE CHEMICAL SHIFT

Let's look at an actual ^{1}H-NMR plot for methyl acetate. Just as in IR and UV-vis spectroscopy, the vertical axis corresponds to intensity of absorbance, the horizontal axis to frequency (typically the vertical axis is not shown in an NMR spectrum).



We see three absorbance signals: two of these correspond to H_a and H_b, while the peak at the far right of the spectrum corresponds to the 12 chemically equivalent protons in tetramethylsilane (TMS), a standard reference compound that was added to our sample.



tetramethylsilane (TMS)

You may be wondering about a few things at this point - why is TMS necessary, and what is the meaning of the `ppm (δ)` label on the horizontal axis? Shouldn't the frequency units be in Hz? Keep in mind that NMR instruments of many different applied field strengths are used in organic chemistry laboratories, and that the proton's resonance frequency range depends on the strength of the applied field. The spectrum above was generated on an instrument with an applied field of approximately 7.1 Tesla, at which strength protons resonate in the neighborhood of 300 million Hz (chemists refer to this as a 300 MHz instrument). If our colleague in another lab takes the NMR spectrum of the same molecule using an instrument with a 2.4 Tesla magnet, the protons will resonate at around 100 million Hz (so we'd call this a 100 MHz instrument). It would be inconvenient and confusing to always have to convert NMR data according to the field strength of the instrument used. Therefore, chemists report resonance frequencies not as absolute values in Hz, but rather as values *relative to a common standard*, generally the signal generated by the protons in TMS. This is where the ppm – parts per million – term comes in. Regardless of

the magnetic field strength of the instrument being used, the resonance frequency of the 12 equivalent protons in TMS is defined as a zero point. The resonance frequencies of protons in the sample molecule are then reported in terms of how much higher they are, in ppm, relative to the TMS signal (almost all protons in organic molecules have a higher resonance frequency than those in TMS, for reasons we shall explore quite soon).

The two proton groups in our methyl acetate sample are recorded as resonating at frequencies 2.05 and 3.67 ppm higher than TMS. One-millionth (1.0 ppm) of 300 MHz is 300 Hz. Thus 2.05 ppm, on this instrument, corresponds to 615 Hz, and 3.67 ppm corresponds to 1101 Hz. If the TMS protons observed by our 7.1 Tesla instrument resonate at exactly 300,000,000 Hz, this means that the protons in our ethyl acetate samples are resonating at 300,000,615 and 300,001,101 Hz, respectively. Likewise, if the TMS protons in our colleague's 2.4 Tesla instrument resonate at exactly 100 MHz, the methyl acetate protons in her sample resonate at 100,000,205 and 100,000,367 Hz (on the 100 MHz instrument, 1.0 ppm corresponds to 100 Hz). The absolute frequency values in each case are not very useful – they will vary according to the instrument used – but the *difference* in resonance frequency from the TMS standard, expressed in parts per million, should be the same regardless of the instrument.

Expressed this way, the resonance frequency for a given proton in a molecule is called its **chemical shift**. A frequently used symbolic designation for chemical shift in ppm is the lower-case Greek letter *delta* (δ). Most protons in organic compounds have chemical shift values between 0 and 12 ppm from TMS, although values below zero and above 12 are occasionally observed. By convention, the left-hand side of an NMR spectrum (higher chemical shift) is called **downfield**, and the right-hand direction is called **upfield**.

In our methyl acetate example we included for illustrative purposes a small amount of TMS standard directly in the sample, as was the common procedure for determining the zero point with older NMR instruments. That practice is generally no longer necessary, as modern NMR instruments are designed to use the deuterium signal from the solvent as a standard reference point, then to extrapolate the 0 ppm baseline that corresponds to the TMS proton signal (in an applied field of 7.1 Tesla, the deuterium atom in $CDCl_3$ resonates at 32 MHz, compared to 300 MHz for the protons in TMS). In the remaining NMR spectra that we will see in this text we will not see an actual TMS signal, but we can always assume that the 0 ppm point corresponds to where the TMS protons *would* resonate if they were present.

EXAMPLE

A proton has a chemical shift (relative to TMS) of 4.56 ppm.

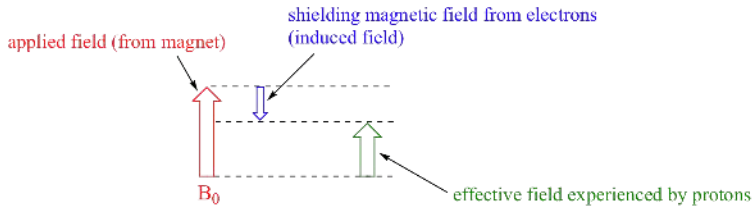
a. a) What is its chemical shift, expressed in Hz, in a 300 MHz instrument? On a 200 MHz instrument?
b. b) What is its resonance frequency, expressed in Hz, in a 300 MHz instrument? On a 200 MHz instrument?

(Assume that in these instruments, the TMS protons resonate at exactly 300 or 200 MHz, respectively)

Solution

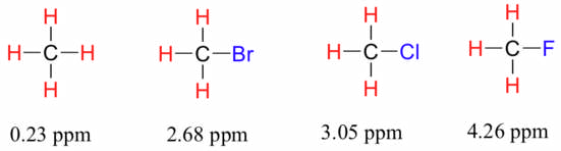
DIAMAGNETIC SHIELDING AND DESHIELDING

We come now to the question of *why* nonequivalent protons have different chemical shifts. The chemical shift of a given proton is determined primarily by its immediate electronic environment. Consider the methane molecule (CH_4), in which the protons have a chemical shift of 0.23 ppm. The valence electrons around the methyl carbon, when subjected to B_0, are induced to circulate and thus generate their own very small magnetic field that *opposes* B_0. This **induced field**, to a small but significant degree, *shields* the nearby protons from experiencing the full force of B_0, an effect known as **local diamagnetic shielding**. The methane protons therefore do not experience the full force of B_0 - what they experience is called B_{eff}, or the **effective field**, which is slightly *weaker* than B_0.

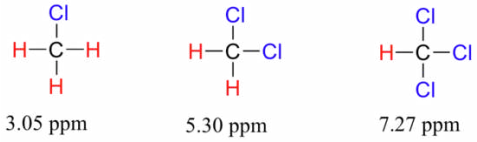


Therefore, their resonance frequency is slightly lower than what it would be if they did not have electrons nearby to shield them.

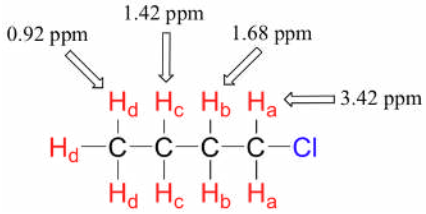
Now consider methyl fluoride, CH_3F, in which the protons have a chemical shift of 4.26 ppm, significantly higher than that of methane. This is caused by something called the **deshielding effect**. Because fluorine is more electronegative than carbon, it pulls valence electrons away from the carbon, effectively *decreasing* the electron density around each of the protons. For the protons, lower electron density means less diamagnetic shielding, which in turn means a greater overall exposure to B_0, a stronger B_{eff}, and a higher resonance frequency. Put another way, the fluorine, by pulling electron density away from the protons, is *deshielding* them, leaving them more exposed to B_0. As the electronegativity of the substituent increases, so does the extent of deshielding, and so does the chemical shift. This is evident when we look at the chemical shifts of methane and three halomethane compounds (remember that electronegativity increases as we move up a column in the periodic table).



To a large extent, then, we can predict trends in chemical shift by considering how much deshielding is taking place near a proton. The chemical shift of trichloromethane is, as expected, higher than that of dichloromethane, which is in turn higher than that of chloromethane.



The deshielding effect of an electronegative substituent diminishes sharply with increasing distance:



The presence of an electronegative oxygen, nitrogen, sulfur, or sp^2-hybridized carbon also tends to shift the NMR signals of nearby protons slightly downfield:

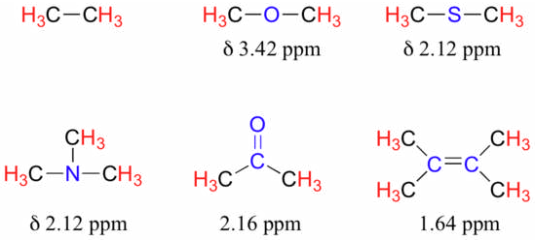
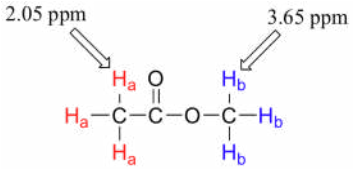
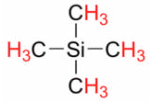


Table 2 lists typical chemical shift values for protons in different chemical environments.

Armed with this information, we can finally assign the two peaks in the the ^{1}H-NMR spectrum of methyl acetate that we saw a few pages back. The signal at 3.65 ppm corresponds to the methyl ester protons (H_b), which are deshielded by the adjacent oxygen atom. The upfield signal at 2.05 ppm corresponds to the acetate protons (H_a), which is deshielded - but to a lesser extent - by the adjacent carbonyl group.



Finally, a note on the use of TMS as a standard in NMR spectroscopy: one of the main reasons why the TMS proton signal was chosen as a zero-point is that the TMS protons are highly shielded: silicon is slightly *less* electronegative than carbon, and therefore *donates* some additional shielding electron density. Very few organic molecules contain protons with chemical shifts that are negative relative to TMS.



This page titled 7.7.2: The Nature of NMR Absorptions is shared under a CC BY-SA 4.0 license and was authored, remixed, and/or curated by Steven Farmer, Dietmar Kennepohl, Tim Soderberg, Lauren Reutenauer, & Lauren Reutenauer.

- **13.1: The Nature of NMR Absorptions** by Dietmar Kennepohl, Lauren Reutenauer, Steven Farmer, Tim Soderberg is licensed CC BY-SA 4.0.

7.7.3: THE CHEMICAL SHIFT

OBJECTIVES

After completing this section, you should be able to

1. describe the delta scale used in NMR spectroscopy.
2. perform calculations based on the relationship between the delta value (in ppm), the observed chemical shift (in Hz), and the operating frequency of an NMR spectrometer (in Hz).

KEY TERMS

Make certain that you can define, and use in context, the key terms below.

- chemical shift
- delta scale
- upfield/downfield

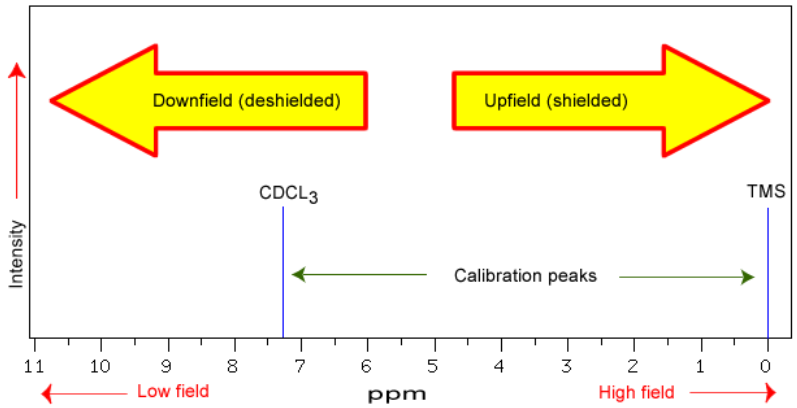
STUDY NOTES

Although the calculations described in this section will help you understand the principles of NMR, it is the actual delta values, not the calculations, which are of greatest importance to the beginning organic chemist. Thus, we shall try to focus on the interpretation of NMR spectra, not the mathematical aspects of the technique.

In Section 13.9 we discuss ^{1}H NMR chemical shifts in more detail. Although you will eventually be expected to associate the approximate region of a ^{1}H NMR spectrum with a particular type of proton, you are expected to use a general table of ^{1}H NMR chemical shifts such as the one shown in Section 13.9.

CHEMICAL SHIFTS

The NMR spectra is displayed as a plot of the applied radio frequency versus the absorption. The applied frequency decreases from left to right, thus the left side of the plot is the low field, downfield or deshielded side and the right side of the plot is the high field, upfield or shielded side (see the figure below). The concept of shielding will be explained shortly.



The position on the plot at which the nuclei absorbs is called the **chemical shift**. Since this has an arbitrary value a standard reference point must be used. The two most common standards are TMS (tetramethylsilane, $(Si(CH_3)_4)$ which has been assigned a chemical shift of zero, and $CDCl_3$ (deuterochloroform) which has a chemical shift of 7.26 for ^{1}H NMR and 77 for ^{13}C NMR. The scale is commonly expressed as parts per million (ppm) which is independent of the spectrometer frequency. The scale is the **delta (δ) scale**.

$$\delta = \frac{\text{frequency of signal} - \text{frequency of standard}}{\text{spectrometerfrequency}} \times 10^{6}$$

The range at which most NMR absorptions occur is quite narrow. Almost all ^{1}H absorptions occur downfield within 10 ppm of TMS. For ^{13}C NMR almost all absorptions occurs within 220 ppm downfield of the C atom in TMS.

SHIELDING IN NMR

Structural features of the molecule will have an effect on the exact magnitude of the magnetic field experienced by a particular nucleus. This means that H atoms which have different chemical environments will have different chemical shifts. This is what makes NMR so useful for structure determination in organic chemistry. There are three main features that will affect the shielding of the nucleus, electronegativity, magnetic anisotropy of π systems and hydrogen bonding.

ELECTRONEGATIVITY

The electrons that surround the nucleus are in motion so they created their own electromagnetic field. This field opposes the the applied magnetic field and so reduces the field experienced by the nucleus. Thus the electrons are said to **shield** the nucleus. Since the magnetic field experienced at the nucleus defines the energy difference between spin states it also defines what the chemical shift will be for that nucleus. Electron with-drawing groups can decrease the electron density at the nucleus, deshielding the nucleus and result in a larger chemical shift. Compare the data in the table below.

Compound, CH_3X	CH_3F	CH_3OH	CH_3Cl	CH_3Br	CH_3I	CH_4	$(CH_3)_4Si$
Electronegativity of X	4.0	3.5	3.1	2.8	2.5	2.1	1.8
Chemical shift δ (ppm)	4.26	3.4	3.05	2.68	2.16	0.23	0

As can be seen from the data, as the electronegativity of X increases the chemical shift, δ increases. This is an effect of the halide atom pulling the electron density away from the methyl group. This exposes the nuclei of both the C and H atoms, "deshielding" the nuclei and shifting the peak downfield.

The effects are cumulative so the presence of more electron withdrawing groups will produce a greater deshielding and therefore a larger chemical shift, *i.e.*

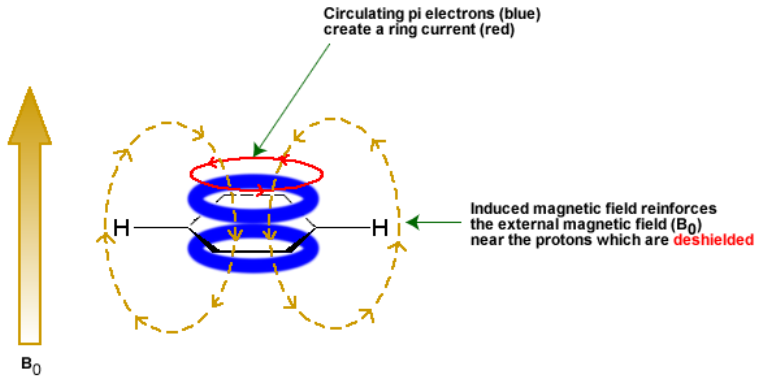
Compound	CH_4	CH_3Cl	CH_2Cl_2	$CHCl_3$
δ (ppm)	0.23	3.05	5.30	7.27

These **inductive effects** are not only felt by the immediately adjacent atoms, but the deshielding can occur further down the chain, *i.e.*

NMR signal	$-CH_2-CH_2-CH_2Br$
δ (ppm)	1.25 1.69 3.30

MAGNETIC ANISOTROPY: Π ELECTRON EFFECTS

The π electrons in a compound, when placed in a magnetic field, will move and generate their own magnetic field. The new magnetic field will have an effect on the shielding of atoms within the field. The best example of this is benzene (see the figure below).

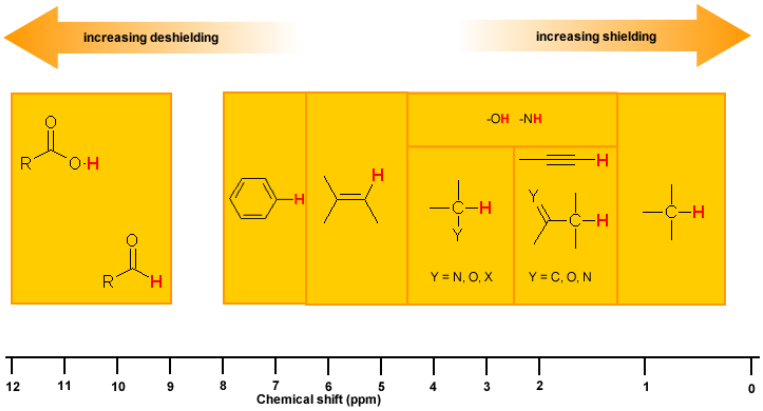


This effect is common for any atoms near a π bond, *i.e.*

Proton Type	Effect	Chemical shift (ppm)
C_6H_5-H	highly deshielded	6.5 - 8
C=C-H	deshielded	4.5 - 6
C≡C-H	shielded*	~2.5
O=C-H	very highly deshielded	9 - 10
* the acetylene H is shielded due to its location relative to the π system		

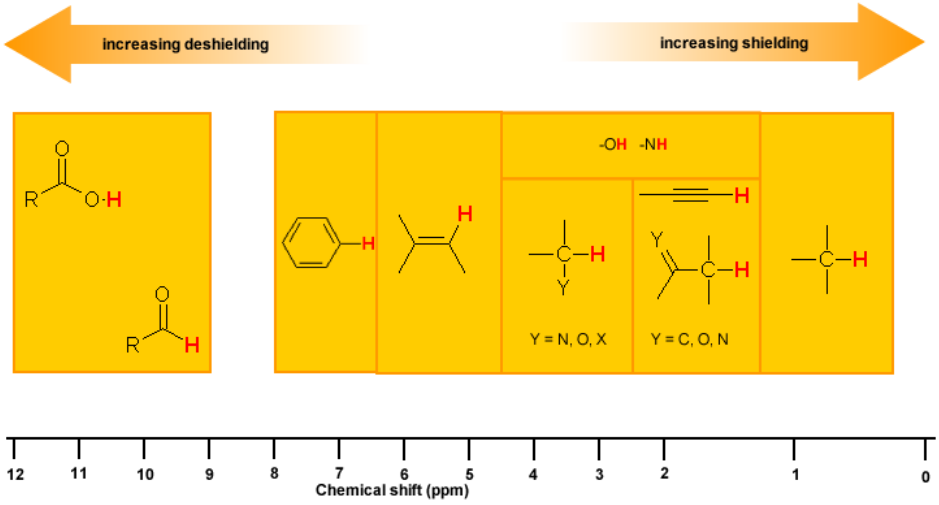
HYDROGEN BONDING

Protons that are involved in hydrogen bonding (*i.e.*-OH or -NH) are usually observed over a wide range of chemical shifts. This is due to the deshielding that occurs in the hydrogen bond. Since hydrogen bonds are dynamic, constantly forming, breaking and forming again, there will be a wide range of hydrogen bonds strengths and consequently a wide range of deshielding. This as well as solvation effects, acidity, concentration and temperature make it very difficult to predict the chemical shifts for these atoms.



Experimentally -OH and -NH can be identified by carrying out a simple D_2O exchange experiment since these protons are exchangeable.

- run the normal H-NMR experiment on your sample
- add a few drops of D_2O
- re-run the H-NMR experiment
- compare the two spectra and look for peaks that have "disappeared"



? EXERCISE 7.7.3.1

The following peaks were from a H^1 NMR spectra from a 400 MHz spectrometer. Convert to δ units

a. $CHCl_3$ 1451 Hz
b. CH_3Cl 610 Hz
c. CH_3OH 693 Hz
d. CH_2Cl_2 1060 Hz

Answer

a. 3.627 ppm
b. 1.525 ppm
c. 1.732 ppm
d. 2.65 ppm

EXERCISE 7.7.3.2

Butan-2-one shows a chemical shift around 2.1 on a 300 MHz spectrometer in the H^1 NMR spectrum.

a. How far downfield is this peak from TMS in Hz?
b. If the spectrum was done with a 400 MHz instrument, would a different chemical shift be seen?
c. On this new 400 MHz spectrum, what would be the difference in Hz from the chemical shift and TMS?

Answer

a. Since TMS is at 0 δ = 0 Hz for reference, the difference between the two would be 630 Hz
b. No not a different chemical shift, but a different frequency would be seen, 840 Hz
c. 840 Hz

This page titled 7.7.3: The Chemical Shift is shared under a CC BY-SA 4.0 license and was authored, remixed, and/or curated by Steven Farmer, Richard Spinney, Dietmar Kennepohl, Lauren Reutenauer, & Lauren Reutenauer.

- **13.2: The Chemical Shift** by Dietmar Kennepohl, Lauren Reutenauer, Richard Spinney, Steven Farmer is licensed CC BY-SA 4.0.

7.7.4: CHEMICAL SHIFTS IN ^{1}H NMR SPECTROSCOPY

OBJECTIVES

After completing this section, you should be able to

1. state the approximate chemical shift (δ) for the following types of protons:
   a. aromatic.
   b. vinylic.
   c. those bonded to carbon atoms which are in turn bonded to a highly electronegative element.
   d. those bonded to carbons which are next to unsaturated centres.
   e. those bonded to carbons which are part of a saturated system.
2. predict the approximate chemical shifts of each of the protons in an organic compound, given its structure and a table of chemical shift correlations.

STUDY NOTES

You should not attempt to memorize the chemical shifts listed in the table of this section, although it is probable that you will need to refer to it quite frequently throughout the remainder of this course. To fulfill Objective 1, above, you should be familiar with the information presented in the figure of chemical shift ranges for organic compounds. If you have an approximate idea of the chemical shifts of some of the most common types of protons, you will find the interpretation of ^{1}H NMR spectra less arduous than it might otherwise be. Notice that we shall not try to understand why aromatic protons are deshielded or why alkynyl protons are not deshielded as much as vinylic protons. These phenomena can be explained, but the focus is on the interpretation of ^{1}H NMR spectra, not on the underlying theory.

^{1}H NMR CHEMICAL SHIFTS

Chemical shifts in NMR (Nuclear Magnetic Resonance) spectroscopy refer to the phenomenon where the resonant frequency of a nucleus in a magnetic field is influenced by its chemical environment. This effect arises from the shielding or deshielding of the nucleus by the surrounding electron cloud. When a nucleus experiences different local electron densities due to nearby atoms or functional groups, its resonant frequency is altered relative to a reference standard, usually tetramethylsilane in organic solvents. This alteration is expressed in parts per million (ppm) and is known as the chemical shift. Tetramethylsilane [TMS;$(CH_3)_4Si$] is generally used for standard to determine chemical shift of compounds: δ_{TMS}=0 ppm. In other words, frequencies for chemicals are measured for a ^{1}H nucleus of a sample from the ^{1}H or resonance of TMS. It is important to understand trend of chemical shift in terms of NMR interpretation. The proton NMR chemical shift is affect by nearness to electronegative atoms (O, N, halogen.) and unsaturated groups (C=C,C=O, aromatic). Electronegative groups move to the down field (left; increase in ppm). Unsaturated groups shift to downfield (left) when affecting nucleus is in the plane of the unsaturation, but reverse shift takes place in the regions above and below this plane. ^{1}H chemical shift play a role in identifying many functional groups. Figure 1. indicates important example to figure out the functional groups.

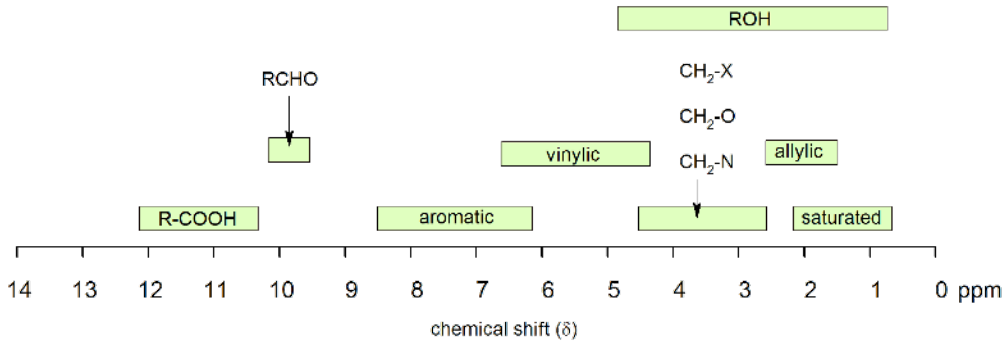
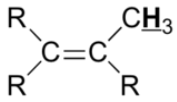
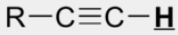
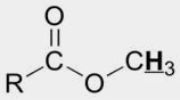
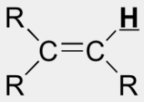
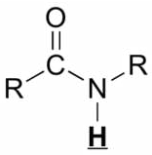
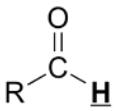
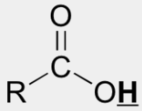


Figure 1. 1H chemical shift ranges for organic compounds

Chemical shift values are in parts per million (ppm) relative to tetramethylsilane.

Table 7.7.4.1: Common Chemical Shift values

Hydrogen type	Chemical shift (ppm)
$RC\underline{H}_3$	0.9 - 1.0
$RC\underline{H}_2R$	1.2 - 1.7
$R_3C\underline{H}$	1.5 – 2.0
	2.0 – 2.3
	1.5 – 1.8
$RN\underline{H}_2$	1 - 3
$ArC\underline{H}_3$	2.2 – 2.4
	2.3 – 3.0
$ROC\underline{H}_3$	3.7 – 3.9
	3.7 – 3.9
$RO\underline{H}$	1 - 5
	3.7 – 6.5
	5 - 9
$Ar\underline{H}$	6.0 – 8.7
	9.5 – 10.0
	10 - 13

EXERCISE 7.7.4.1

The following have one H^1 NMR peak. In each case predict approximately where this peak would be in a spectra.



Answer

A. 5.20 δ; B. 1.50 δ; C. 6.40 δ; D. 1.00 δ

EXERCISE 7.7.4.2

Identify the different equivalent protons in the following molecule and predict their expected chemical shift.



Answer

There are 6 different protons in this molecule

The shifts are (close) to the following: (a) 2 δ; (b) 6 δ; (c) 6.5 δ; (d) 7 δ; (e) 7.5 δ; (f) 7 δ



This page titled 7.7.4: Chemical Shifts in ^{1}H NMR Spectroscopy is shared under a CC BY-SA 4.0 license and was authored, remixed, and/or curated by Steven Farmer, Dietmar Kennepohl, Tim Soderberg, Lauren Reutenauer, & Lauren Reutenauer.

- **13.3: Chemical Shifts in ^{1}H NMR Spectroscopy** by Dietmar Kennepohl, Lauren Reutenauer, Steven Farmer, Tim Soderberg is licensed CC BY-SA 4.0.

7.7.5: INTEGRATION OF ^{1}H NMR ABSORPTIONS - PROTON COUNTING

OBJECTIVES

After completing this section, you should be able to

- explain what information can be obtained from an integrated ^{1}H NMR spectrum, and use this information in the interpretation of such a spectrum.
- use an integrated ^{1}H NMR spectrum to determine the ratio of the different types of protons present in an organic compound.

STUDY NOTES

The concept of peak integration is that the area of a given peak in a ^{1}H NMR spectrum is proportional to the number of (equivalent) protons giving rise to the peak. Thus, a peak which is caused by a single, unique proton has an area which measures one third of the area of a peak resulting from a methyl (CH_3) group in the same spectrum.

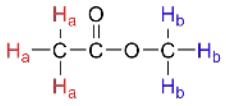
In practice, we do not have to measure these areas ourselves: it is all done electronically by the spectrometer, and an integration curve is superimposed on the rest of the spectrum. The integration curve appears as a series of steps, with the height of each step being proportional to the area of the corresponding absorption peak, and consequently, to the number of protons responsible for the absorption.

As it can be difficult to decide precisely where to start and stop when measuring integrations, you should not expect your ratios to be exact whole numbers.

Signal integration in NMR (Nuclear Magnetic Resonance) spectroscopy is crucial for quantifying the relative number of nuclei contributing to each signal in the spectrum. This process involves measuring the area under each peak in the NMR spectrum, which directly correlates to the abundance of the corresponding nuclei in the sample.

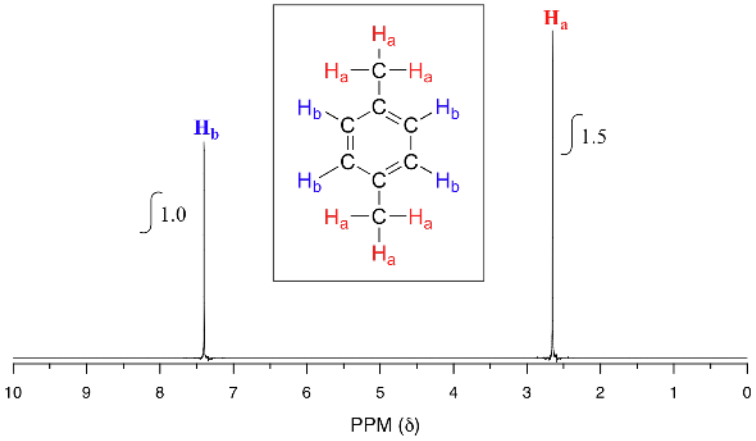
SIGNAL INTEGRATION

The computer in an NMR instrument can be instructed to automatically integrate the area under a signal or group of signals. This is very useful, because *in ^{1}H-NMR spectroscopy the area under a signal is proportional to the number of hydrogens to which the peak corresponds*. In the previous example of methyl acetate from Section 13.2, for example, the Ha and H_b peaks would integrate to approximately the same area, because they both correspond to a set of three equivalent protons.



methyl acetate

Now, take a look next at the spectrum of *para*-xylene (IUPAC name 1,4-dimethylbenzene):



This molecule has two sets of protons: the six methyl (H_a) protons and the four aromatic (H_b) protons. When we instruct the instrument to integrate the areas under the two signals, we find that the area under the peak at 2.6 ppm is 1.5 times greater than the area under the peak at

7.4 ppm, which is the case with 6 methyl protons and 4 aromatic protons. This (along with the actual chemical shift values, which we'll discuss soon) tells us which set of protons corresponds to which NMR signal.

The integration function can also be used to determine the relative amounts of two or more compounds in a *mixed* sample. If we have a sample that is a 50:50 (mole/mole) mixture of benzene and acetone, for example, the acetone signal should integrate to the same value as the benzene sample, because both signals represent six equivalent protons. If we have a 50:50 mixture of acetone and cyclopentane, on the other hand, the ratio of the acetone peak area to the cylopentane peak area will be 3:5 (or 6:10), because the cyclopentane signal represents ten protons.

EXAMPLE 7.7.5.1

You take a ^{1}H-NMR spectrum of a mixed sample of acetone ($CH_3(CO)CH_3$) and dichloromethane (CH_2Cl_2). The integral ratio of the two signals (acetone : dichloromethane) is 2.3 to 1. What is the molar ratio of the two compounds in the sample?

EXAMPLE 7.7.5.2

You take the ^{1}H-NMR spectrum of a mixed sample of 36% *para*-xylene and 64% acetone in $CDCl_3$ solvent (structures are shown earlier in this chapter). How many peaks do you expect to see? What is the expected ratio of integration values for these peaks? (set the acetone peak integration equal to 1.0)

Solutions

EXERCISE 7.7.5.1

Predict how many signals the following molecule would have? Sketch the spectra and estimate the integration of the peaks.



Answer

There will be two peaks. Ideal general spectrum shown with integration.



This page titled 7.7.5: Integration of ^{1}H NMR Absorptions - Proton Counting is shared under a CC BY-SA 4.0 license and was authored, remixed, and/or curated by Steven Farmer, Dietmar Kennepohl, Tim Soderberg, & Tim Soderberg.

- **13.4: Integration of ^{1}H NMR Absorptions - Proton Counting** by Dietmar Kennepohl, Steven Farmer, Tim Soderberg is licensed CC BY-SA 4.0.

7.7.6: SPIN-SPIN SPLITTING IN ^{1}H NMR SPECTRA

OBJECTIVES

After completing this section, you should be able to

1. explain the spin-spin splitting pattern observed in the ^{1}H NMR spectrum of a simple organic compound, such as chloroethane or 2-bromopropane.
2. interpret the splitting pattern of a given ^{1}H NMR spectrum.
3. determine the structure of a relatively simple organic compound, given its ^{1}H NMR spectrum and other relevant information.
4. use coupling constants to determine which groups of protons are coupling with one another in a ^{1}H NMR spectrum.
5. predict the splitting pattern which should be observed in the ^{1}H NMR spectrum of a given organic compound.

KEY TERMS

Make certain that you can define, and use in context, the key terms below.

- coupling constant
- multiplet
- quartet
- triplet
- doublet

STUDY NOTES

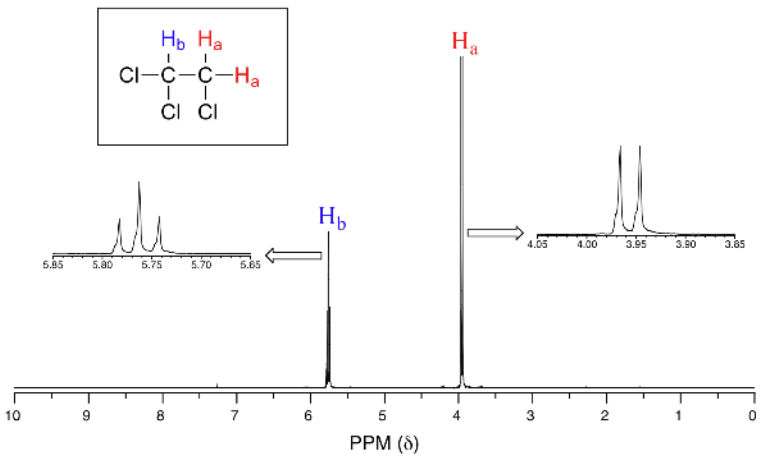
From what we have learned about ^{1}H NMR spectra so far, we might predict that the spectrum of 1,1,2-trichloroethane, $CHCl_2CH_2Cl$, would consist of two peaks—one, at about 2.5-4.0 δ, expected for CH_2-halogen compounds and one shifted downfield because of the presence of an additional electronegative chlorine atom on the second carbon. However, when we look at the spectrum it appears to be much more complex. True, we see absorptions in the regions we predicted, but these absorptions appear as a group of two peaks (a *doublet*) and a group of three peaks (a *triplet*). This complication, which may be disturbing to a student who longs for the simple life, is in fact very useful to the organic chemist, and adds greatly to the power of NMR spectroscopy as a tool for the elucidation of chemical structures. The split peaks (*multiplets*) arise because the magnetic field experienced by the protons of one group is influenced by the spin arrangements of the protons in an adjacent group.

Spin-spin coupling is often one of the more challenging topics for organic chemistry students to master. Remember the $n + 1$ rule and the associated coupling patterns.

THE SOURCE OF SPIN-SPIN COUPLING

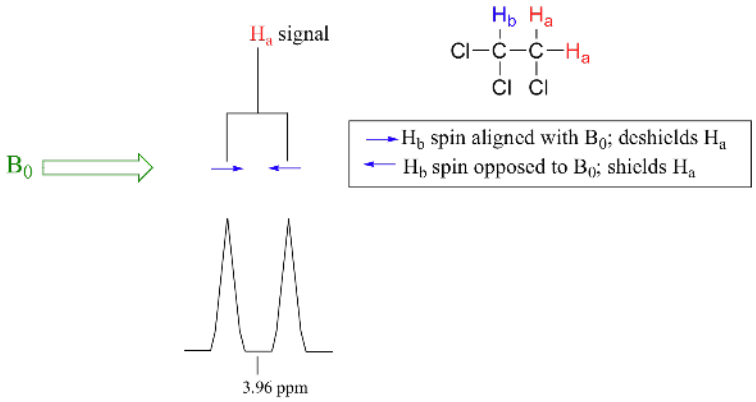
The ^{1}H-NMR spectra that we have seen so far (of methyl acetate and *para*-xylene) are somewhat unusual in the sense that in both of these molecules, each set of protons generates a single NMR signal. In fact, the ^{1}H-NMR spectra of most organic molecules contain proton signals that are 'split' into two or more sub-peaks. Rather than being a complication, however, this splitting behavior actually provides us with more information about our sample molecule.

Consider the spectrum for 1,1,2-trichloroethane. In this and in many spectra to follow, we show enlargements of individual signals so that the signal splitting patterns are recognizable.

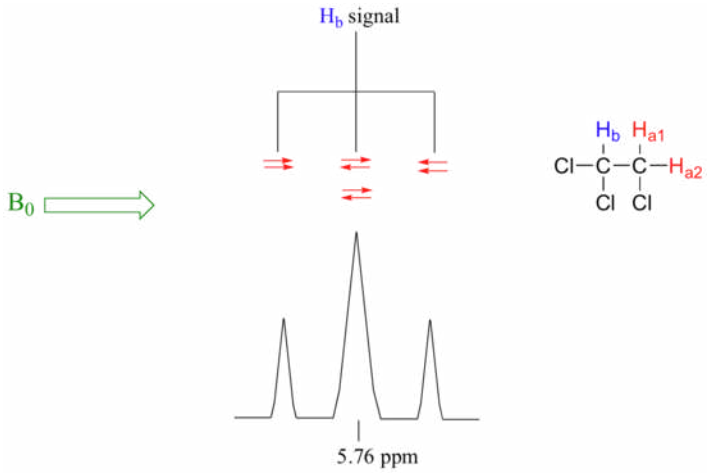


The signal at 3.96 ppm, corresponding to the two H_a protons, is split into two subpeaks of equal height (and area) – this is referred to as a **doublet**. The H_b signal at 5.76 ppm, on the other hand, is split into three sub-peaks, with the middle peak higher than the two outside peaks - if we were to integrate each subpeak, we would see that the area under the middle peak is twice that of each of the outside peaks. This is called a **triplet**.

The source of signal splitting is a phenomenon called **spin-spin coupling**, a term that describes the magnetic interactions between neighboring, non-equivalent NMR-active nuclei. In our 1,1,2 trichloromethane example, the H_a and H_b protons are spin-coupled to each other. Here's how it works, looking first at the H_a signal: in addition to being shielded by nearby valence electrons, each of the H_a protons is also influenced by the small magnetic field generated by H_b next door (remember, each spinning proton is like a tiny magnet). The magnetic moment of H_b will be aligned *with* B_0 in (slightly more than) half of the molecules in the sample, while in the remaining half of the molecules it will be opposed to B_0. The B_{eff} 'felt' by H_a is a slightly weaker if H_b is aligned against B_0, or slightly stronger if H_b is aligned with B_0. In other words, in half of the molecules H_a is *shielded* by H_b (thus the NMR signal is shifted slightly upfield) and in the other half H_a is *deshielded* by H_b(and the NMR signal shifted slightly downfield). What would otherwise be a single H_a peak has been split into two sub-peaks (a doublet), one upfield and one downfield of the original signal. These ideas an be illustrated by a **splitting diagram**, as shown below.

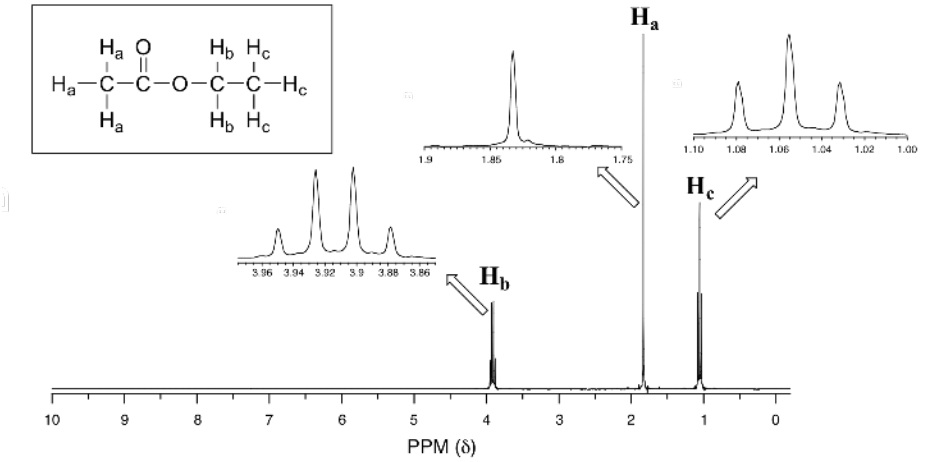


Now, let's think about the $H_b$signal. The magnetic environment experienced by H_b is influenced by the fields of both neighboring H_a protons, which we will call H_{a1} and H_{a2}. There are four possibilities here, each of which is equally probable. First, the magnetic fields of both H_{a1} and H_{a2} could be aligned with B_0, which would deshield H_b, shifting its NMR signal slightly downfield. Second, both the H_{a1} and H_{a2} magnetic fields could be aligned opposed to B_0, which would shield H_b, shifting its resonance signal slightly upfield. Third and fourth, H_{a1} could be with B_0 and H_{a2} opposed, or H_{a1}opposed to B_0 and H_{a2} with B_0. In each of the last two cases, the shielding effect of one H_a proton would cancel the deshielding effect of the other, and the chemical shift of H_b would be unchanged.



So in the end, the signal for H_b is a **triplet**, with the middle peak twice as large as the two outer peaks because there are *two* ways that H_{a1} and H_{a2} can cancel each other out.

Now, consider the spectrum for ethyl acetate:



We see an unsplit '**singlet**' peak at 1.833 ppm that corresponds to the acetyl (H_a) hydrogens – this is similar to the signal for the acetate hydrogens in methyl acetate that we considered earlier. This signal is unsplit because there are no adjacent hydrogens on the molecule. The signal at 1.055 ppm for the H_c hydrogens is split into a triplet by the two H_b hydrogens next door. The explanation here is the same as the explanation for the triplet peak we saw previously for 1,1,2-trichloroethane.

The $H_b$hydrogens give rise to a **quartet** signal at 3.915 ppm – notice that the two middle peaks are taller then the two outside peaks. This splitting pattern results from the spin-coupling effect of the *three* H_c hydrogens next door, and can be explained by an analysis similar to that which we used to explain the doublet and triplet patterns.

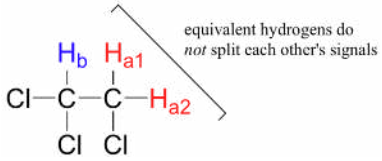
EXAMPLE 13.11.1

a. Explain, using left and right arrows to illustrate the possible combinations of nuclear spin states for the H_c hydrogens, why the H_b signal in ethyl acetate is split into a quartet.
b. The integration ratio of doublets is 1:1, and of triplets is 1:2:1. What is the integration ratio of the H_b quartet in ethyl acetate? (Hint – use the illustration that you drew in part a to answer this question.)

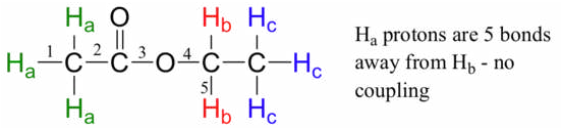
Solution

By now, you probably have recognized the pattern which is usually referred to as the ***n* + 1 rule**: if a set of hydrogens has *n* neighboring, non-equivalent hydrogens, it will be split into *n* + 1 subpeaks. Thus the two H_b hydrogens in ethyl acetate split the H_c signal into a triplet, and the three H_c hydrogens split the H_b signal into a quartet. This is very useful information if we are trying to determine the structure of an unknown molecule: if we see a triplet signal, we know that the corresponding hydrogen or set of hydrogens has two `neighbors`. When we begin to determine structures of unknown compounds using ^{1}H-NMR spectral data, it will become more apparent how this kind of information can be used.

Three important points need to be emphasized here. First, signal splitting only occurs between non-equivalent hydrogens – in other words, H_{a1} in 1,1,2-trichloroethane is *not* split by H_{a2}, and vice-versa.

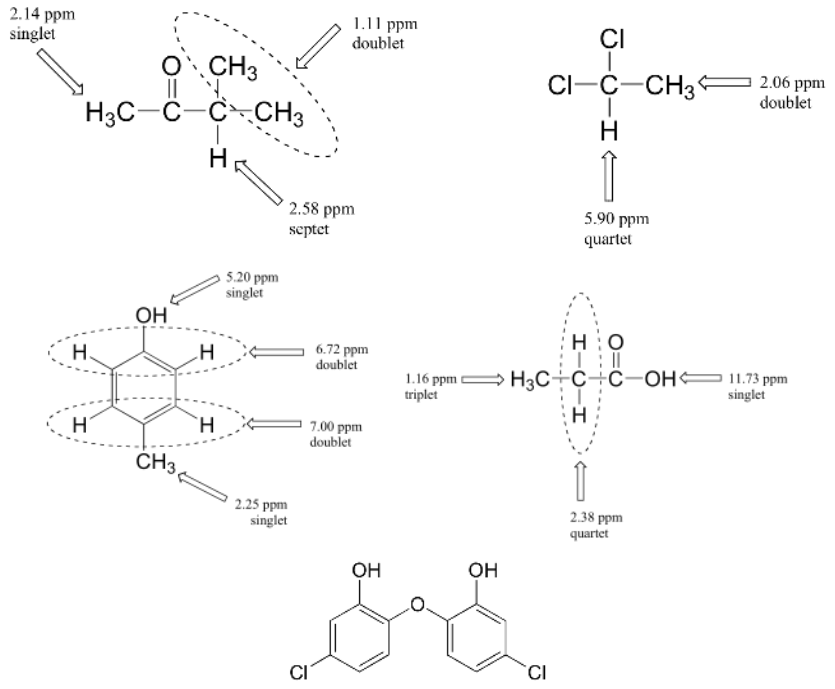


Second, splitting occurs primarily between hydrogens that are separated by three bonds. This is why the H_a hydrogens in ethyl acetate form a singlet– the nearest hydrogen neighbors are five bonds away, too far for coupling to occur.



Occasionally we will see four-bond and even 5-bond splitting, but in these cases the magnetic influence of one set of hydrogens on the other set is much more subtle than what we typically see in three-bond splitting (more details about how we quantify coupling interactions is provided in section 5.5B). Finally, splitting is most noticeable with hydrogens bonded to carbon. Hydrogens that are bonded to heteroatoms (alcohol or amino hydrogens, for example) are coupled weakly - or not at all - to their neighbors. This has to do with the fact that these protons exchange rapidly with solvent or other sample molecules.

Below are a few more examples of chemical shift and splitting pattern information for some relatively simple organic molecules.



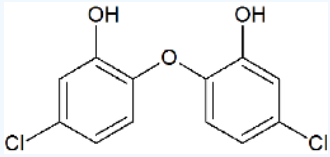
MULTIPLICITY IN PROTON NMR

The number of lines in a peak is always one more (n+1) than the number of hydrogens on the neighboring carbon. This table summarizes coupling patterns that arise when protons have different numbers of neighbors.

# of lines	ratio of lines	term for peak	# of neighbors
1	-	singlet	0
2	1:1	doublet	1
3	1:2:1	triplet	2
4	1:3:3:1	quartet	3
5	1:4:6:4:1	quintet	4
6	1:5:10:10:5:1	sextet	5
7	1:6:15:20:15:6:1	septet	6
8	1:7:21:35:35:21:7:1	octet	7
9	1:8:28:56:70:56:28:8:1	nonet	8

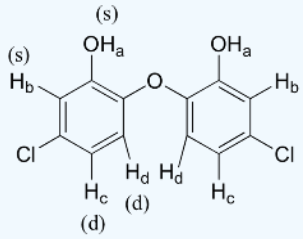
EXAMPLE 13.11.2

How many proton signals would you expect to see in the ^{1}H-NMR spectrum of the structure shown? For each of the proton signals, predict the splitting pattern. Assume that you see only 3-bond coupling.



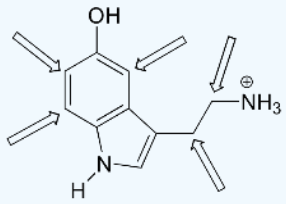
Answer

Because of the symmetry in the molecule, there are only four proton signals. Predicted splitting is indicated.



EXAMPLE 13.11.3

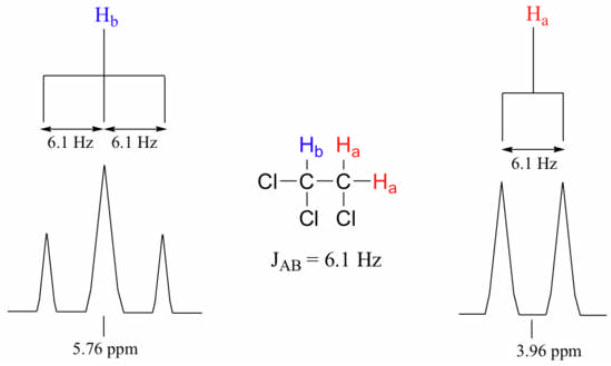
Predict the splitting pattern for the ^{1}H-NMR signals corresponding to the protons at the locations indicated by arrows (the structure is that of the neurotransmitter serotonin).



Solutions

COUPLING CONSTANTS

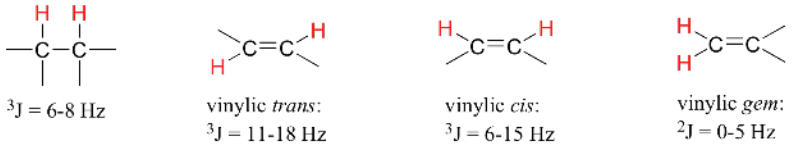
Chemists quantify the spin-spin coupling effect using something called the **coupling constant**, which is abbreviated with the capital letter *J*. The coupling constant is simply the difference, expressed in Hz, between two adjacent sub-peaks in a split signal. For our doublet in the 1,1,2-trichloroethane spectrum, for example, the two subpeaks are separated by 6.1 Hz, and thus we write $^3J_{a\text{-}b}$ = 6.1 Hz.



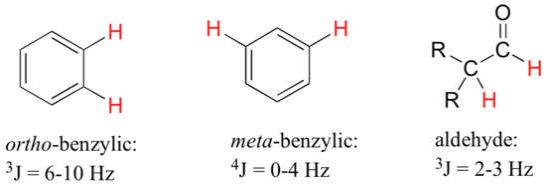
The superscript 3 tells us that this is a three-bond coupling interaction, and the a-b subscript tells us that we are talking about coupling between H_a and H_b. Unlike the chemical shift value, *the coupling constant, expressed in Hz, is the same regardless of the applied field strength of the NMR magnet*. This is because the strength of the magnetic moment of a neighboring proton, which is the source of the spin-spin coupling phenomenon, does *not* depend on the applied field strength.

When we look closely at the triplet signal in 1,1,2-trichloroethane, we see that the coupling constant - the `gap` between subpeaks - is 6.1 Hz, the same as for the doublet. This is an important concept! The coupling constant $^3J_{a\text{-}b}$ quantifies the magnetic interaction between the H_a and H_b hydrogen sets, and *this interaction is of the same magnitude in either direction*. In other words, H_a influences H_b to the same extent that H_b influences H_a. When looking at more complex NMR spectra, this idea of **reciprocal coupling constants** can be very helpful in identifying the coupling relationships between proton sets.

Coupling constants between proton sets on neighboring sp^3-hybridized carbons is typically in the region of 6-8 Hz. With protons bound to sp^2-hybridized carbons, coupling constants can range from 0 Hz (no coupling at all) to 18 Hz, depending on the bonding arrangement.



For vinylic hydrogens in a *trans* configuration, we see coupling constants in the range of ^3J = 11-18 Hz, while *cis* hydrogens couple in the ^3J = 6-15 Hz range. The 2-bond coupling between hydrogens bound to the same alkene carbon (referred to as geminal hydrogens) is very fine, generally 5 Hz or lower. *Ortho* hydrogens on a benzene ring couple at 6-10 Hz, while 4-bond coupling of up to 4 Hz is sometimes seen between *meta* hydrogens.



Fine (2-3 Hz) coupling is often seen between an aldehyde proton and a three-bond neighbor. Table 4 lists typical constant values.

> Remember, chemically equivalent protons do not couple with one another to give spin-spin splitting.

EXERCISE 7.7.6.1

Predict the splitting patterns of the following molecules:



Answer

a. H: Doublet. H: Septet
b. H: Doublet, H: Triplet
c. H: Singlet, H: Quartet, H: Triplet



EXERCISE 7.7.6.2

Draw the following according to the criteria given.

a. C_3H_5O; two triplet, 1 doublet
b. $C_4H_8O_2$; three singlets
c. C_5H_{12}; one singlet

Answer



These are just some drawings, more may be possible.

EXERCISE 7.7.6.3

The following spectrum is for C_3H_8O. Determine the structure.



A triplet; B singlet; C sextet; D triplet

Source: SDBSWeb : http://sdbs.db.aist.go.jp (National Institute of Advanced Industrial Science and Technology, 3 December 2016)

Answer



This page titled 7.7.6: Spin-Spin Splitting in ¹H NMR Spectra is shared under a CC BY-SA 4.0 license and was authored, remixed, and/or curated by Chris Schaller, Steven Farmer, Dietmar Kennepohl, Tim Soderberg, & Tim Soderberg.

- **13.5: Spin-Spin Splitting in ¹H NMR Spectra** by Chris Schaller, Dietmar Kennepohl, Steven Farmer, Tim Soderberg is licensed CC BY-SA 4.0.

7.7.7: ^{1}H NMR SPECTROSCOPY AND PROTON EQUIVALENCE

OBJECTIVES

After completing this section, you should be able to

- identify those protons which are equivalent in a given chemical structure.
- use the ^{1}H NMR spectrum of a simple organic compound to determine the number of equivalent sets of protons present.

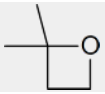
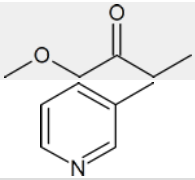
KEY TERMS

Make certain that you can define, and use in context, the key terms below.

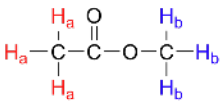
- diastereotopic
- enantiotopic
- homotopic

STUDY NOTES

It is important at this stage to be able to identify equivalent protons in any organic compound given the structure of that compound. Once you know the number of different groups of equivalent protons in a compound, you can predict the number (before coupling) and relative strength of signals. Look at the following examples and make sure you understand how the number and intensity ratio of signals are derived from the structure shown.

Structure	Number of Signals	Ratio of Signals	
$CH_3OCH_2CH_2Br$	3	A : B : C	3 : 2 : 2
	1		
	3	A : B : C	2 : 2 : 6 (or 1 : 1 : 3)
	3	A : B : C	2 : 4 : 2 (or 1 : 2 : 1)
	4	A : B : C : D	3 : 2 : 2 : 3
	5	A : B : C : D : E	3 : 1 : 1 : 1 : 1

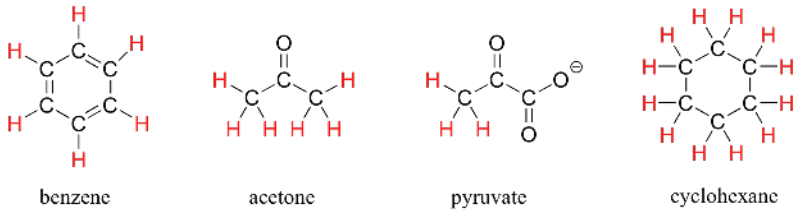
Proton equivalence in proton NMR refers to the concept that not all hydrogen atoms in a molecule produce distinct signals in the NMR spectrum. Instead, chemically equivalent protons, meaning those that occupy identical environments within a molecule, yield the same NMR signal. This concept is essential for interpreting NMR spectra accurately. Chemical equivalence is determined by the molecular structure and symmetry of a molecule. If all protons in all organic molecules had the same resonance frequency in an external magnetic field of a given strength, the information in the previous paragraph would be interesting from a theoretical standpoint, but would not be terribly useful to organic chemists. Fortunately for us, however, resonance frequencies are not uniform for all protons in a molecule. *In an external magnetic field of a given strength, protons in different locations in a molecule have different resonance frequencies, because they are in non-identical electronic environments.* In methyl acetate, for example, there are two 'sets' of protons. The three protons labeled H_a have a different - and easily distinguishable – resonance frequency than the three H_b protons, because the two sets of protons are in non-identical environments: they are, in other words, chemically nonequivalent.



On the other hand, the three H_a protons are all in the same electronic environment, and are chemically equivalent to one another. They have identical resonance frequencies. The same can be said for the three H_b protons. These protons are considered to be homotopic. Homotopic

protons are chemically identical, so electronically equivalent, thus show up as identical NMR absorptions.

The ability to recognize chemical equivalency and nonequivalency among atoms in a molecule will be central to understanding NMR. In each of the molecules below, all protons are chemically equivalent, and therefore will have the same resonance frequency in an NMR experiment.



benzene acetone pyruvate cyclohexane

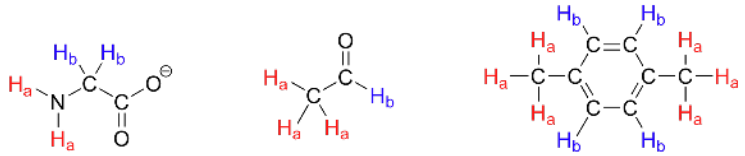
You might expect that the equatorial and axial hydrogens in cyclohexane would be non-equivalent, and would have different resonance frequencies. In fact, an axial hydrogen *is* in a different electronic environment than an equatorial hydrogen. Remember, though, that the molecule rotates rapidly between its two chair conformations, meaning that any given hydrogen is rapidly moving back and forth between equatorial and axial positions. It turns out that, except at extremely low temperatures, this rotational motion occurs on a time scale that is much faster than the time scale of an NMR experiment.



ring-flip process is *fast* compared to the NMR time-scale

In this sense, NMR is like a camera that takes photographs of a rapidly moving object with a slow shutter speed - the result is a blurred image. In NMR terms, this means that all 12 protons in cyclohexane are equivalent.

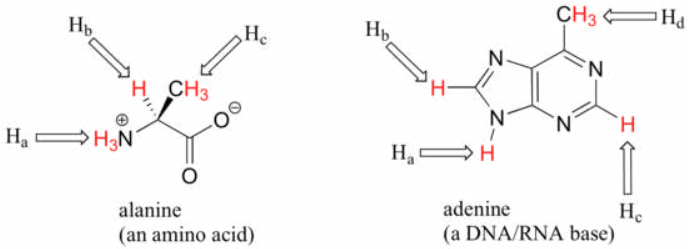
Each the molecules in the next figure contains *two* sets of protons, just like our previous example of methyl acetate, and again in each case the resonance frequency of the H_a protons will be different from that of the H_b protons.



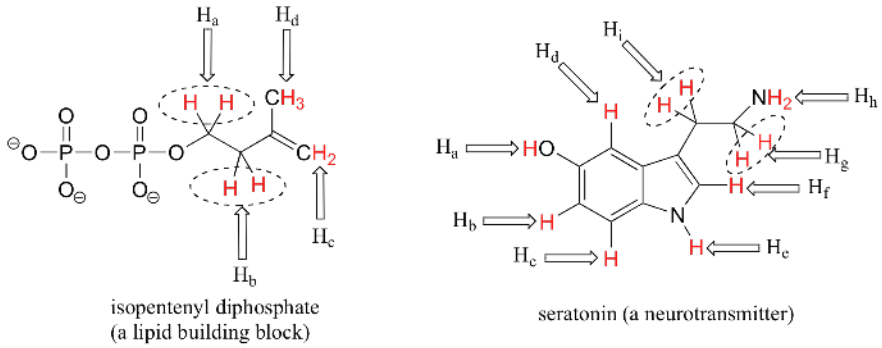
glycine acetaldehyde *para*-xylene

Notice how the symmetry of *para*-xylene results in there being only two different sets of protons.

Most organic molecules have several sets of protons in different chemical environments, and each set, in theory, will have a different resonance frequency in ^{1}H-NMR spectroscopy.

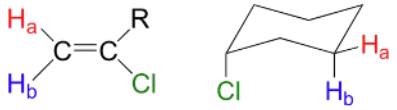


alanine (an amino acid) adenine (a DNA/RNA base)

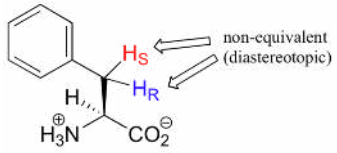


isopentenyl diphosphate (a lipid building block) seratonin (a neurotransmitter)

When stereochemistry is taken into account, the issue of equivalence vs nonequivalence in NMR starts to get a little more complicated. It should be fairly intuitive that hydrogens on different sides of asymmetric ring structures and double bonds are in different electronic environments, and thus are non-equivalent and have different resonance frequencies. In the alkene and cyclohexene structures below, for example, H_a is *trans* to the chlorine substituent, while H_b is *cis* to chlorine.

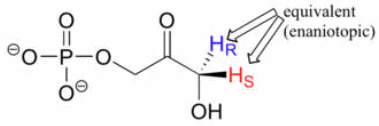


What is not so intuitive is that diastereotopic hydrogens (section 3.10) on chiral molecules are also non-equivalent:

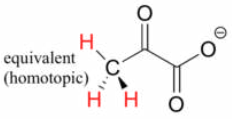


phenylalanine

However, enantiotopic and homotopic hydrogens are chemically equivalent. To determine if protons are homotopic or enantiotopic, you can do a thought experiment by replacing one H with X followed by the other H by X. In pyruvate below, if you replace any of the Hs with an X, then you would get the same molecule. These protons are homotopic. In dihydroxyacetone phosphate, this is not quite the case. If you exchange H_R for X, then you would create a stereocenter with R configuration. If you exchange H_S for X, then you would create a stereocenter with S configuration. The two "new molecules" would have the relationship of being enantiomers. Therefore H_R and H_S are enantiotopic protons. The only way these protons will show up different under NMR experimental conditions would be if you used a solvent that was chiral. Since most common solvents are all achiral, the enantiotopic protons are NMR equivalent and will show up as if they were the same proton.



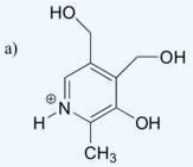
dihydroxyacetone phosphate



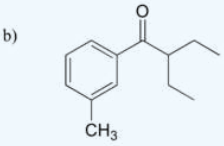
pyruvate

EXAMPLE 13.6.1

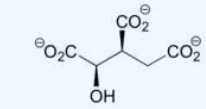
How many different sets of protons do the following molecules contain? (count diastereotopic protons as non-equivalent).



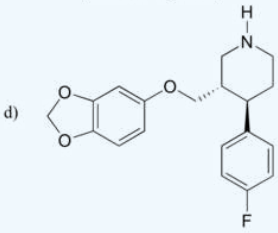
pyridoxine (vitamin B_6)



DEET (an insect repellent)



isocitrate (a citric acid cycle intermediate)



paroxetine (an antianxietry drug, trade name Paxil)

Solution

EXERCISE 7.7.7.1

How many non-equivalent hydrogen are in the following molecules; how many different signals will you see in a H^1 NMR spectrum.

a. $CH_3CH_2CH_2Br$
b. $CH_3OCH_2C(CH_3)_3$
c. Ethyl Benzene
d. 2-methyl-1-hexene

Answer

A. 3; B. 3; C. 5; D. 7

This page titled 7.7.7: ¹H NMR Spectroscopy and Proton Equivalence is shared under a CC BY-SA 4.0 license and was authored, remixed, and/or curated by Steven Farmer, Dietmar Kennepohl, Tim Soderberg, Lauren Reutenauer, & Lauren Reutenauer.

- **13.6: ¹H NMR Spectroscopy and Proton Equivalence** by Dietmar Kennepohl, Lauren Reutenauer, Steven Farmer, Tim Soderberg is licensed CC BY-SA 4.0.

7.7.8: MORE COMPLEX SPIN-SPIN SPLITTING PATTERNS

OBJECTIVES

After completing this section, you should be able to

- explain how multiple coupling can give rise to complex-looking ^{1}H NMR spectra.
- predict the splitting pattern expected in the ^{1}H NMR spectrum of an organic compound in which multiple coupling is possible.
- interpret ^{1}H NMR spectra in which multiple coupling is evident.

KEY TERMS

Make certain that you can define, and use in context, the key term below.

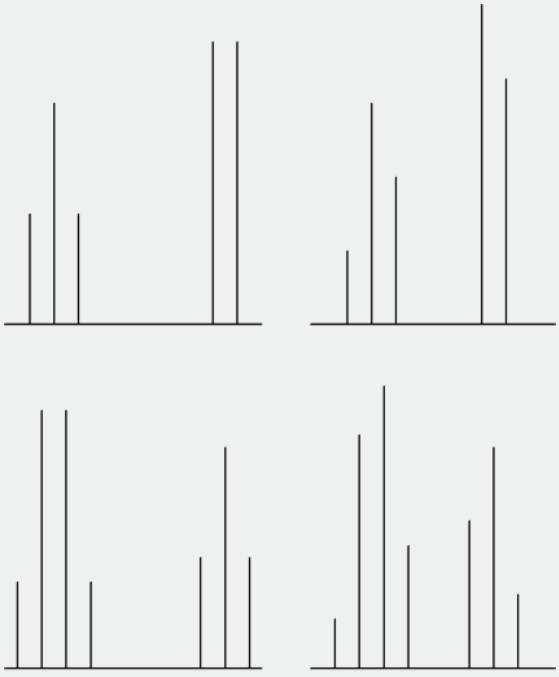
- tree diagram

STUDY NOTES

We saw the effects of spin-spin coupling on the appearance of a ^{1}H NMR signal. These effects can be further complicated when that signal is coupled to several different protons. For example, $BrCH_2CH_2CH_2Cl$ would produce three signals. The hydrogens at C_1 and C_3 would each be triplets because of coupling to the two hydrogens on C_2. However, the hydrogen on C_2 "sees" two different sets of neighboring hydrogens, and would therefore produce a triplet of triplets.

Another effect that can complicate a spectrum is the "closeness" of signals. If signals accidently overlap they can be difficult to identify. In the example above, we expected a triplet of triplets. However, if the coupling is identical (or almost identical) between the hydrogens on C_2 and the hydrogens on both C_1 and C_3, one would observe a quintet in the ^{1}H NMR spectrum. [You can try this yourself by drawing a tree diagram of a triplet of triplets assuming, first, different coupling constants, and then, identical coupling constants.] Keep this point in mind when interpreting real ^{1}H NMR spectra.

Also, when multiplets are well separated, they form patterns. However, when multiplets approach each other in the spectrum they sometimes become distorted. Usually, the inner peaks become larger than the outer peaks. Note the following examples:



Aromatic ring protons quite commonly have overlapping signals and multiplet distortions. Sometimes you cannot distinguish between individual signals, and one or more messy multiplets often appear in the aromatic region.

It is much easier to rationalize the observed ^{1}H NMR spectrum of a known compound than it is to determine the structure of an unknown compound from its ^{1}H NMR spectrum. However, rationalizations can be a useful learning technique as you try to improve your proficiency in spectral interpretation. Remember that when a chemist tries to interpret the ^{1}H NMR spectrum of an unknown compound, he or she usually has additional information available to make the task easier. For example, the chemist will almost certainly have an infrared spectrum of the compound and possibly a mass spectrum too. Details of how the compound was synthesized may be available, together with some indication of its chemical properties, its physical properties, or both.

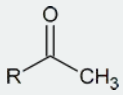
In examinations, you will be given a range of information (IR, MS, UV data and empirical formulae) to aid you with your structural determination using ^{1}H NMR spectroscopy. For example, you may be asked to determine the structure of $C_6H_{12}O$ given the following spectra:

Infrared spectrum: 3000 cm^{-1} and 1720 cm^{-1} absorptions are both strong

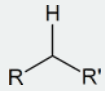
^{1}H NMR

δ (ppm)	Protons	Multiplicity
0.87	6	doublet
1.72	1	broad multiplet
2.00	3	singlet
2.18	2	doublet

To answer this question, you note that the infrared spectrum of $C_6H_{12}O$ shows $C-H$ stretching (3000 cm^{-1}) and $C-O$ stretching (1720 cm^{-1}). Now you have to piece together the information from the ^{1}H NMR spectrum. Notice the singlet with three protons at 2.00 ppm. This signal indicates a methyl group that is not coupled to other protons. It could possibly mean the presence of a methyl ketone functional group.



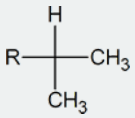
The signal at 1.72 ppm is a broad multiplet, suggesting that a carbon with a single proton is beside carbons with several different protons.



The doublet signal at 2.18 ppm implies that a $-CH_2^-$ group is attached to a carbon having only one proton.

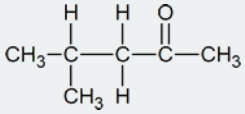


The six protons showing a doublet at 0.87 ppm indicate two equivalent methyl groups attached to a carbon with one proton.



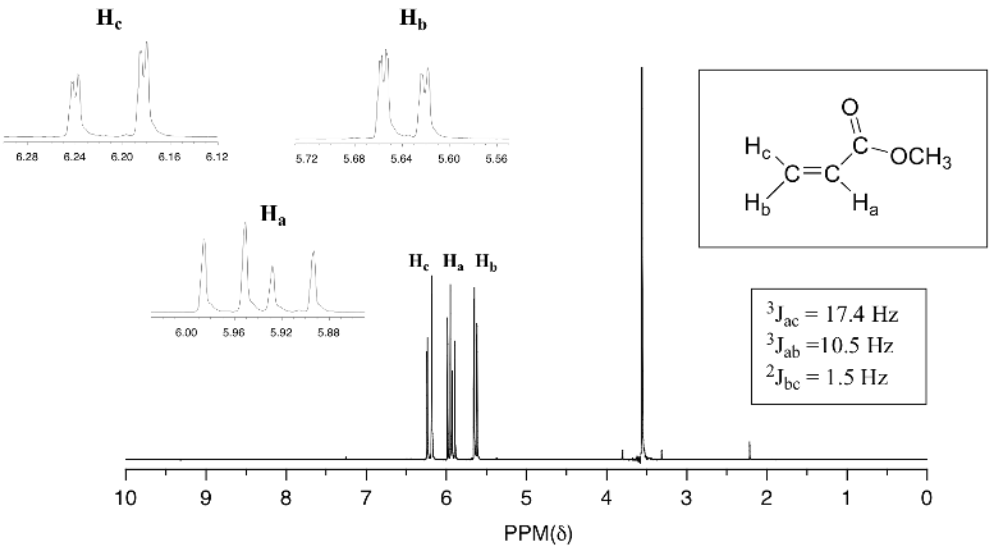
Whenever you see a signal in the 0.7-1.3 ppm range that is a multiplet of three protons (3, 6, 9) it is most likely caused by equivalent methyl groups.

Using trial and error, and with the above observations, you should come up with the correct structure.

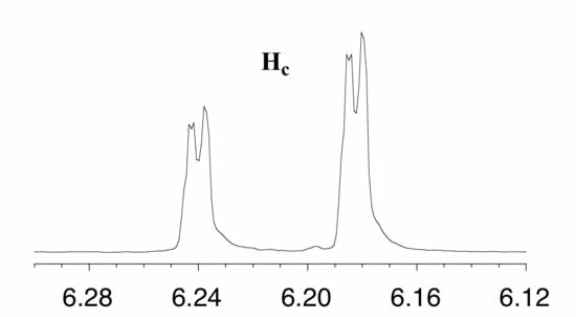


COMPLEX COUPLING

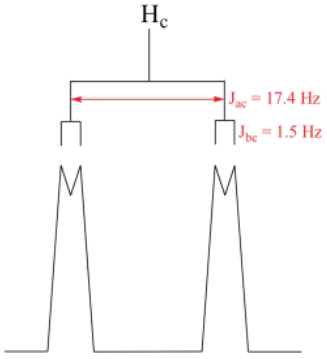
In all of the examples of spin-spin coupling that we have seen so far, the observed splitting has resulted from the coupling of one set of hydrogens to *just one* neighboring set of hydrogens. When a set of hydrogens is coupled to *two or more* sets of nonequivalent neighbors, the result is a phenomenon called **complex coupling**. A good illustration is provided by the ^{1}H-NMR spectrum of methyl acrylate:



First, let's first consider the H_c signal, which is centered at 6.21 ppm. Here is a closer look:

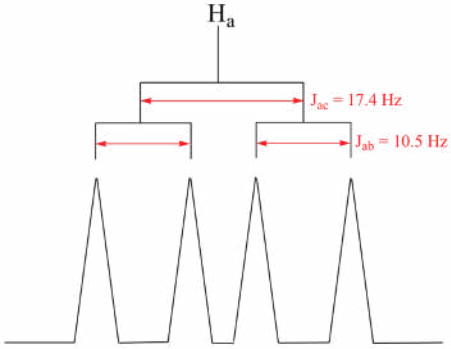


With this enlargement, it becomes evident that the Hc signal is actually composed of four sub-peaks. Why is this? H_c is coupled to both H_a and H_b , but with *two different coupling constants*. Once again, a splitting diagram (or tree diagram) can help us to understand what we are seeing. H_a is *trans* to H_c across the double bond, and splits the H_c signal into a doublet with a coupling constant of $^3J_{ac}$ = 17.4 Hz. In addition, each of these H_c doublet sub-peaks is split again by H_b (*geminal* coupling) into two more doublets, each with a much smaller coupling constant of $^2J_{bc}$ = 1.5 Hz.

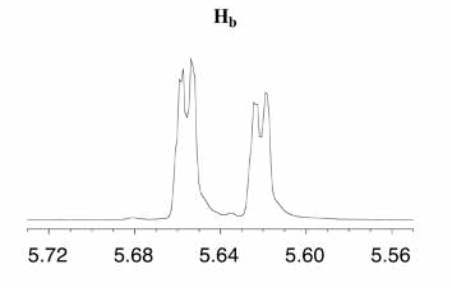


The result of this `double splitting` is a pattern referred to as a **doublet of doublets**, abbreviated `**dd**`.

The signal for H_a at 5.95 ppm is also a doublet of doublets, with coupling constants $^3J_{ac}$= 17.4 Hz and $^3J_{ab}$ = 10.5 Hz.



The signal for H_b at 5.64 ppm is split into a doublet by H_a, a *cis* coupling with $^3J_{ab}$ = 10.4 Hz. Each of the resulting sub-peaks is split again by H_c, with the same *geminal* coupling constant $^2J_{bc}$ = 1.5 Hz that we saw previously when we looked at the H_c signal. The overall result is again a doublet of doublets, this time with the two `sub-doublets` spaced slightly closer due to the smaller coupling constant for the *cis* interaction. Here is a blow-up of the actual $H_b$signal:



EXAMPLE 7.7.8.1

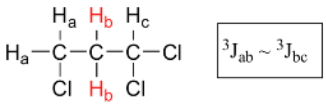
Construct a splitting diagram for the H_b signal in the ^{1}H-NMR spectrum of methyl acrylate. Show the chemical shift value for each sub-peak, expressed in Hz (assume that the resonance frequency of TMS is exactly 300 MHz).

Solution

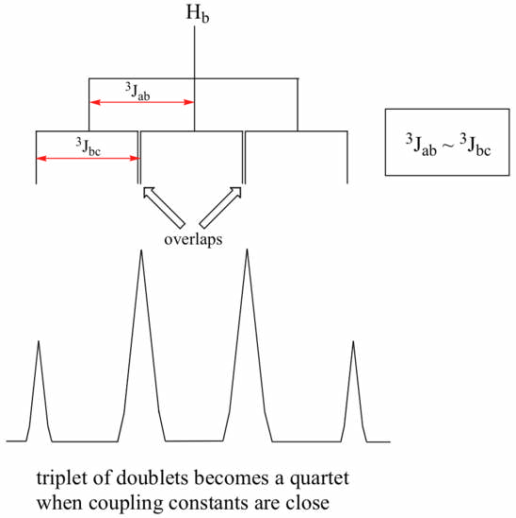
NOTE

When constructing a splitting diagram to analyze complex coupling patterns, it is usually easier to show the larger splitting first, followed by the finer splitting (although the reverse would give the same end result).

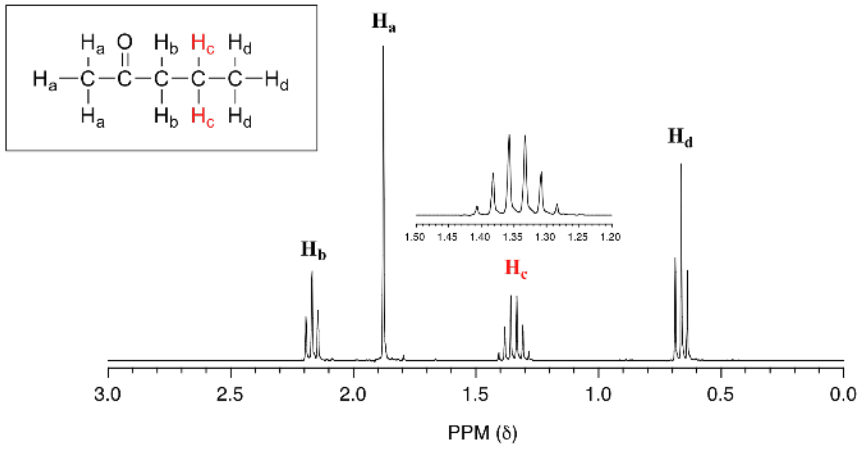
When a proton is coupled to two different neighboring proton sets with identical or very close coupling constants, the splitting pattern that emerges often appears to follow the simple `$n$ + 1 rule` of non-complex splitting. In the spectrum of 1,1,3-trichloropropane, for example, we would expect the signal for H_b to be split into a triplet by H_a, and again into doublets by H_c, resulting in a 'triplet of doublets'.



H_a and H_c are not equivalent (their chemical shifts are different), but it turns out that $^3J_{ab}$ is very close to $^3J_{bc}$. If we perform a splitting diagram analysis for H_b, we see that, due to the overlap of sub-peaks, the signal appears to be a quartet, and for all intents and purposes follows the n + 1 rule.

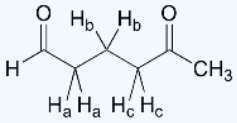


For similar reasons, the H_c peak in the spectrum of 2-pentanone appears as a sextet, split by the five combined H_b and H_d protons. Technically, this 'sextet' could be considered to be a 'triplet of quartets' with overlapping sub-peaks.



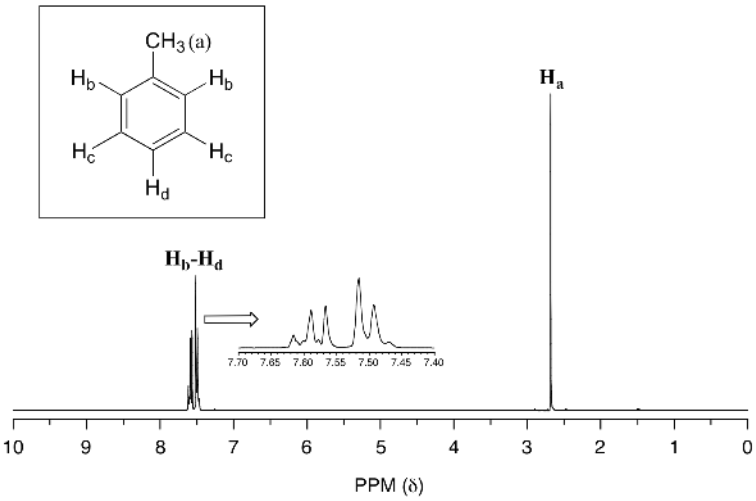
EXAMPLE 7.7.8.2

What splitting pattern would you expect for the signal corresponding to H_b in the molecule below? Assume that $J_{ab} \sim J_{bc}$. Draw a splitting diagram for this signal, and determine the relative integration values of each subpeak.



Solution

In many cases, it is difficult to fully analyze a complex splitting pattern. In the spectrum of toluene, for example, if we consider only 3-bond coupling we would expect the signal for H_b to be a doublet, H_d a triplet, and H_c a triplet.



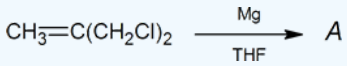
In practice, however, all three aromatic proton groups have very similar chemical shifts and their signals overlap substantially, making such detailed analysis difficult. In this case, we would refer to the aromatic part of the spectrum as a **multiplet**.

When we start trying to analyze complex splitting patterns in larger molecules, we gain an appreciation for why scientists are willing to pay large sums of money (hundreds of thousands of dollars) for higher-field NMR instruments. Quite simply, the stronger our magnet is, the more resolution we get in our spectrum. In a 100 MHz instrument (with a magnet of approximately 2.4 Tesla field strength), the 12 ppm frequency 'window' in which we can observe proton signals is 1200 Hz wide. In a 500 MHz (~12 Tesla) instrument, however, the window is 6000 Hz - five times wider. In this sense, NMR instruments are like digital cameras and HDTVs: better resolution means more information and clearer pictures (and higher price tags!)

? EXERCISE 7.7.8.1

Draw the structures of compound given the information.

An unknown compound *A* was prepared as follows:



Mass spectrum

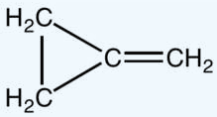
base peak *m*/*e* = 39

parent peak *m*/*e* = 54

^{1}H NMR spectrum

δ (ppm)	Relative Area	Multiplicity
1.0	2	triplet
5.4	1	quintet

Answer



? EXERCISE 7.7.8.2

Draw the structures of compound given the information.

Unknown compound *B* has the molecular formula $C_7H_6O_2$.

Infrared spectrum

3200 cm^{-1} (broad) and 1747 cm^{-1} (strong) absorptions

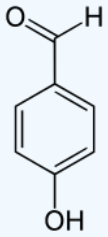
^{1}H NMR spectrum

https://chem.libretexts.org/@go/page/526823

δ (ppm)	Protons
6.9	2
7.4	2
9.8	1
10.9	1

Hint: Aromatic ring currents deshield all proton signals just outside the ring.

Answer



? EXERCISE 7.7.8.3

Draw the structures of compound given the information.

Unknown compound *C* shows no evidence of unsaturation and contains only carbon and hydrogen.

Mass spectrum

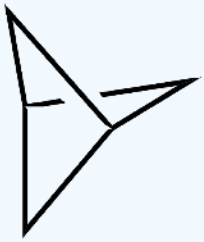
parent peak *m*/*e* = 68

^{1}H NMR spectrum

δ (ppm)	Relative Area	Multiplicity
1.84	3	triplet
2.45	1	septet

Hint: Think three dimensionally!

Answer



? EXERCISE 7.7.8.4

Draw the structures of compound given the information.

Unknown compound *D* ($C_{15}H_{14}O$) has the following spectral properties.

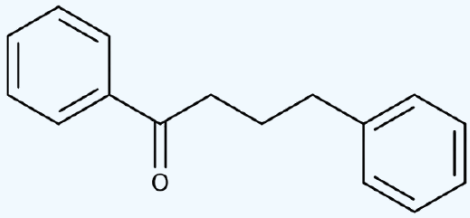
INFRARED SPECTRUM

3010 cm^{-1} (medium)
1715 cm^{-1} (strong)
1610 cm^{-1} (strong)
1500 cm^{-1} (strong)

^{1}H NMR spectrum

δ (ppm)	Relative Area	Multiplicity
3.00	2	triplet
3.07	2	triplet
7.1-7.9	10	Multiplets

Answer



This page titled 7.7.8: More Complex Spin-Spin Splitting Patterns is shared under a CC BY-SA 4.0 license and was authored, remixed, and/or curated by Steven Farmer, Dietmar Kennepohl, Tim Soderberg, & Tim Soderberg.

- **13.7: More Complex Spin-Spin Splitting Patterns** by Dietmar Kennepohl, Steven Farmer, Tim Soderberg is licensed CC BY-SA 4.0.

7.7.9: USES OF ^{1}H NMR SPECTROSCOPY

OBJECTIVE

After completing this section, you should be able to use data from ^{1}H NMR spectra to distinguish between two (or more) possible structures for an unknown organic compound.

There will be cases in which you already know what the structure might be. In these cases:

- You should draw attention to pieces of data that most strongly support your expected structure. This approach will demonstrate evaluative understanding of the data; that means you can look at data and decide what parts are more crucial than others.
- You should also draw attention to negative results: that is, peaks that might be there if this spectrum matched another, possible structure, but that are in fact missing.

One of the most complicated problems to deal with is the analysis of a mixture. This situation is not uncommon when students run reactions in lab and analyse the data.

- Sometimes the spectra show a little starting material mixed in with the product.
- Sometimes solvents show up in the spectrum.
- As you might expect, the minor component usually shows up as smaller peaks in the spectrum. If there are fewer molecules present, then there are usually fewer protons to absorb in the spectrum.
- In this case, you should probably make two completely separate sets of data tables for your analysis, one for each compound, or else one for the main compound and one for impurities.

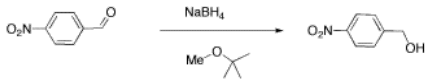
Remember that integration ratios are really only meaningful within a single compound. If your NMR sample contains some benzene (C_6H_6) and some acetone (CH_3COCH_3), and there is a peak at 7.15 that integrates to 1 proton and a peak at 2.10 ppm integrating to 6 protons, it might mean there are 6 protons in acetone and 1 in benzene, but you can tell that isn't true by looking at the structure. There must be six times as many acetone molecules as benzene molecules in the sample.

There are six protons in the benzene, and they should all show up near 7 ppm. There are six protons in acetone, and they should all show up near 2 ppm. Assuming that small integral of 1H for the benzene is really supposed to be 6H, then the large integral of 6H for the acetone must also represent six times as many hydrogens, too. It would be 36 H. There are only six hydrogens in acetone, so it must represent six times as many acetone molecules as there are benzenes.

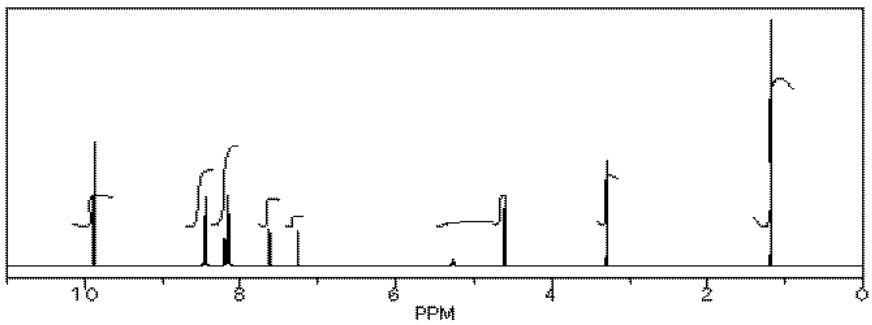
Similarly, if you have decided that you can identify two sets of peaks in the ^{1}H spectrum, analysing them in different tables makes it easy to keep the integration analysis completely separate too ; 1 H in one table will not be the same size integral as 1 H in the other table unless the concentrations of the two compounds in the sample are the same.

However, comparing the ratio of two integrals for two different compounds can give you the ratio of the two compounds in solution, just as we could determine the ratio of benzene to acetone in the mixture described above.

We will look at two examples of sample mixtures that could arise in lab. Results like these are pretty common events in the labIn the first example, a student tried to carry out the following reaction, a borohydride reduction of an aldehyde. The borohydride should give a hydride anion to the C=O carbon; washing with water should then supply a proton to the oxygen, giving an alcohol.

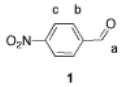
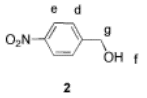
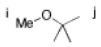


Her reaction produced the following spectrum.



(simulated data)

From this data, she produced the table below.

	shift	integration	int(n)	internal ratio	multiplicity	part structure	assignment
a	9.9 ppm	11 mm	2H	1H	singlet		
b	8.5 ppm	23 mm	4H	2H	doublet		 1
c	8.1 ppm	(20 mm?)	4H	2H	doublet		
d	8.2 ppm	(10 mm?)	2H	2H	doublet		
e	7.6 ppm	9 mm	2H	2H	doublet		 2
f	5.3 ppm	2 mm	0.4H	<1H	singlet	OH	
g	4.7 ppm	12 mm	2H	2H	singlet		
h	7.2 ppm	4 mm	0.8H	1H	singlet	$CHCl_3$	
i	3.3 ppm	8 mm	1.5H	3H	singlet		
j	1.2 ppm	24 mm	4.5H	9H	singlet		
			23.4H total				

Ratio of reactant **1** to product **2** is 2:1 based on peaks at 9.9 and 4.7 ppm (2H / 1H) : (2H / 2H); the reaction is 33% complete [2 / (2+1)]

Ratio of product **2** to TBME is 2:1 based on peaks at 4.7 and 3.3 ppm (2H / 2H) : (1.5H / 3H); the ratio of **1**:**2**:TBME is 2:1:0.5, so the sample is 57% **1** [2/(2+1+0.5)], 29% **2** and 14% TBME.

Notice how she calculated that ratio. She found a peak in molecule 1, the aldehyde, that she was pretty sure corresponded to the aldehydic hydrogen, the H attached to the C=O; in other words, the CH=O. She found another peak from molecule 2, the alcohol, that she was pretty sure represented the two hydrogens on the carbon attached to oxygen, the CH_2-O.

The integrals for those two peaks are equal. They are both 2H in her table. However, she notes that within each molecule, the first integral really represents 1H and the second represents 2H. That means there must be twice as many of molecule 1 as there are molecule 2. That way, there would be 2 x CH=O, and its integral would be the same as the 1 x CH_2-O in the other molecule.

One way to approach this kind of problem is to:

- choose one peak from each of the two compounds you want to compare.
- decide how many hydrogens each peak is supposed to represent in a molecule. Is it supposed to be a CH_2, a CH, a CH_3?
- divide the integral value for that peak by that number of hydrogens it is supposed to represent in a molecule.
- compare the two answers (integral A / ideal # H) vs (integral B / ideal # H).
- the ratio of those two answers is the ratio of the two molecules in the sample.

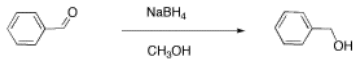
So there is twice as much aldehyde as alcohol in the mixture. In terms of these two compounds alone, she has 33% alcohol and 66% aldehyde. That's (1/(1+2)) x100% for the alcohol, and (2/(1+2)) x100% for the aldehyde. That calculation just represents the amount of individual component divided by the total of the components she wants to compare.

There are a number of things to take note of here.

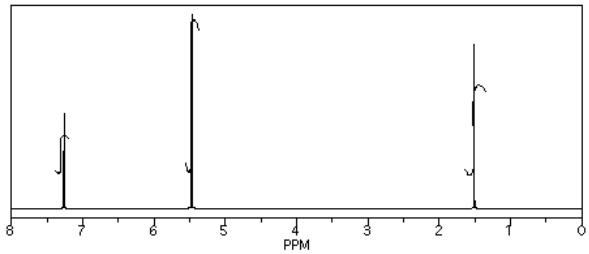
- Her reaction really didn't work very well. She still has majority starting material, not product.
- She will get a good grade on this lab. Although the experiment didn't work well, she has good data, and she has analyzed it very clearly.
- She has separated her data table into different sections for different compounds. Sometimes that makes it easier to analyze things.
- She has noted the actual integral data (she may have measured the integral with a ruler) and also converted it into a more convenient ratio, based on the integral for a peak that she felt certain about.
- She went one step further, and indicated the internal integration ratio within each individual compound.
- She calculated the % completion of the reaction using the integral data for the reactant and product, and she made clear what part of the data she used for that calculation. A similar procedure could be done if a student were just trying to separate two components in a mixture rather than carry out a reaction.
- She also calculated the overall purity of the mixture, including a solvent impurity that she failed to remove.

- However, $CHCl_3$ is not included in her analysis of purity. $CHCl_3$ really isn't part of her sample; it was just present in the NMR solvent, so it doesn't represent anything in the material she ended up with at the end of lab.

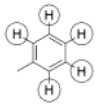
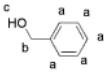
Another student carried out a similar reaction, shown below. He also finished the reaction by washing with water, but because methanol is soluble in water, he had to extract his product out of the water. He chose to use dichloromethane for that purpose.



He obtained the following data.



From this data, he constructed the following table.

	shift	integration	int(n)	multiplicity	partial structure	assignment
a	7.3 ppm	16 mm	5H	singlet		
b	5.4 ppm	64 mm	2H	singlet		
c	1.6 ppm	37 mm	1H	singlet	OH	

There are some things to learn about this table, too.

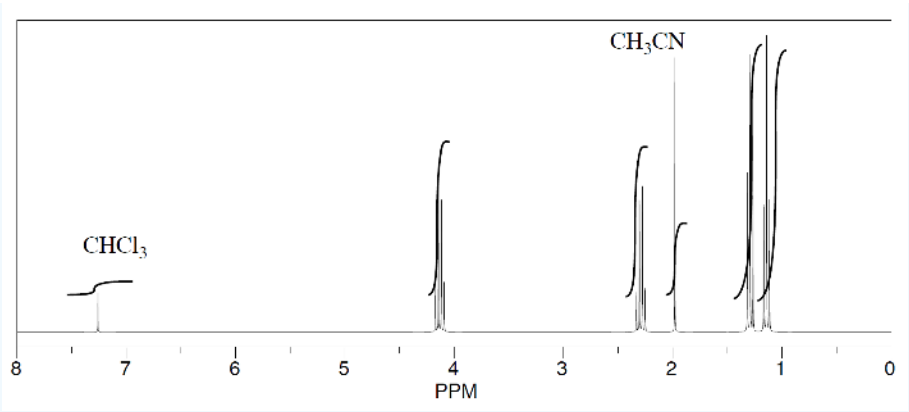
- Does the integration ratio really match the integral data? Or is this just wishful thinking?
- This table might reflect what he wants to see in the data. But what else could be in the data?
- $CHCl_3$ is often seen in NMR spectra if $CDCl_3$ is used for the NMR sample. It's there, at 7.2 ppm.
- "Leftover" or residual solvent is very common in real lab data. There it is, CH_2Cl_2 from the extraction, at 5.4 ppm.
- What about water? Sometimes people don't dry their solutions properly before evaporating the solvent. There is probably water around 1.5 to 1.6 ppm here.

This student might not get a very good grade; the sample does not even show up in the spectrum, so he lost it somewhere. But his analysis is also poor, so he will really get a terrible grade.

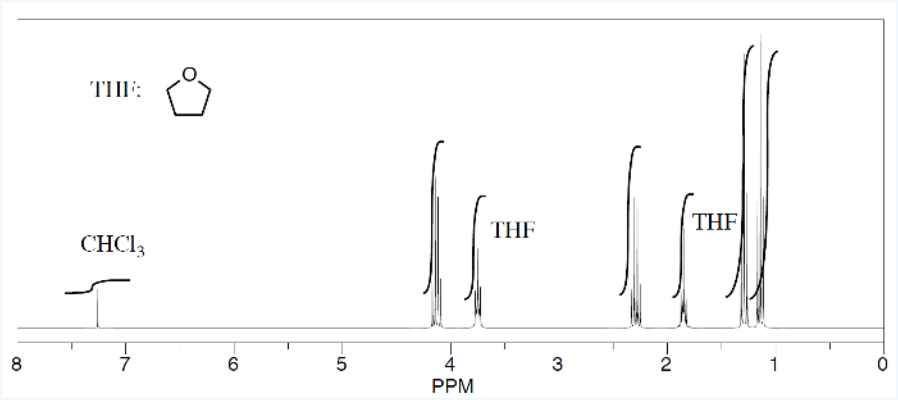
EXAMPLE 7.7.9.1

Three students performed a synthesis of a fragrant ester, ethyl propanoate, $CH_3CH_2CO_2CH_2CH_3$. During their reactions, they each used a different solvent. The students were able to see peaks in the NMR spectrum for ethyl propanoate, as well as peaks for chloroform ($CHCl_3$, in the $CDCl_3$ they used to make their NMR samples).

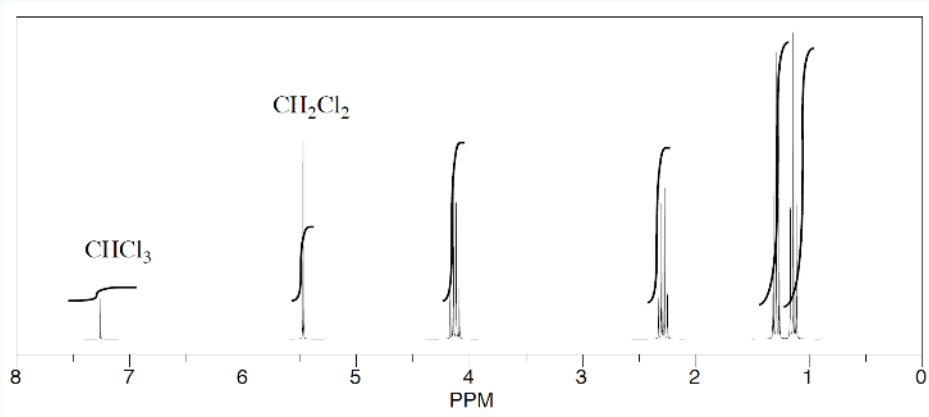
First student's spectrum:



Second student's spectrum:



Third student's spectrum:

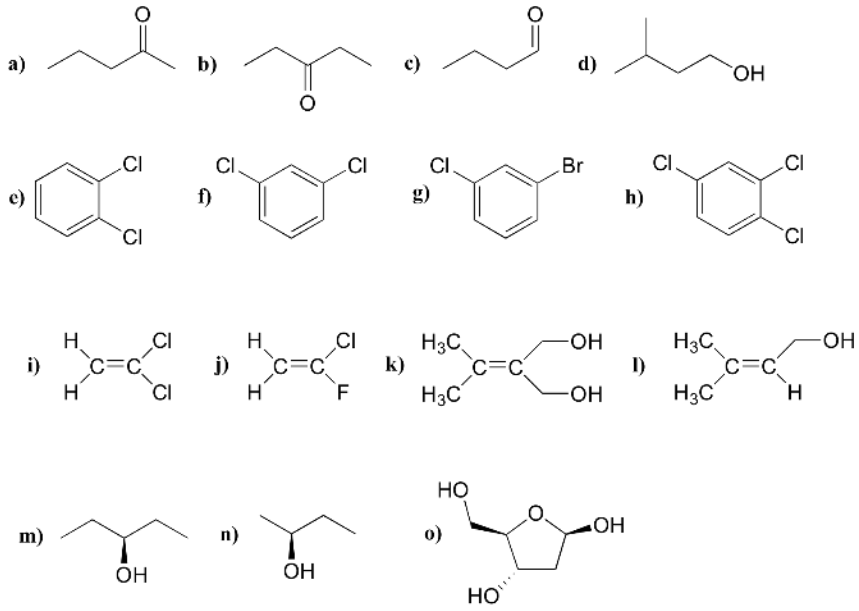


They were also able to determine that they had some leftover solvent in their samples by consulting a useful table of solvent impurities in NMR (which they found in Goldberg et. al., Organometallics 2010, 29, 2176-2179).

1. What is the ratio of leftover solvent to ethyl propanoate in each sample?
2. What is the percent of each sample that is leftover solvent

ADDITIONAL NMR EXAMPLES

For each molecule, predict the number of signals in the ^{1}H-NMR and the ^{13}C-NMR spectra (do not count split peaks - eg. a quartet counts as only one signal). Assume that diastereotopic groups are non-equivalent.

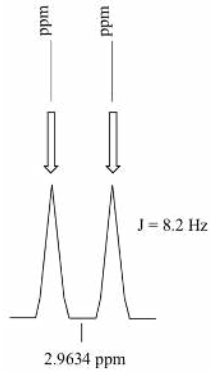


P5.2: For each of the 20 common amino acids, predict the number of signals in the proton-decoupled ^{13}C-NMR spectrum.

P5.3: Calculate the chemical shift value (expressed in Hz, to one decimal place) of each sub-peak on the ^{1}H-NMR doublet signal below. Do this for:

a) a spectrum obtained on a 300 MHz instrument

b) a spectrum obtained on a 100 MHz instrument

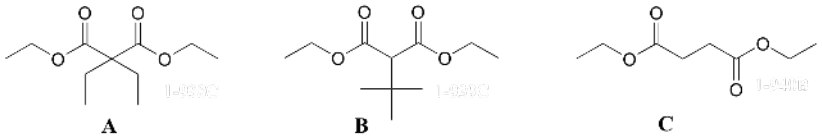


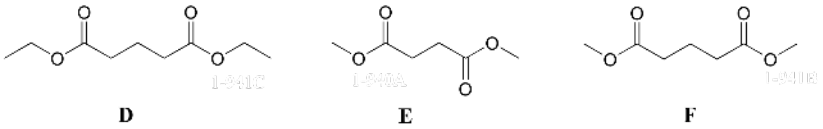
P5.4: Consider a quartet signal in an ^{1}H-NMR spectrum obtained on a 300 MHz instrument. The chemical shift is recorded as 1.7562 ppm, and the coupling constant is J = 7.6 Hz. What is the chemical shift, expressed to the nearest 0.1 Hz, of the furthest downfield sub-peak in the quartet? What is the resonance frequency (again expressed in Hz) of this sub-peak?)

P5.5: One easily recognizable splitting pattern for the aromatic proton signals from disubstituted benzene structures is a pair of doublets. Does this pattern indicate *ortho*, *meta*, or *para* substitution?

P5.6 : Match spectra below to their corresponding structures A-F.

Structures:





Spectrum 1

δ	splitting	integration
4.13	q	2
2.45	t	2
1.94	quintet	1
1.27	t	3

Spectrum 2

δ	splitting	integration
3.68	s	3
2.99	t	2
1.95	quintet	1

Spectrum 3

δ	splitting	integration
4.14	q	1
2.62	s	1
1.26	t	1.5

Spectrum 4

δ	splitting	integration
4.14	q	4
3.22	s	1
1.27	t	6
1.13	s	9

Spectrum 5

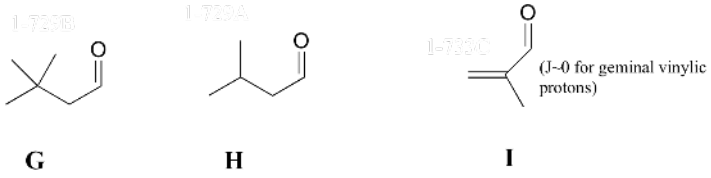
δ	splitting	integration
4.18	q	1
1.92	q	1
1.23	t	1.5
0.81	t	1.5

Spectrum 6

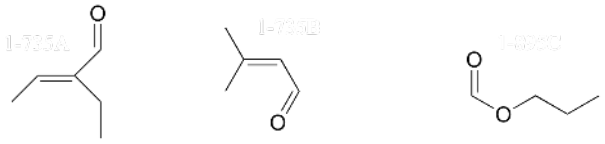
δ	splitting	integration
3.69	s	1.5
2.63	s	1

P5.7: Match spectra 7-12 below to their corresponding structures G-L .

Structures:



G H I



J K L

Spectrum 7:

δ	splitting	integration
9.96	d	1
5.88	d	1
2.17	s	3
1.98	s	3

Spectrum 8:

δ	splitting	integration
9.36	s	1
6.55	q	1
2.26	q	2
1.99	d	3
0.96	t	3

Spectrum 9:

δ	splitting	integration
9.57	s	1
6.30	s	1
6.00	s	1
1.84	s	3

Spectrum 10:

δ	splitting	integration
9.83	t	1
2.27	d	2
1.07	s	9

Spectrum 11:

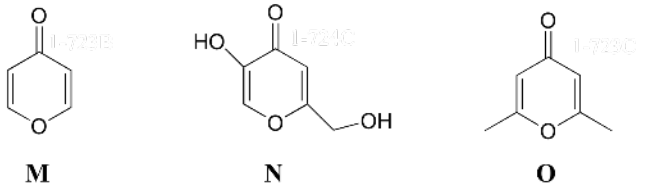
δ	splitting	integration
9.75	t	1
2.30	dd	2
2.21	m	1
0.98	d	6

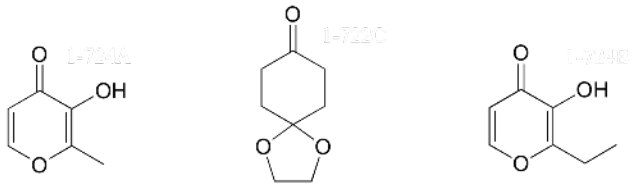
Spectrum 12:

δ	splitting	integration
8.08	s	1
4.13	t	2
1.70	m	2
0.96	t	3

P5.8: Match the ^{1}H-NMR spectra 13-18 below to their corresponding structures M-R .

Structures:





Spectrum 13:

δ	splitting	integration
8.15	d	1
6.33	d	1

Spectrum 14: 1-723C (structure O)

δ	splitting	integration
6.05	s	1
2.24	s	3

Spectrum 15:

δ	splitting	integration
8.57	s (b)	1
7.89	d	1
6.30	d	1
2.28	s	3

Spectrum 16:

δ	splitting	integration
9.05	s (b)	1
8.03	s	1
6.34	s	1
5.68	s (b)	1
4.31	s	2

Spectrum 17:

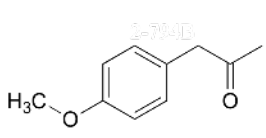
δ	splitting	integration
7.76	d	1
7.57	s (b)	1
6.44	d	1
2.78	q	2
1.25	t	3

Spectrum 18:

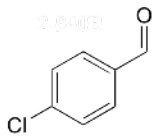
δ	splitting	integration
4.03	s	1
2.51	t	1
2.02	t	1

P5.9: Match the ^{1}H-NMR spectra 19-24 below to their corresponding structures S-X.

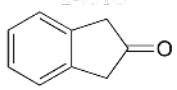
Structures:



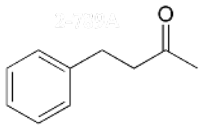
S



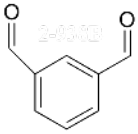
T



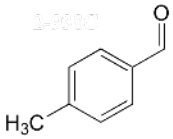
U



V



W



X

Spectrum 19:

δ	splitting	integration
9.94	s	1
7.77	d	2
7.31	d	2
2.43	s	3

Spectrum 20:

δ	splitting	integration
10.14	s	2
8.38	s	1
8.17	d	2
7.75	t	1

Spectrum 21:

δ	splitting	integration
9.98	s	1
7.81	d	2
7.50	d	2

Spectrum 22:

δ	splitting	integration
7.15-7.29	m	2.5
2.86	t	1
2.73	t	1
2.12	s	1.5

Spectrum 23:

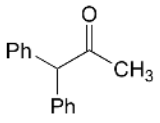
δ	splitting	integration
7.10	d	1
6.86	d	1
3.78	s	1.5
3.61	s	1
2.12	s	1.5

Spectrum 24:

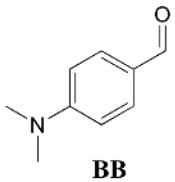
δ	splitting	integration
7.23-7.30	m	1
3.53	s	1

P5.10: Match the ^{1}H-NMR spectra 25-30 below to their corresponding structures AA-FF.

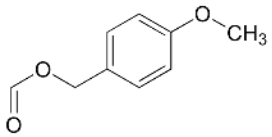
Structures:



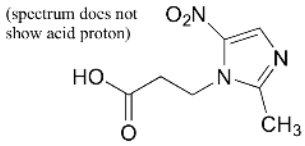
AA



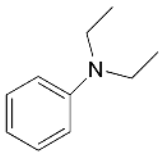
BB



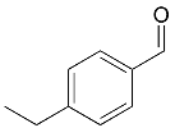
CC



DD



EE



FF

Spectrum 25:

δ	splitting	integration
9.96	s	1
7.79	d	2
7.33	d	2
2.72	q	2
1.24	t	3

Spectrum 26:

δ	splitting	integration
9.73	s	1
7.71	d	2
6.68	d	2
3.06	s	6

Spectrum 27:

δ	splitting	integration
7.20-7.35	m	10
5.12	s	1
2.22	s	3

Spectrum 28:

δ	splitting	integration
8.08	s	1
7.29	d	2
6.87	d	2
5.11	s	2
3.78	s	3

Spectrum 29:

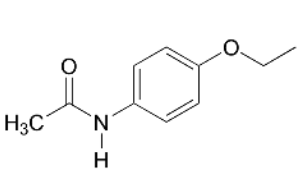
δ	splitting	integration
7.18	d	1
6.65	m	1.5
3.2	q	2
1.13	t	3

Spectrum 30:

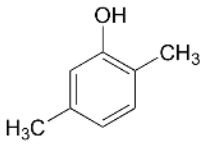
δ	splitting	integration
8.32	s	1
4.19	t	2
2.83	t	2
2.40	s	3

P5.11: Match the ^{1}H-NMR spectra 31-36 below to their corresponding structures GG-LL

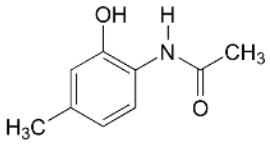
Structures:



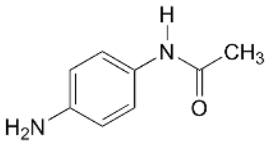
GG



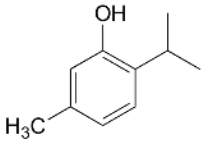
HH



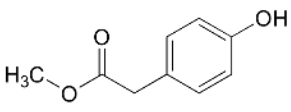
II



JJ



KK



LL

Spectrum 31:

δ	splitting	integration
6.98	d	1
6.64	d	1
6.54	s	1
4.95	s	1
2.23	s	3
2.17	s	3

Spectrum 32:

δ	splitting	integration
7.08	d	1
6.72	d	1
6.53	s	1
4.81	s	1
3.15	7-tet	1
2.24	s	3
1.22	d	6

Spectrum 33:

δ	splitting	integration
7.08	d	2
6.71	d	2
6.54	s	1
3.69	s	3
3.54	s	2

Spectrum 34:

δ	splitting	integration
9.63	s	1
7.45	d	2
6.77	d	2
3.95	q	2
2.05	s	3
1.33	t	3

Spectrum 35:

δ	splitting	integration
9.49	s	1
7.20	d	2
6.49	d	2
4.82	s	2
1.963	s	3

Spectrum 36:

δ	splitting	integration
9.58	s(b)	1
9.31	s	1
7.36	d	1
6.67	s	1
6.55	d	1
2.21	s	3
2.11	s	3

P5.12: Use the NMR data given to deduce structures.

a) Molecular formula: C_5H_8O

^{1}H-NMR:

δ	splitting	integration
9.56	s	1
6.25	d (J~1 Hz)	1
5.99	d (J~1 Hz)	1
2.27	q	2
1.18	t	3

^{13}C-NMR

δ	DEPT
194.60	CH
151.77	C
132.99	CH_2
20.91	CH_2
11.92	CH_3

b) Molecular formula: $C_7H_{14}O_2$

^{1}H-NMR:

δ	splitting	integration
3.85	d	2
2.32	q	2
1.93	m	1
1.14	t	3
0.94	d	6

^{13}C-NMR

δ	DEPT
174.47	C
70.41	CH_2
27.77	CH
27.64	CH_2
19.09	CH_3
9.21	CH_3

c) Molecular formula: $C_5H_{12}O$

^{1}H-NMR:

δ	splitting	integration
3.38	s	2H
2.17	s	1H
0.91	s	9H

^{13}C-NMR

δ	DEPT
73.35	CH_2
32.61	C
26.04	CH_3

d) Molecular formula: $C_{10}H_{12}O$

^{1}H-NMR:

δ	splitting	integration
7.18-7.35	m	2.5
3.66	s	1
2.44	q	1
1.01	t	1.5

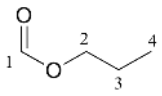
^{13}C-NMR

δ	DEPT
208.79	C
134.43	C
129.31	CH
128.61	CH
126.86	CH
49.77	CH_2
35.16	CH_2
7.75	CH_3

P5.13:

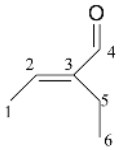
^{13}C-NMR data is given for the molecules shown below. Complete the peak assignment column of each NMR data table.

a)



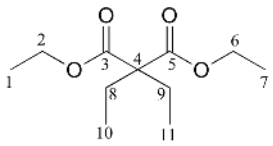
δ	DEPT	carbon #
161.12	CH	
65.54	CH_2	
21.98	CH_2	
10.31	CH_3	

b)



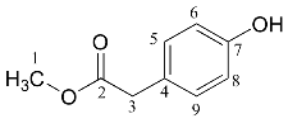
δ	DEPT	carbon #
194.72	C	
149.10	C	
146.33	CH	
16.93	CH_2	
14.47	CH_3	
12.93	CH_3	

c)



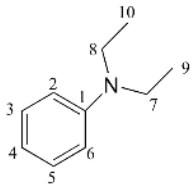
δ	DEPT	carbon #
171.76	C	
60.87	CH_2	
58.36	C	
24.66	CH_2	
14.14	CH_3	
8.35	CH_3	

d)



δ	DEPT	carbon #
173.45	C	
155.01	C	
130.34	CH	
125.34	C	
115.56	CH	
52.27	CH_3	
40.27	CH_2	

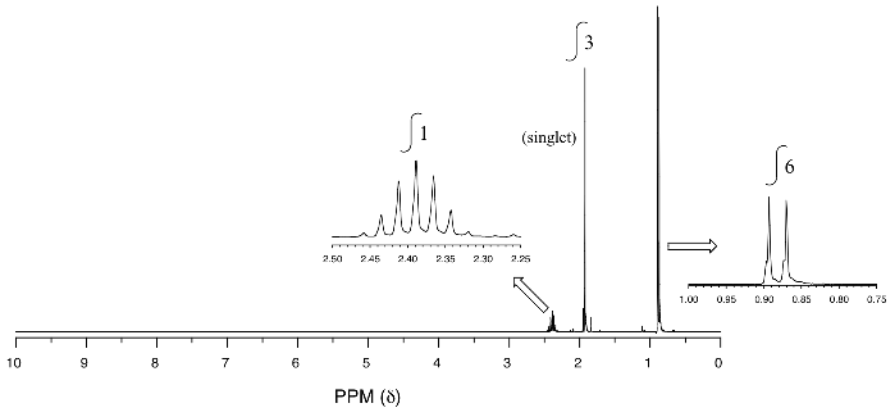
e)



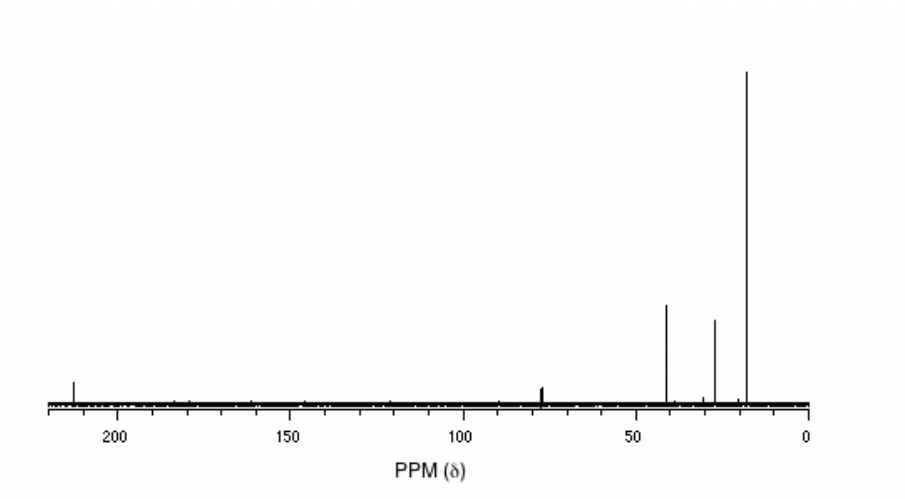
δ	DEPT	carbon #
147.79	C	
129.18	CH	
115.36	CH	
111.89	CH	
44.29	CH_2	
12.57	CH_3	

P5.14: You obtain the following data for an unknown sample. Deduce its structure.

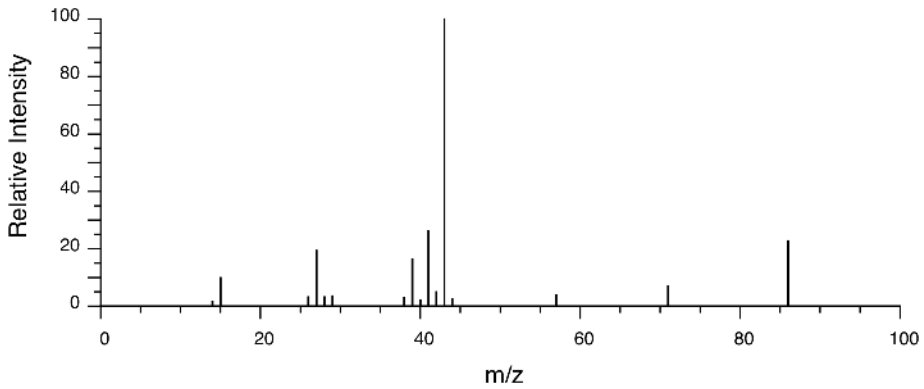
^{1}H-NMR:



^{13}C-NMR:



Mass Spectrometry:



P5.15: You take a ^{1}H-NMR spectrum of a sample that comes from a bottle of 1-bromopropane. However, you suspect that the bottle might be contaminated with 2-bromopropane. The NMR spectrum shows the following peaks:

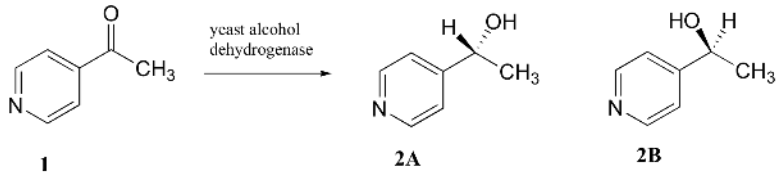
δ	splitting	integration
4.3	septet	0.0735
3.4	triplet	0.661
1.9	sextet	0.665
1.7	doublet	0.441
1.0	triplet	1.00

How badly is the bottle contaminated? Specifically, what percent of the molecules in the bottle are 2-bromopropane?

Challenge problems

C5.1: All of the ^{13}C-NMR spectra shown in this chapter include a signal due to $CDCl_3$, the solvent used in each case. Explain the splitting pattern for this signal.

C5.2: Researchers wanted to investigate a reaction which can be catalyzed by the enzyme alcohol dehydrogenase in yeast. They treated 4'-acylpyridine (1) with living yeast, and isolated the alcohol product(s) (some combination of 2A and 2B).

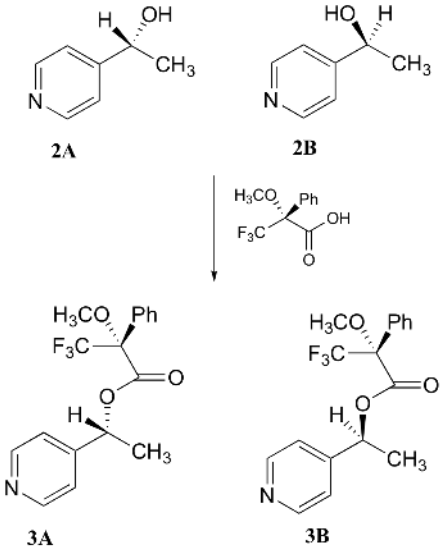


1 **2A** **2B**

a) Will the products 2A and 2B have identical or different ^{1}H-NMR spectra? Explain.

b) Suggest a ^{1}H-NMR experiment that could be used to determine what percent of starting material (1) got turned into product (2A and 2B).

c) With purified 2A/2B, the researchers carried out the subsequent reaction shown below to make 3A and 3B, known as 'Mosher's esters'. Do 3A and 3B have identical or different ^{1}H-NMR spectra? Explain.



2A **2B**

3A **3B**

d) Explain, very specifically, how the researchers could use ^{1}H-NMR to determine the relative amounts of 2A and 2B formed in the reaction catalyzed by yeast enzyme.

This page titled 7.7.9: Uses of ^{1}H NMR Spectroscopy is shared under a CC BY-SA 4.0 license and was authored, remixed, and/or curated by Chris Schaller, Steven Farmer, Dietmar Kennepohl, Tim Soderberg, & Tim Soderberg.

- **13.8: Uses of ^{1}H NMR Spectroscopy** by Chris Schaller, Dietmar Kennepohl, Steven Farmer, Tim Soderberg is licensed CC BY-SA 4.0.

7.7.10: ^{13}C NMR SPECTROSCOPY - SIGNAL AVERAGING AND FT-NMR

OBJECTIVES

After completing this section, you should be able to

- Understand why the nuclei C NMR looks at is ^{13}C and not ^{12}C.
- Know why more scans are needed in ^{13}C NMR than ^{1}H NMR.

Most of what we have learned about ^{1}H-NMR spectroscopy also applies to ^{13}C-NMR, although there are several important differences.

SIGNAL STRENGTH IN ^{13}C-NMR SPECTROSCOPY

The ^{12}C isotope of carbon - which accounts for more than 98% of the carbons in organic molecules - does not have a nuclear magnetic moment, and thus is NMR-inactive. Fortunately for organic chemists, however, the ^{13}C isotope, which accounts for 1.1% of the remaining carbon atoms in nature, has a magnetic moment just like protons.

The magnetic moment of a ^{13}C nucleus is much weaker than that of a proton, meaning that NMR signals from ^{13}C nuclei are inherently much weaker than proton signals. This, combined with the low natural abundance of ^{13}C, means that it is much more difficult to observe carbon signals and there is a much lower signal-to-noise ratio than in ^{1}H NMR. Therefore, more concentrated samples are required to generate a useful spectrum, and often the data from hundreds of scans must be averaged in order to bring the signal-to-noise ratio down to acceptable levels. This type of **signal averaging** works since background noise in a spectrum is typically random while the signal caused by the ^{13}C nuclei is not. Therefore if the spectra from multiple scans is averaged, the noise gets closer to 0 while the signal stays the same, increasing the signal-to-noise ratio.

FOURIER TRANSFORM (FT) NMR

Earlier versions of NMR instruments used variable magnetic fields which required recording of each signal in the spectrum sequentially which is called continuous wave (CW) NMR. The **Fourier Transform** allows recording of all signals simultaneously by introducing a short pulse of all RF frequencies that cause resonance for a given nucleus. This complex signal is then manipulated through complex mathematical processing that creates an NMR spectrum that looks similar to a CW spectrum, but in much less time.

This page titled 7.7.10: ^{13}C NMR Spectroscopy - Signal Averaging and FT-NMR is shared under a CC BY-SA 4.0 license and was authored, remixed, and/or curated by Chris Schaller, Steven Farmer, Layne Morsch, Lauren Reutenauer, & Lauren Reutenauer.

- **13.9: ^{13}C NMR Spectroscopy - Signal Averaging and FT-NMR** by Chris Schaller, Lauren Reutenauer, Layne Morsch, Steven Farmer is licensed CC BY-SA 4.0.

7.7.11: CHARACTERISTICS OF ^{13}C NMR SPECTROSCOPY

OBJECTIVES

After completing this section, you should be able to

- Determine the number of distinct C atoms in a molecule.
- Use the chemical shifts table to determine functional groups present in a molecule.
- Assign a chemical shift to each carbon in a given molecule.

THE BASICS OF ^{13}C-NMR SPECTROSCOPY

Unlike ^{1}H-NMR signals, the area under a ^{13}C-NMR signal cannot be used to determine the number of carbons to which it corresponds. This is because the signals for some types of carbons are inherently weaker than for other types – peaks corresponding to carbonyl carbons, for example, are much smaller than those for methyl or methylene (CH_2) peaks. Peak integration is generally not useful in ^{13}C-NMR spectroscopy, except when investigating molecules that have been enriched with ^{13}C isotope.

The resonance frequencies of ^{13}C nuclei are lower than those of protons in the same applied field - in a 7.05 Tesla instrument, protons resonate at about 300 MHz, while carbons resonate at about 75 MHz. This is fortunate, as it allows us to look at ^{13}C signals using a completely separate 'window' of radio frequencies. This means you will only see the ^{13}C nuclei in a ^{13}C NMR experiment like in the ^{1}H NMR experiments we just looked at, we only saw hydrogens. Just like in ^{1}H-NMR, the standard used in ^{13}C-NMR experiments to define the 0 ppm point is tetramethylsilane (TMS), although of course in ^{13}C-NMR it is the signal from the four equivalent *carbons* in TMS that serves as the standard. Chemical shifts for ^{13}C nuclei in organic molecules are spread out over a much wider range than for protons – up to 200 ppm for ^{13}C compared to 12 ppm for protons (see Table 3 for a list of typical ^{13}C-NMR chemical shifts). This is also fortunate, because it means that the signal from each carbon in a compound can almost always be seen as a distinct peak, without the overlapping that often plagues ^{1}H-NMR spectra. The chemical shift of a ^{13}C nucleus is influenced by essentially the same factors that influence a proton's chemical shift: bonds to electronegative atoms and diamagnetic anisotropy effects tend to shift signals downfield (higher resonance frequency). In addition, sp^2 hybridization results in a large downfield shift. The ^{13}C-NMR signals for carbonyl carbons are generally the furthest downfield (170-220 ppm), due to both sp^2 hybridization and to the double bond to oxygen.

EXAMPLE 7.7.11.1

a. How many sets of non-equivalent carbons are there in each of the molecules shown in exercise 5.1?
b. How many sets of non-equivalent carbons are there in:

- toluene
- 2-pentanone
- para-xylene
- triclosan

(all structures are shown earlier in this chapter)

Solution

a

a) 8 signals (each carbon is different)

b) 11 signals (the two enantiotopic CH_2CH_3 groups are NMR-equivalent)

c) 6 signals (each carbon is different)

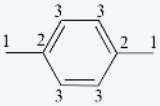
d) 16 signals (the fluorobenzene group only contributes 4 signals due to symmetry)

b

a) 5 signals

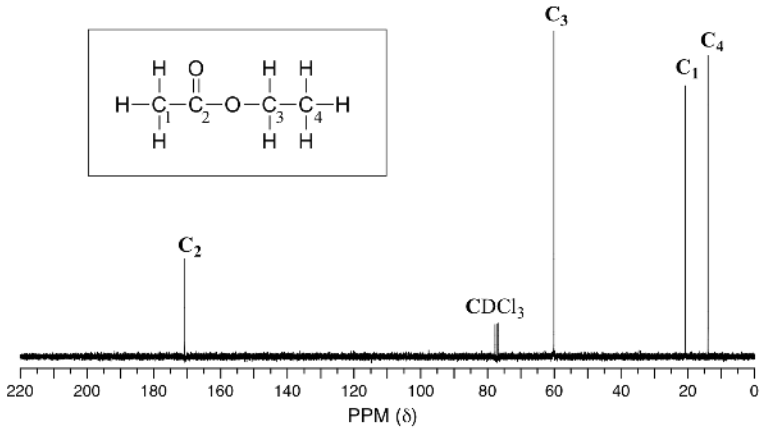
b) 5 signals

c) 3 signals

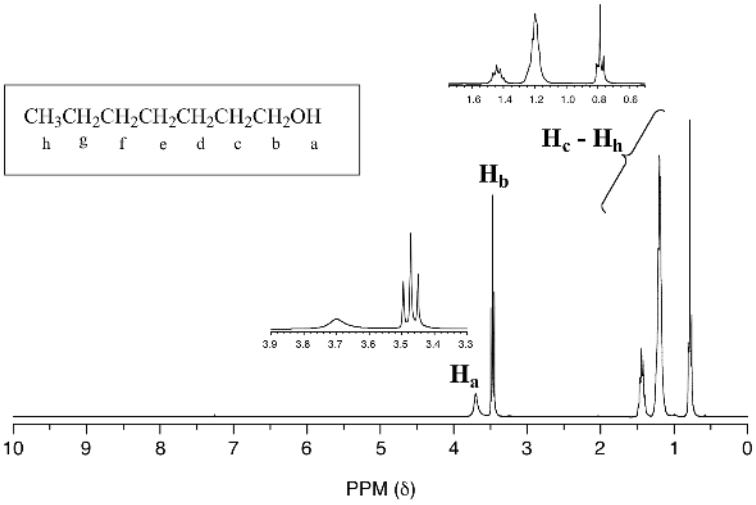


d) 6 signals

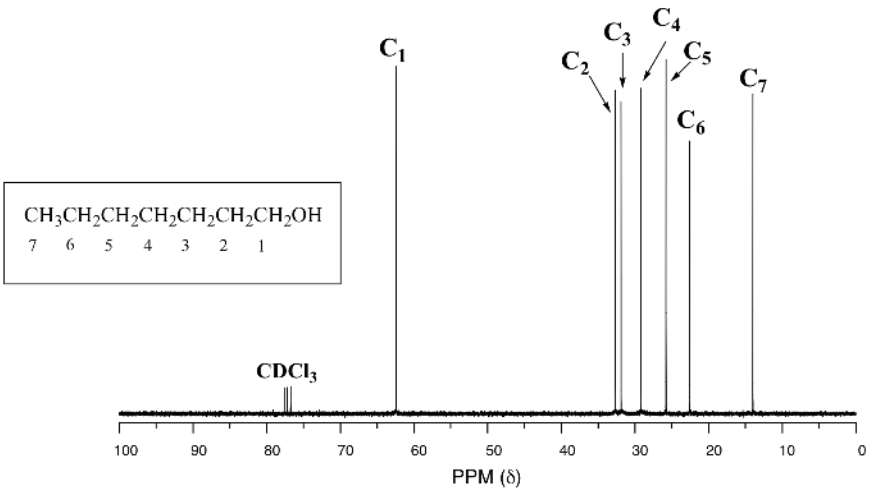
Because of the low natural abundance of ^{13}C nuclei, it is very unlikely to find two ^{13}C atoms near each other in the same molecule, and thus *we do not see spin-spin coupling between neighboring carbons in a ^{13}C-NMR spectrum.* There is, however, **heteronuclear coupling** between ^{13}C carbons and the hydrogens to which they are bound. Carbon-proton coupling constants are very large, on the order of 100 – 250 Hz. For clarity, chemists generally use a technique called **broadband decoupling**, which essentially 'turns off' C-H coupling, resulting in a spectrum in which all carbon signals are singlets. Below is the proton-decoupled^{13}C-NMR spectrum of ethyl acetate, showing the expected four signals, one for each of the carbons.



One of the greatest advantages of ^{13}C-NMR compared to ^{1}H-NMR is the breadth of the spectrum - recall that carbons resonate from 0-220 ppm relative to the TMS standard, as opposed to only 0-12 ppm for protons. Because of this, ^{13}C signals rarely overlap, and we can almost always distinguish separate peaks for each carbon, even in a relatively large compound containing carbons in very similar environments. In the proton spectrum of 1-heptanol, for example, only the signals for the alcohol proton (H_a) and the two protons on the adjacent carbon (H_b) are easily analyzed. The other proton signals overlap, making analysis difficult.



In the ^{13}C spectrum of the same molecule, however, we can easily distinguish each carbon signal, and we know from this data that our sample has seven non-equivalent carbons. (Notice also that, as we would expect, the chemical shifts of the carbons get progressively smaller as they get farther away from the deshielding oxygen.)



This property of ^{13}C-NMR makes it very helpful in the elucidation of larger, more complex structures.

^{13}C NMR CHEMICAL SHIFTS

The Carbon NMR is used for determining functional groups using characteristic shift values. ^{13}C chemical shifts are greatly affected by electronegative effects. If a H atom in an alkane is replaced by substituent X, electronegative atoms (O, N, halogen), ^{13}C signals for nearby carbons shift downfield (left; increase in ppm) with the effect diminishing with distance from the electron withdrawing group. Figure 13.11.1 shows typical ^{13}C chemical shift regions of the major chemical class.

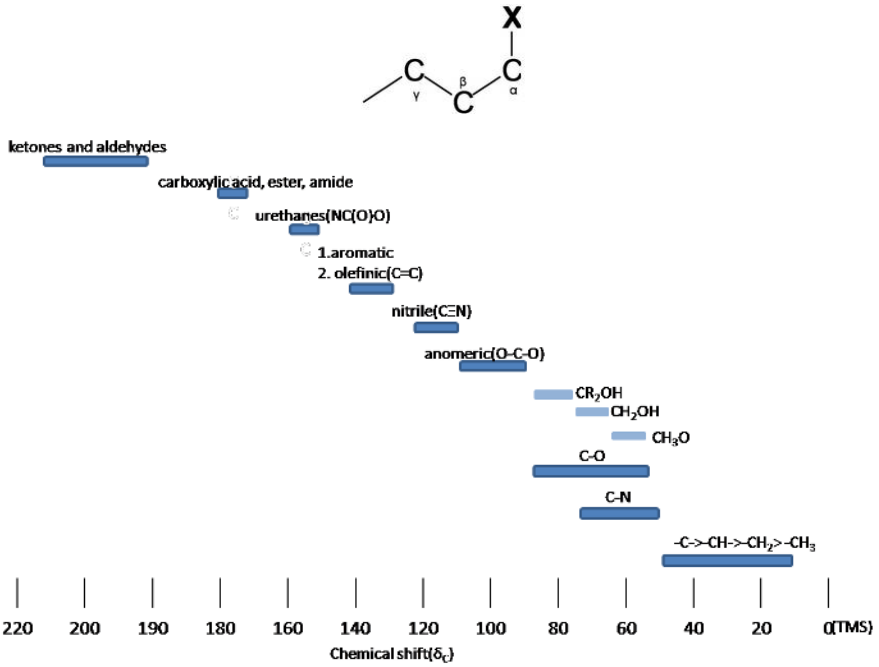


Figure 7.7.11.1: ^{13}C Chemical shift range for organic compound

SPIN-SPIN SPLITTING

Comparing the ^{1}H NMR, there is a big difference thing in the ^{13}C NMR. The ^{13}C-^{13}Cspin-spin splitting rarely exit between adjacent carbons because ^{13}C is naturally lower abundant (1.1%)

- **^{13}C-^{1}H Spin coupling**: ^{13}C-^{1}H Spin coupling provides useful information about the number of protons attached a carbon atom. In case of one bond coupling ($^{1}J_{CH}$), -CH, -CH_2, and CH_3 have respectively doublet, triplet, quartets for the ^{13}C resonances in the spectrum. However, ^{13}C-^{1}H Spin coupling has an disadvantage for ^{13}C spectrum interpretation. ^{13}C-^{1}H Spin coupling is hard to analyze and reveal structure due to a forest of overlapping peaks that result from 100% abundance of ^{1}H.
- **Decoupling**: Decoupling is the process of removing ^{13}C-^{1}H coupling interaction to simplify a spectrum and identify which pair of nuclei is involved in the J coupling. The decoupling ^{13}C spectra shows only one peak(singlet) for each unique carbon in

the molecule (Fig 13.11.2). Decoupling is performed by irradiating at the frequency of one proton with continuous low-power RF.

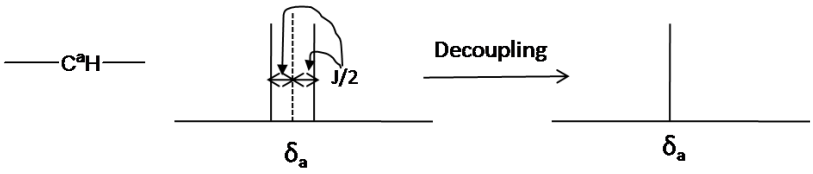


Figure 7.7.11.2: Decoupling in the ^{13}C NMR

SUMMARY

^{13}C NMR (Carbon-13 Nuclear Magnetic Resonance) Spectroscopy is a powerful analytical technique used to study the structure and connectivity of organic molecules. Unlike proton NMR, which detects hydrogen nuclei, ^{13}C NMR specifically targets the carbon nuclei within a molecule. In ^{13}C NMR spectroscopy, carbon atoms resonate at characteristic frequencies based on their local chemical environment, which is influenced by neighboring atoms and functional groups. These resonances appear as peaks in the NMR spectrum, providing valuable information about the types of carbon atoms present and their surroundings. By analyzing the chemical shifts, intensities, and coupling patterns of these peaks, chemists can deduce crucial structural details such as the number and types of carbon atoms, their connectivity, and the presence of certain functional groups. This information is essential for determining the molecular structure and understanding chemical properties and reactivities.

This page titled 7.7.11: Characteristics of ^{13}C NMR Spectroscopy is shared under a CC BY-SA 4.0 license and was authored, remixed, and/or curated by Chris Schaller, Steven Farmer, Dietmar Kennepohl, Layne Morsch, Tim Soderberg, Lauren Reutenauer, & Lauren Reutenauer.

- **13.10: Characteristics of ^{13}C NMR Spectroscopy** by Chris Schaller, Dietmar Kennepohl, Lauren Reutenauer, Layne Morsch, Steven Farmer, Tim Soderberg is licensed CC BY-SA 4.0.

7.7.12: DEPT ^{13}C NMR SPECTROSCOPY

OBJECTIVES

After completing this section, you should be able to

- Understand why the peaks do not have splitting like in ^{1}H NMR.
- Using DEPT, distinguish whether a methyl (CH_3), methylene (CH_2), methine (CH) or quarternary C is present in the molecule and how many.
- Propose a structure based on ^{13}C spectral data.

DEPT (Distortionless Enhancement by Polarization Transfer) ^{13}C NMR Spectroscopy is a powerful technique used in organic chemistry to elucidate the structure of organic molecules. Unlike traditional ^{13}C NMR spectroscopy, which provides only basic information about carbon environments, DEPT enhances signals from specific types of carbon atoms, allowing for more detailed analysis. DEPT works by selectively enhancing signals from three types of carbon atoms: methyl (CH_3), methylene (CH_2), and quaternary carbons (C with no attached hydrogens). This enhancement is achieved through a series of pulse sequences that manipulate the nuclear spins of carbon atoms, resulting in distinct peaks in the NMR spectrum corresponding to each carbon type.

DEPT experiments are used for distinguishing between a CH_3 group (methyl), a CH_2 group (methylene), and a CH group (methine). The proton pulse is set at 45°, 90°, or 135° in the three separate experiments. The different pulses depend on the number of protons attached to a carbon atom. Figure 7.7.12.1 is an example about DEPT spectrum of n-isobutlybutrate.

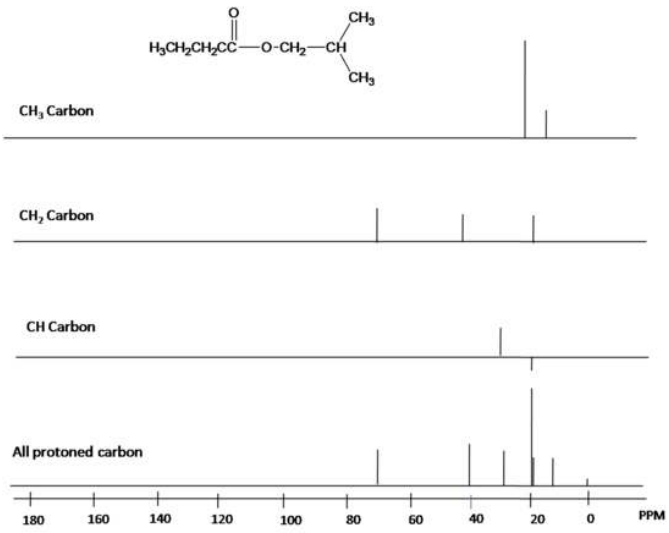


Figure 7.7.12.1: DEPT spectrum of n-isobutlybutrate.

While broadband decoupling results in a much simpler spectrum, useful information about the presence of neighboring protons is lost. However, another modern NMR technique called DEPT (Distortionless Enhancement by Polarization Transfer) allows us to determine how many hydrogens are bound to each carbon. For example, a DEPT experiment tells us that the signal at 171 ppm in the ethyl acetate spectrum is a quaternary carbon (no hydrogens bound, in this case a carbonyl carbon), that the 61 ppm signal is from a methylene (CH_2) carbon, and that the 21 ppm and 14 ppm signals are both methyl (CH_3) carbons. The details of the DEPT experiment are beyond the scope of this text, but DEPT information will often be provided along with ^{13}C spectral data in examples and problems.

Below are two more examples of ^{13}C NMR spectra of simple organic molecules, along with the type of substitution for that carbon which was obtained from a DEPT experiment.

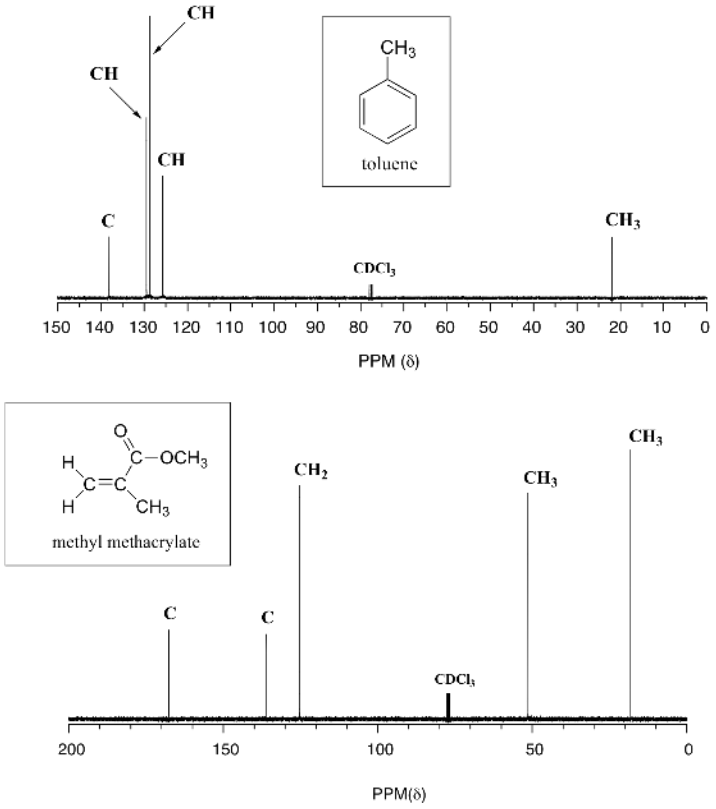
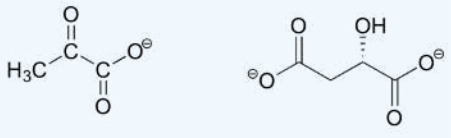


Figure 7.7.12.2: ^{13}C NMR spectra of toluene (left) and meth methacryalate (right)

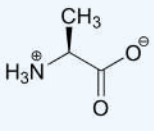
EXERCISE 7.7.12.1

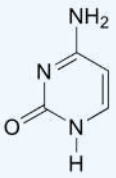
^{13}C-NMR (and DEPT) data for some common biomolecules are shown below (data are from the Aldrich Library of ^{1}H and ^{13}C NMR). Match the NMR data to the correct structure, and make complete peak assignments.

- spectrum a: 168.10 ppm (C), 159.91 ppm (C), 144.05 ppm (CH), 95.79 ppm (CH)
- spectrum b: 207.85 ppm (C), 172.69 ppm (C), 29.29 ppm (CH_3)
- spectrum c: 178.54 ppm (C), 53.25 ppm (CH), 18.95 ppm (CH_3)
- spectrum d: 183.81 ppm (C), 182. 63 ppm (C), 73.06 ppm (CH), 45.35 ppm (CH_2)

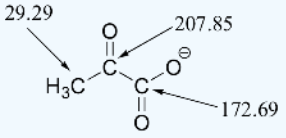

pyruvate

(S)-malate

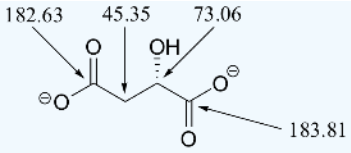

alanine


cytosine

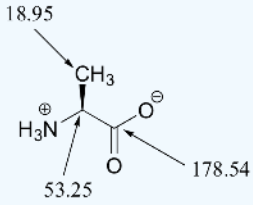
Answer



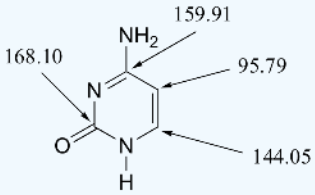
pyruvate: spectrum b



(S)-malate: spectrum d



alanine (spectrum c)



cytosine (spectrum a)

This page titled 7.7.12: DEPT ^{13}C NMR Spectroscopy is shared under a CC BY-SA 4.0 license and was authored, remixed, and/or curated by Chris Schaller, Steven Farmer, Dietmar Kennepohl, Layne Morsch, Tim Soderberg, & Tim Soderberg.

- **13.11: DEPT ^{13}C NMR Spectroscopy** by Chris Schaller, Dietmar Kennepohl, Layne Morsch, Steven Farmer, Tim Soderberg is licensed CC BY-SA 4.0.

7.7.13: USES OF ^{13}C NMR SPECTROSCOPY

OBJECTIVES

After completing this section, you should be able to use data from ^{13}C NMR spectra to distinguish between two (or more) possible structures for an unknown organic compound.

FEATURES OF A ^{13}C NMR SPECTRUM

Butane shows two different peaks in the ^{13}C NMR spectrum, below. Note that: the chemical shifts of these peaks are not very different from methane. The carbons in butane are in a similar environment to the one in methane.

- there are two distinct carbons in butane: the methyl, or CH_3, carbon, and the methylene, or CH_2, carbon.
- the methyl carbon absorbs slightly upfield, or at lower shift, around 10 ppm.
- the methylene carbon absorbs at slightly downfield, or at higher shift, around 20 ppm.
- other factors being equal, methylene carbons show up at slightly higher shift than methyl carbons.

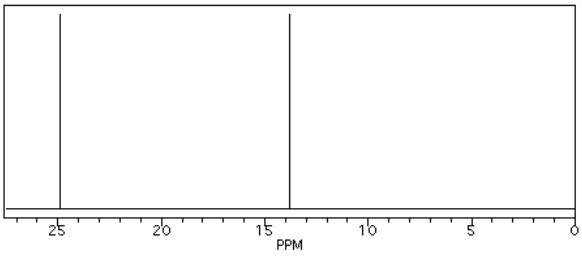


Figure 7.7.13.1. *Simulated ^{13}C NMR spectrum of butane (showing only the upfield portion of the spectrum).*

In the ^{13}C NMR spectrum of pentane (below), you can see three different peaks, even though pentane just contains methyl carbons and methylene carbons like butane. As far as the NMR spectrometer is concerned, pentane contains three different kinds of carbon, in three different environments. That result comes from symmetry.

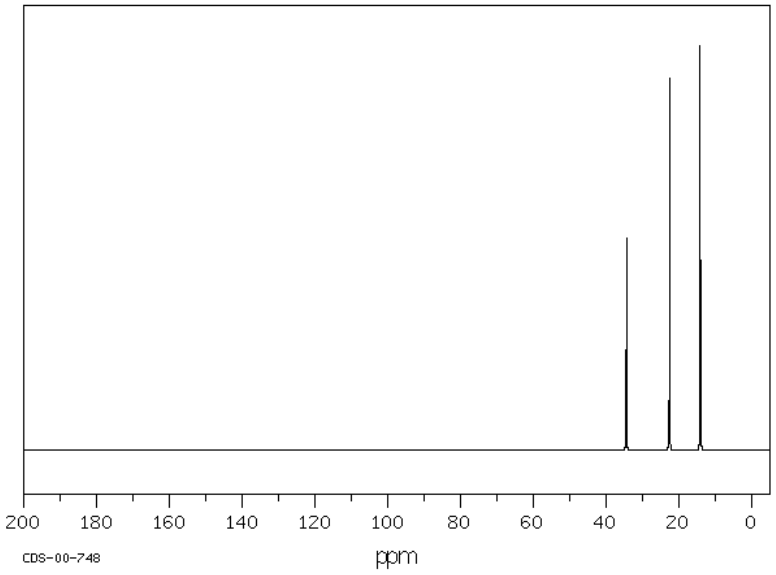


Figure 7.7.13.2 *^{13}C NMR spectrum of pentane. Source: SDBSWeb : http://riodb01.ibase.aist.go.jp/sdbs/ (National Institute of Advanced Industrial Science and Technology of Japan, 15 August 2008)*

Symmetry is an important factor in spectroscopy. Nature says:

- atoms that are symmetry-inequivalent can absorb at different shifts.
- atoms that are symmetry-equivalent must absorb at the same shift.

To learn about symmetry, take a model of pentane and do the following:

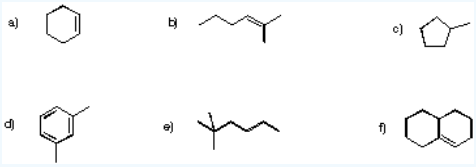
- make sure the model is twisted into the most symmetric shape possible: a nice "W".

- choose one of the methyl carbons to focus on.
- rotate the model 180 degrees so that you are looking at the same "W" but from the other side.
- note that the methyl you were focusing on has simply switched places with the other methyl group. These two carbons are symmetry-equivalent via two-fold rotation.

By the same process, you can see that the second and fourth carbons along the chain are also symmetry-equivalent. However, the middle carbon is not; it never switches places with the other carbons if you rotate the model. There are three different sets of inequivalent carbons; these three groups are not the same as each other according to symmetry.

EXAMPLE 7.7.13.1

Determine how many inequivalent carbons there are in each of the following compounds. How many peaks do you expect in each ^{13}C NMR spectrum?



Practically speaking, there is only so much room in the spectrum from one end to the other. At some point, peaks can get so crowded together that you can't distinguish one from another. You might expect to see ten different peaks in eicosane, a twenty-carbon alkane chain, but when you look at the spectrum you can only see seven different peaks. That may be frustrating, because the experiment does not seem to agree with your expectation. However, you will be using a number of methods together to minimize the problem of misleading data.

Solution

a) Three inequivalent carbons/three peaks. There is a plane of symmetry that bisects the cyclohexene horizontally. The three different carbons are one of the alkene (C1), the CH_2 next to alkene (C3) and C4.

b) Six inequivalent carbons/six peaks. The two methyl groups attached to the alkene are identical.

c) Four inequivalent carbons/four peaks. This molecule has a plane of symmetry through the molecule, including the methyl group. The two carbons adjacent to the methyl group are equivalent (C2 and C5). C3 and C4 are also equivalent.

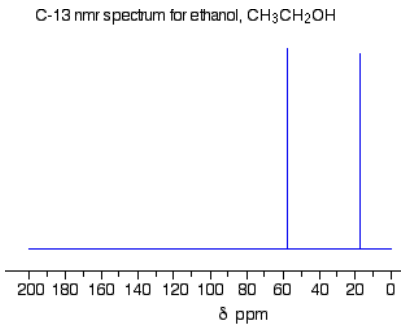
d) Five inequivalent carbons/five peaks. This molecule has a plane of symmetry that passes through the ring carbon between the two methyl groups. The two methyl carbons are identical. The two ring carbons with the methyl groups attached are identical (C1 and C3). C4 and C6 are also equivalent.

e) Six inequivalent carbons/six peaks. The three methyl groups at the end of the molecule are equivalent.

f) Ten inequivalent carbons/ten peaks. There is no symmetry for the carbons in this molecule.

THE ^{13}C NMR SPECTRUM FOR ETHANOL

This is a simple example of a ^{13}C NMR spectrum. Don't worry about the scale for now - we'll look at that in a minute.



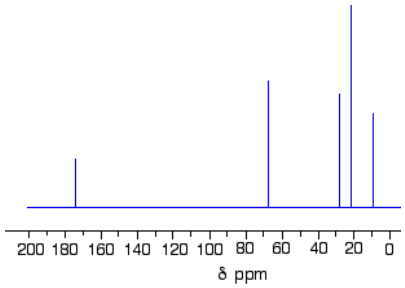
NOTE

Note: The NMR spectra on this page have been produced from graphs taken from the Spectral Data Base System for Organic Compounds (SDBS) at the National Institute of Materials and Chemical Research in Japan.

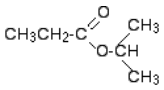
There are two peaks because there are two different environments for the carbons. The carbon in the CH_3 group is attached to 3 hydrogens and a carbon. The carbon in the CH_2 group is attached to 2 hydrogens, a carbon and an oxygen. The two lines are in different places in the NMR spectrum because they need different external magnetic fields to bring them in to resonance at a particular radio frequency.

THE ^{13}C NMR SPECTRUM FOR A MORE COMPLICATED COMPOUND

This is the ^{13}C NMR spectrum for 1-methylethyl propanoate (also known as isopropyl propanoate or isopropyl propionate).



This time there are 5 lines in the spectrum. That means that there must be 5 different environments for the carbon atoms in the compound. Is that reasonable from the structure?



If you count the carbon atoms, there are 6 of them. So why only 5 lines? In this case, two of the carbons are in exactly the same environment. They are attached to exactly the same things. Look at the two CH_3 groups on the right-hand side of the molecule.

You might reasonably ask why the carbon in the CH_3 on the left is not also in the same environment. Just like the ones on the right, the carbon is attached to 3 hydrogens and another carbon. But the similarity is not exact - you have to chase the similarity along the rest of the molecule as well to be sure.

The carbon in the left-hand CH_3 group is attached to a carbon atom which in turn is attached to a carbon with two oxygens on it - and so on down the molecule. That's not exactly the same environment as the carbons in the right-hand CH_3 groups. They are attached to a carbon which is attached to a single oxygen - and so on down the molecule. We'll look at this spectrum again in detail on the next page - and look at some more similar examples as well. This all gets easier the more examples you look at.

For now, all you need to realize is that each line in a ^{13}C NMR spectrum recognizes a carbon atom in one particular environment in the compound. If two (or more) carbon atoms in a compound have exactly the same environment, they will be represented by a single line.

NOTE

You might wonder why all this works, since only about 1% of carbon atoms are ^{13}C. These are the only ones picked up by this form of NMR. If you had a single molecule of ethanol, then the chances are only about 1 in 50 of there being one ^{13}C atom in it, and only about 1 in 10,000 of both being ^{13}C.

But you have got to remember that you will be working with a sample containing huge numbers of molecules. The instrument can pick up the magnetic effect of the ^{13}C nuclei in the carbon of the CH_3 group and the carbon of the CH_2 group even if they are in separate molecules. There's no need for them to be in the same one.

This page titled 7.7.13: Uses of ^{13}C NMR Spectroscopy is shared under a CC BY-SA 4.0 license and was authored, remixed, and/or curated by Steven Farmer, Dietmar Kennepohl, Layne Morsch, Tim Soderberg, William Reusch, Lauren Reutenauer, & Lauren Reutenauer.

- **13.12: Uses of ^{13}C NMR Spectroscopy** by Dietmar Kennepohl, Lauren Reutenauer, Layne Morsch, Steven Farmer, Tim Soderberg, William Reusch is licensed CC BY-SA 4.0.

7.7.S: STRUCTURE DETERMINATION - NUCLEAR MAGNETIC RESONANCE SPECTROSCOPY (SUMMARY)

CONCEPTS & VOCABULARY

13.1 Nuclear Magnetic Resonance Spectroscopy

- An applied magnetic field orients nuclei from random to aligned with or against the field. The nuclei absorb EM radiation of a frequency with energy that matches this energy gap.

13.2 The Nature of NMR Absorptions

- Nuclei in an applied field can align with the magnetic field (+1/2) or against the magnetic field (-1/2). The difference in the energy of these two states is the resonant frequency of that atom.
- To allow comparison between NMR spectra from instruments of differing field strength, the x-axis is reported as chemical shift, rather than frequency.
- **Chemical shift** is defined as the frequency of absorbance (in Hz) divided by the resonant frequency of the instrument (in MHz), thus the units are PPM (parts per million).
- Tetramethylsilane is used as a standard reference with its **chemical shift** set to 0 PPM (since these protons are highly shielded).
- Higher **chemical shifts** are called downfield, while lower shifts are called upfield.
- Nearby electrons shield the nuclei from the induced magnetic field, thus reducing their chemical shift. Atoms of higher electronegativity pull some of this electron density away from the nuclei causing increased **chemical shift**. This is called **deshielding**.

13.3 The Chemical Shift

- Pi electrons in a compound generate their own magnetic field that influences shielding of nearby atoms. This is most clearly exemplified by benzene protons that are highly deshielded (chemical shifts of 6.5-8 PPM).
- Protons that are involved in hydrogen bonding have variable chemical shifts and often do not absorb at one specific frequency, leading to broader peaks.

13.4 Chemical Shifts in ^{1}H NMR Spectroscopy

- Chemical shifts of protons are shifted upfield (higher ppm) by electronegative groups attached to the same carbon (and to a lesser effect when attached to nearby carbons).
- Aromatic protons appear between 6.5 and 8 ppm.
- Chemical shifts of O-H and N-H bonds vary with temperature and concentration.

13.5 Integration of ^{1}H NMR Absorptions - Proton Counting

- The are under a ^{1}H NMR signal is proportional to the number of hydrogens that caused the signal.

13.6 Spin-Spin Splitting in ^{1}H NMR Spectra

- ^{1}H signals are split into multiple peaks by neighboring H atoms whose spins can add to or subtract from the magnetic field.
- Spin-spin coupling yields n+1 peaks where n is the number of neighboring protons.
- Multiplets formed from spin-spin splitting follow specific symmetry based on the number of neighboring protons.
- The distance between peaks in a signal are called coupling constants.

13.7 ^{1}H NMR Spectroscopy and Proton Equivalence

- Equivalent protons (protons in identical electrical environments) only give 1 signal.
- To determine the number of ^{1}H NMR signals expected, symmetry of a molecule needs to be examined to find equivalent protons.
- Protons with different stereochemistry are not equivalent.
- Protons on chiral molecules that are diastereotopic (would create a diastereomer if replaced) are not equivalent.

13.8 More Complex Spin-Spin Splitting Patterns

- ^{1}H NMR signals can overlap making interpretation more difficult.
- Signals can distort where the peaks are not completely symmetrical in shape.
- When neighboring protons are nonequivalent, the coupling constant can be different leading to complex sets of peaks.
- Some complex multiplets can be identified such as a doublet of doublets, but others cannot and are referred to as multiplets.

13.9 Uses of ^{1}H NMR Spectroscopy

- ^{1}H NMR can help identify components of a mixture or determine which product was formed in a reaction.

13.10 ^{13}C NMR Spectroscopy - Signal Averaging and FT-NMR

- NMR signals for ^{13}C NMR are much weaker than for ^{1}H, requiring higher sample concentration and averaging of many scans (hundreds or even thousands).
- **Signal averaging** increases signal-to-noise ratio when running multiple scans in NMR.
- **Fourier Transform** NMR allows the entire spectrum to be acquired at once, rather than one frequency at a time.

13.11 Characteristics of ^{13}C NMR Spectroscopy

- Chemical shifts for ^{13}C NMR are spread over a wider range of frequencies (0-200 ppm).
- Carbons with sp^2 hybridization are shifted far downfield
- Since it is exceptionally rare to have two ^{13}C atoms adjacent to one another, there is no spin-spin coupling in ^{13}C NMR.
- Coupling constants between carbons and hydrogens are large and make interpretation of ^{13}C NMR spectra difficult, so most spectra are run using broadband decoupling. This leads to all signals in ^{13}C NMR appearing as singlets.

13.12 DEPT ^{13}C NMR Spectroscopy

- ^{13}C NMR DEPT experiments are used to identify the number of attached hydrogens each carbon has.

13.13 Uses of ^{13}C NMR Spectroscopy

SKILLS TO MASTER

- Skill 13.1 Interpretation of ^{1}H NMR Spectra.
- Skill 13.2 Interpretation of ^{13}C NMR Spectra.

MEMORIZATION TASKS (MT)

MT 13.1 Memorize chemical shifts patterns in ^{1}H NMR.

MT 13.2 Memorize spin-spin splitting patterns

MT 13.3 Memorize chemical shift patterns in ^{13}C NMR.

This page titled 7.7.S: Structure Determination - Nuclear Magnetic Resonance Spectroscopy (Summary) is shared under a CC BY-SA 4.0 license and was authored, remixed, and/or curated by Layne Morsch.

- **13.S: Structure Determination - Nuclear Magnetic Resonance Spectroscopy (Summary)** by Layne Morsch is licensed CC BY-SA 4.0.

CHAPTER OVERVIEW

8: Molecular Mass Spectrometry

8.1: General Features of Atomic Mass Spectrometry
8.2: Molecular Mass Spectra
8.3: How the Mass Spectrometer Works
8.4: Mass Spectrometers
8.5: Ion Sources
8.5.1: Electrospray Ionization Mass Spectrometry
8.6: Mass Spectrometers
8.6.1: Mass Analyzers (Mass Spectrometry)
8.7: Applications of Molecular Mass Spectrometry
8.7.1: Interpreting a Mass Spectrum
8.7.2: The Molecular Ion (M^+) Peak
8.7.3: The M+1 Peak
8.7.4: The Mass Spectra of Elements
8.7.5: Fragmentation Patterns in Mass Spectra
8.7.6: Mass Spectrometry - Fragmentation Patterns
8.7.7: Organic Compounds Containing Halogen Atoms

This page titled 8: Molecular Mass Spectrometry is shared under a CC BY-NC-SA 4.0 license and was authored, remixed, and/or curated by David Harvey.

8.1: General Features of Atomic Mass Spectrometry

In mass spectrometry—whether of atoms, which is covered in this chapter, or of molecules, which is covered in Chapter 20—we convert the analyte into ions and then separate these ions based on the ratio of their masses to their charges. In this section we give careful attention to what we mean by mass, by charge, and by mass-to-charge ratio. We also give brief consideration to how we generate and measure ions, topics covered in greater detail in subsequent sections.

Atomic Weights in Mass Spectrometry

We trace the modern era of chemistry to John Dalton's development of atomic theory, which made three hypotheses:

1. Elements, which are the smallest division of matter with distinct chemical properties, are composed of atoms. All atoms of a given element are identical—This is not strictly true, as we will see shortly, but we won't hold that against Dalton!—and different from the atoms of other elements. The element carbon is made of carbon atoms, which are different from the atoms of oxygen that make up elemental oxygen.
2. Compounds are composed of atoms from two or more elements. Because atoms cannot be subdivided, the elements that make up a compound are always present in ratios of whole numbers. A compound containing carbon and oxygen, for example, can have 1 carbon atom and 1 oxygen atom (CO) or 1 carbon atom and 2 oxygen atoms (CO_2), but it cannot have 1.5 carbon atoms.
3. In a chemical reaction, the elements that make up the reactants rearrange to make new compounds as products. The atoms that make up these compounds, however, are not destroyed, nor are new atoms created.

Dalton's first hypothesis simply recognized the atom as the basic building block of chemistry. Water, for example, is made from atoms of hydrogen and oxygen. The second hypothesis recognizes that for every compound there is a fixed combination of atoms. Regardless of its source (rain, tears, or a bottle of Evian) a molecule of water always consists of two hydrogen atoms for every atom of oxygen. Dalton's third hypothesis is a statement that atoms are conserved in a reaction; this is more commonly known as the conservation of mass.

The Structure of the Atom

Although Dalton believed that atoms were indivisible, we know now that they are made from three smaller subatomic particles: the electron, the proton, and the neutron. The atom, however, remains the smallest division of matter with distinct chemical properties.

Electrons, Protons, and Neutrons. The characteristic properties of electrons, protons, and neutrons, are shown in Table 8.1.1.

Table 8.1.1. Mass and Charge of Subatomic Particles

particle	mass (g)	unit charge	charge (in Coulombs, C)
electron	9.10939×10^{-28}	-1	-1.6022×10^{-19}
proton	1.67262×10^{-24}	$+1$	$+1.6022 \times 10^{-19}$
neutron	1.67493×10^{-24}	0	0

The proton and the neutron make up the atom's nucleus, which is located at the center of the atom and has a radius of approximately 5×10^{-3} pm. The remainder of the atom, which has radius of approximately 100 pm, is mostly empty space in which the electrons are free to move. Of the three subatomic particles, only the electron and the proton carry a charge, which we can express as a relative unit charge, such as $+1$ or -2, or as an absolute charge in Coulombs. Because elements have no net charge (that is, they are neutral), the number of electrons and protons in an element must be the same.

Atomic Numbers. Why is an atom of carbon different from an atom of hydrogen or helium? One possible explanation is that carbon and hydrogen and helium have different numbers of electrons, protons, or neutrons; Table 8.1.2 provides the relevant numbers.

Table 8.1.2. Comparison of the Elements Hydrogen, Helium, and Carbon

element	number of protons	number of neutrons [1]	number of electrons
hydrogen	1	0, 1, or 2	2
helium	2	2	2

element	number of protons	number of neutrons [1]	number of electrons
carbon	6	6, 7, or 8	6

[1] Only the number of neutrons for the most important naturally occurring forms of these elements are shown here.

Note that although Table 8.1.2 shows that a helium atom has two neutrons, an atom of hydrogen or carbon has three possibilities for the numbers of neutrons. It is even possible for a hydrogen atom to exist without a neutron. Clearly the number of neutrons is not crucial to determining if an atom is carbon, hydrogen, or helium. Although hydrogen, helium, and carbon have different numbers of electrons, the number is not critical to an element's identity. For example, it is possible to strip an electron away from helium to form a helium ion with a charge of $+1$ that has the same number of electrons as hydrogen; nevertheless, it is still helium.

What makes an atom carbon is the presence of six protons, whereas every atom of hydrogen has one proton and every atom of helium has two protons. The number of protons in an atom is called its atomic number, which we represent as *Z*.

Atomic Mass and Isotopes. Protons and neutrons are of similar mass and much heavier than electrons (see Table 8.1.1); thus, most of an atom's mass is in its nucleus. Because not all of an element's atoms necessarily have the same number of neutrons, it is possible for two atoms of an element to differ in mass. For this reason, the sum of an atom's protons and neutrons is known as its mass number (*A*). Carbon, for example, can have a mass number of 12, 13, or 14 (six protons and six, seven, or eight neutrons), and hydrogen can have a mass number of 1, 2, or 3 (one proton and zero, one, or two neutrons).

Atoms of the same element (same *Z*), but with a different number of neutrons (different *A*) are called isotopes. Hydrogen, for example has three isotopes (see Table 8.1.2). The isotope with 0 neutrons is the most abundant, accounting for 99.985% of all stable hydrogen atoms, and is known, somewhat self-referentially, as hydrogen. Deuterium, which accounts for 0.015% of all stable hydrogen atoms, has 1 neutron. The isotope of hydrogen with two neutrons is called tritium. Because tritium is radioactive it is unstable and disappears with time.

The usual way to represent isotopes is with the symbol ${}^{A}_{Z}X$ where *X* is the atomic symbol for the element. The three isotopes of hydrogen, which has an elemental symbol of H, are ${}^{1}_{1}\mathrm{H}$, ${}^{2}_{1}\mathrm{H}$, and ${}^{3}_{1}\mathrm{H}$. Because the elemental symbol (*X*) and the atomic number (*Z*) provide redundant information, we often omit the atomic number; thus, deuterium becomes ${}^{2}\mathrm{H}$. Unlike hydrogen, the isotopes of other elements do not have specific names. Instead they are named by taking the element's name and appending the atomic mass. For example, the isotopes of carbon are called carbon-12, carbon-13, and carbon-14.

Atomic Mass

Individual atoms weigh very little, typically about 10^{-24} g to 10^{-22} g. This amount is so small that there is no easy way to measure the mass of a single atom. To assign masses to atoms it is necessary to assign a mass to one atom and to report the masses of all other atoms relative to that absolute standard. By agreement, atomic mass is stated in terms of atomic mass units (amu) or Daltons (Da), where 1 amu and 1 Da are defined as 1/12 of the mass of an atom of carbon-12. The atomic mass of carbon-12, therefore, is exactly 12 amu. The atomic mass of carbon-13 is 13.00335 amu because the mass of an atom of carbon-13 is $1.0836125\times$greater than the mass of an atom of carbon-12.

Note

If you calculate the masses of carbon-12 and carbon-13 by adding together the masses of each isotope's electrons, neutrons, and protons from Table 8.1.1 you will obtain a mass ratio of 1.08336, not 1.0836125. The reason for this is that the masses in Table 8.1.1 are for "free" electrons, protons, and neutrons; that is, for electrons, protons, and neutrons that are not in an atom. When an atom forms, some of the mass is lost. "Where does it go?," you ask. Remember Einstein and $E = mc^2$? Mass can be converted to energy and the lost mass is the nuclear binding energy that holds the nucleus together.

Average Atomic Mass. Because carbon exists in several isotopes, the atomic mass of an "average" carbon atom is not exactly 12 amu. Instead it is usually reported on periodic tables as 12.01 or 12.011, values that are closer to 12.0 because 98.90% of all carbon atoms are carbon-12. The IUPAC's Commission on Isotopic Abundances and Atomic Weights currently reports its mass as [12.0096, 12.0116] amu where the values in the brackets are the lower and the upper estimates for the average mass in a variety of naturally occurring materials. As shown in the following example, if you know the percent abundance and atomic masses of an element's isotopes, then you can calculate it's average atomic mass.

Example 8.1.1

The element magnesium, Mg, has three stable isotopes with the following atomic masses and percent abundances:

isotope	mass (amu)	percent abundance
^{24}Mg	23.9924	78.70
^{25}Mg	24.9938	10.13
^{26}Mg	25.9898	11.17

Calculate the average atomic mass for magnesium.

Solution

To find the average atomic mass we multiply each isotopes' atomic mass by its fractional abundance (the decimal equivalent of its percent abundance) and add together the results; thus

avg. amu = (0.7870)(23.994 amu) + (0.1013)(24.9938 amu) + (0.1117)(25.9898 amu) avg. amu = 24.32 amu

As the next example shows, we also can work such problems in reverse, using an element's average atomic mass and the atomic masses of its isotopes to find each isotope's percent abundance.

Example 8.1.2

The element gallium, Ga, has two naturally occurring isotopes. The isotope ^{69}Ga has an atomic mass of 68.926 amu and the isotope ^{71}Ga has an atomic mass of 70.926 amu. The average atomic mass for gallium is 69.723. Find the percent abundances for gallium's two isotopes.

Solution

If we let x be the fractional abundance of ^{69}Ga, then the fractional abundance of ^{71}Ga is $1 - x$ (that is, the total amounts of ^{69}Ga and ^{71}Ga must add up to one). Usingthe same general approach as Example 8.1.1, we find that

$$69.723 \text{ amu} = (x)(68.926 \text{ amu}) + (1 - x)(70.926 \text{ amu})$$

$$69.723 \text{ amu} = 68.926x \text{ amu} + 70.926 \text{ amu} - 70.926x \text{ amu}$$

$$2.000x \text{ amu} = 1.203 \text{ amu}$$

$$x = 0.6015$$

$$1 - x = 1 - 0.6015 = 0.3985$$

Thus, 60.15% of naturally occurring gallium is ^{69}Ga and 39.85% is ^{71}Ga.

Note

Although many periodic tables report atomic masses to two decimal places—the periodic table I consult most frequently, for example gives the average atomic mass of carbon as 12.01 amu—the high resolving power of some mass spectrometers allows us to report masses to three or four decimal places.

Mass-to-Charge Ratio

As we will learn later, a mass spectrometer separates ions on the basis of their mass-to-charge ratio (m/z), and not on their mass only or their charge only. As most ions that form during mass spectrometry are singly charged, spectra are often reported using masses (m) instead of mass-to-charge ratios; be sure to remain alert for this when looking at mass spectra.

This page titled 8.1: General Features of Atomic Mass Spectrometry is shared under a CC BY-NC-SA 4.0 license and was authored, remixed, and/or curated by David Harvey.

- **11.1: General Features of Atomic Mass Spectrometry** by David Harvey is licensed CC BY-NC-SA 4.0.

8.2: Molecular Mass Spectra

Figure 8.2.1 shows a mass spectrum for *p*-nitrophenol, $C_6H_5NO_3$, which has a nominal (integer) mass of 139 daltons. If we send a beam of energetic electrons through a gas phase sample of *p*-nitrophenol, it loses an electron, which we write as the reaction

$$C_6H_5NO_3 + e^- \rightarrow C_6H_5NO_3^{+\bullet} + 2e^- \tag{8.2.1}$$

where the product is a radical cation that has a charge of $+1$ and that retains the nominal mass of 139 daltons. We call this the molecular ion—highlighted here in green—and it has a mass-to-charge ratio (*m*/*z*) of 139.

Note

Some of the terminology in this chapter was covered earlier in Chapter 11 on atomic mass spectrometry. See the first section of that chapter for a discussion of atomic mass units (amu) and daltons (Da), and of mass-to-charge ratios.

If reaction 8.2.1 is all that happens when *p*-nitrophenol interacts with an energetic electron, then it would not provide much in the way of useful information. The radical cation $C_6H_5NO_3^{+\bullet}$, however, retains sufficient excess energy from the initial electron-molecule collision that it is in an excited state. In returning to its ground state, the molecular ion undergoes a series of fragmentations that result in the formation of ions—called daughter ions—with different mass-to-charge ratios. A plot that shows the relative intensity of these ions as a function of their mass-to-charge ratios is called a mass spectrum. The most abundant fragment in the spectrum—shown here in red and which is called the base peak—is assigned a relative intensity of 100; the intensity of all other ions is reported relative to the base perk.

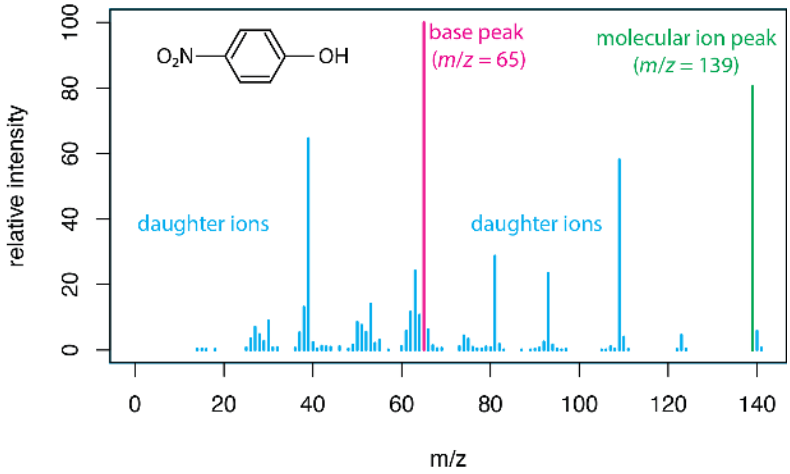


Figure 8.2.1: The mass spectrum for *p*-nitrophenol showing the molecular ion at a m/z of 139 (in green) and the daughter ions (in blue) formed through fragmentation. The most abundant fragment is the base peak at a m/z of 65 (in red). The original data is available here. This particular spectrum was collected using an electron impact source; more on that in Section 20.2.

A molecule's fragmentation patterns provides rich information about its structure. Figure 8.2.2 compares the mass spectra for *o*-nitrophenol, *m*-nitrophenol, and *p*-nitrophenol. All three molecules have clusters of fragment ions at similar mass-to-charge ratios, but the relative abundance of the ions in these clusters varies quite a bit from molecule-to-molecule. For example, the pink rectangle in each spectrum highlights peaks with mass-to-charge ratios from approximately 104 *m*/*z* to 115 *m*/*z*. All three molecules share the property of producing fragment ions with these mass-to-charge ratios; the relative abundance of the fragment ions, however, varies substantially between the three molecules with *o*-nitrophenol and *p*-nitrophenol having a major peak at 109 *m*/*z*, but *m*-nitrophenol showing no more than a trace peak at 109 *m*/*z*. We will return to the use of mass spectrometry for determining structure information later in this chapter.

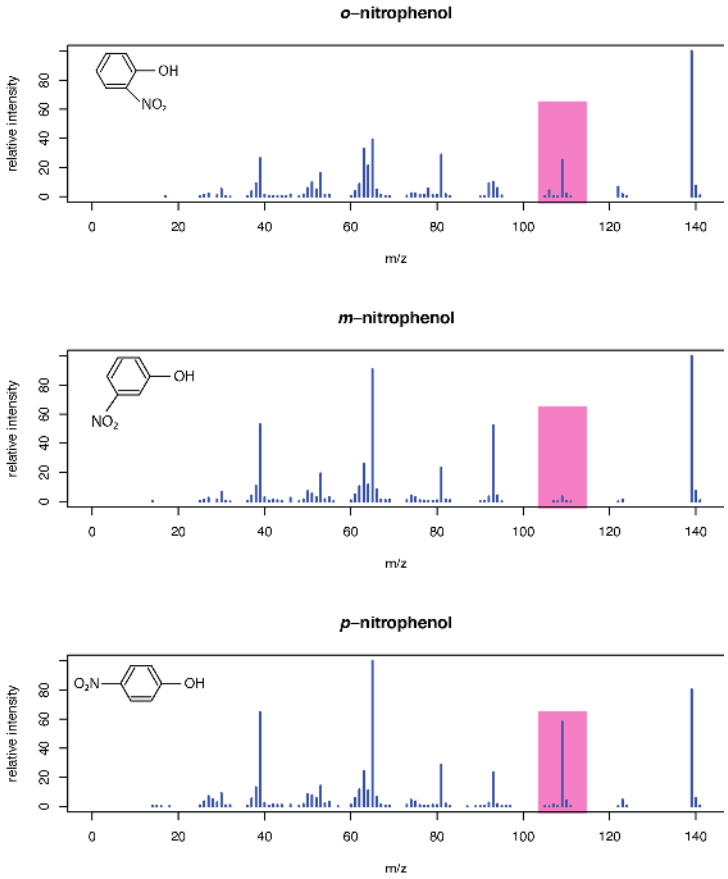


Figure 8.2.2: The mass spectra for *o*-nitrophenol (top), *m*-nitrophenol (middle), and *p*-nitrophenol (bottom). All three molecules show the same pattern of the mass-to-charge ratios where clusters of fragment ions appear; however, the relative abundance of each cluster varies from molecule-to-molecule. The pink rectangle highlights the *m*/*z* values of 104–115. The original data for these spectra are here, here, and here from top-to-bottom.

This page titled 8.2: Molecular Mass Spectra is shared under a CC BY-NC-SA 4.0 license and was authored, remixed, and/or curated by David Harvey.

- **20.1: Molecular Mass Spectra** by David Harvey is licensed CC BY-NC-SA 4.0.

8.3: How the Mass Spectrometer Works

This page describes how a mass spectrum is produced using a mass spectrometer.

How a mass spectrometer works

If something is moving and you subject it to a sideways force, instead of moving in a straight line, it will move in a curve - deflected out of its original path by the sideways force. Suppose you had a cannonball traveling past you and you wanted to deflect it as it went by you. All you've got is a jet of water from a hose-pipe that you can squirt at it. Frankly, its not going to make a lot of difference! Because the cannonball is so heavy, it will hardly be deflected at all from its original course. But suppose instead, you tried to deflect a table tennis ball traveling at the same speed as the cannonball using the same jet of water. Because this ball is so light, you will get a huge deflection.

The amount of deflection you will get for a given sideways force depends on the mass of the ball. If you knew the speed of the ball and the size of the force, you could calculate the mass of the ball if you knew what sort of curved path it was deflected through. The less the deflection, the heavier the ball. You can apply exactly the same principle to atomic sized particles.

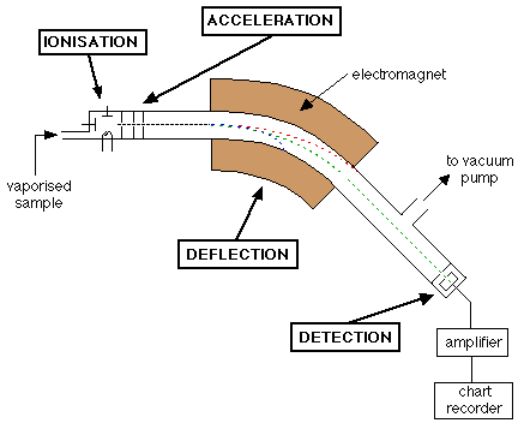
An outline of what happens in a mass spectrometer

Atoms can be deflected by magnetic fields - provided the atom is first turned into an ion. Electrically charged particles are affected by a magnetic field although electrically neutral ones aren't.

The sequence is :

- **Stage 1: Ionization**: The atom is ionised by knocking one or more electrons off to give a positive ion. This is true even for things which you would normally expect to form negative ions (chlorine, for example) or never form ions at all (argon, for example). Mass spectrometers always work with positive ions.
- **Stage 2: Acceleration:** The ions are accelerated so that they all have the same kinetic energy.
- **Stage 3: Deflection:** The ions are then deflected by a magnetic field according to their masses. The lighter they are, the more they are deflected. The amount of deflection also depends on the number of positive charges on the ion - in other words, on how many electrons were knocked off in the first stage. The more the ion is charged, the more it gets deflected.
- **Stage 4: Detection**: The beam of ions passing through the machine is detected electrically.

A full diagram of a mass spectrometer



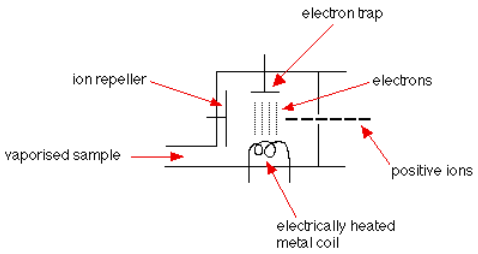
Understanding what's going on

The need for a vacuum

It's important that the ions produced in the ionization chamber have a free run through the machine without hitting air molecules.

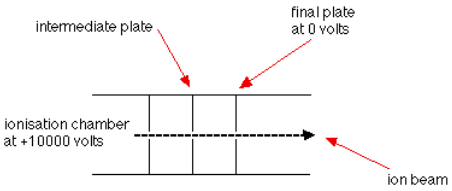
Ionization

The vaporized sample passes into the ionization chamber. The electrically heated metal coil gives off electrons which are attracted to the electron trap which is a positively charged plate.



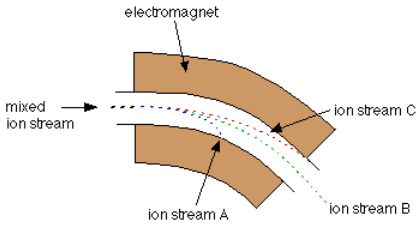
The particles in the sample (atoms or molecules) are therefore bombarded with a stream of electrons, and some of the collisions are energetic enough to knock one or more electrons out of the sample particles to make positive ions. Most of the positive ions formed will carry a charge of +1 because it is much more difficult to remove further electrons from an already positive ion. These positive ions are persuaded out into the rest of the machine by the ion repeller which is another metal plate carrying a slight positive charge.

Acceleration



The positive ions are repelled away from the very positive ionization chamber and pass through three slits, the final one of which is at 0 volts. The middle slit carries some intermediate voltage. All the ions are accelerated into a finely focused beam.

Deflection



Different ions are deflected by the magnetic field by different amounts. The amount of deflection depends on:

- the mass of the ion. Lighter ions are deflected more than heavier ones.
- the charge on the ion. Ions with 2 (or more) positive charges are deflected more than ones with only 1 positive charge.

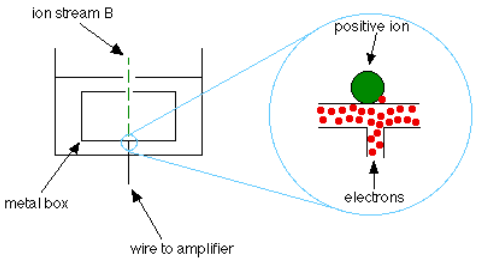
These two factors are combined into the mass/charge ratio. Mass/charge ratio is given the symbol m/z (or sometimes m/e). For example, if an ion had a mass of 28 and a charge of 1+, its mass/charge ratio would be 28. An ion with a mass of 56 and a charge of 2+ would also have a mass/charge ratio of 28.

In the last diagram, ion stream A is most deflected - it will contain ions with the smallest mass/charge ratio. Ion stream C is the least deflected - it contains ions with the greatest mass/charge ratio.

It makes it simpler to talk about this if we assume that the charge on all the ions is 1+. Most of the ions passing through the mass spectrometer will have a charge of 1+, so that the mass/charge ratio will be the same as the mass of the ion. Assuming 1+ ions, stream A has the lightest ions, stream B the next lightest and stream C the heaviest. Lighter ions are going to be more deflected than heavy ones.

Detection

Only ion stream B makes it right through the machine to the ion detector. The other ions collide with the walls where they will pick up electrons and be neutralised. Eventually, they get removed from the mass spectrometer by the vacuum pump.



When an ion hits the metal box, its charge is neutralized by an electron jumping from the metal on to the ion (right hand diagram). That leaves a space amongst the electrons in the metal, and the electrons in the wire shuffle along to fill it. A flow of electrons in the wire is detected as an electric current which can be amplified and recorded. The more ions arriving, the greater the current.

Detecting the other ions

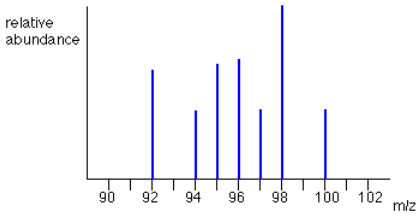
How might the other ions be detected - those in streams A and C which have been lost in the machine?

Remember that stream A was most deflected - it has the smallest value of m/z (the lightest ions if the charge is 1+). To bring them on to the detector, you would need to deflect them less - by using a smaller magnetic field (a smaller sideways force). To bring those with a larger m/z value (the heavier ions if the charge is +1) on to the detector you would have to deflect them more by using a larger magnetic field.

If you vary the magnetic field, you can bring each ion stream in turn on to the detector to produce a current which is proportional to the number of ions arriving. The mass of each ion being detected is related to the size of the magnetic field used to bring it on to the detector. The machine can be calibrated to record current (which is a measure of the number of ions) against m/z directly. The mass is measured on the ^{12}C scale.

What the mass spectrometer output looks like

The output from the chart recorder is usually simplified into a "stick diagram". This shows the relative current produced by ions of varying mass/charge ratio. The stick diagram for molybdenum looks like this:



You may find diagrams in which the vertical axis is labeled as either "relative abundance" or "relative intensity". Whichever is used, it means the same thing. The vertical scale is related to the current received by the chart recorder - and so to the number of ions arriving at the detector: the greater the current, the more abundant the ion.

As you will see from the diagram, the commonest ion has a mass/charge ratio of 98. Other ions have mass/charge ratios of 92, 94, 95, 96, 97 and 100. That means that molybdenum consists of 7 different isotopes. Assuming that the ions all have a charge of 1+, that means that the masses of the 7 isotopes on the carbon-12 scale are 92, 94, 95, 96, 97, 98 and 100.

Contributors and Attributions

- Jim Clark (Chemguide.co.uk)

This page titled 8.3: How the Mass Spectrometer Works is shared under a CC BY-NC 4.0 license and was authored, remixed, and/or curated by Jim Clark.

- **How the Mass Spectrometer Works** by Jim Clark is licensed CC BY-NC 4.0.

8.4: Mass Spectrometers

A mass spectrometer has three essential needs: a means for producing ions, in this case (mostly) singly charged atoms; a means for separating these ions in space or in time by their mass-to-charge ratios; and a means for counting the number of ions for each mass-to-charge ratio. Figure 8.4.1 provides a general view of a mass spectrometer in the same way that we first introduced optical instruments in Chapter 7. The ionization of the sample is analagous to the source of photons in optical spectroscopy as it generates the particles (ions, instead of photons) that ultimately make up the measured signal. The separation of the resulting ions by their mass-to-charge ratios, which is accomplished using a mass analyzer, is analagous to the role of a monochromator in optical spectroscopy. The means for counting ions serves the same role as, for example, a photomultiplier tube in optical spectroscopy. Note that the mass spectrometer is held under vacuum as this allows the ions to travel great distances without undergoing collisions that might alter their charge or energy.

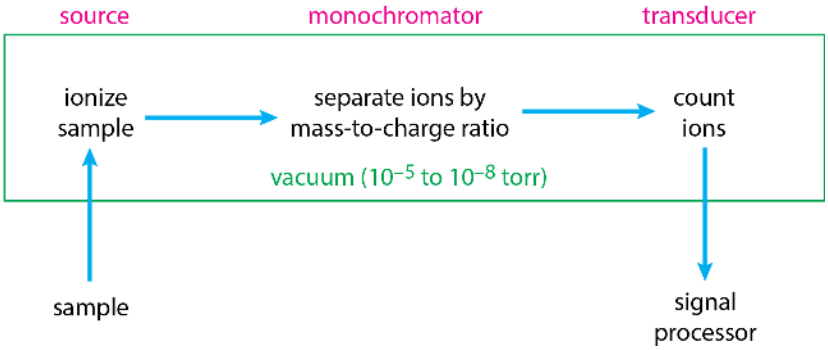


Figure 8.4.1: The basic components of a mass spectrometer. The blue arrows show the direction of sample-to-signal in which the sample is ionized, the ions separated by their mass-to-charge ratio, and ions with the same mass-to-charge ratio counted. The text in red at the top of the figure relates these components to their equivalent in optical spectroscopy.

Sources of Ionization

The most common means for generating ions are plasmas of various sorts, lasers, electrical sparks, and other ions. We will give greater attention to these in the next several sections as we consider specific examples of atomic mass spectrometry.

Transducers for Counting Ions

The transducer for mass spectrometry must be able to report the number of ions that emerge from the mass analyzer. Here we consider two common types of transducers.

Electron Multipliers

In Chapter 7 we introduced the photomultiplier tube as a way to convert photons into electrons, amplifying the signal so that a single photon produces 10^6 to 10^7 electrons, which generates a measurable current. An electron multiplier serves the same role in mass spectrometry. Figure 8.4.2 shows two versions of this transducer. The electron multiplier in Figure 8.4.2a uses a set of individual dynodes. When an ion strikes the first dynode, it generates several electrons, each of which is passed along to the next dynode before arriving at a collecting plate where the current is measured. The result is an amplification, or gain, in the signal of approximately $10^7\times$. The electron multiplier in Figure 8.4.2b uses a horn-shaped cylinder—typically made from glass coated with a thin layer of a semiconducting material—whose surface acts as a single, continuous dynode. When an ion strikes the continuous dynode it generates several electrons that are reflected toward the collector plate where the current is measured. The result is an amplification of 10^5 to $10^8\times$.

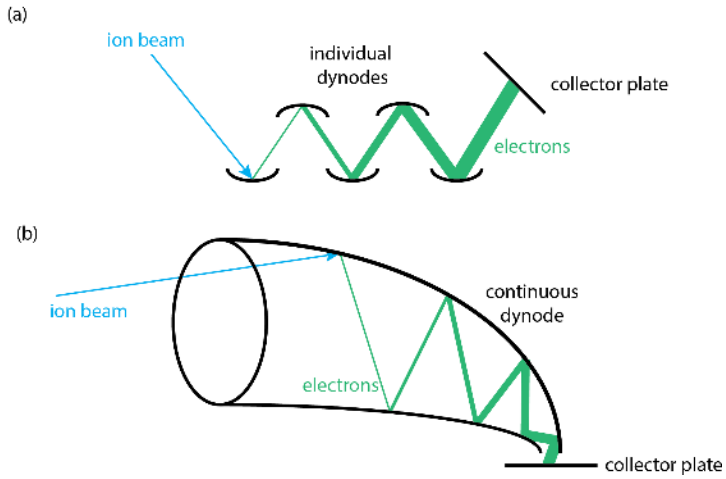


Figure 8.4.2: Electron multipliers using (a) individual, or discrete dynodes, and (b) a single, continuous dynode. The ion beam is represented by the blue arrows and the electrons are represented by the green lines. The increasing thickness of the green lines shows the amplification of the signal.

Faraday Cup

A Faraday cup, as its name suggests, is a simple device shaped like a cup. Ions enter the cup where they strike a collector electrode. A current is directed to the collector plate that is sufficient to neutralize the charge of the ions. The magnitude of this current is proportional to the number of ions. A Faraday cup has the advantage of simplicity, but is less sensitive than an electron multiplier because it lacks the amplification provided by the dynodes.

Separating Ions

Before we can detect the ions, we need to separate them so that we can generate a spectrum that shows the intensity of ions as a function of their mass-to-charge ratio. In this section we consider the three most common mass analyzers for atomic mass spectrometry.

Quadrupole Mass Analyzers

The quadrupole mass analyzer is the most important of the mass analyzers included in this chapter: it is compact in size, low in cost, easy to use, and easy to maintain. As shown in Figure 8.4.3, a quadrapole mass analyzer consists of four cylindrical rods, two of which are connected to the positive terminal of a variable direct current (dc) power supply and two of which are connected to the power supply's negative terminal; the two positive rods are positioned opposite of each other and the two negative rods are positioned opposite of each other. Each pair of rods is also connected to a variable alternating current (ac) source operated such that the alternating currents are 180° out-of-phase with each other. An ion beam from the source is drawn into the channel between the quadrupoles and, depending on the applied dc and ac voltages, ions with only one mass-to-charge ratio successfully travel the length of the mass analyzer and reach the transducer; all other ions collide with one of the four rods and are destroyed.



Figure 8.4.3: Basic arrangement of the quadrupole mass analyzer. The plus and the minus signs on each rod indicate which are connected to the positive terminal of the dc power supply. Not shown here is the circuitry for applying the alternating current. The ion beam enters the channel between the quadrupoles. Depending on the applied dc and ac voltages, some of the ions emerge from this channel and reach the transducer.

To understand how a quadrupole mass analyzer achieves this separation of ions, it helps to consider the movement of an ion relative to just two of the four rods, as shown in Figure 8.4.4 for the poles that carry a positive dc voltage. When the ion beam enters the channel between the rods, the ac voltage causes the ion to begin to oscillate. If, as in the top diagram, the ion is able to

maintain a stable oscillation, it will pass through the mass analyzer and reach the transducer. If, as in the middle diagram, the ion is unable to maintain a stable oscillation, then the ion eventually collides with one of the rods and is destroyed. When the rods have a positive dc voltage, as they do here, ions with larger mass-to-charge ratios will be slow to respond to the alternating ac voltage and will pass through the transducer. The result is shown in the figure at the bottom (and repeated in Figure $8.4.5a$) where we see that ions with a sufficiently large mass-to-charge ratios successfully pass through the transducer; ions with smaller mass-to-charge ratios do not. In this case, the quadrupole mass analyzer acts as a high-pass filter.

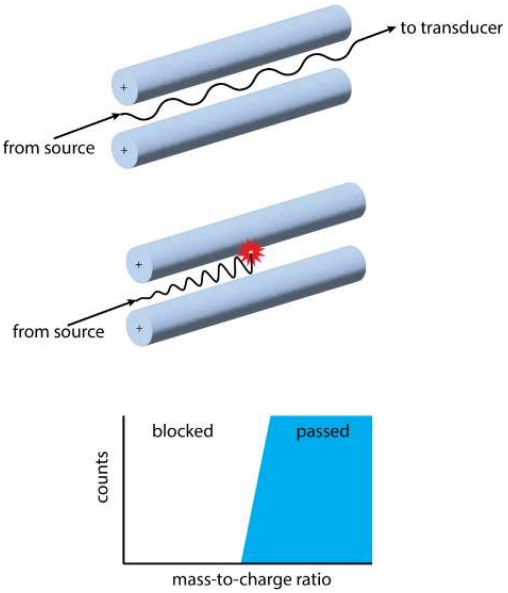


Figure 8.4.4: Illustration of how a quadrupole mass analyzer achieves separation of ions by their mass-to-charge ratio. See the text for additional details.

We can extend this to the behavior of the ions when they interact with rods that carry a negative dc voltage. In this case, the ions are attracted to the rods, but those ions that have a sufficiently small mass-to-charge ratio are able to respond to the alternating current's voltage and remain in the channel between the rods. The ions with larger mass-to-charge ratios move more sluggishly and eventually collide with one of the rods. As shown in Figure $8.4.5b$, in this case, the quadrupole mass analyzer acts as a low-pass filter. Together, as we see in Figure $8.4.5c$, a quadrupole mass analyzer operates as both a high-pass and a low-pass filter, allowing a narrow band of mass-to-charge ratios to pass through the transducer. By varying the applied dc voltage and the applied ac voltage, we can obtain a full mass spectrum.

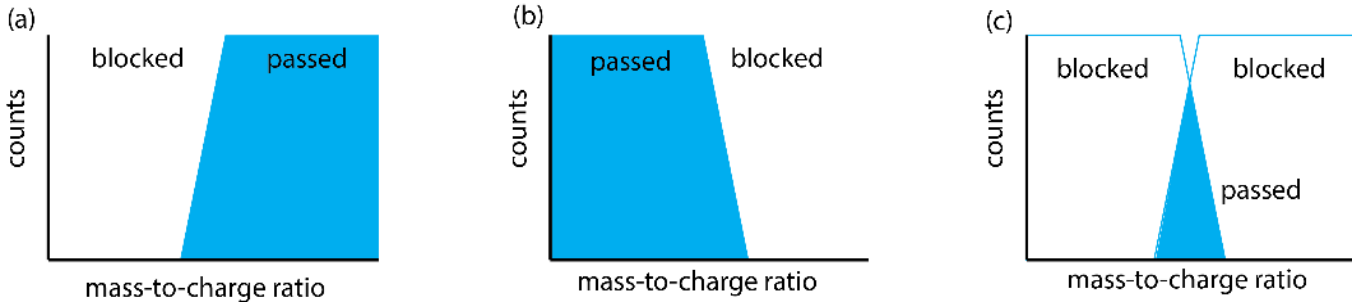


Figure 8.4.5: Illustration that shows how a quadrupole mass analyzer acts as both (a) a high-pass filter and (b) a low pass filter, with the result that it passes only ions with a narrow range of mass-to-charge ratios.

Quadrupole mass analyzers provide a modest mass-to-charge resolution of about 1 amu and extend to m/z ratios of approximately 2000. Quadrupole mass analyzers are particularly useful for sources based on plasmas.

Time-of-Flight (TOF) Mass Analyzers

In a time-of-flight mass analyzers, ions are created in small clusters by applying a periodic pulse of energy to the sample using a laser beam or a beam of energetic particles to ionize the sample. The small cluster of ions are then drawn into a tube by applying an electric field and then allowed to drift through the tube in the absence of any additional applied field; the tube, for obvious reasons, is called a drift tube. All of the ions in the cluster enter the drift tube with the same kinetic energy, KE, which means, given

$$\mathrm{KE} = \frac{1}{2}mv^2 \tag{8.4.1}$$

that the square of an ion's velocity is inversely proportional to the ion's mass. As a result, lighter ions move more quickly than heavier ions. Flight times are typically less than 30 µs. A time-of-flight mass analyzer provide better resolution than a quadrupole mass analyzer, but is limited to sources that can be pulsed.

Double-Focusing Mass Analyzers

In a double-focusing mass analyzer, two mechanisms are used to focus a beam of ions onto the transducer. One of the mechanisms is an electrotatic analyzer that serves to confine the kinetic energy of the ions to a narrow range of energies. The second mechanism is a magnetic sector analyzer that uses an applied magnetic field to separate the ions by their mass-to-charge ratio. The combination of two analyzers allows for a significant resolution. More details on this type of mass analyzer is included in Chapter 20.

This page titled 8.4: Mass Spectrometers is shared under a CC BY-NC-SA 4.0 license and was authored, remixed, and/or curated by David Harvey.

- **11.2: Mass Spectrometers** by David Harvey is licensed CC BY-NC-SA 4.0.

8.5: Ion Sources

Since a mass spectrum shows the relative abundance of ions with different mass-to-charge ratios, a mass spectrometer must include a way to generate ions. More specifically, it needs a method that generates the initial ion as it, once formed, will undergo fragmentation without additional help from the analyst (which does not mean the analyst cannot assist in that fragmentation; see discussion of tandem mass spectrometry in Section 20.4). In this section we consider several common ion sources. We can describe these sources using two characteristic properties: (a) the physical state of the species that is initially ionized (gas, liquid, or solid phase), and (b) whether ionization favors the formation of fragment ions or the formation of molecular ions (hard sources or soft sources).

Electron Ionization Sources (gas phase/hard source)

The electron ionization (EI) source, also known as an electron impact source, uses a beam of energetic electrons to ionize the analyte. As shown in 8.5.1, the sample is volatilized prior to entering the ion source as gas phase molecules, M(*g*). A heated tungsten filament is used to generate electrons, which are pulled toward a positively charged anode. This electron beam intersects with the gas phase molecules at 90° where ionization occurs

$$\mathrm{M}(g) + e^- \rightarrow \mathrm{M}^{+\bullet}(g) + 2e^- \tag{8.5.1}$$

The molecular ions, $\mathrm{M}^{+\bullet}(g)$, are then swept into the mass analyzer using a set of accelerating plates (not shown here).

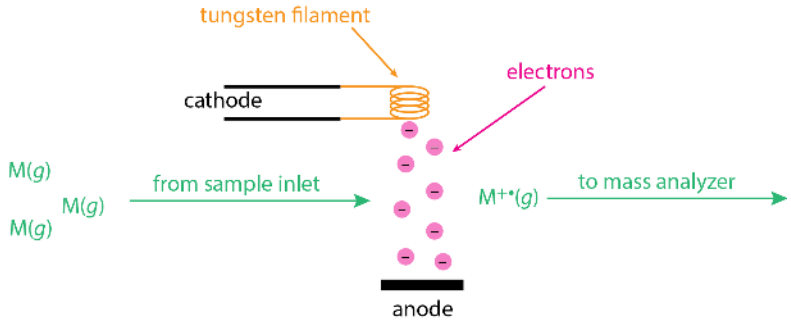


Figure 8.5.1: Illustration of an electron ionization source. The sample is volatilized and brought into the ion source where it intersects with an electron beam, forming the molecular ion, $\mathrm{M}^{+\bullet}$, which is carried on into the mass analyzer.

The electron beam in Figure 8.5.1 has a lot of energy due to the significant potential difference between the cathode and the anode, which may be as much as 70 V. The kinetic energy of these electrons is equivalent to the product of the electron's charge in Coulombs, the applied potential in volts, and Avogadro's number

$$e \times V \times N_A = 1.6 \times 10^{-19} \times 6.022 \times 10^{-23} = 6.7 \times 10^6 \text{ J/mol}$$

or 6,700 kJ/mol. This energy is much greater than typical bond energies, which range from approximately 150–600 kJ/mol for single bonds, from approximately 500–750 kJ/mol for double bonds, and from approximately 800–1100 kJ/mol for triple bonds. The significant difference between the energy of the electrons and bond energies explains why electron ionization spectra are rich in fragment ions, as we saw earlier in Section 20.1 for *o*-nitrophenol, *m*-nitrophenol, and *p*-nitrophenol. This extensive fragmentation is useful in determining an analyte's structure—which is an advantage of a hard ionization method—but at the possible cost of the loss of the molecular ion peak for some analytes. For example, Figure 8.5.2 shows the electron ionization mass spectrum from 1-decanol, $C_{10}H_{22}O$, which has a nominal mass of 158 daltons. The small peak at *m*/*z* = 157 is for the fragment ion $C_{10}H_{21}O^+$; the molecular ion is not observed in this spectrum.

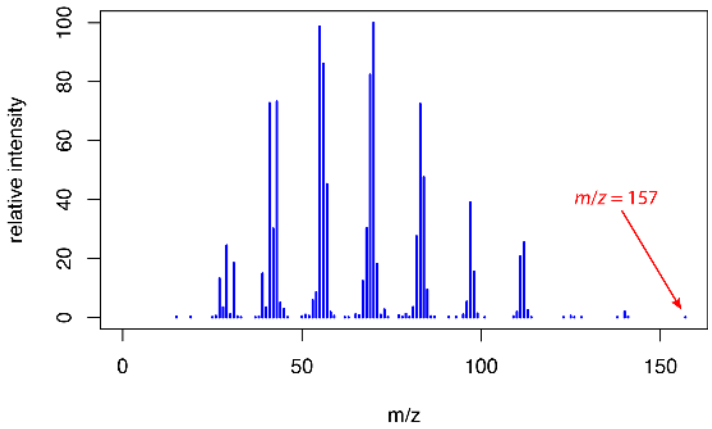


Figure 8.5.2: Mass spectrum for 1-decanol, $C_{10}H_{22}O$, using electron ionization. The peak furthest to the right (*m*/*z* = 157 amu) is one atomic mass unit less than the expected peak for the molecular ion, which does not appear in the spectrum. The original data is available here.

Chemical Ionization Sources (gas phase/soft source)

Electron ionization is a hard source because the electron beam's energy results in easy fragmentation. In chemical ionization, we introduced a reagent molecule, such as methane, into the electron ionization (CI) source so that it is present at level that is $1000\times$ to $10,000\times$ greater than the analyte. At this higher concentration, it is the reagent molecule that is ionized; for example, when using CH_4 as the reagent gas, ions such as CH_4^+ and CH_3^+ form. These ions then react with additional methane molecules

$$CH_4^+(g) + CH_4(g) \rightarrow CH_5^+(g) + CH_3(g) \tag{8.5.2}$$

$$CH_3^+(g) + CH_4(g) \rightarrow C_2H_5^+(g) + H_2(g) \tag{8.5.3}$$

to form CH_5^+ and $C_2H_5^+$, species that are sufficiently reactive that they easily transfer a hydrogen to a molecule of the analyte, MH

$$CH_5^+(g) + MH(g) \rightarrow MH_2^+(g) + CH_4(g) \tag{8.5.4}$$

to give a molecular ion that we identify as $[M + H]^+$ and that has a mass that is one amu unit greater than that for M. Alternatively, they can easily remove a hydrogen from a molecule of the analyte, MH

$$C_2H_5^+(g) + MH(g) \rightarrow M^+(g) + C_2H_6(g) \tag{8.5.5}$$

to give a molecular ion that we identify as $[M - H]^-$ and that has a mass that is one amu less than that for M. Because formation of the molecular ion occurs indirectly and less energetically, fragmentation is suppressed, leading to a mass spectrum with a molecular ion peak and with only a small number of other ions. Figure 8.5.2 shows the mass spectrum for 1-decanol when using chemical ionization with CH_4 as the reagent gas.

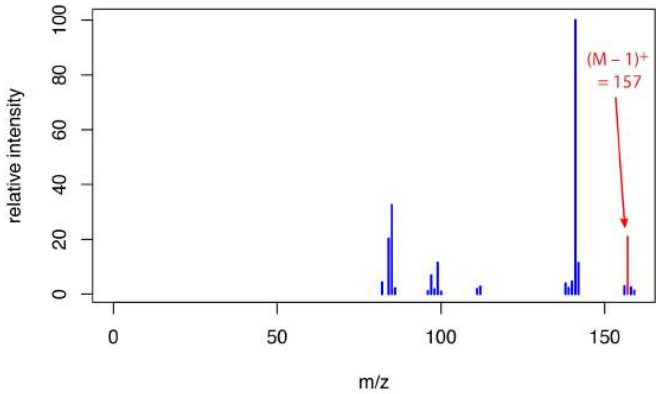


Figure 8.5.3: Mass spectrum for 1-decanol, $C_{10}H_{22}O$, using chemical ionization. The peak highlighted in red is the molecular ion, which has a *m*/*z* ratio of $158 - 1 = 157$ amu. The original data is available here.

Electrospray Ionization Sources (liquid phase/soft source)

Electron impact and chemical ionization are gas phase sources because the sample is volatilized before it enters the mass spectrometer's inlet. In electrospray ionization (ESI), the sample is a liquid and ions desorb from that matrix in the mass spectrometer's inlet system. The liquid sample is pulled into the spectrometer's inlet through a capillary needle, forming a mist of droplets. The application of a large potential across this inlet assures that the droplets carry positive charges. These charged droplets then enter a chamber where they undergo desolvation, which decreases the size of the droplet and increases their charge density (see Figure 8.5.4). As this charge density increases, the droplets eventually become unstable, for reasons that are not fully understood, and ionized gas-phase ions desorb from the droplets and enter into the mass analyzer.

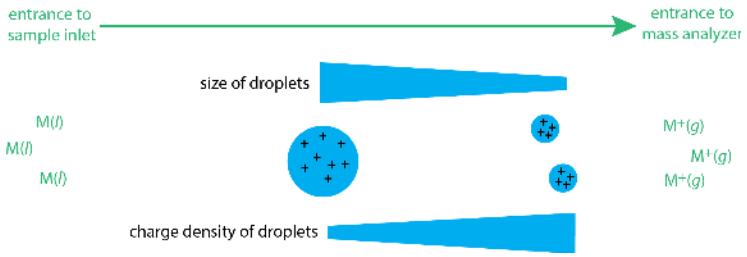


Figure 8.5.4: Illustration showing the change in the size of droplets and the charge density of droplets during electrospray ionization.

A typical electrospray ionization mass spectrum for a small molecule is shown in Figure 8.5.5 for the compound (4-aminophenyl)arsonic acid. As we saw in Figure 8.5.3 for chemical ionization, a soft ionization source results in a limited amount of fragmentation and a strong peak for the molecular ion, which here includes a proton transfer to give the $[M + H]^+$ peak at a *m/z* of 218 amu.

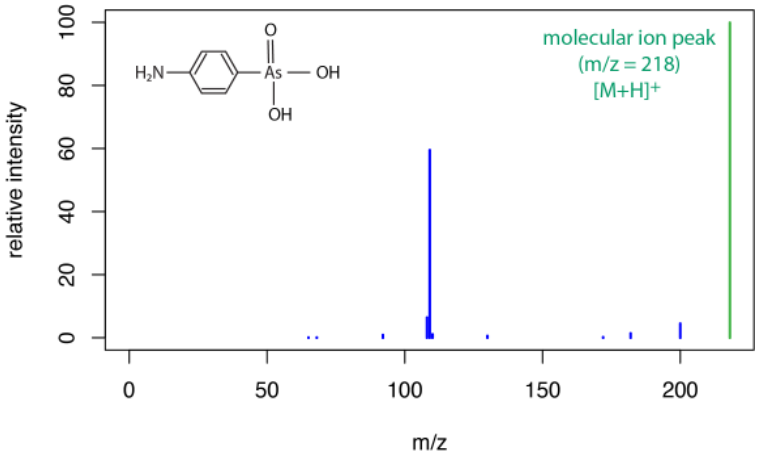


Figure 8.5.5: Mass spectrum for (4-aminophenyl)arsonic acid obtained using electrospray ionization. The spectrum contains only two majors peak: the molecular ion at $m/z = 218$ amu and a fragment at $m/z = 109$ amu. The original data is available here.

Electrospray ionization is particularly useful for biological molecules, such as peptides and proteins, because the soft ionization ensures that molecular weight information is retained. Because these molecules are large, they readily pick up multiple protons, forming multiply charged ions of the general form $[M + zH]^{z+}$ where *z* is the number of protons added. Figure 8.5.6 shows a hypothetical spectrum for the molecule M and Table 8.5.1 provides the corresponding *m/z* values for the mass spectrum's peaks.

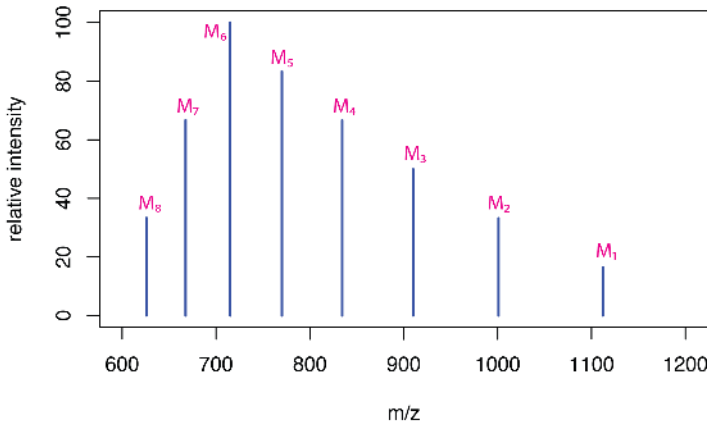


Figure 8.5.6: Simulated electrospray ionization mass spectrum for a molecule, M, that shows eight peaks with mass-to-charge ratios between 600 amu and 1200 amu. The subscripts in the symbols M_i serve to identify the peaks; they are not an indication of charge.

Table 8.5.1. Mass-to-charge ratios for the peaks in Figure 8.5.6.

peak	*m*/*z*
M_1	1112
M_2	1001
M_3	910
M_4	834
M_5	770
M_6	715
M_7	667
M_8	626

If we take the mass-to-charge ratios for any two adjacent peaks, M_i and M_j, where the peak M_i has the greater value for *m*/*z*, and if we assume that M_j has one additional hydrogen atom, giving it a charge that is one unit higher, then

$$Z_i = \frac{M_j - 1}{M_i - M_j} \tag{8.5.6}$$

where Z_i is the charge on the ion M_i. Table 8.5.2 shows the calculated charges for the ions M_1 to M_7.

Note

Here is a derivation for Equation 8.5.6. Suppose the molecule of interest has a molecular weight of m. If the charge on the ion responsible for peak M_i is Z, then it must be the case that the peak's mass is equal to m + Z as it has Z extra hydrogens and it must be the case that its mass-to-charge ratio is

$$M_i = \frac{m + Z}{Z}$$

and its molecular weight, m, is

$$m = (M_i \times Z) - Z$$

In the same way, the peak M_j has a charge of $Z + 1$ and

$$M_j = \frac{m + Z + 1}{Z + 1}$$

$$m = (M_j \times Z) + M_j - Z - 1$$

Setting the two equations for m equal to each other and solving for Z gives

$$(M_i \times Z) - Z = (M_j \times Z) + M_j - Z - 1$$

$$(M_i \times Z) = (M_j \times Z) + M_j - 1$$

$$(M_i \times Z) - (M_j \times Z) = M_j - 1$$

$$Z = \frac{M_j - 1}{M_i - M_j}$$

Table 8.5.2. Calculated charges on the ions for peaks M_1 to M_7

peak	*m*/*z*	Z
M_1	1112	9
M_2	1001	10
M_3	910	11
M_4	834	12
M_5	770	13
M_6	715	14
M_7	667	15
M_8	626	—

The molecular weight, m, is given by the equation

$$m = (M_i \times Z) - Z \tag{8.5.7}$$

Table 8.5.3 shows the molecular weights for the ions M_1 to M_7 and their average value. The simulated mass spectrum was created by setting the molecular weight to 10,000 amu and with charges ranging from +9 to +16.

Table 8.5.3. Calculated molecular weights for the ions M_1 to M_7.

peak	*m*/*z*	Z	m
M_1	1112	9	9,999
M_2	1001	10	10,000
M_3	910	11	9,999
M_4	834	12	9,996
M_5	770	13	9,997
M_6	715	14	9,996
M_7	667	15	10,005
M_8	626	—	—
		average molecular weight	9,999

Matrix-Assisted Laser Desorption/Ionization Sources (solid phase/soft source)

Matrix-assisted laser desorption ionization (MALDI) is a soft ionization source for obtaining the mass spectrum for biologically important molecules, such as proteins and peptides. Figure 8.5.7 illustrates the basic steps in obtaining a MALDI spectrum. The sample is first mixed with a small molecule—which is called the matrix—to form a solution; the matrix usually is present in a 10:1 ratio. A drop of this mixture is placed on a sample probe and allowed to dry, leaving the sample in a solid form. A pulsed laser

beam ($\lambda = 237$ nm is typical) is focused on the solid sample–matrix mixture. The matrix absorbs the laser pulse and the absorption of the laser's energy volatilizes both the matrix and the sample. Ionization of the sample forms molecular ions, usually $[M + H]^+$ ions, which are then swept into the mass analyzer.

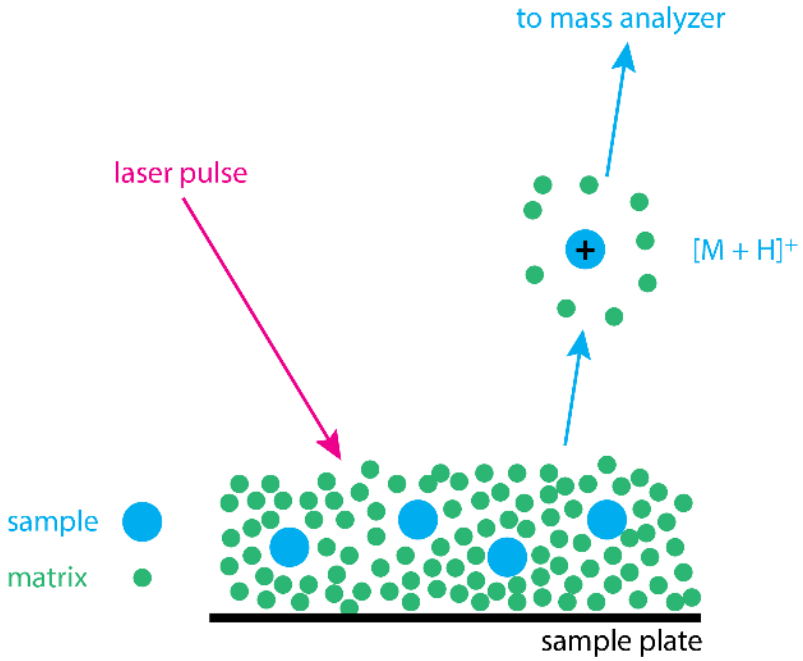


Figure 8.5.7: Illustration of matrix-assisted laser desorption ionization. The sample is dispersed in a liquid matrix and then allowed to dry. A pulsed laser beam is used to vaporize and ionize the sample.

When the sample is a digestion of a protein, then it is a mixture of peptides, each of which appeara as a $[M + H]^+$ peak in the resulting mass spectrum. For example, a peptide with the sequence AWSVAR (alanine–tryptophan–serine–valine–alanine–arginine) will appear as a peak with a mass of 689.8 daltons. To find this value we add together the molecular weights of the amino acids, account for the loss of a molecule of water for each peptide bond that forms, and then account for the hydrogen that gives the $[M + H]^+$ ion. In this case we have

$$[\mathrm{M+H}]^+ = 89.1 + 204.2 + 105.1 + 117.1 + 89.1 + 174.2 - (5 \times 18.0) + 1 = 689.8 \text{ amu}$$

where the term 5×18.0 accounts for the loss of five molecules of $\mathrm{H_2O}$ when forming the five peptide bonds.

Fast Atom Bombardment Sources (liquid phase/soft source)

Fast atom bombardment (FAB) bears some similarity to MALDI: the sample is mixed with a liquid matrix (often glycerol) and bombarded with a beam of xenon or argon atoms (instead of a laser). Desorption of the sample from its matrix forms gas phase ions that are swept into the mass analyzer. Spectra usually contain both a molecular ion and fragmentation patterns.

This page titled 8.5: Ion Sources is shared under a CC BY-NC-SA 4.0 license and was authored, remixed, and/or curated by David Harvey.

- **20.2: Ion Sources** by David Harvey is licensed CC BY-NC-SA 4.0.

8.5.1: Electrospray Ionization Mass Spectrometry

Electrospray ionization is a soft ionization technique that is typically used to determine the molecular weights of proteins, peptides, and other biological macromolecules. Soft ionization is a useful technique when considering biological molecules of large molecular mass, such as the aformetioned, because this process does not fragment the macromolecules into smaller charged particles, rather it turns the macromolecule being ionized into small droplets. These droplets will then be further desolvated into even smaller droplets, which creates molecules with attached protons. These protonated and desolvated molecular ions will then be passed through the mass analyzer to the detector, and the mass of the sample can be determined.

Introduction

Electrospray ionization mass spectrometry is a desorption ionization method. Desorption ionization methods can be performed on solid or liquid samples, and allows for the sample to be nonvolatile or thermally unstable. This means that ionization of samples such as proteins, peptides, olgiopeptides, and some inorganic molecules can be performed. Electrospray ionization mass spectrometry requires that a molecule be of a fairly large mass. The instrument has a small mass range that it is able to detect, so therefore the mass of the unknown injected sample can easily be determined; as it must be in the range of the instrument. This quantitative analysis is done by considering the mass to charge ratios of the various peaks in the spectrum (Figure 1). The spectrum is shown with the mass-to-charge (m/z) ratio on the x-axis, and the relative intensity (%) of each peak shown on the y-axis. Calculations to determine the unknown mass, M_r, from the spectral data can then be performed using

$$p = \frac{m}{z} \tag{8.5.1.1}$$

$$p_1 = \frac{M_r + z_1}{z_1} \tag{8.5.1.2}$$

$$p_2 = \frac{M_r + (z_1 - 1)}{z_1 - 1} \tag{8.5.1.3}$$

where p_1 and p_2 are adjacent peaks. Peak p_1 comes before peak p_2 in the spectrum, and has a lower m/z value. The z_1 value represents the charge of peak one. It should be noted that as the m/z value increases, the number of protons attached to the molecular ion decreases. Figure 1 below illustrates these concepts. Electrospray ionization mass spectrometry research was pioneered by the analytical chemistry professor John Bennet Fenn, who shared the Nobel Prize in Chemistry with Koichi Tanaka in 2002 for his work on the subject.

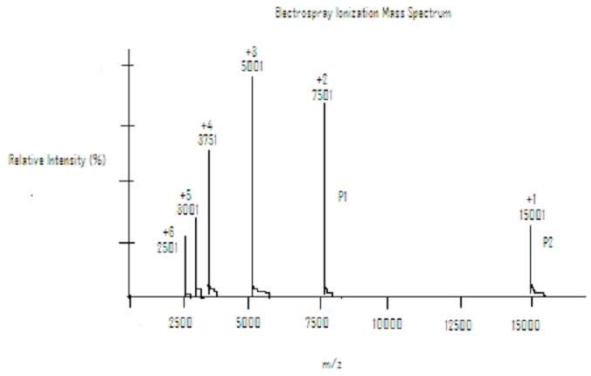


Figure 1. Mass Spectrum Example

Calculations for m/z in spectrum

$[M + 6H]^{6+}$ $[M + 5H]^{5+}$ $[M + 4H]^{4+}$

m/z = 15006/6 = 2501 m/z = 15005/5 = 3001 m/z = 15004/4 = 3751

$$[M + 3H]^{3+}\ [M + 2H]^{2+}\ [M + H]^{1+}$$

$$m/z = 15003/3 = 5001\ m/z = 15002/2 = 7501\ m/z = 15001/1 = 15001$$

Sample Preparation

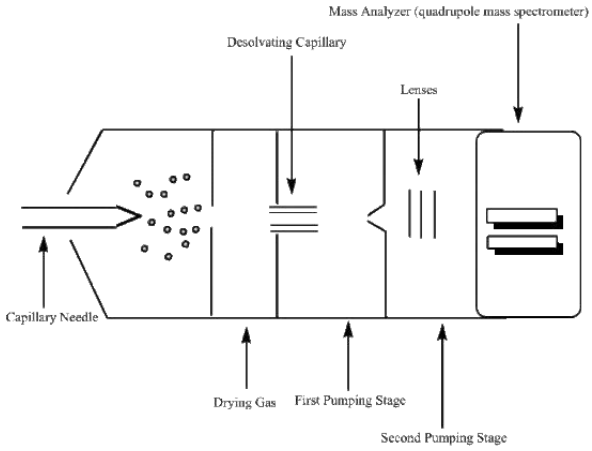
Samples for injection into the electrospray ionization mass spectrometer work the best if they are first purified. The reason purity in a sample is important is because this technique does not work well when mixtures are used as the analyte. For this reason a means of purification is often employed to inject a homogeneous sample into the capillary needle. High performance liquid chromatography, Capillary Electrophoresis, and Liquid-Solid Column Chromatography are methods of choice for this purpose. The chosen purification method is then attached to the capillary needle, and the sample can be introduced directly.

Advantages and Disadvantages

There are some clear advantages to using electrospray ionization mass spectrometry as an analytical method. One advantage is its ability to handle samples that have large masses. Another advantage is that this ionization method is one of the softest ionization methods available, therefore it has the ability to analyze biological samples that are defined by non-covalent interactions. A quadrupole mass analyzer can also be used for this method, which means that a sample's structure can be determined fairly easily. The m/z ratio range of the quadrupole instrument is fairly small, which means that the mass of the sample can be determined to with a high amount of accuracy. Finally, the sensitivity for this instrument is impressive and therefore can be useful in accurate quantitative and qualitative measurements.

Some disadvantages to electrospray ionization mass spectrometry are present as well. A major disadvantage is that this technique cannot analyze mixtures very well, and when forced to do so, the results are unreliable. The apparatus is also very difficult to clean and has a tendency to become overly contaminated with residues from previous experiments. Finally, the multiple charges that are attached to the molecular ions can make for confusing spectral data. This confusion is further fueled by use of a mixed sample, which is yet another reason why mixtures should be avoided when using an electrospray ionization mass spectrometer.

Apparatus



Capillary Needle

The capillary needle is the inlet into the apparatus for the liquid sample. Once in the capillary needle, the liquid sample is nebulized and charged. There is a large amount of pressure being applied to the capillary needle, which in effect nebulizes the liquid sample forming a mist. The stainless steel capillary needle is also surrounded by an electrode that retains a steady voltage of around 4000 volts. This applied voltage will place a charge on the droplets. Therefore, the mist that is ejected from the needle will be comprised of charged molecular ions.

Desolvating Capillary

The molecular ions are oxidized upon entering the desolvating capillary, and a continual voltage is applied to the gas chamber in which this capillary is located. Here the desolvation process begins, through the use of a dry gas or heat, and the desolvation process continues through various pumping stages as the molecular ion travels towards the mass analyzer. An example of a dry gas would be an N_2 gas that has been dehydrated. The gas or heat then provides means of evaporation, or desolvation, for the ionized droplets. As the droplets become smaller in size, their electric field densities become more concentrated. The increase in electric

field density causes the like charges to repel one another, which induces an increase in surface tension. The point where the droplet can no longer support this increase in surface tension is known as the Rayleigh limit. At this point, the droplet divides into smaller droplets of either positive or negative chrage. This process is refered to as either a coulombic explosion or the ions are described as exiting the droplet through the "Taylor cone". Once the molecular ions have reached the entrance to the mass analyzer, they have been effectively reduced through protonation.

Mass Analyzer

Mass Analyzers (Mass Spectrometry) are used to determine the mass-to-charge ratio (m/z), this ratio is used to differentiate between molecular ions that were formed in the desolvating capillary. In order for a mass-to-charge ratio to be determined, the mass analyzer must be able to separate even the smallest masses. The ability of the analyzer to resolve the mass peaks can be defined with the following equation;

$$R = \frac{m}{\Delta m} \tag{8.5.1.4}$$

This equation represents the mass of the first peak (m), divided by the difference between the neighboring peaks Δm. The better the resolution, the more useful the data. The mass analyzer must also be able to measure the ion currents produced by the multiply charged particles that are created in this process.

Mass analyzers use electrostatic lenses to direct the beam of molecular ions to the analyzer. A vacuum system is used to maintain a low pressure environment in order to prevent unwanted interactions between the molecular ions and any components that may be present in the atmosphere. These atmospheric components can effect the determined mass-to-charge ratio, so it is best to keep them to a minimum. The mass-to-charge ratio is then used to determine quantitative and qualitative properties of the liquid sample.

The mass analyzer used for electrospray ionization is a quadrupole mass spectrometer. A quadrupole mass spectrometer uses four charged rods, two negatively charged and two positively charged, that have alternating AC and DC currents. The rods are connected to both the positive terminal of the DC voltage and the negative terminal. Each pair of rods contains a negatively charged rod and a positively charged rod. The molecular ions are then sped through the chamber between these pairs of oppositely charged rods making use of a potential difference to do so. To maintain charge, and ultimately be readable by the detector, the molecular ions must travel through the quadrupole chamber without touching any of the four charged rods. If a molecular ion does run into one of the rods it will deem it neutral and undetectable.

Detector

The molecular ions pass through the mass analyzer to the detector. The detector most commonly used in conjunction with the quadrupole mass analyzer is a high energy dynode (HED), which is a electron multiplier with some slight variations. In an HED detector, the electrons are passed through the system at a high voltage and the electrons are measured at the end of the funnel shaped apparatus; otherwise known as the anode. A HED detector differs from the electron multiplier in that it operates at a much higher sensitivity for samples with a large mass than does the electron multiplier detector. Once the analog signal of the mass-to-charge ratio is recorded, it is then converted to a digital signal and a spectrum representing the data run can be analyzed.

References

1. Skoog, D.A.; Holler, F.J.; Crouch, S.R. Principles of Instrumental Analysis. Sixth Edition, Thomson Brooks/Cole, USA (2007).
2. Siuzdak, G. Mass Spectrometry for Biotechnology. Academic Press, Inc., USA (1996).
3. Chapman, J.R. Mass Spectrometry of Proteins and Peptides. Methods in Molecular Biology volume 146,Humana Press, Totowa, NJ (2000).
4. Snyder, A. P. Biochemical and Biotechnological Applications of Electrospray Ionization Mass Spectrometry. American Chemical Society, Washington, DC (1996).

Problems

Using the above spectrum, calculate the mass of the protein. For $p_{1,}$ shown in spectrum, the m/z is 7501 and for p_2 the m/z is 15001. (Hint: Use the above equations, and the charge of p_1 for z_1)

Contributors and Attributions

- Jennifer Murphy

8.5.1: Electrospray Ionization Mass Spectrometry is shared under a CC BY-NC-SA 4.0 license and was authored, remixed, and/or curated by LibreTexts.

- **Electrospray Ionization Mass Spectrometry** is licensed CC BY-NC-SA 4.0.

8.6: Mass Spectrometers

A mass spectrometer has four essential elements: a means for introducing the sample to the instrument, a means for generating a mixture of ions, a means for separating the ions, and a means for counting the ions. In Chapter 20.2 we introduced some of the most important ways to generate ions. In this section we turn our attention to sample inlet systems and to separating and counting ions. You may wish to review Chapter 11 where we considered these topics in the context of atomic mass spectrometry. As we noted in Chapter 11, a mass spectrometer must operate under a vacuum to ensure that ions can travel long distances without undergoing undesired collisions that affect their ion energy.

Sample Inlet Systems

When the sample is a gas or a volatile liquid, it is easy to transfer a portion of the sample into a reservoir as a gas maintained at a relatively small pressure. The sample is then allowed to enter into the mass spectrometer's ion source through a diaphragm that contains a pin-hole, drawn in by holding the ion source at lower pressure.

Solid and non-volatile liquids are sampled by inserting them directly into the ion source through a vacuum lock that allows the mass spectrometer to remain under vacuum except for the ion source where the sample is inserted. The sample is placed in a capillary tube or a small cup at the end of a sample probe, and then moved into the ion source. The sample probe includes a heating coil that is used, along with the instrument's vacuum, to help volatilize the sample.

Of particular importance are inlet systems that couple a chromatographic or an electrophoretic instrument to a mass spectrometer, providing a way to separate a complex mixture into its individual components and then using the mass spectrometer to determine the composition of those components. The interface between a gas chromatograph and a mass spectrometer (GC-MS) must account for the significant drop in pressure from atmospheric pressure to a pressure of 10^{-8} torr; the interface for LC-MS and for EC-MS must provide a way to remove the liquid eluent, to volatilize the samples, and to account for the drop in pressure. See Chapters 27, 28, and 30 for more details.

Mass Analyzers

The purpose of the mass analyzer is to separate the ions by their mass-to-charge ratios. Ideally we want the mass analyzer to allow us to distinguish between small differences in mass and to do so with a strong signal-to-noise ratio. As we learned in Chapter 7 when introducing optical spectroscopy, these two desires usually are in tension with each other, with improvements in resolution often coming with an increase in noise.

Resolution

The resolution between two peaks, R, in mass spectrometry is defined as the ratio of their average mass to the difference in their masses

$$R = \frac{\overline{m}}{\Delta m} \tag{8.6.1}$$

The following table shows how resolution varies as a function of the average mass and the difference in mass. A resolution of 1,000, for example is sufficient to resolve two ions with an average mass of 100 amu that differ by 0.1 amu, or two ions that have an average mass of 1,000 amu that differ by 1 amu.

Table 8.6.1. Resolution for stated values of $\overline{m}$ and Δm.

$\overline{m} \rightarrow$ $\Delta m \downarrow$	100 amu	1000 amu	10,000 amu
0.1 amu	1,000	10,000	100,000
1 amu	100	1,000	10,000
10 amu	10	100	1,000

Magnetic Sector Mass Analyzers

When a beam of ions passes through a magnetic field, its path is altered, as we see in Figure 8.6.1. The ions experience an acceleration as they exit the ion source and enter the mass analyzer with a kinetic energy that is given by the equations

$$\text{KE} = zeV \tag{8.6.2}$$

$$\text{KE} = \frac{1}{2}mv^2 \tag{8.6.3}$$

where z is the ion's charge (usually +1), e is the electronic charge in Coulombs, V is the applied voltage responsible for the acceleration, m is the ion's mass, and v is the ion's velocity after acceleration. Equation 8.6.2 shows us that all ions with the same charge have the same kinetic energy. Equation 8.6.3, then, tells us that ions with a greater mass will move more slowly.

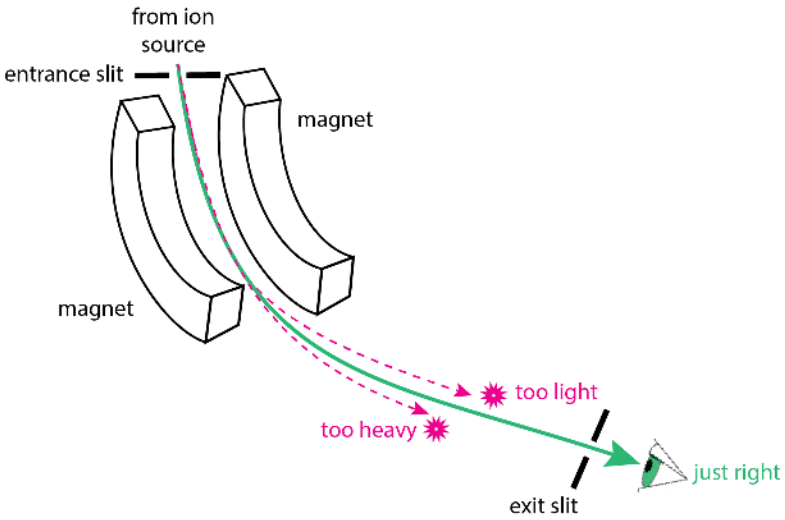


Figure 8.6.1: Illustration of a magnetic sector analyzer for mass spectrometry. Ions from the ion source enter into the mass analyzer. The magnets in the mass analyzer bend the path followed by the ions. For any combination of magnetic field strength and accelerating voltage, only ions with a compatible mass-to-charge ratio are able to leave the mass analyzer through the exit slit; ions that are too heavy or too light, fail to exit the mass analyzer.

An ion's path through the magnetic field is determined by two forces. The first of these forces is the magnetic force, F_M, that acts on the ion, which is

$$F_M = Bzev \tag{8.6.4}$$

where B is the magnetic field strength. The second of these forces is the centripetal force, F_C, that acts on the ion as it moves along its curved path, which is

$$F_C = \frac{mv^2}{r} \tag{8.6.5}$$

where r is the magnet's radius of curvature. An ion can only navigate these opposing forces if F_M and F_C are equal to each other. This requires that

$$Bzev = \frac{mv^2}{r} \tag{8.6.6}$$

Solving for v gives

$$v = \frac{Bzer}{m} \tag{8.6.7}$$

Substituting back into Equation 8.6.3 and solving for the mass-to-charge ratio gives

$$\frac{m}{z} = \frac{B^2r^2e}{2V} \tag{8.6.8}$$

Equation 8.6.8 tells us that for any combinaton of magnetic field strength, B, and accelerating voltage, V, only one mass-to-charge ratio has the correct value of r to reach the director. Ions that are too heavy or ions that are too light, will collide with the sides of the mass analyzer before they reach the detector. The mass spectrum is recorded by holding V and r constant and varying the magnetic field strength, B. The resolution of a magnetic sector instrument is usually less than 2000.

Double-Focusing Mass Analyzers

The resolution of a magnetic sector instrument suffers from limitations that affect its ability to narrow the range of kinetic energies—and, thus, velocities—possessed by the ions when they exit the ion source and enter the mass analyzer. The double-focusing mass analyzer in Figure 8.6.2 compensates for this by placing an electrostatic analyzer before the magnetic analyzer, separating the two by a slit. The electrostatic analyzer consists of two curved metal plates, one of which is held at a positive potential and one at a negative potential. As ions pass betweeen the plates, those ions that have too much energy and those that have too little energy fail to pass through the slit that separates the electrostatic analyzer from the magnetic analyzer. In this way, the distribution of energies—and, thus, velocities—is tightened, improving the resolution achieved by the magnetic sector analyzer. Depending on its design, a double-focusing analyzer can achieve a resolution as large as 100,000.

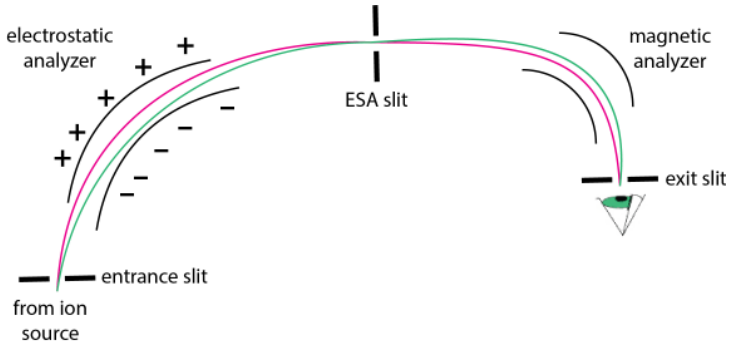


Figure 8.6.2: Illustration of a double-focusing mass analyzer that consists of an electrostatic mass analyzer and a magnetic mass analyzer. Ions that make it through the slit that separates the two analyzers have a smaller range of kinetic energies than the ions in a magnetic sector mass analyzer, which improves resolution.

Quadrupole Mass Analyzers

The quadrupole mass analyzer was introduced in Chapter 11 and the treatment here is largely the same. A quadupole mass analyzer is compact in size, low in cost, easy to use, and easy to maintain. As shown in Figure 8.6.3, it consists of four cylindrical rods, two of which are connected to the positive terminal of a variable direct current (dc) power supply and two of which are connected to the power supply's negative terminal; the two positive rods are positioned opposite of each other and the two negative rods are positioned opposite of each other. Each pair of rods is also connected to a variable alternating current (ac) source operated such that the alternating currents are 180° out-of-phase with each other. An ion beam from the source is drawn into the channel between the quadrupoles and, depending on the applied dc and ac voltages, ions with only one mass-to-charge ratio successfully travel the length of the mass analyzer and reach the transducer; all other ions collide with one of the four rods and are destroyed.

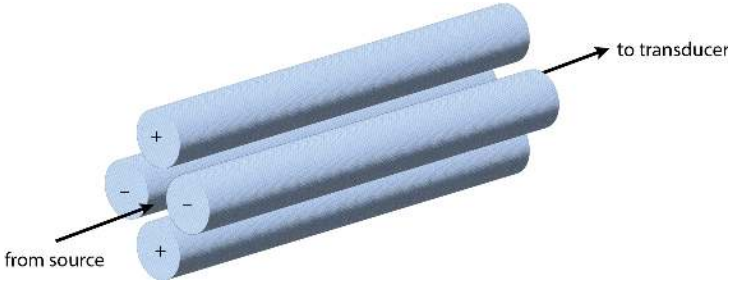


Figure 8.6.3: Basic arrangement of the quadrupole mass analyzer. The plus and the minus signs on each rod indicate which are connected to the positive terminal of the dc power supply. Not shown here is the circuitry for applying the alternating current. The ion beam enters the channel between the quadrupoles. Depending on the applied dc and ac voltages, some of the ions emerge from this channel and reach the transducer.

To understand how a quadrupole mass analyzer achieves this separation of ions, it helps to consider the movement of an ion relative to just two of the four rods, as shown in Figure 8.6.4 for the poles that carry a positive dc voltage. When the ion beam enters the channel between the rods, the ac voltage causes the ion to begin to oscillate. If, as in the top diagram, the ion is able to maintain a stable oscillation, it will pass through the mass analyzer and reach the transducer. If, as in the middle diagram, the ion is

unable to maintain a stable oscillation, then the ion eventually collides with one of the rods and is destroyed. When the rods have a positive dc voltage, as they do here, ions with larger mass-to-charge ratios will be slow to respond to the alternating ac voltage and will pass through the transducer. The result is shown in the figure at the bottom (and repeated in Figure $8.6.5a$) where we see that ions with a sufficiently large mass-to-charge ratios successfully pass through the transducer; ions with smaller mass-to-charge ratios do not. In this case, the quadrupole mass analyzer acts as a high-pass filter.

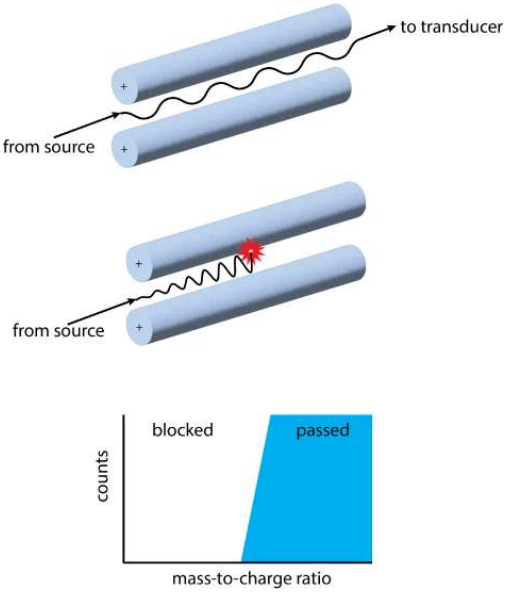


Figure 8.6.4: Illustration of how a quadrupole mass analyzer achieves separation of ions by their mass-to-charge ratio. See the text for additional details.

We can extend this to the behavior of the ions when they interact with rods that carry a negative dc voltage. In this case, the ions are attracted to the rods, but those ions that have a sufficiently small mass-to-charge ratio are able to respond to the alternating current's voltage and remain in the channel between the rods. The ions with larger mass-to-charge ratios move more sluggishly and eventually collide with one of the rods. As shown in Figure $8.6.5b$, in this case, the quadrupole mass analyzer acts as a low-pass filter. Together, as we see in Figure $8.6.5c$, a quadrupole mass analyzer operates as both a high-pass and a low-pass filter, allowing a narrow band of mass-to-charge ratios to pass through the transducer. By varying the applied dc voltage and the applied ac voltage, we can obtain a full mass spectrum.

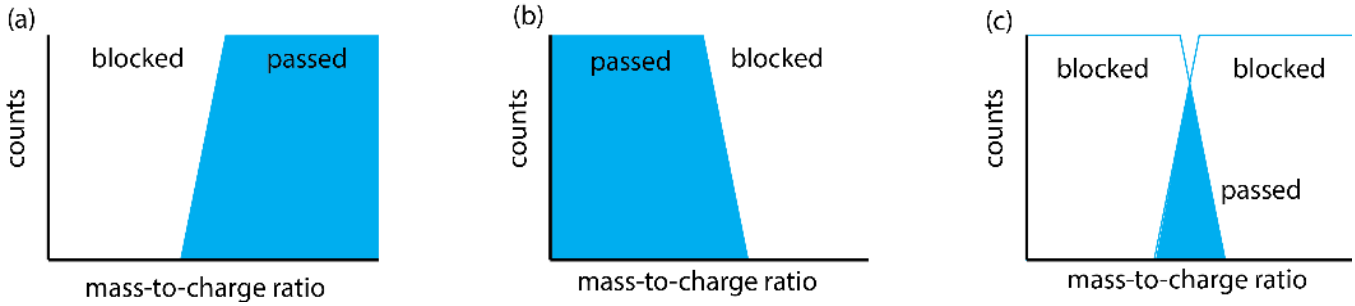


Figure 8.6.5: Illustration that shows how a quadrupole mass analyzer acts as both (a) a high-pass filter and (b) a low pass filter, with the result that it passes only ions with a narrow range of mass-to-charge ratios.

Quadrupole mass analyzers provide a modest mass-to-charge resolution of about 1 amu and extend to m/z ratios of approximately 2000.

Time-Of-Flight Mass Analyzers

In a time-of-flight mass analyzers, Figure $8.6.6$, ions are created in small clusters by applying a periodic pulse of energy to the sample using a laser beam or a beam of energetic particles to ionize the sample. The small cluster of ions are then drawn into a tube by applying an electric field and then allowed to drift through the tube in the absence of any additional applied field; the tube, for obvious reasons, is called a drift tube. All of the ions in the cluster enter the drift tube with the same kinetic energy, KE, which we define as

$$\text{KE} = \frac{1}{2}mv^2 = zeV \tag{8.6.9}$$

The time, T, that it takes the ion to travel the distance, L, to the detector is

$$T = \frac{L}{v} \tag{8.6.10}$$

Substituting Equation 8.6.10 into Equation 8.6.9

$$T = \sqrt{\frac{m}{z}} \times \sqrt{\frac{1}{2eV}} \tag{8.6.11}$$

shows us that the time it takes an ion to travel through the drift tube is proportional to the square rate of its mass-to-charge ratio. As a result, lighter ions move more quickly than heavier ions. Flight times are typically less than 30 µs. A time-of-flight mass analyzer provide better resolution than a quadrupole mass analyzer, but is limited to sources that can be pulsed. A linear time-of-flight analyzer, such as that in Figure 8.6.6, provide a resolution of approximately 4,000; other configurations can achieve resolutions of 10,000 or better. The time-of-flight analyzer is well-suited for MALDI ionization as the time between pulses of the laser provides the time needed for detection to occur.

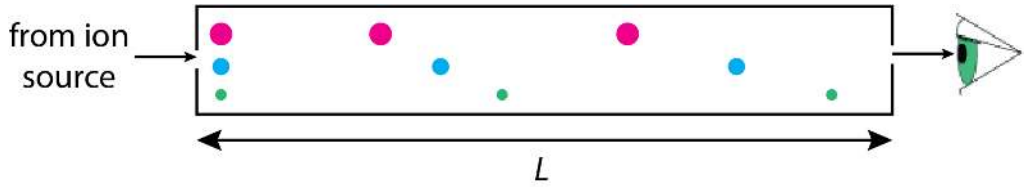


Figure 8.6.6: Illustration of a linear time-of-flight mass analyzer showing three views of the relative positions of three ions with a small (green), medium (blue), and large (red) mass-to-charge ratios as they migrate through the drift tube.

Ion Trap Mass Analyzers

Figure 8.6.7 provides an illustration of an ion trap mass analyzer, which consists of three electrodes—a central ring electrode and two conical end cap electrodes—that create a cavity into which ions are drawn. The ions in the cavity experience stabilizing and destabilizing forces that affect their movement within the cavity. Ions that adopt stable orbits remain in the cavity. By varying the potentials applied to the electrodes, ions with different mass-to-charge ratios enter into destabilizing orbits and exit through a small hole at the bottom of the trap. An ion trap typcially provides a resolution of 1,000.

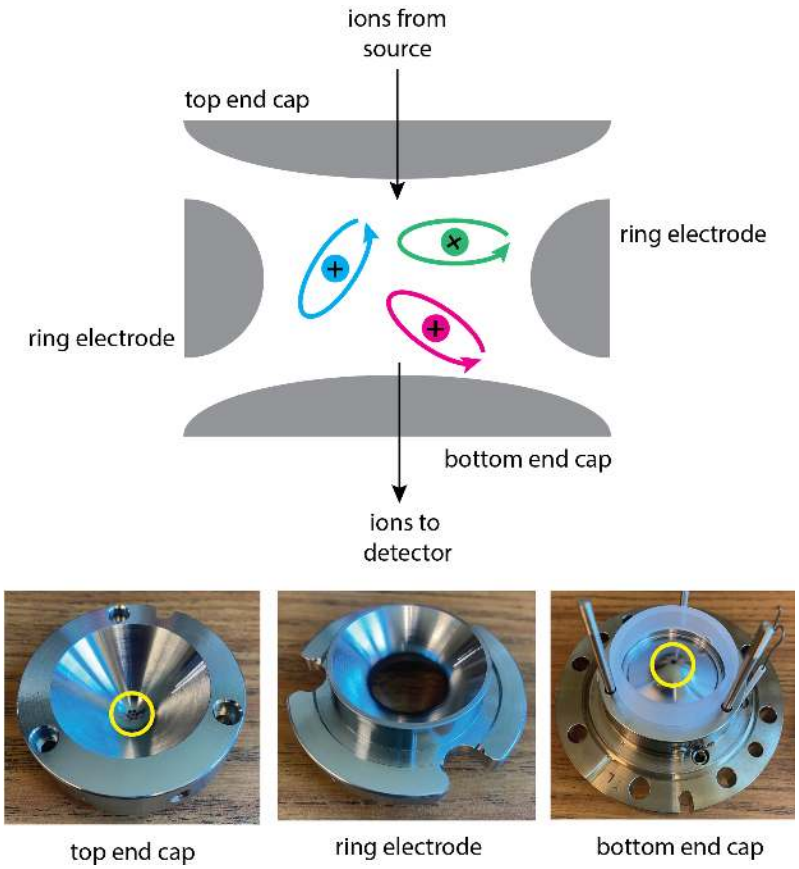


Figure 8.6.7: Illustration of the ion trap mass analyzer showing the cavity defined by the top end cap, the ring electrode, and the bottom end cap. The photographs on the bottom show the conical-shaped top end cap with small holes (inside the yellow circle) that allows ions to enter into the cavity, the ring electrode, and the conical-shaped bottom end cap, which has a small hole (inside the yellow circle) that allows ions to exit the cavity and reach the detector.

Ion Cyclotron Resonance Mass Analyzer

The ion cyclotron resonance (ICR) analyzer is a form of an ion trap but operates in a way that retains all ions within the trap. When a gas phase ion is placed within an applied magnetic field, the ions move in a circular orbit that is perpendicular to the applied field (Figure 8.6.8). In discussing the magnetic sector analyzer, we showed that the velocity, v, of an ion in an applied magnetic field with a strength of B is a function of the radius of the ion's motion, r, and its charge

$$v = \frac{Bzer}{m} \tag{8.6.12}$$

Solving for the ratio v/r gives the ion's cyclotron frequency, w_c, as

$$w_c = \frac{v}{r} = \frac{zeB}{m} \tag{8.6.13}$$

When an ion moving in a circular orbit, as shown by the smaller of the two circular orbits in Figure 8.6.8*a*, absorbs energy equal to its cyclotron frequency, w_c, its velocity, v, and the radius of its orbit, r both increase to maintain a constant value for w_c; the result is an ion that moves in a circular orbit of greater radius. As w_c depends on the mass-to-charge ratio, all ions of equal m/z experience the same change in their orbit, while ions with other mass-to-charge ratios are unaffected. Ions in the larger orbits eventually return to their original circular orbit as a result of collisions in which they lose energy.

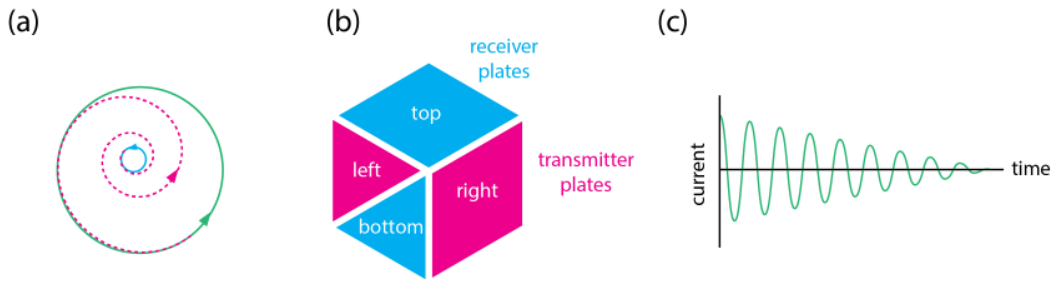


Figure 8.6.8: Illustration of how an ICR mass analyzer works. In (a) an ion originally in a circular orbit with a small radius, shown in blue moves into a circular orbit with a larger radius, shown in green when it absorbs energy equal to its cyclotron frequency, w_c, following the path shown in pink. The ICR cell in (b) consists of two transmitter plates that apply the potential that alters each ion's orbit, and two receiver plates that measure the current generated by the ions; there are two additional plates, one in front and one in back, that provide an entrance for bringing ions into the ICR cell from the ion source and for removing the ions in preparation for the next sample. The signal in (c) decays with time as the ions lose energy through collisions.

The trap itself, as seen in Figure 8.6.8*b*, is defined by two pairs of plates (four in all). The transmitter plates are used to apply the potential that alters the orbits of the ions. Movement of the ions generates a current in the receiver plates that serves as the signal, as seen in Figure 8.6.8*c*, that is positive when the ion is closer to one receiver plate and negative when it is closer to the other receiver plate. The initial magnitude of the current is proportional to the number of ions with the mass-to-charge ratio.

The ion cyclotron resonance analyzer is usually operated by applying a short pulse of energy that varies linearly in its frequency. This sets all ions into motion, with each mass-to-charge ratio yielding a current response similar to that in Figure 8.6.8*c*. Collectively, these individual current-time curves gives a time domain spectrum that we can covert into a frequency domain spectrum by taking the Fourier transform. The frequency domain spectrum yields the mass spectrum through Equation 8.6.13. FT-ICR instruments are capable of achieving resolutions of 1,000,000.

This page titled 8.6: Mass Spectrometers is shared under a CC BY-NC-SA 4.0 license and was authored, remixed, and/or curated by David Harvey.

- **20.3: Mass Spectrometers** by David Harvey is licensed CC BY-NC-SA 4.0.

8.6.1: Mass Analyzers (Mass Spectrometry)

Mass spectrometry is an analytic method that employs ionization and mass analysis of compounds to determine the mass, formula and structure of the compound being analyzed. A mass analyzer is the component of the mass spectrometer that takes ionized masses and separates them based on charge to mass ratios and outputs them to the detector where they are detected and later converted to a digital output.

Introduction

There are six general types of mass analyzers that can be used for the separation of ions in a mass spectrometry.

1. Quadrupole Mass Analyzer
2. Time of Flight Mass Analyzer
3. Magnetic Sector Mass Analyzer
4. Electrostatic Sector Mass Analyzer
5. Quadrupole Ion Trap Mass Analyzers
6. Ion Cyclotron Resonance

Quadrupole Mass Analyzer

The DC bias will cause all the charged molecules to accelerate and move away from the center line, the rate being proportional to their charge to mass ratio. If their course goes off too far they will hit the metal rods or the sides of the container and be absorbed. So the DC bias acts like the magnetic field B of the mass spec and can be tuned to specific charge to mass ratios hitting the detector.

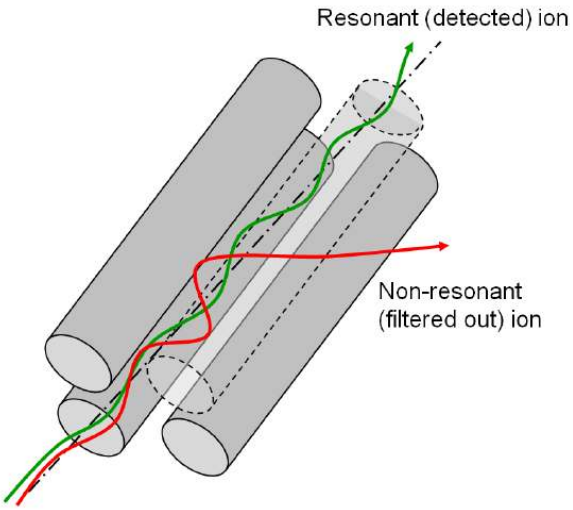


Figure 8.6.1.1: A quadrupole

The two sinusoidal electric fields at 90 orientation and 90 degrees degrees phase shift will cause an electric field which oscillates as a circle over time. So as the charged particles fly down toward the detector, they will be traveling in a spiral, the diameter of the spiral being determined by the charge to mass ratio of the molecule and the frequency and strength of the electric field. The combination of the DC bias and the circularly rotating electric field will be the charge particles will travel in a spiral which is curved. So by timing the peak of the curved spiral to coincide with the position of the detector at the end of the quadrupole, a great deal of selectivity to molecules charge to mass ratio can be obtained.

TOF (Time of Flight) Mass Analyzer

TOF Analyzers separate ions by time without the use of an electric or magnetic field. In a crude sense, TOF is similar to chromatography, except there is no stationary/ mobile phase, instead the separation is based on the kinetic energy and velocity of the ions.

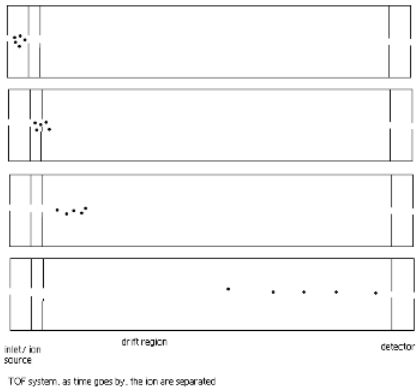


Figure 8.6.1.2: A TOF system. As time evolves, the ions (formed at the source) are separated.

Ions of the same charges have equal kinetic energies; kinetic energy of the ion in the flight tube is equal to the kinetic energy of the ion as it leaves the ion source:

$$KE = \frac{mv^2}{2} = zV \tag{8.6.1.1}$$

The time of flight, or time it takes for the ion to travel the length of the flight tube is:

$$T_f = \frac{L}{v} \tag{8.6.1.2}$$

- with L is the length of tube and
- v is the velocity of the ion

Substituting Equation 1 for kinetic energy in Equation 2 for time of flight:

$$T_f = L\sqrt{\frac{m}{z}}\sqrt{\frac{1}{2V}} \propto \sqrt{\frac{m}{z}} \tag{8.6.1.3}$$

During the analysis, L, length of tube, the Voltage from the ion source V are held constant, which can be used to say that time of flight is directly proportional to the root of the mass to charge ratio.

Unfortunately, at higher masses, resolution is difficult because flight time is longer. Also at high masses, not all of the ions of the same m/z values reach their ideal TOF velocities. To fix this problem, often a **reflectron** is added to the analyzer. The reflectron consists of a series of ring electrodes of very high voltage placed at the end of the flight tube. When an ion travels into the reflectron, it is reflected in the opposite direction due to the high voltage. The reflectron increases resolution by narrowing the broadband range of flight times for a single m/z value. Faster ions travel further into the reflectrons, and slower ions travel less into the reflector. This way both slow and fast ions, of the same m/z value, reach the detector at the same time rather then at different times, narrowing the bandwidth for the output signal.

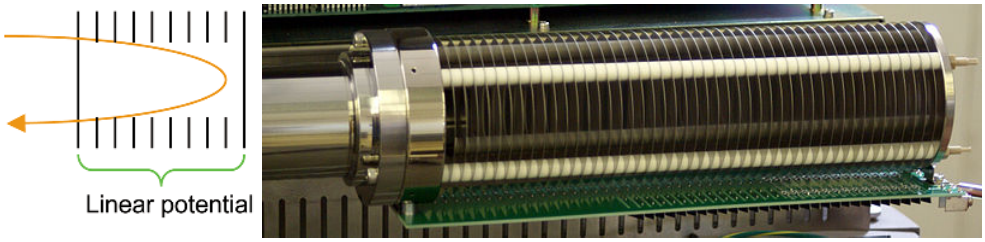


Figure 8.6.1.3: (left) A reflection. from Wikipedia. (right) 4. A photo of a reflectron. An ion mirror (right) attached to a flight tube (left) of the reflectron. Voltages applied to a stack of metal plates create the electric field reflecting the ions back to the flight tube. In this particular design, gaps between the mirror electrodes are too large. This can lead to a distortion of the field inside the mirror caused by a proximity of metal surface of the enveloping vacuum tube. from Wikipedia.

Magnetic Sector Mass Analyzer

Similar to time of flight (TOF) analyzer mentioned earlier,in magnetic sector analyzers ions are accelerated through a flight tube, where the ions are separated by charge to mass ratios. The difference between magnetic sector and TOF is that a magnetic field is

used to separate the ions. As moving charges enter a magnetic field, the charge is deflected to a circular motion of a unique radius in a direction perpendicular to the applied magnetic field. Ions in the magnetic field experience two equal forces; force due to the magnetic field and centripetal force.

$$F_B = zvB = F_c = \frac{mv^2}{r} \tag{8.6.1.4}$$

The above equation can then be rearranged to give:

$$v = \frac{Bzr}{m} \tag{8.6.1.5}$$

If this equation is substituted into the kinetic energy equation:

$$KE = zV = \frac{mv^2}{2} \tag{8.6.1.6}$$

$$\frac{m}{z} = \frac{B^2r^2}{2V} \tag{8.6.1.7}$$

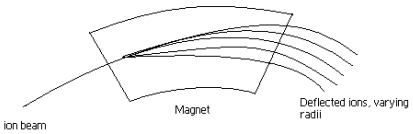


Figure 8.6.1.4: A magnetic sector separator.

Basically the ions of a certain m/z value will have a unique path radius which can be determined if both magnetic field magnitude B, and voltage difference V for region of acceleration are held constant. when similar ions pass through the magnetic field, they all will be deflected to the same degree and will all follow the same trajectory path. Those ions which are not selected by V and B values, will collide with either side of the flight tube wall or will not pass through the slit to the detector. Magnetic sector analyzers are used for mass focusing, they focus angular dispersions.

Electrostatic Sector Mass Analyzer

Is similar to time of flight analyzer in that it separates the ions while in flight, but it separates using an electric field. Electrostatic sector analyzer consists of two curved plates of equal and opposite potential. As the ion travels through the electric field, it is deflected and the force on the ion due to the electric field is equal to the centripetal force on the ion. Here the ions of the same kinetic energy are focused, and ions of different kinetic energies are dispersed.

$$KE = zV = \frac{mv^2}{2} \tag{8.6.1.8}$$

$$F_E = zE = F_c = \frac{mv^2}{R} \tag{8.6.1.9}$$

Electrostatic sector analyzers are energy focusers, where an ion beam is focused for energy. Electrostatic and magnetic sector analyzers when employed individually are single focusing instruments. However when both techniques are used together, it is called a double focusing instrument., because in this instrument both the energies and the angular dispersions are focused.

Quadrupole Ion Trap Mass Analyzers

This analyzer employs similar principles as the quadrupole analyzer mentioned above, it uses an electric field for the separation of the ions by mass to charge ratios. The analyzer is made with a ring electrode of a specific voltage and grounded end cap electrodes. The ions enter the area between the electrodes through one of the end caps. After entry, the electric field in the cavity due to the electrodes causes the ions of certain m/z values to orbit in the space. As the radio frequency voltage increases, heavier mass ion orbits become more stabilized and the light mass ions become less stabilized, causing them to collide with the wall, and eliminating the possibility of traveling to and being detected by the detector.

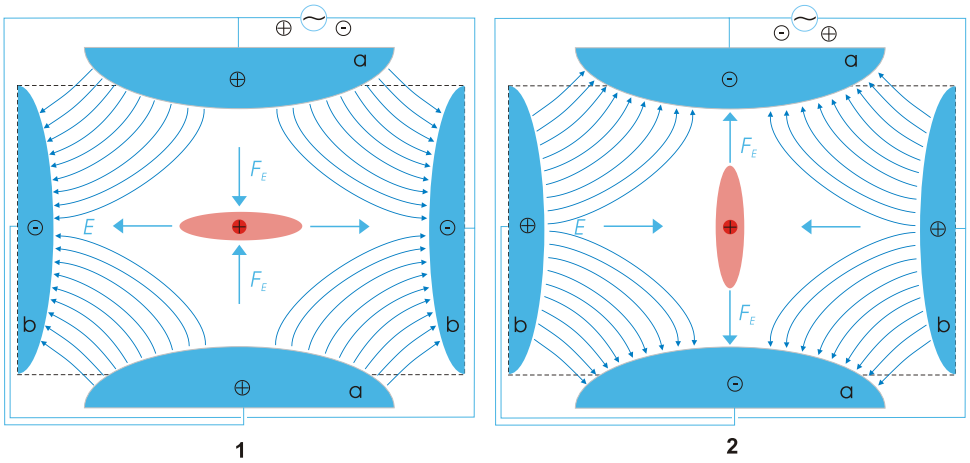


Figure 8.6.1.5: Scheme of a Quadrupole ion trap of classical setup with a particle of positive charge (dark red), surrounded by a cloud of similarly charged particles (light red). The electric field E (blue) is generated by a quadrupole of endcaps (a, positive) and a ring electrode (b). Picture 1 and 2 show two states during an AC cycle. (CC BY 2.5; Arian Kriesch Akriesch via Wikipedia).

The quadrupole ion trap usually runs a mass selective ejection, where selectively it ejects the trapped ions in order of in creasing mass by gradually increasing the applied radio frequency voltage.

Ion Cyclotron Resonance (ICR)

ICR is an ion trap that uses a magnetic field in order to trap ions into an orbit inside of it. In this analyzer there is no separation that occurs rather all the ions of a particular range are trapped inside, and an applied external electric field helps to generate a signal. As mentioned earlier, when a moving charge enters a magnetic field, it experiences a centripetal force making the ion orbit. Again the force on the ion due to the magnetic field is equal to the centripetal force on the ion.

$$zvB = \frac{mv^2}{r} \tag{8.6.1.10}$$

Angular velocity of the ion perpendicular to the magnetic field can be substituted here $w_c = v/r$

$$zB = mw_c \tag{8.6.1.11}$$

$$w_c = \frac{zB}{m} \tag{8.6.1.12}$$

Frequency of the orbit depends on the charge and mass of the ions, not the velocity. If the magnetic field is held constant, the charge to mass ratio of each ion can be determined by measuring the angular velocity ω_c. The relationship is that, at high w_c, there is low m/z value, and at low ω_c, there is a high m/z value. Charges of opposite signs have the same angular velocity, the only difference is that they orbit in the opposite direction.

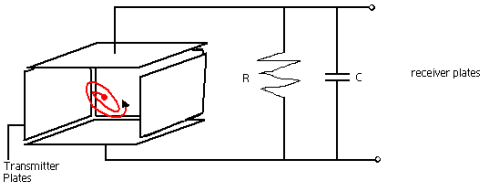


Figure 8.6.1.6: An ICR trap.

To generate an electric signal from the trapped ions, a vary electric field is applied to the ion trap

$$E = E_o \cos(\omega_c t) \tag{8.6.1.13}$$

When the ω_c in the electric field matches the ω_c of a certain ion, the ion absorbs energy making the velocity and orbiting radius of the ion increase. In this high energy orbit, as the ion oscillates between two plates, electrons accumulate at one of the plates over the other inducing an oscillating current, or current image. The current is directly proportional to the number of ions in the cell at a certain frequency.

In a Fourier Transform ICR, all of the ions within the cell are excited simultaneously so that the current image is coupled with the image of all of the individual ion frequencies. A Fourier transform is used to differential the summed signals to produce the desired results.

References

1. K. Downard, *Mass Spectrometry: A Foundation Course*, The Royal Society of Chemistry: UK 2004, Chapter 3
2. Skoog, Holler, Grouch, *Principles of Instrumental Analysis*, Thomson Brooks/Cole 2007, chapter 20
3. C. Herbert, R. Johnstone, *Mass Spectrometry Basics*, CRC Press LLC, 2003 chapter 25, 26, 39
4. E. De Hoffman, V. Stroobant, *Mass Spectrometry: Principles and Applications*, 2nd ed.;Wiley: England, 2001, chapter 2

Contributors and Attributions

- Ommaima Khan

8.6.1: Mass Analyzers (Mass Spectrometry) is shared under a CC BY-NC-SA 4.0 license and was authored, remixed, and/or curated by LibreTexts.

- **Mass Analyzers (Mass Spectrometry)** is licensed CC BY-NC-SA 4.0.

8.7: Applications of Molecular Mass Spectrometry

Qualitative Applications

In a qualitative analysis our interest is in determining the identity of a substance of interest to us. By itself, mass spectrometry is a powerful tool for determining the identity of pure compounds. The analysis of mixtures, however, is possible if we use a mass spectrometer as the detector for a separation technique, such as gas chromatography, or if we string together two or more mass analyzers in sequence.

Identification of Pure Compounds

There are several ways to use a mass spectrum to identify a compound, including identifying its molecular weight, using isotopic ratios, examining fragmentation patterns, and by searching through data bases.

Using Molecular Weight Information. A molecular ion peak, $M^{+\bullet}$, when it is present, a $[M + H]^+$ peak or a $[M - H]^+$ peak, provides information about the compound's molecular weight. When using a low resolution mass analyzer, this may be sufficient to distinguish between molecular ions with, for example, a nominal mass of 95 amu and a nominal mass of 96 amu, but insufficient to distinguish between molecular ions with a more precise mass of 96.0399 amu and 96.0575 amu. When using a high resolution mass analyzer, the difference between the last pair of molecular ions may be feasible.

Using Isotopic Ratios. The molecule cycloheptene has the formula C_7H_{12} and a nominal mass of 96 amu, and the molecule cyclohexenone has the formula C_6H_8O and a nominal mass of 96 amu. Although both molecules will produce a molecular ion with the same nominal mass-to-charge ratio, each will also have a peak with a nominal mass of M + 1 due to the presence of isotopes of carbon, hydrogen, and oxygen. Because cycloheptene and cyclohexenone have different chemical formulas, the relative heights of their M + 1 peaks are different. Here is how we can work this out.

For every 100 atoms of ^{12}C there are 1.08 atoms of ^{13}C (that is, 1.08% of the carbon atoms are ^{13}C), for every 100 atoms of ^{1}H there are 0.015 atoms of ^{2}H, and for every 100 atoms of ^{16}O there are 0.04 atoms of ^{17}O. For cycloheptene, this means that the relative height of its M + 1 peak to its M peak is

$$(7 \times 1.08) + (12 \times 0.015) = 7.74$$

and for cyclohexenone we have

$$(6 \times 1.08) + (8 \times 0.015) + (1 \times 0.04) = 6.64$$

Here we see that a careful examination of the relative height of the M + 1 peak provides a way to distinguish between C_7H_{12} and C_6H_8O even though they have the same nominal masses. On-line calculators are available—this link provides one example—that you can use to calculate the full isotopic abundance patterns, including M + 2, M + 3, and other peaks. Isotopic patterns are particularly useful for identifying the presence of chlorine and bromine in a molecule because each has one isotope with a significant abundance: for chlorine, ^{37}Cl has an abundance of 32.5% relative to ^{35}Cl, and for bromine, ^{81}Br has an abundance of 98.0% of ^{79}Br.

Using Fragmentation Patterns. Figure 8.7.1 shows the mass spectrum of *p*-nitrophenol, which we first considered in Section 20.1. A molecule's mass spectrum is unique and contains information that we can use to deduce its structure. Interpretation of a mass spectrum relies on identifying possible sources for the loss of mass, such as the a Δm of 30 amu corresponding to the loss of NO, or a Δm of 46 amu corresponding to the loss of NO_2. Some mass-to-charge ratios are recognized as evidence for a particular ion, such as $C_5H_5^+$ at a mass-to-charge ratio of 65. The interpretation of fragmentation patterns is covered elsewhere in the curriculum, particularly in organic chemistry, and is not given more consideration here.

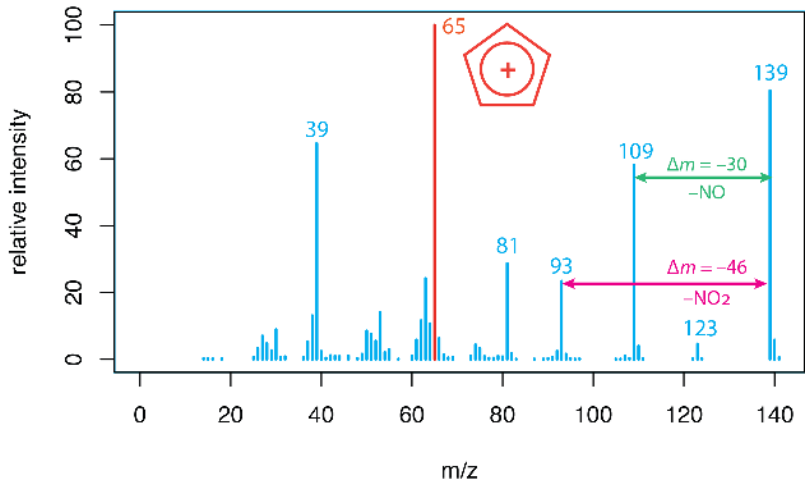


Figure 8.7.1: Mass spectrum of *p*-nitrophenol.

Using Computer Searching. Large databases of mass spectra are available (see here for a source from NIST). A peak table of mass-to-charge ratios and peak intensities for a sample is entered into an algorithm that searches the database and identifies the most likely matches.

Analysis of Mixtures Using MS as a Detector for a GC or LC Separation

Mass spectrometry is a powerful analytical technique when the sample we are analyzing is pure (or if impurities are of sufficiently low concentration that they have little effect on the mass spectrum). For a mixture of two or more analytes, the interpretation of the mass spectrum is difficult, if not impossible. To analyze such a mixture, we need a means of separating the analytes from each other. One approach is to interface a mass spectrometer to a gas chromatograph or a liquid chromatograph. The GC, or LC separates the mixture into its component parts with the mass spectrometer serving as the detector. See Chapter 27 and Chapter 28 for further details about GC-MS and LC-MS.

Analysis of Mixtures Using Tandem Mass Spectrometry

Another approach to working with a complex sample is to use two or more mass analyzers in what is called tandem mass spectrometry. For example, if we place three quadrupole mass analyzers in a sequence, we can use a soft ionization source to generate mostly molecular ions of the form $[M + H]^+$ for each of the sample's analytes, and then let the first quadrupole separate these molecular ions by the differences in their mass-to-charge ratio. The $[M + H]^+$ molecular ions for one of the analytes is then selectively passed into the second quadrupole where it is allowed to undergo fragmentation by collision with a gas, such as He. Finally, these fragment ions are passed along to the third quadrupole where the mass spectrum is obtained. By sequentially passing each of the molecular ions from the first quadrupole through the second and third quadrupoles, we are able to obtain mass spectra for each molecule in the mixture.

Quantitative Applications

As a detector for other instrumental methods, such as gas chromatography and liquid chromatography, mass spectrometry provides for a quantitative analysis by monitoring either the total ion count or by monitoring ions of a single mass-to-charge ratio, which is known as selective ion monitoring. As an Independent method for determining an analyte's concentration, mass spectrometry is less attractive due to the difficulty of controlling the amount of sample or standard introduced into the instrument and the affect of the sample's matrix on fragmentation. The use of an internal standard improves precision and accuracy.

This page titled 8.7: Applications of Molecular Mass Spectrometry is shared under a CC BY-NC-SA 4.0 license and was authored, remixed, and/or curated by David Harvey.

- **20.4: Applications of Molecular Mass Spectrometry** by David Harvey is licensed CC BY-NC-SA 4.0.

8.7.1: Interpreting a Mass Spectrum

Here are a list of steps to follow when interpreting a mass spectrum. This simplified list will help you to interpret many spectra, however there are other mechanisms of fragmentation which cannot be covered in this brief tutorial.

Steps to interpret a mass spectrum

1. Look for the molecular ion peak.

- This peak (if it appears) will be the highest mass peak in the spectrum, except for isotope peaks.
- Nominal MW (meaning=rounded off) will be an even number for compounds containing only C, H, O, S, Si.
- Nominal MW will be an odd number if the compound also contains an odd number of N (1,3,...).

2. Try to calculate the molecular formula:

- The isotope peaks can be very useful, and are best explained with an example.
  - Carbon 12 has an isotope, carbon 13. Their abundances are ^{12}C=100%, ^{13}C=1.1%. This means that for every 100 $^{(12)}C$ atoms there are 1.1 $^{(13)}C$ atoms.
  - If a compound contains 6 carbons, then each atom has a 1.1% abundance of $^{(13)}C$.
  - Therefore, if the molecular ion peak is 100%, then the isotope peak (1 mass unit higher) would be 6x1.1%=6.6%.
  - If the molecular ion peak is not 100% then you can calculate the relative abundance of the isotope peak to the ion peak. For example, if the molecular ion peak were 34% and the isotope peak 2.3%: (2.3/34)x100 = 6.8%. 6.8% is the relative abundance of the isotope peak to the ion peak. Next, divide the relative abundance by the isotope abundance: 6.8/1.1=6 carbons.
- Follow this order when looking for information provided by isotopes: (A simplified table of isotopes is provided in the introduction, more detailed tables can be found in chemistry texts.)
  - Look for A+2 elements: O, Si, S, Cl, Br
  - Look for A+1 elements: C, N
  - "A" elements: H, F, P, I

3. Calculate the total number of rings plus double bonds:

- For the molecular formula: $C_xH_yN_zO_n$
  - rings + double bonds = x - (1/2)y + (1/2)z + 1

4. Postulate the molecular structure consistent with abundance and m/z of fragments.

- More information on specific fragmentation can be found in the quiz for each functional group.

Contributors and Attributions

8.7.1: Interpreting a Mass Spectrum is shared under a CC BY-NC-SA 4.0 license and was authored, remixed, and/or curated by LibreTexts.

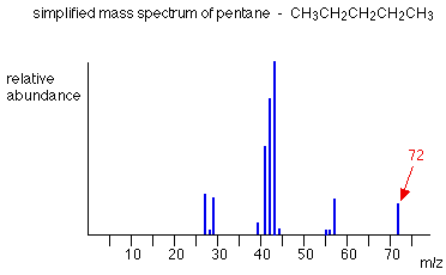
- **Interpreting a Mass Spectrum** is licensed CC BY-NC-SA 4.0.

8.7.2: The Molecular Ion (M^+) Peak

This page explains how to find the relative formula mass (relative molecular mass) of an organic compound from its mass spectrum. It also shows how high resolution mass spectra can be used to find the molecular formula for a compound.

When the vaporised organic sample passes into the ionization chamber of a mass spectrometer, it is bombarded by a stream of electrons. These electrons have a high enough energy to knock an electron off an organic molecule to form a positive ion. This ion is called the molecular ion. The molecular ion is often given the symbol M^+ or$M^{\cdot+}$ - the dot in this second version represents the fact that somewhere in the ion there will be a single unpaired electron. That's one half of what was originally a pair of electrons - the other half is the electron which was removed in the ionization process. The molecular ions tend to be unstable and some of them break into smaller fragments. These fragments produce the familiar stick diagram. Fragmentation is irrelevant to what we are talking about on this page - all we're interested in is the molecular ion.

In the mass spectrum, the heaviest ion (the one with the greatest m/z value) is likely to be the molecular ion. A few compounds have mass spectra which don't contain a molecular ion peak, because all the molecular ions break into fragments. For example, in the mass spectrum of pentane, the heaviest ion has an m/z value of 72.



Because the largest m/z value is 72, that represents the largest ion going through the mass spectrometer - and you can reasonably assume that this is the molecular ion. The relative formula mass of the compound is therefore 72.

Finding the relative formula mass (relative molecular mass) from a mass spectrum is therefore trivial. Look for the peak with the highest value for m/z, and that value is the relative formula mass of the compound. There are, however, complications which arise because of the possibility of different isotopes (either of carbon or of chlorine or bromine) in the molecular ion. These cases are dealt with on separate pages.

Using a mass spectrum to find a molecular formula

So far we've been looking at m/z values in a mass spectrum as whole numbers, but it's possible to get far more accurate results using a high resolution mass spectrometer. You can use that more accurate information about the mass of the molecular ion to work out the molecular formula of the compound.

For normal calculation purposes, you tend to use rounded-off relative isotopic masses. For example, you are familiar with the atomic mass numbers (Z). To 4 decimal places, however, these are the relative isotopic masses.

Isotope	Z	Mass
^{1}H	1	1.0078
^{12}C	12	12.0000
^{14}N	14	14.0031
^{16}O	16	15.9949

The carbon value is 12.0000, of course, because all the other masses are measured on the carbon-12 scale which is based on the carbon-12 isotope having a mass of exactly 12.

Using these accurate values to find a molecular formula

Two simple organic compounds have a relative formula mass of 44 - propane, C_3H_8, and ethanal, CH_3CHO. Using a high resolution mass spectrometer, you could easily decide which of these you had. On a high resolution mass spectrometer, the

molecular ion peaks for the two compounds give the following m/z values:

C_3H_8		44.0624
CH_3CHO		44.0261

You can easily check that by adding up numbers from the table of accurate relative isotopic masses above.

Example 8.7.2.1:

A gas was known to contain only elements from the following list:

^{1}H		1.0078
^{12}C		12.0000
^{14}N		14.0031
^{16}O		15.9949

The gas had a molecular ion peak at m/z = 28.0312 in a high resolution mass spectrometer. What was the gas?

Solution

After a bit of playing around, you might reasonably come up with 3 gases which had relative formula masses of approximately 28 and which contained the elements from the list. They are N_2, CO and C_2H_4. Working out their accurate relative formula masses gives:

N_2		28.0062
CO		27.9949
C_2H_4		28.0312

The gas is obviously C_2H_4.

Contributors and Attributions

- Jim Clark (Chemguide.co.uk)

This page titled 8.7.2: The Molecular Ion (M^+) Peak is shared under a CC BY-NC 4.0 license and was authored, remixed, and/or curated by Jim Clark.

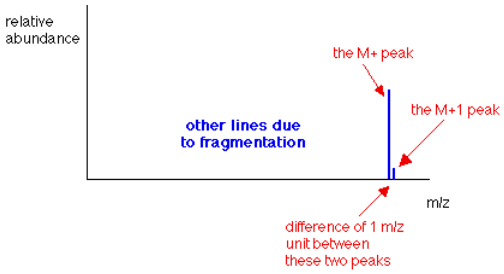
- **The Molecular Ion (M^+) Peak** by Jim Clark is licensed CC BY-NC 4.0.

8.7.3: The M+1 Peak

This page explains how the M+1 peak in a mass spectrum can be used to estimate the number of carbon atoms in an organic compound.

What causes the M+1 peak?

If you had a complete (rather than a simplified) mass spectrum, you will find a small line 1 m/z unit to the right of the main molecular ion peak. This small peak is called the M+1 peak.

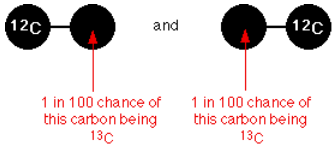


The carbon-13 isotope

The M+1 peak is caused by the presence of the ^{13}C isotope in the molecule. ^{13}C is a stable isotope of carbon - don't confuse it with the ^{14}C isotope which is radioactive. Carbon-13 makes up 1.11% of all carbon atoms. If you had a simple compound like methane, CH_4, approximately 1 in every 100 of these molecules will contain carbon-13 rather than the more common carbon-12. That means that 1 in every 100 of the molecules will have a mass of 17 (13 + 4) rather than 16 (12 + 4). The mass spectrum will therefore have a line corresponding to the molecular ion $[^{13}CH_4]^+$ as well as $[^{12}CH_4]^+$. The line at m/z = 17 will be much smaller than the line at m/z = 16 because the carbon-13 isotope is much less common. Statistically you will have a ratio of approximately 1 of the heavier ions to every 99 of the lighter ones. That's why the M+1 peak is much smaller than the M+ peak.

Using the M+1 peak

Imagine a compound containing 2 carbon atoms. Either of them has an approximately 1 in 100 chance of being ^{13}C.



There's therefore a 2 in 100 chance of the molecule as a whole containing one ^{13}C atom rather than a ^{12}C atom - which leaves a 98 in 100 chance of both atoms being ^{12}C. That means that the ratio of the height of the M+1 peak to the M+ peak will be approximately 2 : 98. That's pretty close to having an M+1 peak approximately 2% of the height of the M+ peak.

Using the relative peak heights to predict the number of carbon atoms

If you measure the peak height of the M+1 peak as a percentage of the peak height of the M+ peak, that gives you the number of carbon atoms in the compound. We've just seen that a compound with 2 carbons will have an M+1 peak approximately 2% of the height of the M+ peak. Similarly, you could show that a compound with 3 carbons will have the M+1 peak at about 3% of the height of the M+ peak. The approximations we are making won't hold with more than 2 or 3 carbons. The proportion of carbon atoms which are ^{13}C isn't 1% - it's 1.11%. And the approximation that a ratio of 2 : 98 is about 2% doesn't hold as the small number increases.

Consider a molecule with 5 carbons in it. You could work out that 5.55 (5 x 1.11) molecules will contain 1 ^{13}C to every 94.45 (100 - 5.55) which contain only ^{12}C atoms. If you convert that to how tall the M+1 peak is as a percentage of the M+ peak, you get an answer of 5.9% (5.55/94.45 x 100). That's close enough to 6% that you might assume wrongly that there are 6 carbon atoms. Above 3 carbon atoms, then, you shouldn't really be making the approximation that the height of the M+1 peak as a percentage of the height of the M+ peak tells you the number of carbons - you will need to do some fiddly sums!

Contributors and Attributions

Jim Clark (Chemguide.co.uk)

This page titled 8.7.3: The M+1 Peak is shared under a CC BY-NC 4.0 license and was authored, remixed, and/or curated by Jim Clark.

- **The M+1 Peak** by Jim Clark is licensed CC BY-NC 4.0.

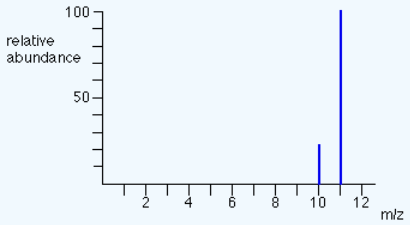
8.7.4: The Mass Spectra of Elements

This page looks at the information you can get from the mass spectrum of an element. It shows how you can find out the masses and relative abundances of the various isotopes of the element and use that information to calculate the relative atomic mass of the element. It also looks at the problems thrown up by elements with diatomic molecules - like chlorine, Cl_2.

The mass spectrum of monatomic elements

Monatomic elements include all those except for things like chlorine, Cl_2, with molecules containing more than one atom.

Example 8.7.4.1: The Mass Spectrum of Boron



The number of isotopes: The two peaks in the mass spectrum shows that there are 2 isotopes of boron - with relative isotopic masses of 10 and 11 on the ^{12}C scale.

The abundance of the isotopes: The relative sizes of the peaks gives you a direct measure of the relative abundances of the isotopes. The tallest peak is often given an arbitrary height of 100 - but you may find all sorts of other scales used. It doesn't matter in the least. You can find the relative abundances by measuring the lines on the stick diagram. In this case, the two isotopes (with their relative abundances) are:

boron-10		23
boron-11		100

Working out the relative atomic mass

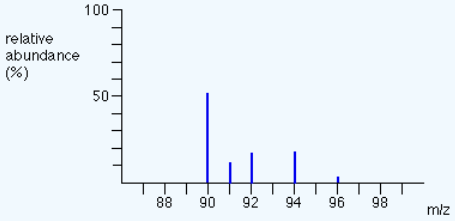
The relative atomic mass (RAM) of an element is given the symbol $\mathbf{A_r}$ and is defined as:

The relative atomic mass of an element is the weighted average of the masses of the isotopes on a scale on which a carbon-12 atom has a mass of exactly 12 units A "weighted average" allows for the fact that there won't be equal amounts of the various isotopes. The example coming up should make that clear.

> Suppose you had 123 typical atoms of boron. 23 of these would be ^{10}B and 100 would be ^{11}B.
>
> The total mass of these would be (23 x 10) + (100 x 11) = 1330
>
> The average mass of these 123 atoms would be 1330 / 123 = 10.8 (to 3 significant figures).
>
> 10.8 is the relative atomic mass of boron.

Notice the effect of the "weighted" average. A simple average of 10 and 11 is, of course, 10.5. Our answer of 10.8 allows for the fact that there are a lot more of the heavier isotope of boron - and so the "weighted" average ought to be closer to that.

Example 8.7.4.2: The Mass Spectrum of Zirconium



The number of isotopes: The 5 peaks in the mass spectrum shows that there are 5 isotopes of zirconium - with relative isotopic masses of 90, 91, 92, 94 and 96 on the ^{12}C scale.

The abundance of the isotopes: This time, the relative abundances are given as percentages. Again you can find these relative abundances by measuring the lines on the stick diagram. In this case, the 5 isotopes (with their relative percentage abundances) are:

zirconium-90		51.5
zirconium-91		11.2
zirconium-92		17.1
zirconium-94		17.4
zirconium-96		2.8

Working out the relative atomic mass

Suppose you had 100 typical atoms of zirconium. 51.5 of these would be ^{90}Zr, 11.2 would be ^{91}Zr and so on.

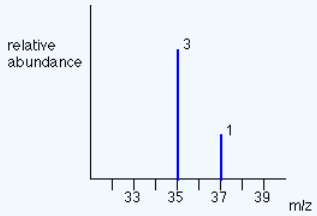
The total mass of these 100 typical atoms would be

$$(51.5 \times 90) + (11.2 \times 91) + (17.1 \times 92) + (17.4 \times 94) + (2.8 \times 96) = 9131.8$$

The average mass of these 100 atoms would be 9131.8 / 100 = 91.3 (to 3 significant figures). 91.3 is the relative atomic mass of zirconium.

Example 8.7.4.3: The Mass Spectrum of Chlorine

Chlorine is taken as typical of elements with more than one atom per molecule. We'll look at its mass spectrum to show the sort of problems involved. Chlorine has two isotopes, ^{35}Cl and ^{37}Cl, in the approximate ratio of 3 atoms of ^{35}Cl to 1 atom of ^{37}Cl. You might suppose that the mass spectrum would look like this:



You would be wrong! The problem is that chlorine consists of molecules, not individual atoms. When chlorine is passed into the ionization chamber, an electron is knocked off the molecule to give a molecular ion, Cl_2^+. These ions won't be particularly stable, and some will fall apart to give a chlorine atom and a Cl^+ ion. The term for this is fragmentation.

$$Cl_2^+ \rightarrow Cl + Cl^+$$

If the Cl atom formed is not then ionized in the ionization chamber, it simply gets lost in the machine - neither accelerated nor deflected.

The Cl^+ ions will pass through the machine and will give lines at 35 and 37, depending on the isotope and you would get exactly the pattern in the last diagram. The problem is that you will also record lines for the unfragmented Cl_2^+ ions.

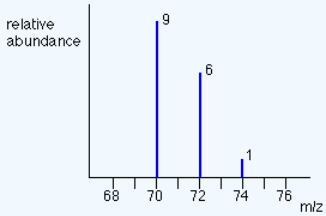
Think about the possible combinations of chlorine-35 and chlorine-37 atoms in a Cl_2^+ ion. Both atoms could be ^{35}Cl, both atoms could be ^{37}Cl, or you could have one of each sort. That would give you total masses of the Cl_2^+ ion of:

35 + 35 = 70

35 + 37 = 72

37 + 37 = 74

That means that you would get a set of lines in the m/z = 70 region looking like this:

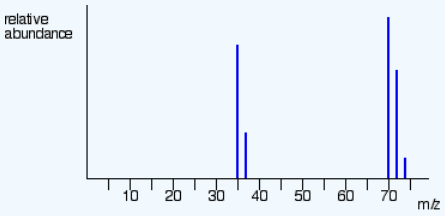


These lines would be in addition to the lines at 35 and 37.

The relative heights of the 70, 72 and 74 lines are in the ratio 9:6:1. If you know the right bit of math, it's very easy to show this. If not, don't worry. Just remember that the ratio is 9:6:1.

What you can't do is make any predictions about the relative heights of the lines at 35/37 compared with those at 70/72/74. That depends on what proportion of the molecular ions break up into fragments. That's why you've got the chlorine mass spectrum in two separate bits so far. You must realise that the vertical scale in the diagrams of the two parts of the spectrum isn't the same.

The overall mass spectrum looks like this:



Contributors and Attributions

- Jim Clark (Chemguide.co.uk)

This page titled 8.7.4: The Mass Spectra of Elements is shared under a CC BY-NC 4.0 license and was authored, remixed, and/or curated by Jim Clark.

- **The Mass Spectra of Elements** by Jim Clark is licensed CC BY-NC 4.0.

8.7.5: Fragmentation Patterns in Mass Spectra

This page looks at how fragmentation patterns are formed when organic molecules are fed into a mass spectrometer, and how you can get information from the mass spectrum.

The formation of molecular ions

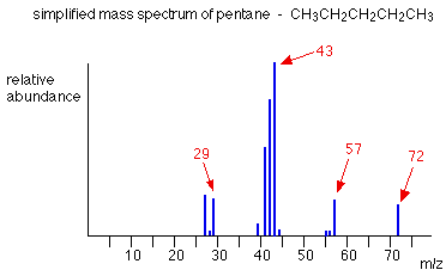
When the vaporized organic sample passes into the ionization chamber of a mass spectrometer, it is bombarded by a stream of electrons. These electrons have a high enough energy to knock an electron off an organic molecule to form a positive ion. This ion is called the **molecular ion - or sometimes the parent ion.** The molecular ion is often given the symbol M^+ or $M^{\cdot+}$ - the dot in this second version represents the fact that somewhere in the ion there will be a single unpaired electron. That's one half of what was originally a pair of electrons - the other half is the electron which was removed in the ionization process.

Fragmentation

The molecular ions are energetically unstable, and some of them will break up into smaller pieces. The simplest case is that a molecular ion breaks into two parts - one of which is another positive ion, and the other is an uncharged free radical.

$$M^{\cdot+} \rightarrow X^+ + Y^{\cdot}$$

The uncharged free radical won't produce a line on the mass spectrum. Only charged particles will be accelerated, deflected and detected by the mass spectrometer. These uncharged particles will simply get lost in the machine - eventually, they get removed by the vacuum pump. The ion, X^+, will travel through the mass spectrometer just like any other positive ion - and will produce a line on the stick diagram. All sorts of fragmentations of the original molecular ion are possible - and that means that you will get a whole host of lines in the mass spectrum. For example, the mass spectrum of pentane looks like this:



It's important to realize that the pattern of lines in the mass spectrum of an organic compound tells you something quite different from the pattern of lines in the mass spectrum of an element. With an element, each line represents a different isotope of that element. With a compound, each line represents a different fragment produced when the molecular ion breaks up.

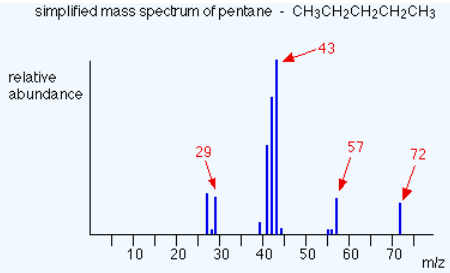
In the stick diagram showing the mass spectrum of pentane, the line produced by the heaviest ion passing through the machine (at m/z = 72) is due to the molecular ion. The tallest line in the stick diagram (in this case at m/z = 43) is called the **base peak**. This is usually given an arbitrary height of 100, and the height of everything else is measured relative to this. The base peak is the tallest peak because it represents the commonest fragment ion to be formed - either because there are several ways in which it could be produced during fragmentation of the parent ion, or because it is a particularly stable ion.

Using fragmentation patterns

This section will ignore the information you can get from the molecular ion (or ions). That is covered in three other pages which you can get at via the mass spectrometry menu. You will find a link at the bottom of the page.

Example 8.7.5.1: Mass Spectrum of Pentane

Let's have another look at the mass spectrum for pentane:



What causes the line at m/z = 57?

Solution

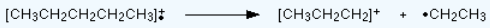
How many carbon atoms are there in this ion? There can't be 5 because 5 x 12 = 60. What about 4? 4 x 12 = 48. That leaves 9 to make up a total of 57. How about $C_4H_9^+$ then?

$C_4H_9^+$ would be $[CH_3CH_2CH_2CH_2]^+$, and this would be produced by the following fragmentation:

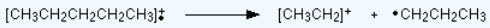


The methyl radical produced will simply get lost in the machine.

The line at m/z = 43 can be worked out similarly. If you play around with the numbers, you will find that this corresponds to a break producing a 3-carbon ion:



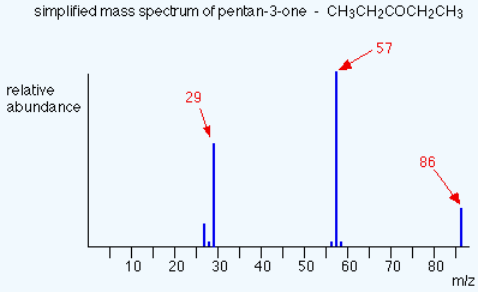
The line at m/z = 29 is typical of an ethyl ion, $[CH_3CH_2]^+$:



The other lines in the mass spectrum are more difficult to explain. For example, lines with m/z values 1 or 2 less than one of the easy lines are often due to loss of one or more hydrogen atoms during the fragmentation process.

Example 8.7.5.2: Pentan-3-one

This time the base peak (the tallest peak - and so the commonest fragment ion) is at m/z = 57. But this isn't produced by the same ion as the same m/z value peak in pentane.

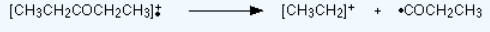


If you remember, the m/z = 57 peak in pentane was produced by $[CH_3CH_2CH_2CH_2]^+$. If you look at the structure of pentan-3-one, it's impossible to get that particular fragment from it.

Work along the molecule mentally chopping bits off until you come up with something that adds up to 57. With a small amount of patience, you'll eventually find $[CH_3CH_2CO]^+$ - which is produced by this fragmentation:



You would get exactly the same products whichever side of the CO group you split the molecular ion. The m/z = 29 peak is produced by the ethyl ion - which once again could be formed by splitting the molecular ion either side of the CO group.



Peak heights and the stability of ions

The more stable an ion is, the more likely it is to form. The more of a particular sort of ion that's formed, the higher its peak height will be. We'll look at two common examples of this.

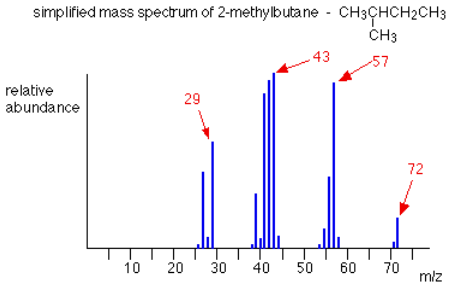
Examples involving carbocations (carbonium ions)

Summarizing the most important conclusion from the page on carbocations:

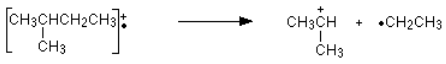
Order of stability of carbocations

primary < secondary < tertiary

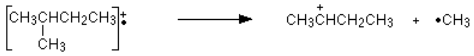
Applying the logic of this to fragmentation patterns, it means that a split which produces a secondary carbocation is going to be more successful than one producing a primary one. A split producing a tertiary carbocation will be more successful still. Let's look at the mass spectrum of 2-methylbutane. 2-methylbutane is an isomer of pentane - isomers are molecules with the same molecular formula, but a different spatial arrangement of the atoms.



Look first at the very strong peak at m/z = 43. This is caused by a different ion than the corresponding peak in the pentane mass spectrum. This peak in 2-methylbutane is caused by:



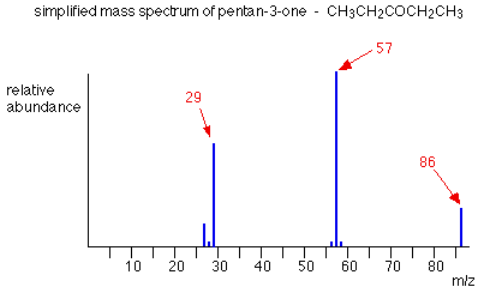
The ion formed is a secondary carbocation - it has two alkyl groups attached to the carbon with the positive charge. As such, it is relatively stable. The peak at m/z = 57 is much taller than the corresponding line in pentane. Again a secondary carbocation is formed - this time, by:



You would get the same ion, of course, if the left-hand CH_3 group broke off instead of the bottom one as we've drawn it. In these two spectra, this is probably the most dramatic example of the extra stability of a secondary carbocation.

Examples involving acylium ions, $[RCO]^+$

Ions with the positive charge on the carbon of a carbonyl group, C=O, are also relatively stable. This is fairly clearly seen in the mass spectra of ketones like pentan-3-one.



The base peak, at m/z=57, is due to the $[CH_3CH_2CO]^+$ ion. We've already discussed the fragmentation that produces this.

Using mass spectra to distinguish between compounds

Suppose you had to suggest a way of distinguishing between pentan-2-one and pentan-3-one using their mass spectra.

pentan-2-one		$CH_3COCH_2CH_2CH_3$
pentan-3-one		$CH_3CH_2COCH_2CH_3$

Each of these is likely to split to produce ions with a positive charge on the CO group. In the pentan-2-one case, there are two different ions like this:

- $[CH_3CO]^+$
- $[COCH_2CH_2CH_3]^+$

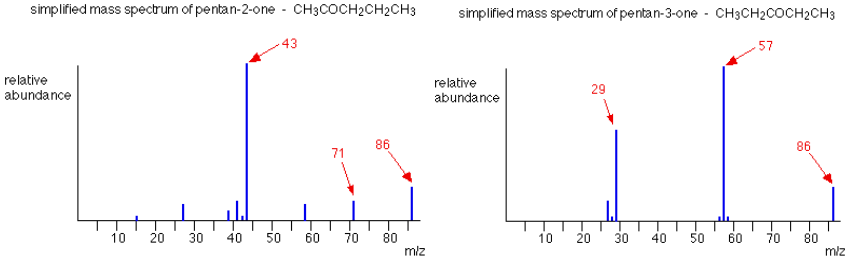
That would give you strong lines at m/z = 43 and 71.

With pentan-3-one, you would only get one ion of this kind:

- $[CH_3CH_2CO]^+$

In that case, you would get a strong line at 57. You don't need to worry about the other lines in the spectra - the 43, 57 and 71 lines give you plenty of difference between the two. The 43 and 71 lines are missing from the pentan-3-one spectrum, and the 57 line is missing from the pentan-2-one one.

The two mass spectra look like this:



Computer matching of mass spectra

As you've seen, the mass spectrum of even very similar organic compounds will be quite different because of the different fragmentations that can occur. Provided you have a computer data base of mass spectra, any unknown spectrum can be computer analysed and simply matched against the data base.

Contributors and Attributions

- Jim Clark (Chemguide.co.uk)

This page titled 8.7.5: Fragmentation Patterns in Mass Spectra is shared under a CC BY-NC 4.0 license and was authored, remixed, and/or curated by Jim Clark.

- **Fragmentation Patterns in Mass Spectra** by Jim Clark is licensed CC BY-NC 4.0.

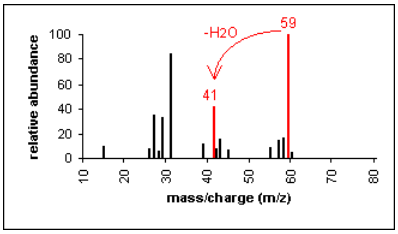
8.7.6: Mass Spectrometry - Fragmentation Patterns

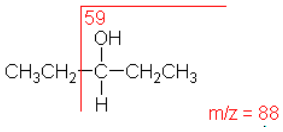
Following are examples of compounds listed by functional group, which demonstrate patterns which can be seen in mass spectra of compounds ionized by electron impact ionization. These examples do not provide information about the fragmentation mechanisms that cause these patterns. Additional information can be found in mass spectrometry reference books.

Alcohol

An alcohol's molecular ion is small or non-existent. Cleavage of the C-C bond next to the oxygen usually occurs. A loss of H_2O may occur as in the spectra below.

3-Pentanol ($C_5H_{12}O$) with MW = 88.15

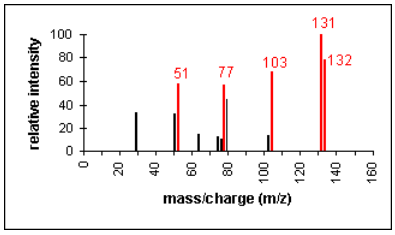


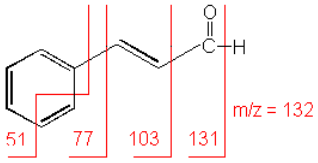


Aldehyde

Cleavage of bonds next to the carboxyl group results in the loss of hydrogen (molecular ion less 1) or the loss of CHO (molecular ion less 29).

3-Phenyl-2-propenal (C_9H_8O) with MW = 132.16

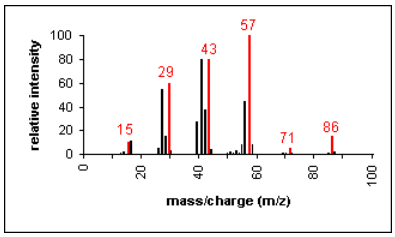


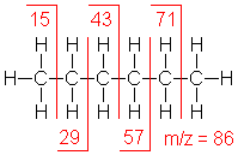


Alkane

Molecular ion peaks are present, possibly with low intensity. The fragmentation pattern contains clusters of peaks 14 mass units apart (which represent loss of (CH2)nCH3).

Hexane (C6H14) with MW = 86.18

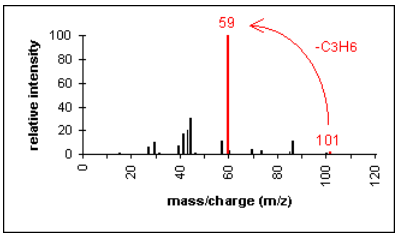


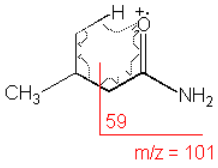


Amide

Primary amides show a base peak due to the McLafferty rearrangement.

3-Methylbutyramide ($C_5H_{11}NO$) with MW = 101.15

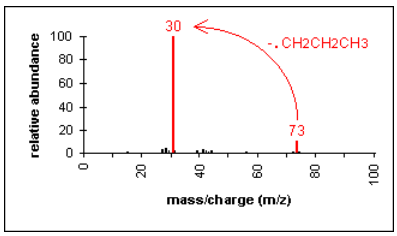


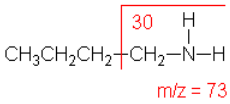


Amine

Molecular ion peak is an odd number. Alpha-cleavage dominates aliphatic amines.

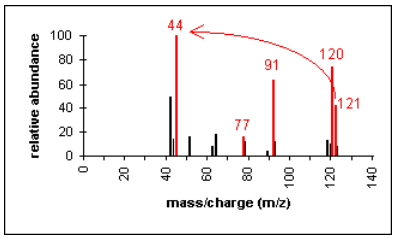
n-Butylamine (C4H11N) with MW = 73.13

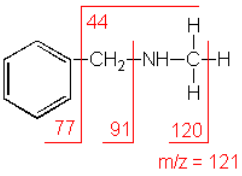




Another example is a secondary amine shown below. Again, the molecular ion peak is an odd number. The base peak is from the C-C cleavage adjacent to the C-N bond.

n-Methylbenzylamine ($C_8H_{11}N$) with MW = 121.18

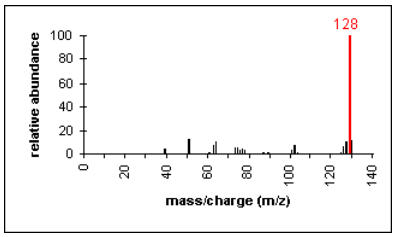


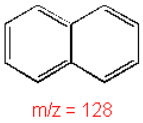


Aromatic

Molecular ion peaks are strong due to the stable structure.

Naphthalene ($C_{10}H_8$) with MW = 128.17

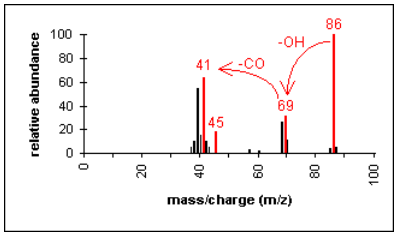


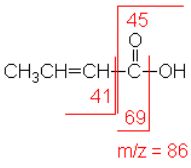


Carboxylic Acid

In short chain acids, peaks due to the loss of OH (molecular ion less 17) and COOH (molecular ion less 45) are prominent due to cleavage of bonds next to C=O.

2-Butenoic acid ($C_4H_6O_2$) with MW = 86.09

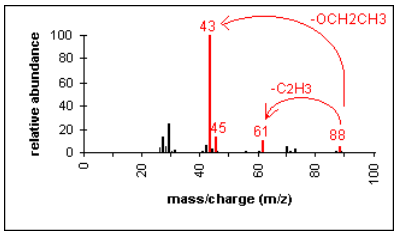


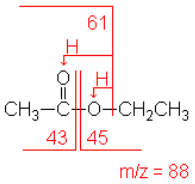


Ester

Fragments appear due to bond cleavage next to C=O (alkoxy group loss, -OR) and hydrogen rearrangements.

Ethyl acetate ($C_4H_8O_2$) with MW = 88.11

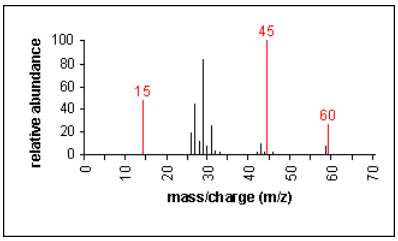


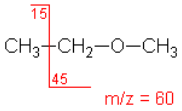


Ether

Fragmentation tends to occur alpha to the oxygen atom (C-C bond next to the oxygen).

Ethyl methyl ether (C_3H_8O) with MW = 60.10

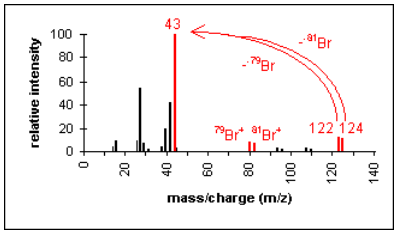


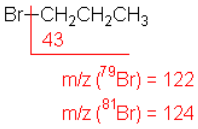


Halide

The presence of chlorine or bromine atoms is usually recognizable from isotopic peaks.

1-Bromopropane (C_3H_7Br) with MW = 123.00

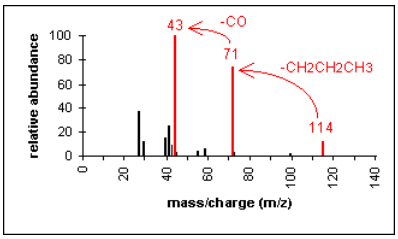


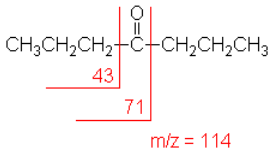


Ketone

Major fragmentation peaks result from cleavage of the C-C bonds adjacent to the carbonyl.

4-Heptanone ($C_7H_{14}O$) with MW = 114.19





Contributors and Attributions

Dr. Linda Breci, Associate Director Arizona Proteomics Consortium University of Arizona

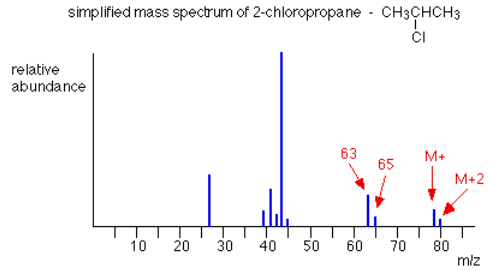
8.7.6: Mass Spectrometry - Fragmentation Patterns is shared under a CC BY-NC-SA 4.0 license and was authored, remixed, and/or curated by LibreTexts.

- **Mass Spectrometry - Fragmentation Patterns** is licensed CC BY-NC-SA 4.0.

8.7.7: Organic Compounds Containing Halogen Atoms

This page explains how the M+2 peak in a mass spectrum arises from the presence of chlorine or bromine atoms in an organic compound. It also deals briefly with the origin of the M+4 peak in compounds containing two chlorine atoms.

One chlorine atom in a compound



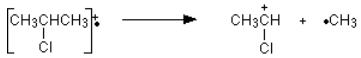
The molecular ion peaks (M+ and M+2) each contain one chlorine atom - but the chlorine can be either of the two chlorine isotopes, ^{35}Cl and ^{37}Cl.

The molecular ion containing the ^{35}Cl isotope has a relative formula mass of 78. The one containing ^{37}Cl has a relative formula mass of 80 - hence the two lines at m/z = 78 and m/z = 80.

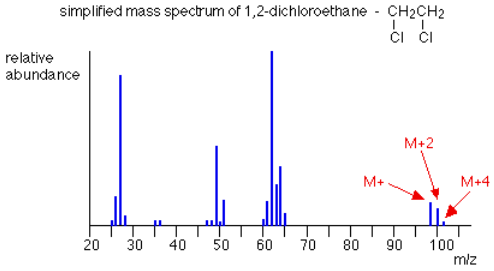
Notice that the peak heights are in the ratio of 3 : 1. That reflects the fact that chlorine contains 3 times as much of the ^{35}Cl isotope as the ^{37}Cl one. That means that there will be 3 times more molecules containing the lighter isotope than the heavier one.

So . . . if you look at the molecular ion region, and find two peaks separated by 2 m/z units and with a ratio of 3 : 1 in the peak heights, that tells you that the molecule contains 1 chlorine atom.

You might also have noticed the same pattern at m/z = 63 and m/z = 65 in the mass spectrum above. That pattern is due to fragment ions also containing one chlorine atom - which could either be ^{35}Cl or ^{37}Cl. The fragmentation that produced those ions was:



Two chlorine atoms in a compound



The lines in the molecular ion region (at m/z values of 98, 100 ands 102) arise because of the various combinations of chlorine isotopes that are possible. The carbons and hydrogens add up to 28 - so the various possible molecular ions could be:

$$28 + 35 + 35 = 98$$

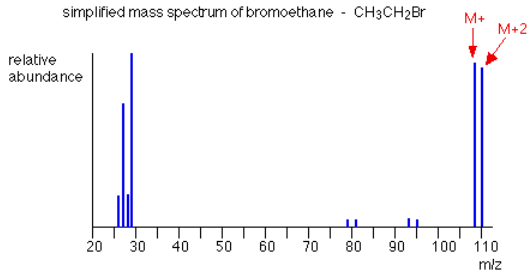
$$28 + 35 + 37 = 100$$

$$28 + 37 + 37 = 102$$

If you have the necessary math, you could show that the chances of these arrangements occurring are in the ratio of 9:6:1 - and this is the ratio of the peak heights. If you don't know the right bit of math, just learn this ratio! So . . . if you have 3 lines in the molecular ion region (M+, M+2 and M+4) with gaps of 2 m/z units between them, and with peak heights in the ratio of 9:6:1, the compound contains 2 chlorine atoms.

Compounds containing bromine atoms

Bromine has two isotopes, ^{79}Br and ^{81}Br in an approximately 1:1 ratio (50.5 : 49.5 if you want to be fussy!). That means that a compound containing 1 bromine atom will have two peaks in the molecular ion region, depending on which bromine isotope the molecular ion contains. Unlike compounds containing chlorine, though, the two peaks will be very similar in height.



The carbons and hydrogens add up to 29. The M+ and M+2 peaks are therefore at m/z values given by:

$$29 + 79 = 108$$

$$29 + 81 = 110$$

Hence, if two lines in the molecular ion region are observed with a gap of 2 m/z units between them and with almost equal heights, this suggests the presence of a bromine atom in the molecule.

Contributors and Attributions

- Jim Clark (Chemguide.co.uk)

This page titled 8.7.7: Organic Compounds Containing Halogen Atoms is shared under a CC BY-NC 4.0 license and was authored, remixed, and/or curated by Jim Clark.

- **Organic Compounds Containing Halogen Atoms** by Jim Clark is licensed CC BY-NC 4.0.

CHAPTER OVERVIEW

9: Atomic Spectroscopy

9.1: Introduction to Atomic Absorption Spectroscopy
9.2: Sample Atomization Techniques
9.3: Atomic Absorption Instrumentation
9.4: Interferences in Absorption Spectroscopy
9.5: Atomic Absorption Techniques
9.6: Atomic Absorption Spectroscopy
9.7: Atomic Emission Spectroscopy
9.7.1: Emission Spectroscopy Based on Flame and Plasma Sources
9.7.2: Atomic Emission Spectroscopy
9.7.3: Inductively Coupled Plasma Mass Spectrometer

This page titled 9: Atomic Spectroscopy is shared under a CC BY-NC-SA 4.0 license and was authored, remixed, and/or curated by David Harvey.

9.1: Introduction to Atomic Absorption Spectroscopy

Brief overview of atomic absorption spectroscopy

History of atomic absorption spectroscopy

The earliest spectroscopy was first described by Marcus Marci von Kronland in 1648 by analyzing sunlight as is passed through water droplets and thus creating a rainbow. Further analysis of sunlight by William Hyde Wollaston (Figure 9.1.1) led to the discovery of black lines in the spectrum, which in 1820 Sir David Brewster (Figure 9.1.2) explained as absorption of light in the sun's atmosphere.



Figure 9.1.1: English chemist and physicist William Hyde Wollaston (1659 - 1724).Figure 9.1.2: Scottish physicist, mathematician, astronomer, inventor, writer and university principal Sir David Brewster (1781 - 1868).

Robert Bunsen (Figure 9.1.3) and Gustav Kirchhoff (Figure 9.1.4) studied the sodium spectrum and came to the conclusion that every element has its own unique spectrum that can be used to identify elements in the vapor phase. Kirchoff further explained the phenomenon by stating that if a material can emit radiation of a certain wavelength, that it may also absorb radiation of that wavelength. Although Bunsen and Kirchoff took a large step in defining the technique of atomic absorption spectroscopy (AAS), it was not widely utilized as an analytical technique except in the field of astronomy due to many practical difficulties.



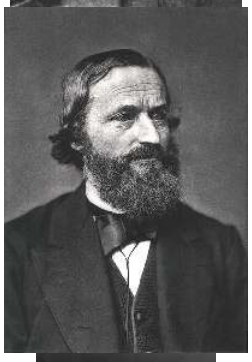




Figure 9.1.3: German chemist Robert Bunsen (1811 - 1899). **Figure** 9.1.4: German physicist Gustav Robert Kirchhoff (1824 - 1887).**Figure** 9.1.5: British physicist Sir Alan Walsh (1916 - 1988).

In 1953, Alan Walsh (Figure 9.1.5) drastically improved the AAS methods. He advocated AAS to many instrument manufacturers, but to no avail. Although he had improved the methods, he hadn't shown how it could be useful in any applications. In 1957, he discovered uses for AAS that convinced manufactures market the first commercial AAS spectrometers. Since that time, AAS's popularity has fluctuated as other analytical techniques and improvements to the methods are made.

Theory of atomic absorption spectroscopy

In order to understand how atomic absorption spectroscopy works, some background information is necessary. Atomic theory began with John Dalton (Figure 9.1.6) in the 18th century when he proposed the concept of atoms, that all atoms of an element are identical, and that atoms of different elements can combine to form molecules. In 1913, Niels Bohr (Figure 9.1.7) revolutionized atomic theory by proposing quantum numbers, a positively charged nucleus, and electrons orbiting around the nucleus in the what became known as the *Bohr model of the atom*. Soon afterward, Louis deBroglie (Figure 9.1.8) proposed quantized energy of electrons, which is an extremely important concept in AAS. Wolfgang Pauli (Figure 9.1.9) then elaborated on deBroglie's theory by stating that no two electrons can share the same four quantum numbers. These landmark discoveries in atomic theory are necessary in understanding the mechanism of AAS.









Figure 9.1.6: English chemist, physicist, and meteorologist John Dalton FRS (1766 - 1844).**Figure** 9.1.7: Danish physicist Niels Henrik David Bohr (1885 - 1962).**Figure** 9.1.8: French physicist and a Nobel laureate Louis de Broglie (1892 - 1987). (public domain).**Figure** 9.1.9: Austrian physicist Wolfgang Pauli (1900 - 1958).

Atoms have valence electrons, which are the outermost electrons of the atom. Atoms can be excited when irradiated, which creates an absorption spectrum. When an atom is excited, the valence electron moves up an energy level. The energies of the various stationary states, or restricted orbits, can then be determined by these emission lines. The resonance line is then defined as the specific radiation absorbed to reach the excited state.

The Maxwell-Boltzmann equation gives the number of electrons in any given orbital. It relates the distribution to the thermal temperature of the system (as opposed to electronic temperature, vibrational temperature, or rotational temperature). Plank proposed radiation emitted energy in discrete packets (quanta),

$$E = h\nu$$

which can be related to Einstein's equation

$$E = mc^2 \tag{9.1.1}$$

Both atomic emission and atomic absorption spectroscopy can be used to analyze samples. Atomic emission spectroscopy measures the intensity of light emitted by the excited atoms, while atomic absorption spectroscopy measures the light absorbed by atomic absorption. This light is typically in the visible or ultraviolet region of the electromagnetic spectrum. The percentage is then compared to a calibration curve to determine the amount of material in the sample. The energy of the system can be used to find the frequency of the radiation, and thus the wavelength through the combination of equations 9.1.1 and 9.1.2.

$$\nu = c/\lambda \tag{9.1.2}$$

Because the energy levels are quantized, only certain wavelengths are allowed and each atom has a unique spectrum. There are many variables that can affect the system. For example, if the sample is changed in a way that increases the population of atoms, there will be an increase in both emission and absorption and *vice versa*. There are also variables that affect the ratio of excited to unexcited atoms such as an increase in temperature of the vapor.

Applications of Atomic Absorption Spectroscopy

There are many applications of atomic absorption spectroscopy (AAS) due to its specificity. These can be divided into the broad categories of biological analysis, environmental and marine analysis, and geological analysis.

Biological analysis

Biological samples can include both human tissue samples and food samples. In human tissue samples, AAS can be used to determine the amount of various levels of metals and other electrolytes, within tissue samples. These tissue samples can be many things including but not limited to blood, bone marrow, urine, hair, and nails. Sample preparation is dependent upon the sample. This is extremely important in that many elements are toxic in certain concentrations in the body, and AAS can analyze what concentrations they are present in. Some examples of trace elements that samples are analyzed for are arsenic, mercury, and lead.

An example of an application of AAS to human tissue is the measurement of the electrolytes sodium and potassium in plasma. This measurement is important because the values can be indicative of various diseases when outside of the normal range. The typical method used for this analysis is atomization of a 1:50 dilution in strontium chloride ($SrCl_2$) using an air-hydrogen flame. The sodium is detected at its secondary line (330.2 nm) because detection at the first line would require further dilution of the sample due to signal intensity. The reason that strontium chloride is used is because it reduces ionization of the potassium and sodium ions, while eliminating phosphate's and calcium's interference.

In the food industry, AAS provides analysis of vegetables, animal products, and animal feeds. These kinds of analyses are some of the oldest application of AAS. An important consideration that needs to be taken into account in food analysis is sampling. The sample should be an accurate representation of what is being analyzed. Because of this, it must be homogenous, and many it is often needed that several samples are run. Food samples are most often run in order to determine mineral and trace element amounts so that consumers know if they are consuming an adequate amount. Samples are also analyzed to determine heavy metals which can be detrimental to consumers.

Environmental and marine analysis

Environmental and marine analysis typically refers to water analysis of various types. Water analysis includes many things ranging from drinking water to waste water to sea water. Unlike biological samples, the preparation of water samples is governed more by laws than by the sample itself. The analytes that can be measured also vary greatly and can often include lead, copper, nickel, and mercury.

An example of water analysis is an analysis of leaching of lead and zinc from tin-lead solder into water. The solder is what binds the joints of copper pipes. In this particular experiment, soft water, acidic water, and chlorinated water were all analyzed. The sample preparation consisted of exposing the various water samples to copper plates with solder for various intervals of time. The

samples were then analyzed for copper and zinc with air-acetylene flame AAS. A deuterium lamp was used. For the samples that had copper levels below 100 µg/L, the method was changed to graphite furnace electrothermal AAS due to its higher sensitivity.

Geological analysis

Geological analysis encompasses both mineral reserves and environmental research. When prospecting mineral reserves, the method of AAS used needs to be cheap, fast, and versatile because the majority of prospects end up being of no economic use. When studying rocks, preparation can include acid digestions or leaching. If the sample needs to have silicon content analyzed, acid digestion is not a suitable preparation method.

An example is the analysis of lake and river sediment for lead and cadmium. Because this experiment involves a solid sample, more preparation is needed than for the other examples. The sediment was first dried, then grounded into a powder, and then was decomposed in a bomb with nitric acid (HNO_3) and perchloric acid ($HClO_4$). Standards of lead and cadmium were prepared. Ammonium sulfate ($[NH_4][SO_4]$]) and ammonium phosphate ($[NH_4][3\,PO_4]$]) were added to the samples to correct for the interferences caused by sodium and potassium that are present in the sample. The standards and samples were then analyzed with electrothermal AAS.

Instrumentation

Atomizer

In order for the sample to be analyzed, it must first be atomized. This is an extremely important step in AAS because it determines the sensitivity of the reading. The most effective atomizers create a large number of homogenous free atoms. There are many types of atomizers, but only two are commonly used: flame and electrothermal atomizers.

Flame atomizer

Flame atomizers (Figure 9.1.10) are widely used for a multitude of reasons including their simplicity, low cost, and long length of time that they have been utilized. Flame atomizers accept an aerosol from a nebulizer into a flame that has enough energy to both volatilize and atomize the sample. When this happens, the sample is dried, vaporized, atomized, and ionized. Within this category of atomizers, there are many subcategories determined by the chemical composition of the flame. The composition of the flame is often determined based on the sample being analyzed. The flame itself should meet several requirements including sufficient energy, a long length, non-turbulent, and safe.

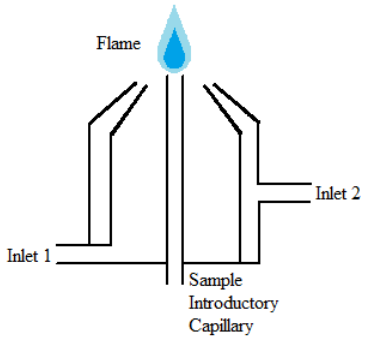


Figure 9.1.10: A schematic diagram of a flame atomizer showing the oxidizer inlet (1) and fuel inlet (2).

Electrothermal atomizer

Although electrothermal atomizers were developed before flame atomizers, they did not become popular until more recently due to improvements made to the detection level. They employ graphite tubes that increase temperature in a stepwise manner. Electrothermal atomization first dries the sample and evaporates much of the solvent and impurities, then atomizes the sample, and then rises it to an extremely high temperature to clean the graphite tube. Some requirements for this form of atomization are the ability to maintain a constant temperature during atomization, have rapid atomization, hold a large volume of solution, and emit minimal radiation. Electrothermal atomization is much less harsh than the method of flame atomization.

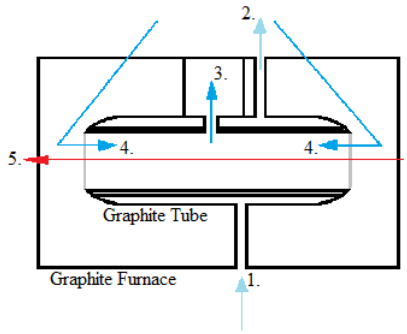


Figure 9.1.11:Schematic diagram of an electrothermal atomizer showing the external gas flow inlet (1), the external gas flow outlet (2), the internal gas flow outlet (3), the internal gas flow inlet (4), and the light beam (5).

Radiation source

The radiation source then irradiates the atomized sample. The sample absorbs some of the radiation, and the rest passes through the spectrometer to a detector. Radiation sources can be separated into two broad categories: line sources and continuum sources. Line sources excite the analyte and thus emit its own line spectrum. Hollow cathode lamps and electrodeless discharge lamps are the most commonly used examples of line sources. On the other hand, continuum sources have radiation that spreads out over a wider range of wavelengths. These sources are typically only used for background correction. Deuterium lamps and halogen lamps are often used for this purpose.

Spectrometer

Spectrometers are used to separate the different wavelengths of light before they pass to the detector. The spectrometer used in AAS can be either single-beam or double-beam. Single-beam spectrometers only require radiation that passes directly through the atomized sample, while double-beam spectrometers (Figure 9.1.12), as implied by the name, require two beams of light; one that passes directly through the sample, and one that does not pass through the sample at all. (Insert diagrams) The single-beam spectrometers have less optical components and therefore suffer less radiation loss. Double-beam monochromators have more optical components, but they are also more stable over time because they can compensate for changes more readily.

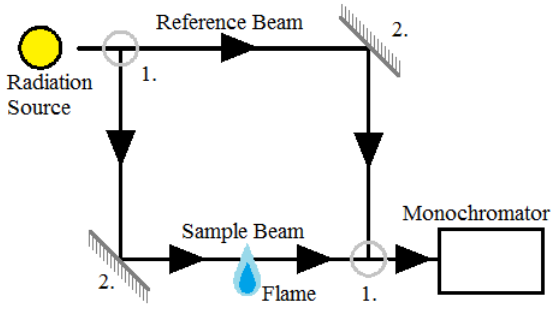


Figure 9.1.12: A schematic of a double-beam spectrometer showing the 50/50 beam splitters (1) and the mirrors (2).

Obtaining Measurements

Sample preparation

Sample preparation is extremely varied because of the range of samples that can be analyzed. Regardless of the type of sample, certain considerations should be made. These include the laboratory environment, the vessel holding the sample, storage of the sample, and pretreatment of the sample.

Sample preparation begins with having a clean environment to work in. AAS is often used to measure trace elements, in which case contamination can lead to severe error. Possible equipment includes laminar flow hoods, clean rooms, and closed, clean vessels for transportation of the sample. Not only must the sample be kept clean, it also needs to be conserved in terms of pH, constituents, and any other properties that could alter the contents.

When trace elements are stored, the material of the vessel walls can adsorb some of the analyte leading to poor results. To correct for this, perfluoroalkoxy polymers (PFA), silica, glassy carbon, and other materials with inert surfaces are often used as the storage

material. Acidifying the solution with hydrochloric or nitric acid can also help prevent ions from adhering to the walls of the vessel by competing for the space. The vessels should also contain a minimal surface area in order to minimize possible adsorption sites.

Pretreatment of the sample is dependent upon the nature of the sample. See Table 9.1.1 for sample pretreatment methods.

Table 9.1.1 Sample pretreatment methods for AAS.

Sample	Examples	Pretreatment method
Aqueous solutions	Water, beverages, urine, blood	Digestion if interference causing substituents are present
Suspensions	Water, beverages, urine, blood	Solid matter must either be removed by filtration, centrifugation or digestion, and then the methods for aqueous solutions can be followed
Organic liquids	Fuels, oils	Either direct measurement with AAS or diltion with organic material followed by measurement with AAS, standards must contain the analyte in the same form as the sample
Solids	Foodstuffs, rocks	Digestion followed by electrothermal AAS

Calibration curve

In order to determine the concentration of the analyte in the solution, calibration curves can be employed. Using standards, a plot of concentration versus absorbance can be created. Three common methods used to make calibration curves are the standard calibration technique, the bracketing technique, and the analyte addition technique.

Standard calibration technique

This technique is the both the simplest and the most commonly used. The concentration of the sample is found by comparing its absorbance or integrated absorbance to a curve of the concentration of the standards versus the absorbances or integrated absorbances of the standards. In order for this method to be applied the following conditions must be met:

- Both the standards and the sample must have the same behavior when atomized. If they do not, the matrix of the standards should be altered to match that of the sample.
- The error in measuring the absorbance must be smaller than that of the preparation of the standards.
- The samples must be homogeneous.

The curve is typically linear and involves at least five points from five standards that are at equidistant concentrations from each other (Figure 9.1.13). This ensures that the fit is acceptable. A least means squares calculation is used to linearly fit the line. In most cases, the curve is linear only up to absorbance values of 0.5 to 0.8. The absorbance values of the standards should have the absorbance value of a blank subtracted.

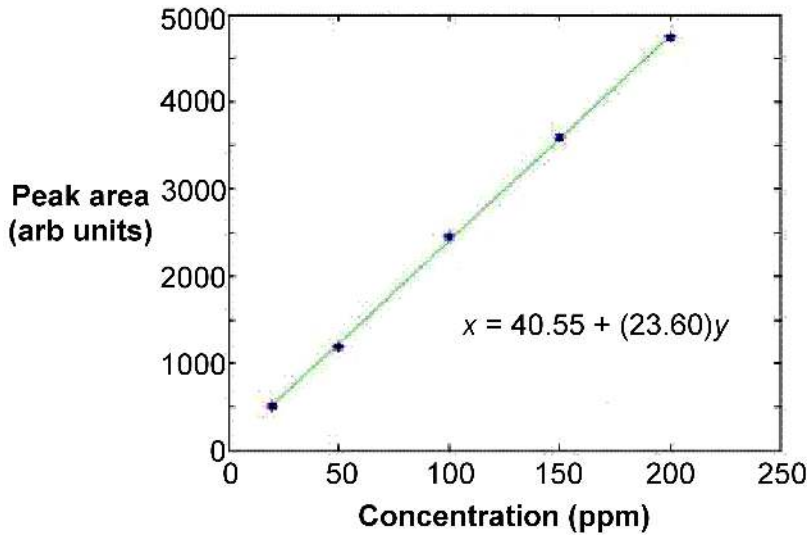


Figure 9.1.13: An example of a calibration curve made for the standard calibration technique.

Bracketing Technique

The bracketing technique is a variation of the standard calibration technique. In this method, only two standards are necessary with concentrations c_1 and c_2. They bracket the approximate value of the sample concentration very closely. Applying Equation 9.1.3 to determines the value for the sample, where c_x and A_x are the concentration and adsorbance of the unknown, and A_1 and A_2 are the adsorbance for c_1 and c_2, respectively.

$$c_x = \frac{(A_x - A_1)(c_1 - c_2)}{A_2 - A_1} + c_1 \tag{9.1.3}$$

This method is very useful when the concentration of the analyte in the sample is outside of the linear portion of the calibration curve because the bracket is so small that the portion of the curve being used can be portrayed as linear. Although this method can be used accurately for nonlinear curves, the further the curve is from linear the greater the error will be. To help reduce this error, the standards should bracket the sample very closely.

Analyte Addition Technique

The analyte addition technique is often used when the concomitants in the sample are expected to create many interferences and the composition of the sample is unknown. The previous two techniques both require that the standards have a similar matrix to that of the sample, but that is not possible when the matrix is unknown. To compensate for this, the analyte addition technique uses an aliquot of the sample itself as the matrix. The aliquots are then spiked with various amounts of the analyte. This technique must be used only within the linear range of the absorbances.

Measurement Interference

Interference is caused by contaminants within the sample that absorb at the same wavelength as the analyte, and thus can cause inaccurate measurements. Corrections can be made through a variety of methods such as background correction, addition of chemical additives, or addition of analyte.

Table 9.1.2: Examples of interference in AAS.

Interference type	Cause of interference	Result	Example	Correction measures
Atomic line overlap	Spectral profile of two elements are within 0.01 nm of each other	Higher experimental absorption value than the real value	Very rare, with the only plausable problem being that of copper (324.754 nm) and europium (324.753 nm)	Typically doesn't occur in practical situations, so there is no established correction method

Interference type	Cause of interference	Result	Example	Correction measures
Molecular band and line overlap	Spectral profile of an element overlaps with molecular band	Higher experimental absorption value than the real value	Calcium hydroxide and barium at 553.6 nm in a air-acetylene flame	Background correction
Ionization (vapor-phase or cation enhancement)	atoms are ionized at the temperature of the flame/furnace, which decreases the amount of free atoms	Lower experimental absorption value than real value	Problems commonly occur with cesium, potassium, and sodium	Add an ionization suppressor (or buffer) to both the sample and the standards
Light scattering	Solid particles scatter the beam of light lowering the intensity of the beam entering the monochromater	Higher experimental absorption value than the real value	High in samples with many refractory elements, highest at UV wavelengths (add specific example)	Matrix modifaction and/or background correction
Chemical	The chemical being analyzed is contained withing a compound in the analyte that is not atomized	Lower experimental absorption value than real value	Calcium and phosphate ions form calcium phosphate which is then converted to calcium pyrophosphate which is stable in high heat	Increase the temperature of the flame if flame AAS is being used, use a releasing chemical, or standard addition for electrothermal AAS
Physical	If physical properties of the sample and the standards are different, atomization can be affected thus affecting the number of free atom population	Can vary in either direction depending upon the conditions	Viscosity differences, surface tension differences, etc	Alter the standards to have similar physical properties to the samples
Volitalization	In electrothermal atomization, interference will occur if the rate of volatilization is not the same for the sample as for the standard, which is often caused by a heavy matrix	Can vary in either direction depending upon the conditions	Chlorides are very volatile, so they need to be converted to a less volatile form. Often this is done by the addition of nitrate or slufate. Zinc and lead are also highly problamatic	Change the matrix by standard addition, or selectively volatileze components of the matrix

Bibliography

- L. Ebon, A. Fisher and S. J. Hill, *An Introduction to Analytical Atomic Spectrometry*, Ed. E. H. Evans, Wiley, New York (1998).
- B. Welz and M. Sperling, *Atomic Absorption Spectrometry*, 3rd Ed, Wiley-VCH, New York (1999).
- J. W. Robinson, *Atomic Spectroscopy*, 2nd Ed. Marcel Dekker, Inc., New York (1996).
- K. S. Subramanian, *Water Res.*, 1995, **29**, 1827.
- M. Sakata and O. Shimoda, *Water Res.*, 1982, **16**, 231.
- J. C. Van Loon, *Analytical Atomic Absorption Spectroscopy Selected Methods*, Academic Press, New York (1980).

This page titled 9.1: Introduction to Atomic Absorption Spectroscopy is shared under a CC BY 4.0 license and was authored, remixed, and/or curated by Pavan M. V. Raja & Andrew R. Barron (OpenStax CNX) via source content that was edited to the style and standards of the LibreTexts platform.

- **1.4: Introduction to Atomic Absorption Spectroscopy** by Pavan M. V. Raja & Andrew R. Barron is licensed CC BY 4.0. Original source: http://cnx.org/contents/ba27839d-5042-4a40-afcf-c0e6e39fb45425.2.

9.2: Sample Atomization Techniques

The process of converting an analyte to a free gaseous atom is called atomization. Converting an aqueous analyte into a free atom requires that we strip away the solvent, volatilize the analyte, and, if necessary, dissociate the analyte into free atoms. Desolvating an aqueous solution of $CuCl_2$, for example, leaves us with solid particulates of $CuCl_2$. Converting the particulate $CuCl_2$ to gas phases atoms of Cu and Cl requires thermal energy.

$$CuCl_2(aq) \rightarrow CuCl_2(s) \rightarrow Cu(g) + 2Cl(g)$$

There are two common atomization methods: flame atomization and electrothermal atomization, although a few elements are atomized using other methods.

Flame Atomization

Figure $9.2.1$ shows a typical flame atomization assembly with close-up views of several key components. In the unit shown here, the aqueous sample is drawn into the assembly by passing a high-pressure stream of compressed air past the end of a capillary tube immersed in the sample. When the sample exits the nebulizer it strikes a glass impact bead, which converts it into a fine aerosol mist within the spray chamber. The aerosol mist is swept through the spray chamber by the combustion gases—compressed air and acetylene in this case—to the burner head where the flame's thermal energy desolvates the aerosol mist to a dry aerosol of small, solid particulates. The flame's thermal energy then volatilizes the particles, producing a vapor that consists of molecular species, ionic species, and free atoms.

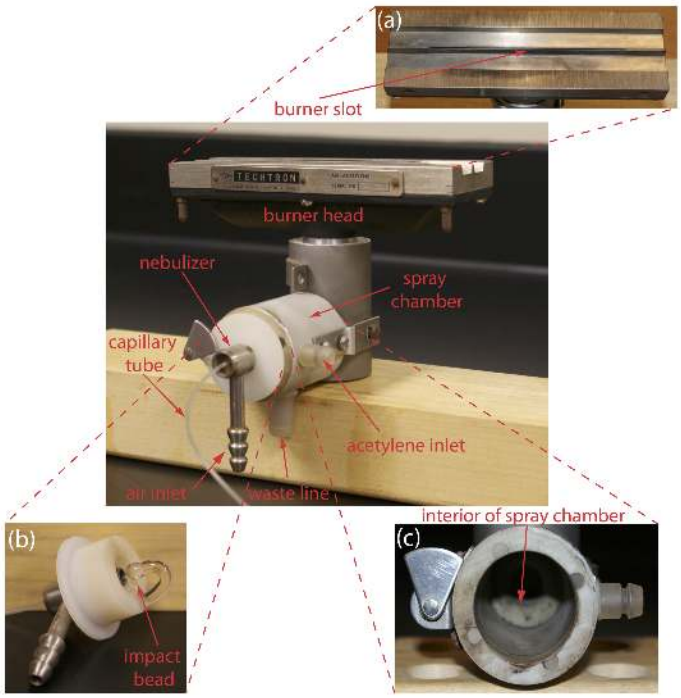


Figure $9.2.1$. Flame atomization assembly with expanded views of (a) the burner head showing the burner slot where the flame is located; (b) the nebulizer's impact bead; and (c) the interior of the spray chamber. Although the unit shown here is from an instrument dating to the 1970s, the basic components of a modern flame AA spectrometer are the same.

Burner. The slot burner in Figure $9.2.1a$ provides a long optical pathlength and a stable flame. Because absorbance is directly proportional to pathlength, a long pathlength provides greater sensitivity. A stable flame minimizes uncertainty due to fluctuations in the flame.

The burner is mounted on an adjustable stage that allows the entire assembly to move horizontally and vertically. Horizontal adjustments ensure the flame is aligned with the instrument's optical path. Vertical adjustments change the height within the flame from which absorbance is monitored. This is important because two competing processes affect the concentration of free atoms in the flame. The more time an analyte spends in the flame the greater the atomization efficiency; thus, the production of free atoms increases with height. On the other hand, a longer residence time allows more opportunity for the free atoms to combine with oxygen to form a molecular oxide. As seen in Figure $9.2.2$, for a metal this is easy to oxidize, such as Cr, the concentration of free

atoms is greatest just above the burner head. For a metal, such as Ag, which is difficult to oxidize, the concentration of free atoms increases steadily with height.

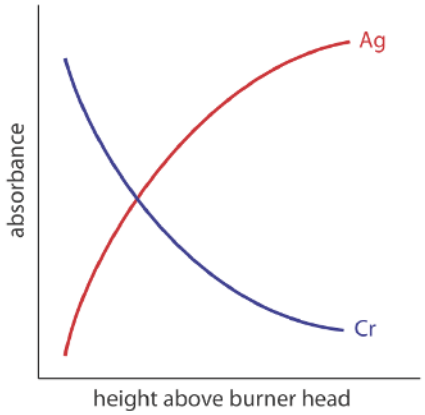


Figure 9.2.2. Absorbance versus height profiles for Ag and Cr in flame atomic absorption spectroscopy.

Flame. The flame's temperature, which affects the efficiency of atomization, depends on the fuel–oxidant mixture, several examples of which are listed in Table 9.2.1. Of these, the air–acetylene and the nitrous oxide–acetylene flames are the most popular. Normally the fuel and oxidant are mixed in an approximately stoichiometric ratio; however, a fuel-rich mixture may be necessary for easily oxidized analytes.

Table 9.2.1. Fuels and Oxidants Used for Flame Combustion

fuel	oxidant	temperature range (^{o}C)
natural gas	air	1700–1900
hydrogen	air	2000–2100
acetylene	air	2100–2400
acetylene	nitrous oxide	2600–2800
acetylene	oxygen	3050–3150

Figure 9.2.3 shows a cross-section through the flame, looking down the source radiation's optical path. The primary combustion zone usually is rich in gas combustion products that emit radiation, limiting is useful- ness for atomic absorption. The interzonal region generally is rich in free atoms and provides the best location for measuring atomic absorption. The hottest part of the flame typically is 2–3 cm above the primary combustion zone. As atoms approach the flame's secondary combustion zone, the decrease in temperature allows for formation of stable molecular species.

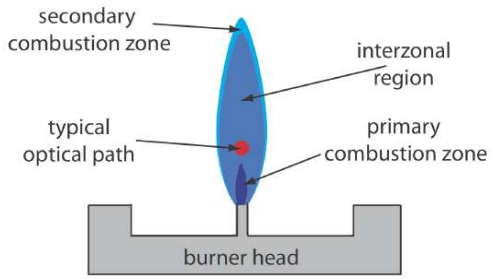


Figure 9.2.3. Profile of typical flame using a slot burner. The relative size of each zone depends on many factors, including the choice of fuel and oxidant, and their relative proportions.

Sample Introduction. The most common means for introducing a sample into a flame atomizer is a continuous aspiration in which the sample flows through the burner while we monitor absorbance. Continuous aspiration is sample intensive, typically requiring from 2–5 mL of sample.

Flame microsampling allows us to introduce a discrete sample of fixed volume, and is useful if we have a limited amount of sample or when the sample's matrix is incompatible with the flame atomizer. For example, continuously aspirating a sample that has a high concentration of dissolved solids—sea water, for example, comes to mind—may build-up a solid de- posit on the burner head that obstructs the flame and that lowers the absorbance. Flame microsampling is accomplished using a micropipet to place 50–250 μL of sample in a Teflon funnel connected to the nebulizer, or by dipping the nebulizer tubing into the sample for a short time. Dip sampling usually is accomplished with an automatic sampler. The signal for flame microsampling is a transitory peak whose height or area is proportional to the amount of analyte that is injected.

Advantages and Disadvantages of Flame Atomization. The principal advantage of flame atomization is the reproducibility with which the sample is introduced into the spectrophotometer; a significant disadvantage is that the efficiency of atomization is quite poor. There are two reasons for poor atomization efficiency. First, the majority of the aerosol droplets produced during nebulization are too large to be carried to the flame by the combustion gases. Consequently, as much as 95% of the sample never reaches the flame, which is the reason for the waste line shown at the bottom of the spray chamber in Figure 9.2.1. A second reason for poor atomization efficiency is that the large volume of combustion gases significantly dilutes the sample. Together, these contributions to the efficiency of atomization reduce sensitivity because the analyte's concentration in the flame may be a factor of 2.5×10^{-6} less than that in solution [Ingle, J. D.; Crouch, S. R. *Spectrochemical Analysis*, Prentice-Hall: Englewood Cliffs, NJ, 1988; p. 275].

Electrothermal Atomization

A significant improvement in sensitivity is achieved by using the resistive heating of a graphite tube in place of a flame. A typical electrothermal atomizer, also known as a graphite furnace, consists of a cylindrical graphite tube approximately 1–3 cm in length and 3–8 mm in diameter. As shown in Figure 9.2.4, the graphite tube is housed in an sealed assembly that has an optically transparent window at each end. A continuous stream of inert gas is passed through the furnace, which protects the graphite tube from oxidation and removes the gaseous products produced during atomization. A power supply is used to pass a current through the graphite tube, resulting in resistive heating.

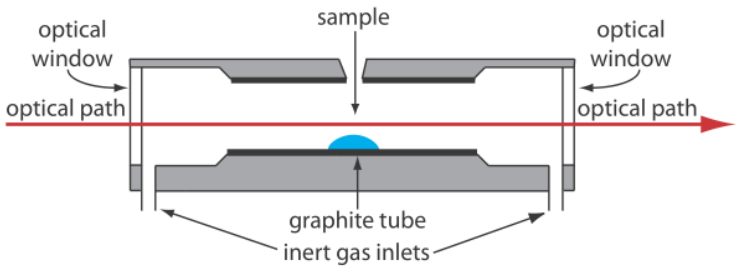


Figure 9.2.4. Diagram showing a cross-section of an electrothermal atomizer, which also is known as a graphite furnace.

Samples of between 5–50 μL are injected into the graphite tube through a small hole at the top of the tube. Atomization is achieved in three stages. In the first stage the sample is dried to a solid residue using a current that raises the temperature of the graphite tube to about 110°C. In the second stage, which is called ashing, the temperature is increased to between 350–1200°C. At these temperatures organic material in the sample is converted to CO_2 and H_2O, and volatile inorganic materials are vaporized. These gases are removed by the inert gas flow. In the final stage the sample is atomized by rapidly increasing the temperature to between 2000–3000°C. The result is a transient absorbance peak whose height or area is proportional to the absolute amount of analyte injected into the graphite tube. Together, the three stages take approximately 45–90 s, with most of this time used for drying and ashing the sample.

Electrothermal atomization provides a significant improvement in sensitivity by trapping the gaseous analyte in the small volume within the graphite tube. The analyte's concentration in the resulting vapor phase is as much as 1000× greater than in a flame atomization [Parsons, M. L.; Major, S.; Forster, A. R. *Appl. Spectrosc.* **1983**, *37*, 411–418]. This improvement in sensitivity—and the resulting improvement in detection limits—is offset by a significant decrease in precision. Atomization efficiency is influenced strongly by the sample's contact with the graphite tube, which is difficult to control reproducibly.

Specialized Atomization Techniques

A few elements are atomized by using a chemical reaction to produce a volatile product. Elements such as As, Se, Sb, Bi, Ge, Sn, Te, and Pb, for example, form volatile hydrides when they react with $NaBH_4$ in the presence of acid. An inert gas carries the volatile hydride to either a flame or to a heated quartz observation tube situated in the optical path. Mercury is determined by the

cold-vapor method in which it is reduced to elemental mercury with $SnCl_2$. The volatile Hg is carried by an inert gas to an unheated observation tube situated in the instrument's optical path.

Flame or Electrothermal Atomization?

The most important factor in choosing a method of atomization is the analyte's concentration. Because of its greater sensitivity, it takes less analyte to achieve a given absorbance when using electrothermal atomization. Table 9.2.2 which compares the amount of analyte needed to achieve an absorbance of 0.20 when using flame atomization and electrothermal atomization, is useful when selecting an atomization method. For example, flame atomization is the method of choice if our samples contain 1–10 mg Zn^{2+}/L, but electrothermal atomization is the best choice for samples that contain 1–10 µg Zn^{2+}/L.

Table 9.2.2. Concentration of Analyte (in mg/L) That Yields an Absorbance of 0.20

element	flame atomization	electrothermal atomization
Ag	1.5	0.0035
Al	40	0.015
As	40	0.050
Ca	0.8	0.003
Cd	0.6	0.001
Co	2.5	0.021
Cr	2.5	0.0075
Cu	1.5	0.012
Fe	2.5	0.006
Hg	70	0.52
Mg	0.15	0.00075
Mn	1	0.003
Na	0.3	0.00023
Ni	2	0.024
Pb	5	0.080
Pt	70	0.29
Sn	50	0.023
Zn	0.3	0.00071

Source: Varian Cookbook, SpectraAA Software Version 4.00 Pro.
As: 10 mg/L by hydride vaporization; Hg: 11.5 mg/L by cold-vapor; and Sn:18 mg/L by hydride vaporization

This page titled 9.2: Sample Atomization Techniques is shared under a CC BY-NC-SA 4.0 license and was authored, remixed, and/or curated by David Harvey.

- **9.1: Sample Atomization Techniques** by David Harvey is licensed CC BY-NC-SA 4.0.

9.3: Atomic Absorption Instrumentation

Atomic absorption spectrophotometers use optical benches similar to those described earlier in Chapter 7, including a source of radiation, a method for introducing the sample (covered in the previous section), a means for isolating the wavelengths of interest, and a way to measure the amount of light absorbed or emitted.

Radiation Sources

Because atomic absorption lines are narrow, we need to use a line source instead of a continuum source to record atomic absorption spectra. Figure 9.3.1 will help us understand why this is necessary. As discussed in Chapter 7, a typical continuum source has an effective bandwidth on the order of 1 nm after passing through a monochromator. An atomic absorption line, as we learned in Chapter 8, has an effective line width on the order of 0.002 nm due to Doppler broadening and pressure broadening that takes place in a flame. If we pass the radiation from a continuum source through the flame, the incident power from the source, P_0, and the power that reaches the detector, P_t, are essentially identical, leading to an absorbance of zero. A line source, which operates a temperature that is lower than a flame, has a line width on the order of 0.001 nm. Passing this source radiation through the flame results in a measurable P_T and a measurable absorbance.

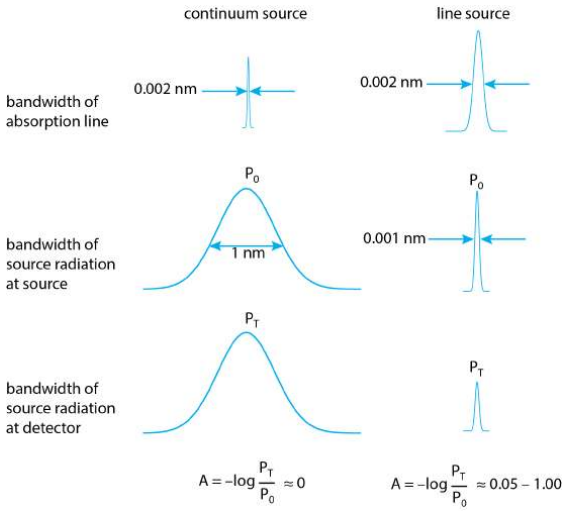


Figure 9.3.1: Illustration showing the effect on absorbance of using a continuum source and a line source for atomic absorption. Note that the peaks in the top row have the same width; thus, the x-axis scale is different for the continuum spectra than for the line source spectra.

The source for atomic absorption is a hollow cathode lamp that consists of a cathode and anode enclosed within a glass tube filled with a low pressure of an inert gas, such as Ne or Ar (Figure 9.3.2). Applying a potential across the electrodes ionizes the filler gas. The positively charged gas ions collide with the negatively charged cathode, sputtering atoms from the cathode's surface. Some of the sputtered atoms are in the excited state and emit radiation characteristic of the metal(s) from which the cathode is manufactured. By fashioning the cathode from the metallic analyte, a hollow cathode lamp provides emission lines that correspond to the analyte's absorption spectrum.

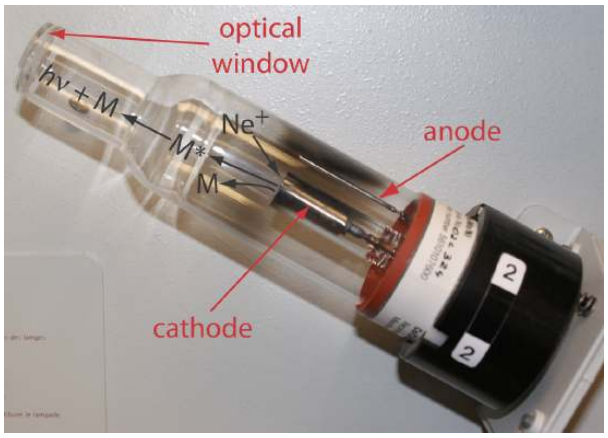


Figure 9.3.2. Photo of a typical multielemental hollow cathode lamp. The cathode in this lamp is fashioned from an alloy of Co, Cr, Cu, Fe, Mn, and Ni, and is surrounded by a glass shield that isolates it from the anode. The lamp is filled with Ne gas. Also shown is the process that leads to atomic emission. Note the black deposit of sputtered metal on the outer wall of the hollow cathode lamp. See the text for additional details.

Each element in a hollow cathode lamp provides several atomic emission lines that we can use for atomic absorption. Usually the wavelength that provides the best sensitivity is the one we choose to use, although a less sensitive wavelength may be more appropriate for a sample that has higher concentration of analyte. For the Cr hollow cathode lamp in Table 9.3.1, the best sensitivity is obtained using a wavelength of 357.9 nm as this line requires the smallest concentration of analyte to achieve an absorbance of 0.20.

Table 9.3.1. Atomic Emission Lines for a Cr Hollow Cathode Lamp

wavelength (nm)	slit width (nm)	mg Cr/L giving A = 0.20	P_0 (relative)
357.9	0.2	2.5	40
425.4	0.2	12	85
429.0	0.5	20	100
520.5	0.2	1500	15
520.8	0.2	500	20

Another consideration is the emission line's intensity, P_0. If several emission lines meet our requirements for sensitivity, we may wish to use the emission line with the largest relative P_0 because there is less uncertainty in measuring P_0 and P_T. When analyzing a sample that is ≈10 mg Cr/L, for example, the first three wavelengths in Table 9.3.1 provide good sensitivity; the wavelengths of 425.4 nm and 429.0 nm, however, have a greater P_0 and will provide less uncertainty in the measured absorbance.

The emission spectrum for a hollow cathode lamp includes, in addition to the analyte's emission lines, additional emission lines from impurities present in the metallic cathode and from the filler gas. These additional lines are a potential source of stray radiation that could result in an instrumental deviation from Beer's law. The monochromator's slit width is set as wide as possible to improve the throughput of radiation and narrow enough to eliminate these sources of stray radiation.

Optical Benches

Atomic absorption spectrometers are available using either a single-beam and a double-beam optical bench. Figure 9.3.3 shows a typical single-beam spectrometer, which consists of a hollow cathode lamp as a source, a flame, a grating monochromator, a detector (usually a photomultiplier tube), and a signal processor. Also included in this design is a chopper that periodically blocks light from the hollow cathode lamp from passing through the flame and reaching the detector. The purpose of the chopper is to provide a means for discriminating against the emission of light from the flame, which will otherwise contribute to the total amount of light that reaches the detector. As shown in Figure 9.3.3, when the chopper is closed, the only light reaching the detector is from the flame; emission from the flame and light from the lamp after it passes through the flame reach the detector when the chopper is open. The difference between the two signals gives the amount of light that reaches the detector after being absorbed by the

sample. An alternative method that accomplishes the same thing is to modulate the amount of radiation emitted by the hollow cathode lamp.

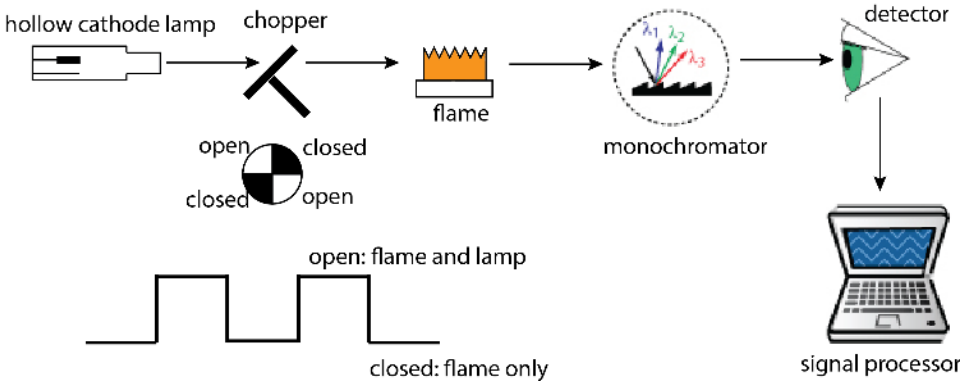


Figure 9.3.3: Typical single-beam optical bench for atomic absorption.

Figure 9.3.4 shows the typical arrangement of a double-beam instrument for atomic absorption spectroscopy. In this design, the chopper alternates between two optical paths: one in which light from the hollow cathode lamp bypasses the flame and that measures the total emission of radiation from the flame and the lamp, and one that passes the hollow light from the hollow cathode lamp through the flame and that measures the emission of light from the flame and the amount of light from the hollow cathode lamp that is not absorbed by the sample. The difference between the two signals gives the amount of light that reaches the detector after being absorbed by the sample.

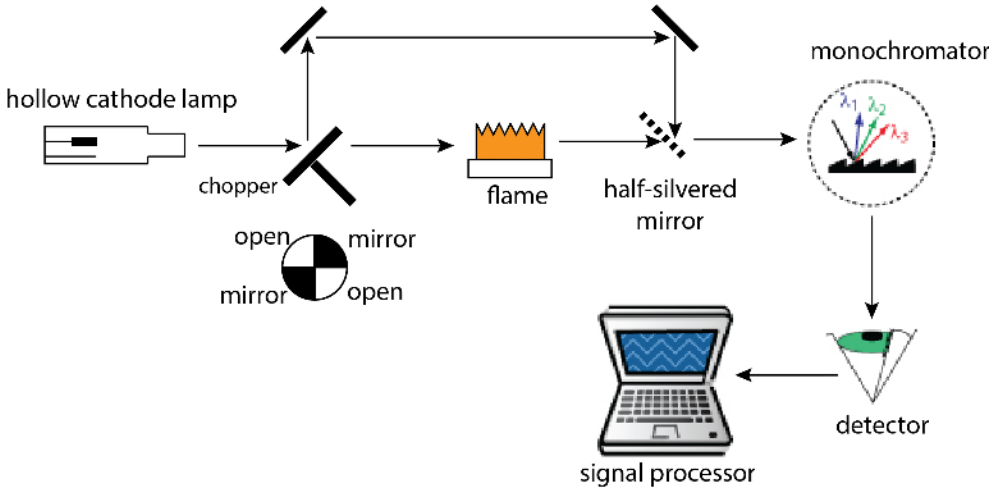


Figure 9.3.4: Typical double-beam optical bench for atomic absorption.

This page titled 9.3: Atomic Absorption Instrumentation is shared under a CC BY-NC-SA 4.0 license and was authored, remixed, and/or curated by David Harvey.

- **9.2: Atomic Absorption Instrumentation** by David Harvey is licensed CC BY-NC-SA 4.0.

9.4: Interferences in Absorption Spectroscopy

In describing the optical benches for atomic absorption spectroscopy, we noted the need to modulate the radiation from the source in order to discriminate against emission of radiation from the flame. In this section we consider additional sources of interference and discuss ways to compensate for them.

Spectral Interferences

A spectral interference occurs when an analyte's absorption line overlaps with an interferent's absorption line or band. Because atomic absorption lines are so narrow, the overlap of two such lines seldom is a problem. On the other hand, a molecule's broad absorption band or the scattering of source radiation is a potentially serious spectral interference.

An important consideration when using a flame as an atomization source is its effect on the measured absorbance. Among the products of combustion are molecular species that exhibit broad absorption bands and particulates that scatter radiation from the source. If we fail to compensate for these spectral interferences, then the intensity of transmitted radiation is smaller than expected. The result is an apparent increase in the sample's absorbance. Fortunately, absorption and scattering of radiation by the flame are corrected by analyzing a blank that does not contain the sample.

Spectral interferences also occur when components of the sample's matrix other than the analyte react to form molecular species, such as oxides and hydroxides. The resulting absorption and scattering constitutes the sample's background and may present a significant problem, particularly at wavelengths below 300 nm where the scattering of radiation becomes more important. If we know the composition of the sample's matrix, then we can prepare our samples using an identical matrix. In this case the background absorption is the same for both the samples and the standards. Alternatively, if the background is due to a known matrix component, then we can add that component in excess to all samples and standards so that the contribution of the naturally occurring interferent is insignificant. Finally, many interferences due to the sample's matrix are eliminated by increasing the atomization temperature. For example, switching to a higher temperature flame helps prevents the formation of interfering oxides and hydroxides.

If the identity of the matrix interference is unknown, or if it is not possible to adjust the flame or furnace conditions to eliminate the interference, then we must find another method to compensate for the background interference. Several methods have been developed to compensate for matrix interferences, and most atomic absorption spectrophotometers include one or more of these methods.

One of the most common methods for background correction is to use a continuum source, such as a D_2 lamp. Because a D_2 lamp is a continuum source, absorbance of its radiation by the analyte's narrow absorption line is negligible. Only the background, therefore, absorbs radiation from the D_2 lamp. Both the analyte and the background, on the other hand, absorb the hollow cathode's radiation. Subtracting the absorbance for the D_2 lamp from that for the hollow cathode lamp gives a corrected absorbance that compensates for the background interference. Although this method of background correction is effective, it does assume that the background absorbance is constant over the range of wavelengths passed by the monochromator. If this is not true, then subtracting the two absorbances underestimates or overestimates the background. A typical optical arrangement is shown in Figure 9.4.1.

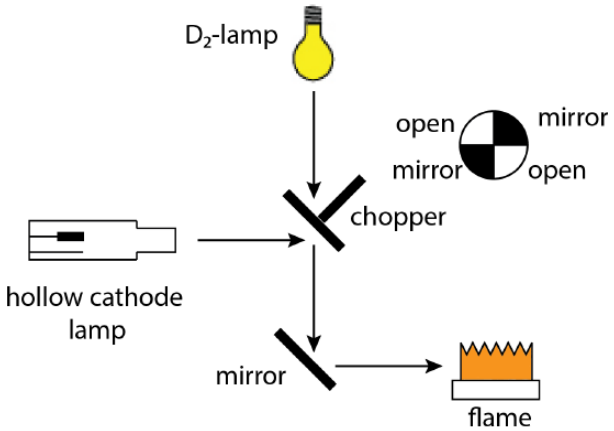


Figure 9.4.1: Illustration showing a modification to the optical bench to allow for background correction using a continuous source, such as a D_2-lamp. The chopper alternates between allowing light from the hollow cathode lamp and light from the D_2-lamp to pass through the flame and reach the detector.

Another approach to removing the background is to take advantage of the Zeeman effect. The basis of the technique is outlined in Figure 9.4.2 and described below in more detail. In the absence of an applied magnetic field—B = 0, where B is the strength of the magnetic field—a $p \rightarrow d$ absorbance by the analyte takes place between two well-defined energy levels and yields a single well-defined absorption line, as seen on the left side of panel (a). When a magnetic field is applied, B > 0, the three equal energy *p*-orbitals split into three closely spaced energy levels and the five equal energy *d*-orbitals split into five closely spaced energy levels. The allowed transitions between these energy levels of $\Delta M_l = 0, \pm 1$ yields three well-defined absorption lines, as seen on the right-side of panel (a), the central one of which ($\Delta M_l = 0$) is at the same wavelength as the absorption line in the absence of the applied magnetic field. This central band is the only wavelength at which the analyte absorbs.

As we see in Figure 9.4.2*b*, *c*, we apply a magnetic field to the instrument's electrothermal atomizer and place a rotating polarizer between it and the hollow cathode lamp. When the rotating polarizer is in one position, radiation from the hollow cathode light is absorbed only by the central absorption line, giving a measure of absorption by both the background and the analyte. when the rotating polarizer is in the other position, radiation from the hollow cathode lamp is absorbed only by the two outside lines, providing a measure of absorption by the background only. The difference in these two absorption values is a function of the analyte's concentration.

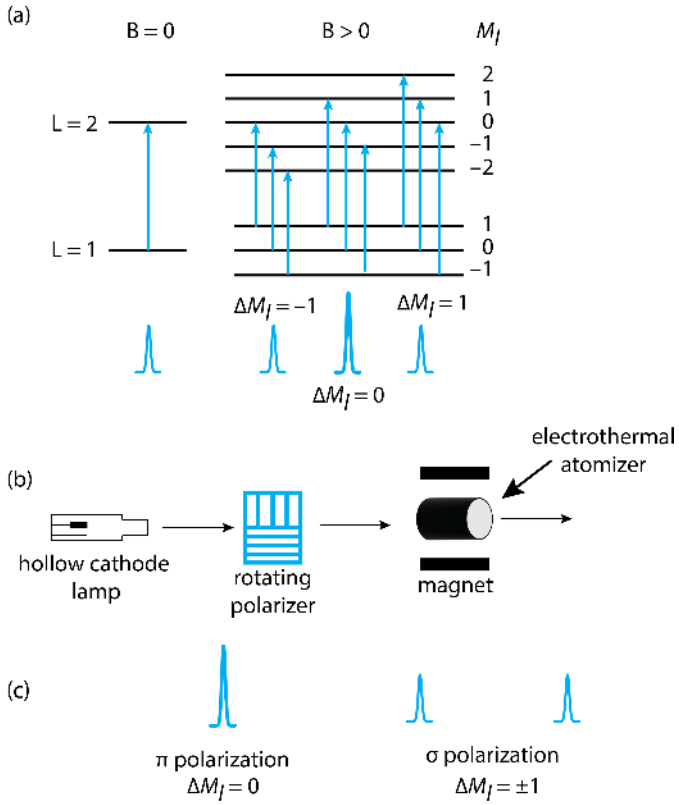


Figure 9.4.2: Illustration of using the Zeeman effect to compensate for background absorption when using an electrothermal atomizer: panel (a) explains the origin of the Zeemen effect; panel (b) shows the modification to the instrument; and panel (c) shows the resulting absorption lines. See the text for more details.

A third method for compensating for background absorption is to take advantage of what happens to the emission intensity of a hollow cathode lamp when it is operated at a high current. As seen in Figure 9.4.3, when using a high current the emission band become significantly broader than when using a normal (low) current and, at the analytical wavelength, the emission intensity from the lamp decreases due to self-absorption, a process in which the ground state atoms in the hollow cathode lamp absorb photons emitted by the excited state atoms in the hollow cathode lamp. When using a low current we measure absorption from both the analyte and the background; when using a high current, absorption is due almost exclusively to the background. This approach is called Smith-Hieftje background corrections.

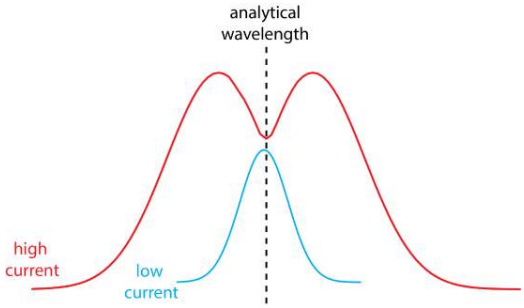


Figure 9.4.1: Illustration showing the basis of Smith-Hieftje background correction.

Chemical Interferences

The quantitative analysis of some elements is complicated by chemical interferences that occur during atomization. The most common chemical interferences are the formation of nonvolatile compounds that contain the analyte and ionization of the analyte.

One example of the formation of a nonvolatile compound is the effect of PO_4^{3-} or Al^{3+} on the flame atomic absorption analysis of Ca^{2+}. In one study, for example, adding 100 ppm Al^{3+} to a solution of 5 ppm Ca^{2+} decreased calcium ion's absorbance from 0.50 to 0.14, while adding 500 ppm PO_4^{3-} to a similar solution of Ca^{2+} decreased the absorbance from 0.50 to 0.38. These interferences are attributed to the formation of nonvolatile particles of $Ca_3(PO_4)_2$ and an Al–Ca–O oxide [Hosking, J. W.; Snell, N. B.; Sturman, B. T. *J. Chem. Educ.* **1977**, *54*, 128–130].

When using flame atomization, we can minimize the formation of non-volatile compounds by increasing the flame's temperature by changing the fuel-to-oxidant ratio or by switching to a different combination of fuel and oxidant. Another approach is to add a releasing agent or a protecting agent to the sample. A releasing agent is a species that reacts preferentially with the interferent, releasing the analyte during atomization. For example, Sr^{2+} and La^{3+} serve as releasing agents for the analysis of Ca^{2+} in the presence of PO_4^{3-} or Al^{3+}. Adding 2000 ppm $SrCl_2$ to the Ca^{2+}/ PO_4^{3-} and to the Ca^{2+}/Al^{3+} mixtures described in the previous paragraph increased the absorbance to 0.48. A protecting agent reacts with the analyte to form a stable volatile complex. Adding 1% w/w EDTA to the Ca^{2+}/ PO_4^{3-} solution described in the previous paragraph increased the absorbance to 0.52.

An ionization interference occurs when thermal energy from the flame or the electrothermal atomizer is sufficient to ionize the analyte

$$M(s) \rightleftharpoons M^+(aq) + e^- \tag{9.4.1}$$

where M is the analyte. Because the absorption spectra for M and M^+ are different, the position of the equilibrium in reaction 9.4.1 affects the absorbance at wavelengths where M absorbs. To limit ionization we add a high concentration of an ionization suppressor, which is a species that ionizes more easily than the analyte. If the ionization suppressor's concentration is sufficient, then the increased concentration of electrons in the flame pushes reaction 9.4.1 to the left, preventing the analyte's ionization. Potassium and cesium frequently are used as an ionization suppressor because of their low ionization energy.

This page titled 9.4: Interferences in Absorption Spectroscopy is shared under a CC BY-NC-SA 4.0 license and was authored, remixed, and/or curated by David Harvey.

- **9.3: Interferences in Absorption Spectroscopy** by David Harvey is licensed CC BY-NC-SA 4.0.

9.5: Atomic Absorption Techniques

Preparing the Sample

Flame and electrothermal atomization require that the analyte is in solution. Solid samples are brought into solution by dissolving in an appropriate solvent. If the sample is not soluble it is digested, either on a hot-plate or by microwave, using HNO_3, H_2SO_4, or $HClO_4$. Alternatively, we can extract the analyte using a Soxhlet extractor. Liquid samples are analyzed directly or the analytes extracted if the matrix is in- compatible with the method of atomization. A serum sample, for instance, is difficult to aspirate when using flame atomization and may produce an unacceptably high background absorbance when using electrothermal atomization. A liquid–liquid extraction using an organic solvent and a chelating agent frequently is used to concentrate analytes. Dilute solutions of Cd^{2+}, Co^{2+}, Cu^{2+}, Fe^{3+}, Pb^{2+}, Ni^{2+}, and Zn^{2+}, for example, are concentrated by extracting with a solution of ammonium pyrrolidine dithiocarbamate in methyl isobutyl ketone.

Standardizing the Method

Because Beer's law also applies to atomic absorption, we might expect atomic absorption calibration curves to be linear. In practice, however, most atomic absorption calibration curves are nonlinear or linear over a limited range of concentrations. Nonlinearity in atomic absorption is a consequence of instrumental limitations, including stray radiation from the hollow cathode lamp and the variation in molar absorptivity across the absorption line. Accurate quantitative work, therefore, requires a suitable means for computing the calibration curve from a set of standards.

When possible, a quantitative analysis is best conducted using external standards. Unfortunately, matrix interferences are a frequent problem, particularly when using electrothermal atomization. For this reason the method of standard additions often is used. One limitation to this method of standardization, however, is the requirement of a linear relationship between absorbance and concentration.

> Most instruments include several different algorithms for computing the calibration curve. The instrument in my lab, for example, includes five algorithms. Three of the algorithms fit absorbance data using linear, quadratic, or cubic polynomial functions of the analyte's concentration. It also includes two algorithms that fit the concentrations of the standards to quadratic functions of the absorbance.

Evaluation of Atomic Absorption Spectroscopy

Scale of Operation

Atomic absorption spectroscopy is ideally suited for the analysis of trace and ultratrace analytes, particularly when using electrothermal atomization. For minor and major analytes, sample are diluted before the analysis. Most analyses use a macro or a meso sample. The small volume requirement for electrothermal atomization or for flame microsampling, however, makes practical the analysis of micro and ultramicro samples.

Accuracy

If spectral and chemical interferences are minimized, an accuracy of 0.5–5% is routinely attainable. When the calibration curve is nonlinear, accuracy is improved by using a pair of standards whose absorbances closely bracket the sample's absorbance and assuming that the change in absorbance is linear over this limited concentration range. Determinate errors for electrothermal atomization often are greater than those obtained with flame atomization due to more serious matrix interferences.

Precision

For an absorbance greater than 0.1–0.2, the relative standard deviation for atomic absorption is 0.3–1% for flame atomization and 1–5% for electrothermal atomization. The principle limitation is the uncertainty in the concentration of free analyte atoms that result from variations in the rate of aspiration, nebulization, and atomization for a flame atomizer, and the consistency of injecting samples for electrothermal atomization.

Sensitivity

The sensitivity of a flame atomic absorption analysis is influenced by the flame's composition and by the position in the flame from which we monitor the absorbance. Normally the sensitivity of an analysis is optimized by aspirating a standard solution of analyte

and adjusting the fuel-to-oxidant ratio, the nebulizer flow rate, and the height of the burner, to give the greatest absorbance. With electrothermal atomization, sensitivity is influenced by the drying and ashing stages that precede atomization. The temperature and time at each stage is optimized for each type of sample.

Sensitivity also is influenced by the sample's matrix. We already noted, for example, that sensitivity is decreased by a chemical interference. An increase in sensitivity may be realized by adding a low molecular weight alcohol, ester, or ketone to the solution, or by using an organic solvent.

Selectivity

Due to the narrow width of absorption lines, atomic absorption provides excellent selectivity. Atomic absorption is used for the analysis of over 60 elements at concentrations at or below the level of μg/L.

Time, Cost, and Equipment

The analysis time when using flame atomization is short, with sample throughputs of 250–350 determinations per hour when using a fully automated system. Electrothermal atomization requires substantially more time per analysis, with maximum sample throughputs of 20–30 determinations per hour. The cost of a new instrument ranges from between $10,000– $50,000 for flame atomization, and from $18,000–$70,000 for electrothermal atomization. The more expensive instruments in each price range include double-beam optics, automatic samplers, and can be programmed for multielemental analysis by allowing the wavelength and hollow cathode lamp to be changed automatically.

This page titled 9.5: Atomic Absorption Techniques is shared under a CC BY-NC-SA 4.0 license and was authored, remixed, and/or curated by David Harvey.

- **9.4: Atomic Absorption Techniques** by David Harvey is licensed CC BY-NC-SA 4.0.

9.6: ATOMIC ABSORPTION SPECTROSCOPY

Guystav Kirchoff and Robert Bunsen first used atomic absorption—along with atomic emission—in 1859 and 1860 as a means for identify atoms in flames and hot gases. Although atomic emission continued to develop as an analytical technique, progress in atomic absorption languished for almost a century. Modern atomic absorption spectroscopy has its beginnings in 1955 as a result of the independent work of A. C. Walsh and C. T. J. Alkemade [(a) Walsh, A. *Anal. Chem.* **1991**, *63*, 933A–941A; (b) Koirtyohann, S. R. *Anal. Chem.* **1991**, *63*, 1024A–1031A; (c) Slavin, W. *Anal. Chem.* **1991**, *63*, 1033A–1038A]. Commercial instruments were in place by the early 1960s, and the importance of atomic absorption as an analytical technique soon was evident.

INSTRUMENTATION

Atomic absorption spectrophotometers use the same single-beam or double-beam optics described earlier for molecular absorption spectrophotometers (see Figure 10.3.2 and Figure 10.3.3). There is, however, an important additional need in atomic absorption spectroscopy: we first must covert the analyte into free atoms. In most cases the analyte is in solution form. If the sample is a solid, then we must bring the analyte into solution before the analysis. When analyzing a lake sediment for Cu, Zn, and Fe, for example, we bring the analytes into solution as Cu^{2+}, Zn^{2+}, and Fe^{3+} by extracting them with a suitable reagent. For this reason, only the introduction of solution samples is considered in this chapter.

> What reagent we choose to use to bring an analyte into solution depends on our research goals. If we need to know the total amount of metal in the sediment, then we might try a microwave digestion using a mixture of concentrated acids, such as HNO_3, HCl, and HF. This destroys the sediment's matrix and brings everything into solution. On the other hand, if our interest is biologically available metals, we might extract the sample under milder conditions using, for example, a dilute solution of HCl or CH_3COOH at room temperature.

ATOMIZATION

The process of converting an analyte to a free gaseous atom is called ***atomization***. Converting an aqueous analyte into a free atom requires that we strip away the solvent, volatilize the analyte, and, if necessary, dissociate the analyte into free atoms. Desolvating an aqueous solution of $CuCl_2$, for example, leaves us with solid particulates of $CuCl_2$. Converting the particulate $CuCl_2$ to gas phases atoms of Cu and Cl requires thermal energy.

$$CuCl_2(aq) \rightarrow CuCl_2(s) \rightarrow Cu(g) + 2Cl(g)$$

There are two common atomization methods: flame atomization and electrothermal atomization, although a few elements are atomized using other methods.

FLAME ATOMIZER

Figure 10.4.1 shows a typical flame atomization assembly with close-up views of several key components. In the unit shown here, the aqueous sample is drawn into the assembly by passing a high-pressure stream of compressed air past the end of a capillary tube immersed in the sample. When the sample exits the nebulizer it strikes a glass impact bead, which converts it into a fine aerosol mist within the spray chamber. The aerosol mist is swept through the spray chamber by the combustion gases—compressed air and acetylene in this case—to the burner head where the flame's thermal energy desolvates the aerosol mist to a dry aerosol of small, solid particulates. The flame's thermal energy then volatilizes the particles, producing a vapor that consists of molecular species, ionic species, and free atoms.

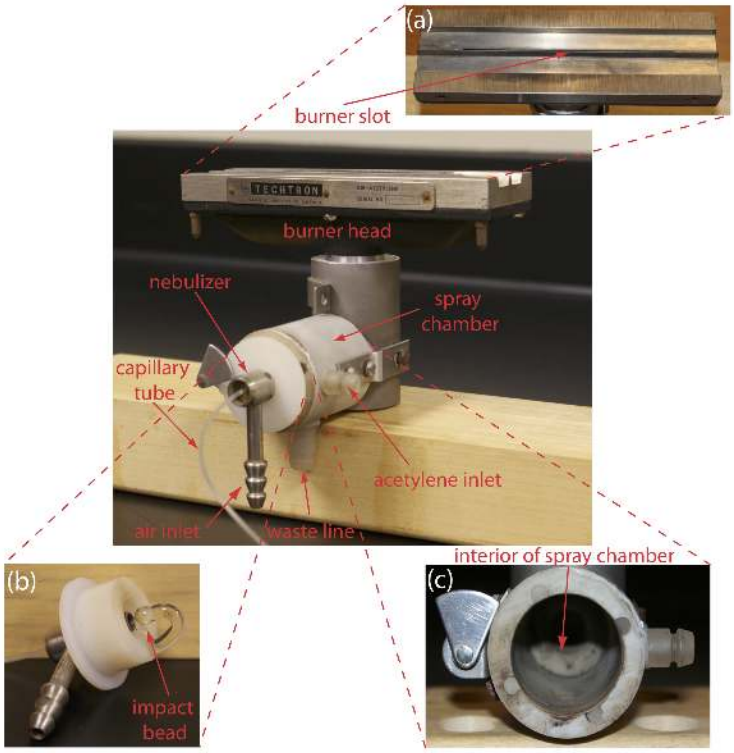


Figure 10.4.1 . Flame atomization assembly with expanded views of (a) the burner head showing the burner slot where the flame is located; (b) the nebulizer's impact bead; and (c) the interior of the spray chamber. Although the unit shown here is from an instrument dating to the 1970s, the basic components of a modern flame AA spectrometer are the same.

Burner. The slot burner in Figure 10.4.1 a provides a long optical pathlength and a stable flame. Because absorbance is directly proportional to pathlength, a long pathlength provides greater sensitivity. A stable flame minimizes uncertainty due to fluctuations in the flame.

The burner is mounted on an adjustable stage that allows the entire assembly to move horizontally and vertically. Horizontal adjustments ensure the flame is aligned with the instrument's optical path. Vertical adjustments change the height within the flame from which absorbance is monitored. This is important because two competing processes affect the concentration of free atoms in the flame. The more time an analyte spends in the flame the greater the atomization efficiency; thus, the production of free atoms increases with height. On the other hand, a longer residence time allows more opportunity for the free atoms to combine with oxygen to form a molecular oxide. As seen in Figure 10.4.2 , for a metal this is easy to oxidize, such as Cr, the concentration of free atoms is greatest just above the burner head. For a metal, such as Ag, which is difficult to oxidize, the concentration of free atoms increases steadily with height.

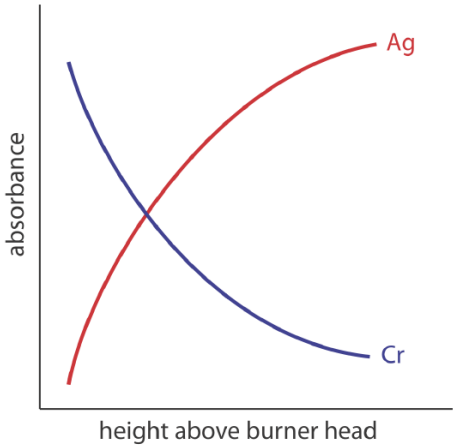


Figure 10.4.2 . Absorbance versus height profiles for Ag and Cr in flame atomic absorption spectroscopy.

Flame. The flame's temperature, which affects the efficiency of atomization, depends on the fuel–oxidant mixture, several examples of which are listed in Table 10.4.1 . Of these, the air–acetylene and the nitrous oxide–acetylene flames are the most popular. Normally the fuel and oxidant are mixed in an approximately stoichiometric ratio; however, a fuel-rich mixture may be necessary for easily oxidized analytes.

Table 10.4.1 . Fuels and Oxidants Used for Flame Combustion

fuel	oxidant	temperature range (°C)
natural gas	air	1700–1900
hydrogen	air	2000–2100
acetylene	air	2100–2400
acetylene	nitrous oxide	2600–2800
acetylene	oxygen	3050–3150

Figure 10.4.3 shows a cross-section through the flame, looking down the source radiation's optical path. The primary combustion zone usually is rich in gas combustion products that emit radiation, limiting is useful- ness for atomic absorption. The interzonal region generally is rich in free atoms and provides the best location for measuring atomic absorption. The hottest part of the flame typically is 2–3 cm above the primary combustion zone. As atoms approach the flame's secondary combustion zone, the decrease in temperature allows for formation of stable molecular species.

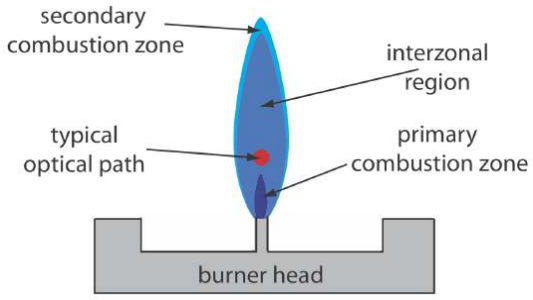


Figure 10.4.3 . Profile of typical flame using a slot burner. The relative size of each zone depends on many factors, including the choice of fuel and oxidant, and their relative proportions.

Sample Introduction. The most common means for introducing a sample into a flame atomizer is a continuous aspiration in which the sample flows through the burner while we monitor absorbance. Continuous aspiration is sample intensive, typically requiring from 2–5 mL of sample.

Flame microsampling allows us to introduce a discrete sample of fixed volume, and is useful if we have a limited amount of sample or when the sample's matrix is incompatible with the flame atomizer. For example, continuously aspirating a sample that has a high concentration of dissolved solids—sea water, for example, comes to mind—may build-up a solid de- posit on the burner head that obstructs the flame and that lowers the absorbance. Flame microsampling is accomplished using a micropipet to place 50–250 μL of sample in a Teflon funnel connected to the nebulizer, or by dipping the nebulizer tubing into the sample for a short time. Dip sampling usually is accomplished with an automatic sampler. The signal for flame microsampling is a transitory peak whose height or area is proportional to the amount of analyte that is injected.

Advantages and Disadvantages of Flame Atomization. The principal advantage of flame atomization is the reproducibility with which the sample is introduced into the spectrophotometer; a significant disadvantage is that the efficiency of atomization is quite poor. There are two reasons for poor atomization efficiency. First, the majority of the aerosol droplets produced during nebulization are too large to be carried to the flame by the combustion gases. Consequently, as much as 95% of the sample never reaches the flame, which is the reason for the waste line shown at the bottom of the spray chamber in Figure 10.4.1 . A second reason for poor atomization efficiency is that the large volume of combustion gases significantly dilutes the sample. Together, these contributions to the efficiency of atomization reduce sensitivity because the analyte's concentration in the flame may be a factor of 2.5×10^{-6} less than that in solution [Ingle, J. D.; Crouch, S. R. *Spectrochemical Analysis*, Prentice-Hall: Englewood Cliffs, NJ, 1988; p. 275].

ELECTROTHERMAL ATOMIZERS

A significant improvement in sensitivity is achieved by using the resistive heating of a graphite tube in place of a flame. A typical electrothermal atomizer, also known as a ***graphite furnace***, consists of a cylindrical graphite tube approximately 1–3 cm in length and 3–8 mm in diameter. As shown in Figure 10.4.4 , the graphite tube is housed in an sealed assembly that has an optically transparent window at each end. A continuous stream of inert gas is passed through the furnace, which protects the graphite tube from oxidation and removes the gaseous products produced during atomization. A power supply is used to pass a current through the graphite tube, resulting in resistive heating.

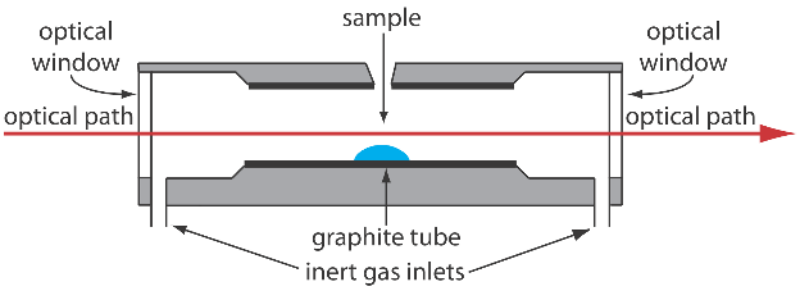


Figure 10.4.4 . Diagram showing a cross-section of an electrothermal analyzer.

Samples of between 5–50 μL are injected into the graphite tube through a small hole at the top of the tube. Atomization is achieved in three stages. In the first stage the sample is dried to a solid residue using a current that raises the temperature of the graphite tube to about 110°C. In the second stage, which is called ashing, the temperature is increased to between 350–1200°C. At these temperatures organic material in the sample is converted to CO_2 and H_2O, and volatile inorganic materials are vaporized. These gases are removed by the inert gas flow. In the final stage the sample is atomized by rapidly increasing the temperature to between 2000–3000°C. The result is a transient absorbance peak whose height or area is proportional to the absolute amount of analyte injected into the graphite tube. Together, the three stages take approximately 45–90 s, with most of this time used for drying and ashing the sample.

Electrothermal atomization provides a significant improvement in sensitivity by trapping the gaseous analyte in the small volume within the graphite tube. The analyte's concentration in the resulting vapor phase is as much as 1000× greater than in a flame atomization [Parsons, M. L.; Major, S.; Forster, A. R. *Appl. Spectrosc.* **1983**, *37*, 411–418]. This improvement in sensitivity—and the resulting improvement in detection limits—is offset by a significant decrease in precision. Atomization efficiency is influenced strongly by the sample's contact with the graphite tube, which is difficult to control reproducibly.

MISCELLANEOUS ATOMIZATION METHODS

A few elements are atomized by using a chemical reaction to produce a volatile product. Elements such as As, Se, Sb, Bi, Ge, Sn, Te, and Pb, for example, form volatile hydrides when they react with $NaBH_4$ in the presence of acid. An inert gas carries the volatile hydride to either a flame or to a heated quartz observation tube situated in the optical path. Mercury is determined by the cold-vapor method in which it is reduced to elemental mercury with $SnCl_2$. The volatile Hg is carried by an inert gas to an unheated observation tube situated in the instrument's optical path.

QUANTITATIVE APPLICATIONS

Atomic absorption is used widely for the analysis of trace metals in a variety of sample matrices. Using Zn as an example, there are standard atomic absorption methods for its determination in samples as diverse as water and wastewater, air, blood, urine, muscle tissue, hair, milk, breakfast cereals, shampoos, alloys, industrial plating baths, gasoline, oil, sediments, and rocks.

Developing a quantitative atomic absorption method requires several considerations, including choosing a method of atomization, selecting the wavelength and slit width, preparing the sample for analysis, minimizing spectral and chemical interferences, and selecting a method of standardization. Each of these topics is considered in this section.

DEVELOPING A QUANTITATIVE METHOD

Flame or Electrothermal Atomization? The most important factor in choosing a method of atomization is the analyte's concentration. Because of its greater sensitivity, it takes less analyte to achieve a given absorbance when using electrothermal atomization. Table 10.4.2 , which compares the amount of analyte needed to achieve an absorbance of 0.20 when using flame atomization and electrothermal atomization, is useful when selecting an atomization method. For example, flame atomization is the method of choice if our samples contain 1–10 mg Zn^{2+}/L, but electrothermal atomization is the best choice for samples that contain 1–10 μg Zn^{2+}/L.

Table 10.4.2 . Concentration of Analyte (in mg/L) That Yields an Absorbance of 0.20

element	flame atomization	electrothermal atomization
Ag	1.5	0.0035
Al	40	0.015
As	40	0.050
Ca	0.8	0.003
Cd	0.6	0.001
Co	2.5	0.021
Cr	2.5	0.0075
Cu	1.5	0.012
Fe	2.5	0.006
Hg	70	0.52
Mg	0.15	0.00075
Mn	1	0.003
Na	0.3	0.00023
Ni	2	0.024
Pb	5	0.080
Pt	70	0.29
Sn	50	0.023
Zn	0.3	0.00071

Source: Varian Cookbook, SpectraAA Software Version 4.00 Pro.
As: 10 mg/L by hydride vaporization; Hg: 11.5 mg/L by cold-vapor; and Sn:18 mg/L by hydride vaporization

Selecting the Wavelength and Slit Width. The source for atomic absorption is a hollow cathode lamp that consists of a cathode and anode enclosed within a glass tube filled with a low pressure of an inert gas, such as Ne or Ar (Figure 10.4.5). Applying a potential across the electrodes ionizes the filler gas. The positively charged gas ions collide with the negatively charged cathode, sputtering atoms from the cathode's surface. Some of the sputtered atoms are in the excited state and emit radiation characteristic of the metal(s) from which the cathode is manufactured. By fashioning the cathode from the metallic analyte, a hollow cathode lamp provides emission lines that correspond to the analyte's absorption spectrum.

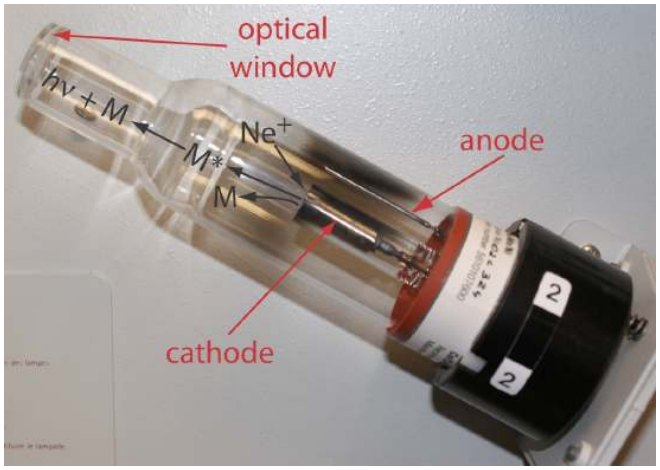


Figure 10.4.5 . Photo of a typical multielemental hollow cathode lamp. The cathode in this lamp is fashioned from an alloy of Co, Cr, Cu, Fe, Mn, and Ni, and is surrounded by a glass shield that isolates it from the anode. The lamp is filled with Ne gas. Also shown is the process that leads to atomic emission. Note the black deposit of sputtered metal on the outer wall of the hollow cathode lamp. See the text for additional details.

Because atomic absorption lines are narrow, we need to use a line source instead of a continuum source (compare, for example, Figure 10.2.4 with Figure 10.2.6). The effective bandwidth when using a continuum source is roughly 1000× larger than an atomic absorption line; thus, $P_T \approx P_0$, $\%T \approx 100$, and $A \approx 0$. Because a hollow cathode lamp is a line source, P_T and P_0 have different values giving a $\%T < 100$ and $A > 0$.

Each element in a hollow cathode lamp provides several atomic emission lines that we can use for atomic absorption. Usually the wavelength that provides the best sensitivity is the one we choose to use, although a less sensitive wavelength may be more appropriate for a sample that has higher concentration of analyte. For the Cr hollow cathode lamp in Table 10.4.3 , the best sensitivity is obtained using a wavelength of 357.9 nm.

Table 10.4.3 . Atomic Emission Lines for a Cr Hollow Cathode Lamp

wavelength (nm)	slit width (nm)	mg Cr/L giving $A = 0.20$	P_0 (relative)
357.9	0.2	2.5	40
425.4	0.2	12	85
429.0	0.5	20	100
520.5	0.2	1500	15
520.8	0.2	500	20

Another consideration is the emission line's intensity. If several emission lines meet our requirements for sensitivity, we may wish to use the emission line with the largest relative P_0 because there is less uncertainty in measuring P_0 and P_T. When analyzing a sample that is ≈10 mg Cr/L, for example, the first three wavelengths in Table 10.4.3 provide an appropriate sensitivity; the wavelengths of 425.4 nm and 429.0 nm, however, have a greater P_0 and will provide less uncertainty in the measured absorbance.

The emission spectrum for a hollow cathode lamp includes, in addition to the analyte's emission lines, additional emission lines from impurities present in the metallic cathode and from the filler gas. These additional lines are a potential source of stray radiation that could result in an instrumental deviation from Beer's law. The monochromator's slit width is set as wide as possible to improve the throughput of radiation and narrow enough to eliminate these sources of stray radiation.

Preparing the Sample. Flame and electrothermal atomization require that the analyte is in solution. Solid samples are brought into solution by dissolving in an appropriate solvent. If the sample is not soluble it is digested, either on a hot-plate or by microwave, using HNO_3, H_2SO_4, or $HClO_4$. Alternatively, we can extract the analyte using a Soxhlet extractor. Liquid samples are analyzed directly or the analytes extracted if the matrix is in- compatible with the method of atomization. A serum sample, for instance, is difficult to aspirate when using flame atomization and may produce an unacceptably high background absorbance when using electrothermal atomization. A liquid–liquid extraction using an organic solvent and a chelating agent frequently is used to concentrate analytes. Dilute solutions of Cd^{2+}, Co^{2+}, Cu^{2+}, Fe^{3+}, Pb^{2+}, Ni^{2+}, and Zn^{2+}, for example, are concentrated by extracting with a solution of ammonium pyrrolidine dithiocarbamate in methyl isobutyl ketone.

Minimizing Spectral Interference. A spectral interference occurs when an analyte's absorption line overlaps with an interferent's absorption line or band. Because they are so narrow, the overlap of two atomic absorption lines seldom is a problem. On the other hand, a molecule's broad absorption band or the scattering of source radiation is a potentially serious spectral interference.

An important consideration when using a flame as an atomization source is its effect on the measured absorbance. Among the products of combustion are molecular species that exhibit broad absorption bands and particulates that scatter radiation from the source. If we fail to compensate for these spectral interferences, then the intensity of transmitted radiation is smaller than expected. The result is an apparent increase in the sample's absorbance. Fortunately, absorption and scattering of radiation by the flame are corrected by analyzing a blank.

Spectral interferences also occur when components of the sample's matrix other than the analyte react to form molecular species, such as oxides and hydroxides. The resulting absorption and scattering constitutes the sample's background and may present a significant problem, particularly at wavelengths below 300 nm where the scattering of radiation becomes more important. If we know the composition of the sample's matrix, then we can prepare our samples using an identical matrix. In this case the background absorption is the same for both the samples and the standards. Alternatively, if the background is due to a known matrix component, then we can add that component in excess to all samples and standards so that the contribution of the naturally occurring interferent is insignificant. Finally, many interferences due to the sample's matrix are eliminated by increasing the atomization temperature. For example, switching to a higher temperature flame helps prevents the formation of interfering oxides and hydroxides.

If the identity of the matrix interference is unknown, or if it is not possible to adjust the flame or furnace conditions to eliminate the interference, then we must find another method to compensate for the background interference. Several methods have been developed to compensate for matrix interferences, and most atomic absorption spectrophotometers include one or more of these methods.

One of the most common methods for ***background correction*** is to use a continuum source, such as a D_2 lamp. Because a D_2 lamp is a continuum source, absorbance of its radiation by the analyte's narrow absorption line is negligible. Only the background, therefore, absorbs radiation from the D_2 lamp. Both the analyte and the background, on the other hand, absorb the hollow cathode's radiation. Subtracting the absorbance for the D_2 lamp from that for the hollow cathode lamp gives a corrected absorbance that compensates for the background interference. Although this method of background correction is effective, it does assume that the background absorbance is constant over the range of wavelengths passed by the monochromator. If this is not true, then subtracting the two absorbances underestimates or overestimates the background.

> Other methods of background correction have been developed, including Zeeman effect background correction and Smith–Hieftje background correction, both of which are included in some commercially available atomic absorption spectrophotometers. Consult the chapter's additional resources for additional information.

Minimizing Chemical Interferences. The quantitative analysis of some elements is complicated by chemical interferences that occur during atomization. The most common chemical interferences are the formation of nonvolatile compounds that contain the analyte and ionization of the analyte.

One example of the formation of a nonvolatile compound is the effect of PO_4^{3-} or Al^{3+} on the flame atomic absorption analysis of Ca^{2+}. In one study, for example, adding 100 ppm Al^{3+} to a solution of 5 ppm Ca^{2+} decreased calcium ion's absorbance from 0.50 to 0.14, while adding 500 ppm PO_4^{3-} to a similar solution of Ca^{2+} decreased the absorbance from 0.50 to 0.38. These interferences are attributed to the formation of nonvolatile particles of $Ca_3(PO_4)_2$ and an Al–Ca–O oxide [Hosking, J. W.; Snell, N. B.; Sturman, B. T. *J. Chem. Educ.* **1977**, *54*, 128–130].

When using flame atomization, we can minimize the formation of non-volatile compounds by increasing the flame's temperature by changing the fuel-to-oxidant ratio or by switching to a different combination of fuel and oxidant. Another approach is to add a releasing agent or a protecting agent to the sample. A ***releasing agent*** is a species that reacts preferentially with the interferent, releasing the analyte during atomization. For example, Sr^{2+} and La^{3+} serve as releasing agents for the analysis of Ca^{2+} in the presence of PO_4^{3-} or Al^{3+}. Adding 2000 ppm $SrCl_2$ to the Ca^{2+}/ PO_4^{3-} and to the Ca^{2+}/Al^{3+} mixtures described in the previous paragraph increased the absorbance to 0.48. A ***protecting agent*** reacts with the analyte to form a stable volatile complex. Adding 1% w/w EDTA to the Ca^{2+}/ PO_4^{3-} solution described in the previous paragraph increased the absorbance to 0.52.

An ionization interference occurs when thermal energy from the flame or the electrothermal atomizer is sufficient to ionize the analyte

$$M(s) \rightleftharpoons M^+(aq) + e^- \tag{9.6.1}$$

where M is the analyte. Because the absorption spectra for M and M^+ are different, the position of the equilibrium in reaction 9.6.1 affects the absorbance at wavelengths where M absorbs. To limit ionization we add a high concentration of an ***ionization suppressor***, which is a species that ionizes more easily than the analyte. If the ionization suppressor's concentration is sufficient, then the increased concentration of electrons in the flame pushes reaction 9.6.1 to the left, preventing the analyte's ionization. Potassium and cesium frequently are used as an ionization suppressor because of their low ionization energy.

Standardizing the Method. Because Beer's law also applies to atomic absorption, we might expect atomic absorption calibration curves to be linear. In practice, however, most atomic absorption calibration curves are nonlinear or linear over a limited range of concentrations. Nonlinearity in atomic absorption is a consequence of instrumental limitations, including stray radiation from the hollow cathode lamp and the variation in molar absorptivity across the absorption line. Accurate quantitative work, therefore, requires a suitable means for computing the calibration curve from a set of standards.

When possible, a quantitative analysis is best conducted using external standards. Unfortunately, matrix interferences are a frequent problem, particularly when using electrothermal atomization. For this reason the method of standard additions often is used. One limitation to this method of standardization, however, is the requirement of a linear relationship between absorbance and concentration.

> Most instruments include several different algorithms for computing the calibration curve. The instrument in my lab, for example, includes five algorithms. Three of the algorithms fit absorbance data using linear, quadratic, or cubic polynomial functions of the analyte's concentration. It also includes two algorithms that fit the concentrations of the standards to quadratic functions of the absorbance.

REPRESENTATIVE METHOD 10.4.1: DETERMINATION OF CU AND ZN IN TISSUE SAMPLES

The best way to appreciate the theoretical and the practical details discussed in this section is to carefully examine a typical analytical method. Although each method is unique, the following description of the determination of Cu and Zn in biological tissues provides an instructive example of a typical procedure. The description here is based on Bhattacharya, S. K.; Goodwin, T. G.; Crawford, A. J. *Anal. Lett.* **1984**, *17*, 1567–1593, and Crawford, A. J.; Bhattacharya, S. K. Varian Instruments at Work, Number AA–46, April 1985.

Description of Method.

Copper and zinc are isolated from tissue samples by digesting the sample with HNO_3 after first removing any fatty tissue. The concentration of copper and zinc in the supernatant are determined by atomic absorption using an air-acetylene flame.

Procedure.

Tissue samples are obtained by a muscle needle biopsy and dried for 24–30 h at 105ºC to remove all traces of moisture. The fatty tissue in a dried sample is removed by extracting overnight with anhydrous ether. After removing the ether, the sample is dried to obtain the fat-free dry tissue weight (FFDT). The sample is digested at 68ºC for 20–24 h using 3 mL of 0.75 M HNO_3. After centrifuging at 2500 rpm for 10 minutes, the supernatant is transferred to a 5-mL volumetric flask. The digestion is repeated two more times, for 2–4 hours each, using 0.9-mL aliquots of 0.75 M HNO_3. These supernatants are added to the 5-mL volumetric flask, which is diluted to volume with 0.75 M HNO_3. The concentrations of Cu and Zn in the diluted supernatant are determined by flame atomic absorption spectroscopy using an air-acetylene flame and external standards. Copper is analyzed at a wavelength of 324.8 nm with a slit width of 0.5 nm, and zinc is analyzed at 213.9 nm

with a slit width of 1.0 nm. Background correction using a D_2 lamp is necessary for zinc. Results are reported as µg of Cu or Zn per gram of FFDT.

Questions.

1. Describe the appropriate matrix for the external standards and for the blank?

The matrix for the standards and the blank should match the matrix of the samples; thus, an appropriate matrix is 0.75 M HNO_3. Any interferences from other components of the sample matrix are minimized by background correction.

2. Why is a background correction necessary for the analysis of Zn, but not for the analysis of Cu?

Background correction compensates for background absorption and scattering due to interferents in the sample. Such interferences are most severe when using a wavelength less than 300 nm. This is the case for Zn, but not for Cu.

3. A Cu hollow cathode lamp has several emission lines, the properties of which are shown in the following table. Explain why this method uses the line at 324.8 nm.

wavelength (nm)	slit width (nm)	mg Cu/L for A = 0.20	P_0 (relative)
217.9	0.2	15	3
218.2	0.2	15	3
222.6	0.2	60	5
244.2	0.2	400	15
249.2	0.5	200	24
324.8	0.5	1.5	100
327.4	0.5	3	87

With 1.5 mg Cu/L giving an absorbance of 0.20, the emission line at 324.8 nm has the best sensitivity. In addition, it is the most intense emission line, which decreases the uncertainty in the measured absorbance.

EXAMPLE 10.4.1

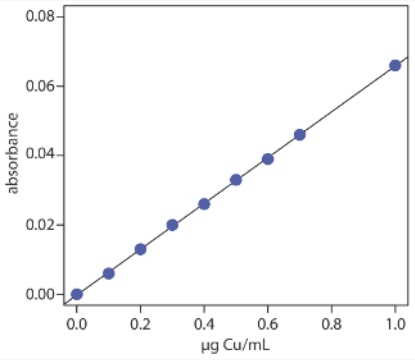
To evaluate the method described in Representative Method 10.4.1, a series of external standard is prepared and analyzed, providing the results shown here [Crawford, A. J.; Bhattacharya, S. K. “Microanalysis of Copper and Zinc in Biopsy-Sized Tissue Specimens by Atomic Absorption Spectroscopy Using a Stoichiometric Air-Acetylene Flame,” Varian Instruments at Work, Number AA–46, April 1985].

µg Cu/mL	absorbance	µg Cu/mL	absorbance
0.000	0.000	0.500	0.033
0.100	0.006	0.600	0.039
0.200	0.013	0.700	0.046
0.300	0.020	1.00	0.066
0.400	0.026		

A bovine liver standard reference material is used to evaluate the method’s accuracy. After drying and extracting the sample, a 11.23-mg FFDT tissue sample gives an absorbance of 0.023. Report the amount of copper in the sample as µg Cu/g FFDT.

Solution

Linear regression of absorbance versus the concentration of Cu in the standards gives the calibration curve shown below and the following calibration equation.



$$A = -0.0002 + 0.0661 \times \frac{\mu\text{g Cu}}{\text{mL}}$$

Substituting the sample's absorbance into the calibration equation gives the concentration of copper as 0.351 μg/mL. The concentration of copper in the tissue sample, therefore, is

$$\frac{\frac{0.351 \mu\text{g Cu}}{\text{mL}} \times 5.000 \text{ mL}}{0.01123 \text{ g sample}} = 156 \ \mu\text{g Cu/g FDT}$$

EVALUATION OF ATOMIC ABSORPTION SPECTROSCOPY

SCALE OF OPERATION

Atomic absorption spectroscopy is ideally suited for the analysis of trace and ultratrace analytes, particularly when using electrothermal atomization. For minor and major analytes, sample are diluted before the analysis. Most analyses use a macro or a meso sample. The small volume requirement for electrothermal atomization or for flame microsampling, however, makes practical the analysis of micro and ultramicro samples.

ACCURACY

If spectral and chemical interferences are minimized, an accuracy of 0.5–5% is routinely attainable. When the calibration curve is nonlinear, accuracy is improved by using a pair of standards whose absorbances closely bracket the sample's absorbance and assuming that the change in absorbance is linear over this limited concentration range. Determinate errors for electrothermal atomization often are greater than those obtained with flame atomization due to more serious matrix interferences.

PRECISION

For an absorbance greater than 0.1–0.2, the relative standard deviation for atomic absorption is 0.3–1% for flame atomization and 1–5% for electrothermal atomization. The principle limitation is the uncertainty in the concentration of free analyte atoms that result from variations in the rate of aspiration, nebulization, and atomization for a flame atomizer, and the consistency of injecting samples for electrothermal atomization.

SENSITIVITY

The sensitivity of a flame atomic absorption analysis is influenced by the flame's composition and by the position in the flame from which we monitor the absorbance. Normally the sensitivity of an analysis is optimized by aspirating a standard solution of analyte and adjusting the fuel-to-oxidant ratio, the nebulizer flow rate, and the height of the burner, to give the greatest absorbance. With electrothermal atomization, sensitivity is influenced by the drying and ashing stages that precede atomization. The temperature and time at each stage is optimized for each type of sample.

Sensitivity also is influenced by the sample's matrix. We already noted, for example, that sensitivity is decreased by a chemical interference. An increase in sensitivity may be realized by adding a low molecular weight alcohol, ester, or ketone to the solution, or by using an organic solvent.

SELECTIVITY

Due to the narrow width of absorption lines, atomic absorption provides excellent selectivity. Atomic absorption is used for the analysis of over 60 elements at concentrations at or below the level of μg/L.

TIME, COST, AND EQUIPMENT

The analysis time when using flame atomization is short, with sample throughputs of 250–350 determinations per hour when using a fully automated system. Electrothermal atomization requires substantially more time per analysis, with maximum sample throughputs of 20–30 determinations per hour. The cost of a new instrument ranges from between $10,000– $50,000 for flame atomization, and from $18,000–$70,000 for electrothermal atomization. The more expensive instruments in each price range include double-beam optics, automatic samplers, and can be programmed for multielemental analysis by allowing the wavelength and hollow cathode lamp to be changed automatically.

This page titled 9.6: Atomic Absorption Spectroscopy is shared under a CC BY-NC-SA 4.0 license and was authored, remixed, and/or curated by David Harvey.

- **10.4: Atomic Absorption Spectroscopy** by David Harvey is licensed CC BY-NC-SA 4.0.

SECTION OVERVIEW

9.7: Atomic Emission Spectroscopy

9.7.1: Emission Spectroscopy Based on Flame and Plasma Sources

9.7.2: Atomic Emission Spectroscopy

9.7.3: Inductively Coupled Plasma Mass Spectrometer

This page titled 9.7: Atomic Emission Spectroscopy is shared under a CC BY-NC-SA 4.0 license and was authored, remixed, and/or curated by David Harvey.

9.7.1: Emission Spectroscopy Based on Flame and Plasma Sources

What is Emission?

An analyte in an excited state possesses an energy, E_2, that is greater than its energy when it is in a lower energy state, E_1. When the analyte returns to its lower energy state—a process we call relaxation—the excess energy, ΔE, is

$$\Delta E = E_2 - E_1$$

There are several ways in which an atom may end up in an excited state, including thermal energy, which is the focus of this chapter. The amount of time an atom, *A*, spends in its excited state—what we call the excited state's lifetime—is short, typically 10^{-5} to 10^{-9} s for an electronic excited state. Relaxation of the atom's excited state, *A**, occurs through several mechanisms, including collisions with other species in the sample and the emission of photons. In the first process, which we call nonradiative relaxation, the excess energy is released as heat.

$$A^* \longrightarrow A + \text{heat}$$

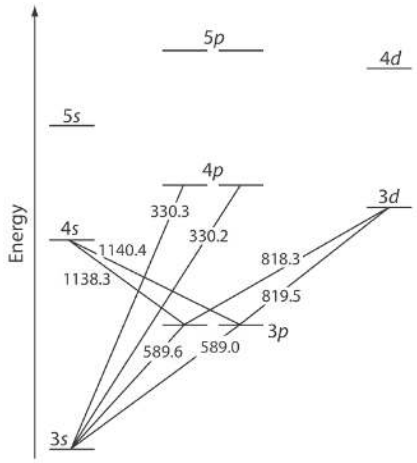
In the second mechanism, the excess energy is released as a photon of electromagnetic radiation.

$$A^* \longrightarrow A + h\nu$$

The release of a photon following thermal excitation is called emission. The focus of this chapter is on the emission of ultraviolet and visible radiation following the thermal excitation of atoms. Atomic emission spectroscopy has a long history. Qualitative applications based on the color of flames were used in the smelting of ores as early as 1550 and were more fully developed around 1830 with the observation of atomic spectra generated by flame emission and spark emission [Dawson, J. B. *J. Anal. At. Spectrosc.* **1991**, *6*, 93–98]. Quantitative applications based on the atomic emission from electric sparks were developed by Lockyer in the early 1870 and quantitative applications based on flame emission were pioneered by Lundegardh in 1930. Atomic emission based on emission from a plasma was introduced in 1964.

Atomic Emission Spectra

Atomic emission occurs when a valence electron in a higher energy atomic orbital returns to a lower energy atomic orbital. Figure 9.7.1.1 shows a portion of the energy level diagram for sodium, which consists of a series of discrete lines at wavelengths that correspond to the difference in energy between two atomic orbitals.



FFigure 9.7.1.1. Valence shell energy level diagram for sodium. The wavelengths corresponding to several transitions are shown.

The intensity of an atomic emission line, I_e, is proportional to the number of atoms, N^*, that populate the excited state

$$I_e = kN^* \tag{9.7.1.1}$$

where *k* is a constant that accounts for the efficiency of the transition. If a system of atoms is in thermal equilibrium, the population of excited state *i* is related to the total concentration of atoms, *N*, by the Boltzmann distribution. For many elements at temperatures of less than 5000 K the Boltzmann distribution is approximated as

$$N^* = N\left(\frac{g_i}{g_0}\right)e^{-E_i/kT} \tag{9.7.1.2}$$

where g_i and g_0 are statistical factors that account for the number of equivalent energy levels for the excited state and the ground state, E_i is the energy of the excited state relative to the ground state, E_0, k is Boltzmann's constant (1.3807×10^{-23} J/K), and T is the temperature in Kelvin. From Equation 9.7.1.2 we expect that excited states with lower energies have larger populations and more intense emission lines. We also expect emission intensity to increase with temperature. The emission spectrum for sodium is shown in Figure 9.7.1.2

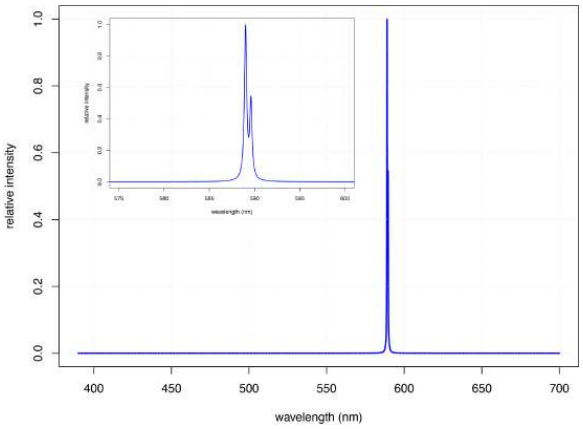


Figure 9.7.1.2: Visible emission spectrum for sodium. The inset shows a close up of the emission lines at 589.0 and 589.6 nm that appear in the energy level diagram in Figure 9.7.1.1.

An atomic emission spectrometer is similar in design to the instrumentation for atomic absorption. In fact, it is easy to adapt most flame atomic absorption spectrometers for atomic emission by turning off the hollow cathode lamp and monitoring the difference between the emission intensity when aspirating the sample and when aspirating a blank. Many atomic emission spectrometers, however, are dedicated instruments designed to take advantage of features unique to atomic emission, including the use of plasmas, arcs, sparks, and lasers as atomization and excitation sources, and an enhanced capability for multielemental analysis.

Flames as a Source

Atomization and excitation in flame atomic emission is accomplished with the same nebulization and spray chamber assembly used in atomic absorption (see Chapter 9). The burner head consists of a single or multiple slots, or a Meker-style burner. Older atomic emission instruments often used a total consumption burner in which the sample is drawn through a capillary tube and injected directly into the flame.

> A Meker burner is similar to the more common Bunsen burner found in most laboratories; it is designed to allow for higher temperatures and for a larger diameter flame.

The Inductively Coupled Plasma Source

A plasma is a hot, partially ionized gas that contains an abundant concentration of cations and electrons. The plasma used in atomic emission is formed by ionizing a flowing stream of argon gas, producing argon ions and electrons. A plasma's high temperature results from resistive heating as the electrons and argon ions move through the gas. Because a plasma operates at a much higher temperature than a flame, it provides for a better atomization efficiency and a higher population of excited states.

A schematic diagram of the inductively coupled plasma source (ICP) is shown in Figure 9.7.1.3 The ICP torch consists of three concentric quartz tubes, surrounded at the top by a radio-frequency induction coil. The sample is mixed with a stream of Ar using a nebulizer, and is carried to the plasma through the torch's central capillary tube. Plasma formation is initiated by a spark from a Tesla coil. An alternating radio-frequency current in the induction coil creates a fluctuating magnetic field that induces the argon ions and the electrons to move in a circular path. The resulting collisions with the abundant unionized gas give rise to resistive heating, providing temperatures as high as 10000 K at the base of the plasma, and between 6000 and 8000 K at a height of 15–20 mm above the coil, where emission usually is measured. At these high temperatures the outer quartz tube must be thermally

isolated from the plasma. This is accomplished by the tangential flow of argon shown in the schematic diagram. Samples are brought into the ICP using the same basic types of nebulization described in Chapter 8 for flame atomic absorption spectroscopy.

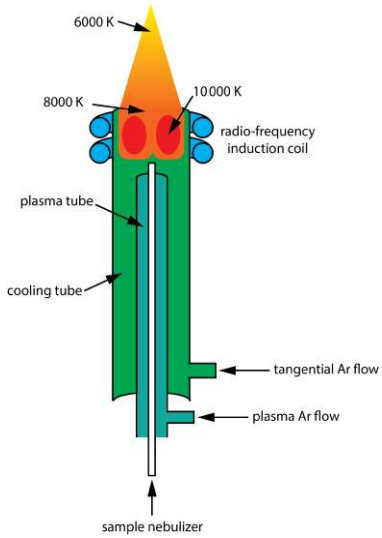


Figure 9.7.1.3. Schematic diagram of an inductively coupled plasma torch for atomic emission.

The Direct Current Plasma Source

An alternative to the inductively coupled plasma source is the direct current (dc) plasma jet, one example of which is illustrated in Figure 9.7.1.4 The argon plasma (shown here in blue) forms between two graphite anodes and a tungsten cathode. The sample is aspirated into the plasma's excitation region where it undergoes atomization, excitation, and emission at temperatures of 5000 K.

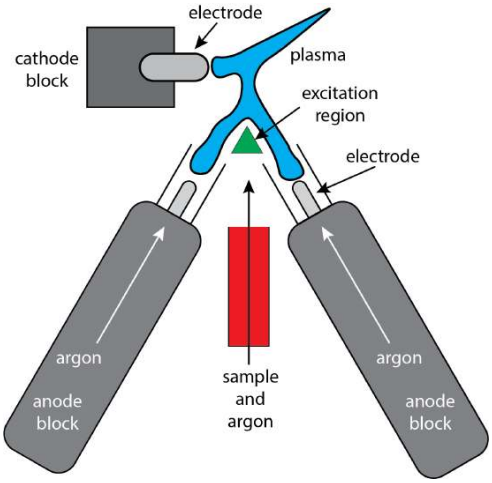


Figure 9.7.1.4: Illustration showing a schematic diagram of a direct current plasma source of atomic emission.

Flame and Plasma Spectrometers

One advantage of atomic emission over atomic absorption is the ease of analyzing samples for multiple analytes. This additional capability arises because atomic emission, unlike atomic absorption, does not need an analyte-specific source of radiation. The two most common types of spectrometers are sequential and multichannel. In a sequential spectrometer the instrument has a single detector and uses the monochromator to move from one emission line to the next. A multichannel spectrometer uses the monochromator to disperse the emission across a field of detectors, each of which measures the emission intensity at a different wavelength.

Sequential Instruments

A sequential instrument uses a programmable scanning monochromator, such as those described in Chapter 7, to rapidly move the monochromator's grating over wavelength regions that are not of interest, and then pauses and scans slowly over the emission lines

of the analytes. Sampling rates of 300 determinations per hour are possible with this configuration. Another option, which is less common, is to move the exit slit and the detector across the monochromator's focal plane, pausing and recording the emission at the desired wavelengths.

Multichannel Instruments

Another approach to a multielemental analysis is to use a multichannel instrument that allows us to monitor simultaneously many analytes. A simple design for a multichannel spectrometer, shown in Figure 9.7.1.5, couples a monochromator with multiple detectors that are positioned in a semicircular array around the monochromator at positions that correspond to the wavelengths for the analytes. A sample throughput of 3000 determinations per hour are possible using a multichannel ICP.

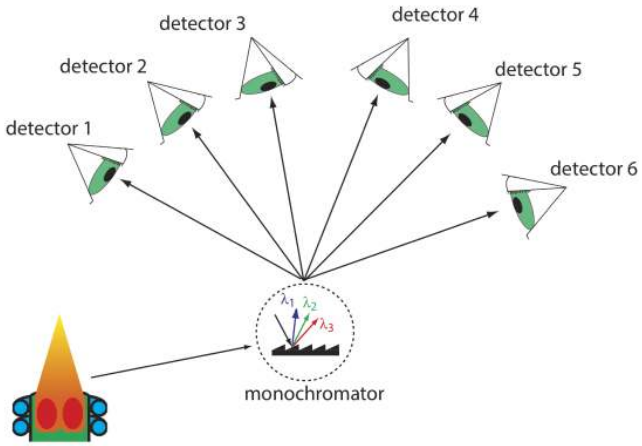


Figure 9.7.1.5. Schematic diagram of a multichannel atomic emission spectrometer for the simultaneous analysis of several elements. Instruments may contain as many as 48–60 detectors.

Another option for a multichannel instrument takes advantage of the charge-injection device, or CID, as a detector (see Chapter 7 for discussion of the charge-coupled device, another type of charge-transfer device used as a detector). Light from the plasma source is dispersed across the CID in two dimensions. The surface of the CID has in excess of 90000 detecting elements, or pixels, that allows for a resolution between detecting elements on the order of 0.04 nm. Light from the atomic emission source is distributed across the detector's surface by a diffraction grating such that each element of interest is detected using its own set of pixels, called a read window. Figure 9.7.1.6 shows that individual read windows consist of a set of detecting elements, nine of which collect photons from the spectral line and 30 of which provide a measurement of the source's background.

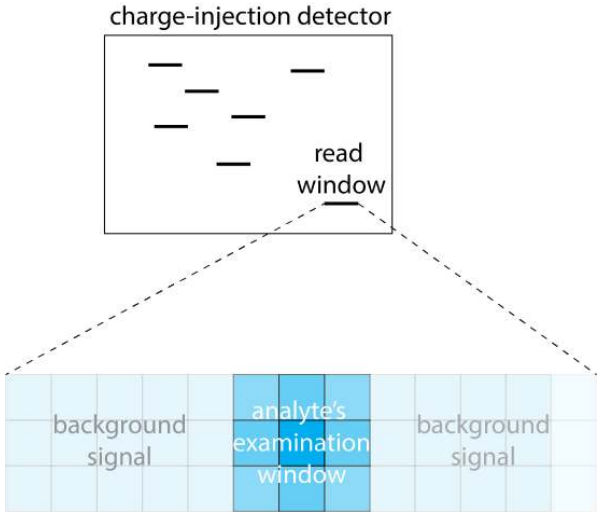


Figure 9.7.1.6: Illustration showing a charge-injection detector. The read window consists of nine central elements that measure the analyte's emission intensity (shown here using blue shading) and 30 of which measure the background emission from the plasma source.

Application of Flame and Plasma Sources

Atomic emission is used widely for the analysis of trace metals in a variety of sample matrices. The development of a quantitative atomic emission method requires several considerations, including choosing a source for atomization and excitation, selecting a wavelength and slit width, preparing the sample for analysis, minimizing spectral and chemical interferences, and selecting a method of standardization.

Choice of Atomization and Excitation Source

Except for the alkali metals, detection limits when using an ICP are significantly better than those obtained with flame emission (Table 9.7.1.1). Plasmas also are subject to fewer spectral and chemical interferences. For these reasons a plasma emission source is usually the better choice.

Table 9.7.1.1. Detection Limits for Atomic Emission

element	detection limit (µg/mL): flame emission	detection limit (µg/mL): ICP
Ag	2	0.2
Al	3	0.2
As	2000	2
Ca	0.1	0.0001
Cd	300	0.07
Co	5	0.1
Cr	1	0.08
Fe	10	0.09
Hg	150	1
K	0.01	30
Li	0.001	0.02
Mg	1	0.02
Mn	1	0.01
Na	0.01	0.1
Ni	10	0.2
Pb	0.2	1
Pt	2000	0.9
Sn	100	3
Zn	1000	0.1

Source: Parsons, M. L.; Major, S.; Forster, A. R.; App. Spectrosc. 1983, 37, 411–418.

Selecting the Wavelength and Slit Width

The choice of wavelength is dictated by the need for sensitivity and the need to avoid interferences from the emission lines of other constituents in the sample. Because an analyte's atomic emission spectrum has an abundance of emission lines—particularly when using a high temperature plasma source—it is inevitable that there will be some overlap between emission lines. For example, an analysis for Ni using the atomic emission line at 349.30 nm is complicated by the atomic emission line for Fe at 349.06 nm.

A narrower slit width provides better resolution, but at the cost of less radiation reaching the detector. The easiest approach to selecting a wavelength is to record the sample's emission spectrum and look for an emission line that provides an intense signal and is resolved from other emission lines.

Preparing the Sample

Flame and plasma sources are best suited for samples in solution and in liquid form. Although a solid sample can be analyzed by directly inserting it into the flame or plasma, they usually are first brought into solution by digestion or extraction.

Minimizing Spectral Interferences

The most important spectral interference is broad, background emission from the flame or plasma and emission bands from molecular species. This background emission is particularly severe for flames because the temperature is insufficient to break down refractory compounds, such as oxides and hydroxides. Background corrections for flame emission are made by scanning over the emission line and drawing a baseline (Figure 9.7.1.7). Because a plasma's temperature is much higher, a background interference due to molecular emission is less of a problem. Although emission from the plasma's core is strong, it is insignificant at a height of 10–30 mm above the core where measurements normally are made.

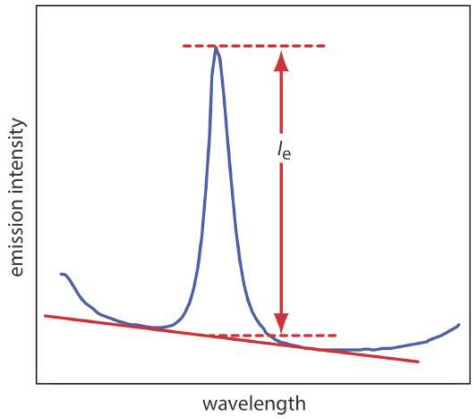


Figure 9.7.1.7. Method for correcting an analyte's emission for the flame's background emission.

Minimizing Chemical Interferences

Flame emission is subject to the same types of chemical interferences as atomic absorption; they are minimized using the same methods: by adjusting the flame's composition and by adding protecting agents, releasing agents, or ionization suppressors. An additional chemical interference results from self-absorption. Because the flame's temperature is greatest at its center, the concentration of analyte atoms in an excited state is greater at the flame's center than at its outer edges. If an excited state atom in the flame's center emits a photon, then a ground state atom in the cooler, outer regions of the flame may absorb the photon, which decreases the emission intensity. For higher concentrations of analyte self-absorption may invert the center of the emission band (Figure 9.7.1.8).

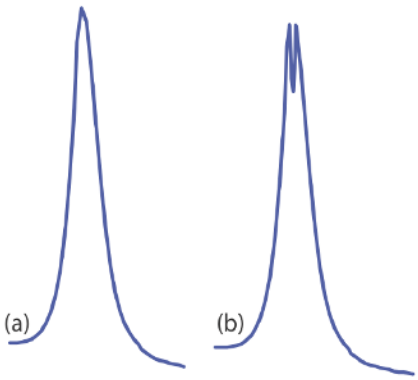


Figure 9.7.1.8. Atomic emission lines for (a) a low concentration of analyte, and (b) a high concentration of analyte showing the effect of self-absorption.

Chemical interferences when using a plasma source generally are not significant because the plasma's higher temperature limits the formation of nonvolatile species. For example, PO_4^{3-} is a significant interferent when analyzing samples for Ca^{2+} by flame emission, but has a negligible effect when using a plasma source. In addition, the high concentration of electrons from the ionization of argon minimizes ionization interferences.

Standardizing the Method

From Equation 9.7.1.1 we know that emission intensity is proportional to the population of the analyte's excited state, N^*. If the flame or plasma is in thermal equilibrium, then the excited state population is proportional to the analyte's total population, N, through the Boltzmann distribution (Equation 9.7.1.2).

A calibration curve for flame emission usually is linear over two to three orders of magnitude, with ionization limiting linearity when the analyte's concentrations is small and self-absorption limiting linearity at higher concentrations of analyte. When using a plasma, which suffers from fewer chemical interferences, the calibration curve often is linear over four to five orders of magnitude and is not affected significantly by changes in the matrix of the standards.

Emission intensity is affected significantly by many parameters, including the temperature of the excitation source and the efficiency of atomization. An increase in temperature of 10 K, for example, produces a 4% increase in the fraction of Na atoms in the 3*p* excited state, an uncertainty in the signal that may limit the use of external standards. The method of internal standards is used when the variations in source parameters are difficult to control. To compensate for changes in the temperature of the excitation source, the internal standard is selected so that its emission line is close to the analyte's emission line. In addition, the internal standard should be subject to the same chemical interferences to compensate for changes in atomization efficiency. To accurately correct for these errors the analyte and internal standard emission lines are monitored simultaneously.

This page titled 9.7.1: Emission Spectroscopy Based on Flame and Plasma Sources is shared under a CC BY-NC-SA 4.0 license and was authored, remixed, and/or curated by David Harvey.

- **10.1: Emission Spectroscopy Based on Flame and Plasma Sources** by David Harvey is licensed CC BY-NC-SA 4.0.

9.7.2: ATOMIC EMISSION SPECTROSCOPY

The focus of this section is on the emission of ultraviolet and visible radiation following the thermal excitation of atoms. Atomic emission spectroscopy has a long history. Qualitative applications based on the color of flames were used in the smelting of ores as early as 1550 and were more fully developed around 1830 with the observation of atomic spectra generated by flame emission and spark emission [Dawson, J. B. *J. Anal. At. Spectrosc.* **1991**, *6*, 93–98]. Quantitative applications based on the atomic emission from electric sparks were developed by Lockyer in the early 1870 and quantitative applications based on flame emission were pioneered by Lundegardh in 1930. Atomic emission based on emission from a plasma was introduced in 1964.

> For an on-line introduction to much of the material in this section, see Atomic Emission Spectroscopy (AES) by Tomas Spudich and Alexander Scheeline, a resource that is part of the Analytical Sciences Digital Library.

ATOMIC EMISSION SPECTRA

Atomic emission occurs when a valence electron in a higher energy atomic orbital returns to a lower energy atomic orbital. Figure 10.7.1 shows a portion of the energy level diagram for sodium, which consists of a series of discrete lines at wavelengths that correspond to the difference in energy between two atomic orbitals.

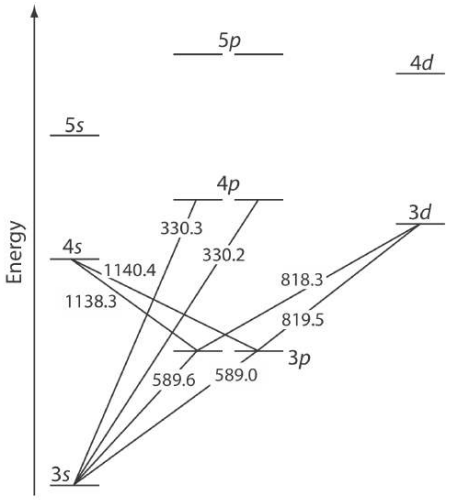


Figure 10.7.1 . Valence shell energy level diagram for sodium. The wavelengths corresponding to several transitions are shown. Note that this is the same energy level diagram as Figure 10.2.5.

The intensity of an atomic emission line, I_e, is proportional to the number of atoms, N^*, that populate the excited state,

$$I_e = kN^* \tag{9.7.2.1}$$

where k is a constant that accounts for the efficiency of the transition. If a system of atoms is in thermal equilibrium, the population of excited state i is related to the total concentration of atoms, N, by the Boltzmann distribution. For many elements at temperatures of less than 5000 K the Boltzmann distribution is approximated as

$$N^* = N\left(\frac{g_i}{g_0}\right)e^{-E_i/kT} \tag{9.7.2.2}$$

where g_i and g_0 are statistical factors that account for the number of equivalent energy levels for the excited state and the ground state, E_i is the energy of the excited state relative to a ground state energy, E_0, k is Boltzmann's constant (1.3807×10^{-23} J/K), and T is the temperature in Kelvin. From Equation 9.7.2.2 we expect that excited states with lower energies have larger populations and more intense emission lines. We also expect emission intensity to increase with temperature.

EQUIPMENT

An atomic emission spectrometer is similar in design to the instrumentation for atomic absorption. In fact, it is easy to adapt most flame atomic absorption spectrometers for atomic emission by turning off the hollow cathode lamp and monitoring the difference between the emission intensity when aspirating the sample and when aspirating a blank. Many atomic emission spectrometers, however, are dedicated instruments designed to take advantage of features unique to atomic emission, including the use of plasmas, arcs, sparks, and lasers as atomization and excitation sources, and an enhanced capability for multielemental analysis.

ATOMIZATION AND EXCITATION

Atomic emission requires a means for converting into a free gaseous atom an analyte that is present in a solid, liquid, or solution sample. The same source of thermal energy used for atomization usually serves as the excitation source. The most common methods are flames and plasmas, both of which are useful for liquid or solution samples. Solid samples are analyzed by dissolving in a solvent and using a flame or plasma atomizer.

FLAME SOURCES

Atomization and excitation in flame atomic emission is accomplished with the same nebulization and spray chamber assembly used in atomic absorption (Figure 10.4.1). The burner head consists of a single or multiple slots, or a Meker-style burner. Older atomic emission instruments often used a total consumption burner in which the sample is drawn through a capillary tube and injected directly into the flame.

> A Meker burner is similar to the more common Bunsen burner found in most laboratories; it is designed to allow for higher temperatures and for a larger diameter flame.

PLASMA SOURCES

A ***plasma*** is a hot, partially ionized gas that contains an abundant concentration of cations and electrons. The plasma used in atomic emission is formed by ionizing a flowing stream of argon gas, producing argon ions and electrons. A plasma's high temperature results from resistive heating as the electrons and argon ions move through the gas. Because a plasma operates at a much higher temperature than a flame, it provides for a better atomization efficiency and a higher population of excited states.

A schematic diagram of the inductively coupled plasma source (ICP) is shown in Figure 10.7.2 . The ICP torch consists of three concentric quartz tubes, surrounded at the top by a radio-frequency induction coil. The sample is mixed with a stream of Ar using a nebulizer, and is carried to the plasma through the torch's central capillary tube. Plasma formation is initiated by a spark from a Tesla coil. An alternating radio-frequency current in the induction coil creates a fluctuating magnetic field that induces the argon ions and the electrons to move in a circular path. The resulting collisions with the abundant unionized gas give rise to resistive heating, providing temperatures as high as 10000 K at the base of the plasma, and between 6000 and 8000 K at a height of 15–20 mm above the coil, where emission usually is measured. At these high temperatures the outer quartz tube must be thermally isolated from the plasma. This is accomplished by the tangential flow of argon shown in the schematic diagram.

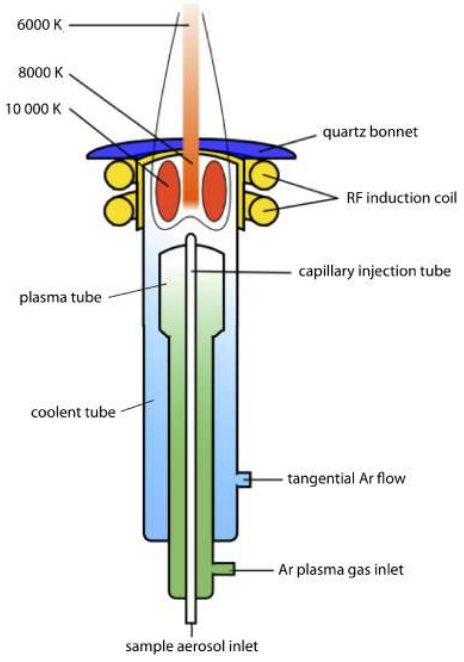


Figure 10.7.2 . Schematic diagram of an inductively coupled plasma torch.

MULTIELEMENTAL ANALYSIS

Atomic emission spectroscopy is ideally suited for a multielemental analysis because all analytes in a sample are excited simultaneously. If the instrument includes a scanning monochromator, we can program it to move rapidly to an analyte's desired wavelength, pause to record its emission intensity, and then move to the next analyte's wavelength. This sequential analysis allows for a sampling rate of 3–4 analytes per minute.

Another approach to a multielemental analysis is to use a multichannel instrument that allows us to monitor simultaneously many analytes. A simple design for a multichannel spectrometer, shown in Figure 10.7.3 , couples a monochromator with multiple detectors that are positioned in a semicircular array around the monochromator at positions that correspond to the wavelengths for the analytes.

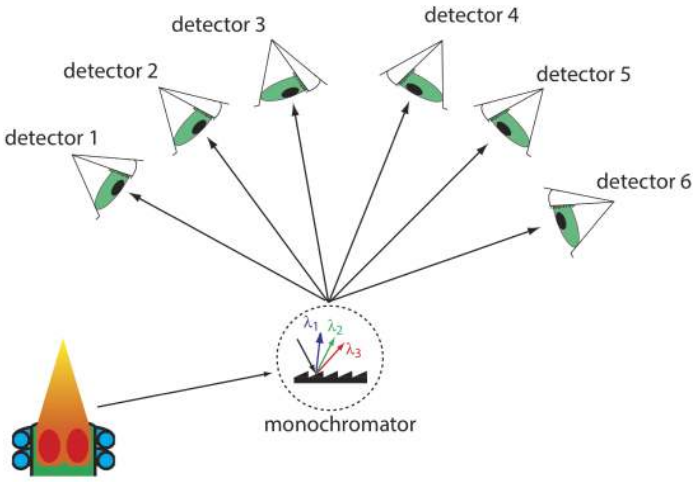


Figure 10.7.3 . Schematic diagram of a multichannel atomic emission spectrometer for the simultaneous analysis of several elements. Instruments may contain as many as 48–60 detectors.

QUANTITATIVE APPLICATIONS

Atomic emission is used widely for the analysis of trace metals in a variety of sample matrices. The development of a quantitative atomic emission method requires several considerations, including choosing a source for atomization and excitation, selecting a wavelength and slit width, preparing the sample for analysis, minimizing spectral and chemical interferences, and selecting a method of standardization.

CHOICE OF ATOMIZATION AND EXCITATION SOURCE

Except for the alkali metals, detection limits when using an ICP are significantly better than those obtained with flame emission (Table 10.7.1). Plasmas also are subject to fewer spectral and chemical interferences. For these reasons a plasma emission source is usually the better choice.

Table \(\PageIndex{1}\). Detection Limits for Atomic Emission

element	detection limit (µg/mL): flame emission	detection limit (µg/mL): ICP
Ag	2	0.2
Al	3	0.2
As	2000	2
Ca	0.1	0.0001
Cd	300	0.07
Co	5	0.1
Cr	1	0.08
Fe	10	0.09
Hg	150	1
K	0.01	30
Li	0.001	0.02
Mg	1	0.02
Mn	1	0.01
Na	0.01	0.1
Ni	10	0.2
Pb	0.2	1
Pt	2000	0.9
Sn	100	3
Zn	1000	0.1
Source: Parsons, M. L.; Major, S.; Forster, A. R.; App. Spectrosc. 1983, 37, 411–418.		

SELECTING THE WAVELENGTH AND SLIT WIDTH

The choice of wavelength is dictated by the need for sensitivity and the need to avoid interferences from the emission lines of other constituents in the sample. Because an analyte's atomic emission spectrum has an abundance of emission lines—particularly when using a

high temperature plasma source—it is inevitable that there will be some overlap between emission lines. For example, an analysis for Ni using the atomic emission line at 349.30 nm is complicated by the atomic emission line for Fe at 349.06 nm.

A narrower slit width provides better resolution, but at the cost of less radiation reaching the detector. The easiest approach to selecting a wavelength is to record the sample's emission spectrum and look for an emission line that provides an intense signal and is resolved from other emission lines.

PREPARING THE SAMPLE

Flame and plasma sources are best suited for samples in solution and in liquid form. Although a solid sample can be analyzed by directly inserting it into the flame or plasma, they usually are first brought into solution by digestion or extraction.

MINIMIZING SPECTRAL INTERFERENCES

The most important spectral interference is broad, background emission from the flame or plasma and emission bands from molecular species. This background emission is particularly severe for flames because the temperature is insufficient to break down refractory compounds, such as oxides and hydroxides. Background corrections for flame emission are made by scanning over the emission line and drawing a baseline (Figure 10.7.4). Because a plasma's temperature is much higher, a background interference due to molecular emission is less of a problem. Although emission from the plasma's core is strong, it is insignificant at a height of 10–30 mm above the core where measurements normally are made.

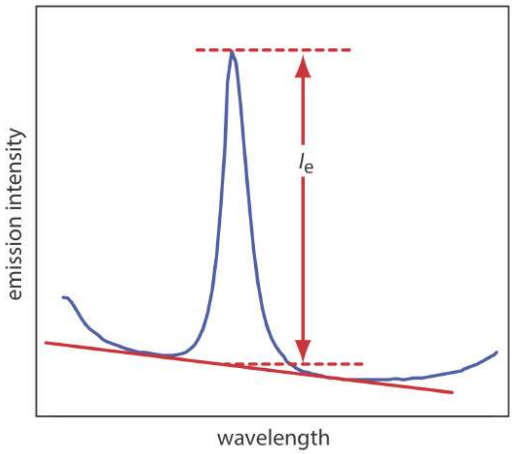


Figure 10.7.4 . Method for correcting an analyte's emission for the flame's background emission.

MINIMIZING CHEMICAL INTERFERENCES

Flame emission is subject to the same types of chemical interferences as atomic absorption; they are minimized using the same methods: by adjusting the flame's composition and by adding protecting agents, releasing agents, or ionization suppressors. An additional chemical interference results from ***self-absorption***. Because the flame's temperature is greatest at its center, the concentration of analyte atoms in an excited state is greater at the flame's center than at its outer edges. If an excited state atom in the flame's center emits a photon, then a ground state atom in the cooler, outer regions of the flame may absorb the photon, which decreases the emission intensity. For higher concentrations of analyte self-absorption may invert the center of the emission band (Figure 10.7.5).

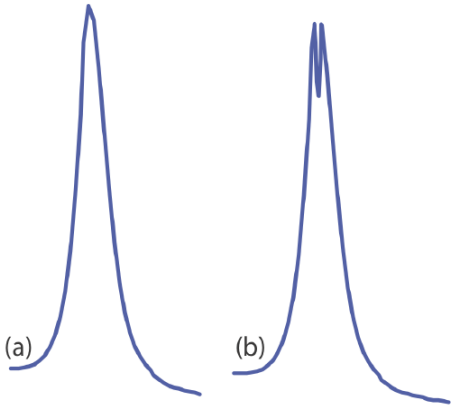


Figure 10.7.5 . Atomic emission lines for (a) a low concentration of analyte, and (b) a high concentration of analyte showing the effect of self-absorption.

Chemical interferences when using a plasma source generally are not significant because the plasma's higher temperature limits the formation of nonvolatile species. For example, PO_4^{3-} is a significant interferent when analyzing samples for Ca^{2+} by flame emission, but has a negligible effect when using a plasma source. In addition, the high concentration of electrons from the ionization of argon minimizes ionization interferences.

STANDARDIZING THE METHOD

From Equation 9.7.2.1 we know that emission intensity is proportional to the population of the analyte's excited state, N^*. If the flame or plasma is in thermal equilibrium, then the excited state population is proportional to the analyte's total population, N, through the Boltzmann distribution (Equation 9.7.2.2).

A calibration curve for flame emission usually is linear over two to three orders of magnitude, with ionization limiting linearity when the analyte's concentrations is small and self-absorption limiting linearity at higher concentrations of analyte. When using a plasma, which suffers from fewer chemical interferences, the calibration curve often is linear over four to five orders of magnitude and is not affected significantly by changes in the matrix of the standards.

Emission intensity is affected significantly by many parameters, including the temperature of the excitation source and the efficiency of atomization. An increase in temperature of 10 K, for example, produces a 4% increase in the fraction of Na atoms in the 3*p* excited state, an uncertainty in the signal that may limit the use of external standards. The method of internal standards is used when the variations in source parameters are difficult to control. To compensate for changes in the temperature of the excitation source, the internal standard is selected so that its emission line is close to the analyte's emission line. In addition, the internal standard should be subject to the same chemical interferences to compensate for changes in atomization efficiency. To accurately correct for these errors the analyte and internal standard emission lines are monitored simultaneously.

REPRESENTATIVE METHOD 10.7.1: DETERMINATION OF SODIUM IN A SALT SUBSTITUTE

The best way to appreciate the theoretical and the practical details discussed in this section is to carefully examine a typical analytical method. Although each method is unique, the following description of the determination of sodium in salt substitutes provides an instructive example of a typical procedure. The description here is based on Goodney, D. E. *J. Chem. Educ.* **1982**, *59*, 875–876.

Description of Method

Salt substitutes, which are used in place of table salt for individuals on low-sodium diets, replaces NaCl with KCl. Depending on the brand, fumaric acid, calcium hydrogen phosphate, or potassium tartrate also are present. Although intended to be sodium-free, salt substitutes contain small amounts of NaCl as an impurity. Typically, the concentration of sodium in a salt substitute is about 100 µg/g The exact concentration of sodium is determined by flame atomic emission. Because it is difficult to match the matrix of the standards to that of the sample, the analysis is accomplished by the method of standard additions.

Procedure

A sample is prepared by placing an approximately 10-g portion of the salt substitute in 10 mL of 3 M HCl and 100 mL of distilled water. After the sample has dissolved, it is transferred to a 250-mL volumetric flask and diluted to volume with distilled water. A series of standard additions is prepared by placing 25-mL portions of the diluted sample into separate 50-mL volumetric flasks, spiking each with a known amount of an approximately 10 mg/L standard solution of Na^+, and diluting to volume. After zeroing the instrument with an appropriate blank, the instrument is optimized at a wavelength of 589.0 nm while aspirating a standard solution of Na^+. The emission intensity is measured for each of the standard addition samples and the concentration of sodium in the salt substitute is reported in µg/g.

Questions

1. Potassium ionizes more easily than sodium. What problem might this present if you use external standards prepared from a stock solution of 10 mg Na/L instead of using a set of standard additions?

Because potassium is present at a much higher concentration than is sodium, its ionization suppresses the ionization of sodium. Normally suppressing ionization is a good thing because it increases emission intensity. In this case, however, the difference between the standard's matrix and the sample's matrix means that the sodium in a standard experiences more ionization than an equivalent amount of sodium in a sample. The result is a determinate error.

2. One way to avoid a determinate error when using external standards is to match the matrix of the standards to that of the sample. We could, for example, prepare external standards using reagent grade KCl to match the matrix to that of the sample. Why is this not a good idea for this analysis?

Sodium is a common contaminant in many chemicals. Reagent grade KCl, for example, may contain 40–50 µg Na/g. This is a significant source of sodium, given that the salt substitute contains approximately 100 µg Na/g.

3. Suppose you decide to use an external standardization. Given the previous questions, is the result of your analysis likely to underestimate or to overestimate the amount of sodium in the salt substitute?

The solid black line in Figure 10.7.6 shows the ideal calibration curve, assuming we match the standard's matrix to the sample's matrix, and that we do so without adding any additional sodium. If we prepare the external standards without adding KCl, the emission for each standard decreases due to increased ionization. This is shown by the lower of the two dashed red lines. Preparing the standards by adding reagent grade KCl increases the concentration of sodium due to its contamination. Because we underestimate the actual concentration of sodium in the standards, the resulting calibration curve is shown by the other dashed red line. In both cases, the sample's emission results in our overestimating the concentration of sodium in the sample.

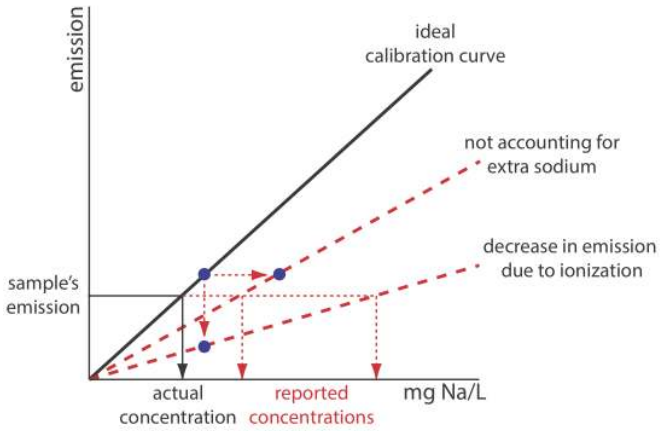


Figure 10.7.6 . External standards calibration curves for the flame atomic emission analysis of Na in a salt substitute. The solid black line shows the ideal calibration curve assuming we match the matrix of the samples and the standards using pure KCl. The lower of the two dashed red lines shows the effect of failing to add KCl to the external standards, which decreases emission. The other dashed red line shows the effect of using KCl that is contaminated with NaCl, which causes us to underestimate the concentration of Na in the standards. In both cases, the result is a positive determinate error in the analysis of samples.

4. One problem with analyzing salt samples is their tendency to clog the aspirator and burner assembly. What effect does this have on the analysis?

Clogging the aspirator and burner assembly decreases the rate of aspiration, which decreases the analyte's concentration in the flame. The result is a decrease in the emission intensity and a negative determinate error.

EXAMPLE 10.7.1

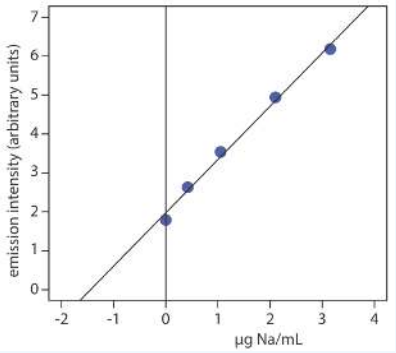
To evaluate the method described in Representative Method 10.7.1, a series of standard additions is prepared using a 10.0077-g sample of a salt substitute. The results of a flame atomic emission analysis of the standards is shown here [Goodney, D. E. *J. Chem. Educ.* **1982**, *59*, 875–876].

added Na (µg/mL)	I_e (arb. units)
0.000	1.79
0.420	2.63
1.051	3.54
2.102	4.94
3.153	6.18

What is the concentration of sodium, in µg/g, in the salt substitute.

Solution

Linear regression of emission intensity versus the concentration of added Na gives the standard additions calibration curve shown below, which has the following calibration equation.



$$I_e = 1.97 + 1.37 \times \frac{\mu g\ Na}{mL}$$

The concentration of sodium in the sample is the absolute value of the calibration curve's *x*-intercept. Substituting zero for the emission intensity and solving for sodium's concentration gives a result of 1.44 μgNa/mL. The concentration of sodium in the salt substitute is

$$\frac{\frac{1.44\ \mu g\ Na}{mL} \times \frac{50.00\ mL}{25.00\ mL} \times 250.0\ mL}{10.0077\ g\ sample} = 71.9\ \mu g\ Na/g$$

EVALUATION OF ATOMIC EMISSION SPECTROSCOPY

SCALE OF OPERATION

The scale of operations for atomic emission is ideal for the direct analysis of trace and ultratrace analytes in macro and meso samples. With appropriate dilutions, atomic emission can be applied to major and minor analytes.

ACCURACY

When spectral and chemical interferences are insignificant, atomic emission can achieve quantitative results with accuracies of 1–5%. For flame emission, accuracy frequently is limited by chemical interferences. Because the higher temperature of a plasma source gives rise to more emission lines, accuracy when using plasma emission often is limited by stray radiation from overlapping emission lines.

PRECISION

For samples and standards in which the analyte's concentration exceeds the detection limit by at least a factor of 50, the relative standard deviation for both flame and plasma emission is about 1–5%. Perhaps the most important factor that affect precision is the stability of the flame's or the plasma's temperature. For example, in a 2500 K flame a temperature fluctuation of ± 2.5 K gives a relative standard deviation of 1% in emission intensity. Significant improvements in precision are realized when using internal standards.

SENSITIVITY

Sensitivity is influenced by the temperature of the excitation source and the composition of the sample matrix. Sensitivity is optimized by aspirating a standard solution of analyte and maximizing the emission by adjusting the flame's composition and the height from which we monitor the emission. Chemical interferences, when present, decrease the sensitivity of the analysis. Because the sensitivity of plasma emission is less affected by the sample matrix, a calibration curve prepared using standards in a matrix of distilled water is possible even for samples that have more complex matrices.

SELECTIVITY

The selectivity of atomic emission is similar to that of atomic absorption. Atomic emission has the further advantage of rapid sequential or simultaneous analysis of multiple analytes.

TIME, COST, AND EQUIPMENT

Sample throughput with atomic emission is rapid when using an automated system that can analyze multiple analytes. For example, sampling rates of 3000 determinations per hour are possible using a multichannel ICP, and sampling rates of 300 determinations per hour when using a sequential ICP. Flame emission often is accomplished using an atomic absorption spectrometer, which typically costs between $10,000–$50,000. Sequential ICP's range in price from $55,000–$150,000, while an ICP capable of simultaneous multielemental analysis costs between $80,000–$200,000. Combination ICP's that are capable of both sequential and simultaneous analysis range in price from $150,000–$300,000. The cost of Ar, which is consumed in significant quantities, can not be overlooked when considering the expense of operating an ICP.

This page titled 9.7.2: Atomic Emission Spectroscopy is shared under a CC BY-NC-SA 4.0 license and was authored, remixed, and/or curated by David Harvey.

- **10.7: Atomic Emission Spectroscopy** by David Harvey is licensed CC BY-NC-SA 4.0.

9.7.3: Inductively Coupled Plasma Mass Spectrometer

In Chapter 10 we introduced the inductively coupled plasma (ICP) as a source for atomic emission. The plasma in ICP is formed by ionizing a flowing stream of argon gas, producing argon ions and electrons. The sample is introduced into the plasma where the high operating temperature of 6000–8000 K is sufficient to atomize and ionize the sample. In optical ICP we measure the emission of photons from the atoms and ions that are in excited states. In ICP-MS we use the plasma as a source of ions that we can send to a mass spectrometer for analysis.

Instrumentation for ICP-MS

An ICP torch operates at room pressure and at an elevated temperature, and a mass spectrometer, as noted in Section 11.2, operates under a vacuum and at room temperature. This difference in pressure and temperature means that a coupling together of these two instrument requires an interface than can bring the pressure and temprature in line with the demands of the mass spectrometer. Figure 9.7.3.1 provides a schematic diagram of a typical ICP-MS instrument with the ICP torch on the right and the mass spectrometer's quadrupole mass analyzer and a continuous electron multiplier on the left. In between the two is a two-stage interface. Note that none of the components in Figure 9.7.3.1are drawn to scale.

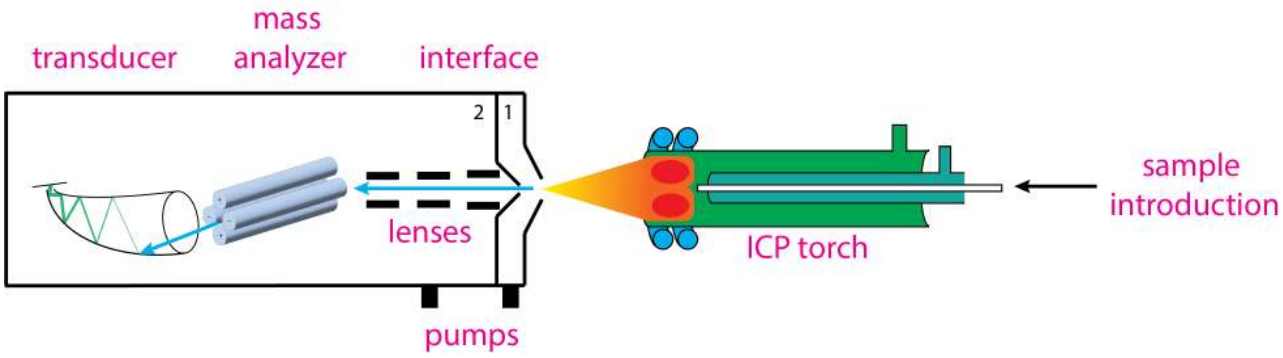


Figure 9.7.3.1. Schematic diagram of an instrument for an inductively coupled plasma mass spectrometer (ICP-MS), showing the torch and the sample nebulizer that make up the ICP on the right, and the mass analyzer and the transducer that make up the MS on the left. Also shown is the interface between the two. The first stage of the interface (1) samples the plasma from the ICP torch and then further reduces the number of particles that are passed along to the second stage (2) a set of ion lenses are used to remove electrons, neutral species, and photons and to focus the ion beam onto the quadrupole.

The first stage of the interface consists of two cone-shaped openings: a sampler cone and a skimmer cone. The hot plasma from the ICP torch enters the first stage of the interface through the sampler cone, which is a pin-hole with a diameter of approximately 1 mm. Samples in solution form are drawn directly into the ICP torch using a nebulizer. Solid samples are vaporized using a laser (a process called laser ablation) and the vapor drawn directly into the ICP torch.

A pump is used to drop the pressure in the first stage to approximately 1 torr. The expansion of the plasma as it enters the first stage results in some cooling of the plasma. The skimmer cone allows a small portion of the plasma in the first stage to pass into the second stage, which is held at the mass spectrometer's operating pressure of approximately 10^{-5} torr. A series of ion lenses are used to narrow the conical dispersion of the plasma, to isolate positive ions from electrons, neutral species, and photons—all of which will generate a signal if they reach the transducer—and to focus the ion beam onto the quadrupole's entrance.

Atomic Mass Spectra and Interferences

Figure 9.7.3.2 shows an example of an ICP-MS spectrum for the analysis of a metal coating using laser ablation to volatilize the sample. The quadrupole mass analyzer operates over a mass-to-charge range of approximately 3 to 300 and can resolve lines that differ by ± 1 m/z. Data are collected either by scanning the quadrupole to provide a survey spectrum of all ions generated in the plasma, as is the case in Figure 9.7.3.2, or by peak hopping in which we gather data for just a few discrete mass-to-charge ratios, adjusting the quadrupole so that it passes only a single mass-to-charge ratio and count the ions for a set period of time before moving to the next mass-to-charge ratio.

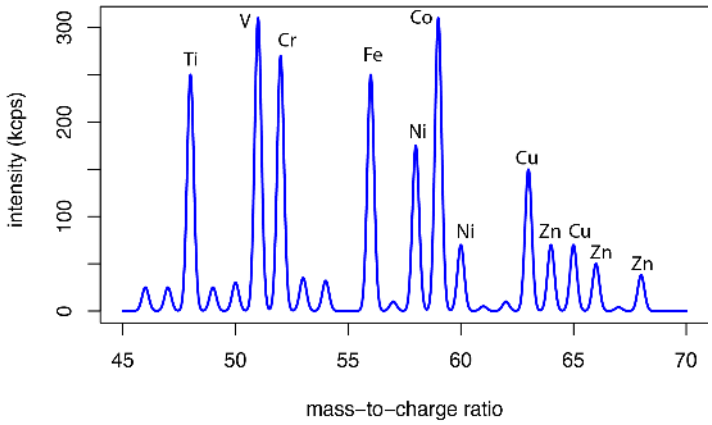


Figure 9.7.3.2. Example of an ICP-MS spectrum of a metal coating using laser ablation to vaporize the sample before drawing it into the ICP torch. The intensity of ions is reported in kilocounts per seconds. The major peaks are identified by element. The data used to construct this figure were extrapolated from the source linked to here.

Spectroscopic Interferences

An ICP-MS spectrum is much simpler than the corresponding ICP atomic emission spectrum because each element in the latter has many emission lines and because the plasma itself has many emission lines. Still, an ICP-MS is not free from interferences, the two most important of which are isobaric ions and polyatomic ions.

Isobaric Ions. Iso- means same and -baric means weight; thus, isobaric means same weight and refers to two (or more) species that have—within the resolution of the mass spectrometer—identical weights and that both contribute to the same peak in the mass spectrum. The source of this interference is the existence of isotopes. For example, the most abundant ions for argon and for calcium are ^{40}Ar and ^{40}Ca, and, given the resolving power of a quadrupole mass analyzer, the two ions appear as a single peak at $m/z = 40$ even though the mass of ^{40}Ar is 39.962383 amu and the mass of ^{40}Ca is 39.962591 amu. We can correct for this interference because the second most abundant isotope of calcium, ^{44}Ca, does not share a m/z with argon (or with another element). Figure 9.7.3.3 shows the ICP-MS spectrum for a sample that contains calcium and argon, and Example 9.7.3.1 shows how we can use this spectrum to determine the contribution of each element.

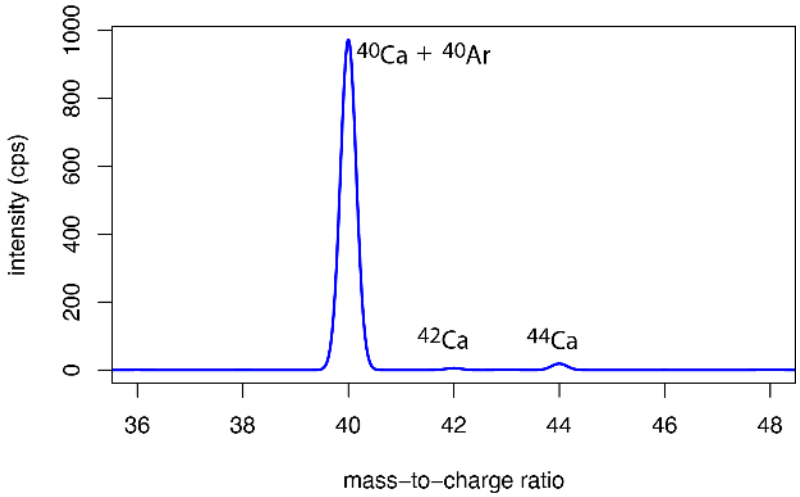


Figure 9.7.3.3: ICP-MS spectrum for a mixture of calcium and argon. The peak at $m/z = 40$ includes contributions from both ^{40}Ca and ^{40}Ar. The other two peaks are for ^{42}Ca and for ^{44}Ca and do not include contributions from argon. The peaks for ^{36}Ar, ^{38}Ar, ^{43}Ca, ^{46}Ca, and ^{48}Ca are too small to appear as peaks in this spectrum.

Example 9.7.3.1

For the spectrum in Figure 9.7.3.3 the intensity at $m/z = 40$ is 972.07 cps and the intensity at $m/z = 44$ is 18.77 cps. Given that the istopic abundance of ^{40}Ca is 96.941% and the isotopic abundance of ^{44}Ca is 2.086%, what is the counts-per-second at $m/z = 40$ for Ca and for Ar.

Solution

Given that only ^{44}Ca contributes to the peak at $m/z = 44$ we can use the relative abundances of ^{40}Ca and ^{44}Ca to determine the expected contribution of ^{40}Ca to the total intensity at $m/z = 40$.

$$18.77 \text{ cps} \times \frac{96.941}{2.086} = 872.28 \text{ cps}$$

Subtracting this result from the total intensity gives the intensity at $m/z = 40$ for argon as

$$972.07 \text{ cps} - 872.28 \text{ cps} = 99.79 \text{ cps}$$

Polyatomic Ions. Compensating for isobaric ions is relatively straightforward because we can rely on the known isotopic abundances of the elements. A more difficult problem is an interference between the isotope of an elemental analyte and a polyatomic ion that has the same mass. Such polyatomic ions may arise from the sample's matrix or from the plasma. For example, the ion $^{40}Ar^{16}O^{+}$ has a mass-to-charge ratio of 56, which overlaps with peak for ^{56}Fe, the most abundant isotope of iron. Although we could choose to monitor iron at a different mass-to-charge ratio, we will lose sensitivity as we are using a less abundant isotope. Corrections can be made using the method outlined in Example 9.7.3.1, although it may require using multiple peaks, which increases the uncertainty of the final result.

Matrix Effects

A matrix effect occurs when the sample's matrix affects the relationship between the signal and the concentration of the analyte. Matrix effects are common in ICP-MS and may lead to either a suppression or an enhancement in the signal. Although not always well understood, matrix effects likely result from how easily an ionizable element affects the ability to ionize other elements. Matrix matching, using the method of standard additions, or using an internal standard can help minimize matrix effects for quantitative work.

Applications of ICP-MS

ICP-MS finds application for analytes in a wide variety of matrices, including both solutions and solids. Solution samples with high concentrations of dissolved ions may present problems due to the deposition of the salts onto the sampler and skimmer cones, which reduces the size of the pinhole that provides entry into the interface between the ICP torch and the mass spectrometer. The use of laser ablation makes it possible to analyzer surfaces—such as glasses, metals, and ceramics—without additional sample preparation.

Qualitative and Semiquantitative Applications. One of the strengths of ICP-MS is its ability to provide a survey scan, such as that in Figure 9.7.3.1, that allows for the identification of the elements present in a sample. Analysis of a single sample that contains known concentrations of these elements is suitable for providing a rough estimate of their concentration in the sample.

Quantitative Analysis. For a more accurate and precise quantitative analysis, one can prepare multiple external standards and prepare a calibration curve. Linearly across approximately six orders of magnitude with detection limits of less than 1 ppb. Including an internal standard in the external standards can help reduce matrix effects. The ideal internal standard will not produce isobaric ions and its primary ionization potential should be similar to that for the analyte; when working with several analytes, it may be necessary to choose a different internal standard for each analyte.

Isotope Ratios. An important advantage of ICP-MS over other analytical methods is its ability to monitor multiple isotopes for a single element.

This page titled 9.7.3: Inductively Coupled Plasma Mass Spectrometer is shared under a CC BY-NC-SA 4.0 license and was authored, remixed, and/or curated by David Harvey.

- **11.3: Inductively Coupled Plasma Mass Spectrometer** by David Harvey is licensed CC BY-NC-SA 4.0.

CHAPTER OVERVIEW

10: CHROMATOGRAPHIC AND ELECTROPHORETIC METHODS

Drawing from an arsenal of analytical techniques—many of which were the subject of the preceding four chapters—analytical chemists design methods that detect increasingly smaller concentrations of analyte in increasingly more complex matrices. Despite the power of these analytical techniques, they often suffer from a lack of selectivity. For this reason, many analytical procedures include a step to separate the analyte from potential interferents. Although effective, each additional step in an analytical procedure increases the analysis time and the cost of the analysis, and introduces uncertainty. In this chapter we consider two analytical techniques that avoid these limitations by combining the separation and analysis: chromatography and electrophoresis.

10.1: Introduction to Chromatographic Separations
- 10.1.1: A General Description of Chromatography
- 10.1.2: Migration Rates of Solutes
- 10.1.3: Zone Broadening and Column Efficiency
- 10.1.4: Chromatography
- 10.1.5: Optimization and Column Performance
- 10.1.6: Summary of Important Relationships for Chromatography
- 10.1.7: Applications of Chromatography

10.2: Gas Chromatography
- 10.2.1: Gas Chromatography

10.3: High-Performance Liquid Chromatography
- 10.3.1: High Performance Liquid Chromatography

10.4: Other Forms of Chromatography
- 10.4.1: Chromatographic Columns

10.5: Capillary Electrophoresis and Capillary Electrochromatography
- 10.5.1: An Overview of Electrophoresis
- 10.5.2: Capillary Electrophoresis
- 10.5.3: Capillary Electrophoresis
  - 10.5.3.1: Ionic Mobility and Electrophoresis
- 10.5.4: Applications of Capillary Electrophoresis

10.6: Problems

10.7: Additional Resources

10.8: Chapter Summary and Key Terms

This page titled 10: Chromatographic and Electrophoretic Methods is shared under a CC BY-NC-SA 4.0 license and was authored, remixed, and/or curated by David Harvey.

SECTION OVERVIEW

10.1: Introduction to Chromatographic Separations

In previous chapters we explored the application of spectroscopy and electroanalytical chemistry to the quantitative analysis of an analyte in a sample. Despite the power of these instrumental methods of analysis, their use is often limited if the sample contains species that will interfere with the analysis. A UV/Vis analysis, for example, is easy to complete if the analyte is the only species present that absorbs light at the analytical wavelength. If two species contribute to the overall absorbance, a quantitative analysis is still possible if we can measure the sample's absorbance at two wavelengths. Things become more complex, however, as the number of analytes or interferents increase or if we do not know the identity of an intereferent.

Chromatography provides a solution to the analysis of complex samples by providing a way to separate the individual species in a sample prior to their analysis by a spectroscopic or electroanalytical method of analysis. In this chapter we provide a general introduction to chromatographic separations. In the four chapters that follow, we will consider specific chromatographic methods.

10.1.1: A General Description of Chromatography

10.1.2: Migration Rates of Solutes

10.1.3: Zone Broadening and Column Efficiency

10.1.4: Chromatography

10.1.5: Optimization and Column Performance

10.1.6: Summary of Important Relationships for Chromatography

10.1.7: Applications of Chromatography

This page titled 10.1: Introduction to Chromatographic Separations is shared under a CC BY-NC-SA 4.0 license and was authored, remixed, and/or curated by David Harvey.

10.1.1: A General Description of Chromatography

In chromatography we pass a sample-free phase, which we call the mobile phase, over a second sample-free stationary phase that remains fixed in space (Figure 10.1.1.1). We inject or place the sample into the mobile phase. As the sample moves with the mobile phase, its components partition between the mobile phase and the stationary phase. A component whose distribution ratio favors the stationary phase requires more time to pass through the system. Given sufficient time and sufficient stationary and mobile phase, we can separate solutes even if they have similar distribution ratios.

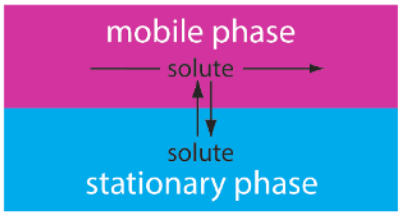


Figure 10.1.1.1. In chromatography we pass a mobile phase over a stationary phase. When we inject a sample into the mobile phase, the sample's components both move with the mobile phase and partition into the stationary phase. The solute that spends the most time in the stationary phase takes the longest time to move through the system.

Classification of Chromatographic Methods

There are many ways in which we can identify a chromatographic separation: by describing the physical state of the mobile phase and the stationary phase; by describing how we bring the stationary phase and the mobile phase into contact with each other; or by describing the chemical or physical interactions between the solute and the stationary phase. Let's briefly consider how we might use each of these classifications.

> We can trace the history of chromatography to the turn of the century when the Russian botanist Mikhail Tswett used a column packed with calcium carbonate and a mobile phase of petroleum ether to separate colored pigments from plant extracts. As the sample moved through the column, the plant's pigments separated into individual colored bands. After effecting the separation, the calcium carbonate was removed from the column, sectioned, and the pigments recovered. Tswett named the technique chromatography, combining the Greek words for "color" and "to write." There was little interest in Tswett's technique until Martin and Synge's pioneering development of a theory of chromatography (see Martin, A. J. P.; Synge, R. L. M. "A New Form of Chromatogram Employing Two Liquid Phases," *Biochem. J.* **1941**, *35*, 1358–1366). Martin and Synge were awarded the 1952 Nobel Prize in Chemistry for this work.

Types of Mobile Phases and Stationary Phases

The mobile phase is a liquid or a gas, and the stationary phase is a solid or a liquid film coated on a solid substrate. We often name chromatographic techniques by listing the type of mobile phase followed by the type of stationary phase. In gas–liquid chromatography, for example, the mobile phase is a gas and the stationary phase is a liquid film coated on a solid substrate. If a technique's name includes only one phase, as in gas chromatography, it is the mobile phase.

Contact Between the Mobile Phase and the Stationary Phase

There are two common methods for bringing the mobile phase and the stationary phase into contact. In column chromatography we pack the stationary phase into a narrow column and pass the mobile phase through the column using gravity or by applying pressure. The stationary phase is a solid particle or a thin liquid film coated on either a solid particulate packing material or on the column's walls.

In planar chromatography the stationary phase is coated on a flat surface—typically, a glass, metal, or plastic plate. One end of the plate is placed in a reservoir that contains the mobile phase, which moves through the stationary phase by capillary action. In paper chromatography, for example, paper is the stationary phase.

Interaction Between the Solute and the Stationary Phase

The interaction between the solute and the stationary phase provides a third method for describing a separation (Figure 10.1.1.2). In adsorption chromatography, solutes separate based on their ability to adsorb to a solid stationary phase. In partition chromatography, the stationary phase is a thin liquid film on a solid support. Separation occurs because there is a difference in the

equilibrium partitioning of solutes between the stationary phase and the mobile phase. A stationary phase that consists of a solid support with covalently attached anionic (e.g., $-SO_3^-$) or cationic (e.g., $-N(CH_3)_3^+$) functional groups is the basis for ion-exchange chromatography in which ionic solutes are attracted to the stationary phase by electrostatic forces. In size-exclusion chromatography the stationary phase is a porous particle or gel, with separation based on the size of the solutes. Larger solutes are unable to penetrate as deeply into the porous stationary phase and pass more quickly through the column.

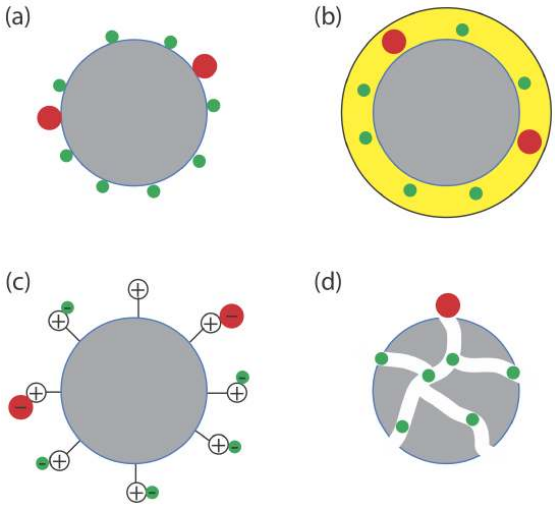


Figure 10.1.1.2. Four examples of interactions between a solute and the stationary phase: (a) adsorption on a solid surface, (b) partitioning into a liquid phase, (c) ion-exchange, and (d) size exclusion. For each example, the smaller, green solute is more strongly retained than the larger, red solute.

There are other interactions that can serve as the basis of a separation. In affinity chromatography the interaction between an antigen and an antibody, between an enzyme and a substrate, or between a receptor and a ligand forms the basis of a separation.

Elution Chromatography on Columns

Of the two methods for bringing the stationary phase and the mobile phases into contact, the most important is column chromatography. In this section we develop a general theory that we may apply to any form of column chromatography.

Figure 10.1.1.3 provides a simple view of a liquid–solid column chromatography experiment. The sample is introduced as a narrow band at the top of the column. Ideally, the solute's initial concentration profile is rectangular (Figure 10.1.1.4a). As the sample moves down (or throught) the column, the solutes begin to separate (Figure 10.1.1.3b,c) and the individual solute bands begin to broaden and develop a Gaussian profile (Figure 10.1.1.4b,c). If the strength of each solute's interaction with the stationary phase is sufficiently different, then the solutes separate into individual bands (Figure 10.1.1.3d and Figure 10.1.1.4d).

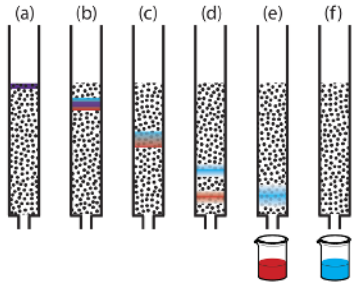


Figure 10.1.1.3. Progress of a column chromatographic separation of a two-component mixture. In (a) the sample is layered on top of the stationary phase. As mobile phase passes through the column, the sample separates into two solute bands (b–d). In (e) and (f), we collect each solute as it elutes from the column.

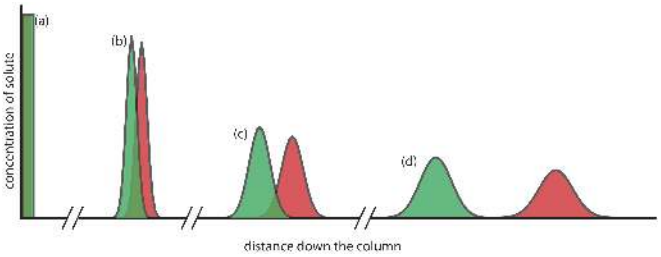


Figure 10.1.1.4. An alternative view of the separation in Figure 10.1.1.3 showing the concentration of each solute as a function of distance down the column.

We can follow the progress of the separation by collecting fractions as they elute from the column (Figure 10.1.1.3e,f), or by placing a suitable detector at the end of the column. A plot of the detector's response as a function of elution time, or as a function of the volume of mobile phase, is known as a chromatogram (Figure 10.1.1.5), and consists of a peak for each solute.

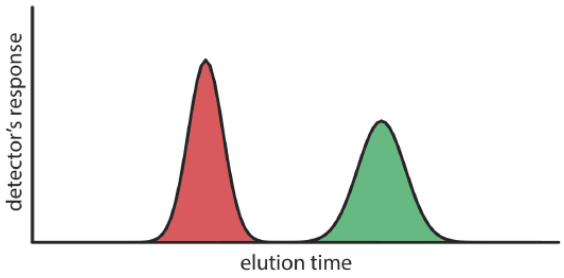


Figure 10.1.1.5. Chromatogram for the separation shown in Figure 10.1.1.3 and Figure 10.1.1.4, showing the detector's response as a function of the elution time.

> There are many possible detectors that we can use to monitor the separation. Later sections of this chapter describe some of the most popular.

This page titled 10.1.1: A General Description of Chromatography is shared under a CC BY-NC-SA 4.0 license and was authored, remixed, and/or curated by David Harvey.

- **26.1: A General Description of Chromatography** by David Harvey is licensed CC BY-NC-SA 4.0.

10.1.2: Migration Rates of Solutes

Our ability to separate two solutes depends on the equilibrium interactions of the solute with the stationary phase and the mobile phase, which effects both the time it takes a solute to travel through the column and the width of the solute's elution profile. In this section we consider the rate at which the solute moves through the column.

Distribution Constants

Let's assume we can describe a solute's distribution between the mobile phase and stationary phase using the following equilibrium reaction

$$S_{\text{m}} \rightleftharpoons S_{\text{s}} \tag{10.1.2.1}$$

where S_{m} is the solute in the mobile phase and S_{s} is the solute in the stationary phase. The equilibrium constant for this reaction is an equilibrium partition coefficient, K_{D}.

$$K_D = \frac{[S_{\text{s}}]}{[S_{\text{m}}]} \tag{10.1.2.2}$$

This is not a trivial assumption. In this section we are, in effect, treating the solute's equilibrium between the mobile phase and the stationary phase as if it is identical to the equilibrium in a simple liquid–liquid extraction carried out in a separatory funnel. You might question whether this is a reasonable assumption. There is an important difference between the two experiments that we need to consider. In a liquid–liquid extraction the two phases remain in contact with each other at all times, allowing for a true equilibrium. In chromatography, however, the mobile phase is in constant motion. A solute that moves into the stationary phase from the mobile phase will equilibrate back into a different portion of the mobile phase; this does not describe a true equilibrium.

So, we ask again: Can we treat a solute's distribution between the mobile phase and the stationary phase as an equilibrium process? The answer is yes, if the mobile phase velocity is slow relative to the kinetics of the solute's movement back and forth between the two phase. In general, this is a reasonable assumption.

Retention Time

We can characterize a chromatographic peak's properties in several ways, two of which are shown in Figure 10.1.2.1. Retention time, t_{r}, is the time between the sample's injection and the maximum response for the solute's peak. A chromatographic peak's baseline width, w, as shown in Figure 10.1.2.1, is determined by extending tangent lines from the inflection points on either side of the peak through the baseline. Although usually we report t_{r} and w using units of time, we can report them using units of volume by multiplying each by the mobile phase's velocity, or report them in linear units by measuring distances with a ruler.

For example, a solute's retention volume,V_{r}, is $t_{\text{r}} \times u$ where u is the mobile phase's velocity through the column.

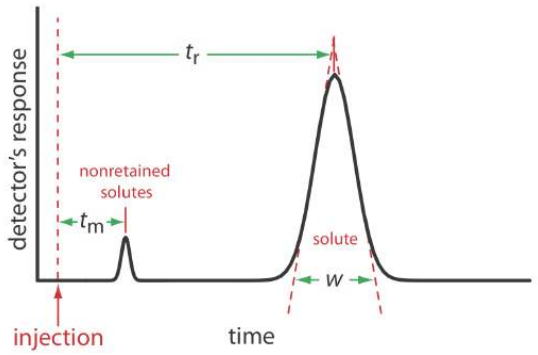


Figure 10.1.2.1. Chromatogram showing a solute's retention time, t_{r}, and baseline width, w, and the column's void time, t_{m}, for nonretained solutes. In this section we focus on retention time; we will consider the width of the solute's peak in Section 26.3.

In addition to the solute's peak, Figure 10.1.2.1 also shows a small peak that elutes shortly after the sample is injected into the mobile phase. This peak contains all nonretained solutes, which move through the column at the same rate as the mobile phase. The time required to elute the nonretained solutes is called the column's void time, t_m.

The Rate of Solute Migration: The Retention Factor

In the absence of any additional equilibrium reactions in the mobile phase or the stationary phase, K_D is equivalent to the distribution ratio, D,

$$D = \frac{[S_0]}{[S_m]} = \frac{(\text{mol S})_s / V_s}{(\text{mol S})_m / V_m} = K_D \tag{10.1.2.3}$$

where V_s and V_m are the volumes of the stationary phase and the mobile phase, respectively.

A conservation of mass requires that the total moles of solute remain constant throughout the separation; thus, we know that the following equation is true.

$$(\text{mol S})_{tot} = (\text{mol S})_m + (\text{mol S})_s \tag{10.1.2.4}$$

Solving Equation 10.1.2.4 for the moles of solute in the stationary phase and substituting into Equation 10.1.2.2 leaves us with

$$D = \frac{\{(\text{mol S})_{tot} - (\text{mol S})_m\} / V_s}{(\text{mol S})_m / V_m} \tag{10.1.2.5}$$

Rearranging this equation and solving for the fraction of solute in the mobile phase, f_m, gives

$$f_m = \frac{(\text{mol S})_m}{(\text{mol S})_{tot}} = \frac{V_m}{DV_s + V_m} \tag{10.1.2.6}$$

Because we may not know the exact volumes of the stationary phase and the mobile phase, we simplify Equation 10.1.2.6 by dividing both the numerator and the denominator by V_m; thus

$$f_m = \frac{V_m / V_m}{DV_s / V_m + V_m / V_m} = \frac{1}{DV_s / V_m + 1} = \frac{1}{1 + k} \tag{10.1.2.7}$$

where k

$$k = D \times \frac{V_s}{V_m} \tag{10.1.2.8}$$

is the solute's retention factor. Note that the larger the retention factor, the more the distribution ratio favors the stationary phase, leading to a more strongly retained solute and a longer retention time.

> Other (older) names for the retention factor are capacity factor, capacity ratio, and partition ratio, and it sometimes is given the symbol k'. Keep this in mind if you are using other resources. Retention factor is the approved name from the IUPAC Gold Book.

We can determine a solute's retention factor from a chromatogram by measuring the column's void time, t_m, and the solute's retention time, t_r (see Figure 10.1.2.1). Solving Equation 10.1.2.7 for k, we find that

$$k = \frac{1 - f_m}{f_m} \tag{10.1.2.9}$$

Earlier we defined f_m as the fraction of solute in the mobile phase. Assuming a constant mobile phase velocity, we also can define f_m as

$$f_m = \frac{\text{time spent in the mobile phase}}{\text{time spent in the stationary phase}} = \frac{t_m}{t_r} \tag{10.1.2.10}$$

Substituting back into Equation 10.1.2.9 and rearranging leaves us with

$$k = \frac{1 - \frac{t_m}{t_r}}{\frac{t_m}{t_r}} = \frac{t_r - t_m}{t_m} = \frac{t'_r}{t_m} \tag{10.1.2.11}$$

where t'_r is the adjusted retention time.

Example 10.1.2.1

In a chromatographic analysis of low molecular weight acids, butyric acid elutes with a retention time of 7.63 min. The column's void time is 0.31 min. Calculate the retention factor for butyric acid.

Solution

$$k_{but} = \frac{t_r - t_m}{t_m} = \frac{7.63 \text{ min} - 0.31 \text{ min}}{0.31 \text{ min}} = 23.6$$

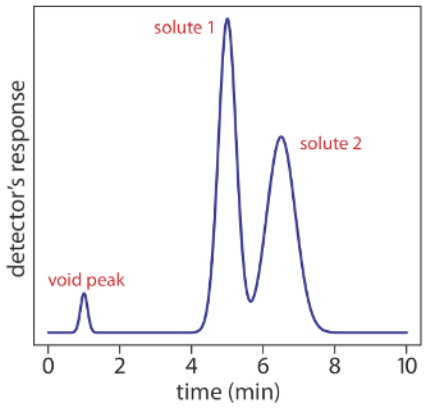


Figure 10.1.2.2. Chromatogram for Exercise 10.1.2.1.

Relative Migration Rates: The Selectivity Factor

Selectivity is a relative measure of the retention of two solutes, which we define using a selectivity factor, α

$$\alpha = \frac{k_B}{k_A} = \frac{t_{r,B} - t_m}{t_{r,A} - t_m} \tag{10.1.2.12}$$

where solute A has the smaller retention time. When two solutes elute with identical retention time, $\alpha = 1.00$; for all other conditions $\alpha > 1.00$.

Example 10.1.2.2

In the chromatographic analysis for low molecular weight acids described in Example 10.1.2.1, the retention time for isobutyric acid is 5.98 min. What is the selectivity factor for isobutyric acid and butyric acid?

Solution

First we must calculate the retention factor for isobutyric acid. Using the void time from Example 10.1.2.1we have

$$k_{iso} = \frac{t_r - t_m}{t_m} = \frac{5.98 \text{ min} - 0.31 \text{ min}}{0.31 \text{ min}} = 18.3$$

The selectivity factor, therefore, is

$$\alpha = \frac{k_{but}}{k_{iso}} = \frac{23.6}{18.3} = 1.29$$

This page titled 10.1.2: Migration Rates of Solutes is shared under a CC BY-NC-SA 4.0 license and was authored, remixed, and/or curated by David Harvey.

- **26.2: Migration Rates of Solutes** by David Harvey is licensed CC BY-NC-SA 4.0.

10.1.3: Zone Broadening and Column Efficiency

Suppose we inject a sample that has a single component. At the moment we inject the sample it is a narrow band of finite width. As the sample passes through the column, the width of this band continually increases in a process we call band broadening. Column efficiency is a quantitative measure of the extent of band broadening.

The Shape of Chromatographic Peaks

When we inject a sample onto a column it has a uniform, or rectangular concentration profile with respect to distance down the column. As the sample passes through the column, the individual solute particles move in and out of the stationary phase, remaining in place when in the stationary phase and moving down the column when in the mobile phase. Because some solute particles will, on average, spend more time in the mobile phase and some will, on average, spend more time in the stationary phase, the original rectangular band increases in width and takes on a Gaussian shape, as we see in Figure 10.1.3.1.

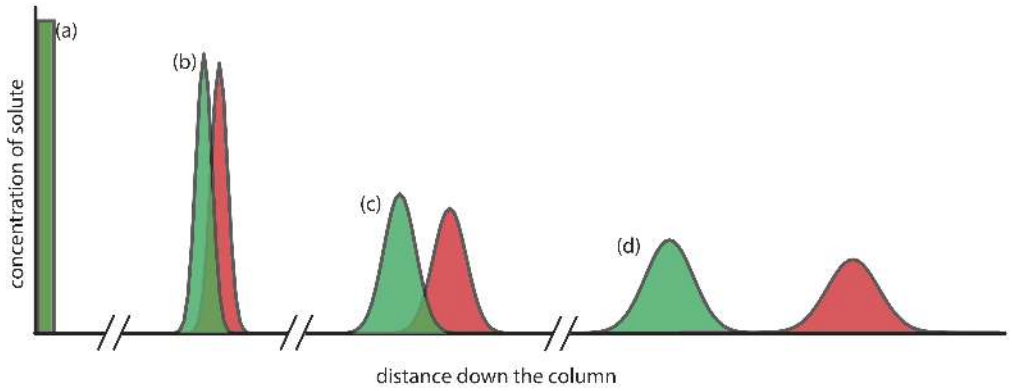


Figure 10.1.3.1. The initial injection of a sample results in the rectangular band of solutes seen in (a). As the sample migrates through the column, the individual components of the sample take on a Gaussian-shaped band profile, as seen in (b-d).

Our treatment of chromatography in this section assumes that a solute elutes as a symmetrical Gaussian peak, such as that shown in Figure 10.1.3.1. This ideal behavior occurs when the solute's partition coefficient, K_D

$$K_D = \frac{[S_s]}{[S_m]} \tag{10.1.3.1}$$

is the same for all concentrations of solute. If this is not the case, then the chromatographic peak has an asymmetric peak shape similar to those shown in Figure 10.1.3.2 The chromatographic peak in Figure 10.1.3.2a is an example of peak tailing, which occurs when some sites on the stationary phase retain the solute more strongly than other sites. Figure 10.1.3.2b, which is an example of peak fronting most often is the result of overloading the column with sample.

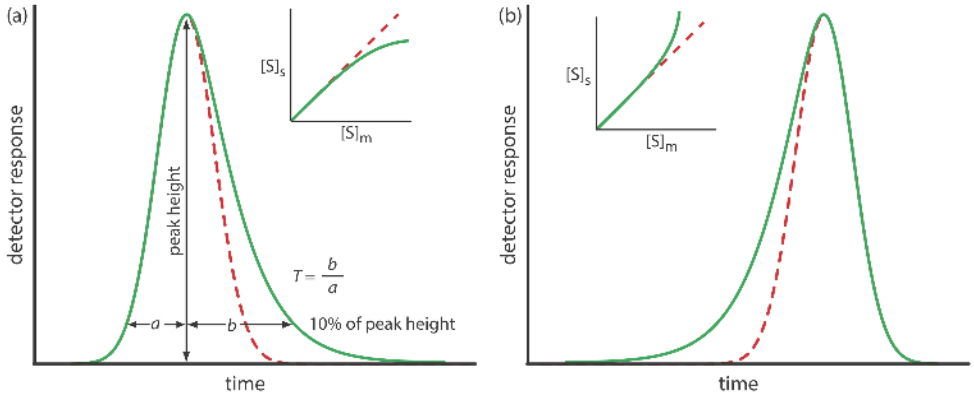


Figure 10.1.3.2. Examples of asymmetric chromatographic peaks showing (a) peak tailing and (b) peak fronting. For both (a) and (b) the green chromatogram is the asymmetric peak and the red dashed chromatogram shows the ideal, Gaussian peak shape. The insets show the relationship between the concentration of solute in the stationary phase, $[S]_s$, and its concentration in the mobile phase, $[S]_m$. The dashed red lines show ideal behavior (K_D is constant for all conditions) and the green lines show nonideal behavior (K_D decreases or increases for higher total concentrations of solute). A quantitative measure of peak tailing, T, is shown in (a).

As shown in Figure 10.1.3.2a, we can report a peak's asymmetry by drawing a horizontal line at 10% of the peak's maximum height and measuring the distance from each side of the peak to a line drawn vertically through the peak's maximum. The asymmetry factor, *T*, is defined as

$$T = \frac{b}{a} \tag{10.1.3.2}$$

Methods for Describing Column Efficiency

In their original theoretical model of chromatography, Martin and Synge divided the chromatographic column into discrete sections, which they called theoretical plates. Within each theoretical plate Martin and Synge assumed that there is an equilibrium between the solute present in the stationary phase and the solute present in the mobile phase [Martin, A. J. P.; Synge, R. L. M. *Biochem. J.* **1941**, *35*, 1358–1366]. They described column efficiency in terms of the number of theoretical plates, *N*,

$$N = \frac{L}{H} \tag{10.1.3.3}$$

where *L* is the column's length and *H* is the height of a theoretical plate. For any given column, the column efficiency improves—and chromatographic peaks become narrower—when there are more theoretical plates.

If we assume that a chromatographic peak has a Gaussian profile, then the extent of band broadening is given by the peak's variance or standard deviation. The height of a theoretical plate is the peak's variance per unit length of the column

$$H = \frac{\sigma^2}{L} \tag{10.1.3.4}$$

where the standard deviation, σ, has units of distance. Because retention times and peak widths usually are measured in seconds or minutes, it is more convenient to express the standard deviation in units of time, τ, by dividing σ by the solute's average linear velocity, $\bar{u}$, which is equivalent to dividing the distance it travels, *L*, by its retention time, t_r.

$$\tau = \frac{\sigma}{\bar{u}} = \frac{\sigma t_r}{L} \tag{10.1.3.5}$$

For a Gaussian peak shape, the width at the baseline, *w*, is four times its standard deviation, τ.

$$w = 4\tau \tag{10.1.3.6}$$

Combining Equation 10.1.3.4, Equation 10.1.3.5, and Equation 10.1.3.6 defines the height of a theoretical plate in terms of the easily measured chromatographic parameters t_r and *w*.

$$H = \frac{Lw^2}{16t_r^2} \tag{10.1.3.7}$$

Combing Equation 10.1.3.7 and Equation 10.1.3.3 gives the number of theoretical plates.

$$N = 16\frac{t_r^2}{w^2} = 16\left(\frac{t_r}{w}\right)^2 \tag{10.1.3.8}$$

Example 10.1.3.4

A chromatographic analysis for the chlorinated pesticide Dieldrin gives a peak with a retention time of 8.68 min and a baseline width of 0.29 min. Calculate the number of theoretical plates? Given that the column is 2.0 m long, what is the height of a theoretical plate in mm?

Solution

Using Equation 10.1.3.8, the number of theoretical plates is

$$N = 16\frac{t_r^2}{w^2} = 16 \times \frac{(8.68\text{ min})^2}{(0.29\text{ min})^2} = 14300\text{ plates}$$

Solving Equation 10.1.3.3 for *H* gives the average height of a theoretical plate as

$$H = \frac{L}{N} = \frac{2.00 \text{ m}}{14300 \text{ plates}} \times \frac{1000 \text{ mm}}{\text{m}} = 0.14 \text{ mm/plate}$$

It is important to remember that a theoretical plate is an artificial construct and that a chromatographic column does not contain physical plates. In fact, the number of theoretical plates depends on both the properties of the column and the solute. As a result, the number of theoretical plates for a column may vary from solute to solute.

The number of theoretical plates for an asymmetric peak shape is approximately

$$N \approx \frac{41.7 \times \frac{t_r^2}{(w_{0.1})^2}}{T + 1.25} = \frac{41.7 \times \frac{t_r^2}{(a+b)^2}}{T + 1.25} \tag{10.1.3.9}$$

where $w_{0.1}$ is the width at 10% of the peak's height [Foley, J. P.; Dorsey, J. G. *Anal. Chem.* **1983**, *55*, 730–737].

Asymmetric peaks have fewer theoretical plates, and the more asymmetric the peak the smaller the number of theoretical plates. For example, the following table gives values for *N* for a solute eluting with a retention time of 10.0 min and a peak width of 1.00 min.

b	*a*	*T*	*N*
0.5	0.5	1.00	1850
0.6	0.4	1.50	1520
0.7	0.3	2.33	1160
0.8	0.2	4.00	790

Kinetic Variables That Affect Zone Broadening

Another approach to understanding the broadening of a solute band as it passes through a column is to consider the factors that affect the rate at which a solute moves through the column and how that is affected by the velocity with which the mobile phase moves through the column. We will consider one approach that considers four contributions: variations in path lengths, longitudinal diffusion, mass transfer in the stationary phase, and mass transfer in the mobile phase.

Multiple Paths: Variations in Path Length

As solute molecules pass through the column they travel paths that differ in length. Because of this difference in path length, two solute molecules that enter the column at the same time will exit the column at different times. The result, as shown in Figure 10.1.3.3, is a broadening of the solute's profile on the column. The contribution of multiple paths to the height of a theoretical plate, H_p, is

$$H_p = 2\lambda d_p \tag{10.1.3.10}$$

where d_p is the average diameter of the particulate packing material and λ is a constant that accounts for the consistency of the packing. A smaller range of particle sizes and a more consistent packing produce a smaller value for λ. For a column without packing material, H_p is zero and there is no contribution to band broadening from multiple paths.

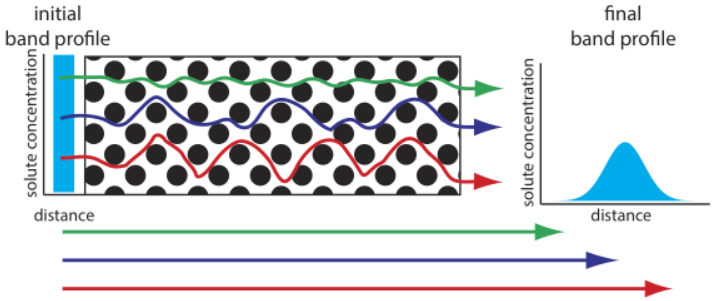


Figure 10.1.3.3. The effect of multiple paths on a solute's band broadening. The solute's initial band profile is rectangular. As this band travels through the column, individual solute molecules travel different paths, three of which are shown by the meandering colored paths (the actual lengths of these paths are shown by the straight arrows at the bottom of the figure). Most solute molecules travel paths with lengths similar to that shown in blue, with a few traveling much shorter paths (green) or much longer paths (red). As a result, the solute's band profile at the end of the column is broader and Gaussian in shape.

An inconsistent packing creates channels that allow some solute molecules to travel quickly through the column. It also can creates pockets that temporarily trap some solute molecules, slowing their progress through the column. A more uniform packing minimizes these problems.

Longitudinal Diffusion

The second contribution to band broadening is the result of the solute's longitudinal diffusion in the mobile phase. Solute molecules are in constant motion, diffusing from regions of higher solute concentration to regions where the concentration of solute is smaller. The result is an increase in the solute's band width (Figure 10.1.3.4). The contribution of longitudinal diffusion to the height of a theoretical plate, H_d, is

$$H_d = \frac{2\gamma D_m}{u} \tag{10.1.3.11}$$

where D_m is the solute's diffusion coefficient in the mobile phase, u is the mobile phase's velocity, and γ is a constant related to the efficiency of column packing. Note that the effect of H_d on band broadening is inversely proportional to the mobile phase velocity: a higher velocity provides less time for longitudinal diffusion. Because a solute's diffusion coefficient is larger in the gas phase than in a liquid phase, longitudinal diffusion is a more serious problem in gas chromatography.

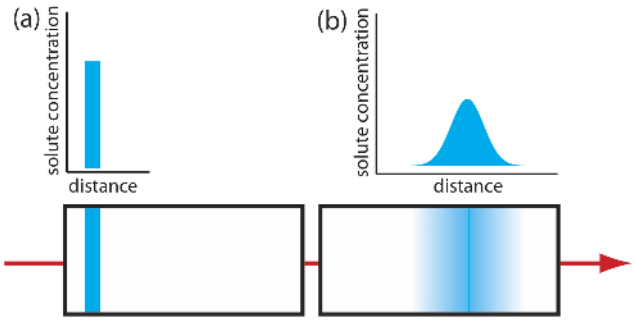


Figure 10.1.3.4. The effect of longitudinal diffusion on a solute's band broadening. Two horizontal cross-sections through the column and the corresponding concentration versus distance profiles are shown, with (a) being earlier in time. The red arrow shows the direction in which the mobile phase is moving.

Mass Transfer

As the solute passes through the column it moves between the mobile phase and the stationary phase. We call this movement between phases mass transfer. As shown in Figure 10.1.3.5, band broadening occurs if the solute's movement within the mobile phase or within the stationary phase is not fast enough to maintain an equilibrium in its concentration between the two phases. On average, a solute molecule in the mobile phase moves some distance down the column before it passes into the stationary phase. A solute molecule in the stationary phase, on the other hand, takes longer than expected to move back into the mobile phase. The contributions of mass transfer in the stationary phase, H_s, and mass transfer in the mobile phase, H_m, are given by the following equations

$$H_s = \frac{qkd_f^2}{(1+k)^2 D_s} u \tag{10.1.3.12}$$

$$H_m = \frac{fn\left(d_p^2, d_c^2\right)}{D_m} u \tag{10.1.3.13}$$

where d_f is the thickness of the stationary phase, d_c is the diameter of the column, D_s and D_m are the diffusion coefficients for the solute in the stationary phase and the mobile phase, k is the solute's retention factor, and q is a constant related to the column packing material. Although the exact form of H_m is not known, it is a function of particle size and column diameter. Note that the effect of H_s and H_m on band broadening is directly proportional to the mobile phase velocity because a smaller velocity provides more time for mass transfer.

> The abbreviation *fn* in Equation 10.1.3.13means "is a function of."

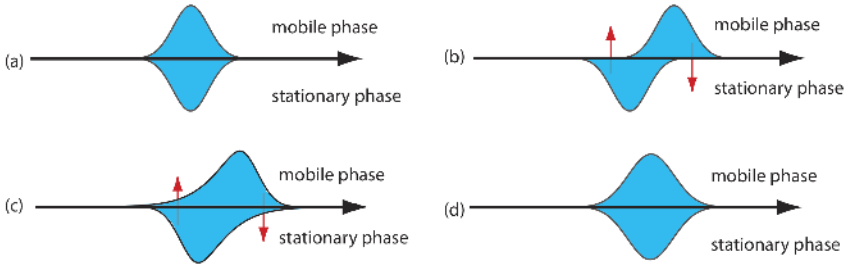


Figure 10.1.3.5. Effect of mass transfer on band broadening: (a) Ideal equilibrium Gaussian profiles for the solute in the mobile phase and in the stationary phase. (b, c) If we allow the solute's band to move a small distance down the column, an equilibrium between the two phases no longer exits. The red arrows show the movement of solute—what we call the mass transfer of solute—from the stationary phase to the mobile phase, and from the mobile phase to the stationary phase. (d) Once equilibrium is reestablished, the solute's band is now broader.

Putting It All Together

The height of a theoretical plate is a summation of the contributions from each of the terms that affect band broadening.

$$H = H_p + H_d + H_s + H_m \tag{10.1.3.14}$$

An alternative form of this equation is the van Deemter equation

$$H = A + \frac{B}{u} + Cu \tag{10.1.3.15}$$

which emphasizes the importance of the mobile phase's velocity. In the van Deemter equation, A accounts for the contribution of multiple paths (H_p), B/u accounts for the contribution of longitudinal diffusion (H_d), and Cu accounts for the combined contribution of mass transfer in the stationary phase and in the mobile phase (H_s and H_m).

There is some disagreement on the best equation for describing the relationship between plate height and mobile phase velocity [Hawkes, S. J. *J. Chem. Educ.* **1983**, *60*, 393–398]. In addition to the van Deemter equation, other equations include

$$H = \frac{B}{u} + (C_s + C_m)\, u \tag{10.1.3.16}$$

where C_s and C_m are the mass transfer terms for the stationary phase and the mobile phase and

$$H = Au^{1/3} + \frac{B}{u} + Cu \tag{10.1.3.17}$$

All three equations, and others, have been used to characterize chromatographic systems, with no single equation providing the best explanation in every case [Kennedy, R. T.; Jorgenson, J. W. *Anal. Chem.* **1989**, *61*, 1128–1135].

To increase the number of theoretical plates without increasing the length of the column, we need to decrease one or more of the terms in Equation 10.1.3.14 The easiest way to decrease H is to adjust the velocity of the mobile phase. For smaller mobile phase velocities, column efficiency is limited by longitudinal diffusion, and for higher mobile phase velocities efficiency is limited by the

two mass transfer terms. As shown in Figure 26.3.6 —which uses the van Deemter equation—the optimum mobile phase velocity is the minimum in a plot of H as a function of u.

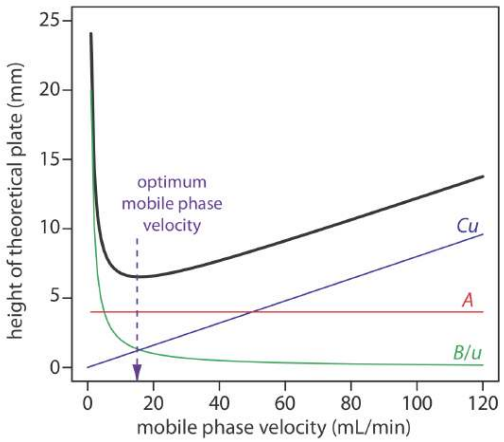


Figure 26.3.6 . Plot showing the relationship between the height of a theoretical plate, H, and the mobile phase's velocity, u, based on the van Deemter equation.

The remaining parameters that affect the terms in Equation 10.1.3.14 are functions of the column's properties and suggest other possible approaches to improving column efficiency. For example, both H_p and H_m are a function of the size of the particles used to pack the column. Decreasing particle size, therefore, is another useful method for improving efficiency.

> For a more detailed discussion of ways to assess the quality of a column, see Desmet, G.; Caooter, D.; Broeckhaven, K. "Graphical Data Represenation Methods to Assess the Quality of LC Columns," *Anal. Chem.* **2015**, *87*, 8593–8602.

Perhaps the most important advancement in chromatography columns is the development of open-tubular, or capillary columns. These columns have very small diameters ($d_c \approx$ 50–500 μm) and contain no packing material ($d_p = 0$). Instead, the capillary column's interior wall is coated with a thin film of the stationary phase. Plate height is reduced because the contribution to H from H_p (Equation 10.1.3.10) disappears and the contribution from H_m (Equation 10.1.3.13) becomes smaller. Because the column does not contain any solid packing material, it takes less pressure to move the mobile phase through the column, which allows for longer columns. The combination of a longer column and a smaller height for a theoretical plate increases the number of theoretical plates by approximately 100×. Capillary columns are not without disadvantages. Because they are much narrower than packed columns, they require a significantly smaller amount of sample, which may be difficult to inject reproducibly. Another approach to improving resolution is to use thin films of stationary phase, which decreases the contribution to H from H_s (Equation 10.1.3.12).

> The smaller the particles, the more pressure is needed to push the mobile phase through the column. As a result, for any form of chromatography there is a practical limit to particle size.

This page titled 10.1.3: Zone Broadening and Column Efficiency is shared under a CC BY-NC-SA 4.0 license and was authored, remixed, and/or curated by David Harvey.

- **26.3: Zone Broadening and Column Efficiency** by David Harvey is licensed CC BY-NC-SA 4.0.

10.1.4: Chromatography

Chromatography is a method by which a mixture is separated by distributing its components between two phases. The stationary phase remains fixed in place while the mobile phase carries the components of the mixture through the medium being used. The stationary phase acts as a constraint on many of the components in a mixture, slowing them down to move slower than the mobile phase. The movement of the components in the mobile phase is controlled by the significance of their interactions with the mobile and/or stationary phases. Because of the differences in factors such as the solubility of certain components in the mobile phase and the strength of their affinities for the stationary phase, some components will move faster than others, thus facilitating the separation of the components within that mixture.

Theory

The distribution of a solute between the mobile and stationary phases in chromatography is described by κ, the partition coefficient, defined by:

$$\kappa = \frac{C_s}{C_m}$$

where C_s is the concentration of solute in the stationary phase and C_m is the concentration of the solute in the mobile phase. The mobile phase serves to carry the sample molecules through the chromatographic column. During the sample molecules transportation through the column, each analyte is retained according to that compound's characteristic affinity for the stationary phase. The time that passes between the sample injection and peak maximum is called the retention time. The area underneath each peak is proportional to the amount of co responding analyte in solution.

Retention Time

The retention time, t_R, is given in seconds by:

$$t_R = t_S + t_M$$

where t_S is the time the analyte spends in the stationary phase and t_M is the time spent in the mobile phase. t_M is often referred to as the dead, or void time, as all components spend t_M in the mobile phase.

Theory of Band Broadening and Column Efficiency

Column efficiency is affected by the amount of band broadening that occurs as the sample passes through the column. Rate theory describes the shapes of the peaks in quantitative terms and is based upon the infinite number of paths that the sample may take in order to elute out of the column. Some molecules will travel through the column quickly due to their accidentally inclusion in the mobile phase while other molecules will severely lag behind because of their accidental inclusion in the stationary phase. The result of these effects is a typical Gaussian shaped chromatographic band with a spread of velocities around the mean value. Furthermore, the width of the peak increases as it move down the column because of the increased opportunity for spreading.

Two additional, undesirable chromatographic features are fronting and tailing. With fronting, the front of the peak is drawn out and the tali is steepened. The opposite is true for tailing. Both effects can be cause by distribution constant that varies with the concentration. These non-ideal effects are unwanted because of they lead to poor separations.

The two terms used to measure column efficiency are plate height, H, and plate count, N. These two terms related by the following equation where L is the length of the column:

$$N = L/H$$

Greater column efficiency is characterized by a large plate count N and a small plate height H. Both H and N can be determined experimentally using the following two equations:

$$H = LW^2/16(t_R)^2$$

$$N = 16(t_R/W)^2$$

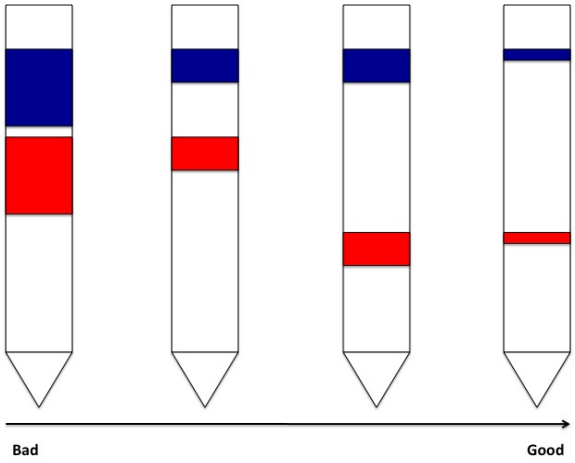
where L is the length of the column packing, W is the width of the magnitude of the base of the triangle and t_R is the retention time of the analyte. Using the theory of band broadening, the efficiency of chromatographic columns can be approximated by the *van Deemter* equation:

$$H = A + \frac{B}{u} + C_S u + C_M u$$

where H is the plate height in centimeters and u is the linear velocity of the mobile phase in centimeters per second. The term A describes the multiple path effect, or eddy diffusion, B describes the longitudinal diffusion coefficient and $C_S u$ and $C_M u$ are the mass-transfer coefficients for the stationary and mobile phases, respectively.

The van Deemter Equation

In chromatography, it is important that the components in solution are adequately separated so that the separate components can be collected in their purest form. This becomes easier to do as the separation between the bands for each component have a greater separation between them. Also, it is ideal to have the bands of the individual components as narrow as possible. This is to say that it is best to have each component occupying as little space as possible within the column:



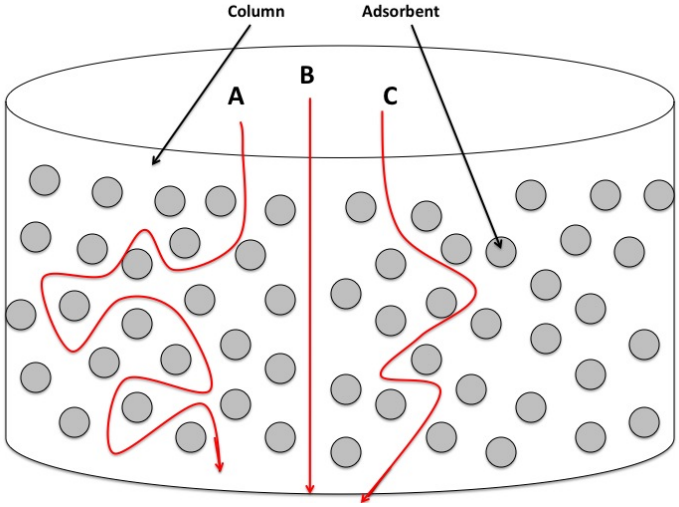
From this figure it can be seen that a better separation between narrow bands of components is ideal for easier collection of the individual samples. Band broadening is an especially important factor for this type of chromatography when separating colored compounds. When the bands of the components are narrow, most of the particles of that component are in close proximity with one another, which makes it easier to see the color of the bands. As the particles diffuse away from one another and broaden the component's band, the color of the band fades and can become more difficult to see, which may also make it harder to collect pure samples of the mixture's components.

The extent of band broadening in chromatography is determined by the Van Deemter equation[3]. This equation relates the efficiency of the chromatography procedure to three different factors. The Van Deemter equation is shown below:

$$H = Au^{1/3} + \frac{B}{u} + Cu$$

Where H is the height equivalent of a theoretical plate[4] (HETP) and u is the velocity (flow rate) of the mobile phase. The lower the resulting value of H is, the greater the efficiency of the procedure. So, ideally, a scientist will want to minimize all three terms in order to minimize H. The other three terms refer to factors that come into play while the chromatography is performed.

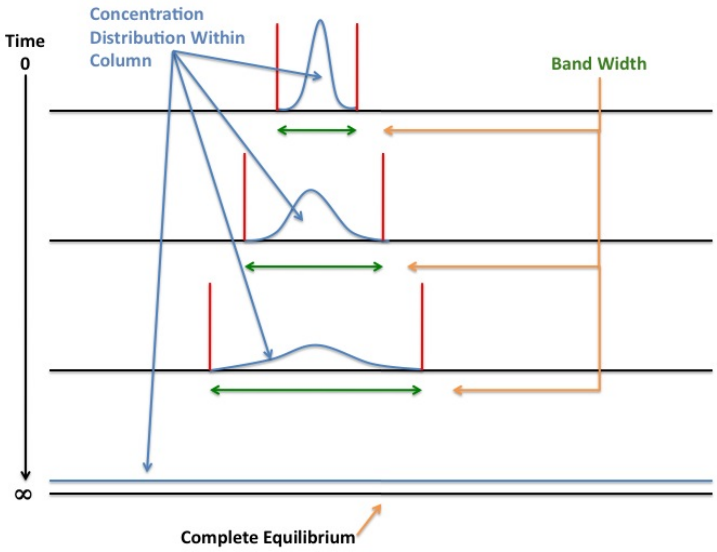
The A factor is determined by a phenomenon called **Eddy Diffusion**[5]. This is also called the multi-path term, as molecular particles of a certain compound have a multitude of options when it comes to finding a pathway through a packed column. The following figure helps in visualizing Eddy diffusion:



Because there is an almost infinite number of different paths that a particle can travel by through a column, some paths will be longer than others. The particles that find the shortest path through the column will be eluted more quickly than those that travel a longer way. In the figure, particle B will be eluted before particle C, and both will be eluted before particle A. Since it is improbable for all particles of one compound to find the shortest path, there will be fractions of the component that will behave like particles A, B, and C. This leads to the broadening of the band. There is little a scientist can do to minimize the Eddy Diffusion factor, as it is influenced by the nature of column being used and by the particles' movement through that column. The A term is loosely affected by the flow rate of the mobile phase, and sometimes the affect of the flow rate is negligible. It is for this reason that sometimes the Van Deemter equation is written as such:

$$H = A + \frac{B}{u} + Cu$$

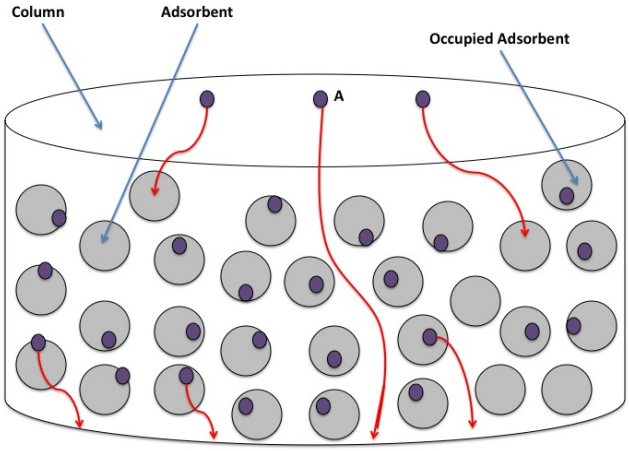
B/u is called the longitudinal diffusion term, and is caused by the components' natural migration from a place of high concentration (the center of the band) to a place of lower concentration (either side of the band) within the column. Diffusion[6] occurs because molecules in a place of high concentration will tend to spread out to areas of lower concentration to achieve equilibrium. Given enough time, diffusion will result in equilibrium of the diffusing fluid via random molecular motion. The figure below helps to visualize this phenomenon:



At time zero in the figure above, the particles of a compound are generally localized in a narrow band within the separating column. If the mobile phase flow rate is too small or if the system is left at rest, the particles begin to separate from one another.

This causes a spread in the concentration distribution of that compound within the column, thus bringing about band broadening for the band of that particular compound. As the time that the system is left still approaches infinity, the compound reaches complete concentration equilibrium throughout the entire column. At this point, there is no definitive band for that component, as a single concentration of that compound is present throughout the entire column. Longitudinal diffusion is a chief cause of band broadening in Gas Chromatography, as the diffusion rates of gaseous species are much higher than those of liquids. It is for this reason that longitudinal diffusion is less of an issue in liquid chromatography. The magnitude of the term B/u can be minimized by increasing the flow rate of the mobile phase. Increasing the velocity of the mobile phase does not allow the components in the column to reach equilibrium, and so will hamper longitudinal diffusion. The flow rate of the mobile phase should not be increased in excess, however, as the term Cu is maximized when u is increased.

Cu is referred to as the mass transfer term. Mass transfer refers to when particles are so strongly adhered to the stationary phase that the mobile phase passes over them without carrying them along. This results is particles of a component being left behind. Since it is likely that more than a single particle of any given compound will undergo this occurrence, band broadening results. This results in a phenomenon called tailing, in which a fraction a component lags behind a more concentrated frontal band. Non-equilibrium effects can be caused by two phenomena: **laminar flow** and **turbulent flow**. Laminar flow[7] occurs in tubular capillaries, and so is most prominent in Capillary Electrophoresis. Turbulent flow occurs as a result of particles becoming overwhelmed by the stationary phase and is more common in column chromatography. This occurrence can be visualized by observing the figure below:



In the above figure, particles of the adsorbent solid become occupied by particles of the sample. If too many particles of the adsorbent are occupied, particle A will have nothing hindering it from flowing through the column. So, the particles of a single compound separate from one another. Also, as the mobile phase moves through the column, particles of the sample leave the stationary phase and migrate with the mobile phase. However, if the flow rate of the mobile phase is too high, many of the sample particles are unable to leave the stationary phase and so get left behind. These occurrences result in band broadening, as the individual particles of a single compound become less closely packed. The high flow rate of the mobile phase makes it more difficult for the components within the column to reach equilibrium between the stationary and mobile phase. It is for this reason that the Cu term is also called the non-equilibrium factor. Minimization of this factor can be achieved by decreasing the flow rate of the mobile phase. Decreasing the flow rate of the mobile phase gives sample components more time to leave the stationary phase and move with the mobile phase, thus reaching equilibrium.

By observing the Van Deemter equation, it can be deduced that an ideal mobile phase flow rate must be determined to yield the best (lowest) value of H. Decreasing the flow rate too much will result in an increase of the longitudinal diffusion factor B/u, while exceedingly increasing the flow rate will increase the significance of the mass transfer term Cu. So, H can be minimized to a finite limit depending on the various parameters involved in the chromatography being performed.

10.1.4: Chromatography is shared under a CC BY-NC-SA 4.0 license and was authored, remixed, and/or curated by Sean Gottlieb.

- **Chromatography** by Sean Gottlieb is licensed CC BY-NC-SA 4.0.

10.1.5: Optimization and Column Performance

The goal of a chromatographic separation is to take a sample with more than one solute and to separate the solutes such that each elutes by itself. Our ability to separate two solutes from each other—to resolve them—is affected by a number of variables; how we can optimize the separation of two solutes is the subject of this section.

Column Resolution

The goal of chromatography is to separate a mixture into a series of chromatographic peaks, each of which constitutes a single component of the mixture. The resolution between two chromatographic peaks, R_{AB}, is a quantitative measure of their separation, and is defined as

$$R_{AB} = \frac{t_{t,B} - t_{t,A}}{0.5\,(w_B + w_A)} = \frac{2\Delta t_r}{w_B + w_A} \tag{10.1.5.1}$$

where B is the later eluting of the two solutes. As shown in Figure 10.1.5.1, the separation of two chromatographic peaks improves with an increase in R_{AB}. If the areas under the two peaks are identical—as is the case in Figure 10.1.5.1—then a resolution of 1.50 corresponds to an overlap of only 0.13% for the two elution profiles. Because resolution is a quantitative measure of a separation's success, it is a useful way to determine if a change in experimental conditions leads to a better separation.

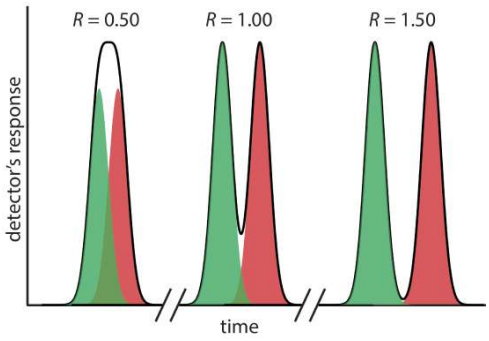


Figure 10.1.5.1. Three examples that show the relationship between resolution and the separation of a two component mixture. The green peak and the red peak are the elution profiles for the two components. The chromatographic peak—which is the sum of the two elution profiles—is shown by the solid black line.

Example 10.1.5.1

In a chromatographic analysis of lemon oil a peak for limonene has a retention time of 8.36 min with a baseline width of 0.96 min. γ-Terpinene elutes at 9.54 min with a baseline width of 0.64 min. What is the resolution between the two peaks?

Solution

Using Equation 10.1.5.1 we find that the resolution is

$$R_{AB} = \frac{2\Delta t_r}{w_B + w_A} = \frac{2(9.54\text{ min} - 8.36\text{ min})}{0.64\text{ min} + 0.96\text{ min}} = 1.48$$

The Effect of Retention and Selectivity Factors on Resolution

Now that we have defined the solute retention factor, selectivity, and column efficiency we are able to consider how they affect the resolution of two closely eluting peaks. Because the two peaks have similar retention times, it is reasonable to assume that their peak widths are nearly identical. If the number of theoretical plates is the same for all solutes—not strictly true, but not a bad assumption—then the ratio t_r/w is a constant. If two solutes have similar retention times, then their peak widths must be similar. Equation 10.1.5.1, therefore, becomes

$$R_{AB} = \frac{t_{r,B} - t_{r,A}}{0.5\,(w_B + w_A)} \approx \frac{t_{r,B} - t_{r,A}}{0.5\,(2w_B)} = \frac{t_{r,B} - t_{r,A}}{w_B} \tag{10.1.5.2}$$

where B is the later eluting of the two solutes. Solving equation 26.3.8 for w_B and substituting into Equation 10.1.5.2 leaves us with the following result.

$$R_{AB} = \frac{\sqrt{N_B}}{4} \times \frac{t_{r,B} - t_{r,A}}{t_{r,B}} \tag{10.1.5.3}$$

Rearranging equation 26.2.11 provides us with the following equations for the retention times of solutes *A* and *B*.

$$t_{r,A} = k_A t_{\mathrm{m}} + t_{\mathrm{m}} \tag{10.1.5.4}$$

$$t_{\mathrm{r},B} = k_B t_{\mathrm{m}} + t_{\mathrm{m}} \tag{10.1.5.5}$$

After substituting these equations into Equation 10.1.5.3 and simplifying, we have

$$R_{AB} = \frac{\sqrt{N_B}}{4} \times \frac{k_B - k_A}{1 + k_B} \tag{10.1.5.6}$$

Finally, we can eliminate solute *A*'s retention factor by substituting in equation 26.2.12. After rearranging, we end up with the following equation for the resolution between the chromatographic peaks for solutes A and B.

$$R_{AB} = \frac{\sqrt{N_B}}{4} \times \frac{\alpha - 1}{\alpha} \times \frac{k_B}{1 + k_B} \tag{10.1.5.7}$$

Although Equation 10.1.5.7 is useful for considering how a change in *N*, α, or *k* qualitatively affects resolution—which suits our purpose here—it is less useful for making accurate quantitative predictions of resolution, particularly for smaller values of *N* and for larger values of *R*. For more accurate predictions use the equation

$$R_{AB} = \frac{\sqrt{N}}{4} \times (\alpha - 1) \times \frac{k_B}{1 + k_{\mathrm{avg}}}$$

where k_{avg} is (k_{A} + k_{B})/2. For a derivation of this equation and for a deeper discussion of resolution in column chromatography, see Foley, J. P. "Resolution Equations for Column Chromatography," *Analyst*, **1991**, *116*, 1275-1279.

Equation 10.1.5.7 contains terms that correspond to column efficiency, selectivity, and the solute retention factor. We can vary these terms, more or less independently, to improve resolution and analysis time. The first term, which is a function of the number of theoretical plates (for Equation 10.1.5.7), accounts for the effect of column efficiency. The second term is a function of α and accounts for the influence of column selectivity. Finally, the third term in both equations is a function of k_B and accounts for the effect of solute *B*'s retention factor. A discussion of how we can use these parameters to improve resolution is the subject of the remainder of this section.

The Effect of Resolution on Retention Time

In addition to resolution, another important factor in chromatography is the amount of time needed to elute a pair of solutes, which we can approximate using the retention time for solute *B*.

$$t_{r,B} = \frac{16 R_{AB}^2 H}{u} \times \left(\frac{\alpha}{\alpha - 1} \right)^2 \times \frac{(1 + k_B)^3}{k_B^2} \tag{10.1.5.8}$$

where *u* is the mobile phase's velocity.

Variables That Affect Column Performance

Using the Retention Factor to Optimize Resolution

One of the simplest ways to improve resolution is to adjust the retention factor for solute *B*. If all other terms in Equation 10.1.5.7 remain constant, an increase in k_B will improve resolution. As shown by the green curve in Figure 26.4.2 , however, the improvement is greatest if the initial value of k_B is small. Once k_B exceeds a value of approximately 10, a further increase produces only a marginal improvement in resolution. For example, if the original value of k_B is 1, increasing its value to 10 gives an 82% improvement in resolution; a further increase to 15 provides a net improvement in resolution of only 87.5%.

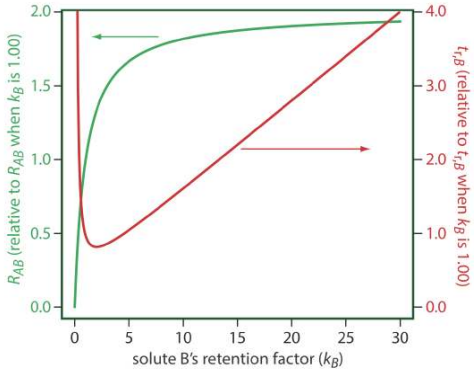


Figure 26.4.2 . Effect of k_B on the resolution for a pair of solutes, R_{AB}, and the retention time for the later eluting solute, $t_{r,B}$. The *y*-axes display the resolution and retention time relative to their respective values when k_B is 1.00.

Any improvement in resolution from increasing the value of k_B generally comes at the cost of a longer analysis time. The red curve in Figure 26.4.2 shows the relative change in the retention time for solute *B* as a function of its retention factor. Note that the minimum retention time is for $k_B = 2$. Increasing k_B from 2 to 10, for example, approximately doubles solute B's retention time.

> The relationship between retention factor and analysis time in Figure 26.4.2 works to our advantage if a separation produces an acceptable resolution with a large k_B. In this case we may be able to decrease k_B with little loss in resolution and with a significantly shorter analysis time.

To increase k_B without changing selectivity, α, any change to the chromatographic conditions must result in a general, nonselective increase in the retention factor for both solutes. In gas chromatography, we can accomplish this by decreasing the column's temperature. Because a solute's vapor pressure is smaller at lower temperatures, it spends more time in the stationary phase and takes longer to elute. In liquid chromatography, the easiest way to increase a solute's retention factor is to use a mobile phase that is a weaker solvent. When the mobile phase has a lower solvent strength, solutes spend proportionally more time in the stationary phase and take longer to elute.

Using Selectivity to Optimize Resolution

A second approach to improving resolution is to adjust the selectivity, α. In fact, for $\alpha \approx 1$ it usually is not possible to improve resolution by adjusting the solute retention factor, k_B, or the column efficiency, N. A change in α often has a more dramatic effect on resolution than a change in k_B. For example, changing α from 1.1 to 1.5, while holding constant all other terms, improves resolution by 267%. In gas chromatography, we adjust α by changing the stationary phase; in liquid chromatography, we change the composition of the mobile phase to adjust α.

To change α we need to selectively adjust individual solute retention factors. Figure 26.4.3 shows one possible approach for the liquid chromatographic separation of a mixture of substituted benzoic acids. Because the retention time of a compound's weak acid form and its weak base form are different, its retention time will vary with the pH of the mobile phase, as shown in Figure 26.4.3 a. The intersections of the curves in Figure 26.4.3 a show pH values where two solutes co-elute. For example, at a pH of 3.8 terephthalic acid and *p*-hydroxybenzoic acid elute as a single chromatographic peak.

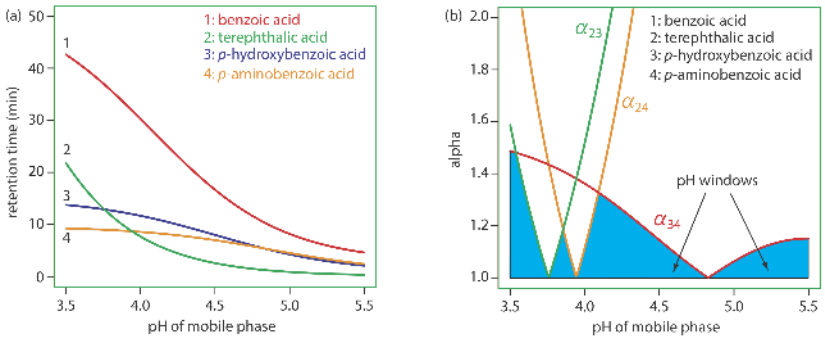


Figure 26.4.3 . Example that shows how the mobile phase pH in liquid chromatography affects selectivity: (a) retention times for four substituted benzoic acids as a function of the mobile phase's pH; (b) alpha values for three pairs of solutes that are difficult to separate. See text for details. The mobile phase is an acetic acid/sodium acetate buffer and the stationary phase is a nonpolar hydrocarbon. Data from Harvey, D. T.; Byerly, S.; Bowman, A.; Tomlin, J. "Optimization of HPLC and GC Separations Using Response Surfaces," *J. Chem. Educ.* **1991**, *68*, 162–168.

Figure 26.4.3 a shows that there are many pH values where some separation is possible. To find the optimum separation, we plot α for each pair of solutes. The red, green, and orange curves in Figure 26.4.3 b show the variation in α with pH for the three pairs of solutes that are hardest to separate (for all other pairs of solutes, $\alpha > 2$ at all pH levels). The blue shading shows windows of pH values in which at least a partial separation is possible—this figure is sometimes called a window diagram—and the highest point in each window gives the optimum pH within that range. The best overall separation is the highest point in any window, which, for this example, is a pH of 3.5. Because the analysis time at this pH is more than 40 min (Figure 26.4.3 a), choosing a pH between 4.1–4.4 might produce an acceptable separation with a much shorter analysis time.

Let's use benzoic acid, C_6H_5COOH, to explain why pH can affect a solute's retention time. The separation uses an aqueous mobile phase and a nonpolar stationary phase. At lower pHs, benzoic acid is predominately in its weak acid form, C_6H_5COOH, and partitions easily into the nonpolar stationary phase. At more basic pHs, however, benzoic acid is in its weak base form, $C_6H_5COO^-$. Because it now carries a charge, its solubility in the mobile phase increases and its solubility in the nonpolar stationary phase decreases. As a result, it spends more time in the mobile phase and has a shorter retention time.

Although the usual way to adjust pH is to change the concentration of buffering agents, it also is possible to adjust pH by changing the column's temperature because a solute's pK_a value is pH-dependent; for a review, see Gagliardi, L. G.; Tascon, M.; Castells, C. B. "Effect of Temperature on Acid–Base Equilibria in Separation Techniques: A Review," *Anal. Chim. Acta*, **2015**, *889*, 35–57.

Using Column Efficiency to Optimize Resolution

A third approach to improve resolution is to adjust the column's efficiency by increasing the number of theoretical plates, *N*. If we have values for k_B and α, then we can use Equation 10.1.5.7 to calculate the number of theoretical plates for any resolution. Table 26.4.1 provides some representative values. For example, if α = 1.05 and k_B = 2.0, a resolution of 1.25 requires approximately 24 800 theoretical plates. If our column provides only 12 400 plates, half of what is needed, then a separation is not possible. How can we double the number of theoretical plates? The easiest way is to double the length of the column, although this also doubles the analysis time. A better approach is to cut the height of a theoretical plate, *H*, in half, providing the desired resolution without changing the analysis time. Even better, if we can decrease *H* by more than 50%, it may be possible to achieve the desired resolution with an even shorter analysis time by also decreasing k_B or α.

Table 26.4.1 . Minimum Number of Theoretical Plates to Achieve Desired Resolution for Selected Values of k_B and α

	R_{AB} = 1.00		R_{AB} = 1.25		R_{AB} = 1.50	
k_B	$\alpha = 1.05$	$\alpha = 1.10$	$\alpha = 1.05$	$\alpha = 1.10$	$\alpha = 1.05$	$\alpha = 1.10$
0.5	63500	17400	99200	27200	143000	39200
1.0	28200	7740	44100	12100	63500	17400

	R_{AB} = 1.00		R_{AB} = 1.25		R_{AB} = 1.50	
k_B	$\alpha = 1.05$	$\alpha = 1.10$	$\alpha = 1.05$	$\alpha = 1.10$	$\alpha = 1.05$	$\alpha = 1.10$
1.5	19600	5380	30600	8400	44100	12100
2.0	15900	4360	24800	6810	35700	9800
3.0	12500	3440	19600	5380	28200	7740
5.0	10200	2790	15900	4360	22900	6270
10.0	8540	2340	13300	3660	19200	5270

The General Elution Problem

Adjusting the retention factor to improve the resolution between one pair of solutes may lead to unacceptably long retention times for other solutes. For example, suppose we need to analyze a four-component mixture with baseline resolution and with a run-time of less than 20 min. Our initial choice of conditions gives the chromatogram in Figure 26.4.4 a. Although we successfully separate components 3 and 4 within 15 min, we fail to separate components 1 and 2. Adjusting conditions to improve the resolution for the first two components by increasing k_2 provides a good separation of all four components, but the run-time is too long (Figure 26.4.4 b). This problem of finding a single set of acceptable operating conditions is known as the general elution problem.

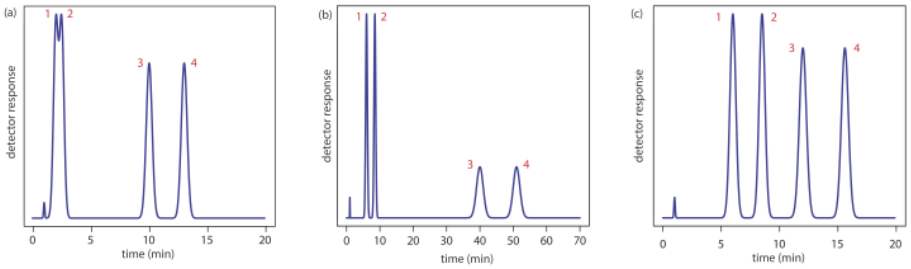


Figure 26.4.4 . Example that shows the general elution problem in chromatography. See text for details.

One solution to the general elution problem is to make incremental adjustments to the retention factor as the separation takes place. At the beginning of the separation we set the initial chromatographic conditions to optimize the resolution for early eluting solutes. As the separation progresses, we adjust the chromatographic conditions to decrease the retention factor—and, therefore, to decrease the retention time—for each of the later eluting solutes (Figure 26.4.4 c). In gas chromatography this is accomplished by temperature programming. The column's initial temperature is selected such that the first solutes to elute are resolved fully. The temperature is then increased, either continuously or in steps, to bring off later eluting components with both an acceptable resolution and a reasonable analysis time. In liquid chromatography the same effect is obtained by increasing the solvent's eluting strength. This is known as a gradient elution. We will have more to say about each of these in later sections of this chapter.

This page titled 10.1.5: Optimization and Column Performance is shared under a CC BY-NC-SA 4.0 license and was authored, remixed, and/or curated by David Harvey.

- **26.4: Optimization and Column Performance** by David Harvey is licensed CC BY-NC-SA 4.0.

10.1.6: Summary of Important Relationships for Chromatography

In this chapter we have introduced many chromatographic variables, some directly measured from the chromatogram, provided by the manufacturer, or from the operating conditions, and some derived from these variables. The following two tables summarize these variables.

Table 10.1.6.1. Chromatographic Variables Directly Measured From Chromatogram, Provided by Manufacturer, or From Operating Conditions

variable	name	source
t_r	retention time for solute	chromatogram
t_m	retention time for non-retained solute	chromatogram
w	peak width	chromatogram
u	mobile phase flow rate	operating conditions
L	length of column's stationary phase	manufacturer
d_c	diameter of column	manufacturer
d_p	diameter of packing material	manufacturer
d_f	thickness of stationary phase	manufacturer
V_s	volume of stationary phase	operating conditions

Table 10.1.6.2. Derived Chromatographic Variables

variable	name	equation to derive value
V_m	volume of mobile phase	$V_m = t_m u$
k	retention factor	$k = \frac{t_r - t_m}{t_m}$
t_r'	adjusted retention time	$t_r' = t_r - t_m$
D	distribution ratio	$D = k \times \frac{V_s}{V_m}$
α	selectivity factor	$\alpha = \frac{k_B}{k_A}$
R_{AB}	resolution	$R_{AB} = \frac{\sqrt{N_B}}{4} \times \frac{\alpha - 1}{\alpha} \times \frac{k_B}{1 + k_B}$
N	number of theoretical plates	$N = 16\left(\frac{t_r}{w}\right)^2$
H	height of theoretical plates	$H = \frac{Lw^2}{16t_r^2} = \frac{L}{N}$
H_p	height due to multiple paths	$H_p = 2\lambda d_p$
H_d	height due to longitudinal diffusion	$H_d = \frac{2\gamma D_m}{u}$
H_s	height due to mass transfer in stationary phase	$H_s = \frac{qkd_f^2}{(1+k)^2 D_s} u$
H_m	height due to mass transfer in mobile phase	$H_m = \frac{fn(d_p^2, d_c^2)}{D_m} u$

This page titled 10.1.6: Summary of Important Relationships for Chromatography is shared under a CC BY-NC-SA 4.0 license and was authored, remixed, and/or curated by David Harvey.

- **26.5: Summary of Important Relationships for Chromatography** by David Harvey is licensed CC BY-NC-SA 4.0.

10.1.7: Applications of Chromatography

Although the primary purpose of chromatography is the separation of a complex mixture into its component parts, as outlined here, a chromatographic separation also provides qualitative and quantitative information about our samples. More detailed examples of qualitative and quantitative applications are found in the chapters that follow.

Qualitative Analysis

As we learned in Section 26.2, solutes migrate through a chromatographic system at rate that is a function of the properties of the mobile phase and the stationary phase. This means that a particular solute will elute with a consistent retention time. If we expect a solute to elute with a retention time of 5.0 min, the presence of a peak at 5.0 min is suggestive of, but not definitive evidence of the solute's presence in our sample; however, the absence of a peak at 5.0 min is strong evidence that the solute is not present in our sample. For a complex mixture, this sort of screening technique is a useful qualitative application of chromatography. As we will see in the chapters that follow, the type of detector used to monitor a chromatographic separation may provide useful qualitative information.

Quantitative Analysis

A chromatographic separation yields a sequence of peaks that, ideally, represent a single solute. These peak's are characterized by an area that is proportional to the amount of analyte injected into the mobile phase. By injecting a series of standards, a calibration curve of peak area as a function of the analyte's concentration provides a way to determine the analyte's concentration in a sample. Any of the calibration strategies discussed in Chapter 1.5—external standards, standard additions, and internal standards—find use in a quantitative chromatographic analysis. Determining a solute's peak area is relatively straight-forward when using a computer-interfaced instrument with appropriate software. Alternatively, peak height, which is easier to measure, can be used as a substitute, although care must be taken to ensure that the peaks are symmetrical and that peak widths are consistent for the standards and the samples.

This page titled 10.1.7: Applications of Chromatography is shared under a CC BY-NC-SA 4.0 license and was authored, remixed, and/or curated by David Harvey.

- **26.6: Applications of Chromatography** by David Harvey is licensed CC BY-NC-SA 4.0.

10.2: GAS CHROMATOGRAPHY

In ***gas chromatography*** (GC) we inject the sample, which may be a gas or a liquid, into an gaseous mobile phase (often called the carrier gas). The mobile phase carries the sample through a packed or a capillary column that separates the sample's components based on their ability to partition between the mobile phase and the stationary phase. Figure 12.4.1 shows an example of a typical gas chromatograph, which consists of several key components: a supply of compressed gas for the mobile phase; a heated injector, which rapidly volatilizes the components in a liquid sample; a column, which is placed within an oven whose temperature we can control during the separation; and a detector to monitor the eluent as it comes off the column. Let's consider each of these components.



Figure 12.4.1 . Example of a typical gas chromatograph with insets showing the heated injection ports—note the symbol indicating that it is hot—and the oven that houses the column. This particular instrument is equipped with an autosampler for injecting samples, a capillary column, and a mass spectrometer (MS) as the detector. Note that the carrier gas is supplied by a tank of compressed gas.

MOBILE PHASE

The most common mobile phases for gas chromatography are He, Ar, and N_2, which have the advantage of being chemically inert toward both the sample and the stationary phase. The choice of carrier gas often is determined by the needs of instrument's detector. For a packed column the mobile phase velocity usually is 25–150 mL/min. The typical flow rate for a capillary column is 1–25 mL/min.

CHROMATOGRAPHIC COLUMNS

There are two broad classes of chromatographic columns: packed columns and capillary columns. In general, a packed column can handle larger samples and a capillary column can separate more complex mixtures.

PACKED COLUMNS

Packed columns are constructed from glass, stainless steel, copper, or aluminum, and typically are 2–6 m in length with internal diameters of 2–4 mm. The column is filled with a particulate solid support, with particle diameters ranging from 37–44 μm to 250–354 μm. Figure 12.4.2 shows a typical example of a packed column.

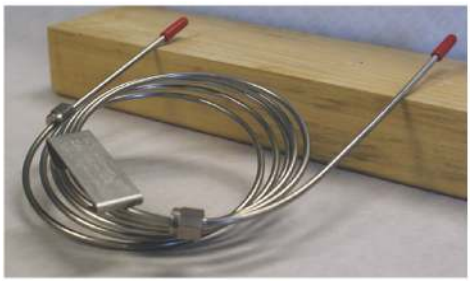


Figure 12.4.2 . Typical example of a packed column for gas chromatography. This column is made from stainless steel and is 2 m long with an internal diameter of 3.2 mm. The packing material in this column has a particle diameter of 149–177 μm. To put this in perspective, beach sand has a typical diameter of 700 μm and the diameter of fine grained sand is 250 μm.

The most widely used particulate support is diatomaceous earth, which is composed of the silica skeletons of diatoms. These particles are very porous, with surface areas ranging from 0.5–7.5 m^2/g, which provides ample contact between the mobile phase and the stationary phase. When hydrolyzed, the surface of a diatomaceous earth contains silanol groups (–SiOH), that serve as active sites for absorbing solute molecules in gas-solid chromatography (GSC).

In ***gas-liquid chromatography*** (GLC), we coat the packing material with a liquid mobile phase. To prevent uncoated packing material from adsorbing solutes, which degrades the quality of the separation, surface silanols are deactivated by reacting them with dimethyldichlorosilane and rinsing with an alcohol—typically methanol—before coating the particles with stationary phase.

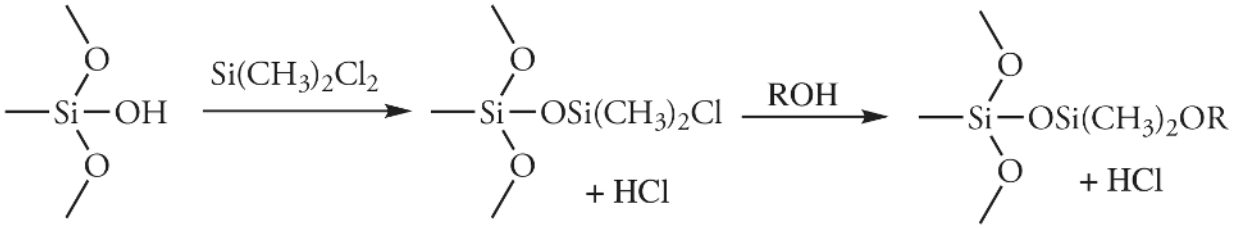


Figure 12.4.2 , for example, has approximately 1800 plates/m, or a total of approximately 3600 theoretical plates. If we assume a V_{max}/V_{min} ≈ 50, then it has a peak capacity (equation 12.2.16) of

$$n_c = 1 + \frac{\sqrt{3600}}{4}\ln(50) \approx 60$$

CAPILLARY COLUMNS

A capillary, or ***open tubular column*** is constructed from fused silica and is coated with a protective polymer coating. Columns range from 15–100 m in length with an internal diameter of approximately 150–300 μm. Figure 12.4.3 shows an example of a typical capillary column.



Figure 12.4.3 . Typical example of a capillary column for gas chromatography. This column is 30 m long with an internal diameter of 247 μm. The interior surface of the capillary has a 0.25 μm coating of the liquid phase.

Capillary columns are of three principal types. In a ***wall-coated open tubular column*** (WCOT) a thin layer of stationary phase, typically 0.25 nm thick, is coated on the capillary's inner wall. In a ***porous-layer open tubular column*** (PLOT), a porous solid support—alumina, silica gel, and molecular sieves are typical examples—is attached to the capillary's inner wall. A ***support-coated open tubular column*** (SCOT) is a PLOT column that includes a liquid stationary phase. Figure 12.4.4 shows the differences between these types of capillary columns.

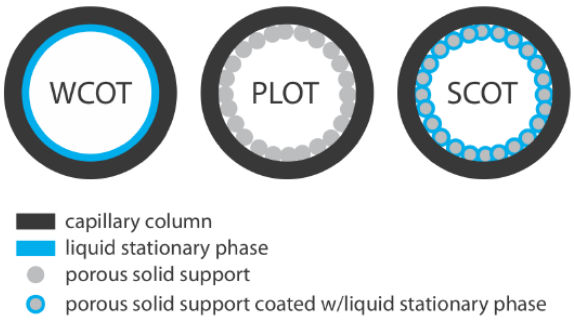


Figure 12.4.4 . Cross sections through the three types of capillary columns.

A capillary column provides a significant improvement in separation efficiency because it has more theoretical plates per meter and is longer than a packed column. For example, the capillary column in Figure 12.4.3 has almost 4300 plates/m, or a total of 129 000 theoretical plates. If we assume a V_{max}/V_{min} ≈ 50, then it has a peak capacity of approximately 350. On the other hand, a packed column can handle a larger sample. Because of its smaller diameter, a capillary column requires a smaller sample, typically less than 10^{-2} μL.

STATIONARY PHASES FOR GAS-LIQUID CHROMATOGRAPHY

Elution order in gas–liquid chromatography depends on two factors: the boiling point of the solutes, and the interaction between the solutes and the stationary phase. If a mixture's components have significantly different boiling points, then the choice of stationary phase is less critical. If two solutes have similar boiling points, then a separation is possible only if the stationary phase selectively interacts with one of the solutes. As a general rule, nonpolar solutes are separated more easily when using a nonpolar stationary phase, and polar solutes are easier to separate when using a polar stationary phase.

There are several important criteria for choosing a stationary phase: it must not react with the solutes, it must be thermally stable, it must have a low volatility, and it must have a polarity that is appropriate for the sample's components. Table 12.4.1 summarizes the properties of several popular stationary phases.

Table 12.4.1 . Selected Examples of Stationary Phases for Gas-Liquid Chromatography

stationary phase	polarity	trade name	temperature limit (°C)	representative applications
squalane	nonpolar	Squalane	150	low-boiling aliphatics hydrocarbons
Apezion L	nonpolar	Apezion L	300	amides, fatty acid methyl esters, terpenoids
polydimethyl siloxane	slightly polar	SE-30	300–350	alkaloids, amino acid derivatives, drugs, pesticides, phenols, steroids
phenylmethyl polysiloxane (50% phenyl, 50% methyl)	moderately polar	OV-17	375	alkaloids, drugs, pesticides, polyaromatic hydrocarbons, polychlorinated biphenyls
trifluoropropylmethyl polysiloxane (50% trifluoropropyl, 50% methyl)	moderately polar	OV-210	275	alkaloids, amino acid derivatives, drugs, halogenated compounds, ketones
cyanopropylphenylmethyl polysiloxane (50%cyanopropyl, 50% phenylmethyl)	polar	OV-225	275	nitriles, pesticides, steroids
polyethylene glycol	polar	Carbowax 20M	225	aldehydes, esters, ethers, phenols

Many stationary phases have the general structure shown in Figure 12.4.5 a. A stationary phase of polydimethyl siloxane, in which all the –R groups are methyl groups, $–CH_3$, is nonpolar and often makes a good first choice for a new separation. The order of elution when using polydimethyl siloxane usually follows the boiling points of the solutes, with lower boiling solutes eluting first. Replacing some of the methyl groups with other substituents increases the stationary phase's polarity and provides greater selectivity. For example, replacing 50% of the $–CH_3$ groups with phenyl groups, $–C_6H_5$, produces a slightly polar stationary phase. Increasing polarity is provided by substituting trifluoropropyl, $–C_3H_6CF$, and cyanopropyl, $–C_3H_6CN$, functional groups, or by using a stationary phase of polyethylene glycol (Figure 12.4.5 b).

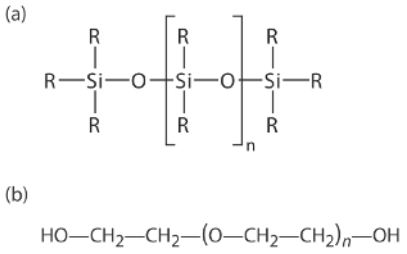


Figure 12.4.5 . General structures of common stationary phases: (a) substituted polysiloxane; (b) polyethylene glycol.

An important problem with all liquid stationary phases is their tendency to elute, or ***bleed*** from the column when it is heated. The temperature limits in Table 12.4.1 minimize this loss of stationary phase. Capillary columns with bonded or cross-linked stationary phases provide superior stability. A bonded stationary phase is attached chemically to the capillary's silica surface. Cross-linking, which is done after the stationary phase is in the capillary column, links together separate polymer chains to provide greater stability.

Another important consideration is the thickness of the stationary phase. From equation 12.3.7 we know that separation efficiency improves with thinner films of stationary phase. The most common thickness is 0.25 μm, although a thicker films is useful for highly volatile solutes, such as gases, because it has a greater capacity for retaining such solutes. Thinner films are used when separating low volatility solutes, such as steroids.

A few stationary phases take advantage of chemical selectivity. The most notable are stationary phases that contain chiral functional groups, which are used to separate enantiomers [Hinshaw, J. V. *LC .GC* **1993**, *11*, 644–648].

SAMPLE INTRODUCTION

Three factors determine how we introduce a sample to the gas chromatograph. First, all of the sample's constituents must be volatile. Second, the analytes must be present at an appropriate concentration. Finally, the physical process of injecting the sample must not degrade the separation. Each of these needs is considered in this section.

PREPARING A VOLATILE SAMPLE

Not every sample can be injected directly into a gas chromatograph. To move through the column, the sample's constituents must be sufficiently volatile. A solute of low volatility, for example, may be retained by the column and continue to elute during the analysis of subsequent samples. A nonvolatile solute will condense at the top of the column, degrading the column's performance.

We can separate a sample's volatile analytes from its nonvolatile components using any of the extraction techniques described in Chapter 7. A liquid–liquid extraction of analytes from an aqueous matrix into methylene chloride or another organic solvent is a common choice. Solid-phase extractions also are used to remove a sample's nonvolatile components.

An attractive approach to isolating analytes is a ***solid-phase microextraction*** (SPME). In one approach, which is illustrated in Figure 12.4.6 , a fused-silica fiber is placed inside a syringe needle. The fiber, which is coated with a thin film of an adsorbent material, such as polydimethyl siloxane, is lowered into the sample by depressing a plunger and is exposed to the sample for a predetermined time. After withdrawing the fiber into the needle, it is transferred to the gas chromatograph for analysis.

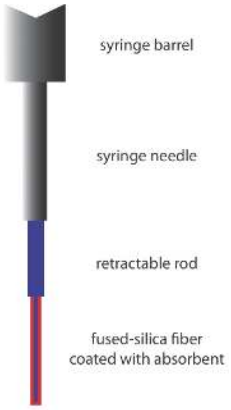


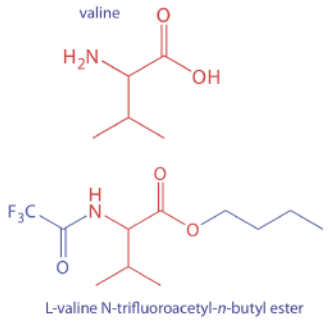
Figure 12.4.6 . Schematic diagram of a solid-phase microextraction device. The absorbent is shown in red.

Two additional methods for isolating volatile analytes are a purge-and-trap and headspace sampling. In a ***purge-and-trap***, we bubble an inert gas, such as He or N_2, through the sample, releasing—or purging—the volatile compounds. These compounds are carried by the purge gas through a trap that contains an absorbent material, such as Tenax, where they are retained. Heating the trap and back-flushing with carrier gas transfers the volatile compounds to the gas chromatograph. In ***headspace sampling*** we place the sample in a closed vial with an overlying air space. After allowing time for the volatile analytes to equilibrate between the sample and the overlying air, we use a syringe to extract a portion of the vapor phase and inject it into the gas chromatograph. Alternatively, we can sample the headspace with an SPME.

Thermal desorption is a useful method for releasing volatile analytes from solids. We place a portion of the solid in a glass-lined, stainless steel tube. After purging with carrier gas to remove any O_2 that might be present, we heat the sample. Volatile analytes are swept from the tube by an inert gas and carried to the GC. Because volatilization is not a rapid process, the volatile analytes often are concentrated at the top of the column by cooling the column inlet below room temperature, a process known as ***cryogenic focusing***. Once volatilization is complete, the column inlet is heated rapidly, releasing the analytes to travel through the column.

> The reason for removing O_2 is to prevent the sample from undergoing an oxidation reaction when it is heated.

To analyze a nonvolatile analyte we must convert it to a volatile form. For example, amino acids are not sufficiently volatile to analyze directly by gas chromatography. Reacting an amino acid, such as valine, with 1-butanol and acetyl chloride produces an esterified amino acid. Subsequent treatment with trifluoroacetic acid gives the amino acid's volatile N-trifluoroacetyl-*n*-butyl ester derivative.



L-valine N-trifluoroacetyl-*n*-butyl ester

ADJUSTING THE ANALYTE'S CONCENTRATION

In an analyte's concentration is too small to give an adequate signal, then we must concentrate the analyte before we inject the sample into the gas chromatograph. A side benefit of many extraction methods is that they often concentrate the analytes. Volatile organic materials isolated from an aqueous sample by a purge-and-trap, for example, are concentrated by as much as 1000×.

If an analyte is too concentrated, it is easy to overload the column, resulting in peak fronting (see Figure 12.2.7) and a poor separation. In addition, the analyte's concentration may exceed the detector's linear response. Injecting less sample or diluting the sample with a volatile solvent, such as methylene chloride, are two possible solutions to this problem.

INJECTING THE SAMPLE

In Chapter 12.3 we examined several explanations for why a solute's band increases in width as it passes through the column, a process we called band broadening. We also introduce an additional source of band broadening if we fail to inject the sample into the minimum possible volume of mobile phase. There are two principal sources of this precolumn band broadening: injecting the sample into a moving stream of mobile phase and injecting a liquid sample instead of a gaseous sample. The design of a gas chromatograph's injector helps minimize these problems.

An example of a simple injection port for a packed column is shown in Figure 12.4.7 . The top of the column fits within a heated injector block, with carrier gas entering from the bottom. The sample is injected through a rubber septum using a microliter syringe, such as the one shown in in Figure 12.4.8 . Injecting the sample directly into the column minimizes band broadening because it mixes the sample with the smallest possible amount of carrier gas. The injector block is heated to a temperature at least 50°C above the boiling point of the least volatile solute, which ensures a rapid vaporization of the sample's components.

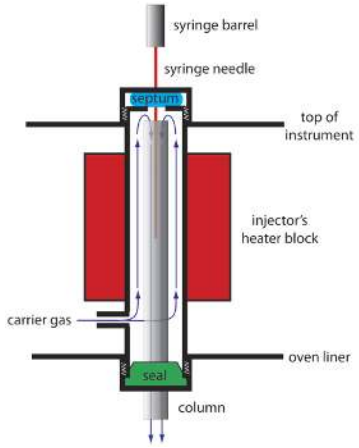


Figure 12.4.7 . Schematic diagram of a heated GC injector port for use with packed columns. The needle pierces a rubber septum and enters into the top of the column, which is located within a heater block.



Figure 12.4.8 . Example of a syringe for injecting samples into a gas chromatograph. This syringe has a maximum capacity of 10 μL with graduations every 0.1 μL.

Because a capillary column's volume is significantly smaller than that for a packed column, it requires a different style of injector to avoid overloading the column with sample. Figure 12.4.9 shows a schematic diagram of a typical split/splitless injector for use with a capillary column.

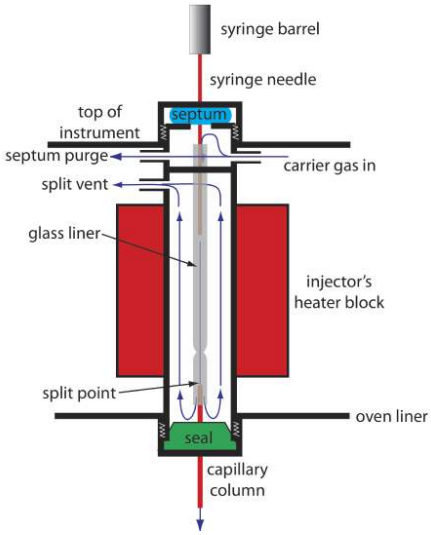


Figure 12.4.9 . Schematic diagram of a split/splitless injection port for use with capillary columns. The needle pierces a rubber septum and enters into a glass liner, which is located within a heater block. In a split injection the split vent is open; the split vent is closed for a splitless injection.

In a ***split injection*** we inject the sample through a rubber septum using a microliter syringe. Instead of injecting the sample directly into the column, it is injected into a glass liner where it mixes with the carrier gas. At the split point, a small fraction of the carrier gas and sample enters the capillary column with the remainder exiting through the split vent. By controlling the flow rate of the carrier gas as it enters the injector, and its flow rate through the septum purge and the split vent, we can control the fraction of sample that enters the capillary column, typically 0.1–10%.

> For example, if the carrier gas flow rate is 50 mL/min, and the flow rates for the septum purge and the split vent are 2 mL/min and 47 mL/min, respectively, then the flow rate through the column is 1 mL/min (= 50 – 2 – 47). The ratio of sample entering the column is 1/50, or 2%.

In a ***splitless injection***, which is useful for trace analysis, we close the split vent and allow all the carrier gas that passes through the glass liner to enter the column—this allows virtually all the sample to enters the column. Because the flow rate through the injector is low, significant precolumn band broadening is a problem. Holding the column's temperature approximately 20–25ºC below the solvent's boiling point allows the solvent to condense at the entry to the capillary column, forming a barrier that traps the solutes. After allowing the solutes to concentrate, the column's temperature is increased and the separation begins.

For samples that decompose easily, an ***on-column injection*** may be necessary. In this method the sample is injected directly into the column without heating. The column temperature is then increased, volatilizing the sample with as low a temperature as is practical.

TEMPERATURE CONTROL

Control of the column's temperature is critical to attaining a good separation when using gas chromatography. For this reason the column is placed inside a thermostated oven (see Figure 12.4.1). In an ***isothermal*** separation we maintain the column at a constant temperature. To increase the interaction between the solutes and the stationary phase, the temperature usually is set slightly below that of the lowest-boiling solute.

One difficulty with an isothermal separation is that a temperature that favors the separation of a low-boiling solute may lead to an unacceptably long retention time for a higher-boiling solute. ***Temperature programming*** provides a solution to this problem. At the beginning of the analysis we set the column's initial temperature below that for the lowest-boiling solute. As the separation progresses, we slowly increase the temperature at either a uniform rate or in a series of steps.

DETECTORS FOR GAS CHROMATOGRAPHY

The final part of a gas chromatograph is the detector. The ideal detector has several desirable features: a low detection limit, a linear response over a wide range of solute concentrations (which makes quantitative work easier), sensitivity for all solutes or selectivity for a specific class of solutes, and an insensitivity to a change in flow rate or temperature.

THERMAL CONDUCTIVITY DETECTOR (TCD)

One of the earliest gas chromatography detectors takes advantage of the mobile phase's thermal conductivity. As the mobile phase exits the column it passes over a tungsten-rhenium wire filament (see Figure 12.4.10 . The filament's electrical resistance depends on its temperature,

which, in turn, depends on the thermal conductivity of the mobile phase. Because of its high thermal conductivity, helium is the mobile phase of choice when using a ***thermal conductivity detector*** (TCD).

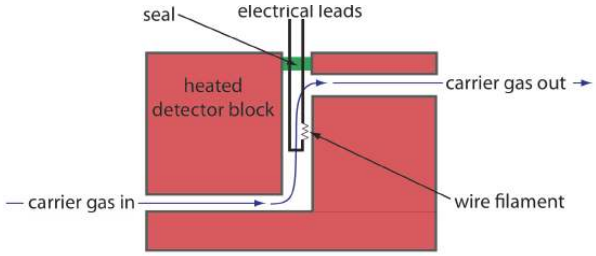


Figure 12.4.10 . Schematic diagram of a thermal conductivity detector showing one cell of a matched pair. The sample cell takes the carrier gas as it elutes from the column. A source of carrier gas that bypasses the column passes through a reference cell.

> Thermal conductivity, as the name suggests, is a measure of how easily a substance conducts heat. A gas with a high thermal conductivity moves heat away from the filament—and, thus, cools the filament—more quickly than does a gas with a low thermal conductivity.

When a solute elutes from the column, the thermal conductivity of the mobile phase in the TCD cell decreases and the temperature of the wire filament, and thus it resistance, increases. A reference cell, through which only the mobile phase passes, corrects for any time-dependent variations in flow rate, pressure, or electrical power, all of which affect the filament's resistance.

Because all solutes affect the mobile phase's thermal conductivity, the thermal conductivity detector is a universal detector. Another advantage is the TCD's linear response over a concentration range spanning 10^4–10^5 orders of magnitude. The detector also is non-destructive, which allows us to recover analytes using a postdetector cold trap. One significant disadvantage of the TCD detector is its poor detection limit for most analytes.

FLAME IONIZATION DETECTOR (FID)

The combustion of an organic compound in an H_2/air flame results in a flame that contains electrons and organic cations, presumably CHO^+. Applying a potential of approximately 300 volts across the flame creates a small current of roughly 10^{-9} to 10^{-12} amps. When amplified, this current provides a useful analytical signal. This is the basis of the popular ***flame ionization detector,*** a schematic diagram of which is shown in Figure 12.4.11 .

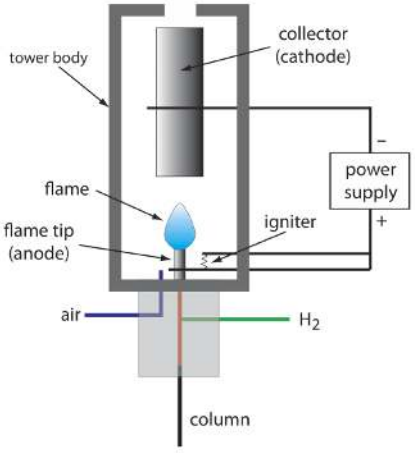


Figure 12.4.11 . Schematic diagram of a flame ionization detector. The eluent from the column mixes with H_2 and is burned in the presence of excess air. Combustion produces a flame that contains electrons and the cation $CHO^{+\cdot}$ Applying a potential between the flame's tip and the collector gives a current that is proportional to the concentration of cations in the flame.

Most carbon atoms—except those in carbonyl and carboxylic groups—generate a signal, which makes the FID an almost universal detector for organic compounds. Most inorganic compounds and many gases, such as H_2O and CO_2, are not detected, which makes the FID detector a useful detector for the analysis of organic analytes in atmospheric and aqueous environmental samples. Advantages of the FID include a detection limit that is approximately two to three orders of magnitude smaller than that for a thermal conductivity detector, and a linear response over 10^6–10^7 orders of magnitude in the amount of analyte injected. The sample, of course, is destroyed when using a flame ionization detector.

ELECTRON CAPTURE DETECTOR (ECD)

The ***electron capture detector*** is an example of a selective detector. As shown in Figure 12.4.12 , the detector consists of a β-emitter, such as ^{63}Ni. The emitted electrons ionize the mobile phase, usually N_2, generating a standing current between a pair of electrodes. When a solute with a high affinity for capturing electrons elutes from the column, the current decreases, which serves as the signal. The ECD is highly selective toward solutes with electronegative functional groups, such as halogens and nitro groups, and is relatively insensitive to amines, alcohols, and hydrocarbons. Although its detection limit is excellent, its linear range extends over only about two orders of magnitude.

> A β-particle is an electron.

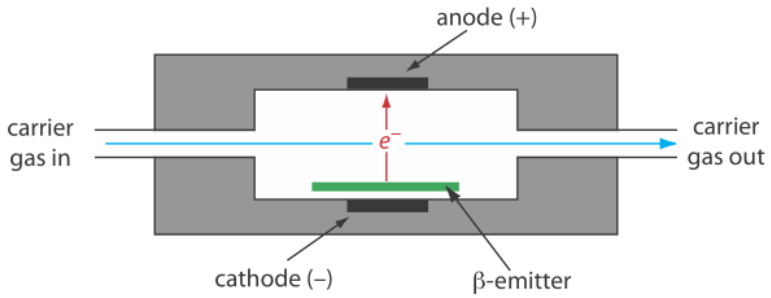


Figure 12.4.12 . Schematic diagram showing an electron capture detector.

MASS SPECTROMETER (MS)

A ***mass spectrometer*** is an instrument that ionizes a gaseous molecule using sufficient energy that the resulting ion breaks apart into smaller ions. Because these ions have different mass-to-charge ratios, it is possible to separate them using a magnetic field or an electrical field. The resulting mass spectrum contains both quantitative and qualitative information about the analyte. Figure 12.4.13 shows a mass spectrum for toluene.

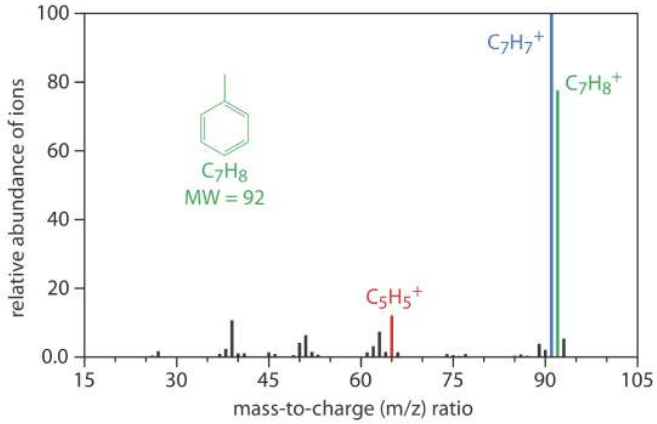


Figure 12.4.13 . Mass spectrum for toluene highlighting the molecular ion in green (m/z=92), and two fragment ions in blue (m/z=91) and in red (m/z= 65). A mass spectrum provides both quantitative and qualitative information: the height of any peak is proportional to the amount of toluene in the mass spectrometer and the fragmentation pattern is unique to toluene.

Figure 12.4.14 shows a block diagram of a typical gas chromatography-mass spectrometer (GC–MS) instrument. The effluent from the column enters the mass spectrometer's ion source in a manner that eliminates the majority of the carrier gas. In the ionization chamber the remaining molecules—a mixture of carrier gas, solvent, and solutes—undergo ionization and fragmentation. The mass spectrometer's mass analyzer separates the ions by their mass-to-charge ratio and a detector counts the ions and displays the mass spectrum.

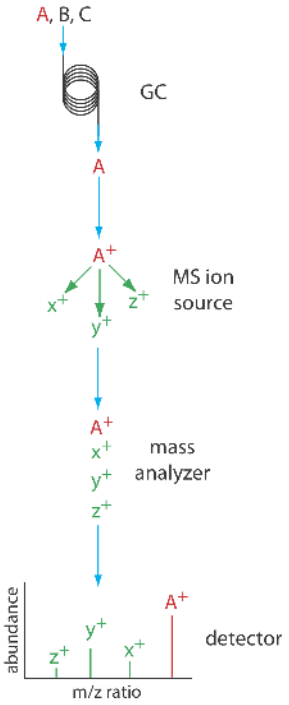


Figure 12.4.14 . Block diagram of GC– MS. A three component mixture enters the GC. When component A elutes from the column, it enters the MS ion source and ionizes to form the parent ion and several fragment ions. The ions enter the mass analyzer, which separates them by their mass-to-charge ratio, providing the mass spectrum shown at the detector.

There are several options for monitoring a chromatogram when using a mass spectrometer as the detector. The most common method is to continuously scan the entire mass spectrum and report the total signal for all ions that reach the detector during each scan. This total ion scan provides universal detection for all analytes. We can achieve some degree of selectivity by monitoring one or more specific mass-to-charge ratios, a process called selective-ion monitoring. A mass spectrometer provides excellent detection limits, typically 25 fg to 100 pg, with a linear range of 10^5 orders of magnitude. Because we continuously record the mass spectrum of the column's eluent, we can go back and examine the mass spectrum for any time increment. This is a distinct advantage for GC–MS because we can use the mass spectrum to help identify a mixture's components.

> For more details on mass spectrometry see Introduction to Mass Spectrometry by Michael Samide and Olujide Akinbo, a resource that is part of the Analytical Sciences Digital Library.

OTHER DETECTORS

Two additional detectors are similar in design to a flame ionization detector. In the flame photometric detector, optical emission from phosphorous and sulfur provides a detector selective for compounds that contain these elements. The thermionic detector responds to compounds that contain nitrogen or phosphorous.

A Fourier transform infrared spectrophotometer (FT–IR) also can serve as a detector. In GC–FT–IR, effluent from the column flows through an optical cell constructed from a 10–40 cm Pyrex tube with an internal diameter of 1–3 mm. The cell's interior surface is coated with a reflecting layer of gold. Multiple reflections of the source radiation as it is transmit- ted through the cell increase the optical path length through the sample. As is the case with GC–MS, an FT–IR detector continuously records the column eluent's spectrum, which allows us to examine the IR spectrum for any time increment.

> See Section 10.3 for a discussion of FT-IR spectroscopy and instrumentation.

QUANTITATIVE APPLICATIONS

Gas chromatography is widely used for the analysis of a diverse array of samples in environmental, clinical, pharmaceutical, biochemical, forensic, food science and petrochemical laboratories. Table 12.4.2 provides some representative examples of applications.

Table 12.4.2 . Representative Applications of Gas Chromatography

area	applications
environmental analysis	green house gases (CO_2, CH_4, NO_x) in air pesticides in water, wastewater, and soil vehicle emissions trihalomethanes in drinking water
clinical analysis	drugs blood alcohols
forensic analysis	analysis of arson accelerants detection of explosives
consumer products	volatile organics in spices and fragrances trace organics in whiskey monomers in latex paint
petrochemical and chemical industry	purity of solvents refinery gas composition of gasoline

QUANTITATIVE CALCULATIONS

In a GC analysis the area under the peak is proportional to the amount of analyte injected onto the column. A peak's area is determined by integration, which usually is handled by the instrument's computer or by an electronic integrating recorder. If two peak are resolved fully, the determination of their respective areas is straightforward.

> Before electronic integrating recorders and computers, two methods were used to find the area under a curve. One method used a manual planimeter; as you use the planimeter to trace an object's perimeter, it records the area. A second approach for finding a peak's area is the cut-and-weigh method. The chromatogram is recorded on a piece of paper and each peak of interest is cut out and weighed. Assuming the paper is uniform in thickness and density of fibers, the ratio of weights for two peaks is the same as the ratio of areas. Of course, this approach destroys your chromatogram.

Overlapping peaks, however, require a choice between one of several options for dividing up the area shared by the two peaks (Figure 12.4.15). Which method we use depends on the relative size of the two peaks and their resolution. In some cases, the use of peak heights provides more accurate results [(a) Bicking, M. K. L. Chromatography Online, April 2006; (b) Bicking, M. K. L. Chromatography Online, June 2006].

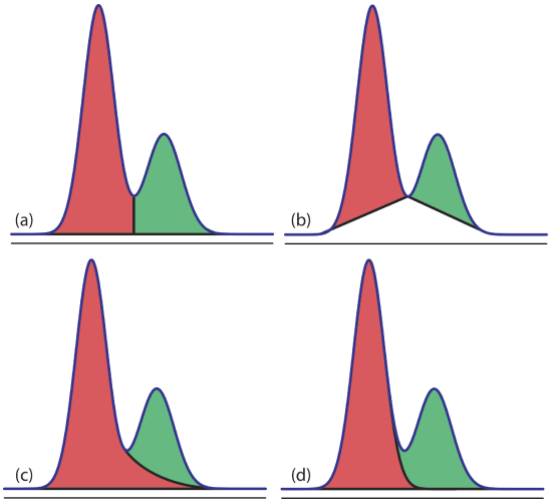


Figure 12.4.15 . Four methods for determining the areas under two overlapping chromatographic peaks: (a) the drop method; (b) the valley method; (c) the exponential skim method; and (d) the Gaussian skim method. Other methods for determining areas also are available.

For quantitative work we need to establish a calibration curve that relates the detector's response to the analyte's concentration. If the injection volume is identical for every standard and sample, then an external standardization provides both accurate and precise results. Unfortunately,even under the best conditions the relative precision for replicate injections may differ by 5%; often it is substantially worse. For quantitative work that requires high accuracy and precision, the use of internal standards is recommended.

> To review the method of internal standards, see Chapter 5.3.

EXAMPLE 12.4.1

Marriott and Carpenter report the following data for five replicate injections of a mixture that contains 1% v/v methyl isobutyl ketone and 1% v/v *p*-xylene in dichloromethane [Marriott, P. J.; Carpenter, P. D. *J. Chem. Educ.* **1996**, *73*, 96–99].

injection	peak	peak area (arb. units)
I	1	48075
	2	78112
II	1	85829
	2	135404
III	1	84136
	2	132332
IV	1	71681
	2	112889
V	1	58054
	2	91287

Assume that *p*-xylene (peak 2) is the analyte, and that methyl isobutyl ketone (peak 1) is the internal standard. Determine the 95% confidence interval for a single-point standardization with and without using the internal standard.

Solution

For a single-point external standardization we ignore the internal standard and determine the relationship between the peak area for *p*-xylene, A_2, and the concentration, C_2, of *p*-xylene.

$$A_2 = kC_2$$

Substituting the known concentration for *p*-xylene (1% v/v) and the appropriate peak areas, gives the following values for the constant *k*.

$$78112 \quad 135404 \quad 132332 \quad 112889 \quad 91287$$

The average value for *k* is 110 000 with a standard deviation of 25 100 (a relative standard deviation of 22.8%). The 95% confidence interval is

$$\mu = \overline{X} \pm \frac{ts}{\sqrt{n}} = 111000 \pm \frac{(2.78)(25100)}{\sqrt{5}} = 111000 \pm 31200$$

For an internal standardization, the relationship between the analyte's peak area, A_2, the internal standard's peak area, A_1, and their respective concentrations, C_2 and C_1, is

$$\frac{A_2}{A_1} = k\frac{C_2}{C_1}$$

Substituting in the known concentrations and the appropriate peak areas gives the following values for the constant *k*.

$$1.5917 \quad 1.5776 \quad 1.5728 \quad 1.5749 \quad 1.5724$$

The average value for *k* is 1.5779 with a standard deviation of 0.0080 (a relative standard deviation of 0.507%). The 95% confidence interval is

$$\mu = \overline{X} \pm \frac{ts}{\sqrt{n}} = 1.5779 \pm \frac{(2.78)(0.0080)}{\sqrt{5}} = 1.5779 \pm 0.0099$$

Although there is a substantial variation in the individual peak areas for this set of replicate injections, the internal standard compensates for these variations, providing a more accurate and precise calibration.

EXERCISE 12.4.1

Figure 12.4.16 shows chromatograms for five standards and for one sample. Each standard and sample contains the same concentration of an internal standard, which is 2.50 mg/mL. For the five standards, the concentrations of analyte are 0.20 mg/mL, 0.40 mg/mL, 0.60 mg/mL, 0.80 mg/mL, and 1.00 mg/mL, respectively. Determine the concentration of analyte in the sample by (a) ignoring the internal standards and creating an external standards calibration curve, and by (b) creating an internal standard calibration curve. For each approach, report the analyte's concentration and the 95% confidence interval. Use peak heights instead of peak areas.

Answer

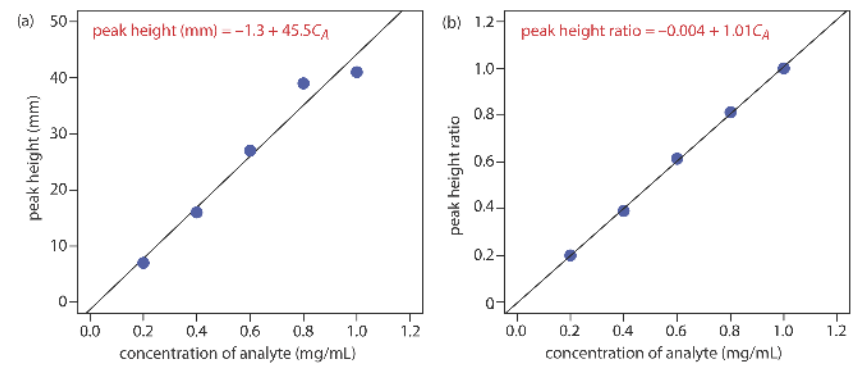
The following table summarizes my measurements of the peak heights for each standard and the sample, and their ratio (although your absolute values for peak heights will differ from mine, depending on the size of your monitor or printout, your relative peak height ratios should be similar to mine).

[standard] (mg/mL)	peak height of standard (mm)	peak height of analyte (mm)	peak height ratio
0.20	35	7	0.20
0.40	41	16	0.39
0.60	44	27	0.61
0.80	48	39	0.81
1.00	41	41	1.00
sample	39	21	0.54

Figure (a) shows the calibration curve and the calibration equation when we ignore the internal standard. Substituting the sample's peak height into the calibration equation gives the analyte's concentration in the sample as 0.49 mg/mL. The 95% confidence interval is ±0.24 mg/mL. The calibration curve shows quite a bit of scatter in the data because of uncertainty in the injection volumes.

Figure (b) shows the calibration curve and the calibration equation when we include the internal standard. Substituting the sample's peak height ratio into the calibration equation gives the analyte's concentration in the sample as 0.54 mg/mL. The 95% confidence interval is ±0.04 mg/mL.

To review the use of Excel or R for regression calculations and confidence intervals, see Chapter 5.5.



The data for this exercise were created so that the analyte's actual concentration is 0.55 mg/mL. Given the resolution of my ruler's scale, my answer is pretty reasonable. Your measurements may be slightly different, but your answers should be close to the actual values.

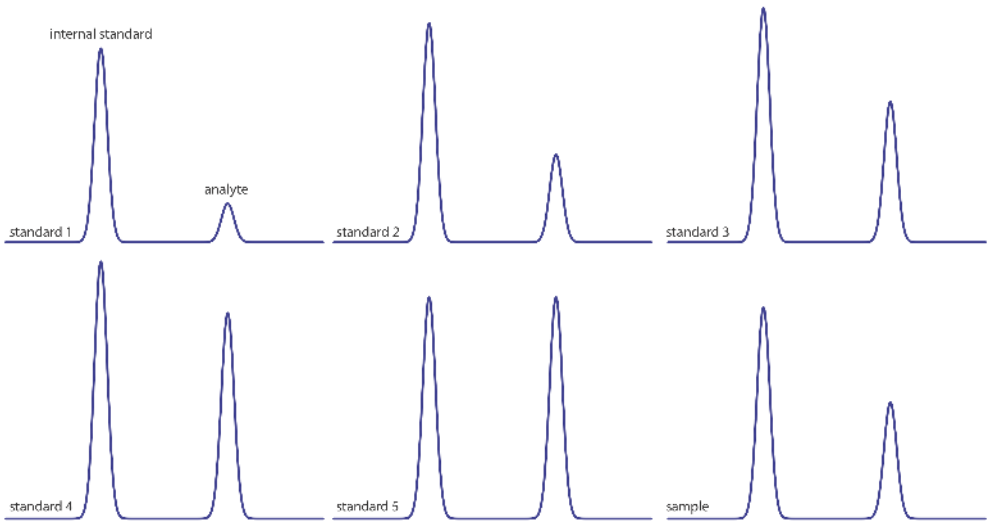


Figure 12.4.16 . Chromatograms for Practice Exercise 12.5.

QUALITATIVE APPLICATIONS

In addition to a quantitative analysis, we also can use chromatography to identify the components of a mixture. As noted earlier, when using an FT–IR or a mass spectrometer as the detector we have access to the eluent's full spectrum for any retention time. By interpreting the spectrum or by searching against a library of spectra, we can identify the analyte responsible for each chromatographic peak.

> In addition to identifying the component responsible for a particular chromatographic peak, we also can use the saved spectra to evaluate peak purity. If only one component is responsible for a chromatographic peak, then the spectra should be identical throughout the peak's elution. If a spectrum at the beginning of the peak's elution is different from a spectrum taken near the end of the peak's elution, then at least two components are co-eluting.

When using a nonspectroscopic detector, such as a flame ionization detector, we must find another approach if we wish to identify the components of a mixture. One approach is to spike a sample with the suspected compound and look for an increase in peak height. We also can compare a peak's retention time to the retention time for a known compound if we use identical operating conditions.

Because a compound's retention times on two identical columns are not likely to be the same—differences in packing efficiency, for example, will affect a solute's retention time on a packed column—creating a table of standard retention times is not possible. ***Kovat's retention index*** provides one solution to the problem of matching retention times. Under isothermal conditions, the adjusted retention times for normal alkanes increase logarithmically. Kovat defined the retention index, I, for a normal alkane as 100 times the number of carbon atoms. For example, the retention index is 400 for butane, C_4H_{10}, and 500 for pentane, C_5H_{12}. To determine the a compound's retention index, I_{cpd}, we use the following formula

$$I_{cpd} = 100 \times \frac{\log t'_{r,cpd} - \log t'_{r,x}}{\log t'_{r,x+1} - \log t'_{r,x}} + I_x \tag{10.2.1}$$

where $t'_{r,cpd}$ is the compound's adjusted retention time, $t'_{r,x}$ and $t'_{r,x+1}$ are the adjusted retention times for the normal alkanes that elute immediately before the compound and immediately after the compound, respectively, and I_x is the retention index for the normal alkane that elutes immediately before the compound. A compound's retention index for a particular set of chromatographic conditions—stationary phase, mobile phase, column type, column length, temperature, etc.—is reasonably consistent from day- to-day and between different columns and instruments.

> Tables of Kovat's retention indices are available; see, for example, the NIST Chemistry Webbook. A search for toluene returns 341 values of I for over 20 different stationary phases, and for both packed columns and capillary columns.

✔ EXAMPLE 12.4.2

In a separation of a mixture of hydrocarbons the following adjusted retention times are measured: 2.23 min for propane, 5.71 min for isobutane, and 6.67 min for butane. What is the Kovat's retention index for each of these hydrocarbons?

Solution

Kovat's retention index for a normal alkane is 100 times the number of carbons; thus, for propane, I = 300 and for butane, I = 400. To find Kovat's retention index for isobutane we use Equation 10.2.1.

$$I_{\text{isobutane}} = 100 \times \frac{\log(5.71) - \log(2.23)}{\log(6.67) - \log(2.23)} + 300 = 386$$

? EXERCISE 12.4.2

When using a column with the same stationary phase as in Example 12.4.2 , you find that the retention times for propane and butane are 4.78 min and 6.86 min, respectively. What is the expected retention time for isobutane?

Answer

Because we are using the same column we can assume that isobutane's retention index of 386 remains unchanged. Using Equation 10.2.1, we have

$$386 = 100 \times \frac{\log x - \log(4.78)}{\log(6.86) - \log(4.78)} + 300$$

where x is the retention time for isobutane. Solving for x, we find that

$$0.86 = \frac{\log x - \log(4.78)}{\log(6.86) - \log(4.78)}$$

$$0.135 = \log x - 0.679$$

$$0.814 = \log x$$

$$x = 6.52$$

the retention time for isobutane is 6.5 min.

The best way to appreciate the theoretical and the practical details discussed in this section is to carefully examine a typical analytical method. Although each method is unique, the following description of the determination of trihalomethanes in drinking water provides an instructive example of a typical procedure. The description here is based on a Method 6232B in *Standard Methods for the Examination of Water and Wastewater*, 20th Ed., American Public Health Association: Washing- ton, DC, 1998.

REPRESENTATIVE METHOD 12.4.1: DETERMINATION OF TRIHALOMETHANES IN DRINKING WATER

Description of Method

Trihalomethanes, such as chloroform, $CHCl_3$, and bromoform, $CHBr_3$, are found in most chlorinated waters. Because chloroform is a suspected carcinogen, the determination of trihalomethanes in public drinking water supplies is of considerable importance. In this method the trihalomethanes $CHCl_3$, $CHBrCl_2$, $CHBr_2Cl$, and $CHBr_3$ are isolated using a liquid–liquid extraction with pentane and determined using a gas chromatograph equipped with an electron capture detector.

Procedure

Collect the sample in a 40-mL glass vial equipped with a screw-cap lined with a TFE-faced septum. Fill the vial until it overflows, ensuring that there are no air bubbles. Add 25 mg of ascorbic acid as a reducing agent to quench the further production of trihalomethanes. Seal the vial and store the sample at 4°C for no longer than 14 days.

Prepare a standard stock solution for each trihalomethane by placing 9.8 mL of methanol in a 10-mL volumetric flask. Let the flask stand for 10 min, or until all surfaces wetted with methanol are dry. Weigh the flask to the nearest ±0.1 mg. Using a 100-µL syringe, add 2 or more drops of trihalomethane to the volumetric flask, allowing each drop to fall directly into the methanol. Reweigh the flask before diluting to volume and mixing. Transfer the solution to a 40-mL glass vial equipped with a TFE-lined screw-top and report the concentration in µg/mL. Store the stock solutions at –10 to –20°C and away from the light.

Prepare a multicomponent working standard from the stock standards by making appropriate dilutions of the stock solution with methanol in a volumetric flask. Choose concentrations so that calibration standards (see below) require no more than 20 µL of working standard per 100 mL of water.

Using the multicomponent working standard, prepare at least three, but preferably 5–7 calibration standards. At least one standard must be near the detection limit and the standards must bracket the expected concentration of trihalomethanes in the samples. Using an appropriate volumetric flask, prepare the standards by injecting at least 10 µL of the working standard below the surface of the water and dilute to volume. Gently mix each standard three times only. Discard the solution in the neck of the volumetric flask and then transfer the remaining solution to a 40-mL glass vial with a TFE-lined screw-top. If the standard has a headspace, it must be analyzed within 1 hr; standards without a headspace may be held for up to 24 hr.

Prepare an internal standard by dissolving 1,2-dibromopentane in hexane. Add a sufficient amount of this solution to pentane to give a final concentration of 30 µg 1,2-dibromopentane/L.

To prepare the calibration standards and samples for analysis, open the screw top vial and remove 5 mL of the solution. Recap the vial and weigh to the nearest ±0.1 mg. Add 2.00 mL of pentane (with the internal standard) to each vial and shake vigorously for 1 min. Allow the two phases to separate for 2 min and then use a glass pipet to transfer at least 1 mL of the pentane (the upper phase) to a 1.8-mL screw top sample vial equipped with a TFE septum, and store at 4°C until you are ready to inject them into the GC. After emptying, rinsing, and drying the sample's original vial, weigh it to the nearest ±0.1 mg and calculate the sample's weight to ±0.1 g. If the density is 1.0 g/mL, then the sample's weight is equivalent to its volume.

Inject a 1–5 µL aliquot of the pentane extracts into a GC equipped with a 2-mm ID, 2-m long glass column packed with a stationary phase of 10% squalane on a packing material of 80/100 mesh Chromosorb WAW. Operate the column at 67°C and a flow rate of 25 mL/min.

A variety of other columns can be used. Another option, for example, is a 30-m fused silica column with an internal diameter of 0.32 mm and a 1 µm coating of the stationary phase DB-1. A linear flow rate of 20 cm/s is used with the following temperature program: hold for 5 min at 35°C; increase to 70°C at 10°C/min; increase to 200°C at 20°C/min.

Questions

1. A simple liquid–liquid extraction rarely extracts 100% of the analyte. How does this method account for incomplete extractions?

Because we use the same extraction procedure for the samples and the standards, we reasonably expect that the extraction efficiency is the same for all samples and standards; thus, the relative amount of analyte in any two samples or standards is unaffected by an incomplete extraction.

2. Water samples are likely to contain trace amounts of other organic compounds, many of which will extract into pentane along with the trihalomethanes. A short, packed column, such as the one used in this method, generally does not do a particularly good job of resolving chromatographic peaks. Why do we not need to worry about these other compounds?

An electron capture detector responds only to compounds, such as the trihalomethanes, that have electronegative functional groups. Because an electron capture detector will not respond to most of the potential interfering compounds, the chromatogram will have relatively few peaks other than those for the trihalomethanes and the internal standard.

3. Predict the order in which the four analytes elute from the GC column.

Retention time should follow the compound's boiling points, eluting from the lowest boiling point to the highest boiling points. The expected elution order is $CHCl_3$ (61.2°C), $CHCl_2Br$ (90°C), $CHClBr_2$ (119°C), and $CHBr_3$ (149.1°C).

4. Although chloroform is an analyte, it also is an interferent because it is present at trace levels in the air. Any chloroform present in the laboratory air, for example, may enter the sample by diffusing through the sample vial's silicon septum. How can we determine whether samples are contaminated in this manner?

A sample blank of trihalomethane-free water is kept with the samples at all times. If the sample blank shows no evidence for chloroform, then we can safely assume that the samples also are free from contamination.

5. Why is it necessary to collect samples without a headspace (a layer of air that overlays the liquid) in the sample vial?

Because trihalomethanes are volatile, the presence of a headspace allows for the loss of analyte from the sample to the headspace, resulting in a negative determinate error.

6. In preparing the stock solution for each trihalomethane, the procedure specifies that we add two or more drops of the pure compound by dropping them into a volumetric flask that contains methanol. When preparing the calibration standards, however, the working standard must be injected below the surface of the methanol. Explain the reason for this difference.

When preparing a stock solution, the potential loss of the volatile trihalomethane is unimportant because we determine its concentration by weight after adding it to the methanol and diluting to volume. When we prepare the calibration standard, however, we must ensure that the addition of trihalomethane is quantitative; thus, we inject it below the surface to avoid the potential loss of analyte.

EVALUATION

SCALE OF OPERATION

Gas chromatography is used to analyze analytes present at levels ranging from major to ultratrace components. Depending on the detector, samples with major and minor analytes may need to be diluted before analysis. The thermal conductivity and flame ionization detectors can handle larger amounts of analyte; other detectors, such as an electron capture detector or a mass spectrometer, require substantially smaller amounts of analyte. Although the injection volume for gas chromatography is quite small—typically about a microliter—the amount of available sample must be sufficient that the injection is a representative subsample. For a trace analyte, the actual amount of injected analyte is often in the picogram range. Using Representative Method 12.4.1 as an example, a 3.0-μL injection of 1 μg/L $CHCl_3$ is equivalent to 15 pg of $CHCl_3$, assuming a 100% extraction efficiency.

ACCURACY

The accuracy of a gas chromatographic method varies substantially from sample-to-sample. For routine samples, accuracies of 1–5% are common. For analytes present at very low concentration levels, for samples with complex matrices, or for samples that require significant processing before analysis, accuracy may be substantially poorer. In the analysis for trihalomethanes described in Representative Method 12.4.1, for example, determinate errors as large as ±25% are possible.

PRECISION

The precision of a gas chromatographic analysis includes contributions from sampling, sample preparation, and the instrument. The relative standard deviation due to the instrument typically is 1–5%, although it can be significantly higher. The principal limitations are detector noise, which affects the determination of peak area, and the reproducibility of injection volumes. In quantitative work, the use of an internal standard compensates for any variability in injection volumes.

SENSITIVITY

In a gas chromatographic analysis, sensitivity is determined by the detector's characteristics. Of particular importance for quantitative work is the detector's linear range; that is, the range of concentrations over which a calibration curve is linear. Detectors with a wide linear range, such as the thermal conductivity detector and the flame ionization detector, can be used to analyze samples over a wide range of concentrations without adjusting operating conditions. Other detectors, such as the electron capture detector, have a much narrower linear range.

SELECTIVITY

Because it combines separation with analysis, chromatographic methods provide excellent selectivity. By adjusting conditions it usually is possible to design a separation so that the analytes elute by themselves, even when the mixture is complex. Additional selectivity is obtained by using a detector, such as the electron capture detector, that does not respond to all compounds.

TIME, COST, AND EQUIPMENT

Analysis time can vary from several minutes for samples that contain only a few constituents, to more than an hour for more complex samples. Preliminary sample preparation may substantially increase the analysis time. Instrumentation for gas chromatography ranges in price from inexpensive (a few thousand dollars) to expensive (>$50,000). The more expensive models are designed for capillary columns, include a variety of injection options, and use more sophisticated detectors, such as a mass spectrometer, or include multiple detectors. Packed columns typically cost <$200, and the cost of a capillary column is typically $300–$1000.

This page titled 10.2: Gas Chromatography is shared under a CC BY-NC-SA 4.0 license and was authored, remixed, and/or curated by David Harvey.

- **12.4: Gas Chromatography** by David Harvey is licensed CC BY-NC-SA 4.0.

10.2.1: Gas Chromatography

Gas chromatography is a term used to describe the group of analytical separation techniques used to analyze volatile substances in the gas phase. In gas chromatography, the components of a sample are dissolved in a solvent and vaporized in order to separate the analytes by distributing the sample between two phases: a stationary phase and a mobile phase. The mobile phase is a chemically inert gas that serves to carry the molecules of the analyte through the heated column. Gas chromatography is one of the sole forms of chromatography that does not utilize the mobile phase for interacting with the analyte. The stationary phase is either a solid adsorbant, termed gas-solid chromatography (GSC), or a liquid on an inert support, termed gas-liquid chromatography (GLC).

Introduction

In early 1900s, Gas chromatography (GC) was discovered by Mikhail Semenovich Tsvett as a separation technique to separate compounds. In organic chemistry, liquid-solid column chromatography is often used to separate organic compounds in solution. Among the various types of gas chromatography, gas-liquid chromatography is the method most commonly used to separate organic compounds. The combination of gas chromatography and mass spectrometry is an invaluable tool in the identification of molecules. A typical gas chromatograph consists of an injection port, a column, carrier gas flow control equipment, ovens and heaters for maintaining temperatures of the injection port and the column, an integrator chart recorder and a detector.

To separate the compounds in gas-liquid chromatography, a solution sample that contains organic compounds of interest is injected into the sample port where it will be vaporized. The vaporized samples that are injected are then carried by an inert gas, which is often used by helium or nitrogen. This inert gas goes through a glass column packed with silica that is coated with a liquid. Materials that are less soluble in the liquid will increase the result faster than the material with greater solubility.The purpose of this module is to provide a better understanding on its separation and measurement techniques and its application.

In GLC, the liquid stationary phase is adsorbed onto a solid inert packing or immobilized on the capillary tubing walls. The column is considered packed if the glass or metal column tubing is packed with small spherical inert supports. The liquid phase adsorbs onto the surface of these beads in a thin layer. In a capillary column, the tubing walls are coated with the stationary phase or an adsorbant layer, which is capable of supporting the liquid phase. However, the method of GSC, has limited application in the laboratory and is rarely used due to severe peak tailing and the semi-permanent retention of polar compounds within the column. Therefore, the method of gas-liquid chromatography is simply shortened to gas chromatography and will be referred to as such here.The purpose of this module is to provide a better understanding on its separation and measurement techniques and its application.

Instrumentation

Sample Injection

A sample port is necessary for introducing the sample at the head of the column. Modern injection techniques often employ the use of heated sample ports through which the sample can be injected and vaporized in a near simultaneous fashion. A calibrated microsyringe is used to deliver a sample volume in the range of a few microliters through a rubber septum and into the vaporization chamber. Most separations require only a small fraction of the initial sample volume and a sample splitter is used to direct excess sample to waste. Commercial gas chromatographs often allow for both split and splitless injections when alternating between packed columns and capillary columns. The vaporization chamber is typically heated 50 °C above the lowest boiling point of the sample and subsequently mixed with the carrier gas to transport the sample into the column.

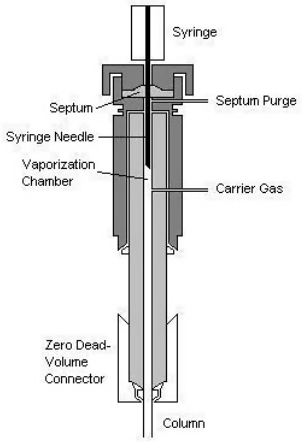


Figure 1: A cross-sectional view of a microflash vaporizer direct injector.

Carrier Gas

The carrier gas plays an important role, and varies in the GC used. Carrier gas must be dry, free of oxygen and chemically inert mobile-phase employed in gas chromatography. Helium is most commonly used because it is safer than, but comprable to hydrogen in efficiency, has a larger range of flow rates and is compatible with many detectors. Nitrogen, argon, and hydrogen are also used depending upon the desired performance and the detector being used. Both hydrogen and helium, which are commonly used on most traditional detectors such as Flame Ionization(FID), thermal conductivity (TCD) and Electron capture (ECD), provide a shorter analysis time and lower elution temperatures of the sample due to higher flow rates and low molecular weight. For instance, hydrogen or helium as the carrier gas gives the highest sensitivity with TCD because the difference in thermal conductivity between the organic vapor and hydrogen/helium is greater than other carrier gas. Other detectors such as mass spectroscopy, uses nitrogen or argon which has a much better advantage than hydrogen or helium due to their higher molecular weights, in which improve vacuum pump efficiency.

All carrier gasses are available in pressurized tanks and pressure regulators, gages and flow meters are used to meticulously control the flow rate of the gas. Most gas supplies used should fall between 99.995% - 99.9995% purity range and contain a low levels (< 0.5 ppm) of oxygen and total hydrocarbons in the tank. The carrier gas system contains a molecular sieve to remove water and other impurities. Traps are another option to keep the system pure and optimum sensitive and removal traces of water and other contaminants. A two stage pressure regulation is required to use to minimize the pressure surges and to monitor the flow rate of the gas. To monitor the flow rate of the gas a flow or pressure regulator was also require onto both tank and chromatograph gas inlet. This applies different gas type will use different type of regulator.The carrier gas is preheated and filtered with a molecular sieve to remove impurities and water prior to being introduced to the vaporization chamber. A carrier gas is typically required in GC system to flow through the injector and push the gaseous components of the sample onto the GC column, which leads to the detector (see more detail in detector section).

Gas Recommendations for Capillary Columns

Detector	Carrier gas	Preferred makeup gas	Second choice	Detector, anode purge, or reference gas
Electron Capture	Hydrogen	Argon/Methane	Nitrogen	Anode purge must be same as makeup
	Helium	Argon/Methane	Nitrogen	
	Nitrogen	Nitrogen	Argon/Methane	
	Argon/Methane	Argon/Methane	Nitrogen	
Flame Ionization	Hydrogen	Nitrogen	Helium	Hydrogen and air for detector
	Helium	Nitrogen	Helium	
	Nitrogen	Nitrogen	Helium	
Flame Photometric	Hydrogen	Nitrogen		Hydrogen and air for detector
	Helium	Nitrogen		
	Nitrogen	Nitrogen		
	Argon	Nitrogen		
Nitrogen-Phosphorus	Helium	Nitrogen	Helium**	Hydrogen and air for detector
	Nitrogen	Nitrogen	Helium**	
Thermal Conductivity	Hydrogen*	Must be same as carrier and reference gas	Must be same as carrier and reference gas	Reference must be same as carrier and makeup
	Helium			
	Nitrogen			

* When using hydrogen with a thermal conductivity detector, vent the detector exhaust to a fume hood or a dedicated exhaust to avoid buildup of hydrogen gas.

**Helium is not recommended as a makeup gas at flow rates > 5 mL/min. Flow rates above 5 mL/min shorten detector life.

Gas Recommendations for Packed Columns

Detector	Carrier gas	Comments	Detector, anode purge, or reference gas
Electron Capture	Nitrogen	Maximum sensitivity	Nitrogen
	Argon/Methane	Maximum dynamic range	Argon/Methane
Flame Ionization	Nitrogen	Maximum sensitivity	Hydrogen and air for detector
	Helium	Acceptable alternative	
Flame Photometric	Hydrogen		Hydrogen and air for detector
	Helium		
	Nitrogen		
	Argon		
Nitrogen-Phosphorus	Helium	Optimum performance	Hydrogen and air for detector
	Nitrogen	Acceptable alternative	
Thermal Conductivity	Helium	General use	Reference must be same as carrier
	Hydrogen	Maximum sensitivity (Note A)	
	Nitrogen	Hydrogen detection (Note B)	
	Argon	Maximum hydrogen sensitivity (Note B)	

Note A: Slightly greater sensitivity than helium. Incompatible with some compounds.
Note B: For analysis of hydrogen or helium. Greatly reduces sensitivity for other compounds.

Figure 3. Gas Recommendations for Packed Columns

Column Oven

The thermostatted oven serves to control the temperature of the column within a few tenths of a degree to conduct precise work. The oven can be operated in two manners: isothermal programming or temperature programming. In isothermal programming, the temperature of the column is held constant throughout the entire separation. The optimum column temperature for isothermal operation is about the middle point of the boiling range of the sample. However, isothermal programming works best only if the boiling point range of the sample is narrow. If a low isothermal column temperature is used with a wide boiling point range, the low boiling fractions are well resolved but the high boiling fractions are slow to elute with extensive band broadening. If the temperature is increased closer to the boiling points of the higher boiling components, the higher boiling components elute as sharp peaks but the lower boiling components elute so quickly there is no separation.

In the temperature programming method, the column temperature is either increased continuously or in steps as the separation progresses. This method is well suited to separating a mixture with a broad boiling point range. The analysis begins at a low temperature to resolve the low boiling components and increases during the separation to resolve the less volatile, high boiling components of the sample. Rates of 5-7 °C/minute are typical for temperature programming separations.

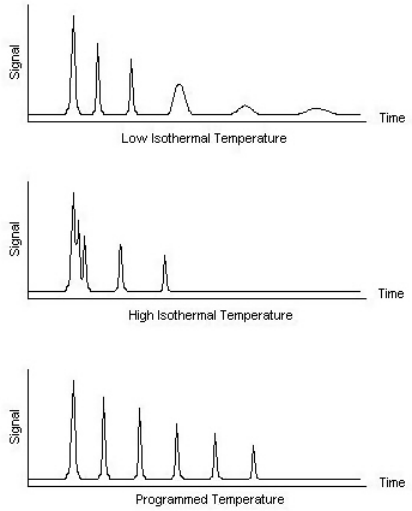


Figure 3. The effect of column temperature on the shape of the peaks.

Open Tubular Columns and Packed Columns

Open tubular columns, which are also known as capillary columns, come in two basic forms. The first is a wall-coated open tubular (WCOT) column and the second type is a support-coated open tubular (SCOT) column. WCOT columns are capillary tubes that have a thin later of the stationary phase coated along the column walls. In SCOT columns, the column walls are first coated with a thin layer (about 30 micrometers thick) of adsorbant solid, such as diatomaceous earth, a material which consists of single-celled, sea-plant skeletons. The adsorbant solid is then treated with the liquid stationary phase. While SCOT columns are capable of holding a greater volume of stationary phase than a WCOT column due to its greater sample capacity, WCOT columns still have greater column efficiencies.

Most modern WCOT columns are made of glass, but T316 stainless steel, aluminum, copper and plastics have also been used. Each material has its own relative merits depending upon the application. Glass WCOT columns have the distinct advantage of chemical etching, which is usually achieved by gaseous or concentrated hydrochloric acid treatment. The etching process gives the glass a rough surface and allows the bonded stationary phase to adhere more tightly to the column surface.

One of the most popular types of capillary columns is a special WCOT column called the fused-silica wall-coated (FSWC) open tubular column. The walls of the fused-silica columns are drawn from purified silica containing minimal metal oxides. These columns are much thinner than glass columns, with diameters as small as 0.1 mm and lengths as long as 100 m. To protect the column, a polyimide coating is applied to the outside of the tubing and bent into coils to fit inside the thermostatted oven of the gas chromatography unit. The FSWC columns are commercially available and currently replacing older columns due to increased chemical inertness, greater column efficiency and smaller sampling size requirements. It is possible to achieve up to 400,000 theoretical plates with a 100 m WCOT column, yet the world record for the largest number of theoretical plates is over 2 million plates for 1.3 km section of column.

Packed columns are made of a glass or a metal tubing which is densely packed with a solid support like diatomaceous earth. Due to the difficulty of packing the tubing uniformly, these types of columns have a larger diameter than open tubular columns and have a limited range of length. As a result, packed columns can only achieve about 50% of the efficiency of a comparable WCOT column. Furthermore, the diatomaceous earth packing is deactivated over time due to the semi-permanent adsorption of impurities within the column. In contrast, FSWC open tubular columns are manufactured to be virtually free of these adsorption problems.

	Type of Column			
	FSWC	WCOT	SCOT	Packed
Length	10 to 1000 m	10 to 1000 m	10 to 100 m	1 to 6 m
Inner Diameter	0.1 to 0.3 mm	0.25 to 0.75 mm	0.5 mm	2 to 4 mm
Efficiency (plates/m)	2000 to 4000	1000 to 4000	600 to 1200	500 to 1000
Sample Size	10 to 75 ng	10 to 1000 ng	10 to 1000 ng	10 to 10^6 ng
Pressure	Low	Low	Low	High
Speed	Fast	Fast	Fast	Slow
Inertness	Best	Good	Fair	Poor

Figure 4. Properties of gas chromatography columns.

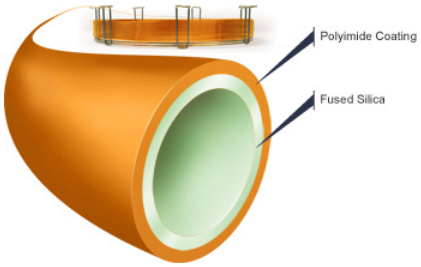


Figure 5. Computer Generated Image of a FSWC column (specialized for measuring BAC levels)

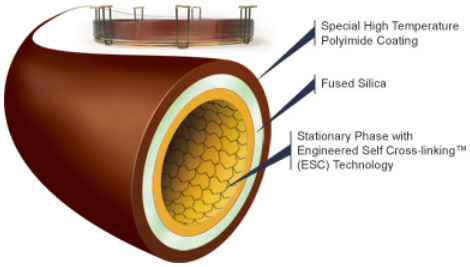


Figure 6. Computer Generated Image of a FSWC column (specialized to withstand extreme heat)

Different types of columns can be applied for different fields. Depending on the type of sample, some GC columns are better than the others. For example, the FSWC column shown in Figure 5 is designed specially for blood alcohol analysis. It produces fast run times with baseline resolution of key components in under 3 minutes. Moreover, it displays enhanced resolutions of ethanol and acetone peaks, which helps with determining the BAC levels. This particular column is known as Zebron-BAC and it made with polyimide coating on the outside and the inner layer is made of fused silica and the inner diameter ranges from .18 mm to .25 mm. There are also many other Zebron brand columns designed for other purposes.

Another example of a Zebron GC column is known as the Zebron-inferno. Its outer layer is coated with a special type of polyimide that is designed to withstand high temperatures. As shown in figure 6, it contains an extra layer inside. It can withstand up to 430 °C to be exact and it is designed to provide true boiling point separation of hydrocarbons distillation methods. Moreover, it is also used for acidic and basic samples.

Detection Systems

The detector is the device located at the end of the column which provides a quantitative measurement of the components of the mixture as they elute in combination with the carrier gas. In theory, any property of the gaseous mixture that is different from the carrier gas can be used as a detection method. These detection properties fall into two categories: bulk properties and specific properties. Bulk properties, which are also known as general properties, are properties that both the carrier gas and analyte possess but to different degrees. Specific properties, such as detectors that measure nitrogen-phosphorous content, have limited applications but compensate for this by their increased sensitivity.

Each detector has two main parts that when used together they serve as transducers to convert the detected property changes into an electrical signal that is recorded as a chromatogram. The first part of the detector is the sensor which is placed as close the the column exit as possible in order to optimize detection. The second is the electronic equipment used to digitize the analog signal so

that a computer may analyze the acquired chromatogram. The sooner the analog signal is converted into a digital signal, the greater the signal-to-noise ratio becomes, as analog signal are easily susceptible to many types of interferences.

An ideal GC detector is distinguished by several characteristics. The first requirement is adequate sensitivity to provide a high resolution signal for all components in the mixture. This is clearly an idealized statement as such a sample would approach zero volume and the detector would need infinite sensitivity to detect it. In modern instruments, the sensitivities of the detectors are in the range of 10^{-8} to 10^{-15} g of solute per second. Furthermore, the quantity of sample must be reproducible and many columns will distort peaks if enough sample is not injected. An ideal column will also be chemically inert and and should not alter the sample in any way. Optimized columns will be able to withstand temperatures in the range of -200 °C to at least 400 °C. In addition, such a column would have a short linear response time that is independent of flow rate and extends for several orders of magnitude. Moreover, the detector should be reliable, predictable and easy to operate.

Understandably, it is not possible for a detector meet all of these requirements. The next subsections will discuss some of the more common types of gas chromatography detectors and the relative advantages and/or disadvantages of each.

Table 7: Typical gas chromatography detectors and their detection limits.

Type of Detector	Applicable Samples	Detection Limit
Mass Spectrometer (MS)	Tunable for any sample	.25 to 100 pg
Flame Ionization (FID)	Hydrocarbons	1 pg/s
Thermal Conductivity (TCD)	Universal	500 pg/ml
Electron-Capture (ECD)	Halogenated hydrocarbons	5 fg/s
Atomic Emission (AED)	Element-selective	1 pg
Chemiluminescence (CS)	Oxidizing reagent	Dark current of PMT
Photoionization (PID)	Vapor and gaseous Compounds	.002 to .02 µg/L

Mass Spectrometry Detectors

Mass Spectrometer (MS) detectors are most powerful of all gas chromatography detectors. In a GC/MS system, the mass spectrometer scans the masses continuously throughout the separation. When the sample exits the chromatography column, it is passed through a transfer line into the inlet of the mass spectrometer . The sample is then ionized and fragmented, typically by an electron-impact ion source. During this process, the sample is bombarded by energetic electrons which ionize the molecule by causing them to lose an electron due to electrostatic repulsion. Further bombardment causes the ions to fragment. The ions are then passed into a mass analyzer where the ions are sorted according to their m/z value, or mass-to-charge ratio. Most ions are only singly charged.

The Chromatogram will point out the retention times and the mass spectrometer will use the peaks to determine what kind of molecules are exist in the mixture. The figure below represents a typical mass spectrum of water with the absorption peaks at the appropriate m/z ratios.

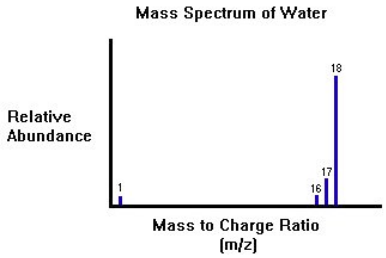


Figure 8. Mass Spectrum of Water

Instrumentation

One of the most common types of mass analyzer in GC/MS is the quadrupole ion-trap analyzer, which allows gaseous anions or cations to be held for long periods of time by electric and magnetic fields. A simple quadrupole ion-trap consists of a hollow ring electrode with two grounded end-cap electrodes as seen in figure #. Ions are allowed into the cavity through a grid in the upper end

cap. A variable radio-frequency is applied to the ring electrode and ions with an appropriate m/z value orbit around the cavity. As the radio-frequency is increased linearly, ions of a stable m/z value are ejected by mass-selective ejection in order of mass. Ions that are too heavy or too light are destabilized and their charge is neutralized upon collision with the ring electrode wall. Emitted ions then strike an electron multiplier which converts the detected ions into an electrical signal. This electrical signal is then picked up by the computer through various programs. As an end result, a chromatogram is produced representing the m/z ratio versus the abundance of the sample.

GC/MS units are advantageous because they allow for the immediate determination of the mass of the analyte and can be used to identify the components of incomplete separations. They are rugged, easy to use and can analyze the sample almost as quickly as it is eluted. The disadvantages of mass spectrometry detectors are the tendency for samples to thermally degrade before detection and the end result of obliterating all the sample by fragmentation.

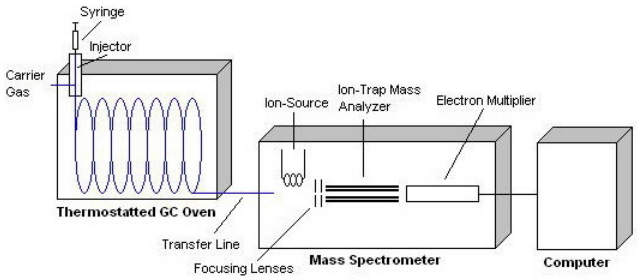


Figure 9. Schematic of the GC/MS system.

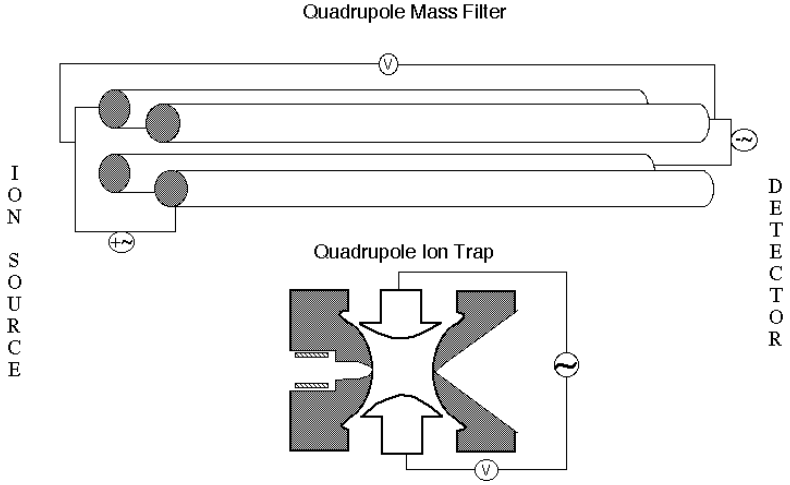


Figure 10. Arrangement of the poles in Quadrupole and Ion Trap Mass spectrometers

Flame Ionization Detectors

Flame ionization detectors (FID) are the most generally applicable and most widely used detectors. In a FID, the sample is directed at an air-hydrogen flame after exiting the column. At the high temperature of the air-hydrogen flame, the sample undergoes pyrolysis, or chemical decomposition through intense heating. Pyrolized hydrocarbons release ions and electrons that carry current. A high-impedance picoammeter measures this current to monitor the sample's elution.

It is advantageous to use FID because the detector is unaffected by flow rate, noncombustible gases and water. These properties allow FID high sensitivity and low noise. The unit is both reliable and relatively easy to use. However, this technique does require flammable gas and also destroys the sample.

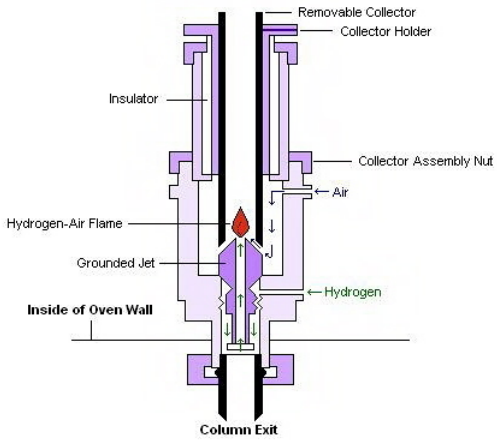


Figure 11. Schematic of a typical flame ionization detector.

Thermal Conductivity Detectors

Thermal conductivity detectors (TCD) were one the earliest detectors developed for use with gas chromatography. The TCD works by measuring the change in carrier gas thermal conductivity caused by the presence of the sample, which has a different thermal conductivity from that of the carrier gas. Their design is relatively simple, and consists of an electrically heated source that is maintained at constant power. The temperature of the source depends upon the thermal conductivities of the surrounding gases. The source is usually a thin wire made of platinum, gold or . The resistance within the wire depends upon temperature, which is dependent upon the thermal conductivity of the gas.

TCDs usually employ two detectors, one of which is used as the reference for the carrier gas and the other which monitors the thermal conductivity of the carrier gas and sample mixture. Carrier gases such as helium and hydrogen has very high thermal conductivities so the addition of even a small amount of sample is readily detected.

The advantages of TCDs are the ease and simplicity of use, the devices' broad application to inorganic and organic compounds, and the ability of the analyte to be collected after separation and detection. The greatest drawback of the TCD is the low sensitivity of the instrument in relation to other detection methods, in addition to flow rate and concentration dependency.

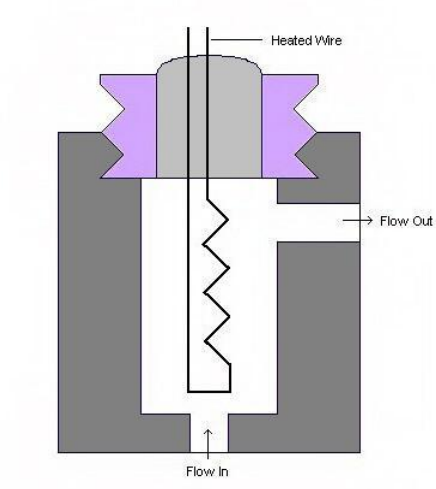


Figure 12. Schematic of thermal conductivity detection cell.

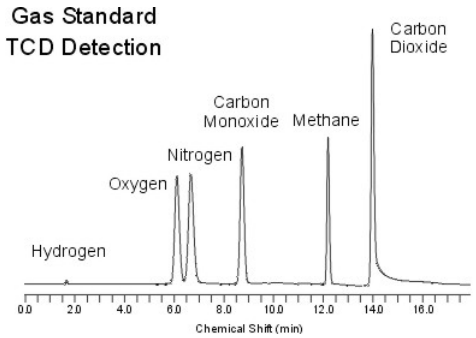


Figure 13. Standard Chromatogram of a Mixture of Gases

Chromatogram

Figure 13 represents a standard chromatogram produced by a TCD detector. In a standard chromatogram regardless of the type detector, the x-axis is the time and the y-axis is the abundance or the absorbance. From these chromatograms, retention times and the peak heights are determined and used to further investigate the chemical properties or the abundance of the samples.

Electron-capture Detectors

Electron-capture detectors (ECD) are highly selective detectors commonly used for detecting environmental samples as the device selectively detects organic compounds with moieties such as halogens, peroxides, quinones and nitro groups and gives little to no response for all other compounds. Therefore, this method is best suited in applications where traces quantities of chemicals such as pesticides are to be detected and other chromatographic methods are unfeasible.

The simplest form of ECD involves gaseous electrons from a radioactive ? emitter in an electric field. As the analyte leaves the GC column, it is passed over this ? emitter, which typically consists of nickle-63 or tritium. The electrons from the ? emitter ionize the nitrogen carrier gas and cause it to release a burst of electrons. In the absence of organic compounds, a constant standing current is maintained between two electrodes. With the addition of organic compounds with electronegative functional groups, the current decreases significantly as the functional groups capture the electrons.

The advantages of ECDs are the high selectivity and sensitivity towards certain organic species with electronegative functional groups. However, the detector has a limited signal range and is potentially dangerous owing to its radioactivity. In addition, the signal-to-noise ratio is limited by radioactive decay and the presence of O2 within the detector.

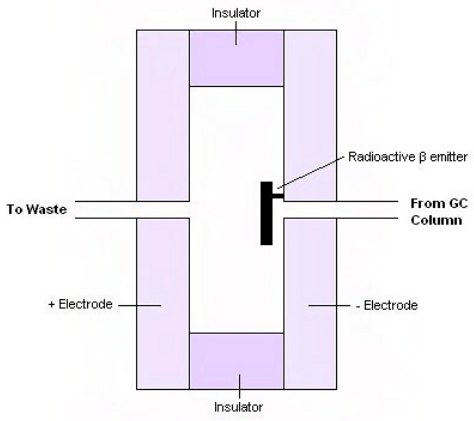


Figure 14. Schematic of an electron-capture detector.

Atomic Emission Detectors

Atomic emission detectors (AED), one of the newest addition to the gas chromatographer's arsenal, are element-selective detectors that utilize plasma, which is a partially ionized gas, to atomize all of the elements of a sample and excite their characteristic atomic emission spectra. AED is an extremely powerful alternative that has a wider applicability due to its based on the detection of atomic emissions.There are three ways of generating plasma: microwave-induced plasma (MIP), inductively coupled plasma (ICP) or direct current plasma (DCP). MIP is the most commonly employed form and is used with a positionable diode array to simultaneously monitor the atomic emission spectra of several elements.

Instrumentation

The components of the Atomic emission detectors include 1) an interface for the incoming capillary GC column to induce plasma chamber,2) a microwave chamber, 3) a cooling system, 4) a diffration grating that associated optics, and 5) a position adjustable photodiode array interfaced to a computer.

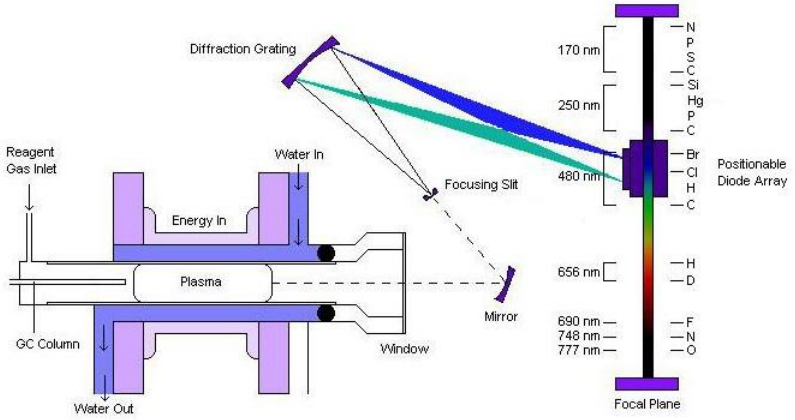


Figure 15. Schematic of atomic emission detector.

GC Chemiluminescence Detectors

Chemiluminescence spectroscopy (CS) is a process in which both qualitative and quantitative properties can be be determined using the optical emission from excited chemical species. It is very similar to AES, but the difference is that it utilizes the light emitted from the energized molecules rather than just excited molecules. Moreover, chemiluminescence can occur in either the solution or gas phase whereas AES is designed for gaseous phases. The light source for chemiluminescence comes from the reactions of the chemicals such that it produces light energy as a product. This light band is used instead of a separate source of light such as a light beam.

Like other methods, CS also has its limitations and the major limitation to the detection limits of CS concerns with the use of a photomultiplier tube (PMT). A PMT requires a dark current in it to detect the light emitted from the analyte.

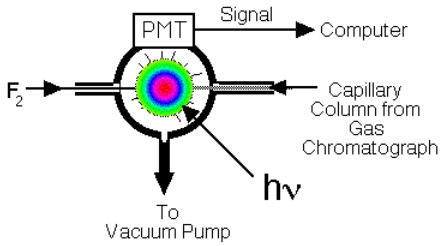


Figure 16. Schematic of a GC Chemiluminescence Detector

Photoionization Detectors

Another different kind of detector for GC is the photoionization detector which utilizes the properties of chemiluminescence spectroscopy. Photoionization detector (PID) is a portable vapor and gas detector that has selective determination of aromatic hydrocarbons, organo-heteroatom, inorganice species and other organic compounds. PID comprise of an ultrviolet lamp to emit photons that are absorbed by the compounds in an ionization chamber exiting from a GC column. Small fraction of the analyte molecules are actually ionized, nondestructive, allowing confirmation analytical results through other detectors. In addition, PIDs are available in portable hand-held models and in a number of lamp configurations. Results are almost immediate. PID is used commonly to detect VOCs in soil, sediment, air and water, which is often used to detect contaminants in ambient air and soil. The disavantage of PID is unable to detect certain hydrocarbon that has low molecular weight, such as methane and ethane.

Instrumentation

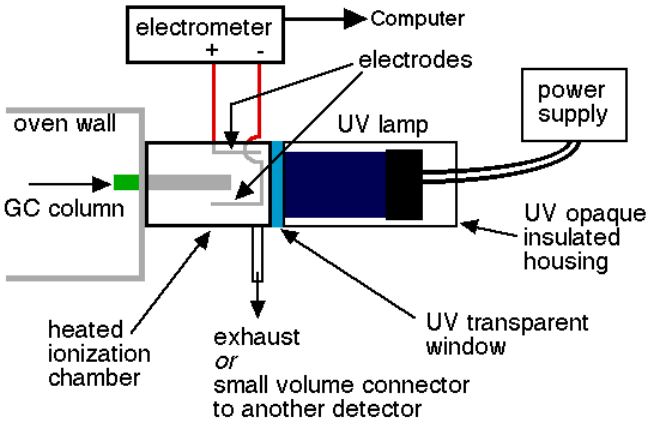


Figure 17. Schematic of a photoionization detector

Limitations

1. Not suitable for detecting semi-volatile compounds
2. Only indicates if volatile organic compounds are presents.
3. High concentration so methane are required for higher performance.
4. Frequent calibration are required.
5. Units of parts per million range
6. Enviromental distraction, especially water vapor.
7. Strong electrical fieldsRapid variation in temperature at the detector and naturally occurring compounds may affect instrumental signal.

Applications

Gas chromatography is a physical separation method in where volatile mixtures are separated. It can be used in many different fields such as pharmaceuticals, cosmetics and even environmental toxins. Since the samples have to be volatile, human breathe, blood, saliva and other secretions containing large amounts of organic volatiles can be easily analyzed using GC. Knowing the amount of which compound is in a given sample gives a huge advantage in studying the effects of human health and of the environment as well.

Air samples can be analyzed using GC. Most of the time, air quality control units use GC coupled with FID in order to determine the components of a given air sample. Although other detectors are useful as well, FID is the most appropriate because of its sensitivity and resolution and also because it can detect very small molecules as well.

GC/MS is also another useful method which can determine the components of a given mixture using the retention times and the abundance of the samples. This method be applied to many pharmaceutical applications such as identifying the amount of chemicals in drugs. Moreover, cosmetic manufacturers also use this method to effectively measure how much of each chemical is used for their products.

Equations

“Height equivalent to a theoretical plate” (HETP) use to calculate the flow rate by usingthe total number of theoretical plates (N) and column length (L). Some application, HETP concepts is used in industrial practice to convert number of theoretical plates to packing height. HETP can be calculate with the Van Deemter equation, which is given by

$$HETP = A + \frac{B}{v} + Cv \tag{1}$$

Where A and B and C are constants and v is the linear velocity (carrier flow rate).

- A is the "Eddy-Diffusion" term and causes the broadening of the solute band.
- B is the "Longitudinal diffusion" term whereby the concentration of the analyte, in which diffuses out from the center to the edges.This causes the broadering of the analyte band.
- C is the "Resistance to Mass Transfer " term and causes the band of the analyte broader.

$$HETP = \frac{L}{N} \tag{2}$$

L is the length of the column, where N is the number of theoretical plates, tR is the retention time, and ω is the width of the elution peak at its base.

$$N = 16\left(\frac{tR}{\omega}\right)^2 \tag{3}$$

In which, the more plates give a better resolution and more efficiency. Resolution can be determined by

$$R = 2\left[\frac{(tR)B - (tR)A}{WA + WB}\right] \tag{4}$$

A relationship between the plates and resolution is giving by,

$$R = (N)1/2/4)(\alpha - \frac{1}{\alpha})(1 + \frac{K'B}{K'B}) \tag{5}$$

Where the selectivity, a, and k' is the capacity factors take places of the two solutes. The selectivity and capacity factors can be control by improving separation, such as changing mobile/ stationary phase composition, column temperature and use a special chemical effect.

References

1. Skoog, D. A.; Holler, F. J.; Crouch, S. R. Principles of Instrumental Analysis. Sixth Edition, Thomson Brooks/Cole, USA, 2007.
2. Krugers, J. Instrumentation in Gas Chromatography. Centrex Publishing Company-Eindhoven, Netherlands, 1968.
3. Hubschmann, H. Handbook of GC/MS: Fundamentals and Applications. Wiley-VCH Verlag, Germany, 2001.
4. Scott, R. P. W. Chromatographic Detectors: Design, Function, and Operation. Marcel Dekker, Inc., USA, 1996.
5. J.N. Driscoll. REview of Photoionization Detection in Gas Chromatography: The first Decade. Journal of CHromatographic Science , Vol 23. November 1985. 488-492.
6. Boer, H. , "Vapour phase Chromatography", ed. Desty, D. H., 169 (Butterworths Sci. Pub., London, 1957).
7. Dimbat, M. , Porter, P. E. , and Stross, F. H. , Anal. Chem., 28, 290 (1956). | Article | ISI | ChemPort |

Contributors and Attributions

- Kyaw Thet (UC Davis), Nancy Woo (UC Davis)

10.2.1: Gas Chromatography is shared under a CC BY-NC-SA 4.0 license and was authored, remixed, and/or curated by LibreTexts.

- **Gas Chromatography** is licensed CC BY-NC-SA 4.0.

10.3: HIGH-PERFORMANCE LIQUID CHROMATOGRAPHY

In ***high-performance liquid chromatography*** (HPLC) we inject the sample, which is in solution form, into a liquid mobile phase. The mobile phase carries the sample through a packed or capillary column that separates the sample's components based on their ability to partition between the mobile phase and the stationary phase. Figure 12.5.1 shows an example of a typical HPLC instrument, which has several key components: reservoirs that store the mobile phase; a pump for pushing the mobile phase through the system; an injector for introducing the sample; a column for separating the sample into its component parts; and a detector for monitoring the eluent as it comes off the column. Let's consider each of these components.

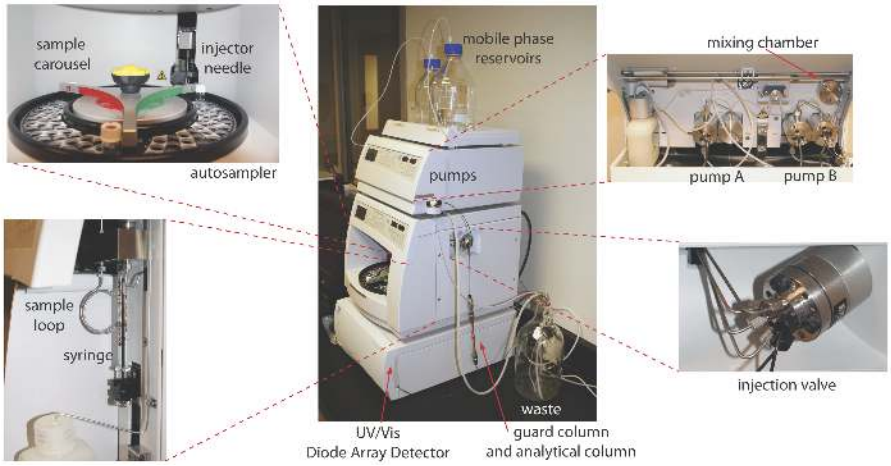


Figure 12.5.1 . Example of a typical high-performance liquid chromatograph with insets showing the pumps that move the mobile phase through the system and the plumbing used to inject the sample into the mobile phase. This particular instrument includes an autosampler. An instrument in which samples are injected manually does not include the features shown in the two left-most insets, and has a different style of loop injection valve.

A solute's retention time in HPLC is determined by its interaction with the stationary phase and the mobile phase. There are several different types of solute/stationary phase interactions, including liquid–solid adsorption, liquid–liquid partitioning, ion-exchange, and size-exclusion. This chapter deals exclusively with HPLC separations based on liquid–liquid partitioning. Other forms of liquid chromatography receive consideration in Chapter 12.6.

HPLC COLUMNS

An HPLC typically includes two columns: an analytical column, which is responsible for the separation, and a guard column that is placed before the analytical column to protect it from contamination.

ANALYTICAL COLUMNS

The most common type of HPLC column is a stainless steel tube with an internal diameter between 2.1 mm and 4.6 mm and a length between 30 mm and 300 mm (Figure 12.5.2). The column is packed with 3–10 µm porous silica particles with either an irregular or a spherical shape. Typical column efficiencies are 40000–60000 theoretical plates/m. Assuming a V_{max}/V_{min} of approximately 50, a 25-cm column with 50 000 plates/m has 12 500 theoretical plates and a peak capacity of 110.



Figure 12.5.2 . Typical packed column for HPLC. This particular column has an internal diameter of 4.6 mm and a length of 150 mm, and is packed with 5 µm particles coated with stationary phase.

Capillary columns use less solvent and, because the sample is diluted to a lesser extent, produce larger signals at the detector. These columns are made from fused silica capillaries with internal diameters from 44–200 µm and lengths of 50–250 mm. Capillary columns packed with 3–5 µm particles have been prepared with column efficiencies of up to 250 000 theoretical plates [Novotony, M. *Science*, **1989**, *246*, 51–57].

One limitation to a packed capillary column is the back pressure that develops when pumping the mobile phase through the small interstitial spaces between the particulate micron-sized packing material (Figure 12.5.3). Because the tubing and fittings that carry the mobile phase have pressure limits, a higher back pressure requires a lower flow rate and a longer analysis time. Monolithic columns, in which the solid

support is a single, porous rod, offer column efficiencies equivalent to a packed capillary column while allowing for faster flow rates. A monolithic column—which usually is similar in size to a conventional packed column, although smaller, capillary columns also are available—is prepared by forming the mono- lithic rod in a mold and covering it with PTFE tubing or a polymer resin. Monolithic rods made of a silica-gel polymer typically have macropores with diameters of approximately 2 μm and mesopores—pores within the macropores—with diameters of approximately 13 nm [Cabrera, K. Chromatography Online, April 1, 2008].

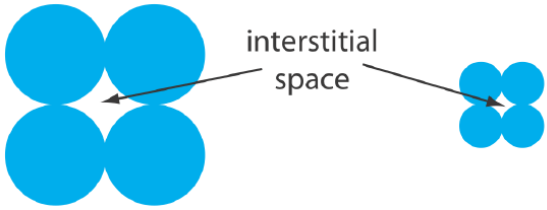


Figure 12.5.3 . The packing of smaller particles creates smaller interstitial spaces than the packing of larger particles. Although reducing particle size by 2× increases efficiency by a factor of 1.4, it also produces a 4-fold increase in back pressure.

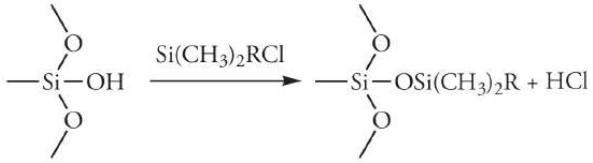
GUARD COLUMNS

Two problems tend to shorten the lifetime of an analytical column. First, solutes that bind irreversibly to the stationary phase degrade the column's performance by decreasing the amount of stationary phase available for effecting a separation. Second, particulate material injected with the sample may clog the analytical column. To minimize these problems we place a guard column before the analytical column. A Guard column usually contains the same particulate packing material and stationary phase as the analytical column, but is significantly shorter and less expensive—a length of 7.5 mm and a cost one-tenth of that for the corresponding analytical column is typical. Because they are intended to be sacrificial, guard columns are replaced regularly.

> If you look closely at Figure 12.5.1 , you will see the small guard column just above the analytical column.

STATIONARY PHASES FOR LIQUID-LIQUID CHROMATOGRAPHY

In liquid–liquid chromatography the stationary phase is a liquid film coated on a packing material, typically 3–10 μm porous silica particles. Because the stationary phase may be partially soluble in the mobile phase, it may elute, or bleed from the column over time. To prevent the loss of stationary phase, which shortens the column's lifetime, it is bound covalently to the silica particles. ***Bonded stationary phases*** are created by reacting the silica particles with an organochlorosilane of the general form $Si(CH_3)_2RCl$, where R is an alkyl or substituted alkyl group.



To prevent unwanted interactions between the solutes and any remaining –SiOH groups, $Si(CH_3)_3Cl$ is used to convert unreacted sites to $-SiOSi(CH_3)_3$; such columns are designated as end-capped.

The properties of a stationary phase depend on the organosilane's alkyl group. If R is a polar functional group, then the stationary phase is polar. Examples of polar stationary phases include those where R contains a cyano ($–C_2H_4CN$), a diol ($–C_3H_6OCH_2CHOHCH_2OH$), or an amino ($–C_3H_6NH_2$) functional group. Because the stationary phase is polar, the mobile phase is a nonpolar or a moderately polar solvent. The combination of a polar stationary phase and a nonpolar mobile phase is called ***normal- phase chromatography***.

In ***reversed-phase chromatography***, which is the more common form of HPLC, the stationary phase is nonpolar and the mobile phase is polar. The most common nonpolar stationary phases use an organochlorosilane where the R group is an *n*-octyl (C_8) or *n*-octyldecyl (C_{18}) hydrocarbon chain. Most reversed-phase separations are carried out using a buffered aqueous solution as a polar mobile phase, or using other polar solvents, such as methanol and acetonitrile. Because the silica substrate may undergo hydrolysis in basic solutions, the pH of the mobile phase must be less than 7.5.

> It seems odd that the more common form of liquid chromatography is identified as reverse-phase instead of normal phase. You might recall that one of the earliest examples of chromatography was Mikhail Tswett's separation of plant pigments using a polar column of calcium carbonate and a nonpolar mobile phase of petroleum ether. The assignment of normal and reversed, therefore, is all about precedence.

MOBILE PHASES

The elution order of solutes in HPLC is governed by polarity. For a normal-phase separation, a solute of lower polarity spends proportionally less time in the polar stationary phase and elutes before a solute that is more polar. Given a particular stationary phase, retention times in normal-phase HPLC are controlled by adjusting the mobile phase's properties. For example, if the resolution between two solutes is poor, switching to a less polar mobile phase keeps the solutes on the column for a longer time and provides more opportunity for their separation. In reversed-phase HPLC the order of elution is the opposite that in a normal-phase separation, with more polar solutes eluting first. Increasing the polarity of the mobile phase leads to longer retention times. Shorter retention times require a mobile phase of lower polarity.

CHOOSING A MOBILE PHASE: USING THE POLARITY INDEX

There are several indices that help in selecting a mobile phase, one of which is the polarity index [Snyder, L. R.; Glajch, J. L.; Kirkland, J. J. *Practical HPLC Method Development*, Wiley-Inter- science: New York, 1988]. Table 12.5.1 provides values of the polarity index, P', for several common mobile phases, where larger values of P' correspond to more polar solvents. Mixing together two or more mobile phases—assuming they are miscible—creates a mobile phase of intermediate polarity. For example, a binary mobile phase made by combining solvent *A* and solvent *B* has a polarity index, P'_{AB}, of

$$P'_{AB} = \Phi_A P'_A + \Phi_B P'_B \tag{10.3.1}$$

where P'_A and P'_B are the polarity indices for solvents *A* and *B*, and Φ_A and Φ_B are the volume fractions for the two solvents.

Table 12.5.1 . Properties of HPLC Mobile Phases

mobile phase	polarity index (P')	UV cutoff (nm)
cyclohexane	0.04	210
n-hexane	0.1	210
carbon tetrachloride	1.6	265
i-propyl ether	2.4	220
toluene	2.4	286
diethyl ether	2.8	218
tetrahydrofuran	4.0	220
ethanol	4.3	210
ethyl acetate	4.4	255
dioxane	4.8	215
methanol	5.1	210
acetonitrile	5.8	190
water	10.2	—

EXAMPLE 12.5.1

A reversed-phase HPLC separation is carried out using a mobile phase of 60% v/v water and 40% v/v methanol. What is the mobile phase's polarity index?

Solution

Using Equation 10.3.1 and the values in Table 12.5.1 , the polarity index for a 60:40 water–methanol mixture is

$$P'_{AB} = \Phi_{\text{water}} P'_{\text{water}} + \Phi_{\text{methanol}} P'_{\text{methanol}}$$

$$P'_{AB} = 0.60 \times 10.2 + 0.40 \times 5.1 = 8.2$$

EXERCISE 12.5.1

Suppose you need a mobile phase with a polarity index of 7.5. Explain how you can prepare this mobile phase using methanol and water.

Answer

If we let *x* be the fraction of water in the mobile phase, then 1 – *x* is the fraction of methanol. Substituting these values into Equation 10.3.1 and solving for *x*

$$7.5 = 10.2x + 5.1(1 - x)$$

$$7.5 = 10.2x + 5.1 - 5.1x$$

$$2.4 = 5.1x$$

gives *x* as 0.47. The mobile phase is 47% v/v water and 53% v/v methanol.

As a general rule, a two unit change in the polarity index corresponds to an approximately 10-fold change in a solute's retention factor. Here is a simple example. If a solute's retention factor, *k*, is 22 when using water as a mobile phase (P' = 10.2), then switching to a mobile phase of 60:40 water–methanol (P' = 8.2) decreases *k* to approximately 2.2. Note that the retention factor becomes smaller because we are switching from a more polar mobile phase to a less polar mobile phase in a reversed-phase separation.

CHOOSING A MOBILE PHASE: ADJUSTING SELECTIVITY

Changing the mobile phase's polarity index changes a solute's retention factor. As we learned in Chapter 12.3, however, a change in *k* is not an effective way to improve resolution when the initial value of *k* is greater than 10. To effect a better separation between two solutes we must improve the selectivity factor, α. There are two common methods for increasing α: adding a reagent to the mobile phase that reacts with the solutes in a secondary equilibrium reaction or switching to a different mobile phase.

Taking advantage of a secondary equilibrium reaction is a useful strategy for improving a separation [(a) Foley, J. P. *Chromatography*, **1987**, *7*, 118–128; (b) Foley, J. P.; May, W. E. Anal. Chem. 1987, 59, 102–109; (c) Foley, J. P.; May, W. E. Anal. Chem. 1987, 59, 110–115]. Figure 12.3.3, which we considered earlier in this chapter, shows the reversed-phase separation of four weak acids—benzoic acid, terephthalic acid, *p*-aminobenzoic acid, and *p*-hydroxybenzoic acid—on a nonpolar C_{18} column using an aqueous buffer of acetic acid and sodium acetate as the mobile phase. The retention times for these weak acids are shorter when using a less acidic mobile phase because each solute is present in an anionic, weak base form that is less soluble in the nonpolar stationary phase. If the mobile phase's pH is sufficiently acidic, the solutes are present as neutral weak acids that are more soluble in the stationary phase and take longer to elute. Because the weak acid solutes do not have identical pK_a values, the pH of the mobile phase has a different effect on each solute's retention time, allowing us to find the optimum pH for effecting a complete separation of the four solutes.

> Acid–base chemistry is not the only example of a secondary equilibrium reaction. Other examples include ion-pairing, complexation, and the interaction of solutes with micelles. We will consider the last of these in Chapter 12.7 when we discuss micellar electrokinetic capillary chromatography.

In Example 12.5.1 we learned how to adjust the mobile phase's polarity by blending together two solvents. A polarity index, however, is just a guide, and binary mobile phase mixtures with identical polarity indices may not resolve equally a pair of solutes. Table 12.5.2 , for example, shows retention times for four weak acids in two mobile phases with nearly identical values for P'. Although the order of elution is the same for both mobile phases, each solute's retention time is affected differently by the choice of organic solvent. If we switch from using acetonitrile to tetrahydrofuran, for example, we find that benzoic acid elutes more quickly and that *p*-hydroxybenzoic acid elutes more slowly. Although we can resolve fully these two solutes using mobile phase that is 16% v/v acetonitrile, we cannot resolve them if the mobile phase is 10% tetrahydrofuran.

Table 12.5.2 . Retention Times for Four Weak Acids in Mobile Phases With Similar Polarity Indexes

retention time (min)	16% acetonitrile (CH_3CN) 84% pH 4.11 aqueous buffer (P' = 9.5)	10% tetrahydrofuran (THF) 90% pH 4.11 aqueous buffer (P' = 9.6)
$t_{r,\,BA}$	5.18	4.01
$t_{r,\,PH}$	1.67	2.91
$t_{r,\,PA}$	1.21	1.05
$t_{r,\,TP}$	0.23	0.54

Key: BA is benzoic acid; PH is *p*-hydroxybenzoic acid; PA is *p*-aminobenzoic acid; TP is terephthalic acid
Source: Harvey, D. T.; Byerly, S.; Bowman, A.; Tomlin, J. "Optimization of HPLC and GC Separations Using Re- sponse Surfaces," *J. Chem. Educ.* **1991**, *68*, 162–168.

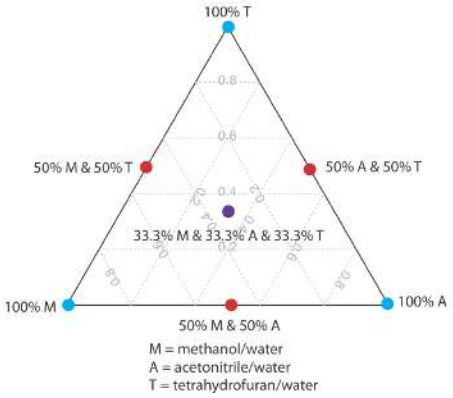


Figure 12.5.4 . Solvent triangle for optimizing a reversed-phase HPLC separation. The three blue circles show mobile phases consisting of an organic solvent and water. The three red circles are binary mobile phases created by combining equal volumes of the pure mobile phases. The ternary mobile phase shown by the purple circle contains all three of the pure mobile phases.

One strategy for finding the best mobile phase is to use the solvent triangle shown in Figure 12.5.4 , which allows us to explore a broad range of mobile phases with only seven experiments. We begin by adjusting the amount of acetonitrile in the mobile phase to produce the best possible separation within the desired analysis time. Next, we use Table 12.5.3 to estimate the composition of methanol/H_2O and tetrahydrofuran/H_2O mobile phases that will produce similar analysis times. Four additional mobile phases are prepared using the binary and ternary mobile phases shown in Figure 12.5.4 . When we examine the chromatograms from these seven mobile phases we may find that one or more provides an adequate separation, or we may identify a region within the solvent triangle where a separation is feasible. Figure 12.5.5 shows a resolution map for the reversed-phase separation of benzoic acid, terephthalic acid, *p*-aminobenzoic acid, and *p*-hydroxybenzoic acid on a nonpolar C_{18} column in which the maximum desired analysis time is set to 6 min [Harvey, D. T.; Byerly, S.; Bowman, A.; Tomlin, J. *J. Chem. Educ.* **1991**, *68*, 162–168]. The areas in blue, green, and red show mobile phase compositions that do not provide baseline resolution. The unshaded area represents mobile phase compositions where a separation is possible.

> The choice to start with acetonitrile is arbitrary—we can just as easily choose to begin with methanol or with tetrahydrofuran.

Table 12.5.3 . Composition of Mobile Phases With Approximately Equal Solvent Strengths

%v/v CH_3OH	% v/v CH_3CN	%v/v THF
0	0	0
10	6	4
20	14	10
30	22	16
40	32	24
50	40	30
6	50	36
70	60	44
80	72	52
90	87	62
100	99	71

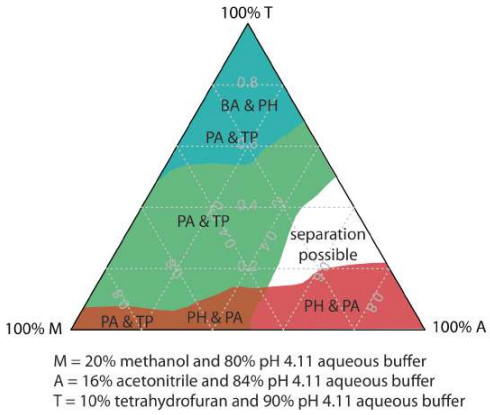


Figure 12.5.5 . Resolution map for the separation of benzoic acid (BA), terephthalic acid (TP), *p*-aminobenzoic acid (PA), and *p*-hydroxybenzoic acid (PH) on a nonpolar C_{18} column subject to a maximum analysis time of 6 min. The shaded areas represent regions where a separation is not possible, with the unresolved solutes identified. A separation is possible in the unshaded area. See Harvey, D. T.; Byerly, S.; Bowman, A.; Tomlin, J. "Optimization of HPLC and GC Separations Using Response Surfaces," *J. Chem. Educ.* **1991**, *68*, 162–168 for details on the mathematical model used to generate the resolution map.

CHOOSING A MOBILE PHASE: ISOCRATIC AND GRADIENT ELUTIONS

A separation using a mobile phase that has a fixed composition is an ***isocratic elution***. One difficulty with an isocratic elution is that an appropriate mobile phase strength for resolving early-eluting solutes may lead to unacceptably long retention times for late-eluting solutes. Optimizing the mobile phase for late-eluting solutes, on the other hand, may provide an inadequate separation of early-eluting solutes. Changing the mobile phase's composition as the separation progresses is one solution to this problem. For a reversed-phase separation we use an initial mobile phase that is more polar. As the separation progresses, we adjust the composition of mobile phase so that it becomes less polar (see Figure 12.5.6). Such separations are called ***gradient elutions***.

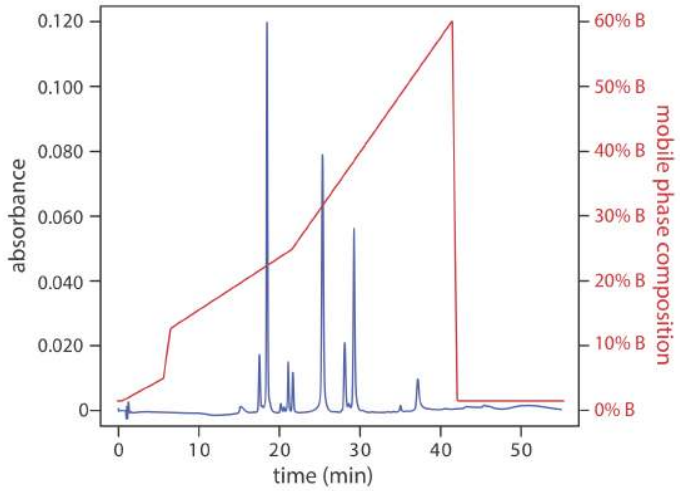


Figure 12.5.6 . Gradient elution separation of a mixture of flavonoids. Mobile phase A is an aqueous solution of 0.1% formic acid and mobile phase B is 0.1% formic acid in acetonitrile. The initial mobile phase is 98% A and 2% B. The percentage of mobile phase B increases in four steps: from 2% to 5% over 5 min, beginning at 0.5 min; from 5% to 12% over 1 min, beginning at 5.5 min; from 12% to 25% over 15 min, beginning at 6.5 min; and from 25% to 60% over 20 min, beginning at 21.5 min. Data provided by Christopher Schardon, Kyle Meinhardt, and Michelle Bushey, Department of Chemistry, Trinty University.

HPLC PLUMBING

In a gas chromatograph the pressure from a compressed gas cylinder is sufficient to push the mobile phase through the column. Pushing a liquid mobile phase through a column, however, takes a great deal more effort, generating pressures in excess of several hundred atmospheres. In this section we consider the basic plumbing needed to move the mobile phase through the column and to inject the sample into the mobile phase.

MOVING THE MOBILE PHASE

A typical HPLC includes between 1–4 reservoirs for storing mobile phase solvents. The instrument in Figure 12.5.1 , for example, has two mobile phase reservoirs that are used for an isocratic elution or a gradient elution by drawing solvents from one or both reservoirs.

Before using a mobile phase solvent we must remove dissolved gases, such as N_2 and O_2, and small particulate matter, such as dust. Because there is a large drop in pressure across the column—the pressure at the column's entrance is as much as several hundred atmospheres, but it is atmospheric pressure at the column's exit—gases dissolved in the mobile phase are released as gas bubbles that may interfere with the detector's response. Degassing is accomplished in several ways, but the most common are the use of a vacuum pump or sparging with an inert gas, such as He, which has a low solubility in the mobile phase. Particulate materials, which may clog the HPLC tubing or column, are removed by filtering the solvents.

> Bubbling an inert gas through the mobile phase releases volatile dissolved gases. This process is called sparging.

The mobile phase solvents are pulled from their reservoirs by the action of one or more pumps. Figure 12.5.7 shows a close-up view of the pumps for the instrument in Figure 12.5.1 . The working pump and the equilibrating pump each have a piston whose back and forth movement maintains a constant flow rate of up to several mL/min and provides the high output pressure needed to push the mobile phase through the chromatographic column. In this particular instrument, each pump sends its mobile phase to a mixing chamber where they combine to form the final mobile phase. The relative speed of the two pumps determines the mobile phase's final composition.

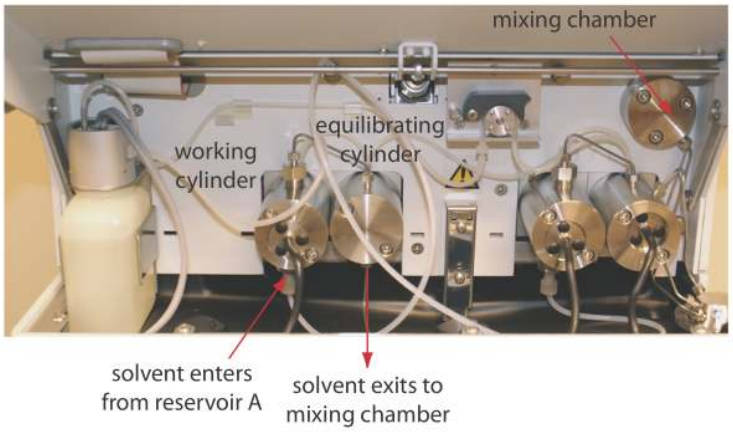


Figure 12.5.7 . Close-up view of the pumps for the instrument shown in Figure 12.5.1 . The working cylinder and the equilibrating cylinder for the pump on the left take solvent from reservoir A and send it to the mixing chamber. The pump on the right moves solvent from reservoir B to the mixing chamber. The mobile phase's flow rate is determined by the combined speeds of the two pumps. By changing the relative speeds of the two pumps, different binary mobile phases can be prepared.

The back and forth movement of a reciprocating pump creates a pulsed flow that contributes noise to the chromatogram. To minimize these pulses, each pump in Figure 12.5.7 has two cylinders. During the working cylinder's forward stoke it fills the equilibrating cylinder and establishes flow through the column. When the working cylinder is on its reverse stroke, the flow is maintained by the piston in the equilibrating cylinder. The result is a pulse-free flow.

> There are other possible ways to control the mobile phase's composition and flow rate. For example, instead of the two pumps in Figure 12.5.7 , we can place a solvent proportioning valve before a single pump. The solvent proportioning value connects two or more solvent reservoirs to the pump and determines how much of each solvent is pulled during each of the pump's cycles. Another approach for eliminating a pulsed flow is to include a pulse damper between the pump and the column. A pulse damper is a chamber filled with an easily compressed fluid and a flexible diaphragm. During the piston's forward stroke the fluid in the pulse damper is compressed. When the piston withdraws to refill the pump, pressure from the expanding fluid in the pulse damper maintains the flow rate.

INJECTING THE SAMPLE

The operating pressure within an HPLC is sufficiently high that we cannot inject the sample into the mobile phase by inserting a syringe through a septum, as is possible in gas chromatography. Instead, we inject the sample using a ***loop injector***, a diagram of which is shown in Figure 12.5.8 . In the load position a sample loop—which is available in a variety of sizes ranging from 0.5 µL to 5 mL—is isolated from the mobile phase and open to the atmosphere. The sample loop is filled using a syringe with a capacity several times that of the sample loop, with excess sample exiting through the waste line. After loading the sample, the injector is turned to the inject position, which redirects the mobile phase through the sample loop and onto the column.

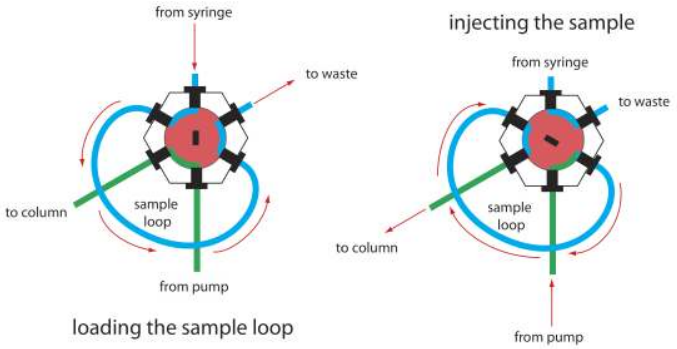


Figure 12.5.8 . Schematic diagram of a manual loop injector. In the load position the flow of mobile phase from the pump to the column (shown in green) is isolated from the sample loop, which is filled using a syringe (shown in blue). Rotating the inner valve (shown in red) to the inject position directs the mobile phase through the sample loop and onto the column.

The instrument in Figure 12.5.1 uses an autosampler to inject samples. Instead of using a syringe to push the sample into the sample loop, the syringe draws sample into the sample loop.

DETECTORS FOR HPLC

Many different types of detectors have been use to monitor HPLC separations, most of which use the spectroscopic techniques from Chapter 10 or the electrochemical techniques from Chapter 11.

SPECTROSCOPIC DETECTORS

The most popular HPLC detectors take advantage of an analyte's UV/Vis absorption spectrum. These detectors range from simple designs, in which the analytical wavelength is selected using appropriate filters, to a modified spectrophotometer in which the sample compartment includes a flow cell. Figure 12.5.9 shows the design of a typical flow cell when using a diode array spectrometer as the detector. The flow cell has a volume of 1–10 μL and a path length of 0.2–1 cm.

To review the details of how we measure absorbance, see Chapter 10.2. More information about different types of instruments, including the diode array spectrometer, is in Chapter 10.3.

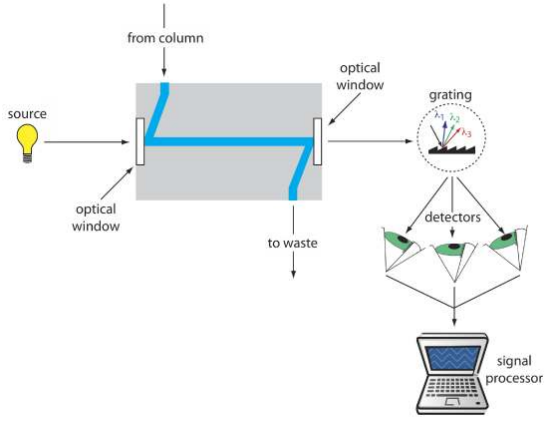


Figure 12.5.9 . Schematic diagram of a flow cell for a detector equipped with a diode array spectrometer.

When using a UV/Vis detector the resulting chromatogram is a plot of absorbance as a function of elution time (see Figure 12.5.10). If the detector is a diode array spectrometer, then we also can display the result as a three-dimensional chromatogram that shows absorbance as a function of wavelength and elution time. One limitation to using absorbance is that the mobile phase cannot absorb at the wavelengths we wish to monitor. Table 12.5.1 lists the minimum useful UV wavelength for several common HPLC solvents. Absorbance detectors provide detection limits of as little as 100 pg–1 ng of injected analyte.

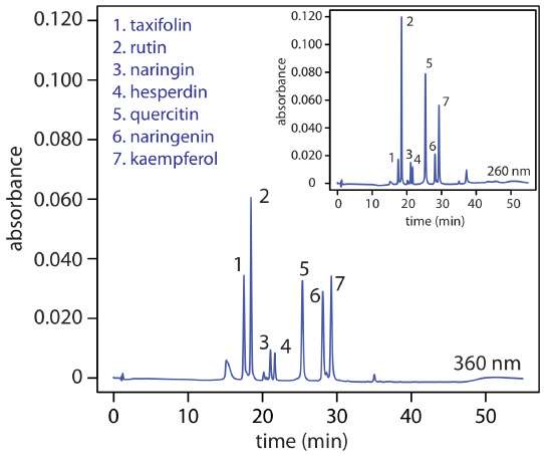


Figure 12.5.10 . HPLC separation of a mixture of flavonoids with UV/Vis detection at 360 nm and, in the inset, at 260 nm. The choice of wavelength affects each analyte's signal. By carefully choosing the wavelength, we can enhance the signal for the analytes of greatest interest. Data provided by Christopher Schardon, Kyle Meinhardt, and Michelle Bushey, Department of Chemistry, Trinty University.

If an analyte is fluorescent, we can place the flow cell in a spectrofluorimeter. As shown in Figure 12.5.11 , a fluorescence detector provides additional selectivity because only a few of a sample's components are fluorescent. Detection limits are as little as 1–10 pg of injected analyte.

> See Chapter 10.6 for a review of fluorescence spectroscopy and spectrofluorimeters.

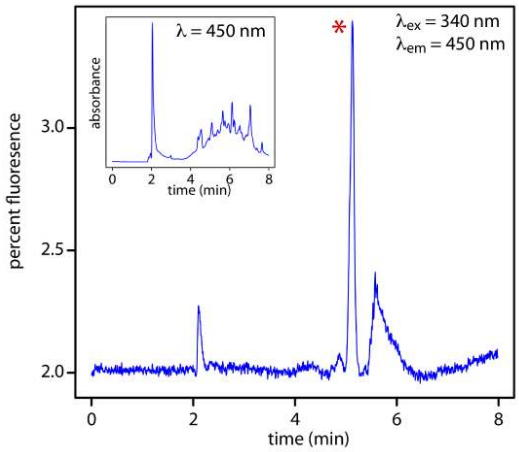


Figure 12.5.11 . HPLC chromatogram for the determination of riboflavin in urine using fluorescence detection with exci-tation at a wavelength of 340 nm and detection at 450 nm. The peak corresponding to riboflavin is marked with a red asterisk (*). The inset shows the same chromatogram when using a less-selective UV/Vis detector at a wavelength of 450 nm. Data provided by Jason Schultz, Jonna Berry, Kaelene Lundstrom, and Dwight Stoll, Department of Chemistry, Gustavus Adolphus College.

ELECTROCHEMICAL DETECTORS

Another common group of HPLC detectors are those based on electrochemical measurements such as amperometry, voltammetry, coulometry, and conductivity. Figure 12.5.12 , for example, shows an amperometric flow cell. Effluent from the column passes over the working electrode—held at a constant potential relative to a downstream reference electrode—that completely oxidizes or reduces the analytes. The current flowing between the working electrode and the auxiliary electrode serves as the analytical signal. Detection limits for amperometric electrochemical detection are from 10 pg–1 ng of injected analyte.

> See Chapter 11.4 for a review of amperometry.

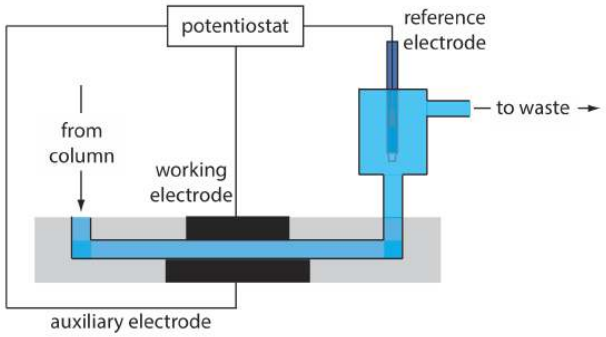


Figure 12.5.12 . Schematic diagram showing a flow cell for an amperometric electrochemical detector.

OTHER DETECTORS

Several other detectors have been used in HPLC. Measuring a change in the mobile phase's refractive index is analogous to monitoring the mobile phase's thermal conductivity in gas chromatography. A refractive index detector is nearly universal, responding to almost all compounds, but has a relatively poor detection limit of 0.1–1 μg of injected analyte. An additional limitation of a refractive index detector is that it cannot be used for a gradient elution unless the mobile phase components have identical refractive indexes.

Another useful detector is a mass spectrometer. Figure 12.5.13 shows a block diagram of a typical HPLC–MS instrument. The effluent from the column enters the mass spectrometer's ion source using an interface the removes most of the mobile phase, an essential need because of the incompatibility between the liquid mobile phase and the mass spectrometer's high vacuum environment. In the ionization chamber the remaining molecules—a mixture of the mobile phase components and solutes—undergo ionization and fragmentation. The mass spectrometer's mass analyzer separates the ions by their mass-to-charge ratio (m/z). A detector counts the ions and displays the mass spectrum.

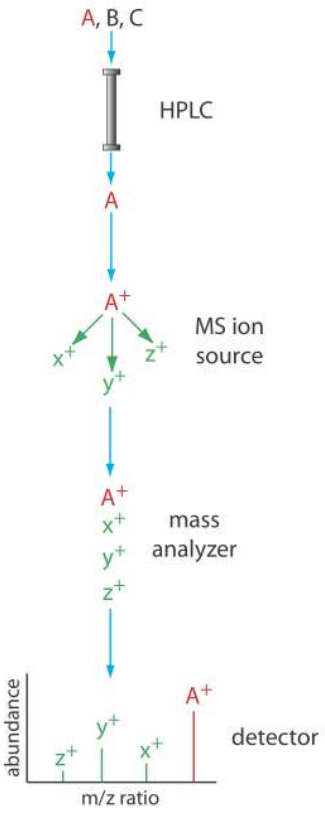


Figure 12.5.13 . Block diagram of an HPLC–MS. A three component mixture enters the HPLC. When component A elutes from the column, it enters the MS ion source and ionizes to form the parent ion and several fragment ions. The ions enter the mass analyzer, which separates them by their mass-to-charge ratio, providing the mass spectrum shown at the detector.

There are several options for monitoring the chromatogram when using a mass spectrometer as the detector. The most common method is to continuously scan the entire mass spectrum and report the total signal for all ions reaching the detector during each scan. This total ion scan

provides universal detection for all analytes. As seen in Figure 12.5.14 , we can achieve some degree of selectivity by monitoring only specific mass-to-charge ratios, a process called selective-ion monitoring.

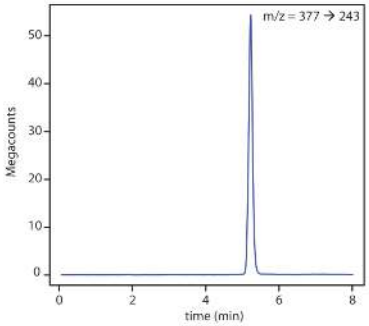


Figure 12.5.14 . HPLC–MS/MS chromatogram for the determination of riboflavin in urine. An initial parent ion with an m/z ratio of 377 enters a second mass spectrometer where it undergoes additional 20 ionization; the fragment ion with an m/z ratio of 243 provides the signal. The selectivity of this detector is evident when you compare this chromatogram to the one in Figure 12.5.11 , which uses fluoresence deterction. Data provided by Jason Schultz, Jonna Berry, Kaelene Lundstrom, and Dwight Stoll, Department of Chemistry, Gustavus Adolphus College.

The advantages of using a mass spectrometer in HPLC are the same as for gas chromatography. Detection limits are very good, typically 0.1–1 ng of injected analyte, with values as low as 1–10 pg for some samples. In addition, a mass spectrometer provides qualitative, structural information that can help to identify the analytes. The interface between the HPLC and the mass spectrometer is technically more difficult than that in a GC–MS because of the incompatibility of a liquid mobile phase with the mass spectrometer's high vacuum requirement.

> For more details on mass spectrometry see Introduction to Mass Spectrometry by Michael Samide and Olujide Akinbo, a resource that is part of the Analytical Sciences Digital Library.

QUANTITATIVE APPLICATIONS

High-performance liquid chromatography is used routinely for both qualitative and quantitative analyses of environmental, pharmaceutical, industrial, forensic, clinical, and consumer product samples.

PREPARING SAMPLES FOR ANALYSIS

Samples in liquid form are injected into the HPLC after a suitable clean-up to remove any particulate materials, or after a suitable extraction to remove matrix interferents. In determining polyaromatic hydrocarbons (PAH) in wastewater, for example, an extraction with CH_2Cl_2 serves the dual purpose of concentrating the analytes and isolating them from matrix interferents. Solid samples are first dissolved in a suitable solvent or the analytes of interest brought into solution by extraction. For example, an HPLC analysis for the active ingredients and the degradation products in a pharmaceutical tablet often begins by extracting the powdered tablet with a portion of mobile phase. Gas samples are collected by bubbling them through a trap that contains a suitable solvent. Organic isocyanates in industrial atmospheres are collected by bubbling the air through a solution of 1-(2-methoxyphenyl)piperazine in toluene. The reaction between the isocyanates and 1-(2-methoxyphenyl)piperazine both stabilizes them against degradation before the HPLC analysis and converts them to a chemical form that can be monitored by UV absorption.

QUANTITATIVE CALCULATIONS

A quantitative HPLC analysis is often easier than a quantitative GC analysis because a fixed volume sample loop provides a more precise and accurate injection. As a result, most quantitative HPLC methods do not need an internal standard and, instead, use external standards and a normal calibration curve.

> An internal standard is necessary when using HPLC–MS because the interface between the HPLC and the mass spectrometer does not allow for a reproducible transfer of the column's eluent into the MS's ionization chamber.

✔ EXAMPLE 12.5.2

The concentration of polynuclear aromatic hydrocarbons (PAH) in soil is determined by first extracting the PAHs with methylene chloride. The extract is diluted, if necessary, and the PAHs separated by HPLC using a UV/Vis or fluorescence detector. Calibration is achieved using one or more external standards. In a typical analysis a 2.013-g sample of dried soil is extracted with 20.00 mL of methylene chloride. After filtering to remove the soil, a 1.00-mL portion of the extract is removed and diluted to 10.00 mL with acetonitrile. Injecting 5 µL of the diluted extract into an HPLC gives a signal of 0.217 (arbitrary units) for the PAH fluoranthene. When

5 µL of a 20.0-ppm fluoranthene standard is analyzed using the same conditions, a signal of 0.258 is measured. Report the parts per million of fluoranthene in the soil.

Solution

For a single-point external standard, the relationship between the signal, *S*, and the concentration, *C*, of fluoranthene is

$$S = kC$$

Substituting in values for the standard's signal and concentration gives the value of *k* as

$$k = \frac{S}{C} = \frac{0.258}{20.0 \text{ ppm}} = 0.0129 \text{ ppm}^{-1}$$

Using this value for *k* and the sample's HPLC signal gives a fluoranthene concentration of

$$C = \frac{S}{k} = \frac{0.217}{0.0129 \text{ ppm}^{-1}} = 16.8 \text{ ppm}$$

for the extracted and diluted soil sample. The concentration of fluoranthene in the soil is

$$\frac{16.8 \text{ g/mL} \times \frac{10.00 \text{ mL}}{1.00 \text{ mL}} \times 20.00 \text{ mL}}{2.013 \text{ g sample}} = 1670 \text{ ppm fluoranthene}$$

EXERCISE 12.5.2

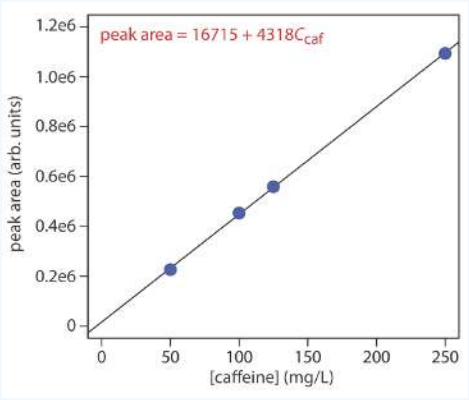
The concentration of caffeine in beverages is determined by a reversed-phase HPLC separation using a mobile phase of 20% acetonitrile and 80% water, and using a nonpolar C_8 column. Results for a series of 10-µL injections of caffeine standards are in the following table.

[caffeine] (mg/L)	peak area (arb. units)
50.0	226724
100.0	453762
125.0	559443
250.0	1093637

What is the concentration of caffeine in a sample if a 10-µL injection gives a peak area of 424195? The data in this problem comes from Kusch, P.; Knupp, G. "Simultaneous Determination of Caffeine in Cola Drinks and Other Beverages by Reversed-Phase HPTLC and Reversed-Phase HPLC," *Chem. Educator*, **2003**, *8*, 201–205.

Answer

The figure below shows the calibration curve and calibration equation for the set of external standards. Substituting the sample's peak area into the calibration equation gives the concentration of caffeine in the sample as 94.4 mg/L.



The best way to appreciate the theoretical and the practical details discussed in this section is to carefully examine a typical analytical method. Although each method is unique, the following description of the determination of fluoxetine in serum provides an instructive example of a typical procedure. The description here is based on Smyth, W. F. *Analytical Chemistry of Complex Matricies*, Wiley Teubner: Chichester, England, 1996, pp. 187–189.

REPRESENTATIVE METHOD 12.5.1: DETERMINATION OF FLUOXETINE IN SERUM

Description of Method

Fluoxetine is another name for the antidepressant drug Prozac. The determination of fluoxetine in serum is an important part of monitoring its therapeutic use. The analysis is complicated by the complex matrix of serum samples. A solid-phase extraction followed by an HPLC analysis using a fluorescence detector provides the necessary selectivity and detection limits.

Procedure

Add a known amount of the antidepressant protriptyline, which serves as an internal standard, to each serum sample and to each external standard. To remove matrix interferents, pass a 0.5-mL aliquot of each serum sample or standard through a C_{18} solid-phase extraction cartridge. After washing the cartridge to remove the interferents, elute the remaining constituents, including the analyte and the internal standard, by washing the cartridge with 0.25 mL of a 25:75 v/v mixture of 0.1 M $HClO_4$ and acetonitrile. Inject a 20-µL aliquot onto a 15-cm × 4.6-mm column packed with a 5 µm C_8-bonded stationary phase. The isocratic mobile phase is 37.5:62.5 v/v acetonitrile and water (that contains 1.5 g of tetramethylammonium perchlorate and 0.1 mL of 70% v/v $HClO_4$). Monitor the chromatogram using a fluorescence detector set to an excitation wave- length of 235 nm and an emission wavelength of 310 nm.

Questions

1. The solid-phase extraction is important because it removes constitutions in the serum that might interfere with the analysis. What types of interferences are possible?

Blood serum, which is a complex mixture of compounds, is approximately 92% water, 6–8% soluble proteins, and less than 1% each of various salts, lipids, and glucose. A direct injection of serum is not advisable for three reasons. First, any particulate materials in the serum will clog the column and restrict the flow of mobile phase. Second, some of the compounds in the serum may absorb too strongly to the stationary phase, degrading the column's performance. Finally, although an HPLC can separate and analyze complex mixtures, an analysis is difficult if the number of constituents exceeds the column's peak capacity.

2. One advantage of an HPLC analysis is that a loop injector often eliminates the need for an internal standard. Why is an internal standard used in this analysis? What assumption(s) must we make when using the internal standard?

An internal standard is necessary because of uncertainties introduced during the solid-phase extraction. For example, the volume of serum transferred to the solid-phase extraction cartridge, 0.5 mL, and the volume of solvent used to remove the analyte and internal standard, 0.25 mL, are very small. The precision and accuracy with which we can measure these volumes is not as good as when we use larger volumes. For example, if we extract the analyte into a volume of 0.24 mL instead of a volume of 0.25 mL, then the analyte's concentration increases by slightly more than 4%. In addition, the concentration of eluted analytes may vary from trial-to-trial due to variations in the amount of solution held up by the cartridge. Using an internal standard compensates for these variation. To be useful we must assume that the analyte and the internal standard are retained completely during the initial loading, that they are not lost when the cartridge is washed, and that they are extracted completely during the final elution.

3. Why does the procedure monitor fluorescence instead of monitoring UV absorption?

Fluorescence is a more selective technique for detecting analytes. Many other commonly prescribed antidepressants (and their metabolites) elute with retention times similar to that of fluoxetine. These compounds, however, either do not fluoresce or are only weakly fluorescent.

4. If the peaks for fluoxetine and protriptyline are resolved insufficiently, how might you alter the mobile phase to improve their separation?

Decreasing the amount of acetonitrile and increasing the amount of water in the mobile will increase retention times, providing more time to effect a separation.

EVALUATION

With a few exceptions, the scale of operation, accuracy, precision, sensitivity, selectivity, analysis time, and cost for an HPLC method are similar to GC methods. Injection volumes for an HPLC method usually are larger than for a GC method because HPLC columns have a greater capacity. Because it uses a loop injection, the precision of an HPLC method often is better than a GC method. HPLC is not limited to volatile analytes, which means we can analyze a broader range of compounds. Capillary GC columns, on the other hand, have more theoretical plates, and can separate more complex mixtures.

This page titled 10.3: High-Performance Liquid Chromatography is shared under a CC BY-NC-SA 4.0 license and was authored, remixed, and/or curated by David Harvey.

- **12.5: High-Performance Liquid Chromatography** by David Harvey is licensed CC BY-NC-SA 4.0.

10.3.1: High Performance Liquid Chromatography

High Performance Liquid Chromotagraphy (HPLC) is an analytical technique used for the separation of compounds soluble in a particular solvent.

History of HPLC

Liquid chromatography was initially discovered as an analytical technique in the early twentieth century and was first used as a method of separating colored compounds. This is where the name **chromatography** *chroma* means color, *graphy* means writing, was derived. A Russian botanist named Mikhail S. Tswett used a rudimentary form of chromatographic separation to purify mixtures of plant pigments into the pure constituents. He separated the pigments based on their interaction with a **stationary phase**, which is essential to any chromatographic separation. The stationary phase he used was powdered chalk and aluminia, the mobile phase in his separation was the solvent. After the solid stationary phase was packed into a glass column (essentially a long, hollow, glass tube) he poured the mixture of plant pigments and solvent in the top of the column. He then poured additional solvent into the column until the samples were eluted at the bottom of the column. The result of this process most crucial to his investigation was that the plant pigments separated into bands of pure components as they passed through the stationary phase. Modern high performance liquid chromatography or HPLC has its roots in this separation, the first form of liquid chromatography. The chromatographic process has been significantly improved over the last hundred years, yielding greater separation efficiency, versatility and speed.

Affinities for Mobile and Stationary Phases

All chromatographic separations, including HPLC operate under the same basic principle; every compound interacts with other chemical species in a characteristic manner. Chromatography separates a sample into its constituent parts because of the difference in the relative affinities of different molecules for the mobile phase and the stationary phase used in the separation.

Distribution Constant

All chemical reactions have a characteristic equilibrium constant. For the reaction

$$A_{aq} + B_s \rightleftharpoons AB_s \tag{10.3.1.1}$$

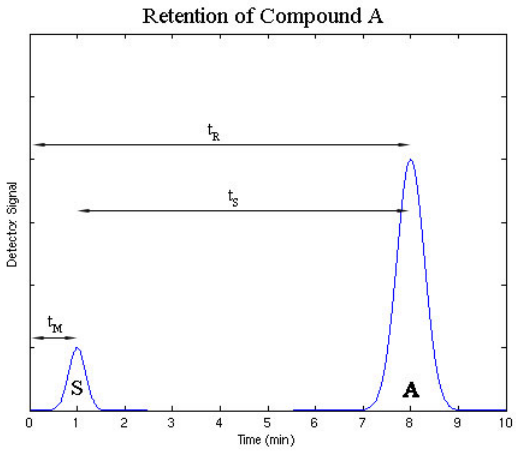
There is a chemical equilibrium constant $\mathbf{K_{eq}}$ that dictates what percentage of compound **A** will be in solution and what percentage will be bound to the stationary compound **B**. During a chromatographic separation, there is similar relationship between compound **A** and the solvent, or **mobile phase**, **C**. This will yield an overall equilibrium equation which dictates the quantity of **A** that will be associated with the stationary phase and the quantity of **A** that will be associated with the mobile phase.

$$A_{mobile} \rightleftharpoons A_{stationary} \tag{10.3.1.2}$$

The equilibrium between the mobile phase and stationary phase is given by the constant $\mathbf{K_c}$.

$$K_c = \frac{(a_A)_S}{(a_A)_M} \approx \frac{c_S}{c_M} \tag{10.3.1.3}$$

Where $\mathbf{K_c}$, the **distribution constant**, is the ratio of the activity of compound **A** in the stationary phase and activity of compound **A** in the mobile phase. In most separations, which contain low concentrations of the species to be separated, the activity of **A** in each is approximately equal to the concentration of **A** in that state. The distribution constant indicates the amount of time that compound **A** spends adsorbed to the stationary phase as the opposed to the amount of time **A** spends solvated by the mobile phase. This relationship determines the amount of time it will take for compound **A** to travel the length of the column. The more time **A** spends adsorbed to the stationary phase, the more time compound **A** will take to travel the length of the column. The amount of time between the injection of a sample and its elution from the column is known as the **retention time**; it is given the symbol $\mathbf{t_R}$.



The amount of time required for a sample that does not interact with the stationary phase, or has a $\mathbf{K_c}$ equal to zero, to travel the length of the column is known as the **void time**, $\mathbf{t_M}$. No compound can be eluted in less than the void time.

Retention Factor

Since $\mathbf{K_c}$ is a factor that is wholly dependent on a particular column and solvent flow rate, a quantitative measure of the affinity of a compound for a particular set of mobile and stationary phases that does not depend on the column geometry is useful. The **retention factor**, **k**, can be derived from $\mathbf{K_c}$ and is independent of the column size and the solvent flow rate.

$$k_C = \frac{K_C V_S}{V_M} \tag{10.3.1.4}$$

The retention factor is calculated by multiplying the distribution constant by the volume of stationary phase in the column and dividing by the volume of mobile phase in the column.

Selectivity

In order to separate two compounds, their respective retention factors must be different, otherwise both compounds would be eluted simultaneously; the **selectivity** factor is the ratio of the retention factors.

$$\alpha = \frac{k_B}{k_A} \tag{10.3.1.5}$$

Where **B** is the compound that is retained more strongly by the column and **A** is the compound with the faster elution time.

Band Broadening

As a compound passes through the column it slowly diffuses away from the initial injection band, which is the area of greatest concentration. The initial, narrow, band that contained all of the sample becomes broader the longer the analyte remains in the column. This **band broadening** increases the time required for complete elution of a particular compound and is generally undesirable. It must be minimized so that overly broad elution bands do not overlap with one another. We will see how this is measured quantitatively when we discuss peak resolution momentarily.

Separation Efficiency

The overriding purpose of a chromatographic separation is just that, to separate two or more compounds contained in solution. In analytical chemistry, a quantitative metric of every experimental parameter is desired, and so separation efficiency is measured in plates. The concept of plates as a separation metric arose from the original method of **fractional distillation**, where compounds were separated based on their volatilities through many simultaneous **simple distillations**, each simple distillation occurred on one of many distillation plates. In chromatography, no actual plates are used, but the concept of a **theoretical plate**, as a distinct region where a single equilibrium is maintained, remains. In a particular liquid chromatographic separation, the number of theoretical plates and the **height equivalent to a theoretical plate (HETP)** are related simply by the length of the column

$$N = \frac{L}{H} \tag{10.3.1.6}$$

Where **N** is the number of theoretical plates, **L** is the length of the column, and **H** is the height equivalent to a theoretical plate. The plate height is given by the **variance** (standard deviation squared) of an elution peak divided by the length of the column.

$$H = \frac{\sigma^2}{L} \tag{10.3.1.7}$$

The standard deviation of an elution peak can be approximated by assuming that a Gaussian elution peak is roughly triangular, in that case the plate height can be given by the width of the elution peak squared times the length of the column over the retention time of the that peak squared times 16.

$$H = \frac{LW^2}{16t_R^2} \tag{10.3.1.8}$$

Using the relationship between plate height and number of plates, the number of plates can also be found in terms of retention time and peak width.

$$N = 16\left(\frac{t_R}{W}\right)^2 \tag{10.3.1.9}$$

In order to optimize separation efficiency, it is necessary in maximize the number of theoretical plates, which requires reducing the plate height. The plate height is related to the **flow rate** of the mobile phase, so for a fixed set of mobile phase, stationary phase, and analytes; separation efficiency can be maximized by optimizing flow rate as dictated by the **van Deemter equation**.

$$H = A + \frac{B}{v} + Cv \tag{10.3.1.10}$$

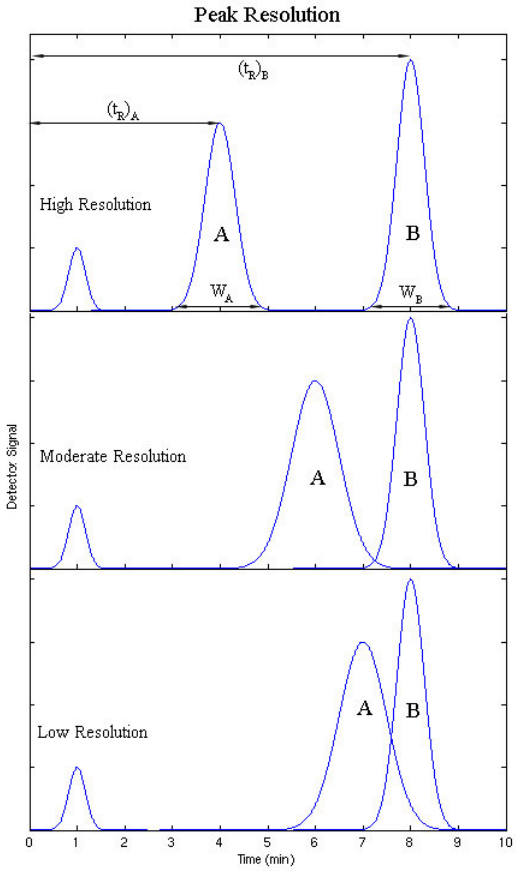
The three constants in the van Deemter equation are factors that describe possible causes of band broadening in a particular separation. A is a constant which represents the different possible paths that can be taken by the analyte through the stationary phase, it decreases if the packing of the column is kept as small as possible. B is a constant that describes the longitudinal diffusion that occurs in the system. C is a constant that describes the rate of adsorption and desorption of the analyte to the stationary phase. A, B and C are constant for any given system (with constant analyte, stationary phase, and mobile phase), so flow rate must be optimized accordingly. If the flow rate is too low, the **longitudinal diffusion factor** ($\frac{B}{v}$) will increase significantly, which will increase plate height. At low flow rates, the analyte spends more time at rest in the column and therefore longitudinal diffusion in a more significant problem. If the flow rate is too high, the **mass transfer term** (Cv) will increase and reduce column efficiency. At high flow rates the adsorption of the analyte to the stationary phase results in some of the sample lagging behind, which also leads to band broadening.

Resolution

The **resolution** of a elution is a quantitative measure of how well two elution peaks can be differentiated in a chromatographic separation. It is defined as the difference in retention times between the two peaks, divided by the combined widths of the elution peaks.

$$R_S = \frac{2\left[(t_R)_B - (t_R)_A\right]}{W_B + W_A} \tag{10.3.1.11}$$

Where **B** is the species with the longer retention time, and $\mathbf{t_R}$ and **W** are the retention time and elution peak width respectively. If the resolution is greater than one, the peaks can usually be differentiated successfully.



HPLC as a solution to efficiency problems

While all of these basic principles hold true for all chromatographic separations, HPLC was developed as method to solve some of the shortcomings of standard liquid chromatography. Classic liquid chromatography has several severe limitations as a separation method. When the solvent is driven by gravity, the separation is very slow, and if the solvent is driven by vacuum, in a standard packed column, the plate height increases and the effect of the vacuum is negated. The limiting factor in liquid chromatography was originally the size of the column packing, once columns could be packed with particles as small as 3 µm, faster separations could be performed in smaller, narrower, columns. High pressure was required to force the mobile phase and sample through these new columns, and previously unneeded apparatus was required to maintain reproducibility of results in this new instruments. The use of high pressures in a narrow column allowed for a more effective separation to be achieved in much less time than was required for previous forms of liquid chromatography.

Apparatus

Specialized apparatus is required for an HPLC separation because of the high pressures and low tolerances under which the separation occurs. If the results are to be reproducible, then the conditions of the separation must also be reproducible. Thus HPLC equipment must be of high quality; it is therefore expensive.

Solvent

The **mobile phase**, or solvent, in HPLC is usually a mixture of polar and non-polar liquid components whose respective concentrations are varied depending on the composition of the sample. As the solvent is passed through a very narrow bore column, any contaminants could at worst plug the column, or at the very least add variability to the retention times during repeated different trials. Therefore HPLC solvent must be kept free of dissolved gases, which could come out of solution mid-separation, and particulates.

Column

In the **HPLC column**, the components of the sample separate based on their differing interactions with the column packing. If a species interacts more strongly with the stationary phase in the column, it will spend more time adsorbed to the column's adsorbent and will therefore have a greater retention time. Columns can be packed with solids such as silica or alumina; these columns are called **homogeneous columns**. If stationary phase in the column is a liquid, the column is deemed a **bonded column**. Bonded columns contain a liquid stationary phase bonded to a sold support, which is again usually silica or alumina. The value of the constant **C** described in the van Deemter equation is proportional, in HPLC, to the diameter of the particles that constitute the column's packing material.

Pump

The **HPLC pump** drives the solvent and sample through the column. To reduce variation in the elution, the pump must maintain a constant, pulse free, flow rate; this is achieved with **multi-piston pumps**. The presence of two pistons allows the flow rate to be controlled by one piston as the other recharges. A **syringe pump** can be used for even greater control of flow rate; however, the syringe pump is unable to produce as much pressure as a piston pump, so it cannot be used in all HPLC applications.

Detector

The **HPLC detector**, located at the end of the column, must register the presence of various components of the sample, but must not detect the solvent. For that reason there is no universal detector that works for all separations. A common HPLC detector is a **UV absorption detector**, as most medium to large molecules absorb UV radiation. Detectors that measure fluorescence and refractive index are also used for special applications. A relatively new development is the combination of an HPLC separation with an **NMR detector**. This allows the pure components of the sample to be identified and quantified by nuclear magnetic resonance after having been separated by HPLC, in one integrated process.

Technique

Normal Phase vs. Reverse Phase

If the stationary phase is more polar than the mobile phase, the separation is deemed **normal phase**. If the stationary phase is less polar than the mobile phase, the separation is **reverse phase**. In reverse phase HPLC the retention time of a compound increases with decreasing polarity of the particular species. The key to an effective and efficient separation is to determine the appropriate ratio between polar and non-polar components in the mobile phase. The goal is for all the compounds to elute in as short a time as possible, while still allowing for the resolution of individual peaks. Typical columns for normal phase separation are packed with alumina or silica. Alkyl, aliphatic or phenyl bonded phases are typically used for reverse phase separation.

Gradient Elution vs. Isocratic Elution

If the composition of the mobile phase remains constant throughout the HPLC separation, the separation is deemed an **isocratic elution**. Often the only way to elute all of the compounds in the sample in a reasonable amount of time, while still maintaining peak resolution, is to change the ratio of polar to non-polar compounds in the mobile phase during the sample run. Known as **gradient chromatography**, this is the technique of choice when a sample contains components of a wide range of polarities. For a **reverse phase gradient**, the solvent starts out relatively polar and slowly becomes more non-polar. The gradient elution offers the most complete separation of the peaks, without taking an inordinate amount of time. A sample containing compounds of a wide range of polarities can be separated by a gradient elution in a shorter time period without a loss of resolution in the earlier peaks or excessive broadening of later peaks. However, gradient elution requires more complex and expensive equipment and it is more difficult to maintain a constant flow rate while there are constant changes in mobile phase composition. Gradient elution, especially at high speeds, brings out the limitations of lower quality experimental apparatus, making the results obtained less reproducible in equipment already prone to variation. If the flow rate or mobile phase composition fluctuates, the results will not be reproducible.

Applications

HPLC can be used in both qualitative and quantitative applications, that is for both compound identification and quantification. Normal phase HPLC is only rarely used now, almost all HPLC separation can be performed in reverse phase. Reverse phase HPLC (RPLC) is ineffective in for only a few separation types; it cannot separate inorganic ions (they can be separated by ion exchange chromatography). It cannot separate polysaccharides (they are too hydrophilic for any solid phase adsorption to occur), nor polynucleotides (they adsorb irreversibly to the reverse phase packing). Lastly, incredibly hydrophobic compounds cannot be separated effectively by RPLC (there is little selectivity). Aside from these few exceptions, RPLC is used for the separation of

almost all other compound varieties. RPLC can be used to effectively separate similar simple and aromatic hydrocarbons, even those that differ only by a single methylene group. RPLC effectively separates simple amines, sugars, lipids, and even pharmaceutically active compounds. RPLC is also used in the separation of amino acids, peptides, and proteins. Finally RPLC is used to separate molecules of biological origin. The determination of caffeine content in coffee products is routinely done by RPLC in commercial applications in order to guarantee purity and quality of ground coffee. HPLC is a useful addition to an analytical arsenal, especially for the separation of a sample before further analysis.

References

1. Skoog, D.; Holler, F.; Crouch, S. *Principles of Instrumental Analysis* **2007**
2. Swadesh, J.K. *HPLC: Practical and Industrial Applications* **2001**
3. Waters Corporation: History of Chromatography (accessed March 3, 2008)

Contributors and Attributions

- Matthew Barkovich (UCD)

10.3.1: High Performance Liquid Chromatography is shared under a CC BY-NC-SA 4.0 license and was authored, remixed, and/or curated by LibreTexts.

- **High Performance Liquid Chromatography** is licensed CC BY-NC-SA 4.0.

10.4: OTHER FORMS OF CHROMATOGRAPHY

At the beginning of Section 12.5, we noted that there are several different types of solute/stationary phase interactions in liquid chromatography, but limited our discussion to liquid–liquid chromatography. In this section we turn our attention to liquid chromatography techniques in which partitioning occurs by liquid–solid adsorption, ion-exchange, and size exclusion.

LIQUID-SOLID CHROMATOGRAPHY

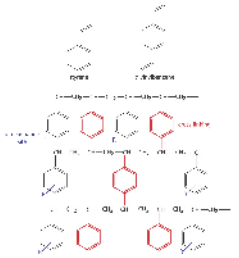
In ***liquid–solid adsorption chromatography*** (LSC) the column packing also serves as the stationary phase. In Tswett's original work the stationary phase was finely divided $CaCO_3$, but modern columns employ porous 3–10 μm particles of silica or alumina. Because the stationary phase is polar, the mobile phase usually is a nonpolar or a moderately polar solvent. Typical mobile phases include hexane, isooctane, and methylene chloride. The usual order of elution—from shorter to longer retention times—is

olefins < aromatic hydrocarbons < ethers < esters, aldehydes, ketones < alcohols, amines < amide < carboxylic acids

Nonpolar stationary phases, such as charcoal-based absorbents, also are used. For most samples, liquid–solid chromatography does not offer any special advantages over liquid–liquid chromatography. One exception is the analysis of isomers, where LSC excels.

ION-EXCHANGE CHROMATOGRAPHY

In ***ion-exchange chromatography*** (IEC) the stationary phase is a cross-linked polymer resin, usually divinylbenzene cross-linked polystyrene, with covalently attached ionic functional groups (see Figure 12.6.1 and Table 12.6.1). The counterions to these fixed charges are mobile and are displaced by ions that compete more favorably for the exchange sites. Ion-exchange resins are divided into four categories: strong acid cation exchangers; weak acid cation exchangers; strong base anion exchangers; and weak base anion exchangers.



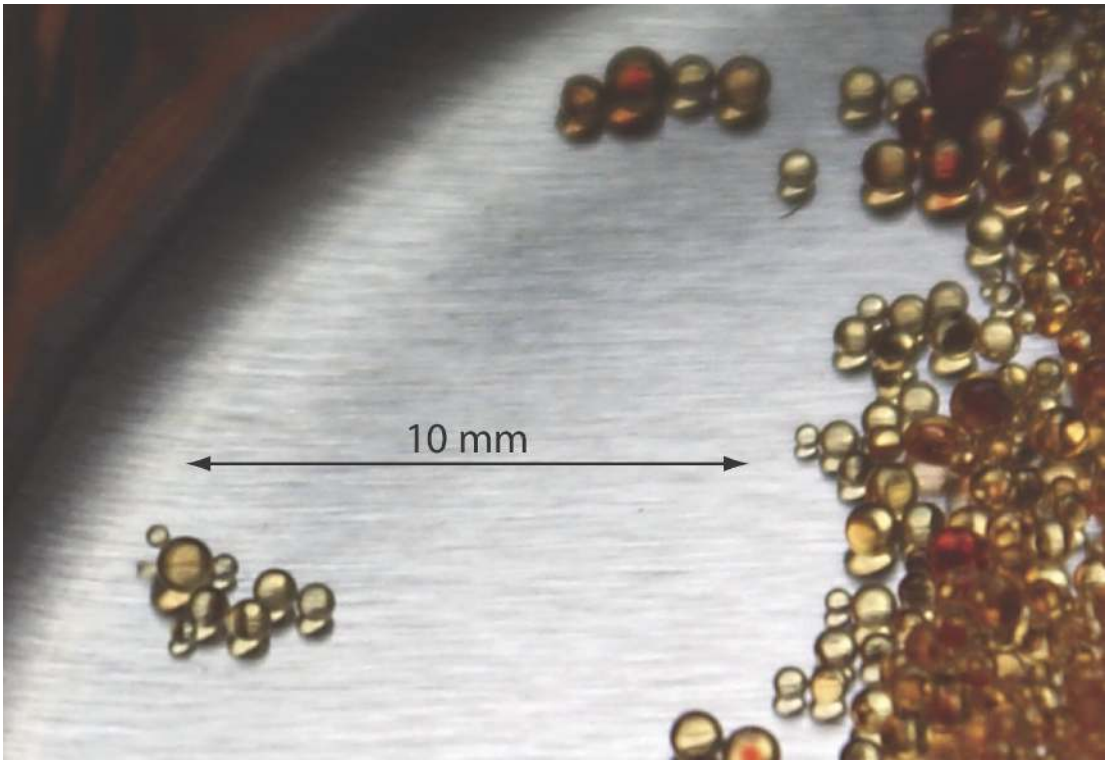


Figure 12.6.1 . Structures of styrene, divinylbenzene, and a styrene–divinylbenzene co-polymer modified for use as an ion-exchange resin are shown on the left. The ion-exchange sites, indicated by R and shown in blue, are mostly in the *para* position and are not necessarily bound to all styrene units. The cross-linking is shown in red. The photo on the right shows an example of the polymer beads. These beads are approximately 0.30–0.85 mm in diameter. Resins for use in ion-exchange chromatography typically are 5–11 μm in diameter.

Table 12.6.1 . Examples of Common Ion-Exchange Resins

type	functional group	examples
strong acid cation exchanger	sulfonic acid	$-SO_3^-$ $-CH_2CH_2SO_3^-$
weak acid cation exchanger	carboxylic acid	$-COO^-$ $-CH_2COO^-$
strong base anion exchanger	quaternary amine	$-CH_2N(CH_3)_3^+$ $-CH_2CH_2N(CH_2CH_3)_3^+$
weak base anion exchanger	amine	$-NH_4^+$ $-CH_2CH_2NH(CH_2CH_3)_3^+$

Strong acid cation exchangers include a sulfonic acid functional group that retains it anionic form—and thus its capacity for ion-exchange—in strongly acidic solutions. The functional groups for a weak acid cation exchanger, on the other hand, are fully protonated at pH levels less then 4 and lose their exchange capacity. The strong base anion exchangers include a quaternary amine, which retains a positive charge even in strongly basic solutions. Weak base anion exchangers remain protonated only at pH levels that are moderately basic. Under more basic conditions a weak base anion exchanger loses a proton and its exchange capacity.

The ion-exchange reaction of a monovalent cation, M^+, exchange site is

$$-SO_3^-H^+(s) + M^+(aq) \rightleftharpoons -SO_3^-M^+(s) + H^+(aq)$$

The equilibrium constant for this ion-exchange reaction, which we call the selectivity coefficient, *K*, is

$$K = \frac{\{-SO_3^-M^+\}\left[H^+\right]}{\{-SO_3^-H^+\}\left[M^+\right]} \tag{10.4.1}$$

where we use curly brackets, { }, to indicate a surface concentration instead of a solution concentration.

> We don't usually think about a solid's concentration. There is a good reason for this. In most cases, a solid's concentration is a constant. If you break a piece of chalk into two parts, for example, the mass and the volume of each piece retains the same proportional relationship as in the original piece of chalk. When we consider an ion binding to a reactive site on the solid's surface, however, the fraction of sites that are bound, and thus the concentration of bound sites, can take on any value between 0 and some maximum value that is proportional to the density of reactive sites.

Rearranging Equation 10.4.1 shows us that the distribution ratio, *D*, for the exchange reaction

$$D = \frac{\text{amount of } M^+ \text{ in the stationary phase}}{\text{amount of } M^+ \text{ in the mobile phase}}$$

$$D = \frac{\{-SO_3^-M^+\}}{\left[M^+\right]} = K \times \frac{\{-SO_3^-H^+\}}{\left[H^+\right]} \tag{10.4.2}$$

is a function of the concentration of H^+ and, therefore, the pH of the mobile phase.

An ion-exchange resin's selectivity is somewhat dependent on whether it includes strong or weak exchange sites and on the extent of cross-linking. The latter is particularly important as it controls the resin's permeability, and, therefore, the accessibility of exchange sites. An approximate order of selectivity for a typical strong acid cation exchange resin, in order of decreasing *D*, is

$$Al^{3+} > Ba^{2+} > Pb^{2+} > Ca^{2+} > Ni^{2+} > Cd^{2+} > Cu^{2+} > Co^{2+} > Zn^{2+} > Mg^{2+} > Ag^+ > K^+ > NH_4^+ > Na^+ > H^+ > Li^+$$

Note that highly charged cations bind more strongly than cations of lower charge, and that for cations of similar charge, those with a smaller hydrated radius (see Table 6.9.1 in Chapter 6), or that are more polarizable, bind more strongly. For a strong base anion exchanger the general elution order is

$$SO_4^{2-} > I^- > HSO_4^- > NO_3^- > Br^- > NO_2^- > Cl^- > HCO_3^- > CH3COO^- > OH^- > F^-$$

Anions of higher charge and of smaller hydrated radius bind more strongly than anions with a lower charge and a larger hydrated radius.

The mobile phase in IEC usually is an aqueous buffer, the pH and ionic composition of which determines a solute's retention time. Gradient elutions are possible in which the mobile phase's ionic strength or pH is changed with time. For example, an IEC separation of cations might use a dilute solution of HCl as the mobile phase. Increasing the concentration of HCl speeds the elution rate for more strongly retained cations because the higher concentration of H^+ allows it to compete more successfully for the ion-exchange sites.

> From Equation 10.4.2, a cation's distribution ratio, *D*, becomes smaller when the concentration of H^+ in the mobile phase increases.

An ion-exchange resin is incorporated into an HPLC column either as 5–11 μm porous polymer beads or by coating the resin on porous silica particles. Columns typically are 250 mm in length with internal diameters ranging from 2–5 mm.

Measuring the conductivity of the mobile phase as it elutes from the column serves as a universal detector for cationic and anionic analytes. Because the mobile phase contains a high concentration of ions—a mobile phase of dilute HCl, for example, contains significant concentrations of H^+ and Cl^-—we need a method for detecting the analytes in the presence of a significant background conductivity.

To minimize the mobile phase's contribution to conductivity, an ***ion-suppressor column*** is placed between the analytical column and the detector. This column selectively removes mobile phase ions without removing solute ions. For example, in cation-exchange chromatography using a dilute solution of HCl as the mobile phase, the suppressor column contains a strong base anion-exchange resin. The exchange reaction

$$H^+(aq) + Cl^-(aq) + \text{Resin}^+OH^-(s) \rightleftharpoons \text{Resin}^+\,Cl^-(s) + H_2O(l)$$

replaces the mobile phase ions H^+ and Cl^- with H_2O. A similar process is used in anion-exchange chromatography where the suppressor column contains a cation-exchange resin. If the mobile phase is a solution of Na_2CO_3, the exchange reaction

$$2Na^+(aq) + CO_3^{2-}(aq) + 2\,\text{Resin}^-\,H^+(s) \rightleftharpoons 2\,\text{Resin}^-\,Na^+(s) + H_2CO_3(aq)$$

replaces a strong electrolyte, Na_2CO_3, with a weak electrolyte, H_2CO_3.

Ion-suppression is necessary when the mobile phase contains a high concentration of ions. ***Single-column ion chromatography***, in which an ion-suppressor column is not needed, is possible if the concentration of ions in the mobile phase is small. Typically the stationary phase is a resin with a low capacity for ion-exchange and the mobile phase is a very dilute solution of methane sulfonic acid for cationic analytes, or potassium benzoate or potassium hydrogen phthalate for anionic analytes. Because the background conductivity is sufficiently small, it is possible to monitor a change in conductivity as the analytes elute from the column.

A UV/Vis absorbance detector can be used if the analytes absorb ultraviolet or visible radiation. Alternatively, we can detect indirectly analytes that do not absorb in the UV/Vis if the mobile phase contains a UV/Vis absorbing species. In this case, when a solute band passes through the detector, a decrease in absorbance is measured at the detector.

Ion-exchange chromatography is an important technique for the analysis of anions and cations in water. For example, an ion-exchange chromatographic analysis for the anions F^-, Cl^-, Br^-, NO_2^-, NO_3^-, PO_4^{3-}, and SO_4^{2-} takes approximately 15 minutes (Figure 12.6.2). A complete analysis of the same set of anions by a combination of potentiometry and spectrophotometry requires 1–2 days. Ion-exchange chromatography also is used for the analysis of proteins, amino acids, sugars, nucleotides, pharmaceuticals, consumer products, and clinical samples.

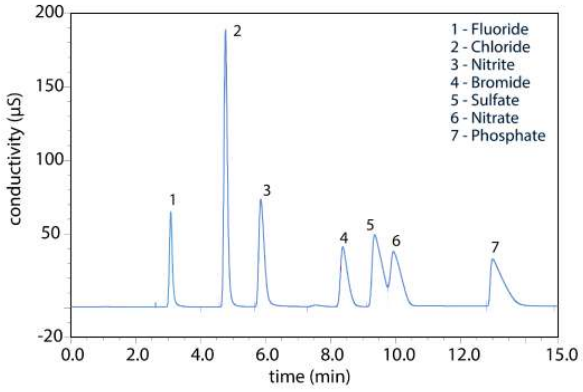


Figure 12.6.2 . Ion-exchange chromatographic analysis of water from Big Walnut Creek in Putnam County, Indiana. Data provided by Jeanette Pope, Department of Geosciences, DePauw University.

SIZE-EXCLUSION CHROMATOGRAPHY

We have considered two classes of micron-sized stationary phases in this section: silica particles and cross-linked polymer resin beads. Both materials are porous, with pore sizes ranging from approximately 5–400 nm for silica particles, and from 5 nm to 100 μm for divinylbenzene cross-linked polystyrene resins. In ***size-exclusion chromatography***—which also is known by the terms molecular-exclusion or gel permeation chromatography—the separation of solutes depends upon their ability to enter into the pores of the stationary phase. Smaller solutes spend proportionally more time within the pores and take longer to elute from the column.

A stationary phase's size selectivity extends over a finite range. All solutes significantly smaller than the pores move through the column's entire volume and elute simultaneously, with a retention volume, V_r, of

$$V_r = V_i + V_o \tag{10.4.3}$$

where V_i is the volume of mobile phase occupying the stationary phase's pore space and V_o is volume of mobile phase in the remainder of the column. The largest solute for which Equation 10.4.3 holds is the column's inclusion limit, or permeation limit. Those solutes too large to enter the pores elute simultaneously with an retention volume of

$$V_r = V_o \tag{10.4.4}$$

Equation 10.4.4 defines the column's ***exclusion limit***.

For a solute whose size is between the inclusion limit and the exclusion limit, the amount of time it spends in the stationary phase's pores is proportional to its size. The retention volume for these solutes is

$$V_r = DV_i + V_o \tag{10.4.5}$$

where D is the solute's distribution ratio, which ranges from 0 at the exclusion limit to 1 at the inclusion limit. Equation 10.4.5 assumes that size-exclusion is the only interaction between the solute and the stationary phase that affects the separation. For this reason, stationary phases using silica particles are deactivated as described earlier, and polymer resins are synthesized without exchange sites.

Size-exclusion chromatography provides a rapid means for separating larger molecules, including polymers and biomolecules. A stationary phase for proteins that consists of particles with 30 nm pores has an inclusion limit of 7500 g/mol and an exclusion limit of 1.2×10^6 g/mol. Mixtures of proteins that span a wider range of molecular weights are separated by joining together in series several columns with different inclusion and exclusion limits.

Another important application of size-exclusion chromatography is the estimation of a solute's molecular weight (MW). Calibration curves are prepared using a series of standards of known molecular weight and measuring each standard's retention volume. As shown in Figure 12.6.3 , a plot of log(MW) versus V_r is roughly linear between the exclusion limit and the inclusion limit. Because a solute's retention volume is influenced by both its size and its shape, a reasonably accurate estimation of molecular weight is possible only if the standards are chosen carefully to minimize the effect of shape.

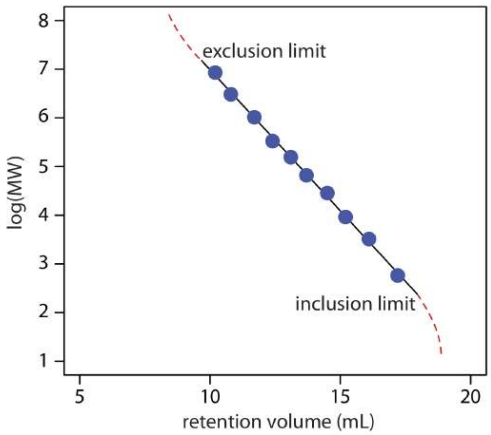


Figure 12.6.3 . Calibration curve for the determination of molecular weight by size-exclusion chromatography. The data shown here are adapted from Rouessac, F.; Rouessac, A. *Chemical Analysis: Modern Instrumentation Methods and Techniques*, Wiley: Chichester, England, 2004, p 141.

Size-exclusion chromatography is carried out using conventional HPLC instrumentation, replacing the HPLC column with an appropriate size-exclusion column. A UV/Vis detector is the most common means for obtaining the chromatogram.

SUPERCRITICAL FLUID CHROMATOGRAPHY

Although there are many analytical applications of gas chromatography and liquid chromatography, they can not separate and analyze all types of samples. Capillary column GC separates complex mixtures with excellent resolution and short analysis times. Its application is limited, however, to volatile analytes or to analytes made volatile by a suitable derivatization reaction. Liquid chromatography separates a wider range of solutes than GC, but the most common detectors—UV, fluorescence, and electrochemical— have poorer detection limits and smaller linear ranges than GC detectors, and are not as universal in their selectivity.

For some samples, ***supercritical fluid chromatography*** (SFC) provides a useful alternative to gas chromatography and liquid chromatography. The mobile phase in supercritical fluid chromatography is a gas held at a temperature and pressure that exceeds its critical point (Figure 12.6.4). Under these conditions the mobile phase is neither a gas nor a liquid. Instead, the mobile phase is a supercritical fluid.

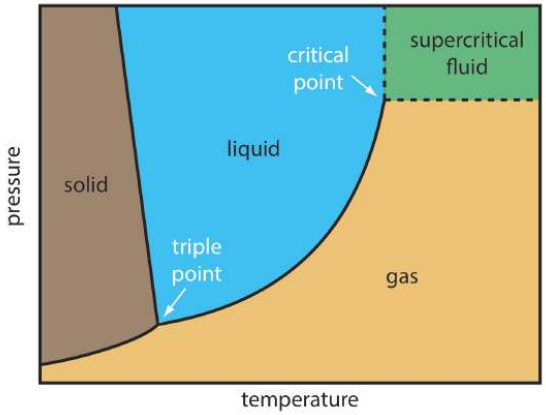


Figure 12.6.4 . Phase diagram showing the combinations of temperature and pres- sure for which a compound is in its solid state, its liquid state, and its gas state. For pressures and temperatures above the critical point, the compound is a supercritical fluid with properties intermediate between a gas and a liquid. Click here to see an interesting video demonstration of supercritical fluids from Nottingham Science City at the University of Nottingham.

Some properties of a supercritical fluid, as shown in Table 12.6.2 , are similar to a gas; other properties, however, are similar to a liquid. The viscosity of a supercritical fluid, for example, is similar to a gas, which means we can move a supercritical fluid through a capillary column or a packed column without the high pressures needed in HPLC. Analysis time and resolution, although not as good as in GC, usually are better than in conventional HPLC. The density of a supercritical fluid, on the other hand, is much closer to that of a liquid, which explains why supercritical fluids are good solvents. In terms of its separation power, a mobile phase in SFC behaves more like the liquid mobile phase in HPLC than the gaseous mobile phase in GC.

Table 12.6.2 . Typical Properties of Gases, Liquids, and Supercritical Fluids

phase	density (g/cm^3)	viscosity ($g\ cm^{-1}\ s^{-1}$)	diffusion coefficient ($cm^2\ s^{-1}$)
gas	$\approx 10^{-3}$	$\approx 10^{-4}$	≈ 0.1
supercritical fluid	$\approx 0.1 - 1$	$\approx 10^{-4} - 10^{-3}$	$\approx 10^{-4} - 10^{-3}$
liquid	≈ 1	$\approx 10^{-2}$	$\approx 10^{-3}$

The most common mobile phase for supercritical fluid chromatography is CO_2. Its low critical temperature of 31.1ºC and its low critical pressure of 72.9 atm are relatively easy to achieve and maintain. Although supercritical CO_2 is a good solvent for nonpolar organics, it is less useful for polar solutes. The addition of an organic modifier, such as methanol, improves the mobile phase's elution strength. Other common mobile phases and their critical temperatures and pressures are listed in Table 12.6.3 .

Table 12.6.3 . Critical Points for Selected Supercritical Fluids

compound	critical temperature (ºC)	critical pressure (atm)
carbon dioxide	31.3	72.9
ethane	32.4	48.3
nitrous oxide	36.5	71.4
ammonia	132.3	111.3
diethyl ether	193.6	36.3
isopropanol	235.3	47.0
methanol	240.5	78.9
ethanol	243.4	63.0
water	374.4	226.8

The instrumentation for supercritical fluid chromatography essentially is the same as that for a standard HPLC. The only important additions are a heated oven for the column and a pressure restrictor downstream from the column to maintain the critical pressure. Gradient elutions are accomplished by changing the applied pressure over time. The resulting change in the mobile phase's density affects its solvent strength. Detection is accomplished using standard GC detectors or HPLC detectors. Supercritical fluid chromatography has many applications in the analysis of polymers, fossil fuels, waxes, drugs, and food products.

This page titled 10.4: Other Forms of Chromatography is shared under a CC BY-NC-SA 4.0 license and was authored, remixed, and/or curated by David Harvey.

- **12.6: Other Forms of Chromatography** by David Harvey is licensed CC BY-NC-SA 4.0.

10.4.1: Chromatographic Columns

Chromatography is an analytical technique that separates components in a mixture. Chromatographic columns are part of the instrumentation that is used in chromatography. Five chromatographic methods that use columns are gas chromatography (GC), liquid chromatography (LC), Ion exchange chromatography (IEC), size exclusion chromatography (SEC), and chiral chromatography. The basic principals of chromatography can be applied to all five methods.

Gas Chromatographic Columns

In gas chromatography the mobile phase is a gas. Gas chromatographic columns are usually between 1 and 100 meters long. *Gas liquid chromatography(GLC):* The liquid stationary phase is bonded or adsorbed onto the surface of an open tubular (capillary) column, or onto a packed solid support inside the column. Matching the polarities of the analyte and stationary phase is not an exact science. The two should have similar polarities. The thickness of the stationary phase ranges between 0.1 and 8 µm. The thicker the layer the more volatile the analyte can be.

High Performance Liquid Chromatographic Columns

High performance liquid chromatography (HPLC) is a type of liquid chromatography that uses a liquid moblie phase. The same basic principals from gas chromatography are applied to liquid chromatography. There are three basic types of liquid chromatographic columns: liquid-liquid, liquid-solid, and ion-exchange. Liquid-liquid chromatographic columns have the liquid stationary phase bonded or absorbed to the surface of the column, or packed material. liquid-liquid chromatographic columns are not as popular because they have limited stability and they are inconvenient. Partitioning occurs between the two different liquids of the mobile and stationary phases. In liquid-solid chromatographic columns the stationary phase is a solid and the analyte absorbs onto the stationary phase which separates the components of the mixture. In ion-exchange chromatographic columns the stationary phase is an ion-exchange resin and partitioning occurs with ion exchanges that occur between the analyte and stationary phase.

Usually HPLC has a guard column ahead of the analytical column to protect and extend the life of the analytical column. The guard column removes particulate matter, contaminants, and molecules that bind irreversibly to the column. The guard column has a stationary phase similar to the analytical column.

The most common HPLC columns are made from stainless steel, but they can be also made out of thick glass, polymers such as polyetherethelketone, a combination of stainless steel and glass, or a combination of stainless steel and polymers. Typical HPLC analytical columns are between 3 and 25 cm long and have a diameter of 1 to 5 mm. The columns are usually straight unlike GC columns. Particles that pack the columns have a typical diameter between 3 to 5 µm. Liquid chromatographic columns will increase in efficiency when the diameter of the packed particles inside the column decreases.

Packing Material

HPLC columns are usually packed with pellicular, or porous particles. Pellicular particles are made from polymer, or glass beads. Pellicular particles are surrounded by a thin uniform layer of silica, polystyrene-divinyl-benzene synthetic resin, alumina, or other type of ion-exchange resin. The diameter of the pellicular beads is between 30 and 40 µm. Porous particles are more commonly used and have diameters between 3 to 10 µm. Porous particles are made up silica, polystyrene-divinyl-benzene synthetic resin, alumina, or other type of ion-exchange resin. Silica is the most common type of porous particle packing material.

Partition HPLC uses liquid bonded phase columns, where the liquid stationary phase is chemically bonded to the packing material. The packing material is usually hydrolyzed silica which reacts with the bond-phase coating. Common bond phase coatings are siloxanes. The relative structure of the siloxane is shown in Figure 10.4.1.1.

Table 10.4.1.1: This table shows the R groups that can be attached to the siloxane and what chromatographic method it is commonly applied to.

R group attached to siloxane	Chromatography method application
Alkyl	Reverse phase
Fluoroalkyl	Reverse phase
Cyano	Normal and reverse phase
Amide	Reverse phase
Amino	Normal and reverse phase

R group attached to siloxane	Chromatography method application
dimethylamine	Weak anion exchanger
Quaternary Amine	Strong anion exchanger
Sulfonic Acid	Strong cation exchanger
Carboxylic Acid	Weak cation exchanger
Diol	reverse phase
Phenyl	Reverse phase
Carbamate	Reverse Phase

Reverse and Normal Phase HPLC

A polar stationary phase and a non-polar mobile phase are used for normal phase HPLC. In normal phase, the most common R groups attached to the siloxane are: diol, amino, cyano, inorganic oxides, and dimethylamino. Normal phase is also a form of liquid-solid chromatography. The most non-polar compounds will elute first when doing normal phase HPLC.

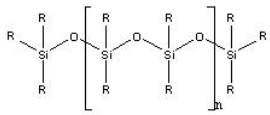


Figure 10.4.1.1: Basic structure of a siloxane. The R groups can be varied depending on the type of column and analyte being analyzed. This figure was created with ChemBioDraw Ultra 12.0.

Reverse phase HPLC uses a polar mobile phase and a non-polar stationary phase. Reverse phase HPLC is the most common liquid chromatography method used. The R groups usually attached to the siloxane for reverse phase HPLC are: C_8, C_{18},or any hydrocarbon. Reverse phase can also use water as the mobile phase, which is advantageous because water is cheap, nontoxic, and invisible in the UV region. The most polar compounds will elute first when performing reverse phase HPLC. Check the animation on the principle of reversed-phase chromatography to understand its principle.

Ion Exchange Chromatographic Columns

Ion exchange columns are used to separate ions and molecules that can be easily ionized. Separation of the ions depends on the ion's affinity for the stationary phase, which creates an ion exchange system. The electrostatic interactions between the analytes, moble phase, and the stationary phase, contribute to the separation of ions in the sample. Only positively or negatively charged complexes can interact with their respective cation or anion exchangers. Common packing materials for ion exchange columns are amines, sulfonic acid, diatomaceous earth, styrene-divinylbenzene, and cross-linked polystyrene resins. Some of the first ion exchangers used were inorganic and made from aluminosilicates (zeolites). Although aluminosilicates are not widely used as ion exchange resins used.

Size Exclusion Chromatographic Columns

Size Exclusion Chromatographic columns separate molecules based upon their size, not molecular weight. A common packing material for these columns is molecular sieves. Zeolites are a common molecular sieve that is used. The molecular sieves have pores that small molecules can go into, but large molecules cannot. This allows the larger molecules to pass through the column faster than the smaller ones. Other packing materials for size exclusion chromatographic columns are polysaccharides and other polymers, and silica. The pore size for size exclusion separations varies between 4 and 200 nm.

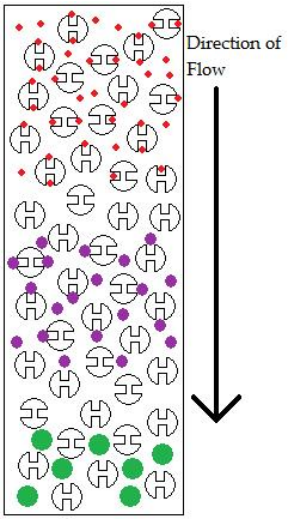


Figure 10.4.1.2: Schematic of a size exclusion column. The larger particles will elute first because they are too big to fit inside the pores. The smallest particles will elute last because they fit very well inside the pores. This figure was created with Microsoft Paint.

Chiral Columns

Chiral columns are used to separate enantiomers. Separation of chiral molecules is based upon steriochemistry. These columns have a stationary phase that selectively interacts with one enantiomer over the other. These types of columns are very useful for separating racemic mixtures. Some Stationary Phases Used to Separate Enantiomer are show in Table 10.4.1.2

Table 10.4.1.2: This table shows some stationary phases that are used to separate enantiomers and the corresponding chromatographic methods that they are applied to.

Stationary Phase	Method(s) Used
Metal Chelates	GC, LC
Amino Acid Derivatives	GC, LC
Proteins	LC
Helical Polymers	LC
Cyclodextrin Derivatives	GC, LC

Column Efficiency

Peak or band broadening causes the column to be less efficient. The ideal situation would to have sharp peaks that are resolved. The longer a substance stays in the column it will cause the peaks to widen. Lengthening the column is a way to improve the separation of different species in the column. A column usually needs to remain at a constant temperature to remain efficient. Plate height and number of theoretical plates determines the efficiency of the column. Improving the efficiency would be to increase the number of plates and decrease the plate height.

The number of plates can be determined from the equation:

$$N = L/H$$

where L is the length of the column and H is the height of each plate. N can also be determined from the equation:

$$N = 16\left(\frac{t_R}{W}\right)^2$$

or

$$N = 5.54\left(\frac{t_R}{W_{1/2}}\right)^2$$

where t_R is the retention time, W is the width of the peak and $W_{1/2}$ is half the width of the peak.

Height equivalent to a theoretical plate (HETP) is determined from the equation:

$$H = L/N$$

or HETP can also be determined by the *van Beemter equation*:

$$H = A + \frac{B}{u} + Cu$$

where H equals HETP, A is the term for eddy diffusion, B is the term for longitudinal diffusion, C is the coefficient for mass-transfer between the stationary and mobile phases, and u is the linear velocity. The equation for HETP is often used to describe the efficiency of the column. An efficient column would have a minimum HETP value. Gas chromatographic columns have plate heights that are at least one order of magnitude greater than liquid chromatographic column plates. However GC columns are longer, which causes them to be more efficient. LC columns have a maximum length of 25 cm whereas GC columns can be 100 meters long.

References

1. Skoog, D., Holler, J., Crouch, S. Principles of Instrumental Analysis, 6th Ed.; Thomson Brooks/Cole: Belmont, 2007.
2. Poole, C.F. The Essence of Chromatography; Elsevier: San Francisco, 2003.
3. Miller, J.J. Chromatography: Concepts and Contrasts, 2nd Ed.; John Wiley & Sons, Inc.: Hoboken, NJ, 2005.
4. Ravindranath, B., Principles and Practice of Chromatography; John Wiley & Sons: New York, 1989.
5. Johnson, E.L., Stevenson, R., Basic Liquid Chromatography; Varian Associates: Palo Alto, CA, 1978.
6. Brown, P.R., Hartwick, R.A., High Performance Liquid Chromatography. In Chemical Analysis; Winefordner, J.D., Ed. John Wiley & Sons: New York, 1989; Vol. 98; p 277-295

10.4.1: Chromatographic Columns is shared under a CC BY-NC-SA 4.0 license and was authored, remixed, and/or curated by LibreTexts.

- **Chromatographic Columns** is licensed CC BY-NC-SA 4.0.

SECTION OVERVIEW

10.2: Capillary Electrophoresis and Capillary Electrochromatography

Electrophoresis is a class of separation techniques in which we separate analytes by their ability to move through a conductive medium—usually an aqueous buffer—in response to an applied electric field. In the absence of other effects, cations migrate toward the electric field's negatively charged cathode. Cations with larger charge-to-size ratios—which favors ions of greater charge and of smaller size—migrate at a faster rate than larger cations with smaller charges. Anions migrate toward the positively charged anode and neutral species do not experience the electrical field and remain stationary. In this chapter we focus on the most important of these techniques, capillary electrophoresis and a few related variants.

10.2.1: An Overview of Electrophoresis

10.2.2: Capillary Electrophoresis

10.2.3: Capillary Electrophoresis

10.2.3.1: Ionic Mobility and Electrophoresis

10.2.4: Applications of Capillary Electrophoresis

This page titled 10.2: Capillary Electrophoresis and Capillary Electrochromatography is shared under a CC BY-NC-SA 4.0 license and was authored, remixed, and/or curated by David Harvey.

10.2.1: An Overview of Electrophoresis

Electrophoresis is a class of separation techniques in which we separate analytes by their ability to move through a conductive medium—usually an aqueous buffer—in response to an applied electric field. In the absence of other effects, cations migrate toward the electric field's negatively charged cathode. Cations with larger charge-to-size ratios—which favors ions of greater charge and of smaller size—migrate at a faster rate than larger cations with smaller charges. Anions migrate toward the positively charged anode and neutral species do not experience the electrical field and remain stationary.

> As we will see shortly, under normal conditions even neutral species and anions migrate toward the cathode.

There are several forms of electrophoresis. In slab gel electrophoresis the conducting buffer is retained within a porous gel of agarose or polyacrylamide. Slabs are formed by pouring the gel between two glass plates separated by spacers. Typical thicknesses are 0.25–1 mm. Gel electrophoresis is an important technique in biochemistry where it frequently is used to separate DNA fragments and proteins. Although it is a powerful tool for the qualitative analysis of complex mixtures, it is less useful for quantitative work.

In capillary electrophoresis the conducting buffer is retained within a capillary tube with an inner diameter that typically is 25–75 μm. The sample is injected into one end of the capillary tube, and as it migrates through the capillary the sample's components separate and elute from the column at different times. The resulting electropherogram looks similar to a GC or an HPLC chromatogram, and provides both qualitative and quantitative information.

This page titled 10.2.1: An Overview of Electrophoresis is shared under a CC BY-NC-SA 4.0 license and was authored, remixed, and/or curated by David Harvey.

- **30.1: An Overview of Electrophoresis** by David Harvey is licensed CC BY-NC-SA 4.0.

10.2.2: Capillary Electrophoresis

Theory of Electrophoresis

In capillary electrophoresis we inject the sample into a buffered solution retained within a capillary tube. When an electric field is applied across the capillary tube, the sample's components migrate as the result of two types of actions: electrophoretic mobility and electroosmotic mobility. Electrophoretic mobility is the solute's response to the applied electrical field in which cations move toward the negatively charged cathode, anions move toward the positively charged anode, and neutral species remain stationary. The other contribution to a solute's migration is electroosmotic flow, which occurs when the buffer moves through the capillary in response to the applied electrical field. Under normal conditions the buffer moves toward the cathode, sweeping most solutes, including the anions and neutral species, toward the negatively charged cathode.

Electrophoretic Mobility

The velocity with which a solute moves in response to the applied electric field is called its electrophoretic velocity, ν_{ep}; it is defined as

$$\nu_{ep} = \mu_{ep} E \tag{10.2.2.1}$$

where μ_{ep} is the solute's electrophoretic mobility, and E is the magnitude of the applied electrical field. A solute's electrophoretic mobility is defined as

$$\mu_{ep} = \frac{q}{6\pi\eta r} \tag{10.2.2.2}$$

where q is the solute's charge, η is the buffer's viscosity, and r is the solute's radius. Using Equation 10.2.2.1 and Equation 10.2.2.2 we can make several important conclusions about a solute's electrophoretic velocity. Electrophoretic mobility and, therefore, electrophoretic velocity, increases for more highly charged solutes and for solutes of smaller size. Because q is positive for a cation and negative for an anion, these species migrate in opposite directions. A neutral species, for which q is zero, has an electrophoretic velocity of zero.

Electroosmotic Mobility

When an electric field is applied to a capillary filled with an aqueous buffer we expect the buffer's ions to migrate in response to their electrophoretic mobility. Because the solvent, H_2O, is neutral we might reasonably expect it to remain stationary. What we observe under normal conditions, however, is that the buffer moves toward the cathode. This phenomenon is called the electroosmotic flow.

Electroosmotic flow occurs because the walls of the capillary tubing carry a charge. The surface of a silica capillary contains large numbers of silanol groups (–SiOH). At a pH level greater than approximately 2 or 3, the silanol groups ionize to form negatively charged silanate ions ($–SiO^–$). Cations from the buffer are attracted to the silanate ions. As shown in Figure 30.2.1 , some of these cations bind tightly to the silanate ions, forming a fixed layer. Because the cations in the fixed layer only partially neutralize the negative charge on the capillary walls, the solution adjacent to the fixed layer—which is called the diffuse layer—contains more cations than anions. Together these two layers are known as the double layer. Cations in the diffuse layer migrate toward the cathode. Because these cations are solvated, the solution also is pulled along, producing the electroosmotic flow.

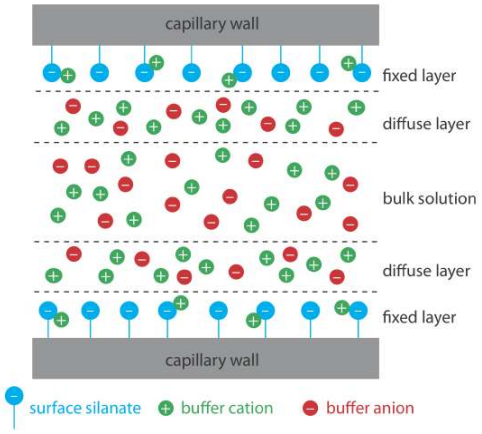


Figure 30.2.1 . Schematic diagram showing the origin of the double layer within a capillary tube. Although the net charge within the capillary is zero, the distribution of charge is not. The walls of the capillary have an excess of negative charge, which decreases across the fixed layer and the diffuse layer, reaching a value of zero in bulk solution.

> The anions in the diffuse layer, which also are solvated, try to move toward the anode. Because there are more cations than anions, however, the cations win out and the electroosmotic flow moves in the direction of the cathode.

The rate at which the buffer moves through the capillary, what we call its electroosmotic flow velocity, ν_{eof}, is a function of the applied electric field, *E*, and the buffer's electroosmotic mobility, μ_{eof}.

$$\nu_{eof} = \mu_{eof} E \tag{10.2.2.3}$$

Electroosmotic mobility is defined as

$$\mu_{eof} = \frac{\varepsilon \zeta}{4 \pi \eta} \tag{10.2.2.4}$$

where ϵ is the buffer dielectric constant, ζ is the zeta potential, and η is the buffer's viscosity.

The zeta potential—the potential of the diffuse layer at a finite distance from the capillary wall—plays an important role in determining the electroosmotic flow velocity. Two factors determine the zeta potential's value. First, the zeta potential is directly proportional to the charge on the capillary walls, with a greater density of silanate ions corresponding to a larger zeta potential. Below a pH of 2 there are few silanate ions and the zeta potential and the electroosmotic flow velocity approach zero. As the pH increases, both the zeta potential and the electroosmotic flow velocity increase. Second, the zeta potential is directly proportional to the thickness of the double layer. Increasing the buffer's ionic strength provides a higher concentration of cations, which decreases the thickness of the double layer and decreases the electroosmotic flow.

> The definition of zeta potential given here admittedly is a bit fuzzy. For a more detailed explanation see Delgado, A. V.; González-Caballero, F.; Hunter, R. J.; Koopal, L. K.; Lyklema, J. "Measurement and Interpretation of Electrokinetic Phenomena," *Pure. Appl. Chem.* **2005**, *77*, 1753–1805. Although this is a very technical report, Sections 1.3–1.5 provide a good introduction to the difficulty of defining the zeta potential and of measuring its value.

The electroosmotic flow profile is very different from that of a fluid moving under forced pressure. Figure 30.2.2 compares the electroosmotic flow profile with the hydrodynamic flow profile in gas chromatography and liquid chromatography. The uniform, flat profile for electroosmosis helps minimize band broadening in capillary electrophoresis, improving separation efficiency.

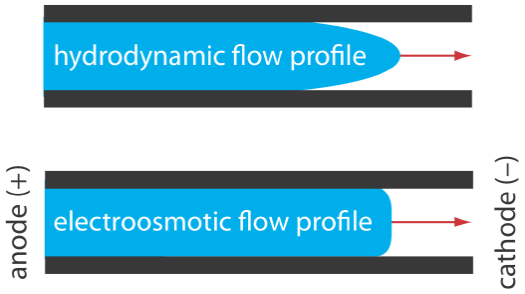


Figure 30.2.2 . Comparison of hydrodynamic flow and electroosmotic flow. The nearly uniform electroosmotic flow profile means that the electroosmotic flow velocity is nearly constant across the capillary.

Total Mobility

A solute's total velocity, ν_{tot}, as it moves through the capillary is the sum of its electrophoretic velocity and the electroosmotic flow velocity.

$$\nu_{tot} = \nu_{ep} + \nu_{eof}$$

As shown in Figure 30.2.3 , under normal conditions the following general relationships hold true.

$$(\nu_{tot})_{cations} > \nu_{eof}$$

$$(\nu_{tot})_{neutrals} = \nu_{eof}$$

$$(\nu_{tot})_{anions} < \nu_{eof}$$

Cations elute first in an order that corresponds to their electrophoretic mobilities, with small, highly charged cations eluting before larger cations of lower charge. Neutral species elute as a single band with an elution rate equal to the electroosmotic flow velocity. Finally, anions are the last components to elute, with smaller, highly charged anions having the longest elution time.

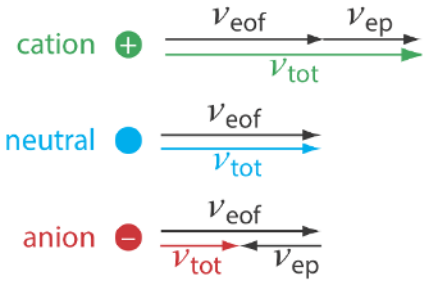


Figure 30.2.3 . Visual explanation for the general elution order in capillary electrophoresis. Each species has the same electroosmotic flow, ν_{eof}. Cations elute first because they have a positive electrophoretic velocity, ν_{ep}. Anions elute last because their negative electrophoretic velocity partially offsets the electroosmotic flow velocity. Neutrals elute with a velocity equal to the electroosmotic flow.

Migration Time

Another way to express a solute's velocity is to divide the distance it travels by the elapsed time

$$\nu_{tot} = \frac{l}{t_m} \tag{10.2.2.5}$$

where l is the distance between the point of injection and the detector, and t_m is the solute's migration time. To understand the experimental variables that affect migration time, we begin by noting that

$$\nu_{tot} = \mu_{tot} E = (\mu_{ep} + \mu_{eof}) E \tag{10.2.2.6}$$

Combining Equation 10.2.2.5 and Equation 10.2.2.6 and solving for t_m leaves us with

$$t_m = \frac{l}{(\mu_{ep} + \mu_{eof}) E} \tag{10.2.2.7}$$

The magnitude of the electrical field is

$$E = \frac{V}{L} \tag{10.2.2.8}$$

where V is the applied potential and L is the length of the capillary tube. Finally, substituting Equation 10.2.2.8 into Equation 10.2.2.7 leaves us with the following equation for a solute's migration time.

$$t_{\mathrm{m}} = \frac{lL}{(\mu_{ep} + \mu_{eof})\,V} \tag{10.2.2.9}$$

To decrease a solute's migration time—which shortens the analysis time—we can apply a higher voltage or use a shorter capillary tube. We can also shorten the migration time by increasing the electroosmotic flow, although this decreases resolution.

Efficiency

As we learned in Chapter 26.3, the efficiency of a separation is given by the number of theoretical plates, N. In capillary electrophoresis the number of theoretic plates is

$$N = \frac{l^2}{2Dt_m} = \frac{(\mu_{ep} + \mu_{eof})\,El}{2DL} \tag{10.2.2.10}$$

where D is the solute's diffusion coefficient. From Equation 10.2.2.10, the efficiency of a capillary electrophoretic separation increases with higher voltages. Increasing the electroosmotic flow velocity improves efficiency, but at the expense of resolution. Two additional observations deserve comment. First, solutes with larger electrophoretic mobilities—in the same direction as the electroosmotic flow—have greater efficiencies; thus, smaller, more highly charged cations are not only the first solutes to elute, but do so with greater efficiency. Second, efficiency in capillary electrophoresis is independent of the capillary's length. Theoretical plate counts of approximately 100 000–200 000 are not unusual.

> It is possible to design an electrophoretic experiment so that anions elute before cations—more about this later—in which smaller, more highly charged anions elute with greater efficiencies.

Selectivity

In chromatography we defined the selectivity between two solutes as the ratio of their retention factors. In capillary electrophoresis the analogous expression for selectivity is

$$\alpha = \frac{\mu_{ep,1}}{\mu_{ep,2}}$$

where $\mu_{ep,1}$ and $\mu_{ep,2}$ are the electrophoretic mobilities for the two solutes, chosen such that $\alpha \geq 1$. We can often improve selectivity by adjusting the pH of the buffer solution. For example, NH_4^+ is a weak acid with a pK_a of 9.75. At a pH of 9.75 the concentrations of NH_4^+ and NH_3 are equal. Decreasing the pH below 9.75 increases its electrophoretic mobility because a greater fraction of the solute is present as the cation NH_4^+. On the other hand, raising the pH above 9.75 increases the proportion of neutral NH_3, decreasing its electrophoretic mobility.

Resolution

The resolution between two solutes is

$$R = \frac{0.177(\mu_{ep,2} - \mu_{ep,1})\sqrt{V}}{\sqrt{D(\mu_{avg} + \mu_{eof})}} \tag{10.2.2.11}$$

where μ_{avg} is the average electrophoretic mobility for the two solutes. Increasing the applied voltage and decreasing the electroosmotic flow velocity improves resolution. The latter effect is particularly important. Although increasing electroosmotic flow improves analysis time and efficiency, it decreases resolution.

Instrumentation

The basic instrumentation for capillary electrophoresis is shown in Figure 30.2.4 and includes a power supply for applying the electric field, anode and cathode compartments that contain reservoirs of the buffer solution, a sample vial that contains the sample, the capillary tube, and a detector. Each part of the instrument receives further consideration in this section.

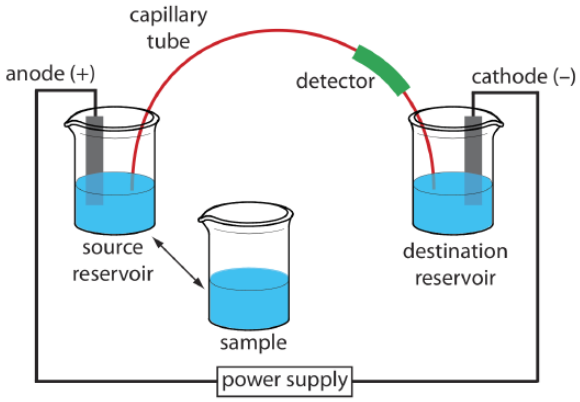


Figure 30.2.4 . Schematic diagram of the basic instrumentation for capillary electrophoresis. The sample and the source reservoir are switched when making injections.

Capillary Tubes

Figure 30.2.5 shows a cross-section of a typical capillary tube. Most capillary tubes are made from fused silica coated with a 15–35 μm layer of polyimide to give it mechanical strength. The inner diameter is typically 25–75 μm, which is smaller than the internal diameter of a capillary GC column, with an outer diameter of 200–375 μm.

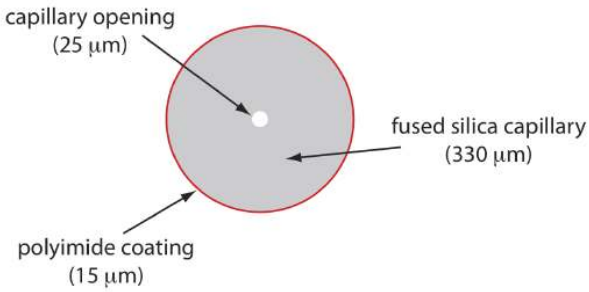


Figure 30.2.5 . Cross section of a capillary column for capillary electrophoresis. The dimensions shown here are typical and are scaled proportionally in this figure.

The capillary column's narrow opening and the thickness of its walls are important. When an electric field is applied to the buffer solution, current flows through the capillary. This current leads to the release of heat, which we call Joule heating. The amount of heat released is proportional to the capillary's radius and to the magnitude of the electrical field. Joule heating is a problem because it changes the buffer's viscosity, with the solution at the center of the capillary being less viscous than that near the capillary walls. Because a solute's electrophoretic mobility depends on its viscosity (see Equation 10.2.2.2), solute species in the center of the capillary migrate at a faster rate than those near the capillary walls. The result is an additional source of band broadening that degrades the separation. Capillaries with smaller inner diameters generate less Joule heating, and capillaries with larger outer diameters are more effective at dissipating the heat. Placing the capillary tube inside a thermostated jacket is another method for minimizing the effect of Joule heating; in this case a smaller outer diameter allows for a more rapid dissipation of thermal energy.

Injecting the Sample

There are two common methods for injecting a sample into a capillary electrophoresis column: hydrodynamic injection and electrokinetic injection. In both methods the capillary tube is filled with the buffer solution. One end of the capillary tube is placed in the destination reservoir and the other end is placed in the sample vial.

Hydrodynamic injection uses pressure to force a small portion of sample into the capillary tubing. A difference in pressure is applied across the capillary either by pressurizing the sample vial or by applying a vacuum to the destination reservoir. The volume

of sample injected, in liters, is given by the following equation

$$V_{\text{inj}} = \frac{\Delta P d^4 \pi t}{128 \eta L} \times 10^3 \tag{10.2.2.12}$$

where ΔP is the difference in pressure across the capillary in pascals, d is the capillary's inner diameter in meters, t is the amount of time the pressure is applied in seconds, η is the buffer's viscosity in kg m^{-1} s^{-1}, and L is the length of the capillary tubing in meters. The factor of 10^3 changes the units from cubic meters to liters.

For a hydrodynamic injection we move the capillary from the source reservoir to the sample. The anode remains in the source reservoir. A hydrodynamic injection also is possible if we raise the sample vial above the destination reservoir and briefly insert the filled capillary.

Example 30.2.1

In a hydrodynamic injection we apply a pressure difference of 2.5×10^3 Pa (a $\Delta P \approx 0.02$ atm) for 2 s to a 75-cm long capillary tube with an internal diameter of 50 μm. Assuming the buffer's viscosity is 10^{-3} kg m^{-1} s^{-1}, what volume and length of sample did we inject?

Solution

Making appropriate substitutions into Equation 10.2.2.12gives the sample's volume as

$$V_{inj} = \frac{\left(2.5 \times 10^3 \text{ kg m}^{-1} \text{ s}^{-2}\right)\left(50 \times 10^{-6} \text{ m}\right)^4 (3.14)(2 \text{ s})}{(128)\left(0.001 \text{ kg m}^{-1} \text{ s}^{-1}\right)(0.75 \text{ m})} \times 10^3 \text{L/m}^3$$

$$V_{inj} = 1 \times 10^{-9} \text{ L} = 1 \text{ nL}$$

Because the interior of the capillary is cylindrical, the length of the sample, l, is easy to calculate using the equation for the volume of a cylinder; thus

$$l = \frac{V_{\text{inj}}}{\pi r^2} = \frac{\left(1 \times 10^{-9} \text{ L}\right)\left(10^{-3} \text{ m}^3/\text{L}\right)}{(3.14)\left(25 \times 10^{-6} \text{ m}\right)^2} = 5 \times 10^{-4} \text{ m} = 0.5 \text{ mm}$$

Exercise 30.2.1

Suppose you need to limit your injection to less than 0.20% of the capillary's length. Using the information from Example 30.2.1 , what is the maximum injection time for a hydrodynamic injection?

Answer

The capillary is 75 cm long, which means that 0.20% of that sample's maximum length is 0.15 cm. To convert this to the maximum volume of sample we use the equation for the volume of a cylinder.

$$V_{inj} = l\pi r^2 = (0.15 \text{ cm})(3.14)\left(25 \times 10^{-4} \text{ cm}\right)^2 = 2.94 \times 10^{-6} \text{ cm}^3$$

Given that 1 cm^3 is equivalent to 1 mL, the maximum volume is 2.94×10^{-6} mL or 2.94×10^{-9} L. To find the maximum injection time, we first solve Equation 10.2.2.12for t

$$t = \frac{128 V_{inj} \eta L}{P d^4 \pi} \times 10^{-3} \text{ m}^3/\text{L}$$

and then make appropriate substitutions.

$$t = \frac{(128)\left(2.94 \times 10^{-9} \text{ L}\right)\left(0.001 \text{ kg m}^{-1} \text{ s}^{-1}\right)(0.75 \text{ m})}{\left(2.5 \times 10^3 \text{ kg m}^{-1} \text{ s}^{-2}\right)\left(50 \times 10^{-6} \text{ m}\right)^4 (3.14)} \times \frac{10^{-3} \text{ m}^3}{\text{L}} = 5.8 \text{ s}$$

The maximum injection time, therefore, is 5.8 s.

In an electrokinetic injection we place both the capillary and the anode into the sample and briefly apply an potential. The volume of injected sample is the product of the capillary's cross sectional area and the length of the capillary occupied by the sample. In turn, this length is the product of the solute's velocity (see Equation 10.2.2.6) and time; thus

$$V_{inj} = \pi r^2 L = \pi r^2 (\mu_{ep} + \mu_{eof}) E' t \tag{10.2.2.13}$$

where r is the capillary's radius, L is the capillary's length, and E' is the effective electric field in the sample. An important consequence of Equation 10.2.2.13is that an electrokinetic injection is biased toward solutes with larger electrophoretic mobilities. If two solutes have equal concentrations in a sample, we inject a larger volume—and thus more moles—of the solute with the larger μ_{ep}.

The electric field in the sample is different that the electric field in the rest of the capillary because the sample and the buffer have different ionic compositions. In general, the sample's ionic strength is smaller, which makes its conductivity smaller. The effective electric field is

$$E' = E \times \frac{\chi_{\text{buffer}}}{\chi_{\text{sample}}}$$

where χ_{buffer} and χ_{sample} are the conductivities of the buffer and the sample, respectively.

When an analyte's concentration is too small to detect reliably, it maybe possible to inject it in a manner that increases its concentration. This method of injection is called stacking. Stacking is accomplished by placing the sample in a solution whose ionic strength is significantly less than that of the buffer in the capillary tube. Because the sample plug has a lower concentration of buffer ions, the effective field strength across the sample plug, E', is larger than that in the rest of the capillary.

We know from Equation 10.2.2.1that electrophoretic velocity is directly proportional to the electrical field. As a result, the cations in the sample plug migrate toward the cathode with a greater velocity, and the anions migrate more slowly—neutral species are unaffected and move with the electroosmotic flow. When the ions reach their respective boundaries between the sample plug and the buffer, the electrical field decreases and the electrophoretic velocity of the cations decreases and that for the anions increases. As shown in Figure 30.2.6 , the result is a stacking of cations and anions into separate, smaller sampling zones. Over time, the buffer within the capillary becomes more homogeneous and the separation proceeds without additional stacking.

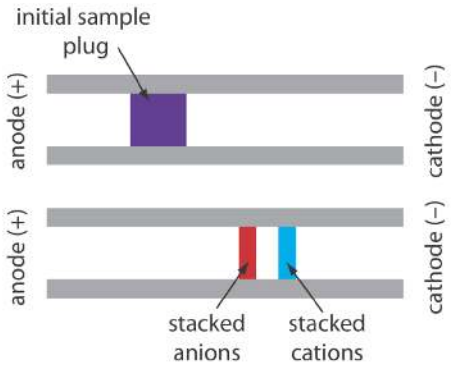


Figure 30.2.6 . The stacking of cations and anions. The top diagram shows the initial sample plug and the bottom diagram shows how the cations and anions are concentrated at opposite sides of the sample plug.

Applying the Electrical Field

Migration in electrophoresis occurs in response to an applied electric field. The ability to apply a large electric field is important because higher voltages lead to shorter analysis times (Equation 10.2.2.9), more efficient separations (Equation 10.2.2.10), and better resolution (Equation 10.2.2.11). Because narrow bored capillary tubes dissipate Joule heating so efficiently, voltages of up to 40 kV are possible.

Because of the high voltages, be sure to follow your instrument's safety guidelines.

Detectors

Most of the detectors used in HPLC also find use in capillary electrophoresis. Among the more common detectors are those based on the absorption of UV/Vis radiation, fluorescence, conductivity, amperometry, and mass spectrometry. Whenever possible, detection is done “on-column” before the solutes elute from the capillary tube and additional band broadening occurs.

UV/Vis detectors are among the most popular. Because absorbance is directly proportional to path length, the capillary tubing’s small diameter leads to signals that are smaller than those obtained in HPLC. Several approaches have been used to increase the pathlength, including a Z-shaped sample cell and multiple reflections (see Figure 30.2.7). Detection limits are about 10^{-7} M.

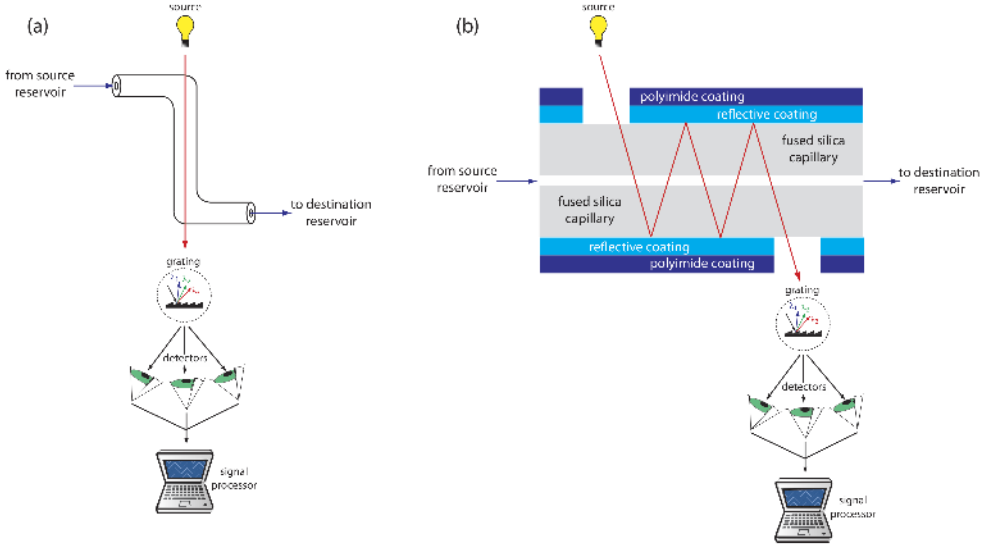


Figure 30.2.7 . Two approaches to on-column detection in capillary electrophoresis using a UV/Vis diode array spectrometer: (a) Z-shaped bend in capillary, and (b) multiple reflections.

Better detection limits are obtained using fluorescence, particularly when using a laser as an excitation source. When using fluorescence detection a small portion of the capillary’s protective coating is removed and the laser beam is focused on the inner portion of the capillary tubing. Emission is measured at an angle of 90º to the laser. Because the laser provides an intense source of radiation that can be focused to a narrow spot, detection limits are as low as 10^{-16} M.

Solutes that do not absorb UV/Vis radiation or that do not undergo fluorescence can be detected by other detectors. Table 30.2.1 provides a list of detectors for capillary electrophoresis along with some of their important characteristics.

Table 30.2.1 . Characteristics of Detectors for Capillary Electrophoresis

detector	selectivity (universal or analyte must ...)	detection limited (moles injected)	detection limit (molarity)	on-column detection?
UV/Vis absorbance	have a UV/Vis chromophore	$10^{-13} - 10^{-16}$	$10^{-5} - 10^{-7}$	yes
indirect absorbancd	universal	$10^{-12} - 10^{-15}$	$10^{-4} - 10^{-6}$	yes
fluoresence	have a favorable quantum yield	$10^{-13} - 10^{-17}$	$10^{-7} - 10^{-9}$	yes
laser fluorescence	have a favorable quantum yield	$10^{-18} - 10^{-20}$	$10^{-13} - 10^{-16}$	yes
mass spectrometer	universal (total ion) selective (single ion)	$10^{-16} - 10^{-17}$	$10^{-8} - 10^{-10}$	no
amperometry	undergo oxidation or reduction	$10^{-18} - 10^{-19}$	$10^{-7} - 10^{-10}$	no
conductivity	universal	$10^{-15} - 10^{-16}$	$10^{-7} - 10^{-9}$	no

detector	selectivity (universal or analyte must ...)	detection limited (moles injected)	detection limit (molarity)	on-column detection?
radiometric	be radioactive	$10^{-17} - 10^{-19}$	$10^{-10} - 10^{-12}$	yes

This page titled 10.2.2: Capillary Electrophoresis is shared under a CC BY-NC-SA 4.0 license and was authored, remixed, and/or curated by David Harvey.

- **30.2: Capillary Electrophoresis** by David Harvey is licensed CC BY-NC-SA 4.0.

10.2.3: Capillary Electrophoresis

Capillary electrophoresis is an analytical technique that separates ions based on their electrophoretic mobility with the use of an applied voltage. The electrophoretic mobility is dependent upon the charge of the molecule, the viscosity, and the atom's radius. The rate at which the particle moves is directly proportional to the applied electric field--the greater the field strength, the faster the mobility. Neutral species are not affected, only ions move with the electric field. If two ions are the same size, the one with greater charge will move the fastest. For ions of the same charge, the smaller particle has less friction and overall faster migration rate. Capillary electrophoresis is used most predominately because it gives faster results and provides high resolution separation. It is a useful technique because there is a large range of detection methods available.[1]

Introduction

Endeavors in capillary electrophoresis (CE) began as early as the late 1800's. Experiments began with the use of glass U tubes and trials of both gel and free solutions.[1] In 1930, Arnes Tiselius first showed the capability of electrophoresis in an experiment that showed the separation of proteins in free solutions.[2] His work had gone unnoticed until Hjerten introduced the use of capillaries in the 1960's. However, their establishments were not widely recognized until Jorgenson and Lukacs published papers showing the ability of capillary electrophoresis to perform separations that seemed unachievable. Employing a capillary in electrophoresis had solved some common problems in traditional electrophoresis. For example, the thin dimensions of the capillaries greatly increased the surface to volume ratio, which eliminated overheating by high voltages. The increased efficiency and the amazing separating capabilities of capillary electrophoresis spurred a growing interest among the scientific society to execute further developments in the technique.

Instrumental Setup

A typical capillary electrophoresis system consists of a high-voltage power supply, a sample introduction system, a capillary tube, a detector and an output device. Some instruments include a temperature control device to ensure reproducible results. This is because the separation of the sample depends on the electrophoretic mobility and the viscosity of the solutions decreases as the column temperature rises.[3] Each side of the high voltage power supply is connected to an electrode. These electrodes help to induce an electric field to initiate the migration of the sample from the anode to the cathode through the capillary tube. The capillary is made of fused silica and is sometimes coated with polyimide.[3] Each side of the capillary tube is dipped in a vial containing the electrode and an electrolytic solution, or aqueous buffer. Before the sample is introduced to the column, the capillary must be flushed with the desired buffer solution. There is usually a small window near the cathodic end of the capillary which allows UV-VIS light to pass through the analyte and measure the absorbance. A photomultiplier tube is also connected at the cathodic end of the capillary, which enables the construction of a mass spectrum, providing information about the mass to charge ratio of the ionic species.

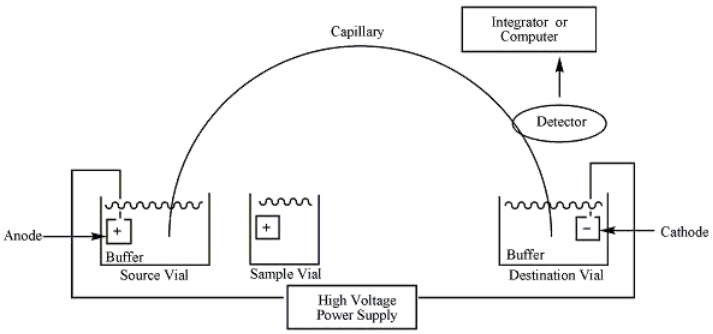


Figure 10.2.3.1: Instrumental Setup. from Wikipedia.

Theory

Electrophoretic Mobility

Electrophoresis is the process in which sample ions move under the influence of an applied voltage. The ion undergoes a force that is equal to the product of the net charge and the electric field strength. It is also affected by a drag force that is equal to the product of f, the translational friction coefficient, and the velocity. This leads to the expression for *electrophoretic mobility*:

$$\mu_{EP} = \frac{q}{f} = \frac{q}{6\pi\eta r} \tag{10.2.3.1}$$

where f for a spherical particle is given by the Stokes' law; η is the viscosity of the solvent, and r is the radius of the atom. The rate at which these ions migrate is dictated by the charge to mass ratio. The actual velocity of the ions is directly proportional to E, the magnitude of the electrical field and can be determined by the following equation[4]:

$$v = \mu_{EP} E \tag{10.2.3.2}$$

This relationship shows that a greater voltage will quicken the migration of the ionic species.

Electroosmotic Flow

The electroosmotic flow (EOF) is caused by applying high-voltage to an electrolyte-filled capillary.[4] This flow occurs when the buffer running through the silica capillary has a pH greater than 3 and the SiOH groups lose a proton to become SiO^- ions. The capillary wall then has a negative charge, which develops a double layer of cations attracted to it. The inner cation layer is stationary, while the outer layer is free to move along the capillary. The applied electric field causes the free cations to move toward the cathode creating a powerful bulk flow. The rate of the electroosmotic flow is governed by the following equation:

$$\mu_{EOF} = \frac{\epsilon}{4\pi\eta} E\zeta \tag{10.2.3.3}$$

where ε is the dielectric constant of the solution, η is the viscosity of the solution, E is the field strength, and ζ is the zeta potential. Because the electrophoretic mobility is greater than the electroosmotic flow, negatively charged particles, which are naturally attracted to the positively charged anode, will separate out as well. The EOF works best with a large zeta potential between the cation layers, a large diffuse layer of cations to drag more molecules towards the cathode, low resistance from the surrounding solution, and buffer with pH of 9 so that all the SiOH groups are ionized.[1]

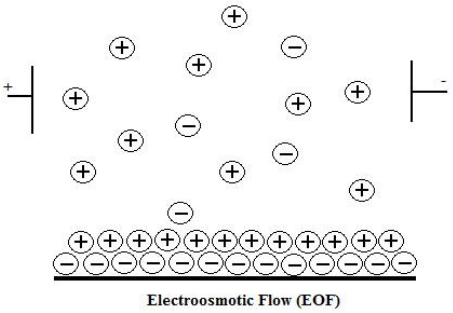


Figure 10.2.3.2:Electroosmotic Flow due to Applied Voltage

Capillary Electroseparation Methods

There are six types of capillary electroseparation available: capillary zone electrophoresis (CZE), capillary gel electrophoresis (CGE), micellar electrokinetic capillary chromatography (MEKC), capillary electrochromatography (CEC), capillary isoelectric focusing (CIEF), and capillary isotachophoresis (CITP). They can be classified into continuous and discontinuous systems as shown in Figure 3. A continuous system has a background electrolyte acting throughout the capillary as a buffer. This can be broken down into kinetic (constant electrolyte composition) and steady-state (varying electrolyte composition) processes. A discontinuous system keeps the sample in distinct zones separated by two different electrolytes.[6]

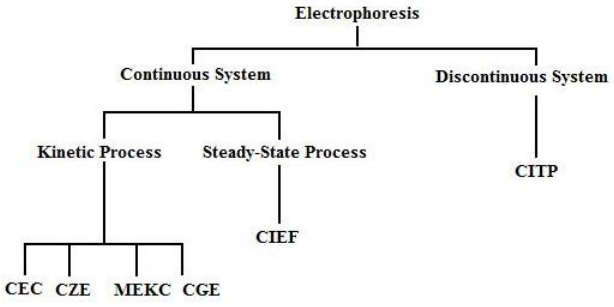


Figure 10.2.3.3: Categorization of Electrophoresis Techniques

Capillary Zone Electrophoresis (CZE)

Capillary Zone Electrophoresis (CZE), also known as free solution capillary electrophoresis, it is the most commonly used technique of the six methods.A mixture in a solution can be separated into its individual components quickly and easily.The separation is based on the differences in electrophoretic mobility, which is directed proportional to the charge on the molecule, and inversely proportional to the viscosity of the solvent and radius of the atom.The velocity at which the ion moves is directly proportional to the electrophoretic mobility and the magnitude of the electric field.[1]

The fused silica capillaries have silanol groups that become ionized in the buffer. The negatively charged SiO^- ions attract positively charged cations, which form two layers—a stationary and diffuse cation layer. In the presence of an applied electric field, the diffuse layer migrates towards the negatively charged cathode creating an electrophoretic flow (μ_{ep}) that drags bulk solvent along with it. Anions in solution are attracted to the positively charged anode, but get swept to the cathode as well. Cations with the largest charge-to-mass ratios separate out first, followed by cations with reduced ratios, neutral species, anions with smaller charge-to-mass ratios, and finally anions with greater ratios. The electroosmotic velocity can be adjusted by altering pH, the viscosity of the solvent, ionic strength, voltage, and the dielectric constant of the buffer.[1]

Capillary Gel Electrophoresis (CGE)

CGE uses separation based on the difference in solute size as the particles migrate through the gel. Gels are useful because they minimize solute diffusion that causes zone broadening, prevent the capillary walls from absorbing the solute, and limit the heat transfer by slowing down the molecules. A commonly used gel apparatus for the separation of proteins is capillary SDS-PAGE. It is a highly sensitive system and only requires a small amount of sample.[1]

Micellar Electrokinetic Capillary Chromatography (MEKC)

MEKC is a separation technique that is based on solutes partitioning between micelles and the solvent. Micelles are aggregates of surfactant molecules that form when a surfactant is added to a solution above the critical micelle concentration. The aggregates have polar negatively charged surfaces and are naturally attracted to the positively charged anode. Because of the electroosmotic flow toward the cathode, the micelles are pulled to the cathode as well, but at a slower rate. Hydrophobic molecules will spend the majority of their time in the micelle, while hydrophilic molecules will migrate quicker through the solvent. When micelles are not present, neutral molecules will migrate with the electroosmotic flow and no separation will occur. The presence of micelles results in a retention time to where the solute has little micelle interaction and retention time tmc where the solute strongly interacts. Neutral molecules will be separated at a time between to and tmc. Factors that affect the electroosmotic flow in MEKC are: pH, surfactant concentration, additives, and polymer coatings of the capillary wall.[1]

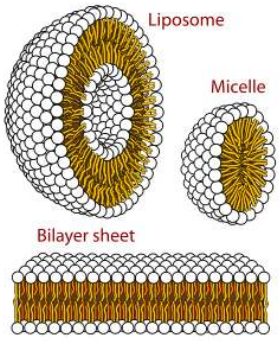


Figure 10.2.3.4: Micelles. from Wikipedia.

Capillary Electrochromatography (CEC)

The separation mechanism is a packed column similar to chromatography. The mobile liquid passes over the silica wall and the particles. An electroosmosis flow occurs because of the charges on the stationary surface. CEC is similar to CZE in that they both have a plug-type flow compared to the pumped parabolic flow that increases band broadening.[1]

Capillary Isoelectric Focusing (CIEF)

CIEF is a technique commonly used to separate peptides and proteins. These molecules are called zwitterionic compounds because they contain both positive and negative charges. The charge depends on the functional groups attached to the main chain and the

surrounding pH of the environment. In addition, each molecule has a specific isoelectric point (pI). When the surrounding pH is equal to this pI, the molecule carries no net charge. To be clear, it is not the pH value where a protein has all bases deprotonated and all acids protonated, but rather the value where positive and negative charges cancel out to zero. At a pH below the pI, the molecule is positive, and then negative when the pH is above the pI. Because the charge changes with pH, a pH gradient can be used to separate molecules in a mixture. During a CIEF separation, the capillary is filled with the sample in solution and typically no EOF is used (EOF is removed by using a coated capillary). When the voltage is applied, the ions will migrate to a region where they become neutral (pH=pI). The anodic end of the capillary sits in acidic solution (low pH), while the cathodic end sits in basic solution (high pH). Compounds of equal isoelectric points are “focused” into sharp segments and remain in their specific zone, which allows for their distinct detection.[6]

Calculating pI

An amino acid with n ionizable groups with their respective pKa values pK_1, pK_2, ... pk_n will have the pI equal to the average of the group pkas: $pI = (pK_1+pK_2+...+pk_n)/n$. Most proteins have many ionizable sidechains in addition to their amino- and carboxy-terminal groups. The pI is different for each protein and it can be theoretically calculated according to the Henderson-Hasselbalch approximation, if we know amino acids composition of protein. In order to experimentally determine a protein's pI 2-Dimensional Electrophoresis (2-DE) can be used. The proteins of a cell lysate are applied to a pH immobilized gradient strip, upon electrophoresis the proteins migrate to their pI within the strip. The second dimension of 2-DE is the separation of proteins by MW using a SDS-gel.

Capillary Isotachorphoresis (CITP)

CITP is the only method to be used in a discontinuous system. The analyte migrates in consecutive zones and each zone length can be measured to find the quantity of sample present.[1]

Capillary Electrophoresis versus High Performance Liquid Chromatography (HPLC)

1. CE has a flat flow, compared to the pumped parabolic flow of the HPLC. The flat flow results in narrower peaks and better resolution (Figure 10.2.3.4).
2. CE has a greater peak capacity when compared to HPLC—CE uses millions of theoretical plates.
3. HPLC is more thoroughly developed and has many mobile and stationary phases that can be implemented.
4. HPLC has more complex instrumentation, while CE is simpler for the operator.
5. HPLC has such a wide variety of column lengths and packing, whereas CE is limited to thin capillaries.
6. Both techniques use similar modes of detection.
7. Can be used complementary to one another.

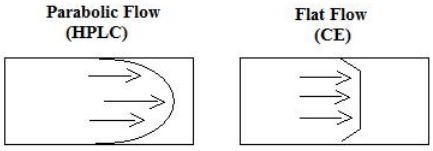


Figure* 10.2.3.4*: *HPLC versus CE flow profiles*

Problems

1. Calculate µEP if q= +1, η is 3.7 (lb s/ft^2) x 10^{-5} and the radius of the atom is 2 nm.
2. How does buffer pH affect the capillary?
3. How does hydrophilicity affect MEKC?
4. What advantages does capillary electrophoresis provide over liquid chromatography?
5. Give reasons why “Analyte A” migrated first, while “Analyte D” migrated last.

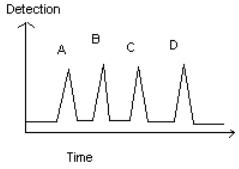


Figure 10.2.3.5: Detection Times

References

1. Li, Sam. Capillary Electrophoresis: Principles, Practice, and Applications. Journal of Chromatography Library; Elsevier Science Publishers: The Netherlands, 1992; Vol 52.
2. Petersen, John R., and Amin A. Mohammad, eds. Clinical and Forensic Applications of Capillary Electrophoresis. New York: Humana P, 2001.
3. Camilleri, Patrick. Capillary Electrophoresis. New York: C R C P LLC, 1997.
4. Altria, Kevin D., Capillary Electrophoresis Guidebook : Principles, Operation and Applications. New York: Humana P, 1995.
5. Landers, James P., Handbook of Capillary Electrophoresis. New York: C R C P LLC, 1996.
6. Weston, A.; Brown, P. HPLC and CE: Principles and Practice; Academic Press: San Diego, 1997.

10.2.3: Capillary Electrophoresis is shared under a CC BY-NC-SA 4.0 license and was authored, remixed, and/or curated by Juliet Precissi.

- **Capillary Electrophoresis** by Juliet Precissi is licensed CC BY-NC-SA 4.0.

10.2.3.1: Ionic Mobility and Electrophoresis

When an electric field is applied to ions in a medium, a phenomenon causes the ions to move with the electric field. The motion of the ion itself can be characterized by charge, shape, and size. The ion moves through the medium and migrates with a characteristic velocity, which is in turn dependent on the characteristics of the ion itself and the properties of the medium. This phenomenon is called **electrophoresis**.

Introduction

Many different biochemical techniques use the principles of electrophoresis to identify compounds of interest in a sample and understand interactions at the molecular and ionic level. The basic concept of the techniques uses an electric field that attracts or repels certain ions, and measurements of the mobility of the ions through the medium (Figure 10.2.3.1.1). The cations move toward the cathode, and the anions move toward the anode. Heavier or bulkier ions move more slowly through the medium. Visual patterns formed on the various media (through the use of dyes and other techniques, such as Coomassie Brilliant Blue G 250 dye) can be analyzed for useful information.

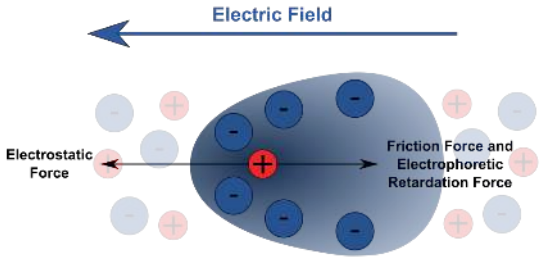


Figure 10.2.3.1.1: Illustration of electrophoresis. (CC-SA-BY 3.0; Daniele Pugliesi)

The velocity of the ion is given by the following equation:

$$v = \frac{E \times q}{f} \tag{10.2.3.1.1}$$

where:

- v is the velocity,
- f is the coefficient of friction,
- E is the applied electric field (Volts/cm), and
- q is the net charge on the ion

The **coefficient of friction** (f) in Equation 10.2.3.1.1is introduced due to the fact that when the ion moves through the medium, the medium exerts a frictional force on the ion that inhibits the movement of the ion. Usually the voltage applied is held constant, so the **mobility** (η) of the ion can be measured; it is defined as follows:

$$\eta = \frac{v}{E} \tag{10.2.3.1.2}$$

where:

- v is the velocity
- E is the applied electric field (Volts/cm)The electric field's properties determine the separation of ions, and is affected by resistance, current, and voltage.

The higher the current, the faster the migration of the ions (due to increased Coulombic attractions). Because current is affected by voltage, as the difference in potential between the electrodes increases, the rate of migration increases. The resistance is dependent on the properties of the medium; a denser or more saturated medium will retard migration, as will a longer or narrower medium. Mediums with different densities can be made from the same compound, and are quite useful for separating and identifying molecules (through molecular sieving, for example). The most common mediums are agar and polyacrylamide gels.

Of key importance is the buffer used. Different compounds have different stability conditions, and the buffer must be chosen carefully so as not to "harm" the molecules' native states. The main factors to consider when choosing a buffer are its concentration

and its pH. Concentration in terms of electrophoresis buffer refers to the ionic strength of the buffer; a buffer with a higher ionic strength will conduct the current more than the sample, leading to slower migration of the molecules. For compounds that have different ionization forms, pH is a major factor in choosing a buffer. The buffer must have a pH that matches the specific ionization forms' pH range.

References

1. Boyer, Rodney. Modern Experimental Biochemistry (Second Edition). Redwood City: The Benjamin/Cummings Publishing Company, Inc., 1993.
2. Williams, Bryan and Wilson, Keith. A Biologist's Guide to Principles and Techniques of Practical Biochemistry. London: Edward Arnold (Publishers) Ltd., 1975
3. Plummer, David. An introduction to Practical Biochemistry (Third Edition). London: McGraw-Hill Book Company (UK) Ltd., 1987

Contributors and Attributions

- Sher Butt

10.2.3.1: Ionic Mobility and Electrophoresis is shared under a CC BY-NC-SA 4.0 license and was authored, remixed, and/or curated by LibreTexts.

- **Ionic Mobility and Electrophoresis** is licensed CC BY-NC-SA 4.0.

10.2.4: Applications of Capillary Electrophoresis

There are several different forms of capillary electrophoresis, each of which has its particular advantages. Several of these methods are described briefly in this section.

Capillary Zone Electrophoresis (CZE)

The simplest form of capillary electrophoresis is capillary zone electrophoresis. In CZE we fill the capillary tube with a buffer and, after loading the sample, place the ends of the capillary tube in reservoirs that contain additional buffer. Usually the end of the capillary containing the sample is the anode and solutes migrate toward the cathode at a velocity determined by their respective electrophoretic mobilities and the electroosmotic flow. Cations elute first, with smaller, more highly charged cations eluting before larger cations with smaller charges. Neutral species elute as a single band. Anions are the last species to elute, with smaller, more negatively charged anions being the last to elute.

We can reverse the direction of electroosmotic flow by adding an alkylammonium salt to the buffer solution. As shown in Figure 30.3.1 , the positively charged end of the alkyl ammonium ions bind to the negatively charged silanate ions on the capillary's walls. The tail of the alkyl ammonium ion is hydrophobic and associates with the tail of another alkyl ammonium ion. The result is a layer of positive charges that attract anions in the buffer. The migration of these solvated anions toward the anode reverses the electroosmotic flow's direction. The order of elution is exactly opposite that observed under normal conditions.

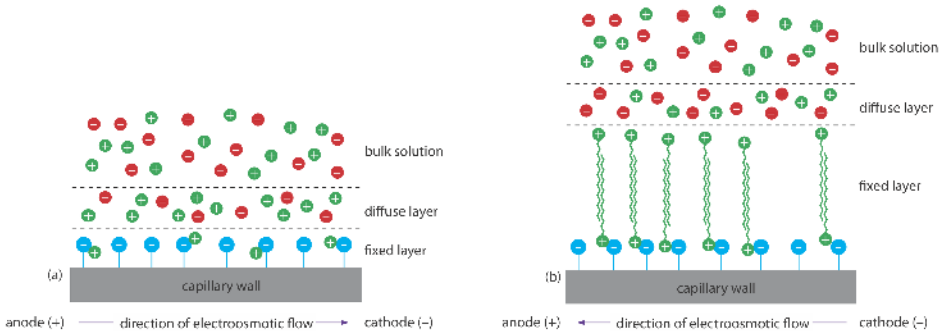


Figure 30.3.1 . Two modes of capillary zone electrophoresis showing (a) normal migration with electroosmotic flow toward the cathode and (b) reversed migration in which the electroosmotic flow is toward the anode.

Coating the capillary's walls with a nonionic reagent eliminates the electroosmotic flow. In this form of CZE the cations migrate from the anode to the cathode. Anions elute into the source reservoir and neutral species remain stationary.

Capillary zone electrophoresis provides effective separations of charged species, including inorganic anions and cations, organic acids and amines, and large biomolecules such as proteins. For example, CZE was used to separate a mixture of 36 inorganic and organic ions in less than three minutes [Jones, W. R.; Jandik, P. *J. Chromatog.* **1992**, *608*, 385–393]. A mixture of neutral species, of course, can not be resolved.

Micellar Electrokinetic Capillary Chromatography (MEKC)

One limitation to CZE is its inability to separate neutral species. Micellar electrokinetic capillary chromatography overcomes this limitation by adding a surfactant, such as sodium dodecylsulfate (Figure 30.3.2 a) to the buffer solution. Sodium dodecylsulfate, or SDS, consists of a long-chain hydrophobic tail and a negatively charged ionic functional group at its head. When the concentration of SDS is sufficiently large a micelle forms. A micelle consists of a spherical agglomeration of 40–100 surfactant molecules in which the hydrocarbon tails point inward and the negatively charged heads point outward (Figure 30.3.2 b).

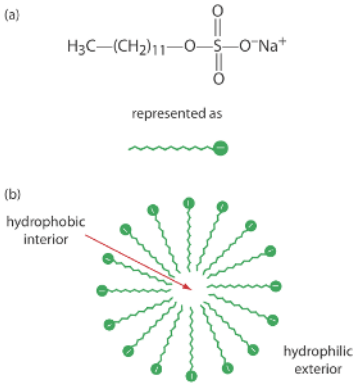


Figure 30.3.2 . (a) Structure of sodium dodecylsulfate and (b) cross section through a micelle showing its hydrophobic interior and its hydrophilic exterior.

Because micelles have a negative charge, they migrate toward the cathode with a velocity less than the electroosmotic flow velocity. Neutral species partition themselves between the micelles and the buffer solution in a manner similar to the partitioning of solutes between the two liquid phases in HPLC. Because there is a partitioning between two phases, we include the descriptive term chromatography in the techniques name. Note that in MEKC both phases are mobile.

The elution order for neutral species in MEKC depends on the extent to which each species partitions into the micelles. Hydrophilic neutrals are insoluble in the micelle's hydrophobic inner environment and elute as a single band, as they would in CZE. Neutral solutes that are extremely hy- drophobic are completely soluble in the micelle, eluting with the micelles as a single band. Those neutral species that exist in a partition equilibrium between the buffer and the micelles elute between the completely hydro- philic and completely hydrophobic neutral species. Those neutral species that favor the buffer elute before those favoring the micelles. Micellar electrokinetic chromatography is used to separate a wide variety of samples, including mixtures of pharmaceutical compounds, vitamins, and explosives.

Capillary Gel Electrophoresis (CGE)

In capillary gel electrophoresis the capillary tubing is filled with a polymeric gel. Because the gel is porous, a solute migrates through the gel with a velocity determined both by its electrophoretic mobility and by its size. The ability to effect a separation using size is helpful when the solutes have similar electrophoretic mobilities. For example, fragments of DNA of varying length have similar charge-to-size ratios, making their separation by CZE difficult. Because the DNA fragments are of different size, a CGE separation is possible.

The capillary used for CGE usually is treated to eliminate electroosmotic flow to prevent the gel from extruding from the capillary tubing. Samples are injected electrokinetically because the gel provides too much resistance for hydrodynamic sampling. The primary application of CGE is the separation of large biomolecules, including DNA fragments, proteins, and oligonucleotides.

Capillary Electrochromatography (CEC)

Another approach to separating neutral species is capillary electrochromatography. In CEC the capillary tubing is packed with 1.5–3 μm particles coated with a bonded stationary phase. Neutral species separate based on their ability to partition between the stationary phase and the buffer, which is moving as a result of the electroosmotic flow; Figure 30.3.3 provides a representative example for the separation of a mixture of hydrocarbons. A CEC separation is similar to the analogous HPLC separation, but without the need for high pressure pumps. Efficiency in CEC is better than in HPLC, and analysis times are shorter.

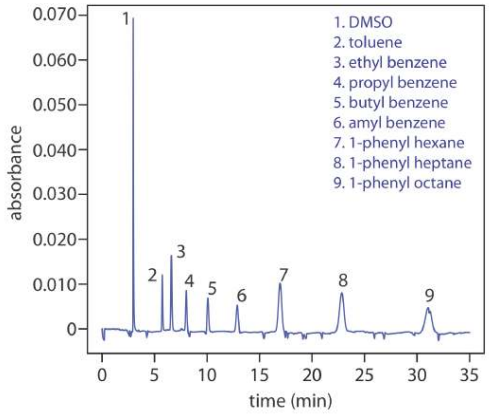


Figure 30.3.3 . Capillary electrochromatographic separation of a mixture of hydrocarbons in DMSO. The column contains a porous polymer of butyl methacrylate and lauryl acrylate (25%:75% mol:mol) with butane dioldacrylate as a crosslinker. Data provided by Zoe LaPier and Michelle Bushey, Department of Chemistry, Trinity University.

This page titled 10.2.4: Applications of Capillary Electrophoresis is shared under a CC BY-NC-SA 4.0 license and was authored, remixed, and/or curated by David Harvey.

- **30.3: Applications of Capillary Electrophoresis** by David Harvey is licensed CC BY-NC-SA 4.0.

10.3: PROBLEMS

1. The following data were obtained for four compounds separated on a 20-m capillary column.

compound	t_r (min)	w (min)
A	8.04	0.15
B	8.26	0.15
C	8.43	0.16

(a) Calculate the number of theoretical plates for each compound and the average number of theoretical plates for the column, in mm.

(b) Calculate the average height of a theoretical plate.

(c) Explain why it is possible for each compound to have a different number of theoretical plates.

2. Using the data from Problem 1, calculate the resolution and the selectivity factors for each pair of adjacent compounds. For resolution, use both equation 12.2.1 and equation 12.3.3, and compare your results. Discuss how you might improve the resolution between compounds B and C. The retention time for an nonretained solute is 1.19 min.

3. Use the chromatogram in Figure 12.8.1 , obtained using a 2-m column, to determine values for t_r, w, t'_r, k, N, and H.

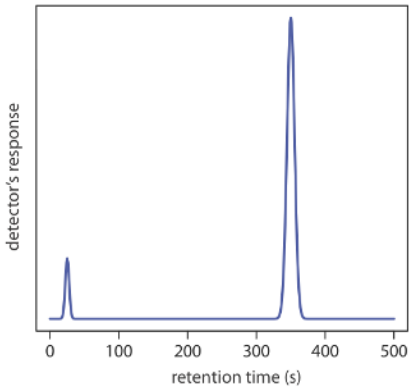


Figure 12.8.1 . Chromatogram for Problem 3.

4. Use the partial chromatogram in Figure 12.8.2 to determine the resolution between the two solute bands.

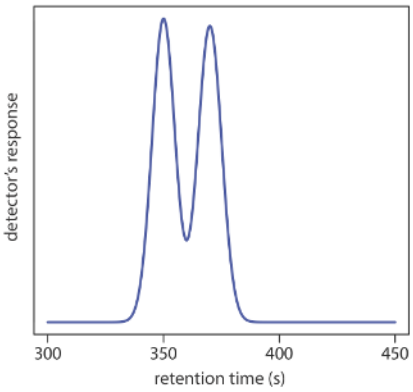


Figure 12.8.2 . Chromatogram for Problem 4.

5. The chromatogram in Problem 4 was obtained on a 2-m column with a column dead time of 50 s. Suppose you want to increase the resolution between the two components to 1.5. Without changing the height of a theoretical plate, what length column do you need? What height of a theoretical plate do you need to achieve a resolution of 1.5 without increasing the column's length?

6. Complete the following table.

N_B	α	k_B	R
100000	1.05	0.50	
10000	1.10		1.50
10000		4.0	1.00
	1.05	3.0	1.75

7. Moody studied the efficiency of a GC separation of 2-butanone on a dinonyl phthalate packed column [Moody, H. W. *J. Chem. Educ.* **1982**, *59*, 218–219]. Evaluating plate height as a function of flow rate gave a van Deemter equation for which *A* is 1.65 mm, *B* is 25.8 mm•mL min^{-1}, and *C* is 0.0236 mm•min mL^{-1}.

(a) Prepare a graph of *H* versus *u* for flow rates between 5 –120 mL/min.

(b) For what range of flow rates does each term in the Van Deemter equation have the greatest effect?

(c) What is the optimum flow rate and the corresponding height of a theoretical plate?

(d) For open-tubular columns the *A* term no longer is needed. If the *B* and *C* terms remain unchanged, what is the optimum flow rate and the corresponding height of a theoretical plate?

(e) Compared to the packed column, how many more theoretical plates are in the open-tubular column?

8. Hsieh and Jorgenson prepared 12–33 µm inner diameter HPLC columns packed with 5.44-µm spherical stationary phase particles [Hsieh, S.; Jorgenson, J. W. *Anal. Chem.* **1996**, *68*, 1212–1217]. To evaluate these columns they measured reduced plate height, *h*, as a function of reduced flow rate, *v*,

$$b = \frac{H}{d_p} \quad v = \frac{ud_p}{D_m}$$

where d_p is the particle diameter and D_m is the solute's diffusion coefficient in the mobile phase. The data were analyzed using van Deemter plots. The following table contains a portion of their results for norepinephrine.

internal diameter (µm)	A	B	C
33	0.63	1.32	0.10
33	0.67	1.30	0.08
23	0.40	1.34	0.09
23	0.58	1.11	0.09
17	0.31	1.47	0.11
17	0.40	1.41	0.11
12	0.22	1.53	0.11
12	0.19	1.27	0.12

(a) Construct separate van Deemter plots using the data in the first row and in the last row for reduced flow rates in the range 0.7–15. Determine the optimum flow rate and plate height for each case given d_p = 5.44 µm and $D_m = 6.23 \times 10^{-6}$ $cm^2\ s^{-1}$.

(b) The *A* term in the van Deemter equation is strongly correlated with the column's inner diameter, with smaller diameter columns providing smaller values of *A*. Offer an explanation for this observation. *Hint: consider how many particles can fit across a capillary of each diameter.*

> When comparing columns, chromatographers often use dimensionless, reduced parameters. By including particle size and the solute's diffusion coefficient, the reduced plate height and reduced flow rate correct for differences between the packing material, the solute, and the mobile phase.

9. A mixture of *n*-heptane, tetrahydrofuran, 2-butanone, and *n*-propanol elutes in this order when using a polar stationary phase such as Carbowax. The elution order is exactly the opposite when using a nonpolar stationary phase such as polydimethyl siloxane. Explain the order of elution in each case.

10. The analysis of trihalomethanes in drinking water is described in Representative Method 12.4.1. A single standard that contains all four trihalomethanes gives the following results.

compound	concentration (ppb)	peak area
$CHCl_3$	1.30	1.35×10^4
$CHCl_2Br$	0.90	6.12×10^4
$CHClBr_2$	4.00	1.71×10^4
$CHBr_3$	1.20	1.52×10^4

Analysis of water collected from a drinking fountain gives areas of 1.56×10^4, 5.13×10^4, 1.49×10^4, and 1.76×10^4 for, respectively, $CHCl_3$, $CHCl_2Br$, $CHClBr_2$, and $CHBr_3$. All peak areas were corrected for variations in injection volumes using an internal standard of 1,2-dibromopentane. Determine the concentration of each of the trihalomethanes in the sample of water.

11. Zhou and colleagues determined the %w/w H_2O in methanol by capillary column GC using a polar stationary phase and a thermal conductivity detector [Zhou, X.; Hines, P. A.; White, K. C.; Borer, M. W. *Anal. Chem.* **1998**, *70*, 390–394]. A series of calibration standards

gave the following results.

%w/w H_2O	peak height (arb. units)
0.00	1.15
0.0145	2.74
0.0472	6.33
0.0951	11.58
0.1757	20.43
0.2901	32.97

(a) What is the %w/w H_2O in a sample that has a peak height of 8.63?

(b) The %w/w H_2O in a freeze-dried antibiotic is determined in the following manner. A 0.175-g sample is placed in a vial along with 4.489 g of methanol. Water in the vial extracts into the methanol. Analysis of the sample gave a peak height of 13.66. What is the %w/w H_2O in the antibiotic?

12. Loconto and co-workers describe a method for determining trace levels of water in soil [Loconto, P. R.; Pan, Y. L.; Voice, T. C. *LC•GC* **1996**, *14*, 128–132]. The method takes advantage of the reaction of water with calcium carbide, CaC_2, to produce acetylene gas, C_2H_2. By carrying out the reaction in a sealed vial, the amount of acetylene produced is determined by sampling the headspace. In a typical analysis a sample of soil is placed in a sealed vial with CaC_2. Analysis of the headspace gives a blank corrected signal of 2.70×10^5. A second sample is prepared in the same manner except that a standard addition of 5.0 mg H_2O/g soil is added, giving a blank-corrected signal of 1.06×10^6. Determine the milligrams H_2O/g soil in the soil sample.

13. Van Atta and Van Atta used gas chromatography to determine the %v/v methyl salicylate in rubbing alcohol [Van Atta, R. E.; Van Atta, R. L. *J. Chem. Educ.* **1980**, *57*, 230–231]. A set of standard additions was prepared by transferring 20.00 mL of rubbing alcohol to separate 25-mL volumetric flasks and pipeting 0.00 mL, 0.20 mL, and 0.50 mL of methyl salicylate to the flasks. All three flasks were diluted to volume using isopropanol. Analysis of the three samples gave peak heights for methyl salicylate of 57.00 mm, 88.5 mm, and 132.5 mm, respectively. Determine the %v/v methyl salicylate in the rubbing alcohol.

14. The amount of camphor in an analgesic ointment is determined by GC using the method of internal standards [Pant, S. K.; Gupta, P. N.; Thomas, K. M.; Maitin, B. K.; Jain, C. L. *LC•GC* **1990**, *8*, 322–325]. A standard sample is prepared by placing 45.2 mg of camphor and 2.00 mL of a 6.00 mg/mL internal standard solution of terpene hydrate in a 25-mL volumetric flask and diluting to volume with CCl_4. When an approximately 2-µL sample of the standard is injected, the FID signals for the two components are measured (in arbitrary units) as 67.3 for camphor and 19.8 for terpene hydrate. A 53.6-mg sample of an analgesic ointment is prepared for analysis by placing it in a 50-mL Erlenmeyer flask along with 10 mL of CCl_4. After heating to 50°C in a water bath, the sample is cooled to below room temperature and filtered. The residue is washed with two 5-mL portions of CCl_4 and the combined filtrates are collected in a 25-mL volumetric flask. After adding 2.00 mL of the internal standard solution, the contents of the flask are diluted to volume with CCl_4. Analysis of an approximately 2-µL sample gives FID signals of 13.5 for the terpene hydrate and 24.9 for the camphor. Report the %w/w camphor in the analgesic ointment.

15. The concentration of pesticide residues on agricultural products, such as oranges, is determined by GC-MS [Feigel, C. *Varian GC/MS Application Note*, Number 52]. Pesticide residues are extracted from the sample using methylene chloride and concentrated by evaporating the methylene chloride to a smaller volume. Calibration is accomplished using anthracene-d_{10} as an internal standard. In a study to determine the parts per billion heptachlor epoxide on oranges, a 50.0-g sample of orange rinds is chopped and extracted with 50.00 mL of methylene chloride. After removing any insoluble material by filtration, the methylene chloride is reduced in volume, spiked with a known amount of the internal standard and diluted to 10 mL in a volumetric flask. Analysis of the sample gives a peak–area ratio ($A_{analyte}/A_{intstd}$) of 0.108. A series of calibration standards, each containing the same amount of anthracene-d_{10} as the sample, gives the following results.

ppb heptachlor epoxide	$A_{analyte}/A_{intstd}$
20.0	0.065
60.0	0.153
200.0	0.637
500.0	1.554
1000.0	3.198

Report the nanograms per gram of heptachlor epoxide residue on the oranges.

16. The adjusted retention times for octane, toluene, and nonane on a particular GC column are 15.98 min, 17.73 min, and 20.42 min, respectively. What is the retention index for each compound?

17. The following data were collected for a series of normal alkanes using a stationary phase of Carbowax 20M.

alkane	t'_r (min)
pentane	0.79
hexane	1.99
heptane	4.47
octane	14.12
nonane	33.11

What is the retention index for a compound whose adjusted retention time is 9.36 min?

18. The following data were reported for the gas chromatographic analysis of *p*-xylene and methylisobutylketone (MIBK) on a capillary column [Marriott, P. J.; Carpenter, P. D. *J. Chem. Educ.* **1996**, *73*, 96–99].

injection mode	compound	t_r (min)	peak area (arb. units)	peak width (min)
split	MIBK	1.878	54285	0.028
	p-xylene	5.234	123483	0.044
splitless	MIBK	3.420	2493005	1.057
	p-xylene	5.795	3396656	1.051

Explain the difference in the retention times, the peak areas, and the peak widths when switching from a split injection to a splitless injection.

19. Otto and Wegscheider report the following retention factors for the reversed-phase separation of 2-aminobenzoic acid on a C_{18} column when using 10% v/v methanol as a mobile phase [Otto, M.; Wegscheider, W. *J. Chromatog.* **1983**, *258*, 11–22].

pH	*k*
2.0	10.5
3.0	16.7
4.0	15.8
5.0	8.0
6.0	2.2
7.0	1.8

Explain the effect of pH on the retention factor for 2-aminobenzene.

20. Haddad and associates report the following retention factors for the reversed-phase separation of salicylamide and caffeine [Haddad, P.; Hutchins, S.; Tuffy, M. *J. Chem. Educ.* **1983**, *60*, 166-168].

%v/v methanol	30%	35%	40%	45%	50%	55%
k_{sal}	2.4	1.6	1.6	1.0	0.7	0.7
k_{caff}	4.3	2.8	2.3	1.4	1.1	0.9

(a) Explain the trends in the retention factors for these compounds.

(b) What is the advantage of using a mobile phase with a smaller %v/v methanol? Are there any disadvantages?

21. Suppose you need to separate a mixture of benzoic acid, aspartame, and caffeine in a diet soda. The following information is available.

	t_r in aqueous mobile phase of pH			
compound	3.0	3.5	4.0	4.5
benzoic acid	7.4	7.0	6.9	4.4
aspartame	5.9	6.0	7.1	8.1
caffeine	3.6	3.7	4.1	4.4

(a) Explain the change in each compound's retention time.

(b) Prepare a single graph that shows retention time versus pH for each compound. Using your plot, identify a pH level that will yield an acceptable separation.

22. The composition of a multivitamin tablet is determined using an HPLC with a diode array UV/Vis detector. A 5-µL standard sample that contains 170 ppm vitamin C, 130 ppm niacin, 120 ppm niacinamide, 150 ppm pyridoxine, 60 ppm thiamine, 15 ppm folic acid, and 10 ppm riboflavin is injected into the HPLC, giving signals (in arbitrary units) of, respectively, 0.22, 1.35, 0.90, 1.37, 0.82, 0.36, and 0.29. The multivitamin tablet is prepared for analysis by grinding into a powder and transferring to a 125-mL Erlenmeyer flask that contains 10 mL of 1% v/v NH_3 in dimethyl sulfoxide. After sonicating in an ultrasonic bath for 2 min, 90 mL of 2% acetic acid is added and the mixture is stirred for 1 min and sonicated at 40°C for 5 min. The extract is then filtered through a 0.45-µm membrane filter. Injection of a 5-µL sample

into the HPLC gives signals of 0.87 for vitamin C, 0.00 for niacin, 1.40 for niacinamide, 0.22 for pyridoxine, 0.19 for thiamine, 0.11 for folic acid, and 0.44 for riboflavin. Report the milligrams of each vitamin present in the tablet.

23. The amount of caffeine in an analgesic tablet was determined by HPLC using a normal calibration curve. Standard solutions of caffeine were prepared and analyzed using a 10-μL fixed-volume injection loop. Results for the standards are summarized in the following table.

concentration (ppm)	signal (arb. units)
50.0	8.354
100.0	16925
150.0	25218
200.0	33584
250.0	42002

The sample is prepared by placing a single analgesic tablet in a small beaker and adding 10 mL of methanol. After allowing the sample to dissolve, the contents of the beaker, including the insoluble binder, are quantitatively transferred to a 25-mL volumetric flask and diluted to volume with methanol. The sample is then filtered, and a 1.00-mL aliquot transferred to a 10-mL volumetric flask and diluted to volume with methanol. When analyzed by HPLC, the signal for caffeine is found to be 21 469. Report the milligrams of caffeine in the analgesic tablet.

24. Kagel and Farwell report a reversed-phase HPLC method for determining the concentration of acetylsalicylic acid (ASA) and caffeine (CAF) in analgesic tablets using salicylic acid (SA) as an internal standard [Kagel, R. A.; Farwell, S. O. *J. Chem. Educ.* **1983**, *60*, 163–166]. A series of standards was prepared by adding known amounts of ace- tylsalicylic acid and caffeine to 250-mL Erlenmeyer flasks and adding 100 mL of methanol. A 10.00-mL aliquot of a standard solution of salicylic acid was then added to each. The following results were obtained for a typical set of standard solutions.

	milligrams of		peak height ratios for	
standard	ASA	CAF	ASA/SA	CAF/SA
1	200.0	20.0	20.5	10.6
2	250.0	40.0	25.1	23.0
3	300.0	60.0	30.9	36.8

A sample of an analgesic tablet was placed in a 250-mL Erlenmeyer flask and dissolved in 100 mL of methanol. After adding a 10.00-mL portion of the internal standard, the solution was filtered. Analysis of the sample gave a peak height ratio of 23.2 for ASA and of 17.9 for CAF.

(a) Determine the milligrams of ASA and CAF in the tablet.

(b) Why is it necessary to filter the sample?

(c) The directions indicate that approximately 100 mL of methanol is used to dissolve the standards and samples. Why is it not necessary to measure this volume more precisely?

(d) In the presence of moisture, ASA decomposes to SA and acetic acid. What complication might this present for this analysis? How might you evaluate whether this is a problem?

25. Bohman and colleagues described a reversed-phase HPLC method for the quantitative analysis of vitamin A in food using the method of standard additions Bohman, O.; Engdahl, K. A.; Johnsson, H. *J. Chem. Educ.* **1982**, *59*, 251–252]. In a typical example, a 10.067-g sample of cereal is placed in a 250-mL Erlenmeyer flask along with 1 g of sodium ascorbate, 40 mL of ethanol, and 10 mL of 50% w/v KOH. After refluxing for 30 min, 60 mL of ethanol is added and the solution cooled to room temperature. Vitamin A is extracted using three 100-mL portions of hexane. The combined portions of hexane are evaporated and the residue containing vitamin A transferred to a 5-mL volumetric flask and diluted to volume with methanol. A standard addition is prepared in a similar manner using a 10.093-g sample of the cereal and spiking with 0.0200 mg of vitamin A. Injecting the sample and standard addition into the HPLC gives peak areas of, respectively, 6.77×10^3 and 1.32×10^4. Report the vitamin A content of the sample in milligrams/100 g cereal.

26. Ohta and Tanaka reported on an ion-exchange chromatographic method for the simultaneous analysis of several inorganic anions and the cations Mg^{2+} and Ca^{2+} in water [Ohta, K.; Tanaka, K. *Anal. Chim. Acta* **1998**, *373*, 189–195]. The mobile phase includes the ligand 1,2,4-benzenetricarboxylate, which absorbs strongly at 270 nm. Indirect detection of the analytes is possible because its absorbance decreases when complexed with an anion.

(a) The procedure also calls for adding the ligand EDTA to the mobile phase. What role does the EDTA play in this analysis?

(b) A standard solution of 1.0 mM $NaHCO_3$, 0.20 mM $NaNO_2$, 0.20 mM $MgSO_4$, 0.10 mM $CaCl_2$, and 0.10 mM $Ca(NO_3)_2$ gives the following peak areas (arbitrary units).

ion	HCO_3^-	Cl^-	NO_2^-	NO_3^-
peak area	373.5	322.5	264.8	262.7
ion	Ca^{2+}	Mg^{2+}	SO_4^{2-}	
peak area	458.9	352.0	341.3	

Analysis of a river water sample (pH of 7.49) gives the following results.

ion	HCO_3^-	Cl^-	NO_2^-	NO_3^-
peak area	310.0	403.1	3.97	157.6
ion	Ca^{2+}	Mg^{2+}	SO_4^{2-}	
peak area	734.3	193.6	324.3	

Determine the concentration of each ion in the sample.

(c) The detection of HCO_3^- actually gives the total concentration of carbonate in solution ($[CO_3^{2-}]+[HCO_3^-]+[H_2CO_3]$). Given that the pH of the water is 7.49, what is the actual concentration of HCO_3^-?

(d) An independent analysis gives the following additional concentrations for ions in the sample: $[Na^+]$ = 0.60 mM; $[NH_4^+]$ = 0.014 mM; and $[K^+]$ = 0.046 mM. A solution's ion balance is defined as the ratio of the total cation charge to the total anion charge. Determine the charge balance for this sample of water and comment on whether the result is reasonable.

27. The concentrations of Cl^-, NO_2^-, and SO_4^{2-} are determined by ion chromatography. A 50-µL standard sample of 10.0 ppm Cl^-, 2.00 ppm NO_2^-, and 5.00 ppm SO_4^{2-} gave signals (in arbitrary units) of 59.3, 16.1, and 6.08 respectively. A sample of effluent from a wastewater treatment plant is diluted tenfold and a 50-µL portion gives signals of 44.2 for Cl^-, 2.73 for NO_2^-, and 5.04 for SO_4^{2-}. Report the parts per million for each anion in the effluent sample.

28. A series of polyvinylpyridine standards of different molecular weight was analyzed by size-exclusion chromatography, yielding the following results.

formula weight	retention volume (mL)
600000	6.42
100000	7.98
30000	9.30
3000	10.94

When a preparation of polyvinylpyridine of unknown formula weight is analyzed, the retention volume is 8.45 mL. Report the average formula weight for the preparation.

29. Diet soft drinks contain appreciable quantities of aspartame, benzoic acid, and caffeine. What is the expected order of elution for these compounds in a capillary zone electrophoresis separation using a pH 9.4 buffer given that aspartame has pK_a values of 2.964 and 7.37, benzoic acid has a pK_a of 4.2, and the pK_a for caffeine is less than 0. Figure 12.8.3 provides the structures of these compounds.

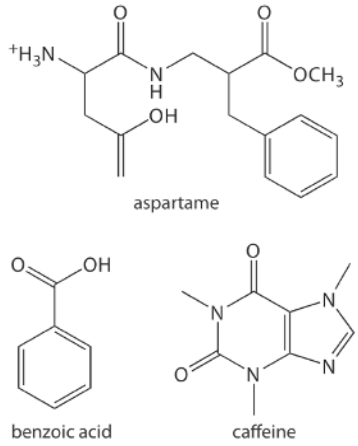


Figure 12.8.3
. Structures for the compounds in Problem 29.

30. Janusa and coworkers describe the determination of chloride by CZE [Janusa, M. A.; Andermann, L. J.; Kliebert, N. M.; Nannie, M. H. *J. Chem. Educ.* **1998**, *75*, 1463–1465]. Analysis of a series of external standards gives the following calibration curve.

$$\text{area} = -883 + 5590 \times \text{ppm } Cl^-$$

A standard sample of 57.22% w/w Cl^- is analyzed by placing 0.1011-g portions in separate 100-mL volumetric flasks and diluting to volume. Three unknowns are prepared by pipeting 0.250 mL, 0.500 mL, an 0.750 mL of the bulk unknown in separate 50-mL volumetric flasks and diluting to volume. Analysis of the three unknowns gives areas of 15 310, 31 546, and 47 582, respectively. Evaluate the accuracy of this analysis.

31. The analysis of NO_3^- in aquarium water is carried out by CZE using IO_4^- as an internal standard. A standard solution of 15.0 ppm NO_3^- and 10.0 ppm IO_4^- gives peak heights (arbitrary units) of 95.0 and 100.1, respectively. A sample of water from an aquarium is diluted 1:100 and sufficient internal standard added to make its concentration 10.0 ppm in IO_4^-. Analysis gives signals of 29.2 and 105.8 for NO_3^- and IO_4^-, respectively. Report the ppm NO_3^- in the sample of aquarium water.

32. Suggest conditions to separate a mixture of 2-aminobenzoic acid (pK_{a1} = 2.08, pK_{a2} = 4.96), benzylamine (pK_a = 9.35), and 4-methylphenol (pK_{a2} = 10.26) by capillary zone electrophoresis. Figure $PageIndex4$ provides the structures of these compounds.

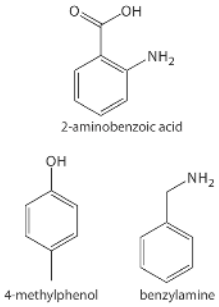


Figure 12.8.4 . Structures for the compounds in Problem 32.

33. McKillop and associates examined the electrophoretic separation of some alkylpyridines by CZE [McKillop, A. G.; Smith, R. M.; Rowe, R. C.; Wren, S. A. C. *Anal. Chem.* **1999**, *71*, 497–503]. Separations were carried out using either 50-µm or 75-µm inner diameter capillaries, with a total length of 57 cm and a length of 50 cm from the point of injection to the detector. The run buffer was a pH 2.5 lithium phosphate buffer. Separations were achieved using an applied voltage of 15 kV. The electroosmotic mobility, μ_{eof}, as measured using a neutral marker, was found to be 6.398×10^{-5} cm^2 V^{-1} s^{-1}. The diffusion coefficient for alkylpyridines is 1.0×10^{-5} cm^2 s^{-1}.

(a) Calculate the electrophoretic mobility for 2-ethylpyridine given that its elution time is 8.20 min.

(b) How many theoretical plates are there for 2-ethylpyridine?

(c) The electrophoretic mobilities for 3-ethylpyridine and 4-ethylpyridine are 3.366×10^{-4} cm^2 V^{-1} s^{-1} and 3.397×10^{-4} cm^2 V^{-1} s^{-1}, respectively. What is the expected resolution between these two alkylpyridines?

(d) Explain the trends in electrophoretic mobility shown in the following table.

alkylpyridine	μ_{ep} (cm^2 V^{-1} s^{-1})
2-methylpyridine	3.581×10^{-4}
2-ethylpyridine	3.222×10^{-4}
2-propylpyridine	2.923×10^{-4}
2-pentylpyridine	2.534×10^{-4}
2-hexylpyridine	2.391×10^{-4}

(e) Explain the trends in electrophoretic mobility shown in the following table.

alkylpyridine	μ_{ep} (cm^2 V^{-1} s^{-1})
2-ethylpyridine	3.222×10^{-4}
3-ethylpyridine	3.366×10^{-4}
4-ethylpyridine	3.397×10^{-4}

(f) The pK_a for pyridine is 5.229. At a pH of 2.5 the electrophoretic mobility of pyridine is 4.176×10^{-4} cm^2 V^{-1} s^{-1}. What is the expected electrophoretic mobility if the run buffer's pH is 7.5?

This page titled 10.3: Problems is shared under a CC BY-NC-SA 4.0 license and was authored, remixed, and/or curated by David Harvey.

- **12.8: Problems** by David Harvey is licensed CC BY-NC-SA 4.0.

10.4: ADDITIONAL RESOURCES

The following set of experiments introduce students to the applications of chromatography and electrophoresis. Experiments are grouped into five categories: gas chromatography, high-performance liquid chromatography, ion-exchange chromatography, size-exclusion chromatography, and electrophoresis.

Gas Chromatography

- Bishop, R. D., Jr. "Using GC–MS to Determine Relative Reactivity Ratios," *J. Chem. Educ.* **1995**, *72*, 743–745.
- Elderd, D. M.; Kildahl, N. K.; Berka, L. H. "Experiments for Modern Introductory Chemistry: Identification of Arson Accelerants by Gas Chromatography," *J. Chem. Educ.* **1996**, *73*, 675–677.
- Fleurat-Lessard, P.; Pointet, K.; Renou-Gonnord, M.-F. "Quantitative Determination of PAHs in Diesel Engine Exhausts by GC–MS," *J. Chem. Educ.* **1999**, *76*, 962–965.
- Galipo, R. C.; Canhoto, A. J.; Walla, M. D.; Morgan, S. L. "Analysis of Volatile Fragrance and Flavor Compounds by Headspace Solid Phase Microextraction and GC–MS," *J. Chem. Educ.* **1999**, *76*, 245–248.
- Graham, R. C.; Robertson, J. K. "Analysis of Trihalomethanes in Soft Drinks," *J. Chem. Educ.* **1988**, *65*, 735–737.
- Heinzen, H.; Moyan, P.; Grompone, A. "Gas Chromatographic Determination of Fatty Acid Compositions," *J. Chem. Educ.* **1985**, *62*, 449–450.
- Kegley, S. E.; Hansen, K. J.; Cunningham, K. L. "Determination of Polychlorinated Biphenyls (PCBs) in River and Bay Sediments," *J. Chem. Educ.* **1996**, *73*, 558–562.
- Kostecka, K. S.; Rabah, A.; Palmer, C. F., Jr. "GC/MS Analysis of the Aromatic Composition of Gasoline," *J. Chem. Educ.* **1995**, *72*, 853–854.
- Quach, D. T.; Ciszkowski, N. A.; Finlayson-Pitts, B. J. "A New GC-MS Experiment for the Undergraduate Instrumental Analysis Laboratory in Environmental Chemistry: Methyl-t-butyl Ether and Benzene in Gasoline," *J. Chem. Educ.* **1998**, *75*, 1595–1598.
- Ramachandran, B. R.; Allen, J. M.; Halpern, A. M. "Air–Water Partitioning of Environmentally Important Organic Compounds," *J. Chem. Educ.* **1996**, *73*, 1058–1061.
- Rice, G. W. "Determination of Impurities in Whiskey Using Internal Standard Techniques," *J. Chem. Educ.* **1987**, *64*, 1055–1056.
- Rubinson, J. F.; Neyer-Hilvert, J. "Integration of GC-MS Instrumentation into the Undergraduate Laboratory: Separation and Identification of Fatty Acids in Commercial Fats and Oils," *J. Chem. Educ.* **1997**, *74*, 1106–1108.
- Rudzinski, W. E.; Beu, S. "Gas Chromatographic Determination of Environmentally Significant Pesticides," *J. Chem. Educ.* **1982**, *59*, 614–615.
- Sobel, R. M.; Ballantine, D. S.; Ryzhov, V. "Quantitation of Phenol Levels in Oil of Wintergreen Using Gas Chromatography–Mass Spectrometry with Selected Ion Monitoring," *J. Chem. Educ.* **2005**, *82*, 601–603.
- Welch, W. C.; Greco, T. G. "An Experiment in Manual Multiple Headspace Extraction for Gas Chromatography," *J. Chem. Educ.* **1993**, *70*, 333–335.
- Williams, K. R.; Pierce, R. E. "The Analysis of Orange Oil and the Aqueous Solubility of d-Limone," *J. Chem. Educ.* **1998**, *75*, 223–226.
- Wong, J. W.; Ngim, K. K.; Shibamoto, T.; Mabury, S. A.; Eiserich, J. P.; Yeo, H. C. H. "Determination of Formaldehyde in Cigarette Smoke," *J. Chem. Educ.* **1997**, *74*, 1100–1103.
- Yang, M. J.; Orton, M. L., Pawliszyn, J. "Quantitative Determination of Caffeine in Beverages Using a Combined SPME-GC/MS Method," *J. Chem. Educ.* **1997**, *74*, 1130–1132.

High-Performance Liquid Chromatography

- Batchelor, J. D.; Jones, B. T. "Determination of the Scoville Heat Value for Hot Sauces and Chilies: An HPLC Experiment," *J. Chem. Educ.* **2000**, *77*, 266–267.
- Beckers, J. L. "The Determination of Caffeine in Coffee: Sense or Nonsense?" *J. Chem. Educ.* **2004**, *81*, 90–93.
- Betts, T. A. "Pungency Quantitation of Hot Pepper Sauces Using HPLC," *J. Chem. Educ.* **1999**, *76*, 240–244.
- Bidlingmeyer, B. A.; Schmitz, S. "The Analysis of Artificial Sweeteners and Additives in Beverages by HPLC," *J. Chem. Educ.* **1991**, *68*, A195–A200.
- Bohman, O.; Engdahl, K.-A.; Johnsson, H. "High Performance Liquid Chromatography of Vitamin A: A Quantitative Determination," *J. Chem. Educ.* **1982**, *59*, 251–252.
- Brenneman, C. A.; Ebeler, S. E. "Chromatographic Separations Using Solid-Phase Extraction Cartridges: Separation of Wine Phenolics," *J. Chem. Educ.* **1999**, *76*, 1710–1711.
- Cantwell, F. F.; Brown, D. W. "Liquid Chromatographic Determination of Nitroanilines," *J. Chem. Educ.* **1981**, *58*, 820–823.
- DiNunzio, J. E. "Determination of Caffeine in Beverages by High Performance Liquid Chromatography," *J. Chem. Educ.* **1985**, *62*, 446–447.

- Ferguson, G. K. “Quantitative HPLC Analysis of an Analgesic/Caffeine Formulation: Determination of Caffeine,” *J. Chem. Educ.* **1998**, *75*, 467–469.
- Ferguson, G. K. “Quantitative HPLC Analysis of a Psychotherapeutic Medication: Simultaneous Determination of Amitriptyline Hydrochloride and Perphenazine,” *J. Chem. Educ.* **1998**, *75*, 1615–1618.
- Goodney, D. E. “Analysis of Vitamin C by High-Pressure Liquid Chromatography,” *J. Chem. Educ.* **1987**, *64*, 187–188.
- Guevremont, R.; Quigley, M. N. “Determination of Paralytic Shellfish Poisons Using Liquid Chromatography,” *J. Chem. Educ.* **1994**, *71*, 80–81.
- Haddad, P.; Hutchins, S.; Tuffy, M. “High Performance Liquid Chromatography of Some Analgesic Compounds,” *J. Chem. Educ.* **1983**, *60*, 166–168.
- Huang, J.; Mabury, S. A.; Sagebiel, J. C. “Hot Chili Peppers: Extraction, Cleanup, and Measurement of Capscaicin,” *J. Chem. Educ.* **2000**, *77*, 1630–1631.
- Joeseph, S. M.; Palasota, J. A. “The Combined Effect of pH and Percent Methanol on the HPLC Separation of Benzoic Acid and Phenol,” *J. Chem. Educ.* **2001**, *78*, 1381–1383.
- Lehame, S. “The Separation of Copper, Iron, and Cobalt Tetramethylene Dithiocarbamates by HPLC,” *J. Chem. Educ.* **1986**, *63*, 727–728.
- Luo, P.; Luo, M. Z.; Baldwin, R. P. “Determination of Sugars in Food Products,” *J. Chem. Educ.* **1993**, *70*, 679–681.
- Mueller, B. L.; Potts, L. W. “HPLC Analysis of an Asthma Medication,” *J. Chem. Educ.* **1988**, *65*, 905–906.
- Munari, M.; Miurin, M.; Goi, G. “Didactic Application to Riboflavin HPLC Analysis,” *J. Chem. Educ.* **1991**, *68*, 78–79.
- Orth, D. L. “HPLC Determination of Taurine in Sports Drinks,” *J. Chem. Educ.* **2001**, *78*, 791– 792.
- Remcho, V. T.; McNair, H. M.; Rasmussen, H. T. “HPLC Method Development with the Photodiode Array Detector,” *J. Chem. Educ.* **1992**, *69*, A117–A119.
- Richardson, W. W., III; Burns, L. “HPLC of the Polypeptides in a Hydrolyzate of Egg-White Lysozyme,” *J. Chem. Educ.* **1988**, *65*, 162–163.
- Silveira, A., Jr.; Koehler, J. A.; Beadel, E. F., Jr.; Monore, P. A. “HPLC Analysis of Chlorophyll a, Chlorophyll b, and β-Carotene in Collard Greens,” *J. Chem. Educ.* **1984**, *61*, 264–265.
- Siturmorang, M.; Lee, M. T. B.; Witzeman, L. K.; Heineman, W. R. “Liquid Chromatography with Electrochemical Detection (LC-EC): An Experiment Using 4-Aminophenol,” *J. Chem. Educ.* **1998**, *75*, 1035–1038.
- Sottofattori, E.; Raggio, R.; Bruno, O. “Milk as a Drug Analysis Medium: HPLC Determination of Isoniazid,” *J. Chem. Educ.* **2003**, *80*, 547–549.
- Strohl, A. N. “A Study of Colas: An HPLC Experiment,” *J. Chem. Educ.* **1985**, *62*, 447–448.
- Tran, C. D.; Dotlich, M. “Enantiomeric Separation of Beta-Blockers by High Performance Liquid Chromatography,” *J. Chem. Educ.* **1995**, *72*, 71–73.
- Van Arman, S. A.; Thomsen, M. W. “HPLC for Undergraduate Introductory Laboratories,” *J. Chem. Educ.* **1997**, *74*, 49–50.
- Wingen, L. M.; Low, J. C.; Finlayson-Pitts, B. J. “Chromatography, Absorption, and Fluorescence: A New Instrumental Analysis Experiment on the Measurement of Polycyclic Aromatic Hydrocarbons in Cigarette Smoke,” *J. Chem. Educ.* **1998**, *75*, 1599–1603.

Ion-Exchange Chromatography

- Bello, M. A.; Gustavo González, A. “Determination of Phosphate in Cola Beverages Using Nonsuppressed Ion Chromatography,” *J. Chem. Educ.* **1996**, *73*, 1174–1176.
- Kieber, R. J.; Jones, S. B. “An Undergraduate Laboratory for the Determination of Sodium, Potassium, and Chloride,” *J. Chem. Educ.* **1994**, *71*, A218–A222.
- Koubek, E.; Stewart, A. E. “The Analysis of Sulfur in Coal,” *J. Chem. Educ.* **1992**, *69*, A146–A148.
- Sinniah, K.; Piers, K. “Ion Chromatography: Analysis of Ions in Pond Water,” *J. Chem. Educ.* **2001**, *78*, 358–362.
- Xia, K.; Pierzynski, G. “Competitive Sorption between Oxalate and Phosphate in Soil: An Environmental Chemistry Laboratory Using Ion Chromatography,” *J. Chem. Educ.* **2003**, *80*, 71–75.

Size-Exchange Chromatography

- Brunauer, L. S.; Davis, K. K. “Size Exclusion Chromatography: An Experiment for High School and Community College Chemistry and Biotechnology Laboratory Programs,” *J. Chem. Educ.* **2008**, *85*, 683–685.
- Saiz, E.; Tarazona, M. P. “Size-Exclusion Chromatography Using Dual Detection,” *Chem. Educator* **2000**, *5*, 324–328.

Electrophoresis

- Almarez, R. T.; Kochis, M. “Microscale Capillary Electrophoresis: A Complete Instrumentation Experiment for Chemistry Students at the Undergraduate Junior or Senior Level,” *J. Chem. Educ.* **2003**, *80*, 316–319.
- Beckers, J. L. “The Determination of Caffeine in Coffee: Sense or Nonsense?” *J. Chem. Educ.* **2004**, *81*, 90–93.
- Beckers, J. L. “The Determination of Vanillin in a Vanilla Extract,” *J. Chem. Educ.* **2005**, *82*, 604– 606.
- Boyce, M. “Separation and Quantification of Simple Ions by Capillary Zone Electrophoresis,” *J. Chem. Educ.* **1999**, *76*, 815–819.

- Conradi, S.; Vogt, C.; Rohde, E. “Separation of Enatiomeric Barbiturates by Capillary Electrophoresis Using a Cyclodextrin-Containing Run Buffer,” *J. Chem. Educ.* **1997**, *74*, 1122–1125.
- Conte, E. D.; Barry, E. F.; Rubinstein, H. “Determination of Caffeine in Beverages by Capillary Zone Electrophoresis,” *J. Chem. Educ.* **1996**, *73*, 1169–1170.
- Demay, S.; Martin-Girardeau, A.; Gonnord, M.-F. “Capillary Electrophoretic Quantitative Analysis of Anions in Drinking Water,” *J. Chem. Educ.* **1999**, *76*, 812–815.
- Emry, R.; Cutright, R. D.; Wright, J.; Markwell, J. “Candies to Dye for: Cooperative, Open-Ended Student Activities to Promote Understanding of Electrophoretic Fractionation,” *J. Chem. Educ.* **2000**, *77*, 1323–1324.
- Gardner, W. P.; Girard, J. E. “Analysis of Common Household Cleaner-Disinfectants by Capillary Electrophoresis,” *J. Chem. Educ.* **2000**, *77*, 1335–1338.
- Gruenhagen, J. A.; Delaware, D.; Ma, Y. “Quantitative Analysis of Non-UV-Absorbing Cations in Soil Samples by High-Performance Capillary Electrophoresis,” *J. Chem. Educ.* **2000**, *77*, 1613–1616.
- Hage, D. S.; Chattopadhyay, A.; Wolfe, C. A. C.; Grundman, J.; Kelter, P. B. “Determination of Nitrate and Nitrite in Water by Capillary Electrophoresis,” *J. Chem. Educ.* **1998**, *75*, 1588–1590.
- Herman, H. B.; Jezorek, J. R.; Tang, Z. “Analysis of Diet Tonic Water Using Capillary Electrophoresis,” *J. Chem. Educ.* **2000**, *77*, 743–744.
- Janusa, M. A.; Andermann, L. J.; Kliebert, N. M.; Nannie, M. H. “Determination of Chloride Concentration Using Capillary Electrophoresis,” *J. Chem. Educ.* **1998**, *75*, 1463–1465.
- McDevitt, V. L.; Rodríguez, A.; Williams, K. R. “Analysis of Soft Drinks: UV Spectrophotometry, Liquid Chromatography, and Capillary Electrophoresis,” *J. Chem. Educ.* **1998**, *75*, 625–629.
- Palmer, C. P. “Demonstrating Chemical and Analytical Concepts in the Undergraduate Laboratory Using Capillary Electrophoresis and Micellar Electrokinetic Chromatography,” *J. Chem. Educ.* **1999**, *76*, 1542–1543.
- Pursell, C. J.; Chandler, B.; Bushey, M. M. “Capillary Electrophoresis Analysis of Cations in Water Samples,” *J. Chem. Educ.* **2004**, *81*, 1783–1786.
- Solow, M. “Weak Acid p*Ka* Determination Using Capillary Zone Electrophoresis,” *J. Chem. Educ.* **2006**, *83*, 1194–1195.
- Thompson, L.; Veening, H.; Strain, T. G. “Capillary Electrophoresis in the Undergraduate Instrumental Analysis Laboratory: Determination of Common Analgesic Formulations,” *J. Chem. Educ.* **1997**, *74*, 1117–1121.
- Vogt, C.; Conradi, S.; Rhode, E. “Determination of Caffeine and Other Purine Compounds in Food and Pharmaceuticals by Micellar Electrokinetic Chromatography” *J. Chem. Educ.* **1997**, *74*, 1126– 1130.
- Weber, P. L.; Buck, D. R. “Capillary Electrophoresis: A Fast and Simple Method for the Determination of the Amino Acid Composition of Proteins,” *J. Chem. Educ.* **1994**, *71*, 609–612.
- Welder, F.; Colyer, C. L. “Using Capillary Electrophoresis to Determine the Purity of Acetylsalicylic Acid Synthesized in the Undergraduate Laboratory,” *J. Chem. Educ.* **2001**, *78*, 1525–1527.
- Williams, K. R.; Adhyaru, B.; German, I.; Russell, T. “Determination of a Diffusion Coefficient by Capillary Electrophoresis,” *J. Chem. Educ.* **2002**, *79*, 1475–1476.

The following texts provide a good introduction to the broad field of separations, including chromatography and electrophoresis.

- Giddings, J. C. *Unified Separation Science*, Wiley-Interscience: New York 1991.
- Karger, B. L.; Snyder, L. R.; Harvath, C. *An Introduction to Separation Science*, Wiley-Interscience: New York, 1973
- Miller, J. M. *Separation Methods in Chemical Analysis*, Wiley-Interscience: New York, 1975.
- Poole, C. F. *The Essence of Chromatography*, Elsevier: Amsterdam, 2003.

A more recent discussion of peak capacity is presented in the following papers.

- Chester, T. L. “Further Considerations of Exact Equations for Peak Capacity in Isocratic Liquid Chromatography,” *Anal. Chem.* **2014**, *86*, 7239–7241.
- Davis, J. M.; Stoll, D. R.; Carr, P. W. “Dependence of Effective Peak Capacity in Comprehensive Two-Dimensional Separations on the Distribution of Peak Capacity between the Two Dimensions,” *Anal. Chem.* **2008**, *80*, 8122–8134.
- Li, X.; Stoll, D. R.; Carr, P. W. “Equation for Peak Capacity Estimation in Two-Dimensional Liquid Chromatography,” *Anal. Chem.* **2009**, *81*, 845–850.
- Shen, Y.; Lee, M. “General Equation for Peak Capacity in Column Chromatography,” *Anal. Chem*. **1998**, *70*, 3853–3856.

The following references may be consulted for more information on gas chromatography.

- Grob, R. L., ed, *Modern Practice of Gas Chromatography*, Wiley-Interscience: New York, 1972.
- Hinshaw, J. V. “A Compendium of GC Terms and Techniques,” *LC•GC* **1992**, *10*, 516–522.
- Ioffe, B. V.; Vitenberg, A. G. *Head-Space Analysis and Related Methods in Gas Chromatography*, Wiley-Interscience: New York, 1982.
- Kitson, F. G.; Larsen, B. S.; McEwen, C. N. *Gas Chromatography and Mass Spectrometry: A Practical Guide*, Academic Press: San Diego, 1996.

- McMaster, M. C. *GC/MS: A Practical User's Guide*, Wiley-Interscience: Hoboken, NJ, 2008.

The following references provide more information on high-performance liquid chromatography.

- Dorschel, C. A.; Ekmanis, J. L.; Oberholtzer, J. E.; Warren, Jr. F. V.; Bidlingmeyer, B. A. "LC Detectors," *Anal. Chem.* **1989**, *61*, 951A–968A.
- Ehlert, S.; Tallarek, U. "High-pressure liquid chromatography in lab-on-a-chip devices," *Anal. Bioanal. Chem.* **2007**, *388*, 517–520.
- Francois, I.; Sandra, K.; Sandra, P. "Comprehensive liquid chromatography: Fundamental aspects and practical considerations—A review," *Anal. Chim. Acta* **2009**, *641*, 14–31.
- Harris, C. M. "Shrinking the LC Landscape," *Anal. Chem.* **2003**, *75*, 64A–69A.
- Meyer, V. R. *Pitfalls and Errors of HPLC in Pictures*, Wiley-VCH: Weinheim, Germany, 2006.
- Pozo, O. J.; Van Eenoo, P.; Deventer, K.; Delbeke, F. T. "Detection and characterization of anabolic steroids in doping analysis by LC–MS," *Trends Anal. Chem.* **2008**, *27*, 657–671.
- Scott, R. P. W. "Modern Liquid Chromatography," *Chem. Soc. Rev.* **1992**, *21*, 137–145.
- Simpson, C. F., ed. *Techniques in Liquid Chromatography*, Wiley-Hayden: Chichester, England; 1982.
- Snyder, L. R.; Glajch, J. L.; Kirkland, J. J. *Practical HPLC Method Development*, Wiley-Interscience: New York,1988.
- van de Merbel, N. C. "Quantitative determination of endogenous compounds in biological samples using chromatographic techniques," *Trends Anal. Chem.* **2008**, *27*, 924–933.
- Yeung, E. S. "Chromatographic Detectors: Current Status and Future Prospects," *LC•GC* **1989**, *7*, 118–128.

The following references may be consulted for more information on ion chromatography.

- Shpigun, O. A.; Zolotov, Y. A. *Ion Chromatography in Water Analysis*, Ellis Horwood: Chichester, England, 1988.
- Smith, F. C. Jr.; Chang, R. C. *The Practice of Ion Chromatography*, Wiley-Interscience: New York, 1983.

The following references may be consulted for more information on supercritical fluid chromatography.

- Palmieri, M. D. "An Introduction to Supercritical Fluid Chromatography. Part I: Principles and Applications," *J. Chem. Educ.* **1988**, *65*, A254–A259.
- Palmieri, M. D. "An Introduction to Supercritical Fluid Chromatography. Part II: Applications and Future Trends," *J. Chem. Educ.* **1989**, *66*, A141–A147.

The following references may be consulted for more information on capillary electrophoresis.

- Baker, D. R. *Capillary Electrophoresis*, Wiley-Interscience: New York, 1995.
- Copper, C. L. "Capillary Electrophoresis: Part I. Theoretical and Experimental Background," *J. Chem. Educ.* **1998**, *75*, 343–347.
- Copper, C. L.; Whitaker, K. W. "Capillary Electrophoresis: Part II. Applications," *J. Chem. Educ.* **1998**, *75*, 347–351.
- DeFrancesco, L. "Capillary Electrophoresis: Finding a Niche," *Today's Chemist at Work*, February 2002, 59–64.
- Ekins, R. P. "Immunoassay, DNA Analysis, and Other Ligand Binding Assay Techniques: From Electropherograms to Multiplexed, Ultrasensative Microarrays on a Chip," *J. Chem. Educ.* **1999**, *76*, 769– 780.
- Revermann, T.; Götz, S.; Künnemeyer, J.; Karst, U. "Quantitative analysis by microchip capillary electrophoresis—current limitations and problem-solving strategies," *Analyst* **2008**, *133*, 167–174.
- Timerbaev, A. R. "Capillary electrophoresis coupled to mass spectrometry for biospeciation analysis: critical evaluation," *Trends Anal. Chem.* **2009**, *28*, 416–425.
- Unger, K. K.; Huber, M.; Hennessy, T. P.; Hearn, M. T. W.; Walhagen, K. "A Critical Appraisal of Capillary Electrochromatography," *Anal. Chem.* **2002**, *74*, 200A–207A.
- Varenne, A.; Descroix, S. "Recent strategies to improve resolution in capillary electrophoresis—A review," *Anal. Chim. Acta* **2008**, *628*, 9–23.
- Vetter, A. J.; McGowan, G. J. "The Escalator—An Analogy for Explaining Electroosmotic Flow," J. Chem. Educ. 2001, 78, 209–211.
- Xu, Y. "Tutorial: Capillary Electrophoresis," *Chem. Educator*, **1996**, *1(2)*, 1–14.

The application of spreadsheets and computer programs for modeling chromatography is described in the following papers.

- Abbay, G. N.; Barry, E. F.; Leepipatpiboon, S.; Ramstad, T.; Roman, M. C.; Siergiej, R. W.; Snyder, L. R.; Winniford, W. L. "Practical Applications of Computer Simulation for Gas Chromatography Method Development," *LC•GC* **1991**, *9*, 100–114.
- Drouen, A.; Dolan, J. W.; Snyder, L. R.; Poile, A.; Schoenmakers, P. J. "Software for Chromatographic Method Development," *LC•GC* **1991**, *9*, 714–724.
- Kevra, S. A.; Bergman, D. L.; Maloy, J. T. "A Computational Introduction to Chromatographic Bandshape Analysis," *J. Chem. Educ.* **1994**, *71*, 1023–1028.
- Rittenhouse, R. C. "HPLC for Windows: A Computer Simulation of High-Performance Liquid Chromatography," *J. Chem. Educ.* **1995**, *72*, 1086–1087.
- Shalliker, R. A.; Kayillo, S.; Dennis, G. R. "Optimizing Chromatographic Separations: An Experiment Using an HPLC Simulator," *J. Chem. Educ.* **2008**, *85*, 1265–1268.

- Sundheim, B. R. “Column Operations: A Spreadsheet Model,” *J. Chem. Educ.* **1992**, *69*, 1003– 1005.

The following papers discuss column efficiency, peak shapes, and overlapping chromatographic peaks.

- Bildingmeyer, B. A.; Warren, F. V., Jr. “Column Efficiency Measurement,” *Anal. Chem.* **1984**, *56*, 1583A–1596A.
- Hawkes, S. J. “Distorted Chromatographic Peaks,” *J. Chem. Educ.* **1994**, *71*, 1032–1033.
- Hinshaw, J. “Pinning Down Tailing Peaks,” *LC•GC* **1992**, *10*, 516–522.
- Meyer, V. K. “Chromatographic Integration Errors: A Closer Look at a Small Peak,” *LC•GC North America* **2009**, *27*, 232–244.
- Reid, V. R.; Synovec, R. E. “High-speed gas chromatography: The importance of instrumentation optimization and the elimination of extra-column band broadening,” *Talanta* **2008**, *76*, 703–717.

This page titled 10.4: Additional Resources is shared under a CC BY-NC-SA 4.0 license and was authored, remixed, and/or curated by David Harvey.

- **12.9: Additional Resources** by David Harvey is licensed CC BY-NC-SA 4.0.

10.5: CHAPTER SUMMARY AND KEY TERMS

CHAPTER SUMMARY

Chromatography and electrophoresis are powerful analytical techniques that both separate a sample into its components and provide a means for determining each component's concentration. Chromatographic separations utilize the selective partitioning of the sample's components between a stationary phase that is immobilized within a column and a mobile phase that passes through the column.

The effectiveness of a chromatographic separation is described by the resolution between two chromatographic bands and is a function of each component's retention factor, the column's efficiency, and the column's selectivity. A solute's retention factor is a measure of its partitioning into the stationary phase, with larger retention factors corresponding to more strongly retained solutes. The column's selectivity for two solutes is the ratio of their retention factors, providing a relative measure of the column's ability to retain the two solutes. Column efficiency accounts for those factors that cause a solute's chromatographic band to increase in width during the separation. Column efficiency is defined in terms of the number of theoretical plates and the height of a theoretical plate, the later of which is a function of a number of parameters, most notably the mobile phase's flow rate. Chromatographic separations are optimized by increasing the number of theoretical plates, by increasing the column's selectivity, or by increasing the solute retention factor.

In gas chromatography the mobile phase is an inert gas and the stationary phase is a nonpolar or polar organic liquid that either is coated on a particulate material and packed into a wide-bore column, or coated on the walls of a narrow-bore capillary column. Gas chromatography is useful for the analysis of volatile components.

In high-performance liquid chromatography the mobile phase is either a nonpolar solvent (normal phase) or a polar solvent (reversed-phase). A stationary phase of opposite polarity, which is bonded to a particulate material, is packed into a wide-bore column. HPLC is applied to a wider range of samples than GC; however, the separation efficiency for HPLC is not as good as that for capillary GC.

Together, GC and HPLC account for the largest number of chromatographic separations. Other separation techniques, however, find specialized applications: of particular importance are ion-exchange chromatography for separating anions and cations; size-exclusion chromatography for separating large molecules; and supercritical fluid chromatography for the analysis of samples that are not easily analyzed by GC or HPLC.

In capillary zone electrophoresis a sample's components are separated based on their ability to move through a conductive medium under the influence of an applied electric field. Positively charged solutes elute first, with smaller, more highly charged cations eluting before larger cations of lower charge. Neutral species elute without undergoing further separation. Finally, anions elute last, with smaller, more negatively charged anions being the last to elute. By adding a surfactant, neutral species can be separated by micellar electrokinetic capillary chromatography. Electrophoretic separations also can take advantage of the ability of polymeric gels to separate solutes by size (capillary gel electrophoresis), and the ability of solutes to partition into a stationary phase (capillary electrochromatography). In comparison to GC and HPLC, capillary electrophoresis provides faster and more efficient separations.

KEY TERMS

adjusted retention time
adsorption chromatography
band broadening
baseline width
bleed
bonded stationary phase
capillary column
capillary electrochromatography
capillary electrophoresis
capillary gel electrophoresis
capillary zone electrophoresis
chromatogram
chromatography
column chromatography
counter-current extraction
cryogenic focusing
electrokinetic injection
electroosmotic flow
electroosmotic flow velocity
electron capture detector
electropherogram
electrophoresis
electrophoretic mobility
electrophoretic velocity
exclusion limit
flame ionization detector
fronting
gas chromatography
gas–liquid chromatography
gas–solid chromatography
general elution problem
guard column
gradient elution
headspace sampling
high-performance liquid chromatography
hydrodynamic injection
inclusion limit
ion-exchange chromatography
ion suppressor column
isocratic elution
isothermal
Joule heating
Kovat's retention index
liquid–solid adsorption chromatography
longitudinal diffusion
loop injector
mass spectrometer
mass spectrum
mass transfer
micelle
micellar electrokinetic capillary chromatography
mobile phase
monolithic column
multiple paths
nonretained solutes
normal-phase chromatography
on-column injection
open tubular column
packed columns
partition chromatography
peak capacity
planar chromatography
polarity index
porous-layer open tubular column
purge-and-trap
resolution
retention factor
retention time
reversed-phase chromatography
selectivity factor
single-column ion chromatography
solid-phase microextraction
split injection
splitless injection
stacking
stationary phase
supercritical fluid chromatography
support-coated open tubular column
tailing
temperature programming
theoretical plate
thermal conductivity detector
van Deemter equation
void time
wall-coated open-tubular column
zeta potential

This page titled 10.5: Chapter Summary and Key Terms is shared under a CC BY-NC-SA 4.0 license and was authored, remixed, and/or curated by David Harvey.

- **12.10: Chapter Summary and Key Terms** by David Harvey is licensed CC BY-NC-SA 4.0.

CHAPTER OVERVIEW

11: Thermal Methods

A thermal method of analysis is a technique in which measure a physical property of a material as we subject it to a change in temperature. In this chapter we consider three examples of thermal methods: thermogravimetry, differential thermal analysis, and differential scanning calorimetry.

11.1: Thermogravimetry

11.2: Differential Thermal Analysis and Differential Scanning Calorimetry

This page titled 11: Thermal Methods is shared under a CC BY-NC-SA 4.0 license and was authored, remixed, and/or curated by David Harvey.

11.1: Thermogravimetry

One method for determining the products of a thermal decomposition is to monitor the sample's mass as a function of temperature, a process called a thermogravimetric analysis (TGA) or thermogravimetry. Figure 31.1.1 shows a typical thermogram in which each change in mass—each "step" in the thermogram—represents the loss of a volatile product. As the following example illustrates, we can use a thermogram to identify a compound's decomposition reactions.

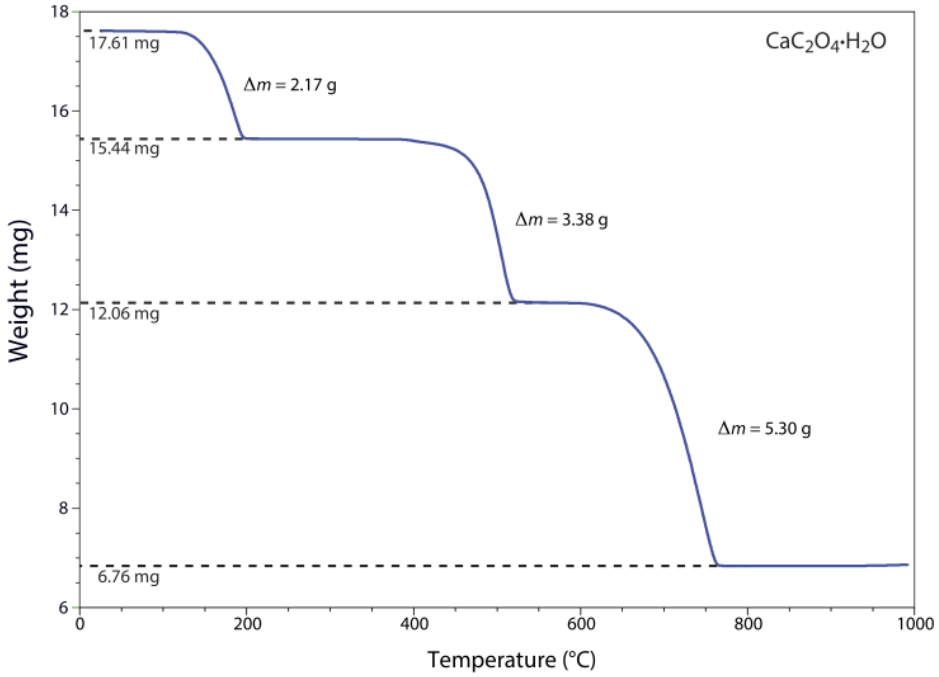


Figure 31.1.1 . Thermogram for CaC_2O_4•H_2O obtained by heating a sample from room temperature to 1000°C at a rate of 20°C/min. Each change in mass results from the loss of a volatile product. The sample's initial mass and its mass after each loss are shown by the dotted lines. See Example 31.1.1 for information on interpreting this thermogram.

Example 31.1.1

The thermogram in Figure 31.1.1 shows the mass of a sample of calcium oxalate monohydrate, CaC_2O_4•H_2O, as a function of temperature. The original sample of 17.61 mg was heated from room temperature to 1000°C at a rate of 20°C per minute. For each step in the thermogram, identify the volatilization product and the solid residue that remains.

Solution

From 100–250°C the sample loses 17.61 mg – 15.44 mg, or 2.17 mg, which is

$$\frac{2.17\text{ mg}}{17.61\text{ mg}} \times 100 = 12.3\%$$

of the sample's original mass. In terms of CaC_2O_4•H_2O, this corresponds to a decrease in the molar mass of

$$0.123 \times 146.11\text{ g/mol} = 18.0\text{ g/mol}$$

The product's molar mass and the temperature range for the decomposition, suggest that this is a loss of $H_2O(g)$, leaving a residue of CaC_2O_4.

The loss of 3.38 mg from 350–550°C is a 19.2% decrease in the sample's original mass, or a decrease in the molar mass of

$$0.192 \times 146.11\text{ g/mol} = 28.1\text{ g/mol}$$

which is consistent with the loss of $CO(g)$ and a residue of $CaCO_3$.

Finally, the loss of 5.30 mg from 600-800°C is a 30.1% decrease in the sample's original mass, or a decrease in molar mass of

$$0.301 \times 146.11 \text{ g/mol} = 44.0 \text{ g/mol}$$

This loss in molar mass is consistent with the release of $CO_2(g)$, leaving a final residue of CaO. The three decomposition reactions are

$$CaC_2O_4 \cdot H_2O(s) \rightarrow CaC_2O_4(s) + 2H_2O(l)$$
$$CaC_2O_4(s) \rightarrow CaCO_3(s) + CO(g)$$
$$CaCO_3(s) \rightarrow CaO(s) + CO_2(g)$$

Identifying the products of a thermal decomposition provides information that we can use to develop an analytical procedure. For example, the thermogram in Figure 31.1.1 shows that we must heat a precipitate of CaC_2O_4•H_2O to a temperature between 250 and 400°C if we wish to isolate and weigh CaC_2O_4. Alternatively, heating the sample to 1000°C allows us to isolate and weigh CaO.

? Exercise 31.1.1

Under the same conditions as Figure 31.1.1 , the thermogram for a 22.16 mg sample of MgC_2O_4•H_2O shows two steps: a loss of 3.06 mg from 100–250°C and a loss of 12.24 mg from 350–550°C. For each step, identify the volatilization product and the solid residue that remains. Using your results from this exercise and the results from Example 31.1.1 , explain how you can use thermogravimetry to analyze a mixture that contains CaC_2O_4•H_2O and MgC_2O_4•H_2O. You may assume that other components in the sample are inert and thermally stable below 1000°C.

Answer

From 100–250°C the sample loses 13.8% of its mass, or a loss of

$$0.138 \times 130.34 \text{ g/mol} = 18.0 \text{ g/mol}$$

which is consistent with the loss of $H_2O(g)$ and a residue of MgC_2O_4.

From 350–550°C the sample loses 55.23% of its original mass, or a loss of

$$0.5523 \times 130.34 \text{ g/mol} = 71.99 \text{ g/mol}$$

This weight loss is consistent with the simultaneous loss of $CO(g)$ and $CO_2(g)$, leaving a residue of MgO.

We can analyze the mixture by heating a portion of the sample to 300°C, 600°C, and 1000°C, recording the mass at each temperature. The loss of mass between 600°C and 1000°C, Δm_2, is due to the loss of $CO_2(g)$ from the decomposition of $CaCO_3$ to CaO, and is proportional to the mass of CaC_2O_4•H_2O in the sample.

$$\text{g } CaC_2O_4 \cdot H_2O = \Delta m_2 \times \frac{1 \text{ mol } CO_2}{44.01 \text{ g } CO_2} \times \frac{146.11 \text{ g } CaC_2O_4 \cdot H_2O}{\text{mol } CO_2}$$

The change in mass between 300°C and 600°C, Δm_1, is due to the loss of $CO(g)$ from CaC_2O_4•H_2O and the loss of $CO(g)$ and $CO_2(g)$ from MgC_2O_4•H_2O. Because we already know the amount of CaC_2O_4•H_2O in the sample, we can calculate its contribution to Δm_1.

$$(\Delta m_1)_{Ca} = \text{g } CaC_2O_4 \cdot H_2O = \Delta m_2 \times \frac{1 \text{ mol CO}}{146.11 \text{ g } CaC_2O_4 \cdot H_2O} \times \frac{28.01 \text{ g CO}}{\text{mol CO}}$$

The change in mass between 300°C and 600°C due to the decomposition of MgC_2O_4•H_2O

$$(m_1)_{Mg} = \Delta m_1 - (\Delta m_1)_{Ca}$$

provides the mass of MgC_2O_4•H_2O in the sample.

$$\text{g } MgC_2O_4 \cdot H_2O = (\Delta m_1)_{Mg} \times \frac{1 \text{ mol } (CO + CO_2)}{130.35 \text{ g } MgC_2O_4 \cdot H_2O} \times \frac{78.02 \text{ g } (CO + CO_2)}{\text{mol } (CO + CO_2)}$$

Instrumentation

In a thermogravimetric analysis, the sample is placed on a small balance pan attached to one arm of an electromagnetic balance (Figure 31.1.2). The sample is lowered into an electric furnace and the furnace's temperature is increased at a fixed rate of a few degrees per minute while monitoring continuously the sample's weight. The instrument usually includes a gas line for purging the volatile decomposition products out of the furnace, and a heat exchanger to dissipate the heat emitted by the furnace.

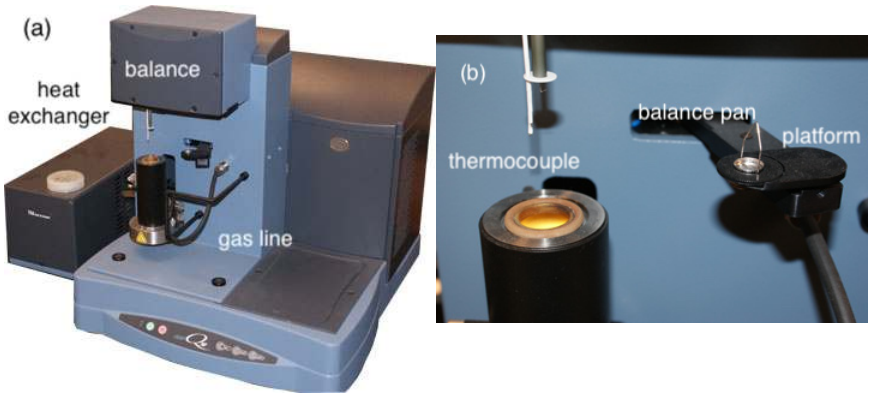


Figure 31.1.2 . (a) Instrumentation for conducting a thermogravimetric analysis. The balance sits on the top of the instrument with the sample suspended below. A gas line supplies an inert gas that sweeps the volatile decomposition products out of the furnace. The heat exchanger dissipates the heat from the furnace to a reservoir of water. (b) Close-up showing the balance pan, which sits on a moving platform, the thermocouple for monitoring temperature, a hook for lowering the sample pan into the furnace, and the opening to the furnace. After placing a small portion of the sample on the balance pan, the platform rotates over the furnace and transfers the balance pan to a hook that is suspended from the balance. Once the balance pan is in place, the platform rotates back to its initial position. The balance pan and the thermocouple are then lowered into the furnace.

Applications

Perhaps the most important application gravimetry is exploring a compound's thermal stability, as illustrated in Figure 11.1.1 and Exercise 11.1.1 for calcium oxalate hydrate. TGA is particularly useful for studying the thermal stability of polymers.

This page titled 11.1: Thermogravimetry is shared under a CC BY-NC-SA 4.0 license and was authored, remixed, and/or curated by David Harvey.

- **31.1: Thermogravimetry** by David Harvey is licensed CC BY-NC-SA 4.0.

11.2: Differential Thermal Analysis and Differential Scanning Calorimetry

Differential thermal analysis (DTA) and differential scanning calorimetry (DSC) are similar methods in which the response of a sample and a reference to a change in temperature. In DTA the temperature applied to the sample is increased linearly and the difference between the temperature of the reference material, T_{ref}, and the temperature of the sample, T_{samp}, is recorded as function of the sample's temperature

$$\Delta T = T_{ref} - T_{samp}$$

When the sample undergoes an exothermic process, such as a crystallization or a chemical reaction, the temperature of the sample increases more than does the temperature of the reference, resulting in a more negative value for ΔT. For an endothermic process, such as melting of a crystalline material or the loss of waters of hydration, the sample's temperature lags behind that for the reference materials, resulting in a more positive value for ΔT. Figure 11.2.1 shows the general shape of DTA curve with negative peaks signaling an endothermic process and positive peaks signaling an exothermic process. Changes in ΔT that are not peaks, but shifts in the baseline—as seen at the far left of the curve in Figure 11.2.1—are the result of a simple phase transition for which $\Delta H = 0$.In DSC the temperature applied to the sample is increased linearly and the relative amount of heat needed to maintain the sample and the reference at the same temperature is measured. For an endothermic process, more heat flows into the sample and for an exothermic process, less heat flows into the sample. The result is a DSC curve that looks similar to that for DTA (see Figure 11.2.1).

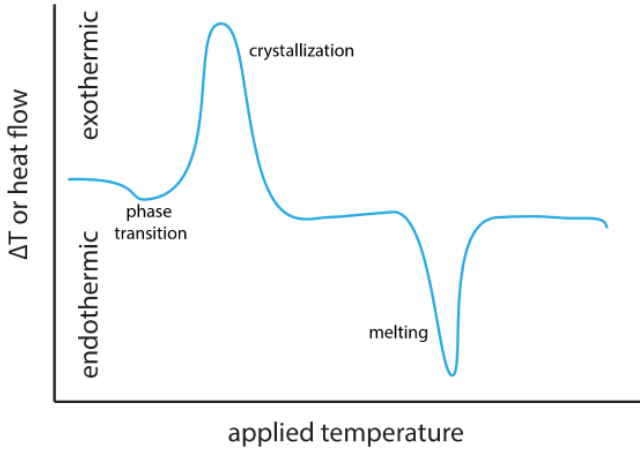


Figure 11.2.1: Illustration showing typical experimental curves for a differential thermal analysis (DTA) or a differential scanning calorimetry analysis (DSC) for a polymeric material. For a DTA analysis, the difference in temperature, ΔT, is measured and for a DSC analysis, the flow of heat is measured. The three responses seen here are, from left-to-right, a phase transition, an exothermic crystallization, and an endothermic melting.

Instrumentation

Figure 11.2.2 shows the basic components of a heat-flux differential scanning calorimeter. The sample and the reference materials are sealed within small aluminum pans and placed on separate platforms within the sample chamber. The two platforms are connected by a metal disk that provides a low resistance path for moving heat between the sample and the reference to maintain a ΔT of zero between the two. Another instrumental design for differential scanning calorimetry, which is called power compensation DSC, places the sample and the reference in separated heating chambers and measures the difference in the power applied to the two chambers needed to maintain a ΔT of zero.

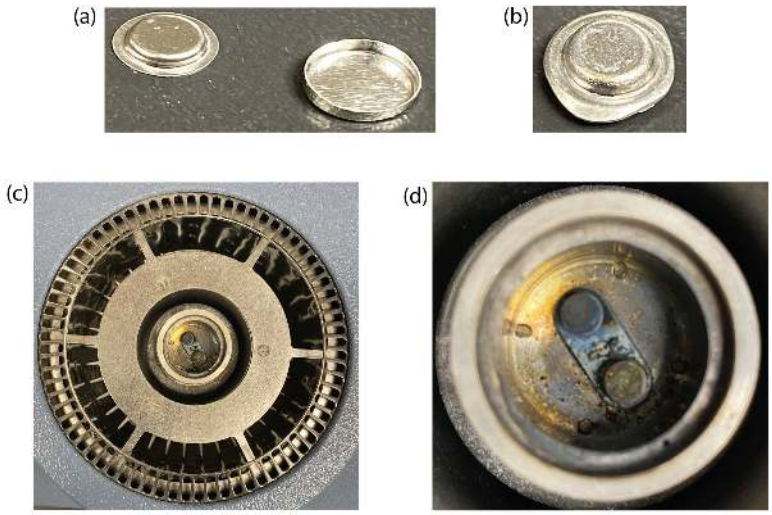


Figure 11.2.2: Components of instrument for a differential scanning calorimetry (DSC) experiment. The sample and the reference material are (a) placed in small aluminum pans, each with a separate lid, and then (b) the lid and the pan are crimped together. The sample chamber in (c) allows for applying heat to the sample and the reference, which are place in the center of the chamber. A close-up of the sample chamber (d) shows two—well-used—platforms on which the sample and the reference are placed. An insulated cap sits on top of the sample chamber. Although the basic set-up shown here is for DSC, it is similar to the instrumentation for a differential thermal analysis. For a sense of scale, the pan in (a) is approximately 5 mm across and has a depth of 1 mm, and the platforms in (d) also are 5 mm across.

Applications

Integrating a peak in DSC or DTA to determine its its area, A, gives a signal that is proportional to ΔH

$$\Delta H = K \times A$$

where the calibration constant, k, is determined using an established reference material. Both DSC and DTA find applications in the study of polymers, liquid crystals, and pharmaceutical compounds.

This page titled 11.2: Differential Thermal Analysis and Differential Scanning Calorimetry is shared under a CC BY-NC-SA 4.0 license and was authored, remixed, and/or curated by David Harvey.

- **31.2: Differential Thermal Analysis and Differential Scanning Calorimetry** by David Harvey is licensed CC BY-NC-SA 4.0.

CHAPTER OVERVIEW

12: EQUILIBRIUM CHEMISTRY

Regardless of the problem on which an analytical chemist is working, its solution requires a knowledge of chemistry and the ability to apply that knowledge to solve a problem. For example, an analytical chemist who is studying the effect of pollution on spruce trees needs to know, or know where to find, the chemical differences between *p*-hydroxybenzoic acid and *p*-hydroxyacetophenone, two common phenols found in the needles of spruce trees.

The ability to "think as a chemist" is a product of your experience in the classroom and in the laboratory. For the most part, the material in this text assumes you are familiar with topics covered in earlier courses; however, because of its importance to analytical chemistry, this chapter provides a review of equilibrium chemistry. Much of the material in this chapter should be familiar to you, although some topics—ladder diagrams and activity, for example—likely afford you with new ways to look at equilibrium chemistry.

12.1: Reversible Reactions and Chemical Equilibria
12.2: Thermodynamics and Equilibrium Chemistry
12.3: Manipulating Equilibrium Constants
12.4: Equilibrium Constants for Chemical Reactions
12.5: Ladder Diagrams
12.6: Problems
12.7: Additional Resources
12.8: Chapter Summary and Key Terms

This page titled 12: Equilibrium Chemistry is shared under a CC BY-NC-SA 4.0 license and was authored, remixed, and/or curated by David Harvey.

12.1: REVERSIBLE REACTIONS AND CHEMICAL EQUILIBRIA

In 1798, the chemist Claude Berthollet accompanied Napoleon's military expedition to Egypt. While visiting the Natron Lakes, a series of salt water lakes carved from limestone, Berthollet made an observation that led him to an important discovery. When exploring the lake's shore, Berthollet found deposits of Na_2CO_3, a result he found surprising. Why did Berthollet find this result surprising and how did it contribute to an important discovery? Answering these questions provides us with an example of chemical reasoning and introduces us to the topic of this chapter.

> Napoleon's expedition to Egypt was the first to include a significant scientific presence. The Commission of Sciences and Arts, which included Claude Berthollet, began with 151 members, and operated in Egypt for three years. In addition to Berthollet's work, other results included a publication on mirages and a detailed catalogs of plant and animal life, mineralogy, and archeology. For a review of the Commission's contributions, see Gillispie, C. G. "Scientific Aspects of the French Egyptian Expedition, 1798-1801," *Proc. Am. Phil. Soc.* **1989**, *133*, 447–474.

At the end of the 18th century, chemical reactivity was explained in terms of elective affinities [Quilez, J. *Chem. Educ. Res. Pract.* **2004**, *5*, 69–87]. If, for example, substance A reacts with substance BC to form AB

$$\mathrm{A + BC \rightarrow AB + C}$$

then A and B were said to have an elective affinity for each other. With elective affinity as the driving force for chemical reactivity, reactions were understood to proceed to completion and to proceed in one direction. Once formed, the compound AB could not revert to A and BC.

$$\mathrm{A + BC \nrightarrow AB + C}$$

From his experience in the laboratory, Berthollet knew that adding solid Na_2CO_3 to a solution of $CaCl_2$ produces a precipitate of $CaCO_3$.

$$\mathrm{Na_2CO_3}(s) + \mathrm{CaCl_2}(aq) \rightarrow 2\mathrm{NaCl}(aq) + \mathrm{CaCO_3}(s)$$

Understanding this, Berthollet was surprised to find solid Na_2CO_3 forming on the edges of the lake, particularly since the deposits formed only when the lake's salt water, NaCl(*aq*), was in contact with solid limestone, $CaCO_3$(*s*). Where the lake was in contact with clay soils, there was little or no Na_2CO_3.

> Natron is another name for the mineral sodium carbonate, Na_2CO_3•$10H_2O$. In nature, it usually contains impurities of $NaHCO_3$ and NaCl. In ancient Egypt, natron was mined and used for a variety of purposes, including as a cleaning agent and in mummification.

Berthollet's important insight was recognizing that the chemistry leading to the formation of Na_2CO_3 is the reverse of that seen in the laboratory.

$$2\mathrm{NaCl}(aq) + \mathrm{CaCO_3}(s) \rightarrow \mathrm{Na_2CO_3}(s) + \mathrm{CaCl_2}(aq)$$

Using this insight Berthollet reasoned that the reaction is reversible, and that the relative amounts of NaCl, $CaCO_3$, Na_2CO_3, and $CaCl_2$ determine the direction in which the reaction occurs and the final composition of the reaction mixture. We recognize a reaction's ability to move in both directions by using a double arrow when we write the reaction.

$$\mathrm{Na_2CO_3}(s) + \mathrm{CaCl_2}(aq) \rightleftharpoons 2\mathrm{NaCl}(aq) + \mathrm{CaCO_3}(s)$$

> For obvious reasons, we call the double arrow, $\rightleftharpoons$, an equilibrium arrow.

Berthollet's reasoning that reactions are reversible was an important step in understanding chemical reactivity. When we mix together solutions of Na_2CO_3 and $CaCl_2$ they react to produce NaCl and $CaCO_3$. As the reaction takes place, if we monitor the mass of Ca^{2+} that remains in solution and the mass of $CaCO_3$ that precipitates, the result looks something like Figure 6.1.1 . At the start of the reaction the mass of Ca^{2+} decreases and the mass of $CaCO_3$ increases. Eventually the reaction reaches a point after which there is no further change in the amounts of these species. Such a condition is called a state of ***equilibrium***.

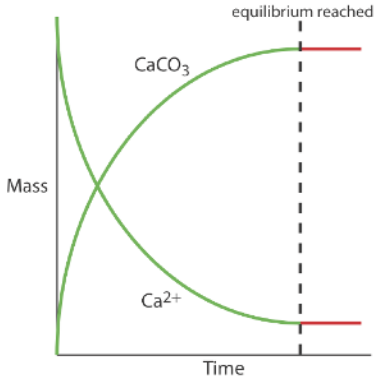


Figure 6.1.1 . Graph showing how the masses of Ca^{2+} and $CaCO_3$ change as a function of time during the precipitation of $CaCO_3$. The dashed line indicates when the reaction reaches equilibrium. Prior to equilibrium the masses of Ca^{2+} and $CaCO_3$ are changing; after equilibrium is reached, their masses remain constant.

Although a system at equilibrium appears static on a macroscopic level, it is important to remember that the forward and the reverse reactions continue to occur. A reaction at equilibrium exists in a ***steady-state***, in which the rate at which a species forms equals the rate at which it is consumed.

This page titled 12.1: Reversible Reactions and Chemical Equilibria is shared under a CC BY-NC-SA 4.0 license and was authored, remixed, and/or curated by David Harvey.

- **6.1: Reversible Reactions and Chemical Equilibria** by David Harvey is licensed CC BY-NC-SA 4.0.

12.2: THERMODYNAMICS AND EQUILIBRIUM CHEMISTRY

Thermodynamics is the study of thermal, electrical, chemical, and mechanical forms of energy. The study of thermodynamics crosses many disciplines, including physics, engineering, and chemistry. Of the various branches of thermodynamics, the most important to chemistry is the study of how energy changes during a chemical reaction.

Consider, for example, the general equilibrium reaction shown in Equation 12.2.1, which involves the species A, B, C, and D, with stoichiometric coefficients of *a*, *b*, *c*, and *d*.

$$aA + bB \rightleftharpoons cC + dD \tag{12.2.1}$$

By convention, we identify the species on the left side of the equilibrium arrow as reactants and those on the right side of the equilibrium arrow as products. As Berthollet discovered, writing a reaction in this fashion does not guarantee that the reaction of A and B to produce C and D is favorable. Depending on initial conditions the reaction may move to the left, it may move to the right, or it may exist in a state of equilibrium. Understanding the factors that determine the reaction's final equilibrium position is one of the goals of chemical thermodynamics.

The direction of a reaction is that which lowers the overall free energy. At a constant temperature and pressure, which is typical of many benchtop chemical reactions, a reaction's free energy is given by the ***Gibb's free energy*** function

$$\Delta G = \Delta H - T\Delta S \tag{12.2.2}$$

where T is the temperature in kelvin, and ΔG, ΔH, and ΔS are the differences in the Gibb's free energy, the enthalpy, and the entropy between the products and the reactants.

Enthalpy is a measure of the flow of energy, as heat, during a chemical reaction. A reaction that releases heat has a negative ΔH and is called exothermic. An endothermic reaction absorbs heat from its surroundings and has a positive ΔH. ***Entropy*** is a measure of energy that is unavailable for useful, chemical work. The entropy of an individual species is always positive and generally is larger for gases than for solids, and for more complex molecules than for simpler molecules. Reactions that produce a large number of simple, gaseous products usually have a positive ΔS.

> For many students, entropy is the most difficult topic in thermodynamics to understand. For a rich resource on entropy, visit the following web site: http://entropysite.oxy.edu/.

The sign of ΔG indicates the direction in which a reaction moves to reach its equilibrium position. A reaction is thermodynamically favorable when its enthalpy, ΔH, decreases and its entropy, ΔS, increases. Substituting the inequalities $\Delta H < 0$ and $\Delta S > 0$ into Equation 12.2.2 shows that a reaction is thermodynamically favorable when ΔG is negative. When ΔG is positive the reaction is unfavorable as written (although the reverse reaction is favorable). A reaction at equilibrium has a ΔG of zero.

> Equation 12.2.2 shows that the sign of ΔG depends on the signs of ΔH and of ΔS, and the temperature, T. The following table summarizes the possibilities.
>
ΔH	ΔS	ΔG
−	+	$\Delta G < 0$ at all temperatures
−	−	$\Delta G < 0$ at low temperatures only
+	+	$\Delta G < 0$ at high temperatures only
+	−	$\Delta G > 0$ at all temperatures
>
> Note that the what constitutes "low temperatures" or "high temperatures" depends on the reaction.

As a reaction moves from its initial, non-equilibrium condition to its equilibrium position, its value of ΔG approaches zero. At the same time, the chemical species in the reaction experience a change in their concentrations. The Gibb's free energy, therefore, must be a function of the concentrations of reactants and products.

As shown in Equation 12.2.3, we can divide the Gibb's free energy, ΔG, into two terms.

$$\triangle G = \Delta G^{\circ} + RT \ln Q_r \tag{12.2.3}$$

The first term, ΔG^{o}, is the change in the Gibb's free energy when each species in the reaction is in its ***standard state***, which we define as follows: gases with unit partial pressures, solutes with unit concentrations, and pure solids and pure liquids. The second term includes the reaction quotient, Q_r, which accounts for non-standard state pressures and concentrations. For reaction 12.2.1 the reaction quotient is

$$Q_r = \frac{[\mathrm{C}]^c[\mathrm{D}]^d}{[\mathrm{A}]^a[\mathrm{B}]^b} \tag{12.2.4}$$

where the terms in brackets are the concentrations of the reactants and products. Note that we define the reaction quotient with the products in the numerator and the reactants in the denominator. In addition, we raise the concentration of each species to a power equivalent to its stoichiometry in the balanced chemical reaction. For a gas, we use partial pressure in place of concentration. Pure solids and pure liquids do not appear in the reaction quotient.

> Although not shown here, each concentration term in Equation 12.2.4 is divided by the corresponding standard state concentration; thus, the term $[\mathrm{C}]^c$ really means
>
> $$\left\{\frac{[\mathrm{C}]}{[\mathrm{C}]^\circ}\right\}$$
>
> where $[\mathrm{C}]^o$ is the standard state concentration for C. There are two important consequences of this: (1) the value of Q is unitless; and (2) the ratio has a value of 1 for a pure solid or a pure liquid. This is the reason that pure solids and pure liquids do not appear in the reaction quotient.

At equilibrium the Gibb's free energy is zero, and Equation 12.2.3 simplifies to

$$\triangle G^\circ = -RT \ln K$$

where K is an ***equilibrium constant*** that defines the reaction's equilibrium position. The equilibrium constant is just the reaction quotient's numerical value when we substitute equilibrium concentrations into Equation 12.2.4.

$$K = \frac{[\mathrm{C}]^c_{\mathrm{eq}}[\mathrm{D}]^d_{\mathrm{eq}}}{[\mathrm{A}]^a_{\mathrm{eq}}[\mathrm{B}]^b_{\mathrm{eq}}} \tag{12.2.5}$$

Here we include the subscript "eq" to indicate a concentration at equilibrium. Although generally we will omit the "eq" when we write an equilibrium constant expressions, it is important to remember that the value of K is determined by equilibrium concentrations.

> As written, Equation 12.2.5 is a limiting law that applies only to infinitely dilute solutions where the chemical behavior of one species is unaffected by the presence of other species. Strictly speaking, Equation 12.2.5 is written in terms of activities instead of concentrations. We will return to this point in Chapter 6.9. For now, we will stick with concentrations as this convention already is familiar to you.

This page titled 12.2: Thermodynamics and Equilibrium Chemistry is shared under a CC BY-NC-SA 4.0 license and was authored, remixed, and/or curated by David Harvey.

- **6.2: Thermodynamics and Equilibrium Chemistry** by David Harvey is licensed CC BY-NC-SA 4.0.

12.3: MANIPULATING EQUILIBRIUM CONSTANTS

We will take advantage of two useful relationships when we work with equilibrium constants. First, if we reverse a reaction's direction, the equilibrium constant for the new reaction is the inverse of that for the original reaction. For example, the equilibrium constant for the reaction

$$\mathrm{A} + 2\mathrm{B} \rightleftharpoons \mathrm{AB_2} \qquad K_1 = \frac{[\mathrm{AB_2}]}{[\mathrm{A}][\mathrm{B}]^2}$$

is the inverse of that for the reaction

$$\mathrm{AB_2} \rightleftharpoons \mathrm{A} + 2\mathrm{B} \qquad K_2 = (K_1)^{-1} = \frac{[\mathrm{A}][\mathrm{B}]^2}{[\mathrm{AB_2}]}$$

Second, if we add together two reactions to form a new reaction, the equilibrium constant for the new reaction is the product of the equilibrium constants for the original reactions.

$$A + C \rightleftharpoons AC \qquad K_3 = \frac{[AC]}{[A][C]}$$

$$\mathrm{AC} + \mathrm{C} \rightleftharpoons \mathrm{AC_2} \qquad K_4 = \frac{[\mathrm{AC_2}]}{[\mathrm{AC}][\mathrm{C}]}$$

$$\mathrm{A} + 2\mathrm{C} \rightleftharpoons \mathrm{AC_2} \qquad K_5 = K_3 \times K_4 = \frac{[\mathrm{AC}]}{[\mathrm{A}][\mathrm{C}]} \times \frac{[\mathrm{AC_2}]}{[\mathrm{AC}][\mathrm{C}]} = \frac{[\mathrm{AC_2}]}{[\mathrm{A}][\mathrm{C}]^2}$$

EXAMPLE 6.3.1

Calculate the equilibrium constant for the reaction

$$2\mathrm{A} + \mathrm{B} \rightleftharpoons \mathrm{C} + 3\mathrm{D}$$

given the following information

$$\begin{aligned} &\mathrm{Rxn\ 1}: A + B \rightleftharpoons D && K_1 = 0.40 \\ &\mathrm{Rxn\ 2}: A + E \rightleftharpoons C + D + F && K_2 = 0.10 \\ &\mathrm{Rxn\ 3}: C + E \rightleftharpoons B && K_3 = 2.0 \\ &\mathrm{Rxn\ 4}: F + C \rightleftharpoons D + B && K_4 = 5.0 \end{aligned}$$

Solution

The overall reaction is equivalent to

$$\mathrm{Rxn\ 1} + \mathrm{Rxn\ 2} - \mathrm{Rxn\ 3} + \mathrm{Rxn\ 4}$$

Subtracting a reaction is equivalent to adding the reverse reaction; thus, the overall equilibrium constant is

$$K = \frac{K_1 \times K_2 \times K_4}{K_3} = \frac{0.40 \times 0.10 \times 5.0}{2.0} = 0.10$$

EXERCISE 6.3.1

Calculate the equilibrium constant for the reaction

$$C + D + F \rightleftharpoons 2A + 3B$$

using the equilibrium constants from Example 6.3.1 .

Answer

The overall reaction is equivalent to

$$\mathrm{Rxn\ 4} - 2 \times \mathrm{Rxn\ 1}$$

Subtracting a reaction is equivalent to adding the reverse reaction; thus, the overall equilibrium constant is

$$K = \frac{K_4}{(K_1)^2} = \frac{(5.0)}{(0.40)^2} = 31.25 \approx 31$$

This page titled 12.3: Manipulating Equilibrium Constants is shared under a CC BY-NC-SA 4.0 license and was authored, remixed, and/or curated by David Harvey.

- **6.3: Manipulating Equilibrium Constants** by David Harvey is licensed CC BY-NC-SA 4.0.

12.4: EQUILIBRIUM CONSTANTS FOR CHEMICAL REACTIONS

Several types of chemical reactions are important in analytical chemistry, either in preparing a sample for analysis or during the analysis. The most significant of these are precipitation reactions, acid–base reactions, complexation reactions, and oxidation–reduction reactions. In this section we review these reactions and their equilibrium constant expressions.

> Another common name for an oxidation–reduction reaction is a redox reaction, where "red" is short for reduction and "ox" is short for oxidation.

PRECIPITATION REACTIONS

In a precipitation reaction, two or more soluble species combine to form an insoluble ***precipitate***. The most common precipitation reaction is a metathesis reaction in which two soluble ionic compounds exchange parts. For example, if we add a solution of lead nitrate, $Pb(NO_3)_2$, to a solution of potassium chloride, KCl, a precipitate of lead chloride, $PbCl_2$, forms. We usually write a precipitation reaction as a net ionic equation, which shows only the precipitate and those ions that form the precipitate; thus, the precipitation reaction for $PbCl_2$ is

$$Pb^{2+}(aq) + 2Cl^-(aq) \rightleftharpoons PbCl_2(s)$$

When we write the equilibrium constant for a precipitation reaction, we focus on the precipitate's solubility; thus, for $PbCl_2$, the solubility reaction is

$$PbCl_2(s) \rightleftharpoons Pb^{2+}(aq) + 2Cl^-(aq)$$

and its equilibrium constant, or ***solubility product***, K_{sp}, is

$$K_{sp} = \left[Pb^{2+}\right]\left[Cl^-\right]^2 \tag{12.4.1}$$

Even though it does not appear in the K_{sp} expression, it is important to remember that Equation 12.4.1 is valid only if $PbCl_2(s)$ is present and in equilibrium with Pb^{2+} and Cl^-. You will find values for selected solubility products in Appendix 10.

ACID–BASE REACTIONS

A useful definition of acids and bases is that independently introduced in 1923 by Johannes Brønsted and Thomas Lowry. In the Brønsted-Lowry definition, an ***acid*** is a proton donor and a ***base*** is a proton acceptor. Note the connection between these definitions—defining a base as a proton acceptor implies there is an acid available to donate the proton. For example, in reaction 12.4.2 acetic acid, CH_3COOH, donates a proton to ammonia, NH_3, which serves as the base.

$$CH_3COOH(aq) + NH_3(aq) \rightleftharpoons NH_4^+(aq) + CH_3COO^-(aq) \tag{12.4.2}$$

When an acid and a base react, the products are a new acid and a new base. For example, the acetate ion, CH_3COO^-, in reaction 12.4.2 is a base that can accept a proton from the acidic ammonium ion, NH_4^+, forming acetic acid and ammonia. We call the acetate ion the conjugate base of acetic acid, and we call the ammonium ion the conjugate acid of ammonia.

STRONG AND WEAK ACIDS

The reaction of an acid with its solvent (typically water) is an acid dissociation reaction. We divide acids into two categories—strong and weak—based on their ability to donate a proton to the solvent. A strong acid, such as HCl, almost completely transfers its proton to the solvent, which acts as the base.

$$HCl(aq) + H_2O(l) \rightarrow H_3O^+(aq) + Cl^-(aq)$$

We use a single arrow ($\rightarrow$) in place of the equilibrium arrow ($\rightleftharpoons$) because we treat HCl as if it dissociates completely in an aqueous solution. In water, the common strong acids are hydrochloric acid (HCl), hydroiodic acid (HI), hydrobromic acid (HBr), nitric acid (HNO_3), perchloric acid ($HClO_4$), and the first proton of sulfuric acid (H_2SO_4).

> The strength of an acid is a function of the acid and the solvent. For example, HCl does not act as a strong acid in methanol. In this case we use the equilibrium arrow when writing the acid–base reaction.
>
> $$HCl + CH_3OH \rightleftharpoons CH_3OH_2^+ + Cl^-$$

A weak acid, of which aqueous acetic acid is one example, does not completely donate its acidic proton to the solvent. Instead, most of the acid remains undissociated with only a small fraction present as the conjugate base.

$$CH_3COOH(aq) + H_2O(l) \rightleftharpoons H_3O^+(aq) + CH_3COO^-(aq)$$

The equilibrium constant for this reaction is an ***acid dissociation constant***, K_a, which we write as

$$K_a = \frac{\left[CH_3COO^-\right]\left[H_3O^+\right]}{\left[CH_3COOH\right]} = 1.75 \times 10^{-5}$$

The magnitude of K provides information about a weak acid's relative strength, with a smaller K_a corresponding to a weaker acid. The ammonium ion, NH_4^+, for example, has a K_a of 5.702×10^{-10} and is a weaker acid than acetic acid.

> Earlier we noted that we omit pure solids and pure liquids from equilibrium constant expressions. Because the solvent, H_2O, is not pure, you might wonder why we have not included it in acetic acid's K_a expression. Recall that we divide each term in an equilibrium constant expression by its standard state value. Because the concentration of H_2O is so large—it is approximately 55.5 mol/L—its concentration as a pure liquid and as a solvent are virtually identical. The ratio
>
> $$\frac{[H_2O]}{[H_2O]^\circ}$$
>
> is essentially 1.00.

A ***monoprotic*** weak acid, such as acetic acid, has only a single acidic proton and a single acid dissociation constant. Other acids, such as phosphoric acid, have multiple acidic protons, each characterized by an acid dissociation constant. We call such acids ***polyprotic***. Phosphoric acid, for example, has three acid dissociation reactions and three acid dissociation constants.

$$H_3PO_4(aq) + H_2O(l) \rightleftharpoons H_3O^+(aq) + H_2PO_4^-(aq)$$

$$K_{a1} = \frac{\left[H_2PO_4^-\right]\left[H_3O^+\right]}{\left[H_3PO_4\right]} = 7.11 \times 10^{-3}$$

$$H_2PO_4^-(aq) + H_2O(l) \rightleftharpoons H_3O^+(aq) + HPO_4^{2-}(aq)$$

$$K_{a2} = \frac{\left[HPO_4^{2-}\right]\left[H_3O^+\right]}{\left[H_2PO_4^-\right]} = 6.32 \times 10^{-8}$$

$$HPO_4^{2-}(aq) + H_2O(l) \rightleftharpoons H_3O^+(aq) + PO_4^{3-}(aq)$$

$$K_{a3} = \frac{\left[PO_4^{3-}\right]\left[H_3O^+\right]}{\left[HPO_4^{2-}\right]} = 4.5 \times 10^{-13}$$

The decrease in the acid dissociation constants from K_{a1} to K_{a3} tells us that each successive proton is harder to remove. Consequently, H_3PO_4 is a stronger acid than $H_2PO_4^-$, and $H_2PO_4^-$ is a stronger acid than HPO_4^{2-}.

STRONG AND WEAK BASES

The most common example of a strong base is an alkali metal hydroxide, such as sodium hydroxide, NaOH, which completely dissociates to produce hydroxide ion.

$$NaOH(s) \rightarrow Na^+(aq) + OH^-(aq)$$

A weak base, such as the acetate ion, CH_3COO^-, only partially accepts a proton from the solvent, and is characterized by a ***base dissociation constant***, K_b. For example, the base dissociation reaction and the base dissociation constant for the acetate ion are

$$CH_3COO^-(aq) + H_2O(l) \rightleftharpoons OH^-(aq) + CH_3COOH(aq)$$

$$K_b = \frac{\left[CH_3COOH\right]\left[OH^-\right]}{\left[CH_3COO^-\right]} = 5.71 \times 10^{-10}$$

A polyprotic weak base, like a polyprotic acid, has more than one base dissociation reaction and more than one base dissociation constant.

AMPHIPROTIC SPECIES

Some species can behave as either a weak acid or as a weak base. For example, the following two reactions show the chemical reactivity of the bicarbonate ion, HCO_3^-, in water.

$$HCO_3^-(aq) + H_2O(l) \rightleftharpoons H_3O^+(aq) + CO_3^{2-}(aq) \tag{12.4.3}$$

$$HCO_3^-(aq) + H_2O(l) \rightleftharpoons OH^-(aq) + H_2CO_3(aq) \tag{12.4.4}$$

A species that is both a proton donor and a proton acceptor is called ***amphiprotic***. Whether an amphiprotic species behaves as an acid or as a base depends on the equilibrium constants for the competing reactions. For bicarbonate, the acid dissociation constant for reaction 12.4.3

$$K_{a2} = \frac{\left[CO_3^{2-}\right]\left[H_3O^+\right]}{\left[HCO_3^-\right]} = 4.69 \times 10^{-11}$$

is smaller than the base dissociation constant for reaction 12.4.4.

$$K_{b2} = \frac{\left[H_2CO_3\right]\left[OH^-\right]}{\left[HCO_3^-\right]} = 2.25 \times 10^{-8}$$

Because bicarbonate is a stronger base than it is an acid, we expect that an aqueous solution of HCO_3^- is basic.

DISSOCIATION OF WATER

Water is an amphiprotic solvent because it can serve as an acid or as a base. An interesting feature of an amphiprotic solvent is that it is capable of reacting with itself in an acid–base reaction.

$$2H_2O(l) \rightleftharpoons H_3O^+(aq) + OH^-(aq) \tag{12.4.5}$$

We identify the equilibrium constant for this reaction as water's dissociation constant, K_w,

$$K_w = \left[H_3O^+\right]\left[OH^-\right] = 1.00 \times 10^{-14} \tag{12.4.6}$$

at a temperature of 24°C. The value of K_w varies substantially with temperature. For example, at 20°C K_w is 6.809×10^{-15} , while at 30°C K_w is 1.469×10^{-14} . At 25°C, K_w is 1.008×10^{-14} , which is sufficiently close to 1.00×10^{-14} that we can use the latter value with negligible error.

An important consequence of Equation 12.4.6 is that the concentration of H_3O^+ and the concentration of OH^- are related. If we know $[H_3O^+]$ for a solution, then we can calculate $[OH^-]$ using Equation 12.4.6.

EXAMPLE 6.4.1

What is the $[OH^-]$ if the $[H_3O^+]$ is 6.12×10^{-5} M?

Solution

$$\left[OH^-\right] = \frac{K_w}{\left[H_3O^+\right]} = \frac{1.00 \times 10^{-14}}{6.12 \times 10^{-5}} = 1.63 \times 10^{-10}$$

THE PH SCALE

Equation 12.4.6 allows us to develop a ***pH scale*** ($pH = -\log[H_3O^+]$) that indicates a solution's acidity. When the concentrations of H_3O^+ and OH^- are equal a solution is neither acidic nor basic; that is, the solution is neutral. Letting

$$\left[H_3O^+\right] = \left[OH^-\right]$$

substituting into Equation 12.4.6

$$K_w = \left[H_3O^+\right]^2 = 1.00 \times 10^{-14}$$

and solving for $[H_3O^+]$ gives

$$\left[H_3O^+\right] = \sqrt{1.00 \times 10^{-14}} = 1.00 \times 10^{-7}$$

A neutral solution of water at 25°C has a hydronium ion concentration of 1.00×10^{-7} M and a pH of 7.00. In an acidic solution the concentration of H_3O^+ is greater than that for OH^-, which means that

$$\left[H_3O^+\right] > 1.00 \times 10^{-7}\text{M}$$

The pH of an acidic solution, therefore, is less than 7.00. A basic solution, on the other hand, has a pH greater than 7.00. Figure 6.4.1 shows the pH scale and pH values for some representative solutions.

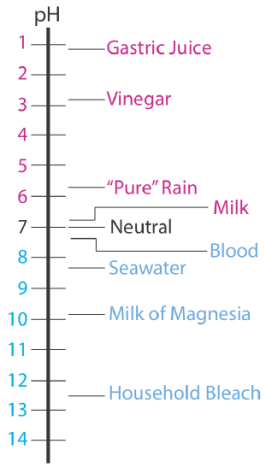


Figure 6.4.1 . Scale showing the pH value for representative solutions. Milk of Magnesia is a saturated solution of $Mg(OH)_2$.

TABULATING VALUES FOR K_A AND K_B

A useful observation about weak acids and weak bases is that the strength of a weak base is inversely proportional to the strength of its conjugate weak acid. Consider, for example, the dissociation reactions of acetic acid and acetate.

$$CH_3COOH(aq) + H_2O(l) \rightleftharpoons H_3O^+(aq) + CH_3COO^-(aq) \tag{12.4.7}$$

$$CH_3COO^-(aq) + H_2O(l) \rightleftharpoons OH^-(aq) + CH_3COOH(aq) \tag{12.4.8}$$

Adding together these two reactions gives the reaction

$$2H_2O(l) \rightleftharpoons H_3O^+(aq) + OH^-(aq)$$

for which the equilibrium constant is K_w. Because adding together two reactions is equivalent to multiplying their respective equilibrium constants, we may express K_w as the product of K_a for CH3COOH and K_b for $CH3COO^-$.

$$K_w = K_{a,CH_3COOH} \times K_{b,CH_3COO^-}$$

For any weak acid, HA, and its conjugate weak base, A^-, we can generalize this to the following equation

$$K_w = K_{a,HA} \times K_{b,A^-} \tag{12.4.9}$$

where HA and A^- are a conjugate acid–base pair. The relationship between K_a and K_b for a conjugate acid–base pair simplifies our tabulation of acid and base dissociation constants. Appendix 11 includes acid dissociation constants for a variety of weak acids. To find the value of K_b for a weak base, use Equation 12.4.9 and the K_a value for its corresponding weak acid.

A common mistake when using Equation 12.4.9 is to forget that it applies to a conjugate acid–base pair only.

EXAMPLE 6.4.2

Using Appendix 11, calculate values for the following equilibrium constants.

a. K_b for pyridine, C_5H_5N
b. K_b for dihydrogen phosphate, $H_2PO_4^-$

Solution

$$\text{(a) } K_{b,C_5H_5N} = \frac{K_w}{K_{a,C_5H_5NH^+}} = \frac{1.00 \times 10^{-14}}{5.90 \times 10^{-6}} = 1.69 \times 10^{-9}$$

$$\text{(b) } K_{b,H_2PO_4^-} = \frac{K_w}{K_{a,H_3PO_4}} = \frac{1.00 \times 10^{-14}}{7.11 \times 10^{-3}} = 1.41 \times 10^{-12}$$

When finding the K_b value for a polyprotic weak base, be careful to choose the correct K_a value. Remember that Equation 12.4.9 applies to a conjugate acid–base pair only. The conjugate acid of $H_2PO_4^-$ is H_3PO_4, not HPO_4^{2-}.

EXERCISE 6.4.1

Using Appendix 11, calculate K_b values for hydrogen oxalate, $HC_2O_4^-$, and for oxalate, $C_2O_4^{2-}$.

Answer

The K_b for hydrogen oxalate is

$$K_{b,HC_2O_4^-} = \frac{K_w}{K_{a,H_2C_2O_4}} = \frac{1.00 \times 10^{-14}}{5.60 \times 10^{-2}} = 1.79 \times 10^{-13}$$

and the K_b for oxalate is

$$K_{b,C_2O_4^{2-}} = \frac{K_w}{K_{a,HC_2O_4^-}} = \frac{1.00 \times 10^{-14}}{5.42 \times 10^{-5}} = 1.85 \times 10^{-10}$$

As we expect, the K_b value for $C_2O_4^{2-}$ is larger than that for $HC_2O_4^-$.

COMPLEXATION REACTIONS

A more general definition of acids and bases was proposed in 1923 by G. N. Lewis. The Brønsted-Lowry definition of acids and bases focuses on an acid's proton-donating ability and a base's proton-accepting ability. Lewis theory, on the other hand, uses the breaking and the forming of covalent bonds to describe acids and bases. In this treatment, an acid is an electron pair acceptor and a base in an electron pair donor. Although we can apply Lewis theory to the treatment of acid–base reactions, it is more useful for treating complexation reactions between metal ions and ligands.

The following reaction between the metal ion Cd^{2+} and the ***ligand*** NH_3 is typical of a complexation reaction.

$$Cd^{2+}(aq) + 4:NH_3(aq) \rightleftharpoons Cd(:NH_3)_4^{2+}(aq) \tag{12.4.10}$$

The product of this reaction is a ***metal–ligand complex***. In writing this reaction we show ammonia as $:NH_3$, using a pair of dots to emphasize the pair of electrons that it donates to Cd^{2+}. In subsequent reactions we will omit this notation.

METAL-LIGAND FORMATION CONSTANTS

We characterize the formation of a metal–ligand complex by a ***formation constant***, K_f. For example, the complexation reaction between Cd^{2+} and NH_3, reaction 12.4.10, has the following equilibrium constant.

$$K_f = \frac{\left[Cd(NH_3)_4^{2+}\right]}{\left[Cd^{2+}\right]\left[NH_3\right]^4} = 5.5 \times 10^7 \tag{12.4.11}$$

The reverse of reaction 12.4.10 is a dissociation reaction, which we characterize by a ***dissociation constant***, K_d, that is the reciprocal of K_f.

Many complexation reactions occur in a stepwise fashion. For example, the reaction between Cd^{2+} and NH_3 involves four successive reactions.

$$Cd^{2+}(aq) + NH_3(aq) \rightleftharpoons Cd(NH_3)^{2+}(aq) \tag{12.4.12}$$

$$Cd(NH_3)^{2+}(aq) + NH_3(aq) \rightleftharpoons Cd(NH_3)_2^{2+}(aq) \tag{12.4.13}$$

$$Cd(NH_3)_2^{2+}(aq) + NH_3(aq) \rightleftharpoons Cd(NH_3)_3^{2+}(aq) \tag{12.4.14}$$

$$Cd(NH_3)_3^{2+}(aq) + NH_3(aq) \rightleftharpoons Cd(NH_3)_4^{2+}(aq) \tag{12.4.15}$$

To avoid ambiguity, we divide formation constants into two categories. A ***stepwise formation constant***, which we designate as K_i for the ith step, describes the successive addition of one ligand to the metal–ligand complex from the previous step. Thus, the equilibrium constants for reactions 12.4.12–12.4.15 are, respectively, K_1, K_2, K_3, and K_4. An overall, or ***cumulative formation constant***, which we designate as β_i, describes the addition of i ligands to the free metal ion. The equilibrium constant in Equation 12.4.11 is correctly identified as β_4, where

$$\beta_4 = K_1 \times K_2 \times K_3 \times K_4$$

In general

$$\beta_n = K_1 \times K_2 \times \cdots \times K_n = \prod_{i=1}^{n} K_i$$

Stepwise and overall formation constants for selected metal–ligand complexes are in Appendix 12.

METAL-LIGAND COMPLEXATION AND SOLUBILITY

A formation constant describes the addition of one or more ligands to a free metal ion. To find the equilibrium constant for a complexation reaction that includes a solid, we combine appropriate K_{sp} and K_f expressions. For example, the solubility of AgCl increases in the presence of excess chloride ions as the result of the following complexation reaction.

$$\mathrm{AgCl}(s) + \mathrm{Cl}^-(aq) \rightleftharpoons \mathrm{Ag(Cl)}_2^-(aq) \tag{12.4.16}$$

We can write this reaction as the sum of three other equilibrium reactions with known equilibrium constants—the solubility of AgCl, which is described by its K_{sp} reaction

$$\mathrm{AgCl}(s) \rightleftharpoons \mathrm{Ag}^+(aq) + \mathrm{Cl}^-(aq)$$

and the stepwise formation of AgCl_2^-, which is described by $K_1$and K_2 reactions.

$$\mathrm{Ag}^+(aq) + \mathrm{Cl}^-(aq) \rightleftharpoons \mathrm{AgCl}(aq)$$

$$\mathrm{AgCl}(aq) + \mathrm{Cl}^-(aq) \rightleftharpoons \mathrm{AgCl}_2^-(aq)$$

The equilibrium constant for reaction 12.4.16, therefore, is $K_{sp} \times K_1 \times K_2$.

EXAMPLE 6.4.3

Determine the value of the equilibrium constant for the reaction

$$\mathrm{PbCl_2}(s) \rightleftharpoons \mathrm{PbCl_2}(aq)$$

Solution

We can write this reaction as the sum of three other reactions. The first of these reactions is the solubility of $PbCl_2$*(s)*, which is described by its K_{sp} reaction.

$$\mathrm{PbCl_2}(s) \rightleftharpoons \mathrm{Pb}^{2+}(aq) + 2\mathrm{Cl}^-(aq)$$

The remaining two reactions are the stepwise formation of $PbCl_2$*(aq)*, which are described by K_1 and K_2.

$$\mathrm{Pb}^{2+}(aq) + \mathrm{Cl}^-(aq) \rightleftharpoons \mathrm{PbCl}^+(aq)$$

$$\mathrm{PbCl}^+(aq) + \mathrm{Cl}^-(aq) \rightleftharpoons \mathrm{PbCl_2}(aq)$$

Using values for K_{sp}, K_1, and K_2 from Appendix 10 and Appendix 12, we find that the equilibrium constant is

$$K = K_{sp} \times K_1 \times K_2 = \left(1.7 \times 10^{-5}\right) \times 38.9 \times 1.62 = 1.1 \times 10^{-3}$$

EXERCISE 6.4.2

What is the equilibrium constant for the following reaction? You will find appropriate equilibrium constants in Appendix 10 and Appendix 12.

$$\mathrm{AgBr}(s) + 2\mathrm{S_2O_3^{2-}}(aq) \rightleftharpoons \mathrm{Ag\,(S_2O_3)_2^{3-}}(aq) + \mathrm{Br}^-(aq)$$

Answer

We can write the reaction as a sum of three other reactions. The first reaction is the solubility of AgBr(s), which we characterize by its K_{sp}.

$$\mathrm{AgBr}(s) \rightleftharpoons \mathrm{Ag}^+(aq) + \mathrm{Br}^-(aq)$$

The remaining two reactions are the stepwise formation of $\mathrm{Ag(S_2O_3)_2^{3-}}$, which we characterize by K_1 and K_2.

$$\mathrm{Ag}^+(aq) + \mathrm{S_2O_3^{2-}}(aq) \rightleftharpoons \mathrm{Ag\,(S_2O_3)^-}(aq)$$

$$\mathrm{Ag\,(S_2O_3)^-}(aq) + \mathrm{S_2O_3^{2-}}(aq) \rightleftharpoons \mathrm{Ag\,(S_2O_3)_2^{3-}}(aq)$$

Using values for K_{sp}, K_1, and K_2 from Appendix 10 and Appendix 12, we find that the equilibrium constant for our reaction is

$$K = K_{sp} \times K_1 \times K_2 = \left(5.0 \times 10^{-13}\right)\left(6.6 \times 10^{8}\right)\left(7.1 \times 10^{4}\right) = 23$$

OXIDATION–REDUCTION (REDOX) REACTIONS

An oxidation–reduction reaction occurs when electrons move from one reactant to another reactant. As a result of this transfer of electrons, the reactants undergo a change in oxidation state. Those reactant that increases its oxidation state undergoes ***oxidation***, and the reactant that decreases its oxidation state undergoes ***reduction***. For example, in the following redox reaction between Fe^{3+} and oxalic acid, $H_2C_2O_4$, iron is reduced because its oxidation state changes from +3 to +2.

$$2Fe^{3+}(aq) + H_2C_2O_4(aq) + 2H_2O(l) \rightleftharpoons 2Fe^{2+}(aq) + 2CO_2(g) + 2H_3O^+(aq) \tag{12.4.17}$$

Oxalic acid, on the other hand, is oxidized because the oxidation state for carbon increases from +3 in $H_2C_2O_4$ to +4 in CO_2.

We can divide a redox reaction, such as reaction 12.4.17, into separate ***half-reactions*** that show the oxidation and the reduction processes.

$$H_2C_2O_4(aq) + 2H_2O(l) \rightleftharpoons 2CO_2(g) + 2H_3O^+(aq) + 2e^-$$

$$Fe^{3+}(aq) + e^- \rightleftharpoons Fe^{2+}(aq)$$

It is important to remember, however, that an oxidation reaction and a reduction reaction always occur as a pair. We formalize this relationship by identifying as a ***reducing agent*** the reactant that is oxidized, because it provides the electrons for the reduction half-reaction. Conversely, the reactant that is reduced is an ***oxidizing agent***. In reaction 12.4.17, Fe^{3+} is the oxidizing agent and $H_2C_2O_4$ is the reducing agent.

The products of a redox reaction also have redox properties. For example, the Fe^{2+} in reaction 12.4.17 is oxidized to Fe^{3+} when CO_2 is reduced to $H_2C_2O_4$. Borrowing some terminology from acid–base chemistry, Fe^{2+} is the conjugate reducing agent of the oxidizing agent Fe^{3+}, and CO_2 is the conjugate oxidizing agent of the reducing agent $H_2C_2O_4$.

THERMODYNAMICS OF REDOX REACTIONS

Unlike precipitation reactions, acid–base reactions, and complexation reactions, we rarely express the equilibrium position of a redox reaction with an equilibrium constant. Because a redox reaction involves a transfer of electrons from a reducing agent to an oxidizing agent, it is convenient to consider the reaction's thermodynamics in terms of the electron.

For a reaction in which one mole of a reactant undergoes oxidation or reduction, the net transfer of charge, *Q*, in coulombs is

$$Q = nF$$

where *n* is the moles of electrons per mole of reactant, and *F* is Faraday's constant (96485 C/mol). The free energy, Δ*G*, to move this charge, *Q*, over a change in ***potential***, *E*, is

$$\triangle G = EQ$$

The change in free energy (in kJ/mole) for a redox reaction, therefore, is

$$\Delta G = -nFE \tag{12.4.18}$$

where Δ*G* has units of kJ/mol. The minus sign in Equation 12.4.18 is the result of a different convention for assigning a reaction's favorable direction. In thermodynamics, a reaction is favored when Δ*G* is negative, but an oxidation-reduction reaction is favored when *E* is positive. Substituting Equation 12.4.18 into equation 6.2.3

$$-nFE = -nFE^\circ + RT \ln Q_r$$

and dividing by –*nF*, leads to the well-known ***Nernst equation***

$$E = E^\circ - \frac{RT}{nF} \ln Q_r$$

where E^o is the potential under standard-state conditions. Substituting appropriate values for *R* and *F*, assuming a temperature of 25 °C (298 K), and switching from *ln* to *log* gives the potential in volts as

$$E = E^o - \frac{0.05916}{n} \log Q_r \tag{12.4.19}$$

STANDARD POTENTIALS

A redox reaction's ***standard potential***, E^o, provides an alternative way of expressing its equilibrium constant and, therefore, its equilibrium position. Because a reaction at equilibrium has a Δ*G* of zero, the potential, *E*, also is zero at equilibrium. Substituting these values into Equation 12.4.19 and rearranging provides a relationship between E^o and *K*

$$E^\circ = \frac{0.05916}{n} \log K \tag{12.4.20}$$

A standard potential is the potential when all species are in their standard states. You may recall that we define standard state conditions as follows: all gases have unit partial pressures, all solutes have unit concentrations, and all solids and liquids are pure.

We generally do not tabulate standard potentials for redox reactions. Instead, we calculate E^o using the standard potentials for the corresponding oxidation half-reaction and reduction half-reaction. By convention, standard potentials are provided for reduction half-reactions. The standard potential for a redox reaction, E^o, is

$$E^\circ = E^\circ_{red} - E^\circ_{ox}$$

where E°_{red} and E°_{ox} are the standard reduction potentials for the reduction half-reaction and the oxidation half-reaction.

Because we cannot measure the potential for a single half-reaction, we arbitrarily assign a standard reduction potential of zero to a reference half-reaction

$$2H_3O^+(aq) + 2e^- \rightleftharpoons 2H_2O(l) + H_2(g)$$

and report all other reduction potentials relative to this reference. Appendix 13 contains a list of selected standard reduction potentials. The more positive the standard reduction potential, the more favorable the reduction reaction is under standard state conditions. For example, under standard state conditions the reduction of Cu^{2+} to Cu (E^o = +0.3419 V) is more favorable than the reduction of Zn^{2+} to Zn (E^o = –0.7618 V).

EXAMPLE 6.4.4

Calculate (a) the standard potential, (b) the equilibrium constant, and (c) the potential when $[Ag^+]$ = 0.020 M and $[Cd^{2+}]$ = 0.050 M, for the following reaction at 25°C.

$$Cd(s) + 2Ag^+(aq) \rightleftharpoons 2Ag(s) + Cd^{2+}(aq)$$

Solution

(a) In this reaction Cd is oxidized and Ag^+ is reduced. The standard cell potential, therefore, is

$$E^\circ = E^\circ_{Ag^+/Ag} - E^\circ_{Cd^{2+}/Cd} = 0.7996 - (-0.4030) = 1.2026 \text{ V}$$

(b) To calculate the equilibrium constant we substitute appropriate values into Equation 12.4.20.

$$E^\circ = 1.2026 \text{ V} = \frac{0.05916 \text{ V}}{2} \log K$$

Solving for K gives the equilibrium constant as

$$\log K = 40.6558$$
$$K = 4.527 \times 10^{40}$$

(c) To calculate the potential when $[Ag^+]$ is 0.020 M and $[Cd^{2+}]$ is 0.050M, we use the appropriate relationship for the reaction quotient, Q_r, in Equation 12.4.19.

$$E = E^\circ - \frac{0.05916 \text{ V}}{n} \log \frac{[Cd^{2+}]}{[Ag^+]^2}$$
$$E = 1.2026 \text{ V} - \frac{0.05916 \text{ V}}{2} \log \frac{0.050}{(0.020)^2} = 1.14 \text{ V}$$

EXERCISE 6.4.3

For the following reaction at 25°C

$$5Fe^{2+}(aq) + MnO_4^-(aq) + 8H^+(aq) \rightleftharpoons 5Fe^{3+}(aq) + Mn^{2+}(aq) + 4H_2O(l)$$

calculate (a) the standard potential, (b) the equilibrium constant, and (c) the potential under these conditions: $[Fe^{2+}]$ = 0.50 M, $[Fe^{3+}]$ = 0.10 M, $[MnO_4^-]$ = 0.025 M, $[Mn^{2+}]$ = 0.015 M, and a pH of 7.00. See Appendix 13 for standard state reduction potentials.

Answer

The two half-reactions are the oxidation of Fe^{2+} and the reduction of MnO_4^-.

$$Fe^{2+}(aq) \rightleftharpoons Fe^{3+}(aq) + e^-$$

$$MnO_4^-(aq) + 8H^+(aq) + 5e^- \rightleftharpoons Mn^{2+}(aq) + 4H_2O(l)$$

From Appendix 13, the standard state reduction potentials for these half-reactions are

$$E^\circ_{Fe^{3+}/Fe^{2+}} = 0.771 \text{ V and } E^\circ_{MnO_4^-/Mn^{2+}} = 1.51 \text{ V}$$

(a) The standard state potential for the reaction is

$$E^\circ = E^\circ_{MnO_4^-/Mn^{2+}} - E^\circ_{Fe^{3+}/Fe^{2+}} = 1.51 \text{ V} - 0.771 \text{ V} = 0.74 \text{ V}$$

(b) To calculate the equilibrium constant we substitute appropriate values into Equation 12.4.20.

$$E^\circ = 0.74 \text{ V} = \frac{0.05916}{5} \log K$$

Solving for *K* gives its value as 3.5×10^{62}.

(c) To calculate the potential under these non-standard state conditions, we make appropriate substitutions into the Nernst equation.

$$E = E^\circ - \frac{RT}{nF} \ln \frac{\left[Mn^{2+}\right]\left[Fe^{3+}\right]^5}{\left[MnO_4^-\right]\left[Fe^{2+}\right]^5\left[H^+\right]^8}$$

$$E = 0.74 - \frac{0.05916}{5} \log \frac{(0.015)(0.10)^5}{(0.025)(0.50)^5\left(1 \times 10^{-7}\right)^8} = 0.12 \text{ V}$$

When writing precipitation, acid–base, and metal–ligand complexation reactions, we represent acidity as H_3O^+. Redox reactions more commonly are written using H^+ instead of H_3O^+. For the reaction in Exercise 6.4.3 , we could replace H^+ with H_3O^+ and increase the stoichiometric coefficient for H_2O from 4 to 12.

This page titled 12.4: Equilibrium Constants for Chemical Reactions is shared under a CC BY-NC-SA 4.0 license and was authored, remixed, and/or curated by David Harvey.

- **6.4: Equilibrium Constants for Chemical Reactions** by David Harvey is licensed CC BY-NC-SA 4.0.

12.5: LADDER DIAGRAMS

When we develop or evaluate an analytical method, we often need to understand how the chemistry that takes place affects our results. Suppose we wish to isolate Ag^+ by precipitating it as AgCl. If we also need to control pH, then we must use a reagent that does not adversely affect the solubility of AgCl. It is a mistake to use NH_3 to adjust the pH, for example, because it increases the solubility of AgCl (see reaction 6.5.4). One of the primary sources of determinate errors in many analytical methods is failing to account for potential chemical interferences.

In this section we introduce the ladder diagram as a simple graphical tool for visualizing equilibrium chemistry. We will use ladder diagrams to determine what reactions occur when we combine several reagents, to estimate the approximate composition of a system at equilibrium, and to evaluate how a change to solution conditions might affect an analytical method.

> Although not specifically on the topic of ladder diagrams as developed in this section, the following papers provide appropriate background information: (a) Runo, J. R.; Peters, D. G. *J. Chem. Educ.* **1993**, *70*, 708–713; (b) Vale, J.; Fernández-Pereira, C.; Alcalde, M. *J. Chem. Educ.* **1993**, *70*, 790–795; (c) Fernández-Pereira, C.; Vale, J. *Chem. Educator* **1996**, *6*, 1–18; (d) Fernández- Pereira, C.; Vale, J.; Alcalde, M. *Chem. Educator* **2003**, *8*, 15–21; (e) Fernández-Pereira, C.; Alcalde, M.; Villegas, R.; Vale, J. *J. Chem. Educ.* **2007**, *84*, 520–525. Ladder diagrams are a great tool for helping you to think intuitively about analytical chemistry. We will make frequent use of them in the chapters to follow.

LADDER DIAGRAMS FOR ACID–BASE EQUILIBRIA

Let's use acetic acid, CH_3COOH, to illustrate the process we will use to draw and to interpret an acid–base ladder diagram. Before we draw the diagram, however, let's consider the equilibrium reaction in more detail. Acetic acid's acid dissociation reaction and equilibrium constant expression are

$$CH_3COOH(aq) + H_2O(l) \rightleftharpoons H_3O^+(aq) + CH_3COO^-(aq)$$

$$K_a = \frac{[CH_3COO^-]\,[H_3O^+]}{[CH_3COOH]} = 1.75 \times 10^{-5}$$

First, let's take the logarithm of each term in this equation and multiply through by –1

$$-\log K_a = 4.76 = -\log[H_3O^+] - \log \frac{[CH_3COO^-]}{[CH_3COOH]}$$

Now, let's replace $-\log[H_3O^+]$ with pH and rearrange the equation to obtain the result shown here.

$$pH = 4.76 + \log \frac{[CH_3COO^-]}{[CH_3COOH]} \tag{12.5.1}$$

Equation 12.5.1 tells us a great deal about the relationship between pH and the relative amounts of acetic acid and acetate at equilibrium. If the concentrations of CH_3COOH and CH_3COO^- are equal, then Equation 12.5.1 reduces to

$$pH = 4.76 + \log(1) = 4.76 + 0 = 4.76$$

If the concentration of CH_3COO^- is greater than that of CH_3COOH, then the log term in Equation 12.5.1 is positive and the pH is greater than 4.76. This is a reasonable result because we expect the concentration of the conjugate base, CH_3COO^-, to increase as the pH increases. Similar reasoning will convince you that the pH is less than 4.76 when the concentration of CH_3COOH exceeds that of CH_3COO^-.

Now we are ready to construct acetic acid's ladder diagram (Figure 6.6.1). First, we draw a vertical arrow that represents the solution's pH, with smaller (more acidic) pH levels at the bottom and larger (more basic) pH levels at the top. Second, we draw a horizontal line at a pH equal to acetic acid's pK_a value. This line, or step on the ladder, divides the pH axis into regions where either CH_3COOH or CH_3COO^- is the predominate species. This completes the ladder diagram.

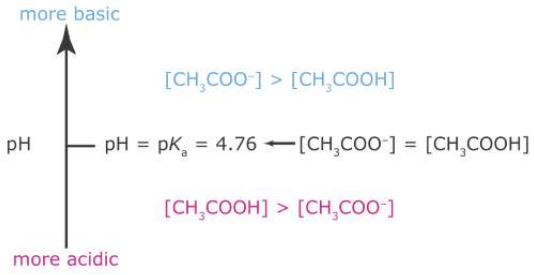


Figure 6.6.1 . Acid–base ladder diagram for acetic acid showing the relative concentrations of CH_3COOH and CH_3COO^-. A simpler version of this ladder diagram dispenses with the equalities and inequalities and shows only the predominate species in each region.

Using the ladder diagram, it is easy to identify the predominate form of acetic acid at any pH. At a pH of 3.5, for example, acetic acid exists primarily as CH_3COOH. If we add sufficient base to the solution such that the pH increases to 6.5, the predominate form of acetic acid is CH_3COO^-.

EXAMPLE 6.6.1

Draw a ladder diagram for the weak base *p*-nitrophenolate and identify its predominate form at a pH of 6.00.

Solution

To draw a ladder diagram for a weak base, we simply draw the ladder diagram for its conjugate weak acid. From Appendix 11, the pK_a for *p*-nitrophenol is 7.15. The resulting ladder diagram is shown in Figure 6.6.2 . At a pH of 6.00, *p*-nitrophenolate is present primarily in its weak acid form.

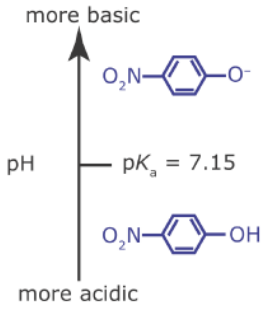


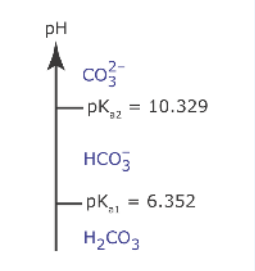
Figure 6.6.2 . Acid–base ladder diagram for *p*-nitrophenolate.

EXERCISE 6.6.1

Draw a ladder diagram for carbonic acid, H_2CO_3. Because H_2CO_3 is a diprotic weak acid, your ladder diagram will have two steps. What is the predominate form of carbonic acid when the pH is 7.00? Relevant equilibrium constants are in Appendix 11.

Answer

From Appendix 11, the pK_a values for H_2CO_3 are 6.352 and 10.329. The ladder diagram for H_2CO_3 is shown below. The predominate form at a pH of 7.00 is HCO_3^-.



https://chem.libretexts.org/@go/page/526622

A ladder diagram is particularly useful for evaluating the reactivity between a weak acid and a weak base. Figure 6.6.3 , for example, shows a single ladder diagram for acetic acid/acetate and for *p*-nitrophenol/*p*-nitrophenolate. An acid and a base can not co-exist if their respective areas of predominance do not overlap. If we mix together solutions of acetic acid and sodium *p*-nitrophenolate, the reaction

$$C_6H_4NO_2^-(aq) + CH_3COOH(aq) \rightleftharpoons CH_3COO^-(aq) + C_6H_4NO_2H(aq) \tag{12.5.2}$$

occurs because the areas of predominance for acetic acid and *p*-nitrophenolate do not overlap. The solution's final composition depends on which species is the limiting reagent. The following example shows how we can use the ladder diagram in Figure 6.6.3 to evaluate the result of mixing together solutions of acetic acid and *p*-nitrophenolate.

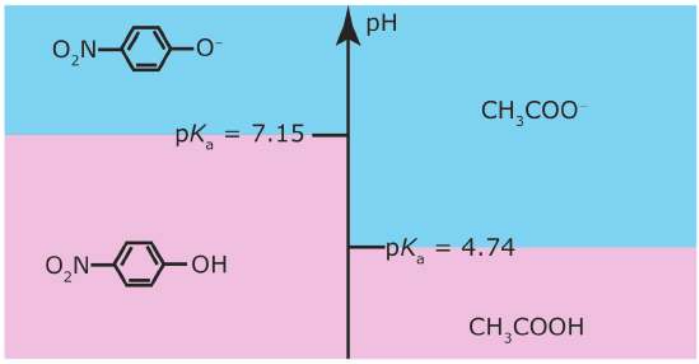


Figure 6.6.3 . Acid–base ladder diagram showing the areas of predominance for acetic acid/acetate and for *p*-nitrophenol/*p*-nitrophenolate. The areas shaded in blue shows the pH range where the weak bases are the predominate species; the weak acid forms are the predominate species in the areas shaded in pink.

EXAMPLE 6.6.2

Predict the approximate pH and the final composition after mixing together 0.090 moles of acetic acid and 0.040 moles of *p*-nitrophenolate.

Solution

The ladder diagram in Figure 6.6.3 indicates that the reaction between acetic acid and *p*-nitrophenolate is favorable. Because acetic acid is in excess, we assume the reaction of *p*-nitrophenolate to *p*-nitrophenol is complete. At equilibrium essentially no *p*-nitrophenolate remains and there are 0.040 mol of *p*-nitrophenol. Converting *p*-nitrophenolate to *p*-nitrophenol consumes 0.040 moles of acetic acid; thus

$$\text{moles } CH_3COOH = 0.090 - 0.040 = 0.050 \text{ mol}$$
$$\text{moles } CH_3COO^- = 0.040 \text{ mol}$$

According to the ladder diagram, the pH is 4.74 when there are equal amounts of CH_3COOH and CH_3COO^-. Because we have slightly more CH_3COOH than CH_3COO^-, the pH is slightly less than 4.74.

EXERCISE 6.6.2

Using Figure 6.6.3 , predict the approximate pH and the composition of the solution formed by mixing together 0.090 moles of *p*-nitrophenolate and 0.040 moles of acetic acid.

Answer

The ladder diagram in Figure 6.6.3 indicates that the reaction between acetic acid and *p*-nitrophenolate is favorable. Because *p*-nitrophenolate is in excess, we assume the reaction of acetic acid to acetate is complete. At equilibrium essentially no acetic acid remains and there are 0.040 moles of acetate. Converting acetic acid to acetate consumes 0.040 moles of *p*-nitrophenolate; thus

$$\text{moles } p\text{-nitrophenolate} = 0.090 - 0.040 = 0.050 \text{ mol}$$

$$\text{moles } p\text{-nitrophenol} = 0.040 \text{ mol}$$

According to the ladder diagram for this system, the pH is 7.15 when there are equal concentrations of *p*-nitrophenol and *p*-nitrophenolate. Because we have slightly more *p*-nitrophenolate than we have *p*-nitrophenol, the pH is slightly greater than 7.15.

If the areas of predominance for an acid and a base overlap, then we do not expect that much of a reaction will occur. For example, if we mix together solutions of CH_3COO^- and *p*-nitrophenol, we do not expect a significant change in the moles of either reagent. Furthermore,

the pH of the mixture must be between 4.76 and 7.15, with the exact pH depending upon the relative amounts of CH_3COO^- and *p*-nitrophenol.

We also can use an acid–base ladder diagram to evaluate the effect of pH on other equilibria. For example, the solubility of CaF_2

$$CaF_2(s) \rightleftharpoons Ca^{2+}(aq) + 2F^-(aq)$$

is affected by pH because F^- is a weak base. From Le Châtelier's principle, we know that converting F^- to HF will increase the solubility of CaF_2. To minimize the solubility of CaF_2 we need to maintain the solution's pH so that F^- is the predominate species. The ladder diagram for HF (Figure 6.6.4) shows us that maintaining a pH of more than 3.17 will minimize solubility losses.

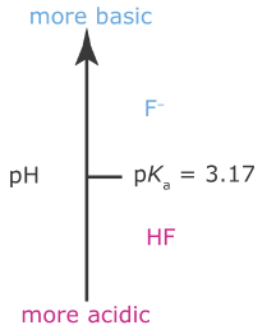


Figure 6.6.4 . Acid–base ladder diagram for HF. To minimize the solubility of CaF_2, we need to keep the pH above 3.17, with more basic pH levels leading to smaller solubility losses. See Chapter 8 for a more detailed discussion.

LADDER DIAGRAMS FOR COMPLEXATION EQUILIBRIA

We can apply the same principles for constructing and interpreting an acid–base ladder diagram to equilibria that involve metal–ligand complexes. For a complexation reaction we define the ladder diagram's scale using the concentration of uncomplexed, or free ligand, pL. Using the formation of $Cd(NH_3)^{2+}$ as an example

$$Cd^{2+}(aq) + NH_3(aq) \rightleftharpoons Cd(NH_3)^{2+}(aq)$$

we can show that $\log K_1$ is the dividing line between the areas of predominance for Cd^{2+} and for $Cd(NH_3)^{2+}$.

$$K_1 = 3.55 \times 10^2 = \frac{\left[Cd(NH_3)^{2+}\right]}{\left[Cd^{2+}\right]\left[NH_3\right]}$$

$$\log K_1 = \log\left(3.55 \times 10^2\right) = \log \frac{\left[Cd(NH_3)^{2+}\right]}{\left[Cd^{2+}\right]} - \log[NH_3]$$

$$\log K_1 = 2.55 = \log \frac{\left[Cd(NH_3)^{2+}\right]}{\left[Cd^{2+}\right]} + pNH_3$$

$$pNH_3 = \log K_1 + \log \frac{\left[Cd^{2+}\right]}{\left[Cd(NH_3)^{2+}\right]} = 2.55 + \log \frac{\left[Cd^{2+}\right]}{\left[Cd(NH_3)^{2+}\right]}$$

Thus, Cd^{2+} is the predominate species when pNH_3 is greater than 2.55 (a concentration of NH_3 smaller than 2.82×10^{-3} M) and for a pNH_3 value less than 2.55, $Cd(NH_3)^{2+}$ is the predominate species. Figure 6.6.5 shows a complete metal–ligand ladder diagram for Cd^{2+} and NH_3 that includes additional Cd–NH_3 complexes.

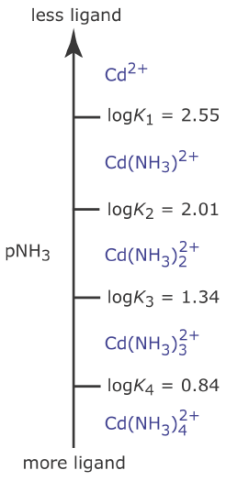


Figure 6.6.5 . Metal–ligand ladder diagram for Cd^{2+}–NH_3 complexation reactions. Note that higher-order complexes form when pNH_3 is smaller (which corresponds to larger concentrations of NH_3).

EXAMPLE 6.6.3

Draw a single ladder diagram for the $Ca(EDTA)^{2-}$ and the $Mg(EDTA)^{2-}$ metal–ligand complexes. Use your ladder diagram to predict the result of adding 0.080 moles of Ca^{2+} to 0.060 moles of $Mg(EDTA)^{2-}$. EDTA is an abbreviation for the ligand ethylenediaminetetraacetic acid.

Solution

Figure 6.6.6 shows the ladder diagram for this system of metal–ligand complexes. Because the predominance regions for Ca^{2+} and $Mg(EDTA)^{2-}$ do not overlap, the reaction

$$Ca^{2+}(aq) + Mg(EDTA)^{2-}(aq) \rightleftharpoons Ca(EDTA)^{2-}(aq) + Mg^{2+}(aq)$$

proceeds essentially to completion. Because Ca^{2+} is the excess reagent, the composition of the final solution is approximately

$$\text{moles } Ca^{2+} = 0.080 - 0.060 = 0.020 \text{ mol}$$

$$\text{moles } Ca(EDTA)^{2-} = 0.060 \text{ mol}$$

$$\text{moles } Mg^{2+} = 0.060 \text{ mol}$$

$$\text{moles } Mg(EDTA)^{2-} = 0 \text{ mol}$$

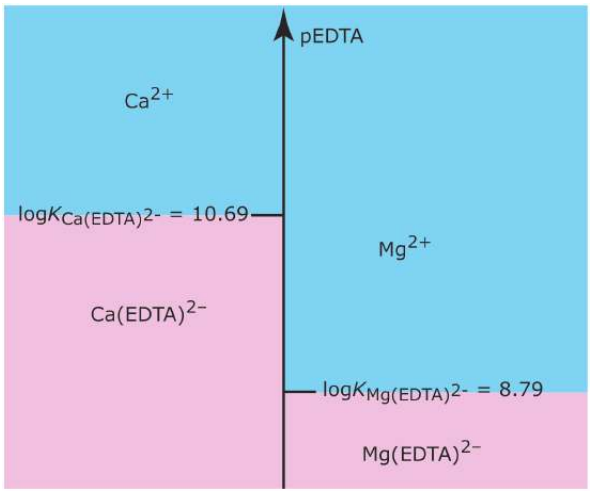


Figure 6.6.6 . Metal–ligand ladder diagram for $Ca(EDTA)^{2-}$ and for $Mg(EDTA)^{2-}$. The areas shaded in blue show the pEDTA range where the free metal ions are the predominate species; the metal–ligand complexes are the predominate species in the areas shaded in pink.

The metal–ligand ladder diagram in Figure 6.6.5 uses stepwise formation constants. We also can construct a ladder diagram using cumulative formation constants. For example, the first three stepwise formation constants for the reaction of Zn^{2+} with NH_3

$$Zn^{2+}(aq) + NH_3(aq) \rightleftharpoons Zn(NH_3)^{2+}(aq) \quad K_1 = 1.6 \times 10^2$$

$$Zn(NH_3)^{2+}(aq) + NH_3(aq) \rightleftharpoons Zn(NH_3)_2^{2+}(aq) \quad K_2 = 1.95 \times 10^2$$

$$Zn(NH_3)_2^{2+}(aq) + NH_3(aq) = Zn(NH_3)_3^{2+}(aq) \quad K_3 = 2.3 \times 10^2$$

suggests that the formation of $Zn(NH_3)_3^{2+}$ is more favorable than the formation of $Zn(NH_3)^{2+}$ or $Zn(NH_3)_2^{2+}$. For this reason, the equilibrium is best represented by the cumulative formation reaction shown here.

$$Zn^{2+}(aq) + 3NH_3(aq) \rightleftharpoons Zn(NH_3)_3^{2+}(aq) \quad \beta_3 = 7.2 \times 10^6$$

Because K_3 is greater than K_2, which is greater than K_1, the formation of the metal-ligand complex $Zn(NH_3)_3^{2+}$ is more favorable than the formation of the other metal ligand complexes. For this reason, at lower values of pNH_3 the concentration of $Zn(NH_3)_3^{2+}$ is larger than the concentrations of $Zn(NH_3)^{2+}$ or $Zn(NH_3)_2^{2+}$. The value of β_3 is

$$\beta_3 = K_1 \times K_2 \times K_3$$

To see how we incorporate this cumulative formation constant into a ladder diagram, we begin with the reaction's equilibrium constant expression.

$$\beta_3 = \frac{\left[Zn(NH_3)_3^{2+}\right]}{\left[Zn^{2+}\right]\left[NH_3\right]^3}$$

Taking the log of each side

$$\log \beta_3 = \log \frac{\left[Zn(NH_3)_3^{2+}\right]}{\left[Zn^{2+}\right]} - 3\log[NH_3]$$

and rearranging gives

$$pNH_3 = \frac{1}{3}\log \beta_3 + \frac{1}{3}\log \frac{\left[Zn^{2+}\right]}{\left[Zn(NH_3)_3^{2+}\right]}$$

When the concentrations of Zn and $Zn(NH_3)_3^{2+}$ are equal, then

$$pNH_3 = \frac{1}{3}\log \beta_3 = 2.29$$

In general, for the metal–ligand complex ML_n, the step for a cumulative formation constant is

$$pL = \frac{1}{n}\log \beta_n$$

Figure 6.6.7 shows the complete ladder diagram for the Zn^{2+}–NH_3 system.

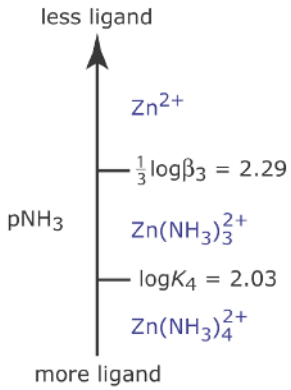


Figure 6.6.7 . Ladder diagram for Zn^{2+}–NH_3 metal–ligand complexation reactions showing both a step based on a cumulative formation constant and a step based on a stepwise formation constant.

LADDER DIAGRAMS FOR OXIDATION/REDUCTION EQUILIBRIA

We also can construct ladder diagrams to help us evaluate redox equilibria. Figure 6.6.8 shows a typical ladder diagram for two half-reactions in which the scale is the potential, *E*.

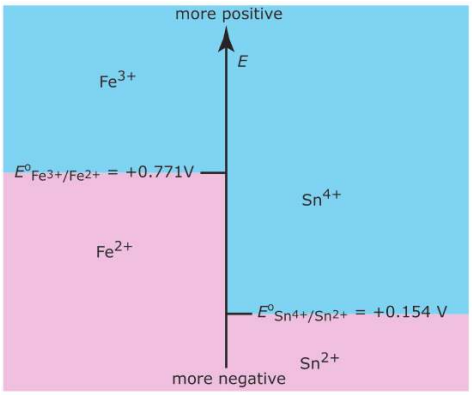


Figure 6.6.8 . Redox ladder diagram for Fe^{3+}/Fe^{2+} and for Sn^{4+}/Sn^{2+}. The areas shaded in blue show the potential range where the oxidized forms are the predominate species; the reduced forms are the predominate species in the areas shaded in pink. Note that a more positive potential favors the oxidized form.

The Nernst equation defines the areas of predominance. Using the Fe^{3+}/Fe^{2+} half-reaction as an example, we write

$$E = E^\circ - \frac{RT}{nF}\ln\frac{\left[\mathrm{Fe^{2+}}\right]}{\left[\mathrm{Fe^{3+}}\right]} = 0.771 - 0.05916\log\frac{\left[\mathrm{Fe^{2+}}\right]}{\left[\mathrm{Fe^{3+}}\right]}$$

At a potential more positive than the standard state potential, the predominate species is Fe^{3+}, whereas Fe^{2+} predominates at potentials more negative than E^o. When coupled with the step for the Sn^{4+}/Sn^{2+} half-reaction we see that Sn^{2+} is a useful reducing agent for Fe^{3+}. If Sn^{2+} is in excess, the potential of the resulting solution is near +0.154 V.

Because the steps on a redox ladder diagram are standard state potentials, a complication arises if solutes other than the oxidizing agent and reducing agent are present at non-standard state concentrations. For example, the potential for the half-reaction

$$\mathrm{UO_2^{2+}}(aq) + 4\mathrm{H_3O^+}(aq) + 2e^- \rightleftharpoons \mathrm{U^{4+}}(aq) + 6\mathrm{H_2O}(l)$$

depends on the solution's pH. To define areas of predominance in this case we begin with the Nernst equation

$$E = +0.327 - \frac{0.05916}{2}\log\frac{\left[\mathrm{U^{4+}}\right]}{\left[\mathrm{UO_2^{2+}}\right]\left[\mathrm{H_3O^+}\right]^4}$$

and factor out the concentration of H_3O^+.

$$E = +0.327 + \frac{0.05916}{2}\log\left[\mathrm{H_3O^+}\right]^4 - \frac{0.05916}{2}\log\frac{\left[\mathrm{U^{4+}}\right]}{\left[\mathrm{UO_2^{2+}}\right]}$$

From this equation we see that the area of predominance for UO_2^{2+} and U^{4+} is defined by a step at a potential where $[U^{4+}] = [UO_2^{2+}]$.

$$E = +0.327 + \frac{0.05916}{2}\log\left[\mathrm{H_3O^+}\right]^4 = +0.327 - 0.1183\mathrm{pH}$$

Figure 6.6.9 shows how pH affects the step for the UO_2^{2+} /U^{4+} half-reaction.

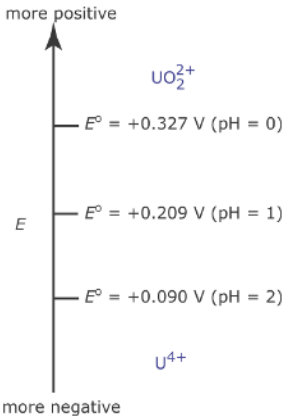


Figure 6.6.9 . Redox ladder diagram for the UO_2^{2+}/U^{4+} half-reaction showing the effect of pH on the step defined by the standard state's potential.

This page titled 12.5: Ladder Diagrams is shared under a CC BY-NC-SA 4.0 license and was authored, remixed, and/or curated by David Harvey.

- **6.6: Ladder Diagrams** by David Harvey is licensed CC BY-NC-SA 4.0.

12.6: PROBLEMS

1. Write equilibrium constant expressions for the following reactions. What is the value for each reaction's equilibrium constant?

(a) $NH_3(aq) + H_3O^+(aq) \rightleftharpoons NH_4^+(aq)$

(b) $PbI_2(s) + S^{2-}(aq) \rightleftharpoons PbS(s) + 2I^-(aq)$

(c) $CdY^{2-}(aq) + 4CN^-(aq) \rightleftharpoons Cd(CN)_4^{2-}(aq) + Y^{4-}(aq)$; *note: Y is the shorthand symbol for EDTA*

(d) $AgCl(s) + 2NH_3(aq) \rightleftharpoons Ag(NH_3)_2^+(aq) + Cl^-(aq)$

(e) $BaCO_3(s) + 2H_3O^+(aq) \rightleftharpoons Ba^{2+}(aq) + H_2CO_3(aq) + 2H_2O(l)$

2. Use a ladder diagram to explain why the first reaction is favorable and why the second reaction is unfavorable.

$$H_3PO_4(aq) + F^-(aq) \rightleftharpoons HF(aq) + H_2PO_4^-(aq)$$

$$H_3PO_4(aq) + 2F^-(aq) \rightleftharpoons 2HF(aq) + HPO_4^{2-}(aq)$$

Determine the equilibrium constant for these reactions and verify that they are consistent with your ladder diagram.

3. Calculate the potential for the following redox reaction for a solution in which [Fe^{3+}] = 0.050 M, [Fe^{2+}] = 0.030 M, [Sn^{2+}] = 0.015 M and [Sn^{4+}] = 0.020 M.

$$2Fe^{3+}(aq) + Sn^{2+}(aq) \rightleftharpoons Sn^{4+}(aq) + 2Fe^{2+}(aq)$$

4. Calculate the standard state potential and the equilibrium constant for each of the following redox reactions. Assume that [H_3O^+] is 1.0 M for an acidic solution and that [OH^-] is 1.0 M for a basic solution. Note that these reactions are not balanced. Reactions (a) and (b) are in acidic solution; reaction (c) is in a basic solution.

(a) $MnO_4^-(aq) + H_2SO_3(aq) \rightleftharpoons Mn^{2+}(aq) + SO_4^{2-}(aq)$

(b) $IO_3^-(aq) + I^-(aq) \rightleftharpoons I_2(aq)$

(c) $ClO^-(aq) + I^-(aq) \rightleftharpoons IO_3^-(aq) + Cl^-(aq)$

5. One analytical method for determining the concentration of sulfur is to oxidize it to SO_4^{2-} and then precipitate it as $BaSO_4$ by adding $BaCl_2$. The mass of the resulting precipitate is proportional to the amount of sulfur in the original sample. The accuracy of this method depends on the solubility of $BaSO_4$, the reaction for which is shown here.

$$BaSO_4(s) \rightleftharpoons Ba^{2+}(aq) + SO_4^{2-}(aq)$$

For each of the following, predict the affect on the solubility of $BaSO_4$: (a) decreasing the solution's pH; (b) adding more $BaCl_2$; and (c) increasing the solution's volume by adding H_2O.

6. Write a charge balance equation and one or more mass balance equations for the following solutions.

(a) 0.10 M NaCl

(b) 0.10 M HCl

(c) 0.10 M HF

(d) 0.10 M NaH_2PO_4

(e) $MgCO_3$ (saturated solution)

(f) 0.10 M $Ag(CN)_2^-$ (prepared using $AgNO_3$ and KCN)

(g) 0.10 M HCl and 0.050 M $NaNO_2$

7. Use the systematic approach to equilibrium problems to calculate the pH of the following solutions. Be sure to state and justify any assumptions you make in solving the problems.

(a) 0.050 M $HClO_4$

(b) 1.00×10^{-7} M HCl

(c) 0.025 M HClO

(d) 0.010 M HCOOH

(e) 0.050 M $Ba(OH)_2$

(f) 0.010 M C_5H_5N

8. Construct ladder diagrams for the following diprotic weak acids (H_2A) and estimate the pH of 0.10 M solutions of H_2A, NaHA, and Na_2A.

(a) maleic acid

(b) malonic acid

(c) succinic acid

9. Use the systematic approach to solving equilibrium problems to calculate the pH of (a) malonic acid, H_2A; (b) sodium hydrogenmalonate, NaHA; and (c) sodium malonate, Na_2A. Be sure to state and justify any assumptions you make in solving the problems.

10. Ignoring activity effects, calculate the molar solubility of Hg_2Br_2 in the following solutions. Be sure to state and justify any assumption you make in solving the problems.

(a) a saturated solution of Hg_2Br_2

(b) 0.025 M $Hg_2(NO_3)_2$ saturated with Hg_2Br_2

(c) 0.050 M NaBr saturated with Hg_2Br_2

11. The solubility of CaF_2 is controlled by the following two reactions

$$\mathrm{CaF_2}(s) \rightleftharpoons \mathrm{Ca^{2+}}(aq) + 2\mathrm{F^-}(aq)$$

$$\mathrm{HF}(aq) + \mathrm{H_2O}(l) \rightleftharpoons \mathrm{H_3O^+}(aq) + \mathrm{F^-}(aq)$$

Calculate the molar solubility of CaF_2 in a solution that is buffered to a pH of 7.00. Use a ladder diagram to help simplify the calculations. How would your approach to this problem change if the pH is buffered to 2.00? What is the solubility of CaF_2 at this pH? Be sure to state and justify any assumptions you make in solving the problems.

12. Calculate the molar solubility of $Mg(OH)_2$ in a solution buffered to a pH of 7.00. How does this compare to its solubility in unbuffered deionized water with an initial pH of 7.00? Be sure to state and justify any assumptions you make in solving the problem.

13. Calculate the solubility of Ag_3PO_4 in a solution buffered to a pH of 9.00. Be sure to state and justify any assumptions you make in solving the problem.

14. Determine the equilibrium composition of saturated solution of AgCl. Assume that the solubility of AgCl is influenced by the following reactions

$$\mathrm{AgCl}(s) \rightleftharpoons \mathrm{Ag^+}(aq) + \mathrm{Cl^-}(aq)$$

$$\mathrm{Ag^+}(aq) + \mathrm{Cl^-}(aq) \rightleftharpoons \mathrm{AgCl}(aq)$$

$$\mathrm{AgCl}(aq) + \mathrm{Cl^-}(aq) \rightleftharpoons \mathrm{AgCl_2^-}(aq)$$

Be sure to state and justify any assumptions you make in solving the problem.

15. Calculate the ionic strength of the following solutions

(a) 0.050 M NaCl

(b) 0.025 M $CuCl_2$

(c) 0.10 M Na_2SO_4

16. Repeat the calculations in Problem 10, this time correcting for the effect of ionic strength. Be sure to state and justify any assumptions you make in solving the problems.

17. Over what pH range do you expect $Ca_3(PO_4)_2$ to have its minimum solubility?

18. Construct ladder diagrams for the following systems, each of which consists of two or three equilibrium reactions. Using your ladder diagrams, identify all reactions that are likely to occur in each system?

(a) HF and H_3PO_4

(b) $\mathrm{Ag(CN)_2^-}$, $\mathrm{Ni(CN)_4^{2-}}$, and $\mathrm{Fe(CN)_6^{3-}}$

(c) $\mathrm{Cr_2O_7^{2-}/Cr^{3+}}$ and $\mathrm{Fe^{3+}/Fe^{2+}}$

19. Calculate the pH of the following acid–base buffers. Be sure to state and justify any assumptions you make in solving the problems.

(a) 100.0 mL of 0.025 M formic acid and 0.015 M sodium formate

(b) 50.00 mL of 0.12 M NH_3 and 3.50 mL of 1.0 M HCl

(c) 5.00 g of Na_2CO_3 and 5.00 g of $NaHCO_3$ diluted to 0.100 L

20. Calculate the pH of the buffers in Problem 19 after adding 5.0 mL of 0.10 M HCl. Be sure to state and justify any assumptions you make in solving the problems.

21. Calculate the pH of the buffers in Problem 19 after adding 5.0 mL of 0.10 M NaOH. Be sure to state and justify any assumptions you make in solving the problems.

22. Consider the following hypothetical complexation reaction between a metal, M, and a ligand, L

$$\mathrm{M}(aq) + \mathrm{L}(aq) \rightleftharpoons \mathrm{ML}(aq)$$

for which the formation constant is 1.5×10^8 . (a) Derive an equation similar to the Henderson–Hasselbalch equation that relates pM to the concentrations of L and ML. (b) What is the pM for a solution that contains 0.010 mol of M and 0.020 mol of L? (c) What is pM if you add 0.002 mol of M to this solution? Be sure to state and justify any assumptions you make in solving the problem.

23. A redox buffer contains an oxidizing agent and its conjugate reducing agent. Calculate the potential of a solution that contains 0.010 mol of Fe^{3+} and 0.015 mol of Fe^{2+}. What is the potential if you add sufficient oxidizing agent to convert 0.002 mol of Fe^{2+} to Fe^{3+}? Be sure to state and justify any assumptions you make in solving the problem.

24. Use either Excel or R to solve the following problems. For these problems, make no simplifying assumptions.

(a) the solubility of CaF_2 in deionized water

(b) the solubility of AgCl in deionized water

(c) the pH of 0.10 M fumaric acid

25. Derive equation 6.10.1 for the rigorous solution to the pH of 0.1 M HF.

This page titled 12.6: Problems is shared under a CC BY-NC-SA 4.0 license and was authored, remixed, and/or curated by David Harvey.

- **6.12: Problems** by David Harvey is licensed CC BY-NC-SA 4.0.

12.7: ADDITIONAL RESOURCES

The following experiments involve the experimental determination of equilibrium constants, the characterization of buffers, and, in some cases, demonstrations of the importance of activity effects.

- "The Effect of Ionic Strength on an Equilibrium Constant (A Class Study)" in *Chemical Principles in Practice*, J. A. Bell, Ed., Addison-Wesley: Reading, MA, 1967.
- "Equilibrium Constants for Calcium Iodate Solubility and Iodic Acid Dissociation" in *Chemical Principles in Practice*, J. A. Bell, Ed., Addison-Wesley: Reading, MA, 1967.
- "The Solubility of Silver Acetate" in *Chemical Principles in Practice*, J. A. Bell, Ed., Addison-Wesley: Reading, MA, 1967.
- Cobb, C. L.; Love, G. A. "Iron(III) Thiocyanate Revisited: A Physical Chemistry Equilibrium Lab Incorporating Ionic Strength Effects," *J. Chem. Educ.* **1998**, *75*, 90–92.
- Green, D. B.; Rechtsteiner, G.; Honodel, A. "Determination of the Thermodynamic Solubility Product, K_{sp}, of PbI_2 Assuming Nonideal Behavior," *J. Chem. Educ.* **1996**, *73*, 789–792.
- Russo, S. O.; Hanania, I. H. "Buffer Capacity," *J. Chem. Educ.* **1987**, *64*, 817–819.
- Stolzberg, R. J. "Discovering a Change in Equilibrium Constant with Change in Ionic Strength," *J. Chem. Educ.* **1999**, *76*, 640–641.
- Wiley, J. D. "The Effect of Ionic Strength on the Solubility of an Electrolyte," *J. Chem. Educ.* **2004**, *81*, 1644–1646.

A nice discussion of Berthollet's discovery of the reversibility of reactions is found in

- Roots-Bernstein, R. S. *Discovering*, Harvard University Press: Cambridge, MA, 1989.

The following texts provide additional coverage of equilibrium chemistry.

- Butler, J. N. *Ionic Equilibria: A Mathematical Approach*; Addison-Wesley: Reading, MA, 1964.
- Butler, J. N. *Solubility and pH Calculations*; Addison-Wesley: Reading, MA, 1973.
- Fernando, Q.; Ryan, M. D. *Calculations in Analytical Chemistry*, Harcourt Brace Jovanovich: New York, 1982.
- Freiser, H.; Fernando, Q. *Ionic Equilibria in Analytical Chemistry*, Wiley: New York, 1963.
- Freiser, H. *Concepts and Calculations in Analytical Chemistry*, CRC Press: Boca Raton, 1992.
- Gordus, A. A. *Schaum's Outline of Analytical Chemistry*; McGraw-Hill: New York, 1985.
- Ramette, R. W. *Chemical Equilibrium and Analysis*, Addison-Wesley: Reading, MA, 1981.

The following papers discuss a variety of general aspects of equilibrium chemistry.

- Cepría, G.; Salvatella, L. "General Procedure for the Easy Calculation of pH in an Introductory Course of General or Analytical Chemistry," *J. Chem. Educ.* **2014**, *91*, 524–530.
- Gordus, A. A. "Chemical Equilibrium I. The Thermodynamic Equilibrium Concept," *J. Chem. Educ.* **1991**, *68*, 138–140.
- Gordus, A. A. "Chemical Equilibrium II. Deriving an Exact Equilibrium Equation," *J. Chem. Educ.* **1991**, *68*, 215–217.
- Gordus, A. A. "Chemical Equilibrium III. A Few Math Tricks," *J. Chem. Educ.* **1991**, *68*, 291–293.
- Gordus, A. A. "Chemical Equilibrium IV. Weak Acids and Bases," *J. Chem. Educ.* **1991**, *68*, 397–399.
- Gordus, A. A. "Chemical Equilibrium VI. Buffer Solutions," *J. Chem. Educ.* **1991**, *68*, 656–658.
- Gordus, A. A. "Chemical Equilibrium VII. Precipitates, "*J. Chem. Educ.* **1991**, *68*, 927–930.
- Reijenga, J.; Van Hoof, A.; van Loon, A.; Teunissen, B. "Development of Methods for the Determination of pK_a Values," *Analytical Chemistry Insights*, **2013**, *8*, 53–71.
- Thomson, B. M.; Kessick, M. A. "On the Preparation of Buffer Solutions," *J. Chem. Educ.* **1981**, *58*, 743–746.
- Weltin, E. "Are the Equilibrium Concentrations for a Chemical Reaction Always Uniquely Determined by the Initial Concentrations?" *J. Chem. Educ.* **1990**, *67*, 548.
- Weltin, E. "Are the Equilibrium Compositions Uniquely Determined by the Initial Compositions? Properties of the Gibbs Free Energy Function," J. Chem. Educ. 1995, 72, 508–511.

Collected here are a papers that discuss a variety of approaches to solving equilibrium problems.

- Ault, A. "Do pH in Your Head," *J. Chem. Educ.* **1999**, *76*, 936–938.
- Chaston, S. "Calculating Complex Equilibrium Concentrations by a Next Guess Factor Method," *J. Chem. Educ.* **1993**, *70*, 622–624.
- Donato, H. "Graphing Calculator Strategies for Solving Chemical Equilibrium Problems," J. Chem. Educ. 1999, 76, 632–634.
- Glaser, R. E. Delarosa, M. A.; Salau, A. O.; Chicone, C. "Dynamical Approach to Multiequilibria Problems for Mixtures of Acids and Their Conjugate Bases," *J. Chem. Educ.* **2014**, *91*, 1009–1016.
- Olivieri, A. C. "Solution of Acid-Base Equilibria by Successive Approximations," *J. Chem. Educ.* **1990**, *67*, 229–231.
- Weltin, E. "A Numerical Method to Calculate Equilibrium Concentrations for Single-Equation Systems," *J. Chem. Educ.* **1991**, *68*, 486–487.
- Weltin, E. "Calculating Equilibrium Concentrations," *J. Chem. Educ.* **1992**, *69*, 393–396.

- Weltin, E. “Calculating Equilibrium Concentrations for Stepwise Binding of Ligands and Polyprotic Acid-Base Systems,” *J. Chem. Educ.* **1993**, *70*, 568–571.
- Weltin, E. “Equilibrium Calculations are Easier Than You Think - But You do Have to Think!” *J. Chem. Educ.* **1993**, *70*, 571–573.
- Weltin, E. “Calculating Equilibrium Concentrations by Iteration: Recycle Your Approximations,” J. Chem. Educ. 1995, 72, 36–38.

Additional historical background on the development of the Henderson-Hasselbalch equation is provided by the following papers.

- de Levie, R. “The Henderson Approximation and the Mass Action Law of Guldberg and Waage,” *Chem. Educator* **2002**, *7*, 132–135.
- de Levie, R. “The Henderson-Hasselbalch Equation: Its History and Limitations,” *J. Chem. Educ.* **2003**, *80*, 146.

A simulation is a useful tool for helping students gain an intuitive understanding of a topic. Gathered here are some simulations for teaching equilibrium chemistry.

- Edmonson, L. J.; Lewis, D. L. “Equilibrium Principles: A Game for Students,” *J. Chem. Educ.* **1999**, *76*, 502.
- Huddle, P. A.; White, M. W.; Rogers, F. “Simulations for Teaching Chemical Equilibrium,” *J. Chem. Educ.* **2000**, *77*, 920–926.

The following papers provide additional resources on ionic strength, activity, and the effect of ionic strength and activity on equilibrium reactions and pH.

- Clark, R. W.; Bonicamp, J. M. “The K_{sp}-Solubility Conundrum,” *J. Chem. Educ.* **1998**, *75*, 1182– 1185.
- de Levie, R. “On Teaching Ionic Activity Effects: What, When, and Where?” *J. Chem. Educ.* **2005**, *82*, 878–884.
- McCarty, C. G.; Vitz, E. “pH Paradoxes: Demonstrating That It Is Not True That pH = –log[H^+],”*J. Chem. Educ.* **2006**, *83*, 752–757.
- Ramshaw, J. D. “Fugacity and Activity in a Nutshell,” *J. Chem. Educ.* **1995**, *72*, 601–603.
- Sastre de Vicente, M. E. “The Concept of Ionic Strength Eighty Years After Its Introduction,” *J. Chem. Educ.* **2004**, *81*, 750–753.
- Solomon, T. “The Definition and Unit of Ionic Strength,” *J. Chem. Educ.* **2001**, *78*, 1691–1692.

For a contrarian’s view of equilibrium chemistry, please see the following papers.

- Hawkes, S. J. “Buffer Calculations Deceive and Obscure,” *Chem. Educator*, **1996**, *1*, 1–8.
- Hawkes, S. J. “What Should We Teach Beginners About Solubility and Solubility Products?” *J. Chem. Educ.* **1998**, *75*, 1179–1181.
- Hawkes, S. J. “Complexation Calculations are Worse Than Useless,” *J. Chem. Educ.* **1999**, *76*, 1099–1100.
- Hawkes, S. J. “Easy Deviation of pH ≈ (pK_{a1} + pK_{a2})/2 Using Autoprotolysis of HA^-: Doubtful Value of the Supposedly More Rigorous Equation,” *J. Chem. Educ.* **2000**, *77*, 1183–1184. See, also, an exchange of letters between J. J. Roberts and S. J. Hawkes, *J. Chem. Educ.* **2002**, *79*, 161–162.

This page titled 12.7: Additional Resources is shared under a CC BY-NC-SA 4.0 license and was authored, remixed, and/or curated by David Harvey.

- **6.13: Additional Resources** by David Harvey is licensed CC BY-NC-SA 4.0.

12.8: CHAPTER SUMMARY AND KEY TERMS

CHAPTER SUMMARY

Analytical chemistry is more than a collection of techniques; it is the application of chemistry to the analysis of samples. As we will see in later chapters, almost all analytical methods use chemical reactivity to accomplish one or more of the following: dissolve a sample, separate analytes from interferents, transform an analyte into a more useful form, or provide a signal. Equilibrium chemistry and thermodynamics provide us with a means for predicting which reactions are likely to be favorable.

The most important types of reactions are precipitation reactions, acid–base reactions, metal-ligand complexation reactions, and oxidation–reduction reactions. In a precipitation reaction two or more soluble species combine to produce an insoluble precipitate, which we characterize using a solubility product.

An acid–base reaction occurs when an acid donates a proton to a base. The reaction's equilibrium position is described using either an acid dissociation constant, K_a, or a base dissociation constant, K_b. The product of K_a and K_b for an acid and its conjugate base is the dissociation constant for water, K_w.

When a ligand donates one or more pairs of electron to a metal ion, the result is a metal–ligand complex. Two types of equilibrium constants are used to describe metal–ligand complexation: stepwise formation constants and overall formation constants. There are two stepwise formation constants for the metal–ligand complex ML_2, each of which describes the addition of one ligand; thus, K_1 represents the addition of the first ligand to M, and K_2 represents the addition of the second ligand to ML. Alternatively, we can use a cumulative, or overall formation constant, β_2, for the metal–ligand complex ML_2, in which both ligands are added to M.

In an oxidation–reduction reaction, one of the reactants is oxidized and another reactant is reduced. Instead of using an equilibrium constants to characterize an oxidation–reduction reactions, we use the potential, positive values of which indicate a favorable reaction. The Nernst equation relates this potential to the concentrations of reactants and products.

Le Châtelier's principle provides a means for predicting how a system at equilibrium responds to a change in conditions. If we apply a stress to a system at equilibrium—by adding a reactant or product, by adding a reagent that reacts with a reactant or product, or by changing the volume—the system will respond by moving in the direction that relieves the stress.

You should be able to describe a system at equilibrium both qualitatively and quantitatively. You can develop a rigorous solution to an equilibrium problem by combining equilibrium constant expressions with appropriate mass balance and charge balance equations. Using this systematic approach, you can solve some quite complicated equilibrium problems. If a less rigorous answer is acceptable, then a ladder diagram may help you estimate the equilibrium system's composition.

Solutions that contain relatively similar amounts of a weak acid and its conjugate base experience only a small change in pH upon the addition of a small amount of strong acid or of strong base. We call these solutions buffers. A buffer can also be formed using a metal and its metal–ligand complex, or an oxidizing agent and its conjugate reducing agent. Both the systematic approach to solving equilibrium problems and ladder diagrams are useful tools for characterizing buffers.

A quantitative solution to an equilibrium problem may give an answer that does not agree with experimental results if we do not consider the effect of ionic strength. The true, thermodynamic equilibrium constant is a function of activities, a, not concentrations. A species' activity is related to its molar concentration by an activity coefficient, γ. Activity coefficients are estimated using the extended Debye-Hückel equation, making possible a more rigorous treatment of equilibria.

KEY TERMS

acid	acid dissociation constant	activity
activity coefficient	amphiprotic	base
base dissociation constant	buffer	buffer capacity
charge balance equation	common ion effect	cumulative formation constant
dissociation constant	enthalpy	entropy
equilibrium	equilibrium constant	extended Debye-Hückel equation
formation constant	Gibb's free energy	half-reaction
Henderson–Hasselbalch equation	ionic strength	ladder diagram
Le Châtelier's principle	ligand	mass balance equation
metal–ligand complex	method of successive approximations	monoprotic
Nernst equation	oxidation	oxidizing agent
pH scale	polyprotic	potential
precipitate	redox reaction	reducing agent
reduction	standard-state	standard potential
steady state	stepwise formation constant	solubility product

This page titled 12.8: Chapter Summary and Key Terms is shared under a CC BY-NC-SA 4.0 license and was authored, remixed, and/or curated by David Harvey.

- **6.14: Chapter Summary and Key Terms** by David Harvey is licensed CC BY-NC-SA 4.0.

CHAPTER OVERVIEW

13: ELECTROCHEMICAL METHODS

In Chapter 10 we examined several spectroscopic techniques that take advantage of the interaction between electromagnetic radiation and matter. In this chapter we turn our attention to electrochemical techniques in which the potential, current, or charge in an electrochemical cell serves as the analytical signal.

Although there are only three fundamental electrochemical signals, there are many possible experimental designs—too many, in fact, to cover adequately in an introductory textbook. The simplest division of electrochemical techniques is between bulk techniques, in which we measure a property of the solution in the electrochemical cell, and interfacial techniques, in which the potential, current, or charge depends on the species present at the interface between an electrode and the solution in which it sits. The measurement of a solution's conductivity, which is proportional to the total concentration of dissolved ions, is one example of a bulk electrochemical technique. A determination of pH using a pH electrode is an example of an interfacial electrochemical technique. Only interfacial electrochemical methods receive further consideration in this chapter.

- 13.1: Overview of Electrochemistry
- 13.2: An Introduction to Electroanalytical Chemistry
  - 13.2.1: Electrochemical Cells
  - 13.2.2: Potentials in Electroanalytical Cells
  - 13.2.3: Electrode Potentials
  - 13.2.4: Calculation of Cell Potentials from Electrode Potentials
  - 13.2.5: Currents in Electrochemical Cells
  - 13.2.6: Types of Electroanalytical Methods
- 13.3: Potentiometry
  - 13.3.1: Standard Electrodes
  - 13.3.2: Standard Potentials
  - 13.3.3: Reference Electrodes
  - 13.3.4: Metallic Indicator Electrodes
  - 13.3.5: Membrane Ion-Selective Electrodes
  - 13.3.6: Molecular-Selective Electrode Systems
  - 13.3.7: Quantitative Potentiometry
- 13.4: Voltammetry
  - 13.4.1: Potential Excitation Signals and Currents in Voltammetry
  - 13.4.2: Voltammetric Instrumentation
  - 13.4.3: Linear Sweep Voltammetry
  - 13.4.4: Cyclic Voltammetry
  - 13.4.5: Polarography
  - 13.4.6: Stripping Methods
  - 13.4.7: Applications of Voltammetry
- 13.5: Problems
- 13.6: Additional Resources
- 13.7: Chapter Summary and Key Terms

This page titled 13: Electrochemical Methods is shared under a CC BY-NC-SA 4.0 license and was authored, remixed, and/or curated by David Harvey.

13.1: OVERVIEW OF ELECTROCHEMISTRY

The focus of this chapter is on analytical techniques that use a measurement of potential, current, or charge to determine an analyte's concentration or to characterize an analyte's chemical reactivity. Collectively we call this area of analytical chemistry ***electrochemistry*** because its originated from the study of the movement of electrons in an oxidation–reduction reaction.

Despite the difference in instrumentation, all electrochemical techniques share several common features. Before we consider individual examples in greater detail, let's take a moment to consider some of these similarities. As you work through the chapter, this overview will help you focus on similarities between different electrochemical methods of analysis. You will find it easier to understand a new analytical method when you can see its relationship to other similar methods.

FIVE IMPORTANT CONCEPTS

To understand electrochemistry we need to appreciate five important and interrelated concepts: (1) the electrode's potential determines the analyte's form at the electrode's surface; (2) the concentration of analyte at the electrode's surface may not be the same as its concentration in bulk solution; (3) in addition to an oxidation–reduction reaction, the analyte may participate in other chemical reactions; (4) current is a measure of the rate of the analyte's oxidation or reduction; and (5) we cannot control simultaneously current and potential.

> The material in this section—particularly the five important concepts—draws upon a vision for understanding electrochemistry outlined by Larry Faulkner in the article "Understanding Electrochemistry: Some Distinctive Concepts," *J. Chem. Educ.* **1983**, *60*, 262–264. See also, Kissinger, P. T.; Bott, A. W. "Electrochemistry for the Non-Electrochemist," *Current Separations*, **2002**, *20:2*, 51–53.

THE ELECTRODE'S POTENTIAL DETERMINES THE ANALYTE'S FORM

In Chapter 6 we introduced the ladder diagram as a tool for predicting how a change in solution conditions affects the position of an equilibrium reaction. Figure 11.1.1 , for example, shows a ladder diagram for the Fe^{3+}/Fe^{2+} and the Sn^{4+}/Sn^{2+} equilibria. If we place an electrode in a solution of Fe^{3+} and Sn^{4+} and adjust its potential to +0.500 V, Fe^{3+} is reduced to Fe^{2+} but Sn^{4+} is not reduced to Sn^{2+}.

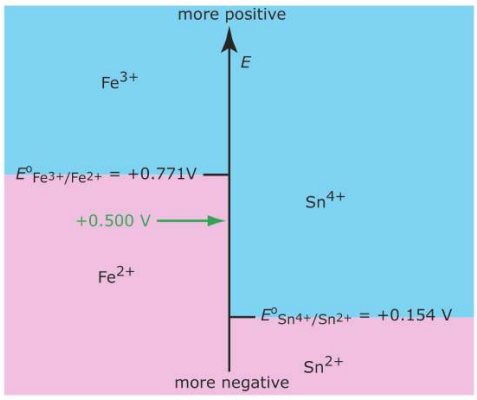


Figure 11.1.1 . Redox ladder diagram for Fe^{3+}/Fe^{2+} and for Sn^{4+}/Sn^{2+} redox couples. The areas in blue show the potential range where the oxidized forms are the predominate species; the reduced forms are the predominate species in the areas shown in pink. Note that a more positive potential favors the oxidized forms. At a potential of +0.500 V (green arrow) Fe^{3+} reduces to Fe^{2+}, but Sn^{4+} remains unchanged. You may wish to review the earlier treatment of oxidation–reduction reactions in Chapter 6.4 and the development of ladder diagrams for oxidation–reduction reactions in Chapter 6.6.

INTERFACIAL CONCENTRATIONS MAY NOT EQUAL BULK CONCENTRATIONS

In Chapter 6 we introduced the Nernst equation, which provides a mathematical relationship between the electrode's potential and the concentrations of an analyte's oxidized and reduced forms in solution. For example, the Nernst equation for Fe^{3+} and Fe^{2+} is

$$E = E_{Fe^{3+}/Fe^{2+}} - \frac{RT}{nF}\ln\frac{[Fe^{2+}]}{[Fe^{3+}]} = \frac{0.05916}{1}\log\frac{[Fe^{2+}]}{[Fe^{3+}]} \tag{13.1.1}$$

where E is the electrode's potential and $E^{\circ}_{Fe^{3+}/Fe^{2+}}$ is the standard-state reduction potential for the reaction $Fe^{3+}(aq) \rightleftharpoons Fe^{2+}(aq) + e^{-}$. Because it is the potential of the electrode that determines the analyte's form at the electrode's surface, the concentration terms in Equation 13.1.1 are those of Fe^{2+} and Fe^{3+} at the electrode's surface, not their concentrations in bulk solution.

This distinction between a species' surface concentration and its bulk concentration is important. Suppose we place an electrode in a solution of Fe^{3+} and fix its potential at 1.00 V. From the ladder diagram in Figure 11.1.1 , we know that Fe^{3+} is stable at this potential and, as shown in Figure 11.1.2 a, the concentration of Fe^{3+} is the same at all distances from the electrode's surface. If we change the electrode's

potential to +0.500 V, the concentration of Fe^{3+} at the electrode's surface decreases to approximately zero. As shown in Figure 11.1.2 b, the concentration of Fe^{3+} increases as we move away from the electrode's surface until it equals the concentration of Fe^{3+} in bulk solution. The resulting concentration gradient causes additional Fe^{3+} from the bulk solution to diffuse to the electrode's surface.

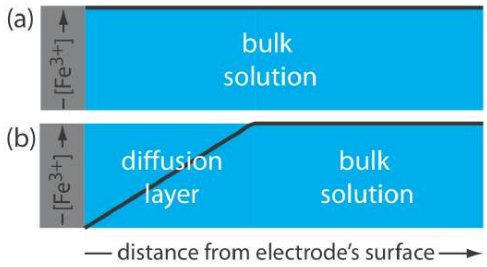


Figure 11.1.2 . Concentration of Fe^{3+} as a function of distance from the electrode's surface at (a) E = +1.00 V and (b) E = +0.500 V. The electrode is shown in gray and the solution in blue.

We call the region of solution that contains this concentration gradient in Fe^{3+} the diffusion layer. We will have more to say about this in Chapter 11.4.

THE ANALYTE MAY PARTICIPATE IN OTHER REACTIONS

Figure 11.1.1 and Figure 11.1.2 shows how the electrode's potential affects the concentration of Fe^{3+} and how the concentration of Fe^{3+} varies as a function of distance from the electrode's surface. The reduction of Fe^{3+} to Fe^{2+}, which is governed by Equation 13.1.1, may not be the only reaction that affects the concentration of Fe^{3+} in bulk solution or at the electrode's surface. The adsorption of Fe^{3+} at the electrode's surface or the formation of a metal–ligand complex in bulk solution, such as $Fe(OH)^{2+}$, also affects the concentration of Fe^{3+}.

CURRENT IS A MEASURE OF RATE

The reduction of Fe^{3+} to Fe^{2+} consumes an electron, which is drawn from the electrode. The oxidation of another species, perhaps the solvent, at a second electrode is the source of this electron. Because the reduction of Fe^{3+} to Fe^{2+} consumes one electron, the flow of electrons between the electrodes—in other words, the current—is a measure of the rate at which Fe^{3+} is reduced. One important consequence of this observation is that the current is zero when the reaction $\mathrm{Fe}^{3+}(aq) \rightleftharpoons \mathrm{Fe}^{2+}(aq) + e^-$ is at equilibrium.

The rate of the reaction $\mathrm{Fe}^{3+}(aq) \rightleftharpoons \mathrm{Fe}^{2+}(aq) + e^-$ is the change in the concentration of Fe^{3+} as a function of time.

WE CANNOT CONTROL SIMULTANEOUSLY BOTH THE CURRENT AND THE POTENTIAL

If a solution of Fe^{3+} and Fe^{2+} is at equilibrium, the current is zero and the potential is given by Equation 13.1.1. If we change the potential away from its equilibrium position, current flows as the system moves toward its new equilibrium position. Although the initial current is quite large, it decreases over time, reaching zero when the reaction reaches equilibrium. The current, therefore, changes in response to the applied potential. Alternatively, we can pass a fixed current through the electrochemical cell, forcing the reduction of Fe^{3+} to Fe^{2+}. Because the concentrations of Fe^{3+} decreases and the concentration of Fe^{2+} increases, the potential, as given by Equation 13.1.1, also changes over time. In short, if we choose to control the potential, then we must accept the resulting current, and we must accept the resulting potential if we choose to control the current.

CONTROLLING AND MEASURING CURRENT AND POTENTIAL

Electrochemical measurements are made in an electrochemical cell that consists of two or more electrodes and the electronic circuitry needed to control and measure the current and the potential. In this section we introduce the basic components of electrochemical instrumentation.

The simplest electrochemical cell uses two electrodes. The potential of one electrode is sensitive to the analyte's concentration, and is called the ***working electrode*** or the ***indicator electrode***. The second electrode, which we call the ***counter electrode***, completes the electrical circuit and provides a reference potential against which we measure the working electrode's potential. Ideally the counter electrode's potential remains constant so that we can assign to the working electrode any change in the overall cell potential. If the counter electrode's potential is not constant, then we replace it with two electrodes: a ***reference electrode*** whose potential remains constant and an ***auxiliary electrode*** that completes the electrical circuit.

Because we cannot control simultaneously the current and the potential, there are only three basic experimental designs: (1) we can measure the potential when the current is zero, (2) we can measure the potential while we control the current, and (3) we can measure the current while we control the potential. Each of these experimental designs relies on ***Ohm's law***, which states that the current, i, passing through an electrical circuit of resistance, R, generates a potential, E.

$$E = iR$$

Each of these experimental designs uses a different type of instrument. To help us understand how we can control and measure current and potential, *we will describe these instruments as if the analyst is operating them manually*. To do so the analyst observes a change in the current or the potential and manually adjusts the instrument's settings to maintain the desired experimental conditions. It is important to understand that modern electrochemical instruments provide an automated, electronic means for controlling and measuring current and potential, and that they do so by using very different electronic circuitry than that described here.

> This point bears repeating: It is important to understand that the experimental designs in Figure 11.1.3 , Figure 11.1.4 , and Figure 11.1.5 do not represent the electrochemical instruments you will find in today's analytical labs. For further information about modern electrochemical instrumentation, see this chapter's additional resources.

POTENTIOMETERS

To measure the potential of an electrochemical cell under a condition of zero current we use a ***potentiometer***. Figure 11.1.3 shows a schematic diagram for a manual potentiometer that consists of a power supply, an electrochemical cell with a working electrode and a counter electrode, an ammeter to measure the current that passes through the electrochemical cell, an adjustable, slide-wire resistor, and a tap key for closing the circuit through the electrochemical cell. Using Ohm's law, the current in the upper half of the circuit is

$$i_{\text{upper}} = \frac{E_{\text{PS}}}{R_{ab}}$$

where E_{PS} is the power supply's potential, and R_{ab} is the resistance between points *a* and *b* of the slide-wire resistor. In a similar manner, the current in the lower half of the circuit is

$$i_{\text{lower}} = \frac{E_{\text{cell}}}{R_{cb}}$$

where E_{cell} is the potential difference between the working electrode and the counter electrode, and R_{cb} is the resistance between the points *c* and *b* of the slide-wire resistor. When $i_{\text{upper}} = i_{\text{lower}} = 0$, no current flows through the ammeter and the potential of the electrochemical cell is

$$E_{\text{coll}} = \frac{R_{cb}}{R_{ab}} \times E_{\text{PS}} \tag{13.1.2}$$

To determine E_{cell} we briefly press the tap key and observe the current at the ammeter. If the current is not zero, then we adjust the slide wire resistor and remeasure the current, continuing this process until the current is zero. When the current is zero, we use Equation 13.1.2 to calculate E_{cell}.

Using the tap key to briefly close the circuit through the electrochemical cell minimizes the current that passes through the cell and limits the change in the electrochemical cell's composition. For example, passing a current of 10^{-9} A through the electrochemical cell for 1 s changes the concentrations of species in the cell by approximately 10^{-14} moles. Modern potentiometers use operational amplifiers to create a high-impedance voltmeter that measures the potential while drawing a current of less than 10^{-9} A.

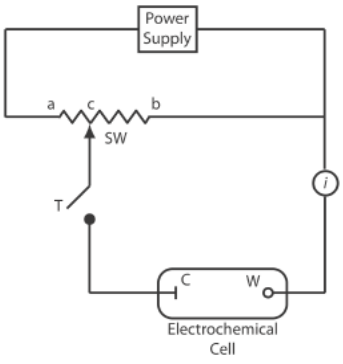


Figure 11.1.3 . Schematic diagram of a manual potentiometer: C is the counter electrode; W is the working electrode; SW is a slide-wire resistor; T is a tap key and *i* is an ammeter for measuring current.

GALVANOSTATS

A ***galvanostat***, a schematic diagram of which is shown in Figure 11.1.4 , allows us to control the current that flows through an electrochemical cell. The current from the power supply through the working electrode is

$$i = \frac{E_{\text{PS}}}{R + R_{\text{cell}}}$$

where E_{PS} is the potential of the power supply, R is the resistance of the resistor, and R_{cell} is the resistance of the electrochemical cell. If $R >> R_{cell}$, then the current between the auxiliary and working electrodes

$$i = \frac{E_{PS}}{R} \approx \text{constant}$$

maintains a constant value. To monitor the working electrode's potential, which changes as the composition of the electrochemical cell changes, we can include an optional reference electrode and a high-impedance potentiometer.

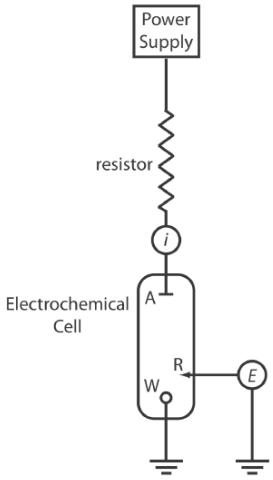


Figure 11.1.4 . Schematic diagram of a galvanostat: A is the auxiliary electrode; W is the working electrode; R is an optional reference electrode, E is a high-impedance potentiometer, and i is an ammeter. The working electrode and the optional reference electrode are connected to a ground.

POTENTIOSTATS

A ***potentiostat***, a schematic diagram of which is shown in Figure 11.1.5 , allows us to control the working electrode's potential. The potential of the working electrode is measured relative to a constant-potential reference electrode that is connected to the working electrode through a high-impedance potentiometer. To set the working electrode's potential we adjust the slide wire resistor that is connected to the auxiliary electrode. If the working electrode's potential begins to drift, we adjust the slide wire resistor to return the potential to its initial value. The current flowing between the auxiliary electrode and the working electrode is measured with an ammeter. Modern potentiostats include waveform generators that allow us to apply a time-dependent potential profile, such as a series of potential pulses, to the working electrode.

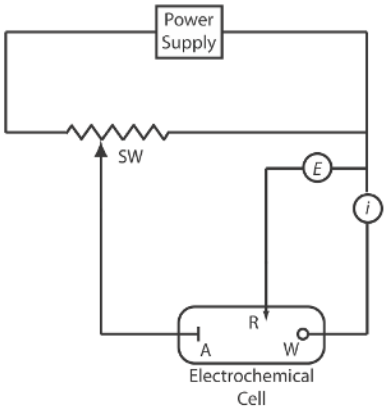


Figure 11.1.5 . Schematic diagram for a manual potentiostat: W is the working electrode; A is the auxiliary electrode; R is the reference electrode; SW is a slide-wire resistor, E is a high-impendance potentiometer; and i is an ammeter.

INTERFACIAL ELECTROCHEMICAL TECHNIQUES

Because interfacial electrochemistry is such a broad field, let's use Figure 11.1.6 to organize techniques by the experimental conditions we choose to use (Do we control the potential or the current? How do we change the applied potential or applied current? Do we stir the solution?) and the analytical signal we decide to measure (Current? Potential?).

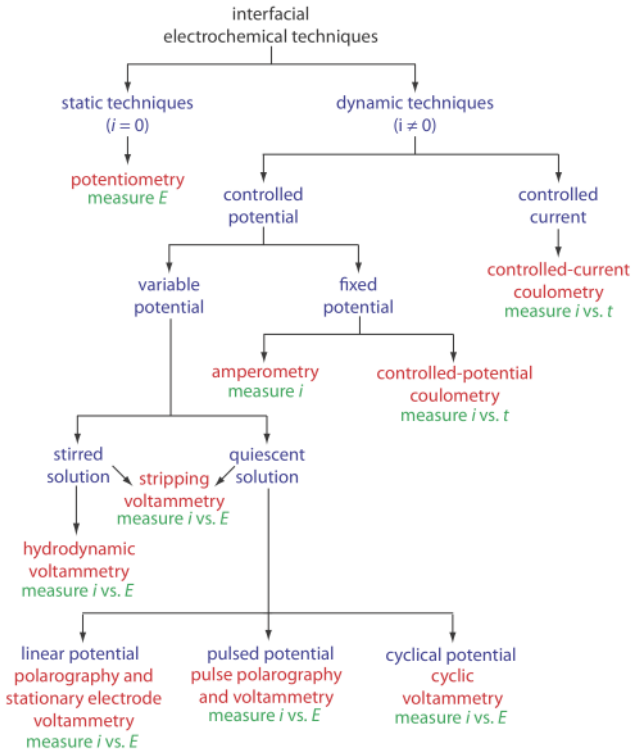


Figure 11.1.6 . Family tree that highlights the similarities and differences between a number of interfacial electrochemical techniques. The specific techniques are shown in red, the experimental conditions are shown in blue, and the analytical signals are shown in green.

At the first level, we divide interfacial electrochemical techniques into static techniques and dynamic techniques. In a static technique we do not allow current to pass through the electrochemical cell and, as a result, the concentrations of all species remain constant. Potentiometry, in which we measure the potential of an electrochemical cell under static conditions, is one of the most important quantitative electrochemical methods and is discussed in detail in Chapter 11.2.

Dynamic techniques, in which we allow current to flow and force a change in the concentration of species in the electrochemical cell, comprise the largest group of interfacial electrochemical techniques. Coulometry, in which we measure current as a function of time, is covered in Chapter 11.3. Amperometry and voltammetry, in which we measure current as a function of a fixed or variable potential, is the subject of Chapter 11.4.

This page titled 13.1: Overview of Electrochemistry is shared under a CC BY-NC-SA 4.0 license and was authored, remixed, and/or curated by David Harvey.

- **11.1: Overview of Electrochemistry** by David Harvey is licensed CC BY-NC-SA 4.0.

SECTION OVERVIEW

13.2: An Introduction to Electroanalytical Chemistry

In Chapters 6–21 we examined a wide range of spectroscopic techniques that take advantage of the interaction between electromagnetic radiation and matter. In this chapter we turn our attention to electrochemical techniques in which the potential, current, or charge in an electrochemical cell serves as the analytical signal.

Although there are only three fundamental electrochemical signals, there are many possible experimental designs—too many, in fact, to cover adequately in an introductory textbook. The simplest division of electrochemical techniques is between bulk techniques, in which we measure a property of the solution in the electrochemical cell, and interfacial techniques, in which the potential, current, or charge depends on the species present at the interface between an electrode and the solution in which it sits. The measurement of a solution's conductivity, which is proportional to the total concentration of dissolved ions, is one example of a bulk electrochemical technique. A determination of pH using a pH electrode is an example of an interfacial electrochemical technique. Only interfacial electrochemical methods receive further consideration in this textbook. In this chapter we provide an introduction to electrochemistry, introducing ideas relevant to understanding the specific electroanalytical methods introduced in Chapters 23–25.

13.2.1: Electrochemical Cells

13.2.2: Potentials in Electroanalytical Cells

13.2.3: Electrode Potentials

13.2.4: Calculation of Cell Potentials from Electrode Potentials

13.2.5: Currents in Electrochemical Cells

13.2.6: Types of Electroanalytical Methods

This page titled 13.2: An Introduction to Electroanalytical Chemistry is shared under a CC BY-NC-SA 4.0 license and was authored, remixed, and/or curated by David Harvey.

13.2.1: Electrochemical Cells

A schematic diagram of a typical electrochemical cell is shown in Figure 13.2.1.1. The electrochemical cell consists of two half-cells, each of which contains an electrode immersed in a solution of ions whose activities determine the electrode's potential. A salt bridge that contains an inert electrolyte, such as KCl, connects the two half-cells. The ends of the salt bridge are fixed with porous frits, which allow the electrolyte's ions to move freely between the half-cells and the salt bridge. This movement of ions in the salt bridge completes the electrical circuit, allowing us to measure the potential using a potentiometer.

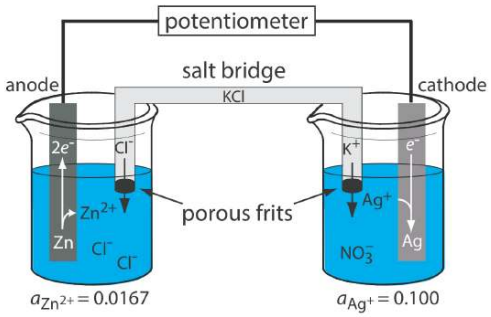


Figure 13.2.1.1. Example of a potentiometric electrochemical cell. The activities of Zn^{2+} and Ag^+ are shown below the two half-cells.

The reason for separating the electrodes is to prevent the oxidation reaction and the reduction reaction from occurring at the same electrode. For example, if we place a strip of Zn metal in a solution of $AgNO_3$, the reduction of Ag^+ to Ag occurs on the surface of the Zn at the same time as a portion of the Zn metal oxidizes to Zn^{2+}. Because the transfer of electrons from Zn to Ag^+ occurs at the electrode's surface, we can not pass them through the potentiometer.

Conduction in a Cell

Current moves through the cell in Figure 13.2.1.1as a result of the movement of two types of charged particles: electrons and ions. First, when zinc, Zn*(s)* underoges an oxidation reaction

$$\mathrm{Zn}(s) \rightleftharpoons \mathrm{Zn}^{2+}(aq) + 2e^- \tag{13.2.1.1}$$

it releases two electrons. These electrons move through the circuit that connects the metallic Zn electrode in the left half-cell to the metallic Ag electrode in the right half-cell, where it effects the reduction of $Ag^+(aq)$.

$$\mathrm{Ag}^+(aq) + e^- \rightleftharpoons \mathrm{Ag}(s) \tag{13.2.1.2}$$

If this is all that happens, then the half-cell on the left will develop an excess of positive charge as $Zn^{2+}(aq)$ ions accumulate and the half-cell on the right will develop an excess of negative charge due to the loss of $Ag^+(aq)$. The salt bridge provides a way to continue the movement of charge, and thus the current, with the K^+ ions moving toward the right half-cell and $Cl^–$ ions moving toward the left half-cell.

Galvanic and Electrolytic Cells

The net reaction for the electrochemical cell in Figure 13.2.1.1is

$$\mathrm{Zn}(s) + 2\mathrm{Ag}^+(aq) \rightleftharpoons 2\mathrm{Ag}(s) + \mathrm{Zn}^{2+}(\mathrm{aq}) \tag{13.2.1.3}$$

which simply is the result of adding together the reactions in the two half-cells after adjusting for the difference in electrons. As shown by the arrows in the figure, when we connect the electrodes to the potentiometer, current spontaneously flows from the left half-cell to the right half-cell. We call this a galvanic cell. If we apply a potential sufficient to reverse the direction of the current flow, resulting in a net reaction of

$$2\mathrm{Ag}(s) + \mathrm{Zn}^{2+}(\mathrm{aq}) \rightleftharpoons \mathrm{Zn}(s) + 2\mathrm{Ag}^+(aq)$$

then we call the system an electrolytic cell. A galvanic cell produces electrical energy and an electrolytic cell consumes electrical energy.

Anodes and Cathodes

The half-cell where oxidation takes place is called the anode and, by convention, it is shown on the left for a galvanic cell. The half-cell where reduction takes place is called the cathode and, by convention, it is shown on the right for a galvanic cell.

Faradaic and Non-Faradaic Currents

When we oxidize or reduce an analyte at the electrode in one half-cell, the electrons pass through the potentiometer to the electrode in the other half-cell where a corresponding reduction or oxidation reaction takes place. In either case, the current from the redox reactions at the two electrodes is called a faradaic current. A faradaic current due to the reduction of an analyte is called a cathodic current and carries a positive sign. An anodic current results from the analyte's oxidation and carries a negative sign.

In addition to the faradaic current from a redox reaction, the current in an electrochemical cell includes non-faradaic sources. Suppose the charge on an electrode is zero and we suddenly change its potential so that the electrode's surface acquires a positive charge. Cations near the electrode's surface will respond to this positive charge by migrating away from the electrode; anions, on the other hand, will migrate toward the electrode. This migration of ions occurs until the electrode's positive surface charge and the excess negative charge of the solution near the electrode's surface are equal. Because the movement of ions and the movement of electrons are indistinguishable, the result is a small, short-lived non-faradaic current that we call the charging current. Every time we change the electrode's potential, a short-lived charging current flows.

Even in the absence of analyte, a small, measurable current flows through an electrochemical cell. This residual current has two components: a faradaic current due to the oxidation or reduction of trace impurities and a non-faradaic charging current. Methods for discriminating between the analyte's faradaic current and the residual current are discussed later in this chapter.

The Electrical Double Layer

As noted in the previous section, when we apply a potential to an electrode it develops a positive or negative surface charge, the magnitude of which is a function of the metal and the applied potential. Because the surface carries a charge, the composition of the layer of solution immediately adjacent to the electrode changes with, for example, the concentration of cations increasing and the concentration of anions decreasing if the electrode's surface carries a negative charge. As we move away from the electrode's surface, the net potential first decreases in a linear manner, due to the imbalance of the cations and anions, and then in an exponential manner until it reaches zero. This structured surface is called the electrical double layer and consists of an inner layer and a diffuse layer. Anytime we change the potential applied to the electrode, the structure of the electrical double layer changes and a small charging current flows.

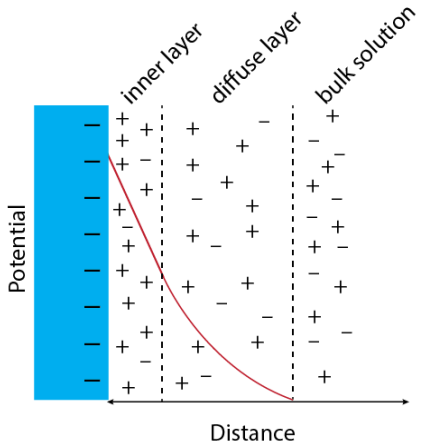


Figure 13.2.1.2: The electrical double layer. When the electrode carries a negative surface charge, the layer of solution immediately in contact with the electrode, the inner layer, becomes enriched with cations and deficient in anions. At greater distances from the electrode's surface, the concentration of cations and anions become more balanced—this is called the diffuse layer—eventually reaching the bulk solution where the net charge are in balance. The potential decreases linearly through the inner layer and exponentially through the diffuse layer.

Mass Transfer in Cells with the Passage of Current

The magnitude of a faradaic current is determined by the rate at which the analyte is oxidized at the anode or reduced at the cathode. Two factors contribute to the rate of an electrochemical reaction: the rate at which the reactants and products are

transported to and from the electrode—what we call mass transport—and the rate at which electrons pass between the electrode and the reactants and products in solution.

There are three modes of mass transport that affect the rate at which reactants and products move toward or away from the electrode surface: diffusion, migration, and convection. Diffusion occurs whenever the concentration of an ion or a molecule at the surface of the electrode is different from that in bulk solution. For example, if we apply a potential sufficient to completely reduce Ag^+ at the electrode surface, the result is a concentration gradient similar to that shown in Figure 13.2.1.3 The region of solution over which diffusion occurs is the diffusion layer. In the absence of other modes of mass transport, the width of the diffusion layer, δ, increases with time as the Ag^+ must diffuse from an increasingly greater distance.

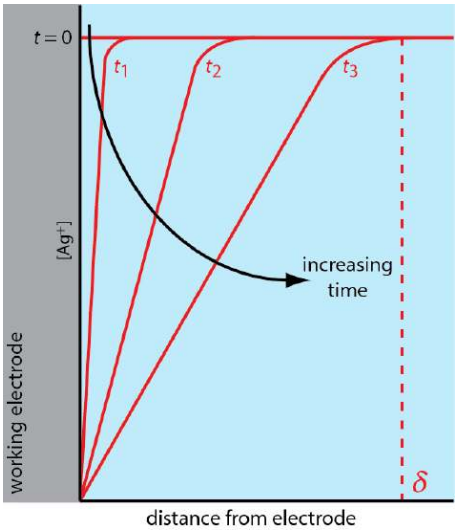


Figure 13.2.1.3. Concentration gradients (in red) for Ag^+ following the application of a potential that completely reduces it to Ag(*s*). Before we apply the potential (t = 0) the concentration of Ag^+ is the same at all distances from the electrode's surface. After we apply the potential, its concentration at the electrode's surface decreases to zero and Ag^+ diffuses to the electrode from bulk solution. The longer we apply the potential, the greater the distance over which diffusion occurs. The dashed red line shows the extent of the diffusion layer at time t_3. These profiles assume that convection and migration do not contribute significantly to the mass transport of Ag^+.

Convection occurs when we mix the solution, which carries reactants toward the electrode and removes products from the electrode. The most common form of convection is stirring the solution with a stir bar; other methods include rotating the electrode and incorporating the electrode into a flow-cell.

The final mode of mass transport is migration, which occurs when a charged particle in solution is attracted to or repelled from an electrode that carries a surface charge. If the electrode carries a positive charge, for example, an anion will move toward the electrode and a cation will move toward the bulk solution. Unlike diffusion and convection, migration affects only the mass transport of charged particles.

Schematic Representations of Cells

Although Figure 13.2.1.1 provides a useful picture of an electrochemical cell, it is not a convenient way to represent it. Imagine having to draw a picture of each electrochemical cell you are using! A more useful way to describe an electrochemical cell is a shorthand notation that uses symbols to identify different phases and that lists the composition of each phase. We use a vertical slash (|) to identify a boundary between two phases where a potential develops, and a comma (,) to separate species in the same phase or to identify a boundary between two phases where no potential develops. Shorthand cell notations begin with the anode and continue to the cathode. For example, we describe the electrochemical cell in Figure 13.2.1.1 using the following shorthand notation.

$$\mathrm{Zn}(s)|\mathrm{ZnCl_2}(aq, a_{\mathrm{Zn^{2+}}} = 0.0167)||\mathrm{AgNO_3}(aq, a_{\mathrm{Ag^+}} = 0.100)|\mathrm{Ag}(s)$$

The double vertical slash (||) represents the salt bridge, the contents of which we usually do not list. Note that a double vertical slash implies that there is a potential difference between the salt bridge and each half-cell.

Example 13.2.1.1

What are the anodic, the cathodic, and the overall reactions responsible for the potential of the electrochemical cell in Figure 13.2.1.4? Write the shorthand notation for the electrochemical cell.

Solution

The oxidation of Ag to Ag^+ occurs at the anode, which is the left half-cell. Because the solution contains a source of Cl^-, the anodic reaction is

$$\mathrm{Ag}(s) + \mathrm{Cl}^-(aq) \rightleftharpoons \mathrm{AgCl}(s) + e^-$$

The cathodic reaction, which is the right half-cell, is the reduction of Fe^{3+} to Fe^{2+}.

$$\mathrm{Fe}^{3+}(aq) + e^- \rightleftharpoons \mathrm{Fe}^{2+}(aq)$$

The overall cell reaction, therefore, is

$$\mathrm{Ag}(s) + \mathrm{Fe}^{3+}(aq) + \mathrm{Cl}^-(aq) \rightleftharpoons \mathrm{AgCl}(s) + \mathrm{Fe}^{2+}(aq)$$

The electrochemical cell's shorthand notation is

$$\mathrm{Ag}(s)|\mathrm{HCl}(aq, a_{\mathrm{Cl}^-} = 0.100), \mathrm{AgCl(sat'd)}||\mathrm{FeCl_2}(aq, a_{\mathrm{Fe}^{2+}} = 0.0100), \mathrm{Fe}^{3+}(aq, a_{\mathrm{Fe}^{3+}} = 0.0500)|\mathrm{Pt}(s)$$

Note that the Pt cathode is an inert electrode that carries electrons to the reduction half-reaction. The electrode itself does not undergo reduction.

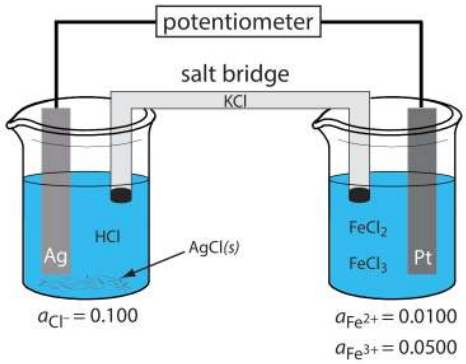


Figure 13.2.1.4. Potentiometric electrochemical cell for Example 13.2.1.1.

This page titled 13.2.1: Electrochemical Cells is shared under a CC BY-NC-SA 4.0 license and was authored, remixed, and/or curated by David Harvey.

- **22.1: Electrochemical Cells** by David Harvey is licensed CC BY-NC-SA 4.0.

13.2.2: Potentials in Electroanalytical Cells

If a Zn*(s)* electrode in a solution of Zn^{2+}*(aq)* in an electrochemical cell is at equilibrium, the current is zero and the potential is fixed in value. If we change the potential from its equilibrium value, current will flow as the system moves to its new equilibrium position. Although the initial current is quite large, it decreases over time, reaching zero when the reaction reaches equilibrium. The current, therefore, changes in response to the applied potential. Alternatively, we can pass a fixed current through the electrochemical cell, forcing the oxidation of Zn*(s)* to Zn^{2+}*(aq)*, effecting a change in the potential. In short, if we choose to control the potential, then we must accept the resulting current, and we must accept the resulting potential if we choose to control the current.

The Thermodynamics of Cell Potentials

Because a redox reaction involves a transfer of electrons from a reducing agent to an oxidizing agent, it is convenient to consider the reaction's thermodynamics in terms of the electron. For a reaction in which one mole of a reactant undergoes oxidation or reduction, the net transfer of charge, *q*, in coulombs is

$$q = nF \tag{13.2.2.1}$$

where *n* is the moles of electrons per mole of reactant, and *F* is Faraday's constant (96485 C/mol). The free energy, Δ*G*, to move this charge given an applied potential, *E*, is

$$\Delta G = Eq \tag{13.2.2.2}$$

The change in free energy (in kJ/mole) for a redox reaction, therefore, is

$$\Delta G = -nFE \tag{13.2.2.3}$$

where Δ*G* has units of kJ/mol. The minus sign in Equation 13.2.2.3is the result of a different convention for assigning a reaction's favorable direction. In thermodynamics, a reaction is favored when Δ*G* is negative, but a redox reaction is favored when *E* is positive. Substituting Equation 13.2.2.3into the thermodynamic equation that relates the free energy to its standard state value

$$\Delta G = \Delta G^{\circ} + RT \ln Q_r \tag{13.2.2.4}$$

gives

$$-nFE = -nFE^{\circ} + RT \ln Q_r \tag{13.2.2.5}$$

Dividing by –*nF* leads to the Nernst equation

$$E = E^{\circ} - \frac{RT}{nF} \ln Q_r \tag{13.2.2.6}$$

where E^{o} is the potential under standard-state conditions (more on this in Section 22.3). Substituting appropriate values for *R* and *F*, assuming a temperature of 25 ºC (298 K), and switching from the natural logarithm (*ln*) to the base 10 logarithm (*log*) gives the potential in volts as

$$E = E^{o} - \frac{0.05916}{n} \log Q_r \tag{13.2.2.7}$$

The term Q_r in the previous equations is the reaction quotient, which has the same mathematical form as the reaction's equilibrium constant expression, but uses the instantaneous amounts of reactants and products in place of their equilibrium values. For the cell in Figure 22.1.1, for example, the overall reaction is

$$\mathrm{Zn}(s) + 2\mathrm{Ag}^{+}(aq) \rightleftharpoons 2\mathrm{Ag}(s) + \mathrm{Zn}^{2+}(\mathrm{aq}) \tag{13.2.2.8}$$

and Equation 13.2.2.7becomes

$$E = E^{\circ} - \frac{0.05916}{2} \log \frac{\left[\mathrm{Zn}^{2+}\right]}{\left[\mathrm{Ag}^{+}\right]^2} \tag{13.2.2.9}$$

Equation 13.2.2.9shows us how the potential changes as the concentrations of Zn^{2+} and Ag^{+} change.

> As we will see in 22.3, 13.2.2.9 actually is expressed in terms of activities instead of concentrations. The appendix in Chapter 35.7 explains what activity is, why it is important to make a distinction between activity and concentration, and when it is reasonable to use concentrations in place of activities.

Liquid Junction Potentials

A junction potential develops at the interface between two ionic solutions if there is a difference in the concentration and the mobility of the ions. Consider, for example, a porous membrane that separates a solution of 0.1 M HCl from a solution of 0.01 M HCl (Figure 13.2.2.1a). Because the concentration of HCl on the membrane's left side is greater than that on the right side of the membrane, H^+ and Cl^- will diffuse in the direction of the arrows. The mobility of H^+, however, is greater than that for Cl^-, as shown by the difference in the lengths of their respective arrows. Because of this difference in mobility, the solution on the right side of the membrane develops an excess concentration of H^+ and a positive charge (Figure 13.2.2.1b). Simultaneously, the solution on the membrane's left side develops a negative charge because there is an excess concentration of Cl^-. We call this difference in potential across the membrane a junction potential and represent it as E_j.

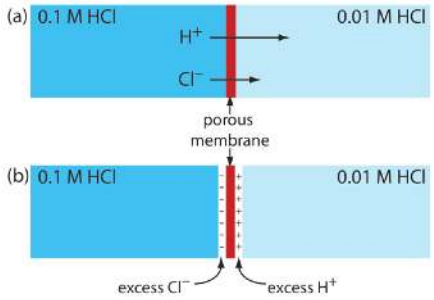


Figure 13.2.2.1. Origin of the junction potential between a solution of 0.1 M HCl and a solution of 0.01 M HCl.

The magnitude of a junction potential depends upon the difference in the concentration of ions on the two sides of the interface, and may be as large as 30–40 mV. For example, a junction potential of 33.09 mV has been measured at the interface between solutions of 0.1 M HCl and 0.1 M NaCl [Sawyer, D. T.; Roberts, J. L., Jr. *Experimental Electrochemistry for Chemists*, Wiley-Interscience: New York, 1974, p. 22]. A salt bridge's junction potential is minimized by using a salt, such as KCl, for which the mobilities of the cation and anion are approximately equal. We also can minimize the junction potential by incorporating a high concentration of the salt in the salt bridge. For this reason salt bridges frequently are constructed using solutions that are saturated with KCl. Nevertheless, a small junction potential, generally of unknown magnitude, is always present.

This page titled 13.2.2: Potentials in Electroanalytical Cells is shared under a CC BY-NC-SA 4.0 license and was authored, remixed, and/or curated by David Harvey.

- **22.2: Potentials in Electroanalytical Cells** by David Harvey is licensed CC BY-NC-SA 4.0.

13.2.3: Electrode Potentials

We began this chapter by examining the electrochemical cell in Figure 22.1.1 where $\mathrm{Zn(s)}$ is oxidized to $\mathrm{Zn^{2+}(aq)}$ and $\mathrm{Ag^{+}(aq)}$ is reduced to $\mathrm{Ag(s)}$, as shown by the following reaction.

$$2\mathrm{Ag}(s) + \mathrm{Zn^{2+}(aq)} \rightleftharpoons \mathrm{Zn}(s) + 2\mathrm{Ag^{+}}(aq)$$

The reaction proceeds as written because the reduction of $\mathrm{Ag^{+}}$*(aq)* to Ag*(s)*

$$\mathrm{Ag^{+}}(aq) + e^{-} \rightleftharpoons \mathrm{Ag}(s) \tag{13.2.3.1}$$

is more thermodynamically favorable than the reduction of $\mathrm{Zn^{2+}(aq)}$ to $\mathrm{Zn(s)}$

$$\mathrm{Zn^{2+}}(aq) + 2e^{-} \rightleftharpoons \mathrm{Zn}(s) \tag{13.2.3.2}$$

But, how do we know this is true? In this section we answer this question by taking a close look at electrode potentials.

Nature of Electrode Potentials

The potential of an electrochemical cell is the difference between the potential at the cathode, E_{cathode}, and the potential at the anode, E_{anode}, where both potentials are defined in terms of a reduction reaction (and are called reduction potentials); thus

$$E_{\text{cell}} = E_{\text{cathode}} - E_{\text{anode}} \tag{13.2.3.3}$$

$$\mathrm{H^{+}}(aq) + e^{-} = \frac{1}{2}\mathrm{H_2}(g) \tag{13.2.3.4}$$

which is the reaction that defines the standard hydrogen electrode, or SHE.

The Standard Hydrogen Electrode (SHE)

The SHE consists of a Pt electrode immersed in a solution in which the activity of hydrogen ion is 1.00 and in which the partial pressure of $\mathrm{H_2}$*(g)* is 1.00 atm (Figure 13.2.3.1). A conventional salt bridge connects the SHE to the indicator half-cell. The short hand notation for the standard hydrogen electrode is

$$\mathrm{Pt}(s),\ \mathrm{H_2}\ (g, f_{\mathrm{H_2}} = 1.00)\ |\ \mathrm{H^{+}}\ (aq, a_{\mathrm{H^{+}}} = 1.00)\ \| \tag{13.2.3.5}$$

and the standard-state potential for the reaction 13.2.3.4is, by definition, 0.000 V at all temperatures.

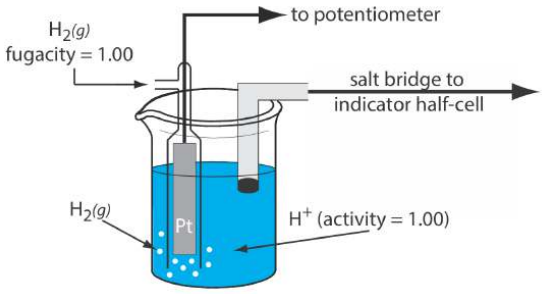


Figure 13.2.3.1. Schematic diagram showing the standard hydrogen electrode.

Practical Reference Electrodes

Although the standard hydrogen electrode is the standard against which all other potentials are referenced, it is not practical for routine use as it is difficult to prepare and maintain. Instead, we use one of several other reference electrodes. The two most common of these alternative reference electrodes are the calomel, or $\mathrm{Hg/Hg_2Cl_2}$ electrode, which is based on the following redox couple between $\mathrm{Hg_2Cl_2}$ and Hg (calomel is the common name for $\mathrm{Hg_2Cl_2}$)

$$\mathrm{Hg_2Cl_2}(s) + 2e^{-} \rightleftharpoons 2\mathrm{Hg}(l) + 2\mathrm{Cl^{-}}(aq)$$

and the Ag/AgCl reference electrode, which is based on the reduction of AgCl to Ag

$$\mathrm{AgCl}(s) + e^{-} \rightleftharpoons \mathrm{Ag}(s) + \mathrm{Cl^{-}}(aq)$$

A more detailed examination of these two reference electrodes is found in Chapter 23.1.

Definition of Electrode Potential

To determine the potential for the reduction of $Zn^{2+}(aq)$ to $Zn(s)$ we make it the cathode in the following electrochemical cell

$$\mathrm{Pt}(s),\ \mathrm{H_2}\ (g, P_{\mathrm{H_2}} = 1.00)\ |\ \mathrm{H^+}\ (aq, a_{\mathrm{H^+}} = 1.00)\ \|\mathrm{Zn^{2+}}\ (aq, a_{\mathrm{Zn^{2+}}} = x)\ |\mathrm{Zn}(s) \tag{13.2.3.6}$$

where x is the activity of Zn^{2+} in its half-cell. For example, when $a_{\mathrm{Zn^{2+}}} = 1.00$, the potential of the electrochemical cell is $-0.763\mathrm{V}$. If we find that the potential for the electrochemical cell

$$\mathrm{Zn}(s)|\mathrm{Zn^{2+}}(aq, a_{\mathrm{Zn^{2+}}} = 1.00)\|\mathrm{Ag^+}(aq, a_{\mathrm{Ag^+}} = 1.00)|\mathrm{Ag}(s)$$

is +1.562 V, then knowing that

$$E_{cell} = E_{\mathrm{Ag^+/Ag}} - E_{\mathrm{Zn^{2+}/Zn}} = E_{\mathrm{Ag^+/Ag}} - (-0.763\mathrm{V})$$

gives $E_{\mathrm{Ag^+/Ag}} = +0.799$. In this way, we can build tables of potentials for individual half-reactions.

Sign Convention for Electrode Potentials

In Section 22.2 we noted the following relationship between an electrochemical potential, E, and the Gibbs free energy, ΔG

$$\Delta G = -nFE \tag{13.2.3.7}$$

which tells us that a positive potential corresponds to a thermodynamically favorable reaction. Knowing that the potential for the electrochemical cell in Equation 13.2.3.6 is $-0.763\mathrm{V}$ tells us that the reduction of $Zn^{2+}(aq)$ to $Zn(s)$ is not thermodynamically favorable relative to the reduction of $H^+(aq)$ to $H_2(g)$; that is, we do not expect the reaction

$$\mathrm{Zn^{2+}}(aq) + \mathrm{H_2}(g) \rightleftharpoons 2\mathrm{H^+}(aq) + \mathrm{Zn}(s) \tag{13.2.3.8}$$

to occur; however, with a potential of +0.799 V, we do expect the reaction

$$2\mathrm{Ag^+}(aq) + \mathrm{H_2}(g) \rightleftharpoons 2\mathrm{H^+}(aq) + 2\mathrm{Ag}(s) \tag{13.2.3.9}$$

to occur. Or, looking at this another way, we expect that $Zn(s)$, but not $Ag(s)$, will dissolve in acid.

Effect of Activity on Electrode Potentials

In Chapter 22.2 we wrote the Nernst equation for the reaction

$$\mathrm{Zn}(s) + 2\mathrm{Ag^+}(aq) \rightleftharpoons 2\mathrm{Ag}(s) + \mathrm{Zn^{2+}(aq)} \tag{13.2.3.10}$$

in terms of the concentrations of $Zn^{2+}(aq)$ and $Ag^+(aq)$

$$E = E^\circ - \frac{0.05916}{2}\log\frac{\left[\mathrm{Zn^{2+}}\right]}{\left[\mathrm{Ag^+}\right]^2} \tag{13.2.3.11}$$

Although there are times when we will write the Nernst equation in terms of concentrations, thermodynamic functions are more correctly written in terms of the activities of ions. Under ideal conditions, individual ions and molecules of gases behave as independent particles. When this is true, then an ion's activity and concentration are equal and we can write the Nernst equation using concentrations; under other conditions, then the Nernst equation is more correctly written in terms of activities

$$E = E^\circ - \frac{0.05916}{2}\log\frac{a_{\mathrm{Zn^{2+}}}}{\left(a_{\mathrm{Ag^+}}\right)^2} \tag{13.2.3.12}$$

where $a_{\mathrm{Zn^{2+}}}$ and $a_{\mathrm{Ag^+}}$ are the activities of Zn^{2+} and Ag^+. Equation 13.2.3.12 shows us how the potential changes as the activities of Zn^{2+} and Ag^+ change.

> If you are not familiar with activity, or need a reminder on the relationship between activity and concentration, then see the appendix in Chapter 35.7, which explains what activity is, why it is important to make a distinction between activity and concentration, and when it is reasonable to use concentrations in place of activities.

The Standard Electrode Potential E°

The standard electrode potential, E°, for a half-reaction is the potential when all species are present at unit activity or, for gases, unit fugacity. Its value is independent of how we choose to write the half-reaction; that is, the standard state potential for the reduction of $Ag^+(aq)$ to $Ag(s)$, which is the cathode in the electrochemical cell in Figure 22.1.1, is +0.799 V whether we write the half-reacation as

$$Ag^+(aq) + e^- \rightleftharpoons Ag(s) \tag{13.2.3.13}$$

or as

$$2Ag^+(aq) + e^- \rightleftharpoons 2Ag(s) \tag{13.2.3.14}$$

At first glance, this seems counterintuitive; however, if we calculate the potential when the activity of Ag+ is 0.50 we get

$$E = E^\circ - \frac{0.05916}{1}\log\frac{1}{a_{Ag^+}} = 0.799 - \frac{0.05916}{1}\log\frac{1}{0.50} = 0.781\text{V}$$

when using reaction 13.2.3.13, and

$$E = E^\circ - \frac{0.05916}{2}\log\frac{1}{(a_{Ag^+})^2} = 0.799 - \frac{0.05916}{2}\log\frac{1}{0.50^2} = 0.781\text{V}$$

The appendix in Chapter 35.8 provides a table of standard state reduction potentials for a wide variety of half-reactions at 298 K.

Some Limitations to the Use of Standard Electrode Potentials

Although standard electrode potentials are valuable, they are several important limitations to their use, which we outline here.

Substitution of Concentration for Activities

One important limitation is that that the Nernst equation is defined in terms of the activity of ions instead of their concentrations. Although it is easy to prepare a solution for which the concentration of Na^+ is 0.100 M using NaCl—just weigh out 5.844 g of NaCl and dissolve in 1.00 L of water—it is much more challenging to prepare a solution for which the activity of Na^+ is 0.100. For this reason, in calculations we usually substitute concentrations for activities when using the Nernst equation. This simplification generally is okay for dilute solutions where the difference between activities and concentrations are small.

Effect of Other Equilibrium Reactions

A standard state potential tells us about the equilibrium position of a redox half-reaction reaction under standard state conditions. If one or more of the species in the half-reaction are involved in other equilibrium reactions, then these reactions will affect the value of the standard potential. For example, Fe^{2+} and Fe^{3+} form a variety of metal-ligand complexes with Cl^- which explains why $E^\circ_{Fe^{3+}/Fe^{2+}}$ is 0.771 in the absence of chloride ion, but is 0.70 in 1 M HCl.

Formal Potentials

One way to compensate for using concentrations and partial pressures in place of activities and fugacities, and to compensate for other equilibrium reactions, is to replace the standard state potentials, E° with a formal potential, $E^{\circ\prime}$, that is measured using concentrations of 1.00 for ions, partial pressures of 1.00 for gases, and for a specific concentration of other reagents. The table below, which is adapted from the appendix in Chapter 35.8, provides formal potentials for Fe^{3+}/Fe^{2+} half-reaction in five different solvents.

iron	E° (V)	$E^{\circ\prime}$ (V)
$Fe^{3+} + e^- \rightleftharpoons Fe^{2+}$	0.771	0.70 in 1 M HCl 0.767 in 1 M $HClO_4$ 0.746 in 1 M HNO_3 0.68 in 1 M H_2SO_4 0.44 in 0.3 M H_3PO_4

Reaction Rates

The reduction of Fe^{3+} to Fe^{2+} consumes an electron, which is drawn from the electrode. The oxidation of another species, perhaps the solvent, at a second electrode is the source of this electron. Because the reduction of Fe^{3+} to Fe^{2+} consumes one electron, the flow of electrons between the electrodes—in other words, the current—is a measure of the rate at which Fe^{3+} is reduced. One important consequence of this observation is that the current is zero when the reaction $\mathrm{Fe}^{3+}(aq) \rightleftharpoons \mathrm{Fe}^{2+}(aq) + e^-$ is at equilibrium. If redox half-reaction cannot maintain an equilibrium because the reaction in one direction is too slow, then we cannot measure a meaningful standard state potential.

This page titled 13.2.3: Electrode Potentials is shared under a CC BY-NC-SA 4.0 license and was authored, remixed, and/or curated by David Harvey.

- **22.3: Electrode Potentials** by David Harvey is licensed CC BY-NC-SA 4.0.

13.2.4: Calculation of Cell Potentials from Electrode Potentials

The potential of an electrochemical cell is the difference between the electrode potentials of the cathode and the anode

$$E_{\text{cell}} = E_{\text{cathode}} - E_{\text{anode}} \tag{13.2.4.1}$$

where E_{cathode} and E_{anode} are both reduction potentials. Given a set of conditions, we can use the Nernst equation to calculate the cell potential, as shown by the following example.

Example 13.2.4.1

Calculate (a) the standard state potential and (b) the potential when [Ag^+] = 0.0020 M and [Cd^{2+}] = 0.0050 M, for the following reaction at 25°C.

$$\text{Cd}(s) + 2\text{Ag}^+(aq) \rightleftharpoons 2\text{Ag}(s) + \text{Cd}^{2+}(aq)$$

For part (b), calculate the potential twice, once using concentrations and once using activities assuming that the solution's ionic strength is 0.100.

Solution

(a) In this reaction Cd is oxidized at the anode and Ag^+ is reduced at the cathode. Using standard state electrode potentials from Appendix 3, we find that the standard state potential is

$$E^\circ = E^\circ_{\text{Ag}^+/\text{Ag}} - E^\circ_{\text{Cd}^{2+}/\text{Cd}} = 0.7996 - (-0.4030) = 1.2026 \text{ V}$$

(b) To calculate the potential when [Ag^+] is 0.0020 M and [Cd^{2+}] is 0.0050 M, we use the appropriate relationship for the reaction quotient, Q_r, when writing the Nernst equation

$$E = E^\circ - \frac{0.05916 \text{ V}}{n} \log \frac{[\text{Cd}^{2+}]}{[\text{Ag}^+]^2}$$

$$E = 1.2026 \text{ V} - \frac{0.05916 \text{ V}}{2} \log \frac{0.050}{(0.020)^2} = 1.14 \text{ V}$$

To calculate the potential using activities, we first calculate the activity coefficients for Cd^{2+} and Ag^+. Following the approach outlined in the appendix in Chapter 35.7 gives

$$\log \gamma_{\text{Cd}^{2+}} = \frac{-0.51 \times (+2)^2 \times \sqrt{0.100}}{1 + 3.3 \times 0.50 \times \sqrt{0.100}} = -0.2078$$

$$]log\gamma_{\text{Ag}^+} = \frac{-0.51 \times (+1)^2 \times \sqrt{0.100}}{1 + 3.3 \times 0.25 \times \sqrt{0.100}} = -0.1279$$

$$a_{\text{Cd}^{2+}} = \gamma_{\text{Cd}^{2+}} \times [\text{Cd}^{2+}] = 0.6197 \times 0.0050 = 0.003098$$

$$a_{\text{Ag}^+} = \gamma_{\text{Ag}^+} \times [\text{Ag}^+] = 7449 \times 0.0020 = 0.00149$$

Finally, we substitute activities for concentrations in the Nernst equation to arrive at a potential of

$$E = 1.2026 \text{ V} - \frac{0.05916 \text{ V}}{2} \log \frac{0.003098}{(0.00149)^2} = 1.11 \text{ V}$$

This page titled 13.2.4: Calculation of Cell Potentials from Electrode Potentials is shared under a CC BY-NC-SA 4.0 license and was authored, remixed, and/or curated by David Harvey.

- **22.4: Calculation of Cell Potentials from Electrode Potentials** by David Harvey is licensed CC BY-NC-SA 4.0.

13.2.5: Currents in Electrochemical Cells

Most electrochemical techniques rely on either controlling the current and measuring the resulting potential, or controlling the potential and measuring the resulting current; only potentiometry (see Chapter 23) measures a potential under conditions where there is essentially no current. Understanding the relationship between current, *i*, and potential, *E*, is important. Although we learned in Sections 22.3 and 22.4 how to calculated electrode potentials and cell potentials using the Nernst equation, the experimentally measured potentials may differ from their thermodynamic values for a variety of reasons that we outline here.

iR drop

The movement of an electrical charge in an electrochemical cell generates a potential, E_{ir} defined by Ohm's law

$$E_{ir} = iR \tag{13.2.5.1}$$

where *i* is the current and *R* is the solution's resistance. To account for this, we can include an additional term to the equation for the electrochemical cell's potential

$$E_{\text{cell}} = E_{\text{cathode}} - E_{\text{anode}} - E_{ir} = E_{\text{Nernst}} - iR \tag{13.2.5.2}$$

where E_{Nernst} is the potential from the Nernst equation. The resulting decease in the potential from its idealized value is called the *iR* drop.

Polarization

Equation 13.2.5.2indicates that we expect a linear relationship between an electrochemical cell's potential, E_{cell}. When this is not the case, the electrochemical cell is said to be polarized. There are several sources that contribute to polarization, which we consider in this section; first, however, we define ideal polarized and nonpolarized electrodes.

Ideal Polarized and Nonpolarized Electrodes and Electrochemical Cells

An ideal polarized electrode is one in which a change in potential over a fairly wide range has no effect on the current that flows through the electrode, as we see in Figure $13.2.5.1a$for the range of potentials defined by the solid green line. Such electrodes are useful because they do not themselves undergo oxidation or reduction—they are electrochemically inert—which makes them a good choice for studying the electrochemical behavior of other species.

An ideal nonpolarized electrode is one in which a change in current has no effect on the electrode's potential, as we see in Figure $13.2.5.1b$between the limits defined by the solid red line with deviations shown by the dashed red line. Such electrodes are useful because the provided a stable potential against which we can reference the redox potential of other species.

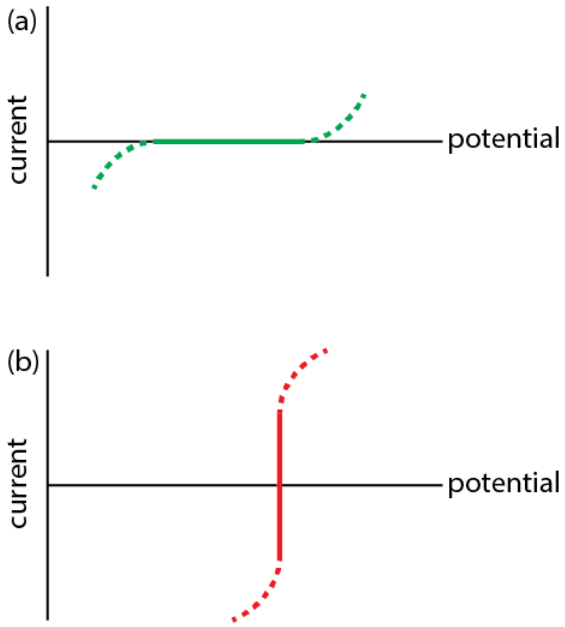


Figure 13.2.5.1: Current-potential curves for (a) an ideal polarized electrode and for (b) an ideal nonpolarized electrode. For both, the solid line shows the range of (a) potentials or (b) currents where the electrode shows ideal behavior.

Overpotential

The magnitude of polarization when drawing a current is called the overpotential, η and expressed as the difference between the applied potential, E, and the potential from the Nernst equation.

$$\eta = E - E_{\text{Nernst}} \tag{13.2.5.3}$$

The overpotential can be subdivided into a variety of sources, a few of which are discussed below.

Concentration Polarization

The reduction of Fe^{3+} to Fe^{2+} in an electrochemical cell consumes an electron, which is drawn from the electrode. The oxidation of another species, perhaps the solvent, at a second electrode is the source of this electron. Because the reduction of Fe^{3+} to Fe^{2+} consumes one electron, the flow of electrons between the electrodes—in other words, the current—is a measure of the rate at which Fe^{3+} is reduced.

> The rate of the reaction $\mathrm{Fe}^{3+}(aq) \rightleftharpoons \mathrm{Fe}^{2+}(aq) + e^-$ is the change in the concentration of Fe^{3+} as a function of time.

In order for the reduction of Fe^{3+} to Fe^{2+} to take place, Fe^{3+} must move from the bulk solution into the layer of solution immediately adjacent to the electrode and then diffuse to the electrode's surface; this is called the diffusion layer. Once the reduction takes place, the Fe^{2+} produced must diffuse away from the electrode's surface and enter into the bulk solution. These two processes are called mass transfer and if we try to change the electrode's potential too quickly, mass transfer may result in concentrations of Fe^{3+} to Fe^{2+} at the electrode's surface that are different from that in bulk solution, resulting in concentration polarization.

Let's use the reduction of Fe^{3+} to Fe^{2+} at the cathode of a galvanic cell to think though how concentration polarization affects the potential we measure. From the Nernst equation we know that

$$E = E^\circ_{\mathrm{Fe}^{3+}/\mathrm{Fe}^{2+}} - \frac{0.05916}{1}\log\frac{[\mathrm{Fe}^{2+}]}{[\mathrm{Fe}^{3+}]} = +0.771 - \frac{0.05916}{1}\log\frac{[\mathrm{Fe}^{2+}]}{[\mathrm{Fe}^{3+}]} \tag{13.2.5.4}$$

If the mass transfer of Fe^{3+} from bulk solution to the electrode's surface is slow and if mass transfer of Fe^{2+} from the electrode's surface to bulk solution is slow, then the concentration of Fe^{3+} at the electrode's surface is smaller than in bulk solution and the concentration of Fe^{2+} at the electrode's surface is greater than in the bulk solution. As a result, the ratio $\frac{[\mathrm{Fe}^{2+}]}{[\mathrm{Fe}^{3+}]}$ is greater than that

predicted by the bulk concentrations of Fe^{3+} and Fe^{2+} and the potential of the cathode is smaller (less positive) than the value +0.771 V predicted by the bulk concentrations of Fe^{3+} and Fe^{2+}. The resulting potential of the electrochemical cell

$$E_{\text{cell}} = E_{\text{cathode}} - E_{\text{anode}} \tag{13.2.5.5}$$

is less positive than that predicted by the bulk concentrations of Fe^{3+} and Fe^{2+} due to this concentration polarization.

Other kinetic processes can contribute to polarization, including the rate of chemical reactions that take place within the layer of solution near the electrode's surface, the kinetics of reactions in which the electroactive species absorb or desorb from the electrode's surface, and the kinetics of the electron transfer process itself. More details on these are included in later chapters covering specific electrochemical techniques.

This page titled 13.2.5: Currents in Electrochemical Cells is shared under a CC BY-NC-SA 4.0 license and was authored, remixed, and/or curated by David Harvey.

- **22.5: Currents in Electrochemical Cells** by David Harvey is licensed CC BY-NC-SA 4.0.

13.2.6: Types of Electroanalytical Methods

In the next three chapters we will consider a variety of different interfacial electrochemical experiments; that is, experiments in which the redox reaction takes place at the surface of an electrode. Because electrochemistry is such a broad field, let's use Figure 13.2.6.1to organize these techniques by the experimental conditions we choose to use (Do we control the potential or the current? How do we change the applied potential or applied current? Do we stir the solution?) and the analytical signal we decide to measure (Current? Potential?).

At the first level, we divide electrochemical techniques into static techniques and dynamic techniques. In a static technique we do not allow current to pass through the electrochemical cell and, as a result, the concentrations of all species remain constant. Potentiometry, in which we measure the potential of an electrochemical cell under static conditions, is one of the most important quantitative electrochemical methods and is discussed in Chapter 23.

Dynamic techniques, in which we allow current to flow and force a change in the concentration of species in the electrochemical cell, comprise the largest group of interfacial electrochemical techniques. Coulometry, in which we measure current as a function of time, is covered Chapter 24. Voltammetry and amperometry, in which we measure current as a function of a fixed or variable potential, are the subjects of Chapter 25.

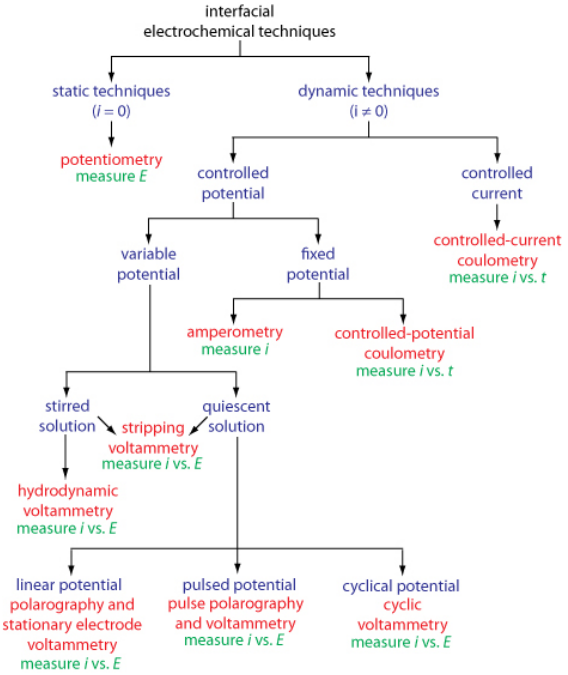


Figure 13.2.6.1: Family tree that highlights the similarities and differences between a number of interfacial electrochemical techniques. The specific instrumental methods are shown in red, the experimental conditions are shown in blue, and the analytical signals are in green.

This page titled 13.2.6: Types of Electroanalytical Methods is shared under a CC BY-NC-SA 4.0 license and was authored, remixed, and/or curated by David Harvey.

- **22.6: Types of Electroanalytical Methods** by David Harvey is licensed CC BY-NC-SA 4.0.

SECTION OVERVIEW

13.3: Potentiometry

In potentiometry we measure the potential of an electrochemical cell under static conditions. Because no current—or only a negligible current—flows through the electrochemical cell, its composition remains unchanged. For this reason, potentiometry is a useful quantitative method of analysis. The first quantitative potentiometric applications appeared soon after the formulation, in 1889, of the Nernst equation, which relates an electrochemical cell's potential to the concentration of electroactive species in the cell [Stork, J. T. *Anal. Chem.* **1993**, *65*, 344A–351A].

Potentiometry initially was restricted to redox equilibria at metallic electrodes, which limited its application to a few ions. In 1906, Cremer discovered that the potential difference across a thin glass membrane is a function of pH when opposite sides of the membrane are in contact with solutions that have different concentrations of H_3O^+. This discovery led to the development of the glass pH electrode in 1909. Other types of membranes also yield useful potentials. For example, in 1937 Kolthoff and Sanders showed that a pellet of AgCl can be used to determine the concentration of Ag^+. Electrodes based on membrane potentials are called ion-selective electrodes, and their continued development extends potentiometry to a diverse array of analytes.

13.3.1: Standard Electrodes

13.3.2: Standard Potentials

13.3.3: Reference Electrodes

13.3.4: Metallic Indicator Electrodes

13.3.5: Membrane Ion-Selective Electrodes

13.3.6: Molecular-Selective Electrode Systems

13.3.7: Quantitative Potentiometry

This page titled 13.3: Potentiometry is shared under a CC BY-NC-SA 4.0 license and was authored, remixed, and/or curated by David Harvey.

13.3.1: Standard Electrodes

An electrode by definition is a point where current enters and leaves the electrolyte. When the current leaves the electrodes it is known as the cathode and when the current enters it is known as the anode. Electrodes are vital components of electrochemical cells. They transport produced electrons from one half-cell to another, which produce an electrical charge. This charge is based off a standard electrode system (SHE) with a reference potential of 0 volts and serves as a medium for any cell potential calculation.

What are the mechanics of an electrode?

What processes are going on?

An electrode is a metal whose surface serves as the location where oxidation-reduction equilibrium is established between the metal and what is in the solution. The electrode can either be an anode or a cathode. An anode receives current or electrons from the electrolyte mixture, thus becoming oxidized. When the atoms or molecules get close enough to the surface of the electrode, the solution in which the electrode is placed into, donates electrons. This causes the atoms/molecules to become positive ions.



The opposite occurs with the cathode. Here the electrons are released from the electrode and the solution around it is reduced.

What is an electrode made of?

An electrode has to be a good electrical conductor so it is usually a metal. Now what this metal is made out of is dependent on whether or not it is involved in the reaction. Some reactions require an inert electrode that does not participate. An example of this would be platinum in the SHE reaction(described later). While other reactions utilize solid forms of the reactants, making them the electrodes. An example of this type of cell would be:

(left side is the anode) $Cu(s)|Cu(NO_3)_2(aq)$ (0.1M)$||AgNO_3(aq)$ (.01M)$|Ag(s)$ (right side is cathode)

(In the above cell set up: the outside components are the electrodes for the reaction while the inner parts are the solutions they are immersed in)

Here you can see that a solid form of the reactant, copper, is used. The copper, as well as the silver, are participating as reactants and electrodes.

Examples of Electrodes

Some commonly used inert electrodes: graphite(carbon), platinum, gold, and rhodium.

Some commonly used reactive (or involved) electrodes: copper, zinc, lead, and silver.

Standard Hydrogen Electrode

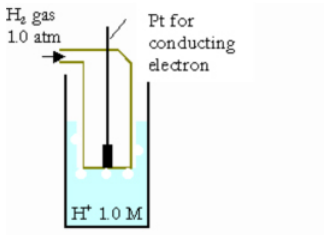
A Standard Hydrogen Electrode (SHE) is an electrode that scientists use for reference on all half-cell potential reactions. The value of the standard electrode potential is zero, which forms the basis one needs to calculate cell potentials using different electrodes or different concentrations. It is important to have this common reference electrode just as it is important for the International Bureau of Weights and Measures to keep a sealed piece of metal that is used to reference the S.I. Kilogram.

What is a SHE made of?

SHE is composed of a 1.0 M $H^+(aq)$ solution containing a square piece of platinized platinum (connected to a platinum wire where electrons can be exchanged) inside a tube. During the reaction, hydrogen gas is then passed through the tube and into the solution

causing the reaction:

$$2H^+(aq) + 2e^- <==> H_2(g).$$



Standard Hydrogen Electrode (SHE)

Platinum is used because it is inert and does not react much with hydrogen.

What is going on in this process?

First an initial discharge allows electrons to fill into the highest occupied energy level of Pt. As this is done, some of the H+ ions form H_3O^+ ions with the water molecules in the solution. These hydrogen and hydronium ions then get close enough to the Pt electrode (on the platinized surface of this electrode) to where a hydrogen is attracted to the electrons in the metal and forms a hydrogen atom. Then these combine with other hydrogen atoms to create H2(g). This hydrogen gas is released from the system. In order to keep the reaction going, the electrode requires a constant flow of H_2(g). The Pt wire is connected to a similar electrode in which the opposite process is occurring, thus producing a charge that is referenced at 0 volts. Other standard electrodes are usually preferred because the SHE can be a difficult electrode to set up. The difficulty arises in the preparation of the platinized surface and in controlling the concentration of the reactants. For this reason the SHE is referred to as a hypothetical electrode.

Three Electrode System

The three electrode system is made up of the working electrode, reference electrode, and the auxiliary electrode. The three electrode system is important in voltammetry. All three of these electrodes serve a unique roll in the three electrode system. A reference electrode refers to an electrode that has an established electrode potential. In an electrochemical cell, the reference electrode can be used as a half cell. When the reference electrode acts as a half cell, the other half cell's electrode potential can be discovered. An auxiliary electrode is an electrode makes sure that current does not pass through the reference cell. It makes sure the current is equal to that of the working electrode's current. The working electrode is the electrode that transports electrons to and from the substances that are present. Some examples of reference cells include:

Calomel electrode: This reference electrode consists of a mercury and mercury-chloride molecules. This electrode can be relatively easier to make and maintain compared to the SHE. It is composed of a solid paste of Hg_2Cl_2 and liquid elemental mercury attached to a rod that is immersed in a saturated KCl solution. It is necessary to have the solution saturated because this allows for the activity to be fixed by the potassium chloride and the voltage to be lower and closer to the SHE. This saturated solution allows for the exchange of chlorine ions to take place. All this is usually placed inside a tube that has a porous salt bridge to allow the electrons to flow back through and complete the circuit.

$$\frac{1}{2}Hg_2Cl_{2(s)} + e- \rightleftharpoons Hg_{(l)} + Cl^-_{(aq)}$$

Silver-Silver Chloride electrode: An electrode of this sort precipitates a salt in the solution that participates in the electrode reaction. This electrode consists, of solid silver and its precipitated salt AgCl. This a widely used reference electrode because it is inexpensive and not as toxic as the Calomel electrode that contains mercury. A Silver-Silver Chloride electrode is made by taking a wire of solid silver and coding it in AgCl. Then it is placed in a tube of KCl and AgCl solution. This allows ions to be formed (and the opposite) as electrons flow in and out of the electrode system.

$$AgCl_{(s)} + e^- \rightleftharpoons Ag^+_{(aq)} + Cl^-_{(aq)}$$

References

1. Ives, David J. G., and George John. Janz. "2. The Hydrogen Electrode." *Reference Electrodes.*New York [usw.]: Acad. Pr., 1961. Print.

2. Allmand, A., and Harold Johann Thomas. Ellingham. "Chapter 4: The Electrolysis Bath." *The Principles of Applied Electrochemistry,*. New York: Longmans, Green, 1924. Print
3. The Standard Hydrogen Electrode: A misrepresented concept, http://pubs.acs.org/doi/pdf/10.1021/ed050p604

Problems

1. Which electrode oxidizes the solution in the half-cell? Anode or Cathode?

2. Why is the Standard Hydrogen Electrode important to calculating cell potentials?

3. Identify the which side is the cathode and which side is the anode.

Ag(s) | Ag+(aq)(.5M) || Ag^{+}(aq) (.05M) | Ag(s)

4. Why is it important to use an inert electrode in situations like the SHE?

5. What is the standard half cell potential for the SHE?

Answers (highlight to see):

1.

2.

3.

4.

5.

Contributors and Attributions

- Michael Devengenzo (UCD)

13.3.1: Standard Electrodes is shared under a CC BY-NC-SA 4.0 license and was authored, remixed, and/or curated by LibreTexts.

- **Standard Electrodes** is licensed CC BY-NC-SA 4.0.

13.3.2: Standard Potentials

Learning Objectives

- To use redox potentials to predict whether a reaction is spontaneous.
- To balance redox reactions using half-reactions.

In a galvanic cell, current is produced when electrons flow externally through the circuit from the anode to the cathode because of a difference in potential energy between the two electrodes in the electrochemical cell. In the Zn/Cu system, the valence electrons in zinc have a substantially higher potential energy than the valence electrons in copper because of shielding of the s electrons of zinc by the electrons in filled d orbitals. Hence electrons flow spontaneously from zinc to copper(II) ions, forming zinc(II) ions and metallic copper. Just like water flowing spontaneously downhill, which can be made to do work by forcing a waterwheel, the flow of electrons from a higher potential energy to a lower one can also be harnessed to perform work.

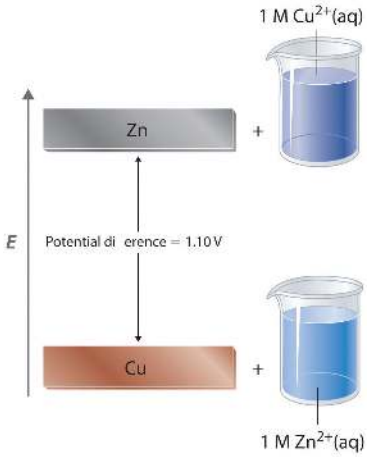


Figure 13.3.2.1: Potential Energy Difference in the Zn/Cu System. The potential energy of a system consisting of metallic Zn and aqueous Cu^{2+} ions is greater than the potential energy of a system consisting of metallic Cu and aqueous Zn^{2+} ions. Much of this potential energy difference is because the valence electrons of metallic Zn are higher in energy than the valence electrons of metallic Cu. Because the Zn(s) + Cu^{2+}(aq) system is higher in energy by 1.10 V than the Cu(s) + Zn^{2+}(aq) system, energy is released when electrons are transferred from Zn to Cu^{2+} to form Cu and Zn^{2+}.

Because the potential energy of valence electrons differs greatly from one substance to another, the voltage of a galvanic cell depends partly on the identity of the reacting substances. If we construct a galvanic cell similar to the one in part (a) in Figure 19.3 but instead of copper use a strip of cobalt metal and 1 M Co^{2+} in the cathode compartment, the measured voltage is not 1.10 V but 0.51 V. Thus we can conclude that the difference in potential energy between the valence electrons of cobalt and zinc is less than the difference between the valence electrons of copper and zinc by 0.59 V.

The measured potential of a cell also depends strongly on the concentrations of the reacting species and the temperature of the system. To develop a scale of relative potentials that will allow us to predict the direction of an electrochemical reaction and the magnitude of the driving force for the reaction, the potentials for oxidations and reductions of different substances must be measured under comparable conditions. To do this, chemists use the **standard cell potential** ($E°_{cell}$), defined as the potential of a cell measured under standard conditions—that is, with all species in their standard states (1 M for solutions,Concentrated solutions of salts (about 1 M) generally do not exhibit ideal behavior, and the actual standard state corresponds to an activity of 1 rather than a concentration of 1 M. Corrections for nonideal behavior are important for precise quantitative work but not for the more qualitative approach that we are taking here. 1 atm for gases, pure solids or pure liquids for other substances) and at a fixed temperature, usually 25°C.

Note

Measured redox potentials depend on the potential energy of valence electrons, the concentrations of the species in the reaction, and the temperature of the system.

Measuring Standard Electrode Potentials

It is physically impossible to measure the potential of a single electrode: only the difference between the potentials of two electrodes can be measured. (This is analogous to measuring absolute enthalpies or free energies. Recall that only differences in enthalpy and free energy can be measured.) We can, however, compare the standard cell potentials for two different galvanic cells that have one kind of electrode in common. This allows us to measure the potential difference between two dissimilar electrodes. For example, the measured standard cell potential (E°) for the Zn/Cu system is 1.10 V, whereas E° for the corresponding Zn/Co system is 0.51 V. This implies that the potential difference between the Co and Cu electrodes is 1.10 V − 0.51 V = 0.59 V. In fact, that is exactly the potential measured under standard conditions if a cell is constructed with the following cell diagram:

$$Co_{(s)} \mid Co^{2+}(aq, 1M) \parallel Cu^{2+}(aq, 1M) \mid Cu(s) \qquad E^\circ = 0.59\ V \tag{13.3.2.1}$$

This cell diagram corresponds to the oxidation of a cobalt anode and the reduction of Cu^{2+} in solution at the copper cathode.

All tabulated values of standard electrode potentials by convention are listed for a reaction written as a reduction, not as an oxidation, to be able to compare standard potentials for different substances (Table P1). The standard cell potential ($E°_{cell}$) is therefore the difference between the tabulated reduction potentials of the two half-reactions, not their sum:

$$E^\circ_{cell} = E^\circ_{cathode} - E^\circ_{anode} \tag{13.3.2.2}$$

In contrast, recall that half-reactions are written to show the reduction and oxidation reactions that actually occur in the cell, so the overall cell reaction is written as the sum of the two half-reactions. According to Equation 13.3.2.2, when we know the standard potential for any single half-reaction, we can obtain the value of the standard potential of many other half-reactions by measuring the standard potential of the corresponding cell.

Note

The overall cell reaction is the sum of the two half-reactions, but the cell potential is the difference between the reduction potentials:

$$E^\circ_{cell} = E^\circ_{cathode} - E^\circ_{anode} \tag{13.3.2.3}$$

Although it is impossible to measure the potential of any electrode directly, we can choose a reference electrode whose potential is defined as 0 V under standard conditions. The **standard hydrogen electrode (SHE)** is universally used for this purpose and is assigned a standard potential of 0 V. It consists of a strip of platinum wire in contact with an aqueous solution containing 1 M H^+. The $[H^+]$ in solution is in equilibrium with H_2 gas at a pressure of 1 atm at the Pt-solution interface (Figure 13.3.2.2). Protons are reduced or hydrogen molecules are oxidized at the Pt surface according to the following equation:

$$2H^+_{(aq)} + 2e^- \rightleftharpoons H_{2(g)} \tag{13.3.2.4}$$

One especially attractive feature of the SHE is that the Pt metal electrode is not consumed during the reaction.

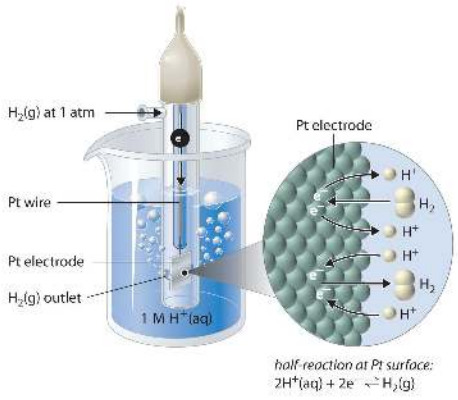


Figure 13.3.2.2: The Standard Hydrogen Electrode. The SHE consists of platinum wire that is connected to a Pt surface in contact with an aqueous solution containing 1 M H^+ in equilibrium with H_2 gas at a pressure of 1 atm. In the molecular view, the Pt surface catalyzes the oxidation of hydrogen molecules to protons or the reduction of protons to hydrogen gas. (Water is omitted for clarity.) The standard potential of the SHE is arbitrarily assigned a value of 0 V.

Figure 13.3.2.3shows a galvanic cell that consists of a SHE in one beaker and a Zn strip in another beaker containing a solution of Zn^{2+} ions. When the circuit is closed, the voltmeter indicates a potential of 0.76 V. The zinc electrode begins to dissolve to form Zn^{2+}, and H^+ ions are reduced to H_2 in the other compartment. Thus the hydrogen electrode is the cathode, and the zinc electrode is the anode. The diagram for this galvanic cell is as follows:

$$Zn_{(s)} \mid Zn^{2+}_{(aq)} \parallel H^+(aq, 1M) \mid H_2(g, 1atm) \mid Pt_{(s)} \tag{13.3.2.5}$$

The half-reactions that actually occur in the cell and their corresponding electrode potentials are as follows:

- cathode:

$$2H^+_{(aq)} + 2e^- \rightarrow H_{2(g)} \qquad E^\circ{}_{cathode} = 0V \tag{13.3.2.6}$$

- anode:

$$Zn_{(s)} \rightarrow Zn^{2+}_{(aq)} + 2e^- \qquad E^\circ{}_{anode} = -0.76\ V \tag{13.3.2.7}$$

- overall:

$$Zn_{(s)} + 2H^+_{(aq)} \rightarrow Zn^{2+}_{(aq)} + H_{2(g)} \tag{13.3.2.8}$$

$$E^\circ{}_{cell} = E^\circ{}_{cathode} - E^\circ{}_{anode} = 0.76\ V \tag{13.3.2.9}$$

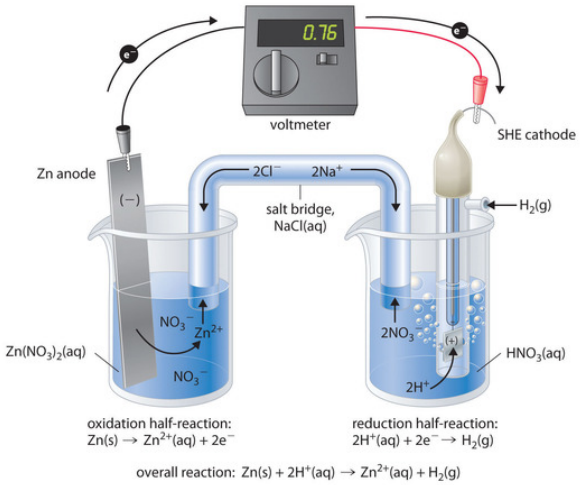


Figure 13.3.2.3: Determining a Standard Electrode Potential Using a Standard Hydrogen Electrode. The voltmeter shows that the standard cell potential of a galvanic cell consisting of a SHE and a Zn/Zn^{2+} couple is $E°_{cell}$ = 0.76 V. Because the zinc electrode in this cell dissolves spontaneously to form $Zn^{2+}(aq)$ ions while $H^+(aq)$ ions are reduced to H_2 at the platinum surface, the standard electrode potential of the Zn^{2+}/Zn couple is −0.76 V.

Although the reaction at the anode is an oxidation, by convention its tabulated E° value is reported as a reduction potential. The potential of a half-reaction measured against the SHE under standard conditions is called the **standard electrode potential** for that half-reaction.In this example, the standard reduction potential for $Zn^{2+}(aq) + 2e^- \rightarrow Zn(s)$ is −0.76 V, which means that the standard electrode potential for the reaction that occurs at the anode, the oxidation of Zn to Zn^{2+}, often called the Zn/Zn^{2+} redox couple, or the Zn/Zn^{2+} couple, is −(−0.76 V) = 0.76 V. We must therefore subtract $E°_{anode}$ from $E°_{cathode}$ to obtain $E°_{cell}$: 0 − (−0.76 V) = 0.76 V.

Because electrical potential is the energy needed to move a charged particle in an electric field, standard electrode potentials for half-reactions are intensive properties and do not depend on the amount of substance involved. Consequently, E° values are independent of the stoichiometric coefficients for the half-reaction, and, most important, the coefficients used to produce a balanced overall reaction do not affect the value of the cell potential.

Note

E° values do **NOT** depend on the stoichiometric coefficients for a half-reaction, because it is an *intensive* property.

Standard Electrode Potentials

To measure the potential of the Cu/Cu^{2+} couple, we can construct a galvanic cell analogous to the one shown in Figure 13.3.2.3 but containing a Cu/Cu^{2+} couple in the sample compartment instead of Zn/Zn^{2+}. When we close the circuit this time, the measured potential for the cell is negative (−0.34 V) rather than positive. The negative value of $E°_{cell}$ indicates that the direction of spontaneous electron flow is the opposite of that for the Zn/Zn^{2+} couple. Hence the reactions that occur spontaneously, indicated by a positive $E°_{cell}$, are the reduction of Cu^{2+} to Cu at the copper electrode. The copper electrode gains mass as the reaction proceeds, and H_2 is oxidized to H^+ at the platinum electrode. In this cell, the copper strip is the cathode, and the hydrogen electrode is the anode. The cell diagram therefore is written with the SHE on the left and the Cu^{2+}/Cu couple on the right:

$$Pt_{(s)} \mid H_2(g, 1atm) \mid H^+(aq, 1\ M) \parallel Cu^{2+}(aq, 1M) \mid Cu_{(s)} \tag{13.3.2.10}$$

The half-cell reactions and potentials of the spontaneous reaction are as follows:

- Cathode:

$$Cu^{2+}(aq) + 2e^- \rightarrow Cu_{(g)} \quad E^\circ{}_{cathode} = 0.34\ V \tag{13.3.2.11}$$

- Anode:

$$H_{2(g)} \rightarrow 2H^+_{(aq)} + 2e^- \quad E^\circ{}_{anode} = 0\ V \tag{13.3.2.12}$$

- Overall:

$$H_{2(g)} + Cu^{2+}_{(aq)} \rightarrow 2H^+_{(aq)} + Cu_{(s)} \tag{13.3.2.13}$$

$$E^\circ{}_{cell} = E^\circ{}_{cathode} - E^\circ{}_{anode} = 0.34\ V \tag{13.3.2.14}$$

Thus the standard electrode potential for the Cu^{2+}/Cu couple is 0.34 V.



Electrode Potentials and ECell: https://youtu.be/zeeAXleT1c0

Balancing Redox Reactions Using the Half-Reaction Method

Previously, we described a method for balancing redox reactions using oxidation numbers. Oxidation numbers were assigned to each atom in a redox reaction to identify any changes in the oxidation states. Here we present an alternative approach to balancing redox reactions, the half-reaction method, in which the overall redox reaction is divided into an oxidation half-reaction and a reduction half-reaction, each balanced for mass and charge. This method more closely reflects the events that take place in an electrochemical cell, where the two half-reactions may be physically separated from each other.

We can illustrate how to balance a redox reaction using half-reactions with the reaction that occurs when Drano, a commercial solid drain cleaner, is poured into a clogged drain. Drano contains a mixture of sodium hydroxide and powdered aluminum, which in solution reacts to produce hydrogen gas:

$$Al_{(s)} + OH^-_{(aq)} \rightarrow Al(OH)^-_{4(aq)} + H_{2(g)} \tag{13.3.2.15}$$

In this reaction, $Al_{(s)}$ is oxidized to Al^{3+}, and H^+ in water is reduced to H_2 gas, which bubbles through the solution, agitating it and breaking up the clogs.

The overall redox reaction is composed of a reduction half-reaction and an oxidation half-reaction. From the standard electrode potentials listed Table P1, we find the corresponding half-reactions that describe the reduction of H^+ ions in water to $H_2$and the oxidation of Al to Al^{3+} in basic solution:

- reduction:

$$2H_2O_{(l)} + 2e^- \rightarrow 2OH^-_{(aq)} + H_{2(g)} \tag{13.3.2.16}$$

- oxidation:

$$Al_{(s)} + 4OH^-_{(aq)} \rightarrow Al(OH)^-_{4(aq)} + 3e^- \tag{13.3.2.17}$$

The half-reactions chosen must exactly reflect the reaction conditions, such as the basic conditions shown here. Moreover, the physical states of the reactants and the products must be identical to those given in the overall reaction, whether gaseous, liquid, solid, or in solution.

In Equation 13.3.2.16, two H^+ ions gain one electron each in the reduction; in Equation 13.3.2.17, the aluminum atom loses three electrons in the oxidation. The charges are balanced by multiplying the reduction half-reaction (Equation 13.3.2.16) by 3 and the oxidation half-reaction (Equation 13.3.2.17) by 2 to give the same number of electrons in both half-reactions:

- Adding the two half-reactions,

$$6H_2O_{(l)} + 2Al_{(s)} + 8OH^-_{(aq)} \rightarrow 2Al(OH)^-4(aq) + 3H_{2(g)} + 6OH^-_{(aq)} \tag{13.3.2.18}$$

Simplifying by canceling substances that appear on both sides of the equation,

$$6H_2O_{(l)} + 2Al_{(s)} + 2OH^-_{(aq)} \rightarrow 2Al(OH)^-_{4(aq)} + 3H_{2(g)} \tag{13.3.2.19}$$

We have a −2 charge on the left side of the equation and a −2 charge on the right side. Thus the charges are balanced, but we must also check that atoms are balanced:

$$2Al + 8O + 14H = 2Al + 8O + 14H \tag{13.3.2.20}$$

The atoms also balance, so Equation 13.3.2.19is a balanced chemical equation for the redox reaction depicted in Equation 13.3.2.15.

> **Note**
>
> The half-reaction method requires that half-reactions exactly reflect reaction conditions, and the physical states of the reactants and the products must be identical to those in the overall reaction.

We can also balance a redox reaction by first balancing the atoms in each half-reaction and then balancing the charges. With this alternative method, we do not need to use the half-reactions listed in Table P1 but instead focus on the atoms whose oxidation states change, as illustrated in the following steps:

Step 1: Write the reduction half-reaction and the oxidation half-reaction.

For the reaction shown in Equation 13.3.2.15, hydrogen is reduced from H^+ in OH^- to H_2, and aluminum is oxidized from Al° to Al^{3+}:

- **Step 2:** Balance the atoms by balancing elements other than O and H. Then balance O atoms by adding H_2O and balance H atoms by adding H^+.

  Elements other than O and H in the previous two equations are balanced as written, so we proceed with balancing the O atoms. We can do this by adding water to the appropriate side of each half-reaction:

  - Balancing H atoms by adding H^+, we obtain the following:
    - We have now balanced the atoms in each half-reaction, but the charges are not balanced.

      Step 3: Balance the charges in each half-reaction by adding electrons.

Two electrons are gained in the reduction of H^+ ions to H_2, and three electrons are lost during the oxidation of Al° to Al^{3+}:

- **Step 4:** Multiply the reductive and oxidative half-reactions by appropriate integers to obtain the same number of electrons in both half-reactions.

  In this case, we multiply Equation ??? (the reductive half-reaction) by 3 and Equation ??? (the oxidative half-reaction) by 2 to obtain the same number of electrons in both half-reactions:

  - **Step 5:** Add the two half-reactions and cancel substances that appear on both sides of the equation.

    Adding and, in this case, canceling $8H^+$, $3H_2O$, and $6e^-$,

    $$2Al_{(s)} + 5H_2O_{(l)} + 3OH^-_{(aq)} + H^+_{(aq)} \rightarrow 2Al(OH)^-_{4(aq)} + 3H_{2(g)} \quad (13.3.2.21)$$

    We have three OH^- and one H^+ on the left side. Neutralizing the H^+ gives us a total of $5H_2O + H_2O = 6H_2O$ and leaves $2OH^-$ on the left side:

    $$2Al_{(s)} + 6H_2O_{(l)} + 2OH^-_{(aq)} \rightarrow 2Al(OH)^-_{4(aq)} + 3H_{2(g)} \quad (13.3.2.22)$$

    Step 6: Check to make sure that all atoms and charges are balanced.

    Equation 13.3.2.22 is identical to Equation 13.3.2.19, obtained using the first method, so the charges and numbers of atoms on each side of the equation balance.

Example 13.3.2.1

In acidic solution, the redox reaction of dichromate ion ($Cr_2O^{2-}_7$) and iodide (I^-) can be monitored visually. The yellow dichromate solution reacts with the colorless iodide solution to produce a solution that is deep amber due to the presence of a green $Cr^{3+}_{(aq)}$ complex and brown I_2(aq) ions (Figure 13.3.2.4):

$$Cr_2O^{2-}_{7(aq)} + I^-_{(aq)} \rightarrow Cr^{3+}_{(aq)} + I_{2(aq)} \quad (13.3.2.23)$$

Balance this equation using half-reactions.

Given: redox reaction and Table P1

Asked for: balanced chemical equation using half-reactions

Strategy:

Follow the steps to balance the redox reaction using the half-reaction method.

Solution

From the standard electrode potentials listed in Table P1 we find the half-reactions corresponding to the overall reaction:

- reduction:

$$Cr_2O^{2-}_{7(aq)} + 14H^+_{(aq)} + 6e^- \rightarrow 2Cr^{3+}{}_{(aq)} + 7H_2O_{(l)} \quad (13.3.2.24)$$

- oxidation:

$$2I^-_{(aq)} \rightarrow I_{2(aq)} + 2e^- \quad (13.3.2.25)$$

Balancing the number of electrons by multiplying the oxidation reaction by 3,

- oxidation:

$$6I^-_{(aq)} \rightarrow 3I_{2(aq)} + 6e^- \quad (13.3.2.26)$$

Adding the two half-reactions and canceling electrons,

$$Cr_2O^{2-}_{7(aq)} + 14H^+_{(aq)} + 6I^-_{(aq)} \rightarrow 2Cr^{3+}_{(aq)} + 7H_2O_{(l)} + 3I_{2(aq)} \quad (13.3.2.27)$$

We must now check to make sure the charges and atoms on each side of the equation balance:

$$(-2) + 14 + (-6) = +6$$
$$+6 = +6$$
$$2Cr + 7O + 14H + 6I = 2Cr + 7O + 14H + 6I$$

The charges and atoms balance, so our equation is balanced.

We can also use the alternative procedure, which does not require the half-reactions listed in Table P1.

Step 1: Chromium is reduced from Cr^{6+} in $Cr_2O_7^{2-}$ to Cr^{3+}, and I^- ions are oxidized to I_2. Dividing the reaction into two half-reactions,

- reduction:

$$Cr_2O_{7(aq)}^{2-} \rightarrow Cr_{(aq)}^{3+} \tag{13.3.2.28}$$

- oxidation:

$$I_{(aq)}^{-} \rightarrow I_{2(aq)} \tag{13.3.2.29}$$

Step 2: Balancing the atoms other than oxygen and hydrogen,

- reduction:

$$Cr_2O_{7(aq)}^{2-} \rightarrow 2Cr_{(aq)}^{3+} \tag{13.3.2.30}$$

- oxidation:

$$2I_{(aq)}^{-} \rightarrow I_{2(aq)} \tag{13.3.2.31}$$

We now balance the O atoms by adding H_2O—in this case, to the right side of the reduction half-reaction. Because the oxidation half-reaction does not contain oxygen, it can be ignored in this step.

- reduction:

$$Cr_2O_{7(aq)}^{2-} \rightarrow 2Cr_{(aq)}^{3+} + 7H_2O_{(l)} \tag{13.3.2.32}$$

Next we balance the H atoms by adding H^+ to the left side of the reduction half-reaction. Again, we can ignore the oxidation half-reaction.

- reduction:

$$Cr_2O_{7(aq)}^{2-} + 14H_{(aq)}^{+} \rightarrow 2Cr_{(aq)}^{3+} + 7H_2O_{(l)} \tag{13.3.2.33}$$

Step 3: We must now add electrons to balance the charges. The reduction half-reaction ($2Cr^{+6}$ to $2Cr^{+3}$) has a +12 charge on the left and a +6 charge on the right, so six electrons are needed to balance the charge. The oxidation half-reaction ($2I^-$ to I_2) has a −2 charge on the left side and a 0 charge on the right, so it needs two electrons to balance the charge:

- reduction: $Cr_2O_7^{2-}(aq) + 14H^+(aq) + 6e^- \rightarrow 2Cr^{3+}(aq) + 7H_2O(l)$
- oxidation: $2I^-(aq) \rightarrow I_2(aq) + 2e^-$

Step 4: To have the same number of electrons in both half-reactions, we must multiply the oxidation half-reaction by 3:

- oxidation: $6I^-(aq) \rightarrow 3I_2(s) + 6e^-$

Step 5: Adding the two half-reactions and canceling substances that appear in both reactions,

- $Cr_2O_7^{2-}(aq) + 14H^+(aq) + 6I^-(aq) \rightarrow 2Cr^{3+}(aq) + 7H_2O(l) + 3I_2(aq)$

Step 6: This is the same equation we obtained using the first method. Thus the charges and atoms on each side of the equation balance.

? Exercise 13.3.2.1

Copper is found as the mineral covellite (CuS). The first step in extracting the copper is to dissolve the mineral in nitric acid (HNO_3), which oxidizes sulfide to sulfate and reduces nitric acid to NO:

$$CuS_{(s)} + HNO_{3(aq)} \rightarrow NO_{(g)} + CuSO_{4(aq)} \tag{13.3.2.34}$$

Balance this equation using the half-reaction method.



Figure by Didier Descouens. Image used by permission of Wikipedia

Answer

$$3CuS_{(s)} + 8HNO3(aq) \rightarrow 8NO_{(g)} + 3CuSO_{4(aq)} + 4H_2O_{(l)} \tag{13.3.2.35}$$



Balancing a Redox Reaction in Acidic Conditions: https://youtu.be/IB-fWLsI0lc

Calculating Standard Cell Potentials

The standard cell potential for a redox reaction ($E°_{cell}$) is a measure of the tendency of reactants in their standard states to form products in their standard states; consequently, it is a measure of the driving force for the reaction, which earlier we called voltage. We can use the two standard electrode potentials we found earlier to calculate the standard potential for the Zn/Cu cell represented by the following cell diagram:

$$Zn(s) \mid Zn^{2+}(aq, 1M) \parallel Cu^{2+}(aq, 1M) \mid Cu_{(s)} \tag{13.3.2.36}$$

We know the values of $E°_{anode}$ for the reduction of Zn^{2+} and $E°_{cathode}$ for the reduction of Cu^{2+}, so we can calculate $E°_{cell}$:

$$E^\circ_{cell} = E^\circ_{cathode} - E^\circ_{anode} = 1.10\ V \tag{13.3.2.37}$$

This is the same value that is observed experimentally. If the value of $E°_{cell}$ is positive, the reaction will occur spontaneously as written. If the value of $E°_{cell}$ is negative, then the reaction is not spontaneous, and it will not occur as written under standard conditions; it will, however, proceed spontaneously in the opposite direction. As we shall see, this does not mean that the reaction cannot be made to occur at all under standard conditions. With a sufficient input of electrical energy, virtually any reaction can be forced to occur. Example 4 and its corresponding exercise illustrate how we can use measured cell potentials to calculate standard potentials for redox couples.

Note

A positive $E°_{cell}$ means that the reaction will occur spontaneously as written. A negative $E°_{cell}$ means that the reaction will proceed spontaneously in the opposite direction.

Example 13.3.2.2

A galvanic cell with a measured standard cell potential of 0.27 V is constructed using two beakers connected by a salt bridge. One beaker contains a strip of gallium metal immersed in a 1 M solution of $GaCl_3$, and the other contains a piece of nickel immersed in a 1 M solution of $NiCl_2$. The half-reactions that occur when the compartments are connected are as follows:

$$\text{cathode: } Ni^{2+}(aq) + 2e^- \rightarrow Ni(s)$$

$$\text{anode: } Ga(s) \rightarrow Ga^{3+}(aq) + 3e^-$$

If the potential for the oxidation of Ga to Ga^{3+} is 0.55 V under standard conditions, what is the potential for the oxidation of Ni to Ni^{2+}?

Given: galvanic cell, half-reactions, standard cell potential, and potential for the oxidation half-reaction under standard conditions

Asked for: standard electrode potential of reaction occurring at the cathode

Strategy:

A. Write the equation for the half-reaction that occurs at the anode along with the value of the standard electrode potential for the half-reaction.

B. Use Equation 13.3.2.2to calculate the standard electrode potential for the half-reaction that occurs at the cathode. Then reverse the sign to obtain the potential for the corresponding oxidation half-reaction under standard conditions.

Solution

A We have been given the potential for the oxidation of Ga to Ga^{3+} under standard conditions, but to report the standard electrode potential, we must reverse the sign. For the reduction reaction $Ga^{3+}(aq) + 3e^- \rightarrow Ga(s)$, $E°_{anode} = -0.55$ V.

B Using the value given for $E°_{cell}$ and the calculated value of $E°_{anode}$, we can calculate the standard potential for the reduction of Ni^{2+} to Ni from Equation 13.3.2.2

$$E°_{cell} = E°_{cathode} - E°_{anode}$$
$$0.27 \text{ V} = E°_{cathode} - (-0.55 \text{ V})$$
$$E°_{cathode} = -0.28 \text{ V}$$

This is the standard electrode potential for the reaction $Ni^{2+}(aq) + 2e^- \rightarrow Ni(s)$. Because we are asked for the potential for the oxidation of Ni to Ni^{2+} under standard conditions, we must reverse the sign of $E°_{cathode}$. Thus $E° = -(-0.28 \text{ V}) = 0.28$ V for the oxidation. With three electrons consumed in the reduction and two produced in the oxidation, the overall reaction is not balanced. Recall, however, that standard potentials are independent of stoichiometry.

Exercise 13.3.2.2

A galvanic cell is constructed with one compartment that contains a mercury electrode immersed in a 1 M aqueous solution of mercuric acetate $Hg(CH_3CO_2)_2$ and one compartment that contains a strip of magnesium immersed in a 1 M aqueous solution of $MgCl_2$. When the compartments are connected, a potential of 3.22 V is measured and the following half-reactions occur:

- cathode: $Hg^{2+}(aq) + 2e^- \rightarrow Hg(l)$
- anode: $Mg(s) \rightarrow Mg^{2+}(aq) + 2e^-$

If the potential for the oxidation of Mg to Mg^{2+} is 2.37 V under standard conditions, what is the standard electrode potential for the reaction that occurs at the anode?

Answer 0.85 V

We can use this procedure described to measure the standard potentials for a wide variety of chemical substances, some of which are listed in Table P2. These data allow us to compare the oxidative and reductive strengths of a variety of substances. The half-reaction for the standard hydrogen electrode (SHE) lies more than halfway down the list in Table 13.3.2.1. All reactants that lie below the SHE in the table are stronger oxidants than H^+, and all those that lie above the SHE are weaker. The strongest oxidant in the table is F_2, with a standard electrode potential of 2.87 V. This high value is consistent with the high electronegativity of fluorine and tells us that fluorine has a stronger tendency to accept electrons (it is a stronger oxidant) than any other element.

Table 13.3.2.1: Standard Potentials for Selected Reduction Half-Reactions at 25°C

Half-Reaction	E° (V)
$Li^+(aq) + e^- \rightleftharpoons Li(s)$	–3.040
$Be^{2+}(aq) + 2e^- \rightleftharpoons Be(s)$	–1.99
$Al^{3+}(aq) + 3e^- \rightleftharpoons Al(s)$	–1.676
$Zn^{2+}(aq) + 2e^- \rightleftharpoons Zn(s)$	–0.7618
$Ag_2S(s) + 2e^- \rightleftharpoons 2Ag(s) + S^{2-}(aq)$	–0.71
$Fe^{2+}(aq) + 2e^- \rightleftharpoons Fe(s)$	–0.44
$Cr^{3+}(aq) + e^- \rightleftharpoons Cr^{2+}(aq)$	–0.424
$Cd^{2+}(aq) + 2e^- \rightleftharpoons Cd(s)$	–0.4030
$PbSO_4(s) + 2e^- \rightleftharpoons Pb(s) + SO_4^{2-}(aq)$	–0.356
$Ni^{2+}(aq) + 2e^- \rightleftharpoons Ni(s)$	–0.257
$2SO_4^{2-}(aq) + 4H^+(aq) + 2e^- \rightleftharpoons S_2O_6^{2-}(aq) + 2H_2O(l)$	–0.25
$Sn^{2+}(aq) + 2e^- \rightleftharpoons Sn(s)$	−0.14
$2H^+(aq) + 2e^- \rightleftharpoons H_2(g)$	0.00
$Sn^{4+}(aq) + 2e^- \rightleftharpoons Sn^{2+}(aq)$	0.154
$Cu^{2+}(aq) + e^- \rightleftharpoons Cu^+(aq)$	0.159
$AgCl(s) + e^- \rightleftharpoons Ag(s) + Cl^-(aq)$	0.2223
$Cu^{2+}(aq) + 2e^- \rightleftharpoons Cu(s)$	0.3419
$O_2(g) + 2H_2O(l) + 4e^- \rightleftharpoons 4OH^-(aq)$	0.401
$H_2SO_3(aq) + 4H^+(aq) + 4e^- \rightleftharpoons S(s) + 3H_2O(l)$	0.45
$I_2(s) + 2e^- \rightleftharpoons 2I^-(aq)$	0.5355
$MnO_4^{2-}(aq) + 2H_2O(l) + 2e^- \rightleftharpoons MnO_2(s) + 4OH^-(aq)$	0.60
$O_2(g) + 2H^+(aq) + 2e^- \rightleftharpoons H_2O_2(aq)$	0.695
$H_2SeO_3(aq) + 4H^+ + 4e^- \rightleftharpoons Se(s) + 3H_2O(l)$	0.74
$Fe^{3+}(aq) + e^- \rightleftharpoons Fe^{2+}(aq)$	0.771
$Ag^+(aq) + e^- \rightleftharpoons Ag(s)$	0.7996
$NO_3^-(aq) + 3H^+(aq) + 2e^- \rightleftharpoons HNO_2(aq) + H_2O(l)$	0.94
$Br_2(aq) + 2e^- \rightleftharpoons 2Br^-(aq)$	1.087
$MnO_2(s) + 4H^+(aq) + 2e^- \rightleftharpoons Mn^{2+}(aq) + 2H_2O(l)$	1.23
$O_2(g) + 4H^+(aq) + 4e^- \rightleftharpoons 2H_2O(l)$	1.229

Half-Reaction	E° (V)
$Cr_2O_7^{2-}(aq) + 14H^+(aq) + 6e^- \rightleftharpoons 2Cr^{3+}(aq) + 7H_2O(l)$	1.36
$Cl_2(g) + 2e^- \rightleftharpoons 2Cl^-(aq)$	1.396
$Ce^{4+}(aq) + e^- \rightleftharpoons Ce^{3+}(aq)$ (13.3.2.38)	1.44
$PbO_2(s) + HSO_4^-(aq) + 3H^+(aq) + 2e^- \rightleftharpoons PbSO_4(s) + 2H_2O(l)$	1.690
$H_2O_2(aq) + 2H^+(aq) + 2e^- \rightleftharpoons 2H_2O(l)$	1.763
$F_2(g) + 2e^- \rightleftharpoons 2F^-(aq)$	2.87

Similarly, all species in Table 13.3.2.1 that lie above H_2 are stronger reductants than H_2, and those that lie below H_2 are weaker. The strongest reductant in the table is thus metallic lithium, with a standard electrode potential of −3.04 V. This fact might be surprising because cesium, not lithium, is the least electronegative element. The apparent anomaly can be explained by the fact that electrode potentials are measured in aqueous solution, where intermolecular interactions are important, whereas ionization potentials and electron affinities are measured in the gas phase. Due to its small size, the Li^+ ion is stabilized in aqueous solution by strong electrostatic interactions with the negative dipole end of water molecules. These interactions result in a significantly greater $\Delta H_{hydration}$ for Li^+ compared with Cs^+. Lithium metal is therefore the strongest reductant (most easily oxidized) of the alkali metals in aqueous solution.

Note

Species in Talbe Table 13.3.2.1 (or Table P2) that lie above H_2 are stronger reducing agents (more easily oxidized) than H_2. Species that lie below H_2 are stronger oxidizing agents.

Because the half-reactions shown in Table 13.3.2.1 are arranged in order of their E° values, we can use the table to quickly predict the relative strengths of various oxidants and reductants. Any species on the left side of a half-reaction will spontaneously oxidize any species on the right side of another half-reaction that lies below it in the table. Conversely, any species on the right side of a half-reaction will spontaneously reduce any species on the left side of another half-reaction that lies above it in the table. We can use these generalizations to predict the spontaneity of a wide variety of redox reactions ($E°_{cell} > 0$), as illustrated below.

Example 13.3.2.3

The black tarnish that forms on silver objects is primarily Ag_2S. The half-reaction for reversing the tarnishing process is as follows:

$$Ag_2S(s) + 2e^- \rightarrow 2Ag(s) + S^{2-}(aq) \quad E° = -0.69\ V$$

a. Referring to Table 13.3.2.1, predict which species—$H_2O_2(aq)$, $Zn(s)$, $I^-(aq)$, $Sn^{2+}(aq)$—can reduce Ag_2S to Ag under standard conditions.
b. Of these species—$H_2O_2(aq)$, $Zn(s)$, $I^-(aq)$, $Sn^{2+}(aq)$, identify which is the strongest reducing agent in aqueous solution and thus the best candidate for a commercial product.
c. From the data in Table 13.3.2.1, suggest an alternative reducing agent that is readily available, inexpensive, and possibly more effective at removing tarnish.



Given: reduction half-reaction, standard electrode potential, and list of possible reductants

Asked for: reductants for Ag_2S, strongest reductant, and potential reducing agent for removing tarnish

Strategy:

A From their positions in Table 13.3.2.1, decide which species can reduce Ag_2S. Determine which species is the strongest reductant.

B Use Table 13.3.2.1 to identify a reductant for Ag_2S that is a common household product.

Solution

We can solve the problem in one of two ways: (1) compare the relative positions of the four possible reductants with that of the Ag_2S/Ag couple in Table 13.3.2.1 or (2) compare E° for each species with E° for the Ag_2S/Ag couple (−0.69 V).

a. **A** The species in Table 13.3.2.1 are arranged from top to bottom in order of increasing reducing strength. Of the four species given in the problem, $I^-(aq)$, $Sn^{2+}(aq)$, and $H_2O_2(aq)$ lie above Ag_2S, and one [Zn(s)] lies below it. We can therefore conclude that Zn(s) can reduce $Ag_2S(s)$ under standard conditions, whereas $I^-(aq)$, $Sn^{2+}(aq)$, and $H_2O_2(aq)$ cannot. $Sn^{2+}(aq)$ and $H_2O_2(aq)$ appear twice in the table: on the left side (oxidant) in one half-reaction and on the right side (reductant) in another.
b. The strongest reductant is Zn(s), the species on the right side of the half-reaction that lies closer to the bottom of Table 13.3.2.1 than the half-reactions involving $I^-(aq)$, $Sn^{2+}(aq)$, and $H_2O_2(aq)$. (Commercial products that use a piece of zinc are often marketed as a “miracle product” for removing tarnish from silver. All that is required is to add warm water and salt for electrical conductivity.)
c. **B** Of the reductants that lie below Zn(s) in Table 13.3.2.1, and therefore are stronger reductants, only one is commonly available in household products: Al(s), which is sold as aluminum foil for wrapping foods.

Example 13.3.2.4

Use the data in Table 13.3.2.1 to determine whether each reaction is likely to occur spontaneously under standard conditions:

a. $Sn(s) + Be^{2+}(aq) \rightarrow Sn^{2+}(aq) + Be(s)$
b. $MnO_2(s) + H_2O_2(aq) + 2H^+(aq) \rightarrow O_2(g) + Mn^{2+}(aq) + 2H_2O(l)$

Given: redox reaction and list of standard electrode potentials (Table P2)

Asked for: reaction spontaneity

Strategy:

A. Identify the half-reactions in each equation. Using Table 13.3.2.1, determine the standard potentials for the half-reactions in the appropriate direction.
B. Use Equation 13.3.2.2 to calculate the standard cell potential for the overall reaction. From this value, determine whether the overall reaction is spontaneous.

Solution

a. **A** Metallic tin is oxidized to $Sn^{2+}(aq)$, and $Be^{2+}(aq)$ is reduced to elemental beryllium. We can find the standard electrode potentials for the latter (reduction) half-reaction (−1.85 V) and for the former (oxidation) half-reaction (−0.14 V) directly from Table 13.3.2.1.

B Adding the two half-reactions gives the overall reaction:

$$\begin{aligned}\text{cathode: } &Be^{2+}(aq) + 2e^- \rightarrow Be(s)\\ \text{anode: } &Sn(s) \rightarrow Sn^{2+}(s) + 2e^-\\ \text{total: } &Sn(s) + Be^{2+}(aq) \rightarrow Sn^{2+}(aq) + Be(s)\end{aligned}$$

$$\begin{aligned}E^\circ_{\text{cathode}} &= -1.99\text{ V}\\ E^\circ_{\text{anode}} &= -0.14\text{ V}\\ E^\circ_{\text{cell}} &= E^\circ_{\text{cathode}} - E^\circ_{\text{anode}}\\ &= -1.85\text{ V}\end{aligned}$$

The standard cell potential is quite negative, so the reaction will not occur spontaneously as written. That is, metallic tin cannot reduce Be^{2+} to beryllium metal under standard conditions. Instead, the reverse process, the reduction of stannous ions (Sn^{2+}) by metallic beryllium, which has a positive value of $E°_{cell}$, will occur spontaneously.

b. **A** MnO_2 is the oxidant (Mn^{4+} is reduced to Mn^{2+}), while H_2O_2 is the reductant (O^{2-} is oxidized to O_2). We can obtain the standard electrode potentials for the reduction and oxidation half-reactions directly from Table 13.3.2.1.

B The two half-reactions and their corresponding potentials are as follows

$$\begin{aligned}\text{cathode:} &MnO_2(s) + 4H^+(aq) + 2e^- \rightarrow Mn^{2+}(aq) + 2H_2O(l)\\ \text{anode:} &H_2O_2(aq) \rightarrow O_2(g) + 2H^+(aq) + 2e^-\\ \text{overall:} &MnO_2(s) + H_2O_2(aq) + 2H^+(aq) \rightarrow O_2(g) + Mn^{2+}(aq) + 2H_2O(l)\end{aligned}$$

$$\begin{aligned}E^\circ_{\text{cathode}} &= 1.22\text{ V}\\ E^\circ_{\text{anode}} &= 0.70\text{ V}\\ E^\circ_{\text{cell}} &= E^\circ_{\text{cathode}} - E^\circ_{\text{anode}}\\ &= -0.53\text{ V}\end{aligned}$$

The standard potential for the reaction is positive, indicating that under standard conditions, it will occur spontaneously as written. Hydrogen peroxide will reduce MnO_2, and oxygen gas will evolve from the solution.

? Exercise 13.3.2.4

Use the data in Table 13.3.2.1to determine whether each reaction is likely to occur spontaneously under standard conditions:

1. $2Ce^{4+}(aq) + 2Cl^-(aq) \rightarrow 2Ce^{3+}(aq) + Cl_2(g)$
2. $4MnO_2(s) + 3O_2(g) + 4OH^-(aq) \rightarrow 4MnO_4^-(aq) + 2H_2O$

Answer

1. spontaneous ($E°_{cell}$ = 0.36 V)
2. nonspontaneous ($E°_{cell}$ = −0.20 V)

Although the sign of $E°_{cell}$ tells us whether a particular redox reaction will occur spontaneously under standard conditions, it does not tell us to what extent the reaction proceeds, and it does not tell us what will happen under nonstandard conditions. To answer these questions requires a more quantitative understanding of the relationship between electrochemical cell potential and chemical thermodynamics.

Reference Electrodes and Measuring Concentrations

When using a galvanic cell to measure the concentration of a substance, we are generally interested in the potential of only one of the electrodes of the cell, the so-called **indicator electrode**, whose potential is related to the concentration of the substance being measured. To ensure that any change in the measured potential of the cell is due to only the substance being analyzed, the potential of the other electrode, the **reference electrode**, must be constant. You are already familiar with one example of a reference electrode: the SHE. The potential of a reference electrode must be unaffected by the properties of the solution, and if possible, it should be physically isolated from the solution of interest. To measure the potential of a solution, we select a reference electrode and an appropriate indicator electrode. Whether reduction or oxidation of the substance being analyzed occurs depends on the potential of the half-reaction for the substance of interest (the sample) and the potential of the reference electrode.

Note

The potential of any reference electrode should **not** be affected by the properties of the solution to be analyzed, and it should also be physically isolated.

There are many possible choices of reference electrode other than the SHE. The SHE requires a constant flow of highly flammable hydrogen gas, which makes it inconvenient to use. Consequently, two other electrodes are commonly chosen as reference electrodes. One is the **silver–silver chloride electrode**, which consists of a silver wire coated with a very thin layer of AgCl that is dipped into a chloride ion solution with a fixed concentration. The cell diagram and reduction half-reaction are as follows:

$$Cl^-_{(aq)} \mid AgCl_{(s)} \mid Ag_{(s)} \tag{13.3.2.39}$$

$$AgCl_{(s)} + e^- \rightarrow Ag_{(s)} + Cl^-_{(aq)} \tag{13.3.2.40}$$

If a saturated solution of KCl is used as the chloride solution, the potential of the silver–silver chloride electrode is 0.197 V versus the SHE. That is, 0.197 V must be subtracted from the measured value to obtain the standard electrode potential measured against the SHE.

A second common reference electrode is the **saturated calomel electrode (SCE)**, which has the same general form as the silver–silver chloride electrode. The SCE consists of a platinum wire inserted into a moist paste of liquid mercury (Hg_2Cl_2; called calomel in the old chemical literature) and KCl. This interior cell is surrounded by an aqueous KCl solution, which acts as a salt bridge between the interior cell and the exterior solution (part (a) in Figure 13.3.2.4). Although it sounds and looks complex, this cell is actually easy to prepare and maintain, and its potential is highly reproducible. The SCE cell diagram and corresponding half-reaction are as follows:

$$Pt_{(s)} \mid Hg_2Cl_{2(s)} \mid KCl_{(aq,sat)} \tag{13.3.2.41}$$

$$Hg_2Cl_{2(s)} + 2e^- \rightarrow 2Hg_{(l)} + 2Cl^-(aq) \tag{13.3.2.42}$$

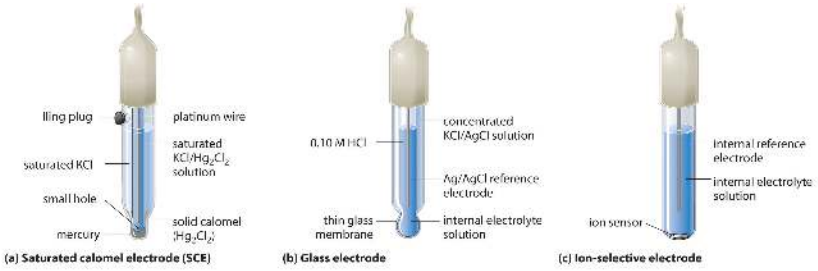


Figure 13.3.2.4: Three Common Types of Electrodes. (a) The SCE is a reference electrode that consists of a platinum wire inserted into a moist paste of liquid mercury (calomel; Hg_2Cl_2) and KCl. The interior cell is surrounded by an aqueous KCl solution, which acts as a salt bridge between the interior cell and the exterior solution. (b) In a glass electrode, an internal Ag/AgCl electrode is immersed in a 1 M HCl solution that is separated from the sample solution by a very thin glass membrane. The potential of the electrode depends on the H^+ ion concentration of the sample. (c) The potential of an ion-selective electrode depends on the concentration of only a single ionic species in solution.

At 25°C, the potential of the SCE is 0.2415 V versus the SHE, which means that 0.2415 V must be subtracted from the potential versus an SCE to obtain the standard electrode potential.

One of the most common uses of electrochemistry is to measure the H^+ ion concentration of a solution. A **glass electrode** is generally used for this purpose, in which an internal Ag/AgCl electrode is immersed in a 0.10 M HCl solution that is separated from the solution by a very thin glass membrane (part (b) in Figure 13.3.2.5). The glass membrane absorbs protons, which affects the measured potential. The extent of the adsorption on the inner side is fixed because $[H^+]$ is fixed inside the electrode, but the adsorption of protons on the outer surface depends on the pH of the solution. The potential of the glass electrode depends on $[H^+]$ as follows (recall that pH = −log$[H^+]$:

$$E_{glass} = E' + (0.0591\ V \times \log[H^+]) = E' - 0.0591\ V \times pH \tag{13.3.2.43}$$

The voltage E′ is a constant that depends on the exact construction of the electrode. Although it can be measured, in practice, a glass electrode is calibrated; that is, it is inserted into a solution of known pH, and the display on the pH meter is adjusted to the known value. Once the electrode is properly calibrated, it can be placed in a solution and used to determine an unknown pH.

Ion-selective electrodes are used to measure the concentration of a particular species in solution; they are designed so that their potential depends on only the concentration of the desired species (part (c) in Figure 13.3.2.5). These electrodes usually contain an internal reference electrode that is connected by a solution of an electrolyte to a crystalline inorganic material or a membrane, which acts as the sensor. For example, one type of ion-selective electrode uses a single crystal of Eu-doped LaF_3 as the inorganic material. When fluoride ions in solution diffuse to the surface of the solid, the potential of the electrode changes, resulting in a so-called fluoride electrode. Similar electrodes are used to measure the concentrations of other species in solution. Some of the species whose concentrations can be determined in aqueous solution using ion-selective electrodes and similar devices are listed in Table 13.3.2.2

Table 13.3.2.2: Some Species Whose Aqueous Concentrations Can Be Measured Using Electrochemical Methods

Species	Type of Sample
H^+	laboratory samples, blood, soil, and ground and surface water
NH_3/NH_4^+	wastewater and runoff water
K^+	blood, wine, and soil
CO_2/HCO_3^-	blood and groundwater
F^-	groundwater, drinking water, and soil
Br^-	grains and plant extracts
I^-	milk and pharmaceuticals
NO_3^-	groundwater, drinking water, soil, and fertilizer



The Standard Hydrogen Electrode (SHE): https://youtu.be/GS-SE7IDDtY

Summary

The flow of electrons in an electrochemical cell depends on the identity of the reacting substances, the difference in the potential energy of their valence electrons, and their concentrations. The potential of the cell under standard conditions (1 M for solutions, 1 atm for gases, pure solids or liquids for other substances) and at a fixed temperature (25°C) is called the standard cell potential ($E°_{cell}$). Only the difference between the potentials of two electrodes can be measured. By convention, all tabulated values of standard electrode potentials are listed as standard reduction potentials. The overall cell potential is the reduction potential of the reductive half-reaction minus the reduction potential of the oxidative half-reaction ($E°_{cell} = E°_{cathode} - E°_{anode}$). The potential of the standard hydrogen electrode (SHE) is defined as 0 V under standard conditions. The potential of a half-reaction measured against the SHE under standard conditions is called its standard electrode potential. The standard cell potential is a measure of the driving force for a given redox reaction. All E° values are independent of the stoichiometric coefficients for the half-reaction. Redox reactions can be balanced using the half-reaction method, in which the overall redox reaction is divided into an oxidation half-reaction and a reduction half-reaction, each balanced for mass and charge. The half-reactions selected from tabulated lists must

exactly reflect reaction conditions. In an alternative method, the atoms in each half-reaction are balanced, and then the charges are balanced. Whenever a half-reaction is reversed, the sign of E° corresponding to that reaction must also be reversed.

The oxidative and reductive strengths of a variety of substances can be compared using standard electrode potentials. Apparent anomalies can be explained by the fact that electrode potentials are measured in aqueous solution, which allows for strong intermolecular electrostatic interactions, and not in the gas phase.

If $E°_{cell}$ is positive, the reaction will occur spontaneously under standard conditions. If $E°_{cell}$ is negative, then the reaction is not spontaneous under standard conditions, although it will proceed spontaneously in the opposite direction. The potential of an indicator electrode is related to the concentration of the substance being measured, whereas the potential of the reference electrode is held constant. Whether reduction or oxidation occurs depends on the potential of the sample versus the potential of the reference electrode. In addition to the SHE, other reference electrodes are the silver–silver chloride electrode; the saturated calomel electrode (SCE); the glass electrode, which is commonly used to measure pH; and ion-selective electrodes, which depend on the concentration of a single ionic species in solution. Differences in potential between the SHE and other reference electrodes must be included when calculating values for E°.

Contributors and Attributions

- Anonymous
- cathode:

$$Cu^{2+}_{(aq)} + 2e^- \rightarrow Cu_{(s)} \qquad E^\circ{}_{cathode} = 0.34\ V \tag{13.3.2.44}$$

- anode:

$$Zn_{(s)} \rightarrow Zn^{2+}(aq, 1M) + 2e^- \qquad E^\circ{}_{anode} = -0.76\ V \tag{13.3.2.45}$$

- overall:

$$Zn_{(s)} + Cu^{2+}_{(aq)} \rightarrow Zn^{2+}_{(aq)} + Cu_{(s)} \tag{13.3.2.46}$$

- Redox reactions can be balanced using the half-reaction method.
- The standard cell potential is a measure of the driving force for the reaction.
- The relative strengths of various oxidants and reductants can be predicted using E° values.

13.3.2: Standard Potentials is shared under a CC BY-NC-SA 4.0 license and was authored, remixed, and/or curated by LibreTexts.

- **20.2: Standard Electrode Potentials** is licensed CC BY-NC-SA 4.0.

13.3.3: Reference Electrodes

In potentiometry we measure the difference between the potential of two electrodes. The potential of one electrode—the working or indicator electrode—responds to the analyte's activity and the other electrode—the counter or reference electrode—has a known, fixed potential. By convention, the reference electrode is the anode; thus, the short hand notation for a potentiometric electrochemical cell is

$$\text{reference electrode} \,||\, \text{indicator electrode}$$

and the cell potential is

$$E_{\text{cell}} = E_{\text{ind}} - E_{\text{ref}}$$

The ideal reference electrode provides a stable, known potential so that we can attribute any change in E_{cell} to the analyte's effect on the indicator electrode's potential. In addition, the reference electrode should be easy to make and easy to use. Although the standard hydrogen electrode is the reference electrode used to define electrode potentials, it use is not common. Instead, the two reference electrodes discussed in this section find the most applications.

Calomel Electrodes

A calomel reference electrode is based on the following redox couple between Hg_2Cl_2 and Hg (calomel is the common name for Hg_2Cl_2)

$$Hg_2Cl_2(s) + 2e^- \rightleftharpoons 2Hg(l) + 2Cl^-(aq)$$

for which the potential is

$$E = E^{\circ}_{Hg_2Cl_2/Hg} - \frac{0.05916}{2}\log\left(a_{Cl^-}\right)^2 = +0.2682\text{V} - \frac{0.05916}{2}\log\left(a_{Cl^-}\right)^2$$

The potential of a calomel electrode, therefore, depends on the activity of Cl^- in equilibrium with Hg and Hg_2Cl_2.

As shown in Figure 13.3.3.1, in a saturated calomel electrode (SCE) the concentration of Cl^- is determined by the solubility of KCl. The electrode consists of an inner tube packed with a paste of Hg, Hg_2Cl_2, and KCl, situated within a second tube that contains a saturated solution of KCl. A small hole connects the two tubes and a porous wick serves as a salt bridge to the solution in which the SCE is immersed. A stopper in the outer tube provides an opening for adding addition saturated KCl. The short hand notation for this cell is

$$Hg(l)|Hg_2Cl_2(s), KCl(aq,\ \text{sat'd}\,)||$$

Because the concentration of Cl^- is fixed by the solubility of KCl, the potential of an SCE remains constant even if we lose some of the inner solution to evaporation. A significant disadvantage of the SCE is that the solubility of KCl is sensitive to a change in temperature. At higher temperatures the solubility of KCl increases and the electrode's potential decreases. For example, the potential of the SCE is +0.2444 V at 25°C and +0.2376 V at 35°C. The potential of a calomel electrode that contains an unsaturated solution of KCl is less dependent on the temperature, but its potential changes if the concentration, and thus the activity of Cl^-, increases due to evaporation.

> For example, the potential of a calomel electrode is +0.280 V when the concentration of KCl is 1.00 M and +0.336 V when the concentration of KCl is 0.100 M. If the activity of Cl^- is 1.00, the potential is +0.2682 V.

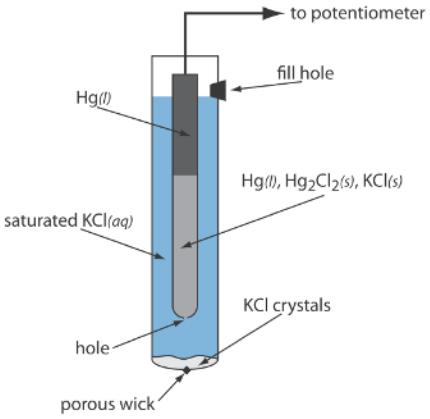


Figure 13.3.3.1. Schematic diagram showing the saturated calomel electrode.

Silver/Silver Chloride Electrodes

Another common reference electrode is the silver/silver chloride electrode, which is based on the reduction of AgCl to Ag.

$$\mathrm{AgCl}(s) + e^- \rightleftharpoons \mathrm{Ag}(s) + \mathrm{Cl}^-(aq)$$

As is the case for the calomel electrode, the activity of Cl^- determines the potential of the Ag/AgCl electrode; thus

$$E = E^\circ_{\mathrm{AgCl/Ag}} - 0.05916 \log a_{\mathrm{Cl}^-} = 0.2223\ \mathrm{V} - 0.05916 \log a_{\mathrm{Cl}^-}$$

When prepared using a saturated solution of KCl, the electrode's potential is +0.197 V at 25°C. Another common Ag/AgCl electrode uses a solution of 3.5 M KCl and has a potential of +0.205 V at 25°C. As you might expect, the potential of a Ag/AgCl electrode using a saturated solution of KCl is more sensitive to a change in temperature than an electrode that uses an unsaturated solution of KCl.

A typical Ag/AgCl electrode is shown in Figure $13.3.3.2$and consists of a silver wire, the end of which is coated with a thin film of AgCl, immersed in a solution that contains the desired concentration of KCl. A porous plug serves as the salt bridge. The electrode's short hand notation is

$$\mathrm{Ag}(s) | \mathrm{Ag\,Cl}(s), \mathrm{KCl}\,(aq, a_{\mathrm{Cl}^-} = x) \,||$$

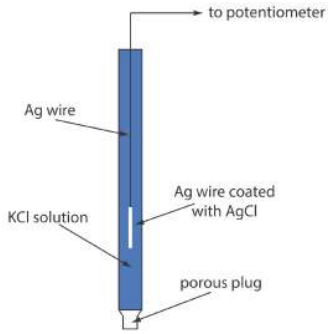


Figure 13.3.3.2. Schematic diagram showing a Ag/AgCl electrode. Because the electrode does not contain solid KCl, this is an example of an unsaturated Ag/AgCl electrode.

Converting Potentials Between Reference Electrodes

The standard state reduction potentials in most tables are reported relative to the standard hydrogen electrode's potential of +0.00 V. Because we rarely use the SHE as a reference electrode, we need to convert an indicator electrode's potential to its equivalent value when using a different reference electrode. As shown in the following example, this is easy to do.

Example 13.3.3.1

The potential for an Fe^{3+}/Fe^{2+} half-cell is +0.750 V relative to the standard hydrogen electrode. What is its potential if we use a saturated calomel electrode or a saturated silver/silver chloride electrode?

Solution

When we use a standard hydrogen electrode the potential of the electrochemical cell is

$$E_{\text{cell}} = E_{\text{Fe}^{3+}/\text{Fe}^{2+}} - E_{\text{SHE}} = 0.750\ \text{V} - 0.000\ \text{V} = 0.750\ \text{V}$$

We can use the same equation to calculate the potential if we use a saturated calomel electrode

$$E_{\text{cell}} = E_{\text{Fe}^{3+}/\text{Fe}^{2+}} - E_{\text{SHE}} = 0.750\ \text{V} - 0.2444\ \text{V} = 0.506\ \text{V}$$

or a saturated silver/silver chloride electrode

$$E_{\text{cell}} = E_{\text{Fe}^{3+}/\text{Fe}^{2+}} - E_{\text{SHE}} = 0.750\ \text{V} - 0.197\ \text{V} = 0.553\ \text{V}$$

Figure 13.3.3.3provides a pictorial representation of the relationship between these different potentials.

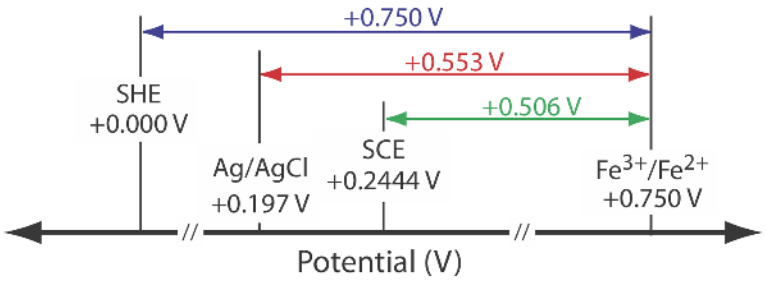


Figure 13.3.3.3. Relationship between the potential of an Fe^{3+}/Fe^{2+} half-cell relative to the reference electrodes in Example 13.3.3.1. The potential relative to a standard hydrogen electrode is shown in blue, the potential relative to a saturated silver/silver chloride electrode is shown in red, and the potential relative to a saturated calomel electrode is shown in green.

This page titled 13.3.3: Reference Electrodes is shared under a CC BY-NC-SA 4.0 license and was authored, remixed, and/or curated by David Harvey.

- **23.1: Reference Electrodes** by David Harvey is licensed CC BY-NC-SA 4.0.

13.3.4: Metallic Indicator Electrodes

In potentiometry, the potential of the indicator electrode is proportional to the analyte's activity. Two classes of indicator electrodes are used to make potentiometric measurements: metallic electrodes, which are the subject of this section, and ion-selective electrodes, which are covered in the next section.

Electrodes of the First Kind

If we place a copper electrode in a solution that contains Cu^{2+}, the electrode's potential due to the reaction

$$Cu^{2+}(aq) + 2e^- \rightleftharpoons Cu(s)$$

is determined by the activity of Cu^{2+}.

$$E = E^{\circ}_{Cu^{2+}/Cu} - \frac{0.05916}{2}\log\frac{1}{a_{Cu^{2+}}} = +0.3419\text{V} - \frac{0.05916}{2}\log\frac{1}{a_{Cu^{2+}}}$$

If copper is the indicator electrode in a potentiometric electrochemical cell that also includes a saturated calomel reference electrode

$$\text{SCE}\|Cu^{2+}\,(aq, a_{Cu^{2+}} = x)\,|Cu(s)$$

then we can use the cell potential to determine an unknown activity of Cu^{2+} in the indicator electrode's half-cell

$$E_{\text{cell}} = E_{\text{ind}} - E_{\text{SCE}} = +0.3419\text{V} - \frac{0.05916}{2}\log\frac{1}{a_{Cu^{2+}}} - 0.2224\text{V}$$

An indicator electrode in which the metal is in contact with a solution containing its ion is called an electrode of the first kind. In general, if a metal, *M*, is in a solution of M^{n+}, the cell potential is

$$E_{\text{call}} = K - \frac{0.05916}{n}\log\frac{1}{a_{M^{n+}}} = K + \frac{0.05916}{n}\log a_{M^{n+}}$$

where *K* is a constant that includes the standard-state potential for the M^{n+}/M redox couple and the potential of the reference electrode.

For a variety of reasons—including the slow kinetics of electron transfer at the metal–solution interface, the formation of metal oxides on the electrode's surface, and interfering reactions—electrodes of the first kind are limited to the following metals: Ag, Bi, Cd, Cu, Hg, Pb, Sn, Tl, and Zn.

> Many of these electrodes, such as Zn, cannot be used in acidic solutions because they are easily oxidized by H^+.
>
> $$Zn(s) + 2H^+(aq) \rightleftharpoons H_2(g) + Zn^{2+}(aq)$$

Electrodes of the Second Kind

The potential of an electrode of the first kind responds to the activity of M^{n+}. We also can use this electrode to determine the activity of another species if it is in equilibrium with M^{n+}. For example, the potential of a Ag electrode in a solution of Ag^+ is

$$E = 0.7996\text{V} + 0.05916\log a_{Ag^+} \tag{13.3.4.1}$$

If we saturate the indicator electrode's half-cell with AgI, the solubility reaction

$$AgI(s) \rightleftharpoons Ag^+(aq) + I^-(aq) \tag{13.3.4.2}$$

determines the concentration of Ag^+; thus

$$a_{Ag^+} = \frac{K_{\text{sp,AgI}}}{a_{I^-}} \tag{13.3.4.3}$$

where $K_{\text{sp,AgI}}$ is the solubility product for AgI. Substituting Equation 13.3.4.3into Equation 13.3.4.1

$$E = 0.7996 \text{ V} + 0.05916 \log \frac{K_{\text{sp, AgI}}}{a_{\text{I}^-}} \tag{13.3.4.4}$$

shows that the potential of the silver electrode is a function of the activity of I^-. If we incorporate this electrode into a potentiometric electrochemical cell with a saturated calomel electrode

$$\text{SCE} \| \text{AgI}(s),\ \text{I}^-\ (aq, a_{\text{I}^-} = x) \,| \text{Ag(s)} \tag{13.3.4.5}$$

then the cell potential is

$$E_{\text{cell}} = K - 0.05916 \log a_{\text{I}^-} \tag{13.3.4.6}$$

where K is a constant that includes the standard-state potential for the Ag^+/Ag redox couple, the solubility product for AgI, and the reference electrode's potential.

If an electrode of the first kind responds to the activity of an ion in equilibrium with M^{n+}, we call it an electrode of the second kind. Two common electrodes of the second kind are the calomel and the silver/silver chloride reference electrodes.

> In an electrode of the second kind we link together a redox reaction and another reaction, such as a solubility reaction. You might wonder if we can link together more than two reactions. The short answer is yes. An electrode of the third kind, for example, links together a redox reaction and two other reactions. Such electrodes are less common and we will not consider them in this text.

Metallic Redox Electrodes

An electrode of the first kind or the second kind develops a potential as the result of a redox reaction that involves the metallic electrode. An electrode also can serve as a source of electrons or as a sink for electrons in an unrelated redox reaction, in which case we call it a redox electrode. The Pt cathode in 13.3.4.1is a redox electrode because its potential is determined by the activity of Fe^{2+} and Fe^{3+} in the indicator half-cell. Note that a redox electrode's potential often responds to the activity of more than one ion, which limits its usefulness for direct potentiometry.

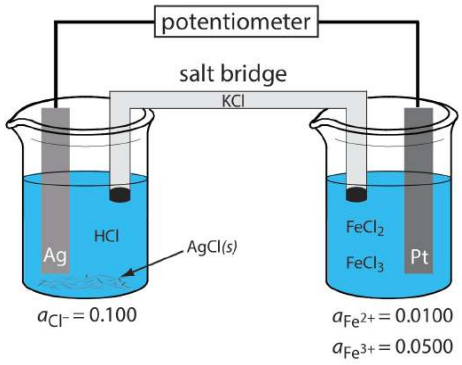


Figure 13.3.4.1. Potentiometric electrochemical cell in which the anode is a metallic electrode of the first kind (Ag) and the cathode is a metallic redox electrode (Pt).

This page titled 13.3.4: Metallic Indicator Electrodes is shared under a CC BY-NC-SA 4.0 license and was authored, remixed, and/or curated by David Harvey.

- **23.2: Metallic Indicator Electrodes** by David Harvey is licensed CC BY-NC-SA 4.0.

13.3.5: Membrane Ion-Selective Electrodes

If metals were the only useful materials for constructing indicator electrodes, then there would be few useful applications of potentiometry. In 1906, Cremer discovered that the potential difference across a thin glass membrane is a function of pH when opposite sides of the membrane are in contact with solutions that have different concentrations of H_3O^+. The existence of this membrane potential led to the development of a new class of indicator electrodes, which we call ion-selective electrodes (ISEs). In addition to the glass pH electrode, ion-selective electrodes are available for a wide range of ions. It also is possible to construct a membrane electrode for a neutral analyte by using a chemical reaction to generate an ion that is monitored with an ion-selective electrode. The development of new ion-selective membrane electrodes continues to be an active area of research.

Classification of Ions-Selective Membranes

There are two broad classes of materials that are used as membranes: crystalline solid-state membranes and non-crystalline membranes. Examples of crystalline solid-state membranes are single crystals of LaF_3 and polycrystalline AgS. Examples non-crystalline membranes are glass and hydrophobic membranes that hold a liquid ion-exchanger. Each of these are considered below.

Properties of Ion-Selective Membranes

To be useful, an ion-selective membrane must be structurally stable (a crystalline membrane that is soluble, for example, is not structurally stable), capable of being machined to a suitable size and shape that can be incorporated into the indicator electrode in a potentiometric electrochemical cell, electrically conductive so it is possible to measure the electrochemical cell's potential, and selective toward the analyte.

The Membrane's Boundary Potential

Figure 13.3.5.1 shows a typical potentiometric electrochemical cell equipped with an ion-selective electrode. The short hand notation for this cell is

$$\text{ref (sample)} \; \| \text{A}_{\text{samp}} \; \left(aq, a_{\text{A}_{\text{samp}}} = x\right) | \text{membrane} | \text{A}_{\text{int}} \; \left(aq, a_{\text{A}_{\text{int}}} = y\right) \| \; \text{ref (internal)}$$

where the ion-selective membrane separates the two solutions that contain analyte with activities of *x* and *y*: the sample solution and the ion-selective electrode's internal solution. The potential of this electrochemical cell

$$E_{\text{cell}} = E_{\text{ref(int)}} - E_{\text{ref(samp)}} + E_{\text{mem}} \tag{13.3.5.1}$$

includes the potential of each reference electrode and the difference in potential across the membrane, E_{mem}, which is the membrane's boundary potential. The notations ref(sample) and ref(internal) represent a reference electrode immersed in the sample and a reference electrode immersed in the ion-selective electrode's internal solution. Because the potential of the two reference electrodes are constant, any change in E_{cell} reflects a change in the membrane's boundary potential.

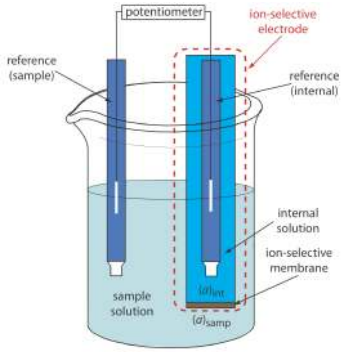


Figure 13.3.5.1. Schematic diagram that shows a typical potentiometric cell with an ion-selective electrode. The ion-selective electrode's membrane separates the sample, which contains the analyte at an activity of $(a_A)_{\text{samp}}$, from an internal solution that contains the analyte with an activity of $(a_A)_{\text{int}}$.

The analyte's interaction with the membrane generates a boundary potential if there is a difference in its activity on the membrane's two sides. Current is carried through the membrane by the movement of either the analyte or an ion already present in the membrane's matrix. The membrane potential is given by the following Nernst-like equation

$$E_{\text{mem}} = E_{\text{asym}} - \frac{RT}{zF}\ln\frac{(a_A)_{\text{int}}}{(a_A)_{\text{samp}}} \tag{13.3.5.2}$$

where $(a_A)_{\text{samp}}$ is the analyte's activity in the sample, $(a_A)_{\text{int}}$ is the analyte's activity in the ion-selective electrode's internal solution, and z is the analyte's charge. Ideally, E_{mem} is zero when $(a_A)_{\text{int}} = (a_A)_{\text{samp}}$. The term E_{asym}, which is an asymmetry potential, accounts for the fact that E_{mem} usually is not zero under these conditions.

> For now we simply note that a difference in the analyte's activity results in the membrane's boundary potential. As we consider different types of ion-selective electrodes, we will explore more specifically the source of the membrane potential.

Substituting Equation 13.3.5.2into Equation 13.3.5.1, assuming a temperature of 25°C, and rearranging gives

$$E_{\text{cell}} = K + \frac{0.05916}{z}\log(a_A)_{\text{samp}} \tag{13.3.5.3}$$

where K is a constant that includes the potentials of the two reference electrodes, the asymmetry potential, and the analyte's activity in the internal solution. Equation 13.3.5.3is a general equation and applies to all types of ion-selective electrodes.

Membrane Selectivity

The membrane's boundary potential results from a chemical interaction between the analyte and active sites on the membrane's surface. Because the signal depends on a chemical process, most membranes are not selective toward a single analyte. Instead, the membrane's boundary potential is proportional to the concentration of each ion that interacts with the membrane's active sites. We can rewrite Equation 13.3.5.3to include the contribution to the potential of an interferent, I

$$E_{\text{cell}} = K + \frac{0.05916}{z_A}\log\left\{a_A + K_{A,I}(a_I)^{z_A/z_I}\right\} \tag{13.3.5.4}$$

where z_A and z_I are the charges of the analyte and the interferent, and $K_{A,I}$ is a selectivity coefficient that accounts for the relative response of the interferent. The selectivity coefficient is defined as

$$K_{A,I} = \frac{(a_A)_e}{(a_I)_e^{z_A/z_I}} \tag{13.3.5.5}$$

where $(a_A)_e$ and $(a_I)_e$ are the activities of analyte and the interferent that yield identical cell potentials. When the selectivity coefficient is 1.00, the membrane responds equally to the analyte and the interferent. A membrane shows good selectivity for the analyte when $K_{A,I}$ is significantly less than 1.00.

Selectivity coefficients for most commercially available ion-selective electrodes are provided by the manufacturer. If the selectivity coefficient is not known, it is easy to determine its value experimentally by preparing a series of solutions, each of which contains the same activity of interferent, $(a_I)_{\text{add}}$, but a different activity of analyte. As shown in Figure 13.3.5.2, a plot of cell potential versus the log of the analyte's activity has two distinct linear regions. When the analyte's activity is significantly larger than $K_{A,I} \times (a_I)_{\text{add}}$, the potential is a linear function of $\log(a_A)$, as given by Equation 13.3.5.3. If $K_{\text{A,I}} \times (a_I)_{\text{add}}$ is significantly larger than the analyte's activity, however, the cell's potential remains constant. The activity of analyte and interferent at the intersection of these two linear regions is used to calculate $K_{\text{A,I}}$.

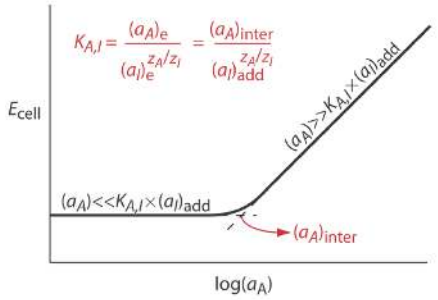


Figure 13.3.5.2. Diagram showing the experimental determination of an ion-selective electrode's selectivity for an analyte. The activity of analyte that corresponds to the intersection of the two linear portions of the curve, $(a_A)_{\text{inter}}$, produces a cell potential identical to that of the interferent. The equation for the selectivity coefficient, $K_{\text{A,I}}$, is shown in red.

Example 13.3.5.1

Sokalski and co-workers described a method for preparing ion-selective electrodes with significantly improved selectivities [Sokalski, T.; Ceresa, A.; Zwicki, T.; Pretsch, E. *J. Am. Chem. Soc.* **1997**, *119*, 11347–11348]. For example, a conventional Pb^{2+} ISE has a $\log K_{Pb^{2+}/Mg^{2+}}$ of –3.6. If the potential for a solution in which the activity of Pb^{2+} is 4.1×10^{-12} is identical to that for a solution in which the activity of Mg^{2+} is 0.01025, what is the value of $\log K_{Pb^{2+}/Mg^{2+}}$ for their ISE?

Solution

Making appropriate substitutions into Equation 13.3.5.5, we find that

$$K_{Pb^{2+}/Mg^{2+}} = \frac{(a_{Pb^{2+}})_e}{(a_{Mg^{2+}})_e^{z_{Pb^{2+}}/z_{Mg^{2+}}}} = \frac{4.1 \times 10^{-12}}{(0.01025)^{+2/+2}} = 4.0 \times 10^{-10}$$

The value of $\log K_{Pb^{2+}/Mg^{2+}}$, therefore, is –9.40.

The Glass Electrode for pH Measurements

The earliest ion-selective electrodes were based on the observation that a thin glass membrane separating two solutions with different levels of acidity develops a measurable difference in potential on opposite sides of the membrane. Incorporating the glass electrode into a potentiometer along with a reference electrode provides a way to measure the potential. Commercial glass membrane pH electrodes often are available in a combination form that includes both the indicator electrode and the reference electrode. The use of a single electrode greatly simplifies the measurement of pH. An example of a typical combination electrode is shown in Figure 13.3.5.3

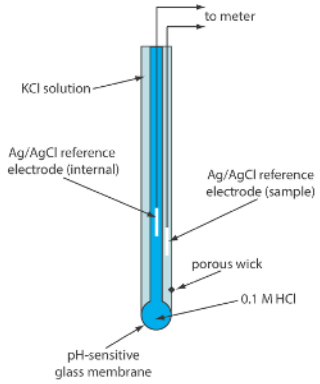


Figure 13.3.5.3. Schematic diagram showing a combination glass electrode for measuring pH. The indicator electrode consists of a pH-sensitive glass membrane and an internal Ag/AgCl reference electrode in a solution of 0.1 M HCl. The sample's reference electrode is a Ag/AgCl electrode in a solution of KCl (which may be saturated with KCl or contain a fixed concentration of KCl). A porous wick serves as a salt bridge between the sample and its reference electrode.

The Composition and Structure of Glass Membranes

The first commercial glass electrodes were manufactured using Corning 015, a glass with a composition that is approximately 22% Na_2O, 6% CaO, and 72% SiO_2. Membranes fashioned from Corning 015 have an excellent selectivity for hydrogen ions, H^+, below a pH of 9; above this pH the membrane becomes more selective for other cations and the measured pH value deviates from its actual value. Replacing Na_2O and CaO with Li_2O and BaO extends the useful pH range of glass membranes to pH levels greater than 12.

Origin of the Boundary Potential for a Glass Membrane

When immersed in an aqueous solution for several hours, the outer approximately 10 nm of the glass membrane's surface becomes hydrated, resulting in the formation of negatively charged sites, —SiO^-. Sodium ions, Na^+, serve as counter ions. Because H^+ binds more strongly to —SiO^- than does Na^+, they displace the sodium ions on both sides of the membrane.

$$H^+ + -SiO^-Na^+ \rightleftharpoons -SiO^-H^+ + Na^+ \qquad (13.3.5.6)$$

explaining the membrane's selectivity for H^+. The transport of charge across the membrane is carried by the Na^+ ions within the glass membrane. The potential of a glass electrode obeys the equation

$$E_{cell} = K + 0.05916 \log a_{H^+} \tag{13.3.5.7}$$

Alkaline and Acid Errors

As noted above, at sufficiently basic pH values a glass electrode no longer provides an accurate measure of a sample's pH as the membrane becomes more selective for other monovalent cations, such as Na^+ and K^+.

Example 13.3.5.2

For a Corning 015 glass membrane, the selectivity coefficient K_{H^+/Na^+} is $\approx 10^{-11}$. What is the expected error if we measure the pH of a solution in which the activity of H^+ is 2×10^{-13} and the activity of Na^+ is 0.05?

Solution

A solution in which the activity of H^+, $(a_{H^+})_{act}$, is 2×10^{-13} has a pH of 12.7. Because the electrode responds to both H^+ and Na^+, the apparent activity of H^+, $(a_{H^+})_{app}$, is

$$(a_{H^+})_{app} = (a_{H^+})_{act} + (K_{H^+/Na^+} \times a_{Na^+}) = 2 \times 10^{-13} + (10^{-11} \times 0.05) = 7 \times 10^{-13}$$

The apparent activity of H^+ is equivalent to a pH of 12.2, an error of –0.5 pH units.

Glass pH electrodes also show deviations from ideal behavior at pH levels less than 0.5, although the reasons for this are not clear. Still, a glass electrode has a wide dynamic range for measuring pH.

Other Limitations to Glass Electrodes

Because an ion-selective electrode's glass membrane is very thin—it is only about 50 μm thick—they must be handled with care to avoid cracks or breakage. Glass electrodes usually are stored in a storage buffer recommended by the manufacturer, which ensures that the membrane's outer surface remains hydrated. If a glass electrode dries out, it is reconditioned by soaking for several hours in a solution that contains the analyte. The composition of a glass membrane will change over time, which affects the electrode's performance. The average lifetime for a typical glass electrode is several years.

Glass Electrodes for Other Cations

The observation that the Corning 015 glass membrane responds to ions other than H^+ led to the development of glass membranes with a greater selectivity for other cations. For example, a glass membrane with a composition of 11% Na_2O, 18% Al_2O_3, and 71% SiO_2 is used as an ion-selective electrode for Na^+. Other glass ion-selective electrodes have been developed for the analysis of Li^+, K^+, Rb^+, Cs^+, NH_4^+, Ag^+, and Tl^+. Table 13.3.5.1provides several examples.

Table 13.3.5.1. Representative Examples of Glass Membrane Ion-Selective Electrodes for Analytes Other Than H^+

analyte	membrane composition	selectivity coefficients
Na^+	11% Na_2O, 18% Al_2O_3, 71% SiO_2	$K_{Na^+/H^+} = 1000$ $K_{Na^+/K^+} = 0.001$ $K_{Na^+/Li^+} = 0.001$
Li^+	15% Li_2O, 25% Al_2O_3, 60% SiO_2	$K_{Li^+/Na^+} = 0.3$ $K_{Li^+/K^+} = 0.001$
K^+	27% Na_2O, 5% Al_2O_3, 68% SiO_2	$K_{K^+/Na^+} = 0.05$

Selectivity coefficients are approximate; values found experimentally may vary substantially from the listed values. See Cammann, K. *Working With Ion-Selective Electrodes*, Springer-Verlag: Berlin, 1977.

Crystalline Membrane Electrodes

A solid-state ion-selective electrode has a membrane that consists of either a polycrystalline inorganic salt or a single crystal of an inorganic salt. We can fashion a polycrystalline solid-state ion-selective electrode by sealing a 1–2 mm thick pellet of AgS—or a mixture of AgS and a second silver salt or another metal sulfide—into the end of a nonconducting plastic cylinder, filling the

cylinder with an internal solution that contains the analyte, and placing a reference electrode into the internal solution. Figure 13.3.5.4shows a typical design.

> The NaCl in a salt shaker is an example of polycrystalline material because it consists of many small crystals of sodium chloride. The NaCl salt plates used in IR spectroscopy, on the other hand, are an example of a single crystal of sodium chloride.

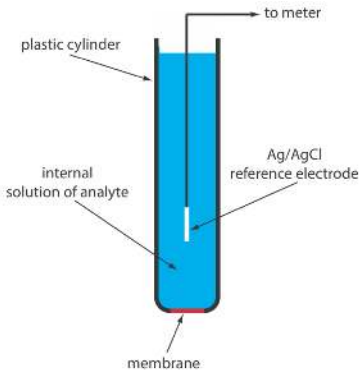


Figure 13.3.5.4. Schematic diagram of a solid-state electrode. The internal solution contains a solution of analyte of fixed activity.

The membrane potential for a Ag_2S pellet develops as the result of a difference in the extent of the solubility reaction

$$Ag_2S(s) \rightleftharpoons 2Ag^+(aq) + S^{2-}(aq) \tag{13.3.5.8}$$

on the membrane's two sides, with charge carried across the membrane by Ag^+ ions. When we use the electrode to monitor the activity of Ag^+, the cell potential is

$$E_{cell} = K + 0.05916 \log a_{Ag^+} \tag{13.3.5.9}$$

The membrane also responds to the activity of S^{2-}, with a cell potential of

$$E_{cell} = K - \frac{0.05916}{2} \log a_{S^{2-}} \tag{13.3.5.10}$$

If we combine an insoluble silver salt, such as AgCl, with the Ag_2S, then the membrane potential also responds to the concentration of Cl^-, with a cell potential of

$$E_{cell} = K - 0.05916 \log a_{Cl^-} \tag{13.3.5.11}$$

By mixing Ag_2S with CdS, CuS, or PbS, we can make an ion-selective electrode that responds to the activity of Cd^{2+}, Cu^{2+}, or Pb^{2+}. In this case the cell potential is

$$E_{cell} = K + \frac{0.05916}{2} \ln a_{M^{2+}} \tag{13.3.5.12}$$

where $a_{M^{2+}}$ is the activity of the metal ion.

Table 13.3.5.2provides examples of polycrystalline, Ag_2S-based solid-state ion-selective electrodes. The selectivity of these ion-selective electrodes depends on the relative solubility of the compounds. A Cl^- ISE using a Ag_2S/AgCl membrane is more selective for Br^- ($K_{Cl^-/Br^-} = 10^2$) and for I^- ($K_{Cl^-/I^-} = 10^6$) because AgBr and AgI are less soluble than AgCl. If the activity of Br^- is sufficiently high, AgCl at the membrane/solution interface is replaced by AgBr and the electrode's response to Cl^- decreases substantially. Most of the polycrystalline ion-selective electrodes listed in Table 13.3.5.2 operate over an extended range of pH levels. The equilibrium between S^{2-} and HS^- limits the analysis for S^{2-} to a pH range of 13–14.

13.3.5.2. Representative Examples of Polycrystalline Solid-State Ion-Selective Electrodes

analyte	membrane composition	selectivity coefficients

analyte	membrane composition	selectivity coefficients
Ag^+	Ag_2S	$K_{Ag^+/Cu^{2+}} = 10^{-6}$ $K_{Ag^+/Pb^{2+}} = 10^{-10}$ Hg^{2+} interferes
Cd^{2+}	CdS/Ag_2S	$K_{Cd^{2+}/Fe^{2+}} = 200$ $K_{Cd^{2+}/Pb^{2+}} = 6$ Ag^+, Hg^{2+}, and Cu^{2+} must be absent
Cu^{2+}	CuS/Ag_2S	$K_{Cu^{2+}/Fe^{3+}} = 10$ $K_{Cu^{2+}/Cu^+} = 10^{-6}$ Ag^+ and Hg^{2+} must be absent
Pb^{2+}	PbS/Ag_2S	$K_{Pb^{2+}/Fe^{3+}} = 1$ $K_{Pb^{2+}/Cd^{2+}} = 1$ Ag^+, Hg^{2+}, and Cu^{2+} must be absent
Br^-	$AgBr/Ag_2S$	$K_{Br^-/I^-} = 5000$ $K_{Br^-/Cl^-} = 0.005$ $K_{Br^-/OH^-} = 10^{-5}$ S^{2-} must be absent
Cl^-	$AgCl/Ag_2S$	$K_{Cl^-/I^-} = 10^6$ $K_{Cl^-/Br^-} = 100$ $K_{Cl^-/OH^-} = 0.01$ S^{2-} must be absent
I^-	AgI/Ag_2S	$K_{I^-/S^{2-}} = 30$ $K_{I^-/Br^-} = 10^{-4}$ $K_{I^-/Cl^-} = 10^{-6}$ $K_{I^-/OH^-} = 10^{-7}$
SCN^-	$AgSCN/Ag_2S$	$K_{SCN^-/I^-} = 10^3$ $K_{SCN^-/Br^-} = 100$ $K_{SCN^-/Cl^-} = 0.1 K_{SCN^-/OH^-} = 0.01$ S^{2-} must be absent
S^{2-}	Ag_2S	Hg^{2+} must be absent

Selectivity coefficients are approximate; values found experimentally may vary substantially from the listed values. See Cammann, K. *Working With Ion-Selective Electrodes*, Springer-Verlag: Berlin, 1977.

The membrane of a F^- ion-selective electrode is fashioned from a single crystal of LaF_3, which usually is doped with a small amount of EuF_2 to enhance the membrane's conductivity. Because EuF_2 provides only two F^- ions—compared to the three F^- ions in LaF_3—each EuF_2 produces a vacancy in the crystal's lattice. Fluoride ions pass through the membrane by moving into adjacent vacancies. As shown in Figure 13.3.5.4, the LaF_3 membrane is sealed into the end of a non-conducting plastic cylinder, which contains a standard solution of F^-, typically 0.1 M NaF, and a Ag/AgCl reference electrode.

The membrane potential for a F^- ISE results from a difference in the solubility of LaF_3 on opposite sides of the membrane, with the potential given by

$$E_{cell} = K - 0.05916 \log a_{F^-} \qquad (13.3.5.13)$$

One advantage of the F^- ion-selective electrode is its freedom from interference. The only significant exception is OH^- (K_{F^-/OH^-} = 0.1), which imposes a maximum pH limit for a successful analysis. Below a pH of 4 the predominate form of fluoride in solution is HF, which does not contribute to the membrane potential. For this reason, an analysis for fluoride is carried out at a pH greater than 4.

Example 13.3.5.3

What is the maximum pH that we can tolerate if we need to analyze a solution in which the activity of F^- is 1×10^{-5} with an error of less than 1%?

Solution

In the presence of OH^- the cell potential is

$$E_{\text{cell}} = K - 0.05916 \left\{ a_{F^-} + K_{F^-/OH^-} \times a_{OH^-} \right\}$$

To achieve an error of less than 1%, the term $K_{F^-/OH^-} \times a_{OH^-}$ must be less than 1% of a_{F^-}; thus

$$K_{F^-/OH^-} \times a_{OH^-} \leq 0.01 \times a_{F^-}$$

$$0.10 \times a_{OH^-} \leq 0.01 \times \left(1.0 \times 10^{-5}\right)$$

Solving for a_{OH^-} gives the maximum allowable activity for OH^- as 1×10^{-6}, which corresponds to a pH of less than 8.

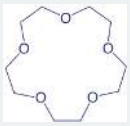
Unlike a glass membrane ion-selective electrode, a solid-state ISE does not need to be conditioned before it is used, and it may be stored dry. The surface of the electrode is subject to poisoning, as described above for a Cl^- ISE in contact with an excessive concentration of Br^-. If an electrode is poisoned, it can be returned to its original condition by sanding and polishing the crystalline membrane.

Poisoning simply means that the surface has been chemically modified, such as AgBr forming on the surface of a AgCl membrane.

Liquid Membrane Electrodes

Another class of ion-selective electrodes uses a hydrophobic membrane that contains a liquid organic complexing agent that reacts selectively with the analyte. Three types of organic complexing agents have been used: cation exchangers, anion exchangers, and neutral ionophores. A membrane potential exists if the analyte's activity is different on the two sides of the membrane. Current is carried through the membrane by the analyte.

An ionophore is a ligand whose exterior is hydrophobic and whose interior is hydrophilic. The crown ether shown here is one example of a neutral ionophore.



One example of a liquid-based ion-selective electrode is that for Ca^{2+}, which uses a porous plastic membrane saturated with the cation exchanger di-(*n*-decyl) phosphate. As shown in Figure 13.3.5.5, the membrane is placed at the end of a non-conducting cylindrical tube and is in contact with two reservoirs. The outer reservoir contains di-(*n*-decyl) phosphate in di-*n*-octylphenylphosphonate, which soaks into the porous membrane. The inner reservoir contains a standard aqueous solution of Ca^{2+} and a Ag/AgCl reference electrode. Calcium ion-selective electrodes also are available in which the di-(*n*-decyl) phosphate is immobilized in a polyvinyl chloride (PVC) membrane that eliminates the need for the outer reservoir.

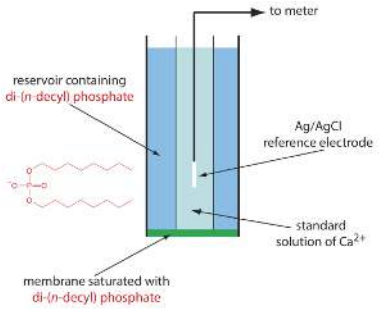


Figure 13.3.5.5. Schematic diagram showing a liquid-based ion-selective electrode for Ca^{2+}. The structure of the cation exchanger, di-(*n*-decyl) phosphate, is shown in red.

The membrane potential for the Ca^{2+} ISE develops as the result of a difference in the extent of the complexation reaction

$$Ca^{2+}(aq) + 2(C_{10}H_{21}O)_2PO_2^-(mem) \rightleftharpoons Ca[(C_{10}H_{21}O)_2PO_2]_2(mem) \tag{13.3.5.14}$$

on the two sides of the membrane, where (*mem*) indicates a species that is present in the membrane. The cell potential for the Ca^{2+} ion-selective electrode is

$$E_{cell} = K + \frac{0.05916}{2}\log a_{ca^{2+}} \tag{13.3.5.15}$$

The selectivity of this electrode for Ca^{2+} is very good, with only Zn^{2+} showing greater selectivity.

Table 13.3.5.3 lists the properties of several liquid-based ion-selective electrodes. An electrode using a liquid reservoir can be stored in a dilute solution of analyte and needs no additional conditioning before use. The lifetime of an electrode with a PVC membrane, however, is proportional to its exposure to aqueous solutions. For this reason these electrodes are best stored by covering the membrane with a cap along with a small amount of wetted gauze to maintain a humid environment. Before using the electrode it is conditioned in a solution of analyte for 30–60 minutes.

Table 13.3.5.3. Representative Examples of Liquid-Based Ion-Selective Electrodes

analyte	membrane composition	selectivity coefficients
Ca^{2+}	di-(*n*-decyl) phosphate in PVC	$K_{Ca^{2+}/Zn^{2+}} = 1-5$ $K_{Ca^{2+}/Al^{3+}} = 0.90$ $K_{Ca^{2+}/Mn^{2+}} = 0.38$ $K_{Ca^{2+}/Cu^{2+}} = 0.070$ $K_{Ca^{2+}/Mg^{2+}} = 0.032$
K^+	valinomycin in PVC	$K_{K^+/Rb^+} = 1.9$ $K_{K^+/Cs^+} = 0.38$ $K_{K^+/Li^+} = 10^{-4}$
Li^+	ETH 149 in PVC	$K_{Li^+/H^+} = 1$ $K_{Li^+/Na^+} = 0.03$ $K_{Li^+/K^+} = 0.007$
NH_4^+	nonactin and monactin in PVC	$K_{NH_4^+/K^+} = 0.12$ $K_{NH_4^+/H^+} = 0.016$ $K_{NH_4^+/Li^+} = 0.0042$ $K_{NH_4^+/Na^+} = 0.002$
ClO_3^-	$Fe(o\text{-phen})_3^{3+}$ in *p*-nitrocymene with porous membrane	$K_{ClO_4^-/OH^-} = 1$ $K_{ClO_4^-/I^-} = 0.012$ $K_{ClO_4^-/NO_3^-} = 0.0015$ $K_{ClO_4^-/Br^-} = 5.6\times10^{-4}$ $K_{ClO_4^-/Cl^-} = 2.2\times10^{-4}$

analyte	membrane composition	selectivity coefficients
NO_3^-	tetradodecyl ammonium nitrate in pVC	$K_{NO_3^-/Cl^-} = 0.006$ $K_{NO_3^-/F^-} = 9 \times 10^{-4}$

Selectivity coefficients are approximate; values found experimentally may vary substantially from the listed values. See Cammann, K. *Working With Ion-Selective Electrodes*, Springer-Verlag: Berlin, 1977.

This page titled 13.3.5: Membrane Ion-Selective Electrodes is shared under a CC BY-NC-SA 4.0 license and was authored, remixed, and/or curated by David Harvey.

- **23.3: Membrane Ion-Selective Electrodes** by David Harvey is licensed CC BY-NC-SA 4.0.

13.3.6: Molecular-Selective Electrode Systems

The electrodes in Chapter 23.3 are selective toward ions. In this section we consider how we can incorporate an ion-selective electrode into an electrode that responds to neutral species, such as volatile analytes, such as CO_2 and NH_3, and biochemically important compounds, such as amino acids and urea.

Gas-Sensing Membrane Electrodes

A number of membrane electrodes respond to the concentration of a dissolved gas. The basic design of a gas-sensing electrode, as shown in Figure 13.3.6.1, consists of a thin membrane that separates the sample from an inner solution that contains an ion-selective electrode. The membrane is permeable to the gaseous analyte, but impermeable to nonvolatile components in the sample's matrix. The gaseous analyte passes through the membrane where it reacts with the inner solution, producing a species whose concentration is monitored by the ion-selective electrode. For example, in a CO_2 electrode, CO_2 diffuses across the membrane where it reacts in the inner solution to produce H_3O^+.

$$\mathrm{CO_2}(aq) + 2\mathrm{H_2O}(l) \rightleftharpoons \mathrm{HCO_3^-}(aq) + \mathrm{H_3O^+}(aq) \tag{13.3.6.1}$$

The change in the activity of H_3O^+ in the inner solution is monitored with a pH electrode, for which the cell potential, from Chapter 23.3, is

$$E_{\text{cell}} = K + 0.05916 \log a_{\mathrm{H^+}} \tag{13.3.6.2}$$

To find the relationship between the activity of H_3O^+ in the inner solution and the activity of CO_2 in the inner solution we rearrange the equilibrium constant expression for reaction 13.3.6.1; thus

$$a_{\mathrm{H_3O^+}} = K_{\text{a}} \times \frac{a_{\mathrm{CO_2}}}{a_{\mathrm{HCO_3^-}}} \tag{13.3.6.3}$$

where K_{a} is the equilibrium constant. If the activity of $\mathrm{HCO_3^-}$ in the internal solution is sufficiently large, then its activity is not affected by the small amount of CO_2 that passes through the membrane. Substituting Equation 13.3.6.3 into Equation 13.3.6.2 gives

$$E_{\text{cell}} = K' + 0.05916 \log a_{\mathrm{co_2}} \tag{13.3.6.4}$$

where K' is a constant that includes the constant for the pH electrode, the equilibrium constant for reaction 13.3.6.1 and the activity of $\mathrm{HCO_3^-}$ in the inner solution.

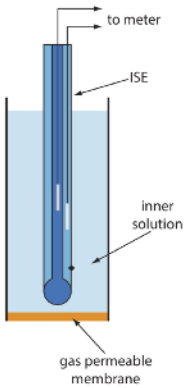


Figure 13.3.6.1. Schematic diagram of a gas-sensing membrane electrode.

Table 13.3.6.1 lists the properties of several gas-sensing electrodes. The composition of the inner solution changes with use, and both the inner solution and the membrane must be replaced periodically. Gas-sensing electrodes are stored in a solution similar to the internal solution to minimize their exposure to atmospheric gases.

Table 13.3.6.1. Representative Examples of Gas-Sensing Electrodes

analyte	inner solution	reaction in inner solution	ion-selective electrode

analyte	inner solution	reaction in inner solution	ion-selective electrode
CO_2	10 mM $NaHCO_3$ 10 mM NaCl	$CO_2(aq) + 2H_2O(l) \rightleftharpoons HCO_3^-(aq) + H_3O^+(aq)$	glass pH ISE
HCN	10 mM $KAg(CN)_2$	$HCN(aq) + H_2O(l) \rightleftharpoons CN^-(aq) + H_3O^+(aq)$	Ag_2S solid-state ISE
HF	1 M H_3O^+	$HF(aq) + H_2O(l) \rightleftharpoons F^-(aq) + H_3O^+(aq)$	F^- solid-state ISE
H_2S	pH 5 citrate buffer	$H_2S(aq) + H_2O(l) \rightleftharpoons HS^-(aq) + H_3O^+(aq)$	Ag_2S solid state ISE
NH_3	10 mM NH_4Cl 0.1 M KNO_3	$NH_3(aq) + H_2O(l) \rightleftharpoons NH_4^+(aq) + OH^-(aq)$	glass pH ISE
NO_2	20 mM $NaNO_2$ 0.1 M KNO_3	$2NO_2(aq) + 3H_2O(l) \rightleftharpoons NO_3^-(aq) + NO_2^-(aq) + 2H_3O^+(aq)$	glass pH ISE
SO_2	1 mM $NaHSO_3$ pH 5	$SO_2(aq) + 2H_2O(l) \rightleftharpoons HSO_3^-(aq) + H_3O^+(aq)$	glass pH ISE

Source: Cammann, K. *Working With Ion-Selective Electrodes*, Springer-Verlag: Berlin, 1977.

Biocatalytic Membrane Electrodes

The approach for developing gas-sensing electrodes can be modified to create potentiometric electrodes that respond to a biochemically important species. The most common class of potentiometric biosensors are enzyme electrodes, in which we trap or immobilize an enzyme at the surface of a potentiometric electrode. The analyte's reaction with the enzyme produces a product whose concentration is monitored by the potentiometric electrode. Potentiometric biosensors also have been designed around other biologically active species, including antibodies, bacterial particles, tissues, and hormone receptors.

One example of an enzyme electrode is the urea electrode, which is based on the catalytic hydrolysis of urea by urease

$$CO(NH_2)_2(aq) + 2H_2O(l) \rightleftharpoons 2NH_4^+(aq) + CO_3^-(aq) \tag{13.3.6.5}$$

Figure 13.3.6.2 shows one version of the urea electrode, which modifies a gas-sensing NH_3 electrode by adding a dialysis membrane that traps a pH 7.0 buffered solution of urease between the dialysis membrane and the gas permeable membrane [(a) Papastathopoulos, D. S.; Rechnitz, G. A. *Anal. Chim. Acta* **1975**, *79*, 17–26; (b) Riechel, T. L. *J. Chem. Educ.* **1984**, *61*, 640–642]. An NH_3 electrode, as shown in Table 13.3.6.1, uses a gas-permeable membrane and a glass pH electrode. The NH_3 diffuses across the membrane where it changes the pH of the internal solution.

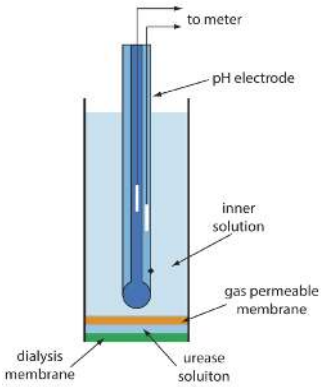


Figure 13.3.6.2. Schematic diagram showing an enzyme-based potentiometric biosensor for urea. A solution of the enzyme urease is trapped between a dialysis membrane and a gas permeable membrane. Urea diffuses across the dialysis membrane and reacts with urease, producing NH_3 that diffuses across the gas permeable membrane. The resulting change in the internal solution's pH is measured with the pH electrode.

When immersed in the sample, urea diffuses through the dialysis membrane where it reacts with the enzyme urease to form the ammonium ion, NH_4^+, which is in equilibrium with NH_3.

$$NH_4^+(aq) + H_2O(l) \rightleftharpoons H_3O^+(aq) + NH_3(aq) \tag{13.3.6.6}$$

The NH_3, in turn, diffuses through the gas permeable membrane where a pH electrode measures the resulting change in pH. The electrode's response to the concentration of urea is

$$E_{cell} = K - 0.05916 \log a_{urea} \tag{13.3.6.7}$$

Another version of the urea electrode (Figure 13.3.6.3) immobilizes the enzyme urease in a polymer membrane formed directly on the tip of a glass pH electrode [Tor, R.; Freeman, A. *Anal. Chem.* **1986**, *58*, 1042–1046]. In this case the response of the electrode is

$$pH = K a_{urea} \tag{13.3.6.8}$$

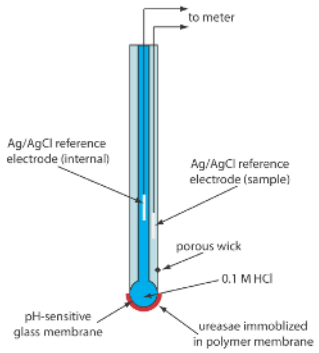


Figure 13.3.6.3. Schematic diagram of an enzyme-based potentiometric biosensor for urea in which urease is immobilized in a polymer membrane coated onto the pH-sensitive glass membrane of a pH electrode.

Few potentiometric biosensors are available commercially. As shown in Figure 13.3.6.2 and Figure 13.3.6.3, however, it is possible to convert an ion-selective electrode or a gas-sensing electrode into a biosensor. Several representative examples are described in Table 13.3.6.2, and additional examples can be found in this chapter's additional resources.

Table 13.3.6.2. Representative Examples of Potentiometric Biosensors

analyte	biologically active phase	substance determined
5′-AMP	AMP-deaminase (E)	NH_3
L-arginine	arginine and urease (E)	NH_3
asparagine	asparaginase (E)	NH_4^+
L-cysteine	*Proteus morganii* (B)	H_2S
L-glutamate	yellow squash (T)	CO_2
L-glutamine	*Sarcina flava* (B)	NH_3
oxalate	oxalate decarboxylase (E)	CO_2
penicillin	penicllinase (E)	H_3O^+
L-phenylalanine	L-amino acid oxidase/horseradish peroxidase (E)	I^-
sugars	bacteria from dental plaque (B)	H_3O^+
urea	urease (E)	NH_3 or H_3O^+

Source: Complied from Cammann, K. *Working With Ion-Selective Electrodes*, Springer-Verlag: Berlin, 1977 and Lunte, C. E.; Heineman, W. R. "Electrochemical techniques in Bioanalysis," in Steckham, E. ed. *Topics in Current Chemistry*, Vol. 143, Springer-Verlag: Berlin, 1988, p.8.
Abbreviations for biologically active phase: E = enzyme; B = bacterial particle; T = tissue.

This page titled 13.3.6: Molecular-Selective Electrode Systems is shared under a CC BY-NC-SA 4.0 license and was authored, remixed, and/or curated by David Harvey.

- **23.4: Molecular-Selective Electrode Systems** by David Harvey is licensed CC BY-NC-SA 4.0.

13.3.7: Quantitative Potentiometry

The most important application of potentiometry is determining the concentration of an analyte in solution. Most potentiometric electrodes are selective toward the free, uncomplexed form of the analyte, and do not respond to any of the analyte's complexed forms. This selectivity provides potentiometric electrodes with a significant advantage over other quantitative methods of analysis if we need to determine the concentration of free ions. For example, calcium is present in urine both as free Ca^{2+} ions and as protein-bound Ca^{2+} ions. If we analyze a urine sample using atomic absorption spectroscopy, the signal is propor- tional to the total concentration of Ca^{2+} because both free and bound calcium are atomized. Analyzing urine with a Ca^{2+} ISE, however, gives a signal that is a function of only free Ca^{2+} ions because the protein-bound Ca^{2+} can not interact with the electrode's membrane. In this section, we consider several important aspects of quantiative potentiometry.

The Relationship Between Concentration and Potential

In Chapter 23.3, we showed that the potential of an ion-selective electrode for an ion with a charge of *z* is

$$E_{\text{cell}} = K + \frac{0.05916}{z} \log \left(a_A\right)_{\text{samp}} \tag{13.3.7.1}$$

where *K* is a constant that includes the potentials of the ion-selective electrode's internal and external reference electrodes, any asymmetry potential associated with the ion-selective electrode's membrane, and the analyte's activity in the ion-selective electrode's internal solution. Equation 13.3.7.1 is a general equation and applies to all types of ion-selective electrodes. Note that when the analyte is a cation, an increase in the analyte's activity results in results in an increase in the potential; when the analyte is an anion, which makes *z* a negative number, an increase in the analyte's activity results in a decrease in the potential.

As the concentrations of ions in solution often are reported as pX values, where

$$\text{pX} = -\log a_{\text{X}} \tag{13.3.7.2}$$

it is convenient to substitute Equation 13.3.7.2 into Equation 13.3.7.1

$$E_{\text{cell}} = K - \frac{0.05916}{z}\ \text{pA} \tag{13.3.7.3}$$

Note that for a cation, an increase in pA results in a decrease in the potential; when the analyte is an anion, an increase in pA results in an increase in the potential.

Calibrating Potentiometric Electrodes

To use Equation 13.3.7.3 we need to determine the value of *K*, which we can do using one or more external standards or by the method of standard addition, both of which were covered in Chapter 1.5. One complication, of course, is that potential is a function of the analyte's activity instead of its concentration.

Activity and Concentration

Equation 13.3.7.1 is written in terms of the analyte's activity. When we use a potentiometric electrode, however, our goal is to determine the analyte's concentration. As we learned in Chapter 22, an ion's activity is the product of its concentration, $[M^{n+}]$, and a matrix-dependent activity coefficient, $\gamma_{Mn^{n+}}$.

$$a_{M^{n+}} = \left[M^{n+}\right] \gamma_{M^{n+}} \tag{13.3.7.4}$$

Substituting Equation 13.3.7.4 into Equation 13.3.7.1 and rearranging, gives

$$E_{\text{cell}} = K + \frac{0.05916}{n} \log \gamma_{M^{n+}} + \frac{0.05916}{n} \log \left[M^{n+}\right] \tag{13.3.7.5}$$

We can solve Equation 13.3.7.5 for the metal ion's concentration if we know the value for its activity coefficient. Unfortunately, if we do not know the exact ionic composition of the sample's matrix—which is the usual situation—then we cannot calculate the value of $\gamma_{Mn^{n+}}$. There is a solution to this dilemma. If we design our system so that the standards and the samples have an identical matrix, then the value of $\gamma_{Mn^{n+}}$ remains constant and Equation 13.3.7.5 simplifies to

$$E_{\text{cell}} = K' + \frac{0.05916}{n} \log \left[M^{n+}\right] \tag{13.3.7.6}$$

where K' includes the activity coefficient.

Calibration Using External Standards

In the absence of interferents, a calibration curve of E_{cell} versus $\log a_A$, where A is the analyte, is a straight-line. A plot of E_{cell} versus $\log[A]$, however, may show curvature at higher concentrations of analyte as a result of a matrix-dependent change in the analyte's activity coefficient. To maintain a consistent matrix we add a high concentration of an inert electrolyte to all samples and standards. If the concentration of added electrolyte is sufficient, then the difference between the sample's matrix and the matrix of the standards will not affect the ionic strength and the activity coefficient essentially remains constant. The inert electrolyte added to the sample and the standards is called a total ionic strength adjustment buffer (TISAB).

Example 13.3.7.1

The concentration of Ca^{2+} in a water sample is determined using the method of external standards. The ionic strength of the samples and the standards is maintained at a nearly constant level by making each solution 0.5 M in KNO_3. The measured cell potentials for the external standards are shown in the following table.

$[Ca^{2+}]$ (M)	E_{cell} (V)
1.00×10^{-5}	–0.125
5.00×10^{-5}	–0.103
1.00×10^{-4}	–0.093
5.00×10^{-4}	–0.072
1.00×10^{-3}	–0.063
5.00×10^{-3}	–0.043
1.00×10^{-2}	–0.033

What is the concentration of Ca^{2+} in a water sample if its cell potential is found to be –0.084 V?

Solution

Linear regression gives the calibration curve in Figure 13.3.7.1, with an equation of

$$E_{cell} = 0.027 + 0.0303 \log\left[Ca^{2+}\right]$$

Substituting the sample's cell potential gives the concentration of Ca^{2+} as 2.17×10^{-4} M. Note that the slope of the calibration curve, which is 0.0303, is slightly larger than its ideal value of 0.05916/2 = 0.02958; this is not unusual and is one reason for using multiple standards. One reason that it is not unusual to find that the experimental slope deviates from its ideal value of 0.05916/*n* is that this ideal value assumes that the temperature is 25°C.

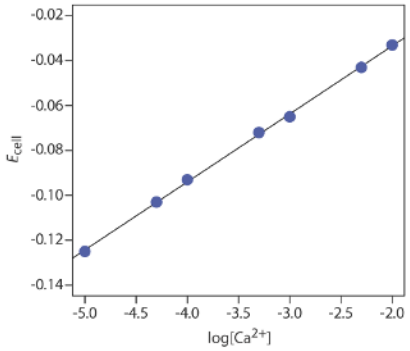


Figure 13.3.7.1. Calibration curve for the data in Example 13.3.7.1.

Calibration Using Standard Additions

Another approach to calibrating a potentiometric electrode is the method of standard additions, which was introduced in Chapter 1.5. First, we transfer a sample with a volume of V_{samp} and an analyte concentration of C_{samp} into a beaker and measure the potential, $(E_{cell})_{samp}$. Next, we make a standard addition by adding to the sample a small volume, V_{std}, of a standard that contains a known concentration of analyte, C_{std}, and measure the potential, $(E_{cell})_{std}$. If V_{std} is significantly smaller than V_{samp}, then we can safely ignore the change in the sample's matrix and assume that the analyte's activity coefficient is constant. Example 13.3.7.9 demonstrates how we can use a one-point standard addition to determine the concentration of analyte in a sample.

Example 13.3.7.2

The concentration of Ca^{2+} in a sample of sea water is determined using a Ca ion-selective electrode and a one-point standard addition. A 10.00-mL sample is transferred to a 100-mL volumetric flask and diluted to volume. A 50.00-mL aliquot of the sample is placed in a beaker with the Ca ISE and a reference electrode, and the potential is measured as –0.05290 V. After adding a 1.00-mL aliquot of a 5.00×10^{-2} M standard solution of Ca^{2+} the potential is –0.04417 V. What is the concentration of Ca^{2+} in the sample of sea water?

Solution

To begin, we write the Nernst equation before and after adding the standard addition. The cell potential for the sample is

$$(E_{cell})_{samp} = K + \frac{0.05916}{2} \log C_{samp}$$

and that following the standard addition is

$$(E_{cell})_{std} = K + \frac{0.05916}{2} \log \left\{ \frac{V_{samp}}{V_{tot}} C_{samp} + \frac{V_{std}}{V_{tot}} C_{std} \right\}$$

where V_{tot} is the total volume (V_{samp} + V_{std}) after the standard addition. Subtracting the first equation from the second equation gives

$$\Delta E = (E_{cell})_{std} - (E_{cell})_{samp} = \frac{0.05916}{2} \log \left\{ \frac{V_{samp}}{V_{tot}} C_{samp} + \frac{V_{std}}{V_{tot}} C_{std} \right\} - \frac{0.05916}{2} \log C_{samp}$$

Rearranging this equation leaves us with

$$\frac{2\Delta E_{cell}}{0.05916} = \log \left\{ \frac{V_{samp}}{V_{tot}} + \frac{V_{std} C_{std}}{V_{tot} C_{samp}} \right\}$$

Substituting known values for ΔE, V_{samp}, V_{std}, V_{tot} and C_{std},

$$\frac{2 \times \{-0.04417 - (-0.05290)\}}{0.05916} =$$

$$\log \left\{ \frac{50.00\ \text{mL}}{51.00\ \text{mL}} + \frac{(1.00\ \text{mL})(5.00 \times 10^{-2}\text{M})}{(51.00\ \text{mL}) C_{samp}} \right\}$$

$$0.2951 = \log \left\{ 0.9804 + \frac{9.804 \times 10^{-4}}{C_{samp}} \right\}$$

and taking the inverse log of both sides gives

$$1.973 = 0.9804 + \frac{9.804 \times 10^{-4}}{C_{samp}}$$

Finally, solving for C_{samp} gives the concentration of Ca^{2+} as 9.88×10^{-4} M. Because we diluted the original sample of seawater by a factor of 10, the concentration of Ca^{2+} in the seawater sample is 9.88×10^{-3} M.

The Operational Definition of pH

With the availability of inexpensive glass pH electrodes and pH meters, the determination of pH is one of the most common quantitative analytical measurements. The potentiometric determination of pH, however, is not without complications, several of which we discuss in this section.

One complication is confusion over the meaning of pH [Kristensen, H. B.; Saloman, A.; Kokholm, G. *Anal. Chem.* **1991**, *63*, 885A–891A]. The conventional definition of pH in most general chemistry textbooks is given in terms of the concentration of H^+

$$\mathrm{pH} = -\log\left[\mathrm{H}^+\right] \tag{13.3.7.7}$$

As we now know, when we measure pH it actually is a measure of the activity of H^+.

$$\mathrm{pH} = -\log a_{\mathrm{H}^+} \tag{13.3.7.8}$$

> Try this experiment—find several general chemistry textbooks and look up *pH* in each textbook's index. Turn to the appropriate pages and see how it is defined. Next, look up *activity* or *activity coefficient* in each textbook's index and see if these terms are indexed.

Equation 13.3.7.7only approximates the true pH. If we calculate the pH of 0.1 M HCl using Equation 13.3.7.7, we obtain a value of 1.00; the solution's actual pH, as defined by Equation 13.3.7.8, is 1.1 [Hawkes, S. J. *J. Chem. Educ.* **1994**, *71*, 747–749]. The activity and the concentration of H^+ are not the same in 0.1 M HCl because the activity coefficient for H^+ is not 1.00 in this matrix. Figure 13.3.7.2shows a more colorful demonstration of the difference between activity and concentration.

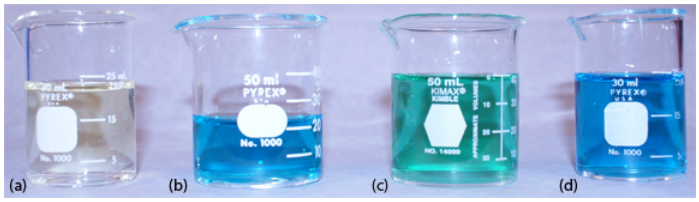


Figure 13.3.7.2. A demonstration of the difference between activity and concentration using the indicator methyl green. The indicator is pale yellow in its acid form (beaker a: 1.0 M HCl) and is blue in its base form (beaker d: H_2O). In 10 mM HCl the indicator is in its base form (beaker b: 20 mL of 10 mM HCl with 3 drops of methyl green). Adding 20 mL of 5 M LiCl to this solution shifts the indicator's color to green (beaker c); although the concentration of HCl is cut in half to 5 mM, the activity of H^+ has increased as evidenced by the green color that is intermediate between the indicator's pale yellow, acid form and its blue, base form. The demonstration shown here is adapted from McCarty, C. G.; Vitz, E. "pH Paradoxes: Demonstrating That It Is Not True That pH ≡ –log[H^+]," *J. Chem. Educ.* **2006**, *83*, 752–757. This paper provides several additional demonstrations that illustrate the difference between concentration and activity.

A second complication in measuring pH is the uncertainty in the relationship between potential and activity. For a glass membrane electrode, the cell potential, $(E_{\text{cell}})_{\text{samp}}$, for a sample of unknown pH is

$$(E_{\text{cell}})_{\text{samp}} = K - \frac{RT}{F}\ln\frac{1}{a_{\mathrm{H}^+}} = K - \frac{2.303RT}{F}\mathrm{pH}_{\text{samp}} \tag{13.3.7.9}$$

where K includes the potential of the reference electrode, the asymmetry potential of the glass membrane, and any junction potentials in the electrochemical cell. All the contributions to K are subject to uncertainty, and may change from day-to-day, as well as from electrode-to-electrode. For this reason, before using a pH electrode we calibrate it using a standard buffer of known pH. The cell potential for the standard, $(E_{\text{cell}})_{\text{std}}$, is

$$(E_{\text{ccll}})_{\text{std}} = K - \frac{2.303RT}{F}\mathrm{pH}_{\text{std}} \tag{13.3.7.10}$$

where pH_{std} is the standard's pH. Subtracting Equation ??? from Equation 13.3.7.9and solving for $\mathrm{pH}_{\text{samp}}$ gives

$$\mathrm{pH}_{\text{samp}} = \mathrm{pH}_{\text{std}} - \frac{\left\{(E_{\text{cell}})_{\text{samp}} - (E_{\text{cell}})_{\text{std}}\right\}F}{2.303RT} \tag{13.3.7.11}$$

which is the operational definition of pH adopted by the International Union of Pure and Applied Chemistry [Covington, A. K.; Bates, R. B.; Durst, R. A. *Pure & Appl. Chem.* **1985**, *57*, 531–542].

Calibrating a pH electrode presents a third complication because we need a standard with an accurately known activity for H^+. Table 13.3.7.1provides pH values for several primary standard buffer solutions accepted by the National Institute of Standards and Technology.

Table 13.3.7.1. pH Values for Selected NIST Primary Standard Buffers

temp (°C)	saturated (at 25°C) KHC_4H4O_7 (tartrate)	0.05 m $KH_2C_6H_5O_7$ (citrate)	0.05 m $KHC_8H_4O_4$ (phthlate)	0.025 m KH_2PO_4, 0.025 m $NaHPO_4$	0.008695 m KH_2PO_4, 0.03043 m Na_2HPO_4	0.01 m $Na_4B_4O_7$	0.025 m $NaHCO_3$, 0.025 m Na_2CO_3
0	—	3.863	4.003	6.984	7.534	9.464	10.317
5	—	3.840	3.999	6.951	7.500	9.395	10.245
10	—	3.820	3.998	6.923	7.472	9.332	10.179
15	—	3.802	3.999	6.900	7.448	9.276	10.118
20	—	3.788	4.002	6.881	7.429	9.225	10.062
25	3.557	3.776	4.008	6.865	7.413	9.180	10.012
30	3.552	3.766	4.015	6.854	7.400	9.139	9.966
35	3.549	3.759	4.024	6.844	7.389	9.012	9.925
40	3.547	3.753	4.035	6.838	7.380	9.068	9.889
45	3.547	3.750	4.047	6.834	7.373	9.038	9.856
50	3.549	3.749	4.060	6.833	7.367	9.011	9.828

Source: Values taken from Bates, R. G. *Determination of pH: Theory and Practice*, 2nd ed. Wiley: New York, 1973. See also Buck, R. P., et. al."Measurement of pH. Definition, Standards, and Procedures," *Pure. Appl. Chem.* **2002**, *74*, 2169–2200. All concentrations are molal (m).

To standardize a pH electrode using two buffers, choose one near a pH of 7 and one that is more acidic or basic depending on your sample's expected pH. Rinse your pH electrode in deionized water, blot it dry with a laboratory wipe, and place it in the buffer with the pH closest to 7. Swirl the pH electrode and allow it to equilibrate until you obtain a stable reading. Adjust the "Standardize" or "Calibrate" knob until the meter displays the correct pH. Rinse and dry the electrode, and place it in the second buffer. After the electrode equilibrates, adjust the "Slope" or "Temperature" knob until the meter displays the correct pH.

Some pH meters can compensate for a change in temperature. To use this feature, place a temperature probe in the sample and connect it to the pH meter. Adjust the "Temperature" knob to the solution's temperature and calibrate the pH meter using the "Calibrate" and "Slope" controls. As you are using the pH electrode, the pH meter compensates for any change in the sample's temperature by adjusting the slope of the calibration curve using a Nernstian response of $2.303RT/F$.

This page titled 13.3.7: Quantitative Potentiometry is shared under a CC BY-NC-SA 4.0 license and was authored, remixed, and/or curated by David Harvey.

- **23.6: Quantitative Potentiometry** by David Harvey is licensed CC BY-NC-SA 4.0.

SECTION OVERVIEW

13.4: Voltammetry

In voltammetry we apply a time-dependent potential to an electrochemical cell and measure the resulting current as a function of that potential. We call the resulting plot of current versus applied potential a voltammogram, and it is the electrochemical equivalent of a spectrum in spectroscopy, providing quantitative and qualitative information about the species involved in the oxidation or reduction reaction [Maloy, J. T. *J. Chem. Educ.* **1983**, *60*, 285–289]. The earliest voltammetric technique is polarography, developed by Jaroslav Heyrovsky in the early 1920s—an achievement for which he was awarded the Nobel Prize in Chemistry in 1959. Since then, many different forms of voltammetry have been developed. Before we examine some these techniques and their applications in more detail, we must first consider the basic experimental design for voltammetry and the factors influencing the shape of the resulting voltammogram.

13.4.1: Potential Excitation Signals and Currents in Voltammetry

13.4.2: Voltammetric Instrumentation

13.4.3: Linear Sweep Voltammetry

13.4.4: Cyclic Voltammetry

13.4.5: Polarography

13.4.6: Stripping Methods

13.4.7: Applications of Voltammetry

This page titled 13.4: Voltammetry is shared under a CC BY-NC-SA 4.0 license and was authored, remixed, and/or curated by David Harvey.

13.4.1: Potential Excitation Signals and Currents in Voltammetry

In voltammetry we apply a time-dependent potential to an electrochemical cell and measure the resulting current as a function of that potential.

Potential Excitation Signals

As shown in Figure 13.4.1.1, the potential may consist of (a) a linear scan or (b) a series of pulses. For the linear scan in (a), the direction of the scan can be reversed and repeated for additional cycles. The series of pulses in (b) shows just one of several different pulsed potential excitation signals; we will consider other pulse trains in the section on polarography.

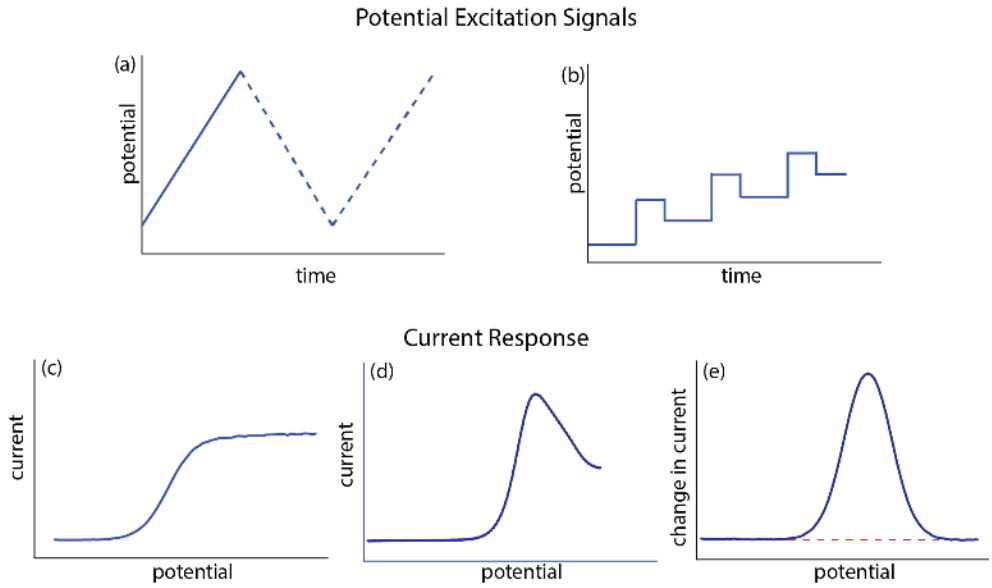


Figure 13.4.1.1: Two examples of potential excitation signals and three examples of current responses. In (a) the potential varies linearly with time and, as shown by the dashed line, the direction of the scan may be changed and repeated. In (b) the potential is changed by applying a series of pulses. The nature of the current response depends on both the potential excitation signal and other experimental conditions, such as if the solution is stirred.

Current

The current responses in Figure 13.4.1.1show the three common types of signals. In (c) and (d) the current is monitored directly as the potential is changed. In (e) a change in current is recorded using the current immediately before and after the application of a potential pulse. The current itself has three components: faradic current from the oxidation or reduction of the analyte, a charging current, and residual currents.

Faradaic Current

Faradic current is the result of oxidation or reduction of the analyte at the working electrode. The ease with which electrons move between the electrode and the species that reacts at the electrode affects the faradiac current. When electron transfer kinetics are fast, the redox reaction is at equilibrium. Under these conditions the redox reaction is electrochemically reversible and the Nernst equation applies. If the electron transfer kinetics are sufficiently slow, the concentration of reactants and products at the electrode surface—and thus the magnitude of the faradaic current—are not what is predicted by the Nernst equation. In this case the system is electrochemically irreversible.

Charging Currents

In addition to the faradaic current from a redox reaction, the current in an electrochemical cell includes other, nonfaradaic sources. Suppose the charge on an electrode is zero and we suddenly change its potential so that the electrode's surface acquires a positive charge. Cations near the electrode's surface will respond to this positive charge by migrating away from the electrode; anions, on the other hand, will migrate toward the electrode. This migration of ions occurs until the electrode's positive surface charge and the negative charge of the solution near the electrode are equal. Because the movement of ions and the movement of electrons are

indistinguishable, the result is a small, short-lived nonfaradaic current that we call the charging current. Every time we change the electrode's potential, a transient charging current flows.

The migration of ions in response to the electrode's surface charge leads to the formation of a structured electrode-solution interface that we call the electrical double layer, or EDL. When we change an electrode's potential, the charging current is the result of a restructuring of the EDL. The exact structure of the electrical double layer is not important in the context of this text, but you can consult this chapter's additional resources for additional information. See Chapter 22.1 for additional details.

Residual Current

Even in the absence of analyte, a small, measurable current flows through an electrochemical cell. In addition to the charging current discussed above, the residual current includes a faradaic current from the oxidation or reduction of trace impurities in the sample. Methods for discriminating between the analyte's faradaic current and the residual current are discussed later in this chapter.

This page titled 13.4.1: Potential Excitation Signals and Currents in Voltammetry is shared under a CC BY-NC-SA 4.0 license and was authored, remixed, and/or curated by David Harvey.

- **25.1: Potential Excitation Signals and Currents in Voltammetry** by David Harvey is licensed CC BY-NC-SA 4.0.

13.4.2: Voltammetric Instrumentation

Although early voltammetric methods used only two electrodes, a modern voltammeter makes use of a three-electrode potentiostat, such as that shown in Figure 13.4.2.1. The potential of the working electrode is measured relative to a constant-potential reference electrode that is connected to the working electrode through a high-impedance potentiometer. The auxiliary electrode generally is a platinum wire and the reference electrode usually is a SCE or a Ag/AgCl electrode. We apply a time-dependent potential excitation signal to the working electrode—changing its potential relative to the fixed potential of the reference electrode—and measure the current that flows between the working electrode and the auxiliary electrode. Modern potentiostats include waveform generators that allow us to apply a time-dependent potential profile, such as a series of potential pulses, to the working electrode.

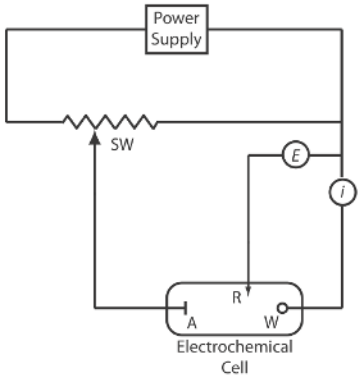


Figure 13.4.2.1. Schematic diagram for a manual potentiostat: W is the working electrode; A is the auxiliary electrode; R is the reference electrode; SW is a slide-wire resistor, *E* is a high-impendance potentiometer; and *i* is an ammeter.

Working Electrodes

For the working electrode we can choose among several different materials, including mercury, platinum, gold, silver, and carbon. The earliest voltammetric techniques used a mercury working electrode. Because mercury is a liquid, the working electrode usually is a drop suspended from the end of a capillary tube. In the hanging mercury drop electrode, or HMDE, we extrude the drop of Hg by rotating a micrometer screw that pushes the mercury from a reservoir through a narrow capillary tube (Figure 13.4.2.2a).

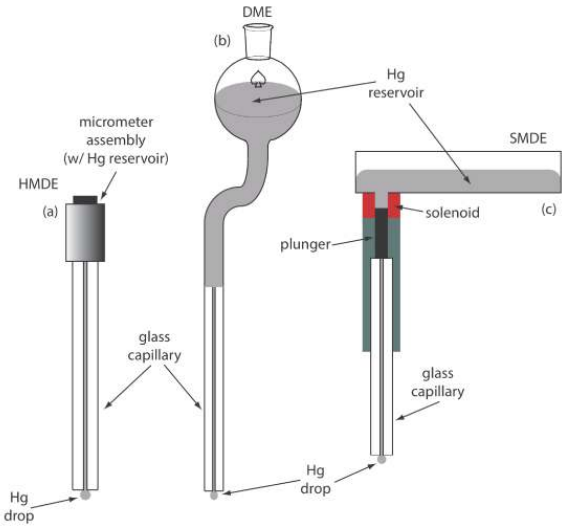


Figure 13.4.2.2. Three examples of mercury electrodes: (a) hanging mercury drop electrode, or HMDE; (b) dropping mercury electrode, or DME; and (c) static mercury drop electrode, or SMDE.

In the dropping mercury electrode, or DME, mercury drops form at the end of the capillary tube as a result of gravity (Figure 13.4.2.2b). Unlike the HMDE, the mercury drop of a DME grows continuously—as mercury flows from the reservoir under the influence of gravity—and has a finite lifetime of several seconds. At the end of its lifetime the mercury drop is dislodged, either manually or on its own, and is replaced by a new drop. The static mercury drop electrode, or SMDE, uses a solenoid driven plunger to control the flow of mercury (Figure 13.4.2.2c). Activation of the solenoid momentarily lifts the plunger, allowing mercury to

flow through the capillary, forming a single, hanging Hg drop. Repeated activation of the solenoid produces a series of Hg drops. In this way the SMDE may be used as either a HMDE or a DME. There is one additional type of mercury electrode: the mercury film electrode. A solid electrode—typically carbon, platinum, or gold—is placed in a solution of Hg^{2+} and held at a potential where the reduction of Hg^{2+} to Hg is favorable, depositing a thin film of mercury on the solid electrode's surface.

Mercury has several advantages as a working electrode. Perhaps its most important advantage is its high overpotential for the reduction of H_3O^+ to H_2, which makes accessible potentials as negative as –1 V versus the SCE in acidic solutions and –2 V versus the SCE in basic solutions (Figure 13.4.2.3). A species such as Zn^{2+}, which is difficult to reduce at other electrodes without simultaneously reducing H_3O^+, is easy to reduce at a mercury working electrode. Other advantages include the ability of metals to dissolve in mercury—which results in the formation of an amalgam—and the ability to renew the surface of the electrode by extruding a new drop. One limitation to mercury as a working electrode is the ease with which it is oxidized. Depending on the solvent, a mercury electrode can not be used at potentials more positive than approximately –0.3 V to +0.4 V versus the SCE.

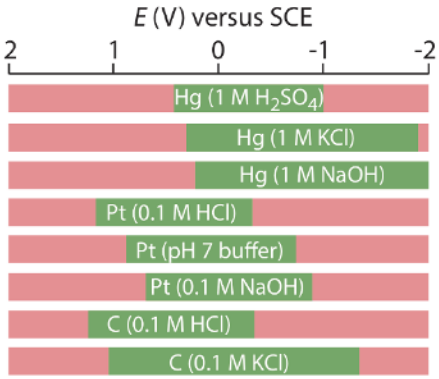


Figure 13.4.2.3. Approximate potential windows for mercury, platinum, and carbon (graphite) electrodes in acidic, neutral, and basic aqueous solvents. The useful potential windows are shown in green; potentials in red result in the oxidation or the reduction of the solvent or the electrode. Complied from Adams, R. N. *Electrochemistry at Solid Electrodes*, Marcel Dekker, Inc.: New York, 1969 and Bard, A. J.; Faulkner, L. R. *Electro- chemical Methods*, John Wiley & Sons: New York, 1980.

Solid electrodes constructed using platinum, gold, silver, or carbon may be used over a range of potentials, including potentials that are negative and positive with respect to the SCE (Figure 13.4.2.3). For example, the potential window for a Pt electrode extends from approximately +1.2 V to –0.2 V versus the SCE in acidic solutions, and from +0.7 V to –1 V versus the SCE in basic solutions. A solid electrode can replace a mercury electrode for many voltammetric analyses that require negative potentials, and is the electrode of choice at more positive potentials. Except for the carbon paste electrode, a solid electrode is fashioned into a disk and sealed into the end of an inert support with an electrical lead (Figure 13.4.2.4). The carbon paste electrode is made by filling the cavity at the end of the inert support with a paste that consists of carbon particles and a viscous oil. Solid electrodes are not without problems, the most important of which is the ease with which the electrode's surface is altered by the adsorption of a solution species or by the formation of an oxide layer. For this reason a solid electrode needs frequent reconditioning, either by applying an appropriate potential or by polishing.

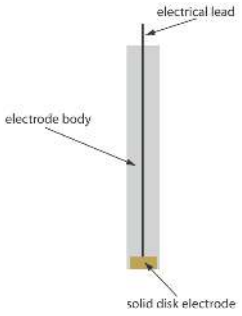


Figure 13.4.2.4. Schematic showing a solid electrode. The electrode is fashioned into a disk and sealed in the end of an inert polymer support along with an electrical lead.

Electrochemical Cells

A typical arrangement for a voltammetric electrochemical cell is shown in Figure 13.4.2.5. In addition to the working electrode, the reference electrode, and the auxiliary electrode, the cell also includes a N_2-purge line for removing dissolved O_2, and an

optional stir bar. Electrochemical cells are available in a variety of sizes, allowing the analysis of solution volumes ranging from more than 100 mL to as small as 50 µL.

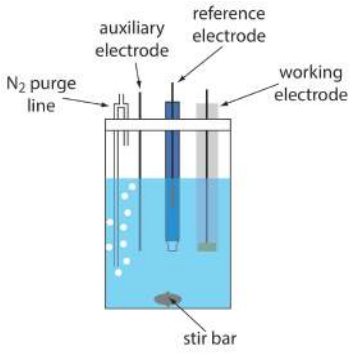


Figure 13.4.2.5. Typical electrochemical cell for voltammetry.

This page titled 13.4.2: Voltammetric Instrumentation is shared under a CC BY-NC-SA 4.0 license and was authored, remixed, and/or curated by David Harvey.

- **25.2: Voltammetric Instrumentation** by David Harvey is licensed CC BY-NC-SA 4.0.

13.4.3: Linear Sweep Voltammetry

In the simplest voltammetric experiment we apply a linear potential ramp as an excitation signal and record the current that flows in response to the change in potential. Among the experimental variables under our control are the initial potential, the final potential, the scan rate, and whether we choose to stir the solution or leave it unstirred. We call this linear sweep voltammetry.

To illustrate how linear sweep voltammetry works, let's consider what happens when we reduce $\mathrm{Fe(CN)_6^{3-}}$ to $\mathrm{Fe(CN)_6^{4-}}$ at the working electrode. The relationship between the concentrations of $\mathrm{Fe(CN)_6^{3-}}$, the concentration of $\mathrm{Fe(CN)_6^{4-}}$, and the potential is given by the Nernst equation

$$E = +0.356\ \mathrm{V} - 0.05916 \log \frac{\left[\mathrm{Fe(CN)_6^{4-}}\right]_{x=0}}{\left[\mathrm{Fe(CN)_6^{3-}}\right]_{x=0}} \tag{13.4.3.1}$$

where +0.356V is the standard-state potential for the $\mathrm{Fe(CN)_6^{3-}/Fe(CN)_6^{4-}}$ redox couple, and x = 0 indicates that the concentrations of $\mathrm{Fe(CN)_6^{3-}}$ and $\mathrm{Fe(CN)_6^{4-}}$ are those at the surface of the working electrode. We use surface concentrations instead of bulk concentrations because the equilibrium position for the redox reaction

$$\mathrm{Fe(CN)_6^{3-}}(aq) + e^- \rightleftharpoons \mathrm{Fe(CN)_6^{4-}}(aq) \tag{13.4.3.2}$$

is established at the electrode's surface.

Let's assume we have a solution for which the initial concentration of $\mathrm{Fe(CN)_6^{3-}}$ is 1.0 mM and that $\mathrm{Fe(CN)_6^{4-}}$ is absent. Figure 13.4.3.1shows the relationship between the applied potential and the species that are stable at the electrode's surface.

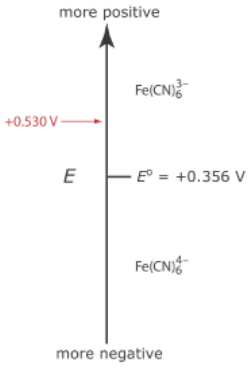


Figure 13.4.3.1. Potential diagram for the $\mathrm{Fe(CN)_6^{3-}/Fe(CN)_6^{4-}}$ redox half-reaction showing the potentials where $\mathrm{Fe(CN)_6^{3-}}$ and where $\mathrm{Fe(CN)_6^{4-}}$ are the dominate species. At a potential of +0.30 V, only $\mathrm{Fe(CN)_6^{3-}}$ is stable at the electrode's surface.

If we apply a potential of +0.530 V to the working electrode, the concentrations of $\mathrm{Fe(CN)_6^{3-}}$ and $\mathrm{Fe(CN)_6^{4-}}$ at the surface of the electrode are unaffected, and no faradaic current is observed. If we switch the potential to +0.356 V some of the $\mathrm{Fe(CN)_6^{3-}}$ at the electrode's surface is reduced to $\mathrm{Fe(CN)_6^{4-}}$until we reach a condition where

$$\left[\mathrm{Fe(CN)_6^{3-}}\right]_{x=0} = \left[\mathrm{Fe(CN)_6^{4-}}\right]_{x=0} = 0.50\ \mathrm{mM} \tag{13.4.3.3}$$

If this is all that happens after we apply the potential, then there would be a brief surge of faradaic current that quickly returns to zero, which is not the most interesting of results (although this is the basis for chronoamperometry, an electrochemical method we will not consider in this text). Although the concentrations of $\mathrm{Fe(CN)_6^{3-}}$ and $\mathrm{Fe(CN)_6^{4-}}$ at the electrode surface are 0.50 mM, their concentrations in bulk solution remains unchanged.

Because of this difference in concentration, there is a concentration gradient between the electrode's surface and the bulk solution. This concentration gradient creates a driving force that transports $\mathrm{Fe(CN)_6^{4-}}$ away from the electrode and that transports $\mathrm{Fe(CN)_6^{3-}}$ to the electrode (Figure 13.4.3.2). As the $\mathrm{Fe(CN)_6^{3-}}$ arrives at the electrode it, too, is reduced to $\mathrm{Fe(CN)_6^{4-}}$. A faradaic current continues to flow until there is no difference between the concentrations of $\mathrm{Fe(CN)_6^{3-}}$ and $\mathrm{Fe(CN)_6^{4-}}$ at the electrode and their concentrations in bulk solution (although this might take a long time!).

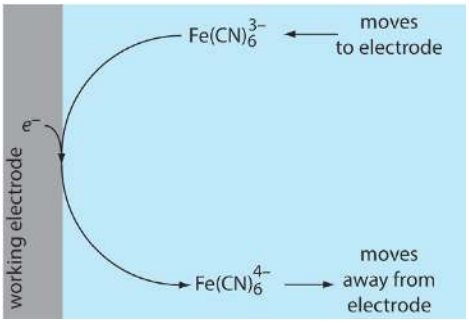


Figure 13.4.3.2. Schematic diagram showing the transport of $\mathrm{Fe(CN)_6^{4-}}$ away from the electrode's surface and the transport of $\mathrm{Fe(CN)_6^{3-}}$ toward the electrode's surface following the reduction of $\mathrm{Fe(CN)_6^{3-}}$ to $\mathrm{Fe(CN)_6^{4-}}$.

Although the potential at the working electrode determines if a faradaic current flows, the magnitude of the current is determined by the rate of the resulting oxidation or reduction reaction. Two factors contribute to the rate of the electrochemical reaction: the rate at which the reactants and products are transported to and from the electrode—what we call mass transport—and the rate at which electrons pass between the electrode and the reactants and products in solution.

Concentration Profiles at the Working Electrode

There are three modes of mass transport that affect the rate at which reactants and products move toward or away from the electrode surface: diffusion, migration, and convection. Diffusion occurs whenever the concentration of an ion or a molecule at the surface of the electrode is different from that in bulk solution. If we apply a potential sufficient to completely reduce $\mathrm{Fe(CN)_6^{3-}}$ at the electrode surface, the result is a concentration gradient similar to that shown in Figure 13.4.3.3 The region of solution over which diffusion occurs is the diffusion layer. In the absence of other modes of mass transport, the width of the diffusion layer, δ, increases with time as the $\mathrm{Fe(CN)_6^{3-}}$ must diffuse from an increasingly greater distance.

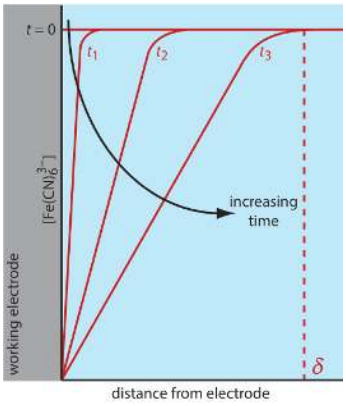


Figure 13.4.3.3. Concentration gradients (in red) for $\mathrm{Fe(CN)_6^{3-}}$ following the application of a potential that completely reduces it to $\mathrm{Fe(CN)_6^{4-}}$. Before we apply the potential (t = 0) the concentration of $\mathrm{Fe(CN)_6^{3-}}$ is the same at all distances from the electrode's surface. After we apply the potential, its concentration at the electrode's surface decreases to zero and $\mathrm{Fe(CN)_6^{3-}}$ diffuses to the electrode from bulk solution. The longer we apply the potential, the greater the distance over which diffusion occurs. The dashed red line shows the extent of the diffusion layer at time t_3. These profiles assume that convection and migration do not contribute significantly to the mass transport of $\mathrm{Fe(CN)_6^{3-}}$.

Convection occurs when we mix the solution, which carries reactants toward the electrode and removes products from the electrode. The most common form of convection is stirring the solution with a stir bar; other methods include rotating the electrode and incorporating the electrode into a flow-cell.

The final mode of mass transport is migration, which occurs when a charged particle in solution is attracted to or repelled from an electrode that carries a surface charge. If the electrode carries a positive charge, for example, an anion will move toward the electrode and a cation will move toward the bulk solution. Unlike diffusion and convection, migration affects only the mass transport of charged particles.

The movement of material to and from the electrode surface is a complex function of all three modes of mass transport. In the limit where diffusion is the only significant form of mass transport, the current, i, in a voltammetric cell is proportional to the slope of

the concentration profile in Figure 13.4.3.3

$$i \propto \frac{\partial C}{\partial x} \tag{13.4.3.4}$$

where C is the concentration of $\mathrm{Fe(CN)_6^{3-}}$ and x is distance.

For Equation 13.4.3.4 to be valid, convection and migration must not interfere with the formation of a diffusion layer. We can eliminate migration by adding a high concentration of an inert supporting electrolyte. Because ions of similar charge are equally attracted to or repelled from the surface of the electrode, each has an equal probability of undergoing migration. A large excess of an inert electrolyte ensures that few reactants or products experience migration. Although it is easy to eliminate convection by not stirring the solution, there are experimental designs where we cannot avoid convection, either because we must stir the solution or because we are using an electrochemical flow cell. Fortunately, as shown in Figure 13.4.3.4 the dynamics of a fluid moving past an electrode results in a small diffusion layer—typically 1–10 μm in thickness—in which the rate of mass transport by convection drops to zero.

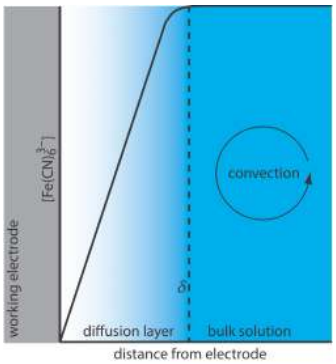


Figure 13.4.3.4. Concentration gradient for $\mathrm{Fe(CN)_6^{3-}}$ when stirring the solution. Diffusion is the only significant form of mass transport close to the electrode's surface. At distances greater than δ, convection is the only significant form of mass transport, maintaining a homogeneous solution in which the concentration of $\mathrm{Fe(CN)_6^{3-}}$ at δ is the same as its concentration in bulk solution.

Concentration Profiles in an Unstirred Solution

Figure 13.4.3.5 shows the linear sweep voltammogram (the center image, which shows the current as a function of time) and eight snapshots of the concentration profiles for the reduction of $\mathrm{Fe(CN)_6^{3-}}$ to $\mathrm{Fe(CN)_6^{4-}}$ in an unstirred solution. The initial potential was set to +0.530 V and the final potential was set to +0.182 V with a scan rate of 0.050 V/s.

At the initial potential, only $\mathrm{Fe(CN)_6^{3-}}$ is stable at the electrode surface, and no current flows. After 0.696 s the potential is 0.495 V (image to the left of the linear sweep voltammogram) and, because $\mathrm{Fe(CN)_6^{3-}}$ remains stable at the electrode surface, no current flows. Moving clockwise around the linear sweep voltammogram, the applied potential becomes smaller and the concentration of $\mathrm{Fe(CN)_6^{3-}}$ at the electrode surface decreases and the concentration of $\mathrm{Fe(CN)_6^{4-}}$ increases. Initially the slope of the concentration gradient, and, therefore, the current increases; as the concentration of $\mathrm{Fe(CN)_6^{3-}}$ at the electrode surface approaches zero, however, the concentration gradient becomes less steep and the current decreases. The result is the linear sweep voltammogram in the center of the diagram.

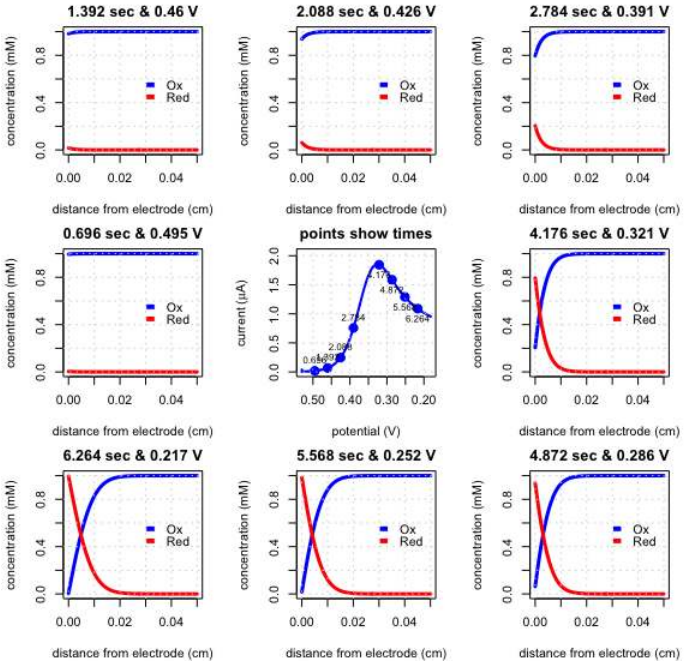


Figure 13.4.3.5: The central image shows the linear sweep voltammogram in an unstirred solution for the reduction of $Fe(CN)_6^{3-}$ to $Fe(CN)_6^{4-}$. The remaining images show the concentration profiles for $Fe(CN)_6^{3-}$ (in blue) and for $Fe(CN)_6^{4-}$ (in red) as the potential is swept from +0.530 V to +0.182 V (arranged clockwise, beginning immediately left of the linear sweep voltammogram.

Concentration Profiles in a Stirred Solution

If we run the same experiment as in Figure 13.4.3.5, but stir the solution, the resulting linear sweep voltammogram and concentration profiles are those in Figure 13.4.3.6. Stirring the solution, as we saw in Figure 13.4.3.4 creates a diffusion layer whose thickness is independent of time.

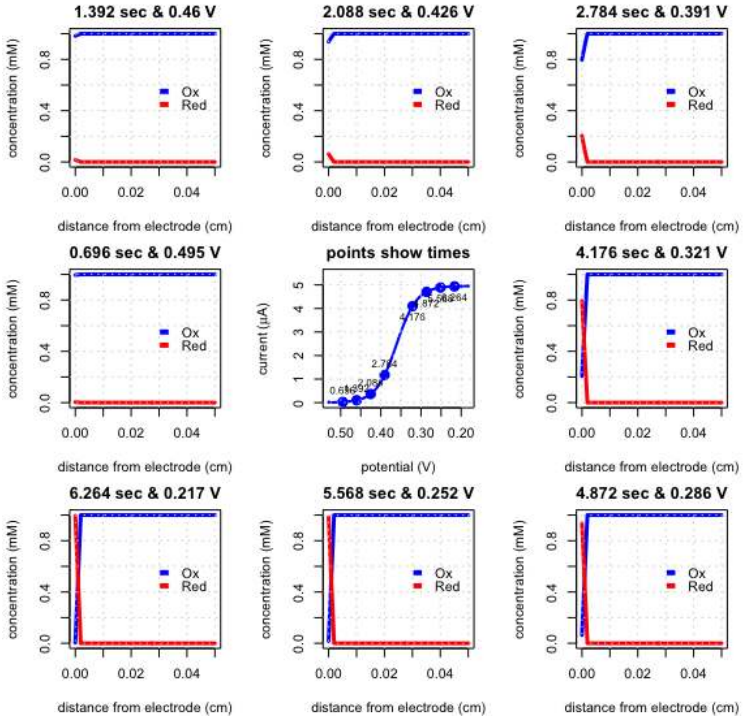


Figure 13.4.3.6: The central image shows the linear sweep voltammogram in a stirred solution for the reduction of $Fe(CN)_6^{3-}$ to $Fe(CN)_6^{4-}$. The remaining images show the concentration profiles for $Fe(CN)_6^{3-}$ (in blue) and for $Fe(CN)_6^{4-}$ (in red) as the potential is swept from +0.530 V to +0.182 V (arranged clockwise, beginning immediately left of the linear sweep voltammogram.

https://chem.libretexts.org/@go/page/532688

As a result, instead of the peak current in Figure 13.4.3.5, the current reaches a steady-state value, which we call the limiting current, i_l. The linear sweep voltammogram also has a characteristic half-wave potential, $E_{1/2}$, when the current is 50% of the limiting current. Figure 13.4.3.7shows how the limiting current and half-wave potential are measured.

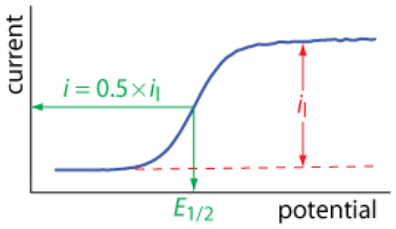


Figure 13.4.3.7: The limiting current and half-wave potential for a linear sweep voltammetry experiment in a stirred solution.

Voltammetric Currents

Earlier we noted, in Equation 13.4.3.4, that the current in linear sweep voltammetry is proportional to the slope of the concentration profile. The current is also a function of other variables, as shown here for the reduction of $\mathrm{Fe(CN)_6^{3-}}$ to $\mathrm{Fe(CN)_6^{4-}}$

$$i = \frac{nFAD\left(\left[\mathrm{Fe(CN)_6^{3-}}\right]_{\text{bulk}} - \left[\mathrm{Fe(CN)_6^{3-}}\right]_{x=0}\right)}{\delta} \tag{13.4.3.5}$$

where *n* the number of electrons in the redox reaction, *F* is Faraday's constant, *A* is the area of the electrode, *D* is the diffusion coefficient for $\mathrm{Fe(CN)_6^{3-}}$, δ is the thickness of the diffusion layer, and $\left(\left[\mathrm{Fe(CN)_6^{3-}}\right]_{\text{bulk}} - \left[\mathrm{Fe(CN)_6^{3-}}\right]_{x=0}\right)$ is the difference in the concentration of $\mathrm{Fe(CN)_6^{3-}}$ between the bulk solution and the electrode's surface.

Because n, F, A, and D are constants, and because δ is a constant if we stir the solution, we can write Equation 13.4.3.5as

$$i = K_{\mathrm{Fe(CN)_6^{3-}}}\left(\left[\mathrm{Fe(CN)_6^{3-}}\right]_{\text{bulk}} - \left[\mathrm{Fe(CN)_6^{3-}}\right]_{x=0}\right) \tag{13.4.3.6}$$

where $K_{\mathrm{Fe(CN)_6^{3-}}}$ is a constant. If we use the limiting current, then $\left[\mathrm{Fe(CN)_6^{3-}}\right]_{x=0}$ is zero, and Equation 13.4.3.6becomes

$$i_l = K_{\mathrm{Fe(CN)_6^{3-}}}\left[\mathrm{Fe(CN)_6^{3-}}\right]_{\text{bulk}} \tag{13.4.3.7}$$

Current/Voltage Relationships for Reversible Reactions

A reversible electrochemical reaction is one in which the concentration of the oxidized and reduced species at the electrode surface remain in thermodynamic equilibrium with each other. When this is true, the Nernst equation explains the relationship between the applied potential, their concentration, and the standard state potential.

Equation 13.4.3.7shows us that the limiting current is a measure of the concentration of $\mathrm{Fe(CN)_6^{3-}}$ in bulk solution, which means we can use the limiting current for quantitative work. Figure 13.4.3.7also shows that there is a qualitative relationship between the half-wave potential, $E_{1/2}$, and the limiting current; however, it is not yet clear what the half-wave potential represents.

If we solve Equation 13.4.3.7for $\left[\mathrm{Fe(CN)_6^{3-}}\right]_{\text{bulk}}$ and substitute into Equation 13.4.3.6and rearrange, we have

$$\left[\mathrm{Fe(CN)_6^{3-}}\right]_{x=0} = \frac{i_l - i}{K_{\mathrm{Fe(CN)_6^{3-}}}} \tag{13.4.3.8}$$

If we take the same approach with $\mathrm{Fe(CN)_6^{4-}}$, which forms at the electrode solution, then we have

$$i = -\frac{nFAD\left(\left[\mathrm{Fe(CN)_6^{4-}}\right]_{\text{bulk}} - \left[\mathrm{Fe(CN)_6^{4-}}\right]_{x=0}\right)}{\delta} = K_{\mathrm{Fe(CN)_6^{4-}}}\left[\mathrm{Fe(CN)_6^{4-}}\right]_{x=0} \tag{13.4.3.9}$$

$$\left[\mathrm{Fe(CN)_6^{4-}}\right]_{x=0} = \frac{-i}{K_{\mathrm{Fe(CN)_6^{4-}}}} \tag{13.4.3.10}$$

where the minus sign accounts for the concentration profile having a negative slope. Substituting Equation 13.4.3.9and Equation 13.4.3.10into Equation 13.4.3.1, which is the Nersnt equation, gives

$$E = E^\circ - 0.05916 \log \frac{-i/K_{\text{Fe(CN)}_6^{4-}}}{(i_l - i)/K_{\text{Fe(CN)}_6^{3-}}} \tag{13.4.3.11}$$

$$E = E^\circ + 0.05916 \log \frac{K_{\text{Fe(CN)}_6^{3-}}}{K_{\text{Fe(CN)}_6^{4-}}} - 0.05916 \log \frac{i}{i_l - i} \tag{13.4.3.12}$$

When $i = \frac{i_l - i}{2}$, which is the definition of $E_{1/2}$, Equation 13.4.3.12simplifies to

$$E_{1/2} = E^\circ + 0.05916 \log \frac{K_{\text{Fe(CN)}_6^{3-}}}{K_{\text{Fe(CN)}_6^{4-}}} \tag{13.4.3.13}$$

The only difference between $K_{\text{Fe(CN)}_6^{3-}}$ and $K_{\text{Fe(CN)}_6^{4-}}$ are the diffusion coefficients, D, for Fe(CN)_6^{3-} and for Fe(CN)_6^{4-}. As these values should be similar, we have

$$E_{1/2} \approx E^\circ \tag{13.4.3.14}$$

and $E_{1/2}$ provides an estimate for the standard state reduction potential.

Current/Voltage Relationships for Irreversible Reactions

When an electrochemical reaction is not reversible, the Nernst equation no longer applies, which means we can no longer assume that the half-wave potential provides an estimate for the standard state reduction potential. The relationship between the limiting current and the concentration of the electroactive species in bulk solution still holds true and quantitative work remains possible.

Oxygen Waves

The presence of dissolved oxygen creates a complication as it is capable of undergoing reduction reactions at the electrode's surface that may interfere with the determination of the analyte's limiting current or half-wave potential. For example, O_2 is reduced to H_2O_2 with a standard state potential of +0.695 V

$$\text{O}_2(g) + 2\text{H}^+(aq) + 2e^- \rightleftharpoons \text{H}_2\text{O}_2(aq) \tag{13.4.3.15}$$

and H_2O_2 subsequently is reduced to H_2O at a standard state potential of +1.763 V.

$$\text{H}_2\text{O}_2(aq) + 2\text{H}^+(aq) + 2e^- \rightleftharpoons 2\text{H}_2\text{O}(aq) \tag{13.4.3.16}$$

This is the reason that a typical cell for voltammetry (see Figure 25.2.5) includes the ability to pass N_2 through the solution to remove dissolved O_2. Once the solution is deaerated, N_2 is allowed to flow over the solution to prevent O_2 from reentering the solution.

Applications of Linear Sweep Voltammetry

As we learned in the previous section, the limiting current in linear sweep voltammetry is proportional to the concentration of the species undergoing oxidation or reduction at the electrode surface, which makes it a useful tool for a quantitative analysis. Because we are interested only in the limiting current, most quantitative methods simply hold the potential of the working electrode at a fixed value and measure the limiting current. Because we are measuring the current as a function of time instead of potential, these are called amperometric methods (where ampere is the unit for current). Several examples of amperometic methods are gathered here.

Amperometric Detectors in Chromatography and Flow-Injection Analysis

One important detector for high-performance liquid chromatography (HPLC) is one in which the mobile phase eluting from the column passes through a small volume electrochemical cell in which the working electrode is held at a potential that will oxidize or reduce the analytes. The resulting current is plotted as function of time to yield the chromatogram. A similar arrangement is used in flow-injection analysis (FIA). See Chapter 28 (HPLC) and Chapter 33 (FIA) for further details.

Amperometric Senors

One important application of amperometry is in the construction of chemical sensors. One of the first amperometric sensors was developed in 1956 by L. C. Clark to measure dissolved O_2 in blood. Figure 13.4.3.9shows the sensor's design, which is similar to a potentiometric membrane electrode. A thin, gas-permeable membrane is stretched across the end of the sensor and is separated

from the working electrode and the counter electrode by a thin solution of KCl. The working electrode is a Pt disk cathode, and a Ag ring anode serves as the counter electrode. Although several gases can diffuse across the membrane, including O_2, N_2, and CO_2, only oxygen undergoes reduction at the cathode

$$O_2(g) + 4H_3O^+(aq) + 4e^- \rightleftharpoons 6H_2O(l) \tag{13.4.3.17}$$

with its concentration at the electrode's surface quickly reaching zero. The concentration of O_2 at the membrane's inner surface is fixed by its diffusion through the membrane, which creates a limiting current. The result is a steady-state current that is proportional to the concentration of dissolved oxygen. Because the electrode consumes oxygen, the sample is stirred to prevent the depletion of O_2 at the membrane's outer surface.

The oxidation of the Ag anode is the other half-reaction.

$$Ag(s) + Cl^-(aq) \rightleftharpoons AgCl(s) + e^-$$

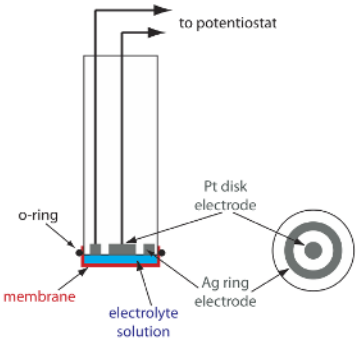


Figure 13.4.3.9. Clark amperometric sensor for determining dissolved O_2. The diagram on the right is a cross-section through the electrode, which shows the Ag ring electrode and the Pt disk electrode.

Another example of an amperometric sensor is a glucose sensor. In this sensor the single membrane in Figure 13.4.3.10is replaced with three membranes. The outermost membrane of polycarbonate is permeable to glucose and O_2. The second membrane contains an immobilized preparation of glucose oxidase that catalyzes the oxidation of glucose to gluconolactone and hydrogen peroxide.

$$\beta - D - \text{glucose}\,(aq) + O_2(aq) + H_2O(l) \rightleftharpoons \text{gluconolactone}\,(aq) + H_2O_2(aq) \tag{13.4.3.18}$$

The hydrogen peroxide diffuses through the innermost membrane of cellulose acetate where it undergoes oxidation at a Pt anode.

$$H_2O_2(aq) + 2OH^-(aq) \rightleftharpoons O_2(aq) + 2H_2O(l) + 2e^- \tag{13.4.3.19}$$

Figure 13.4.3.10summarizes the reactions that take place in this amperometric sensor. FAD is the oxidized form of flavin adenine nucleotide—the active site of the enzyme glucose oxidase—and $FADH_2$ is the active site's reduced form. Note that O_2 serves a mediator, carrying electrons to the electrode.

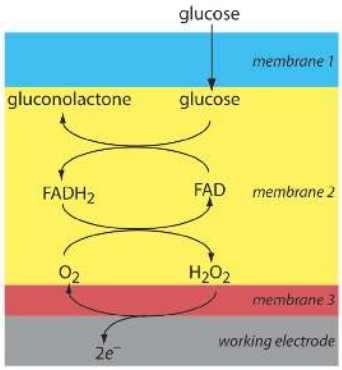


Figure 13.4.3.10. Schematic showing the reactions by which an amperometric biosensor responds to glucose.

By changing the enzyme and mediator, it is easy to extend to the amperometric sensor in Figure 13.4.3.10to the analysis of other analytes. For example, a CO_2 sensor has been developed using an amperometric O_2 sensor with a two-layer membrane, one of

which contains an immobilized preparation of autotrophic bacteria [Karube, I.; Nomura, Y.; Arikawa, Y. *Trends in Anal. Chem.* **1995**, *14*, 295–299]. As CO_2 diffuses through the membranes it is converted to O_2 by the bacteria, increasing the concentration of O_2 at the Pt cathode.

This page titled 13.4.3: Linear Sweep Voltammetry is shared under a CC BY-NC-SA 4.0 license and was authored, remixed, and/or curated by David Harvey.

- **25.3: Linear Sweep Voltammetry** by David Harvey is licensed CC BY-NC-SA 4.0.

13.4.4: Cyclic Voltammetry

In linear sweep voltammetry we scan the potential in one direction, either to more positive potentials or to more negative potentials. In cyclic voltammetry we complete a scan in both directions. Figure 13.4.4.1a shows a typical potential-excitation signal. In this example, we first scan the potential to more positive values, resulting in the following oxidation reaction for the species *R*.

$$R \rightleftharpoons O + ne^- \tag{13.4.4.1}$$

When the potential reaches a predetermined switching potential, we reverse the direction of the scan toward more negative potentials. Because we generated the species *O* on the forward scan, during the reverse scan it reduces back to *R*.

$$O + ne^- \rightleftharpoons R \tag{13.4.4.2}$$

Cyclic voltammetry is carried out in an unstirred solution, which, as shown in Figure 13.4.4.1b, results in peak currents instead of limiting currents. The voltammogram has separate peaks for the oxidation reaction and for the reduction reaction, each characterized by a peak potential and a peak current.

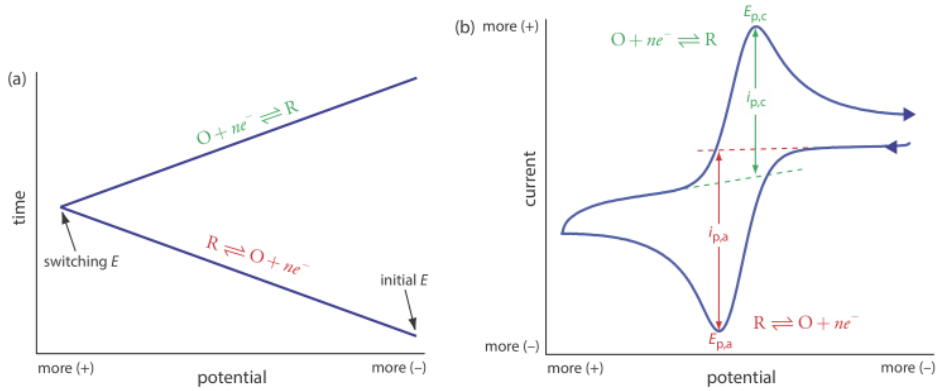


Figure 13.4.4.1. Details for cyclic voltammetry. (a) One cycle of the triangular potential-excitation signal showing the initial potential and the switching potential. A cyclic voltammetry experiment can consist of one cycle or many cycles. Although the initial potential in this example is the negative switching potential, the cycle can begin with an intermediate initial potential and cycle between two limits. (b) The resulting cyclic voltammogram showing the measurement of the peak currents and peak potentials.

The peak current in cyclic voltammetry is given by the Randles-Sevcik equation

$$i_p = \left(2.69 \times 10^5\right) n^{3/2} A D^{1/2} \nu^{1/2} C_A \tag{13.4.4.3}$$

where *n* is the number of electrons in the redox reaction, *A* is the area of the working electrode, *D* is the diffusion coefficient for the electroactive species, ν is the scan rate, and C_A is the concentration of the electroactive species at the electrode. For a well-behaved system, the anodic and the cathodic peak currents are equal, and the ratio $i_{p,a}/i_{p,c}$ is 1.00. The half-wave potential, $E_{1/2}$, is midway between the anodic and cathodic peak potentials.

$$E_{1/2} = \frac{E_{p,a} + E_{p,c}}{2} \tag{13.4.4.4}$$

Scanning the potential in both directions provides an opportunity to explore the electrochemical behavior of species generated at the electrode. This is a distinct advantage of cyclic voltammetry over other voltammetric techniques. Figure 13.4.4.2 shows the cyclic voltammogram for the same redox couple at both a faster and a slower scan rate. At the faster scan rate, 13.4.4.2a, we see two peaks. At the slower scan rate in Figure 13.4.4.2b, however, the peak on the reverse scan disappears. One explanation for this is that the products from the reduction of *R* on the forward scan have sufficient time to participate in a chemical reaction whose products are not electroactive.

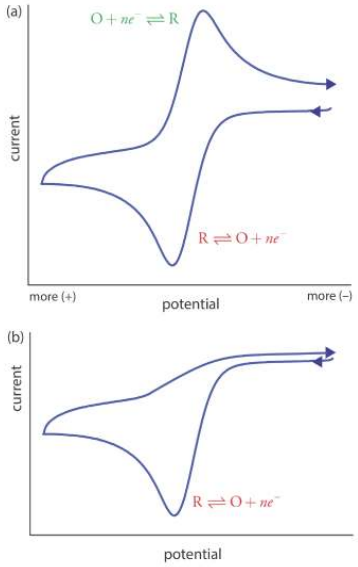


Figure 13.4.4.2. Cyclic voltammograms for *R* obtained at (a) a faster scan rate and at (b) a slower scan rate. One of the principal uses of cyclic voltammetry is to study the chemical and electrochemical behavior of compounds. See this chapter's additional resources for further information.

This page titled 13.4.4: Cyclic Voltammetry is shared under a CC BY-NC-SA 4.0 license and was authored, remixed, and/or curated by David Harvey.

- **25.4: Cyclic Voltammetry** by David Harvey is licensed CC BY-NC-SA 4.0.

13.4.5: Polarography

The first important voltammetric technique to be developed—polarography—uses the dropping mercury (DME) electrode as the working electrode (see Figure 25.2.2 for a schematic diagram of the DME as well as two other types of Hg electrodes). In polarography, as in linear sweep voltammetry, we vary the potential and measure the current. The change in potential can be in the form of a linear ramp, as was the case for linear sweep voltammetry, or it can involve a series of pulses.

Normal Polarography

As shown in Figure 13.4.5.1, the current is measured while applying a linear potential ramp.

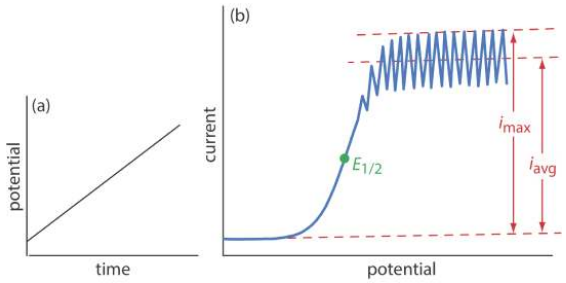


Figure 13.4.5.1. Details of normal polarography: (a) the linear potential-excitation signal, and (b) the resulting voltammogram.

Although polarography takes place in an unstirred solution, we obtain a limiting current instead of a peak current. When a Hg drop separates from the glass capillary and falls to the bottom of the electrochemical cell, it mixes the solution. Each new Hg drop, therefore, grows into a solution whose composition is identical to the bulk solution. The oscillations in the current are a result of the Hg drop's growth, which leads to a time-dependent change in the area of the working electrode. The limiting current—which also is called the diffusion current—is measured using either the maximum current, i_{max}, or from the average current, i_{avg}. The relationship between the analyte's concentration, C_A, and the limiting current is given by the Ilkovic equations

$$i_{\max} = 706nD^{1/2}m^{2/3}t^{1/6}C_A = K_{\max}C_A \tag{13.4.5.1}$$

$$i_{avg} = 607nD^{1/2}m^{2/3}t^{1/6}C_A = K_{\text{avg}}C_A \tag{13.4.5.2}$$

where n is the number of electrons in the redox reaction, D is the analyte's diffusion coefficient, m is the flow rate of Hg, t is the drop's lifetime and K_{max} and K_{avg} are constants. The half-wave potential, $E_{1/2}$, provides qualitative information about the redox reaction.

Pulse Polarography

Normal polarography has been replaced by various forms of pulse polarography, several examples of which are shown in Figure 13.4.5.2 [see Osteryoung, J. *J. Chem. Educ.* **1983**, *60*, 296–298 for a comprehensive review]. Normal pulse polarography (Figure 13.4.5.2a), for example, uses a series of potential pulses characterized by a cycle of time τ, a pulse-time of t_p, a pulse potential of ΔE_p, and a scan rate of $\Delta E/\Delta t$. Typical experimental conditions for normal pulse polarography are $\tau \approx 1\ \text{s}$, $t_p \approx 50$ ms, and $\Delta E/\Delta t \approx 2\ \text{mV/s}$. The initial value of $\Delta E_p \approx 2\ \text{mV}$, and it increases by ≈ 2 mV with each pulse. The current is sampled at the end of each potential pulse for approximately 17 ms before returning the potential to its initial value. The shape of the resulting voltammogram is similar to Figure 13.4.5.1, but without the current oscillations. Because we apply the potential for only a small portion of the drop's lifetime, there is less time for the analyte to undergo oxidation or reduction and a smaller diffusion layer. As a result, the faradaic current in normal pulse polarography is greater than in the polarography, resulting in better sensitivity and smaller detection limits.

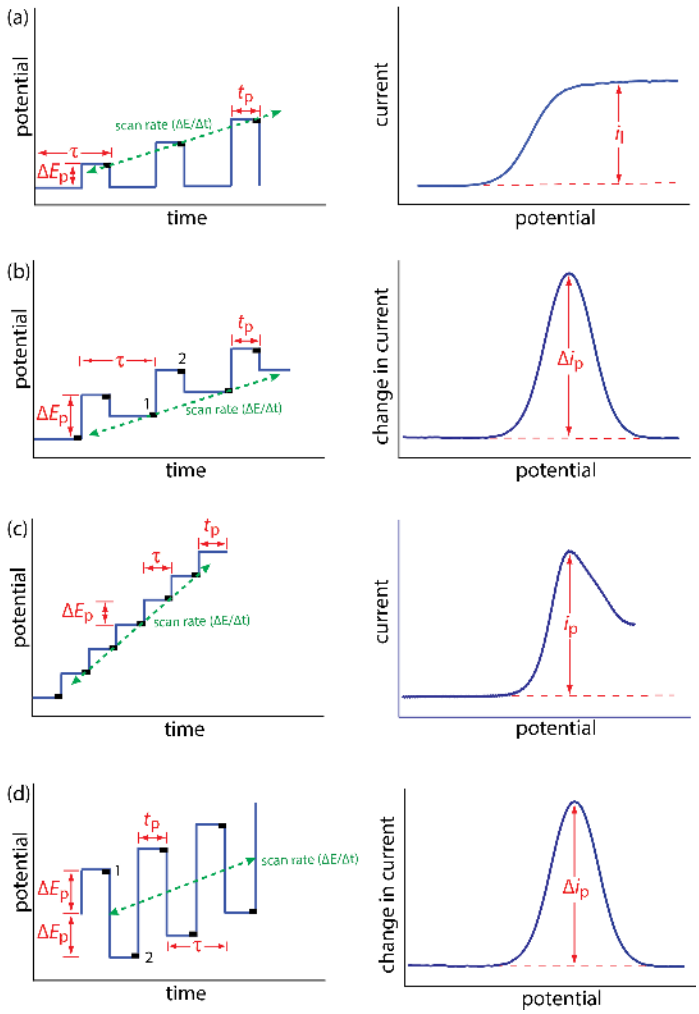


Figure 13.4.5.2. Potential-excitation signals and voltammograms for (a) normal pulse polarography, (b) differential pulse polarography, (c) staircase polarography, and (d) square-wave polarography. The current is sampled at the time intervals shown by the black rectangles. When measuring a change in current, Δi, the current at point 1 is subtracted from the current at point 2. The symbols in the diagrams are as follows: τ is the cycle time; ΔE_p is a fixed or variable pulse potential relative to the beginning of the cycle; and t_p is the pulse time. The scan rate (change in potential per unit time) is shown by the dashed arrow.

In differential pulse polarography (Figure 13.4.5.2b) the current is measured twice per cycle: for approximately 17 ms before applying the pulse and for approximately 17 ms at the end of the cycle. The difference in the two currents gives rise to the peak-shaped voltammogram. Typical experimental conditions for differential pulse polarography are $\tau \approx 1$ s, $t_p \approx 50$ ms, $\Delta E_p \approx 50$ mV, and $\Delta E/\Delta t \approx 2$ mV/s.

> The voltammogram for differential pulse polarography is approximately the first derivative of the voltammogram for normal pulse polarography. To see why this is the case, note that the change in current over a fixed change in potential, $\Delta i/\Delta E$, approximates the slope of the voltammogram for normal pulse polarography. You may recall that the first derivative of a function returns the slope of the function at each point. The first derivative of a sigmoidal function is a peak-shaped function.

Other forms of pulse polarography include staircase polarography (Figure 13.4.5.2c) and square-wave polarography (Figure 13.4.5.2d). One advantage of square-wave polarography is that we can make τ very small—perhaps as small as 5 ms, compared to 1 s for other forms of pulse polarography—which significantly decreases analysis time. For example, suppose we need to scan a potential range of 400 mV. If we use normal pulse polarography with a $\Delta E/\Delta t$ of 2 mV/cycle and a τ of 1 s/cycle, then we need 200 s to complete the scan. If we use square-wave polarography with a $\Delta E/\Delta t$ of 2 mV/cycle and a τ of 5 ms/cycle, we can complete the scan in 1 s. At this rate, we can acquire a complete voltammogram using a single drop of Hg!

Applications

Polarography is used extensively for the analysis of metal ions and inorganic anions, such as IO_3^- and NO_3^-. We also can use polarography to study organic compounds with easily reducible or oxidizable functional groups, such as carbonyls, carboxylic acids, and carbon-carbon double bonds.

This page titled 13.4.5: Polarography is shared under a CC BY-NC-SA 4.0 license and was authored, remixed, and/or curated by David Harvey.

- **25.5: Polarography** by David Harvey is licensed CC BY-NC-SA 4.0.

13.4.6: Stripping Methods

Another important voltammetric technique is stripping voltammetry, which consists of three related techniques: anodic stripping voltammetry, cathodic stripping voltammetry, and adsorptive stripping voltammetry. Because anodic stripping voltammetry is the more widely used of these techniques, we will consider it in greatest detail.

Anodic stripping voltammetry consists of two steps (Figure 13.4.6.1). The first step is a controlled potential electrolysis in which we hold the working electrode—usually a hanging mercury drop or a mercury film electrode—at a cathodic potential sufficient to deposit the metal ion on the electrode. For example, when analyzing Cu^{2+} the deposition reaction is

$$Cu^{2+} + 2e^- \rightleftharpoons Cu(Hg) \tag{13.4.6.1}$$

where Cu(Hg) indicates that the copper is amalgamated with the mercury. This step serves as a means of concentrating the analyte by transferring it from the larger volume of the solution to the smaller volume of the electrode. During most of the electrolysis we stir the solution to increase the rate of deposition. Near the end of the deposition time we stop the stirring—eliminating convection as a mode of mass transport—and allow the solution to become quiescent. Typical deposition times of 1–30 min are common, with analytes at lower concentrations requiring longer times.

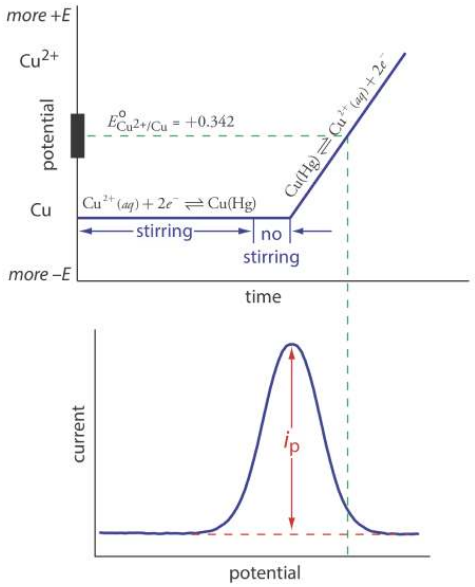


Figure 13.4.6.1. Potential-excitation signal and voltammogram for anodic stripping voltammetry at a hanging mercury drop electrode or a mercury film electrode.

In the second step, we scan the potential anodically—that is, toward a more positive potential. When the working electrode's potential is sufficiently positive, the analyte is stripped from the electrode, returning to solution in its oxidized form.

$$Cu(Hg) \rightleftharpoons Cu^{2+} + 2e^- \tag{13.4.6.2}$$

Monitoring the current during the stripping step gives a peak-shaped voltammogram, as shown in Figure 13.4.6.1. The peak current is proportional to the analyte's concentration in the solution. Because we are concentrating the analyte in the electrode, detection limits are much smaller than other electrochemical techniques. An improvement of three orders of magnitude—the equivalent of parts per billion instead of parts per million—is routine.

Applications

Anodic stripping voltammetry is very sensitive to experimental conditions, which we must carefully control to obtain results that are accurate and precise. Key variables include the area of the mercury film or the size of the hanging Hg drop, the deposition time, the rest time, the rate of stirring, and the scan rate during the stripping step. Anodic stripping voltammetry is particularly useful for metals that form amalgams with mercury, several examples of which are listed in Table 13.4.6.1.

Table 13.4.6.1. Representative Examples of Analytes Determined by Stripping Voltammetry

anodic stripping voltammetry	cathodic stripping voltammetry	adsorptive stripping voltammetry

anodic stripping voltammetry	cathodic stripping voltammetry	adsorptive stripping voltammetry
Bi^{3+}	Br^-	bilirubin
Cd^{2+}	Cl^-	codeine
Cu^{2+}	I^-	cocaine
Ga^{3+}	mercaptans (RSH)	digitoxin
In^{3+}	S^{2-}	dopamine
Pb^{2+}	SCN^-	heme
Tl^+		monesin
Sn^{2+}		testosterone
Zn^{2+}		

Source: Compiled from Peterson, W. M.; Wong, R. V. *Am. Lab.* November 1981, 116–128; Wang, J. *Am. Lab.* May 1985, 41–50.

The experimental design for cathodic stripping voltammetry is similar to anodic stripping voltammetry with two exceptions. First, the deposition step involves the oxidation of the Hg electrode to Hg_2^{2+}, which then reacts with the analyte to form an insoluble film at the surface of the electrode. For example, when Cl^- is the analyte the deposition step is

$$2Hg(l) + 2Cl^-(aq) \rightleftharpoons Hg_2Cl_2(s) + 2e^- \tag{13.4.6.3}$$

Second, stripping is accomplished by scanning cathodically toward a more negative potential, reducing Hg_2^{2+} back to Hg and returning the analyte to solution.

$$Hg_2Cl_2(s) + 2e^- \rightleftharpoons 2Hg(l) + 2Cl^-(aq) \tag{13.4.6.4}$$

Table 13.4.6.1lists several analytes analyzed successfully by cathodic stripping voltammetry.

In adsorptive stripping voltammetry, the deposition step occurs without electrolysis. Instead, the analyte adsorbs to the electrode's surface. During deposition we maintain the electrode at a potential that enhances adsorption. For example, we can adsorb a neutral molecule on a Hg drop if we apply a potential of –0.4 V versus the SCE, a potential where the surface charge of mercury is approximately zero. When deposition is complete, we scan the potential in an anodic or a cathodic direction, depending on whether we are oxidizing or reducing the analyte. Examples of compounds that have been analyzed by absorptive stripping voltammetry also are listed in Table 13.4.6.1.

This page titled 13.4.6: Stripping Methods is shared under a CC BY-NC-SA 4.0 license and was authored, remixed, and/or curated by David Harvey.

- **25.6: Stripping Methods** by David Harvey is licensed CC BY-NC-SA 4.0.

13.4.7: Applications of Voltammetry

Voltammetry finds use for both quantitative analyses and characterization analyses. Examples of each are highlighted in this section.

Quantitative Applications

Voltammetry has been used for the quantitative analysis of a wide variety of samples, including environmental samples, clinical samples, pharmaceutical formulations, steels, gasoline, and oil.

Selecting the Voltammetric Technique

The choice of which voltammetric technique to use depends on the sample's characteristics, including the analyte's expected concentration and the sample's location. For example, amperometry is ideally suited for detecting analytes in flow systems, including the *in vivo* analysis of a patient's blood or as a selective sensor for the rapid analysis of a single analyte. The portability of amperometric sensors, which are similar to potentiometric sensors, also make them ideal for field studies. Although cyclic voltammetry is used to determine an analyte's concentration, other methods described in this chapter are better suited for quantitative work.

Pulse polarography and stripping voltammetry frequently are interchangeable. The choice of which technique to use often depends on the analyte's concentration and the desired accuracy and precision. Detection limits for normal pulse polarography generally are on the order of 10^{-6} M to 10^{-7} M, and those for differential pulse polarography, staircase, and square wave polarography are between 10^{-7} M and 10^{-9} M. Because we concentrate the analyte in stripping voltammetry, the detection limit for many analytes is as little as 10^{-10} M to 10^{-12} M. On the other hand, the current in stripping voltammetry is much more sensitive than pulse polarography to changes in experimental conditions, which may lead to poorer precision and accuracy. We also can use pulse polarography to analyze a wider range of inorganic and organic analytes because there is no need to first deposit the analyte at the electrode surface.

Stripping voltammetry also suffers from occasional interferences when two metals, such as Cu and Zn, combine to form an intermetallic compound in the mercury amalgam. The deposition potential for Zn is sufficiently negative that any Cu^{2+} in the sample also deposits into the mercury drop or film, leading to the formation of intermetallic compounds such as CuZn and $CuZn_2$. During the stripping step, zinc in the intermetallic compounds strips at potentials near that of copper, decreasing the current for zinc at its usual potential and increasing the apparent current for copper. It is possible to overcome this problem by adding an element that forms a stronger intermetallic compound with the interfering metal. Thus, adding Ga^{3+} minimizes the interference of Cu when analyzing for Zn by forming an intermetallic compound of Cu and Ga.

Correcting for the Residual Current

In any quantitative analysis we must correct the analyte's signal for signals that arise from other sources. The total current, i_{tot}, in voltammetry consists of two parts: the current from the analyte's oxidation or reduction, i_A, and a background or residual current, i_r.

$$i_{tot} = i_A + i_r \tag{13.4.7.1}$$

The residual current, in turn, has two sources. One source is a faradaic current from the oxidation or reduction of trace interferents in the sample, i_{int}. The other source is the charging current, i_{ch}, that accompanies a change in the working electrode's potential.

$$i_r = i_{\text{int}} + i_{ch} \tag{13.4.7.2}$$

We can minimize the faradaic current due to impurities by carefully preparing the sample. For example, one important impurity is dissolved O_2, which undergoes a two-step reduction: first to H_2O_2 at a potential of –0.1 V versus the SCE, and then to H_2O at a potential of –0.9 V versus the SCE. Removing dissolved O_2 by bubbling an inert gas such as N_2 through the sample eliminates this interference. After removing the dissolved O_2, maintaining a blanket of N_2 over the top of the solution prevents O_2 from reentering the solution.

There are two methods to compensate for the residual current. One method is to measure the total current at potentials where the analyte's faradaic current is zero and extrapolate it to other potentials. This is the method shown in Figure 25.3.7. One advantage of extrapolating is that we do not need to acquire additional data. An important disadvantage is that an extrapolation assumes that any change in the residual current with potential is predictable, which may not be the case. A second, and more rigorous approach, is to obtain a voltammogram for an appropriate blank. The blank's residual current is then subtracted from the sample's total current.

Analysis for Single Components

The analysis of a sample with a single analyte is straightforward using any of the standardization methods discussed in Chapter 1.

Example 13.4.7.1

The concentration of As(III) in water is determined by differential pulse polarography in 1 M HCl. The initial potential is set to –0.1 V versus the SCE and is scanned toward more negative potentials at a rate of 5 mV/s. Reduction of As(III) to As(0) occurs at a potential of approximately –0.44 V versus the SCE. The peak currents for a set of standard solutions, corrected for the residual current, are shown in the following table.

[As(III)] (μM)	i_p (μM)
1.00	0.298
3.00	0.947
6.00	1.83
9.00	2.72

What is the concentration of As(III) in a sample of water if its peak current is 1.37 μA?

Solution

Linear regression gives the calibration curve shown in Figure 13.4.7.1, with an equation of

$$i_p = 0.0176 + 3.01 \times [\text{As(III)}]$$

Substituting the sample's peak current into the regression equation gives the concentration of As(III) as 4.49 μM.

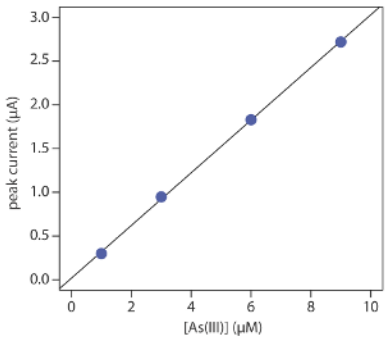


Figure 13.4.7.1. Calibration curve for the data in Example 13.4.7.1.

Multicomponent Analysis

Voltammetry is a particularly attractive technique for the analysis of samples that contain two or more analytes. Provided that the analytes behave independently, the voltammogram of a multicomponent mixture is a summation of each analyte's individual voltammograms. As shown in Figure 13.4.7.2, if the separation between the half-wave potentials or between the peak potentials is sufficient, we can determine the presence of each analyte as if it is the only analyte in the sample. The minimum separation between the half-wave potentials or peak potentials for two analytes depends on several factors, including the type of electrode and the potential-excitation signal. For normal polarography the separation is at least ±0.2–0.3 V, and differential pulse voltammetry requires a minimum separation of ±0.04–0.05 V.

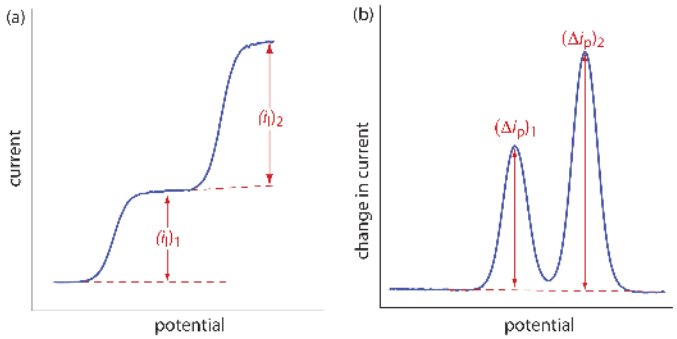


Figure 13.4.7.2. Voltammograms for a sample that contains two analytes showing the measurement of (a) limiting currents, and (b) peak currents.

If the voltammograms for two analytes are not sufficiently separated, a simultaneous analysis may be possible. An example of this approach is outlined the following example.

Example 13.4.7.2

The differential pulse polarographic analysis of a mixture of indium and cadmium in 0.1 M HCl is complicated by the overlap of their respective voltammograms [Lanza P. *J. Chem. Educ.* **1990**, *67*, 704–705]. The peak potential for indium is at –0.557 V and that for cadmium is at –0.597 V. When a 0.800-ppm indium standard is analyzed, Δi_p (in arbitrary units) is 200.5 at –0.557 V and 87.5 at –0.597 V relative to a saturated Ag/AgCl reference electorde. A standard solution of 0.793 ppm cadmium has a Δi_p of 58.5 at –0.557 V and 128.5 at –0.597 V. What is the concentration of indium and cadmium in a sample if Δi_p is 167.0 at a potential of –0.557 V and 99.5 at a potential of –0.597V.

Solution

The change in current, Δi_p, in differential pulse polarography is a linear function of the analyte's concentration

$$\Delta i_p = k_A C_A$$

where k_A is a constant that depends on the analyte and the applied potential, and C_A is the analyte's concentration. To determine the concentrations of indium and cadmium in the sample we must first find the value of k_A for each analyte at each potential. For simplicity we will identify the potential of –0.557 V as E_1, and that for –0.597 V as E_2. The values of k_A are

$$k_{\text{In},E_1} = \frac{200.5}{0.800 \text{ ppm}} = 250.6 \text{ ppm}^{-1}$$
$$k_{\text{In},E_2} = \frac{87.5}{0.800 \text{ ppm}} = 109.4 \text{ ppm}^{-1}$$
$$k_{\text{Cd}E_1} = \frac{58.5}{0.793 \text{ ppm}} = 73.8 \text{ ppm}^{-1}$$
$$k_{\text{Cd}E_2} = \frac{128.5}{0.793 \text{ ppm}} = 162.0 \text{ ppm}^{-1}$$

Next, we write simultaneous equations for the current at the two potentials.

$$\Delta i_{E_1} = 167.0 = 250.6 \text{ ppm}^{-1} \times C_{\text{In}} + 73.8 \text{ ppm}^{-1} \times C_{\text{Cd}}$$
$$\triangle i_{E_2} = 99.5 = 109.4 \text{ ppm}^{-1} \times C_{\text{In}} + 162.0 \text{ ppm}^{-1} \times C_{\text{Cd}}$$

Solving the simultaneous equations, which is left as an exercise, gives the concentration of indium as 0.606 ppm and the concentration of cadmium as 0.205 ppm.

Environmental Samples

Voltammetry is one of several important analytical techniques for the analysis of trace metals in environmental samples, including groundwater, lakes, rivers and streams, seawater, rain, and snow. Detection limits at the parts-per-billion level are routine for many trace metals using differential pulse polarography, with anodic stripping voltammetry providing parts-per-trillion detection limits for some trace metals.

One interesting environmental application of anodic stripping voltammetry is the determination of a trace metal's chemical form within a water sample. Speciation is important because a trace metal's bioavailability, toxicity, and ease of transport through the environment often depends on its chemical form. For example, a trace metal that is strongly bound to colloidal particles generally is not toxic because it is not available to aquatic lifeforms. Unfortunately, anodic stripping voltammetry can not distinguish a trace metal's exact chemical form because closely related species, such as Pb^{2+} and $PbCl^{+}$, produce a single stripping peak. Instead, trace metals are divided into "operationally defined" categories that have environmental significance.

> Operationally defined means that an analyte is divided into categories by the specific methods used to isolate it from the sample. There are many examples of operational definitions in the environmental literature. The distribution of trace metals in soils and sediments, for example, often is defined in terms of the reagents used to extract them; thus, you might find an operational definition for Zn^{2+} in a lake sediment as that extracted using 1.0 M sodium acetate, or that extracted using 1.0 M HCl.

Although there are many speciation schemes in the environmental literature, we will consider one proposed by Batley and Florence [see (a) Batley, G. E.; Florence, T. M. *Anal. Lett.* **1976**, *9*, 379–388; (b) Batley, G. E.; Florence, T. M. *Talanta* **1977**, *24*, 151–158; (c) Batley, G. E.; Florence, T. M. *Anal. Chem.* **1980**, *52*, 1962–1963; (d) Florence, T. M., Batley, G. E.; *CRC Crit. Rev. Anal. Chem.* **1980**, *9*, 219–296]. This scheme, which is outlined in Table 13.4.7.2, combines anodic stripping voltammetry with ion-exchange and UV irradiation, dividing soluble trace metals into seven groups. In the first step, anodic stripping voltammetry in a pH 4.8 acetic acid buffer differentiates between labile metals and nonlabile metals. Only labile metals—those present as hydrated ions, weakly bound complexes, or weakly adsorbed on colloidal surfaces—deposit at the electrode and give rise to a signal. Total metal concentration are determined by ASV after digesting the sample in 2 M HNO_3 for 5 min, which converts all metals into an ASV-labile form.

Table 13.4.7.1. Operational Speciation of Soluble Trace Metals

method	speciation of soluble metals						
ASV	labile metals			nonlabile or bound metals			
Ion-Exchange	removed	not removed		removed		not removed	
UV Irradiation		released	not released	released	not released	released	not released
Groups	I	II	III	IV	V	VI	VII
Group I: free metal ions; weaker labile organic complexes and inorganic complexes							
Group II: stronger labile organic complexes; labile metals absorbed on organic solids							
Group III: stronger labile inorganic complexes; labile metals absorbed on inorganic solids							
Group IV: weaker nonlabile organic complexes							
Group V: weaker nonlabile inorganic complexes							
Group VI: stronger nonlabile organic complexes; nonlabile metals absorbed on organic solids							
Group VII: stronger nonlabile inorganic complexes; nonlabile metals absorbed on inorganic solids							
Operational definitions of speciation from (a)Batley,G.E.;Florence,T.M.*Anal.Lett.***1976**,*9*,379–388; (b)Batley,G.E.;Florence,T.M.*Talanta***1977**,*24*,151–158; (c) Batley, G. E.; Florence, T. M. *Anal. Chem.* **1980**, *52*, 1962–1963; (d) Florence, T. M., Batley, G. E.; *CRC Crit. Rev. Anal. Chem.* **1980**, *9*, 219–296.							

A Chelex-100 ion-exchange resin further differentiates between strongly bound metals—usually metals bound to inorganic and organic solids, but also those tightly bound to chelating ligands—and more loosely bound metals. Finally, UV radiation differentiates between metals bound to organic phases and inorganic phases. The analysis of seawater samples, for example, suggests that cadmium, copper, and lead are present primarily as labile organic complexes or as labile adsorbates on organic colloids (Group II in Table 13.4.7.1).

Differential pulse polarography and stripping voltammetry are used to determine trace metals in airborne particulates, incinerator fly ash, rocks, minerals, and sediments. The trace metals, of course, are first brought into solution using a digestion or an

extraction.

Amperometric sensors also are used to analyze environmental samples. For example, the dissolved O_2 sensor described earlier is used to determine the level of dissolved oxygen and the biochemical oxygen demand, or BOD, of waters and wastewaters. The latter test—which is a measure of the amount of oxygen required by aquatic bacteria as they decompose organic matter—is important when evaluating the efficiency of a wastewater treatment plant and for monitoring organic pollution in natural waters. A high BOD suggests that the water has a high concentration of organic matter. Decomposition of this organic matter may seriously deplete the level of dissolved oxygen in the water, adversely affecting aquatic life. Other amperometric sensors are available to monitor anionic surfactants in water, and CO_2, H_2SO_4, and NH_3 in atmospheric gases.

Clinical Samples

Differential pulse polarography and stripping voltammetry are used to determine the concentration of trace metals in a variety of clinical samples, including blood, urine, and tissue. The determination of lead in blood is of considerable interest due to concerns about lead poisoning. Because the concentration of lead in blood is so small, anodic stripping voltammetry frequently is the more appropriate technique. The analysis is complicated, however, by the presence of proteins that may adsorb to the mercury electrode, inhibiting either the deposition or stripping of lead. In addition, proteins may prevent the electrodeposition of lead through the formation of stable, nonlabile complexes. Digesting and ashing the blood sample mini- mizes this problem. Differential pulse polarography is useful for the routine quantitative analysis of drugs in biological fluids, at concentrations of less than 10^{-6} M [Brooks, M. A. “Application of Electrochemistry to Pharmaceutical Analysis,” Chapter 21 in Kissinger, P. T.; Heinemann, W. R., eds. *Laboratory Techniques in Electroanalytical Chemistry*, Marcel Dekker, Inc.: New York, 1984, pp 539–568.]. Amperometric sensors using enzyme catalysts also have many clinical uses, several examples of which are shown in Table 13.4.7.2

Table 13.4.7.2. Representative Amperometric Biosensors

analyte	enzyme	species detected
choline	choline oxidase	H_2O_2
ethanol	alcohol oxidase	H_2O_2
formaldehyde	formaldehyde dehydrogenase	NADH
glucose	glucose oxidase	H_2O_2
glutamine	glutaminase, glutamine oxidase	H_2O_2
glycerol	glycerol dehydrogenase	NADH, O_2
lactate	lactate oxidase	H_2O_2
phenol	polyphenol oxidase	quinone
inorganic phosphorous	nucleoside phosphoylase	O_2

Source: Cammann, K.; Lemke, U.; Rohen, A.; Sander, J.; Wilken, H.; Winter, B. *Angew. Chem. Int. Ed. Engl.* **1991**, *30*, 516–539.

Miscellaneous Samples

In addition to environmental samples and clinical samples, differential pulse polarography and stripping voltammetry are used for the analysis of trace metals in other sample, including food, steels and other alloys, gasoline, gunpowder residues, and pharmaceuticals. Voltammetry is an important technique for the quantitative analysis of organics, particularly in the pharmaceutical industry where it is used to determine the concentration of drugs and vitamins in formulations. For example, voltammetric methods are available for the quantitative analysis of vitamin A, niacinamide, and riboflavin. When the compound of interest is not electroactive, it often can be derivatized to an electroactive form. One example is the differential pulse polarographic determination of sulfanilamide, which is converted into an electroactive azo dye by coupling with sulfamic acid and 1-napthol.

In the previous section we learned how to use voltammetry to determine an analyte’s concentration in a variety of different samples. We also can use voltammetry to characterize an analyte’s properties, including verifying its electrochemical reversibility, determining the number of electrons transferred during its oxidation or reduction, and determining its equilibrium constant in a coupled chemical reaction.

Characterization Applications

In a characterization application we study the properties of a system. Three examples are described here: determining if a redox reaction is electrochemically reversible, determining the number of electrons involved in the redox reaction, and studying metal-ligand complexation.

Electrochemical Reversibility and Determination of *n*

Earlier in this chapter we derived a relationship between $E_{1/2}$ and the standard-state potential for a redox couple using the Nernst equation, noting that a redox reaction must be electrochemically reversible. How can we tell if a redox reaction is reversible by looking at its voltammogram? As we learned in Chapter 25.3, for a reversible redox reaction the relationship between potential and current is

$$E = E_{½} - \frac{0.05916}{n} \log \frac{i}{i_l - i} \tag{13.4.7.3}$$

If a reaction is electrochemically reversible, a plot of E versus $\log \frac{i}{i_l - i}$ is a straight line with a slope of –0.05916/n. In addition, the slope should yield an integer value for n.

Example 13.4.7.3

The following data were obtained from a linear scan hydrodynamic voltammogram of a reversible reduction reaction.

E (V vs. SCE)	current (μA)
–0.358	0.37
–0.372	0.95
–0.382	1.71
–0.400	3.48
–0.410	4.20
–0.435	4.97

The limiting current is 5.15 μA. Show that the reduction reaction is reversible, and determine values for n and for $E_{1/2}$.

Solution

Figure 13.4.7.3 shows a plot of E versus $\log \frac{i}{i_l - i}$. Because the result is a straight-line, we know the reaction is electrochemically reversible under the conditions of the experiment. A linear regression analysis gives the equation for the straight line as

$$E = -0.391\text{V} - 0.0300 \log \frac{i}{i_l - i}$$

From Equation 13.4.7.3, the slope is equivalent to –0.05916/n; solving for n gives a value of 1.97, or 2 electrons. From Equation 13.4.7.3we also know that $E_{1/2}$ is the y-intercept for a plot of E versus $\log \frac{i}{i_l - i}$; thus, $E_{1/2}$ for the data in this example is –0.391 V versus the SCE.

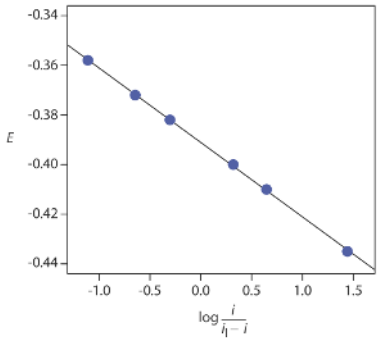


Figure 13.4.7.3. Determination of electrochemical reversibility for the data in Example 13.4.7.3.

We also can use cyclic voltammetry to evaluate electrochemical reversibility by looking at the difference between the peak potentials for the anodic and the cathodic scans. For an electrochemically reversible reaction, the following equation holds true.

$$\Delta E_p = E_{p,a} - E_{p,c} = \frac{0.05916 \text{ V}}{n} \tag{13.4.7.4}$$

As an example, for a two-electron reduction we expect a ΔE_p of approximately 29.6 mV. For an electrochemically irreversible reaction the value of ΔE_p is larger than expected.

Determining Equilibrium Constants for Coupled Chemical Reactions

Another important application of voltammetry is determining the equilibrium constant for a solution reaction that is coupled to a redox reaction. The presence of the solution reaction affects the ease of electron transfer in the redox reaction, shifting $E_{1/2}$ to a more negative or to a more positive potential. Consider, for example, the reduction of *O* to R

$$O + ne^- \rightleftharpoons R \tag{13.4.7.5}$$

the voltammogram for which is shown in Figure 13.4.7.4 If we introduce a ligand, *L*, that forms a strong complex with *O*, then we also must consider the reaction

$$O + pL \rightleftharpoons OL_p \tag{13.4.7.6}$$

In the presence of the ligand, the overall redox reaction is

$$OL_p + ne^- \rightleftharpoons R + pL \tag{13.4.7.7}$$

Because of its stability, the reduction of the OL_p complex is less favorable than the reduction of *O*. As shown in Figure 13.4.7.4 the resulting voltammogram shifts to a potential that is more negative than that for *O*. Furthermore, the shift in the voltammogram increases as we increase the ligand's concentration.

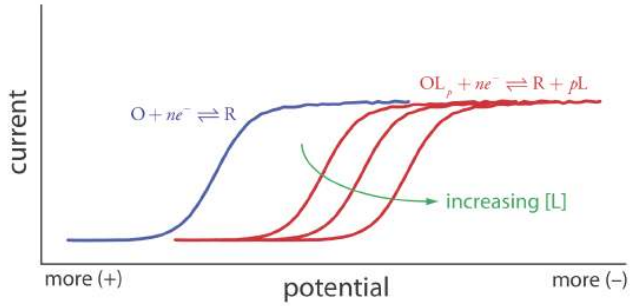


Figure 13.4.7.4. Effect of a metal-ligand complexation reaction on a voltammogram. The voltammogram in blue is for the reduction of *O* in the absence of ligand. Adding the ligand shifts the potentials to more negative potentials, as shown by the voltammograms in red.

We can use this shift in the value of $E_{1/2}$ to determine both the stoichiometry and the formation constant for a metal-ligand complex. To derive a relationship between the relevant variables we begin with two equations: the Nernst equation for the reduction of *O*

$$E = E^{\circ}_{O/R} - \frac{0.05916}{n} \log \frac{[R]_{x=0}}{[O]_{x=0}} \tag{13.4.7.8}$$

and the stability constant, β_p for the metal-ligand complex at the electrode surface.

$$\beta_p = \frac{[OL_p]_{x=0}}{[O]_{x=0}[L]^p_{x=0}} \tag{13.4.7.9}$$

In the absence of ligand the half-wave potential occurs when $[R]_{x = 0}$ and $[O]_{x = 0}$ are equal; thus, from the Nernst equation we have

$$\left(E_{1/2}\right)_{nc} = E^{\circ}_{O/R} \tag{13.4.7.10}$$

where the subscript "*nc*" signifies that the complex is not present. When ligand is present we must account for its effect on the concentration of *O*. Solving Equation 13.4.7.9 for $[O]_{x = 0}$ and substituting into the Equation 13.4.7.8 gives

$$E = E^{\circ}_{O/R} - \frac{0.05916}{n} \log \frac{[R]_{x=0}[L]^p_{x=0}\beta_p}{[OL_p]_{x=0}} \tag{13.4.7.11}$$

If the formation constant is sufficiently large, such that essentially all *O* is present as the complex OL_p, then $[R]_{x=0}$ and $[OL_p]_{x=0}$ are equal at the half-wave potential, and Equation 13.4.7.11 simplifies to

$$\left(E_{1/2}\right)_c = E^{\circ}_{O/R} - \frac{0.05916}{n} \log [L]^p_{x=0}\beta_p \tag{13.4.7.12}$$

where the subscript "*c*" indicates that the complex is present. Defining $\Delta E_{1/2}$ as

$$\triangle E_{1/2} = \left(E_{1/2}\right)_c - \left(E_{1/2}\right)_{nc} \tag{13.4.7.13}$$

and substituting Equation 13.4.7.10 and Equation 13.4.7.12 and expanding the log term leaves us with the following equation.

$$\Delta E_{1/2} = -\frac{0.05916}{n} \log \beta_p - \frac{0.05916p}{n} \log [L] \tag{13.4.7.14}$$

A plot of $\Delta E_{1/2}$ versus log[L] is a straight-line, with a slope that is a function of the metal-ligand complex's stoichiometric coefficient, *p*, and a *y*-intercept that is a function of its formation constant β_p.

Example 13.4.7.4

A voltammogram for the two-electron reduction (n = 2) of a metal, *M*, has a half-wave potential of –0.226 V versus the SCE. In the presence of an excess of ligand, *L*, the following half-wave potentials are recorded.

[L] (M)	$(E_{1/2})_c$ (V vs. SCE)
0.020	–0.494
0.040	–0.512
0.060	–0.523
0.080	–0.530
0.100	–0.536

Determine the stoichiometry of the metal-ligand complex and its formation constant.

Solution

We begin by calculating values of $\Delta E_{1/2}$ using Equation 13.4.7.13, obtaining the values in the following table.

[L] (M)	$\Delta E_{1/2}$ (V vs. SCE)
0.020	–0.268
0.040	–0.286

[L] (M)	$\Delta E_{1/2}$ (V vs. SCE)
0.020	–0.308
0.040	–0.318
0.060	–0.297
0.080	–0.304
0.100	–0.310

Figure 13.4.7.5 shows the resulting plot of $\Delta E_{1/2}$ as a function of log[L]. A linear regression analysis gives the equation for the straight line as

$$\triangle E_{1/2} = -0.370\text{V} - 0.0601 \log [L]$$

From Equation 13.4.7.14 we know that the slope is equal to –0.05916p/n. Using the slope and n = 2, we solve for p obtaining a value of 2.03 ≈ 2. The complex's stoichiometry, therefore, is ML_2. We also know, from Equation 13.4.7.14, that the y-intercept is equivalent to –(0.05916/n)logβ_p. Solving for β_2 gives a formation constant of 3.2×10^{12}.

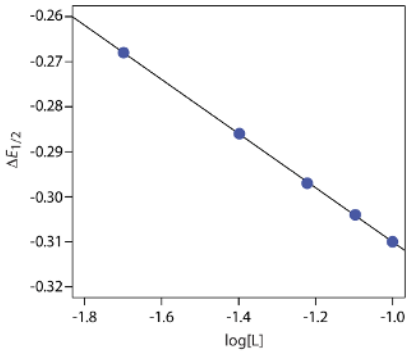


Figure 13.4.7.5. Determination of the stoichiometry and formation constant for a metal-ligand complex using the data in Example 13.4.7.4.

Cyclic voltammetry is one of the most powerful electrochemical techniques for exploring the mechanism of coupled electrochemical and chemical reactions. The treatment of this aspect of cyclic voltammetry is beyond the level of this text, although you can consult this chapter's additional resources for additional information.

This page titled 13.4.7: Applications of Voltammetry is shared under a CC BY-NC-SA 4.0 license and was authored, remixed, and/or curated by David Harvey.

- **25.7: Applications of Voltammetry** by David Harvey is licensed CC BY-NC-SA 4.0.

13.5: PROBLEMS

1. Identify the anode and the cathode for the following electrochemical cells, and identify the oxidation or the reduction reaction at each electrode.

(a) Pt| $FeCl_2$ (*aq*, 0.015), $FeCl_3$ (*aq*, 0.045) || $AgNO_3$ (*aq*, 0.1) | Ag

(b) Ag | AgBr(*s*), NaBr (*aq*, 1.0) || $CdCl_2$ (*aq*, 0.05) | Cd

(c) Pb | $PbSO_4$ (*s*), H_2SO_4 (*aq*, 1.5) || H_2SO_4 (*aq*, 2.0), $PbSO_4$ (*s*) | PbO_2

2. Calculate the potential for each electrochemical cell in problem 1. The values in parentheses are the activities of the associated species.

3. Calculate the activity of KI, *x*, in the following electrochemical cell if the potential is +0.294 V.

$$\text{Ag | AgCl (}s\text{), NaCl (}aq\text{, 0.1) || KI (aq, }x\text{), I}_2\text{ (}s\text{) | Pt}$$

4. What reaction prevents us from using Zn as an electrode of the first kind in an acidic solution? Which other metals do you expect to behave in the same manner as Zn when immersed in an acidic solution?

5. Creager and colleagues designed a salicylate ion-selective electrode using a PVC membrane impregnated with tetraalkylammonium salicylate [Creager, S. E.; Lawrence, K. D.; Tibbets, C. R. *J. Chem. Educ.* **1995**, *72*, 274–276]. To determine the ion-selective electrode's selectivity coefficient for benzoate, they prepared a set of salicylate calibration standards in which the concentration of benzoate was held constant at 0.10 M. Using the following data, determine the value of the selectivity coefficient.

[salicylate] (M)	potential (mV)
1.0	20.2
1.0×10^{-1}	73.5
1.0×10^{-2}	126
1.0×10^{-3}	168
1.0×10^{-4}	182
1.0×10^{-5}	182
1.0×10^{-6}	177

What is the maximum acceptable concentration of benzoate if you plan to use this ion-selective electrode to analyze a sample that contains as little as 10^{-5} M salicylate with an accuracy of better than 1%?

6. Watanabe and co-workers described a new membrane electrode for the determination of cocaine, a weak base alkaloid with a pK_a of 8.64 [Watanabe, K.; Okada, K.; Oda, H.; Furuno, K.; Gomita, Y.; Katsu, T. *Anal. Chim. Acta* **1995**, *316*, 371–375]. The electrode's response for a fixed concentration of cocaine is independent of pH in the range of 1–8, but decreases sharply above a pH of 8. Offer an explanation for this pH dependency.

7. Figure 11.2.14 shows a schematic diagram for an enzyme electrode that responds to urea by using a gas-sensing NH_3 electrode to measure the amount of ammonia released following the enzyme's reaction with urea. In turn, the NH_3 electrode uses a pH electrode to monitor the change in pH due to the ammonia. The response of the urea electrode is given by equation 11.2.12. Beginning with equation 11.2.19, which gives the potential of a pH electrode, show that equation 11.2.12 for the urea electrode is correct.

8. Explain why the response of an NH_3-based urea electrode (Figure 11.2.14 and equation 11.2.12) is different from the response of a urea electrode in which the enzyme is coated on the glass membrane of a pH electrode (Figure 11.2.15 and equation 11.2.13).

9. A potentiometric electrode for HCN uses a gas-permeable membrane, a buffered internal solution of 0.01 M $KAg(CN)_2$, and a Ag_2S ISE electrode that is immersed in the internal solution. Consider the equilibrium reactions that take place within the internal solution and derive an equation that relates the electrode's potential to the concentration of HCN in the sample. To check your work, search on-line for US Patent 3859191 and consult Figure 2.

10. Mifflin and associates described a membrane electrode for the quantitative analysis of penicillin in which the enzyme penicillinase is immobilized in a polyacrylamide gel coated on the glass membrane of a pH electrode [Mifflin, T. E.; Andriano, K. M.; Robbins, W. B. *J. Chem. Educ.* **1984**, *61*, 638–639]. The following data were collected using a set of penicillin standards.

[penicillin] (M)	potential (mV)
1.0×10^{-2}	220
2.0×10^{-3}	204
1.0×10^{-3}	190
2.0×10^{-4}	153
1.0×10^{-4}	135
1.0×10^{-5}	96
1.0×10^{-6}	80

(a) Over what range of concentrations is there a linear response?

(b) What is the calibration curve's equation for this concentration range?

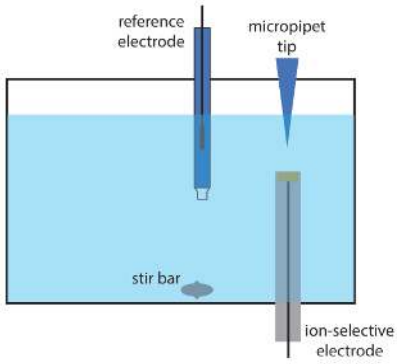
(c) What is the concentration of penicillin in a sample that yields a potential of 142 mV?

11. An ion-selective electrode can be placed in a flow cell into which we inject samples or standards. As the analyte passes through the cell, a potential spike is recorded instead of a steady-state potential. The concentration of K^+ in serum has been determined in this fashion using standards prepared in a matrix of 0.014 M NaCl [Meyerhoff, M. E.; Kovach, P. M. *J. Chem. Educ.* **1983**, *9*, 766–768].

$[K^+]$ (mM)	*E* (arb. units)	$[K^+]$ (mM)	*E* (arb. units)
0.10	25.5	0.60	58.7
0.20	37.2	0.80	64.0
0.40	50.8	1.00	66.8

A 1.00-mL sample of serum is diluted to volume in a 10-mL volumetric flask and analyzed, giving a potential of 51.1 (arbitrary units). Report the concentration of K^+ in the sample of serum.

12. Wang and Taha described an interesting application of potentiometry, which they call batch injection [Wang, J.; Taha, Z. *Anal. Chim. Acta* **1991**, *252*, 215–221]. As shown in the figure below, an ion-selective electrode is placed in an inverted position in a large volume tank, and a fixed volume of a sample or a standard solution is injected toward the electrode's surface using a micropipet. The response of the electrode is a spike in potential that is proportional to the analyte's concentration. The following data were collected using a pH electrode and a set of pH standards.



pH	potential (mV)
2.0	+300
3.0	+240
4.0	+168
5.0	+81
6.0	+35
8.0	–92
9.0	–168
10.0	–235
11.0	–279

Determine the pH of the following samples given the recorded peak potentials: tomato juice, 167 mV; tap water, –27 mV; coffee, 122 mV.

13. The concentration of NO_3^- in a water sample is determined by a one-point standard addition using a NO_3^- ion-selective electrode. A 25.00-mL sample is placed in a beaker and a potential of 0.102 V is measured. A 1.00-mL aliquot of a 200.0-mg/L standard solution of NO_3^- is added, after which the potential is 0.089 V. Report the mg NO_3^-/L in the water sample.

14. In 1977, when I was an undergraduate student at Knox College, my lab partner and I completed an experiment to determine the concentration of fluoride in tap water and the amount of fluoride in toothpaste. The data in this problem are from my lab notebook.

(a) To analyze tap water, we took three 25.0-mL samples and added 25.0 mL of TISAB to each. We measured the potential of each solution using a F^- ISE and an SCE reference electrode. Next, we made five 1.00-mL additions of a standard solution of 100.0 ppm F^- to each sample, and measured the potential after each addition, recording the potential three times.

mL of standard added	potential (mV), replicate 1	potential (mV), replicate 2	potential (mV), replicate 3
0.00	–79	–82	–83
1.00	–119	–119	–118
2.00	–133	–133	–133
3.00	–142	–142	–142
4.00	–149	–148	–148
5.00	–154	–153	–153

Report the parts-per-million of F^- in the tap water.

(b) To analyze the toothpaste, we measured 0.3619 g into a 100-mL volumetric flask, added 50.0 mL of TISAB, and diluted to volume with distilled water. After we ensured that the sample was thoroughly mixed, we transferred three 20.0-mL portions into separate beakers and measured the potential of each using a F^- ISE and an SCE reference electrode. Next, we made five 1.00-mL additions of a standard solution of 100.0 ppm F^- to each sample, and measured the potential after each addition, recording the potential three times.

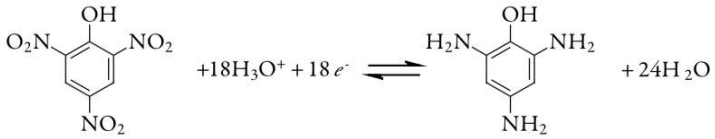
mL of standard added	potential (mV), replicate 1	potential (mV), replicate 2	potential (mV), replicate 3
0.00	–55	–54	–55
1.00	–82	–82	–83
2.00	–94	–94	–94
3.00	–102	–103	–102
4.00	–108	–108	–109
5.00	–112	–112	–113

Report the parts-per-million F^- in the toothpaste.

15. You are responsible for determining the amount of KI in iodized salt and decide to use an I^- ion-selective electrode. Describe how you would perform this analysis using external standards and how you would per-form this analysis using the method of standard additions.

16. Explain why each of the following decreases the analysis time in controlled-potential coulometry: a larger surface area for the working electrode; a smaller volume of solution; and a faster stirring rate.

17. The purity of a sample of picric acid, $C_6H_3N_3O_7$, is determined by controlled-potential coulometry, converting picric acid to triaminophenol, $C_6H_9N_3O$.



A 0.2917-g sample of picric acid is placed in a 1000-mL volumetric flask and diluted to volume. A 10.00-mL portion of this solution is transferred to a coulometric cell and sufficient water added so that the Pt cathode is immersed. An exhaustive electrolysis of the sample requires 21.67 C of charge. Report the purity of the picric acid.

18. The concentration of H_2S in the drainage from an abandoned mine is determined by a coulometric titration using KI as a mediator and I_3^- as the titrant.

$$H_2S(aq) + I_3^-(aq) + 2H_2O(l) \rightleftharpoons 2H_3O^+(aq) + 3I^-(aq) + S(s)$$

A 50.00-mL sample of water is placed in a coulometric cell, along with an excess of KI and a small amount of starch as an indicator. Electrolysis is carried out at a constant current of 84.6 mA, requiring 386 s to reach the starch end point. Report the concentration of H_2S in the sample in μg/mL.

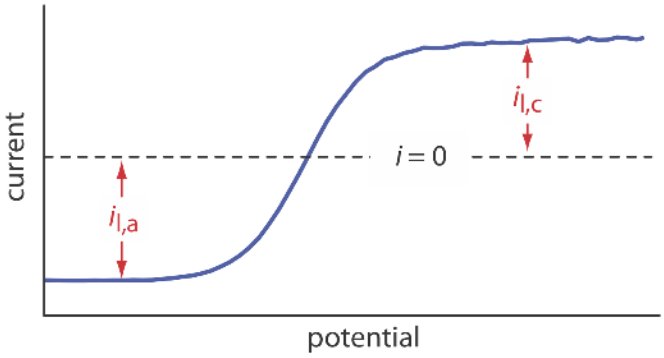
19. One method for the determination of a given mass of H_3AsO_3 is a coulometric titration using I_3^- as a titrant. The relevant standard-state reactions and potentials are summarized here

$$H_3AsO_4(aq) + 2H^+(aq) + 2e^- \rightleftharpoons H_3AsO_3(aq) + H_2O(l)$$
$$I_3^-(aq) + 2e^- \rightleftharpoons 3I^-(aq)$$

with standard state reduction potentials of, respectively, +0.559 V and +0.536 V. Explain why the coulometric titration is carried out in a neutral solution (pH ≈ 7) instead of in a strongly acidic solution (pH < 0).

20. The production of adiponitrile, $NC(CH_2)_4CN$, from acrylonitrile, CH_2=CHCN, is an important industrial process. A 0.594-g sample of acrylonitrile is placed in a 1-L volumetric flask and diluted to volume. An exhaustive controlled-potential electrolysis of a 1.00-mL portion of the diluted acrylonitrile requires 1.080 C of charge. What is the value of *n* for the reduction of acrylonitrile to adiponitrile?

21. The linear-potential scan hydrodynamic voltammogram for a mixture of Fe^{2+} and Fe^{3+} is shown in the figure below where $i_{l,a}$ and $i_{l,c}$ are the anodic and cathodic limiting currents.



(a) Show that the potential is given by

$$E = E^{\circ}_{Fe^{3+}/Fe^{2+}} - 0.05916 \log \frac{K_{Fe^{3+}}}{K_{Fe^{2+}}} - 0.05916 \log \frac{i - i_{l,a}}{i_{l,c} - i}$$

(b) What is the potential when i = 0 for a solution that is 0.100 mM Fe^{3+} and 0.050 mM Fe^{2+}?

22. The amount of sulfur in aromatic monomers is determined by differential pulse polarography. Standard solutions are prepared for analysis by dissolving 1.000 mL of the purified monomer in 25.00 mL of an electrolytic solvent, adding a known amount of sulfur, deaerating, and measuring the peak current. The following results were obtained for a set of calibration standards.

µg S added	peak current (µA)
0	0.14
28	0.70
56	1.23
112	2.41
168	3.42

Analysis of a 1.000-mL sample, treated in the same manner as the standards, gives a peak current of 1.77 µA. Report the mg S/mL in the sample.

23. The purity of a sample of $K_3Fe(CN)_6$ is determined using linear-potential scan hydrodynamic voltammetry at a glassy carbon electrode. The following data were obtained for a set of external calibration standards.

$[K_3Fe(CN)_6]$ (mM)	limiting current (µA)
2.0	127
4.0	252
6.0	376
8.0	500
10.0	624

A sample of impure $K_3Fe(CN)_6$ is prepared for analysis by diluting a 0.246-g portion to volume in a 100-mL volumetric flask. The limiting current for the sample is 444 µA. Report the purity of this sample of $K_3Fe(CN)_6$.

24. One method for determining whether an individual recently fired a gun is to look for traces of antimony in residue collected from the individual's hands. Anodic stripping voltammetry at a mercury film electrode is ideally suited for this analysis. In a typical analysis a sample is collected from a suspect using a cotton-tipped swab wetted with 5% v/v HNO_3. After returning to the lab, the swab is placed in a vial that contains 5.0 mL of 4 M HCl that is 0.02 M in hydrazine sulfate. After soaking the swab, a 4.0-mL portion of the solution is transferred to an electrochemical cell along with 100 µL of 0.01 M $HgCl_2$. After depositing the thin film of mercury and the antimony, the stripping step gives a peak current of 0.38 µA. After adding a standard addition of 100 µL of 5.00×10^2 ppb Sb, the peak current increases to 1.14 µA. How many nanograms of Sb were collected from the suspect's hand?

25. Zinc is used as an internal standard in an analysis of thallium by differential pulse polarography. A standard solution of 5.00×10^{-5} M Zn^{2+} and 2.50×10^{-5} M Tl^{+} has peak currents of 5.71 µA and 3.19 µA, respectively. An 8.713-g sample of a zinc-free alloy is dissolved in acid, transferred to a 500-mL volumetric flask, and diluted to volume. A 25.0-mL portion of this solution is mixed with 25.0 mL of 5.00×10^{-4} M Zn^{2+}. Analysis of this solution gives peak currents of 12.3 µA and of 20.2 µA for Zn^{2+} and Tl^{+}, respectively. Report the %w/w Tl in the alloy.

26. Differential pulse voltammetry at a carbon working electrode is used to determine the concentrations of ascorbic acid and caffeine in drug formulations [Lau, O.; Luk, S.; Cheung, Y. *Analyst* **1989**, *114*, 1047–1051]. In a typical analysis a 0.9183-g tablet is crushed and ground into a fine powder. A 0.5630-g sample of this powder is transferred to a 100-mL volumetric flask, brought into solution, and diluted to volume. A 0.500-mL portion of this solution is then transferred to a voltammetric cell that contains 20.00 mL of a suitable supporting electrolyte. The resulting voltammogram gives peak currents of 1.40 μA and 3.88 μA for ascorbic acid and for caffeine, respectively. A 0.500-mL aliquot of a standard solution that contains 250.0 ppm ascorbic acid and 200.0 ppm caffeine is then added. A voltammogram of this solution gives peak currents of 2.80 μA and 8.02 μA for ascorbic acid and caffeine, respectively. Report the milligrams of ascorbic acid and milligrams of caffeine in the tablet.

27. Ratana-ohpas and co-workers described a stripping analysis method for determining tin in canned fruit juices [Ratana-ohpas, R.; Kanatharana, P.; Ratana-ohpas, W.; Kongsawasdi, W. *Anal. Chim. Acta* **1996**, *333*, 115–118]. Standards of 50.0 ppb Sn^{4+}, 100.0 ppb Sn^{4+}, and 150.0 ppb Sn^{4+} were analyzed giving peak currents (arbitrary units) of 83.0, 171.6, and 260.2, respectively. A 2.00-mL sample of lychee juice is mixed with 20.00 mL of 1:1 HCl/HNO_3. A 0.500-mL portion of this mixture is added to 10 mL of 6 M HCl and the volume adjusted to 30.00 mL. Analysis of this diluted sample gave a signal of 128.2 (arbitrary units). Report the parts-per-million Sn^{4+} in the original sample of lychee juice.

28. Sittampalam and Wilson described the preparation and use of an amperometric sensor for glucose [Sittampalam, G.; Wilson, G. S. *J. Chem. Educ.* **1982**, *59*, 70–73]. The sensor is calibrated by measuring the steady-state current when it is immersed in standard solutions of glucose. A typical set of calibration data is shown here.

[glucose] (mg/100 mL)	current (arb. units)
2.0	17.2
4.0	32.9
6.0	52.1
8.0	68.0
10.0	85.8

A 2.00-mL sample is diluted to 10 mL in a volumetric flask and a steady-state current of 23.6 (arbitrary units) is measured. What is the concentration of glucose in the sample in mg/100 mL?

29. Differential pulse polarography is used to determine the concentrations of lead, thallium, and indium in a mixture. Because the peaks for lead and thallium, and for thallium and indium overlap, a simultaneous analysis is necessary. Peak currents (in arbitrary units) at –0.385 V, –0.455 V, and –0.557 V are measured for a single standard solution, and for a sample, giving the results shown in the following table. Report the mg/mL of Pb^{2+}, Tl^{+} and In^{3+} in the sample.

analyte	[standard] (μg/mL)	peak current at –0.385 V	peak current at –0.455 V	peak current at –0.557 V
Pb^{2+}	1.0	26.1	2.9	0
Tl^{+}	2.0	7.8	23.5	3.2
In^{3+}	0.4	0	0	22.9
sample		60.6	28.8	54.1

30. Abass and co-workers developed an amperometric biosensor for NH_4^+ that uses the enzyme glutamate dehydrogenase to catalyze the following reaction

$$2\text{-oxyglutarate}\,(aq) + NH_4^+(aq) + NADH(aq) \rightleftharpoons \text{glutamate}\,(aq) + NAD^+(aq) + H_2O(l)$$

where NADH is the reduced form of nicotinamide adenine dinucleotide [Abass, A. K.; Hart, J. P.; Cowell, D. C.; Chapell, A. *Anal. Chim. Acta* **1988**, *373*, 1–8]. The biosensor actually responds to the concentration of NADH, however, the rate of the reaction depends on the concentration of NH_4^+. If the initial concentrations of 2-oxyglutarate and NADH are the same for all samples and standards, then the signal is proportional to the concentration of NH_4^+. As shown in the following table, the sensitivity of the method is dependent on pH.

pH	sensitivity (nA S^{-1} M^{-1})
6.2	1.67×10^3
6.75	5.00×10^3
7.3	9.33×10^3
7.7	1.04×10^4
8.3	1.27×10^4
9.3	2.67×10^3

Two possible explanations for the effect of pH on the sensitivity of this analysis are the acid–base chemistry of NH_4^+ and the acid–base chemistry of the enzyme. Given that the pK_a for NH_4^+ is 9.244, explain the source of this pH-dependent sensitivity.

31. The speciation scheme for trace metals in Table 11.4.2 divides them into seven operationally defined groups by collecting and analyzing two samples following each of four treatments, requiring a total of eight samples and eight measurements. After removing insoluble particulates by filtration (treatment 1), the solution is analyzed for the concentration of ASV labile metals and for the total concentration of metals. A portion of the filtered solution is then passed through an ion-exchange column (treatment 2), and the concentrations of ASV metal and of total metal are determined. A second portion of the filtered solution is irradiated with UV light (treatment 3), and the concentrations of ASV metal and of total metal are measured. Finally, a third portion of the filtered solution is irradiated with UV light and passed through an ion-exchange column (treatment 4), and the concentrations of ASV labile metal and of total metal again are determined. The groups that are included in each measurement are summarized in the following table.

treatment	groups removed by treatement	groups contributing to ASV-labile metals	groups contributing to total metals
1	none	I, II, III	I, II, III, IV, V, VI, VII
2	I, IV, V	II, III	II, III, V1, VII
3	none	I, II, III, IV, VI	I, II, III, IV, V, VI, VII
4	I, II, IV, V, VI	III	III, VII

(a) Explain how you can use these eight measurements to determine the concentration of metals present in each of the seven groups identified in Table 11.4.2.

(b) Batley and Florence report the following results for the speciation of cadmium, lead, and copper in a sample of seawater [Batley, G. E.; Florence, T. M. *Anal. Lett.* **1976**, *9*, 379–388]. Determine the speciation of each metal in comment on your results.

measurement treatement: ASV-labile or total	ppb Cd^{2+}	ppb Pb^{2+}	ppb Cu^{2+}
1: ASV-labile	0.24	0.39	0.26
2: total	0.28	0.50	0.40
2: ASV-labile	0.21	0.33	0.17
2: total	0.26	0.43	0.24
3: ASV-labile	0.26	0.37	0.33
3: total	0.28	0.5	0.43
4: ASV-labile	0.00	0.00	0.00
4: total	0.02	0.12	0.10

32. The concentration of Cu^{2+} in seawater is determined by anodic stripping voltammetry at a hanging mercury drop electrode after first releasing any copper bound to organic matter. To a 20.00-mL sample of seawater is added 1 mL of 0.05 M HNO_3 and 1 mL of 0.1% H_2O_2. The sample is irradiated with UV light for 8 hr and then diluted to volume in a 25-mL volumetric flask. Deposition of Cu^{2+} takes place at –0.3 V versus an SCE for 10 min, producing a peak current of 26.1 (arbitrary units). A second 20.00-mL sample of the seawater is treated identically, except that 0.1 mL of a 5.00 μM solution of Cu^{2+} is added, producing a peak current of 38.4 (arbitrary units). Report the concentration of Cu^{2+} in the seawater in mg/L.

33. Thioamide drugs are determined by cathodic stripping analysis [Davidson, I. E.; Smyth, W. F. Anal. Chem. 1977, 49, 1195–1198]. Deposition occurs at +0.05 V versus an SCE. During the stripping step the potential is scanned cathodically and a stripping peak is observed at –0.52 V. In a typical application a 2.00-mL sample of urine is mixed with 2.00 mL of a pH 4.78 buffer. Following a 2.00 min deposition, a peak current of 0.562 μA is measured. A 0.10-mL addition of a 5.00 μM solution of the drug is added to the same solution. A peak current of 0.837 μA is recorded using the same deposition and stripping conditions. Report the drug's molar concentration in the urine sample.

34. The concentration of vanadium (V) in sea water is determined by adsorptive stripping voltammetry after forming a complex with catechol [van der Berg, C. M. G.; Huang, Z. Q. *Anal. Chem.* **1984**, *56*, 2383–2386]. The catechol-V(V) complex is deposited on a hanging mercury drop electrode at a potential of –0.1 V versus a Ag/AgCl reference electrode. A cathodic potential scan gives a stripping peak that is proportional to the concentration of V(V). The following standard additions are used to analyze a sample of seawater.

$[V(V)]_{added}$ (M)	peak current (μA)
2.0×10^{-8}	24
4.0×10^{-8}	33
8.0×10^{-8}	52
1.2×10^{-7}	69
1.8×10^{-7}	97
2.8×10^{-7}	140

Determine the molar concentration of V (V) in the sample of sea water, assuming that the standard additions result in a negligible change in the sample's volume.

35. The standard-state reduction potential for Cu^{2+} to Cu is +0.342 V versus the SHE. Given that Cu^{2+} forms a very stable complex with the ligand EDTA, do you expect that the standard-state reduction potential for $Cu(EDTA)^{2-}$ is greater than +0.342 V, less than +0.342 V, or equal to +0.342 V? Explain your reasoning.

36. The polarographic half-wave potentials (versus the SCE) for Pb^{2+} and for Tl^{+} in 1 M HCl are, respectively, –0.44 V and –0.45 V. In an electrolyte of 1 M NaOH, however, the half-wave potentials are –0.76 V for Pb^{2+} and –0.48 V for Tl^{+}. Why does the change in electrolyte have such a significant effect on the half-wave potential for Pb^{2+}, but not on the half-wave potential for Tl^{+}?

37. The following data for the reduction of Pb^{2+} were collected by normal-pulse polarography.

potential (V vs. SCE)	current (μA)
–0.345	0.16
–0.370	0.98
–0.383	2.05
–0.393	3.13
–0.409	4.62
–0.420	5.16

The limiting current was 5.67 μA. Verify that the reduction reaction is reversible and determine values for n and $E_{1/2}$. The half-wave potentials for the normal-pulse polarograms of Pb^{2+} in the presence of several different concentrations of OH^{-} are shown in the following table.

$[OH^{-}]$ (M)	$E_{1/2}$ (V vs. SCE)	$[OH^{-}]$ (M)	$E_{1/2}$ (V vs. SCE)
0.050	–0.646	0.150	–0.689
0.100	–0.673	0.300	–0.715

Determine the stoichiometry of the Pb-hydroxide complex and its formation constant.

38. In 1977, when I was an undergraduate student at Knox College, my lab partner and I completed an experiment to study the voltammetric behavior of Cd^{2+} (in 0.1 M KNO_3) and Ni^{2+} (in 0.2 M KNO_3) at a dropping mercury electrode. The data in this problem are from my lab notebook. All potentials are relative to an SCE reference electrode.

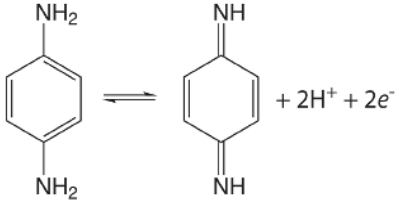
potential for Cd^{2+} (V)	current for Cd^{2+} (μA)	potential for Ni^{2+} (V)	current for Ni^{2+} (μA)
–0.60	4.5	–1.07	1.90
–0.58	3.4	–1.05	1.75
–0.56	2.1	–1.03	1.50
–0.54	0.6	–1.02	1.25
–0.52	0.2	–1.00	1.00

The limiting currents for Cd^{2+} was 4.8 μA and that for Ni^{2+} was 2.0 μA. Evaluate the electrochemical reversibility for each metal ion and comment on your results.

39. Baldwin and co-workers report the following data from a cyclic voltammetry study of the electrochemical behavior of *p*-phenylenediamine in a pH 7 buffer [Baldwin, R. P.; Ravichandran, K.; Johnson, R. K. *J. Chem. Educ.* **1984**, *61*, 820–823]. All potentials are measured relative to an SCE.

scan rate (mV/s)	$E_{p,a}$ (V)	$E_{p,c}$ (V)	$i_{p,a}$ (mA)	$i_{p,c}$ (mA)
2	0.148	0.104	0.34	0.30
5	0.149	0.098	0.56	0.53
10	0.152	0.095	1.00	0.04
20	0.161	0.095	1.44	1.44
50	0.167	0.082	2.12	1.81
100	0.180	0.063	2.50	2.19

The initial scan is toward more positive potentials, leading to the oxidation reaction shown here.



Use this data to show that the reaction is electrochemically irreversible. A reaction may show electrochemical irreversibility because of slow electron transfer kinetics or because the product of the oxidation reaction participates in a chemical reaction that produces an nonelectroactive species. Based on the data in this problem, what is the likely source of *p*-phenylenediamine's electrochemical irreversibility?

This page titled 13.5: Problems is shared under a CC BY-NC-SA 4.0 license and was authored, remixed, and/or curated by David Harvey.

- **11.5: Problems** by David Harvey is licensed CC BY-NC-SA 4.0.

13.6: ADDITIONAL RESOURCES

The following set of experiments introduce students to the applications of electrochemistry. Experiments are grouped into four categories: general electrochemistry, preparation of electrodes, potentiometry, coulometry, and voltammetry and amperometry.

General Electrochemistry

- Chatmontree, A.; Chairam, S.; Supasorn, S.; Amatatongchai, M.; Jarujamrus, P; Tamuang, S.; Somsook E. "Student Fabriaction and Use of Simple, Low-Cost, Paper-Based Galvanic Cells to Investigate Electrochemistry," *J. Chem. Educ.* **2015**, *92*, 1044–1048.
- Mills, K. V.; Herrick, R. S.; Guilmette, L. W.; Nestor, L. P.; Shafer, H.; Ditzler, M. A. "Introducing Undergraduate Students to Electrochemistry: A Two-Week Discovery Chemistry Experiment," *J. Chem. Educ.* **2008**, *85*, 1116–119.

Preparation of Electrodes

- Christopoulos, T. K.; Diamandis, E. P. "Use of a Sintered Glass Crucible for Easy Construction of Liquid-Membrane Ion-Selective Electrodes," *J. Chem. Educ.* **1988**, *65*, 648.
- Fricke, G. H.; Kuntz, M. J. "Inexpensive Solid-State Ion-Selective Electrodes for Student Use," *J. Chem. Educ.* **1977**, *54*, 517–520.
- Inamdar, S. N.; Bhat, M. A.; Haram, S. K. "Construction of Ag/AgCl Reference Electrode form Used Felt-Tipped Pen Barrel for Undergraduate Laboratory," *J. Chem. Educ.* **2009**, *86*, 355–356.
- Lloyd, B. W.; O'Brien, F. L.; Wilson, W. D. "Student Preparation and Analysis of Chloride and Calcium Ion Selective Electrodes," *J. Chem. Educ.* **1976**, *53*, 328–330.
- Mifflin, T. E.; Andriano, K. M.; Robbins, W. B. "Determination of Penicillin Using an Immobilized Enzyme Electrode," *J. Chem. Educ.* **1984**, *61*, 638–639.
- Palanivel, A.; Riyazuddin, P. "Fabrication of an Inexpensive Ion-Selective Electrode," *J. Chem. Educ.* **1984**, *61*, 290.
- Ramaley, L; Wedge, P. J.; Crain, S. M. "Inexpensive Instrumental Analysis: Part 1. Ion-Selective Electrodes," *J. Chem. Educ.* **1994**, *71*, 164–167.
- Selig, W. S. "Potentiometric Titrations Using Pencil and Graphite Sensors," *J. Chem. Educ.* **1984**, *61*, 80–81.

Potentiometry

- Chan, W. H; Wong, M. S.; Yip, C. W. "Ion-Selective Electrode in Organic Analysis: A Salicylate Electrode," *J. Chem. Educ.* **1986**, *63*, 915–916.
- Harris, T. M. "Potentiometric Measurement in a Freshwater Aquarium," *J. Chem. Educ.* **1993**, *70*, 340–341.
- Kauffman, C. A.; Muza, A. L.; Porambo, M. W.; Marsh, A. L. "Use of a Commercial Silver-Silver Chloride Electrode for the Measurement of Cell Potentials to Determine Mean Ionic Activity Coefficients," *Chem. Educator* **2010**, *15*, 178–180.
- Martínez-Fàbregas, E.; Alegret, S. "A Practical Approach to Chemical Sensors through Potentiometric Transducers: Determination of Urea in Serum by Means of a Biosensor," *J. Chem. Educ.* **1994**, *71*, A67–A70.
- Moresco, H.; Sansón, P.; Seoane, G. "Simple Potentiometric Determination of Reducing Sugars," *J. Chem. Educ.* **2008**, *85*, 1091–1093.
- Radic, N.; Komijenovic, J. "Potentiometric Determination of an Overall Formation Constant Using an Ion-Selective Membrane Electrode," *J. Chem. Educ.* **1993**, *70*, 509–511.
- Riyazuddin, P.; Devika, D. "Potentiometric Acid–Base Titrations with Activated Graphite Electrodes,"*J. Chem. Educ.* **1997**, *74*, 1198–1199.

Coulometry

- Bertotti, M.; Vaz, J. M.; Telles, R. "Ascorbic Acid Determination in Natural Orange Juice," *J. Chem. Educ.* **1995**, *72*, 445–447.
- Kalbus, G. E.; Lieu, V. T. "Dietary Fat and Health: An Experiment on the Determination of Iodine Number of Fats and Oils by Coulometric Titration," *J. Chem. Educ.* **1991**, *68*, 64–65.
- Lötz, A. "A Variety of Electrochemical Methods in a Coulometric Titration Experiment," *J. Chem. Educ.* **1998**, *75*, 775–777.
- Swim, J.; Earps, E.; Reed, L. M.; Paul, D. "Constant-Current Coulometric Titration of Hydrochloric Acid," *J. Chem. Educ.* **1996**, *73*, 679–683.

Voltammetry and Amperometry

- Blanco-López, M. C.; Lobo-Castañón, M. J.; Miranda-Ordieres, A. J. "Homemade Bienzymatic-Amperometric Biosensor for Beverages Analysis," *J. Chem. Educ.* **2007**, *84*, 677–680.
- García-Armada, P.; Losada, J.; de Vicente-Pérez, S. "Cation Analysis Scheme by Differential Pulse Polarography," *J. Chem. Educ.* **1996**, *73*, 544–547.
- Herrera-Melián, J. A.; Doña-Rodríguez, J. M.; Hernández-Brito, J.; Pérez-Peña, J. "Voltammetric Determination of Ni and Co in Water Samples," *J. Chem. Educ.* **1997**, *74*, 1444–1445.
- King, D.; Friend, J.; Kariuki, J. "Measuring Vitamin C Content of Commercial Orange Juice Using a Pencil Lead Electrode," *J. Chem. Educ.* **2010**, *87*, 507–509.

- Marin, D.; Mendicuti, F. “Polarographic Determination of Composition and Thermodynamic Stability Constant of a Complex Metal Ion,” *J. Chem. Educ.* **1988**, *65*, 916–918.
- Messersmith, S. J. “Cyclic Voltammetry Simulations with DigiSim Software: An Upper-Level Undergraduate Experiment,” *J. Chem. Educ.* **2014**, *91*, 1498–1500.
- Sadik, O. A.; Brenda, S.; Joasil, P.; Lord, J. “Electropolymerized Conducting Polymers as Glucose Sensors,” *J. Chem. Educ.* **1999**, *76*, 967–970.
- Sittampalam, G.; Wilson, G. S. “Amperometric Determination of Glucose at Parts Per Million Levels with Immobilized Glucose Oxidase,” *J. Chem. Educ.* **1982**, *59*, 70–73.
- Town, J. L.; MacLaren, F.; Dewald, H. D. “Rotating Disk Voltammetry Experiment,” *J. Chem. Educ.* **1991**, *68*, 352–354.
- Wang, J. “Sensitive Electroanalysis Using Solid Electrodes,” *J. Chem. Educ.* **1982**, *59*, 691–692.
- Wang, J. “Anodic Stripping Voltammetry,” *J. Chem. Educ.* **1983**, *60*, 1074–1075.
- Wang, J.; Maccà, C. “Use of Blood-Glucose Test Strips for Introducing Enzyme Electrodes and Modern Biosensors,” *J. Chem. Educ.* **1996**, *73*, 797–800.
- Wang, Q.; Geiger, A.; Frias, R; Golden, T. D. “An Introduction to Electrochemistry for Undergraduates: Detection of Vitamin C (Ascorbic Acid) by Inexpensive Electrode Sensors,” *Chem. Educator* **2000**, *5*, 58–60.

The following general references providing a broad introduction to electrochemistry.

- Adams, R. N. *Electrochemistry at Solid Surfaces*, Marcel Dekker: New York, 1969.
- Bard, A. J.; Faulkner, L. R. *Electrochemical Methods*, Wiley: New York, 1980.
- Faulkner, L. R. “Electrochemical Characterization of Chemical Systems” in Kuwana, T. E., ed. *Physical Methods in Modern Chemical Analysis*, Vol. 3, Academic Press: New York, 1983, pp. 137–248.
- Kissinger, P. T.; Heineman, W. R. *Laboratory Techniques in Electroanalytical Chemistry*, Marcel Dekker: New York, 1984.
- Lingane, J. J. *Electroanalytical Chemistry*, 2nd Ed., Interscience: New York, 1958.
- Sawyer, D. T.; Roberts, J. L., Jr. *Experimental Electrochemistry for Chemists*, Wiley-Interscience: New York, 1974.
- Vassos, B. H.; Ewing, G. W. *Electroanalytical Chemistry*, Wiley-Interscience: New York, 1983.

These short articles provide a good introduction to important principles of electrochemistry.

- Faulkner, L. R. “Understanding Electrochemistry: Some Distinctive Concepts,” *J. Chem. Educ.* **1983**, *60*, 262–264.
- Huddle, P. A.; White, M. D.; Rogers, F. “Using a Teaching Model to Correct Known Misconceptions in Electrochemistry,” *J. Chem. Educ.* **2000**, *77*, 104–110.
- Maloy, J. T. “Factors Affecting the Shape of Current-Potential Curves,” *J. Chem. Educ.* **1983**, *60*, 285–289.
- Miles, D. T. “Run-D.M.C.: A Mnemonic Aid for Explaining Mass Transfer in Electrochemical Systems,” *J. Chem. Educ.* **2013**, *90*, 1649–1653.
- Thompson, R. Q.; Craig, N. C. “Unified Electroanalytical Chemistry: Application of the Concept of Equilibrium,” *J. Chem. Educ.* **2001**, *78*, 928–934.
- Zoski, C. G. “Charging Current Discrimination in Analytical Voltammetry,” *J. Chem. Educ.* **1986**, *63*, 910–914.

Additional information on potentiometry and ion-selective electrodes can be found in the following sources.

- Bakker, E.; Diamond, D.; Lewenstam, A.; Pretsch, E. “Ions Sensors: Current Limits and New Trends,” *Anal. Chim. Acta* **1999**, *393*, 11–18.
- Bates, R. G. *Determination of pH: Theory and Practice*, 2nd ed., Wiley: New York, 1973.
- Bobacka, J.; Ivaska, A.; Lewenstam, A. “Potentiometric Ion Sensors,” *Chem. Rev.* **2008**, *108*, 329–351.
- Buck, R. P. “Potentiometry: pH Measurements and Ion Selective Electrodes” in Weissberger, A., ed. *Physical Methods of Organic Chemistry*, Vol. 1, Part IIA, Wiley: New York, 1971, pp. 61–162.
- Cammann, K. *Working With Ion-Selective Electrodes*, Springer-Verlag: Berlin, 1977.
- Evans, A. P*otentiometry and Ion-Selective Electrodes*, Wiley: New York, 1987.
- Frant, M. S. “Where Did Ion Selective Electrodes Come From?” *J. Chem. Educ.* **1997**, *74*, 159–166.
- Light, T. S. “Industrial Use and Application of Ion-Selective Electrodes,” *J. Chem. Educ.* **1997**, *74*, 171–177.
- Rechnitz, G. A. “Ion and Bio-Selective Membrane Electrodes,” *J. Chem. Educ.* **1983**, *60*, 282–284.
- Ruzicka, J. “The Seventies—Golden Age for Ion-Selective Electrodes,” *J. Chem. Educ.* **1997**, *74*, 167– 170.
- Young, C. C. “Evolution of Blood Chemistry Analyzers Based on Ion Selective Electrodes,” *J. Chem. Educ.* **1997**, *74*, 177–182.

The following sources provide additional information on electrochemical biosensors.

- Alvarez-Icasa, M.; Bilitewski, U. “Mass Production of Biosensors,” *Anal. Chem.* **1993**, *65*, 525A– 533A.
- Meyerhoff, M. E.; Fu, B.; Bakker, E. Yun, J-H; Yang, V. C. “Polyion-Sensititve Membrane Electrodes for Biomedical Analysis,” *Anal. Chem.* **1996**, *68*, 168A–175A.

- Nicolini, C.; Adami, M; Antolini, F.; Beltram, F.; Sartore, M.; Vakula, S. “Biosensors: A Step to Bioelectronics,” *Phys. World*, May 1992, 30–34.
- Rogers, K. R.; Williams. L. R. “Biosensors for Environmental Monitoring: A Regulatory Perspective,” *Trends Anal. Chem.* **1995**, *14*, 289–294.
- Schultz, J. S. “Biosensors,” *Sci. Am.* August 1991, 64–69.
- Thompson, M.; Krull, U. “Biosensors and the Transduction of Molecular Recognition,” *Anal. Chem.* **1991**, *63*, 393A–405A.
- Vadgama, P. “Designing Biosensors,” *Chem. Brit.* **1992**, *28*, 249–252.

A good source covering the clinical application of electrochemistry is listed below.

- Wang, J. *Electroanalytical Techniques in Clinical Chemistry and Laboratory Medicine*, VCH: New York, 1998.

Coulometry is covered in the following texts.

- Rechnitz, G. A. *Controlled-Potential Analysis*, Macmillan: New York, 1963.
- Milner, G. W. C.; Philips, G. *Coulometry in Analytical Chemistry*, Pergamon: New York, 1967.

For a description of electrogravimetry, see the following resource.

- Tanaka, N. “Electrodeposition”, in Kolthoff, I. M.; Elving, P. J., eds. *Treatise on Analytical Chemistry, Part I: Theory and Practice*, Vol. 4, Interscience: New York, 1963.

The following sources provide additional information on polarography and pulse polarography.

- Flato, J. B. “The Renaissance in Polarographic and Voltammetric Analysis,” *Anal. Chem.* **1972**, *44(11)*, 75A–87A.
- Kolthoff, I. M.; Lingane, J. J. *Polarography*, Interscience: New York, 1952.
- Osteryoung, J. “Pulse Voltammetry,” *J. Chem. Educ.* **1983**, *60*, 296–298.

Additional Information on stripping voltammetry is available in the following text.

- Wang, J. *Stripping Analysis*, VCH Publishers: Deerfield Beach, FL, 1985.

The following papers discuss the numerical simulation of voltammetry.

- Bozzini, B. “A Simple Numerical Procedure for the Simulation of “Lifelike” Linear-Sweep Voltammo- grams,” *J. Chem. Educ.* **2000**, *77*, 100–103.
- Howard, E.; Cassidy, J. “Analysis with Microelectrodes Using Microsoft Excel Solver,” *J. Chem. Educ.* **2000**, *77*, 409–411.
- Kätelhön, E.; Compton, R. G. “Testing and Validating Electroanalytical Simulations,” *Analyst*, **2015**, *140*, 2592–2598.
- Messersmith, S. J. “Cyclic Voltammetry Simulations with DigiSim Software: An Upper-Level Undergraduate Experiment,” *J. Chem. Educ.* **2014**, *91*, 1498–1500.

Gathered together here are many useful resources for cyclic voltammetry, including experiments.

- Carriedo, G. A. “The Use of Cyclic Voltammetry in the Study of the Chemistry of Metal–Carbonyls,” *J. Chem. Educ.* **1988**, *65*, 1020–1022.
- García-Jareño, J. J.; Benito, D.; Navarro-Laboulais, J.; Vicente, F. “Electrochemical Behavior of Electrodeposited Prussian Blue Films on ITO Electrodes,” *J. Chem. Educ.* **1998**, *75*, 881–884.
- Gilles de Pelichy, L. D.; Smith, E. T. “A Study of the Oxidation Pathway of Adrenaline by Cyclic Voltammetry,” *Chem. Educator* **1997**, *2(2)*, 1–13.
- Gomez, M. E.; Kaifer, A. E. “Voltammetric Behavior of a Ferrocene Derivative,” *J. Chem. Educ.* **1992**, *69*, 502–505.
- Heffner, J. E.; Raber, J. C.; Moe, O. A.; Wigal, C. T. “Using Cyclic Voltammetry and Molecular Modeling to Determine Substituent Effects in the One-Electron Reduction of Benzoquinones,” *J. Chem. Educ.* **1998**, *75*, 365–367.
- Heinze, J. “Cyclic Voltammetry—Electrochemical Spectroscopy,” *Angew. Chem, Int. Ed. Eng.* **1984**, *23*, 831–918.
- Holder, G. N.; Farrar, D. G.; McClure, L. L. “Voltammetric Reductions of Ring-Substituted Acetophenones. 1. Determination of an Electron-Transfer Mechanism Using Cyclic Voltammetry and Computer Modeling: The Formation and Fate of a Radical Anion,” *Chem. Educator* **2001**, *6*, 343–349.
- Ibanez, J. G.; Gonzalez, I.; Cardenas, M. A. “The Effect of Complex Formation Upon the Redox Potentials of Metal Ions: Cyclic Voltammetry Experiments,” *J. Chem. Educ.* **1988**, *65*, 173–175.
- Ito, T.; Perara, D. M. N. T.; Nagasaka, S. “Gold Electrodes Modified with Self-Assembled Monolayers for Measuring l-Ascobric acid,” *J. Chem. Educ.* **2008**, *85*, 1112–1115.
- Kissinger, P. T.; Heineman, W. R. “Cyclic Voltammetry,” *J. Chem. Educ.* **1983**, *60*, 702–706.
- Mabbott, G. A. “An Introduction to Cyclic Voltammetry,” *J. Chem. Educ.* **1983**, *60*, 697–702.
- Petrovic, S. “Cyclic Voltammetry of Hexachloroiridate (IV): An Alternative to the Electrochemical Study of the Ferricyanide Ion,” *Chem. Educator* **2000**, *5*, 231–235.

- Toma, H. E.; Araki, K.; Dovidauskas, S. “A Cyclic Voltammetry Experiment Illustrating Redox Potentials, Equilibrium Constants and Substitution Reaction in Coordination Chemistry,” *J. Chem. Educ.* **2000**, *77*, 1351–1353.
- Walczak, M. W.; Dryer, D. A.; Jacobson, D. D,; Foss, M. G.; Flynn, N. T. “pH-Dependent Redox Couple: Illustrating the Nernst Equation Using Cyclic Voltammetry,” *J. Chem. Educ.* **1997**, *74*, 1195–1197.

This page titled 13.6: Additional Resources is shared under a CC BY-NC-SA 4.0 license and was authored, remixed, and/or curated by David Harvey.

- **11.6: Additional Resources** by David Harvey is licensed CC BY-NC-SA 4.0.

13.7: CHAPTER SUMMARY AND KEY TERMS

CHAPTER SUMMARY

In this chapter we introduced three electrochemical methods of analysis: potentiometry, coulometry, and voltammetry. In potentiometry we measure the potential at an indicator electrode without allowing any significant current to pass through the electrochemical cell, and use the Nernst equation to calculate the analyte's activity after accounting for junction potentials.

There are two broad classes of potentiometric electrodes: metallic electrodes and membrane electrodes. The potential of a metallic electrode is the result of a redox reaction at the electrode's surface. An electrode of the first kind responds to the concentration of its cation in solution; thus, the potential of a Ag wire is determined by the activity of Ag^+ in solution. If another species is in equilibrium with the metal ion, the electrode's potential also responds to the concentration of that species. For example, the potential of a Ag wire in a solution of $Cl^–$ responds to the concentration of $Cl^–$ because the relative concentrations of Ag^+ and $Cl^–$ are fixed by the solubility product for AgCl. We call this an electrode of the second kind.

The potential of a membrane electrode is determined by a difference in the composition of the solution on each side of the membrane. Electrodes that use a glass membrane respond to ions that bind to negatively charged sites on the membrane's surface. A pH electrode is one example of a glass membrane electrode. Other kinds of membrane electrodes include those that use insoluble crystalline solids or liquid ion-exchangers incorporated into a hydrophobic membrane. The $F^–$ ion-selective electrode, which uses a single crystal of LaF_3 as the ion-selective membrane, is an example of a solid-state electrode. The Ca^{2+} ion-selective electrode, in which the chelating ligand di-(*n*-decyl)phosphate is immobilized in a PVC membrane, is an example of a liquid-based ion-selective electrode.

Potentiometric electrodes are designed to respond to molecules by using a chemical reaction that produces an ion whose concentration is determined using a traditional ion-selective electrode. A gas-sensing electrode, for example, includes a gas permeable membrane that isolates the ion-selective electrode from the gas. When a gas-phase analyte diffuses across the membrane it alters the composition of the inner solution, which is monitored with an ion-selective electrode. An enzyme electrodes operate in the same way.

Coulometric methods are based on Faraday's law that the total charge or current passed during an electrolysis is proportional to the amount of reactants and products participating in the redox reaction. If the electrolysis is 100% efficient—which means that only the analyte is oxidized or reduced—then we can use the total charge or total current to determine the amount of analyte in a sample. In controlled-potential coulometry we apply a constant potential and measure the resulting current as a function of time. In controlled-current coulometry the current is held constant and we measure the time required to completely oxidize or reduce the analyte.

In voltammetry we measure the current in an electrochemical cell as a function of the applied potential. There are several different voltammetric methods that differ in terms of the choice of working electrode, how we apply the potential, and whether we include convection (stirring) as a means for transporting of material to the working electrode.

Polarography is a voltammetric technique that uses a mercury electrode and an unstirred solution. Normal polarography uses a dropping mercury electrode, or a static mercury drop electrode, and a linear potential scan. Other forms of polarography include normal pulse polarography, differential pulse polarography, staircase polarography, and square-wave polarography, all of which use a series of potential pulses.

In hydrodynamic voltammetry the solution is stirred using either a magnetic stir bar or by rotating the electrode. Because the solution is stirred a dropping mercury electrode is not used; instead we use a solid electrode. Both linear potential scans and potential pulses can be applied.

In stripping voltammetry the analyte is deposited on the electrode, usually as the result of an oxidation or reduction reaction. The potential is then scanned, either linearly or using potential pulses, in a direction that removes the analyte by a reduction or oxidation reaction.

Amperometry is a voltammetric method in which we apply a constant potential to the electrode and measure the resulting current. Amperometry is most often used in the construction of chemical sensors for the quantitative analysis of single analytes. One important example is the Clark O_2 electrode, which responds to the concentration of dissolved O_2 in solutions such as blood and water.

KEY TERMS

amalgam	amperometry	anode
anodic current	asymmetry potential	auxiliary electrode
cathode	cathodic current	charging current
controlled-current coulometry	controlled-potential coulometry	convection
coulometric titrations	coulometry	counter electrode
current efficiency	cyclic voltammetry	diffusion
diffusion layer	dropping mercury electrode	electrical double layer
electrochemically irreversible	electrochemically reversible	electrode of the first kind
electrode of the second kind	electrochemistry	electrogravimetry
enzyme electrodes	faradaic current	Faraday's law
galvanostat	gas-sensing electrode	glass electrode
hanging mercury drop electrode	hydrodynamic voltammetry	indicator electrode
ionophore	ion selective electrode	junction potential
limiting current	liquid-based ion-selective electrode	mass transport
mediator	membrane potential	mercury film electrode
migration	nonfaradaic current	Ohm's law
overpotential	peak current	polarography
potentiometer	potentiostat	pulse polarography
redox electrode	reference electrode	residual current
salt bridge	saturated calomel electrode	selectivity coefficient
silver/silver chloride electrode	solid-state ion-selective electrodes	standard hydrogen electrode
static mercury drop electrode	stripping voltammetry	total ionic strength adjustment buffer
voltammetry	voltammogram	working electrode

13.7: Chapter Summary and Key Terms is shared under a not declared license and was authored, remixed, and/or curated by LibreTexts.

- **11.7: Chapter Summary and Key Terms** has no license indicated.

CHAPTER OVERVIEW

14: Surface Characterization by Spectroscopy and Microscopy

14.1: Introduction to the Study of Surfaces
14.2: Scanning Electron Microscopy
14.2.1: Scanning electron microscopy (SEM)
14.2.2: Transmission Electron Microscopy
14.3: Scanning Probe Microscopes
14.3.1: Scanning Tunneling Microscopy
14.3.2: Scanning Tunneling Microscopy (STM)
14.3.3: Atomic Force Microscopy
14.3.4: Atomic Force Microscopy (AFM)
14.4: Spectroscopic Surface Methods
14.4.1: X-ray Photoelectron Spectroscopy
14.4.2: Auger Electron Spectroscopy

This page titled 14: Surface Characterization by Spectroscopy and Microscopy is shared under a CC BY-NC-SA 4.0 license and was authored, remixed, and/or curated by David Harvey.

14.1: Introduction to the Study of Surfaces

Thus far we have considered methods for analyzing the bulk properties of samples, such as determining the identity or concentration of an ion in a solution, of a molecule in a gas, or of several elements in a solid. In doing so, we did not concern ourselves with the sample's homogeneity or heterogeneity. In this chapter we give consideration to how we can gather information about the composition of a sample's surface and how it differs from the sample's bulk composition. But first, let's consider several important questions.

What Is A Surface?

A surface is a boundary, or interface, between two phases, such as a solid and a gas (the type of interface of particular interest to us in this chapter). This is a helpful, but not a sufficient description. Also of interest is the question of depth. Is a surface just the outermost layer of atoms, ions, or molecules, or does it extend several layers into the sample? In what ways might the composition of a sample at the surface differ from its composition in the sample's bulk interior? And, what about variations in composition across a surface? Is the surface itself homogeneous or heterogeneous in its composition? Different analytical methods will sample the surface to different depths and with different surface areas, which means the volume of sample analyzed will vary from method-to-method. For this reason, we usually define a sample's surface as what is analyzed by the analytical method we are using.

Why Are Surfaces of interest?

Figure 14.1.1 shows the crystal structure of AgCl(*s*), which consists of a repeating pattern of Ag^+ ions and Cl^- ions. If you look at the ions in interior of the structure, you will see that each Ag^+ ion is surrounded by six Cl^- ions, and each Cl^- ion is surrounded by six Ag^+ ions. On the surface, however, we see that Cl^- ions and Ag^+ ions no longer are surrounded by six ions of opposite charge. As a result, the Ag^+ ions and Cl^- ions on the surface are more chemically reactive than those in the interior and can serve as sites for interesting chemistry. The chemical and physical properties of a sample's surface are likely to be very different than the sample's bulk properties.

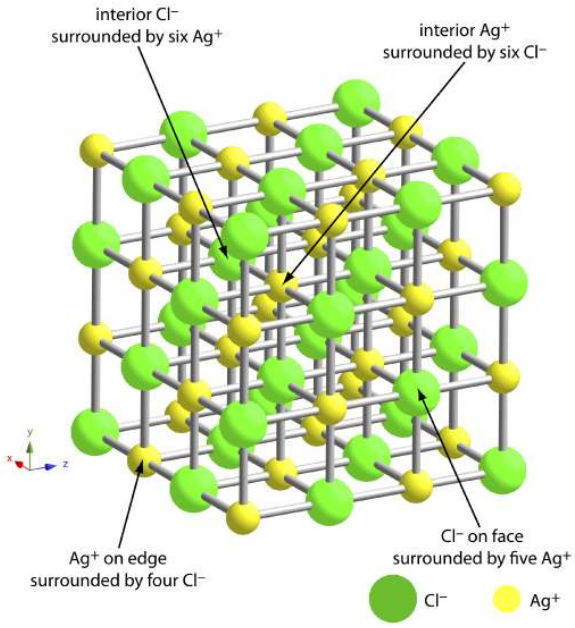


Figure 14.1.1: Ball-and-stick model showing the lattice structure of AgCl. Each silver ion in the lattice's interior binds with six chloride ions and each chloride ion in the interior binds with six silver ions. Those ions on the lattice's surface or edges bind to fewer than six ions and carry a partial charge. A silver ion on the surface, for example, carries a partial positive charge. These charges, for example, make the surface of a precipitate of AgCl an active site for chemical and physical interactions.

What Challenges Does a Surface Present?

Suppose we are interested in studying the surface of a piece of zinc metal using a probe that samples just the outermost layer of atoms and that samples a circular surface area that is 1 μm^2. How many atoms of Zn might we expect our probe to encounter? Here is some useful information about zinc: it has a molar mass of 65.38 g/mol, it has a density of 7.14 g/cm^3, and it has an atomic radius of approximately 0.13 nm. From this we calculate the atoms per unit volume as

$$\frac{7.14\text{ g}}{\text{cm}^3}\times\frac{100\text{ cm}}{\text{m}}\times\frac{1\text{m}}{10^9\text{ nm}}\times\frac{1\text{ mol}}{65.38\text{ g}}\times\frac{6.022\times10^{23}\text{ atoms}}{\text{mol}}=\frac{6.6\times10^{15}\text{ atoms}}{\text{cm}^2\text{ nm}}$$

The units in the denominator may look odd to you, but writing them this way emphasizes that we are interested both in the depth from which information is received (given here in nanometers, nm) and in the surface area from which information is received (given here in square centimeters, cm^2). Multiplying this value by the thickness of an atomic layer of zinc, which is twice its atomic radius, suggests we are analyzing approximately

$$\frac{6.6\times10^{15}\text{ atoms}}{\text{cm}^2\text{ nm}}\times0.26\text{ nm}=1.7\times10^{15}\frac{\text{atoms}}{\text{cm}^2}$$

If we multiply this value by the surface area that we are sampling from, then we are interacting with approximately

$$1.7\times10^{15}\frac{\text{atoms}}{\text{cm}^2}\times\left(\frac{100\text{ cm}^2}{\text{m}}\right)^2\times\left(\frac{1\text{m}}{10^6\mu\text{m}}\right)^2=1.7\times10^7\text{ atoms of Zn}$$

Although 17 million may seem like a large number, it is not a particularly large number of atoms on which to carry out an analysis. Now, suppose the surface has a 10 ppm impurity of copper atoms; that is, there are 10 copper atoms for every 10^6 zinc atoms. In this case, our probe of the sample involves just

$$1.7\times10^7\text{ atoms of Zn}\times\frac{10\text{ atoms of Cu}}{10^6\text{ atoms of Zn}}=170\text{ atoms of Cu}$$

As a comparison, if we analyze a sample in which the analyte is present at a concentration that is $1\times10^{-6}\text{ mol/L}$ using an analytical method that gathers information from a volume that is just 1 mm^3, then we are sampling

$$\frac{1\times10^{-6}\text{ mol}}{\text{L}}\times\frac{1\text{L}}{1000\text{ cm}^3}\times\left(\frac{1\text{cm}}{10\text{ mm}}\right)^3\times1\text{ mm}^3\times6.022\times10^{23}\text{ mol}^{-1}=6.0\times10^{11}\text{ particles of analyte}$$

An additional challenge when we attempt to analyze a surface is that a freshly exposed surface becomes contaminated with an absorbed layer of gas molecules almost instantly when sitting on a laboratory bench, and in a few seconds to a few minutes at pressures in the range of 10^{-6} torr to 10^{-8} torr. Analysis of a surface requires careful attention to how the surface is prepared.

What Opportunities Does a Surface Present?

Compared to many of the methods in Chapters 6–20 and in Chapters 22–34, the use of a probe that samples from a small area allows for moving the probe across the surface—this is called rastering—developing a two-dimensional image of the surface. When using an energetic beam that can etch a hole in the sample, we can obtain information at depth—a process called depth profilling—that provides information in a third dimension. These are particularly important strengths of surface analytical methods.

How Can We Probe the Surface?

To study a surface, we put energy into it in the form of a beam of photons, electrons, or ions and then we measure the energy that exits the surface in the form of a beam of photons, electrons, or ions. Table 14.1.1shows some of the possibilities. Also included in this table are methods in which an applied field generates a response from the surface. Entries in **bold** receive attention in this chapter. Surface enhanced Raman spectroscopy received a brief mention in Chapter 18. Note that Auger electron spectroscopy appears twice as the emission of electrons can follow the input of X-ray photons or electrons.

Table 14.1.1. Classifying surface analysis methods based on the input energy and the output energy.

energy out → energy in ↓	photon	electron	ion	field
photon	surface enhanced Raman spectroscopy (SERS) extended X-ray absorption fine structure (EXAFS)	**X-ray photoelectron spectroscopy (XPS)** **Auger electron spectroscopy (AES)** UV-photoelectron spectroscopy (UPS)	laser-microprobe mass spectrometry (LAMMA)	—

energy out → energy in ↓	photon	electron	ion	field
electron	energy dispersive X-ray spectroscopy (EDS) electron microprobe (EM)	**Auger electron spectroscopy (AES)** **scanning electron microscopy (SEM)** low energy electron diffraction (LEED)	—	—
ion	—	—	Rutherford back scattering (RBS) **secondary ion mass spectrometry (SIMS)**	
field	—	**scanning tunneling microscopy (STM)**	—	**atomic force microscopy (AFM)**

Note

There are other ways to probe a surface by putting energy into it, including the application of thermal energy and the use of neutral species. See the text *Methods of Surface Analysis*, Czanderna, A. Editor, Elsevier: Amsterdam (1975) and the article "Analytical Chemistry of Surfaces" by D. M. Hercules and S. H. Hercules, *J. Chem. Educ.* 1984, *61*, 402–409 for detailed reviews. Although neither is a recent publication, both provide an excellent introduction to surface analysis.

This page titled 14.1: Introduction to the Study of Surfaces is shared under a CC BY-NC-SA 4.0 license and was authored, remixed, and/or curated by David Harvey.

- **21.1: Introduction to the Study of Surfaces** by David Harvey is licensed CC BY-NC-SA 4.0.

14.2: Scanning Electron Microscopy

In optical microscopy we use photons to provide images of a sample. Although extraordinarily useful and powerful, the ability to resolve features in optical microscopy is limited by the source of light; in general, we can distinguish between two objects if they are separated by a distance that is greater than the wavelength of the photons being used. The maximum resolution for an optical microscope is about 0.2 μm (200 nm), which means we can use an optical microscope to view a human hair (20-200 μm), an eukaryotic cell (10-100 μm), a chloroplast (5-8 μm), and a mitochondrion (1-3 μm), but not a ribosome (0.01 μm-0.02 μm). In this section we will consider the electron microscope, which has a resolution limit of approximately 0.2 nm, or approximately 1000× more than an optical microscope. In Section 21.4, we will examine two additional types of non-optical microscopy.

Instrumentation

In scanning electron microscopy we raster a beam of high-energy electrons over a surface using a two-dimensional grid. Figure 14.2.1 shows the basic instrumental needs. The electron gun usually is just a simple tungsten wire that releases electrons when it is heated resistively. Other sources include solid-state crystals of lanthanum hexaboride (LaB_6) or cerium hexaboride (CeB_6) and the field emission gun, which uses a tungsten wire with a tip that has a radius of about 100 μm. Regardless of their source, these electrons are accelerated to an energy of 1-40 keV and passed through a series of lens that narrow and focus them into a beam with a diameter that falls within a range of 1 nm to 1000 nm (0.001 μm to 1 μm). A set of coiled scan controls deflects the electron beam in a raster pattern across the sample's surface (see inset at the bottom left of Figure 14.2.1). An electron detector monitors the electrons that scatter back from the sample; the type of detector used varies with the type of emission from the sample that we choose to monitor—see the next sub-heading for types of emission—but typically are scintillation devices when monitoring electrons and energy-dispersive detectors when monitoring X-rays.

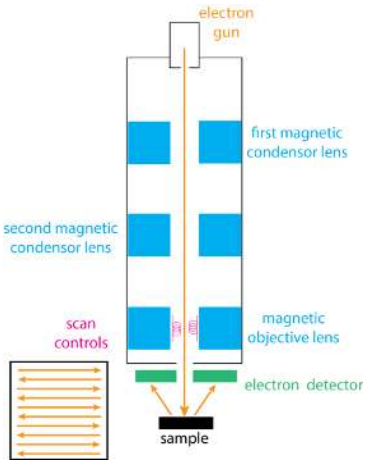


Figure 14.2.1: Schematic diagram of an instrument for scanning electron microscopy, which consists of an electron gun, a system of magnetic lenses, a scan control, and a detector. The inset on the lower left shows a raster pattern in which the electron beam is scanned back-and-forth across the sample's surface.

Interaction of Electron Beams With Solids

Figure 14.2.1 suggests that the only type of signal is the measurement of electrons that are scattered back toward the detector. The interaction between the electron beam and the sample, however creates a variety of signals, including both electrons and X-rays. Figure 14.2.2 illustrates the types of emission that follows from the interaction of the electron beam with the sample. The electron beam penetrates approximately 1-2 μm into the sample. As you might expect from the previous section on electron spectroscopy, the interaction of an electron beam with a sample results in the emission of some Auger electrons; these electrons come from a volume near the vacuum-sample interface. Of more importance are secondary electrons and backscattered electrons.

As the electron beam penetrates into the sample, the electrons undergo collisions with the sample's atoms. Some of these collisions are elastic in which the electron changes its direction, but retains its kinetic energy. With sufficient time, these electrons eventually undergo a collision in which they cross the sample-vacuum interface and exit the solid. These backscattered electrons are collected and passed along to the detector. Other electrons undergo inelastic collisions, losing kinetic energy and, eventually, become embedded in the sample. Backscattered electrons come from a depth as great as 50% of the depth to which the electron beam penetrates. Another source of electrons comes from a process in which the electron beam induces the ejection of electrons from the

sample's conduction band. These secondary electrons are less numerous than backscattered electrons and they also come from a much shallower depth, typically 5-50 nm.

The electron beam also stimulates the release of X-rays, including the characteristic X-rays of the sample's elements, a broad continuum, and fluorescent X-ray emission. See Chapter 12 for more details about atomic X-ray emission.

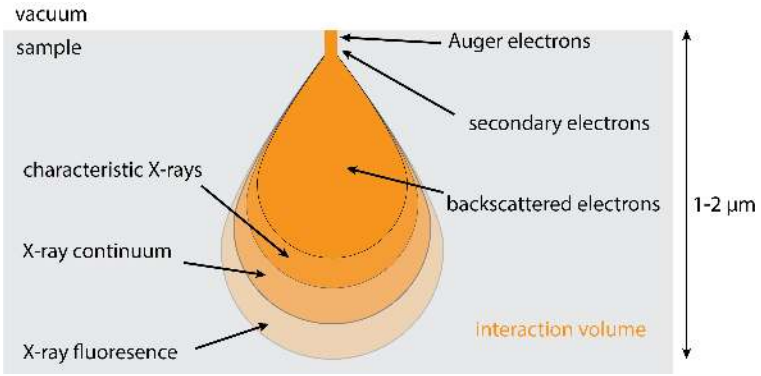


Figure 14.2.2: Illustration showing the types of emission that results from the interaction of an electron beam with a sample. The electron beam penetrates to a depth of approximately 1-2 µm, with the interaction volume increasing with depth. X-rays are emitted from deeper in the sample than are electrons.

As the electron beam is rastered across the sample, the intensity of the backscattered electrons from a specific position on the sample that reaches the detector is stored in the corresponding pixel on the instrument's monitor. The image created in this way is not an optical picture, but a digitized electronic reproduction of the sample's surface. The extent of magnification depends on the length of the detector's monitor relative to the length of a single scan across the sample; scanning a shorter distance results in a greater magnification. An optical microscope usually provides a maximum magnification of $1000\times$; an SEM can achieve a magnification of $1,000,000\times$

Applications

Figure $14.2.3$ shows four examples of applications of scanning electron microscopy for the measurement of particle size (upper left), for the evaluation of nanowires (upper right), for characterizing the channels in a microfluidic device (lower left), and for examining the tip of a cantilever and tip used for atomic force microscopy. Other applications include biological samples, films and coatings, fibers, and powders, to name a few.

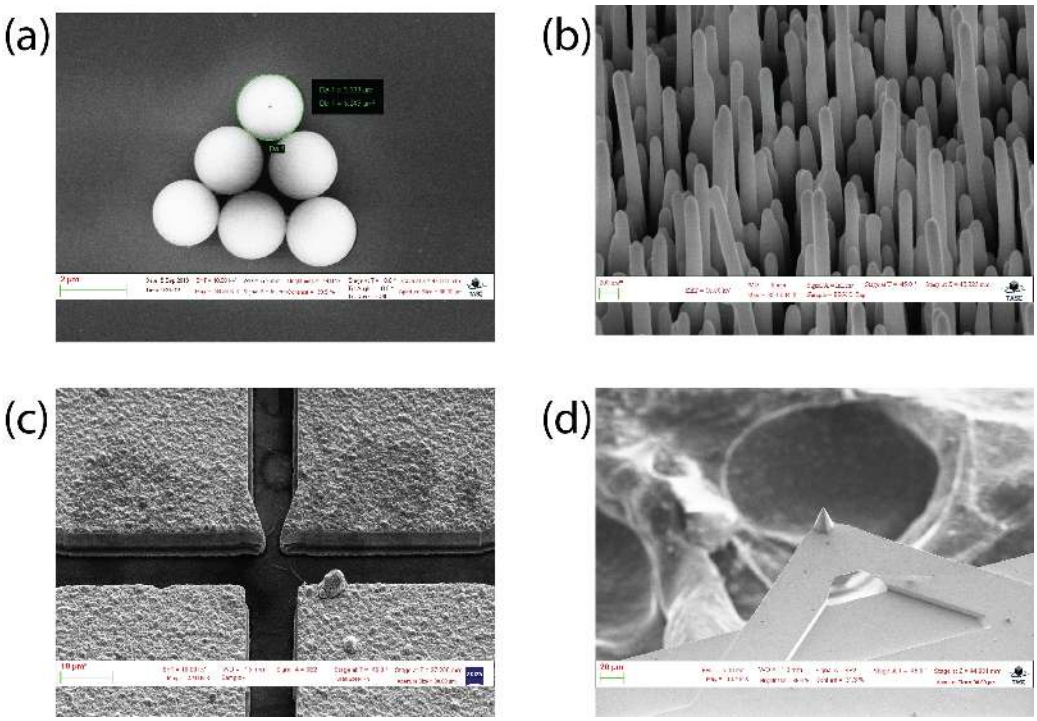


Figure 14.2.3: Scanning electron microscope images. The image in (a) shows six particulate spheres with diameters of about 2 µm each. The image in (b) shows a cluster of nanowires, each with a diameter of approximately 200 nm. The image in (c) shows the intersection of channels in a microfluidic device. The channels have widths of approximately 10 µm, although the upper channel narrows to about 2-4 µm at the intersection of the channels. The image in (d) is the tip of a cantilever used for atomic force microscopy, which we will explore in more detail in Section 21.4. All images are released under a CC-BY license and are available here.

This page titled 14.2: Scanning Electron Microscopy is shared under a CC BY-NC-SA 4.0 license and was authored, remixed, and/or curated by David Harvey.

- **21.3: Scanning Electron Microscopy** by David Harvey is licensed CC BY-NC-SA 4.0.

14.2.1: Scanning electron microscopy (SEM)

Student author: Emily Nagle 2019

How SEM works

In an SEM, an electron beam is emitted from an electron gun, then narrowed to a size of approximately 0.4-5 nm in diameter through the use of one or two condenser lenses. The beam then passes through a pair of deflection coils in the electron column to deflect the beam in the x and y axes before interacting with the sample. This deflection ensures that the scan is in a raster fashion, which means it is a rectangular image capture pattern of the sample. When the electron beam interacts with the sample, it loses energy due to random scattering and absorption by the sample. A schematic showing the components of SEM and how it works is shown in Figure 1. Additionally, a video explaining how SEM works is provided.

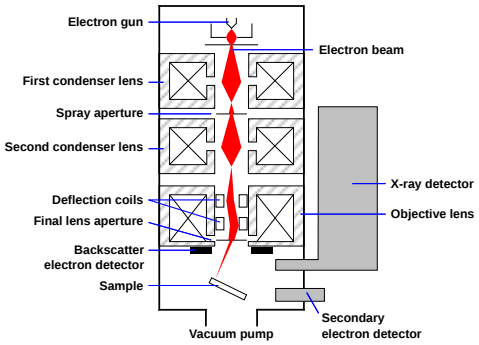
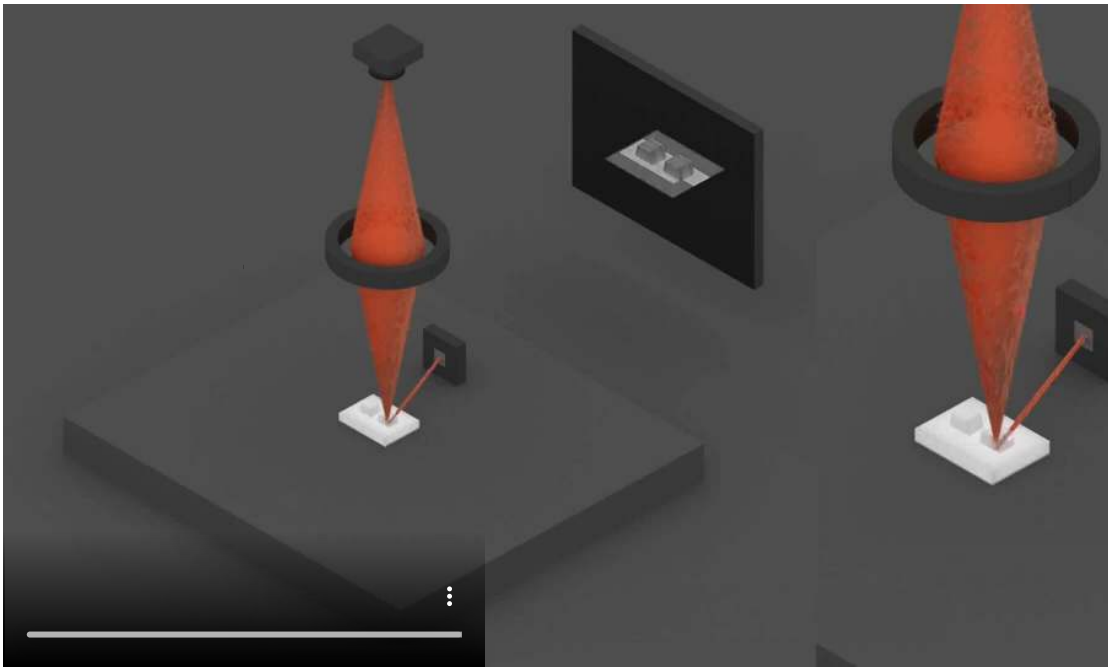


Figure 14.2.1.1: Schematic of how an SEM works (Figure courtesy of Creative Commons license and can be found at https://en.Wikipedia.org/wiki/File:Schema_MEB_(en).svg)



Video 14.2.1.1: Illustration of how SEM works coutresy of Creative Commons license and found at https://en.Wikipedia.org/wiki/File:Scanning_Electron_Microscope.ogv#filehistory

The electron beam of a scanning electron microscope interacts with atoms at different depths within the sample to produce different signals including secondary electrons, back-scattered electrons, and characteristic X-rays. Each of these signals has its own detector in the SEM, as seen in Figure 1. Secondary electrons are low energy electrons that are ejected from the valence or conduction bands of atoms in the sample through inelastic scattering from the beam electrons. Back-scattered electrons are electrons from the beam that are reflected through elastic scattering interactions with atoms in the sample. The intensity of the back-scattered electron signal is dependent upon the atomic number so it can provide information about the distribution of different elements in a sample. The characteristic X-rays are emitted when the electron beam interacts with the sample and removes an inner shell electron, resulting in a higher-energy electron filling the shell and releasing energy. The energy or wavelength of these X-rays can be measured by Energy-dispersive X-Ray Spectroscopy to identify and measure the abundance and distribution of elements in the sample. The electron beam absorbed by the sample is detected and used to create an image of the sample distribution. The resulting image is a map displaying the intensity of signal emitted from the area of the sample being scanned, as seen in Figure 2. Additionally, EDS detectors can be attached to the SEM for elemental analysis.

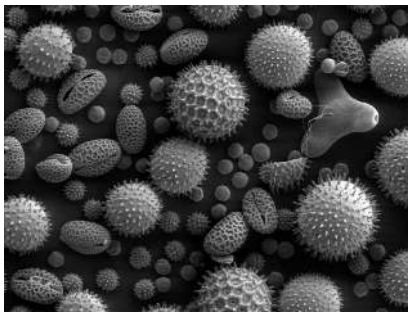


Figure 14.2.1.2 SEM image of pollen grains. Image released to the public domain by original author Dartmouth College Electron Microscope Facility and found at https://upload.wikimedia.org/Wikipedia/commons/a/a4/Misc_pollen.jpg

In order to obtain SEM images, the sample must be electrically conductive at the surface as well as electrically grounded so that it does not accumulate charge. Samples are mounted onto the specimen holder using a conductive adhesive. Metal samples require minimal sample preparation other than conductively mounting the sample to the stage. Non-conductive materials typically undergo ultrathin coating with electrically conductive materials such as gold, platinum, chromium, or graphite. The coating is accomplished through sputter-coating or evaporation under high vacuum.

How to Interpret the Data

Different SEM images can be produced based on the type of detector being used and these image can be used to see what the sample looks like on the nanoscale. The most typical detector used detects the secondary electrons that are emitted from the sample by inelastic scattering. The number of secondary electrons detected represents the signal intensity and is combined with the position of the beam to produce a gray-scale images showing the sample's topography, as seen in Figure 2. Back-scattered electrons can also be used to get an image since elements will reflect a different number of electrons. Therefore, the intensity of back-scattered electrons will vary throughout a sample depending on the elements present. An SEM image produced from the intensity of back-scattered electrons and the beam position can show the distribution of different elements in the sample. Elements that are heavier and reflect more electrons will appear brighter in the image so back-scattered electrons can show contrasts in chemical composition. However, the identity of the different elements cannot be determined with SEM alone, an EDS attachment would have to be used to quantify the relative abundance of different elements.

Good Literature Examples

1. Nehl, C. L., Liao, H. & Hafner, J. H. Optical properties of star-shaped gold nanoparticles. *Nano Lett.* **6,** 683–688 (2006).
2. Burnside, S. D. *et al*. Self-Organization of TiO2 Nanoparticles in Thin Films. *Chem. Mater.* **10,** 2419–2425 (1998).

Works Cited

1. https://en.Wikipedia.org/wiki/Scanning_electron_microscope
2. Nehl, C. L., Liao, H. & Hafner, J. H. Optical properties of star-shaped gold nanoparticles. *Nano Lett.* **6,** 683–688 (2006).
3. Burnside, S. D. *et al*. Self-Organization of TiO2 Nanoparticles in Thin Films. *Chem. Mater.* **10,** 2419–2425 (1998).

Useful Resources for In-Depth Reading

1. McMullan, D. Scanning electron microscopy 1928-1965. *Scanning* **17,** 175–185 (2006).
2. Smith, K. C. A. & Oatley, C. W. The scanning electron microscope and its fields of application. *Br. J. Appl. Phys.* **6,** 391–399 (1955).
3. https://www.atascientific.com.au/sem-imaging-applications-practical-uses-scanning-electron-microscopes/

14.2.1: Scanning electron microscopy (SEM) is shared under a CC BY-NC-SA 4.0 license and was authored, remixed, and/or curated by LibreTexts.

14.2.2: Transmission Electron Microscopy

TEM: An Overview

Transmission electron microscopy (TEM) is a form of microscopy which in which a beam of electrons transmits through an extremely thin specimen, and then interacts with the specimen when passing through it. The formation of images in a TEM can be explained by an optical electron beam diagram in Figure 14.2.2.1. TEMs provide images with significantly higher resolution than visible-light microscopes (VLMs) do because of the smaller de Broglie wavelength of electrons. These electrons allow for the examination of finer details, which are several thousand times higher than the highest resolution in a VLM. Nevertheless, the magnification provide in a TEM image is in contrast to the absorption of the electrons in the material, which is primarily due to the thickness or composition of the material.

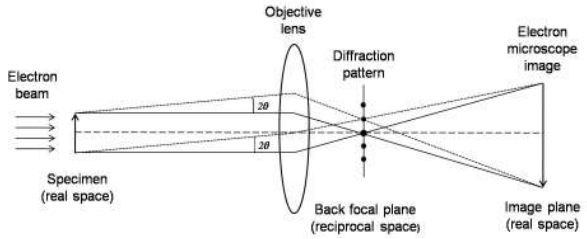


Figure 14.2.2.1 The optical electron beam diagram of TEM.

When a crystal lattice spacing (d) is investigated with electrons with wavelength λ, diffracted waves will be formed at specific angles 2θ, satisfying the Bragg condition, 14.2.2.1.

$$2dsin\theta = \lambda \tag{14.2.2.1}$$

The regular arrangement of the diffraction spots, the so-called diffraction pattern (DP), can be observed. While the transmitted and the diffracted beams interfere on the image plane, a magnified image (electron microscope image) appears. The plane where the DP forms is called the reciprocal space, which the image plane is called the real space. A Fourier transform can mathematically transform the real space to reciprocal space.

By adjusting the lenses (changing their focal lengths), both electron microscope images and DP can be observed. Thus, both observation modes can be successfully combined in the analysis of the microstructures of materials. For instance, during investigation of DPs, an electron microscope image is observed. Then, by inserting an aperture (selected area aperture), adjusting the lenses, and focusing on a specific area that we are interested in, we will get a DP of the area. This kind of observation mode is called a selected area diffraction. In order to investigate an electron microscope image, we first observe the DP. Then by passing the transmitted beam or one of the diffracted beams through a selected aperture and changing to the imaging mode, we can get the image with enhanced contrast, and precipitates and lattice defects can easily be identified.

Describing the resolution of a TEM in terms of the classic Rayleigh criterion for VLMs, which states that the smallest distance that can be investigated, δ, is given approximately by 14.2.2.2, where λ is the wavelength of the electrons, μ is the refractive index of the viewing medium, and β is the semi-angle of collection of the magnifying lens.

$$\delta = \frac{0.61\lambda}{\mu\, sin\beta} \tag{14.2.2.2}$$

ccording to de Broglie's ideas of the wave-particle duality, the particle momentum p is related to its wavelength λ through Planck's constant h, 14.2.2.3.

$$\lambda = \frac{h}{p} \tag{14.2.2.3}$$

Momentum is given to the electron by accelerating it through a potential drop, V, giving it a kinetic energy, eV. This potential energy is equal to the kinetic energy of the electron, 14.2.2.4.

$$eV = \frac{m_o u^2}{2} \tag{14.2.2.4}$$

Based upon the foregoing, we can equate the momentum (p) to the electron mass (mo), multiplied by the velocity (v) and substituting for v from 14.2.2.5i.e., 14.2.2.6.

$$p = m_o u = (2m_o eV)^{\frac{1}{2}} \tag{14.2.2.5}$$

These equations define the relationship between the electron wavelength, λ, and the accelerating voltage of the electron microscope (V), Eq. However, we have to consider about the relative effects when the energy of electron more than 100 keV. So in order to be exact we must modify 14.2.2.6to give 14.2.2.7.

$$\lambda = \frac{h}{(2m_o eV)^{\frac{1}{2}}} \tag{14.2.2.6}$$

$$\lambda = \frac{h}{[2m_o eV(1 + \frac{eV}{2m_o e^2})]^{\frac{1}{2}}} \tag{14.2.2.7}$$

From 14.2.2.2and 14.2.2.3, if a higher resolution is desired a decrease in the electron wavelength is accomplished by increasing the accelerating voltage of the electron microscope. In other words, the higher accelerating rating used, the better resolution obtained.

Why the Specimen Should be Thin

The scattering of the electron beam through the material under study can form different angular distribution (Figure 14.2.2.2) and it can be either forward scattering or back scattering. If an electron is scattered < 90o, then it is forward scattered, otherwise, it is backscattered. If the specimen is thicker, fewer electrons are forward scattered and more are backscattered. Incoherent, backscattered electrons are the only remnants of the incident beam for bulk, non-transparent specimens. The reason that electrons can be scattered through different angles is related to the fact that an electron can be scattered more than once. Generally, the more times of scattering happen, the greater the angle of scattering.

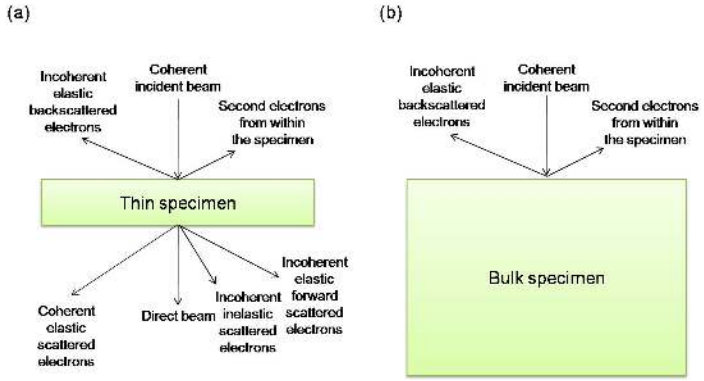


Figure 14.2.2.2 Two different kinds of electron scattering form (a) a thin specimen and (b) a bulk specimen.

All scattering in the TEM specimen is often approximated as a single scattering event since it is the simplest process. If the specimen is very thin, this assumption will be reasonable enough. If the electron is scattered more than once, it is called ‘plural scattering.’ It is generally safe to assume single scattering occurs, unless the specimen is particularly thick. When the times of scattering increase, it is difficult to predict what will happen to the electron and to interpret the images and DPs. So, the principle is ‘thinner is better’, i.e., if we make thin enough specimens so that the single-scattering assumption is plausible, and the TEM research will be much easier.

In fact, forward scattering includes the direct beam, most elastic scattering, refraction, diffraction, particularly Bragg diffraction, and inelastic scattering. Because of forward scattering through the thin specimen, a DP or an image would be showed on the viewing screen, and an X-ray spectrum or an electron energy-loss spectrum can be detected outside the TEM column. However, backscattering still cannot be ignored, it is an important imagine mode in the SEM.

Limitations of TEM

Interpreting Transmission Images

One significant problem that might encounter when TEM images are analyzed is that the TEM present us with 2D images of a 3D specimen, viewed in transmission. This problem can be illustrated by showing a picture of two rhinos side by side such that the head of one appears attached to the rear of the other (Figure 14.2.2.3).

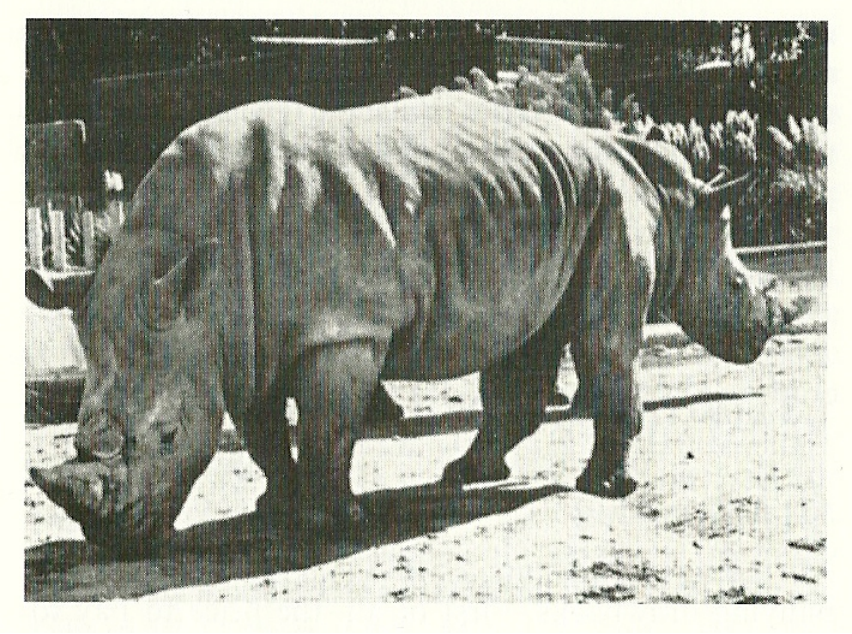


Figure 14.2.2.3 In projection, this photograph of two rhinos appears as one two-headed beast, because sometimes people have difficulty to translate a 2D image to a 3D image. Adapted from D. B. Williams and C. B. Carter, Transmission Electron Microscopy: A Textbook for Material Science, 2nd Ed., Springer, New York (2009).

One aspect of this particular drawback is that a single TEM images has no depth sensitivity. There often is information about the top and bottom surfaces of the specimen, but this is not immediately apparent. There has been progress in overcoming this limitation, by the development of electron tomography, which uses a sequence of images taken at different angles. In addition, there has been improvement in specimen-holder design to permit full 360o rotation and, in combination with easy data storage and manipulation; nanotechnologists have begun to use this technique to look at complex 3D inorganic structures such as porous materials containing catalyst particles.

Electron Beam Damage

A detrimental effect of ionizing radiation is that it can damage the specimen, particularly polymers (and most organics) or certain minerals and ceramics. Some aspects of beam damage made worse at higher voltages. Figure 14.2.2.4shows an area of a specimen damaged by high-energy electrons. However, the combination of more intense electron sources with more sensitive electron detectors, and the use computer enhancement of noisy images, can be used to minimize the total energy received by the sample.

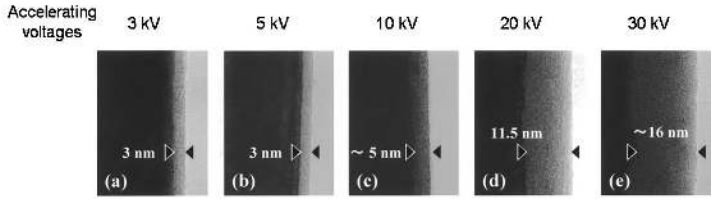


Figure 14.2.2.4 High-resolution TEM images at the slit edge of the GaAs samples prepared by slit focused ion beam. GaAs samples prepared at (a) 3 kV, (b) 5 kV, (c) 10 kV, (d) 20 kV, and (e) 30 kV. The thickness of the amorphous layer produced by focused ion beam is shown in each image. Adapted from Y. Yabuuchi, S. Tametou, T. Okano, S. Inazato, S. Sadayamn, and Y. Tamamoto, *J. Electron Micros.*, 2004, **53**, 5.

Sample Preparation

The specimens under study have to be thin if any information is to be obtained using transmitted electrons in the TEM. For a sample to be transparent to electrons, the sample must be thin enough to transmit sufficient electrons such that enough intensity falls on the screen to give an image. This is a function of the electron energy and the average atomic number of the elements in the

sample. Typically for 100 keV electrons, a specimen of aluminum alloy up to ~ 1 μm would be thin, while steel would be thin up to about several hundred nanometers. However, thinner is better and specimens < 100 nm should be used wherever possible.

The method to prepare the specimens for TEM depends on what information is required. In order to observe TEM images with high resolution, it is necessary to prepare thin films without introducing contamination or defects. For this purpose, it is important to select an appropriate specimen preparation method for each material, and to find an optimum condition for each method.

Crushing

A specimen can be crushed with an agate mortar and pestle. The flakes obtained are suspended in an organic solvent (e.g., acetone), and dispersed with a sonic bath or simply by stirring with a glass stick. Finally, the solvent containing the specimen flakes is dropped onto a grid. This method is limited to materials which tend to cleave (e.g., mica).

Electropolishing

Slicing a bulk specimen into wafer plates of about 0.3 mm thickness by a fine cutter or a multi-wire saw. The wafer is further thinned mechanically down to about 0.1 mm in thickness. Electropolishing is performed in a specific electrolyte by supplying a direct current with the positive pole at the thin plate and the negative pole at a stainless steel plate. In order to avoid preferential polishing at the edge of the specimen, all the edges are cover with insulating paint. This is called the window method. The electropolishing is finished when there is a small hole in the plate with very thin regions around it (Figure 14.2.2.5). This method is mainly used to prepare thin films of metals and alloys.

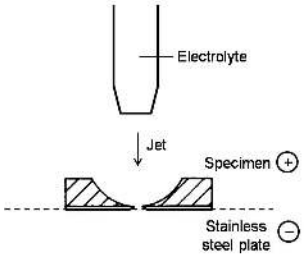


Figure 14.2.2.5 Principle of jet electropolishing method. The specimen and the stainless steel plate is electronic positive and negative, respectively.

Chemical Polishing

Thinning is performed chemically, i.e., by dipping the specimen in a specific solution. As for electropolishing, a thin plate of 0.1~0.2 mm in thickness should be prepared in advance. If a small dimple is made in the center of the plate with a dimple grinder, a hole can be made by etching around the center while keeping the edge of the specimen relatively thick. This method is frequently used for thinning semiconductors such as silicon. As with electro-polishing, if the specimen is not washed properly after chemical etching, contamination such as an oxide layer forms on the surface.

Ultramicrotomy

Specimens of thin films or powders are usually fixed in an acrylic or epoxy resin and trimmed with a glass knife before being sliced with a diamond knife. This process is necessary so that the specimens in the resin can be sliced easily by a diamond knife. Acrylic resins are easily sliced and can be removed with chloroform after slicing. When using an acrylic resin, a gelatin capsule is used as a vessel. Epoxy resin takes less time to solidify than acrylic resins, and they remain strong under electron irradiation. This method has been used for preparing thin sections of biological specimens and sometimes for thin films of inorganic materials which are not too hard to cut.

Ion Milling

A thin plate (less than 0.1 mm) is prepared from a bulk specimen by using a diamond cutter and by mechanical thinning. Then, a disk 3 mm in diameter is made from the plate using a diamond knife or a ultrasonic cutter, and a dimple is formed in the center of the surface with a dimple grinder. If it is possible to thin the disk directly to 0.03 mm in thickness by mechanical thinning without using a dimple grinder, the disk should be strengthened by covering the edge with a metal ring. Ar ions are usually used for the sputtering, and the incidence angle against the disk specimen and the accelerating voltage are set as 10 - 20o and a few kilovolts, respectively. This method is widely used to obtain thin regions of ceramics and semiconductors in particular, and also for cross section of various multilayer films.

Focused Ion Beam (FIB)

This method was originally developed for the purpose of fixing semiconductor devices. In principle, ion beams are sharply focused on a small area, and the specimen in thinned very rapidly by sputtering. Usually Ga ions are used, with an accelerating voltage of about 30 kV and a current of about 10 A/cm2. The probe size is several tens of nanometers. This method is useful for specimens containing a boundary between different materials, where it may be difficult to homogeneously thin the boundary region by other methods such as ion milling.

Vacuum Evaporation

The specimen to be studied is set in a tungsten-coil or basket. Resistance heating is applied by an electric current passing through the coil or basket, and the specimen is melted, then evaporated (or sublimed), and finally deposited onto a substrate. The deposition process is usually carried under a pressure of 10-3-10-4 Pa, but in order to avoid surface contamination, a very high vacuum is necessary. A collodion film or cleaved rock salt is used as a substrate. Rock salt is especially useful in forming single crystals with a special orientation relationship between each crystal and the substrate. Salt is easily dissolved in water, and then the deposited films can be fixed on a grid. Recently, as an alternative to resistance heating, electron beam heating or an ion beam sputtering method has been used to prepare thin films of various alloys. This method is used for preparing homogeneous thin films of metals and alloys, and is also used for coating a specimen with the metal of alloy.

The Characteristics of the Grid

The types of TEM specimens that are prepared depend on what information is needed. For example, a self-supporting specimen is one where the whole specimen consists of one material (which may be a composite). Other specimens are supported on a grid or on a Cu washer with a single slot. Some grids are shown in Figure 14.2.2.6 Usually the specimen or grid will be 3 mm in diameter.

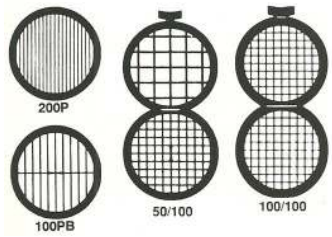


Figure 14.2.2.6 TEM sample support mesh grids. A diameter of a grid is usually 3.05 mm, however, some grids with diameters of 2.30 mm are also be used for earlier microscopes. Adapted from D. B. Williams and C. B. Carter, Transmission Electron Microscopy: A Textbook for Material Science, 2nd Ed., Springer, New York (2009).

TEM specimen stage designs include airlocks to allow for insertion of the specimen holder into the vacuum with minimal increase in pressure in other areas of the microscope. The specimen holders are adapted to hold a standard size of grid upon which the sample is placed or a standard size of self-supporting specimen. Standard TEM grid sizes is a 3.05 mm diameter ring, with a thickness and mesh size ranging from a few to 100 µm. The sample is placed onto the inner meshed area having diameter of approximately 2.5 mm. The grid materials usually are copper, molybdenum, gold or platinum. This grid is placed into the sample holder which is paired with the specimen stage. A wide variety of designs of stages and holders exist, depending upon the type of experiment being performed. In addition to 3.05 mm grids, 2.3 mm grids are sometimes, if rarely, used. These grids were particularly used in the mineral sciences where a large degree of tilt can be required and where specimen material may be extremely rare. Electron transparent specimens have a thickness around 100 nm, but this value depends on the accelerating voltage.

Once inserted into a TEM, the sample is manipulated to allow study of the region of interest. To accommodate this, the TEM stage includes mechanisms for the translation of the sample in the XY plane of the sample, for Z height adjustment of the sample holder, and usually at least one rotation degree of freedom. Most TEMs provide the ability for two orthogonal rotation angles of movement with specialized holder designs called double-tilt sample holders.

A TEM stage is required to have the ability to hold a specimen and be manipulated to bring the region of interest into the path of the electron beam. As the TEM can operate over a wide range of magnifications, the stage must simultaneously be highly resistant to mechanical drift as low as a few nm/minute while being able to move several µm/minute, with repositioning accuracy on the order of nanometers.

Transmission Electron Microscopy Image for Multilayer-Nanomaterials

Although, TEMs can only provide 2D analysis for a 3D specimen; magnifications of 300,000 times can be routinely obtained for many materials making it an ideal methodfor the study of nanomaterials. Besides from the TEM images, darker areas of the image show that the sample is thicker or denser in these areas, so we can observe the different components and structures of the specimen by the difference of color. For investigating multilayer-nanomaterials, a TEM is usually the first choice, because not only does it provide a high resolution image for nanomaterials but also it can distinguish each layer within a nanostructured material.

Observations of Multilayer-nanomaterials

TEM was been used to analyze the depth-graded W/Si multilayer films. Multilayer films were grown on polished, 100 mm thick Si wafers by magnetron sputtering in argon gas. The individual tungsten and silicon layer thicknesses in periodic and depth-graded multilayers are adjusted by varying the computer-controlled rotational velocity of the substrate platen. The deposition times required to produce specific layer thicknesses were determined from detailed rate calibrations. Samples for TEM were prepared by focused ion beam milling at liquid N2 temperature to prevent any beam heating which might result in re-crystallization and/or re-growth of any amorphous or fine grained polycrystalline layers in the film.

TEM measurements were made using a JEOL-4000 high-resolution transmission electron microscope operating at 400 keV; this instrument has a point-to-point resolution of 0.16 nm. Large area cross-sectional images of a depth-graded multilayer film obtained under medium magnification (~100 kX) were acquired at high resolution. A cross-sectional TEM image showed 150 layers W/Si film with the thickness of layers in the range of 3.33 ~ 29.6 nm (Figure 14.2.2.7 shows a part of layers). The dark layers are tungsten and the light layers are silicon and they are separated by the thin amorphous W–Si interlayers (gray bands). By the high resolution of the TEM and the nature characteristics of the material, each layer can be distinguished clearly with their different darkness.

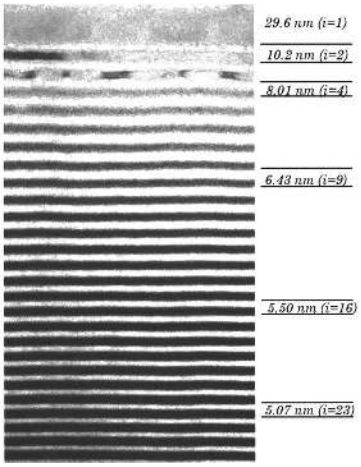


Figure 14.2.2.7 Cross-sectional transmission electron micrograph of the top portion of a depth-graded W/Si multilayer structure. Selected bilayer indices and thicknesses are indicated. The tungsten (dark bands) and silicon (light bands) layers are separated by thin amorphous W–Si interlayers (gray bands). The topmost silicon layer is not completely visible in this image. Adapted from D. L. Windt, F. E. Christensen, W. W. Craig, C. Hailey, F. A. Harrison, M. Jimenez-Garate, R. Kalyanaraman, and P. H. Mao, J. Appl. Phys., 2000, 88, 460.

Not all kinds of multilayer nanomaterials can be observed clearly under TEM. A materials consist of pc-Si:H multilayers were prepared by a photo-assisted chemical vapor deposition (photo-CVD) using a low-pressure mercury lamp as an UV light source to dissociate the gases. The pc-Si:H multilayer included low H2-diluted a-Si:H sublayers (SL's) and highly H2-diluted a-Si:H sublayers (SH's). Control of the CVD gas flow (H2|SiH4) under continuous UV irradiation resulted in the deposition of multilayer films layer by layer.

For a TEM measurement, a 20 nm thick undiluted a-Si:H film on a c-Si wafer before the deposition of multilayer to prevent from any epitaxial growth. Figure 14.2.2.8 shows a cross-sectional TEM image of a six-cycled pc-Si:H multilayer specimen. The white dotted lines are used to emphasize the horizontal stripes, which have periodicity in the TEM image. As can be seen, there are no significant boundaries between SL and SH could be observed because all sublayers are prepared in H2 gas. In order to get the more accurate thickness of each sublayer, other measurements might be necessary.

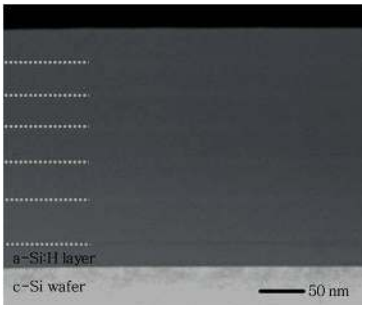


Figure 14.2.2.8 Cross-sectional TEM image of a 6-cycled pc-Si:H multilayer. Before the multilayer deposition, a 20 nm thick a-Si:H was deposited on a c-Si substrate. Adapted from S. W. Kwon, J. Kwak, S. Y. Myong, and K. S. Lim, *J. Non-Cryst. Solid*, 2006, **352**, 1132.

TEM Imaging of Carbon Nanomaterials

Transmission electron microscopy (TEM) is a form of microscopy that uses an high energy electron beam (rather than optical light). A beam of electrons is transmitted through an ultra thin specimen, interacting with the specimen as it passes through. The image (formed from the interaction of the electrons with the sample) is magnified and focused onto an imaging device, such as a photographic film, a fluorescent screen,or detected by a CCD camera. In order to let the electrons pass through the specimen, the specimen has to be ultra thin, usually thinner than 10 nm.

The resolution of TEM is significantly higher than light microscopes. This is because the electron has a much smaller de Broglie wavelength than visible light (wavelength of 400~700 nm). Theoretically, the maximum resolution, d, has been limited by λ, the wavelength of the detecting source (light or electrons) and NA, the numerical aperture of the system.

$$d = \frac{\lambda}{2n\ sin\alpha} \approx \frac{\lambda}{2NA} \tag{14.2.2.8}$$

For high speed electrons (in TEM, electron velocity is close to the speed of light, c, so that the special theory of relativity has to be considered), the λe:

$$\lambda_e = \frac{h}{\sqrt{2m_0E(1+E/2m_0c^2)}} \tag{14.2.2.9}$$

According to this formula, if we increase the energy of the detecting source, its wavelength will decrease, and we can get higher resolution. Today, the energy of electrons used can easily get to 200 keV, sometimes as high as 1 MeV, which means the resolution is good enough to investigate structure in sub-nanometer scale. Because the electrons is focused by several electrostatic and electromagnetic lenses, like the problems optical camera usually have, the image resolution is also limited by aberration, especially the spherical aberration called Cs. Equipped with a new generation of aberration correctors, transmission electron aberration-corrected microscope (TEAM) can overcome spherical aberration and get to half angstrom resolution.

Although TEAM can easily get to atomic resolution, the first TEM invented by Ruska in April 1932 could hardly compete with optical microscope, with only 3.6×4.8 = 14.4 magnification. The primary problem was the electron irradiation damage to sample in poor vacuum system. After World War II, Ruska resumed his work in developing high resolution TEM. Finally, this work brought him the Nobel Prize in physics 1986. Since then, the general structure of TEM hasn't changed too much as shown in Figure 14.2.2.9. The basic components in TEM are: electron gun, condenser system, objective lens (most important len in TEM which determines the final resolution), diffraction lens, projective lenses (all lens are inside the equipment column, between apertures), image recording system (used to be negative films, now is CCD cameras) and vacuum system.

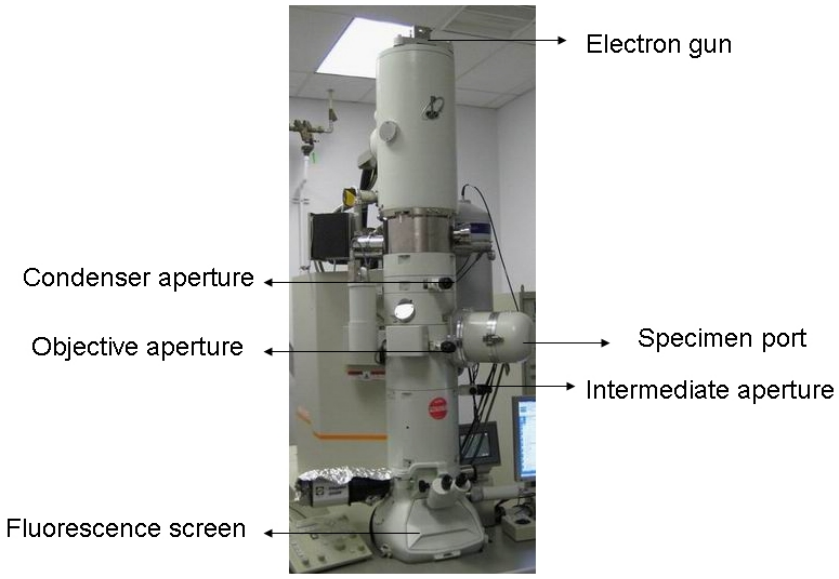


Figure 14.2.2.9 Position of the basic components in a TEM.

The Family of Carbon Allotropes and Carbon Nanomaterials

Common carbon allotropes include diamond, graphite, amorphrous C (a-C), fullerene (also known as buckyball), carbon nanotube (CNT, including single wall CNT and multi wall CNT), graphene. Most of them are chemically inert and have been found in nature. We can also define carbon as sp2 carbon (which is graphite), sp3 carbon (which is diamond) or hybrids of sp2 and sp3 carbon. As shown in Figure, (a) is the structure of diamond, (b) is the structure of graphite, (c) graphene is a single sheet of graphite, (d) is amorphous carbon, (e) is C60, and (f) is single wall nanotube. As for carbon nanomaterials, fullerene, CNT and graphene are the three most well investigated, due to their unique properties in both mechanics and electronics. Under TEM, these carbon nanomaterials will display three different projected images.

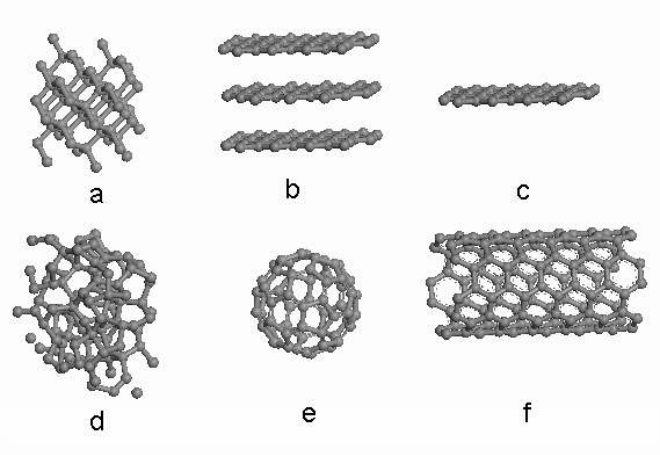


Figure 14.2.2.10 Six allotropes of carbon: a) diamond, b) graphite, c) graphene, d) amorphous carbon, e) C60 (Buckminsterfullerene or buckyball), f) single-wall carbon nanotube or buckytube.

Atomic Structure of Carbon Nanomaterials under TEM

All carbon naomaterials can be investigated under TEM. Howerver, because of their difference in structure and shape, specific parts should be focused in order to obtain their atomic structure.

For C60, which has a diameter of only 1 nm, it is relatively difficult to suspend a sample over a lacey carbon grid (a common kind of TEM grid usually used for nanoparticles). Even if the C60 sits on a thin a-C film, it also has some focus problems since the surface profile variation might be larger than 1 nm. One way to solve this problem is to encapsulate the C60 into single wall CNTs, which is known as nano peapods. This method has two benefits:

CNT helps focus on C60. Single wall is aligned in a long distance (relative to C60). Once it is suspended on lacey carbon film, it is much easier to focus on it. Therefore, the C60 inside can also be caught by minor focus changes.
The CNT can protect C60 from electron irradiation. Intense high energy electrons can permanently change the structure of the CNT. For C60, which is more reactive than CNTs, it can not survive after exposing to high dose fast electrons.
In studying CNT cages, C92 is observed as a small circle inside the walls of the CNT. While a majority of electron energy is absorbed by the CNT, the sample is still not irradiation-proof. Thus, as is seen in Figure 14.2.2.11, after a 123 s exposure, defects can be generated and two C92 fused into one new larger fullerene.

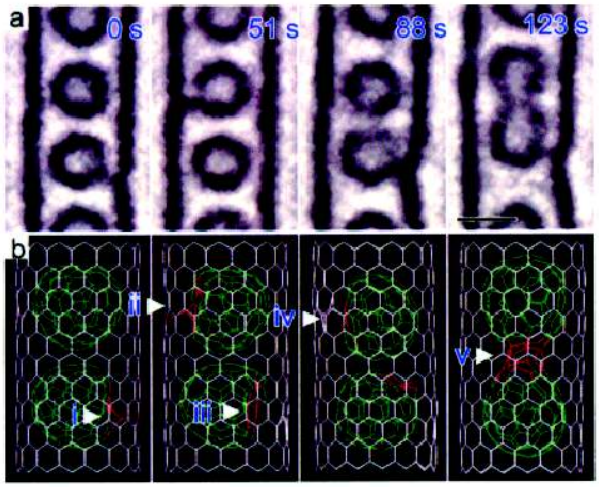


Figure 14.2.2.11 C_{92} encapsulated in SWNTs under different electron irradiation time. Courtesy of Dr. Kazutomo SUENAGA, adapted from K. Urita, Y. Sato, K. Suenaga, A. Gloter, A. Hasimoto, M. Ishida, T. Shimada, T. Shinohara, S. Iijima, *Nano Lett.*, 2004, **4**, 2451. Copyright American Chemical Society (2004).

Although, the discovery of C_{60} was first confirmed by mass spectra rather than TEM. When it came to the discovery of CNTs, mass spectra was no longer useful because CNTs shows no individual peak in mass spectra since any sample contains a range of CNTs with different lengths and diameters. On the other hand, HRTEM can provide a clear image evidence of their existence. An example is shown in Figure 14.2.2.12

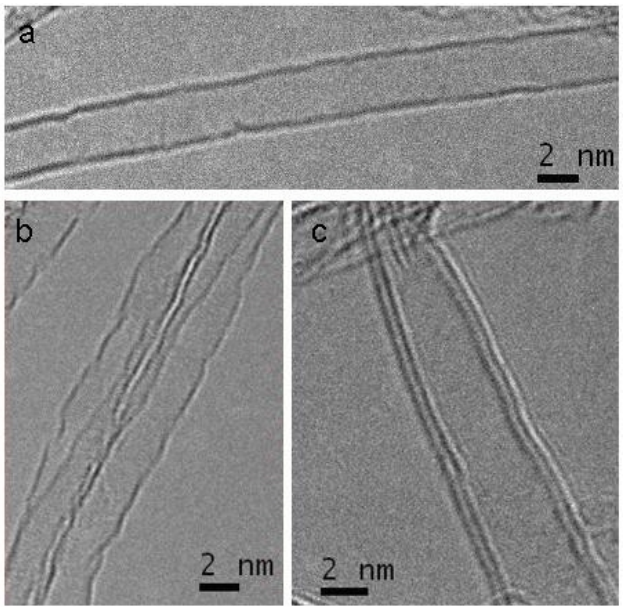


Figure 14.2.2.11 TEM images of SWNT and DWCNTs. Parallel dark lines corresponds to (002) lattice image of graphite. (a) and (b) SWNTs have 1 layer graphene sheet, diameter 3.2 nm. (c) DWCNT, diameter 4.0 nm.

Graphene is a planar fullerene sheet. Until recently, Raman, AFM and optical microscopy (graphene on 300 nm SiO2 wafer) were the most convenient methods to characterize samples. However, in order to confirm graphene's atomic structure and determine the

difference between mono-layer and bi-layer, TEM is still a good option. In Figure 14.2.2.13 a monolayer suspended graphene is observed with its atomic structure clearly shown. Inset is the FFT of the TEM image, which can be used as a filter to get an optimized structure image. High angle annular dark field (HAADF) image usually gives better contrast for different particles on it. It is also sensitive with changes of thickness, which allows a determination of the number of graphene layers.

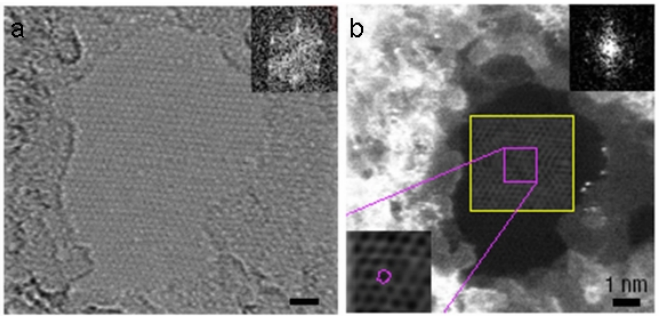


Figure 14.2.2.13 HRTEM of monolayer graphene. (a) Bright filed. (b) High Angle Annular Dark Field. Courtesy of Dr M. H. Gass, adapted from M. H. Gass, U. Bangert, A. L. Bleloch, P. Wang, R. R. Nair, and A. K. Geim, Nature Nanotechnol., 2008, 3, 676.

Graphene Stacking and Edges Direction

Like the situation in CNT, TEM image is a projected image. Therefore, even with exact count of edge lines, it is not possible to conclude that a sample is a single layer graphene or multi-layer. If folding graphene has AA stacking (one layer is superposed on the other), with a projected direction of [001], one image could not tell the thickness of graphene. In order to distinguish such a bilayer of graphene from a single layer of graphene, a series of tilting experiment must be done. Different stacking structures of graphene are shown in Figure 14.2.2.13a.

Theoretically, graphene has the potential for interesting edge effects. Based upon its sp2 structure, its edge can be either that of a zigzag or armchair configuration. Each of these possess different electronic properties similar to that observed for CNTs. For both research and potential application, it is important to control the growth or cutting of graphene with one specific edge. But before testing its electronic properties, all the edges have to be identified, either by directly imaging with STM or by TEM. Detailed information of graphene edges can be obtained with HRTEM, simulated with fast fourier transform (FFT). In Figure 14.2.2.14b, armchair directions are marked with red arrow respectively. A clear model in Figurec shows a 30 degree angle between zigzag edge and armchair edge.

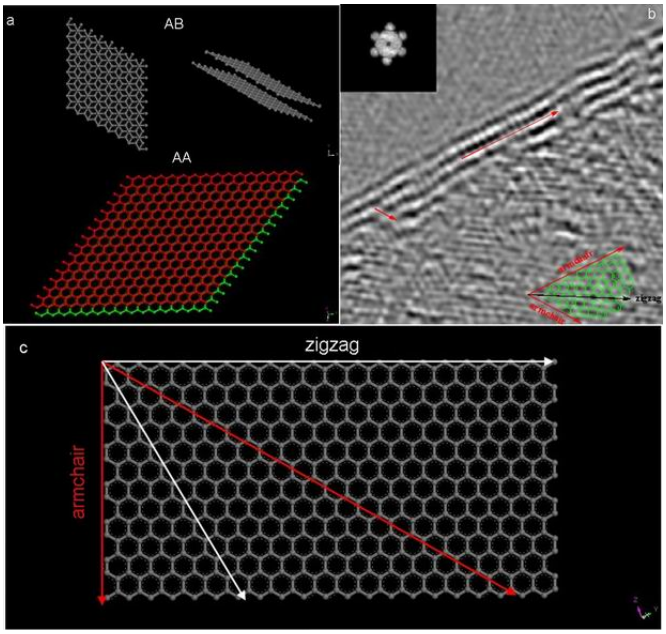


Figure 14.2.2.14 (a) Graphene stacking structure; (b) HRTEM image of graphene edges: zigzag and armchain (inset is FFT); (c) graphene edge model, a 30° angle between zigzag and armchair direction.

Transmission Electron Energy Loss Spectroscopy

Electron energy loss spectroscopy (EELS) is a technique that measures electronic excitations within solid-state materials. When an electron beam with a narrow range of kinetic energy is directed at a material some electrons will be inelastically scattered, resulting in a kinetic energy loss. Electrons can be inelastically scattered from phonon excitations, plasmon excitations, interband transitions, or inner shell ionization. EELS measures the energy loss of these inelastically scattered electrons and can yield information on atomic composition, bonding, electronic properties of valance and conduction bands and surface properties. An example of atomic level composition mapping is shown in Figure 14.2.2.15a. EELS has even been used to measure pressure and temperature within materials.

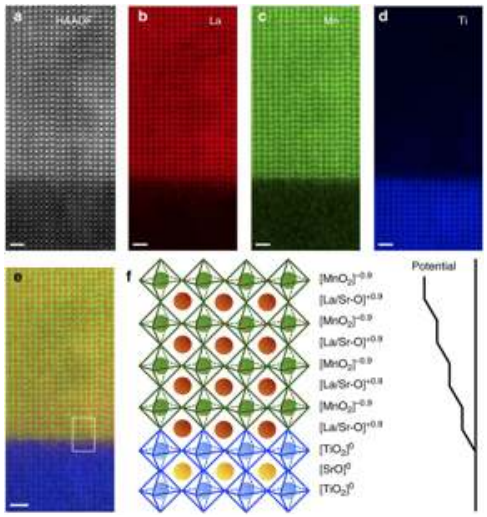


Figure 14.2.2.15 EEL Map showing atomic composition with atomic scale spatial resolution. (a) Shows a high angle annular dark field (HAADF) image with atomic resolution of a LaxSr1-xMnO3 film grow on TiO2. (b) La (c) Mn (d) Ti elemental data obtain from a STEM-EELS measurement. (e) Overlayed image of b-d showing relative positions of La, Mn, and Ti compared to atomic resolution imaging. (f) Model of theoretical packing in LaxSr1-xMnO3 film. Reproduced from J. A. Mundy, et al., Nat. Commun., 2014, 5, 3464. Copyright Nature Publishing Group 2015.

The EEl Spectrum

An idealized EEL spectrum is show in Figure 14.2.2.16 The most prominent feature of any EEL spectrum is the zero loss peak (ZLP). The ZLP is due to those electrons from the electron beam that do not inelastically scatter and reach the detector with their original kinetic energy; typically 100-300 keV. By definition the ZLP is set to 0 eV for further analysis and all signals arising from inelastically scatter electrons occur at >0 eV. The second largest feature is often the plasmon resonance - the collective excitation of conduction band electrons within a material. The plasmon resonance and other peaks attributed to weakly bound, or outer shell electrons, occur in the “low-loss” region of the spectrum. The low-loss regime is typically thought of as energy loss <50 eV, but this cut-off from low-loss to high-loss is arbitrary. Shown in the inset of Figure 14.2.2.16is an edge from atom core-loss and further fine structure. Inner shell ionizations, represented by the core-loss peaks, are useful in determining elemental compositions as these peaks can act as fingerprints for specific elements. For example, if there is a peak at 532 eV in a EEL spectrum, there is a high probability that the sample contains a considerable amount of oxygen because this is known to be the energy needed to remove an inner shell electron from oxygen. This idea is further explored by looking at sudden changes in the bulk plasmon for aluminum in different chemical environments as shown in Figure 14.2.2.16

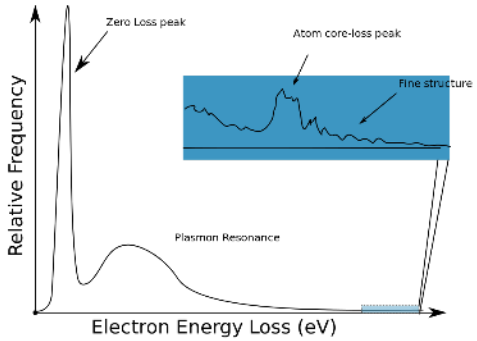


Figure 14.2.2.16 Idealized electron energy loss spectrum (EELS). Inset shows core loss and fine structure. This image is filed under the Creative Commons Attribution-Share Alike 3.0 Unported License. Original Author Hat'n'Coat.

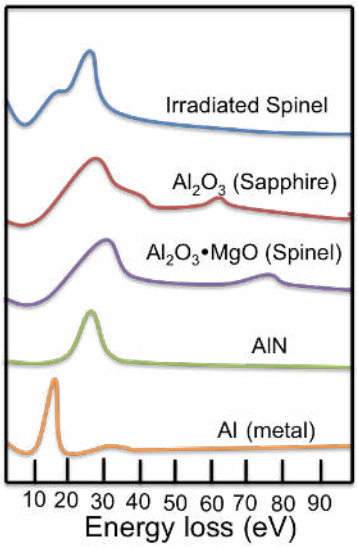


Figure 14.2.2.17 Slight shifts in the plasmon peak of pure Al, AlN, and various aluminum oxides. Slight shifts in peak shape and energy can allow EEL spectroscopists to determine slight variations in chemical and electron enviroments. Adapted from D.B. William, C.B. Carter. Transmission Electron Microscopy: A Textbook for Materials Science. Springer, New York, NY, 2nd Ed., 2009. 760p.

Of course, there are several other techniques available for probing atomic compositions many of which are covered in this text. These include Energy dispersive X-ray spectroscopy, X-ray photoelectron spectroscopy, and Auger electron spectroscopy. Please reference these chapters thorough introduction to these techniques.

Electron Energy Loss Spectroscopy Versus Energy Dispersive X-ray Spectroscopy

As a technique EELS is most frequently compared to energy dispersive X-ray spectroscopy (EDX) also known as energy dispersive spectroscopy (EDS). Energy dispersive X-ray detectors are commonly found as analytical probes on both scanning and transmission electron microscopes. The popularity of EDS can be understood by recognizing the simplicity of compositional analysis using this technique. However, EELS data can offer complementary compositional analysis while also generally yielding further insight into the solid-state physics and chemistry in a system at the cost of a steeper learning curve. EDS and EELS spectra are both derived from the electronic excitations of materials, however, EELS probes the initial excitation while EDS looks at X-ray emissions from the decay of this excited state. As a result, EEL spectra investigate energy ranges from 0-3 keV while EDS spectra analyze a wider energy range from 1-40 keV. The difference in ranges makes EDS suited particularly well for heavy elements while EELS complements measurement elements lighter than Zn.

History and Implementation

In the early 1940s, James Hillier (Figure 14.2.2.18) and R.F. Baker were looking to develop a method for pairing the size, shape, and structure available from electron microscopes to a convenient method for "determining the composition of individual particles in a mixed specimen". Their instrument, shown in Figure 14.2.2.19, reported in the Journal of Applied Physics in September 1994 was the first electron-optical instrument used to measure the velocity distribution in an electron beam transmitting through a sample.



Figure 14.2.2.18 Dr. James Hillier (August 22, 1915 – January 15, 2007) received his Ph.D. in Physics from the University of Toronto. He is recognized as a pioneer in the field of electron microscopy and as a graduate student in 1938 designed and built the first successful electron microscope in the western hemisphere. Dr. Hillier authored 150 papers on both technical subjects and management and held 41 patents for his inventions. He was inducted into the National Inventors Hall of Fame for the electron microscope in 1980.

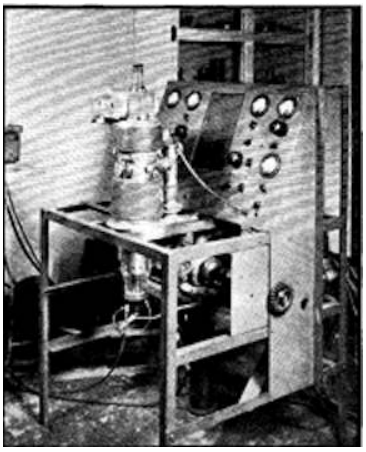


Figure 14.2.2.19 The first instrument capable of performing electron energy loss spectroscopy built by Hillier and Baker in 1944. Reproduced from J. Hillier and R. F. Baker, *J. Appl. Phys.*, 1944, **15**, 663–675. Copyright AIP Publishing LLC

The instrument was built from a repurposed transmission electron microscope (TEM). It consisted of an electron source and three electromagnetic focusing lenses, standard for TEMs at the time, but also incorporated a magnetic deflecting lenses, which when turned on, would redirect the electrons 180° into a photographic plate. The electrons with varying kinetic energies dispersed across the photographic plate and could be correlated to the energy loss of each peak depending on position. In this groundbreaking work, Hillier and Baker were able to find the discrete energy loss corresponding to the K levels of both carbon and oxygen.

The vast majority of EEL spectrometers are found as secondary analyzers in transmission electron microscopes. It wasn't until the 1990s when EELS became a widely used research tool because of advances in electron beam aberration correction and vacuum technologies. Today, EELS is capable of spatial resolutions down to the single atom level, and if the electron beam is monochromated energy resolution can be as low as 0.01eV. Figure 14.2.2.20depicts the typical layout of an EEL spectrometer at the base of a TEM.

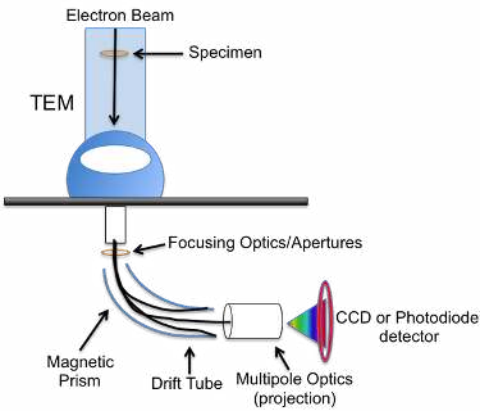


Figure 14.2.2.20 Schematic to show the simplified positions of standard EELS components in a standard TEM.

This page titled 14.2.2: Transmission Electron Microscopy is shared under a CC BY 4.0 license and was authored, remixed, and/or curated by Pavan M. V. Raja & Andrew R. Barron (OpenStax CNX) via source content that was edited to the style and standards of the LibreTexts platform.

- **8.2: Transmission Electron Microscopy** by Pavan M. V. Raja & Andrew R. Barron is licensed CC BY 4.0. Original source: http://cnx.org/contents/ba27839d-5042-4a40-afcf-c0e6e39fb45425.2.

14.3: Scanning Probe Microscopes

in the last section we considered how we can image a surface using an electron beam. In this section we consider a very different approach to developing an image of a surface, one in which we bring a probe close to the surface and examine how the probe interacts with the surface. One advantage of this approach is that the interaction between the probe and the surface can include attraction and repulsion, which opens up a third dimension to the image.

Scanning Tunneling Microscope (STM)

In the scanning tunneling microscope we take advantage of the ability of a current to pass through the gap between the tip of a conducting probe and a conducting sample when the probe and the sample are held at different potentials. Figure 14.3.1 shows the basic arrangement in which the probe has, ideally, a single atom at its tip. The tunneling current, I_t is given by

$$I_t = Ve^{-Cd} \tag{14.3.1}$$

where V is the applied voltage, d is the distance between the probe's tip and the sample, and C is a constant whose value depends upon the composition of the probe and the sample. The exponential decrease in the tunneling current with distance means that a small change in the position of probe's tip relative to the sample results in a significant change in the signal, providing vertical resolution on the order of 0.1 nm. Probes are fashioned using tungsten wires or platinum-iridium wires.

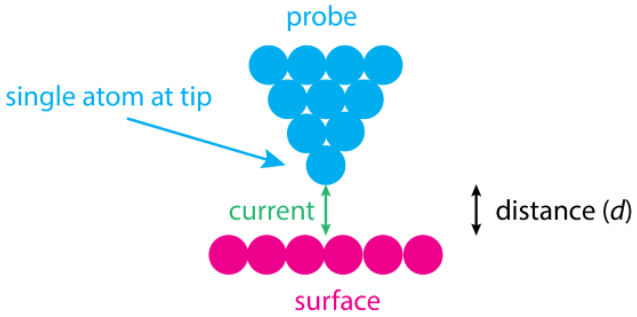


Figure 14.3.1: Illustration showing the relationship between the sample and the tip of the probe in scanning tunneling microscopy.

Scanning tunneling microscopy images are created by moving the probe back-and-forth across the sample while measuring the current. The signal is acquired in one of two modes: constant current or constant height. In constant current mode, the probe's tip is brought near the surface and the current measured, which establishes a setpoint. As the probe moves across the sample, it is raised or lowered to maintain the setpoint current. The result is measure of the distance, d, between the probe's tip and the sample along the *z*-axis as a function of the *xy* position of the probe's tip. In constant height mode, the distance, d, between the probe's tip and the sample is held constant, and the current, I_t, is measured as a function of the *xy* position of the probe's tip. Constant height mode allows for faster data acquisition, but is limited to samples that have flat surfaces.

Positioning of the sample and the probe's tip relative to each other is accomplished by either moving the probe or moving the sample. In either case, the control of movement in accomplished using a piezoelectric scanner. A piezoelectric material, as shown in Figure 14.3.2 experiences a change in its length when a dc potential is applied across its sides, either extending its length or contracting its length.

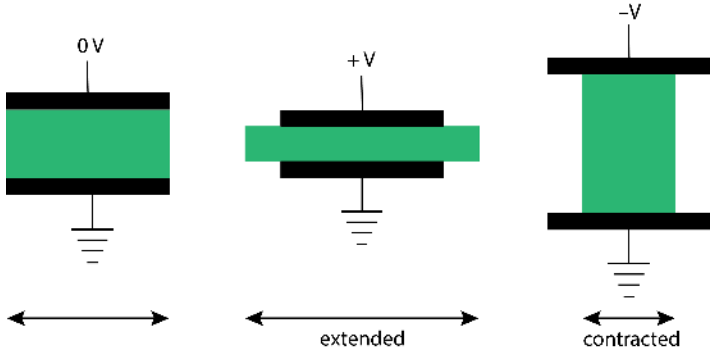


Figure 14.3.2: Illustration showing the behavior of a piezoelectric material when a dc potential is applied to it. The extension and contraction shown here are, of course, exaggerated.

Figure 14.3.3 shows a configuration of cylindrical piezoelectric scanner in which the cylinder's upper half controls movement along the *z*-axis, and the cylinder's lower half is used to control movement along the *x*-axis, the *y*-axis, or both.

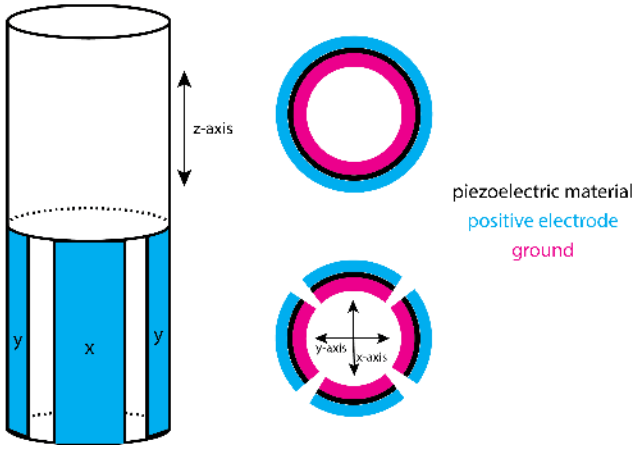


Figure 14.3.3: Illustration that shows the design of a piezoelectric scanner. The top half of the scanner controls movement along the *z*-axis and the lower half of the scanner controls movement along the *x*-axis and the *y*-axis. The piezoelectric material is shown in black, the positive electrodes in blue, and the ground in red.

One limitation of STM is that the sample must be conductive. It is possible to image a non-conducting sample if it first coated with a conductive material, such as gold, although such coatings can mask surface features.

Atomic Force Microscope (AFM)

Unlike the scanning tunneling microscope, the atomic force microscope does not require a conducting sample and imaging is achieved without a current flowing between the sample and the tip of the probe. Instead, as shown in Figure 14.3.4, the probe is attached to the end of a flexible cantilever. The tip of the probe (see photograph in Figure 14.3.3) is pyramidal in shape and extends about 10 µm from its base on the cantilever. The tip of the probe has a diameter on the order of 10 nm and is made of silicon, Si, or silicon nitride, Si_3N_4. The cantilever typically is 100-500 µm in length. The probe is scanned across the sample's surface and the position of the probe relative to the surface is determined by reflecting the beam from a diode laser off the probe-end of the cantilever to a detector.



Figure 14.3.4: The figure on the left illustrates how the position of the cantilever and the probe's tip is monitored in atomic force microscopy. The photo on the right shows an SEM image of a typical cantilever and probe tip. The photograph is released under a CC-BY license and is available here.

The force in atomic force is the interaction between the probe's tip and the sample, which may be a force of attraction or a force of repulsion. When the probe's tip is in contact with the sample—known as contact mode—there is a force of repulsion between them. Because the cantilever has a smaller force constant than the atoms in the probe's tip, the cantilever bends. Moving the sample stage to maintain a constant deflection of the laser off of the cantilever provides an image of the sample's surface. Contact mode allows for rapid scanning and work well for samples with rough surfaces, although it may damage samples with softer surfaces.

In non-contact mode, the probe's tip is brought close to the sample's surface, but not allowed to come into contact with it. The cantilever is place into an oscillatory motion. The amplitude of this oscillation is proportional to the force of attraction between the probe's tip and the sample, which varies with the distance between the probe's tip and the sample. Moving the sample stage to

maintain a constant oscillation provides an image of the sample's surface. Non-contact mode AFM generally provides lower resolution images, but is less damaging to the sample.

A third mode for collecting data is called intermittent or tapping mode. In this mode the cantilever is set to oscillate at its resonant frequency with the probe's tip coming into contact with the sample's surface when it reaches the bottom of the cantilever's oscillation. The frequency of the oscillation is sensitive to the distance between the probe's tip and the sample. Moving the sample stage to maintain the resonant frequency provides an image of the sample's surface.

You can view a gallery of scanning tunneling microscopy images here, and a gallery of atomic force microscopy images here.

This page titled 14.3: Scanning Probe Microscopes is shared under a CC BY-NC-SA 4.0 license and was authored, remixed, and/or curated by David Harvey.

- **21.4: Scanning Probe Microscopes** by David Harvey is licensed CC BY-NC-SA 4.0.

14.3.1: Scanning Tunneling Microscopy

Scanning tunneling microscopy (STM) is a powerful instrument that allows one to image the sample surface at the atomic level. As the first generation of scanning probe microscopy (SPM), STM paves the way for the study of nano-science and nano-materials. For the first time, researchers could obtain atom-resolution images of electrically conductive surfaces as well as their local electric structures. Because of this milestone invention, Gerd Binnig (Figure 14.3.1.1) and Heinrich Rohrer (Figure 14.3.1.2) won the Nobel Prize in Physics in 1986.



Figure 14.3.1.1 German physicist Gerd Binnig (1947 -).

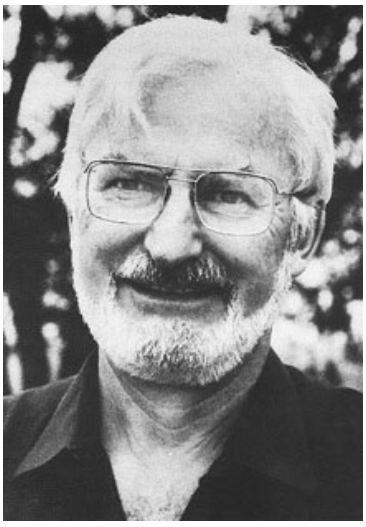


Figure 14.3.1.2 Swiss physicist Heinrich Rohrer (1933 -)

Principles of Scanning Tunneling Microscopy

The key physical principle behind STM is the tunneling effect. In terms of their wave nature, the electrons in the surface atoms actually are not as tightly bonded to the nucleons as the electrons in the atoms of the bulk. More specifically, the electron density is not zero in the space outside the surface, though it will decrease exponentially as the distance between the electron and the surface increases (Figure 14.3.1.3a). So, when a metal tip approaches to a conductive surface within a very short distance, normally just a few Å, their perspective electron clouds will starting to overlap, and generate tunneling current if a small voltage is applied between them, as shown in Figure \(\PageIndex{3}) b.

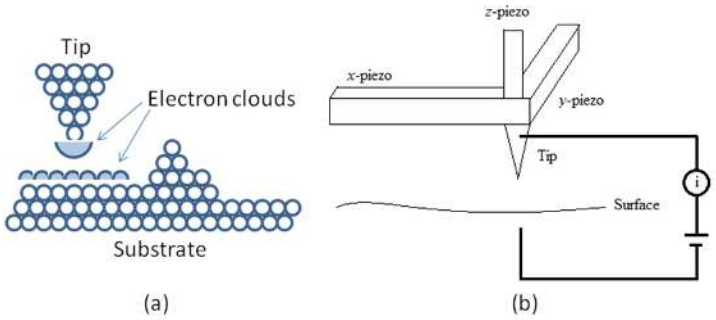


Figure 14.3.1.3 Schematic diagram of the principles of AFM showing (a) the interactions between tip and surface and (b) the tunneling current generated from tip and surface is measured and used as feedback to control the movement of the tip.

When we consider the separation between the tip and the surface as an ideal one-dimensional tunneling barrier, the tunneling probability, or the tunneling current I, will depend largely on s, the distance between the tip and surface, 14.3.1.1, where m is the electron mass, e the electron charge, h the Plank constant, ϕ the averaged work function of the tip and the sample, and V the bias voltage.

$$I \propto e^{-2s\,[2m/h^2(<\phi> - e|V|/2)]^{1/2}} \tag{14.3.1.1}$$

A simple calculation will show us how strongly the tunneling current is affected by the distance (s). If s is increased by Δs = 1 Å, 14.3.1.2and 14.3.1.3

$$\Delta I = e^{-2k_0\Delta s} \tag{14.3.1.2}$$

$$k_0 = [2m/h^2(<\phi> - e|V|/2)]^{1/2} \tag{14.3.1.3}$$

Usually (<ϕ> −e|V|/2) is about 5 eV, which k_0 about 1 Å^{-1}, then ΔI/I = $^1/_8$. That means, if *s* changes by 1 Å, the current will change by one order of the magnitude. That's the reason why we can get atom-level image by measuring the tunneling current between the tip and the sample.

In a typical STM operation process, the tip is scanning across the surface of sample in *x*-*y* plain, the instrument records the *x*-*y* position of the tip, measures the tunneling current, and control the height of the tip via a feedback circuit. The movements of the tip in *x*, *y* and *z* directions are all controlled by piezo ceramics, which can be elongated or shortened according to the voltage applied on them.

Normally, there are two modes of operation for STM, *constant height mode* and *constant current mode*. In constant height mode, the tip stays at a constant height when it scans through the sample, and the tunneling current is measured at different (*x*, *y*) position (Figure 14.3.1.4b). This mode can be applied when the surface of sample is very smooth. But, if the sample is rough, or has some large particles on the surface, the tip may contact with the sample and damage the surface. In this case, the constant current mode is applied. During this scanning process, the tunneling current, namely the distance between the tip and the sample, is settled to an unchanged target value. If the tunneling current is higher than that target value, that means the height of the sample surface is increasing, the distance between the tip and sample is decreasing. In this situation, the feedback control system will respond quickly and retract the tip. Conversely, if the tunneling current drops below the target value, the feedback control will have the tip closer to the surface. According to the output signal from feedback control, the surface of the sample can be imaged.

Comparison of Atomic Force Microscopy (AFM) and Scanning Tunneling Microscopy (STM)

Both AFM and STM are widely used in nano-science. According to the different working principles though, they have their own advantages and disadvantages when measuring specific properties of sample (Table 14.3.1.1). STM requires an electric circuit including the tip and sample to let the tunneling current go through. That means, the sample for STM must be conducting. In case of AFM however, it just measures the deflection of the cantilever caused by the van der Waals forces between the tip and sample. Thus, in general any kind of sample can be used for AFM. But, because of the exponential relation of the tunneling current and distance, STM has a better resolution than AFM. In STM image one can actually "see" an individual atom, while in AFM it's almost impossible, and the quality of AFM image is largely depended on the shape and contact force of the tip. In some cases, the measured signal would be rather complicated to interpret into morphology or other properties of sample. On the other side, STM can give straight forward electric property of the sample surface.

Table 14.3.1.1 Comparison of AFM and STM

	AFM	STM
Sample Requirement	-	Conducting
Work environment	Air, liquid	Vacuum
Lateral resolution	~1 nm	~0.1 nm
Vertical resolution	~0.05 nm	~0.05 nm
Working mode	Tapping, contact	Constant current, constant height

Applications of Scanning Tunneling Microscopy in Nanoscience

STM provides a powerful method to detect the surface of conducting and semi-conducting materials. Recently STM can also be applied in the imaging of insulators, superlattice assemblies and even the manipulation of molecules on surface. More importantly, STM can provide the surface structure and electric property of surface at atomic resolution, a true breakthrough in the development of nano-science. In this sense, the data collected from STM could reflect the local properties even of single molecule and atom. With these valuable measurement data, one could give a deeper understanding of structure-property relations in nanomaterials.

An excellent example is the STM imaging of graphene on Ru(0001), as shown in Figure 14.3.1.4 Clearly seen is the superstructure with a periodicity of ~30 Å , coming from the lattice mismatch of 12 unit cells of the graphene and 11 unit cells of the underneath Ru(0001) substrate. This so-called moiré structure can also be seen in other systems when the adsorbed layers have strong chemical bonds within the layer and weak interaction with the underlying surface. In this case, the periodic superstructure seen in graphene tells us that the formed graphene is well crystallized and expected to have high quality.

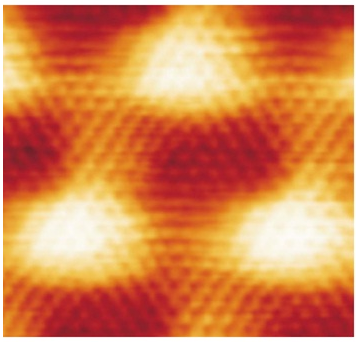


Figure 14.3.1.4 Atomically resolved image of the graphene overlayer. The scanning area is 40 x 40 Å, the operation mode is constant current mode, I_t is l nA, V_{Bias} is -0.05 V. Adapted with permission from S. Marchini, S. Gunther, and J. Wintterlin, *Phys. Rev. B*, 2007, **76**, 075429. Copyrighted by the American Physical Society.

Another good example is shown to see that the measurement from STM could tell us the bonding information in single-molecular level. In thiol- and thiophene-functionalization of single-wall carbon nanotubes (SWNTs), the use of Au nanoparticles as chemical markers for AFM gives misleading results, while STM imaging could give correct information of substituent location. From AFM image, Au-thiol-SWNT (Figure 14.3.1.6a) shows that most of the sidewalls are unfunctionalized, while Au-thiophene-SWNT (Figure 14.3.1.6 c)shows long bands of continuous functionalized regions on SWNT. This could lead to the estimation that thiophene is better functionalized to SWNT than thiol. Yet, if we look up to the STM image (Figure 14.3.1.6b and d), in thiol-SWNTs the multiple functional groups are tightly bonded in about 5 - 25 nm, while in thiophene-SWNTs the functionalization is spread out uniformly along the whole length of SWNT. This information indicates that actually the functionalization levels of thiol- and thiophene-SWNTs are comparable. The difference is that, in thiol-SWNTs, functional groups are grouped together and each group is bonded to a single gold nanoparticle, while in thiophene-SWNTs, every individual functional group is bonded to a nanoparticle.

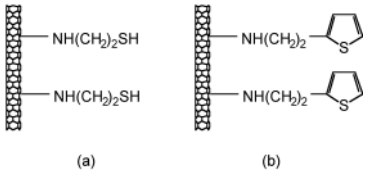


Figure 14.3.1.5 Structure of (a) thiol-functionalized SWNTs and thiophene-functionalized SWNTs.

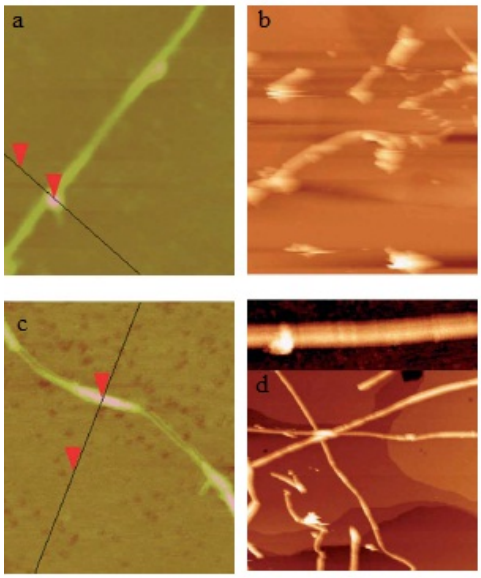


Figure 14.3.1.6 Difference between AFM and STM images of functionalized SWNTs. (a) and (c) are tapping mode AFM images and height profiles of thiol- and thiophene-SWNTs. (b) and (d) are STM images of thiol-SWNTs (scanning area is 4560 x 4000 Å, the operation mode is constant current mode, I_t is 3.25 pA, V_{Bias} is -0.5 V) and thiophene-SWNTs (scanning area is 4560 x 4000 Å, the operation mode is constant current mode, I_t is 5.66 pA, V_{Bias} is -0.8 V). Inset in (d) is a higher resolution image of the local defects on thiophene-SWNT (500 x 140 Å, the operation mode is constant current mode, I_t is 25.5 pA, V_{Bias} is -0.8 V). Adapted from L. Zhang, J. Zhang, N. Schmandt, J. Cratty, V. N. Khabashesku, K. F. Kelly, and A. R. Barron, *Chem. Commun.*, 2005, 5429 (http://dx.doi.org/10.1039/b509257d). Reproduced by permission of The Royal Society of Chemistry.

Adaptations to Scanning Tunneling Microscopy

Scanning tunneling microscopy (STM) is a relatively recent imaging technology that has proven very useful for determining the topography of conducting and semiconducting samples with angstrom (Å) level precision. STM was invented by Gerd Binnig (Figure 14.3.1.7) and Heinrich Rohrer (Figure 14.3.1.8), who both won the 1986 Nobel Prize in physics for their technological advances.



Figure 14.3.1.7 German physicist Gerd Binnig (1947 -).

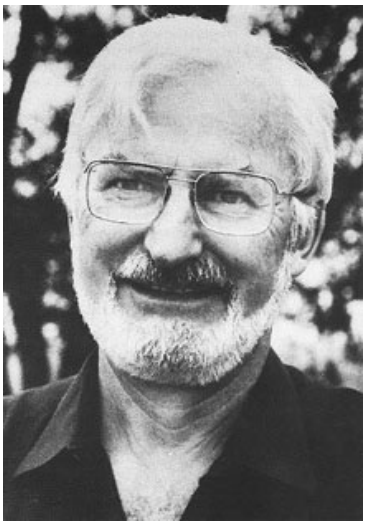


Figure 14.3.1.8 Swiss physicist Heinrich Rohrer (1933 -).

The main component of a scanning tunneling microscope is a rigid metallic probe tip, typically composed of tungsten, connected to a piezodrive containing three perpendicular piezoelectric transducers (Figure 14.3.1.9). The tip is brought within a fraction of a nanometer of an electrically conducting sample. At close distances, the electron clouds of the metal tip overlap with the electron clouds of the surface atoms (Figure 14.3.1.9 inset). If a small voltage is applied between the tip and the sample a tunneling current is generated. The magnitude of this tunneling current is dependent on the bias voltage applied and the distance between the tip and the surface. A current amplifier can covert the generated tunneling current into a voltage. The magnitude of the resulting voltage as compared to the initial voltage can then be used to control the piezodrive, which controls the distance between the tip and the surface (i.e., the *z* direction). By scanning the tip in the *x* and *y* directions, the tunneling current can be measured across the entire sample. The STM system can operate in either of two modes: Constant height or constant current

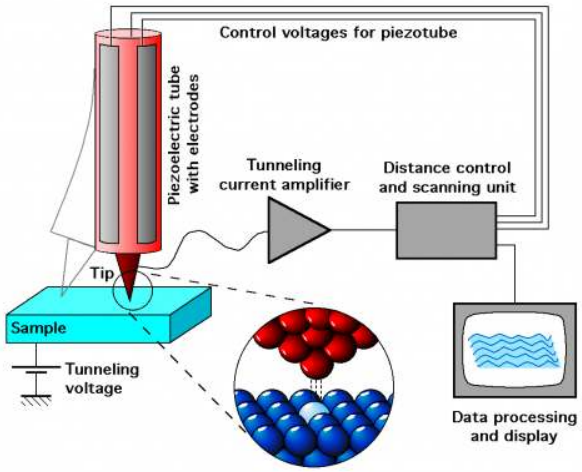


Figure 14.3.1.9 Schematic drawing of a STM apparatus.

In constant height mode, the tip is fixed in the *z* direction and the change in tunneling current as the tip changes in the *x*,*y* direction is collected and plotted to describe the change in topography of the sample. This method is dangerous for use in samples with fluctuations in height as the fixed tip might contact and destroy raised areas of the sample. A common method for non-uniformly smooth samples is constant current mode. In this mode, a target current value, called the set point, is selected and the tunneling current data gathered from the sample is compared to the target value. If the collected voltage deviates from the set point, the tip is moved in the *z* direction and the voltage is measured again until the target voltage is reached. The change in the *z* direction required to reach the set point is recorded across the entire sample and plotted as a representation of the topography of the sample. The height data is typically displayed as a gray scale image of the topography of the sample, where lighter areas typically indicate raised sample areas and darker spots indicate protrusions. These images are typically colored for better contrast.

The standard method of STM, described above, is useful for many substances (including high precision optical components, disk drive surfaces, and buckyballs) and is typically used under ultrahigh vacuum to avoid contamination of the samples from the surrounding systems. Other sample types, such as semiconductor interfaces or biological samples, need some enhancements to the traditional STM apparatus to yield more detailed sample information. Three such modifications, spin-polarized STM (SP-STM), ballistic electron emission microscopy (BEEM) and photon STM (PSTM) are summarized in Table 14.3.1.2 and in described in detail below.

Table 14.3.1.2 Comparison of conventional and altered STM types

Name	Alterations to Conventional STM	Sample Types	Limitations
STM	None	Conducting surface	Rigidity of probe
SP-STM	Magnetized STM tip	Magnetic	Needs to be overlaid with STM, magnetized tip type
BEEM	Three-terminal with base electrode and current collector	Interfaces	Voltage, changes due to barrier height
PSTM	Optical fiber tip	Biological	Optical tip and psrim manufacture

Spin Polarized STM

Spin-polarized scanning tunneling microscopy (SP-STM) can be used to provide detailed information of magnetic phenomena on the single-atom scale. This imaging technique is particularly important for accurate measurement of superconductivity and high-density magnetic data storage devices. In addition, SP-STM, while sensitive to the partial magnetic moments of the sample, is not a field-sensitive technique and so can be applied in a variety of different magnetic fields.

Device setup and sample preparation

In SP-STM, the STM tip is coated with a thin layer of magnetic material. As with STM, voltage is then applied between tip and sample resulting in tunneling current. Atoms with partial magnetic moments that are aligned in the same direction as the partial magnetic moment of the atom at the very tip of the STM tip show a higher magnitude of tunneling current due to the interactions between the magnetic moments. Likewise, atoms with partial magnetic moments opposite that of the atom at the tip of the STM tip demonstrate a reduced tunneling current (Figure 14.3.1.10). A computer program can then translate the change in tunneling current to a topographical map, showing the spin density on the surface of the sample.

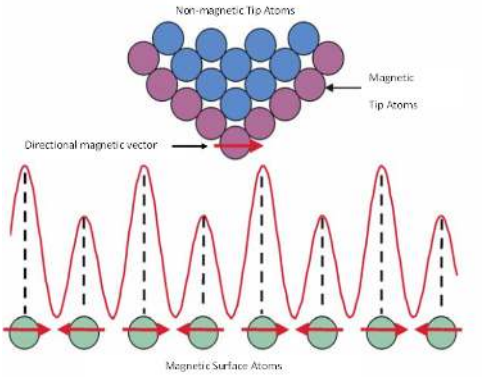


Figure 14.3.1.10 Schematic illustration of magnetized tip for SP-STM.

The sensitivity to magnetic moments depends greatly upon the direction of the magnetic moment of the tip, which can be controlled by the magnetic properties of the material used to coat the outermost layer of the tungsten STM probe. A wide variety of magnetic materials have been studied as possible coatings, including both ferromagnetic materials, such as a thin coat of iron or of gadolinium, and antiferromagnetic materials such as chromium. Another method that has been used to make a magnetically sensitive probe tip is irradiation of a semiconducting GaAs tip with high energy circularly polarized light. This irradiation causes a splitting of electrons in the GaAs valence band and population of the conduction band with spin-polarized electrons. These spin-

polarized electrons then provide partial magnetic moments which in turn influence the tunneling current generated by the sample surface.

Sample preparation for SP-STM is essentially the same as for STM. SP-STM has been used to image samples such as thin films and nanoparticle constructs as well as determining the magnetic topography of thin metallic sheets such as in Figure 14.3.1.11 The upper image is a traditional STM image of a thin layer of cobalt, which shows the topography of the sample. The second image is an SP-STM image of the same layer of cobalt, which shows the magnetic domain of the sample. The two images, when combined provide useful information about the exact location of the partial magnetic moments within the sample.

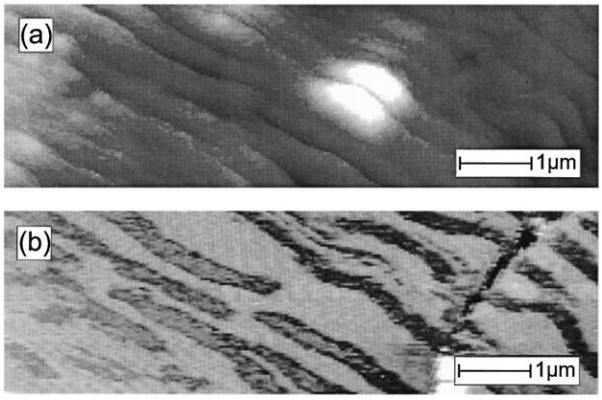


Figure 14.3.1.11 A thin layer of Co(0001) as imaged by (a) STM, showing the topography, and (b) SP-STM, showing the magnetic domain structure. Image adapted from W. Wulfhekel and J. Kirschner, Appl. Phys. Lett., 1999, 75, 1944.

Limitations

One of the major limitations with SP-STM is that both distance and partial magnetic moment yield the same contrast in a SP-STM image. This can be corrected by combination with conventional STM to get multi-domain structures and/or topological information which can then be overlaid on top of the SP-STM image, correcting for differences in sample height as opposed to magnetization.

The properties of the magnetic tip dictate much of the properties of the technique itself. If the outermost atom of the tip is not properly magnetized, the technique will yield no more information than a traditional STM. The direction of the magnetization vector of the tip is also of great importance. If the magnetization vector of the tip is perpendicular to the magnetization vector of the sample, there will be no spin contrast. It is therefore important to carefully choose the coating applied to the tungsten STM tip in order to align appropriately with the expected magnetic moments of the sample. Also, the coating makes the magnetic tips more expensive to produce than standard STM tips. In addition, these tips are often made of mechanically soft materials, causing them to wear quickly and require a high cost of maintenance.

Ballistic Electron Emission Microscopy

Ballistic electron emission microscopy (BEEM) is a technique commonly used to image semiconductor interfaces. Conventional surface probe techniques can provide detailed information on the formation of interfaces, but lack the ability to study fully formed interfaces due to inaccessibility to the surface. BEEM allows for the ability to obtain a quantitative measure of electron transport across fully formed interfaces, something necessary for many industrial applications.

Device Setup and Sample Preparation

BEEM utilizes STM with a three-electrode configuration, as seen in Figure 14.3.1.12 In this technique, ballistic electrons are first injected from a STM tip into the sample, traditionally composed of at least two layers separated by an interface, which rests on three indium contact pads that provide a connection to a base electrode (Figure 14.3.1.12). As the voltage is applied to the sample, electrons tunnel across the vacuum and through the first layer of the sample, reaching the interface, and then scatter. Depending on the magnitude of the voltage, some percentage of the electrons tunnel through the interface, and can be collected and measured as a current at a collector attached to the other side of the sample. The voltage from the STM tip is then varied, allowing for measurement of the barrier height. The barrier height is defined as the threshold at which electrons will cross the interface and are measurable as a current in the far collector. At a metal/n-type semiconductor interface this is the difference between the conduction band minimum and the Fermi level. At a metal/p-type semiconductor interface this is the difference between the valence band maximum of the semiconductor and the metal Fermi level. If the voltage is less than the barrier height, no electrons will cross the

interface and the collector will read zero. If the voltage is greater than the barrier height, useful information can be gathered about the magnitude of the current at the collector as opposed to the initial voltage.

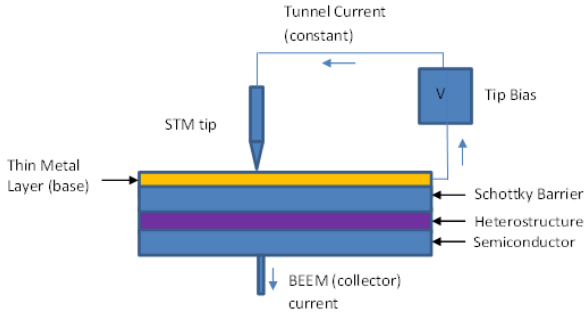


Figure 14.3.1.12 Diagram of a STM/BEEM system. The tip is maintained at the tunneling voltage, V, and the tunneling current, It = VI/RF, is held constant by the STM feedback circuit. The sample base layer is grounded and current into the semiconductor is measured by a virtual ground current amplifier.

Samples are prepared from semiconductor wafers by chemical oxide growth-strip cycles, ending with the growth of a protective oxide layer. Immediately prior to imaging the sample is spin-etched in an inert environment to remove oxides of oxides and then transferred directly to the ultra-high vacuum without air exposure. The BEEM apparatus itself is operated in a glove box under inert atmosphere and shielded from light.

Nearly any type of semiconductor interface can be imaged with BEEM. This includes both simple binary interfaces such as Au/n-Si(100) and more chemically complex interfaces such as Au/n-GaAs(100), such as seen in Figure 14.3.1.13

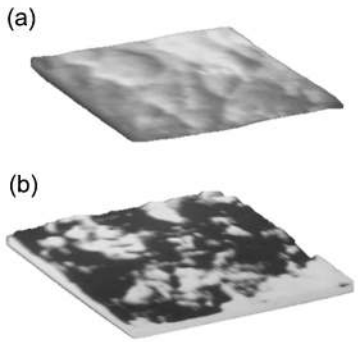


Figure 14.3.1.13 Images of Au/n-GaAs(100) layer (image area 510 Å x 390 Å) showing (a) the topography of the Au surface and (b) the BEEM grey-scale interface image. Image adapted from M. H. Hecht, L. D. Bell, W. J. Kaiser, and F. J. Grunthaner, Appl. Phys. Lett., 1989, 55, 780.

Limitations

Expected barrier height matters a great deal in the desired setup of the BEEM apparatus. If it is necessary to measure small collector currents, such as with an interface of high-barrier-height, a high-gain, low-noise current preamplifier can be added to the system. If the interface is of low-barrier-height, the BEEM apparatus can be operated at very low temperatures, accomplished by immersion of the STM tip in liquid nitrogen and enclosure of the BEEM apparatus in a nitrogen-purged glove box.

Photon STM

Photon scanning tunneling microscopy (PSTM) measures light to determine more information about characteristic sample topography. It has primarily been used as a technique to measure the electromagnetic interaction of two metallic objects in close proximity to one another and biological samples, which are both difficult to measure using many other common surface analysis techniques.

Device Setup and Sample Preparation

This technique works by measuring the tunneling of photons to an optical tip. The source of these photons is the evanescent field generated by the total internal reflection (TIR) of a light beam from the surface of the sample (Figure 14.3.1.14). This field is characteristic of the sample material on the TIR surface, and can be measured by a sharpened optical fiber probe tip where the light intensity is converted to an electrical signal (Figure 14.3.1.15). Much like conventional STM, the force of this electrical signal

modifies the location of the tip in relation to the sample. By mapping these modifications across the entire sample, the topography can be determined to a very accurate degree as well as allowing for calculations of polarization, emission direction and emission time.

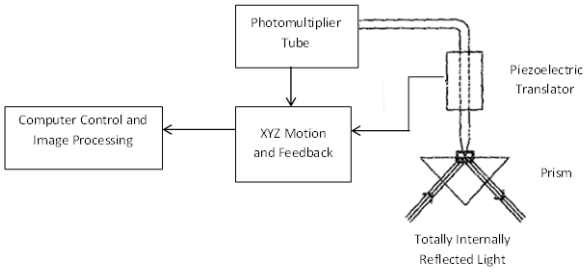


Figure 14.3.1.14 A schematic of a PSTM system

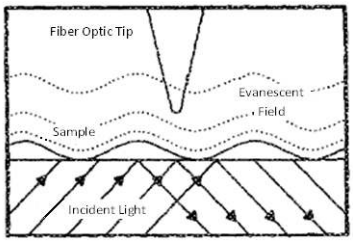


Figure 14.3.1.15 A TIR light beam generates an evanescent field which is modulated by the sample. A sharpened fiber optic probe tip receives light from the evanescent field and spatial variations in evanescent field intensity form the basis for imaging.

In PSTM, the vertical resolution is governed only by the noise, as opposed to conventional STM where the vertical resolution is limited by the tip dimensions. Therefore, this technique provides advantages over more conventional STM apparatus for samples where subwavelength resolution in the vertical dimension is a critical measurement, including fractal metal colloid clusters, nanostructured materials and simple organic molecules.

Samples are prepared by placement on a quartz or glass slide coupled to the TIR face of a triangular prism containing a laser beam, making the sample surface into the TIR surface (Figure 14.3.1.16). The optical fiber probe tips are constructed from UV grade quartz optical fibers by etching in HF acid to have nominal end diameters of 200 nm or less and resemble either a truncated cone or a paraboloid of revolution (Figure 14.3.1.16).

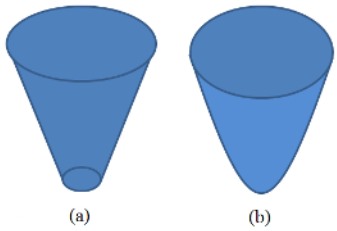


Figure 14.3.1.16 Possible optical fiber tip configurations: (a) truncated cone and (b) paraboloid of rotation.

PSTM shows much promise in the imaging of biological materials due to the increase in vertical resolution and the ability to measure a sample within a liquid environment with a high index TIR substrate and probe tip. This would provide much more detailed information about small organisms than is currently available.

Limitations

The majority of the limitations in this technique come from the materials and construction of the optical fibers and the prism used in the sample collection. The sample needs to be kept at low temperatures, typically around 100K, for the duration of the imaging and therefore cannot decompose or be otherwise negatively impacted by drastic temperature changes.

Conclusion

Scanning tunneling microscopy can provide a great deal of information into the topography of a sample when used without adaptations, but with adaptations, the information gained is nearly limitless. Depending on the likely properties of your sample surface, SP-STM, BEEM and PSTM can provide much more accurate topographical pictures than conventional forms of STM

(Table 14.3.1.2). All of these adaptations to STM have their limitations and all work within relatively specialized categories and subsets of substances, but they are very strong tools that are constantly improving to provide more useful information about materials to the nanometer scale.

Scanning Transmission Electron Microscope- Electron Energy Loss Spectroscopy (STEM-EELS)

History

STEM-EELS is a terminology abbreviation for scanning transmission electron microscopy (STEM) coupled with electron energy loss spectroscopy (EELS). It works by combining two instruments, obtaining an image through STEM and applying EELS to detect signals on the specific selected area of the image. Therefore, it can be applied for many research, such as characterizing morphology, detecting different elements, and different valence state. The first STEM was built by Baron Manfred von Arden (Figure 14.3.1.17) in around 1983, since it was just the prototype of STEM, it was not as good as transmission electron microscopy (TEM) by that time. Development of STEM was stagnant until the field emission gun was invented by Albert Crewe (Figure 14.3.1.18) in 1970s; he also came with the idea of annular dark field detector to detect atoms. In 1997, its resolution increased to 1.9 Å, and further increased to 1.36 Å in 2000. 4D STEM-EELS was developed recently, and this type of 4D STEM-EELS has high brightness STEM equipped with a high acquisition rate EELS detector, and a rotation holder. The rotation holder plays quite an important role to achieve this 4D aim, because it makes observation of the sample in 360° possible, the sample could be rotated to acquire the sample's thickness. High acquisition rate EELS enables this instrument the acquisition of the pixel spectrum in a few minutes.



Figure 14.3.1.17 German physicist and inventor Baron Manfred von Arden (1907–1997).



Figure 14.3.1.18 British physicist Albert Crewe (1927–2009).

Basics of STEM-EELS

Interaction between Electrons and Sample

When electrons interact with the samples, the interaction between those two can be classified into two types, namely, elastic and inelastic interactions (Figure 14.3.1.19). In the elastic interaction, if electrons do not interact with the sample and pass through it, these electrons will contribute to the direct beam. The direct beam can be applied in STEM. In another case, electrons' moving direction in the sample is guided by the Coulombic force; the strength of the force is decided by charge and the distance between

electrons and the core. In both cases, these is no energy transfer from electrons to the samples, that's the reason why it is called elastic interaction. In inelastic interaction, energy transfers from incident electrons to the samples, thereby, losing energy. The lost energy can be measured and how many electrons amounted to this energy can also be measured, and these data yield the electron energy loss spectrum (EELS).

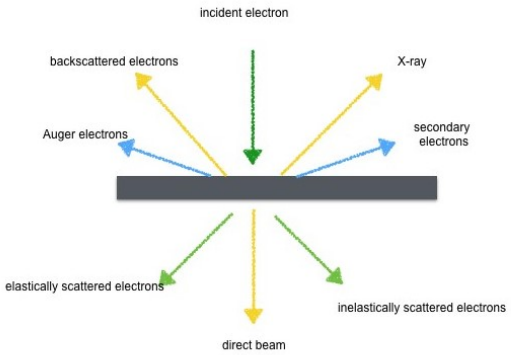


Figure 14.3.1.19 Demonstration of interaction between sample and electrons. Adapted from http://www.microscopy.ethz.ch/downlo...teractions.pdf

How do TEM, STEM and STEM-EELS work?

In transmission electron microscopy (TEM), a beam of electrons is emitted from tungsten source and then accelerated by electromagnetic field. Then with the aid of lens condenser, the beam will focus on and pass through the sample. Finally, the electrons will be detected by a charge-coupled device (CCD) and produce images, Figure 14.3.1.20 STEM works differently from TEM, the electron beam focuses on a specific spot of the sample and then raster scans the sample pixel by pixel, the detector will collect the transmitted electrons and visualize the sample. Moreover, STEM-EELS allows to analyze these electrons, the transmitted electrons could be characterized by adding a magnetic prism, the more energy the electrons lose, the more they will be deflected. Therefore, STEM-EELS can be used to characterize the chemical properties of thin samples.

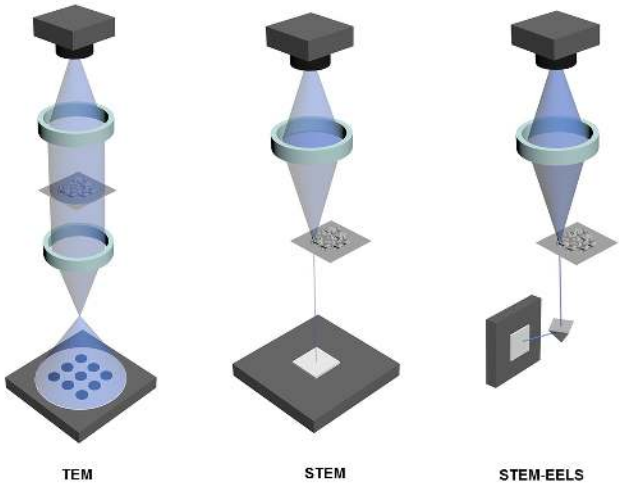


Figure 14.3.1.20 Scheme of TEM, STEM and STEM-EELS experiments. Adapted from http://toutestquantique.fr/en/scanning-electron/.

Principles of STEM-EELS

A brief illustration of STEM-EELS is displayed in Figure 14.3.1.21 The electron source provides electrons, and it usually comes from a tungsten source located in a strong electrical field. The electron field will provide electrons with high energy. The condenser and the object lens also promote electrons forming into a fine probe and then raster scanning the specimen. The diameter of the probe will influence STEM's spatial resolution, which is caused by the lens aberrations. Lens aberration results from the refraction difference between light rays striking the edge and center point of the lens, and it also can happen when the light rays pass through

with different energy. Base on this, an aberration corrector is applied to increase the objective aperture, and the incident probe will converge and increase the resolution, then promote sensitivity to single atoms. For the annular electron detector, the installment sequence of detectors is a bright field detector, a dark field detector and a high angle annular dark field detector. Bright field detector detects the direct beam that transmits through the specimen. Annular dark field detector collects the scattered electrons, which only go through at an aperture. The advantage of this is that it will not influence the EELS to detect signals from direct beam. High angle annular dark field detector collects electrons which are Rutherford scattering (elastic scattering of charged electrons), and its signal intensity is related with the square of atomic number (Z). So, it is also named as Z-contrast image. The unique point about STEM in acquiring image is that the pixels in image are obtained in a point by point mode by scanning the probe. EELS analysis is based on the energy loss of the transmitted electrons, so the thickness of the specimen will influence the detecting signal. In other words, if the specimen is too thick, the intensity of plasmon signal will decrease and may cause difficulty distinguishing these signals from the background.

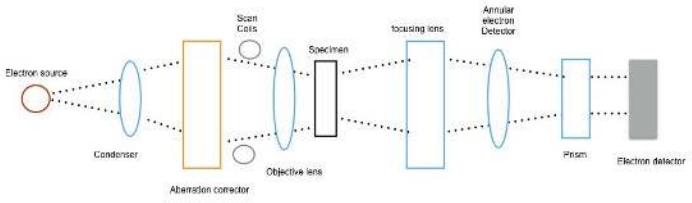


Figure 14.3.1.21 Schematic representation of STEM-EELS.

Typical features of EELS Spectra

As shown in Figure 14.3.1.22, a significant peak appears at energy zero in EELS spectra and is therefore called zero-loss peak. Zero-loss peak represents the electrons which undergo elastic scattering during the interaction with specimen. Zero-loss peak can be used to determine the thickness of specimen according to 14.3.1.4, where t stands for the thickness, λ_{inel} is inelastic mean free path, It stands for the total intensity of the spectrum and IZLP is the intensity of zero loss peak.

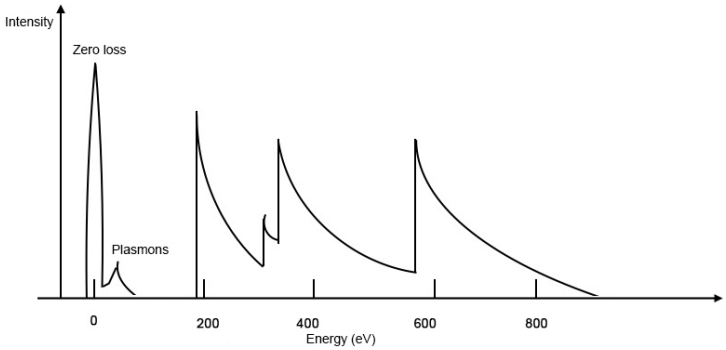


Figure 14.3.1.22 Typical features of EELS spectra. Adapted from http://www.mardre.com/homepage/mic/t...ls/sld001.html.

$$t = \lambda_{inel}\, ln[I_t/I_{ZLP}] \tag{14.3.1.4}$$

The low loss region is also called valence EELS. In this region,valence electrons will be excited to the conduction band. Valence EELS can provide the information about band structure, bandgap, and optical properties. In the low loss region, plasmon peak is the most important. Plasmon is a phenomenon originates from the collective oscillation of weakly bound electrons. Thickness of the sample will influence the plasmon peak. The incident electrons will go through inelastic scattering several times when they interact with a very thick sample, and then result in convoluted plasmon peaks. It is also the reason why STEM-EELS favors sample with low thickness (usually less than 100 nm).

The high loss region is characterized by the rapidly increasing intensity with a gradually falling, which called ionization edge. The onset of ionization edges equals to the energy that inner shell electron needs to be excited from the ground state to the lowest unoccupied state. The amount of energy is unique for different shells and elements. Thus, this information will help to understand the bonding, valence state, composition and coordination information.

Energy resolution affects the signal to background ratio in the low loss region and is used to evaluate EELS spectrum. Energy resolution is based on the full width at half maximum of zero-loss peak.

Background signal in the core-loss region is caused by plasmon peaks and core-loss edges, and can be described by the following power law, 14.3.1.5, where IBG stands for the background signal, E is the energy loss, A is the scaling constant and r is the slope exponent:

$$I_{BG} = AE^{-r} \tag{14.3.1.5}$$

Therefore, when quantification the spectra data, the background signal can be removed by fitting pre-edge region with the above-mentioned equation and extrapolating it to the post-edge region.

Advantages and Disadvantages of STEM-EELS

STEM-EELS has advantages over other instruments, such as the acquisition of high resolution of images. For example, the operation of TEM on samples sometimes result in blurring image and low contrast because of chromatic aberration. STEM-EELS equipped with aberration corrector, will help to reduce the chromatic aberration and obtain high quality image even at atomic resolution. It is very direct and convenient to understand the electron distributions on surface and bonding information. STEM-EELS also has the advantages in controlling the spread of energy. So, it becomes much easier to study the ionization edge of different material.

Even though STEM-EELS does bring a lot of convenience for research in atomic level, it still has limitations to overcome. One of the main limitation of STEM-EELS is controlling the thickness of the sample. As discussed above, EELS detects the energy loss of electrons when they interact with samples and the specimen, then the thickness of samples will impact on the energy lost detection. Simplify, if the sample is too thick, then most of the electrons will interact with the sample, signal to background ratio and edge visibility will decrease. Thus, it will be hard to tell the chemical state of the element. Another limitation is due to EELS needs to characterize low-loss energy electrons, which high vacuum condition is essential for characterization. To achieve such a high vacuum environment, high voltage is necessary. STEM-EELS also requires the sample substrates to be conductive and flat.

Application of STEM-EELS

STEM-EELS can be used to detect the size and distribution of nanoparticles on a surface. For example, CoO on MgO catalyst nanoparticles may be prepared by hydrothermal methods. The size and distribution of nanoparticles will greatly influence the catalytic properties, and the distribution and morphology change of CoO nanoparticles on MgO is important to understand. Co L3/L2 ratios display uniformly around 2.9, suggesting that Co2+ dominates the electron state of Co. The results show that the ratios of O:(Co+Mg) and Mg:(Co+Mg) are not consistence, indicating that these three elements are in a random distribution. STEM-EELS mapping images results further confirm the non-uniformity of the elemental distribution, consistent with a random distribution of CoO on the MgO surface (Figure 14.3.1.23).

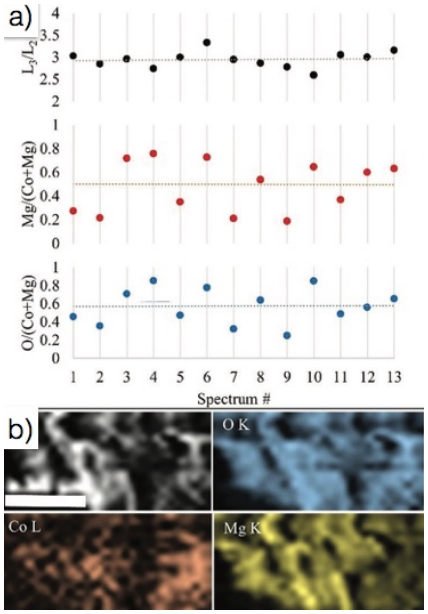


Figure 14.3.1.23 EELS data for a CoO/MgO sample. (a) EELS signal ratio of Co L3/L2, and O and Mg EELS signals relative to combined Co + Mg signals. (b) STEM image and EELS maps acquired at O K, Co L and Mg K edges. Reproduced from S. Alayoglu, D. J. Rosenberg, and M. Ahmed, Dalton Trans., 2016, 45, 9932 with permission of The Royal Society of Chemistry.

Figure 14.3.1.24shows the K-edge absorption of carbon and transition state information could be concluded. Typical carbon based materials have the features of the transition state, such that 1s transits to π* state and 1s to σ* states locate at 285 and 292 eV, respectively. The two-transition state correspond to the electrons in the valence band electrons being excited to conduction state. Epoxy exhibits a sharp peak around 285.3 eV compared to GO and GNPs. Meanwhile, GNPs have the sharpest peak around 292 eV, suggesting the most C atoms in GNPs are in 1s to σ* state. Even though GO is in oxidation state, part of its carbon still behaves 1s transits to π*.

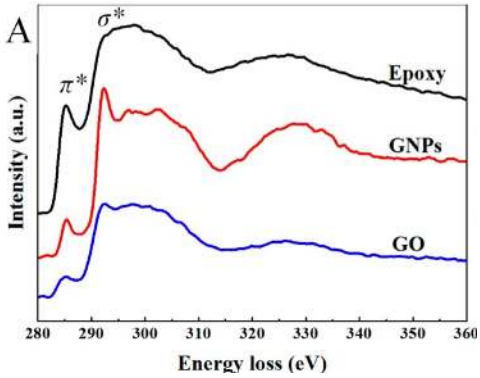


Figure 14.3.1.24 EELS spectrum of graphene nanoplatelets (GNPs), graphene oxide (GO) in comparison with an epoxide resin. Reprinted with permission from Y. Liu, A. L. Hamon, P. Haghi-Ashtiani, T. Reiss, B. Fan, D. He, and J. Bai, ACS Appl. Mater. Inter., 2016, 8, 34151). Copyright (2017) American Chemical Society.

The annular dark filed (ADF) mode of STEM provides information about atomic number of the elements in a sample. For example, the ADF image of La1.2Sr1.8Mn2O7 (Figure 14.3.1.25a and b) along [010] direction shows bright spots and dark spots, and even for bright spots (p and r), they display different levels of brightness. This phenomenon is caused by the difference in atomic numbers. Bright spots are La and Sr, respectively. Dark spots are Mn elements. O is too light to show on the image. EELS result shows the core-loss edge of La, Mn and O (Figure 14.3.1.25c), but the researchers did not give information on core-loss edge of Sr, Sr has N2,3 edge at 29 eV and L3 edge at 1930 eV and L2 edge at 2010 eV.

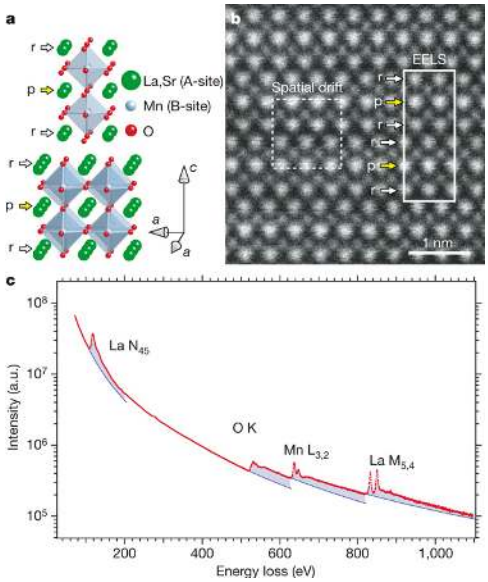


Figure 14.3.1.25 (a) Crystal structure of La1.2Sr21.8Mn2O7, (b) the ADF image of the specimen observed along the [010] direction , and (c) STEM-EELS data of La1.2Sr21.8Mn2O7 obtained from rectangular area of (b) and the blue area equals the core-loss of each element. Reproduced from K. Kimoto, T. Asaka, T. Nagai, M. Saito, Y. Matsui, K. Ishizuka, Nature, 2007, 450, 702. Copyright © 2007, Rights Managed by Nature Publishing Group

This page titled 14.3.1: Scanning Tunneling Microscopy is shared under a CC BY 4.0 license and was authored, remixed, and/or curated by Pavan M. V. Raja & Andrew R. Barron (OpenStax CNX) via source content that was edited to the style and standards of the LibreTexts platform.

- **8.3: Scanning Tunneling Microscopy** by Pavan M. V. Raja & Andrew R. Barron is licensed CC BY 4.0. Original source: http://cnx.org/contents/ba27839d-5042-4a40-afcf-c0e6e39fb45425.2.

14.3.2: Scanning Tunneling Microscopy (STM)

HOW DOES THE STM WORK?

The STM doesn't work the way a conventional microscope does, using optics to magnify a sample. Instead a sharp (1-10 nm) probe that is electrically conductive is scanned just above the surface of an electrically conductive sample. The principle of STM is based on tunneling of electrons between this conductive sharp probe and sample.

What is Tunneling?

Tunneling is a phenomenon that describes how electrons flow (or tunnel) across two objects of differing electric potentials when they are brought into close proximity to each other. When a voltage is applied between probe and surface electrons will flow across the gap (probe-sample distance) generating a measurable current.

The tunneling phenomena can be explained by quantum mechanics. Tunneling originates from the wavelike properties of electrons. When two conductors are close enough there is an overlapping of the electron wavefunctions. Electrons can then diffuse across the barrier between the probe (tip-terminating ideally in a single atom) and the sample when a small voltage is applied. The resulting diffusion of electrons is called tunneling. A more detailed quantum mechanics explanation can be found.[1]

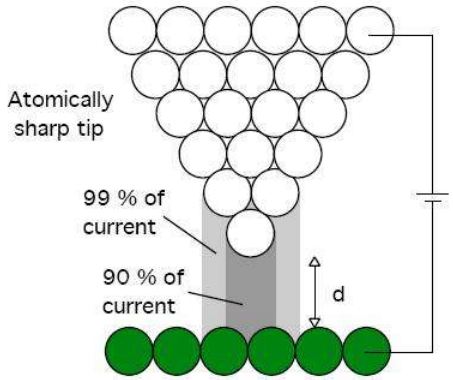


Figure 1. Tunneling of electrons from an etched STM probe (i.e. tungsten wire) to a conductive surface.

An important characteristic of tunneling is that the amplitude of the current exhibits an exponential decay with the distance, d. One way to describe this relationship is by the equation:

$$I \sim Ve^{-cd}$$

- I = Tunneling current
- V = voltage between probe and sample
- c = constant
- d = probe-sample separation distance

Key factor for STM: Very small changes in the probe-sample separation induce large changes in the tunneling current! (i.e. at a separation of a few Å the current rapidly decreases)

This dependency on tunneling current and probe-sample distance allows for precise control of probe-sample separation, resulting in high *vertical resolution(<1 Å)* . Furthermore, *tunneling* is only carried out by the outermost single atom of the probe. This allows for high *lateral resolution (<1 Å).*

How are the sharp STM probes made?

Commercial probes are available but often users make their own probes. A common method is to electrochemically etch tungsten, W, wire in NaOH to create a sharp probe. A problem with W probes is that they oxidize over time. Platinum iridium (Pt-Ir) is preferred for use in air because platinum does not easily oxidize. The tiny fraction of Iridium in the alloy makes it much harder. The Pt-Ir tips are usually shaped by cutting Pt-Ir wire with a wire cutter.

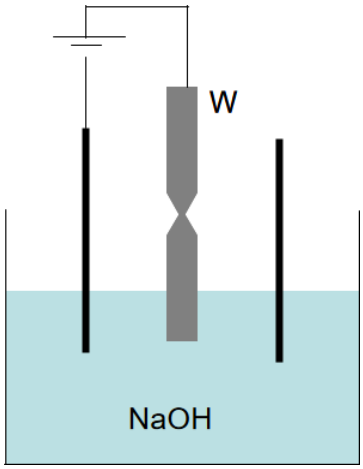
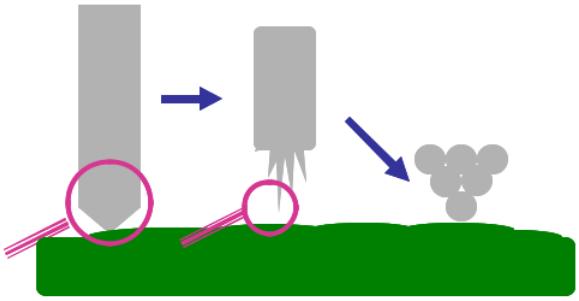


Figure 2. Set up for etching W probe for STM.

It should be noted that a tip does not necessarily have to be one perfect point.

STM Probe


Figure 3. STM probe magnified to an atomic scale.

How does the probe move across the surface?

A simple analogy to describe SPM is to think of a stylus of a turntable scanning across a record, Figure 4. However unlike the stylus in a turntable, the probe in SPM *does not* make direct contact with the surface.


Figure 4. A probe in SPM is similar to the stylus in a turntable used by DJs to fade/mix music.

In STM a voltage is applied between the metallic probe and the sample, typically (0-3 V). When the probe is close to the surface (2-4 *Å*) the voltage will result in a current, due to tunneling between the probe and sample. When the probe is far away from the surface, the current is zero. The tunneling current produced is low (pA-nA) but can be monitored using amplifiers. A 3D scanner with an electronic *feedback loop* is used to raster the probe across the sample to obtain a topographical image and monitor the tunneling current.

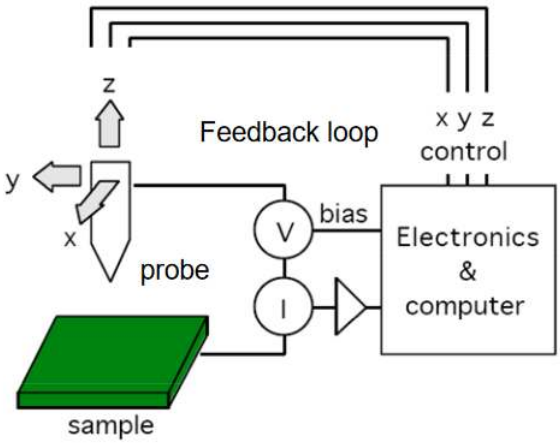


Figure 5. Schematic of STM with a piezoelectric scanner and feedback loop.

Piezoelectric 3D Scanner

The probe is attached to a 3-D *piezoelectric scanner*. By adjusting the voltage applied to the scanner the position of the probe can be controlled. This is due to the unique properties of piezoelectric materials that are incorporated into the scanner.

Piezoelectric materials have a permanent dipole moment across unit cell (Example: $PbZrTiO_3$ (PZT)). If the dipoles are oriented, the material changes length in applied electric field. Each scanner responds differently to applied voltage because of the differences in the material properties and dimensions of each piezoelectric element. Sensitivity is a measure of this response, a ratio of how far the piezo extends or contracts per applied volt. A 10^{-4} to 10^{-7} % length change per V allows < 1 Å positioning.

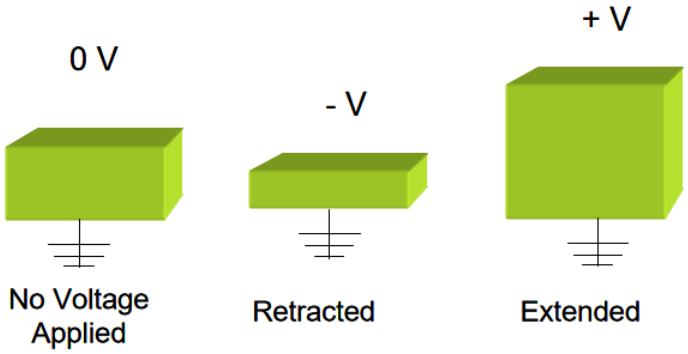


Figure 6. Schematic of piezoelectric materials in response to a voltage. Whether they expand or contract depends on the polarity of the voltage.

Most SPM instruments use a piezoelectric scan tube technology which combines independent piezos to control directions in the x, y, and z. AC voltages applied to the different electrodes produce a scanning (raster) motion in x and y. This motion is controlled by a computer.

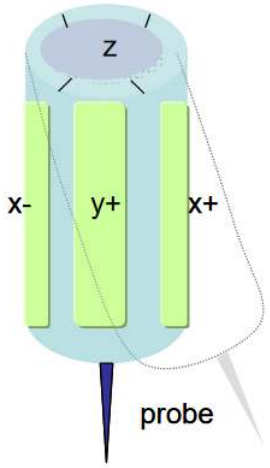


Figure 7. Schematic of a tube piezoelectric scanner. Each quadrant can move together or independently. If all four quadrants move together you have motion in z. If the x quadrants move together or separately this allows for x, y scanning. For example, the y- side may become longer and the y+ may become shorter, allowing for scanning in the y-direction.

Notes:

1. Rastering involves rendering the surface image, pixel by pixel, by sweeping in a vertical and horizontal motion, similar to drawing lines in the dirt with rake.
2. The set up described here can also be reversed and the sample can be rastered with piezoelectric scanners underneath the SPM probe.

There are some factors to consider with piezoelectric scanners:

Hysteresis: piezo scanners are more sensitive at the end of travel. Therefore opposite scans will behave differently and display some hysteresis.

Creep: Drift of piezo displacement may occur with large changes in x, y offsets

Aging: Piezoelectric materials' sensitivity to voltages decreases over time. Therefore scanners need to be calibrated on a standard basis

Bow: This is due to the scanner swinging in an arc motion to measure x,y displacement. This is often compensated with the z piezo or by using flattening algorithms.

Imaging Methods

There are two methods of imaging in STM:

1) Constant Current

A constant tunneling current is maintained during scanning (typically 1 nA). This is done by vertically (z) moving the probe at each (x,y) data point until a “setpoint” current is reached. The vertical position of the probe at each (x,y) data point is stored by the computer to form the topographic image of the sample surface. This method is most common in STM.

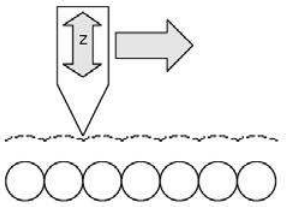


Figure 8. Constant current imaging with STM.

2) Constant Height

In this approach the probe-sample distance is fixed. A variation in tunneling current forms the image. This approaching allows for faster imaging, but only works for flat samples.

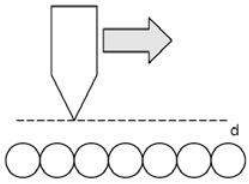


Figure 9. Constant height imaging with STM. (d= fixed probe-sample distance).

Online Interactive Tools

To view an interactive STM model and see how the STM probe moves across a surface you can go to the following website: http://www.iap.tuwien.ac.at/www/_media/surface/stm_gallery/stm_animated.gif

To see how you could possibly build your own STM go here: http://www.e-basteln.de/index_m.htm

WHAT ARE THE LIMITATIONS OF STM?

Although the STM itself does not need vacuum to operate (it works in air as well as under liquids), ultrahigh vacuum (UHV) is required to avoid contamination of the samples from the surrounding medium.

- Complex and expensive instrumentation - especially (UHV) version
- Subject to noise (electrical, vibration)
- Must fabricate probes - dull probes or multiple tips at the end of probe can create serious artifacts
- *Only works for conductive samples: metals, semiconductors*
    - samples can be “altered” to be conductive by coating with Au, but this coating can mask/hide certain features or degrade imaging resolution

References

1. For more detail on tunneling and quantum mechanics you can go here: http://www.chembio.uoguelph.ca/educmat/chm729/STMpage/stmdet.htm
2. Bonnell, D. A., Ed. *Scanning Probe Microscopy and Spectroscopy: Theory, Techniques, and Applications*; Wiley-VCH: New York, 2001.

This page titled 14.3.2: Scanning Tunneling Microscopy (STM) is shared under a CC BY-NC-SA 2.5 license and was authored, remixed, and/or curated by Heather A. Bullen & Robert A. Wilson via source content that was edited to the style and standards of the LibreTexts platform.

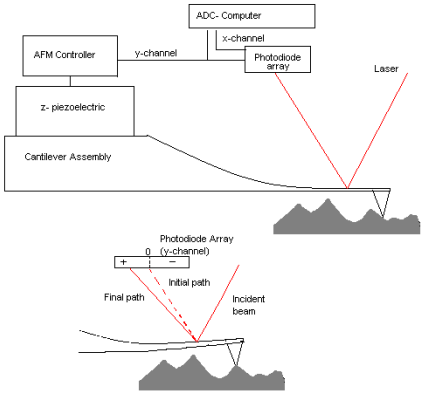
- **Scanning Tunneling Microscopy (STM)** by Heather A. Bullen, Robert A. Wilson is licensed CC BY-NC-SA 2.5. Original source: https://asdlib.org.

14.3.3: Atomic Force Microscopy

Atomic force microscopy utilizes a microscale probe to produce three dimensional image of surfaces at sub nanometer scales. The atomic force microscope obtains images by measurement of the attractive and repulsive forces acting on a microscale probe interacting with the surface of a sample. Ideally the interaction occurs at an atomically fine probe tip being attracted and repulsed by the atoms of the surface giving atomically resolved surface images.

Introduction

The atomic force microscope (AFM) probe is mounted onto a flexible cantilever that is manipulated by a vertical piezoelectric into interacting with the sample. The piezoelectric expands and exerts a force on the cantilever proportional to the potential voltage. The force is balanced by those acting on the probe by its interaction with the surface and the stain on the cantilever.



The flexible cantilever will bend proportionally to the force acting upon it in accordance to Hooke's law. By measuring the reflection of a laser source on the cantilever it is possible to determine the degree of the bend and by a feedback loop control the force exerted by the cantilever. By using the strain as a restoring force, a piezoelectric element can be used to drive the probe as a mechanical oscillator with a calculable resonate frequency, allowing for tapping mode microscopy. The laser acts on a photodiode array to give measurement of the deflection both horizontally and vertically. Using the deflection it is possible to calculate the quantity of force acting on the probe in both the horizontal and vertical directions. From the force applied by the vertical piezoelectric and the force acting on the probe it is possible to obtain a measure of the relative height of the probe.

As the probe encounters a feature, it raises with the feature, causing a deflection measured by the photodiode and a change in the force on the vertical piezoelectric. The potential may be adjusted to minimize the deflection, by feedback from the photodiode array, knowing the expansion rate of the vertical piezoelectric allows for a direct computation of the height, this is the z-sensor. By computation from the total deflection and thus strain on the cantilever, it is also possible to obtain the relative height of the feature given a known spring constant of the cantilever.

The probe is scanned across the surface, with either the probe or the sample being moved by piezoelectric elements. This allows for the measure of the interaction of the forces across the entire sample, allowing the surface to be rendered as a three dimensional image. The force exerted by the probe has the potential to alter the surface by etching or simply moving loosely bound surface features. As such, this microscopy technique can be potentially used to write (etch) as well as read, atomic scale surface features. The strain on the probe tip may cause deformation that leads to loss in resolution due to flattening or the generation of artifacts due to secondary tips.

The probe tip is idealized to be an atomically perfect spherical surface with a nanoscopic radius of curvature, leading to a single point of contact between the probe tip and the surface. Tips however may have multiple points of contact, leading to image artifacts such as doubled images or shadowing. Alternatively tips may be flattened or event indented, causing a lower resolution as smaller surface features are passed over. Significant error may arise from the expansion of the piezoelectric materials as they become heated. This problem is typically mitigated by attempting to maintain an isothermal environment. Drift may be measured and accounted for by repeat measurement of a known point and normalizing the data from that known height.

Modes of Operation

There are mutiple methods of imaging a surface using an atomic force microscope, these imaginging modes uniquely utilize the probe and its interaction with the surface to obtain data.

Contact

If a constant potential is maintained for the vertical piezoelectric, the probe will maintain continuous contact with the surface. It is then possible to use deflection and z-sensor to yield accurate height information of surface features.

Friction

When the probe is in contact with the sample the resistance acting on the probe's horizontal motion causes it to be strained horizontally. This strain is proportional to the resistance, friction, allowing for a direct measurement of the friction of the sample and probe surface.

Adhesion

Also known as non-contact mode, this method utilizes the attractive forces acting on the probe. To measure this, the probe is pulled from the sample by the vertical piezoelectric with a set force, as a feature is encountered the attractive force acting on the probe increases causing it to deflect downward. The downward deflection is counteracted by the vertical piezoelectric in a similar manner to contact mode, reaching the same equilibrium of forces acting on the cantilever.

Tapping

By using a piezoelectric device it is possible to use the cantilever as a harmonic oscillator with a resonance frequency proportional to the known spring constant. The probe then moves with an amplitude proportional to the driving force which is controlled and a frequency which is proportional to the spring constant. When the probe tip contact the surface the effective restoring force increases, increasing the frequency.

The total change in frequency is proportional to the feature's height, and vertical piezoelectric can then be used to raise the cantilever and restore the frequency to the original giving additional data from the z-sensor regarding the feature's height.

Additionally, as the probe contacts the surface it acts as a driving force, deforming the surface which is restored by the internal stress (that acts on the probe to repel it). The phenomenon is proportional to the Young's modulus of compressibility of the sample and will case a phase shift between the oscillation of the piezoelectric driver of the probe and the probe itself.

Other uses of AFM

Use of specialized probes allows a further expansion of atomic force microscopy's role in nanoscience. By alterations in probe design it is possible to: directly obtain data about the surface interaction with other functional groups, alter the surface by etching or causing chemical change, or deposit substrates onto a surface; all at the nanoscopic scale.

Chemical Force Microscopy

Functionalizing a probe can be accomplished by binding a protein or functional groups to the probe tip surface. The probe now takes direct measure of the iteration between the surface and the functional group. This technique is particularly useful for biological application, e.g. affinity of a protein to the binding site of a membrane.

Etching

The strain exerted by the tip on the surface has the potential to manipulate or alter the surface features, allowing for the mechanical etching of the system. By using specialized thermal tips, it becomes possible to heat the surface. Either technique can be used to precisely carve into or otherwise alter a surface at the scales necessary for many nanotechnologic advances.

Depositing

Use of a special tip similar to a fountain pen head, it is possible to deposit units of a substrate onto a surface. Precise deposition allows for building very precise surface structures, e.g. protien binding sites, onto an atomically flat surface.

Data recording

AFM has been demonstrated as a potential means of data storage by the IBM corperation. By using a heated tip it is possible to alter a polymer surface by a reversible polymerization reaction. The indentation created may be read by contact or tapping mode allowing for written data to be read. Data may be erased by use of the thermal tip to cause a polymerization on the surface, sealing the indentation.

14.3.3: Atomic Force Microscopy is shared under a CC BY-NC-SA 4.0 license and was authored, remixed, and/or curated by LibreTexts.

- **Atomic Force Microscopy** is licensed CC BY-NC-SA 4.0.

14.3.4: Atomic Force Microscopy (AFM)

HOW DOES THE AFM WORK?

AFM provides a 3D profile of the surface on a nanoscale, by measuring *forces* between a sharp probe (<10 nm) and surface at very short distance (0.2-10 nm probe-sample separation). The probe is supported on a flexible cantilever. The AFM tip "gently" touches the surface and records the small force between the probe and the surface.

How are Forces Measured?

The probe is placed on the end of a cantilever (which one can think of as a spring). The amount of force between the probe and sample is dependant on the *spring constant* (stiffness) of the cantilever and the distance between the probe and the sample surface. This force can be described using Hooke's Law:

$$F = -k \cdot x$$

F = Force

k = spring constant

x = cantilever deflection

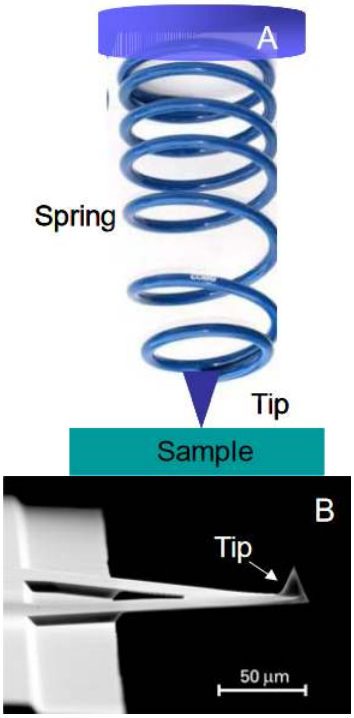


Figure 1. a) Spring depiction of cantilever b) SEM image of triangular SPM cantilever with probe (tip). (Image from MikroMasch)[1]

If the spring constant of cantilever (typically ~ 0.1-1 N/m) is less than surface, the cantilever bends and the deflection is monitored.

This typically results in forces ranging from nN (10^{-9}) to µN (10^{-6}) in the open air.

What are probes made of?

Probes are typically made from Si_3N_4, or Si. Different cantilever lengths, materials, and shapes allow for varied spring constants and resonant frequencies. A description of the variety of different probes can be found at various vendor sites.[2] Probes may be coated with other materials for additional SPM applications such as chemical force microscopy (CFM) and magnetic force microscopy (MFM).

Instrumentation

The motion of the probe across the surface is controlled similarly to the STM using *feedback loop* and *piezoelectronic scanners*. **(See STM basic theory)** The primary difference in instrumentation design is how the forces between the probe and sample surface

are monitored. The deflection of the probe is typically measure by a *"beam bounce" method*. A semiconductor diode laser is bounced off the back of the cantilever onto a position sensitive photodiode detector. This detector measures the bending of cantilever during the tip is scanned over the sample. The measured cantilever deflections are used to generate a map of the surface topography.

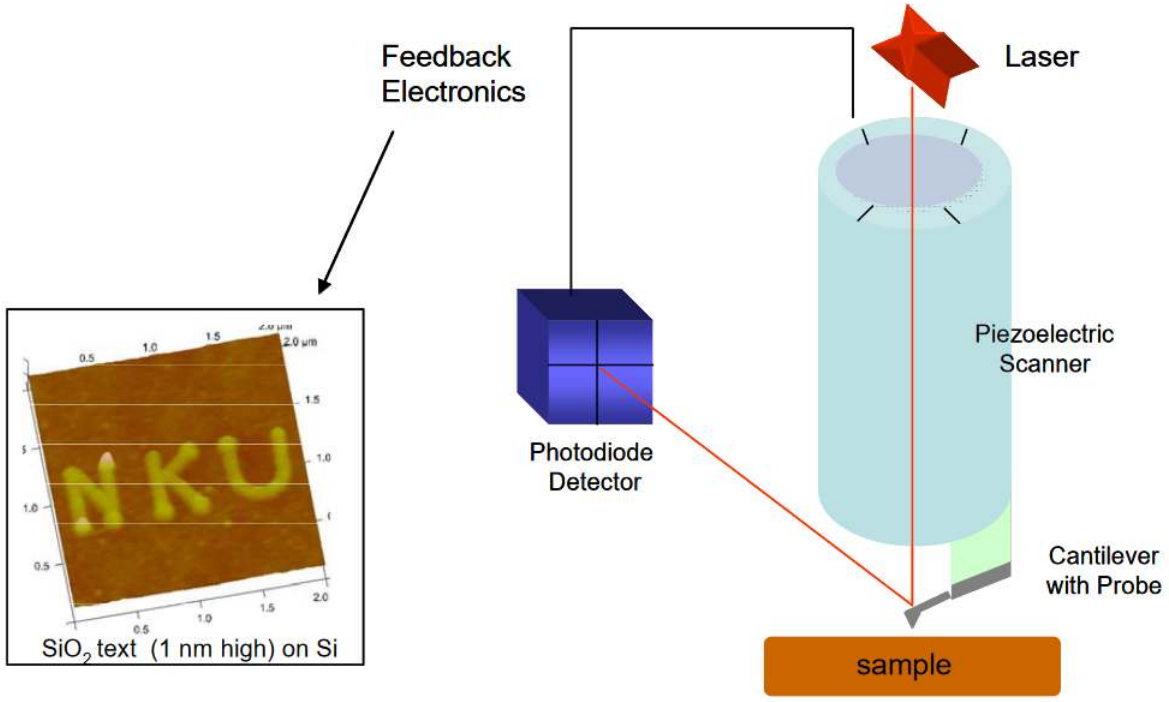


Figure 2. Schematic of AFM instrument showing "beam bounce" method of detection using a laser and position sensitive photodiode detector.

For a visual depiction of the "beam bounce" method of detection in AFM you can refer to the following web resource which utilizes Legos ®, magnetics, and a laser pointer to demonstrate this concept.

Imaging Methods

What types of forces are measured?

The dominant interactions at short probe-sample distances in the AFM are Van der Waals (VdW) interactions. However long-range interactions (i.e. capillary, electrostatic, magnetic) are significant further away from the surface. These are important in other SPM methods of analysis.

During contact with the sample, the probe predominately experiences *repulsive Van der Waals forces* (contact mode). This leads to the tip deflection described previously. As the tip moves further away from the surface *attractive Van der Waals forces* are dominant (non-contact mode).

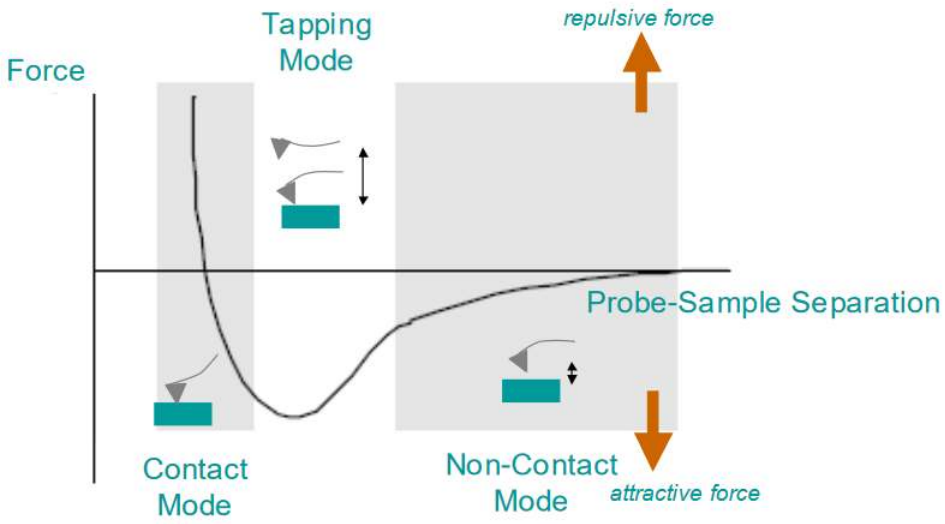


Figure 3. Plot of force as a function of probe-sample separation.

Modes of Operation

There are 3 primary imaging modes in AFM:

1. < 0.5 nm probe-surface separation
2. 0.5-2 nm probe-surface separation
3. 0.1-10 nm probe-surface separation

Primary Modes of Imaging:

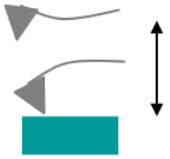
1. **Contact Mode AFM:** (*repulsive VdW*) When the spring constant of cantilever is less than surface, the cantilever bends. The force on the tip is repulsive. By maintaining a constant cantilever deflection (using the feedback loops) the force between the probe and the sample remains constant and an image of the surface is obtained.



Advantages: fast scanning, good for rough samples, used in friction analysis

Disadvantages: at time forces can damage/deform soft samples (however imaging in liquids often resolves this issue)

2. **Intermittent Mode (Tapping):** The imaging is similar to contact. However, in this mode the cantilever is oscillated at its *resonant frequency*, Figure 4. The probe lightly "taps" on the sample surface during scanning, contacting the surface at the bottom of its swing. By maintaining a constant oscillation amplitude a constant tip-sample interaction is maintained and an image of the surface is obtained.



Oscillation Amplitude: 20-100 nm

Advantages: allows high resolution of samples that are easily damaged and/or loosely held to a surface; Good for biological samples

Disadvantages: more challenging to image in liquids, slower scan speeds needed

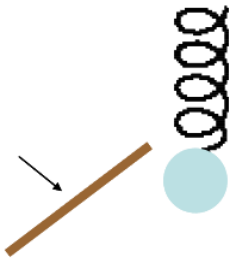


Figure 4. Resonant frequency is a natural frequency of vibration determined by the physical parameters of the vibrating object. For example if you hit a spring with a mass at the end (probe) the main response will be a bob up and down at its natural frequency.

3. **Non-contact Mode:** *(attractive VdW)* The probe does not contact the sample surface, but oscillates above the adsorbed fluid layer on the surface during scanning. *(Note: all samples unless in a controlled UHV or environmental chamber have some liquid adsorbed on the surface).* Using a feedback loop to monitor changes in the amplitude due to attractive VdW forces the surface topography can be measured.



Advantages: VERY low force exerted on the sample(10^{-12} N), extended probe lifetime

Disadvantages: generally lower resolution; contaminant layer on surface can interfere with oscillation; usually need ultra high vacuum (UHV) to have best imaging

What are Force Curves?

Force curves measure the amount of force felt by the cantilever as the probe tip is brought close to - and even indented into - a sample surface and then pulled away. In a force curve analysis the probe is repeatedly brought towards the surface and then retracted, Figure 5. Force curve analyses can be used to determine chemical and mechanical properties such as adhesion, elasticity, hardness and rupture bond lengths.

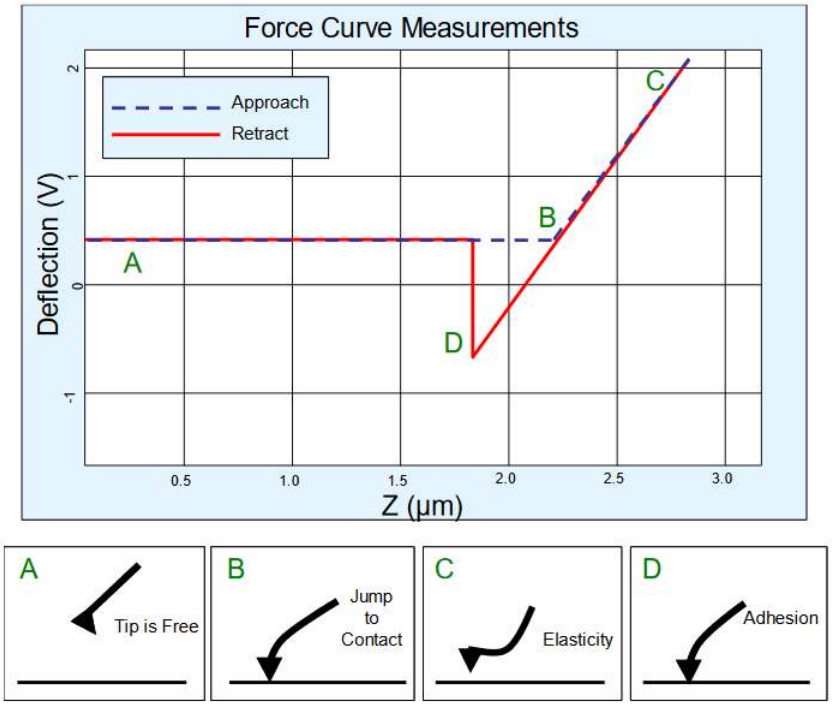


Figure 5. A typical force curve showing the various probe-sample interactions.

The slope of the deflection (C) provides information on the hardness of a sample. The adhesion (D) provides information on the interaction between the probe and sample surface as the probe is trying to break free. Direct measurements of the interactions between molecules and molecular assemblies can be achieved by functionlizing probes with molecules of interest (see Chemical Force Microscopy).

Interactive Tools:

An interactive force curve analysis can be found here: https://www.ntmdt-si.com/resources/spm-principles/afm-spectroscopies/force-distance-curves

WHAT ARE THE LIMITATIONS OF AFM?

The AFM can be used to study a wide variety of samples (i.e. plastic, metals, glasses, semiconductors, and biological samples such as the walls of cells and bacteria). *Unlike STM or scanning electron microscopy it does not require a conductive sample.* However there are limitations in achieving atomic resolution. The physical probe used in AFM imaging is not ideally sharp. As a consequence, an AFM image does not reflect the true sample topography, but rather represents the interaction of the probe with the sample surface. This is called tip convolution, Figure 6.

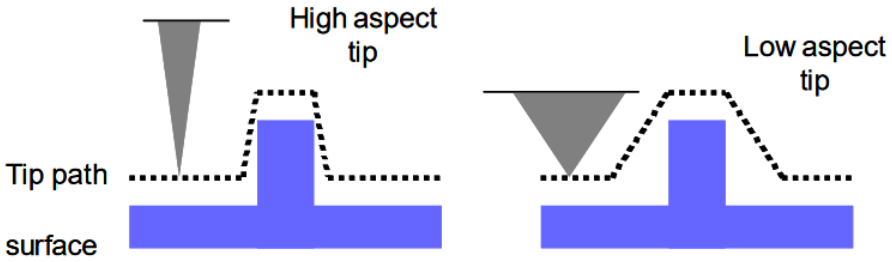


Figure 6. Ideally a probe (tip) with a high aspect ratio will give the best resolution. The radius of curvature of the probe leads to tip convolution. This does not often influence the height of a feature but the lateral resolution.

Commercially available probes are becoming more widely available that have very high aspect ratios. These are made with materials such as carbon nanotubes or tungsten spikes.[3] However these probes are still very expensive to use for every day image analysis.

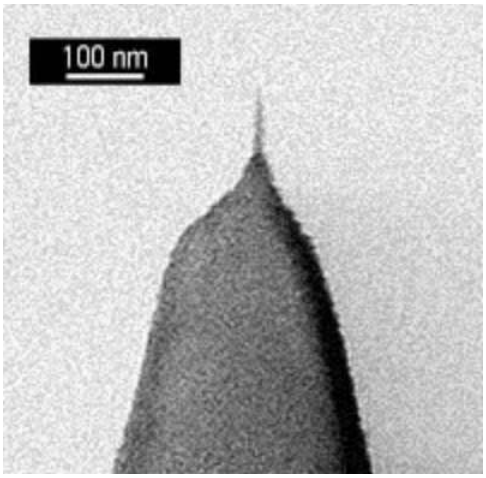


Figure 7. Example of High aspect probes from MikroMasch (1nm radius of curvature HI'RES-W probe).[3]

Online Resources

Another useful source on the principles of SPM:

http://ip.physics.leidenuniv.nl/index.php/component/content/article/15-cat-info/46-stmprinciples

Another useful source on how AFM works

http://stm2.nrl.navy.mil/how-afm/how-afm.html#General%20concept

References:

1. MikroMasch http://www.spmtips.com/products/cantilevers/datasheets/sc11/ (Accessed 11/06/06).
2. Nanosensors Homepage http://www.nanosensors.com (Accessed 11/06/06).
3. MikroMasch http://www.spmtips.com/products/cantilevers/datasheets/hi-res-w/ (Accessed 1/26/07).

This page titled 14.3.4: Atomic Force Microscopy (AFM) is shared under a CC BY-NC-SA 2.5 license and was authored, remixed, and/or curated by Heather A. Bullen & Robert A. Wilson via source content that was edited to the style and standards of the LibreTexts platform.

- **Atomic Force Microscopy (AFM)** by Heather A. Bullen, Robert A. Wilson is licensed CC BY-NC-SA 2.5. Original source: https://asdlib.org.

14.4: Spectroscopic Surface Methods

In this section we consider three representative surface analytical methods: X-ray photoelectron spectroscopy, in which the input is a beam of X-ray photons and the output is electrons; Auger electron spectroscopy, in which the input is either a beam of electrons or of X-ray photons and the output is electrons; and secondary-ion mass spectrometry, in which the input is a beam of ions and the output is ions.

X-Ray Photoelectron Spectroscopy (XPS)

In X-ray photoelectron spectroscopy, which is also known as electron spectroscopy for chemical analysis (ESCA), we measure the kinetic energy of electrons ejected from a sample following the absorption of X-ray photons. The resulting spectrum is a count of these emitted electrons as a function of their energy.

Principles of XPS

We can explain the origin of X-ray photoelectron spectroscopy using the photoelectric effect. Figure $14.4.1a$ shows the energy level diagram for an element's 1*s*, 2*s*, and 2*p* core-level electrons along with their KLM designations (see Chapter 12.1 for a previous discussion of this way of designating electrons). A nearly monoenergetic X-ray beam of known energy is focused on the sample, which results in the ejection of a core-level photoelectron, as shown in Figure $14.4.1b$ The kinetic energy of this emitted electron, E_{KE}, is related to its binding energy to the nucleus, E_{BE}, by the equation

$$E_{KE} = h\nu - E_{EB} - \Phi_w \tag{14.4.1}$$

where $h\nu$ is the energy of the X-ray photon and Φ_w is the spectrometer's work function (the energy needed to remove the electron from the surface and into the vacuum). The most common sources of X-rays are the Mg K_α line with an energy of 1253.6 eV or the Al $K\alpha$ line with an energy of 1486.6 eV.

The core-level vacancy created by the photoelectron leaves the atom with an unstable electron configuration. Relaxation to the ground state occurs when this vacancy is filled by an electron from a higher energy shell, with the excess energy released as either the emission of a second electron or the fluorescent emission of a characteristic X-ray, as seen in Figure $14.4.1c$ The secondary electron in Figure $14.4.1c$is called an Auger electron.

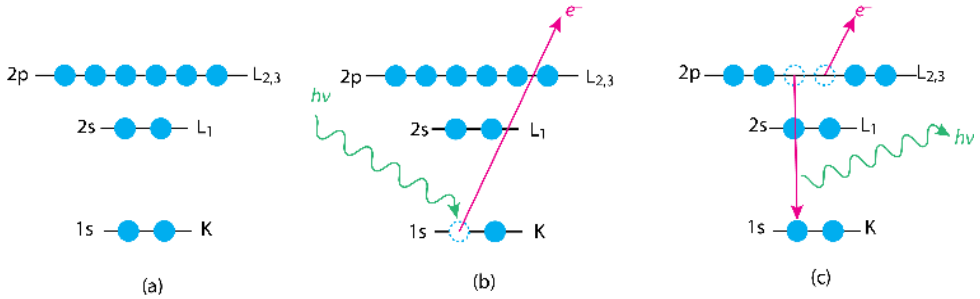


Figure 14.4.1: Energy level diagrams for X-ray photoelectron spectroscopy. In (a) we see the 1*s*, 2*s*, and 2*p* electrons along with their KLM designations. When a photon of sufficient energy is absorbed by the sample (b), a core-level electron is ejected as a photoelectron leaving an unstable electron configuration in which there is a vacancy in the 1s orbital. In (c) an electron from a higher energy orbital moves into the vacancy created by the initial photon with the remaining energy released as a secondary electron or as an X-ray photon.

Figure $14.4.2$provides an example of an XPS survey spectrum for aluminum oxide, Al_2O_3, using the K_α line for aluminum as the source of X-rays. The peak table gives the binding energies of the peaks for aluminum and for oxygen using the K_α for Al and, for comparison, the K_α line for Mg. Note the difference in how the major peaks are labeled. The photoelectrons ejected in the process shown in Figure $14.4.1b$are designated by the element and the *ns* notation that specifies the orbital from which the electron was ejected. Auger electrons are designated using the KLM notation, specifying the initial vacancy created by the absorbed photon, the source of the electron that fills that vacancy, and the source of the ejected Auger electron. The O_{KLL} peak in this spectrum is consistent with the scheme shown in Figure $14.4.1c$ When the source of the second and third electrons is from the valance shell, then notation is sometimes written as KVV; the O_{KLL} peak here could be designated as O_{KVV}.

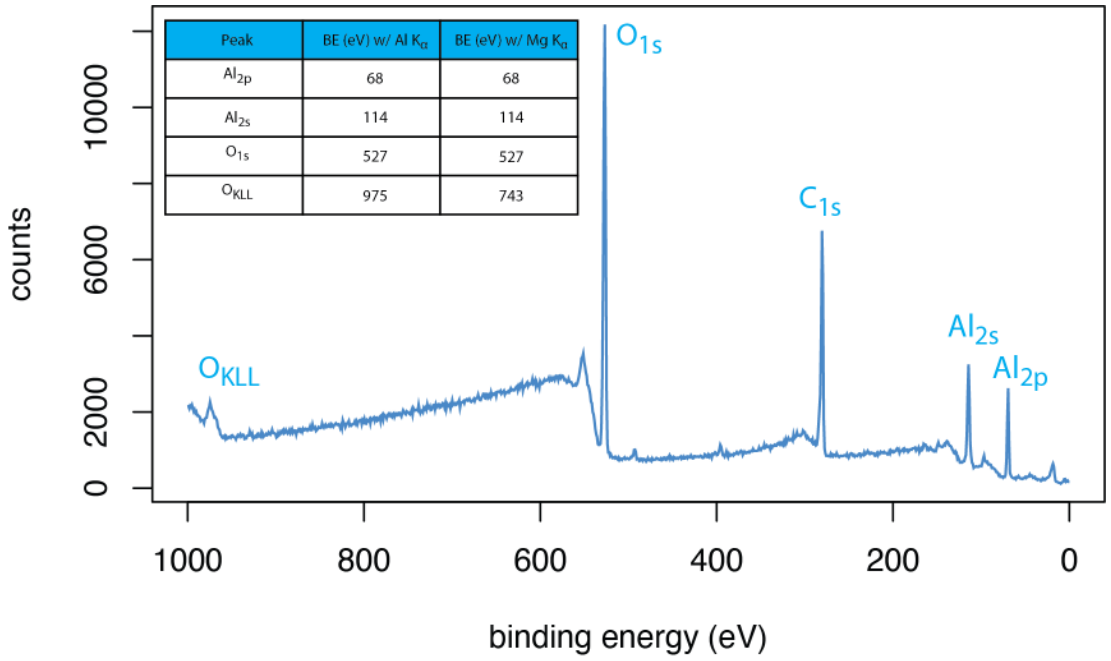


Figure 14.4.2: The XPS spectrum for Al_2O_3 using the Al K_α line, with the major peaks labeled. A spectrum such as this, which spans a wide range of energies, is called a survey spectrum. The source of each peak is shown above or next to the spectrum's peaks. The peak table provides the binding energies for aluminum and for oxygen using both the K_α for Al and the K_α for Mg. The original data used to create this figure is from the xpslibrary.

There are a few additional interesting features to note in the survey spectrum for Al_2O_3. One is the presence of a peak for carbon even though the sample, Al_2O_3, does not contain carbon. The prevalence of carbon in the atmosphere means that trace levels of carbon appear in almost all XPS spectra.

A second feature is the increase in the signal on the high binding energy (low kinetic energy) side of peaks, which is particularly visible here for the O_{1s} peak the C_{1s} peak, and the Al_{2s} peak. The source of this background is electrons that fail to escape the sample without undergoing inelastic collisions that result in a loss of kinetic energy and, given Equation 14.4.1, are recorded as if they have a larger than expected binding energy. Because X-rays penetrate more deeply into the sample than the depth from which electrons can travel without undergoing an inelastic collision, this background is unavoidable. Note that the background is more significant at higher binding energies (smaller kinetic energies).

A third feature is that the binding energy of an XPS peak is independent of the X-ray source, but the binding energy for an Auger peak varies with the X-ray source's energy (see table in Figure 14.4.2). The kinetic energy of the O_{1s}, Al_{2s}, and Al_{2p} photoelectrons is the difference between the energy of the X-ray photon, $h\nu$, and each electron's binding energy, BE; if we change the X-ray source, then $h\nu$ and KE increase in value, but the BE remains fixed. For the O_{KLL} Auger electron, the kinetic energy depends on the difference in the binding energies of the three electrons involved

$$\text{KE} \approx \text{BE}_K - \text{BE}_L - \text{BE}_L \tag{14.4.2}$$

and is, therefore, independent of the energy of the X-ray source. Given Equation 14.4.1, if the KE remains constant, then an increase in the energy of the X-ray photon, $h\nu$, means that the apparent BE must increase. This shift in binding energy when using a different source is one way to identify a peak as resulting from Auger electrons.

Instrumentation

The basic instrumentation for XPS is shown in Figure 14.4.3. The most common X-ray sources, as noted above, are Mg (1253.6 eV) and Al (1486.6 ev), which have the advantage of relatively narrow line-widths (0.7 and 0.9 eV, respectively) and, therefore, a relatively narrow range of energies. Higher energy sources are available, such as Ag (2984.4 ev), but at the cost of a wider line-width (2.6 eV). A system of electron lenses collects and focuses the ejected electrons onto the entrance slit of a hemispherical analyzer. The path of an electron through the analyzer depends upon its kinetic energy. By varying the potentials applied to the hemispherical analyzer's inner and outer plates, electrons of different kinetic energies reach the detector. A sputtering gun is an optional feature that can be used to clean the surface of the sample or to remove successive layers of the sample, allowing for the gathering of spectra at various depths within the sample. Calibration of the spectrometer's binding energy scale, which accounts for

the spectrometer's work function, is made using specific lines for one or more conductive metals; examples include Au $4f_{7/2}$ at 83.95 eV and Cu $2p_{3/2}$ at 932.63 ev. The peak for carbon that appears in almost all XPS spectra provides an additional way to check the calibration of the binding energy scale.

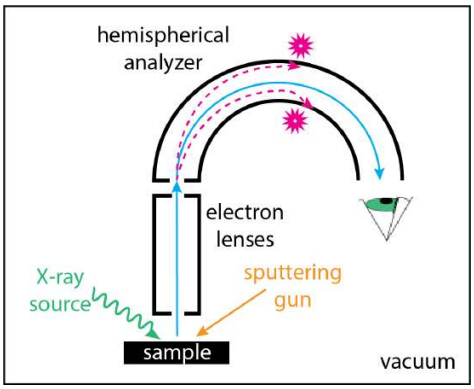


Figure 14.4.3: Schematic diagram of the basic instrumentation for X-ray photoelectron spectroscopy: an X-ray source for generating photoelectrons; a sputtering gun for cleaning the sample's surface or for removing layers of the sample; a set of electron lenses for collecting and focusing the photoelectrons; a hemispherical analyzer for isolating electrons by their kinetic energies; and a transducer to count electrons. The entire instrument is held under a vacuum.

Applications

X-ray photoelectron spectroscopy is a particularly useful tool for determining the composition and structure of a sample. XPS also can provide information about how the composition of a sample varies with depth and quantitative information about a sample's components.

Qualitative Analysis. One of the strengths of X-ray photoelectron spectroscopy is the ability to determine the elements that make up a sample's surface. Figure 14.4.4 shows a survey scan from 0 eV to 1100 eV of a ceramic material. In addition to the O1s peak, we see strong peaks for Si and Al—probably an aluminosilicate ceramic—and small peaks for a variety of elements: La, Ba, Mn, Sn, Ca, Cl, P, and Mg. NIST maintains an extensive, and searchable, database of XPS peaks that help in identifying the elements in a sample.

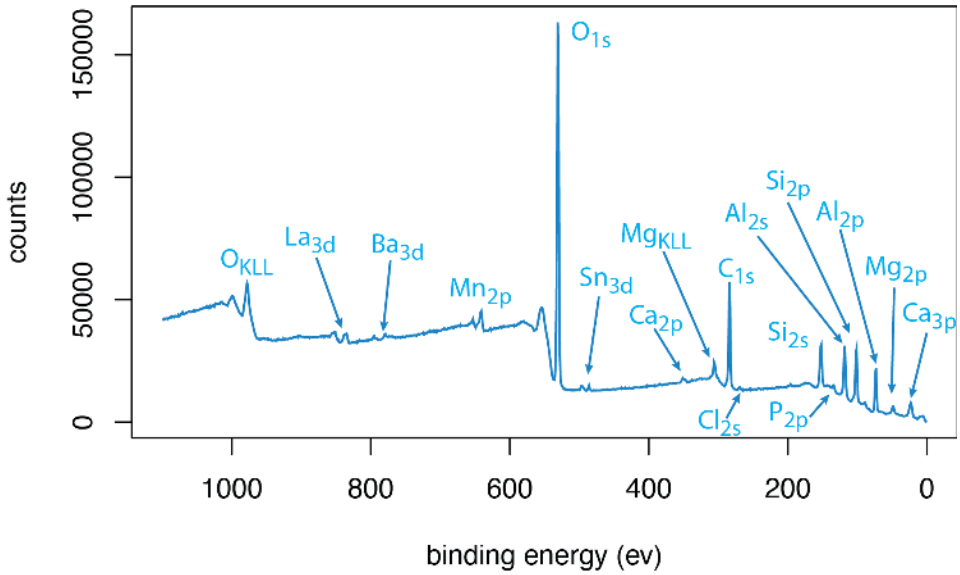


Figure 14.4.4: X-ray photoelectron survey spectrum for an unidentified ceramic material showing the peak assignments, which include major elements that we might reasonably expect from a ceramic (oxygen, magnesium, aluminum, calcium, and silicon) and a variety of trace elements (lanthinum, barium, manganese, tin, chlorine, and phosphorous). The original data used to create this figure is from the xpslibrary.

Chemical Shifts. An element's binding energy is sensitive to its chemical environment, particularly with respect to oxidation states and structure. For example, Table 14.4.1 provides the binding energy for chlorine's 2p line in three potassium salts drawn from the NIST database with all values from the same literature source. Using KCl, in which chlorine has an oxidation state of –1, as a baseline, the Cl 2p peak for $KClO_3$ is shifted by +8.4 eV and the Cl 2p peak for $KClO_4$ is shifted by +10.3 eV. The direction of the shift makes sense, as we expect that it will require more energy to remove an electron from an element that has a more positive oxidation state.

Table 14.4.1. Binding energies for the Cl 2p XPS peak as a function of chlorine's oxidation state.

compound	oxidation state for chlorine	binding energy (eV) for Cl 2p line	ΔBE relative to KCl
KCl	–1	198.1	—
$KClO_3$	+5	206.5	+8.4
$KClO_4$	+7	208.4	+10.3

Chemical shifts also reflect changes in chemical structure. Figure 14.4.5, for example, shows a high resolution scan for the oxygen 2p peak for same sample of aluminum oxide, Al_2O_3, in Figure 14.4.1. The surface of a metal oxide often has three distinct sources of oxygen: oxides, which make up the bulk of the sample, hydroxides that form at the surface following the chemisorption of water, and water that is physically absorbed to the surface. Curve-fitting of the raw data shows the contribution of each type of oxygen to the raw data and, through the peak areas, their relative abundance.

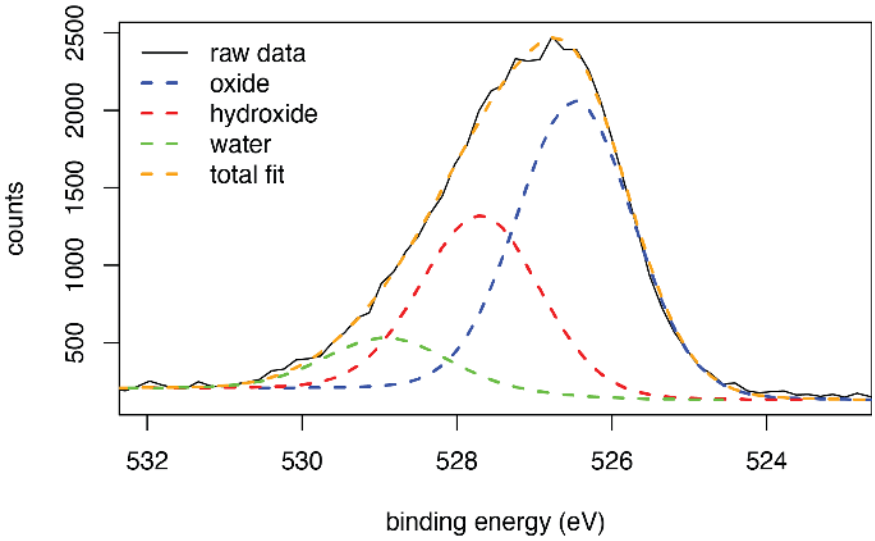


Figure 14.4.5: The results of curve-fitting to determine the relative contribution of different sources of oxygen—oxides, hydroxides, and water—to the O_{2p} peak for aluminum oxide. The original data used to create this figure is from the xpslibrary.

Wagner Plots. Both the binding energy of an X-ray photoelectron and the kinetic energy of an Auger electron convey information about the element from which the electrons were emitted. A Wagner plot shows both the binding energy for a photoelectron that leaves a particular core-level vacancy and the kinetic energy of the Auger electron whose origin arises from the filling of this core-level vacancy. Figure 14.4.6 shows an example of a Wagner plot for copper based on its $2p_{3/2}$ X-ray photoelectron and its LMM Auger electron. The diagonal lines are called the modified Auger parameter, which is defined as the sum of the XPS binding energy and the AES kinetic energy. Values for 20 compounds are included in this plot. Of interest here is the clustering of the individual compounds. For example, all of the samples for which copper has an oxidation state of +1 (shown as magenta squares) have similar binding energies between 932 eV and 933 eV, but with more variable kinetic energies, which range from 914 eV to 917 eV. Most of the compounds in which copper has an oxidation state of +2 (shown as blue diamonds) have modified Auger parameters between approximately 1850 eV and 1851 eV, although there is signifiant variation in their individual binding energies and kinetic energies. The two metals (shown as green circles) and the commpounds CuS and CuSe occupy a similar space within the Wagner plot. Interestingly, both CuS and CuSe are transition metal chalcogenides and have semiconducting properties.

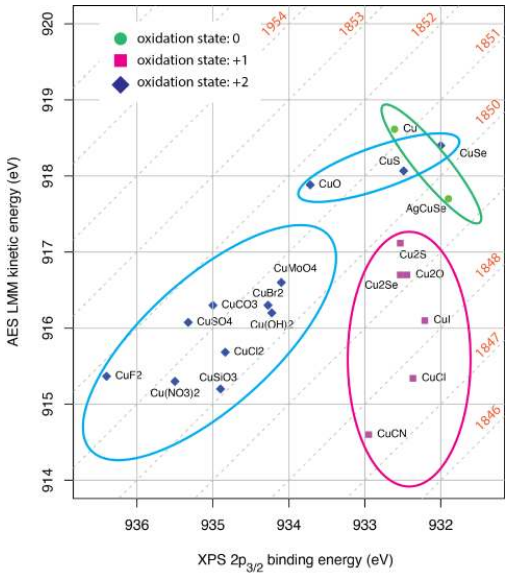


Figure 14.4.6: Wagner plot for 20 copper compounds. The raw data is from https://srdata.nist.gov/xps/Default.aspx and includes 140 measurements of binding energies and 99 measurements of kinetic energies. Compounds are identified by the oxidation state of copper.

Information at Depth. X-rays penetrate into a sample to a depth that is greater than the distance the photoelectron can travel without losing energy to inelastic collisions. We can take advantage of this to vary the depth from which we gather information. Figure 14.4.7 shows how this is accomplished by changing the angle from which we collect and analyze photoelectrons. The length of the solid black line is the distance an electron can travel without losing energy in an inelastic collision. When the detector is placed at 90° to the sample's surface, the sampling depth is at its greatest. Adjusting the detector so that it is at 30° to the surface, results in its detecting electrons from a depth that is just half of that when the detector is at 90°.

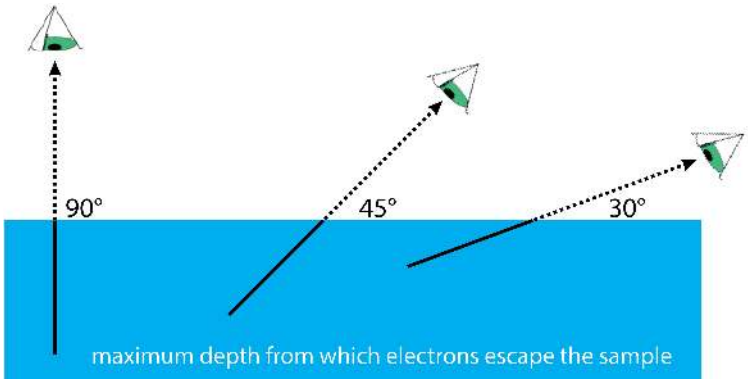


Figure 14.4.7: Illustration showing the measurement of the photoelectron's angle of emission. See text for explanation for how this affects sampling depth.

Quantitative Analysis. The intensity of an XPS peak—either is peak height or its peak area—is proportional to the number of atoms of the element responsible for the peak. This allows for determining the relative concentration, C_x, of an element in a sample; thus

$$C_x = \frac{I_x / S_x}{\sum (I_i / S_i)} \tag{14.4.3}$$

where I_x is the peak intensity for the element, S_x is the sensitivity factor for the element, and I_i and S_i are the peak intensities and sensitivity factors for all other elements in the sample. Sensitivity factors account for differences in the ease with which photoelectrons are produced and escape from the sample. Published tables of sensitivity factors are available, although they may vary some from instrument-to-instrument. Sensitivity factors are referenced to a standard line, typically C_{1s}, which is assigned a sensitivity factor of 1.00.

In many cases we are interested only in the relative concentration of just two elements. In this case, we write Equation 14.4.3 as

$$\frac{C_x}{C_y} = \frac{I_x / S_x}{I_y / S_y} \tag{14.4.4}$$

where x and y are the two elements. For example, using the data in Figure 14.4.4, the Si_{2p} peak has a height of 30 mm and the Al_{2p} peak has a peak height of 20 mm. Their sensitivity factors are, respectively 0.817 and 0.737. Using these values, we find that

$$\frac{C_{Si}}{C_{Al}} = \frac{30/0.817}{20/0.737} = 1.4$$

there are approximately $1.4\times$ as many atoms of silicon as there are atoms of aluminum.

Auger Electron Spectroscopy (AES)

In Figure 14.4.2 we learned that following the ejection of a photoelectron from an atom's core, the now unstable atom releases energy by either emitting a secondary electron from a higher energy orbital or by releasing a photon. In XPS we measure the intensity of the ejected photoejected electrons as a function of their binding energy; in Auger spectroscopy we measure the intensity of these secondary electrons as a function of their kinetic energies.

The instrumentation for AES can be coupled with an XPS spectrometer or be a stand-alone instrument. In either case, the basic instrumentation is similar to that shown in Figure 14.4.3, although AES spectra are usually initiated using an electron gun as a source instead of an X-ray source. One advantage to using an electron gun is that it can be focused into a smaller beam and can then easily rastered across a surface, allowing for imaging of the sample's surface. Depth profiling, using an ion beam to remove layers of the sample, is another common use of AES.

Figure 14.4.8 provides an example of a typical AES spectrum, in this case for the mineral calcite, $CaCO_3$. The raw data, on the left, shows the intensity of the signal as a count of electrons with a particular kinetic energy. The large background signal is from electrons that lose kinetic energy as the result of inelastic collisions. The two broad features between approximately 100 eV and 600 eV are the Auger peaks for calcium and for oxygen. The peaks in this case are easy to see because the two analytes are present in bulk. For a trace-level analyte, the Auger peaks in a normal plot may be difficult to see. For this reason, Auger spectra are usually presented by plotting the derivative of the raw data giving the spectrum on the right.

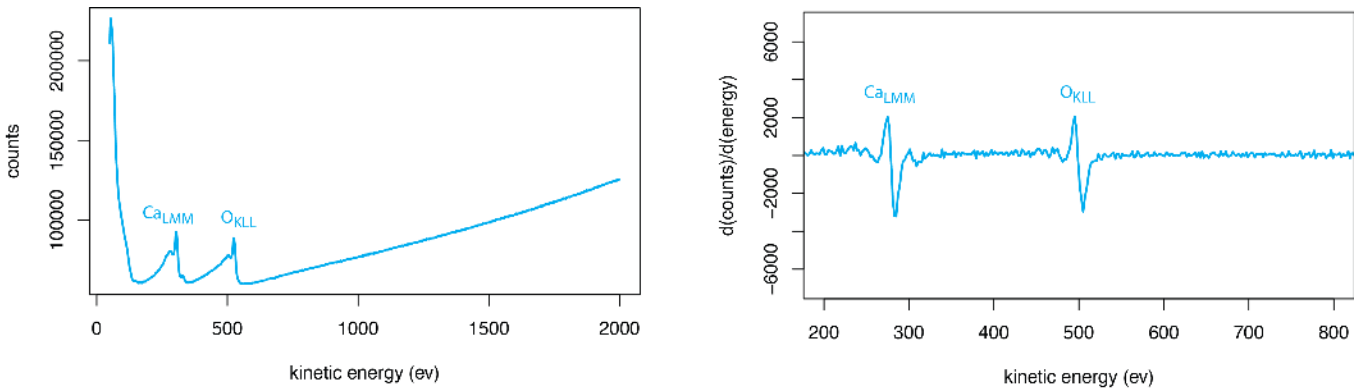


Figure 14.4.8: AES spectrum for the mineral calcite, $CaCO_3$. The figure on the left shows the spectrum as initially recorded and the figure on the right shows the data after taking the derivative of counts as a function of energy. The original data used to create thid figure is from the xpslibrary.

Figure 14.4.9 provides an example of how AES is used to study changes in the composition of a single crystal of $CaCO_3$ that was allowed to equilibrate with a solution containing Mg^{2+} ions. The sample was mounted on a sample probe and the AES spectrum recorded. An Ar^+ ion beam was used to remove layers of the sample while the spectrometer was used to record spectra of the sample. As expected, the surface is enriched in Mg^{2+} ions that diffused into the crystal with the relative concentration of Mg^{2+} decreasing. The relative abundance of Ca^{2+} increases with depth; the relative concentration of oxygen remains more or less constant with depth.

https://chem.libretexts.org/@go/page/532667

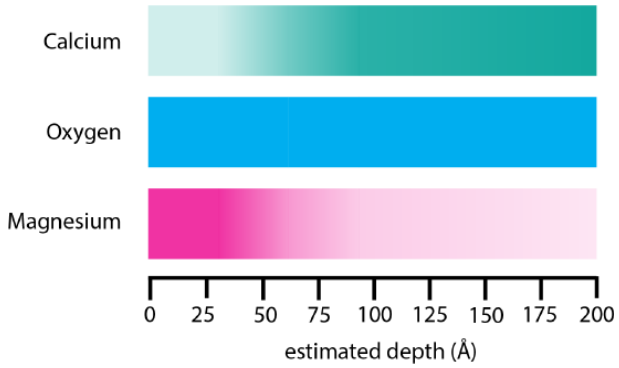


Figure 14.4.9: Depth profiles for calcium, oxygen, and magnesium in a sample of $CaCO_3$ that was suspended in a solution of Mg2+ ion. The shading for each element shows the relative abundance of the element with depth. See Mucci, A.; Morse, J. W.; Kaminsky, M. S. "Auger Spectroscopy Analysis of Magnesian Calcite Overgrowths Precipitated From Seawater and Solutions of Similar Composition," *Am. J. Sci*. **1985**, 289-305 for the paper suggesting this figure.

Secondary-Ion Mass Spectrometry (SIMS)

In SIMS we bombard the surface of a sample with an energetic primary beam—typically 5-20 keV—of an ion, such as Ar^+, O_2^+, or Cs^+. The primary ion penetrates the sample's surface, ejecting a variety of particles, including neutral atoms, electrons, and, more importantly, secondary ions (singly-charged or multiply charged cations and anions, and clusters of ions). These secondary ions are characterized by their mass-to-charge ratios and by their kinetic energies. The use of a primary ion beam of Cs^+ favors the formation of secondary ions that are anions, and a primary beam of O_2^+ favors the formation of secondary ions that are cations.

The instrumentation for SIMS includes an ion gun for generating the primary beam and a mass spectrometer for analyzing the secondary ions. In static mode, the primary ion beam is run using a low current density that minimizes the extent to which the sample's outermost layers are removed. In dynamic mode, the primary beam is run at a higher current density that removes more of the sample's surface. Dynamic SIMS is well suited to depth profiling. High mass resolution is obtained using a time-of-flight mass analyzer or a double-focusing mass analyzer; see Chapter 20 for a discussion of different types of mass analyzers.

SIMS is well suited for imaging as the positively charged primary ion can be rastered across the sample's surface. Figure 14.4.10 provides an example of imaging a surface using SIMS by measuring the yield of $^{14}N^{12}C$ ions while rastering the primary ion beam across a 10 μm × 10 μm section of the sample.

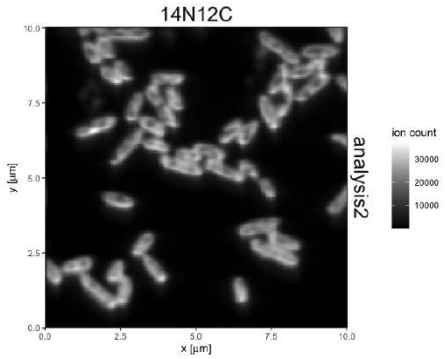


Figure 14.4.10: Image created using the R package lans2r ["lans2r: Work with Look at NanoSims Data in R", Sebastian Kopf, R package version 1.1.0, 2020]. The image shows the analysis of a 10 μm by 10 μm portion of a surface for the $^{14}N^{12}C$ ion, the two major isotopes of carbon and nitrogen. The bright areas have larger total ion counts.

This page titled 14.4: Spectroscopic Surface Methods is shared under a CC BY-NC-SA 4.0 license and was authored, remixed, and/or curated by David Harvey.

- **21.2: Spectroscopic Surface Methods** by David Harvey is licensed CC BY-NC-SA 4.0.

14.4.1: X-ray Photoelectron Spectroscopy

XPS Analysis of Modified Substances

Introduction

X-Ray photoelectron spectroscopy (XPS), also known as electron spectroscopy for chemical analysis (ESCA), is one of the most widely used surface techniques in materials science and chemistry. It allows the determination of atomic composition of the sample in a non-destructive manner, as well as other chemical information, such as binding constants, oxidation states and speciation. The sample under study is subjected to irradiation by a high energy X-ray source. The X-rays penetrate only 5 – 20 Å into the sample, allowing for surface specific, rather than bulk chemical, analysis. As an atom absorbs the X-rays, the energy of the X-ray will cause a K-shell electron to be ejected, as illustrated by Figure 14.4.1.1. The K-shell is the lowest energy shell of the atom. The ejected electron has a kinetic energy (KE) that is related to the energy of the incident beam (hv), the electron binding energy (BE), and the work function of the spectrometer (φ) (14.4.1.1). Thus, the binding energy of the electron can be calculated.

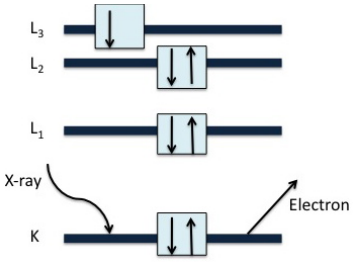


Figure 14.4.1.1 Excitation of an electron from an atom's K-shell.

$$BE = h\nu - KE - \psi_s \tag{14.4.1.1}$$

Table 14.4.1.1 shows the binding energy of the ejected electron, and the orbital from which the electron is ejected, which is characteristic of each element. The number of electrons detected with a specific binding energy is proportional to the number of corresponding atoms in the sample. This then provides the percent of each atom in the sample.

Table 14.4.1.1 Binding energies for select elements in their elemental forms.

Element	Binding Energy (eV)
Carbon (C) (1s)	284.5 - 285.1
Nitrogen (N) (1s)	396.1 - 400.5
Oxygen (O) (1s)	526.2 - 533.5
Silicon (Si) (2p)	98.8 - 99.5
Sulfur (S) ($2p_{3/2}$)	164.0 - 164.3
Iron (Fe) ($2p_{3/2}$)	706.8 - 707.2
Gold (Au) ($4f_{7/2}$)	83.8 - 84.2

The chemical environment and oxidation state of the atom can be determined through the shifts of the peaks within the range expected (Table 14.4.1.2). If the electrons are shielded then it is easier, or requires less energy, to remove them from the atom, i.e., the binding energy is low. The corresponding peaks will shift to a lower energy in the expected range. If the core electrons are not shielded as much, such as the atom being in a high oxidation state, then just the opposite occurs. Similar effects occur with electronegative or electropositive elements in the chemical environment of the atom in question. By synthesizing compounds with known structures, patterns can be formed by using XPS and structures of unknown compounds can be determined.

Table 14.4.1.2 Binding energies of electrons in various compounds.

Compound	Binding Energy (eV)
COH (C 1s)	286.01 - 286.8

Compound	Binding Energy (eV)
CHF (C 1s)	287.5 - 290.2
Nitride (N 1s)	396.2 - 398.3
Fe_2O_3 (from O, 1s)	529.5 - 530.2
Fe_2O_3 (from Fe, $2p_{3/2}$)	710.7 - 710.9
FeO (from Fe $2p_{3/2}$)	709.1 - 709.5
SiO_2 (from O, 2s)	532.5 - 533.3
SiO_2 (from Si, 2p)	103.2 - 103.9

Sample preparation is important for XPS. Although the technique was originally developed for use with thin, flat films, XPS can be used with powders. In order to use XPS with powders, a different method of sample preparation is required. One of the more common methods is to press the powder into a high purity indium foil. A different approach is to dissolve the powder in a quickly evaporating solvent, if possible, which can then be drop-casted onto a substrate. Using sticky carbon tape to adhere the powder to a disc or pressing the sample into a tablet are an option as well. Each of these sample preparations are designed to make the powder compact, as powder not attached to the substrate will contaminate the vacuum chamber. The sample also needs to be completely dry. If it is not, solvent present in the sample can destroy the necessary high vacuum and contaminate the machine, affecting the data of the current and future samples.

Analyzing Functionalized Surfaces

Depth Profiling

When analyzing a sample (Figure 14.4.1.2a) by XPS, questions often arise that deal with layers of the sample. For example, is the sample homogenous, with a consistent composition throughout, or layered, with certain elements or components residing in specific places in the sample? (Figure 14.4.1.2b,c). A simple way to determine the answer to this question is to perform a depth analysis. By sputtering away the sample, data can be collected at different depths within the sample. It should be noted that sputtering is a destructive process. Within the XPS instrument, the sample is subjected to an Ar^+ ion beam that etches the surface. This creates a hole in the surface, allowing the X-rays to hit layers that would not have otherwise been analyzed. However, it should be realized that different surfaces and layers may be etched at different rates, meaning the same amount of etching does not occur during the same amount of time, depending on the element or compound currently being sputtered.

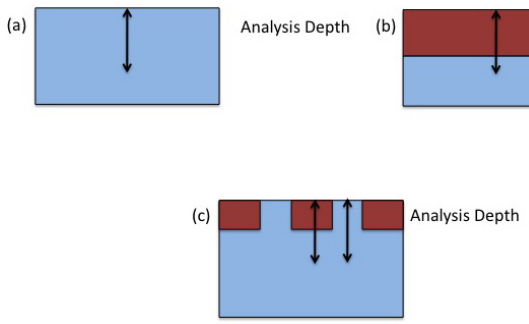


Figure 14.4.1.2 Schematic representation of analysis of (a) an homogeneous sample, as compared to (b) an homogeneous layers in a sample, and (c) an inhomogeneous layers in a sample.

It is important to note that hydrocarbons sputter very easily and can contaminate the high vacuum of the XPS instrument and thus later samples. They can also migrate to a recently sputtered (and hence unfunctionalized) surface after a short amount of time, so it is imperative to sputter and take a measurement quickly, otherwise the sputtering may appear to have had no effect.

Functionalized Films

When running XPS, it is important that the sample is prepared correctly. If it is not, there is a high chance of ruining not only data acquisition, but the instrument as well. With organic functionalization, it is very important to ensure the surface functional group (or as is the case with many functionalized nanoparticles, the surfactant) is immobile on the surface of the substrate. If it is removed easily in the vacuum chamber, it not only will give erroneous data, but it will contaminate the machine, which may then

contaminate future samples. This is particularly important when studying thiol functionalization of gold samples, as thiol groups bond strongly with the gold. If there is any loose thiol group contaminating the machine, the thiol will attach itself to any gold sample subsequently placed in the instrument, providing erroneous data. Fortunately, with the above exception, preparing samples that have been functionalized is not much different than standard preparation procedures. However, methods for analysis may have to be modified in order to obtain good, consistent data.

A common method for the analysis of surface modified material is angle resolved X-ray photoelectron spectroscopy (ARXPS). ARXPS is a non-destructive alternative to sputtering, as it relies upon using a series of small angles to analyze the top layer of the sample, giving a better picture of the surface than standard XPS. ARXPS allows for the analysis of the topmost layer of atoms to be analyzed, as opposed to standard XPS, which will analyze a few layers of atoms into the sample, as illustrated in Figure 14.4.1.3 ARXPS is often used to analyze surface contaminations, such as oxidation, and surface modification or passivation. Though the methodology and limitations are beyond the scope of this module, it is important to remember that, like normal XPS, ARXPS assumes homogeneous layers are present in samples, which can give erroneous data, should the layers be heterogeneous.

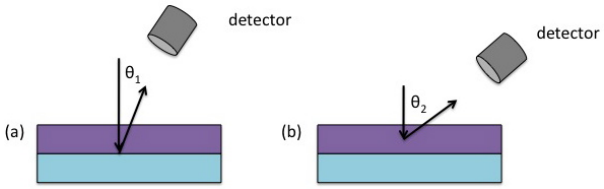


Figure 14.4.1.3 Schematic representation of (a) a standard XPS analysis and (b) ARXPS on a multilayer sample.

Limitations of XPS

There are many limitations to XPS that are not based on the samples or preparation, but on the machine itself. One such limitation is that XPS cannot detect hydrogen or helium. This, of course, leads to a ratio of elements in the sample that is not entirely accurate, as there is always some amount of hydrogen. It is a common fallacy to assume the percent of atoms obtained from XPS data are completely accurate due to this presence of undetected hydrogen (Table 14.4.1.1).

It is possible to indirectly measure the amount of hydrogen in a sample using XPS, but it is not very accurate and has to be done in a roundabout, often time consuming manner. If the sample contains hydrogen with a partial positive charge (i.e. OH), the sample can be washed in sodium naphthalenide ($C_{10}H_8Na$). This replaces this hydrogen with sodium, which can then be measured. The sodium to oxygen ratio that is obtained infers the hydrogen to oxygen ratio, assuming that all the hydrogen atoms have reacted.

XPS can only give an average measurement, as the electrons lower down in the sample will lose more energy as they pass other atoms while the electrons on the surface retain their original kinetic energy. The electrons from lower layers can also undergo inelastic or elastic scattering, seen in Figure 14.4.1.4 This scattering may have a significant impact on data at higher angles of emission. The beam itself is also relatively wide, with the smallest width ranging from 10 – 200 μm, lending to the observed average composition inside the beam area. Due to this, XPS cannot differentiate sections of elements if the sections are smaller than the size of the beam.

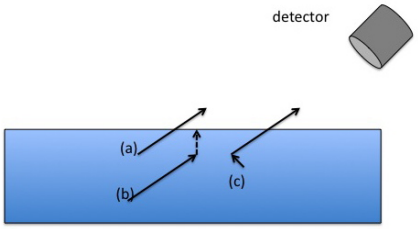


Figure 14.4.1.4: Schematic representation of (a) no scattering, (b) inelastic scattering, and (c) elastic scattering.

Sample reaction or degredation are important considerations. Caution should be exercised when analyzing polymers, as they are often chemically active and X-rays will provide energy to start degrading the polymer, altering the properties of the sample. One method found to help overcome this particular limitation is to use angle-resolved X-ray photoelectron spectroscopy (ARXPS). XPS can often reduce certain metal salts, such as Cu^{2+}. This reduction will give peaks that indicate a certain set of properties or chemical environments when it could be completely different. It needs to be understood that charges can build up on the surface of the sample due to a number of reasons, specifically due to the loss of electrons during the XPS experiment. The charge on the surface will interact with the electrons escaping from the sample, affecting the data obtained. If the charge collecting is positive, the electrons that have been knocked off will be attracted to the charge, slowing the electrons. The detector will pick up a lower kinetic

energy of the electrons, and thus calculate a different binding energy than the one expected, giving peaks which could be labeled with an incorrect oxidation state or chemical environment. To overcome this, the spectra must be charge referenced by one of the following methods: using the naturally occurring graphite peak as a reference, sputtering with gold and using the gold peak as a reference or flooding the sample with the ion gun and waiting until the desired peak stops shifting.

Limitations with Surfactants and Sputtering

While it is known that sputtering is destructive, there are a few other limitations that are not often considered. As mentioned above, the beam of X-rays is relatively large, giving an average composition in the analysis. Sputtering has the same limitation. If the surfactant or layers are not homogeneous, then when the sputtering is finished and detection begins, the analysis will show a homogeneous section, due to the size of both the beam and sputtered area, while it is actually separate sections of elements.

The chemistry of the compounds can be changed with sputtering, as it removes atoms that were bonded, changing the oxidation state of a metal or the hybridization of a non-metal. It can also introduce charges if the sample is non-conducting or supported on a non-conducting surface.

Using XPS to Analyze Metal Nanoparticles

Introduction

X-ray photoelectron spectroscopy (XPS) is a surface technique developed for use with thin films. More recently, however, it has been used to analyze the chemical and elemental composition of nanoparticles. The complication of nanoparticles is that they are neither flat nor larger than the diameter of the beam, creating issues when using the data obtained at face value. Samples of nanoparticles will often be large aggregates of particles. This creates problems with the analysis acquisition, as there can be a variety of cross-sections, as seen in Figure 14.4.1.5 This acquisition problem is also compounded by the fact that the surfactant may not be completely covering the particle, as the curvature of the particle creates defects and divots. Even if it is possible to create a monolayer of particles on a support, other issues are still present. The background support will be analyzed with the particle, due to their small size and the size of the beam and the depth at which it can penetrate.

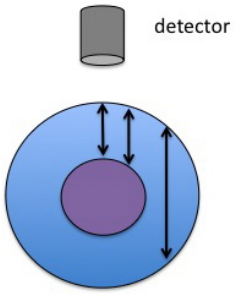


Figure 14.4.1.5 Different cross-sections of analysis possible on a nanoparticle.

Many other factors can introduce changes in nanoparticles and their properties. There can be probe, environmental, proximity, and sample preparation effects. The dynamics of particles can wildly vary depending on the reactivity of the particle itself. Sputtering can also be a problem. The beam used to sputter will be roughly the same size or larger than the particles. This means that what appears in the data is not a section of particle, but an average composition of several particles.

Each of these issues needs to be taken into account and preventative measures need to be used so the data is the best representation possible.

Sample Preparation

Sample preparation of nanoparticles is very important when using XPS. Certain particles, such as iron oxides without surfactants, will interact readily with oxygen in the air. This causes the particles to gain a layer of oxygen contamination. When the particles are then analyzed, oxygen appears where it should not and the oxidation state of the metal may be changed. As shown by these particles, which call for handling, mounting and analysis without exposure to air, knowing the reactivity of the nanoparticles in the sample is very important even before starting analysis. If the reactivity of the nanoparticle is known, such as the reactivity of oxygen and iron, then preventative steps can be taken in sample preparation in order to obtain the best analysis possible.

When preparing a sample for XPS, a powder form is often used. This preparation, however, will lead to aggregation of nanoparticles. If analysis is performed on such a sample, the data obtained will be an average of composition of each nanoparticle. If composition of a single particle is what is desired, then this average composition will not be sufficient. Fortunately, there are

other methods of sample preparation. Samples can be supported on a substrate, which will allow for analysis of single particles. A pictorial representation in Figure 14.4.1.6shows the different types of samples that can occur with nanoparticles.

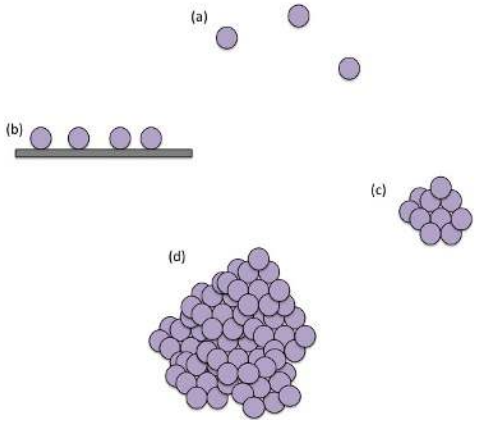


Figure 14.4.1.6 Representation of (a) a theoretical isolated nanoparticles, (b) nanoparticles suspended on a substrate, (c) an aggregate of nanoparticles, and (d) a powdered form of nanoparticles.

Analysis Limitations

Nanoparticles are dynamic; their properties can change when exposed to new chemical environments, leading to a new set of applications. It is the dynamics of nanoparticles that makes them so useful and is one of the reasons why scientists strive to understand their properties. However, it is this dynamic ability that makes analysis difficult to do properly. Nanoparticles are easily damaged and can change properties over time or with exposure to air, light or any other environment, chemical or otherwise. Surface analysis is often difficult because of the high rate of contamination. Once the particles are inserted into XPS, even more limitations appear.

Probe Effects

There are often artifacts introduced from the simple mechanism of conducting the analysis. When XPS is used to analyze the relatively large surface of thin films, there is small change in temperature as energy is transferred. The thin films, however, are large enough that this small change in energy has to significant change to its properties. A nanoparticle is much smaller. Even a small amount of energy can drastically change the shape of particles, in turn changing the properties, giving a much different set of data than expected.

The electron beam itself can affect how the particles are supported on a substrate. Theoretically, nanoparticles would be considered separate from each other and any other chemical environments, such as solvents or substrates. This, however, is not possible, as the particles must be suspended in a solution or placed on a substrate when attempting analysis. The chemical environment around the particle will have some amount of interaction with the particle. This interaction will change characteristics of the nanoparticles, such as oxidation states or partial charges, which will then shift the peaks observed. If particles can be separated and suspended on a substrate, the supporting material will also be analyzed due to the fact that the X-ray beam is larger than the size of each individual particle. If the substrate is made of porous materials, it can adsorb gases and those will be detected along with the substrate and the particle, giving erroneous data.

Environmental Effects

Nanoparticles will often react, or at least interact, with their environments. If the particles are highly reactive, there will often be induced charges in the near environment of the particle. Gold nanoparticles have a well-documented ability to undergo plasmon interactions with each other. When XPS is performed on these particles, the charges will change the kinetic energy of the electrons, shifting the apparent binding energy. When working with nanoparticles that are well known for creating charges, it is often best to use an ion gun or a coating of gold. The purpose of the ion gun or gold coating is to try to move peaks back to their appropriate energies. If the peaks do not move, then the chance of there being no induced charge is high and thus the obtained data is fairly reliable.

Proximity Effects

The proximity of the particles to each other will cause interactions between the particles. If there is a charge accumulation near one particle, and that particle is in close proximity with other particles, the charge will become enhanced as it spreads, affecting the

signal strength and the binding energies of the electrons. While the knowledge of charge enhancement could be useful to potential applications, it is not beneficial if knowledge of the various properties of individual particles is sought.

Less isolated (i.e., less crowded) particles will have different properties as compared to more isolated particles. A good example of this is the plasmon effect in gold nanoparticles. The closer gold nanoparticles are to each other, the more likely they will induce the plasmon effect. This can change the properties of the particles, such as oxidation states and partial charges. These changes will then shift peaks seen in XPS spectra. These proximity effects are often introduced in the sample preparation. This, of course, shows why it is important to prepare samples correctly to get desired results.

Conclusions

Unfortunately there is no good general procedure for all nanoparticles samples. There are too many variables within each sample to create a basic procedure. A scientist wanting to use XPS to analyze nanoparticles must first understand the drawbacks and limitations of using their sample as well as how to counteract the artifacts that will be introduced in order to properly use XPS.

One must never make the assumption that nanoparticles are flat. This assumption will only lead to a misrepresentation of the particles. Once the curvature and stacking of the particles, as well as their interactions with each other are taken into account, XPS can be run.

This page titled 14.4.1: X-ray Photoelectron Spectroscopy is shared under a CC BY 4.0 license and was authored, remixed, and/or curated by Pavan M. V. Raja & Andrew R. Barron (OpenStax CNX) via source content that was edited to the style and standards of the LibreTexts platform.

- **1.13: X-ray Photoelectron Spectroscopy** by Pavan M. V. Raja & Andrew R. Barron is licensed CC BY 4.0. Original source: http://cnx.org/contents/ba27839d-5042-4a40-afcf-c0e6e39fb45425.2.

14.4.2: Auger Electron Spectroscopy

Basic Principles

Auger electron spectroscopy (AES) is one of the most commonly employed surface analysis techniques. It uses the energy of emitted electrons to identify the elements present in a sample, similar to X-ray photoelectron spectroscopy (XPS). The main difference is that XPS uses an X-ray beam to eject an electron while AES uses an electron beam to eject an electron. In AES, the sample depth is dependent on the escape energy of the electrons. It is not a function of the excitation source as in XPS. In AES, the collection depth is limited to 1-5 nm due to the small escape depth of electrons, which permits analysis of the first 2 - 10 atomic layers. In addition, a typical analysis spot size is roughly 10 nm. A representative AES spectrum illustrating the number of emitted electrons, N, as a function of kinetic energy, E, in direct form (red) and in differentiated form (black) is shown in Figure 14.4.2.1.

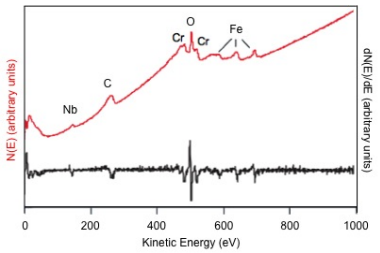


Figure 14.4.2.1 AES survey spectrum (red) and differentiated spectrum (black) of an oxidized Fe-Cr-Nb alloy. Adapted from H. J. Mathieu in *Surface Analysis: The Principal Techniques*, 2nd Edition, Ed. J. C. Vickerman, Wiley-VCH, Weinheim (2011).

Like XPS, AES measures the kinetic energy (E_k) of an electron to determine its binding energy (E_b). The binding energy is inversely proportional to the kinetic energy and can be found from 14.4.2.1, where hν is the energy of the incident photon and ΔΦ is the difference in work function between the sample and the detector material.

$$E_b = h\nu - E_k + \Delta\Phi \tag{14.4.2.1}$$

Since the E_b is dependent on the element and the electronic environment of the nucleus, AES can be used to distinguish elements and their oxidation states. For instance, the energy required to remove an electron from Fe^{3+} is more than in Fe^0. Therefore, the Fe^{3+} peak will have a lower E_k than the Fe^0 peak, effectively distinguishing the oxidation states.

Auger Process

An Auger electron comes from a cascade of events. First, an electron beam comes in with sufficient energy to eject a core electron creating a vacancy (see Figure 14.4.2.2a). Typical energies of the primary electrons range from 3 - 30 keV. A secondary electron (imaging electron) of higher energy drops down to fill the vacancy (see Figure 14.4.2.2b) and emits sufficient energy to eject a tertiary electron (Auger electron) from a higher shell (see Figure 14.4.2.2c).

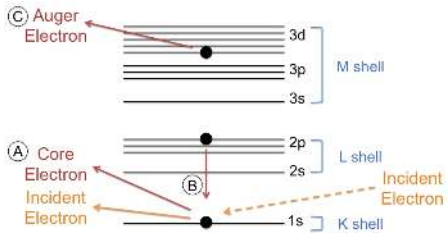


Figure 14.4.2.2 Schematic diagram of the Auger process.

The shells from which the electrons move from lowest to highest energy are described as the K shell, L shell, and M shell. This nomenclature is related to quantum numbers. Explicitly, the K shell represents the 1s orbital, the L shell represents the 2s and 2p orbitals, and the M shell represents the 3s, 3p, and 3d orbitals. The cascade of events typically begins with the ionization of a K shell electron, followed by the movement of an L shell electron into the K shell vacancy. Then, either an L shell electron or M shell electron is ejected. It depends on the element, which peak is prevalent but often both peaks will be present. The peak seen in the spectrum is labeled according to the shells involved in the movement of the electrons. For example, an electron ejected from a gold atom could be labeled as Au KLL or Au KLM.

The intensity of the peak depends on the amount of material present, while the peak position is element dependent. Auger transitions characteristic of each elements can be found in the literature. Auger transitions of the first forty detectable elements are

listed in Table 14.4.2.1

Table 14.4.2.1 Selected AES transitions and their corresponding kinetic energy. Adapted from H. J. Mathieu in *Surface Analysis: The Principal Techniques*, Second Edition, Ed. J. C. Vickerman, Wiley-VCH, Weinheim (2011).

Atomic Number	Element	AES transition	Kinetic Energy of Transition (eV)
3	Li	KLL	43
4	Be	KLL	104
5	B	KLL	179
6	C	KLL	272
7	N	KLL	379
8	O	KLL	508
9	F	KLL	647
11	Na	KLL	990
12	Mg	KLL	1186
13	Al	LMM	68
14	Si	LMM	92
15	P	LMM	120
16	S	LMM	152
17	Cl	LMM	181
19	K	KLL	252
20	Ca	LMM	291
21	Sc	LMM	340
22	Ti	LMM	418
23	V	LMM	473
24	Cr	LMM	529
25	Mn	LMM	589
26	Fe	LMM	703
27	Co	LMM	775
28	Ni	LMM	848
29	Cu	LMM	920
30	Zn	LMM	994
31	Ga	LMM	1070
32	Ge	LMM	1147
33	As	LMM	1228
34	Se	LMM	1315
35	Br	LMM	1376
39	Y	MNN	127

Atomic Number	Element	AES transition	Kinetic Energy of Transition (eV)
40	Zr	MNN	147
41	Nb	MNN	167
42	Mo	MNN	186

Instrumentation

Important elements of an Auger spectrometer include a vacuum system, an electron source, and a detector. AES must be performed at pressures less than 10^{-3} pascal (Pa) to keep residual gases from adsorbing to the sample surface. This can be achieved using an ultra-high-vacuum system with pressures from 10^{-8} to 10^{-9} Pa. Typical electron sources include tungsten filaments with an electron beam diameter of 3 - 5 µm, LaB_6 electron sources with a beam diameter of less than 40 nm, and Schottky barrier filaments with a 20 nm beam diameter and high beam current density. Two common detectors are the cylindrical mirror analyzer and the concentric hemispherical analyzer discussed below. Notably, concentric hemispherical analyzers typically have better energy resolution.

Cylindrical Mirror Analyzer (CMA)

A CMA is composed of an electron gun, two cylinders, and an electron detector (Figure 14.4.2.2). The operation of a CMA involves an electron gun being directed at the sample. An ejected electron then enters the space between the inner and outer cylinders (IC and OC). The inner cylinder is at ground potential, while the outer cylinder's potential is proportional to the kinetic energy of the electron. Due to its negative potential, the outer cylinder deflects the electron towards the electron detector. Only electrons within the solid angle cone are detected. The resulting signal is proportional to the number of electrons detected as a function of kinetic energy.

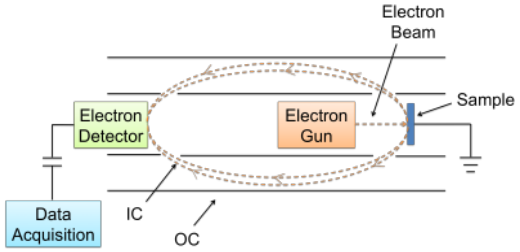


Figure 14.4.2.3 Schematic of a cylindrical mirror analyzer.

Concentric Hemispherical Analyzer (CHA)

A CHA contains three parts (Figure 14.4.2.4):

1. A retarding and focusing input lens assembly
2. An inner and outer hemisphere (IH and OH)
3. An electron detector

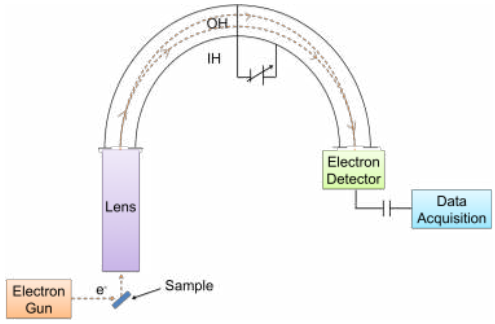


Figure 14.4.2.4 Schematic of a concentric hemispherical analyzer.

Electrons ejected from the surface enter the input lens, which focuses the electrons and retards their energy for better resolution. Electrons then enter the hemispheres through an entrance slit. A potential difference is applied on the hemispheres so that only electrons with a small range of energy differences reach the exit. Finally, an electron detector analyzes the electrons.

Applications

AES has widespread use owing to its ability to analyze small spot sizes with diameters from 5 μm down to 10 nm depending on the electron gun. For instance, AES is commonly employed to study film growth and surface-chemical composition, as well as grain boundaries in metals and ceramics. It is also used for quality control surface analyses in integrated circuit production lines due to short acquisition times. Moreover, AES is used for areas that require high spatial resolution, which XPS cannot achieve. AES can also be used in conjunction with transmission electron microscopy (TEM) and scanning electron microscopy (SEM) to obtain a comprehensive understanding of microscale materials, both chemically and structurally. As an example of combining techniques to investigate microscale materials, Figure 14.4.2.5shows the characterization of a single wire from a Sn-Nb multi-wire alloy. Figure 14.4.2.5a is a SEM image of the singular wire and Figure 14.4.2.5b is a schematic depicting the distribution of Nb and Sn within the wire. Point analysis was performed along the length of the wire to determine the percent concentrations of Nb and Sn.

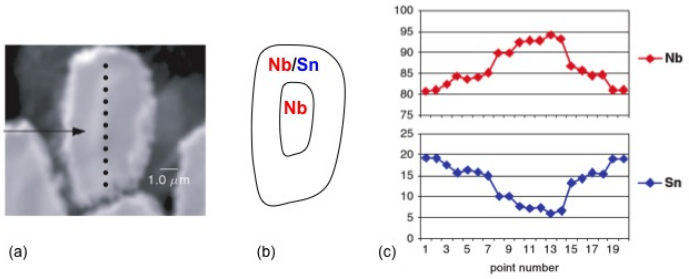


Figure 14.4.2.5 Analysis of a Sn-Nb wire. (a) SEM image of the wire, (b) schematic of the elemental distribution, and (c) graphical representation of point analysis giving the percent concentration of Nb and Sn. Adapted from H. J. Mathieu in *Surface Analysis: The Principal Techniques*, Second Edition, Ed. J. C. Vickerman, Wiley-VCH, Weinheim (2011).

AES is widely used for depth profiling. Depth profiling allows the elemental distributions of layered samples 0.2 – 1 μm thick to be characterized beyond the escape depth limit of an electron. Varying the incident and collection angles, and the primary beam energy controls the analysis depth. In general, the depth resolution decreases with the square root of the sample thickness. Notably, in AES, it is possible to simultaneously sputter and collect Auger data for depth profiling. The sputtering time indicates the depth and the intensity indicates elemental concentrations. Since, the sputtering process does not affect the ejection of the Auger electron, helium or argon ions can be used to sputter the surface and create the trench, while collecting Auger data at the same time. The depth profile does not have the problem of diffusion of hydrocarbons into the trenches. Thus, AES is better for depth profiles of reactive metals (e.g., gold or any metal or semiconductor). Yet, care should be taken because sputtering can mix up different elements, changing the sample composition.

Limitations

While AES is a very valuable surface analysis technique, there are limitations. Because AES is a three-electron process, elements with less than three electrons cannot be analyzed. Therefore, hydrogen and helium cannot be detected. Nonetheless, detection is better for lighter elements with fewer transitions. The numerous transition peaks in heavier elements can cause peak overlap, as can the increased peak width of higher energy transitions. Detection limits of AES include 0.1 – 1% of a monolayer, 10^{-16} – 10^{-15} g of material, and 10^{12} – 10^{13} atoms/cm^2.

Another limitation is sample destruction. Although focusing of the electron beam can improve resolution; the high-energy electrons can destroy the sample. To limit destruction, beam current densities of greater than 1 mA/cm^2 should be used. Furthermore, charging of the electron beam on insulating samples can deteriorate the sample and result in high-energy peak shifts or the appearance of large peaks.

This page titled 14.4.2: Auger Electron Spectroscopy is shared under a CC BY 4.0 license and was authored, remixed, and/or curated by Pavan M. V. Raja & Andrew R. Barron (OpenStax CNX) via source content that was edited to the style and standards of the LibreTexts platform.

- **1.14: Auger Electron Spectroscopy** by Pavan M. V. Raja & Andrew R. Barron is licensed CC BY 4.0. Original source: http://cnx.org/contents/ba27839d-5042-4a40-afcf-c0e6e39fb45425.2.

Index

A

absorbance
5.2: Calibrating the Signal
6.3: Spectroscopy Based on Absorption
6.12.1: Mid-Infrared Absorption Spectometry
6.14: Problems
6.16: Chapter Summary and Key Terms
9.4: Interferences in Absorption Spectroscopy

absorption
1.4: Types of Instrumental Methods
6.11: An Introduction to Infrared Spectrometry

absorption spectra
6.3: Spectroscopy Based on Absorption

absorption spectrometry
6.12: Applications of Infrared Spectrometry

absorption spectroscopy
3.2: Techniques, Methods, Procedures, and Protocols
6.1: Overview of Spectroscopy
6.3: Spectroscopy Based on Absorption

absorption spectrum
6.5: UV/Vis and IR Spectroscopy

accuracy
1.2: The Analytical Perspective
3.4: Selecting an Analytical Method
3.5: Developing the Procedure
3.6: Protocols
3.10: Chapter Summary and Key Terms
4.2: Characterizing Experimental Errors
4.10: Additional Resources
5.2: Calibrating the Signal
6.5: UV/Vis and IR Spectroscopy

accuracy verification
3.6: Protocols

acetic acid
12.5: Ladder Diagrams

acid dissociation
12.5: Ladder Diagrams

acid dissociation constant
12.8: Chapter Summary and Key Terms

acidic solution reaction
13.5: Problems

acrylonitrile reduction
13.5: Problems

activity coefficient
12.8: Chapter Summary and Key Terms

activity effects
12.7: Additional Resources

adsorption
10.1.1: A General Description of Chromatography

adsorptive stripping voltammetry
13.4.6: Stripping Methods

affinity chromatography
10.1.1: A General Description of Chromatography

AFM
14.3: Scanning Probe Microscopes

Ag electrode
13.3.4: Metallic Indicator Electrodes

alternative hypothesis
4.5: Statistical Analysis of Data
4.6: Statistical Methods for Normal Distributions
4.11: Chapter Summary and Key Terms

American Chemical Society
5.1: Analytical Signals

American Society for Testing and Materials
5.2: Calibrating the Signal

amperometric sensors
13.4.3: Linear Sweep Voltammetry

amperometry
13.1: Overview of Electrochemistry
13.2.6: Types of Electroanalytical Methods
13.4.7: Applications of Voltammetry
13.6: Additional Resources
13.7: Chapter Summary and Key Terms

amphiprotic
12.4: Equilibrium Constants for Chemical Reactions

analysis
1.4: Types of Instrumental Methods
3.1: Analysis, Determination, and Measurement
3.6: Protocols
10.1.6: Summary of Important Relationships for Chromatography
11: Thermal Methods
13.3: Potentiometry
14: Surface Characterization by Spectroscopy and Microscopy

analysis time
3.4: Selecting an Analytical Method

analysis_time
10.1.5: Optimization and Column Performance

analyte
3.1: Analysis, Determination, and Measurement
3.3: Classifying Analytical Techniques
3.10: Chapter Summary and Key Terms
4.7: Detection Limits
6.3: Spectroscopy Based on Absorption
6.7: Emission Spectroscopy
9: Atomic Spectroscopy
9.3: Atomic Absorption Instrumentation
10.1: Introduction to Chromatographic Separations
13.4.1: Potential Excitation Signals and Currents in Voltammetry

analyte calculation
5.9: Chapter Summary and Key Terms

analyte concentration
3.8: Problems
5.4: Linear Regression and Calibration Curves
5.5: Compensating for the Reagent Blank
5.7: Problems
9.2: Sample Atomization Techniques
13.4.6: Stripping Methods

analyte dissolution
3.8: Problems

analyte extraction
9.5: Atomic Absorption Techniques

analyte sensitivity
5.3: Determining the Sensitivity

analytematrix
9.4: Interferences in Absorption Spectroscopy

analytical balance
2.10: Chapter Summary and Key Terms
5.2: Calibrating the Signal

analytical chemistry
1.1: What is Analytical Chemistry
1.2: The Analytical Perspective
1.3: Common Analytical Problems
1.6: Additional Resources
1.7: Chapter Summary and Key Terms
2.1: Measurements in Analytical Chemistry
2.2: Concentration
2.3: Stoichiometric Calculations
2.5: Preparing Solutions
2.9: Additional Resources
2.10: Chapter Summary and Key Terms
3.2: Techniques, Methods, Procedures, and Protocols
3.5: Developing the Procedure
3.8: Problems
3.9: Additional Resources
4.2: Characterizing Experimental Errors
4.3: Propagation of Uncertainty
4.5: Statistical Analysis of Data
4.6: Statistical Methods for Normal Distributions
4.7: Detection Limits
4.9: Problems
4.10: Additional Resources
5.3: Determining the Sensitivity
5.7: Problems
5.8: Additional Resources
6.14: Problems
6.15: Additional Resources
9.5: Atomic Absorption Techniques
10.3: Problems
12.4: Equilibrium Constants for Chemical Reactions
12.5: Ladder Diagrams
12.6: Problems
12.7: Additional Resources
12.8: Chapter Summary and Key Terms
13.1: Overview of Electrochemistry

analytical chemistry equipment
2.4: Basic Equipment

Analytical Chemistry review
1.3: Common Analytical Problems

analytical chemists
5.5: Compensating for the Reagent Blank

analytical measurements
2.4: Basic Equipment

analytical method
5.1: Analytical Signals
6.6: Signals and Noise
9.7.2: Atomic Emission Spectroscopy

analytical method validation
4.6: Statistical Methods for Normal Distributions

analytical methodology
3.9: Additional Resources

analytical methods
1.1: What is Analytical Chemistry
1.7: Chapter Summary and Key Terms
2.6: Spreadsheets and Computational Software
2.8: Problems
3.2: Techniques, Methods, Procedures, and Protocols
3.4: Selecting an Analytical Method
3.7: The Importance of Analytical Methodology
5.5: Compensating for the Reagent Blank
6.14: Problems
14.1: Introduction to the Study of Surfaces

analytical methods classification
3.9: Additional Resources

analytical procedure
3.5: Developing the Procedure
3.8: Problems

analytical procedures
3.9: Additional Resources

analytical processes
1.1: What is Analytical Chemistry

analytical sciences
9.7.2: Atomic Emission Spectroscopy

analytical signal
13.2: An Introduction to Electroanalytical Chemistry
analytical signals
13.2.6: Types of Electroanalytical Methods
analytical technique
9.6: Atomic Absorption Spectroscopy
analytical techniques
10.5: Chapter Summary and Key Terms
13.4.7: Applications of Voltammetry
analytical terminology
3.9: Additional Resources
analyticalchemistry
9.4: Interferences in Absorption Spectroscopy
anion detection
10.3: Problems
anode
13.5: Problems
anodic stripping voltammetry
13.4.6: Stripping Methods
ANOVA
5.6: Using Excel and R for a Linear Regression
Antabuse analysis
2.3: Stoichiometric Calculations
applications
14.2: Scanning Electron Microscopy
aqueous samples
6.13.2: Instrumentation
archaeological research
1.3: Common Analytical Problems
arsenic titration
13.5: Problems
ascorbic acid analysis
13.5: Problems
atmospheric chemistry
6.15: Additional Resources
atomic absorption
6.14: Problems
6.15: Additional Resources
6.16: Chapter Summary and Key Terms
9: Atomic Spectroscopy
9.3: Atomic Absorption Instrumentation
9.7.1: Emission Spectroscopy Based on Flame and Plasma Sources
atomic absorption accuracy
9.6: Atomic Absorption Spectroscopy
atomic absorption precision
9.6: Atomic Absorption Spectroscopy
atomic absorption spectroscopy
3.4: Selecting an Analytical Method
9.3: Atomic Absorption Instrumentation
9.5: Atomic Absorption Techniques
9.6: Atomic Absorption Spectroscopy
atomic emission
6.15: Additional Resources
9.6: Atomic Absorption Spectroscopy
9.7: Atomic Emission Spectroscopy
atomic emission lines
9.6: Atomic Absorption Spectroscopy
atomic emission spectra
9.7.2: Atomic Emission Spectroscopy
atomic emission spectroscopy
6.16: Chapter Summary and Key Terms
9.7.2: Atomic Emission Spectroscopy
atomic force microscopy
14.3.3: Atomic Force Microscopy
atomic spectra
9.7.1: Emission Spectroscopy Based on Flame and Plasma Sources
atomic theory
8.1: General Features of Atomic Mass Spectrometry
atomic transitions
6.3: Spectroscopy Based on Absorption
atomic weight
2.8: Problems
AtomicSpectroscopy
9.4: Interferences in Absorption Spectroscopy
atomization
3.2: Techniques, Methods, Procedures, and Protocols
9: Atomic Spectroscopy
9.2: Sample Atomization Techniques
9.7.2: Atomic Emission Spectroscopy
atomization methods
9.6: Atomic Absorption Spectroscopy
atoms
8.1: General Features of Atomic Mass Spectrometry
attenuated total reflectance Fourier transform infrared spectroscopy
6.2.1: ATR-FTIR
attenuated total reflectance spectrometry
6.12.2: Mid-Infrared Reflection Spectrometry
Auger
14: Surface Characterization by Spectroscopy and Microscopy
Auger Electron Spectroscopy
14.4.2: Auger Electron Spectroscopy

B

background correction
6.16: Chapter Summary and Key Terms
9.6: Atomic Absorption Spectroscopy
bacterial colonies
3.1: Analysis, Determination, and Measurement
balance
5.2: Calibrating the Signal
base dissociation constant
12.8: Chapter Summary and Key Terms
base peak
8.2: Molecular Mass Spectra
8.7.5: Fragmentation Patterns in Mass Spectra
base SI units
2.1: Measurements in Analytical Chemistry
batch injection
13.5: Problems
Beer’s law
6.14: Problems
6.16: Chapter Summary and Key Terms
Beer's law
6.3: Spectroscopy Based on Absorption
bias
4.2: Characterizing Experimental Errors
4.11: Chapter Summary and Key Terms
binomial distribution
4.4: The Distribution of Measurements and Results
4.8: Using Excel and R to Analyze Data
4.11: Chapter Summary and Key Terms
bioluminescence
6.7: Emission Spectroscopy
biosensors
13.6: Additional Resources
blank correction
5.5: Compensating for the Reagent Blank
blank determination
5.1: Analytical Signals
blood glucose concentration
4.5: Statistical Analysis of Data
box plot
4.8: Using Excel and R to Analyze Data
4.11: Chapter Summary and Key Terms
buffer characterization
12.7: Additional Resources
buffers
12.8: Chapter Summary and Key Terms
bulk properties
14.1: Introduction to the Study of Surfaces
Bureau International des Poids and Measures
2.9: Additional Resources

C

C13 NMR
7.7.11: Characteristics of ^{13}C NMR Spectroscopy
7.7.13: Uses of ^{13}C NMR Spectroscopy
CaCl2
12.1: Reversible Reactions and Chemical Equilibria
CaCO3
12.1: Reversible Reactions and Chemical Equilibria
caffeine analysis
13.5: Problems
Calc
2.6: Spreadsheets and Computational Software
calculations
2.2: Concentration
2.8: Problems
calibration
1.2: The Analytical Perspective
2.4: Basic Equipment
3.5: Developing the Procedure
3.6: Protocols
3.10: Chapter Summary and Key Terms
4.2: Characterizing Experimental Errors
5.2: Calibrating the Signal
5.9: Chapter Summary and Key Terms
6.5: UV/Vis and IR Spectroscopy
calibration blank
5.5: Compensating for the Reagent Blank
calibration curve
3.5: Developing the Procedure
3.6: Protocols
3.10: Chapter Summary and Key Terms
5.3: Determining the Sensitivity
5.4: Linear Regression and Calibration Curves
5.5: Compensating for the Reagent Blank
5.9: Chapter Summary and Key Terms
6.13.3: Applications of Raman Spectroscopy
6.14: Problems
9.5: Atomic Absorption Techniques
9.7.1: Emission Spectroscopy Based on Flame and Plasma Sources
9.7.2: Atomic Emission Spectroscopy
10.1.7: Applications of Chromatography
10.3: Problems
13.3.5: Membrane Ion-Selective Electrodes
calibration curves
5.7: Problems
5.8: Additional Resources
6.3: Spectroscopy Based on Absorption
calibration instructions
5.2: Calibrating the Signal
calibration standards
6.14: Problems
calibration techniques
5.8: Additional Resources
calomel electrodes
13.3.3: Reference Electrodes
cantilever
14.3: Scanning Probe Microscopes

capillary electrochromatography
10.2: Capillary Electrophoresis and Capillary Electrochromatography
10.2.4: Applications of Capillary Electrophoresis
capillary electrophoresis
10.2: Capillary Electrophoresis and Capillary Electrochromatography
10.2.2: Capillary Electrophoresis
10.2.3: Capillary Electrophoresis
10.5: Chapter Summary and Key Terms
capillary gel electrophoresis
10.2.3: Capillary Electrophoresis
10.2.4: Applications of Capillary Electrophoresis
capillary zone electrophoresis
10.2.3: Capillary Electrophoresis
10.2.4: Applications of Capillary Electrophoresis
10.3: Problems
10.5: Chapter Summary and Key Terms
carbohydrates
6.13.3: Applications of Raman Spectroscopy
carbon dioxide
6.11.1: Theory of Infrared Absorption Spectrometry
cathode
13.5: Problems
cathodic stripping voltammetry
13.4.6: Stripping Methods
cell potential
13.2.4: Calculation of Cell Potentials from Electrode Potentials
central limit theorem
4.4: The Distribution of Measurements and Results
4.11: Chapter Summary and Key Terms
central tendency
4.11: Chapter Summary and Key Terms
CGE
10.2.4: Applications of Capillary Electrophoresis
characterization analysis
1.7: Chapter Summary and Key Terms
characterizing composition
1.1: What is Analytical Chemistry
charge balance
10.3: Problems
12.6: Problems
charge balance equations
12.8: Chapter Summary and Key Terms
charge measurement
13.1: Overview of Electrochemistry
charge transfer
6.3: Spectroscopy Based on Absorption
Chauvenet’s criterion
4.11: Chapter Summary and Key Terms
Chauvenet's criterion
4.6: Statistical Methods for Normal Distributions
chemCal package
5.6: Using Excel and R for a Linear Regression
chemical analysis
1.1: What is Analytical Chemistry
6.12: Applications of Infrared Spectrometry
6.14: Problems
7.3: NMR Spectrometers
10.4: Additional Resources
13.6: Additional Resources
chemical analysis methods
10.3: Problems
chemical calculations
2.3: Stoichiometric Calculations
chemical concentrations
2.8: Problems
chemical education
12.7: Additional Resources
chemical equilibrium
12.1: Reversible Reactions and Chemical Equilibria
12.7: Additional Resources
chemical formulas
8.7: Applications of Molecular Mass Spectrometry
chemical interference
9.6: Atomic Absorption Spectroscopy
chemical interferences
1.2: The Analytical Perspective
3.4: Selecting an Analytical Method
6.16: Chapter Summary and Key Terms
9.7.2: Atomic Emission Spectroscopy
12.5: Ladder Diagrams
chemical kinetics
12.2: Thermodynamics and Equilibrium Chemistry
chemical measurement
5.8: Additional Resources
chemical measurements
1.1: What is Analytical Chemistry
chemical properties
1.7: Chapter Summary and Key Terms
chemical reaction
2.10: Chapter Summary and Key Terms
chemical reactions
2.3: Stoichiometric Calculations
8.2: Molecular Mass Spectra
12.2: Thermodynamics and Equilibrium Chemistry
12.3: Manipulating Equilibrium Constants
12.4: Equilibrium Constants for Chemical Reactions
12.5: Ladder Diagrams
12.7: Additional Resources
chemical reactivity
12.1: Reversible Reactions and Chemical Equilibria
12.8: Chapter Summary and Key Terms
14.1: Introduction to the Study of Surfaces
chemical selectivity
13.3.5: Membrane Ion-Selective Electrodes
chemical separation
10.3: Problems
chemical shift
7.2.2: The Basis for Differences in Chemical Shift
7.7.3: The Chemical Shift
7.7.4: Chemical Shifts in ^{1}H NMR Spectroscopy
chemical shifts
7.2: Environmental Effects on NMR Spectra
7.5: Carbon-13 NMR
chemical signal
3.3: Classifying Analytical Techniques
chemical stoichiometry
2.3: Stoichiometric Calculations
chemical structure
1.3: Common Analytical Problems
chemical systems
1.1: What is Analytical Chemistry
chemical techniques
3.2: Techniques, Methods, Procedures, and Protocols
chemicalinterferences
9.4: Interferences in Absorption Spectroscopy
chemicalShifts
7.4: Applications of Proton NMR
chemiluminescence
1.4: Types of Instrumental Methods
6.1: Overview of Spectroscopy
6.7: Emission Spectroscopy
6.9: Analytical Chemiluminescence
chemist perspective
2.9: Additional Resources
chemistry
8.1: General Features of Atomic Mass Spectrometry
10.1: Introduction to Chromatographic Separations
12.2: Thermodynamics and Equilibrium Chemistry
chemistry concepts
12.3: Manipulating Equilibrium Constants
chemistry education
4.7: Detection Limits
10.4: Additional Resources
chemistry research
1.1: What is Analytical Chemistry
chemistry skills
2.6: Spreadsheets and Computational Software
Chesapeake Bay
3.7: The Importance of Analytical Methodology
chromatogram analysis
10.3: Problems
chromatographic analysis
10.3: Problems
chromatography
8.6: Mass Spectrometers
10.1: Introduction to Chromatographic Separations
10.1.1: A General Description of Chromatography
10.1.5: Optimization and Column Performance
10.1.6: Summary of Important Relationships for Chromatography
10.1.7: Applications of Chromatography
10.4: Additional Resources
10.5: Chapter Summary and Key Terms
chromophores
6.3: Spectroscopy Based on Absorption
circulating penny
4.1: Characterizing Measurements and Results
Clark O2 electrode
13.7: Chapter Summary and Key Terms
classical techniques
3.3: Classifying Analytical Techniques
Claude Berthollet
12.1: Reversible Reactions and Chemical Equilibria
clinical applications
6.5: UV/Vis and IR Spectroscopy
clinical assays
1.2: The Analytical Perspective
1.6: Additional Resources
cocaine detection
13.5: Problems
coefficient of friction
10.2.3.1: Ionic Mobility and Electrophoresis
collaboration
1.2: The Analytical Perspective
ColloidalParticles
6.13.4: Other Types of Raman Spectroscopy
colorimetric assays
1.6: Additional Resources
column efficiency
10.1.3: Zone Broadening and Column Efficiency
10.5: Chapter Summary and Key Terms
column selectivity
10.5: Chapter Summary and Key Terms
combustion gases
9.2: Sample Atomization Techniques
Commission of Sciences and Arts
12.1: Reversible Reactions and Chemical Equilibria
compensating for interferences
3.5: Developing the Procedure
complex materials
1.7: Chapter Summary and Key Terms
complexation equilibria
12.5: Ladder Diagrams
complexation reactions
12.4: Equilibrium Constants for Chemical Reactions
12.6: Problems

complexation titrimetric method
3.4: Selecting an Analytical Method
compounds
8.1: General Features of Atomic Mass Spectrometry
computational packages
5.8: Additional Resources
computational software
2.6: Spreadsheets and Computational Software
concentration
2.2: Concentration
2.10: Chapter Summary and Key Terms
12.2: Thermodynamics and Equilibrium Chemistry
concentration calculation
2.5: Preparing Solutions
5.3: Determining the Sensitivity
13.5: Problems
concentration determination
10.3: Problems
concentration measurement
4.3: Propagation of Uncertainty
concentration method
3.8: Problems
concentration technique
3.10: Chapter Summary and Key Terms
concentration techniques
3.3: Classifying Analytical Techniques
concentration units
2.5: Preparing Solutions
2.8: Problems
conductivity
13.2: An Introduction to Electroanalytical Chemistry
confidence in detection
4.7: Detection Limits
confidence interval
4.5: Statistical Analysis of Data
4.6: Statistical Methods for Normal Distributions
4.11: Chapter Summary and Key Terms
5.4: Linear Regression and Calibration Curves
confidence intervals
4.4: The Distribution of Measurements and Results
confidence level
4.5: Statistical Analysis of Data
conservation of mass
8.1: General Features of Atomic Mass Spectrometry
constant determinate error
4.2: Characterizing Experimental Errors
constant error
5.5: Compensating for the Reagent Blank
continuing calibration verification
3.6: Protocols
Contract Laboratory Program
3.6: Protocols
cooperative venture
3.7: The Importance of Analytical Methodology
copper electrode
13.3.4: Metallic Indicator Electrodes
correlation_spectroscopy
7: Nuclear Magnetic Resonance Spectroscopy
cost
3.4: Selecting an Analytical Method
COSY
7.6: Two-Dimensional Fourier Transform NMR
coulometric methods
13.7: Chapter Summary and Key Terms
coulometry
13.1: Overview of Electrochemistry
13.2.6: Types of Electroanalytical Methods
13.5: Problems
13.6: Additional Resources
13.7: Chapter Summary and Key Terms
coupling constant
7.7.6: Spin-Spin Splitting in ^{1}H NMR Spectra
CRAN
2.6: Spreadsheets and Computational Software
critical value
4.6: Statistical Methods for Normal Distributions
Cu analysis
2.5: Preparing Solutions
Cu2+
13.3.4: Metallic Indicator Electrodes
current
13.4: Voltammetry
13.4.1: Potential Excitation Signals and Currents in Voltammetry
current control
13.1: Overview of Electrochemistry
current measurement
13.1: Overview of Electrochemistry
13.2: An Introduction to Electroanalytical Chemistry
13.4.2: Voltammetric Instrumentation
currentmeasurement
14.3: Scanning Probe Microscopes
curvilinear regression
5.4: Linear Regression and Calibration Curves
cyclic voltammetry
13.4: Voltammetry
13.4.4: Cyclic Voltammetry
13.4.7: Applications of Voltammetry
13.5: Problems
13.6: Additional Resources

D

D2lamp
9.4: Interferences in Absorption Spectroscopy
data analysis
2.6: Spreadsheets and Computational Software
4.8: Using Excel and R to Analyze Data
4.9: Problems
4.11: Chapter Summary and Key Terms
5.5: Compensating for the Reagent Blank
5.6: Using Excel and R for a Linear Regression
5.8: Additional Resources
6.6: Signals and Noise
data collection
3.7: The Importance of Analytical Methodology
data evaluation
4.10: Additional Resources
data processing
7.3: NMR Spectrometers
data sets
4.8: Using Excel and R to Analyze Data
data spread
4.11: Chapter Summary and Key Terms
data visualization
4.8: Using Excel and R to Analyze Data
4.10: Additional Resources
data visualization techniques
4.10: Additional Resources
degrees of freedom
4.4: The Distribution of Measurements and Results
4.6: Statistical Methods for Normal Distributions
4.11: Chapter Summary and Key Terms
delta scale
7.7.3: The Chemical Shift
density
2.8: Problems
DEPT
7.7.12: DEPT ^{13}C NMR Spectroscopy
depth profiling
14.1: Introduction to the Study of Surfaces
derived SI units
2.1: Measurements in Analytical Chemistry
descriptive statistics
4.8: Using Excel and R to Analyze Data
desiccant
2.4: Basic Equipment
2.10: Chapter Summary and Key Terms
desiccator
2.4: Basic Equipment
2.10: Chapter Summary and Key Terms
design criteria
3.4: Selecting an Analytical Method
detection
8.6: Mass Spectrometers
detection limit
3.6: Protocols
3.10: Chapter Summary and Key Terms
4.7: Detection Limits
4.11: Chapter Summary and Key Terms
detection limits
3.7: The Importance of Analytical Methodology
4.10: Additional Resources
6.8: Photoluminescent Spectroscopy
9.7.2: Atomic Emission Spectroscopy
13.4.6: Stripping Methods
detection of outliers
4.10: Additional Resources
DetectionLimits
6.13.4: Other Types of Raman Spectroscopy
detector
6.10.2: Radiation Transducers
9.3: Atomic Absorption Instrumentation
determinate error
4.6: Statistical Methods for Normal Distributions
determinate errors
4.2: Characterizing Experimental Errors
4.11: Chapter Summary and Key Terms
5.2: Calibrating the Signal
5.9: Chapter Summary and Key Terms
determination
3.1: Analysis, Determination, and Measurement
3.10: Chapter Summary and Key Terms
developing regions
1.2: The Analytical Perspective
diamagnetic anisotropy
7.2.2: The Basis for Differences in Chemical Shift
diamagnetic deshielding
7.2.2: The Basis for Differences in Chemical Shift
diamagnetic shielding
7.2.2: The Basis for Differences in Chemical Shift
diastereotopic
7.7.7: ^{1}H NMR Spectroscopy and Proton Equivalence
differential amplifier
6.6.3: Signal-to-Noise Enhancement
differential pulse polarography
13.4.7: Applications of Voltammetry
differential scanning calorimetry
11: Thermal Methods
11.2: Differential Thermal Analysis and Differential Scanning Calorimetry

differential thermal analysis
11: Thermal Methods
11.2: Differential Thermal Analysis and Differential Scanning Calorimetry
diffuse reflectance spectrometry
6.12.2: Mid-Infrared Reflection Spectrometry
diffusion layer
13.1: Overview of Electrochemistry
digital micropipet
2.4: Basic Equipment
dilution
2.5: Preparing Solutions
2.10: Chapter Summary and Key Terms
dilution series
2.8: Problems
dipole
6.11: An Introduction to Infrared Spectrometry
direct current plasma
9.7: Atomic Emission Spectroscopy
dispersive instruments
6.13.2: Instrumentation
dissociation of water
12.4: Equilibrium Constants for Chemical Reactions
Distortions Enhancement by Polarization Transfer
7.7.12: DEPT ^{13}C NMR Spectroscopy
distribution constant
10.1.2: Migration Rates of Solutes
disulfiram analysis
2.3: Stoichiometric Calculations
dot chart
4.8: Using Excel and R to Analyze Data
4.11: Chapter Summary and Key Terms
doublet
7.7.6: Spin-Spin Splitting in ^1H NMR Spectra
drinking water
3.1: Analysis, Determination, and Measurement
3.2: Techniques, Methods, Procedures, and Protocols
3.4: Selecting an Analytical Method
drying ovens
2.4: Basic Equipment
drying samples
2.4: Basic Equipment
duplicate samples
3.6: Protocols
dynamic techniques
13.1: Overview of Electrochemistry
13.2: An Introduction to Electroanalytical Chemistry
13.2.6: Types of Electroanalytical Methods

E

Eddy Diffusion Broadening
10.1.4: Chromatography
education
1.6: Additional Resources
13.6: Additional Resources
educational experiments
10.4: Additional Resources
effective nuclear charge
6.4.5: Semiconductors
Egypt
12.1: Reversible Reactions and Chemical Equilibria
elastic scattering
6.13: Raman Spectroscopy
elective affinities
12.1: Reversible Reactions and Chemical Equilibria
electrical
6.11: An Introduction to Infrared Spectrometry
electroanalytical
10.1: Introduction to Chromatographic Separations
electrochemical
13.3: Potentiometry
13.4: Voltammetry
13.4.1: Potential Excitation Signals and Currents in Voltammetry
electrochemical analysis
13.7: Chapter Summary and Key Terms
electrochemical cell
13.2.1: Electrochemical Cells
13.3.4: Metallic Indicator Electrodes
13.3.5: Membrane Ion-Selective Electrodes
electrochemical cell potential
13.5: Problems
electrochemical cells
13.1: Overview of Electrochemistry
13.2: An Introduction to Electroanalytical Chemistry
13.4.2: Voltammetric Instrumentation
13.5: Problems
electrochemical experiments
13.2.6: Types of Electroanalytical Methods
electrochemical irreversibility
13.5: Problems
electrochemical methods
3.4: Selecting an Analytical Method
13.6: Additional Resources
electrochemical techniques
1.4: Types of Instrumental Methods
13.1: Overview of Electrochemistry
13.2: An Introduction to Electroanalytical Chemistry
13.4.6: Stripping Methods
electrochemistry
3.3: Classifying Analytical Techniques
13.1: Overview of Electrochemistry
13.2: An Introduction to Electroanalytical Chemistry
13.2.6: Types of Electroanalytical Methods
13.4.2: Voltammetric Instrumentation
13.4.7: Applications of Voltammetry
13.6: Additional Resources
13.7: Chapter Summary and Key Terms
electrode
13.4.1: Potential Excitation Signals and Currents in Voltammetry
electrode oxidation
13.4.2: Voltammetric Instrumentation
electrode potential
13.1: Overview of Electrochemistry
electrode potentials
13.2: An Introduction to Electroanalytical Chemistry
electrodes
13.1: Overview of Electrochemistry
13.2.1: Electrochemical Cells
13.3: Potentiometry
13.4.2: Voltammetric Instrumentation
13.6: Additional Resources
electrolytic cell
13.2.1: Electrochemical Cells
electromagnetic radiation
6.1: Overview of Spectroscopy
6.3: Spectroscopy Based on Absorption
6.16: Chapter Summary and Key Terms
electromagnetic spectrum
6.1: Overview of Spectroscopy
electron
6.10.2: Radiation Transducers
electron configurations
6.8: Photoluminescent Spectroscopy
electron spectroscopy for chemical analysis
14.4.1: X-ray Photoelectron Spectroscopy
electronbeam
14.3: Scanning Probe Microscopes
electronic balance
2.4: Basic Equipment
5.2: Calibrating the Signal
electronic energy levels
6.3: Spectroscopy Based on Absorption
electronic transition
6.7: Emission Spectroscopy
electronmicroscope
14.2: Scanning Electron Microscopy
electrons
8.1: General Features of Atomic Mass Spectrometry
14.2: Scanning Electron Microscopy
electroosmotic flow
10.2.3: Capillary Electrophoresis
electroosmotic mobility
10.2.2: Capillary Electrophoresis
electrophoresis
10.2.1: An Overview of Electrophoresis
10.2.3.1: Ionic Mobility and Electrophoresis
10.3: Problems
10.4: Additional Resources
10.5: Chapter Summary and Key Terms
electrophoretic mobility
10.2.2: Capillary Electrophoresis
10.2.3: Capillary Electrophoresis
10.3: Problems
Electrospray Mass Spectrometry
8.5.1: Electrospray Ionization Mass Spectrometry
electrothermal atomization
9: Atomic Spectroscopy
9.2: Sample Atomization Techniques
9.5: Atomic Absorption Techniques
9.6: Atomic Absorption Spectroscopy
elemental analysis
1.3: Common Analytical Problems
9.2: Sample Atomization Techniques
elements
8.1: General Features of Atomic Mass Spectrometry
elution chromatography
10.1.1: A General Description of Chromatography
emission
1.4: Types of Instrumental Methods
6.7: Emission Spectroscopy
9.7.1: Emission Spectroscopy Based on Flame and Plasma Sources
emission intensity
6.14: Problems
emission lines
9.3: Atomic Absorption Instrumentation
emission spectroscopy
6.1: Overview of Spectroscopy
9.7: Atomic Emission Spectroscopy
emission spectrum
6.8: Photoluminescent Spectroscopy
enantiotopic
7.7.7: ^1H NMR Spectroscopy and Proton Equivalence
endothermic
12.2: Thermodynamics and Equilibrium Chemistry
energy
12.2: Thermodynamics and Equilibrium Chemistry
energy changes
12.2: Thermodynamics and Equilibrium Chemistry
energy level diagram
9.7.2: Atomic Emission Spectroscopy
energy release
6.7: Emission Spectroscopy

energy transfer
1.4: Types of Instrumental Methods
6.1: Overview of Spectroscopy
engineering
12.2: Thermodynamics and Equilibrium Chemistry
enhancement
6.6: Signals and Noise
enthalpy
12.2: Thermodynamics and Equilibrium Chemistry
entropy
12.2: Thermodynamics and Equilibrium Chemistry
environmental analysis
3.2: Techniques, Methods, Procedures, and Protocols
6.12.1: Mid-Infrared Absorption Spectometry
environmental applications
6.5: UV/Vis and IR Spectroscopy
environmental chemistry
4.7: Detection Limits
6.15: Additional Resources
environmental exposure
1.2: The Analytical Perspective
environmental monitoring
3.7: The Importance of Analytical Methodology
environmental noise
6.6.2: Sources of Instrumental Noise
environmental problem solving
2.9: Additional Resources
Environmental Protection Agency
3.6: Protocols
environmental samples
13.4.7: Applications of Voltammetry
environmental system
3.7: The Importance of Analytical Methodology
environmental_effects
7: Nuclear Magnetic Resonance Spectroscopy
enzyme electrodes
13.7: Chapter Summary and Key Terms
EPA protocols
3.2: Techniques, Methods, Procedures, and Protocols
EPA standards
3.7: The Importance of Analytical Methodology
equilibrium
12.2: Thermodynamics and Equilibrium Chemistry
equilibrium arrow
12.1: Reversible Reactions and Chemical Equilibria
equilibrium calculations
12.3: Manipulating Equilibrium Constants
equilibrium chemistry
12.5: Ladder Diagrams
12.7: Additional Resources
12.8: Chapter Summary and Key Terms
equilibrium concentrations
12.7: Additional Resources
equilibrium constant
6.14: Problems
12.2: Thermodynamics and Equilibrium Chemistry
12.4: Equilibrium Constants for Chemical Reactions
12.6: Problems
equilibrium constants
1.3: Common Analytical Problems
6.5: UV/Vis and IR Spectroscopy
12.3: Manipulating Equilibrium Constants
12.5: Ladder Diagrams
12.7: Additional Resources
equilibrium problems
12.6: Problems
equilibrium relationships
12.3: Manipulating Equilibrium Constants
equilibrium simulations
12.7: Additional Resources
equilibrium system
12.8: Chapter Summary and Key Terms
equipment
3.4: Selecting an Analytical Method
5.2: Calibrating the Signal
error analysis
4.10: Additional Resources
5.8: Additional Resources
error detection
4.2: Characterizing Experimental Errors
error estimation
4.3: Propagation of Uncertainty
error propagation
4.10: Additional Resources
errors
4.11: Chapter Summary and Key Terms
errors in x
5.4: Linear Regression and Calibration Curves
errors in y
5.4: Linear Regression and Calibration Curves
ESCA
14.4.1: X-ray Photoelectron Spectroscopy
estimation
2.6: Spreadsheets and Computational Software
ethanol
6.11.1: Theory of Infrared Absorption Spectrometry
ethanol analysis
2.8: Problems
examples
2.2: Concentration
Excel
4.8: Using Excel and R to Analyze Data
5.6: Using Excel and R for a Linear Regression
Excel functions
4.8: Using Excel and R to Analyze Data
Excel statistics
4.10: Additional Resources
excitation
9.7.2: Atomic Emission Spectroscopy
excitation spectrum
6.8: Photoluminescent Spectroscopy
excited state
6.7: Emission Spectroscopy
exothermic
12.2: Thermodynamics and Equilibrium Chemistry
experimental data
4.10: Additional Resources
5.8: Additional Resources
experimental design
1.2: The Analytical Perspective
3.7: The Importance of Analytical Methodology
experimental error
4.3: Propagation of Uncertainty
experimental errors
4.2: Characterizing Experimental Errors
experimental methods
4.9: Problems
experimental optimization
2.6: Spreadsheets and Computational Software
experiments
13.6: Additional Resources
exploratory data analysis
4.5: Statistical Analysis of Data
external standardization
5.4: Linear Regression and Calibration Curves
external standards
5.3: Determining the Sensitivity
5.8: Additional Resources
5.9: Chapter Summary and Key Terms

F

faradaic current
13.2.1: Electrochemical Cells
Faraday's law
13.7: Chapter Summary and Key Terms
Fe3+ reaction
2.3: Stoichiometric Calculations
fecal coliform bacteria
3.1: Analysis, Determination, and Measurement
feedback loop
1.2: The Analytical Perspective
fiber optic probes
6.13.2: Instrumentation
field
6.11: An Introduction to Infrared Spectrometry
field bioassays
1.2: The Analytical Perspective
filtering
6.6.3: Signal-to-Noise Enhancement
filtration
3.8: Problems
flame atomization
9: Atomic Spectroscopy
9.2: Sample Atomization Techniques
9.5: Atomic Absorption Techniques
9.6: Atomic Absorption Spectroscopy
flame emission
9.7.2: Atomic Emission Spectroscopy
flameatomization
9.4: Interferences in Absorption Spectroscopy
flicker noise
6.6.2: Sources of Instrumental Noise
flow rate
10.1.6: Summary of Important Relationships for Chromatography
flow rate optimization
10.3: Problems
fluorescence
6.8: Photoluminescent Spectroscopy
6.13.2: Instrumentation
6.14: Problems
6.15: Additional Resources
6.16: Chapter Summary and Key Terms
fluorescence accuracy
6.8: Photoluminescent Spectroscopy
fluorescence precision
6.8: Photoluminescent Spectroscopy
fluorescence probability
6.8: Photoluminescent Spectroscopy
fluorescence spectroscopy
6.8: Photoluminescent Spectroscopy
fluoridation
2.8: Problems
fluoride analysis
13.5: Problems
fluorimeter
6.8: Photoluminescent Spectroscopy
forensic science
1.3: Common Analytical Problems
formality
2.2: Concentration
2.10: Chapter Summary and Key Terms
formation constant
12.6: Problems

formation constants
12.4: Equilibrium Constants for Chemical Reactions
12.8: Chapter Summary and Key Terms
Fourier transforms
6.15: Additional Resources
Fourier_transform
7: Nuclear Magnetic Resonance Spectroscopy
fragmentation
8: Molecular Mass Spectrometry
8.2: Molecular Mass Spectra
Fragmentation Pattern (Mass Spectroscopy)
8.7.4: The Mass Spectra of Elements
8.7.5: Fragmentation Patterns in Mass Spectra
fragmentation patterns
8.7: Applications of Molecular Mass Spectrometry
Fragmentation Patterns (mass spec)
8.7.6: Mass Spectrometry - Fragmentation Patterns
French Egyptian expedition
12.1: Reversible Reactions and Chemical Equilibria
FTIR
6.11.3: FTIR- Hardware
fundamental analysis
1.3: Common Analytical Problems
1.7: Chapter Summary and Key Terms

G

galvanic cell
13.2.1: Electrochemical Cells
galvanostat
13.1: Overview of Electrochemistry
gas chromatography
8: Molecular Mass Spectrometry
8.7: Applications of Molecular Mass Spectrometry
10.3: Problems
10.4: Additional Resources
10.5: Chapter Summary and Key Terms
gas lasers
6.4.1: Gas Lasers
GFAAS
3.2: Techniques, Methods, Procedures, and Protocols
Gibbs free energy
12.2: Thermodynamics and Equilibrium Chemistry
12.7: Additional Resources
glassware
5.1: Analytical Signals
glassware calibration
2.4: Basic Equipment
glucose concentration
1.3: Common Analytical Problems
13.5: Problems
glucose sensor
13.5: Problems
glycolic acid analysis
3.8: Problems
GMP
3.9: Additional Resources
Google Sheets
2.6: Spreadsheets and Computational Software
graduated cylinder
2.4: Basic Equipment
2.10: Chapter Summary and Key Terms
graph preparation
2.6: Spreadsheets and Computational Software
graphite furnace atomic absorption spectroscopy
3.2: Techniques, Methods, Procedures, and Protocols
3.6: Protocols
gravimetric method
3.4: Selecting an Analytical Method
gravimetry
3.3: Classifying Analytical Techniques
Grubb’s test
4.11: Chapter Summary and Key Terms
Grubb's test
4.6: Statistical Methods for Normal Distributions
guidelines
3.6: Protocols

H

H2SO4
2.3: Stoichiometric Calculations
hanging mercury drop
13.4.6: Stripping Methods
hardware
6.6: Signals and Noise
histogram
4.8: Using Excel and R to Analyze Data
4.11: Chapter Summary and Key Terms
historical development
9.7.2: Atomic Emission Spectroscopy
history of analytical chemistry
1.6: Additional Resources
history of chemistry
1.1: What is Analytical Chemistry
hollow cathode lamp
9.3: Atomic Absorption Instrumentation
9.6: Atomic Absorption Spectroscopy
homotopic
7.7.7: ^{1}H NMR Spectroscopy and Proton Equivalence
Horowitz ratio
4.2: Characterizing Experimental Errors
HPLC
10.3: Problems
hydrodynamic voltammetry
13.7: Chapter Summary and Key Terms
hydrodynamic voltammogram
13.5: Problems
hydrogen sulfide concentration
13.5: Problems
hydroxide complex
13.5: Problems
hypothesis testing
4.5: Statistical Analysis of Data
4.6: Statistical Methods for Normal Distributions
hypoxanthine analysis
3.8: Problems

I

identification
8.7: Applications of Molecular Mass Spectrometry
imagingtechniques
14.3: Scanning Probe Microscopes
improving methods
1.1: What is Analytical Chemistry
impurities
5.1: Analytical Signals
14.1: Introduction to the Study of Surfaces
incubation
3.1: Analysis, Determination, and Measurement
indeterminate error
4.6: Statistical Methods for Normal Distributions
4.11: Chapter Summary and Key Terms
indeterminate errors
4.2: Characterizing Experimental Errors
4.11: Chapter Summary and Key Terms
5.4: Linear Regression and Calibration Curves
indicator electrodes
13.3.4: Metallic Indicator Electrodes
inductively coupled plasma
9.7: Atomic Emission Spectroscopy
industrial applications
6.5: UV/Vis and IR Spectroscopy
inelastic scattering
6.13: Raman Spectroscopy
inferential data analysis
4.5: Statistical Analysis of Data
infrared
6.11: An Introduction to Infrared Spectrometry
6.11.1: Theory of Infrared Absorption Spectrometry
infrared radiation
6.1: Overview of Spectroscopy
infrared spectra
6.3: Spectroscopy Based on Absorption
infrared spectromters
6.11.4: Infrared Instruments
infrared spectroscopy
1.3: Common Analytical Problems
6.5: UV/Vis and IR Spectroscopy
6.11.1: Theory of Infrared Absorption Spectrometry
6.12: Applications of Infrared Spectrometry
6.12.1: Mid-Infrared Absorption Spectometry
infrared transducer
6.11.2: Infrared Sources and Transducers
initial calibration verification
3.6: Protocols
inorganic analytes
6.8: Photoluminescent Spectroscopy
inorganic compounds
6.13.3: Applications of Raman Spectroscopy
inorganic ions
1.3: Common Analytical Problems
instrumental analysis
1.6: Additional Resources
6.15: Additional Resources
instrumental limitations
6.3: Spectroscopy Based on Absorption
6.14: Problems
instrumental methods
1.4: Types of Instrumental Methods
instrumental techniques
1.3: Common Analytical Problems
3.3: Classifying Analytical Techniques
instrumentation
5.2: Calibrating the Signal
6.5: UV/Vis and IR Spectroscopy
6.13: Raman Spectroscopy
6.13.2: Instrumentation
9.6: Atomic Absorption Spectroscopy
9.7.2: Atomic Emission Spectroscopy
14.2: Scanning Electron Microscopy
instruments
6.11: An Introduction to Infrared Spectrometry
13.3: Potentiometry
intensity ratio
7.2: Environmental Effects on NMR Spectra
interdisciplinary
1.6: Additional Resources
interfacial techniques
13.2.6: Types of Electroanalytical Methods
interference
3.5: Developing the Procedure
3.10: Chapter Summary and Key Terms

interference analysis
3.8: Problems
interferencecompensation
9.4: Interferences in Absorption Spectroscopy
interferences
9: Atomic Spectroscopy
interferent
3.10: Chapter Summary and Key Terms
interferometer
6.1: Overview of Spectroscopy
interlaboratory exercises
4.10: Additional Resources
internal conversion
6.8: Photoluminescent Spectroscopy
internal reflection
6.12.2: Mid-Infrared Reflection Spectrometry
internal standard
10.3: Problems
internal standardization
5.7: Problems
internal standards
5.3: Determining the Sensitivity
5.8: Additional Resources
5.9: Chapter Summary and Key Terms
internalStandard
7.4: Applications of Proton NMR
intersystem crossing
6.8: Photoluminescent Spectroscopy
introduction to analytical chemistry
1.6: Additional Resources
intuitive thinking
2.6: Spreadsheets and Computational Software
2.9: Additional Resources
inverse reaction
12.3: Manipulating Equilibrium Constants
iodized salt analysis
13.5: Problems
ion activity
13.3.5: Membrane Ion-Selective Electrodes
ion chromatography
10.3: Problems
ionic activity
12.7: Additional Resources
ionic strength
12.6: Problems
12.7: Additional Resources
12.8: Chapter Summary and Key Terms
ionization
8.6: Mass Spectrometers
ions
8: Molecular Mass Spectrometry
8.6: Mass Spectrometers
iR drop
13.2.5: Currents in Electrochemical Cells
IR radiation
6.12.1: Mid-Infrared Absorption Spectometry
6.16: Chapter Summary and Key Terms
IR spectroscopy
6.15: Additional Resources
IR spectrum
6.11.1: Theory of Infrared Absorption Spectrometry
isotope ratios
9.7.3: Inductively Coupled Plasma Mass Spectrometer
IUPAC
3.9: Additional Resources
4.7: Detection Limits

J

J. Chem. Educ.
6.15: Additional Resources
John Dalton
8.1: General Features of Atomic Mass Spectrometry

K

Ka
12.4: Equilibrium Constants for Chemical Reactions
Kb
12.4: Equilibrium Constants for Chemical Reactions
KBrO3 preparation
2.5: Preparing Solutions
kernel density plot
4.8: Using Excel and R to Analyze Data
4.11: Chapter Summary and Key Terms
KI analysis
13.5: Problems
kidney stones
2.3: Stoichiometric Calculations
kilogram
2.9: Additional Resources

L

laboratory
3.6: Protocols
laboratory equipment
2.10: Chapter Summary and Key Terms
laboratory experiments
6.15: Additional Resources
laboratory notebook
2.9: Additional Resources
laboratory reports
2.9: Additional Resources
ladder diagrams
12.5: Ladder Diagrams
12.6: Problems
lasers
6.4: Lasers
6.4.3: Overview of Lasers
Le Chatelier's principle
12.8: Chapter Summary and Key Terms
lead analysis
3.2: Techniques, Methods, Procedures, and Protocols
lead detection
3.4: Selecting an Analytical Method
5.3: Determining the Sensitivity
lead reduction
13.5: Problems
ligand detection
10.3: Problems
light absorption
9: Atomic Spectroscopy
light behavior
6.1: Overview of Spectroscopy
light scattering
6.14: Problems
limit of identification
4.7: Detection Limits
4.11: Chapter Summary and Key Terms
limit of quantitation
4.7: Detection Limits
4.11: Chapter Summary and Key Terms
limitations to Beer's law
6.3: Spectroscopy Based on Absorption
linear regression
5.3: Determining the Sensitivity
5.4: Linear Regression and Calibration Curves
5.6: Using Excel and R for a Linear Regression
5.7: Problems
5.8: Additional Resources
5.9: Chapter Summary and Key Terms
linear regression model
5.4: Linear Regression and Calibration Curves
linear regresssion
5.6: Using Excel and R for a Linear Regression
linear sweep
13.4: Voltammetry
Linear Sweep Voltammetry
13.4.3: Linear Sweep Voltammetry
liquid chromatography
8.7: Applications of Molecular Mass Spectrometry
Liquid Junction Potentials
13.2.2: Potentials in Electroanalytical Cells
long term trends
3.7: The Importance of Analytical Methodology
low concentrations
1.7: Chapter Summary and Key Terms
luminescence
6.15: Additional Resources

M

M+1 peak (mass spec)
8.7.3: The M+1 Peak
magnetic field
7.2: Environmental Effects on NMR Spectra
7.3: NMR Spectrometers
magnetogyric ratio
7.5: Carbon-13 NMR
magnification
14.2: Scanning Electron Microscopy
mass
14: Surface Characterization by Spectroscopy and Microscopy
mass analyzers
8.6: Mass Spectrometers
8.6.1: Mass Analyzers (Mass Spectrometry)
mass and amount
2.9: Additional Resources
mass balance
12.6: Problems
mass balance equations
12.8: Chapter Summary and Key Terms
mass measurement
2.4: Basic Equipment
5.2: Calibrating the Signal
mass of a penny
4.1: Characterizing Measurements and Results
mass spectrometers
8: Molecular Mass Spectrometry
mass spectrometry
1.3: Common Analytical Problems
1.4: Types of Instrumental Methods
8: Molecular Mass Spectrometry
8.1: General Features of Atomic Mass Spectrometry
8.6: Mass Spectrometers
8.7: Applications of Molecular Mass Spectrometry
14.1: Introduction to the Study of Surfaces
mass spectrum
8.2: Molecular Mass Spectra
math in chemistry
4.3: Propagation of Uncertainty
Mathematica
2.6: Spreadsheets and Computational Software

Matlab
2.6: Spreadsheets and Computational Software
matrix
3.1: Analysis, Determination, and Measurement
3.10: Chapter Summary and Key Terms
matrix effect
5.5: Compensating for the Reagent Blank
9.7.3: Inductively Coupled Plasma Mass Spectrometer
matrix effects
5.3: Determining the Sensitivity
matrix interference
9.5: Atomic Absorption Techniques
9.6: Atomic Absorption Spectroscopy
matrix matching
5.9: Chapter Summary and Key Terms
maximum contaminant level
3.1: Analysis, Determination, and Measurement
mean
4.1: Characterizing Measurements and Results
4.8: Using Excel and R to Analyze Data
4.11: Chapter Summary and Key Terms
mean comparison
4.6: Statistical Methods for Normal Distributions
measurement
3.1: Analysis, Determination, and Measurement
3.3: Classifying Analytical Techniques
3.10: Chapter Summary and Key Terms
6.6: Signals and Noise
measurement error
4.11: Chapter Summary and Key Terms
measurement errors
4.2: Characterizing Experimental Errors
measurement precision
4.2: Characterizing Experimental Errors
measurement strategies
1.1: What is Analytical Chemistry
measurement uncertainty
2.1: Measurements in Analytical Chemistry
measurements
1.7: Chapter Summary and Key Terms
2.1: Measurements in Analytical Chemistry
2.10: Chapter Summary and Key Terms
13.4.1: Potential Excitation Signals and Currents in Voltammetry
measures of central tendency
4.1: Characterizing Measurements and Results
measures of spread
4.1: Characterizing Measurements and Results
median
4.1: Characterizing Measurements and Results
4.8: Using Excel and R to Analyze Data
4.11: Chapter Summary and Key Terms
medication efficacy
4.5: Statistical Analysis of Data
MEKC
10.2.4: Applications of Capillary Electrophoresis
membrane electrode
13.5: Problems
membrane electrodes
13.7: Chapter Summary and Key Terms
membrane potential
13.3.5: Membrane Ion-Selective Electrodes
meniscus
2.10: Chapter Summary and Key Terms
mercury film electrode
13.4.6: Stripping Methods
metal ion deposition
13.4.6: Stripping Methods
metal ion reversibility
13.5: Problems
metallic electrodes
13.3.4: Metallic Indicator Electrodes
13.7: Chapter Summary and Key Terms
metals
6.13.4: Other Types of Raman Spectroscopy
method
3.10: Chapter Summary and Key Terms
method blank
3.5: Developing the Procedure
3.6: Protocols
3.10: Chapter Summary and Key Terms
4.7: Detection Limits
method development
3.2: Techniques, Methods, Procedures, and Protocols
3.5: Developing the Procedure
method error
4.11: Chapter Summary and Key Terms
5.5: Compensating for the Reagent Blank
method errors
4.2: Characterizing Experimental Errors
method of standard additions
5.9: Chapter Summary and Key Terms
method selectivity
3.8: Problems
method specificity
3.4: Selecting an Analytical Method
method standardization
5.3: Determining the Sensitivity
method validation
3.5: Developing the Procedure
method's sensitivity
4.7: Detection Limits
micellar electrokinetic capillary chromatography
10.2.4: Applications of Capillary Electrophoresis
10.5: Chapter Summary and Key Terms
microfluidic devices
1.2: The Analytical Perspective
1.3: Common Analytical Problems
1.6: Additional Resources
microscopy
14: Surface Characterization by Spectroscopy and Microscopy
Microsoft Excel
2.6: Spreadsheets and Computational Software
minerals
6.13.3: Applications of Raman Spectroscopy
mobile phase
10.1: Introduction to Chromatographic Separations
10.1.1: A General Description of Chromatography
10.1.6: Summary of Important Relationships for Chromatography
10.1.7: Applications of Chromatography
10.5: Chapter Summary and Key Terms
mobile_phase
10.1.5: Optimization and Column Performance
modern analytical chemistry
1.6: Additional Resources
modulation
6.6.3: Signal-to-Noise Enhancement
molality
2.2: Concentration
2.10: Chapter Summary and Key Terms
molar absorptivity
6.14: Problems
molar concentration
6.14: Problems
molarity
2.2: Concentration
2.5: Preparing Solutions
2.8: Problems
2.10: Chapter Summary and Key Terms
molecular analysis
6.5: UV/Vis and IR Spectroscopy
molecular fluorescence analysis
6.8: Photoluminescent Spectroscopy
molecular ion
8.2: Molecular Mass Spectra
8.7.2: The Molecular Ion (M^+) Peak
8.7.5: Fragmentation Patterns in Mass Spectra
molecular mass spectra
8: Molecular Mass Spectrometry
molecular structure
7.5: Carbon-13 NMR
molecular transitions
6.3: Spectroscopy Based on Absorption
molecular vibrations
6.11.1: Theory of Infrared Absorption Spectrometry
molecular weight
2.3: Stoichiometric Calculations
8.7: Applications of Molecular Mass Spectrometry
molecular weight analysis
10.3: Problems
monochromator
6.1: Overview of Spectroscopy
9.3: Atomic Absorption Instrumentation
monoprotic acids
12.4: Equilibrium Constants for Chemical Reactions
muffle furnace
2.4: Basic Equipment
multicomponent samples
6.3: Spectroscopy Based on Absorption
multidisciplinary research
1.1: What is Analytical Chemistry
multielemental analysis
9.7.1: Emission Spectroscopy Based on Flame and Plasma Sources
9.7.2: Atomic Emission Spectroscopy
multiplet
7.7.6: Spin-Spin Splitting in ^{1}H NMR Spectra
multivariate calibration
5.8: Additional Resources
multivariate regression
5.4: Linear Regression and Calibration Curves
municipal water department
3.1: Analysis, Determination, and Measurement

N

Na2CO3
12.1: Reversible Reactions and Chemical Equilibria
Na2S2O3 reaction
2.3: Stoichiometric Calculations
NaCl
12.1: Reversible Reactions and Chemical Equilibria
NaCl solutions
2.8: Problems
nanotechnology
14.3: Scanning Probe Microscopes
nanowires
14.2: Scanning Electron Microscopy
NaOH
5.1: Analytical Signals
NaOH solution
2.5: Preparing Solutions

Napoleon's expedition
12.1: Reversible Reactions and Chemical Equilibria
National Institute for Standards and Technology
5.2: Calibrating the Signal
National Institute of Standards and Technology
2.9: Additional Resources
Natron
12.1: Reversible Reactions and Chemical Equilibria
Natron Lakes
12.1: Reversible Reactions and Chemical Equilibria
natural pigments
6.13.3: Applications of Raman Spectroscopy
nebulizer
9.2: Sample Atomization Techniques
nephelometry
6.16: Chapter Summary and Key Terms
Nernst
13.3: Potentiometry
Nernst equation
12.4: Equilibrium Constants for Chemical Reactions
12.5: Ladder Diagrams
12.8: Chapter Summary and Key Terms
13.1: Overview of Electrochemistry
Nernst_equation
13.4.1: Potential Excitation Signals and Currents in Voltammetry
NH3 dilution
2.5: Preparing Solutions
NH3 gas sensing
13.5: Problems
nitrate concentration
13.5: Problems
nitrophenols
7.5: Carbon-13 NMR
NMR
7: Nuclear Magnetic Resonance Spectroscopy
7.2: Environmental Effects on NMR Spectra
7.2.1: Spin-Spin Coupling
7.2.2: The Basis for Differences in Chemical Shift
7.3: NMR Spectrometers
NMR_spectra
7: Nuclear Magnetic Resonance Spectroscopy
NMR_spectrometers
7: Nuclear Magnetic Resonance Spectroscopy
NMRpeak
7.4: Applications of Proton NMR
noise
6.6: Signals and Noise
6.6.1: The Signal-to-Noise Ratio
normal distribution
4.4: The Distribution of Measurements and Results
4.5: Statistical Analysis of Data
4.6: Statistical Methods for Normal Distributions
4.8: Using Excel and R to Analyze Data
4.11: Chapter Summary and Key Terms
normality
2.2: Concentration
2.10: Chapter Summary and Key Terms
nuclear magnetic resonance
1.3: Common Analytical Problems
7.2: Environmental Effects on NMR Spectra
7.7.1: Nuclear Magnetic Resonance Spectroscopy
nuclear magnetic resonance spectroscopy
7.1: Theory of Nuclear Magnetic Resonance
nuclear overhauser enhancement
7.5: Carbon-13 NMR
nuclear_magnetic_resonance
7: Nuclear Magnetic Resonance Spectroscopy
null hypothesis
4.5: Statistical Analysis of Data
4.6: Statistical Methods for Normal Distributions
4.11: Chapter Summary and Key Terms
nutrient broth
3.1: Analysis, Determination, and Measurement
nutrients
3.7: The Importance of Analytical Methodology

O

OpenOffice.org
2.6: Spreadsheets and Computational Software
optical bench
6.13.2: Instrumentation
optical benches
9: Atomic Spectroscopy
optical materials
6.1: Overview of Spectroscopy
opticalbenches
9.4: Interferences in Absorption Spectroscopy
opticalmicroscopy
14.2: Scanning Electron Microscopy
optimization
6.6: Signals and Noise
10.1.5: Optimization and Column Performance
optrodes
6.5: UV/Vis and IR Spectroscopy
organic analytes
6.8: Photoluminescent Spectroscopy
organic functional groups
1.3: Common Analytical Problems
organic molecules
6.12: Applications of Infrared Spectrometry
organicchemistry
7.4: Applications of Proton NMR
oscillation
6.11: An Introduction to Infrared Spectrometry
outliers
4.6: Statistical Methods for Normal Distributions
4.11: Chapter Summary and Key Terms
oxalic acid
2.3: Stoichiometric Calculations
oxidation
13.2.1: Electrochemical Cells
13.5: Problems

P

paired data
4.11: Chapter Summary and Key Terms
paired data analysis
4.6: Statistical Methods for Normal Distributions
parent ion
8.7.5: Fragmentation Patterns in Mass Spectra
particle properties
6.1: Overview of Spectroscopy
particle size
1.3: Common Analytical Problems
parts per billion
2.2: Concentration
2.10: Chapter Summary and Key Terms
parts per million
2.2: Concentration
2.10: Chapter Summary and Key Terms
pathogenic organisms
3.1: Analysis, Determination, and Measurement
peak area
10.1.7: Applications of Chromatography
peak splitting
7.2: Environmental Effects on NMR Spectra
peak width
10.1.6: Summary of Important Relationships for Chromatography
penny mass
4.4: The Distribution of Measurements and Results
performance characteristics
3.9: Additional Resources
personal error
4.11: Chapter Summary and Key Terms
personal errors
4.2: Characterizing Experimental Errors
pesticide residue analysis
10.3: Problems
pH
2.2: Concentration
13.3: Potentiometry
13.3.5: Membrane Ion-Selective Electrodes
pH calculation
2.8: Problems
12.6: Problems
12.7: Additional Resources
pH control
12.5: Ladder Diagrams
pH effects
2.6: Spreadsheets and Computational Software
pH measurement
13.2: An Introduction to Electroanalytical Chemistry
pH meter
5.2: Calibrating the Signal
pH paradoxes
12.7: Additional Resources
pH scale
12.4: Equilibrium Constants for Chemical Reactions
pharmaceuticals
13.4.7: Applications of Voltammetry
phosphorescence
6.8: Photoluminescent Spectroscopy
6.14: Problems
6.15: Additional Resources
6.16: Chapter Summary and Key Terms
phosphorescence instrumentation
6.8: Photoluminescent Spectroscopy
phosphorescence lifetime
6.8: Photoluminescent Spectroscopy
photoelectron
14: Surface Characterization by Spectroscopy and Microscopy
photoluminescence
1.4: Types of Instrumental Methods
6.1: Overview of Spectroscopy
6.7: Emission Spectroscopy
6.8: Photoluminescent Spectroscopy
6.16: Chapter Summary and Key Terms
photoluminescent applications
6.8: Photoluminescent Spectroscopy
photometer
6.5: UV/Vis and IR Spectroscopy
photomultiplier
6.10.2: Radiation Transducers
photon absorption
6.13: Raman Spectroscopy
photon emission
6.13: Raman Spectroscopy
photon transducers
6.1: Overview of Spectroscopy

photon's
6.11: An Introduction to Infrared Spectrometry
photons
14.2: Scanning Electron Microscopy
photovoltaic cell
6.10.2: Radiation Transducers
physical interferences
1.2: The Analytical Perspective
physical properties
1.7: Chapter Summary and Key Terms
11: Thermal Methods
physical signal
3.3: Classifying Analytical Techniques
physics
12.2: Thermodynamics and Equilibrium Chemistry
picric acid purity
13.5: Problems
piezoelectric
14.3: Scanning Probe Microscopes
pipet calibration
4.3: Propagation of Uncertainty
pKa
12.5: Ladder Diagrams
plasma emission
9.7.2: Atomic Emission Spectroscopy
polarity
10.5: Chapter Summary and Key Terms
polarography
13.4: Voltammetry
13.4.1: Potential Excitation Signals and Currents in Voltammetry
13.4.5: Polarography
13.5: Problems
13.7: Chapter Summary and Key Terms
polynomial regression
5.4: Linear Regression and Calibration Curves
polyprotic acids
12.4: Equilibrium Constants for Chemical Reactions
population vs sample
4.4: The Distribution of Measurements and Results
portable device
1.2: The Analytical Perspective
potassium analysis
13.5: Problems
potassium dichromate
2.8: Problems
potassium hydrogen phthalate
5.1: Analytical Signals
potential
13.4: Voltammetry
13.4.1: Potential Excitation Signals and Currents in Voltammetry
13.4.2: Voltammetric Instrumentation
potential control
13.1: Overview of Electrochemistry
13.2: An Introduction to Electroanalytical Chemistry
potential measurement
13.1: Overview of Electrochemistry
potentiometer
13.1: Overview of Electrochemistry
13.2.1: Electrochemical Cells
potentiometric electrode
13.5: Problems
potentiometric electrodes
13.7: Chapter Summary and Key Terms
potentiometry
13.1: Overview of Electrochemistry
13.2.6: Types of Electroanalytical Methods
13.3: Potentiometry
13.3.4: Metallic Indicator Electrodes
13.3.5: Membrane Ion-Selective Electrodes
13.6: Additional Resources
13.7: Chapter Summary and Key Terms
potentiostat
13.1: Overview of Electrochemistry
13.4.2: Voltammetric Instrumentation
ppm
2.5: Preparing Solutions
precipitate formation
12.6: Problems
precipitation
2.8: Problems
precipitation reactions
12.4: Equilibrium Constants for Chemical Reactions
12.8: Chapter Summary and Key Terms
precision
1.2: The Analytical Perspective
3.4: Selecting an Analytical Method
3.5: Developing the Procedure
3.6: Protocols
3.10: Chapter Summary and Key Terms
4.2: Characterizing Experimental Errors
4.10: Additional Resources
6.5: UV/Vis and IR Spectroscopy
9.5: Atomic Absorption Techniques
preparing solutions
2.4: Basic Equipment
pressure
12.2: Thermodynamics and Equilibrium Chemistry
primary literature
1.6: Additional Resources
primary standard
5.1: Analytical Signals
5.9: Chapter Summary and Key Terms
primary standards
5.1: Analytical Signals
probability
4.5: Statistical Analysis of Data
4.7: Detection Limits
4.9: Problems
probability distribution
4.4: The Distribution of Measurements and Results
4.11: Chapter Summary and Key Terms
probability distributions
4.8: Using Excel and R to Analyze Data
probe
14: Surface Characterization by Spectroscopy and Microscopy
procedure
3.10: Chapter Summary and Key Terms
procedure validation
3.2: Techniques, Methods, Procedures, and Protocols
procedures
3.6: Protocols
propagation of uncertainty
4.3: Propagation of Uncertainty
4.11: Chapter Summary and Key Terms
5.7: Problems
propanal
7.4: Applications of Proton NMR
propane
7.2: Environmental Effects on NMR Spectra
proportional determinate error
4.2: Characterizing Experimental Errors
4.11: Chapter Summary and Key Terms
protocol
3.6: Protocols
3.10: Chapter Summary and Key Terms
proton decoupling
7.5: Carbon-13 NMR
protonNMR
7.4: Applications of Proton NMR
public health
3.2: Techniques, Methods, Procedures, and Protocols
pulse polarography
13.4.5: Polarography
pure compounds
8.7: Applications of Molecular Mass Spectrometry

Q

QA/QC
3.6: Protocols
3.10: Chapter Summary and Key Terms
quadrupole
8.6: Mass Spectrometers
qualitative
8.7: Applications of Molecular Mass Spectrometry
qualitative analysis
1.1: What is Analytical Chemistry
1.3: Common Analytical Problems
1.7: Chapter Summary and Key Terms
6.5: UV/Vis and IR Spectroscopy
6.11.1: Theory of Infrared Absorption Spectrometry
6.12: Applications of Infrared Spectrometry
6.12.1: Mid-Infrared Absorption Spectometry
6.13: Raman Spectroscopy
8: Molecular Mass Spectrometry
10.1.7: Applications of Chromatography
qualitative applications
6.13.3: Applications of Raman Spectroscopy
9.7.2: Atomic Emission Spectroscopy
qualitativeAnalysis
7.4: Applications of Proton NMR
quality assurance
3.6: Protocols
quality control
3.6: Protocols
4.1: Characterizing Measurements and Results
quantitative analysis
1.1: What is Analytical Chemistry
1.3: Common Analytical Problems
1.7: Chapter Summary and Key Terms
3.8: Problems
4.9: Problems
5.4: Linear Regression and Calibration Curves
5.9: Chapter Summary and Key Terms
6.5: UV/Vis and IR Spectroscopy
6.11.1: Theory of Infrared Absorption Spectrometry
6.12: Applications of Infrared Spectrometry
6.12.1: Mid-Infrared Absorption Spectometry
6.13: Raman Spectroscopy
6.14: Problems
7.3: NMR Spectrometers
8: Molecular Mass Spectrometry
9.7.1: Emission Spectroscopy Based on Flame and Plasma Sources
9.7.2: Atomic Emission Spectroscopy
10.1: Introduction to Chromatographic Separations
10.1.7: Applications of Chromatography
13.4: Voltammetry
quantitative applications
6.13.3: Applications of Raman Spectroscopy
9.7.2: Atomic Emission Spectroscopy
quantitative potentiometry
13.3.7: Quantitative Potentiometry
quantitative transfer
2.10: Chapter Summary and Key Terms

quantitativeAnalysis
7.4: Applications of Proton NMR
quantitive analysis
9.6: Atomic Absorption Spectroscopy
quantum yield
6.8: Photoluminescent Spectroscopy
quantum_mechanics
7: Nuclear Magnetic Resonance Spectroscopy
quartet
7.7.6: Spin-Spin Splitting in ^{1}H NMR Spectra
quinine analysis
6.8: Photoluminescent Spectroscopy

R

R
2.6: Spreadsheets and Computational Software
4.8: Using Excel and R to Analyze Data
R functions
4.8: Using Excel and R to Analyze Data
R programming
4.8: Using Excel and R to Analyze Data
4.10: Additional Resources
5.6: Using Excel and R for a Linear Regression
radiation
9: Atomic Spectroscopy
radical cation
8.2: Molecular Mass Spectra
raman spectroscopy
6.13: Raman Spectroscopy
6.13.1: Theory of Raman Spectroscopy
6.13.2: Instrumentation
6.13.3: Applications of Raman Spectroscopy
Raman spectrum
6.13: Raman Spectroscopy
RamanSpectroscopy
6.13.4: Other Types of Raman Spectroscopy
range
4.1: Characterizing Measurements and Results
4.11: Chapter Summary and Key Terms
Rayleigh scattering
6.13: Raman Spectroscopy
reaction constants addition
12.3: Manipulating Equilibrium Constants
reaction equilibrium
12.3: Manipulating Equilibrium Constants
reaction quotient
12.2: Thermodynamics and Equilibrium Chemistry
reaction rate
13.1: Overview of Electrochemistry
reagent blank
5.2: Calibrating the Signal
5.5: Compensating for the Reagent Blank
5.9: Chapter Summary and Key Terms
reagent dispensing
4.3: Propagation of Uncertainty
reagent grade
5.9: Chapter Summary and Key Terms
reagent grade chemicals
5.1: Analytical Signals
reagent quality
5.1: Analytical Signals
redox
13.3: Potentiometry
13.4.7: Applications of Voltammetry
redox buffer
12.6: Problems
redox equilibria
12.5: Ladder Diagrams
redox reaction
13.3.4: Metallic Indicator Electrodes
13.7: Chapter Summary and Key Terms
redox reactions
2.3: Stoichiometric Calculations
12.4: Equilibrium Constants for Chemical Reactions
12.6: Problems
13.1: Overview of Electrochemistry
13.2.1: Electrochemical Cells
redox_reaction
13.4.1: Potential Excitation Signals and Currents in Voltammetry
reduction
13.2.1: Electrochemical Cells
13.5: Problems
reference
13.3: Potentiometry
reference electrodes
13.3.3: Reference Electrodes
reference spectra
6.13.3: Applications of Raman Spectroscopy
reflection spectrometry
6.12: Applications of Infrared Spectrometry
regression equation
5.4: Linear Regression and Calibration Curves
regression model
5.6: Using Excel and R for a Linear Regression
regulatory environment
3.9: Additional Resources
relaxation
6.7: Emission Spectroscopy
repeatability
4.2: Characterizing Experimental Errors
4.11: Chapter Summary and Key Terms
representative samples
3.5: Developing the Procedure
reproducibility
4.2: Characterizing Experimental Errors
4.11: Chapter Summary and Key Terms
research
13.3.5: Membrane Ion-Selective Electrodes
research goals
1.2: The Analytical Perspective
research methodology
4.9: Problems
research program
3.7: The Importance of Analytical Methodology
residual error
5.4: Linear Regression and Calibration Curves
5.9: Chapter Summary and Key Terms
residual plots
5.7: Problems
residuals
5.6: Using Excel and R for a Linear Regression
resolution
8.6: Mass Spectrometers
10.1.5: Optimization and Column Performance
10.1.6: Summary of Important Relationships for Chromatography
10.3: Problems
10.5: Chapter Summary and Key Terms
14: Surface Characterization by Spectroscopy and Microscopy
14.2: Scanning Electron Microscopy
ResonanceRamanSpectroscopy
6.13.4: Other Types of Raman Spectroscopy
retention factor
10.1.2: Migration Rates of Solutes
10.5: Chapter Summary and Key Terms
retention time
10.1.2: Migration Rates of Solutes
10.1.6: Summary of Important Relationships for Chromatography
10.1.7: Applications of Chromatography
10.3: Problems
retention_time
10.1.5: Optimization and Column Performance
reversible reactions
12.1: Reversible Reactions and Chemical Equilibria
RF_radiation
7: Nuclear Magnetic Resonance Spectroscopy
rhubarb analysis
2.3: Stoichiometric Calculations
robust estimate
4.1: Characterizing Measurements and Results
robust regression
5.8: Additional Resources
robustness
3.4: Selecting an Analytical Method
3.10: Chapter Summary and Key Terms
rounding
2.8: Problems
ruggedness
3.4: Selecting an Analytical Method
3.10: Chapter Summary and Key Terms

S

Safe Drinking Water Act
3.1: Analysis, Determination, and Measurement
3.2: Techniques, Methods, Procedures, and Protocols
salt bridge
13.2.1: Electrochemical Cells
sample
3.10: Chapter Summary and Key Terms
10.1: Introduction to Chromatographic Separations
sample analysis
1.2: The Analytical Perspective
2.3: Stoichiometric Calculations
3.4: Selecting an Analytical Method
4.4: The Distribution of Measurements and Results
sample digestion
3.8: Problems
sample handling
6.12.1: Mid-Infrared Absorption Spectometry
sample inlet systems
8: Molecular Mass Spectrometry
sample introduction
9.2: Sample Atomization Techniques
sample matrix
5.5: Compensating for the Reagent Blank
sample preparation
6.5: UV/Vis and IR Spectroscopy
9.5: Atomic Absorption Techniques
9.6: Atomic Absorption Spectroscopy
9.7.2: Atomic Emission Spectroscopy
sample probe
7.3: NMR Spectrometers
samples
3.6: Protocols
sampling error
4.11: Chapter Summary and Key Terms
sampling errors
4.2: Characterizing Experimental Errors
sampling strategy
3.5: Developing the Procedure
saturated calomel reference electrode
13.3.4: Metallic Indicator Electrodes

scale of operation
3.4: Selecting an Analytical Method
scanning
14: Surface Characterization by Spectroscopy and Microscopy
scanning tunneling microscopy
14.1: Introduction to the Study of Surfaces
Scanning Tunneling Microscopy (STM)
14.3.2: Scanning Tunneling Microscopy (STM)
scanningelectronmicroscopy
14.2: Scanning Electron Microscopy
Scattering
6.13.4: Other Types of Raman Spectroscopy
scattering intensity
6.13.2: Instrumentation
scientific data
2.6: Spreadsheets and Computational Software
scientific discovery
12.1: Reversible Reactions and Chemical Equilibria
scientific notation
2.1: Measurements in Analytical Chemistry
2.10: Chapter Summary and Key Terms
scientific notation prefixes
2.1: Measurements in Analytical Chemistry
scientific techniques
10.4: Additional Resources
secondary standard
5.1: Analytical Signals
5.9: Chapter Summary and Key Terms
secondary standards
5.1: Analytical Signals
selectivity
3.4: Selecting an Analytical Method
3.10: Chapter Summary and Key Terms
6.5: UV/Vis and IR Spectroscopy
6.8: Photoluminescent Spectroscopy
10.1.5: Optimization and Column Performance
selectivity coefficient
3.4: Selecting an Analytical Method
3.8: Problems
3.10: Chapter Summary and Key Terms
13.3.5: Membrane Ion-Selective Electrodes
selectivity factor
10.1.2: Migration Rates of Solutes
10.1.6: Summary of Important Relationships for Chromatography
selectivity factors
10.3: Problems
semiconductor
6.10.2: Radiation Transducers
Semiconductor Lasers
6.4.4: Semiconductor and Solid-state lasers
Sensitivity
1.2: The Analytical Perspective
3.4: Selecting an Analytical Method
3.10: Chapter Summary and Key Terms
5.9: Chapter Summary and Key Terms
6.5: UV/Vis and IR Spectroscopy
6.8: Photoluminescent Spectroscopy
6.10.2: Radiation Transducers
6.13.4: Other Types of Raman Spectroscopy
9.2: Sample Atomization Techniques
9.3: Atomic Absorption Instrumentation
sensitivity analysis
3.8: Problems
sensitivity debate
3.9: Additional Resources
sensitivity in atomic absorption
9.6: Atomic Absorption Spectroscopy
sensors
13.6: Additional Resources
separation
10.1.1: A General Description of Chromatography
10.1.5: Optimization and Column Performance
10.5: Chapter Summary and Key Terms
separation technique
10.1.7: Applications of Chromatography
separation techniques
10.3: Problems
serial dilution
5.1: Analytical Signals
5.7: Problems
5.9: Chapter Summary and Key Terms
SERS
6.13.4: Other Types of Raman Spectroscopy
shielding
7.2: Environmental Effects on NMR Spectra
shot noise
6.6.2: Sources of Instrumental Noise
SI Units
2.1: Measurements in Analytical Chemistry
2.9: Additional Resources
2.10: Chapter Summary and Key Terms
signal
3.10: Chapter Summary and Key Terms
6.6: Signals and Noise
signal averaging
6.15: Additional Resources
7.7.10: ^{13}C NMR Spectroscopy - Signal Averaging and FT-NMR
signal detection
4.7: Detection Limits
signal integration
7.7.5: Integration of ^{1}H NMR Absorptions - Proton Counting
signal intensity
7.5: Carbon-13 NMR
signal measurement
3.8: Problems
5.2: Calibrating the Signal
5.9: Chapter Summary and Key Terms
signal processing
6.15: Additional Resources
7.3: NMR Spectrometers
signal processor
6.1: Overview of Spectroscopy
significance level
5.7: Problems
significance test
4.6: Statistical Methods for Normal Distributions
4.11: Chapter Summary and Key Terms
significance testing
4.5: Statistical Analysis of Data
significance tests
4.6: Statistical Methods for Normal Distributions
4.8: Using Excel and R to Analyze Data
significant figures
2.1: Measurements in Analytical Chemistry
2.3: Stoichiometric Calculations
2.5: Preparing Solutions
2.8: Problems
2.10: Chapter Summary and Key Terms
4.10: Additional Resources
significant figures in calculations
2.1: Measurements in Analytical Chemistry
silicon photodiode
6.10.2: Radiation Transducers
singlet state
6.8: Photoluminescent Spectroscopy
slope
5.7: Problems
small samples
1.7: Chapter Summary and Key Terms
sodium carbonate
12.1: Reversible Reactions and Chemical Equilibria
sodium in serum
4.1: Characterizing Measurements and Results
software
6.6: Signals and Noise
software download
2.6: Spreadsheets and Computational Software
solubility
2.6: Spreadsheets and Computational Software
12.4: Equilibrium Constants for Chemical Reactions
12.5: Ladder Diagrams
12.6: Problems
12.7: Additional Resources
solubility product
12.8: Chapter Summary and Key Terms
solubility products
12.7: Additional Resources
solute
2.2: Concentration
10.1.1: A General Description of Chromatography
10.1.5: Optimization and Column Performance
10.1.7: Applications of Chromatography
solutes
10.5: Chapter Summary and Key Terms
solution
2.2: Concentration
solution preparation
2.5: Preparing Solutions
2.8: Problems
solvent
2.2: Concentration
solvents
5.1: Analytical Signals
spark emission
9.7.2: Atomic Emission Spectroscopy
specific analytes
3.9: Additional Resources
specificity
3.10: Chapter Summary and Key Terms
spectral interference
9.6: Atomic Absorption Spectroscopy
spectral interferences
9.7.2: Atomic Emission Spectroscopy
spectral searching
6.12.1: Mid-Infrared Absorption Spectometry
spectrofluorometer
6.8: Photoluminescent Spectroscopy
spectrofluorometry
6.14: Problems
spectrometer
6.2: Spectrometer
9.7.2: Atomic Emission Spectroscopy
spectrometry
6.12.1: Mid-Infrared Absorption Spectometry
spectrophotometer
5.2: Calibrating the Signal
6.5: UV/Vis and IR Spectroscopy
6.14: Problems
9.2: Sample Atomization Techniques
spectrophotometer accuracy
5.2: Calibrating the Signal
spectrophotometers
9.3: Atomic Absorption Instrumentation
spectrophotometric analysis
5.3: Determining the Sensitivity

spectrophotometric determination
6.14: Problems
spectrophotometry
6.15: Additional Resources
6.16: Chapter Summary and Key Terms
9.6: Atomic Absorption Spectroscopy
spectroscopic measurements
6.16: Chapter Summary and Key Terms
spectroscopy
1.4: Types of Instrumental Methods
3.3: Classifying Analytical Techniques
6.1: Overview of Spectroscopy
6.5: UV/Vis and IR Spectroscopy
6.7: Emission Spectroscopy
6.10.2: Radiation Transducers
6.11: An Introduction to Infrared Spectrometry
6.14: Problems
6.15: Additional Resources
7: Nuclear Magnetic Resonance Spectroscopy
7.2: Environmental Effects on NMR Spectra
7.2.1: Spin-Spin Coupling
7.2.2: The Basis for Differences in Chemical Shift
7.3: NMR Spectrometers
7.5: Carbon-13 NMR
9: Atomic Spectroscopy
9.7.1: Emission Spectroscopy Based on Flame and Plasma Sources
10.1: Introduction to Chromatographic Separations
14: Surface Characterization by Spectroscopy and Microscopy
spike tests
3.6: Protocols
split samples
3.6: Protocols
spreadsheets
2.6: Spreadsheets and Computational Software
2.9: Additional Resources
standard addition method
10.3: Problems
standard additions
5.3: Determining the Sensitivity
5.5: Compensating for the Reagent Blank
5.8: Additional Resources
9.5: Atomic Absorption Techniques
9.7.2: Atomic Emission Spectroscopy
standard additions calibration
5.7: Problems
standard deviation
4.1: Characterizing Measurements and Results
4.4: The Distribution of Measurements and Results
4.6: Statistical Methods for Normal Distributions
4.7: Detection Limits
4.8: Using Excel and R to Analyze Data
4.11: Chapter Summary and Key Terms
5.4: Linear Regression and Calibration Curves
standard deviation about regression
5.4: Linear Regression and Calibration Curves
standard deviation about the regression
5.9: Chapter Summary and Key Terms
standard error of the mean
4.11: Chapter Summary and Key Terms
standard hydrogen electrode
13.2.3: Electrode Potentials
standard methods
3.8: Problems
standard potentials
12.4: Equilibrium Constants for Chemical Reactions
standard reference material
4.11: Chapter Summary and Key Terms
standard solution
5.1: Analytical Signals
standard state
12.2: Thermodynamics and Equilibrium Chemistry
standardization
1.2: The Analytical Perspective
5.1: Analytical Signals
5.5: Compensating for the Reagent Blank
standardization methods
5.8: Additional Resources
9.6: Atomic Absorption Spectroscopy
standardization strategies
5.9: Chapter Summary and Key Terms
standards
3.6: Protocols
static techniques
13.1: Overview of Electrochemistry
13.2.6: Types of Electroanalytical Methods
stationary phase
10.1: Introduction to Chromatographic Separations
10.1.1: A General Description of Chromatography
10.1.6: Summary of Important Relationships for Chromatography
10.1.7: Applications of Chromatography
10.5: Chapter Summary and Key Terms
statistical analysis
1.2: The Analytical Perspective
2.6: Spreadsheets and Computational Software
4.1: Characterizing Measurements and Results
4.2: Characterizing Experimental Errors
4.4: The Distribution of Measurements and Results
4.5: Statistical Analysis of Data
4.6: Statistical Methods for Normal Distributions
4.10: Additional Resources
4.11: Chapter Summary and Key Terms
statistical calculations
4.8: Using Excel and R to Analyze Data
statistical errors
4.5: Statistical Analysis of Data
statistical methods
5.8: Additional Resources
statistical significance
4.4: The Distribution of Measurements and Results
4.9: Problems
4.10: Additional Resources
statistical summary
4.8: Using Excel and R to Analyze Data
5.6: Using Excel and R for a Linear Regression
statistical tests
4.9: Problems
statistics
4.9: Problems
5.6: Using Excel and R for a Linear Regression
STM
14.3: Scanning Probe Microscopes
stock solution
2.10: Chapter Summary and Key Terms
stock solutions
2.5: Preparing Solutions
stoichiometry
2.3: Stoichiometric Calculations
2.10: Chapter Summary and Key Terms
5.1: Analytical Signals
6.14: Problems
12.2: Thermodynamics and Equilibrium Chemistry
stripping methods
13.4: Voltammetry
stripping voltammetry
13.7: Chapter Summary and Key Terms
strong acids
12.4: Equilibrium Constants for Chemical Reactions
strong bases
12.4: Equilibrium Constants for Chemical Reactions
student experiments
13.6: Additional Resources
subatomic particles
8.1: General Features of Atomic Mass Spectrometry
sulfur concentration
13.5: Problems
supercritical fluid chromatography
10.5: Chapter Summary and Key Terms
surface analysis
14.1: Introduction to the Study of Surfaces
surface properties
14.1: Introduction to the Study of Surfaces
surface structure
1.3: Common Analytical Problems
SurfaceEnhancedRamanSpectroscopy
6.13.4: Other Types of Raman Spectroscopy
surfaceimaging
14.3: Scanning Probe Microscopes
surfaces
14: Surface Characterization by Spectroscopy and Microscopy
synthetic organic pigments
6.13.3: Applications of Raman Spectroscopy

T

tandem mass spectrometry
8.7: Applications of Molecular Mass Spectrometry
tare
2.10: Chapter Summary and Key Terms
tare weight
2.4: Basic Equipment
technique
3.10: Chapter Summary and Key Terms
telemedicine
1.2: The Analytical Perspective
temperature
11: Thermal Methods
12.2: Thermodynamics and Equilibrium Chemistry
test statistic
4.5: Statistical Analysis of Data
textbooks
1.6: Additional Resources
thallium analysis
13.5: Problems
theoretical plates
10.1.6: Summary of Important Relationships for Chromatography
10.3: Problems
10.5: Chapter Summary and Key Terms
theoretical_plates
10.1.5: Optimization and Column Performance
theory limitations
1.3: Common Analytical Problems
thermal excitation
9.7.1: Emission Spectroscopy Based on Flame and Plasma Sources
thermal methods
11: Thermal Methods
thermal noise
6.6.2: Sources of Instrumental Noise
thermal transducers
6.1: Overview of Spectroscopy
thermodynamic solubility product
12.7: Additional Resources
thermodynamics
12.2: Thermodynamics and Equilibrium Chemistry
12.8: Chapter Summary and Key Terms
thermogravimetry
11: Thermal Methods
11.1: Thermogravimetry

thioamide drug analysis
13.5: Problems
time scales
1.7: Chapter Summary and Key Terms
tin concentration
13.5: Problems
titration
2.3: Stoichiometric Calculations
5.1: Analytical Signals
titrimetry
3.3: Classifying Analytical Techniques
TOCSY
7.6: Two-Dimensional Fourier Transform NMR
total analysis method
3.8: Problems
total analysis technique
3.10: Chapter Summary and Key Terms
total analysis techniques
3.3: Classifying Analytical Techniques
toxic pollutants
3.7: The Importance of Analytical Methodology
trace detection
1.3: Common Analytical Problems
trace metals
3.6: Protocols
9.7.1: Emission Spectroscopy Based on Flame and Plasma Sources
13.4.7: Applications of Voltammetry
trace metals analysis
9.6: Atomic Absorption Spectroscopy
9.7.2: Atomic Emission Spectroscopy
transducer
6.10.2: Radiation Transducers
transmittance
6.3: Spectroscopy Based on Absorption
6.5: UV/Vis and IR Spectroscopy
6.11.1: Theory of Infrared Absorption Spectrometry
6.14: Problems
6.16: Chapter Summary and Key Terms
tree diagram
7.7.8: More Complex Spin-Spin Splitting Patterns
triplet
7.7.6: Spin-Spin Splitting in ^{1}H NMR Spectra
triplet state
6.8: Photoluminescent Spectroscopy
TunableLaser
6.13.4: Other Types of Raman Spectroscopy
tunnelingcurrent
14.3: Scanning Probe Microscopes
turbidimetry
6.16: Chapter Summary and Key Terms
type 1 error
4.5: Statistical Analysis of Data
4.7: Detection Limits
4.11: Chapter Summary and Key Terms
type 2 error
4.5: Statistical Analysis of Data
4.7: Detection Limits
4.11: Chapter Summary and Key Terms

U

ultraviolet radiation
6.1: Overview of Spectroscopy
uncertainties
2.8: Problems
uncertainty
4.2: Characterizing Experimental Errors
5.6: Using Excel and R for a Linear Regression
6.6: Signals and Noise
uncertainty analysis
4.3: Propagation of Uncertainty
4.10: Additional Resources
uncertainty calculation
4.3: Propagation of Uncertainty
uncertainty propagation
4.9: Problems
undergraduate experiments
6.15: Additional Resources
unit conversions
2.1: Measurements in Analytical Chemistry
United States Mint
4.1: Characterizing Measurements and Results
United States penny
4.1: Characterizing Measurements and Results
unpaired data
4.11: Chapter Summary and Key Terms
unpaired data analysis
4.6: Statistical Methods for Normal Distributions
unweighted linear regression
5.9: Chapter Summary and Key Terms
unweighted regression
5.4: Linear Regression and Calibration Curves
urea enzyme electrode
13.5: Problems
uv vis spectroscopy
6.13.2: Instrumentation
UV/Vis
6.16: Chapter Summary and Key Terms
UV/Vis absorption
6.5: UV/Vis and IR Spectroscopy
UV/Vis analysis
10.1: Introduction to Chromatographic Separations
UV/Vis spectra
6.3: Spectroscopy Based on Absorption
UV/Vis spectroscopy
6.15: Additional Resources

V

v/v percentage
2.5: Preparing Solutions
vacuum
8.6: Mass Spectrometers
validation
1.2: The Analytical Perspective
3.10: Chapter Summary and Key Terms
van Deemter equation
10.1.4: Chromatography
10.3: Problems
vanadium concentration
13.5: Problems
variance
4.1: Characterizing Measurements and Results
4.4: The Distribution of Measurements and Results
4.8: Using Excel and R to Analyze Data
4.11: Chapter Summary and Key Terms
variance comparison
4.6: Statistical Methods for Normal Distributions
vibrational
6.11: An Introduction to Infrared Spectrometry
Vibrational Energy Levels
6.3: Spectroscopy Based on Absorption
vibrational energy states
6.11.1: Theory of Infrared Absorption Spectrometry
vibrational relaxation
6.7: Emission Spectroscopy
6.8: Photoluminescent Spectroscopy
vibrational spectroscopy
1.3: Common Analytical Problems
visible radiation
6.1: Overview of Spectroscopy
visualization
5.6: Using Excel and R for a Linear Regression
vitamin analysis
10.3: Problems
volatile components
10.5: Chapter Summary and Key Terms
voltammetric behavior
13.5: Problems
voltammetric determination
5.7: Problems
voltammetric methods
13.7: Chapter Summary and Key Terms
voltammetric techniques
13.4.2: Voltammetric Instrumentation
13.4.6: Stripping Methods
voltammetry
13.1: Overview of Electrochemistry
13.2.6: Types of Electroanalytical Methods
13.4: Voltammetry
13.4.1: Potential Excitation Signals and Currents in Voltammetry
13.4.2: Voltammetric Instrumentation
13.4.7: Applications of Voltammetry
13.6: Additional Resources
13.7: Chapter Summary and Key Terms
voltammogram
13.4: Voltammetry
volume measurement
2.4: Basic Equipment
volume percent
2.2: Concentration
2.10: Chapter Summary and Key Terms
volumetric flask
2.4: Basic Equipment
2.5: Preparing Solutions
2.10: Chapter Summary and Key Terms
volumetric glassware
4.3: Propagation of Uncertainty
volumetric pipet
2.4: Basic Equipment
2.10: Chapter Summary and Key Terms

W

water analysis
3.6: Protocols
water testing
3.1: Analysis, Determination, and Measurement
wave properties
6.1: Overview of Spectroscopy
waveform generator
13.4.2: Voltammetric Instrumentation
wavelength selection
6.1: Overview of Spectroscopy
9.6: Atomic Absorption Spectroscopy
weak acids
12.4: Equilibrium Constants for Chemical Reactions
12.5: Ladder Diagrams
weak bases
12.4: Equilibrium Constants for Chemical Reactions
12.5: Ladder Diagrams
weight percent
2.2: Concentration
2.10: Chapter Summary and Key Terms
5.7: Problems
weight vs mass
2.4: Basic Equipment

weighted linear regression
5.7: Problems
5.9: Chapter Summary and Key Terms
weighted regression
5.4: Linear Regression and Calibration Curves
5.6: Using Excel and R for a Linear Regression

X
XPS
14.4: Spectroscopic Surface Methods
14.4.1: X-ray Photoelectron Spectroscopy

Y
Youden blank
5.5: Compensating for the Reagent Blank
5.9: Chapter Summary and Key Terms

Z
Zeemaneffect
9.4: Interferences in Absorption Spectroscopy
zinc concentration analysis
4.6: Statistical Methods for Normal Distributions
Zn2+ standard solution
2.5: Preparing Solutions

Glossary

Sample Word 1 | Sample Definition 1

Detailed Licensing

Overview

Title: Instrumental Analysis (CHEM 311)

Webpages: 230

Applicable Restrictions: Noncommercial

All licenses found:

- CC BY-NC-SA 4.0: 80% (184 pages)
- CC BY-SA 4.0: 9.1% (21 pages)
- Undeclared: 5.2% (12 pages)
- CC BY-NC 4.0: 2.6% (6 pages)
- CC BY 4.0: 2.2% (5 pages)
- CC BY-NC-SA 2.5: 0.9% (2 pages)

By Page

- Instrumental Analysis (CHEM 311) - *Undeclared*
  - Front Matter - *Undeclared*
    - TitlePage - *Undeclared*
    - InfoPage - *Undeclared*
    - Table of Contents - *Undeclared*
    - Licensing - *Undeclared*
  - 1: Introduction to Analytical Chemistry - *CC BY-NC-SA 4.0*
    - 1.1: What is Analytical Chemistry - *CC BY-NC-SA 4.0*
    - 1.2: The Analytical Perspective - *CC BY-NC-SA 4.0*
    - 1.3: Common Analytical Problems - *CC BY-NC-SA 4.0*
    - 1.4: Types of Instrumental Methods - *CC BY-NC-SA 4.0*
    - 1.5: Problems - *CC BY-NC-SA 4.0*
    - 1.6: Additional Resources - *CC BY-NC-SA 4.0*
    - 1.7: Chapter Summary and Key Terms - *CC BY-NC-SA 4.0*
  - 2: Basic Tools of Analytical Chemistry - *CC BY-NC-SA 4.0*
    - 2.1: Measurements in Analytical Chemistry - *CC BY-NC-SA 4.0*
    - 2.2: Concentration - *CC BY-NC-SA 4.0*
    - 2.3: Stoichiometric Calculations - *CC BY-NC-SA 4.0*
    - 2.4: Basic Equipment - *CC BY-NC-SA 4.0*
    - 2.5: Preparing Solutions - *CC BY-NC-SA 4.0*
    - 2.6: Spreadsheets and Computational Software - *CC BY-NC-SA 4.0*
    - 2.7: The Laboratory Notebook - *CC BY-NC-SA 4.0*
    - 2.8: Problems - *CC BY-NC-SA 4.0*
    - 2.9: Additional Resources - *CC BY-NC-SA 4.0*
    - 2.10: Chapter Summary and Key Terms - *CC BY-NC-SA 4.0*
  - 3: The Vocabulary of Analytical Chemistry - *CC BY-NC-SA 4.0*
    - 3.1: Analysis, Determination, and Measurement - *CC BY-NC-SA 4.0*
    - 3.2: Techniques, Methods, Procedures, and Protocols - *CC BY-NC-SA 4.0*
    - 3.3: Classifying Analytical Techniques - *CC BY-NC-SA 4.0*
    - 3.4: Selecting an Analytical Method - *CC BY-NC-SA 4.0*
    - 3.5: Developing the Procedure - *CC BY-NC-SA 4.0*
    - 3.6: Protocols - *CC BY-NC-SA 4.0*
    - 3.7: The Importance of Analytical Methodology - *CC BY-NC-SA 4.0*
    - 3.8: Problems - *CC BY-NC-SA 4.0*
    - 3.9: Additional Resources - *CC BY-NC-SA 4.0*
    - 3.10: Chapter Summary and Key Terms - *CC BY-NC-SA 4.0*
  - 4: Evaluating Analytical Data - *CC BY-NC-SA 4.0*
    - 4.1: Characterizing Measurements and Results - *CC BY-NC-SA 4.0*
    - 4.2: Characterizing Experimental Errors - *CC BY-NC-SA 4.0*
    - 4.3: Propagation of Uncertainty - *CC BY-NC-SA 4.0*
    - 4.4: The Distribution of Measurements and Results - *CC BY-NC-SA 4.0*
    - 4.5: Statistical Analysis of Data - *CC BY-NC-SA 4.0*
    - 4.6: Statistical Methods for Normal Distributions - *CC BY-NC-SA 4.0*
    - 4.7: Detection Limits - *CC BY-NC-SA 4.0*
    - 4.8: Using Excel and R to Analyze Data - *CC BY-NC-SA 4.0*

- 4.9: Problems - *CC BY-NC-SA 4.0*
- 4.10: Additional Resources - *CC BY-NC-SA 4.0*
- 4.11: Chapter Summary and Key Terms - *CC BY-NC-SA 4.0*

5: Standardizing Analytical Methods - *CC BY-NC-SA 4.0*
- 5.1: Analytical Signals - *CC BY-NC-SA 4.0*
- 5.2: Calibrating the Signal - *CC BY-NC-SA 4.0*
- 5.3: Determining the Sensitivity - *CC BY-NC-SA 4.0*
- 5.4: Linear Regression and Calibration Curves - *CC BY-NC-SA 4.0*
- 5.5: Compensating for the Reagent Blank - *CC BY-NC-SA 4.0*
- 5.6: Using Excel and R for a Linear Regression - *CC BY-NC-SA 4.0*
- 5.7: Problems - *CC BY-NC-SA 4.0*
- 5.8: Additional Resources - *CC BY-NC-SA 4.0*
- 5.9: Chapter Summary and Key Terms - *CC BY-NC-SA 4.0*

6: Spectroscopic Methods - *CC BY-NC-SA 4.0*
- 6.1: Overview of Spectroscopy - *CC BY-NC-SA 4.0*
- 6.2: Spectrometer - *CC BY-NC-SA 4.0*
  - 6.2.1: ATR-FTIR - *CC BY-NC-SA 4.0*
- 6.3: Spectroscopy Based on Absorption - *CC BY-NC-SA 4.0*
- 6.4: Lasers - *CC BY-NC-SA 4.0*
  - 6.4.1: Gas Lasers - *CC BY-NC-SA 4.0*
  - 6.4.2: Laser Theory - *CC BY-NC-SA 4.0*
  - 6.4.3: Overview of Lasers - *CC BY-NC-SA 4.0*
  - 6.4.4: Semiconductor and Solid-state lasers - *CC BY-NC-SA 4.0*
  - 6.4.5: Semiconductors - *CC BY-NC-SA 4.0*
- 6.5: UV/Vis and IR Spectroscopy - *CC BY-NC-SA 4.0*
- 6.6: Signals and Noise - *CC BY-NC-SA 4.0*
  - 6.6.1: The Signal-to-Noise Ratio - *CC BY-NC-SA 4.0*
  - 6.6.2: Sources of Instrumental Noise - *CC BY-NC-SA 4.0*
  - 6.6.3: Signal-to-Noise Enhancement - *CC BY-NC-SA 4.0*
- 6.7: Emission Spectroscopy - *CC BY-NC-SA 4.0*
- 6.8: Photoluminescent Spectroscopy - *CC BY-NC-SA 4.0*
- 6.9: Analytical Chemiluminescence - *CC BY-SA 4.0*
  - 6.9.1: Introduction to Chemiluminescence - *CC BY-SA 4.0*
    - 6.9.1.1: Electronic transitions and luminescence - *CC BY-SA 4.0*
    - 6.9.1.2: Chemiluminescence Spectroscopy - *CC BY-SA 4.0*
  - 6.9.2: Instrumentation - *CC BY-SA 4.0*
    - 6.9.2.1: Detection of chemiluminescence - *CC BY-SA 4.0*
- 6.10: Detectors - *CC BY-NC-SA 4.0*
  - 6.10.1: Detectors of Light - *CC BY-NC-SA 4.0*
  - 6.10.2: Radiation Transducers - *CC BY-NC-SA 4.0*
- 6.11: An Introduction to Infrared Spectrometry - *CC BY-NC-SA 4.0*
  - 6.11.1: Theory of Infrared Absorption Spectrometry - *CC BY-NC-SA 4.0*
  - 6.11.2: Infrared Sources and Transducers - *CC BY-NC-SA 4.0*
  - 6.11.3: FTIR- Hardware - *CC BY-NC-SA 4.0*
  - 6.11.4: Infrared Instruments - *CC BY-NC-SA 4.0*
- 6.12: Applications of Infrared Spectrometry - *CC BY-NC-SA 4.0*
  - 6.12.1: Mid-Infrared Absorption Spectometry - *CC BY-NC-SA 4.0*
  - 6.12.2: Mid-Infrared Reflection Spectrometry - *CC BY-NC-SA 4.0*
  - 6.12.3: Near-Infrared and Far-Infrared Spectroscopy - *CC BY-NC-SA 4.0*
- 6.13: Raman Spectroscopy - *CC BY-NC-SA 4.0*
  - 6.13.1: Theory of Raman Spectroscopy - *CC BY-NC-SA 4.0*
  - 6.13.2: Instrumentation - *CC BY-NC-SA 4.0*
  - 6.13.3: Applications of Raman Spectroscopy - *CC BY-NC-SA 4.0*
  - 6.13.4: Other Types of Raman Spectroscopy - *CC BY-NC-SA 4.0*
- 6.14: Problems - *CC BY-NC-SA 4.0*
- 6.15: Additional Resources - *CC BY-NC-SA 4.0*
- 6.16: Chapter Summary and Key Terms - *CC BY-NC-SA 4.0*

7: Nuclear Magnetic Resonance Spectroscopy - *CC BY-NC-SA 4.0*
- 7.1: Theory of Nuclear Magnetic Resonance - *CC BY-NC-SA 4.0*
- 7.2: Environmental Effects on NMR Spectra - *CC BY-NC-SA 4.0*
  - 7.2.1: Spin-Spin Coupling - *CC BY-NC-SA 4.0*
  - 7.2.2: The Basis for Differences in Chemical Shift - *CC BY-NC-SA 4.0*
- 7.3: NMR Spectrometers - *CC BY-NC-SA 4.0*
- 7.4: Applications of Proton NMR - *CC BY-NC-SA 4.0*
- 7.5: Carbon-13 NMR - *CC BY-NC-SA 4.0*
- 7.6: Two-Dimensional Fourier Transform NMR - *CC BY-NC-SA 4.0*
- 7.7: Structure Determination - Nuclear Magnetic Resonance Spectroscopy - *CC BY-SA 4.0*

- 7.7.1: Nuclear Magnetic Resonance Spectroscopy - *CC BY-SA 4.0*
- 7.7.2: The Nature of NMR Absorptions - *CC BY-SA 4.0*
- 7.7.3: The Chemical Shift - *CC BY-SA 4.0*
- 7.7.4: Chemical Shifts in ^{1}H NMR Spectroscopy - *CC BY-SA 4.0*
- 7.7.5: Integration of ^{1}H NMR Absorptions - Proton Counting - *CC BY-SA 4.0*
- 7.7.6: Spin-Spin Splitting in ^{1}H NMR Spectra - *CC BY-SA 4.0*
- 7.7.7: ^{1}H NMR Spectroscopy and Proton Equivalence - *CC BY-SA 4.0*
- 7.7.8: More Complex Spin-Spin Splitting Patterns - *CC BY-SA 4.0*
- 7.7.9: Uses of ^{1}H NMR Spectroscopy - *CC BY-SA 4.0*
- 7.7.10: ^{13}C NMR Spectroscopy - Signal Averaging and FT-NMR - *CC BY-SA 4.0*
- 7.7.11: Characteristics of ^{13}C NMR Spectroscopy - *CC BY-SA 4.0*
- 7.7.12: DEPT ^{13}C NMR Spectroscopy - *CC BY-SA 4.0*
- 7.7.13: Uses of ^{13}C NMR Spectroscopy - *CC BY-SA 4.0*
- 7.7.S: Structure Determination - Nuclear Magnetic Resonance Spectroscopy (Summary) - *CC BY-SA 4.0*

8: Molecular Mass Spectrometry - *CC BY-NC-SA 4.0*

- 8.1: General Features of Atomic Mass Spectrometry - *CC BY-NC-SA 4.0*
- 8.2: Molecular Mass Spectra - *CC BY-NC-SA 4.0*
- 8.3: How the Mass Spectrometer Works - *CC BY-NC 4.0*
- 8.4: Mass Spectrometers - *CC BY-NC-SA 4.0*
- 8.5: Ion Sources - *CC BY-NC-SA 4.0*
  - 8.5.1: Electrospray Ionization Mass Spectrometry - *CC BY-NC-SA 4.0*
- 8.6: Mass Spectrometers - *CC BY-NC-SA 4.0*
  - 8.6.1: Mass Analyzers (Mass Spectrometry) - *CC BY-NC-SA 4.0*
- 8.7: Applications of Molecular Mass Spectrometry - *CC BY-NC-SA 4.0*
  - 8.7.1: Interpreting a Mass Spectrum - *CC BY-NC-SA 4.0*
  - 8.7.2: The Molecular Ion (M^+) Peak - *CC BY-NC 4.0*
  - 8.7.3: The M+1 Peak - *CC BY-NC 4.0*
  - 8.7.4: The Mass Spectra of Elements - *CC BY-NC 4.0*
  - 8.7.5: Fragmentation Patterns in Mass Spectra - *CC BY-NC 4.0*
  - 8.7.6: Mass Spectrometry - Fragmentation Patterns - *CC BY-NC-SA 4.0*
  - 8.7.7: Organic Compounds Containing Halogen Atoms - *CC BY-NC 4.0*

9: Atomic Spectroscopy - *CC BY-NC-SA 4.0*

- 9.1: Introduction to Atomic Absorption Spectroscopy - *CC BY 4.0*
- 9.2: Sample Atomization Techniques - *CC BY-NC-SA 4.0*
- 9.3: Atomic Absorption Instrumentation - *CC BY-NC-SA 4.0*
- 9.4: Interferences in Absorption Spectroscopy - *CC BY-NC-SA 4.0*
- 9.5: Atomic Absorption Techniques - *CC BY-NC-SA 4.0*
- 9.6: Atomic Absorption Spectroscopy - *CC BY-NC-SA 4.0*
- 9.7: Atomic Emission Spectroscopy - *CC BY-NC-SA 4.0*
  - 9.7.1: Emission Spectroscopy Based on Flame and Plasma Sources - *CC BY-NC-SA 4.0*
  - 9.7.2: Atomic Emission Spectroscopy - *CC BY-NC-SA 4.0*
  - 9.7.3: Inductively Coupled Plasma Mass Spectrometer - *CC BY-NC-SA 4.0*

10: Chromatographic and Electrophoretic Methods - *CC BY-NC-SA 4.0*

- 10.1: Introduction to Chromatographic Separations - *CC BY-NC-SA 4.0*
  - 10.1.1: A General Description of Chromatography - *CC BY-NC-SA 4.0*
  - 10.1.2: Migration Rates of Solutes - *CC BY-NC-SA 4.0*
  - 10.1.3: Zone Broadening and Column Efficiency - *CC BY-NC-SA 4.0*
  - 10.1.4: Chromatography - *CC BY-NC-SA 4.0*
  - 10.1.5: Optimization and Column Performance - *CC BY-NC-SA 4.0*
  - 10.1.6: Summary of Important Relationships for Chromatography - *CC BY-NC-SA 4.0*
  - 10.1.7: Applications of Chromatography - *CC BY-NC-SA 4.0*
- 10.2: Capillary Electrophoresis and Capillary Electrochromatography - *CC BY-NC-SA 4.0*
  - 10.2.1: An Overview of Electrophoresis - *CC BY-NC-SA 4.0*
  - 10.2.2: Capillary Electrophoresis - *CC BY-NC-SA 4.0*

- 10.2.3: Capillary Electrophoresis - *CC BY-NC-SA 4.0*
  - 10.2.3.1: Ionic Mobility and Electrophoresis - *CC BY-NC-SA 4.0*
- 10.2.4: Applications of Capillary Electrophoresis - *CC BY-NC-SA 4.0*
- 10.3: Problems - *CC BY-NC-SA 4.0*
- 10.4: Additional Resources - *CC BY-NC-SA 4.0*
- 10.5: Chapter Summary and Key Terms - *CC BY-NC-SA 4.0*

11: Thermal Methods - *CC BY-NC-SA 4.0*
- 11.1: Thermogravimetry - *CC BY-NC-SA 4.0*
- 11.2: Differential Thermal Analysis and Differential Scanning Calorimetry - *CC BY-NC-SA 4.0*

12: Equilibrium Chemistry - *CC BY-NC-SA 4.0*
- 12.1: Reversible Reactions and Chemical Equilibria - *CC BY-NC-SA 4.0*
- 12.2: Thermodynamics and Equilibrium Chemistry - *CC BY-NC-SA 4.0*
- 12.3: Manipulating Equilibrium Constants - *CC BY-NC-SA 4.0*
- 12.4: Equilibrium Constants for Chemical Reactions - *CC BY-NC-SA 4.0*
- 12.5: Ladder Diagrams - *CC BY-NC-SA 4.0*
- 12.6: Problems - *CC BY-NC-SA 4.0*
- 12.7: Additional Resources - *CC BY-NC-SA 4.0*
- 12.8: Chapter Summary and Key Terms - *CC BY-NC-SA 4.0*

13: Electrochemical Methods - *CC BY-NC-SA 4.0*
- 13.1: Overview of Electrochemistry - *CC BY-NC-SA 4.0*
- 13.2: An Introduction to Electroanalytical Chemistry - *CC BY-NC-SA 4.0*
  - 13.2.1: Electrochemical Cells - *CC BY-NC-SA 4.0*
  - 13.2.2: Potentials in Electroanalytical Cells - *CC BY-NC-SA 4.0*
  - 13.2.3: Electrode Potentials - *CC BY-NC-SA 4.0*
  - 13.2.4: Calculation of Cell Potentials from Electrode Potentials - *CC BY-NC-SA 4.0*
  - 13.2.5: Currents in Electrochemical Cells - *CC BY-NC-SA 4.0*
  - 13.2.6: Types of Electroanalytical Methods - *CC BY-NC-SA 4.0*
- 13.3: Potentiometry - *CC BY-NC-SA 4.0*
  - 13.3.1: Standard Electrodes - *CC BY-NC-SA 4.0*
  - 13.3.2: Standard Potentials - *CC BY-NC-SA 4.0*
  - 13.3.3: Reference Electrodes - *CC BY-NC-SA 4.0*
  - 13.3.4: Metallic Indicator Electrodes - *CC BY-NC-SA 4.0*
  - 13.3.5: Membrane Ion-Selective Electrodes - *CC BY-NC-SA 4.0*
  - 13.3.6: Molecular-Selective Electrode Systems - *CC BY-NC-SA 4.0*
  - 13.3.7: Quantitative Potentiometry - *CC BY-NC-SA 4.0*
- 13.4: Voltammetry - *CC BY-NC-SA 4.0*
  - 13.4.1: Potential Excitation Signals and Currents in Voltammetry - *CC BY-NC-SA 4.0*
  - 13.4.2: Voltammetric Instrumentation - *CC BY-NC-SA 4.0*
  - 13.4.3: Linear Sweep Voltammetry - *CC BY-NC-SA 4.0*
  - 13.4.4: Cyclic Voltammetry - *CC BY-NC-SA 4.0*
  - 13.4.5: Polarography - *CC BY-NC-SA 4.0*
  - 13.4.6: Stripping Methods - *CC BY-NC-SA 4.0*
  - 13.4.7: Applications of Voltammetry - *CC BY-NC-SA 4.0*
- 13.5: Problems - *CC BY-NC-SA 4.0*
- 13.6: Additional Resources - *CC BY-NC-SA 4.0*
- 13.7: Chapter Summary and Key Terms - *Undeclared*

14: Surface Characterization by Spectroscopy and Microscopy - *CC BY-NC-SA 4.0*
- 14.1: Introduction to the Study of Surfaces - *CC BY-NC-SA 4.0*
- 14.2: Scanning Electron Microscopy - *CC BY-NC-SA 4.0*
  - 14.2.1: Scanning electron microscopy (SEM) - *CC BY-NC-SA 4.0*
  - 14.2.2: Transmission Electron Microscopy - *CC BY 4.0*
- 14.3: Scanning Probe Microscopes - *CC BY-NC-SA 4.0*
  - 14.3.1: Scanning Tunneling Microscopy - *CC BY 4.0*
  - 14.3.2: Scanning Tunneling Microscopy (STM) - *CC BY-NC-SA 2.5*
  - 14.3.3: Atomic Force Microscopy - *CC BY-NC-SA 4.0*
  - 14.3.4: Atomic Force Microscopy (AFM) - *CC BY-NC-SA 2.5*
- 14.4: Spectroscopic Surface Methods - *CC BY-NC-SA 4.0*
  - 14.4.1: X-ray Photoelectron Spectroscopy - *CC BY 4.0*
  - 14.4.2: Auger Electron Spectroscopy - *CC BY 4.0*

Back Matter - *Undeclared*
- Index - *Undeclared*
- Glossary - *Undeclared*
- Detailed Licensing - *Undeclared*

- Detailed Licensing - *Undeclared*

Detailed Licensing

Overview

Title: Instrumental Analysis (CHEM 311)

Webpages: 230

Applicable Restrictions: Noncommercial

All licenses found:

- CC BY-NC-SA 4.0: 80% (184 pages)
- CC BY-SA 4.0: 9.1% (21 pages)
- Undeclared: 5.2% (12 pages)
- CC BY-NC 4.0: 2.6% (6 pages)
- CC BY 4.0: 2.2% (5 pages)
- CC BY-NC-SA 2.5: 0.9% (2 pages)

By Page

- Instrumental Analysis (CHEM 311) - *Undeclared*
  - Front Matter - *Undeclared*
    - TitlePage - *Undeclared*
    - InfoPage - *Undeclared*
    - Table of Contents - *Undeclared*
    - Licensing - *Undeclared*
  - 1: Introduction to Analytical Chemistry - *CC BY-NC-SA 4.0*
    - 1.1: What is Analytical Chemistry - *CC BY-NC-SA 4.0*
    - 1.2: The Analytical Perspective - *CC BY-NC-SA 4.0*
    - 1.3: Common Analytical Problems - *CC BY-NC-SA 4.0*
    - 1.4: Types of Instrumental Methods - *CC BY-NC-SA 4.0*
    - 1.5: Problems - *CC BY-NC-SA 4.0*
    - 1.6: Additional Resources - *CC BY-NC-SA 4.0*
    - 1.7: Chapter Summary and Key Terms - *CC BY-NC-SA 4.0*
  - 2: Basic Tools of Analytical Chemistry - *CC BY-NC-SA 4.0*
    - 2.1: Measurements in Analytical Chemistry - *CC BY-NC-SA 4.0*
    - 2.2: Concentration - *CC BY-NC-SA 4.0*
    - 2.3: Stoichiometric Calculations - *CC BY-NC-SA 4.0*
    - 2.4: Basic Equipment - *CC BY-NC-SA 4.0*
    - 2.5: Preparing Solutions - *CC BY-NC-SA 4.0*
    - 2.6: Spreadsheets and Computational Software - *CC BY-NC-SA 4.0*
    - 2.7: The Laboratory Notebook - *CC BY-NC-SA 4.0*
    - 2.8: Problems - *CC BY-NC-SA 4.0*
    - 2.9: Additional Resources - *CC BY-NC-SA 4.0*
    - 2.10: Chapter Summary and Key Terms - *CC BY-NC-SA 4.0*
  - 3: The Vocabulary of Analytical Chemistry - *CC BY-NC-SA 4.0*
    - 3.1: Analysis, Determination, and Measurement - *CC BY-NC-SA 4.0*
    - 3.2: Techniques, Methods, Procedures, and Protocols - *CC BY-NC-SA 4.0*
    - 3.3: Classifying Analytical Techniques - *CC BY-NC-SA 4.0*
    - 3.4: Selecting an Analytical Method - *CC BY-NC-SA 4.0*
    - 3.5: Developing the Procedure - *CC BY-NC-SA 4.0*
    - 3.6: Protocols - *CC BY-NC-SA 4.0*
    - 3.7: The Importance of Analytical Methodology - *CC BY-NC-SA 4.0*
    - 3.8: Problems - *CC BY-NC-SA 4.0*
    - 3.9: Additional Resources - *CC BY-NC-SA 4.0*
    - 3.10: Chapter Summary and Key Terms - *CC BY-NC-SA 4.0*
  - 4: Evaluating Analytical Data - *CC BY-NC-SA 4.0*
    - 4.1: Characterizing Measurements and Results - *CC BY-NC-SA 4.0*
    - 4.2: Characterizing Experimental Errors - *CC BY-NC-SA 4.0*
    - 4.3: Propagation of Uncertainty - *CC BY-NC-SA 4.0*
    - 4.4: The Distribution of Measurements and Results - *CC BY-NC-SA 4.0*
    - 4.5: Statistical Analysis of Data - *CC BY-NC-SA 4.0*
    - 4.6: Statistical Methods for Normal Distributions - *CC BY-NC-SA 4.0*
    - 4.7: Detection Limits - *CC BY-NC-SA 4.0*
    - 4.8: Using Excel and R to Analyze Data - *CC BY-NC-SA 4.0*

- 4.9: Problems - *CC BY-NC-SA 4.0*
- 4.10: Additional Resources - *CC BY-NC-SA 4.0*
- 4.11: Chapter Summary and Key Terms - *CC BY-NC-SA 4.0*

5: Standardizing Analytical Methods - *CC BY-NC-SA 4.0*
- 5.1: Analytical Signals - *CC BY-NC-SA 4.0*
- 5.2: Calibrating the Signal - *CC BY-NC-SA 4.0*
- 5.3: Determining the Sensitivity - *CC BY-NC-SA 4.0*
- 5.4: Linear Regression and Calibration Curves - *CC BY-NC-SA 4.0*
- 5.5: Compensating for the Reagent Blank - *CC BY-NC-SA 4.0*
- 5.6: Using Excel and R for a Linear Regression - *CC BY-NC-SA 4.0*
- 5.7: Problems - *CC BY-NC-SA 4.0*
- 5.8: Additional Resources - *CC BY-NC-SA 4.0*
- 5.9: Chapter Summary and Key Terms - *CC BY-NC-SA 4.0*

6: Spectroscopic Methods - *CC BY-NC-SA 4.0*
- 6.1: Overview of Spectroscopy - *CC BY-NC-SA 4.0*
- 6.2: Spectrometer - *CC BY-NC-SA 4.0*
  - 6.2.1: ATR-FTIR - *CC BY-NC-SA 4.0*
- 6.3: Spectroscopy Based on Absorption - *CC BY-NC-SA 4.0*
- 6.4: Lasers - *CC BY-NC-SA 4.0*
  - 6.4.1: Gas Lasers - *CC BY-NC-SA 4.0*
  - 6.4.2: Laser Theory - *CC BY-NC-SA 4.0*
  - 6.4.3: Overview of Lasers - *CC BY-NC-SA 4.0*
  - 6.4.4: Semiconductor and Solid-state lasers - *CC BY-NC-SA 4.0*
  - 6.4.5: Semiconductors - *CC BY-NC-SA 4.0*
- 6.5: UV/Vis and IR Spectroscopy - *CC BY-NC-SA 4.0*
- 6.6: Signals and Noise - *CC BY-NC-SA 4.0*
  - 6.6.1: The Signal-to-Noise Ratio - *CC BY-NC-SA 4.0*
  - 6.6.2: Sources of Instrumental Noise - *CC BY-NC-SA 4.0*
  - 6.6.3: Signal-to-Noise Enhancement - *CC BY-NC-SA 4.0*
- 6.7: Emission Spectroscopy - *CC BY-NC-SA 4.0*
- 6.8: Photoluminescent Spectroscopy - *CC BY-NC-SA 4.0*
- 6.9: Analytical Chemiluminescence - *CC BY-SA 4.0*
  - 6.9.1: Introduction to Chemiluminescence - *CC BY-SA 4.0*
    - 6.9.1.1: Electronic transitions and luminescence - *CC BY-SA 4.0*
    - 6.9.1.2: Chemiluminescence Spectroscopy - *CC BY-SA 4.0*
  - 6.9.2: Instrumentation - *CC BY-SA 4.0*
    - 6.9.2.1: Detection of chemiluminescence - *CC BY-SA 4.0*
- 6.10: Detectors - *CC BY-NC-SA 4.0*
  - 6.10.1: Detectors of Light - *CC BY-NC-SA 4.0*
  - 6.10.2: Radiation Transducers - *CC BY-NC-SA 4.0*
- 6.11: An Introduction to Infrared Spectrometry - *CC BY-NC-SA 4.0*
  - 6.11.1: Theory of Infrared Absorption Spectrometry - *CC BY-NC-SA 4.0*
  - 6.11.2: Infrared Sources and Transducers - *CC BY-NC-SA 4.0*
  - 6.11.3: FTIR- Hardware - *CC BY-NC-SA 4.0*
  - 6.11.4: Infrared Instruments - *CC BY-NC-SA 4.0*
- 6.12: Applications of Infrared Spectrometry - *CC BY-NC-SA 4.0*
  - 6.12.1: Mid-Infrared Absorption Spectometry - *CC BY-NC-SA 4.0*
  - 6.12.2: Mid-Infrared Reflection Spectrometry - *CC BY-NC-SA 4.0*
  - 6.12.3: Near-Infrared and Far-Infrared Spectroscopy - *CC BY-NC-SA 4.0*
- 6.13: Raman Spectroscopy - *CC BY-NC-SA 4.0*
  - 6.13.1: Theory of Raman Spectroscopy - *CC BY-NC-SA 4.0*
  - 6.13.2: Instrumentation - *CC BY-NC-SA 4.0*
  - 6.13.3: Applications of Raman Spectroscopy - *CC BY-NC-SA 4.0*
  - 6.13.4: Other Types of Raman Spectroscopy - *CC BY-NC-SA 4.0*
- 6.14: Problems - *CC BY-NC-SA 4.0*
- 6.15: Additional Resources - *CC BY-NC-SA 4.0*
- 6.16: Chapter Summary and Key Terms - *CC BY-NC-SA 4.0*

7: Nuclear Magnetic Resonance Spectroscopy - *CC BY-NC-SA 4.0*
- 7.1: Theory of Nuclear Magnetic Resonance - *CC BY-NC-SA 4.0*
- 7.2: Environmental Effects on NMR Spectra - *CC BY-NC-SA 4.0*
  - 7.2.1: Spin-Spin Coupling - *CC BY-NC-SA 4.0*
  - 7.2.2: The Basis for Differences in Chemical Shift - *CC BY-NC-SA 4.0*
- 7.3: NMR Spectrometers - *CC BY-NC-SA 4.0*
- 7.4: Applications of Proton NMR - *CC BY-NC-SA 4.0*
- 7.5: Carbon-13 NMR - *CC BY-NC-SA 4.0*
- 7.6: Two-Dimensional Fourier Transform NMR - *CC BY-NC-SA 4.0*
- 7.7: Structure Determination - Nuclear Magnetic Resonance Spectroscopy - *CC BY-SA 4.0*

- 7.7.1: Nuclear Magnetic Resonance Spectroscopy - *CC BY-SA 4.0*
- 7.7.2: The Nature of NMR Absorptions - *CC BY-SA 4.0*
- 7.7.3: The Chemical Shift - *CC BY-SA 4.0*
- 7.7.4: Chemical Shifts in ^{1}H NMR Spectroscopy - *CC BY-SA 4.0*
- 7.7.5: Integration of ^{1}H NMR Absorptions - Proton Counting - *CC BY-SA 4.0*
- 7.7.6: Spin-Spin Splitting in ^{1}H NMR Spectra - *CC BY-SA 4.0*
- 7.7.7: ^{1}H NMR Spectroscopy and Proton Equivalence - *CC BY-SA 4.0*
- 7.7.8: More Complex Spin-Spin Splitting Patterns - *CC BY-SA 4.0*
- 7.7.9: Uses of ^{1}H NMR Spectroscopy - *CC BY-SA 4.0*
- 7.7.10: ^{13}C NMR Spectroscopy - Signal Averaging and FT-NMR - *CC BY-SA 4.0*
- 7.7.11: Characteristics of ^{13}C NMR Spectroscopy - *CC BY-SA 4.0*
- 7.7.12: DEPT ^{13}C NMR Spectroscopy - *CC BY-SA 4.0*
- 7.7.13: Uses of ^{13}C NMR Spectroscopy - *CC BY-SA 4.0*
- 7.7.S: Structure Determination - Nuclear Magnetic Resonance Spectroscopy (Summary) - *CC BY-SA 4.0*

8: Molecular Mass Spectrometry - *CC BY-NC-SA 4.0*

- 8.1: General Features of Atomic Mass Spectrometry - *CC BY-NC-SA 4.0*
- 8.2: Molecular Mass Spectra - *CC BY-NC-SA 4.0*
- 8.3: How the Mass Spectrometer Works - *CC BY-NC 4.0*
- 8.4: Mass Spectrometers - *CC BY-NC-SA 4.0*
- 8.5: Ion Sources - *CC BY-NC-SA 4.0*
  - 8.5.1: Electrospray Ionization Mass Spectrometry - *CC BY-NC-SA 4.0*
- 8.6: Mass Spectrometers - *CC BY-NC-SA 4.0*
  - 8.6.1: Mass Analyzers (Mass Spectrometry) - *CC BY-NC-SA 4.0*
- 8.7: Applications of Molecular Mass Spectrometry - *CC BY-NC-SA 4.0*
  - 8.7.1: Interpreting a Mass Spectrum - *CC BY-NC-SA 4.0*
  - 8.7.2: The Molecular Ion (M^{+}) Peak - *CC BY-NC 4.0*
  - 8.7.3: The M+1 Peak - *CC BY-NC 4.0*
  - 8.7.4: The Mass Spectra of Elements - *CC BY-NC 4.0*
  - 8.7.5: Fragmentation Patterns in Mass Spectra - *CC BY-NC 4.0*
  - 8.7.6: Mass Spectrometry - Fragmentation Patterns - *CC BY-NC-SA 4.0*
  - 8.7.7: Organic Compounds Containing Halogen Atoms - *CC BY-NC 4.0*

9: Atomic Spectroscopy - *CC BY-NC-SA 4.0*

- 9.1: Introduction to Atomic Absorption Spectroscopy - *CC BY 4.0*
- 9.2: Sample Atomization Techniques - *CC BY-NC-SA 4.0*
- 9.3: Atomic Absorption Instrumentation - *CC BY-NC-SA 4.0*
- 9.4: Interferences in Absorption Spectroscopy - *CC BY-NC-SA 4.0*
- 9.5: Atomic Absorption Techniques - *CC BY-NC-SA 4.0*
- 9.6: Atomic Absorption Spectroscopy - *CC BY-NC-SA 4.0*
- 9.7: Atomic Emission Spectroscopy - *CC BY-NC-SA 4.0*
  - 9.7.1: Emission Spectroscopy Based on Flame and Plasma Sources - *CC BY-NC-SA 4.0*
  - 9.7.2: Atomic Emission Spectroscopy - *CC BY-NC-SA 4.0*
  - 9.7.3: Inductively Coupled Plasma Mass Spectrometer - *CC BY-NC-SA 4.0*

10: Chromatographic and Electrophoretic Methods - *CC BY-NC-SA 4.0*

- 10.1: Introduction to Chromatographic Separations - *CC BY-NC-SA 4.0*
  - 10.1.1: A General Description of Chromatography - *CC BY-NC-SA 4.0*
  - 10.1.2: Migration Rates of Solutes - *CC BY-NC-SA 4.0*
  - 10.1.3: Zone Broadening and Column Efficiency - *CC BY-NC-SA 4.0*
  - 10.1.4: Chromatography - *CC BY-NC-SA 4.0*
  - 10.1.5: Optimization and Column Performance - *CC BY-NC-SA 4.0*
  - 10.1.6: Summary of Important Relationships for Chromatography - *CC BY-NC-SA 4.0*
  - 10.1.7: Applications of Chromatography - *CC BY-NC-SA 4.0*
- 10.2: Capillary Electrophoresis and Capillary Electrochromatography - *CC BY-NC-SA 4.0*
  - 10.2.1: An Overview of Electrophoresis - *CC BY-NC-SA 4.0*
  - 10.2.2: Capillary Electrophoresis - *CC BY-NC-SA 4.0*

- 10.2.3: Capillary Electrophoresis - *CC BY-NC-SA 4.0*
  - 10.2.3.1: Ionic Mobility and Electrophoresis - *CC BY-NC-SA 4.0*
- 10.2.4: Applications of Capillary Electrophoresis - *CC BY-NC-SA 4.0*
- 10.3: Problems - *CC BY-NC-SA 4.0*
- 10.4: Additional Resources - *CC BY-NC-SA 4.0*
- 10.5: Chapter Summary and Key Terms - *CC BY-NC-SA 4.0*

11: Thermal Methods - *CC BY-NC-SA 4.0*
- 11.1: Thermogravimetry - *CC BY-NC-SA 4.0*
- 11.2: Differential Thermal Analysis and Differential Scanning Calorimetry - *CC BY-NC-SA 4.0*

12: Equilibrium Chemistry - *CC BY-NC-SA 4.0*
- 12.1: Reversible Reactions and Chemical Equilibria - *CC BY-NC-SA 4.0*
- 12.2: Thermodynamics and Equilibrium Chemistry - *CC BY-NC-SA 4.0*
- 12.3: Manipulating Equilibrium Constants - *CC BY-NC-SA 4.0*
- 12.4: Equilibrium Constants for Chemical Reactions - *CC BY-NC-SA 4.0*
- 12.5: Ladder Diagrams - *CC BY-NC-SA 4.0*
- 12.6: Problems - *CC BY-NC-SA 4.0*
- 12.7: Additional Resources - *CC BY-NC-SA 4.0*
- 12.8: Chapter Summary and Key Terms - *CC BY-NC-SA 4.0*

13: Electrochemical Methods - *CC BY-NC-SA 4.0*
- 13.1: Overview of Electrochemistry - *CC BY-NC-SA 4.0*
- 13.2: An Introduction to Electroanalytical Chemistry - *CC BY-NC-SA 4.0*
  - 13.2.1: Electrochemical Cells - *CC BY-NC-SA 4.0*
  - 13.2.2: Potentials in Electroanalytical Cells - *CC BY-NC-SA 4.0*
  - 13.2.3: Electrode Potentials - *CC BY-NC-SA 4.0*
  - 13.2.4: Calculation of Cell Potentials from Electrode Potentials - *CC BY-NC-SA 4.0*
  - 13.2.5: Currents in Electrochemical Cells - *CC BY-NC-SA 4.0*
  - 13.2.6: Types of Electroanalytical Methods - *CC BY-NC-SA 4.0*
- 13.3: Potentiometry - *CC BY-NC-SA 4.0*
  - 13.3.1: Standard Electrodes - *CC BY-NC-SA 4.0*
  - 13.3.2: Standard Potentials - *CC BY-NC-SA 4.0*
  - 13.3.3: Reference Electrodes - *CC BY-NC-SA 4.0*
  - 13.3.4: Metallic Indicator Electrodes - *CC BY-NC-SA 4.0*
  - 13.3.5: Membrane Ion-Selective Electrodes - *CC BY-NC-SA 4.0*
  - 13.3.6: Molecular-Selective Electrode Systems - *CC BY-NC-SA 4.0*
  - 13.3.7: Quantitative Potentiometry - *CC BY-NC-SA 4.0*
- 13.4: Voltammetry - *CC BY-NC-SA 4.0*
  - 13.4.1: Potential Excitation Signals and Currents in Voltammetry - *CC BY-NC-SA 4.0*
  - 13.4.2: Voltammetric Instrumentation - *CC BY-NC-SA 4.0*
  - 13.4.3: Linear Sweep Voltammetry - *CC BY-NC-SA 4.0*
  - 13.4.4: Cyclic Voltammetry - *CC BY-NC-SA 4.0*
  - 13.4.5: Polarography - *CC BY-NC-SA 4.0*
  - 13.4.6: Stripping Methods - *CC BY-NC-SA 4.0*
  - 13.4.7: Applications of Voltammetry - *CC BY-NC-SA 4.0*
- 13.5: Problems - *CC BY-NC-SA 4.0*
- 13.6: Additional Resources - *CC BY-NC-SA 4.0*
- 13.7: Chapter Summary and Key Terms - *Undeclared*

14: Surface Characterization by Spectroscopy and Microscopy - *CC BY-NC-SA 4.0*
- 14.1: Introduction to the Study of Surfaces - *CC BY-NC-SA 4.0*
- 14.2: Scanning Electron Microscopy - *CC BY-NC-SA 4.0*
  - 14.2.1: Scanning electron microscopy (SEM) - *CC BY-NC-SA 4.0*
  - 14.2.2: Transmission Electron Microscopy - *CC BY 4.0*
- 14.3: Scanning Probe Microscopes - *CC BY-NC-SA 4.0*
  - 14.3.1: Scanning Tunneling Microscopy - *CC BY 4.0*
  - 14.3.2: Scanning Tunneling Microscopy (STM) - *CC BY-NC-SA 2.5*
  - 14.3.3: Atomic Force Microscopy - *CC BY-NC-SA 4.0*
  - 14.3.4: Atomic Force Microscopy (AFM) - *CC BY-NC-SA 2.5*
- 14.4: Spectroscopic Surface Methods - *CC BY-NC-SA 4.0*
  - 14.4.1: X-ray Photoelectron Spectroscopy - *CC BY 4.0*
  - 14.4.2: Auger Electron Spectroscopy - *CC BY 4.0*

Back Matter - *Undeclared*
- Index - *Undeclared*
- Glossary - *Undeclared*
- Detailed Licensing - *Undeclared*

- Detailed Licensing - *Undeclared*